INFLUENCE OF RUBBING ON ROTOR DYNAMICS

NASA Contract No. NAS8–36719

FINAL REPORT

Part 1 of 2

Prepared for George C. Marshall Space Flight Center
Marshall Space Flight Center,
Alabama 35812

by

Agnes Muszynska
Donald E. Bently
Wesley D. Franklin
Robert D. Hayashida
Lori M. Kingsley
Arthur E. Curry

Bently Rotor Dynamics Research Corporation

BENTLY NEVADA CORPORATION
P.O. Box 157
MINDEN, NEVADA 89423

March 1989

SUMMARY

The results of analytical and experimental research on rotor–to–stationary element rubbing in rotating machines are presented in this report. A characterization of physical phenomena associated with rubbing, as well as literature survey on the subject of rub is given.

The experimental results were obtained from two rubbing rotor rigs: one, which dynamically simulates the space shuttle main engine high pressure fuel turbo pump (HPFTP), and the second one, much simpler, a two–mode–rotor rig, designed for more generic studies on rotor–to–stator rubbing. The experiments brought a wide array of results, confirming the richness of rotor–to–stator rub occurrences. Some dynamic phenomena observed during the experiments, such as fluid induced instabilities and internal friction instability which were not correlated to rubbing are also mentioned in this report.

The study on the influence of rubbing on rotor dynamics can be divided into two parts: (i) generic rotor–to–stator rub–related dynamic phenomena affecting rotating machine behavior, and (ii) applications to the space shuttle HPFTP. The characterization of rotor–to–stator rub phenomena in rotating machines brought a very rich array of factors and parameters which affect the rotating system responses. The influence of several parameters was investigated during this study. The main interest was placed into rotor lateral vibrational responses modified by rotor rubbing against the stationary part. The emphasis was in the lowest modes, as these modes are vital in rotor dynamics. Two most thoroughly investigated factors affecting rub–related rotor dynamics were the rotor rotative speed versus the system natural frequency spectrum, and the radial preload force. It is shown that rotor vibrational patterns vary for different values of these parameters. The effects of other factors, such as rubbing element materials and their surface finishes and hardness, rotor unbalance, geometry of the stator rubbing area, rubbing at several axial locations were also studied.

An outline of application of the Dynamic Stiffness methodology for identification of rotor/bearing system modal parameters is given. Such identification was necessary for appropriate interpretation of consequently obtained experimental data on rubbing rotor.

The mathematical model of rotor/bearing/seal system under rub condition is given. The computer program was developed to calculate rotor responses. Compared with experimental results the computed results prove an adequacy of the model.

In the Conclusions a discussion on influence of rubbing on rotating machine dynamics is summarized. Some recommendations concerning rub prevention, use of vibration measuring and data processing instrumentation, as well as rub diagnostic hints are given.

In the Appendix of this report the data from the SS HPFTP hot fire tests reduced and evaluated by using Bently Nevada methodology are included. Also included is the paper on the influence of rubbing on rotor dynamics presented on the 1988 Conference on Advanced Earth–to–Orbit Propulsion Technology.

At the end of this report the information on the electronic instrumentation used in the experiments is attached.

TABLE OF CONTENTS

PART 1

1. INTRODUCTION.

1.1 Original Scope of the Research on "Influence of Rubbing on Rotor Dynamics" Solicited by NASA

The interest in rotor–to stator rub analysis in rotating machines continues to grow as machines become ever more complex and dynamically "active." Rubbing cannot only increase energy losses and cause premature wear of machine elements, but can also cause a devastating failure of the entire machine.

The objectives of the program, "Influence of Rubbing on Rotor Dynamics," as solicited by NASA in 1985 were:

- Delineate and characterize various rubbing sources in high performance turbomachinery.
- Develop mathematical models to depict the significant factors which rubbing contributes to rotor dynamical responses.
- Perform laboratory tests to demonstrate significant rubbing mechanisms for comparison with mathematical model results.
- Demonstrate how the simulation methods can be applied to high performance rotating machinery to assess the severity of rubbing during operational conditions.

The objective of the research performed at Bently Nevada Corporation was to gain an improved understanding of the rubbing phenomena in rotating machines, in order to properly diagnose the malfunction and prevent rub–related damages and failures.

The end product of the effort is a contribution to vibration diagnostic techniques of machines, improved prediction of operational limits, and improved design criteria for high performance rotating machinery.

1.2 Scope of This Report

In the present report the summary of the two–year research effort on the subject of "Influence of Rubbing on Rotor Dynamics" is given. In the following chapters the obtained theoretical, analytical, and experimental results are presented. Following the NASA suggestion formulated at the time when the research contract was granted to Bently Nevada Corporation, the investigation of rotor–to–stator rub phenomena was concentrated on those occurring in the high–pressure fuel turbopump (HPFTP) of the Space Shuttle. An experimental rig simulating HPFTP was built, and the majority of experiments were performed on this rig.

Another smaller and easier to control rig was also built in order to perform more generic studies on rotor–to–stator rubs.

Following the theoretical predictions and experimental observations, the computer program was designed to calculate rotor response in case of rotor–to–stator rubbing contact. This program or its elements can be incorporated in most complex rotordynamic programs for rotating machines.

The chapters in this report are put in order in "historical" rather than "topical" sequence. Pertinent figures are included at the end of each chapter. The report is divided into two integral parts; the page numbering is maintained continous.

The second chapter gives the literature overview on rotor–to–stationary element rubbing phenomena. The third chapter provides more specific characterization of rubs. From these two chapters one may conclude how rich is rotor–to–stator rub in terms of dynamic occurrences. Chapter 4 describes the initial design assumptions and data for the experimental rig which simulates the space shuttle main engine high pressure fuel turbo pump (HPFTP). The simulation is based on similarity of mode shapes and scaled natural frequencies for the lowest modes.

In Chapter 5 the results of seal–simulating bearing tests are described. The oil–lubricated bearings with controlled oil pressure are used in the HPFTP–simulating rotor rig. The bearings simulate the interstage seals.

Chapter 6 gives the general description of the HPFTP–simulating rig and instrumentation used for dynamic testing.

In Chapter 7 some preliminary results from the HPFTP–simulating rig are described.

Chapter 8 provides the results of dry friction coefficient measurements and analysis of surface damaging effects of rubbing.

In Chapter 9 the second, smaller, two–bending mode rotor rig is described, and the identification of its dynamic characteristics is given. Being simpler and much easier to operate and control its dynamic processes than the HPFTP–simulating rig, this rig is used for more generic rub tests.

In Chapter 10 the results of rotor–to–stator rubbing obtained from the two–mode–rig are given.

In Chapter 11 the mathematical model of rubbing rotor/bearing/seal/stator system is described.

Chapter 12 provides results of the rotor–to–stator rubbing obtained on the HPFTP–simulating rig.

In Chapter 13 the experimental results of the rotor–to–stator rubbing contact are analyzed.

Chapter 14 gives the description of the computer code for obtaining numerical calculations of rotor–to–stator rubbing system dynamic responses, and Chapter 15 provides some computer–generated results.

In Appendix 1 the reduced dynamic data from HPFTP hot fire tests are given. The data provided by NASA were reduced by using Bently Nevada data–processing systems. The results provide some significant conclusions.

In Appendix 2 the copy of the paper presented at the Third Conference on Advanced Earth–to–Orbit Propulsion Technology in 1988 is included. Some results obtained during the rotor–to–stator rubbing study were summarized in this paper.

Finally, Appendix 3 contains information on the electronic instrumentation used in experimental testing.

2. ROTOR–TO–STATIONARY ELEMENT RUB–RELATED VIBRATION PHENOMENA IN ROTATING MACHINERY. LITERATURE SURVEY.

Rotor–to–stationary element rub is a serious malfunction in rotating machinery which may lead to a catastrophic failure of the machine. Dynamic phenomena occurring during rubbing such as friction, impacting, stiffening, and coupling effects are discussed in this chapter. The literature survey on rub–related phenomena in rotating machinery is presented.

2.1 Introduction

In spite of the fact that the importance of rotor–to–stationary element rub phenomena in rotating machinery has been recognized for over a half of the century, the literature on this subject is relatively scarce and incoherent. This is probably due to the fact that rotor–to–stator rub–related phenomena are very complex, involving several physical mechanisms, thus, they represent a wide spectrum of rotating machinery dynamic problems.

The major physical phenomena occurring during rotor–to–stator rubs, and the literature survey on the subject of rub, both are outlined below.

2.2 Rub Malfunction in Rotating Machinery

The normal operation of a rotating machine results from an appropriate torque/load balance and consists of main rotative motion of the shaft (together with all rotating elements associated with the shaft) performed with an appropriate rotative speed and around the appropriate axis. This main motion can be accompanied by a limited level of lateral/torsional/longitudinal vibrations ("parasitic motion") of the rotor itself, and a limited level of vibration of stationary (nonrotating) parts.

Rub in a rotating machine is a malfunction condition associated with the physical contact of rotating and stationary parts which otherwise should not be touching. As a result of the rotor–to–stator rub, the "normal operation" of the machine is affected. Rub changes the system force balance and dynamic stiffness; this results in modifications of the machine motion. The effect is usually associated with a decrease of the amount of energy provided to maintain the main motion, and an increase in the level of "parasitic" vibrations.

The rotor–to–stator rub is a secondary phenomenon usually resulting from a primary cause which perturbs the "normal operation conditions." This primary cause can originate from various sources, such as unbalance, thermal and/or assembly misalignment, stator/casing motion, fluid dynamic forces in main flow, bearings, and/or seals, leading to instability and self–excited vibrations. The occurrence of the "primary source" results in changes of shaft centerline position and/or shaft vibrations (most often at the lateral mode).

Rub occurs at a rotor axial location at which, for the given rotative speed and the shaft bow mode, the sum of the shaft centerline displacement plus vibrations amplitude exceeds the available clearance within the stator or seal. Once the rotor starts rubbing, the system becomes modified and the vibrations level usually increases. This may lead to rubbing at other locations.

Most often rub occurs at seals. Seldom, but more dangerous conditions occur when a blade rubs against the stator or a vane. Rub phenomena may also result when a magnetically

suspended rotor touches upon its emergency bearings. Rub also occurs in friction dampers installed to limit high lateral vibrations of rotors (most often resonant vibrations while passing balance resonances, critical speeds).

2.3 Thermal Effect of Rub

The earliest publications on rub phenomena reported a thermal effect of rub in turbomachinery. The phenomenon is often referred to as "Newkirk effect." Newkirk [67] pointed out that when a rubbing rotor is running below its first balance resonance speed, the rub–induced vibrations tend to increase in time. Later this effect was studied by several authors [20,24–27,42–48,64,75,82] who confirmed that vibrations can grow in amplitude and phase, resulting in "spiral vibrations" [26,48,51]. When an unbalanced shaft runs at a speed slightly lower than the first balance resonance, the rub usually takes place at the seal with the smallest clearance and located closest to the shaft antinodal position. The rub occurs at the shaft "high spot" (radial location under highest tension stress). At a constant rotative speed, for the mode of vibration predominantly synchronous with a circular or slightly elliptical orbit, the rubbing high spot occurs always at the same shaft location at each turn. The rub causes friction–related heating and local thermal expansion. Due to normal or accidental presence of fluids in the rotor/stator clearance areas, the rub–generated heat can be transferred by the fluid flow, so that shaft heating and thermal expansion may be relatively slow. Due to local expansion, the shaft bows, causing an additional imbalance in the system. At the rotative speed lower than the first balance resonance, the phase angle between the high spot and heavy spot (unbalance) is less than 90 degrees. The additional bow–related imbalance adds, therefore, to the existing one. The result is an increase of rotor synchronous vibrations. The relationship between the new imbalance and original one explains phase rotation. The increase of total value unbalance causes higher vibration amplitudes which result in stronger rubbing and larger amount of generated heat. Finally, due to local thermal expansion, the elastic stress limit is exceeded, and shaft becomes permanently bowed due to local plastic deformations. At that stage the shaft does not qualify any more for further operation.

Kellenberger [48] proposed a model of the rub thermal phenomenon. He introduced parameters describing the flow of heat into and out of the shaft. Used in equations, these parameters model well the rub thermal effect resulting in spiral motion of the shaft. Dimarogonas [24,26] identified an additional type of rub thermal effect–related shaft vibrations — an oscillating mode occurring during the transition from the spiraling to the steady–state mode.

Smalley [75] pointed out that rotor low angular acceleration when passing through the first balance resonance speed, as well as extended operation just below this critical speed lead to aggravation of the rub–related conditions of the turbomachine.

The described rub–related thermal effects of rotors are particularly important for big machinery with relatively high thermal inertia. Field experience in observing the rub–related thermally induced vibration effects on turbomachinery was reported in several papers [20,64]. State of the Art review on thermal effects of rub is given in [27].

2.4 Dry Whip

More observations of rotating machinery dynamic behavior led to identification of several other effects than the thermally induced vibrational effect of rub described above. The most important among them is the self–excited backward precession of the shaft, known as "dry whip" [7,8,15,16,23,24,30,31,35,45,56,61–63]. In this mode the shaft rolls while sliding against the seal in the direction opposite to the direction of rotation, and maintains the

contact with the seal. High normal forces and corresponding friction forces at the contacting surfaces may lead to extremely severe damage in merely a few seconds [34,35,39,45,47]. Most often seals are damaged or destroyed [35,45]. Due to the backward mode of precession, the shaft is also under severe stress condition which may lead to failure. The seal damage may trigger a sequence of catastrophic events: a violation of the design integrity of the machine at the seal level causes a further increase of rotor vibrations and rotating load levels, which may cause further damage to bearings or blades (including blade loss). Catastrophic failures of rotating machines are often disastrous, as a high amount of energy is suddenly released, endangering the environment as well as human lives. Rotor rub–related failures occur quite often. In particular, the U. S. Department of Transportation reported that 10.2% of all uncontained engine rotor failures during 417 million engine flight hours in the period from 1962 to 1976 were caused by rotor rubbing against stationary parts [47].

2.5 Physical Phenomena Occurring During Rubbing

Rotor–to–stator rub involves several physical phenomena, the most important among them being friction, impacting, coupling, and stiffening effects.

2.5.1 Friction

Friction accompanies the relative motion of rotor/stationary element during their contact. It produces the usual friction–related effects: wear (grinding, pitting) of the rubbing surfaces, together with heat generation (up to metal melting temperatures). The local heating effects of rub were discussed in the previous section. Very often the rubbing surface relative tangential velocity is high, and the normal forces significant, the destructive effects of friction can, therefore, be extremely strong in a very short time. Due to the wear effect, the surface rubbing conditions change very fast with time. This may lead to either widening clearances and resulting elimination of the rotor–to–stator contact, or to an enlargement of the contact surface area (breaking–in effect). Therefore, in a limited time either rub stops (causing some short–time transient conditions for the rotor system) or rub continues with further continuous modification of conditions and dynamic responses.

2.5.2 Impacting

Impact conditions occur when the low normal contact force of rotor/stationary part occurs instantaneously with relatively high incoming speed. An impact generates a wide frequency spectrum of exciting forces. The system response contains then components with natural frequencies. Repetitive periodic impacts can result in a definite spectrum of periodic excitation and periodic responses of the system.

Impacts create an "after impact" instantaneous response — most often a rebounding motion of the rotor (separation from the stator) with the initial direction depending on impact conditions and relative tangential velocities in particular[5, 60].

The impacting motion of high speed rotors with significant elastic properties, together with high friction at the contacting surfaces promoting an "adhesive mechanism," creates conditions for a "superball effect" [52,81,87]. During the impact, the shaft incoming speed (precessional speed) is less important than the rotative speed. During a short time adhesive contact (with no relative motion), the shaft rotative energy becomes transferred into vibrational energy of the rebounding motion (precessional energy). The direction and velocity of rebounded motion depends on the amount of tangential moment generated by shaft rotation.

2.5.3 Torsional Load

Rub causes an additional torsional load in the system. It usually results in a decrease of rotative speed and/or an increase of required power.

2.5.4 Coupling Effect

Due to the physical contact of the rotating and stationary part, the dynamic state of mechanical structure involved in motion changes. This effect is similar to coupling an additional structure to the existing ("normal") structure. Since the rub–related coupling is usually time dependent (on/off periodic type), the system dynamic stiffness also becomes periodically time dependent. The rub coupling effect varies with contact normal forces, contact surface area, flexibility (degrees of freedom) of the contacting elements, dynamic stiffnesses of the "normally operating" structure, and the additional, coupled structure (strong/weak coupling), and the time of contact versus time of separation.

2.5.5 Stiffening Effect

An additional effect of rub coupling may result in stiffening of the shaft as it is forced to rotate in a bent configuration. This results in an increase of the system rigidity and an increase of the natural frequencies of the system.

2.5.6 Other Effects

In fluid–handling machines rub at seals, and following seal wear, cause an increase of clearances and changes in the flow pattern of the working fluid. This generates new fluid dynamic forces and possible modifications of thermal conditions which, in turn, can change clearance situations due to thermal expansion. Both effects affect system dynamics when rub results in the conditions of slowly or rapidly changing clearances.

2.6 Analysis of Rubbing Rotors

In order to predict and prevent rub–related phenomena, mathematical modelization of rub conditions attracted the attention of many researchers [7–9,13,15–19,21,24,30,44, 46,55,59–63,65,69,79–81]. The complexity of the phenomena and their local/global nature usually prevented the authors from treating general cases. Most publications discuss some particular aspect of rotor–to–stator rubs.

Initial important assumptions in the analyses are the dynamic characteristics of the considered rotating machine: number of degrees of freedom (modes) of the rotor, stator (seal) susceptibility, and external constants as well as rotating loads. The assumptions regarding the rotative machine model lead to the determination of characteristics of the system. Simple rotor models most often allow for analytical results and provide qualitative features of rotating system steady–state and transient response modifications due to rub. In papers [59–62] it was shown how different amounts of rub–related friction, impacting, and system stiffness modification resulted in significantly different steady–state vibrational patterns. At the extremes of the rub–related steady–state vibrational responses are "full annular rub," i.e., the above–mentioned "dry whip," and "partial rub" [5,6,29,59,60,88]. The latter type of rub means that the rotor enters into contact with a stationary part (stator, seal) only occasionally and maintains this contact during a small fraction of its precessional period. Rub may occur only at one axial and radial location of the shaft, or it may occur at several locations ("multiple partial rub"). In the partial rub mode, the most pronounced physical phenomenon is impacting, followed by rotor free vibration. Normal contact forces and friction are relatively low, thus, the rubbing surface damage is not

significant, allowing for maintained steady–state conditions of vibration. During the full annular rub ("dry whip"), the friction and vibrating system stiffness modifications are considerable. The steady–state full annular rub occurrence cannot be maintained for a prolonged period of time, as it rapidly leads to surface damage and changes in rub conditions, followed by subsequent dynamic transients.

During each local rotor–to–stator rub event several phases can be distinguished: (i) no rub, (ii) rub initiation with impact, (iii) rub interaction in the form of stick–slip chattering motion (transition phase), (iv) rub interaction in the form of a sliding/rolling contact, (v) separation. At each phase, the contribution of rub–related physical phenomena is different. Each rub event may comprise all or only a few phases. The adequacy of obtained analytical results to observable dynamic phenomena is determined by an appropriate modelization of the global and local rub effects. The chaos theory found an interesting application in modelling complex rub–related phenomena [79]. Application of this theory allows for prediction of structural instabilities (Feigenbaum scenario) which result in chaotic regions in wide ranges of system parameters.

The effect of dry surface friction is taken into account in several publications [8,9,11,13,15–20,44,45,60–63,66]. Most often the simple Coulomb friction model is considered [8,11,16,19,20,45,60,63,66]. The more advanced nonlocal dynamic friction law which takes into account a weighting function that distributes the influence of normal surface stress has been proposed in [77]. Friction at rubbing surfaces generates heat. Local temperatures may increase high enough to melt the seal metal (such as brass) [35,63]. In the condition of the fluid presence (melted metal), the "dry friction" model of the phenomenon is no longer adequate. The friction model must, therefore, be adjusted following the conditions at the rubbing surfaces. Friction forces become heat transfer–related functions of dynamic parameters of the system.

Friction introduces a usual damping effect considered in papers [28,55,58,74,89], as well as a structure coupling effect [3,59,73]. The conditions of stick–slip motion were discussed in papers [30,50,72]. The corresponding mathematical models of friction include nonlinear terms.

Damping effects of rub provided an objective for designing special emergency dampers which allow rotors to pass critical speeds [28,89]. These dampers physically restrict the shaft lateral motion while providing dry friction as an energy dissipating mechanism.

Friction is the main mechanism of surface wear (fretting). A few research reports [38,78,83,86] provide recommendations regarding material selection, surface finish, and surface coatings in order to reduce the rub–related severity of load, wear, and debris generation. The continuous changes in rubbing surface conditions and clearance increase due to wear should be taken into account in more sophisticated rub models. The increased clearance as a result of wear can lead to a less violent version of the rotor rub–related problems [34].

With the assistance of computers, more complex rotor system configurations with rub effects could be modeled using both finite element [21,49,70] and/or modal synthesis techniques [18,55,65,66]. Nonlinear effects can be included in both schemes. The analyses most often provide results of numerical integration, i.e., timebase vibration waveforms of transient processes [2,16–18,20,44,46,55,66,69,81,88], leading eventually to limit cycles of rub–induced rotor self–excited vibrations (partial rub or dry whip) [2,16,81]. The final results of such analyses depend significantly on how the local effects of rub were modeled, and what ranges of parameters were considered. Some of these studies have been limited in scope to the onset of rub wherein the rotor vibration amplitude (most often an unbalance

response and possibly steady radial force–related displacements) just exceeds the stator or seal clearance.

In publications [15–19,44–46,59,69] on rotor–to–stator rub interactions the results of series of studies were presented. These studies were undertaken in order to define the role of stator stiffness, friction effect, and magnitudes of suddenly applied forces (such as an unbalance force due to a blade loss), as well as the effect of various rub models on the system responses. Several rub models were considered in the numerical studies [44,46]: (i) abradable model based on energy loss per unit volume, (ii) smearing model based on viscous hydrodynamic theory, (iii) dry friction model. The analysis of rotor vibrations using these models provided comparable results: in the case of each model there exist "critical values" of rub–related parameters which lead to most destructive rotor backward dry whip. A special class of rotating systems prone to rubs are high speed rigid gyroscopes and gyro pendulums [53,79–81,84,85]. When an obstacle, against which the rotor rubs at its originally conical mode, is a flat surface, the friction acts as a negative damping [81]. In addition, the friction forces at the rubbing surfaces become amplified by the gyroscopic effect [53,79–81]. The resulting self–excited vibrations (with possible multiple limit cycles) may gather into an extremely violent form [79–81].

The impacting phase is most often modeled by applying straight impact theory with the restitution coefficient which quantifies the loss of energy [59,60,71]. The advanced model of the rotor impact includes the "superball effect" resulting from the tangential momentum [52,81,87]. A "tangential coefficient of restitution" representing the adhesive friction is used to model the superball impact losses [52,87]. In the superball effect the vibrational energy provided by rotation is usually much larger than the energy dissipated by the classical impact mechanism. In the typical rub with the superball effect the shaft/stator contact after the impact is extremely short, possibly followed by an equally short period of sliding and rolling. During these short phases a significant local deformation of rubbing elements occurs. When the contact is broken, the rotation–related rebounding velocity initiating the shaft free motion often directs the shaft into backward precession regions, thus the phase of motion becomes reversed. Since the impact period in time scale is much shorter than other phases of rub, the piece–wise continuous numerical integration used in order to obtain rotor response must include variable step code.

More advanced rub models may take into consideration local surface deformation, contact stress, and elastic wave effects for more adequate prediction of pitting (surface fatigue failure) [10]. To the authors' knowledge, they have not yet been applied, however, in rotor–to–stator rub analysis.

2.7 Vibration Response of Rubbing Rotors

Rotor–to–stator rub represents a strongly nonlinear phenomenon. In terms of rotor vibrational response, rub generates a wide spectrum of components. The steady–state regimes then existing for a relatively short time may have as fundamental the subsynchronous frequencies corresponding to even fractions of the rotative speed [2,5,11,29,59,60,62], and/or frequencies corresponding to the rub–modified system natural frequencies [63]. The transient process involve free vibrational responses, thus are characterized by frequencies being system natural frequencies. Rub–related steady–state occurrences are never long–lasting due to continuously changing rubbing surface conditions (grinding effect) which produce variable radial load conditions, thus very often can be accompanied or alternated by transient processes. Each fundamental frequency vibration component is accompanied by higher harmonics. Amplitudes of higher harmonic vibrational components increase with the severity of rub (mostly involving higher friction and nonlinear radial stiffness forces).

The appearance and strength of higher harmonics in the rotor vibrational spectrum can be used as a diagnostic tool to detect rotor–to–stator rub. The method allows for determination of limits between light to severe rotor–to–stator contact with rub, excessive wear, and initiation of destructive dry whip mode [4]. The method was effectively used in rub detection in testing of the liquid oxygen turbopump MK48–0 [68].

The appearance of the higher harmonics in the rotor vibrational spectrum leads to a generation of a wide frequency kinematical excitation for the machine stationary elements, as well as for the environment (through elastic and acoustic waves). High frequency excitation may lead to structural resonances and an overall increase of the machine vibration level. The latter may cause further changes in the system, such as loosening friction–tightened bolts and other frictional joints [35]. Affected integrity leads to an aggravation of the machine condition. To make things worse, the entire scenario usually occurs in a very short time.

Vibration monitoring and data processing systems installed on rotating machines provide more and more information on rub–related vibrations and help in the prevention of machine catastrophic failures. Reported field case histories bring insights on the symptoms and severity of rotor–to–stator rub–related phenomena in pumps [1,9,40,50,56], turbogenerators [2,20], and compressors [36].

Vibration signals carry important diagnostic information: frequency content, modes of shaft centerline, vibration component amplitudes, phases of synchronous vibration and its harmonic components. An orbital presentation of shaft motion is a useful diagnostic tool for rub detection. Most machine malfunctions are characterized by forward precession (the same direction as rotation). Rub is among a minority of phenomena which produce backward components. In orbital presentation these components result in external loops most often superimposed on the synchronous orbit (forward components produce internal loops). The existence of strong higher harmonics generates quite complex orbital pattern of the rotor response, thus rub is relatively easy to detect. The diagnosis of the rub location is, however, more difficult.

2.8 Dead Band Malfunction — Twin Brother of Rub

The rotor–to–stator rub is an abnormal situation which (among other phenomena) provides an increase in the vibrating system stiffness. This effect is often referred to as the "normal–tight" situation. There exists a "twin brother" effect consisting of a decrease in the system stiffness, when a normally contacting element of the rotating system becomes loose. The latter situation often occurs when the bearing clearance becomes too large, and is usually referred to as "normal–loose" or "dead band" phenomenon [4,6,8,11,14,22,33,41, 43,55,57]. The effect of vibrating system stiffness modifications in both "normal–tight" and "normal–loose" situations is very similar, as described by Bently [5]. Both cause periodically variable stiffness, thus provide conditions for classical parametric excitation, which may lead to rotor instability [9,13,30]. In the "dead band" phenomenon the friction contribution is usually much lower [4].

2.9 Summary

To summarize this survey on rotor–to–stator rub vibrational phenomena, one should realize that rub is a very complex phenomenon involving a wide spectrum of dynamic events. Rub occurs usually as a secondary effect of some other machine malfunction (such as unbalance, misalignment, thermal mismatch, fluid–induced self–excited vibrations of whirl or whip type) which results in either rotor high vibration amplitudes or changes in rotor centerline position. More seldom rub occurs as a secondary effect of stator/casing

vibrations such as caused by foundation motion when the machine operates on a ship or off–shore platform, or caused by seismic events. Unlike other secondary effects, rub, however, immediately becomes dominant in the rotating machine dynamic behavior, leading quickly to further changes in the machine mechanical system. Very often these changes mean an ultimate failure of a system component and a catastrophic failure of the entire machine.

Building adequate models of rub and incorporating them into the machine dynamic analysis, in order to predict rub dynamic phenomena and to evaluate their possible severity, are important and urgent tasks. It is also necessary to work out an efficient diagnostic methodology and establish acceptable tolerances for rub–related vibrations of rotating machines.

2.10 References

1. Allaire, P. E., Martinez, L. C., Barrett, L. E., Bosi, D. M., Flack, R. D., "Vibration Analysis of Reactor Recirculation Pump Problems," Reactor Coolant Pump Recirculation Pump Monitoring Workshop, Proceedings EPRI, M&DC. Toronto, Canada, March 1988.

2. Allaire, P. E., Lee, C. C., "Vibrations of Rotating Machinery Undergoing Rub," Fifth Annual ROMAC Short Course, Washington, D.C., August 1987.

3. Bazan, E., Bielak, J., Griffin, J. H., "An Efficient Method for Predicting the Vibrating Response of Linear Structures With Friction Interfaces," 86–GT–88, Journ. of Engineering for Gas Turbines and Power, 1986.

4. Beatty, R. F., "Differentiating Rotor Response Due to Radial Rubbing," ASME J. of Vibration, Acoustics, Stress, and Reliability in Design, v. 107, April 1985.

5. Bently, D. E., "Forced Subrotative Speed Dynamic Action of Rotating Machinery," ASME Publication, 74–Pet–16, Petroleum Mechanical Engineering Conference, Dallas, Texas, September 1984.

6. Bently Nevada Applications Note, "Exact Subrotative (1/2X, 1/3X, 2/3X, 1/4X, etc.) Machinery Vibration Behavior. Part I: The Normal/Tight Mathieu Rub, Part II: The Normal/Loose Mathieu Malfunction," Machinery Protection and Diagnostics Topics, 1977.

7. Billet, R. A., "Shaft Whirl Induced by Dry Friction," The Engineer, v. 220, No. 57, October 1965, pp. 713–714.

8. Black. H. F., "Interaction of a Whirling Rotor With a Vibrating Stator Across a Clearance Annulus," Journal Mechanical Engineering Science, v. 10., No. 1, 1968, pp. 1–12.

9. Black, H. F., "Synchronous Whirling of a Shaft Within a Radially Flexible Annulus Having Small Radial Clearance," IMechE, Paper 4, v. 181, No. 65, March 1966/67.

10. Castleberry, G. A., "The Little Things Count in Designing for Contact Stresses," Machine Design, August 1985, pp. 75–78.

11. Childs, D. W., "Fractional — Frequency Rotor Motion Due to Nonsymmetric Clearance Effects," ASME Publication, 81–GT–145, International Gas Turbine Conference and Products Show, Houston, Texas, Journal of Engineering for Power, 1981.

12. Childs, D. W., "The Space Shuttle Main Engine High Pressure Fuel Turbopump Rotordynamic Instability Problem," ASME Journal of Engineering for Power, v. 100, 1978, pp. 48–57.

13 Childs, D. W., "Rub–Induced Parametric Excitation in Rotors," ASME Journal of Mechanical Design, Paper 79–WA, DE–14, ASME Trans., v. 101, October 1979, pp. 640–644.

14. Childs, D., Moyer, D. S., "Vibration Characteristics of the HPOTP of the SSME," Journal of Engineering for Gas Turbines and Power, v. 107, January 1985.

15. Choy, F. K., Padovan, J., "Investigation of Rub Effects on Rotor–Bearing–Casing System Response," Proceedings of the 40th Mechanical Failures Prevention Group Symposium, National Bureau of Standards, Gaithersburg, Maryland, April 1985.

16. Choy, F. K., Padovan, J., "Nonlinear Transient Analysis of Rotor Casing Rub Events," Journal of Sound and Vibration, v. 113, No. 3, 1987.

17 Choy, F. K., Padovan, J., Li, W. H., "Rub in High Performance Turbomachinery, Modelling, Solution Methodology, Signature Analysis," The University of Akron, P/165/87, 1987.

18. Choy, F. K., Padovan, J., Batur, C., "Rub Interactions of Flexible Casing Rotor Systems with Base Excitations," Rotating Machinery Dynamics, DE–Vol. 2, ASME HO400B, Proceedings of the 11th Biennial ASME Design Engineering Division Conference on Vibration and Noise, Boston, Massachussetts, September 1987.

19. Choy, F. K., Padovan, J., Li, W., "Seismic Induced Nonlinear Rotor–Bearing–Casing Interaction of Rotating Nuclear Component," Proceedings of the ASME 1986 PVP Conference, Chicago, Illinois, PVP–vol. 108, July, 1986.

20. Curami, A., Pizzigoni, B., Vania, A., "On the Rubbing Phenomena in Turbomachinery," International Conference on Rotordynamics, Tokyo, Japan, 1986.

21. Davis, R. R., "Enhanced Rotor Modelling Tailored for Rub Dynamic Stability Analysis and Simulation," The Fifth Workshop on Rotordynamic Instability Problems in High–Performance Turbomachinery, Texas A&M University, College Station, Texas, May 1988.

22. Davis, R. R., Vallance, C. S., "Incorporating General Race and Housing Flexibility and Dead Band in Rolling Element Bearing Analysis," The Second International Symposium on Transport Phenomena, Dynamics, and Design of Rotating Machinery, Honolulu, Hawaii, April 1988.

23. Den Hartog, I. P., "Mechanical Vibration," McGraw Hill, 1956, pp. 291–293.

24. Dimarogonas, A. D., Paipetis, S. A., "Analytical Methods in Rotor Dynamics," Applied Science Publishers, London & New York, 1983.

25. Dimarogonas, A. D., "Heat Distribution and Flash Temperatures in Radial Seals," Wear, v. 23, No. 1, 1973.

26. Dimarogonas, A. D., "Newkirk Effect: Thermally Induced Dynamic Instability of High–Speed Rotors," International Gas Turbine Conference, ASME Paper No. 73–GT–26, Washington, D.C., 1973, pp. 1–11.

27. Dimarogonas, A. D., Sandor, G. N., "Packing Rub Effect in Rotating Machinery, A State–of–the–Art Review," Wear, v. 12, 1969.

28. Edbauer, R. Meinke, P., Müller, P. C., Wauer, J., "Passive Means for Passing the Critical Speeds of Lateral Vibrations of Elastic Rotors" (German: Passive Durchlaufhilfen beim Durchfahren beige kritisher Drehzahlen elastischer Rotoren), VDI–Report No. 456, 1982, pp. 157–166.

29. Ehrich, F. F., "Animated Vibrations," ASME 10th Biennial Conference on Mechanical Vibration and Noise, Cincinnati, Ohio, September 1985.

30. Ehrich, F. F., "The Dynamic Stability of Rotor/Stator Radial Rubs in Rotating Machinery," Journal of Engineering for Industry, November 1969, pp. 1025–1028.

31. Ehrich, F. F., "Self–Excited Vibrations," Chapter 5, Shock and Vibration Handbook, Editors: C. M. Harris and C. E. Crede, McGraw–Hill Book Co., 1976.

32. Ehrich, F. F., O'Connor, J. J. "Stator Whirl With Rotors in Bearing Clearance," ASME WA/MD–8, Paper 66, 1966.

33. Ehrich, F. F., "Subharmonic Vibration of Rotors in Bearing Clearance," Design Engineering Conference and Show, Chicago, Illinois, 9–12 May 1966, ASME Publication No. 66–MD–1, 1966, pp. 1–4.

34. Ek, M. C., "Solving Subsynchronous Whirl in the High–Pressure Hydrogen Turbomachinery of the SSME," Paper 78–1002, AIAA/SAE 14th Joint Propulsion Conference, Las Vegas, Nevada, July 25–27, 1978, 78–1002R, J. Spacecraft, v. 17, No. 3, 1980, pp.1–11.

35. "Full Annular Rub," Video Tape, Bently Rotordynamics Research Corporation/Bently Nevada Corporation Production, 1984.

36. Gao Tin Ti, Qui Qui Min, "Rotor to Stator Rub Vibration in Centrifugal Compressor," Symposium on Instability in Rotating Machinery, NASA CP2409, Carson City, Nevada, 1985.

37. Grissom, R., "Partial Rotor to Stator Rub Demonstration," NASA CP2409, 1985.

38. Grossklus, W., Shell, J., "Investigation and Characterization of Blade Tip Shroud Rub Interaction," AFWAL/MLLM, Report No. F33615–81–C–5073, 1981.

39. Gunter, E. J., Jr., Allaire, P. E., et al, "The Dynamic Analysis of the Space Shuttle Main Engine High Pressure Fuel Turbopump," Univ. of Virginia, Report No. ME–4012–101–76 52814.0/ME76/102, 103, 104, June–September 1976.

40. Guy, K. R., "Boiler Feed Pump Vibration (Rubbing and Friction Whirl)," Proceedings of the Vibration Institute Annual Conference, Las Vegas, Nevada, June 1986.

41. Haines, R. S., "Theory of Contact Loss at Resolute Joints With Clearance," Journal Mechanical Engineering Science, IMechE, v. 22, No. 3, 1980, pp. 129–136.

42. Hashemi, Y., "Vibration Problems With Thermally Induced Distortions in Turbine–Generator Rotors," Vibrations in Rotating Machinery, Third International Conference Proceedings, IMechE., C271/84, York, 1984.

43. Johnson, D. C., "Synchronous Whirl of a Vertical Shaft Having Clearance in One Bearing," J. Mech. Eng., Sci., v. 85, No. 1, 1962, pp. 85–93.

44. Kascak, A. F., Tomko, J. J., "Effects of Different Rub Models on Simulated Rotor Dynamics," NASA Lewis Res. Ctr., Report No. E–1801, NASA–TP–2220, ASME Applied Mechanics, Bioengineering and Fluids Engineering Conference, Houston, Texas, June 1983.

45. Kascak, A. F., "The Response of Turbine Engine Rotors to Interference Rubs," The 1980 Army Science Conference, West Point, New York, June 17–19, 1980, NASA Technical Memorandum 81518, AVRADCOM Technical Report 80–C–14–1980, pp. 1–16.

46. Kascak, A. F., Palazzolo, A., Montague, G., "Transient Rotor Dynamic Rub Phenomena; Theory of Test," Rotating Machinery Dynamics, DE–Vol. 2, ASME HO400B, Proceedings of the 11th Biennial ASME Design Engineering Division Conference on Vibration and Noise, Boston, Massachussetts, September 1987.

47. Keith, L. A., "Design Considerations for Minimizing Hazards Caused by Uncontained Turbine Engine and Auxiliary Power Unit Rotor and Fan Blade Failures," U. S. Dept. of Transportation Advisory Circular, FAA Aircraft Certification Division, ANM–100, 1986.

48. Kellenberger, W., "Spiral Vibrations Due to the Seal Rings in Turbogenerators Thermally Induced Interaction Betweeen Rotor and Stator," Journal of Mechanical Design, v. 102, January 1980, pp. 177–184.

49. Kennedy, F. E., "Single Pass Rub Phenomena — Analysis and Experiment," ASME Paper 81 – Lub – 55, J. of Lubrication Technology, October 1982.

50. Kiryn, K., Yanai, T., Matsumoto, S., Koga, T., "An Analysis of "Ringing Phenomena" in a Water Pump Mechanical Seal," Parts I and II, ASLE Trans., v. 29, No. 1, January 1986.

51. Kroon, R. P., Williams, W. A., "Spiral Vibration of Rotating Machinery," 5th Int. Conference of Applied Mechanics, Wiley, New York, 1939, p. 712.

52. Lehmann, T., "Elements of Mechanics," Part III (German: Elemente der Mechanik III), Vieweg, Braunschweig, 1977.

53. Mansour, W. M., Pavlow, D., Douainish, M. A., "The Mechanism of Gyroscopic Tracking: Parts 1 & 2, "Journal of Engineering for Industry, Transactions of ASME, May 1973, pp. 430–444.

54. Marscher, W. D., "Test Simulation of Turbomachinery Rotor–Stator Interactions," ASLE paper presented as ASLE Annual Meeting, 1982.

55. Matsushita, O., Takagi, M., Kikuchi, K., Kaga, M., "Rotor Vibration Caused by External Excitation and Rub," Rotordynamic Instability Problems in High Performance Turbomachinery, NASA CP2250, 1982.

56. Maxwell, J. H., "Pump Failure Caused by Dry Friction Whip Vibrations," v. 3, No. 2, September 1987, pp. 11–14.

57. Morris, J., "The Impact of Bearing Clearances on Shaft Stability; a New Approach to Shaft Balancing," Aircr. Engineering, v. 29, December 1957.

58. Muszynska, A., "Damping of Flexural Vibrations of Rotating Shafts by Means of Elastic–Frictional Dampers" (in Polish), Archiwum Budowy Maszyn, v. 20, No. 1, Warsaw, Poland, 1973.

59. Muszynska, A., Franklin, W. D., Hayashida, R. D., "Influence of Rubbing on Rotor Dynamics," NASA 3rd Conference on Advanced Earth–to–Orbit Propulsion Technology, Huntsville, Alabama, May 1980.

60. Muszynska, A., "Partial Lateral Rotor to Stator Rubs," Third International Conference on Vibrations in Rotating Machinery, C281/84, IMechE, York, United Kingdom, 1984.

61. Muszynska, A., "Rotor/Seal Full Annular Rub," Proc. of Senior Mechanical Engineering Seminar, Bently Nevada Corp., Carson City, Nevada, June 1984.

62. Muszynska, A., "Rub — An Important Malfunction in Rotating Machinery," Proc. of Senior Mechanical Engineering Seminar, Bently Nevada Corporation, Carson City, Nevada, June, 1983.

63. Muszynska, A., "Synchronous and Self–Excited Rotor Vibrations Caused by a Full Annular Rub," Modal Analysis and Vibrations. Diagnostics in Machinery, Proceedings of the Eighth Machinery Dynamics Seminar, NRC, Halifax, Nova Scotia, Canada, October 1–2, 1984.

64. Nathoo, N. S., Crenwelge, O. E., "Case History of a Steam Turbine Rotordynamic Problem: Theoretical Versus Experimental Results," Vibration Institute Proceedings, Machinery Vibration Monitoring & Analysis, April 1983, pp. 81–89.

65. Nelson, H. D., Meacham, W. L., Fleming, D. P., Kascak, A. F., "Nonlinear Analysis of Rotor–Bearing Systems Using Component Mode Synthesis," ASME Journal of Engineering for Power, v. 105, 1983, pp. 606–614.

66. Nelson, H. D., et. al., "Transient Response of Rotor–Bearing System Using Component Mode Synthesis," ERC–R81016–1, March 1981.

67. Newkirk, B. L., "Shaft Rubbing. Relative Freedom of Rotor Shafts From Sensitiveness to Rubbing Contact When Running Above Their Critical Speeds," Mechanical Engineering, v. 48, No. 8, August 1926, pp. 830–832.

68. Nielson, C. E., "Liquid Oxygen Turbopump Technology," NASA CR–165487, November 1981.

69. Padovan, J., Choy, F. K., "Nonlinear Dynamics of Rotor/Blade/Casing Rub Interactions," ASME 86–DE–6, Journal of Turbomachinery, Trans, ASME, v. 109, No. 4, October 1987.

70. Padovan, J., Adams, M. L., Fertis, D., Zeid, I., Lam, P., "Nonlinear Transient Finite Element Analysis of Rotor–Bearing Stator Systems," Journal of Computers and Structures, v. 18, 1984, pp. 629–639.

71. Pielorz, A., Nadolski, W., "Criterion of Multiple Collisions in a Simple Mechanical System With Viscous Damping and Dry Friction," International Journal Nonlin. Mech., v. 18, No. 6, 1983.

72. Pratt, T. K., Williams, R., "Nonlinear Analysis of Stick/Slip Motion," J. Sound and Vibration, v. 74, No. 4, 1981.

73. Schiehlen, W., "Constrains With Friction by Multibody Systems" (German: Reibungs behaftete Bindungen in Melhrk Örpersystem), Ingeuieur–Archiv, 53, 1983 265–273.

74. Sinha, A., Griffin, J. H., "Effects of Friction Dampers on Aerodynamically Unstable Rotor Stages," AIAA Journal, v. 23, No. 2, February 1985.

75. Smalley, A. J., "The Dynamic Response of Rotors to Rubs During Start–Up," Rotating Machinery Dynamics, DE–Vol. 2, ASME HO0400B, Proceedings of the 11th Biennial ASME Design Engineering Division Conference on Vibration and Noise, Boston, Massachussetts, 20–27 September 1987.

76. Sohre, J. S., "Turbomachinery Problems and Their Corrections," Turbomachinery International Publication Division of Business Journals, Inc., 1983.

77. Srinivasan, A. V., Cassenti, B. N., "A Nonlinear Theory of Dynamic Systems With Dry Friction Forces," 86–GT–8, Journal of Engineering for Gas Turbines and Power, 1986.

78. Srinivasan, A. V., Cassenti, B. N., Cutts, D. G., "Study of Characteristics of Dry Friction Damping," Final Report to the Air Force Office of Scientific Research, R85–956479–2, 1985.

79. Szczygielski, W. M., "Applicaion of Chaos–Theory to the Contacting Dynamics of High–Speed Rotors, Rotating Machinery Dynamics," DE–Vol 1, ASME HO400A, 11th Biennial ASME Conference on Vibration and Noise, Boston, Massachussetts, September 1987.

80. Szczygielski, W. M., "Dynamical Behavior of a High–Speed Rotor Touching a Boundary" (German: Dynamisches Verhalten eines schnell drehenden Rotors bei Anstreifvorgangen), Dissertation No. 8094, Swiss Federal Institute of Technology (ETH), Zurich, Switzerland, 1986.

81. Szczygielski, W. M., Schweitzer, G., "Dynamics of a High–Speed Rotor Touching a Boundary," Proceedings on Dynamics of Multibody Systems IUTAM/IFTOMM Symposium, Udine, Italy 1985, Springer–Verlag 1986, pp. 287–298.

82. Taylor, H. D., "Rubbing Shafts Above and Below the Resonance Speed (Critical Speed)," GE Company, R–16709, Schenectady, New York, April 1924.

83. Tschegg, E. K., Ritchie, R. O., McClintock, F. A., "On the Influence of Rubbing Fracture Surfaces on Fatigue Crack Propagation in Mode III," International Journal Fatigue, v. 5, No. 1, January 1983.

84. Von Magnus, K., "Contribution of the Kinematics of a Gyroscope Tracking" (German: Beitrage zur Kinetik des Kurvenkreisels), Ingenieur–Archiv v. 43, 1974, pp. 145–157.

85. Von Magnus, K., "Gyroscope, Theory and Applications" (German: Kreisel, Theorie und Anwendungen), Berlin–Heidelberg– New York, Springer–Verlag 1971.

86. Wisander, D. W., Johnson, R. L., "Friction and Wear of Nine Selected Polymers With Various Fillers in Liquid Hydrogen," NASA TN D–5073, Washington, D.C., March 1969.

87. Witt, J., A Rough, "Almost Elastic Impact of a Super Ball; Design of a Catapult" (German: Det rauche, fast elastische Stoss beim Superball. Entwurf einer Wurfeinrichtung), Institute of Mechanics, Technical University of Stuttgart, September 1983.

88. Zia Songbo, Lue Zhangsheng, Wang Guangming, Wu Xinhua, "Diagnosis of the Rub Malfunction of Rotors," Int. Conference on Machine Diagnostic Techniques, Shenyang, PRCh, September 1988.

89. Zippe, G., Meinke, P., "Approach and Device for Passing Critical Speeds by Slender Rotors" (German: Verfahren und Vorrichtungen zum Durchlaufen kritischer Drehzahlen banggestrecter Rotoren), Patentschrift DE 263 32586 C2 (Patent in W. Germany), 1986.

3. CHARACTERIZATION OF RUB PHENOMENA IN ROTATING MACHINERY.

In this chapter the rotor–to–stationary element rub phenomena in rotating machines are characterized from the point of view of conditions leading to rub, physical mechanisms involved during rubbing, and dynamic effects of rub on the rotating machine performance. The parameters of concern for mathematical modelization of the rub–related phenomena are outlined.

3.1 Definitions

The normal operation of a rotating machine is related to the appropriate torque/load balance and consists of motion of the shaft (together with all rotating elements associated with the shaft) performed with an appropriate rotative speed and around the appropriate axis. This main motion can be accompanied by a limited level of lateral/torsional/longitudinal vibrations ("parasitic motion") of the rotor itself and a limited level of vibration of stationary (nonrotating) parts.

Rub in a rotating machine is a malfunction condition associated with the physical contact of rotating and stationary parts which otherwise should not be in contact. As a result of rub, the "normal operation" of the machine is affected. Rub changes the system force balance and dynamic stiffness, which results in modifications of the machine motion. The effect is usually associated with a decrease of the amount of energy in the main motion and an increase in the level of "parasitic" motion.

3.2 Rub–Related Changes in the Rotating Machine Force Balance and Dynamic Stiffness

3.2.1 Coupling Effect

Due to the physical contact of the rotating and stationary parts, the mechanical structure which is involved in motion changes. This effect is similar to coupling an additional structure to the existing ("normal") structure. Since the rub–related coupling is usually time dependent (on/off periodic type), the system dynamic stiffness also becomes periodically time dependent. The rub coupling effect will vary with:

- contact normal forces
- contact surface area
- flexibility (degrees of freedom) of the contacting elements
- dynamic stiffnesses of the "normal operation" structure and the additional, coupled structure (strong/weak coupling)
- time of contact versus time of separation.

Parameters of concern for mathematical modelization are:

- "normal operation system" and "coupled system" spectra of natural frequencies and corresponding modes
- function of coupling and decoupling relationship versus time and its relation to rotor unbalance.

3.2.2 Stiffening Effect

An additional effect of rub–coupling results in stiffening of the shaft as it is forced to rotate in a bent position (Fig. 3.1). This results in an increase of the system rigidity and a slight increase of the natural frequencies.

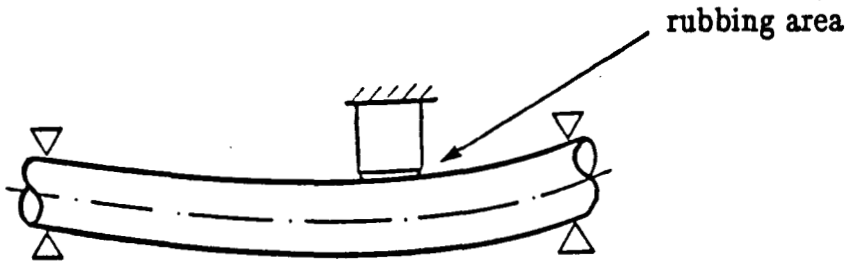

FIGURE 3.1 SHAFT BOW DUE TO RUB

Parameters of concern for mathematical modelization:

- stiffnesses of the normally supported shaft and bent shaft.

3.2.3 Friction Effect

Friction accompanies the relative motion of rotor/stationary parts during their contact. It produces the usual friction–related effects: wear (grinding,pitting) of the rubbing surfaces together with heat generation (up to metal melting temperatures). Since the rubbing surface relative tangential velocity is usually high, the destructive effects of friction can be extremely strong in a very short time. Friction is a nonlinear phenomenon. Due to the wear effect, the surface rubbing conditions change very fast with time. This may lead to either widening clearances and elimination of the contact or to an enlargement of the contact surface area (breaking–in effect). Therefore, in a short time either rub stops (causing some short–time transient conditions for the rotor system) or rub will continue with further continuous modification of conditions and dynamic responses.

Parameters of concern for mathematical modelization:

- normal forces at the contact surfaces and contact stresses
- surface area of contact
- friction conditions (dry/fluid lubricated) leading to a realistic model of the friction force
- time intervals of contact/separation.

3.2.4 Impacting Effect

Impact conditions occur when the contact of rotor/stationary part occurs instantaneously. An impact generates a wide frequency spectrum of exciting forces; however, repetitive periodic impacts may result in a definite spectrum of periodic excitation.

Impacts create an "after impact" response — most often, a rebounding motion (separation) with the initial direction depending on impact conditions and relative tangential velocities.

Impacting is a highly nonlinear phenomenon.

Parameters of concern for mathematical modelization:

- impact surface conditions, restitution coefficient/function, incoming velocities
- time intervals of contact/separation.

3.2.5 Fluid Dynamic Forces and Thermal Unbalance

Rub–related wear of seal surfaces causes an increase of clearances and changes in the flow pattern of the working fluid. This generates new fluid dynamic forces and modifications of thermal conditions which, in turn, can change clearance situations due to thermal expansion. Both effects have to be investigated when rub results in the conditions of slowly or rapidly increasing clearances.

3.3 Rub Location

Generally rub location can be classified in terms of occurrence along the shaft axis:

- at one axial location
- at several axial locations.

At each axial location, rub can occur:

- at one radial location (seals or other stationary parts) with determined area of contact
- at several radial locations (e.g., rebounding motion inside a seal)
- continuously maintaining the shaft/seal contact (for an obviously limited time).

Relating to the shaft axis, the rubbing surfaces can be located (Fig. 3.2)

- radially
- axially
- "conically."

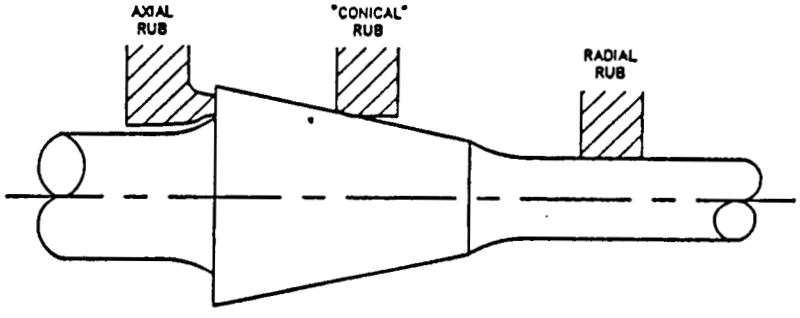

FIGURE 3.2 RUB LOCATION

3.4 Conditions Leading to Rub

Rub is a secondary phenomenon usually resulting from a primary cause which perturbs the "normal operation conditions." This primary cause can originate from various sources (such as unbalance, misalignment, fluid dynamic forces in main flow/bearings/seals leading to instability, etc.). The occurrence of the "primary source" results in:

- changes of shaft centerline position
- and/or shaft vibrations (most often lateral mode).

The amount of the centerline displacement and the vibration amplitude have to be considered in relationship to clearance values (together with their tolerances). By taking

into account the most probable mode of the shaft centerline bow for the operational conditions, the most probable "weak" point susceptible to rub, can be determined. The first "weak point" is the one where rub starts. This causes a modification in system properties which eventually may lead to rubbing in other locations. The conditions leading to rub must, therefore, be considered in a sequential form.

3.5 Transient Character of Rub–Related Effects

Most of rub–related dynamic phenomena are characterized by continuously changing conditions due to "grinding effect" at the rubbing surfaces. Steady–state conditions can be maintained during significantly long (but limited) time only if:

- rub is very light (short contact time and low contact normal forces), or
- there are full annular backward rub conditions (the vibrational process which is most often destructive for the machine, i.e., the "steady state" lasts a limited time before transforming into a transient process of destruction).

3.6 Rub–Related Modifications of the Rotating Machine Vibrational Response

3.6.1 Frequency

The starting point is no–rub machine operation. The frequencies of the machine vibrational response of interest are:

- shaft actual rotative speed, ω
- spectrum of machine natural frequencies, ω_n, n = 1, 2, 3, . . .

Rub can cause machine element vibrational responses with frequencies being:

- a fraction (p/r) of the rotative speed ω (p, r are integers)
- one (or more) system natural frequencies ω_n (note the coupling and stiffening effects causing modifications in the natural frequency spectrum)
- higher harmonics (multiples) of the lowest frequency component ($q\omega(p/r)$ and/or $q\omega_n$; q = 2, 3, 4, . . .)
- combinations of the above.

Note: Higher harmonics (multiples) are generated (or significantly magnified if they already exist in limited amount in the vibrational response) due to strong nonlinear effects of rub–related friction, impacting, and the on/off type of motion.

3.6.2 Amplitude, Phase

Both amplitude and phase (the latter for synchronous 1× and multiples of synchronous 2×, 3×, . . . components) of the system responses are modified by rub.

3.6.3 Mode of Shaft Centerline

Rub can modify the shaft–centerline modal deflection shape. The information can be significant for localization of rub area.

Response frequency content, amplitudes, phases of the response components, static displacement position, and shaft orbital motion carry significant rub–diagnostics information.

3.7 Summary

Characterization of rotor–to–stationary element rub dynamic phenomena in rotating machines is outlined in this chapter. This characterization is schematically presented in Figures 3.3 to 3.7.

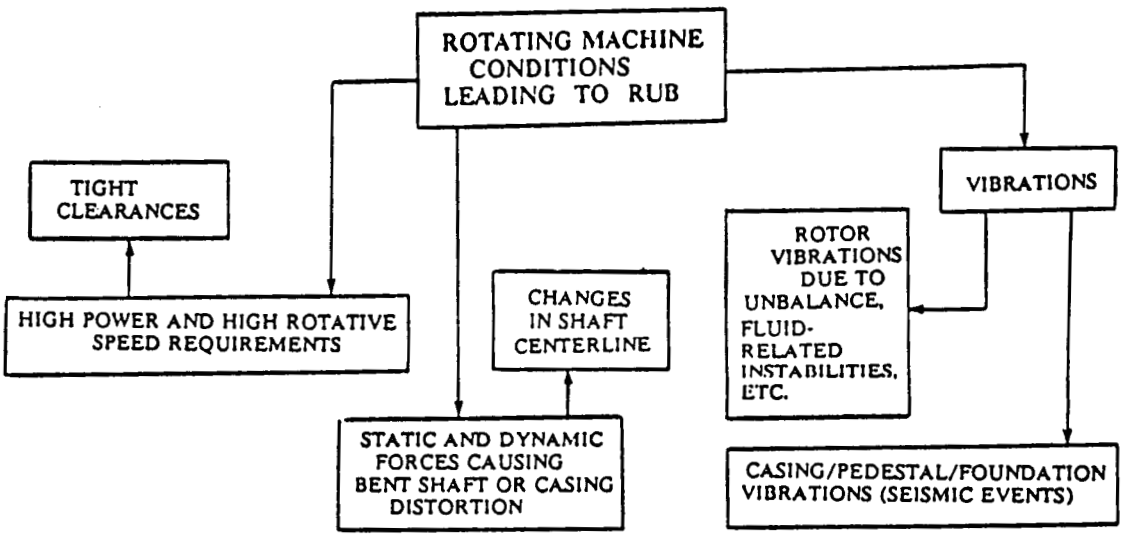

FIGURE 3.3 ROTATING MACHINE CONDITIONS LEADING TO ROTOR–TO–STATIONARY ELEMENT RUB.

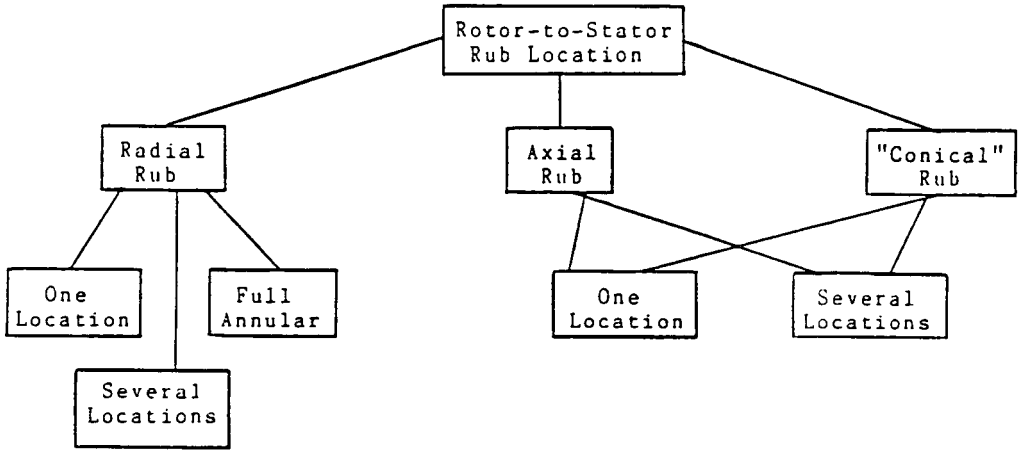

FIGURE 3.4 ROTOR–TO–STATIONARY ELEMENT RUB LOCATION.

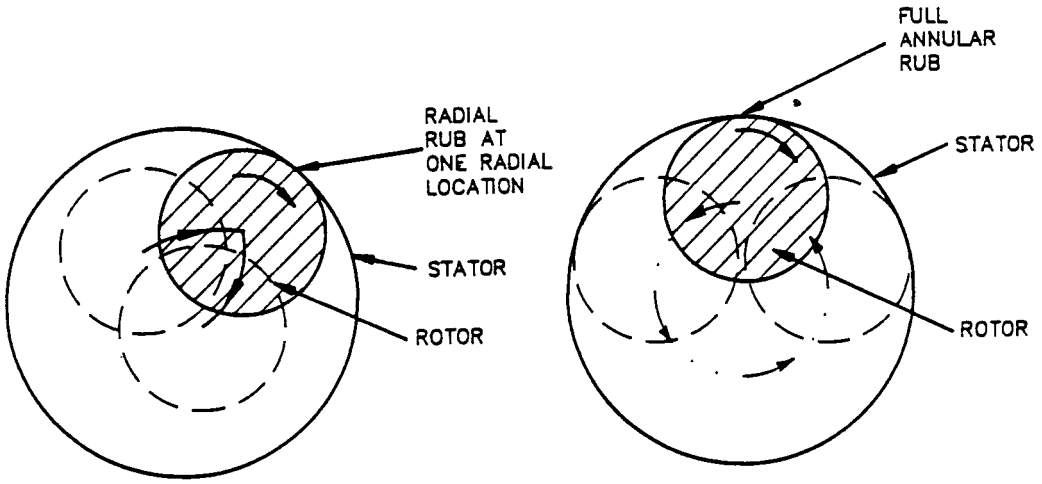

FIGURE 3.5 ROTOR–TO–STATIONARY ELEMENT RUB CASES.

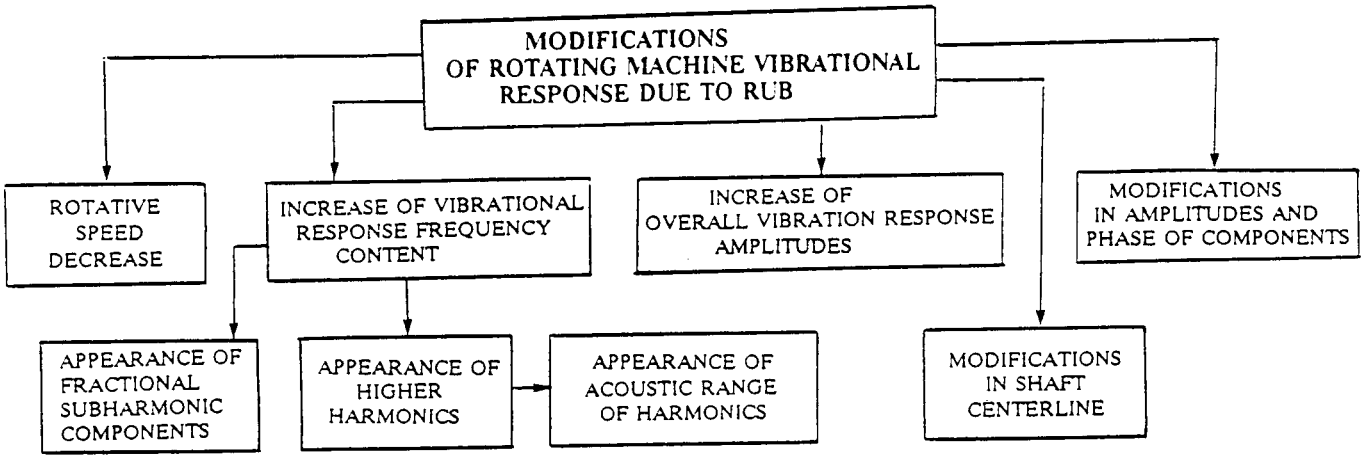

FIGURE 3.6 MODIFICATIONS OF ROTATING MACHINE VIBRATIONAL RESPONSE DUE TO ROTOR–TO–STATIONARY ELEMENT RUB.

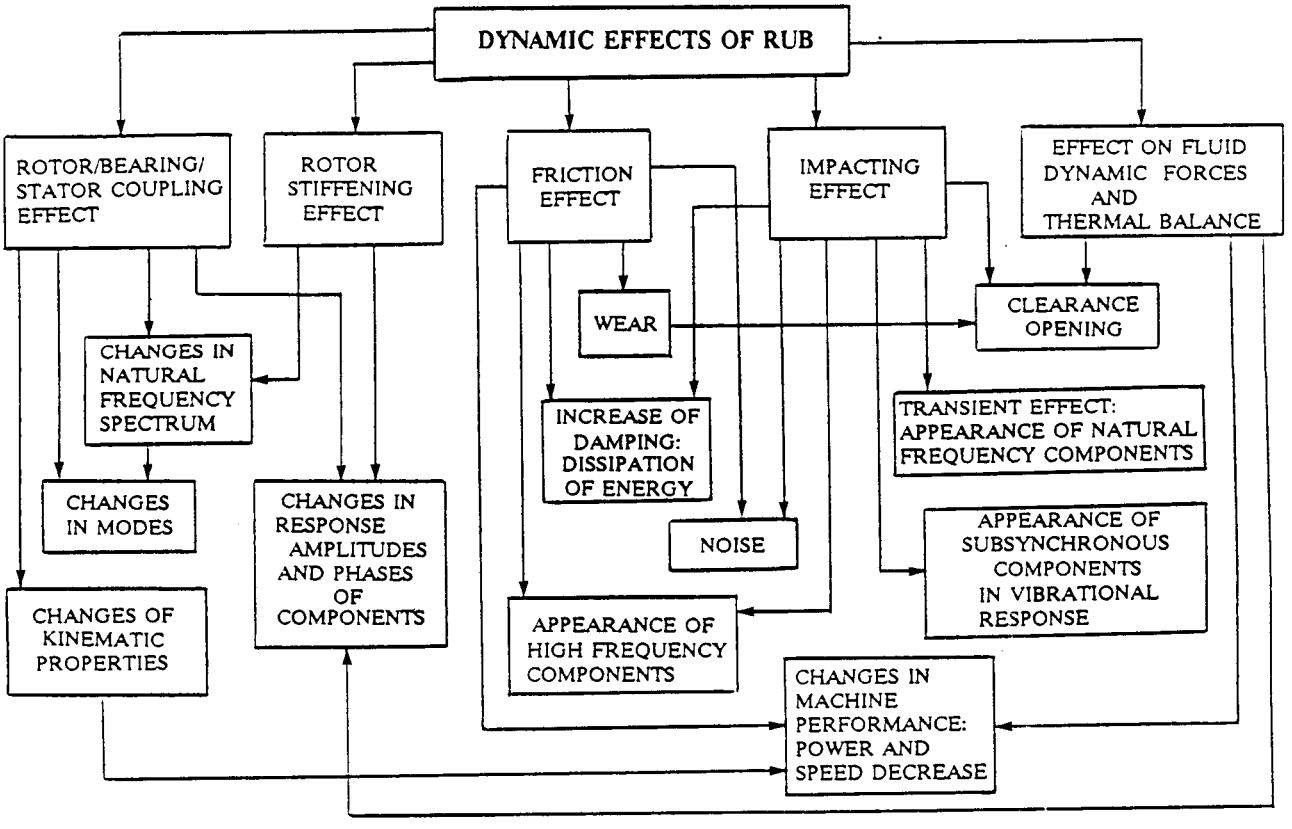

FIGURE 3.7 DYNAMIC EFFECTS OF ROTOR–TO–STATIONARY ELEMENT RUB.

4. HPFTP SIMULATING RUBBING ROTOR RIG INITIAL DESIGN DATA.

Since the space shuttle's high pressure fuel turbopump (HPFTP) resonant frequencies are too high to produce a safe rotor model to study rotor–to–seal rubs, it was decided to design a rotor model with reduced resonant rotative speeds. In order to obtain data that is representative of the HPFTP, the resonant speed ratios and the corresponding mode shapes at the resonances of the rotor rig should match those of the HPFTP. The other rotor rig requirement of interest is its robustness and durability. Since the rig will be subjected to continuous rubbing, if the model parameters continue changing with use, it will be difficult to correlate rotor response with the data obtained from mathematical models. This requires the use of replaceable wear surfaces and/or light force per unit area values in locations subject to rubs.

4.1 Modelling Data for HPFTP

The data regarding HPFTP supplied by NASA are as follows:

1st mode natural frequency = 16800 rpm	
bearing stiffness	8.4×10^5 lb/in
1st seal radial stiffness kyy	4.0×10^4 lb/in
2nd seal radial stiffness kyy	4.0×10^4 lb/in
2nd mode natural frequency = 30880 rpm	
bearing stiffness	6.5×10^5 lb/in
1st seal radial stiffness kyy	1.8×10^5 lb/in
2nd seal radial stiffness kyy	2.3×10^5 lb/in
3rd mode natural frequency = 46290 rpm	
bearing stiffness	4.2×10^5 lb/in
1st seal radial stiffness kyy	3.8×10^5 lb/in
2nd seal radial stiffness kyy	3.8×10^5 lb/in

All bearing stiffnesses and the seal stiffnesses at the 2nd mode were interpolated from HPFTP modelling data sent to Bently Nevada Corporation on March 4, 1987. The seal stiffnesses for the 1st and 3rd mode were taken from graph curves supplied on February 17, 1987. The values at the 2nd mode didn't correspond exactly with the numbers of 4 March 1987 data, so a scaling factor was determined based on these two values. The values for the 1st and 3rd modes were then taken from the 17 February data and scaled using the determined scaling factor. The turbine interstage seal stiffness was so small compared to the turbine bearing stiffness that it was neglected in the rubbing rotor rig.

4.2 Scaled Rotor Rig Model Data

The next step was to determine the ratios of the stiffnesses and resonant frequencies so they could be scaled. The ratios of the resonant frequencies were 1.0, 1.84, and 2.76 using the 1st mode as the reference, the ratios for the bearing stiffnesses were 1.0, 0.77, and 0.5 using the 1st mode bearing stiffness as the reference. Taking the bearing stiffness for each mode as the reference, the ratios of seal stiffness to bearing stiffness for each mode were as follows:

Mode	Bearing Stiffness	1st Seal	2nd Seal
1st mode	1	0.05	0.05
2nd mode	1	0.28	0.35
3rd mode	1	0.90	0.90

These stiffness ratios were used in the rubbing rotor rig model to keep the same relationships between parameters. The rotor rig maintains the same axial dimensions as the HPFTP. The rig shaft diameter is reduced to 0.375" and the disks representing the impellers are attached to the shaft. The disk masses were sized to obtain the correct shape for the 3rd mode. The bearing stiffnesses were then determined to get the proper ratios for the resonant frequencies. The resonant frequencies and stiffnesses for the rotor rig are as follows:

1st mode natural frequency — 1729 rpm	
bearing stiffness	150 lb/in
1st seal radial stiffness	7 lb/in
2nd seal radial stiffness	7 lb/in
2nd mode natural frequency — 3193 rpm	
bearing stiffness	115 lb/in
1st seal radial stiffness	32 lb/in
2nd seal radial stiffness	40 lb/in
3rd mode natural frequency — 4725 rpm	
bearing stiffness	75 lb/in
1st seal radial stiffness	68 lb/in
2nd seal radial stiffness	68 lb/in

The support bearings are implemented by suspending a rolling element bearing on springs from a rigid frame. The bearing stiffnesses are controllable by using springs with different stiffness rates. The seals are modelled using pressurized fluid lubricated bearing systems. The stiffness is varied by changing the oil supply pressure and the damping varied by fluid selection and/or temperature variations. There is also a replaceable rub ring at each of the pressurized bearings. The bearings can be moved to any axial locations along the shaft.

The rotor rig is mounted on a solid base supported by a steel/concrete foundation. This arrangement simulates the rigid casing mode of the HPFTP.

4.3 Computer Calculation of Natural Frequencies and Mode Shapes

A transfer matrix computer program calculating undamped natural frequencies and modes of rotating systems was used to generate data for the designed rubbing rotor rig. Twenty–three rotor stations were used in the calculations. The results are presented in Figures 4.1 to 4.4. The simulation rig rotor mode shapes along with the HPFTP mode shapes supplied by NASA are shown. Also shown is the resonant speed ratio for both model and HPFTP data.

4.4 Summary

The scaling principle of the rubbing rotor rig to HPFTP was associated with natural frequencies and corresponding first three modes. The scaling factor for the natural frequencies was 1:9. The mode shapes were maintained as close as possible. The summary of the natural frequency data is given in Table 4.1.

	Natural Frequency		
Mode	HPFTP [rpm]	SCALED HPFTP [rpm]	Rubbing Rotor (Calculated) [rpm]
1st	16828	1870	1729
2nd	30881	3435	3109
3rd	46286	5150	5389

TABLE 4.1

Summary of Natural Frequencies for HPFTP and Rubbing Rotor Rig

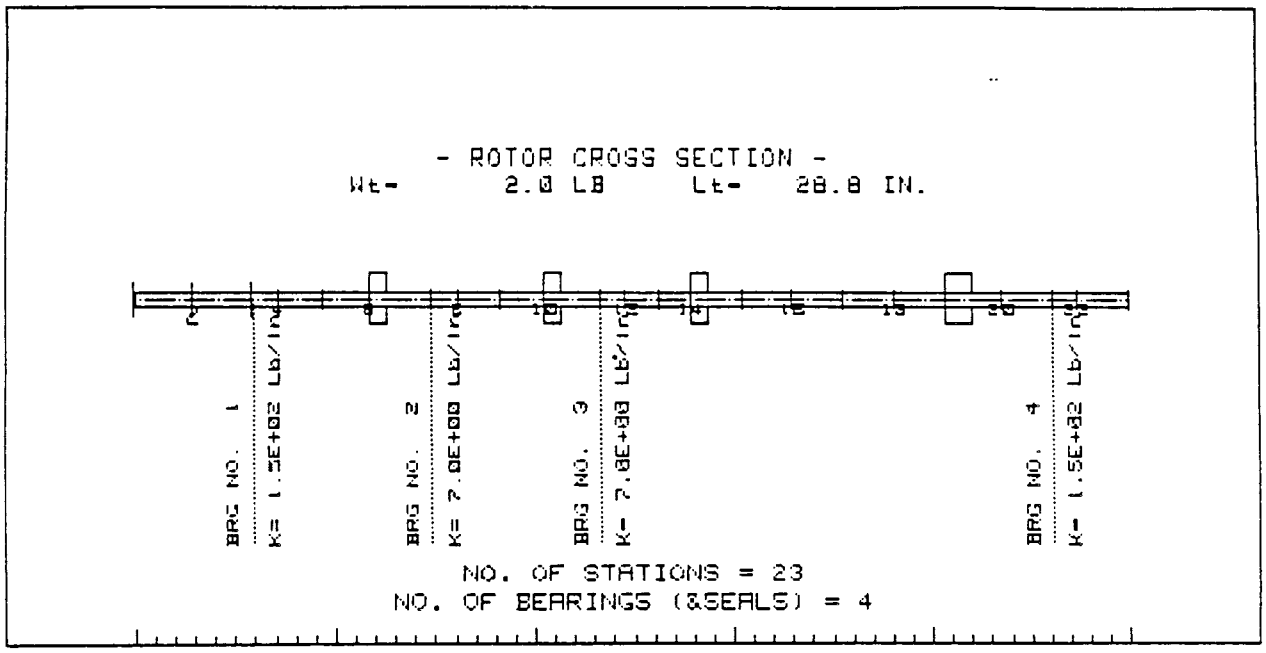

FIGURE 4.1 COMPUTER–GENERATED MODEL OF THE RUBBING ROTOR RIG.

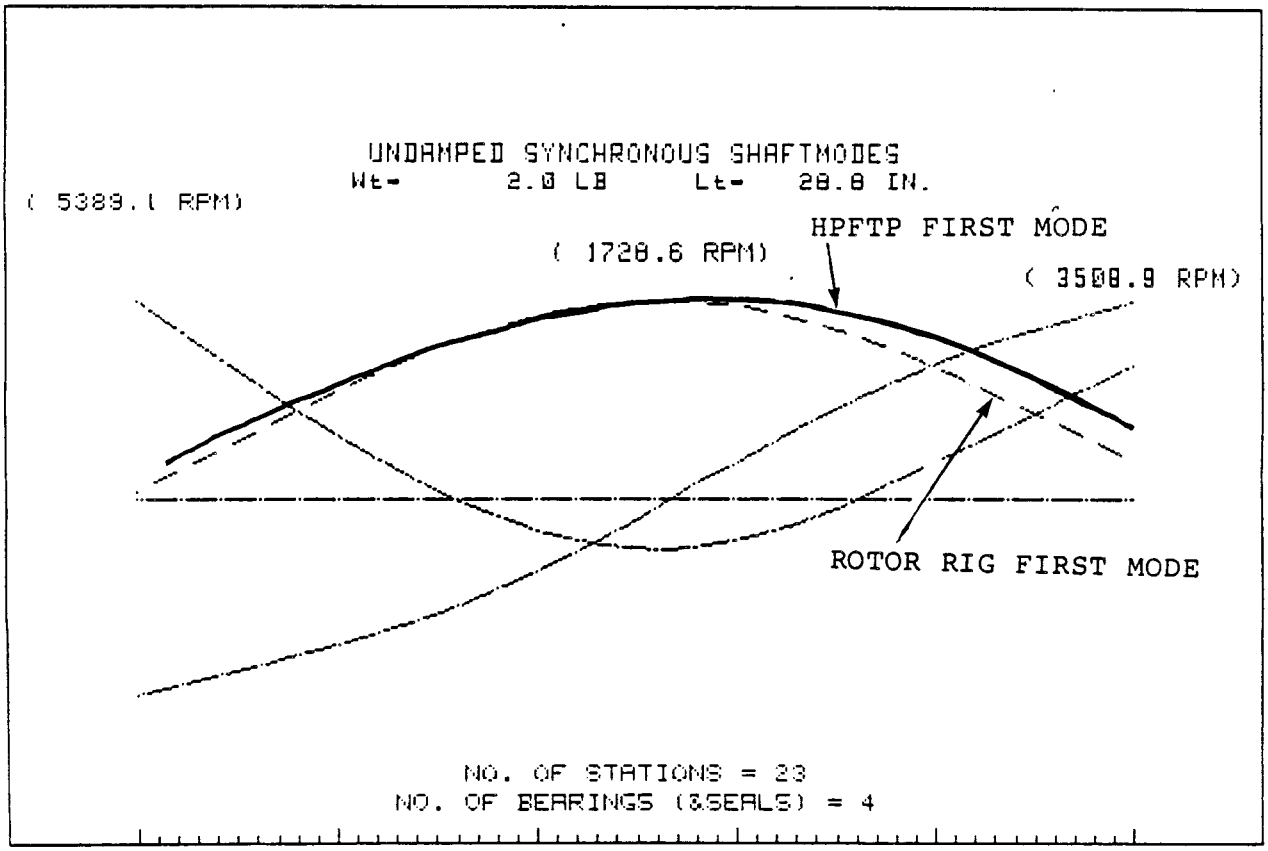

FIGURE 4.2 COMPUTER–GENERATED NATURAL FREQUENCIES AND MODES OF THE RUBBING ROTOR RIG. COMPARISON WITH THE HPFTP FIRST MODE.

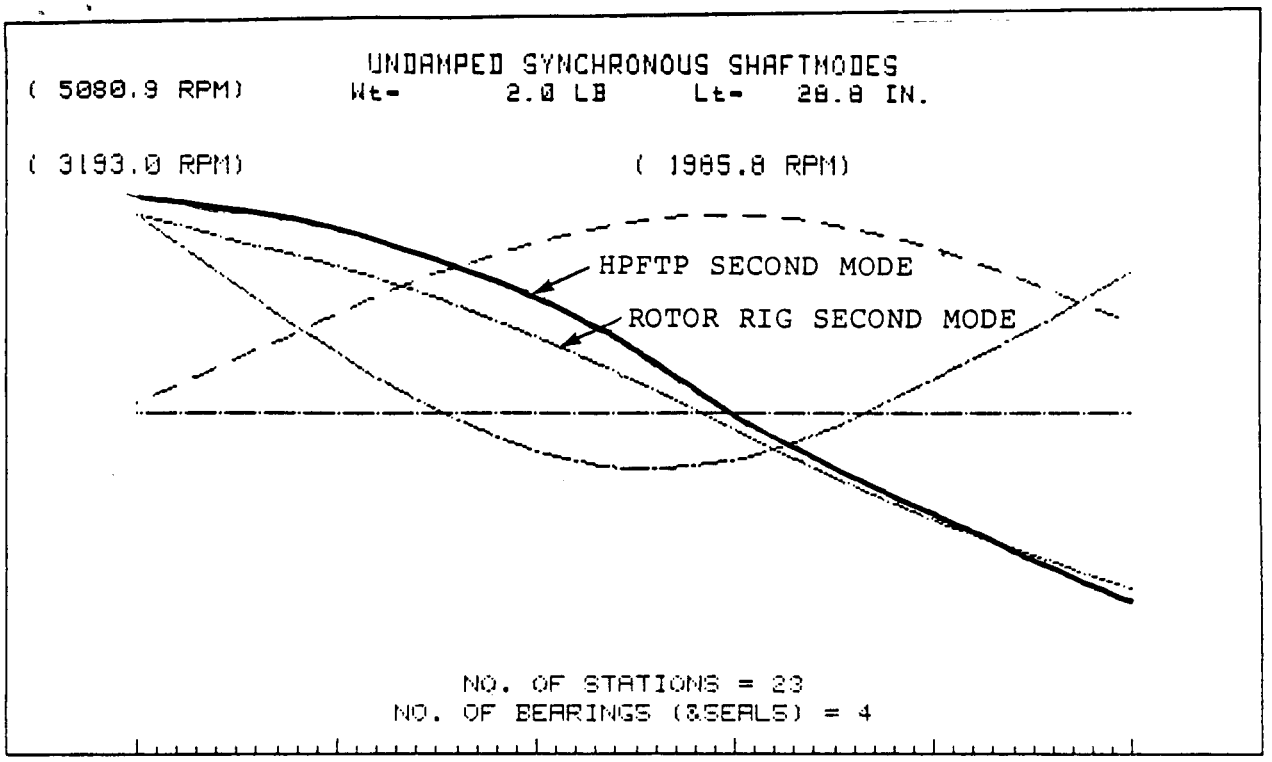

FIGURE 4.3 COMPUTER–GENERATED NATURAL FREQUENCIES AND MODES OF THE RUBBING ROTOR RIG. COMPARISON WITH THE HPFTP SECOND MODE.

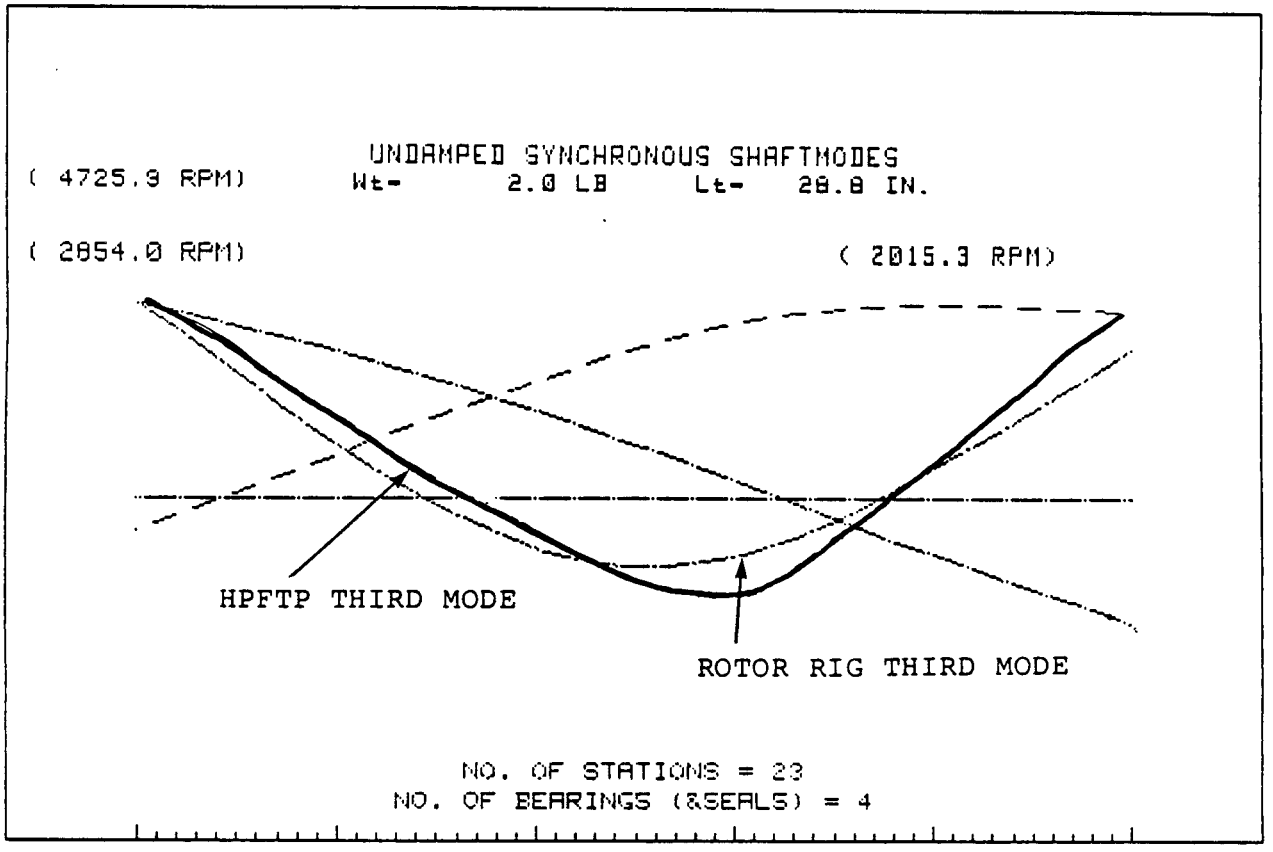

FIGURE 4.4 COMPUTER–GENERATED NATURAL FREQUENCIES AND MODES OF THE RUBBING ROTOR RIG. COMPARISON WITH THE HPFTP THIRD MODE.

5. HPFTP SEAL–SIMULATING OIL–LUBRICATED BEARING SELECTION AND TESTS.

5.1 Introduction

The interstage seals in HPFTP introduce a significant stiffening effect which modifies the pump dynamic response. In order to maintain the dynamic similarity, the simulating HPFTP rubbing rotor rig was equipped with two oil–lubricated bearings. By varying oil pressure in the bearings the variation of fluid film radial stiffness was achieved.

5.2 Seal–Simulating Oil Bearing Tests

5.2.1 Introduction

The purpose of these tests is to verify and document the stiffness characteristics of the pressurized bearings used on the rub rotor rig to simulate the interstage seals in the HPFTP. A cylindrical bearing with a 0.52 diameter–to–length ratio was designed (Fig. 5.1). In a preliminary tested bearing the radial clearance was 2.5 mils. When installed in the rubbing rotor rig, too low clearance bearing caused problems with rotor alignment. The bearings were then redesigned for increased radial clearance of 5.5 mils. The stiffness versus oil pressure, the main control relationship, was determined using the static and dynamic tests.

5.2.2 Test Procedure

The bearing test setup is shown in Figure 5.2. It consists of a 0.375 inch diameter shaft supported at one end in a radially rigid bearing and at the other end in the oil lubricated cylindrical bearing under test (Fig. 5.1). The lubricant is T10 oil (Chevron GST Oil 132, ISO–VG–32). The shaft is centered in the test bearing using a rolling element bearing mounted to the rigid frame through calibrated springs. This arrangement is placed as far from the bearing under test as possible to reduce its dynamic effect on the measured values.

5.2.3 Static Test

The static radial load force is applied to the shaft using another rolling element bearing connected to a weight carriage with a string routed through a series of pulleys. The static test on the bearing consisted of varying the load in the weight carriage and measuring the resultant displacement of the shaft in the bearing by using two noncontacting eddy current displacement probes mounted in the XY orientation. The force vector (amplitude and phase) was then divided by the resultant motion response vector to obtain the dynamic stiffness. Then the stiffness was resolved into two components, one in the same direction as the applied force, the "direct stiffness," and another at right angles to the applied force, the "quadrature stiffness." The mathematical model of the system and the corresponding analytical relationships are discussed in Section 5.3.

Since the force cannot be applied directly to the shaft at the bearing and resultant motion cannot be measured at the same location, the experimental values determined by the raw force and motion vectors must be modified by a geometric/modal correction factor.

5.2.4 Dynamic Tests

The dynamic test setup was arranged by replacing the rolling element bearing, pulley, and weight carriage assembly of the static setup with a light disk, into which unbalance masses could be inserted at a 1.2–inch radius. The test consisted of measuring the rotating shaft

vibration response due to the rotating unbalance mass over the perturbation speed range of 200 to 6000 rpm. The measuring transducers were located at the bearing. Again, the force vector resulting from the rotating unbalance mass was divided by the vibration response vector to produce the dynamic stiffness. The mathematical model of the system and the corresponding analytical relationships are discussed in Section 5.3.

5.2.5 Results of Static Perturbation Testing of the 2.5 Mil Radial Clearance Bearing

The test was performed at two conditions regarding the rotative speed, namely, 0 and 1000 rpm. The results from 0 rpm run are presented in Figures 5.3 and 5.4 and from the 1000 rpm run, in Figures 5.5 and 5.6. They indicate that the fluid film radial stiffness is linearly dependent on the oil pressure with a coefficient of proportionality of approximately 5.5 lb/in/psi while the quadrature stiffness is very small and practically independent of oil pressure. Since the force is not applied to the shaft within the bearing, the stiffness values need to be adjusted by a geometric/modal factor equal to 0.65 to get the actual bearing fluid film radial stiffness. This factor reduces the bearing stiffness slope versus pressure to 3.6 lb/in/psi. With the maximum oil supply pressure of 25 psi, this produces a maximum radial stiffness of 90 lb/in. Since the rotor rub rig required values from 0 to 75 lb/in., this bearing gave a slight over range capability while still providing good setpoint resolution. The data also indicates that the bearing radial stiffness is independent of rotative speed, within a limited range of shaft eccentricity inside the bearing clearance, starting from zero to a certain value, determined by the shaft rotation–related circumferential flow inside the clearance area. This value varies, depending on the actual rotating speed. The useful range of eccentricities is smallest for 0 rpm rotative speed. However, as the bearing would be used predominantly above 1000 rpm, the useful displacement range of the shaft within the bearing will be well over 1.5 mils, which corresponds to the eccentricity ratio of 0.6.

5.2.6 Results of Dynamic Perturbation Testing of the 2.5 Mil Radial Clearance Bearing

The results of the dynamic tests of the 2.5 mil clearance bearing are shown in Figures 5.7 and 5.8. The stiffness values can be determined from the data by extrapolating the values of direct dynamic stiffness at 0 rpm perturbation frequency. The slope of the direct dynamic stiffness is determined by the effective (modal) system mass while the slope of the quadrature stiffness is determined by the system damping. These latter values are not important in this application and are, therefore, not evaluated. The bearing radial stiffness values determined using the dynamic forcing function confirm the values obtained using the static forcing function in the previous test.

5.2.7 Results of Static Perturbation Testing of the 5.5 Mil Radial Clearance Bearing

The results of the static perturbation testing of the 5.5 mil clearance seal–simulating bearing are presented in Figure 5.9. The experimental data indicate the coefficient of fluid film radial stiffness is 3.75 lb/in/psi, which becomes 5.8 lb/in/psi when modified by the geometric correction factor. For this particular test setup, this factor was 1.54 (see Fig. 5.2). The quadrature stiffness is very small and practically independent of oil pressure. With the maximum system oil pressure of 20 psi, this gives a stiffness range of 115 lb/in which is compatible with the required range of 80 lb/in determined from critical speed computations for the rubbing rotor rig. The useful linear range of eccentricities has been increased from the original 1.5 mils pk to approximately 5.0 mils pk before the fluid film nonlinearity causes the stiffness to increase independently of oil pressure.

5.3 Mathematical Model Used for Oil Lubricated Bearing Test Data Interpretation

The considered rotor/bearing system lateral motion model for the first mode is as follows:

$$M\ddot{z} + D_s\dot{z} + D(\dot{z} - zj\omega\ \lambda) + Kz + K_o(p)z = F \qquad (5.1)$$

$$\cdot = d/dt \qquad j = \sqrt{-1}$$

where

M is system generalized (modal) mass for the first mode.

$z = x + jy$ is shaft lateral displacement at the bearing location (x – horizontal, y – vertical) in a form of complex number.

D_s is external viscous damping.

λ is lubricated bearing fluid average circumferential velocity ratio.

D is bearing fluid film radial damping coefficient.

ω is shaft rotative speed.

K is system generalized (modal) stiffness (including stiffness of supporting springs).

p is the fluid pressure.

$K_o(p)$ is bearing fluid film radial stiffness as function of pressure p.

F is perturbation force. For the static test $F = Pe^{j\sigma} = \text{const}$, where P is amplitude and σ is angular position of the static force, and for the dynamic test $F = mr\omega_p^2 e^{j\omega_p t}$, where ω_p is perturbation frequency, and m and r are mass and radius of perturbation unbalance respectively. The force F includes the geometric/modal factor adjustment. The latter takes into consideration the fact that the force is not applied directly to the journal, but to the shaft at a certain distance from the journal.

t is time.

e = 2.718 . . .

The objective of the test is identification of the fluid film radial stiffness K_o as a function of oil pressure p.

5.3.1 Static test: $F = \text{const} = Pe^{j\sigma}$.

The solution of Eq. (5.1) with $F = Pe^{j\sigma}$ is

$$z(t) = Be^{j\beta} \tag{5.2}$$

where B and β are amplitude and angular position of the shaft static response respectively. They are measured in the test. Taking (5.2) into consideration, the following equation results from (5.1):

$$Be^{j\beta}\,[-Dj\omega\ \lambda + K + K_o(p)] = Pe^{j\sigma} \tag{5.3}$$

By splitting the real and imaginary parts Eq. (5.3) can be solved for dynamic stiffness (DS) components:

$$\text{Direct DS} = K + K_o(p) = \frac{P}{B}\cos(\beta - \sigma)$$

$$\text{Quad DS} = D\lambda\omega\ = \frac{P}{B}\sin(\beta - \sigma) \tag{5.4}$$

The right–hand side expressions of Eqs. (5.4) contain measured parameters, thus, the left–hand side parameters can be identified.

In the static the test variables were rotative speed (two data points, namely, ω = O and ω = 1000 rpm), bearing fluid pressure, p, and the force amplitude P.

5.3.2 Dynamic test: $F = mr\omega_p^2 e^{j\omega_p t}$

The solution of Eq. (5.1) with $F = mr\omega_p^2 e^{j\omega_p t}$ is

$$z(t) = Ae^{j(\omega_p t+\alpha)} \tag{5.5}$$

where A and α are amplitude and phase respectively of the shaft forced response due to perturbation force with synchronous–to–perturbation frequency ω_p.

Expression (5.5) introduced to Eq. (5.1) gives the following algebraic equation:

$$Ae^{j\alpha}\,[-M\omega_p^2 + D_s j\omega_p + Dj(\omega_p - \lambda\omega\ ) + K + K_o(p)] = mr\omega_p^2 \tag{5.6}$$

Again Eq. (5.6) can be solved for dynamic stiffness (DS) components:

$$\text{Direct DS} = -M\omega_p^2 + K + K_o(p) = \frac{mr\omega_p^2}{A}\cos\alpha \tag{5.7}$$

$$\text{Quad DS} = D_s\omega_p + D(\omega_p - \lambda\omega) = -\frac{mr\omega_p^2}{A}\sin\alpha$$

The right–hand side expressions of Eqs. (5.7) contain again the measured parameters, so that the left–hand side coefficients can be identified. In this test the synchronous perturbation was used, i.e., $\omega_p = \omega$.

Variable parameters in the dynamic test were shaft rotative/perturbation speed ω , and bearing fluid pressure, p.

5.4 Summary

The performed tests show that the bearings designed to simulate the HPFTP interstage seals on the rub rotor rig are appropriate for use in the system. They provide a slight over range capability while producing good setpoint resolution of the fluid film radial stiffness within the required range of 0 to 75 lb/in. Both static and dynamic tests provide comparable data. The perturbation testing proved to be very useful and efficient.

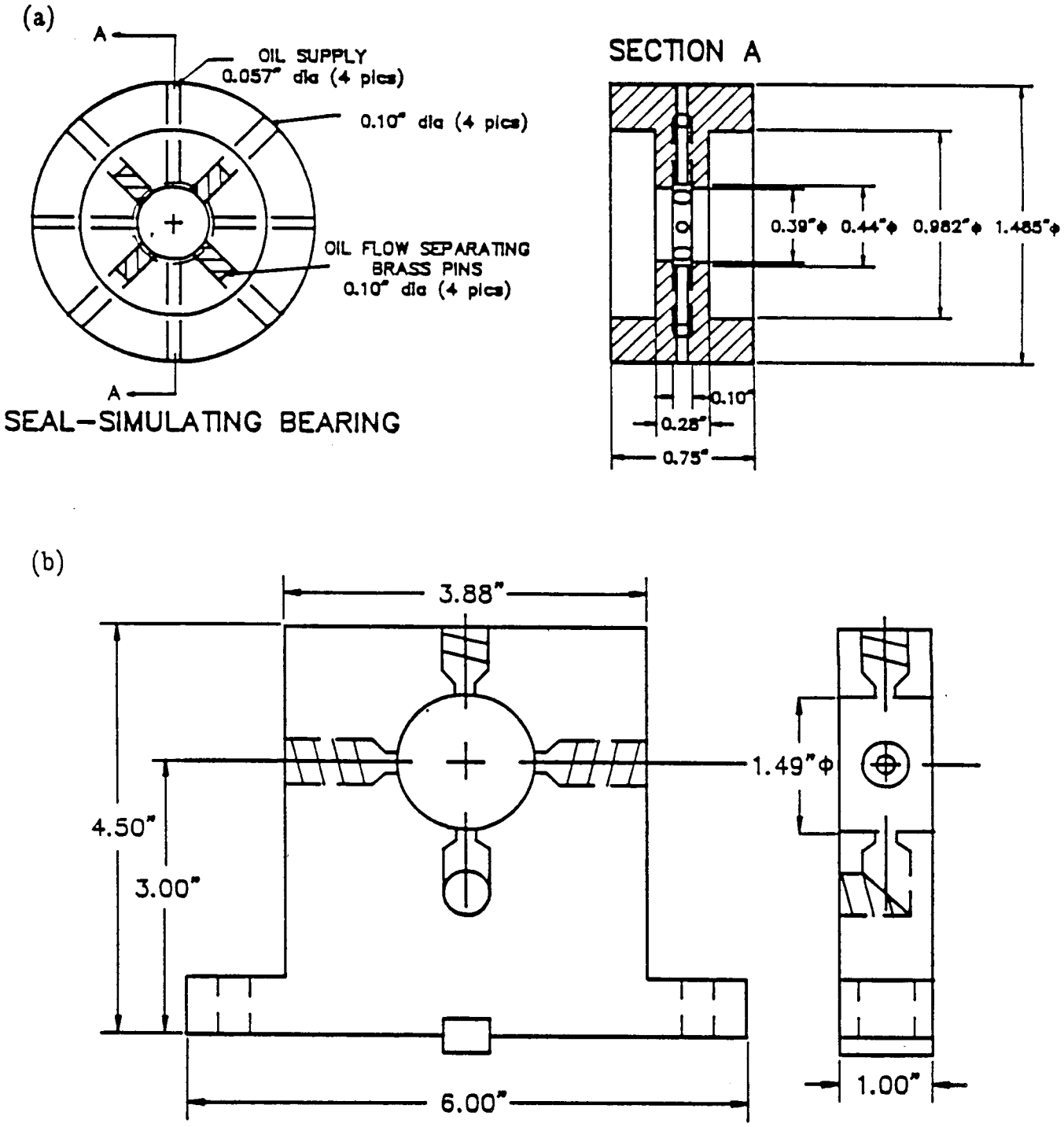

FIGURE 5.1 OIL–LUBRICATED BEARING SIMULATING A SEAL IN THE RUBBING ROTOR RIG. (a) BEARING (b) BEARING HOUSING.

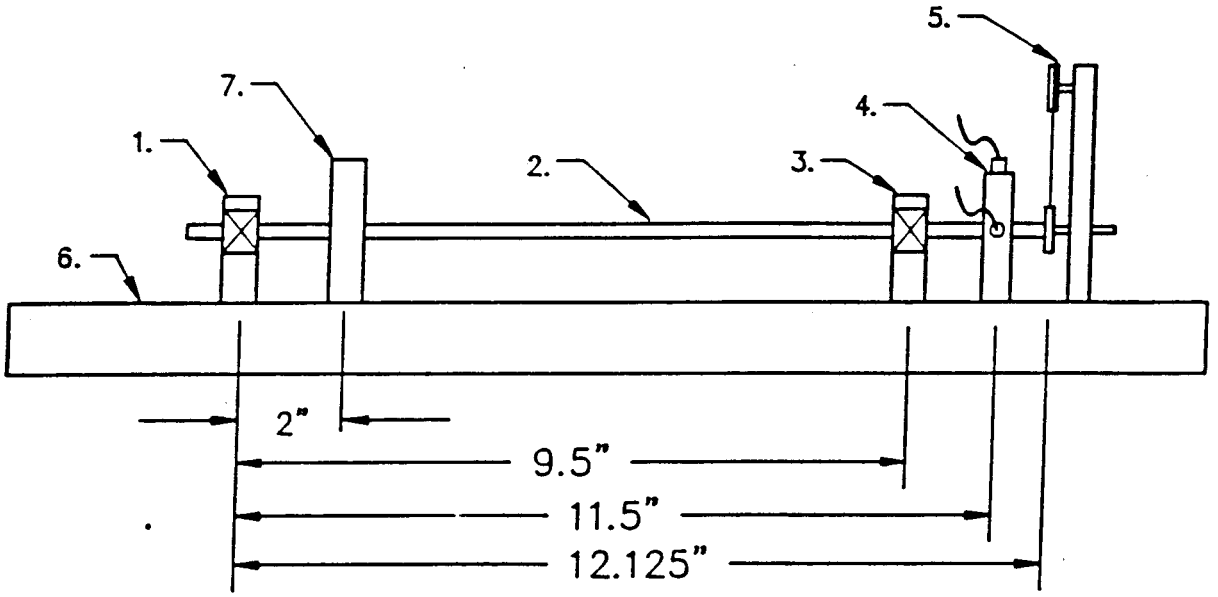

1. Rigid Anti–Friction Bearing
2. 0.375" Steel Shaft
3. Pressurized Oil Bearing Under Test
4. X–Y Eddy Current Displacement Probes
5. Pulley Arrangement To Generate Input Force
6. Base
7. Centering Springs

FIGURE 5.2 TEST SETUP FOR BEARING FLUID FILM RADIAL STIFFNESS MEASUREMENTS USING PERTURBATION TESTING.

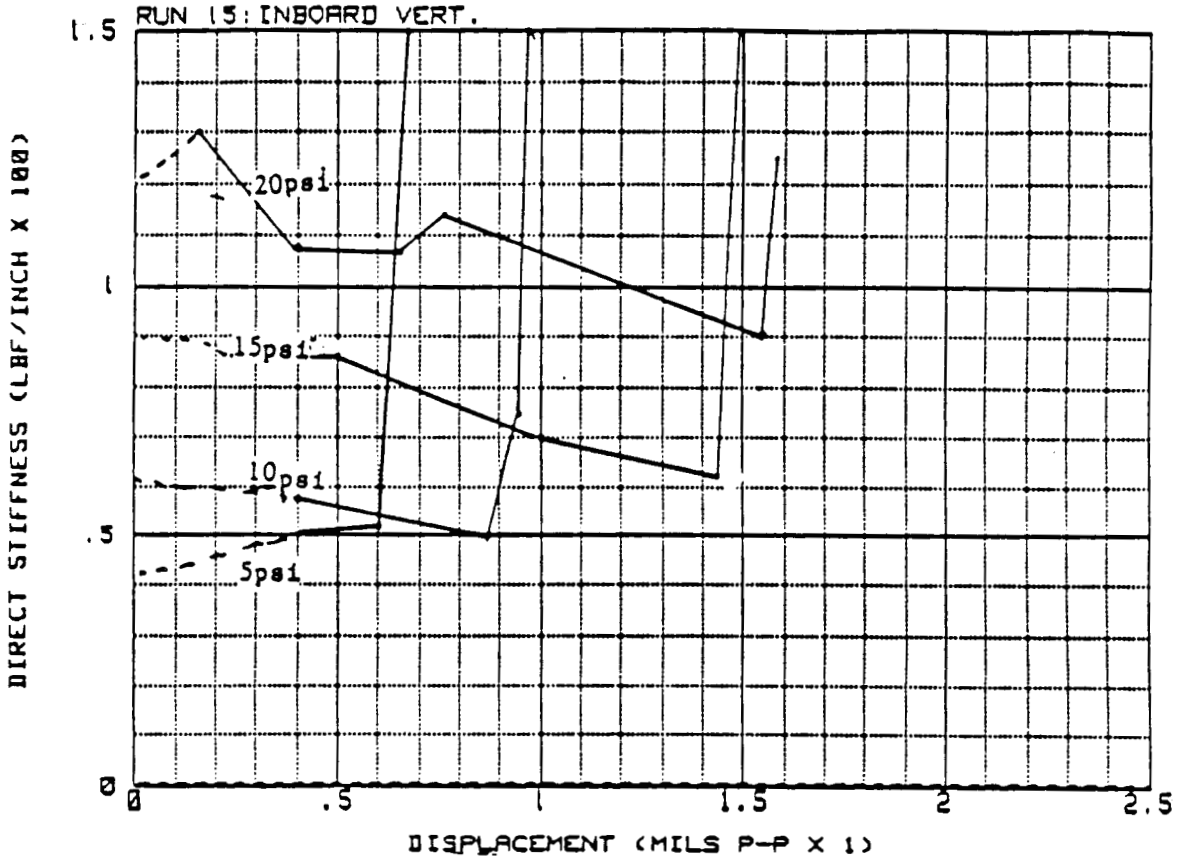

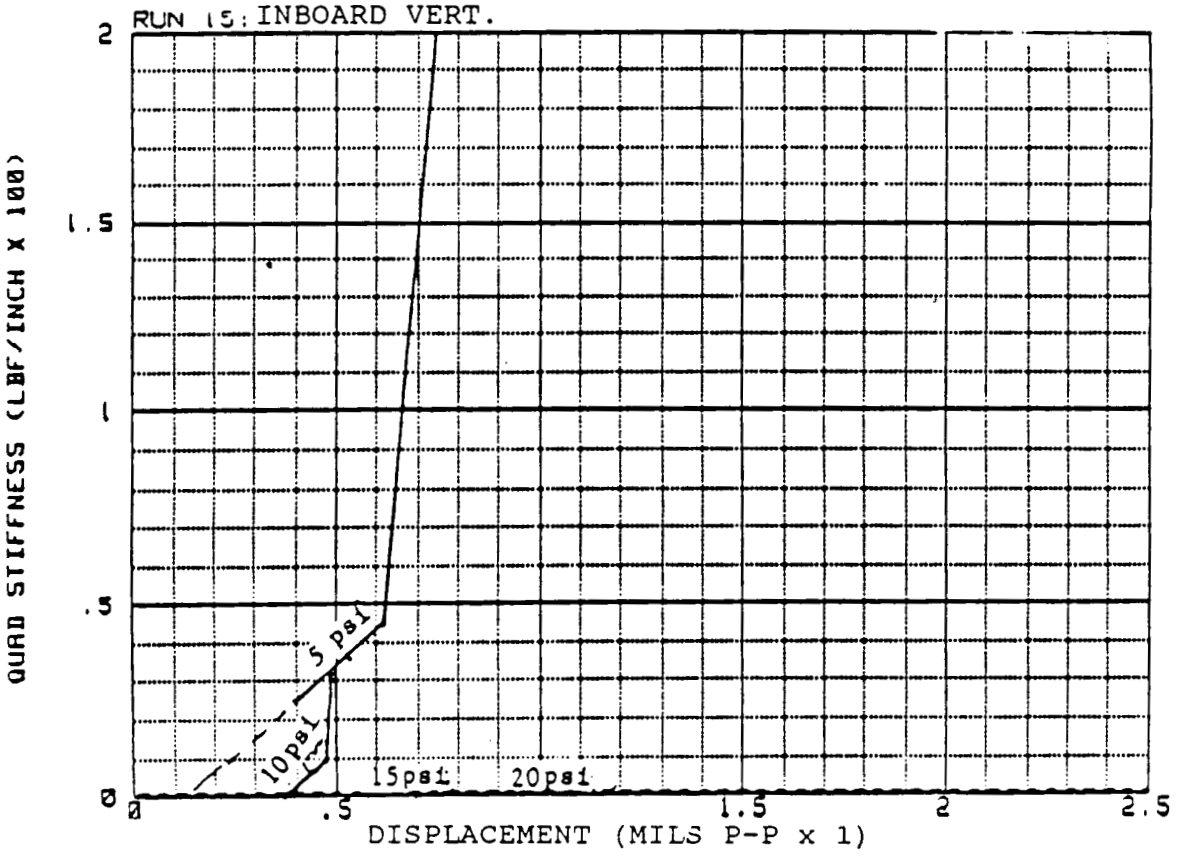

FIGURE 5.3 SEAL–SIMULATING OIL–LUBRICATED BEARING STATIC INBOARD DIRECT AND QUADRATURE STIFFNESSES AT 0 RPM AND FOR VARIOUS OIL SUPPLY PRESSURE.

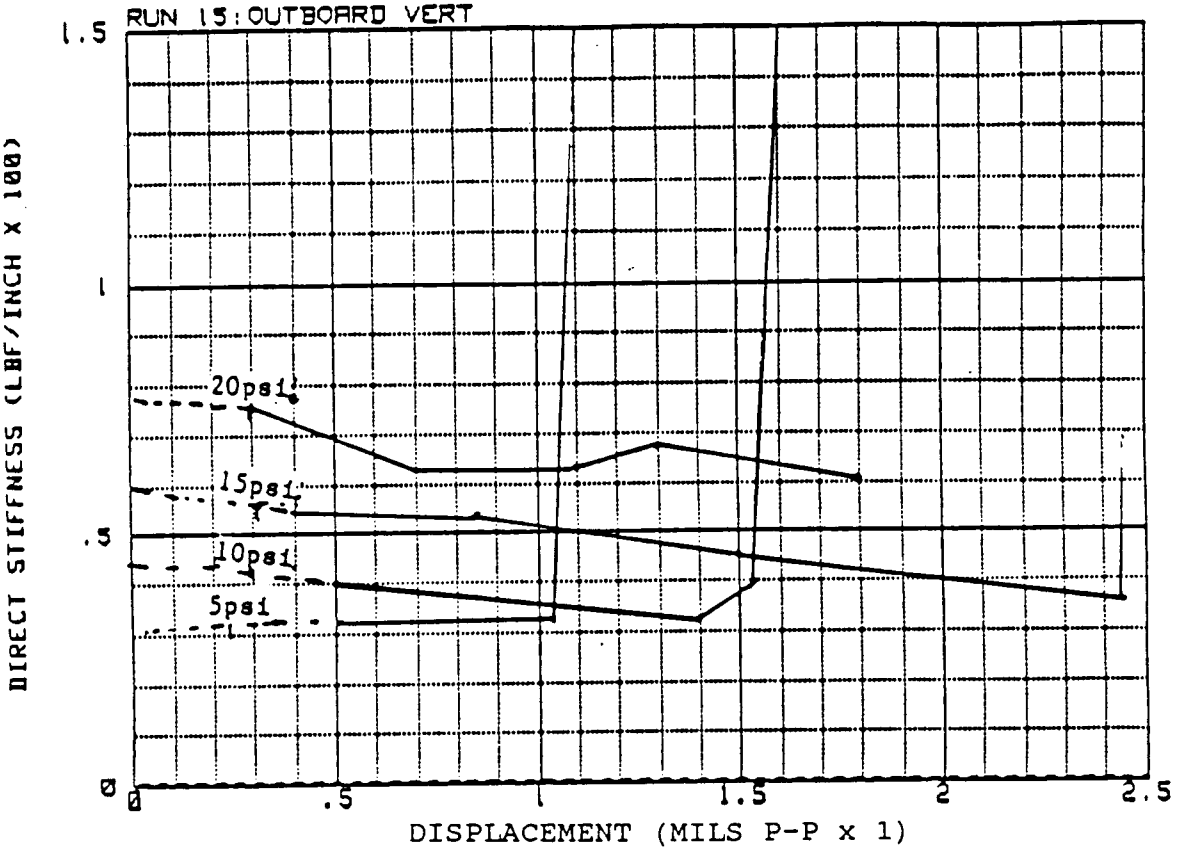

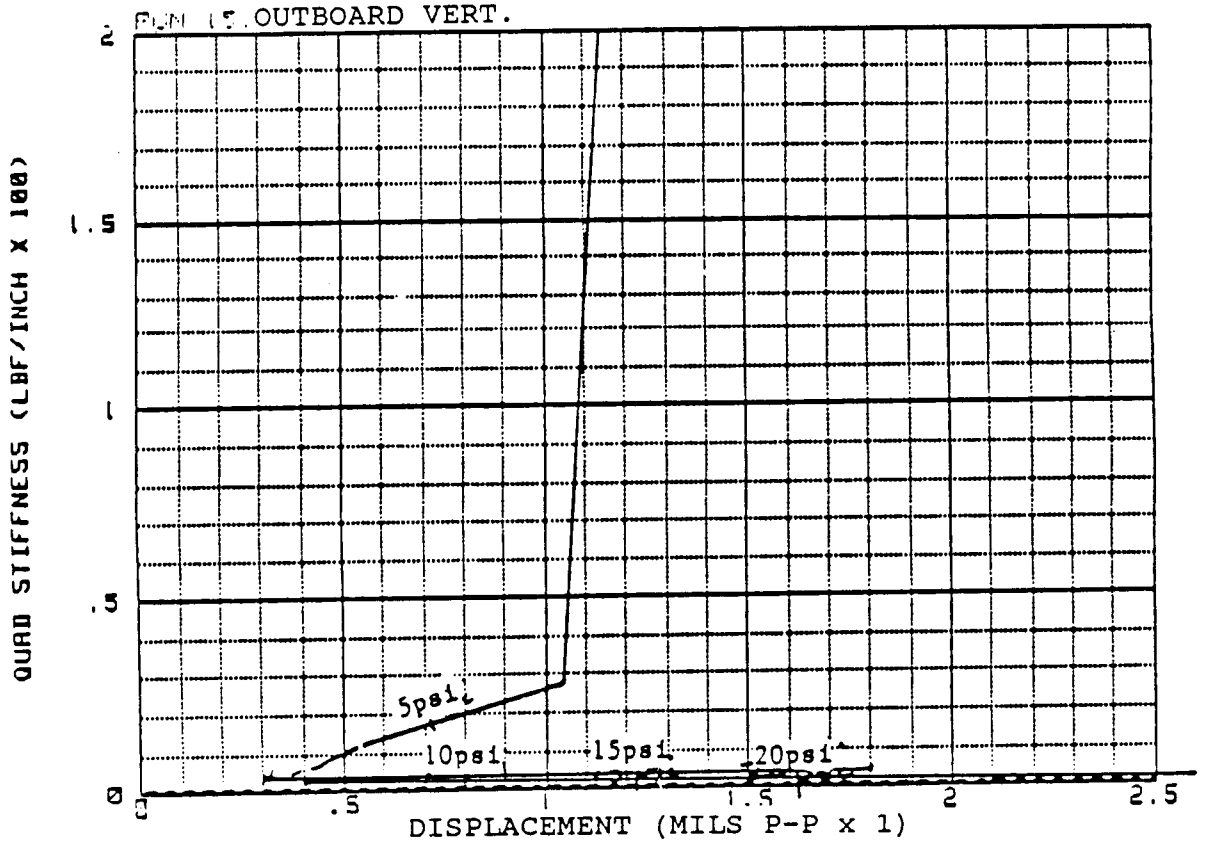

FIGURE 5.4 SEAL–SIMULATING OIL–LUBRICATED BEARING STATIC OUTBOARD DIRECT AND QUADRATURE STIFFNESS AT 0 RPM AND VARIOUS OIL SUPPLY PRESSURE.

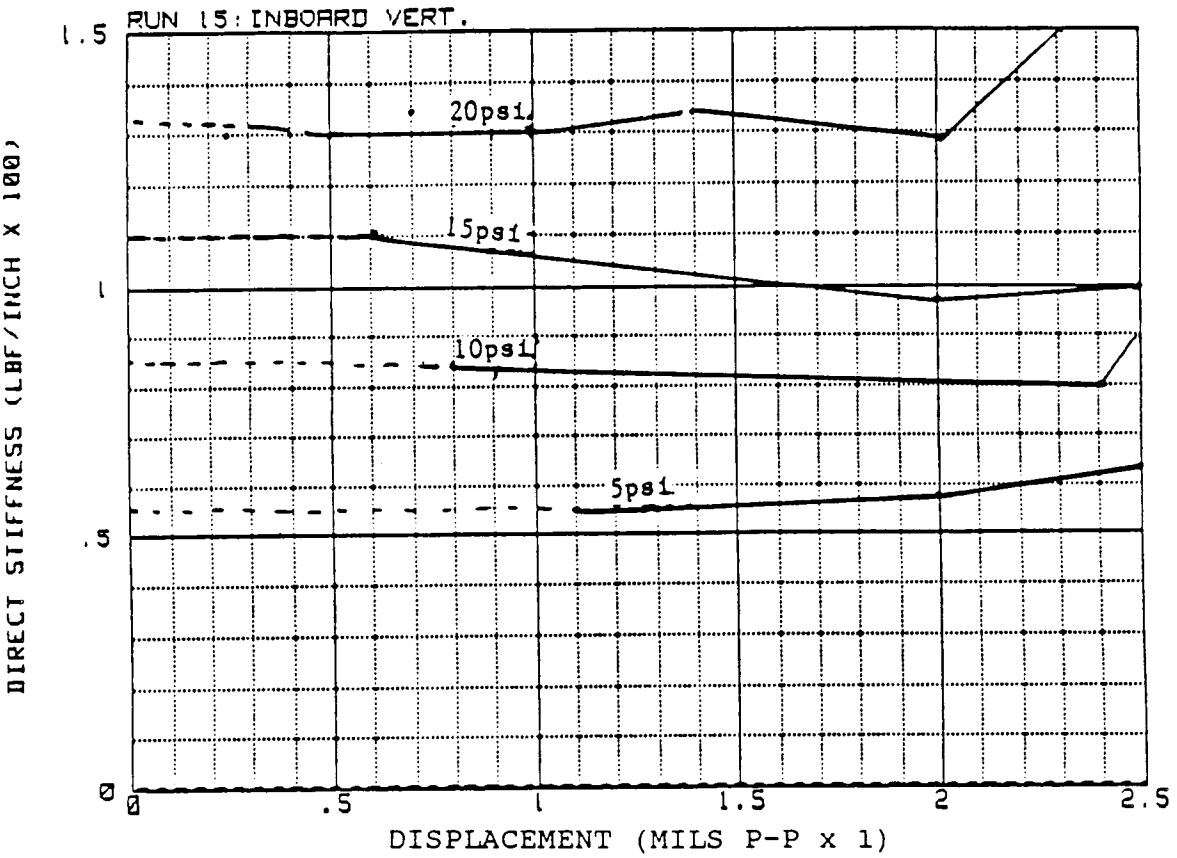

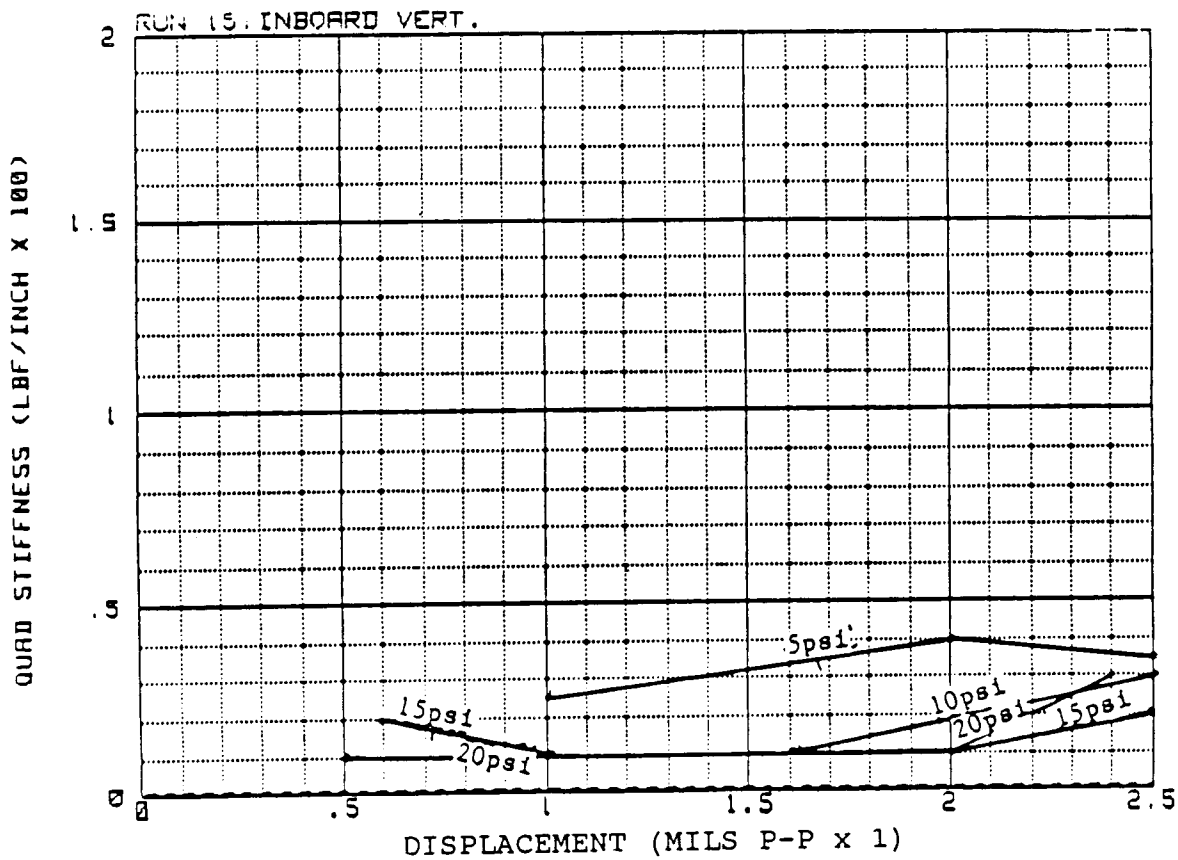

FIGURE 5.5 SEAL–SIMULATING OIL–LUBRICATED BEARING STATIC INBOARD DIRECT AND QUADRATURE STIFFNESS AT 1000 RPM AND VARIOUS OIL SUPPLY PRESSURES.

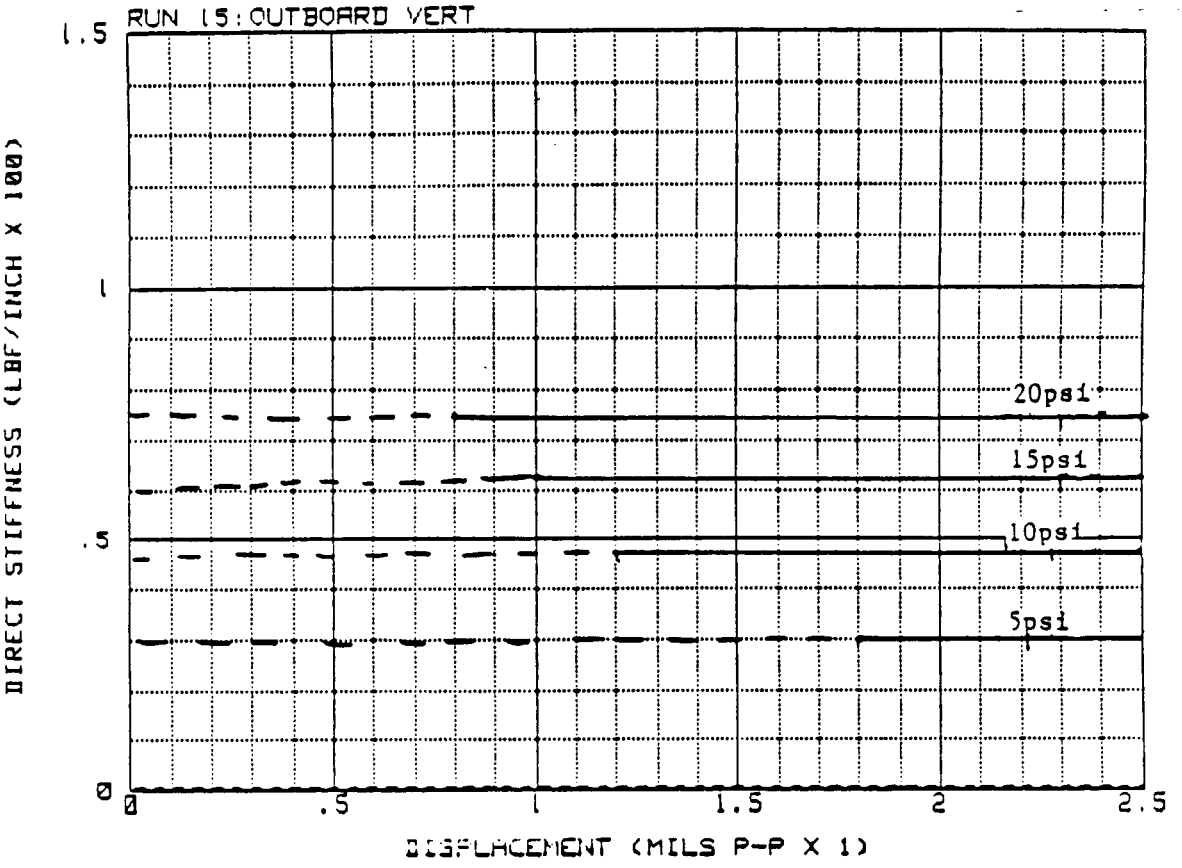

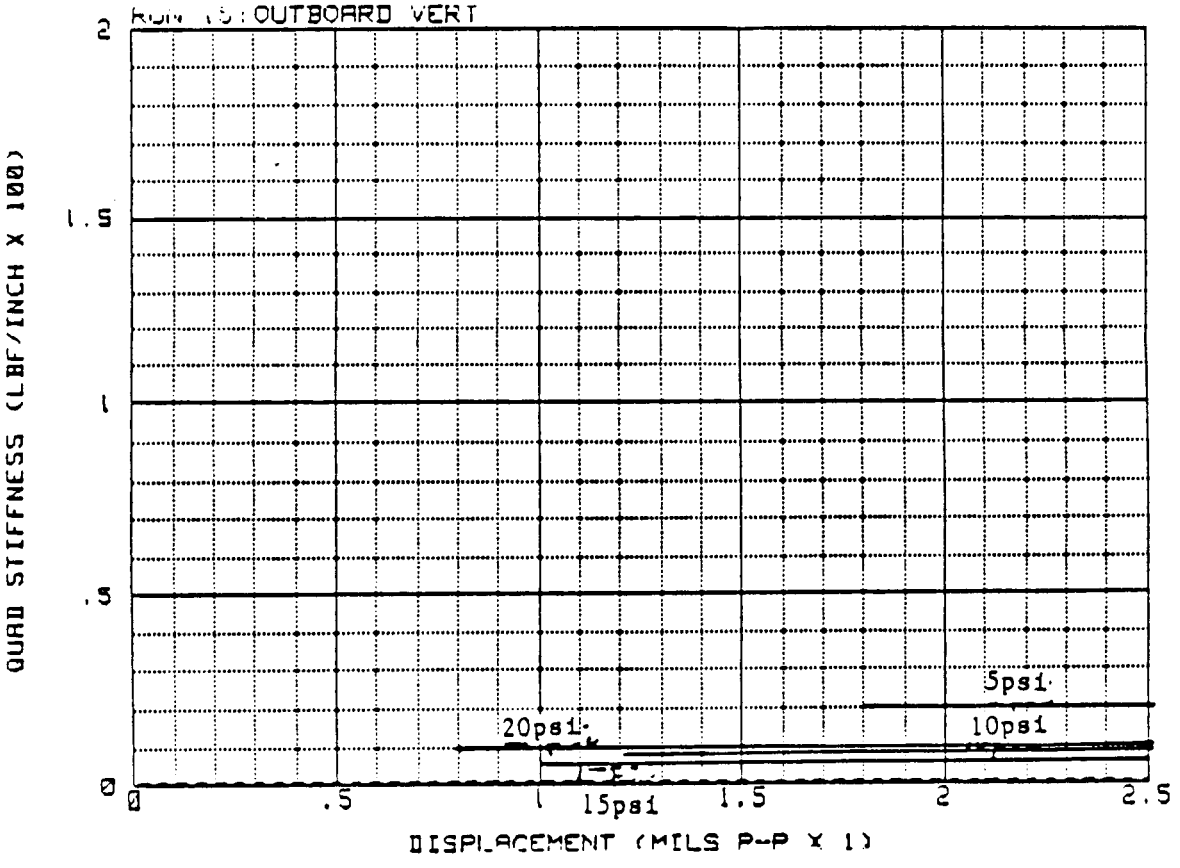

FIGURE 5.6 SEAL–SIMULATING OIL–LUBRICATED BEARING STATIC OUTBOARD DIRECT AND QUADRATURE STIFFNESS AT 1000 RPM AND VARIOUS OIL SUPPLY PRESSURE.

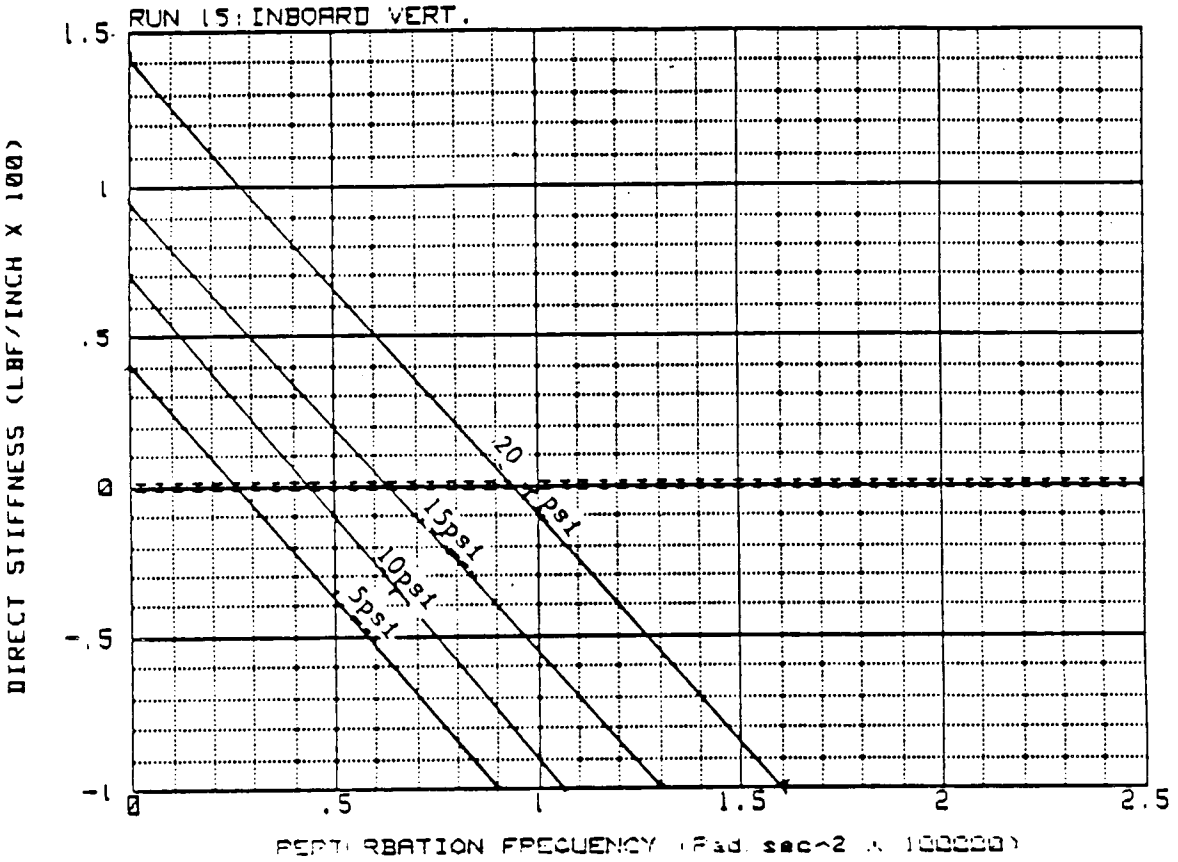

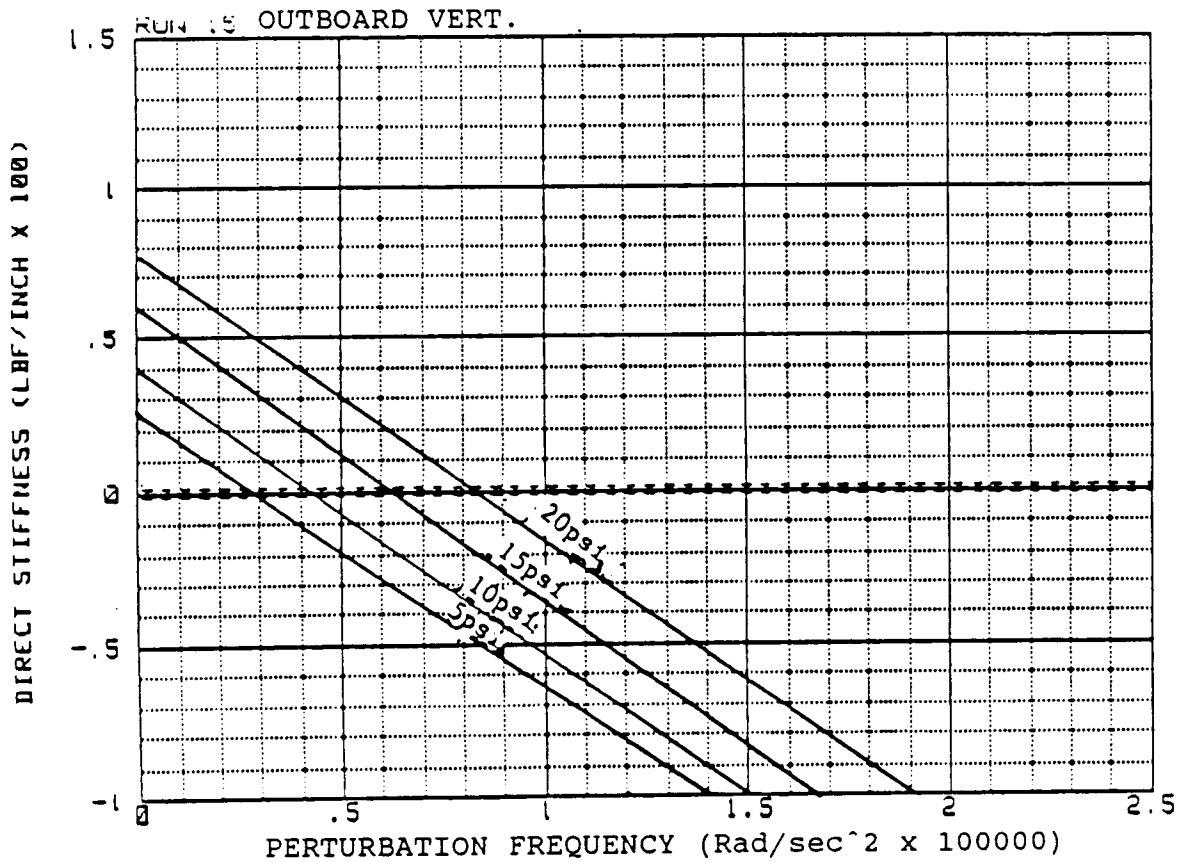

FIGURE 5.7 SEAL–SIMULATING OIL–LUBRICATED BEARING DYNAMIC DIRECT STIFFNESS AS MEASURED BY THE INBOARD AND OUTBOARD VERTICAL PROBES.

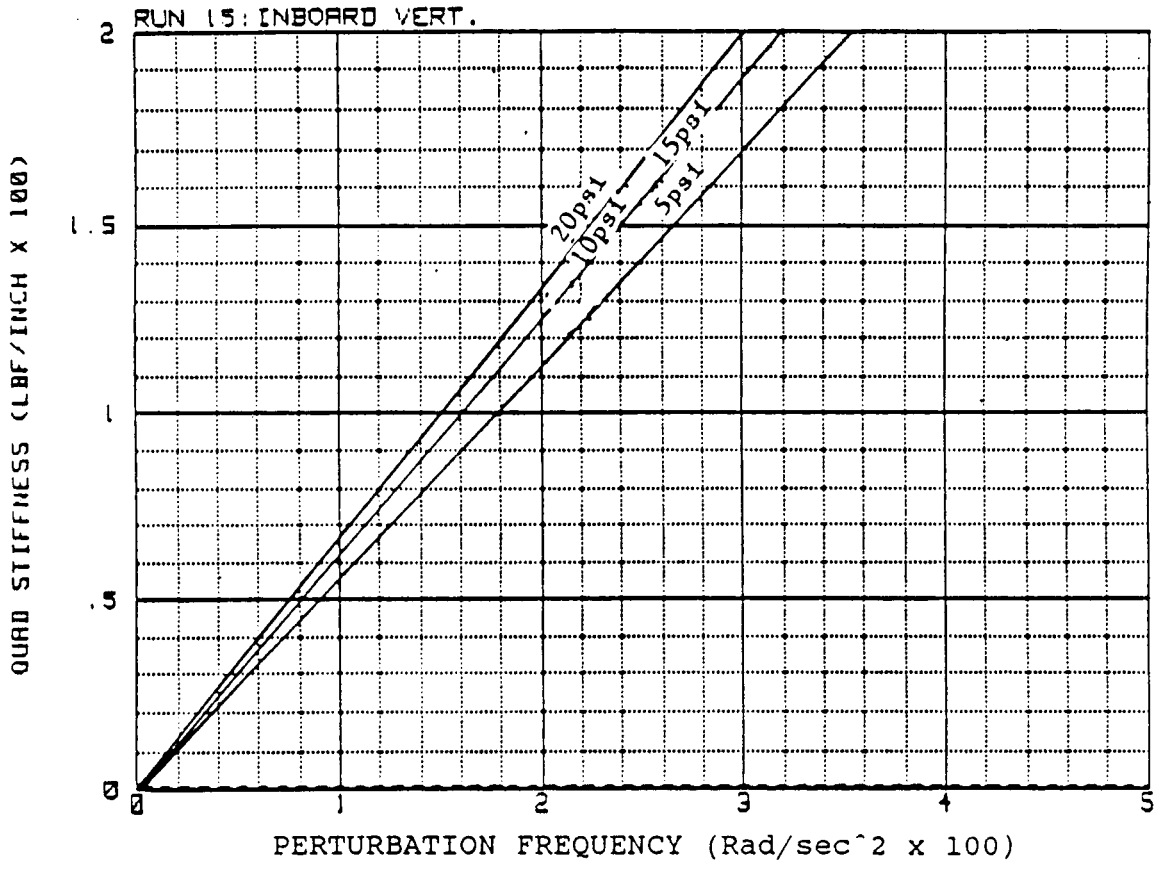

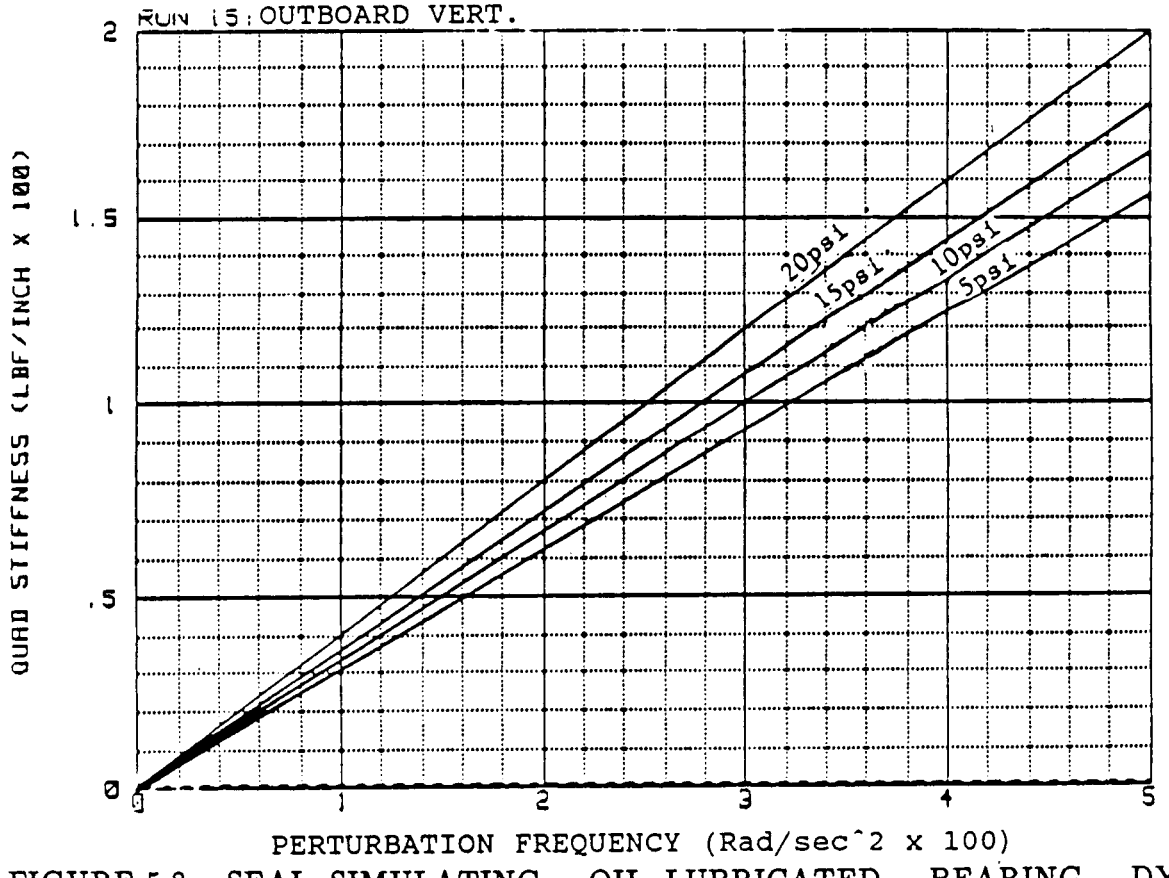

FIGURE 5.8 SEAL–SIMULATING OIL–LUBRICATED BEARING DYNAMIC QUADRATURE STIFFNESS AS MEASURED BY THE INBOARD AND OUTBOARD VERTICAL PROBES.

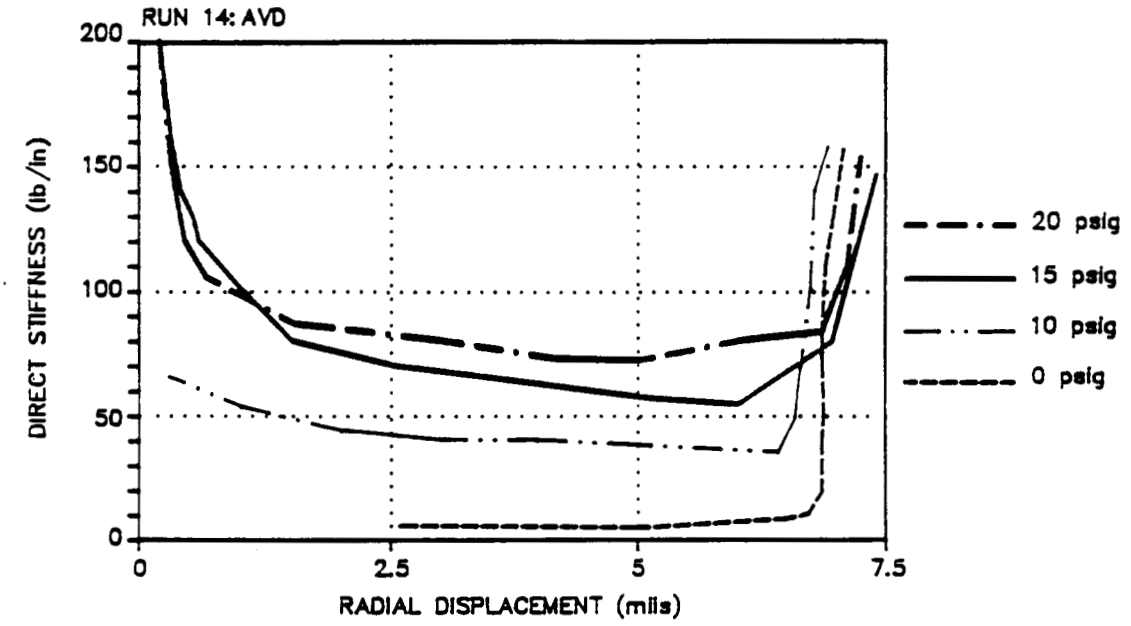

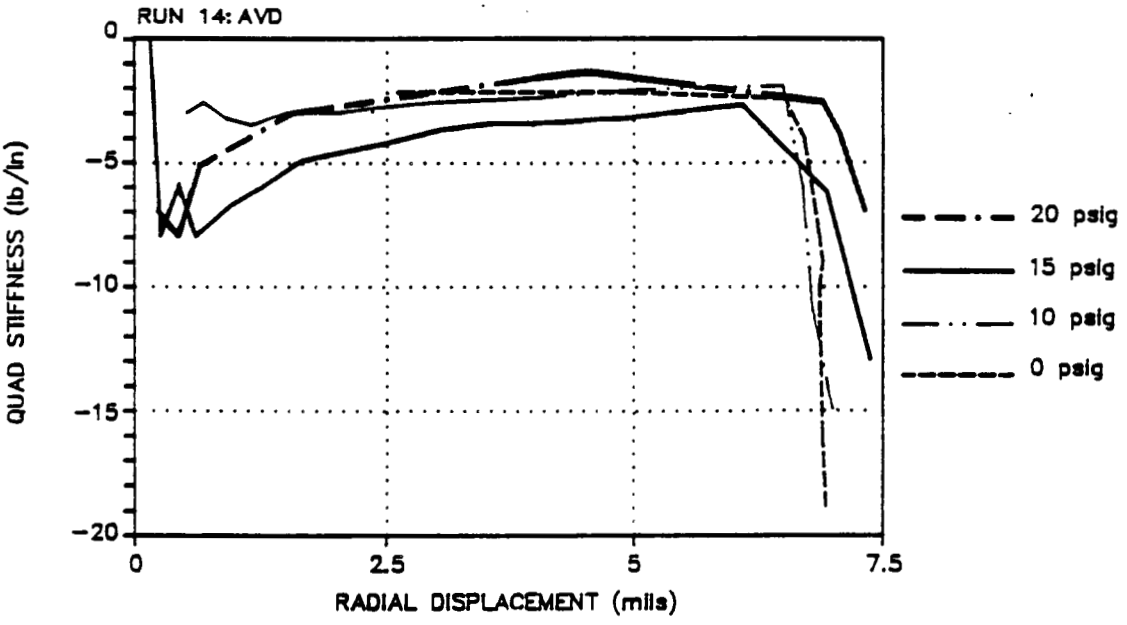

FIGURE 5.9 SEAL–SIMULATING 5.5 MIL CLEARANCE OIL–LUBRICATED BEARING STATIC DIRECT AND QUADRATURE STIFFNESS VERSUS SHAFT POSITION INSIDE THE BEARING AND OIL PRESSURE.

6.◦ RUBBING ROTOR RIG SIMULATING HPFTP.

6.1 Rotor Rig

The rotor rig designed to simulate the HPFTP rotor for rub testing is shown in Figures 6.1 and 6.2. The rig consists of a 0.375–inch–diameter shaft with four disks to simulate the lumped mass contributed by the pump impellers and turbine blading. The shaft is supported by rolling element bearings suspended from a rigid housing with four matched springs. This system provides a relatively soft, lightly damped support structure similar to the support characteristic of the HPFTP. Fluid lubricated cylindrical bearings with T10 (Chevron GST Oil 32, ISO–VG–32) oil supplied from an adjustable pressure source are used to simulate the additional radial stiffness created by the HPFTP seals. The picture of the rotor rig is given in Figure 6.3 with a key in Figure 6.4.

6.2 Instrumentation of the Rubbing Rotor Rig Simulating HPFTP

The HPFTP simulation rotor rig was equipped with a monitoring system to provide time, rotative speed, and vibrational response at several axial locations along the shaft. See Figure 6.2 for transducer locations and associated data paths and Figures 6.5 and 6.6 for monitoring system. The individual components of the system are discussed in more detail in the following paragraphs. The information on the electronic instrumention used in the experiments is included in the Appendix A3 of this report.

6.2.1 Vibration Transducers

The lateral displacements of the rotor are converted to electrical signals by the vibration transducers. A Bently Nevada Corporation 300 Series 190 proximity transducer system was used to obtain the shaft relative vibrational motion at the different axial locations. Bently Nevada Corporation high frequency accelerometers and interface modules were used to monitor absolute motion when necessary. (See Section 9.2.1 and Appendix A3.)

6.2.2 Data Acquisition and Processing Instrumentation

The majority of the final vibrational data of the rubbing rotor rig was obtained by reducing the vibrational signals from the transducers using a BENTLY NEVADA 108 DAI. The DAI (Data Acquisition and Instrumentation) provided data acquisition, synchronous filtration, plus amplitude scaling. Timebase information suitable for processing into narrow band spectrum data was also obtained by the 108 DAI. The instrument was connected to an IBM compatible personal computer system via an RS232 interface bus.

The computer system was operated with ADRE III® software developed by BENTLY NEVADA. The computer processed and stored the data, and produced the hard copy via an external printer.

The remaining data was acquired by reducing the vibrational data with a BENTLY NEVADA DVF–II and a HEWLETT PACKARD 3582 spectrum analyzer. The DVF–II provided the synchronous filtration and amplitude scaling, while the HP3582 spectrum analyzer produced the narrow band spectrum information. These instruments were connected to a HEWLETT PACKARD 9836C computer via an IEEE–488 interface bus. The computer system was operated with ADRE II or special software developed for Bently Rotor Dynamics Research Corporation to provide data presentation formats, data storage, or additional data manipulation. Hard copy was produced within this system using an external printer, a HEWLETT PACKARD 9876A. Since this system can only process two channels of information at one time, a TEAC SR–51 or HEWLETT PACKARD 3868A multi–channel FM tape recorder was used in conjunction with a BENTLY NEVADA 5248

–02 amplifier rack to capture the necessary data. This data was then played back into the signal processing system two channels at one time until all the data from all the channels was processed.

6.2.3 Description of Data Presentation Formats

Machinery vibration characteristics are conveniently presented on several distinct types of hard copy data plots. To provide an overview on the specific data presentation formats, the following descriptions are presented.

Steady–State Data Formats: The first format is the observation of shaft vibration signals in the time domain. This is normally combined with a shaft orbit when mutually perpendicular radial probes are observing the shaft motion, and phase is referenced with a once–per–turn Keyphasor® signal provided by the Keyphasor® probe. During data acquisition, this information can be observed directly on the oscilloscope screen as timebase waveforms and orbits. Both have once–per–turn Keyphasor marks, bright dots preceded by blanc spots.

Transient Data Formats: The second major category of data addresses the presentation of transient, variable rotative speed information. Typically this data is viewed in terms of the synchronous rotative speed vectors, as processed through the BENTLY NEVADA DAI 108, plus frequency spectra. Both types of data are required to provide the necessary overview of synchronous vector changes, plus the overall variation of frequency distribution.

The rotative speed vectors are accommodated by the Bodé plot where a running speed filtered vibration amplitude and phase angle are simultaneously plotted as a function of machine speed. The same information as in the Bodé plot can be presented in a polar plot format. The polar plot describes the locus of the shaft response vectors with variable rotative speed during a rotor start–up or shutdown operation. Although both of these plots provide the same basic data array, the Bodé provides excellent visibility of changes with respect to rotative speed, and the polar plot yields improved resolution of phase variation. Data of this type is essential for identifying rotor critical speeds (balance resonance speeds), and the influence of secondary resonances during variable speed response testing. In all cases, the synchronous vectors are plotted with amplitudes in mils, and phase angles expressed in terms of degrees of phase lag. Under machine conditions where significant sub or super synchronous vibration components are generated, it is desirable to generate a cascade plot of individual spectra at incremental operating speeds. This type of data presentation provides an excellent overview of the frequency content of the vibration signals as a function of rotative speed.

6.2.4 Auxiliary Instrumentation

In addition to the eddy current displacement transducers, accelerometers, and the computerized data acquisition and processing system used to document the vibration response of the rotor rig, other instrumentation was used to monitor secondary process variables. A digital scale was used to measure the magnitude of the masses used to produce the synchronous excitation forces. Dial pressure gauges were used to monitor the oil pressure in the seal simulation bearings. Measurement scales were used to evaluate the amount of preload applied to the rotor. In addition to these, other electronic lab instruments were used as needed such as oscilloscopes to monitor vibration signals, Digital Multimeters to check and set probe gaps, and Current Limited power supplies to provide the voltage potentials used to monitor rotor–to–stator contact.

6.3 Summary

Following the initial design criteria to dynamically simulate the HPFTP, the rotor rig was built. The rig geometry and the instrumentation for vibration data acquisition and processing is described in this chapter.

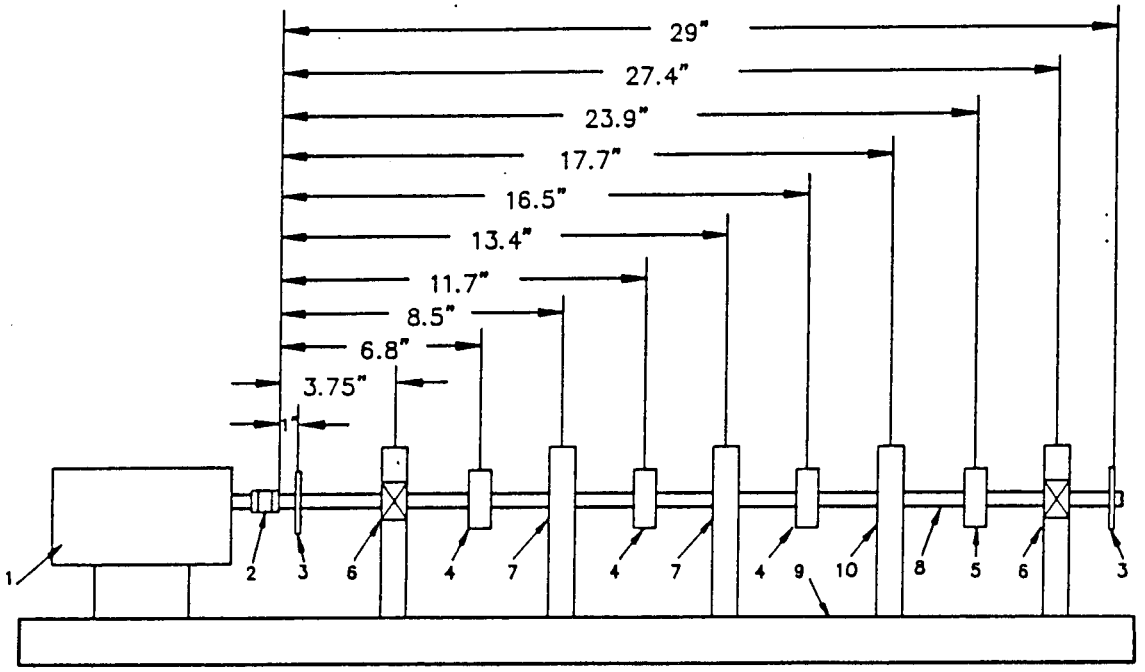

1. ELECTRIC MOTOR
2. FLEXIBLE COUPLING
3. BALANCING DISK
4. PUMP IMPELLER DISK
5. TURBINE IMPELLER DISK
6. SUPPORT BEARINGS
7. SEAL SIMULATING BEARINGS
8. 0.375" DIAMETER SHAFT
9. ROTOR BASE
10. PRELOAD SPRING

FIGURE 6.1 HPFTP SIMULATION RUBBING ROTOR RIG STRUCTURAL DIMENSIONS.

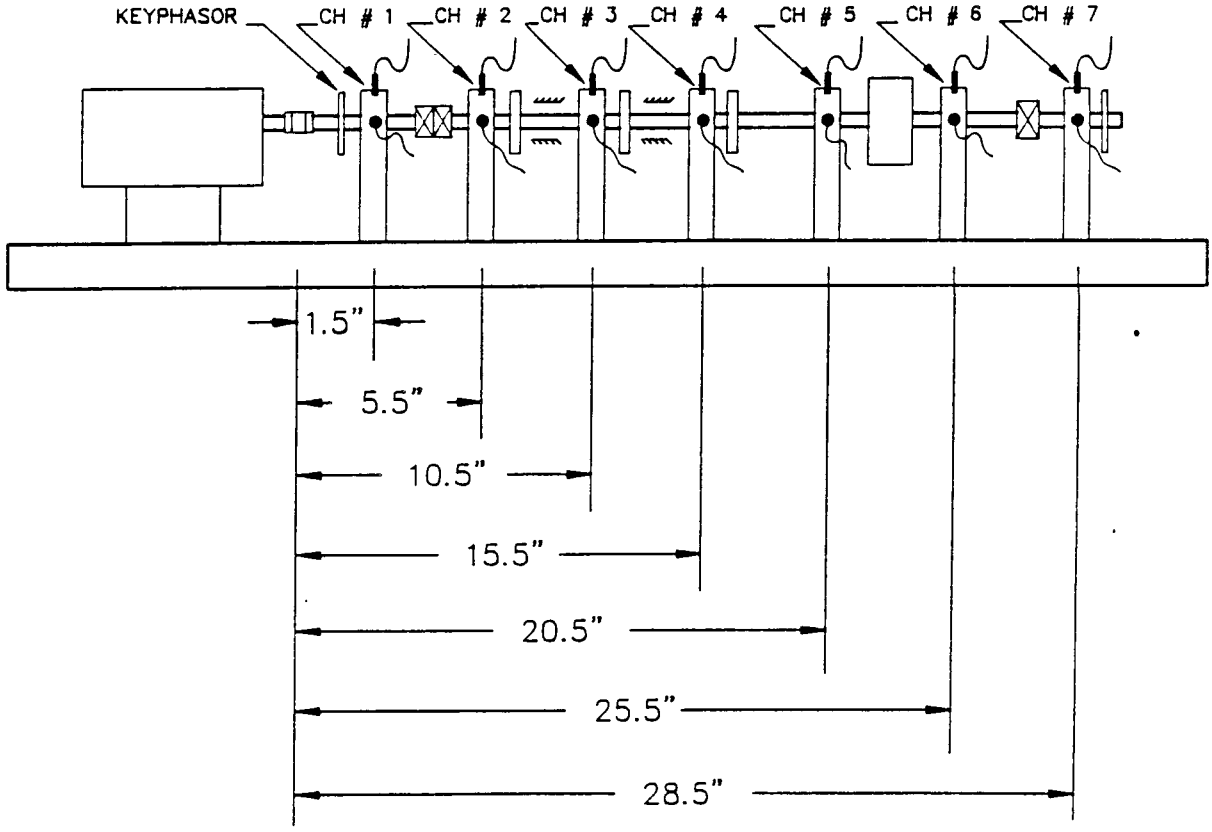

FIGURE 6.2 HPFTP SIMULATION RUBBING ROTOR RIG DISPLACEMENT PROBE LOCATIONS

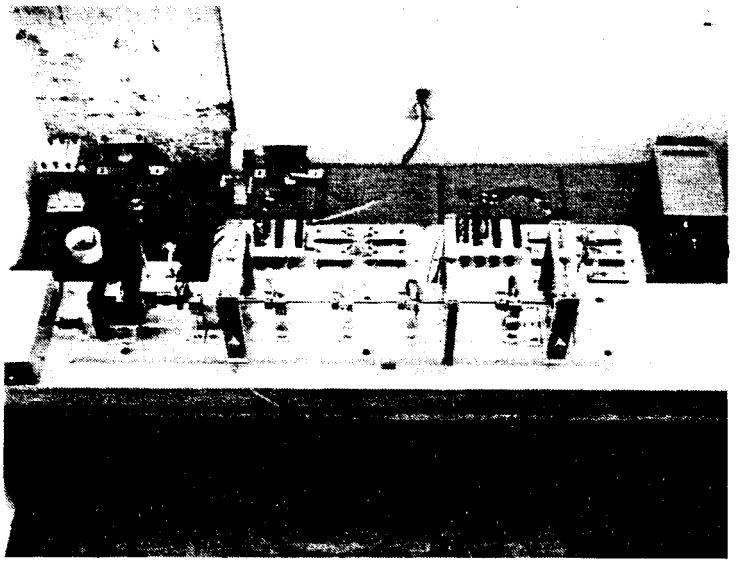

FIGURE 6.3 ROTOR TEST RIG (OIL LUBRICATED BEARINGS SIMULATING INTERSTAGE SEALS NOT INSTALLED APPEAR BEHIND THE ROTOR RIG).

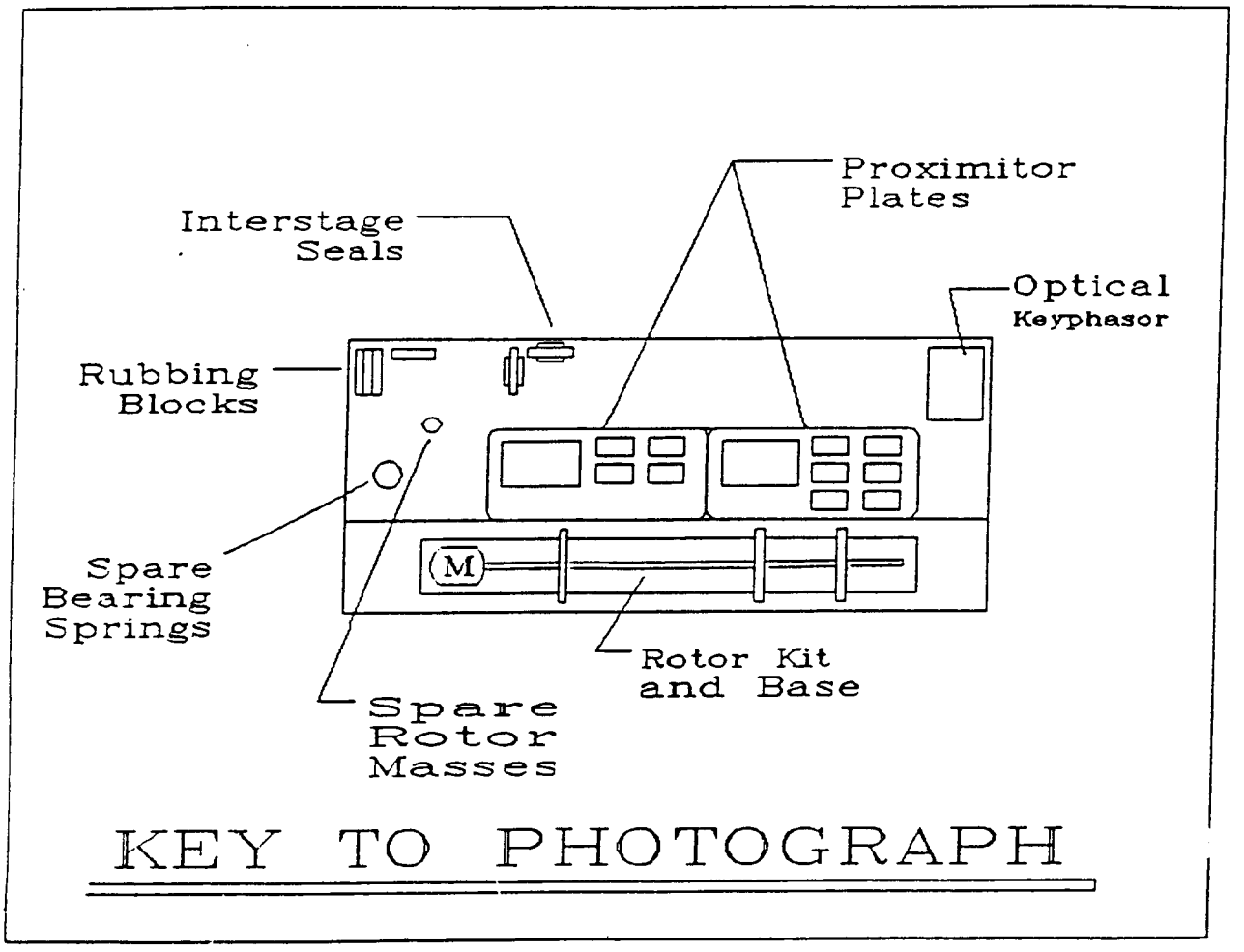

FIGURE 6.4 RUBBING ROTOR RIG LAYOUT.

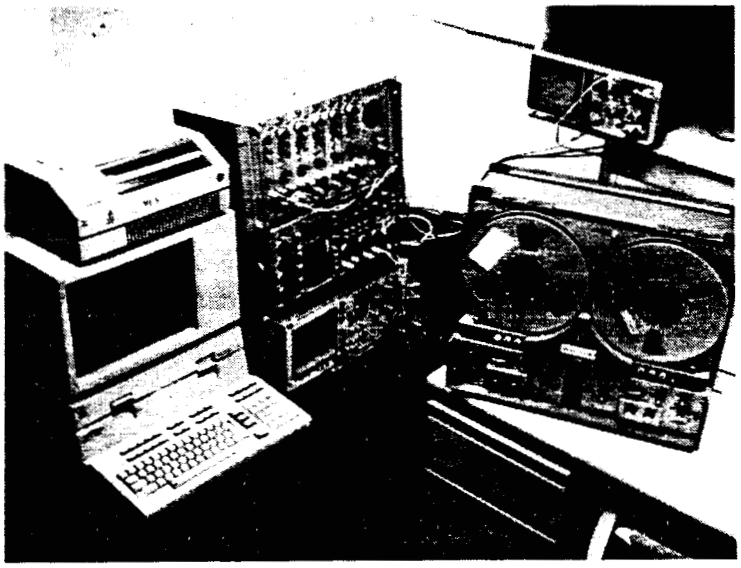

FIGURE 6.5 INSTRUMENTATION FOR DATA ACQUISITION/REDUCTION (HP COMPUTER WITH PLOTTER, AMPLIFIER, DIGITAL VECTOR FILTER, SPECTRUM ANALYZER, OSCILLOSCOPE, AND TAPE RECORDER).

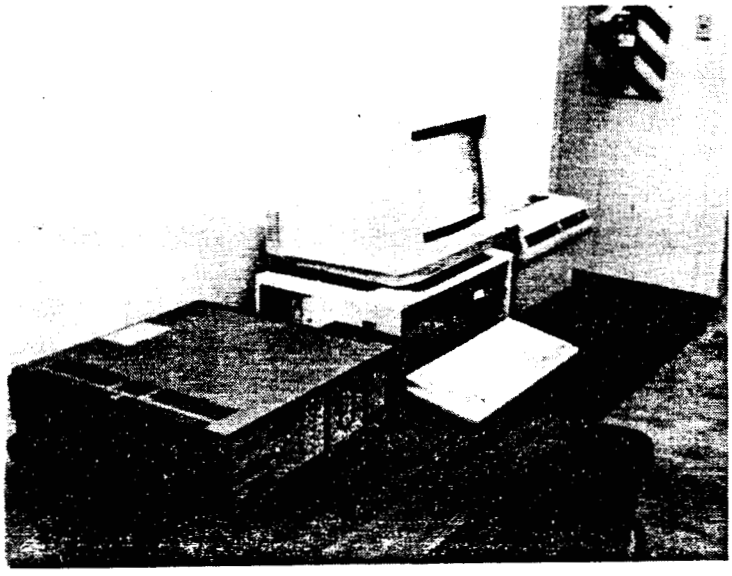

FIGURE 6.6 INSTRUMENTATION FOR DATA ACQUISITION/REDUCTION: ADRE 3 PACKAGE (IBM COMPUTER WITH PLOTTER AND INTERFACING DIGITIZING INSTRUMENT).

7. HPFTP SIMULATING RUBBING ROTOR RIG PRELIMINARY EXPERIMENTAL RESULTS.

7.1 Test Objective and Experiment Conditions

The rotor rig simulating the HPFTP was scaled down to reduce the forces, and hence increase the safety factor during the experiments. In order to verify that the dynamic behavior of the rotor rig simulates that of the HPFTP a series of tests were performed. These tests consisted of transient run–up data monitoring over the frequency range of interest for different seal simulation bearing pressures. This data was then reduced to get the resonant frequencies and the associated vibrational mode shapes at each frequency. The obtained mode shapes can be directly compared with those expected from the HPFTP while the resonant frequencies must be modified by a scale factor before comparison. If the relationship between the resonant frequencies of the rig and the mode shape at each frequency matches that of the HPFTP then the dynamic vibration response of the rotor rig should predict how the HPFTP would react under the same conditions.

7.2 Test Results

Figures 7.1 to 7.56 present the vibration data obtained from the HPFTP simulating rubbing rotor rig for four values of oil pressures in the seal simulating bearings between 0 psi and 15 psi. The probe locations indicated in the plot headings are referenced to their axial locations along the shaft in Figure 6.2. The synchronous vibration data indicate three resonant frequencies within the frequency range of interest. The mode shapes for the first three natural frequencies are shown in Figures 7.57 to 7.59 along with the predicted mode shapes for the HPFTP with a rigid casing. As can be seen from the figures, the mode shapes for the rubbing rig are very similar to those of the HPFTP supplied by NASA. By far the largest discrepancy occurs at the first mode for high oil pressures at the seal simulating bearings. The mode shape becomes pinched in the center because at high oil pressures the seal stiffness is greater than the support bearing stiffness. At normal simulation conditions the oil pressures for this rotative speed range are less than 3 psi. The rubbing rotor rig mode shape is then almost identical with the one predicted for the HPFTP. The second mode shows a slight restriction at the pump end of the shaft, caused by the additional restraint of the coupling used to connect the shaft to the drive motor. Since the deviation from the predicted mode shape is minor, and also at a noncritical axial location along the shaft, it does not significantly modify the rig vibrational response during rub testing. The third mode matches the predicted mode shape very well for all operating conditions. The resonant rotative speeds are shown in Table 7.1 along with those predicted by NASA. This data shows that the rub rig resonant speeds have been scaled down from the actual HPFTP resonances by a factor of nine; note the scaled HPFTP resonant speeds are also included in Table 7.1 for comparison. Even though the resonant speeds for the rub rig have been scaled down for safety during the experiments, the data in the table clearly shows that the relationship between the resonant speeds and the mode shape at each natural frequency are the same for both the HPFTP and the rubbing rotor rig, the data taken on the rig should be representative of that from the HPFTP.

A phenomenon of interest, but not pertinent to this rub research, is the occurrence of rotor oil whirl/whip self–excited vibrations at rotative speeds above 3200 rpm and oil pressures in seal simulating bearings below 10 psi. This hopefully will not create any significant problem during rub tests since the oil pressure can be controlled to eliminate the instability at the rotative speed of interest. When even a light rotor–to–stator rub occurs, it causes enough change in the system dynamic stiffness at the seal simulation locations to re–stabilize the rotor (see the paper in Appendix 2, for the experimental data and

conclusions regarding the effect of rub on oil whirl/whip instabilities). In this aspect the rub provides a positive effect.

The rig can be run over the full operating range without oil whirl/whip at 0 psi pressure, if all the oil is blown out of the seal clearance area using compressed air before the rub experiment begins.

The experimental data also shows the presence of a very small 2x vibrational component at all measurement planes. This is probably caused by an asymmetry produced by the disk mounts. The disks used to simulate the pump impellers and turbine blading are positioned along the shaft and then secured in place using a set screw tightened against the shaft. Previous experience with rotor systems has indicated that this causes a slight asymmetry in the rotor lateral stiffness characteristics in two orthogonal directions. Coupled with the preload due to gravity or the radial preload applied to the rotor, the shaft asymmetry causes the 2x component to appear in the vibrational response. As can be seen from the data, this component is very small and will not interfere with the data obtained from the rub experiments.

	Natural Frequency					
Mode	HPFTP [rpm]	SCALED [rpm]	0 psi	5 psi	10 psi	15 psi
1st	16828	1870	1650	1900	2200	2300
2nd	30881	3435	3000	3100	3350	3750
3rd	46286	5150	5400	4800	5100	5200

TABLE 7.1

Summary of Natural Frequencies for HPFTP and Rubbing Rotor Rig at Different Seal Pressures

7.3 Internal Friction Instability

During initial checkout and debugging of the HPFTP simulation rotor rig, a vibrational instability with a limit cycle subsynchronous vibrations of the frequency equal to the system first natural frequency was noted for rotative speeds above 5500 rpm, (see Figures 7.8 to 7.14). The seal simulation bearings were run without oil, which eliminated the possibility of fluid–related whirl/whip instability. After some careful checking to ensure that the vibration was not caused by forces coupled through the supporting structure, it was concluded that the instability was caused by the internal/structural friction of the rotor. Since the disks simulating the pump and turbine impeller masses were slipped onto the shaft and secured in place with a setscrew pressed against the shaft, it was assumed that they would be the major contributing factors to the internal/structural friction.

In order to circumvent the time–consuming alignment procedure required for the simulation rotor rig after each disassembly/reassembly process, a second rotor was constructed from spare parts. Initially the new rotor was suspended in standard bronze Oilite rotor kit bearing bushings. In this configuration the test rotor would not duplicate the instability observed on the HPFTP simulation rotor rig. When the Oilite bearings were replaced with standard anti–friction rolling element bearings, the test rotor then duplicated the symptoms originally observed. The disks were then bonded to the shaft with a cyanoacrylate glue. This resulted with no change in the stability threshold and subsynchronous vibrations. Gluing does not produce a friction–free joint; however, the probability of getting the same friction coefficient for the disks glued to the shaft or secured with a setscrew seems small. Therefore, it was assumed that the disk mounting technique was probably not the main factor contributing to the instability. To verify this, a shaft was run with no disks attached. This produced the same instability pattern, but with a slightly higher rotative speed threshold.

Since the instability occurred outside the desired operating speed range and, therefore, was not creating a significant problem, the internal friction studies were discontinued at this point.

7.4 Summary

In order to secure a safe environment to perform the rub tests, the HPFTP needed to be replaced with a model which produced lower energy levels during rotor–to–stator contact. This was accomplished by reducing both the rotative speed and the mass of the simulation rub rig. Tests were then performed which verified that the simulation rub rig retained the same ratios between natural frequencies as the HPFTP. The results of these tests are discussed in this chapter. The tests indicated the mode shapes at the natural frequencies matched those of the HPFTP. Based on these test results, it was concluded that the simulation rub rig would produce comparable vibration responses as the original HPFTP.

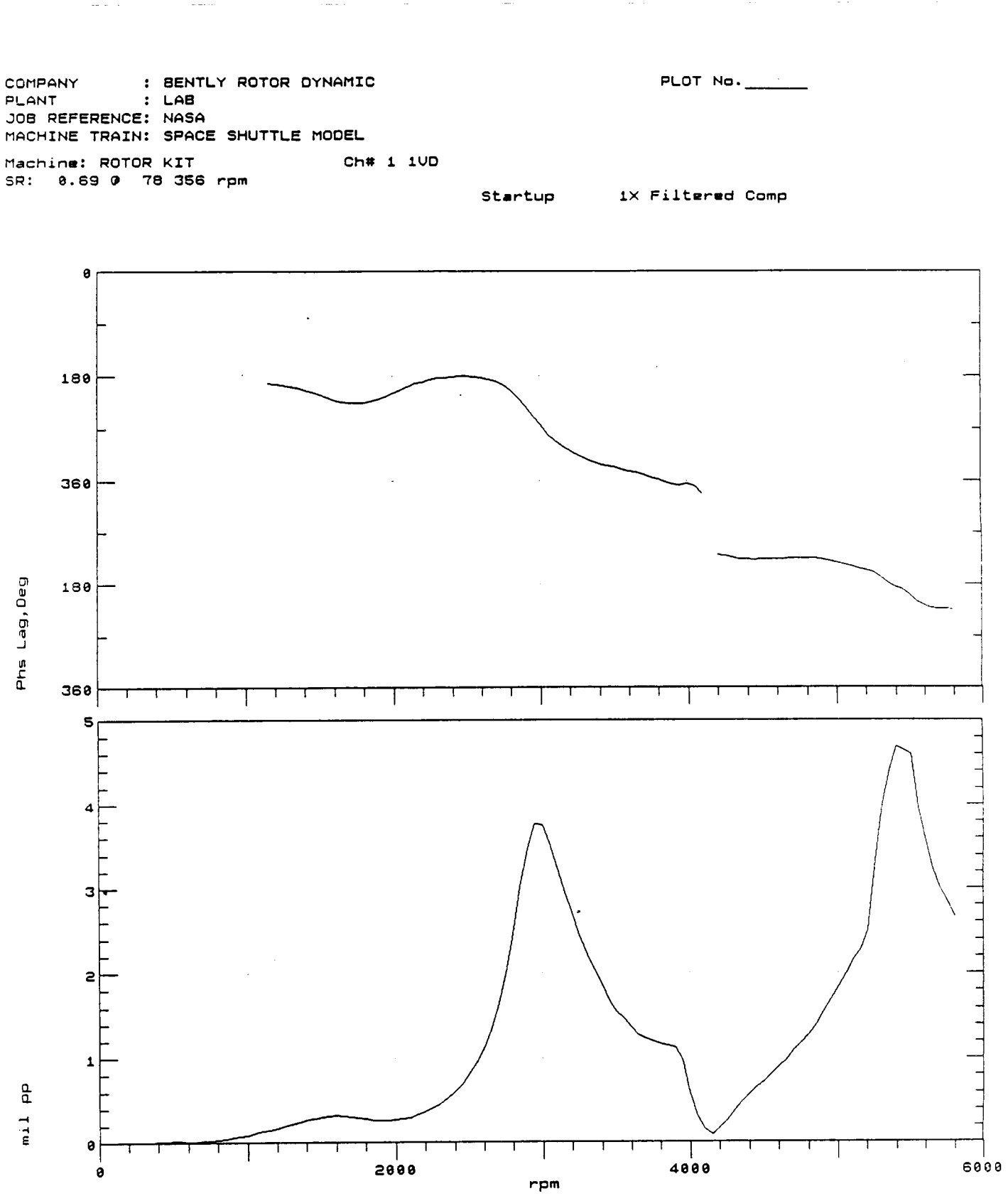

FIGURE 7.1 BODÉ PLOT OF ROTOR SYNCHRONOUS VIBRATION MEASURED AT CHANNEL #1. 0.0 PSI OIL PRESSURE AT SEAL SIMULATION BEARINGS. 0.0 INCH PRELOAD.

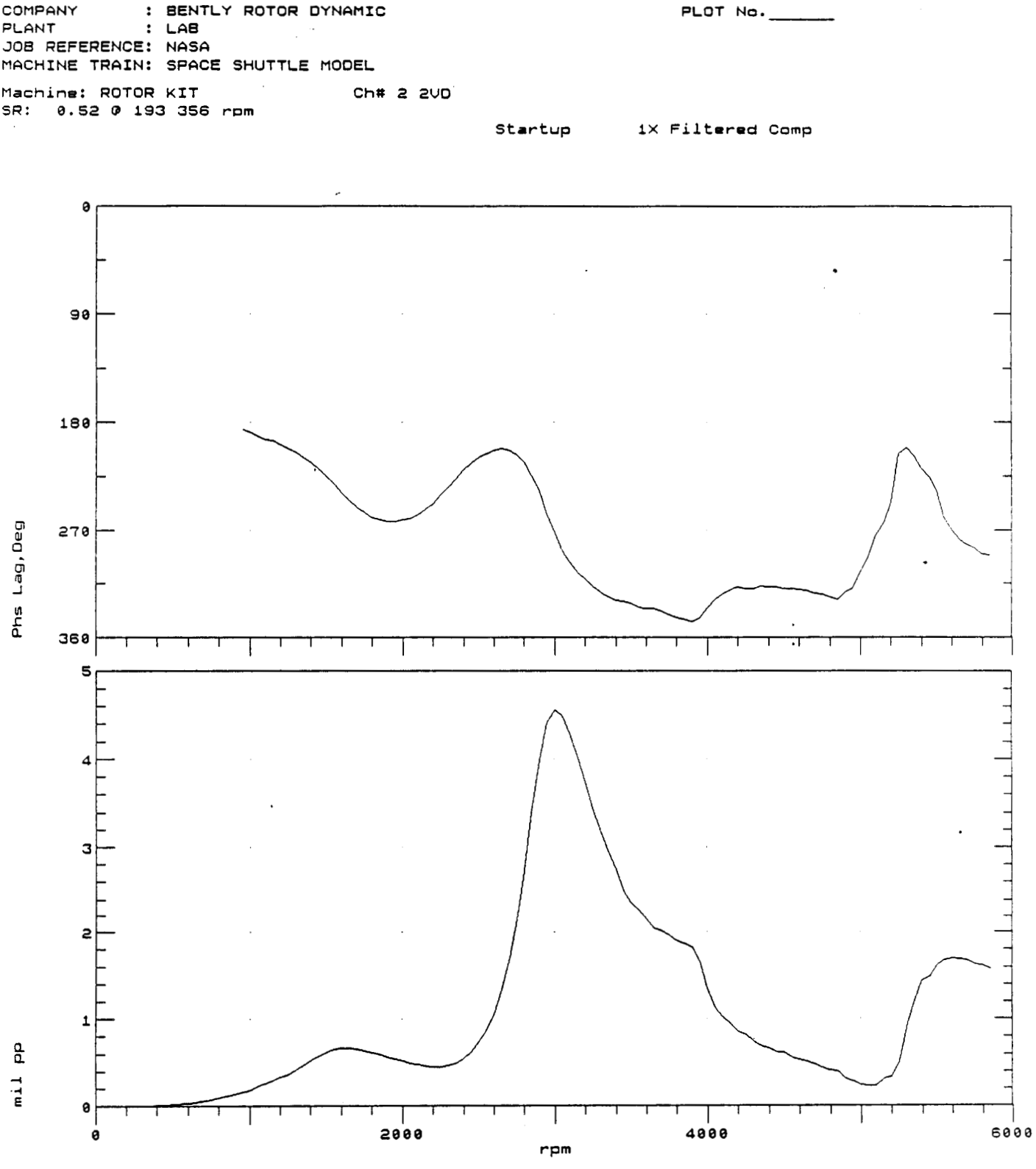

FIGURE 7.2 BODÉ PLOT OF ROTOR SYNCHRONOUS VIBRATION MEASURED AT CHANNEL #2. 0.0 PSI OIL PRESSURE AT SEAL SIMULATION BEARINGS. 0.0 INCH PRELOAD.

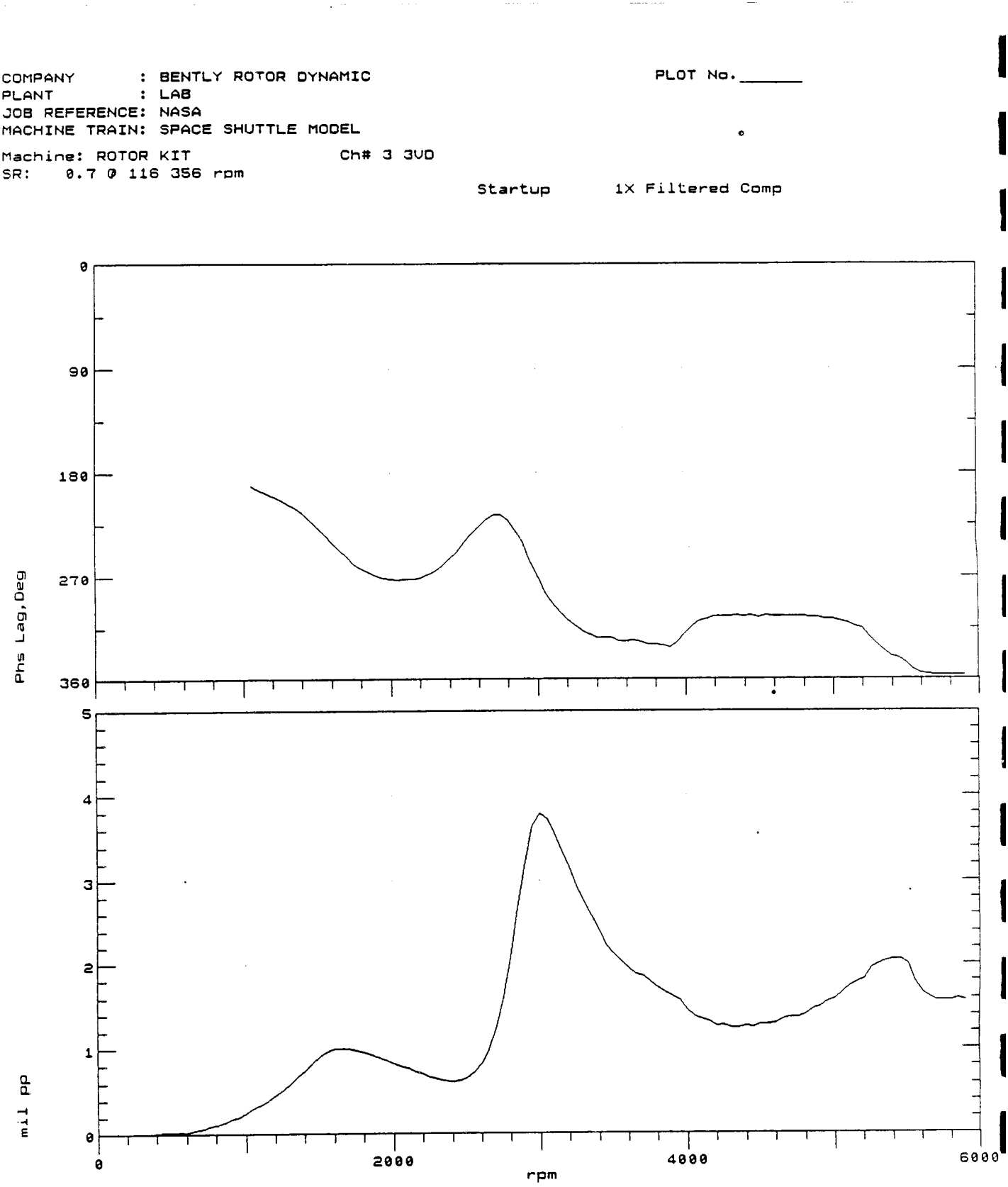

FIGURE 7.3 BODÉ PLOT OF ROTOR SYNCHRONOUS VIBRATION MEASURED AT CHANNEL #3. 0.0 PSI OIL PRESSURE AT SEAL SIMULATION BEARINGS. 0.0 INCH PRELOAD.

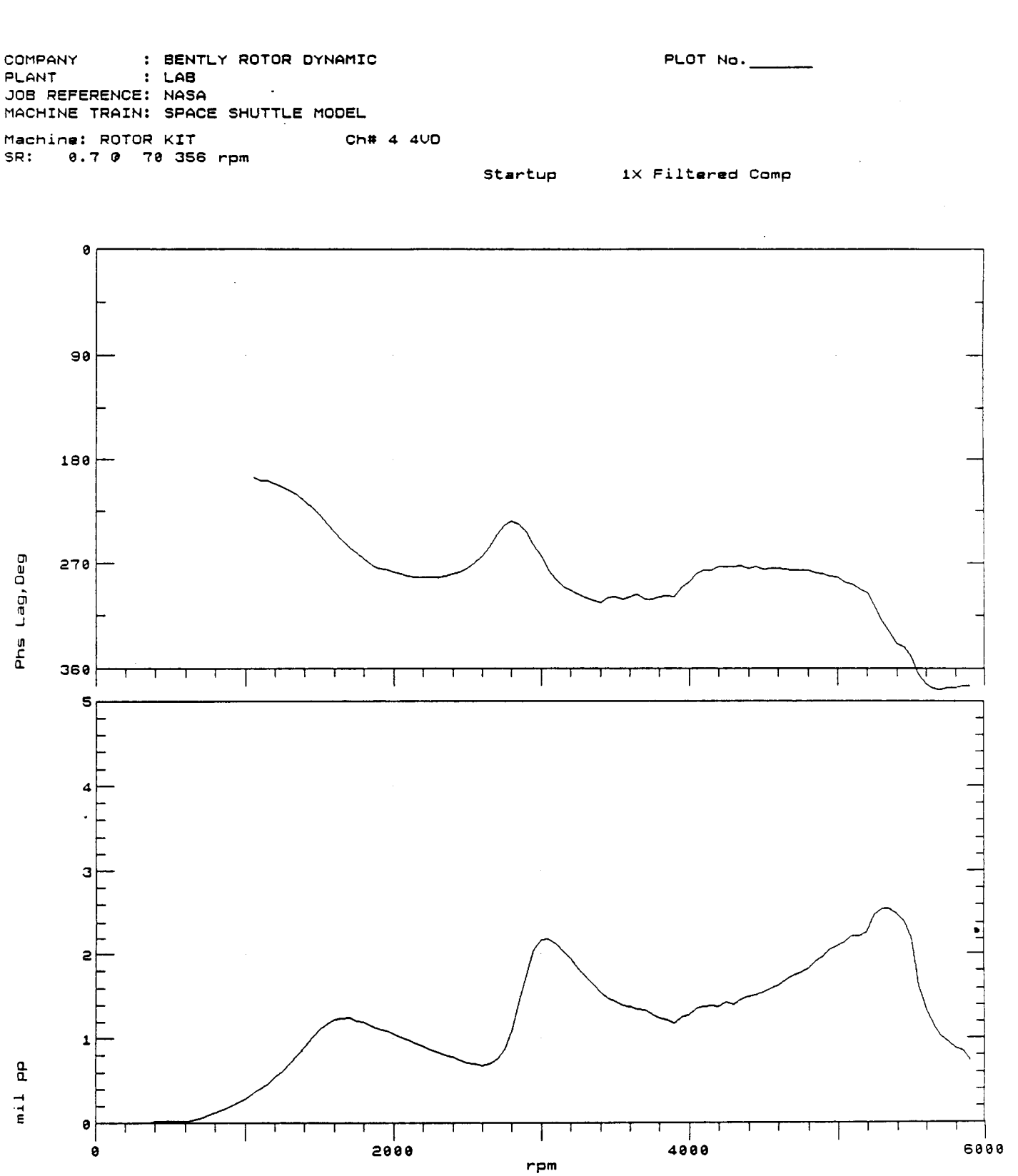

FIGURE 7.4 BODÉ PLOT OF ROTOR SYNCHRONOUS VIBRATION MEASURED AT CHANNEL #4. 0.0 PSI OIL PRESSURE AT SEAL SIMULATION BEARINGS. 0.0 INCH PRELOAD.

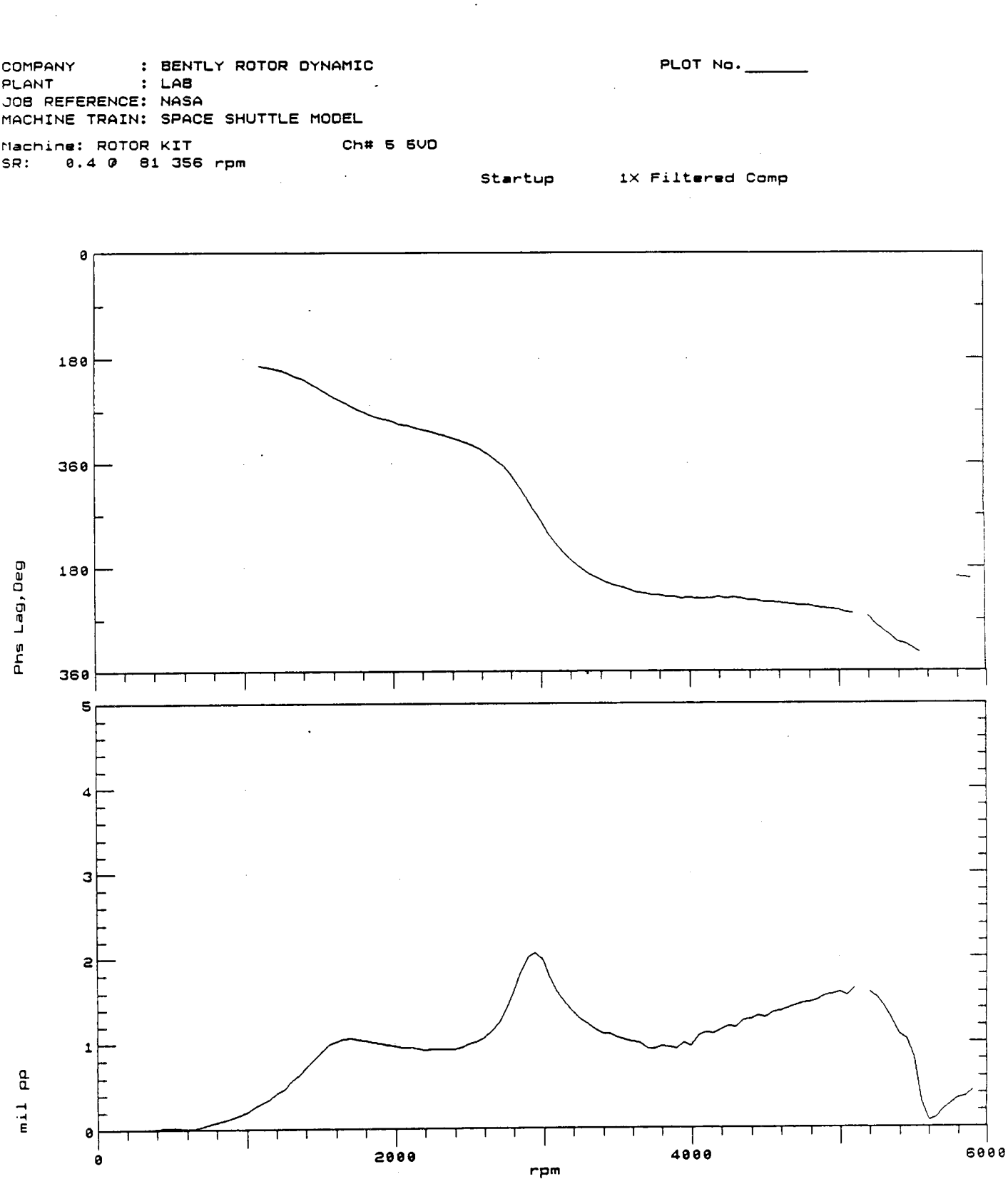

FIGURE 7.5 BODÉ PLOT OF ROTOR SYNCHRONOUS VIBRATION MEASURED AT CHANNEL #5. 0.0 PSI OIL PRESSURE AT SEAL SIMULATION BEARINGS. 0.0 INCH PRELOAD.

COMPANY : BENTLY ROTOR DYNAMIC PLOT No._____
PLANT : LAB
JOB REFERENCE: NASA
MACHINE TRAIN: SPACE SHUTTLE MODEL

Machine: ROTOR KIT Ch# 6 6VD
SR: 0.6 @ 26 356 rpm

Startup 1X Filtered Comp

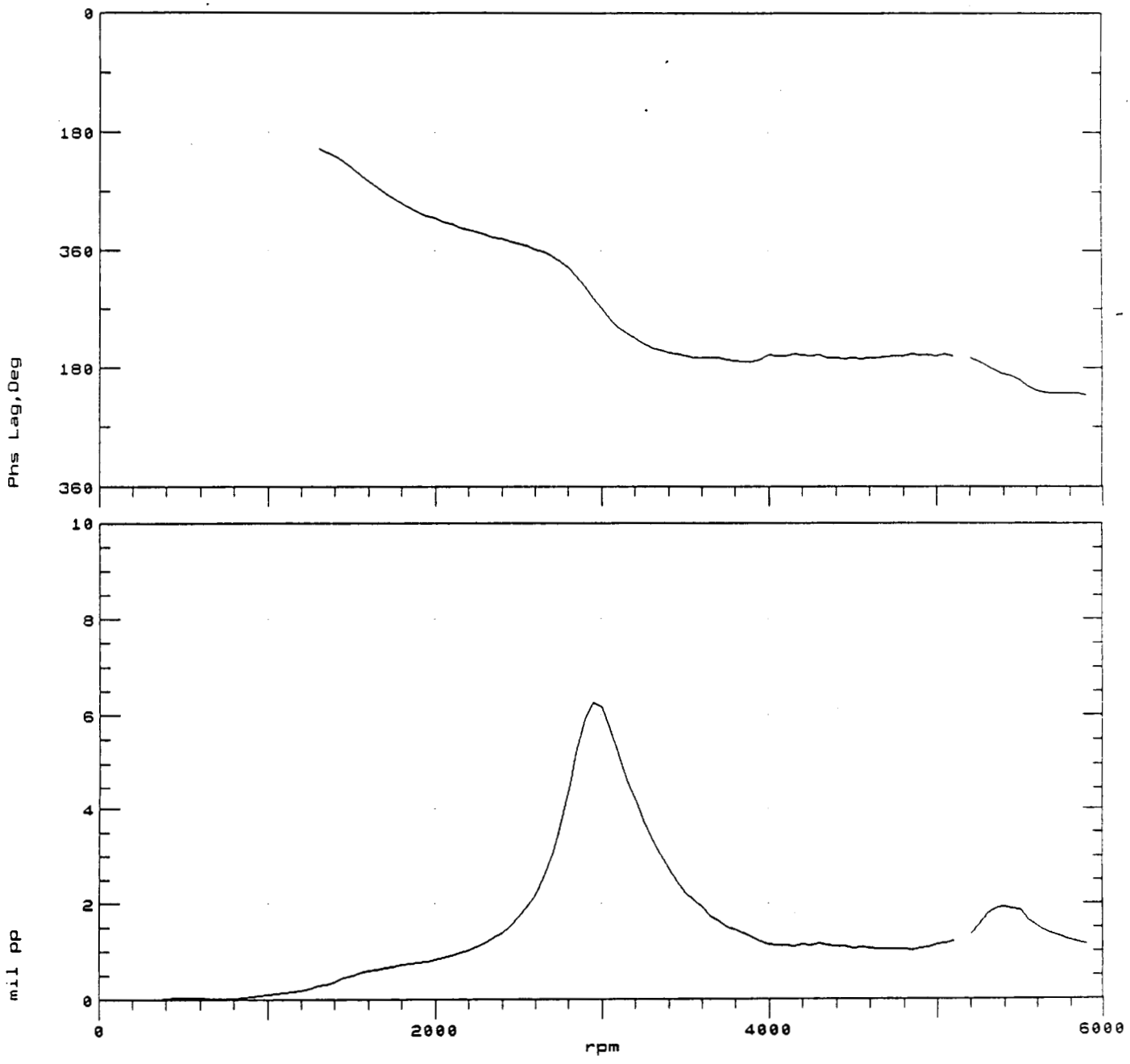

FIGURE 7.6 BODÉ PLOT OF ROTOR SYNCHRONOUS VIBRATION MEASURED AT CHANNEL #6. 0.0 PSI OIL PRESSURE AT SEAL SIMULATION BEARINGS. 0.0 INCH PRELOAD.

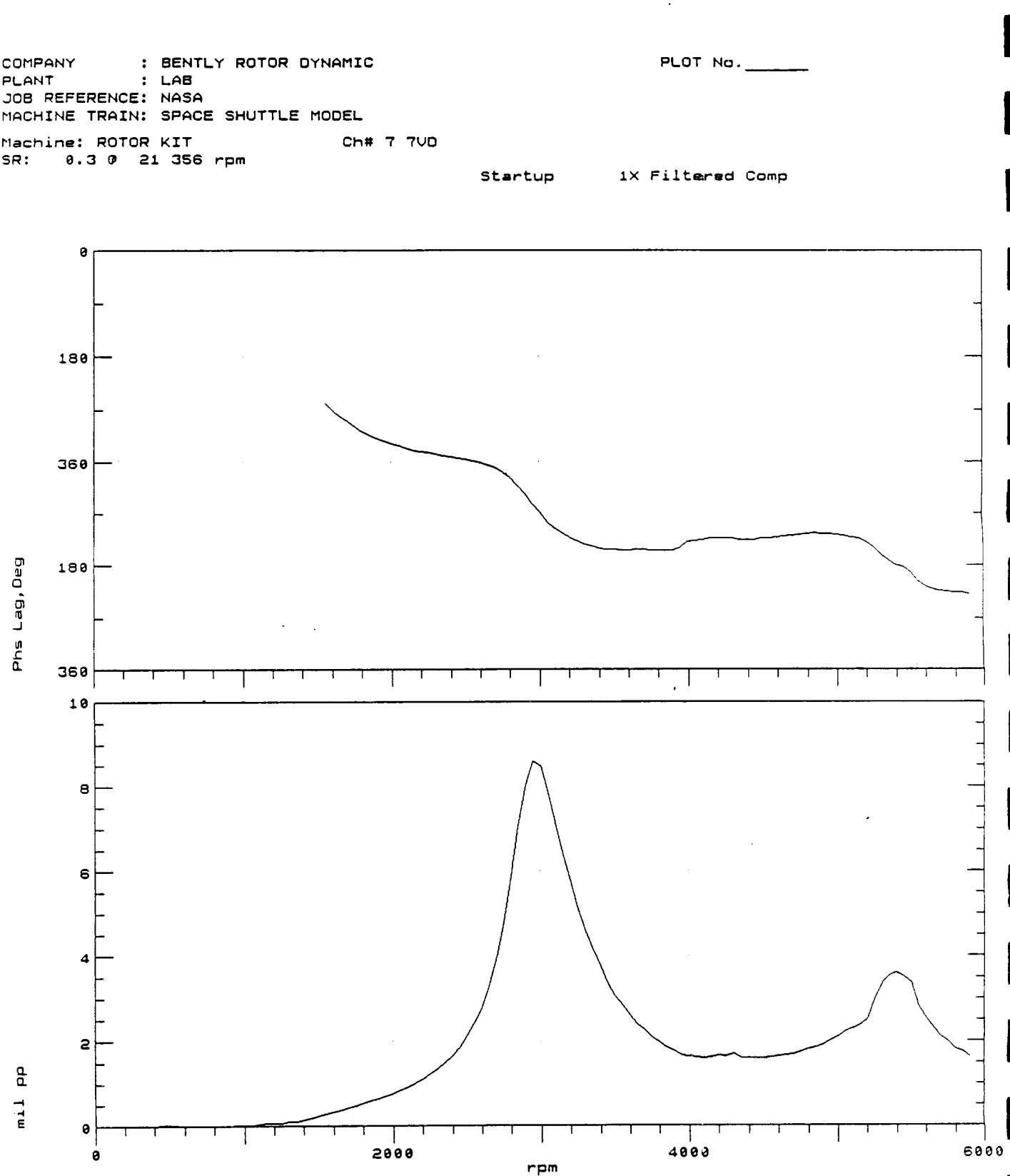

FIGURE 7.7 BODÉ PLOT OF ROTOR SYNCHRONOUS VIBRATION MEASURED AT CHANNEL #7. 0.0 PSI OIL PRESSURE AT SEAL SIMULATION BEARINGS. 0.0 INCH PRELOAD.

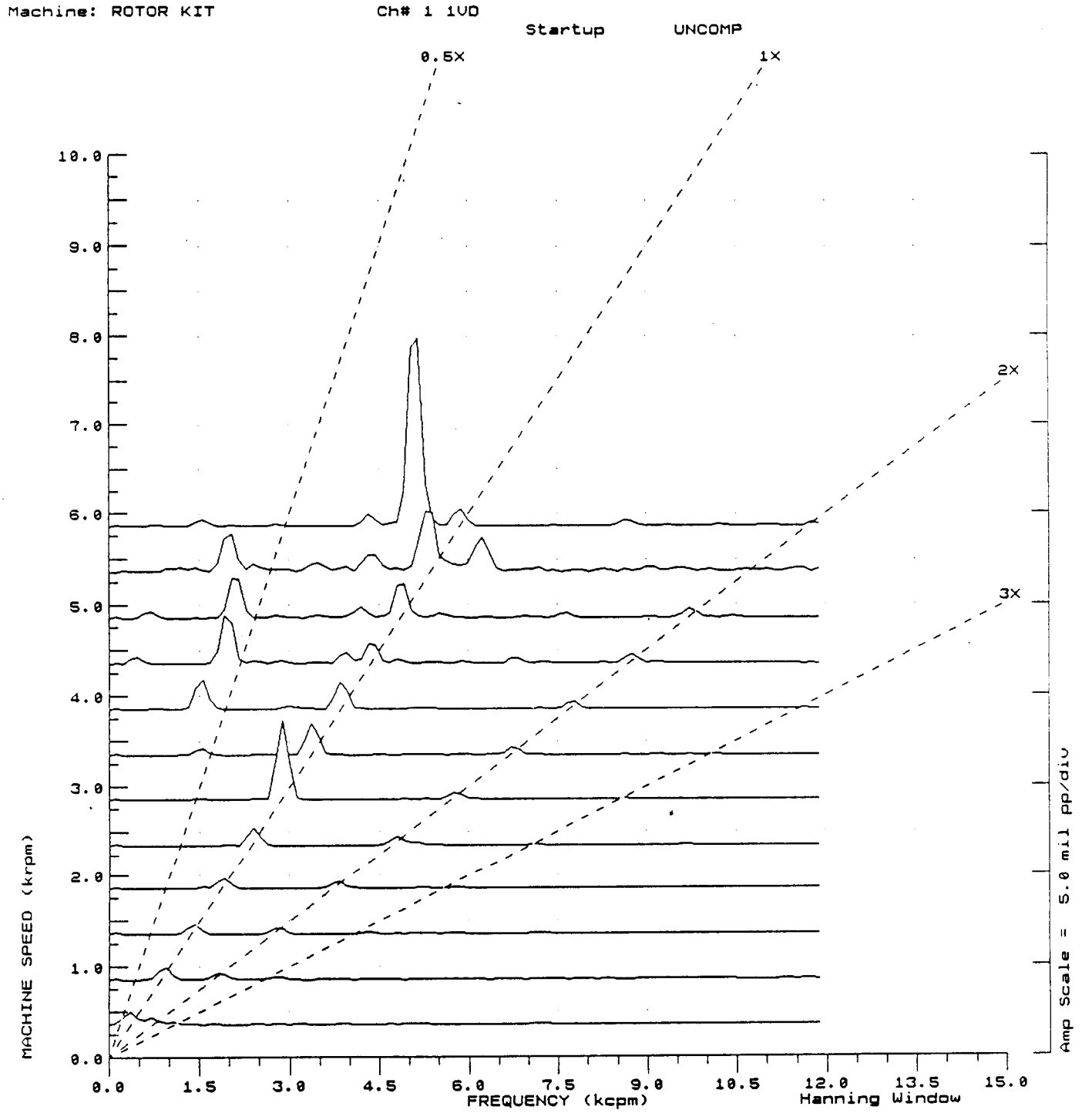

FIGURE 7.8 SPECTRUM CASCADE OF ROTOR VERTICAL VIBRATIONS DURING START–UP MEASURED AT CHANNEL #1. 0.0 PSI OIL PRESSURE AT SEAL SIMULATION BEARINGS. 0.0 INCH PRELOAD.

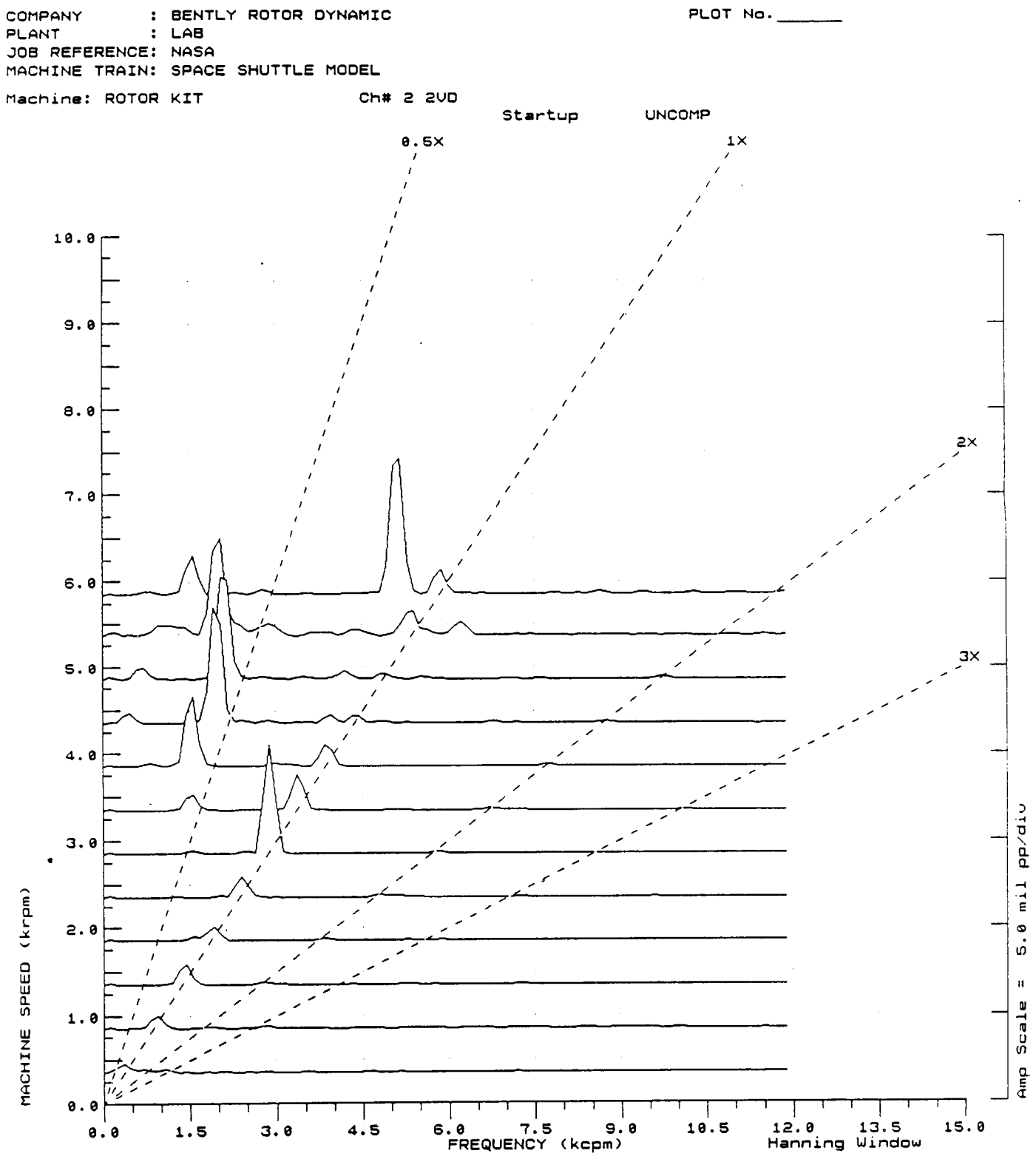

FIGURE 7.9 SPECTRUM CASCADE OF ROTOR VERTICAL VIBRATIONS DURING START-UP MEASURED AT CHANNEL #2. 0.0 PSI OIL PRESSURE AT SEAL SIMULATION BEARINGS. 0.0 INCH PRELOAD.

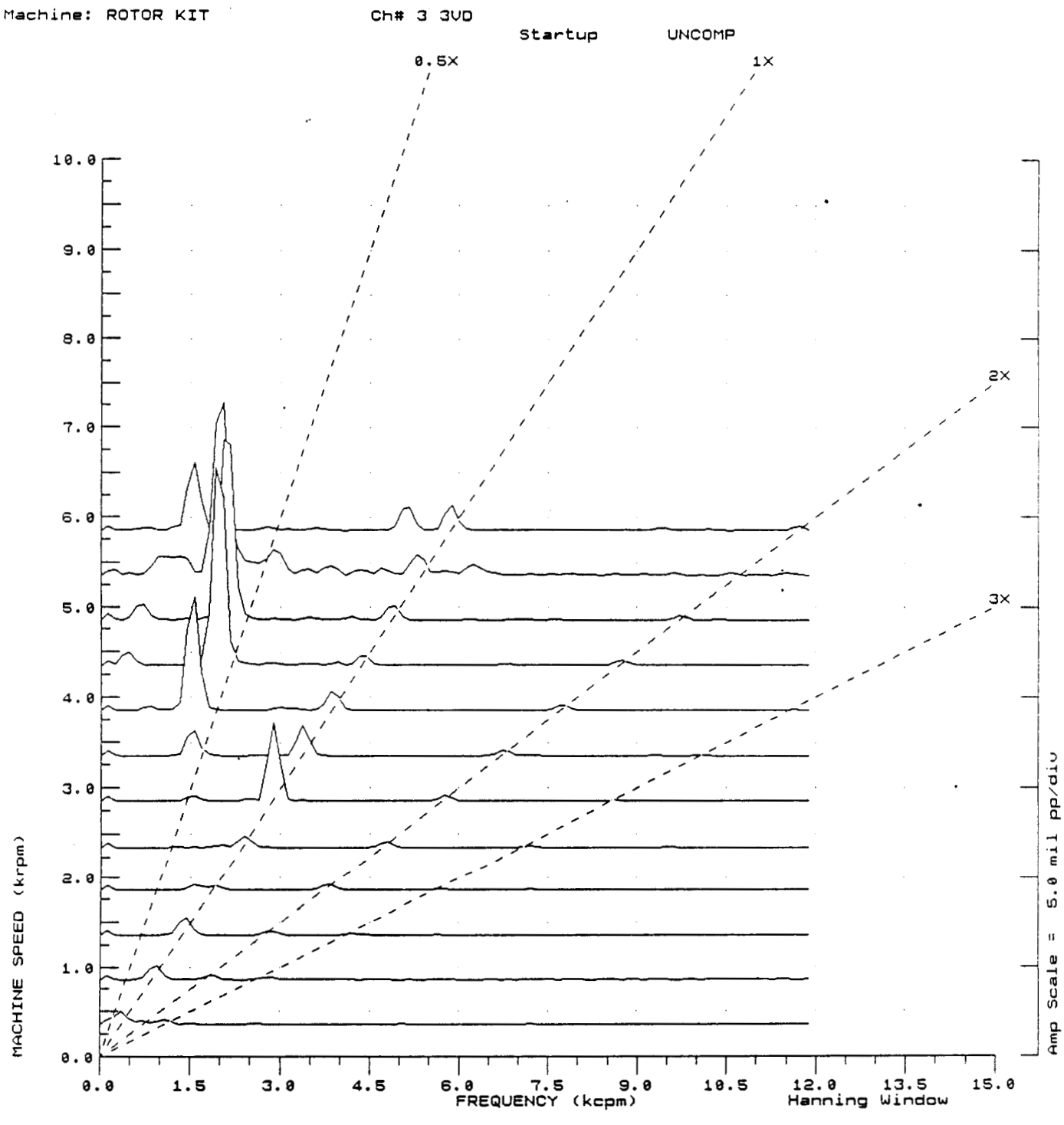

FIGURE 7.10 SPECTRUM CASCADE OF ROTOR VERTICAL VIBRATIONS DURING START–UP MEASURED AT CHANNEL #3. 0.0 PSI OIL PRESSURE AT SEAL SIMULATION BEARINGS. 0.0 INCH PRELOAD.

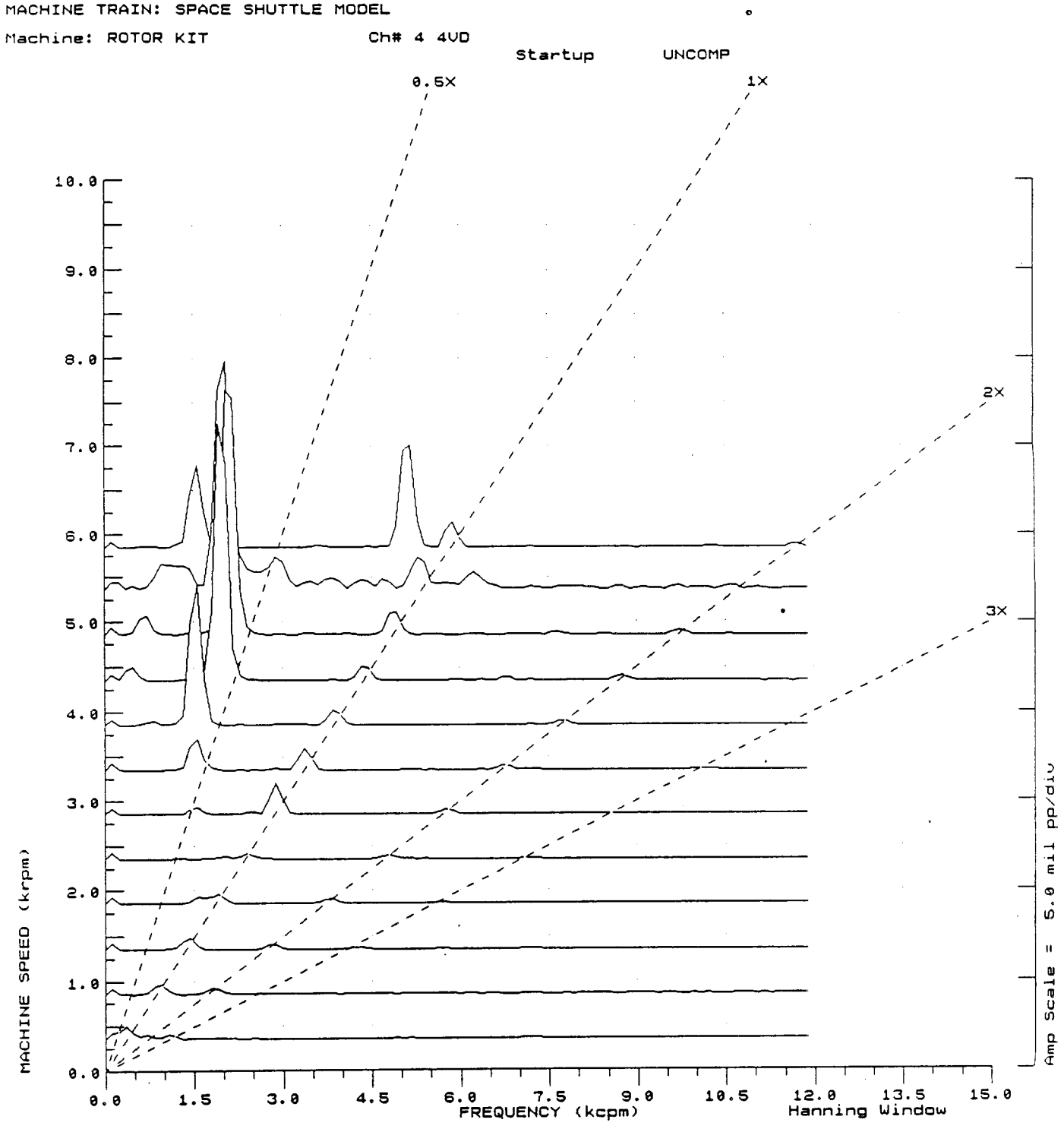

FIGURE 7.11 SPECTRUM CASCADE OF ROTOR VERTICAL VIBRATIONS DURING START–UP MEASURED AT CHANNEL #4. 0.0 PSI OIL PRESSURE AT SEAL SIMULATION BEARINGS. 0.0 INCH PRELOAD.

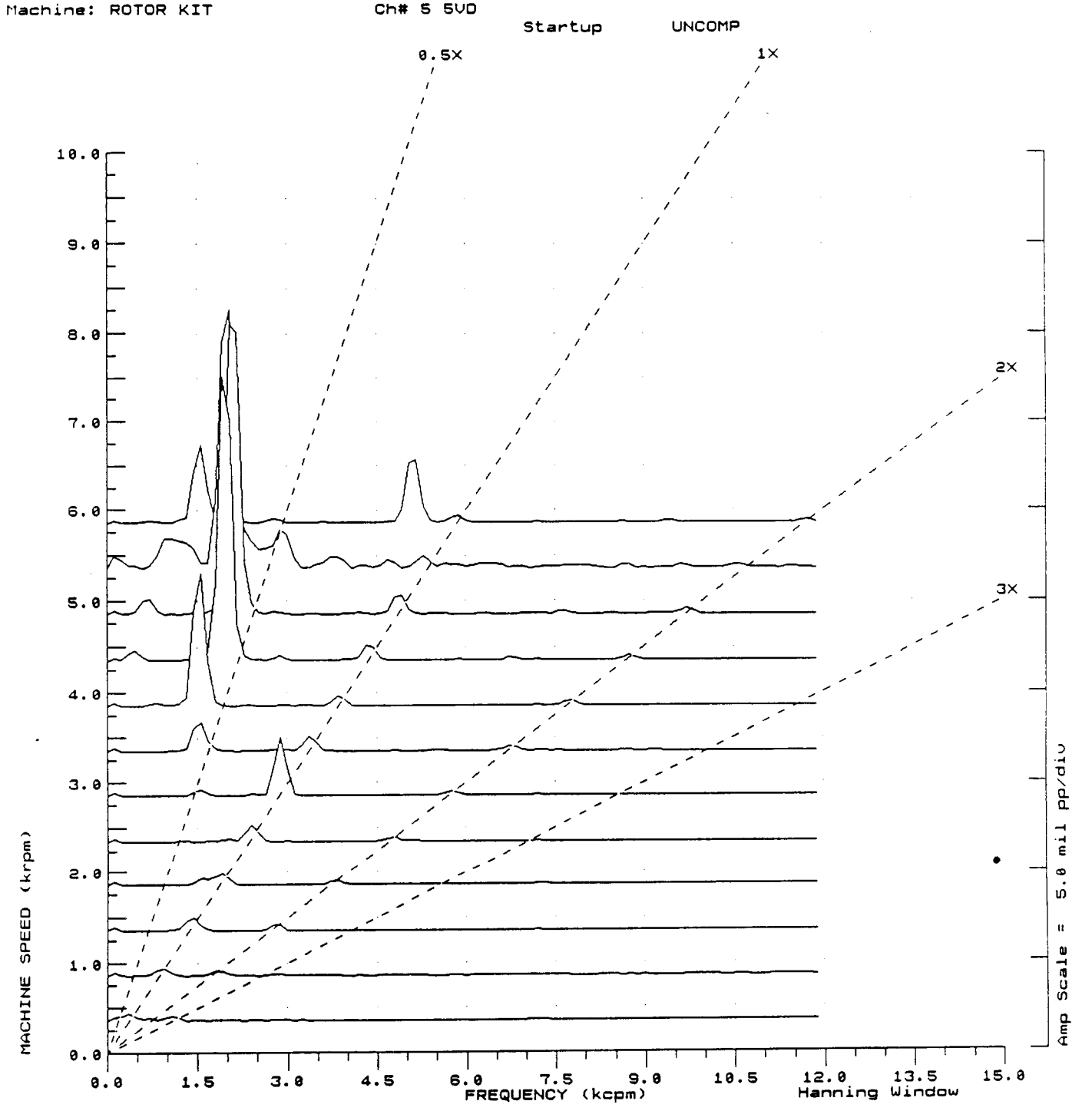

FIGURE 7.12 SPECTRUM CASCADE OF ROTOR VERTICAL VIBRATIONS DURING START–UP MEASURED AT CHANNEL #5. 0.0 PSI OIL PRESSURE AT SEAL SIMULATION BEARINGS. 0.0 INCH PRELOAD.

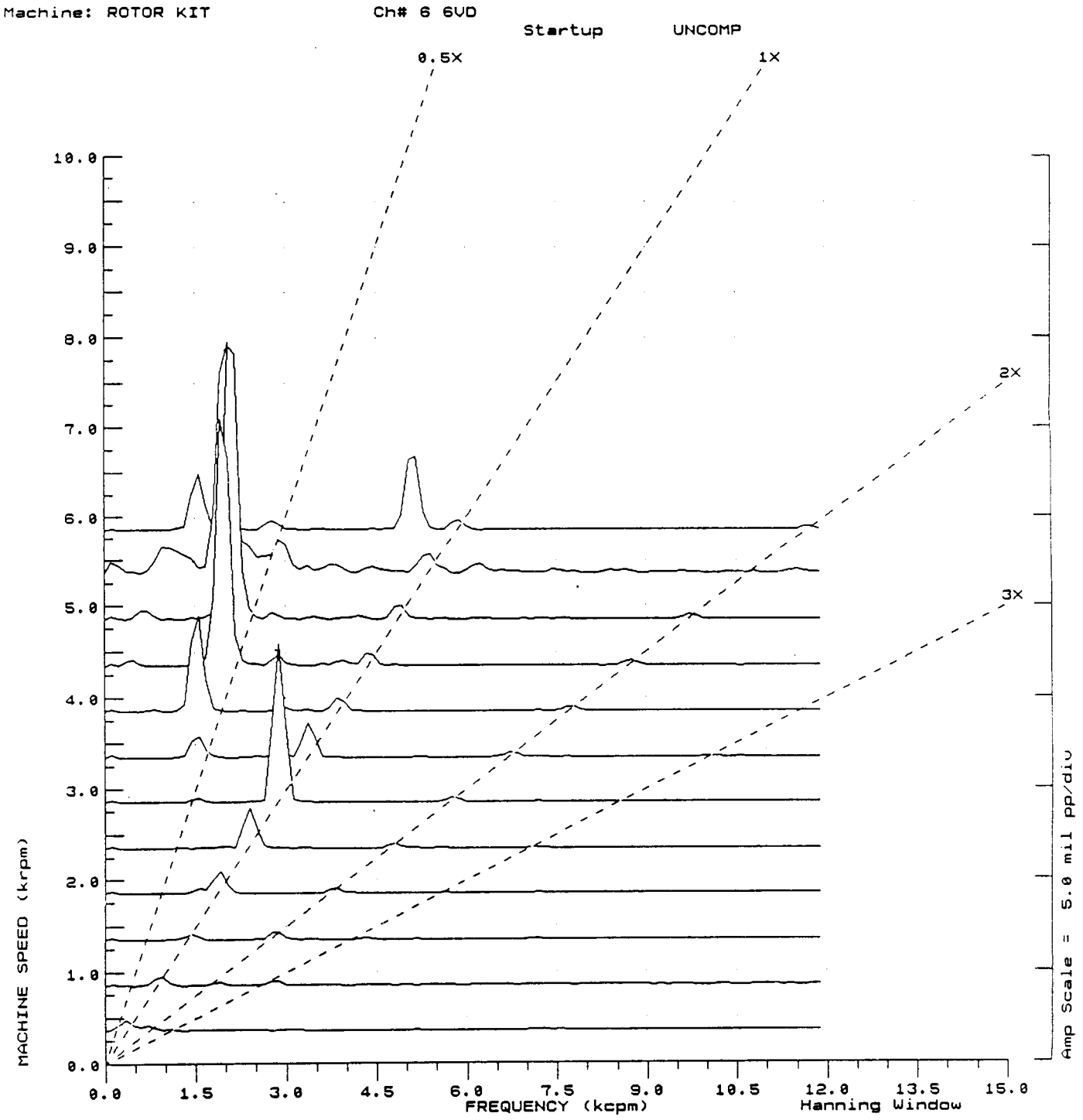

FIGURE 7.13 SPECTRUM CASCADE OF ROTOR VERTICAL VIBRATIONS DURING START–UP MEASURED AT CHANNEL #6. 0.0 PSI OIL PRESSURE AT SEAL SIMULATION BEARINGS. 0.0 INCH PRELOAD.

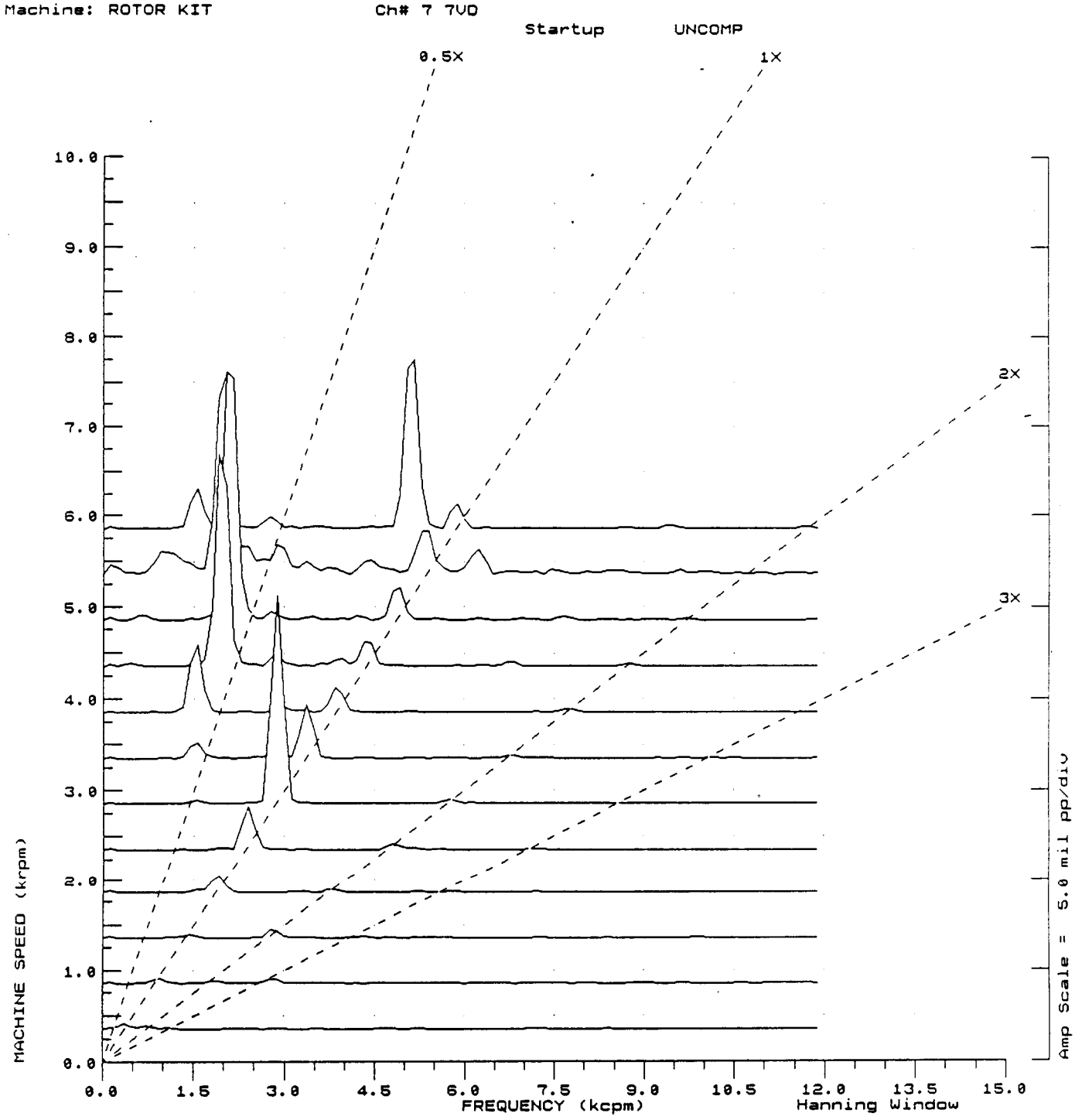

FIGURE 7.14 SPECTRUM CASCADE OF ROTOR VERTICAL VIBRATIONS DURING START-UP MEASURED AT CHANNEL #7. 0.0 PSI OIL PRESSURE AT SEAL SIMULATION BEARINGS. 0.0 INCH PRELOAD.

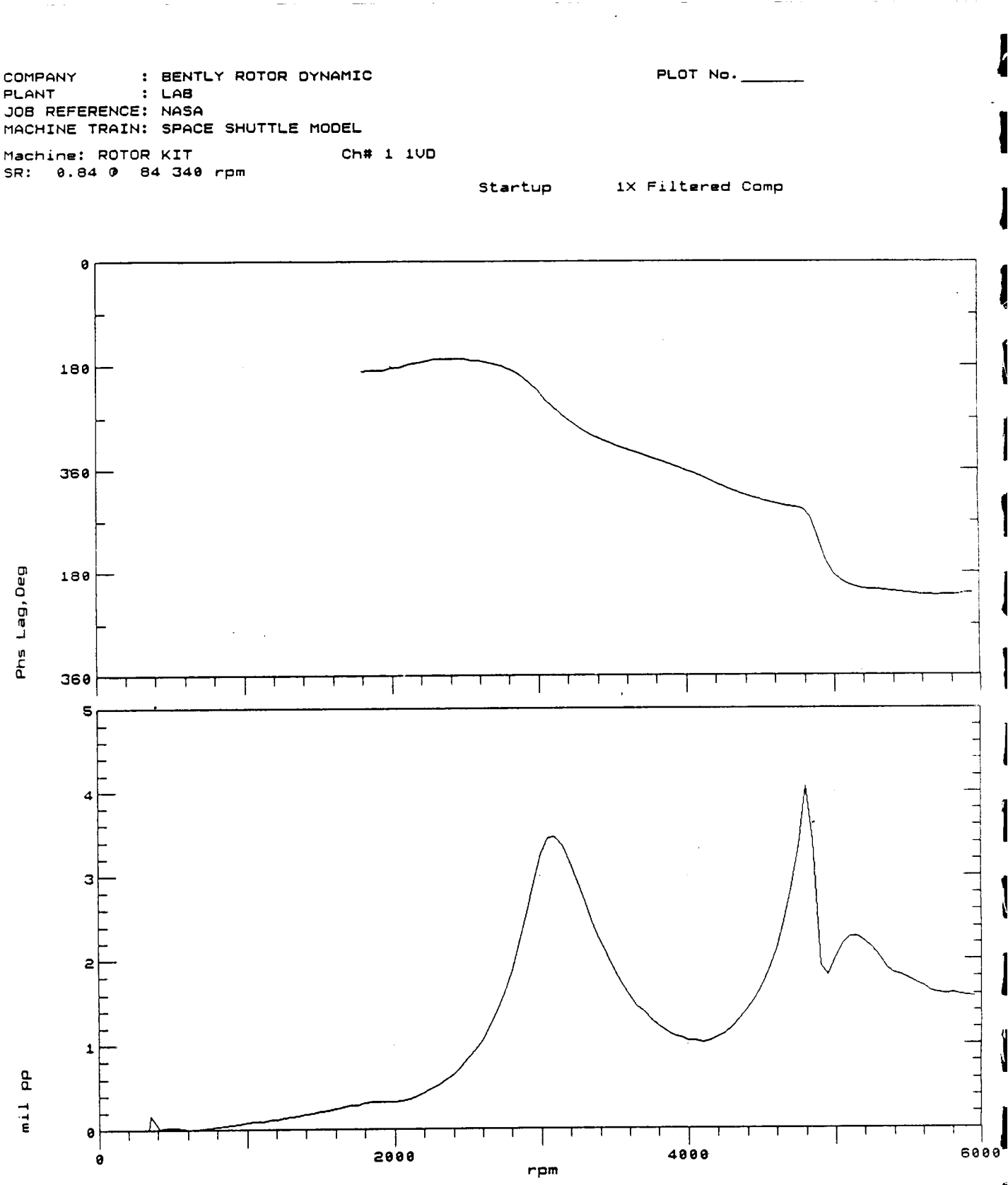

FIGURE 7.15 BODÉ PLOT OF ROTOR SYNCHRONOUS VIBRATION MEASURED AT CHANNEL #1. 5 PSI OIL PRESSURE. 0.0 INCH PRELOAD.

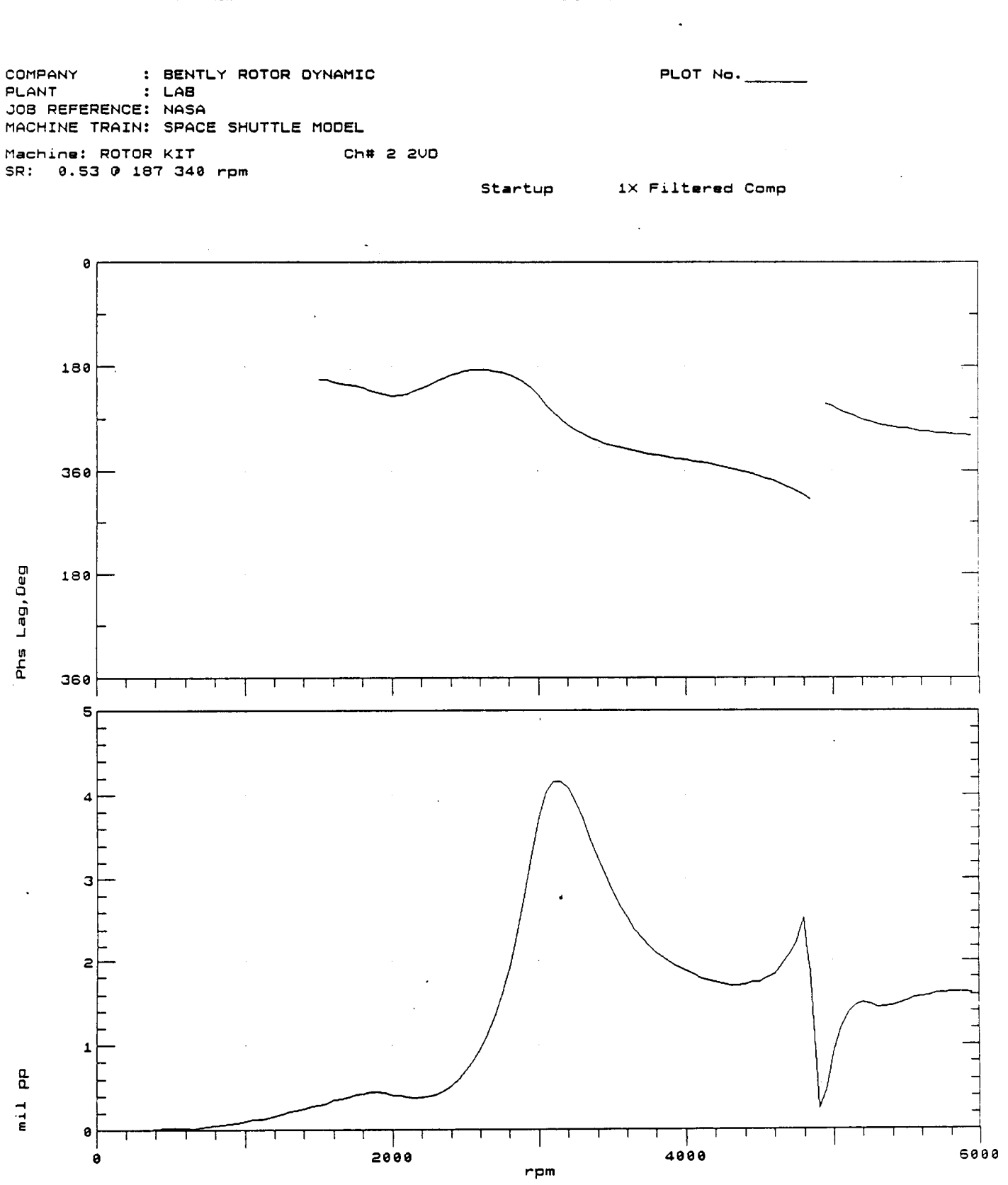

FIGURE 7.16 BODÉ PLOT OF ROTOR SYNCHRONOUS VIBRATION MEASURED AT CHANNEL #2. 5 PSI OIL PRESSURE AT SEAL SIMULATION BEARINGS. 0.0 INCH PRELOAD.

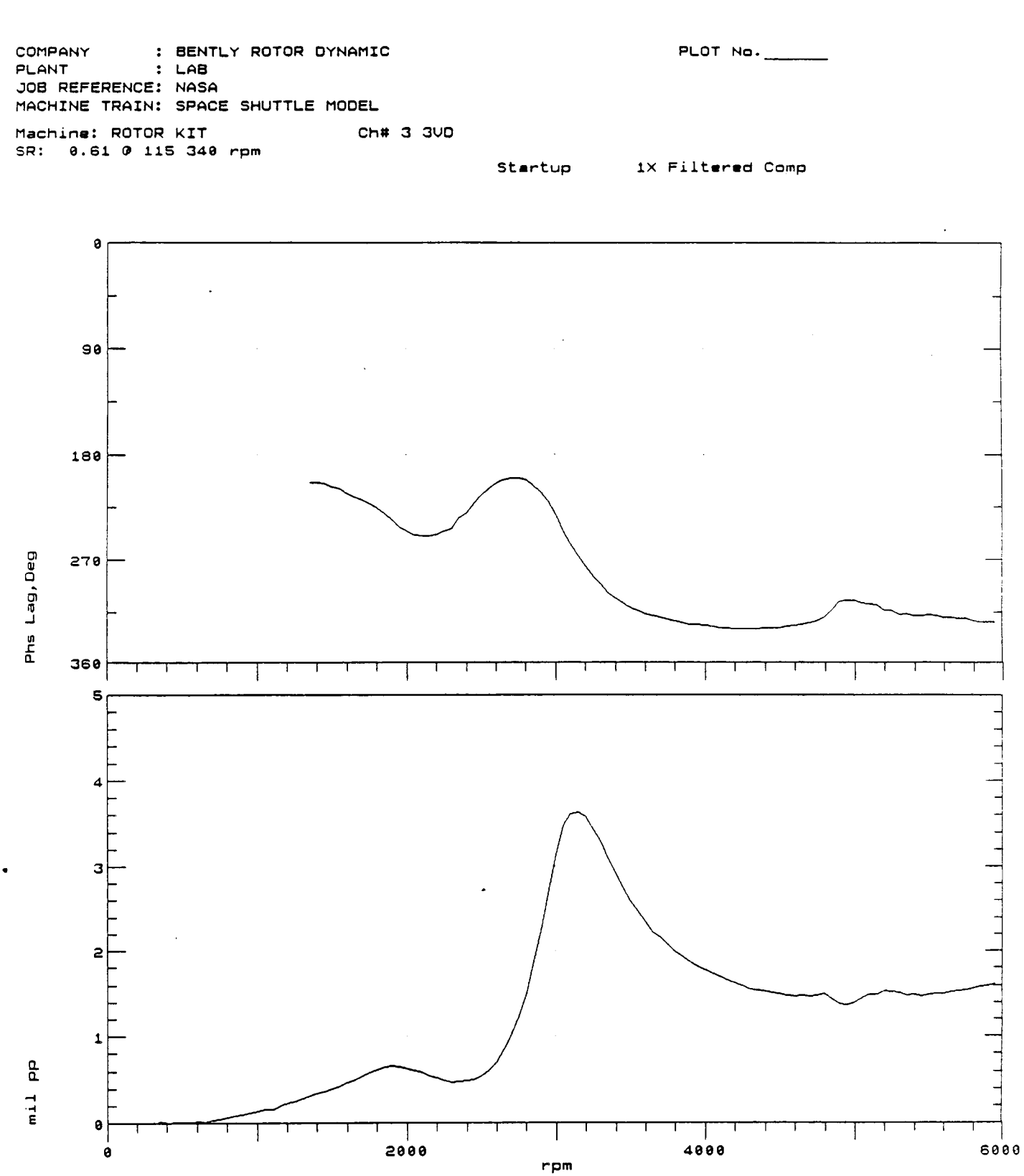

FIGURE 7.17 BODÉ PLOT OF ROTOR SYNCHRONOUS VIBRATION MEASURED AT CHANNEL #3. 5 PSI OIL PRESSURE AT SEAL SIMULATION BEARINGS. 0.0 INCH PRELOAD.

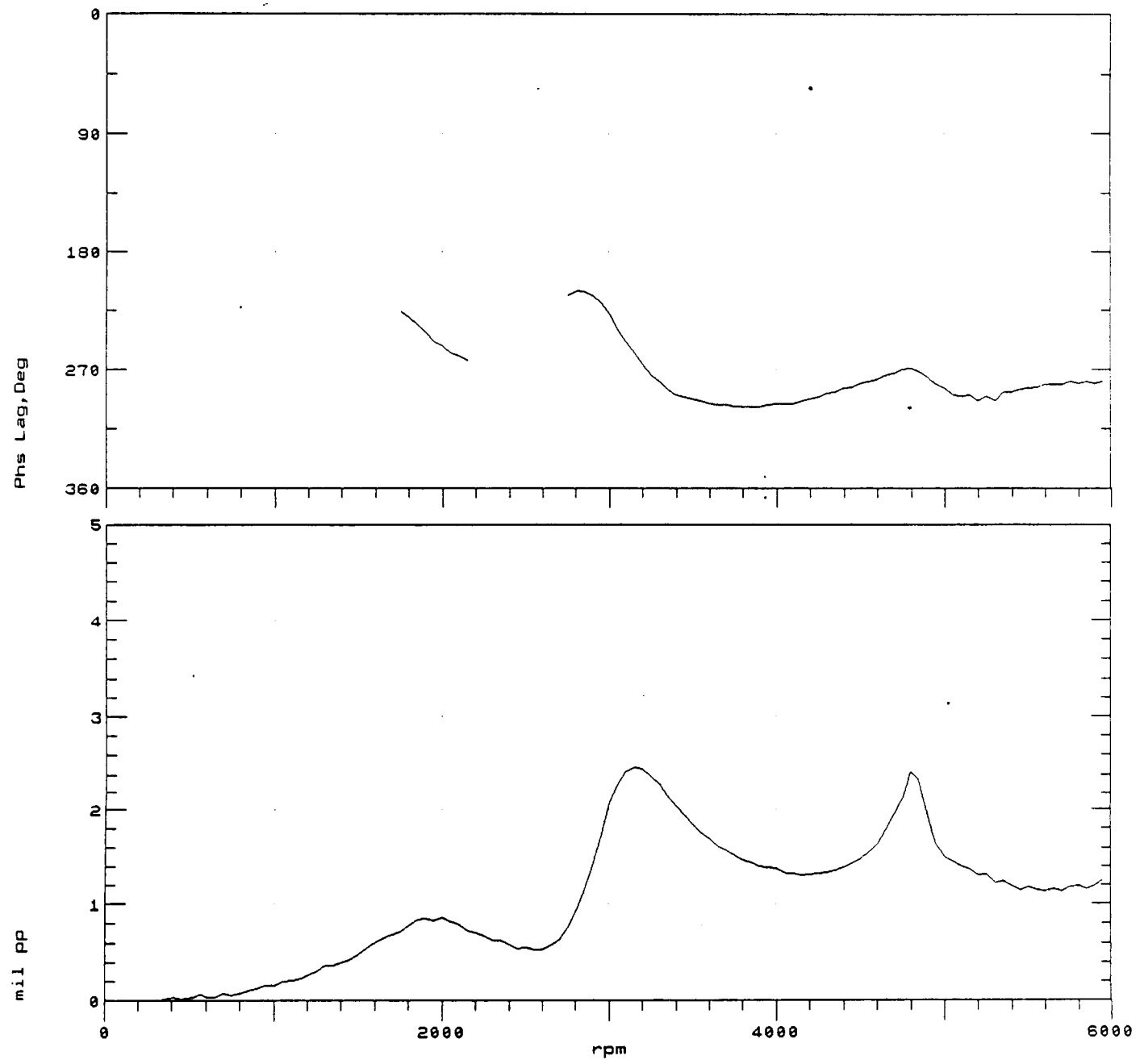

FIGURE 7.18 BODÉ PLOT OF ROTOR SYNCHRONOUS VIBRATION MEASURED AT CHANNEL #4. 5 PSI OIL PRESSURE AT SEAL SIMULATION BEARINGS. 0.0 INCH PRELOAD.

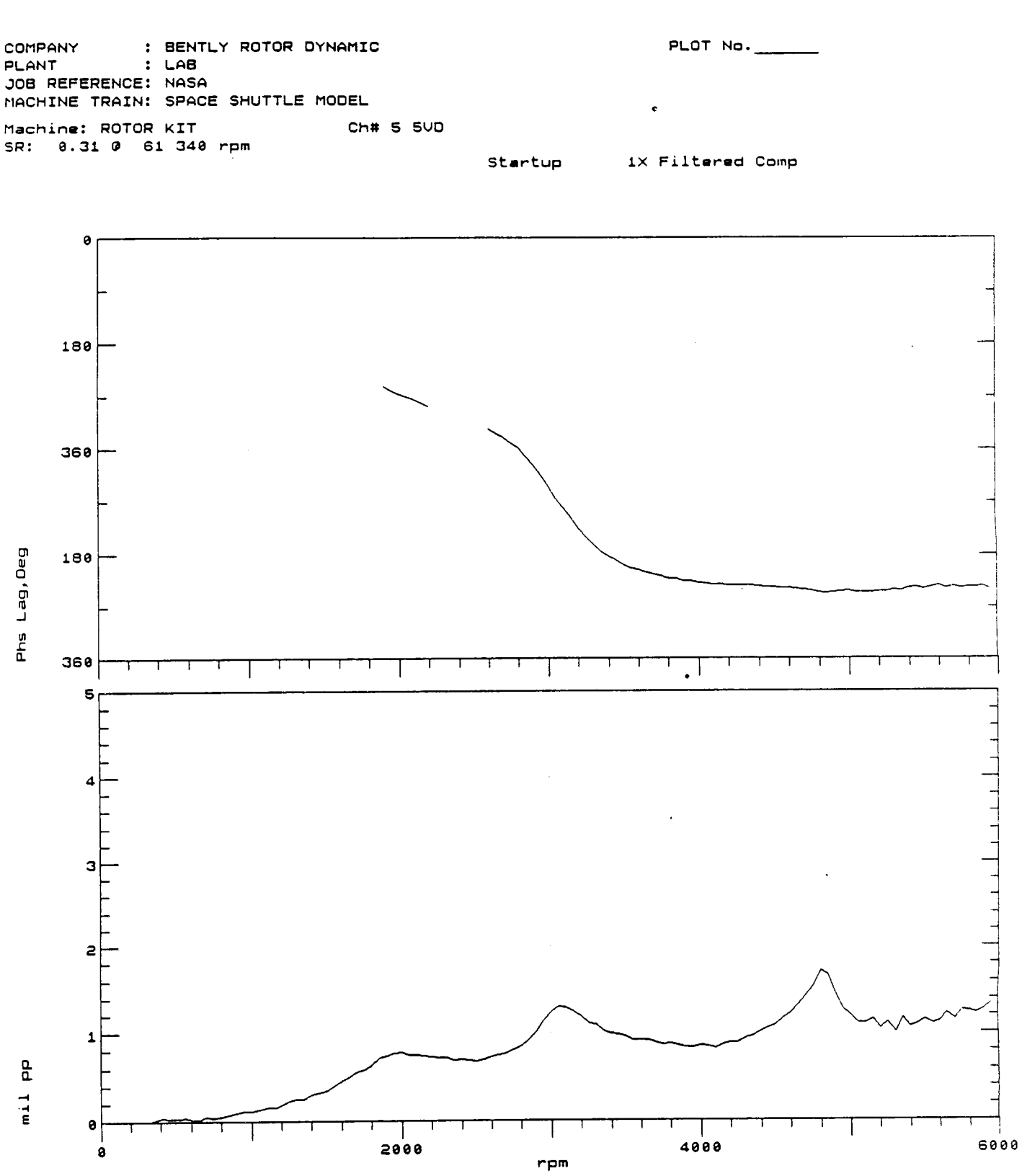

FIGURE 7.19 BODÉ PLOT OF ROTOR SYNCHRONOUS VIBRATION MEASURED AT CHANNEL #5. 5 PSI OIL PRESSURE AT SEAL SIMULATION BEARINGS. 0.0 INCH PRELOAD.

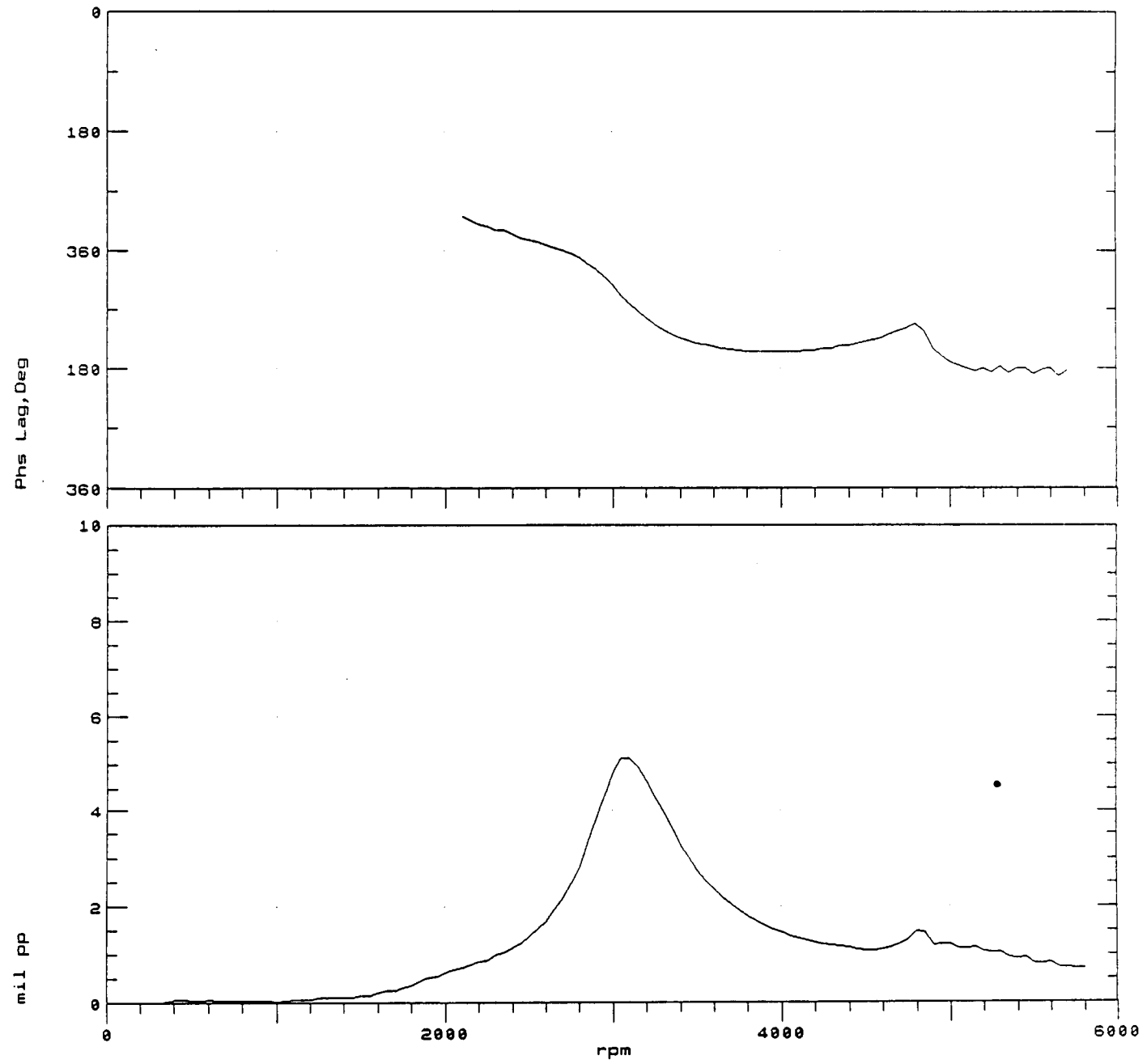

FIGURE 7.20 BODÉ PLOT OF ROTOR SYNCHRONOUS VIBRATION MEASURED AT CHANNEL #6. 5 PSI OIL PRESSURE AT SEAL SIMULATION BEARINGS. 0.0 INCH PRELOAD.

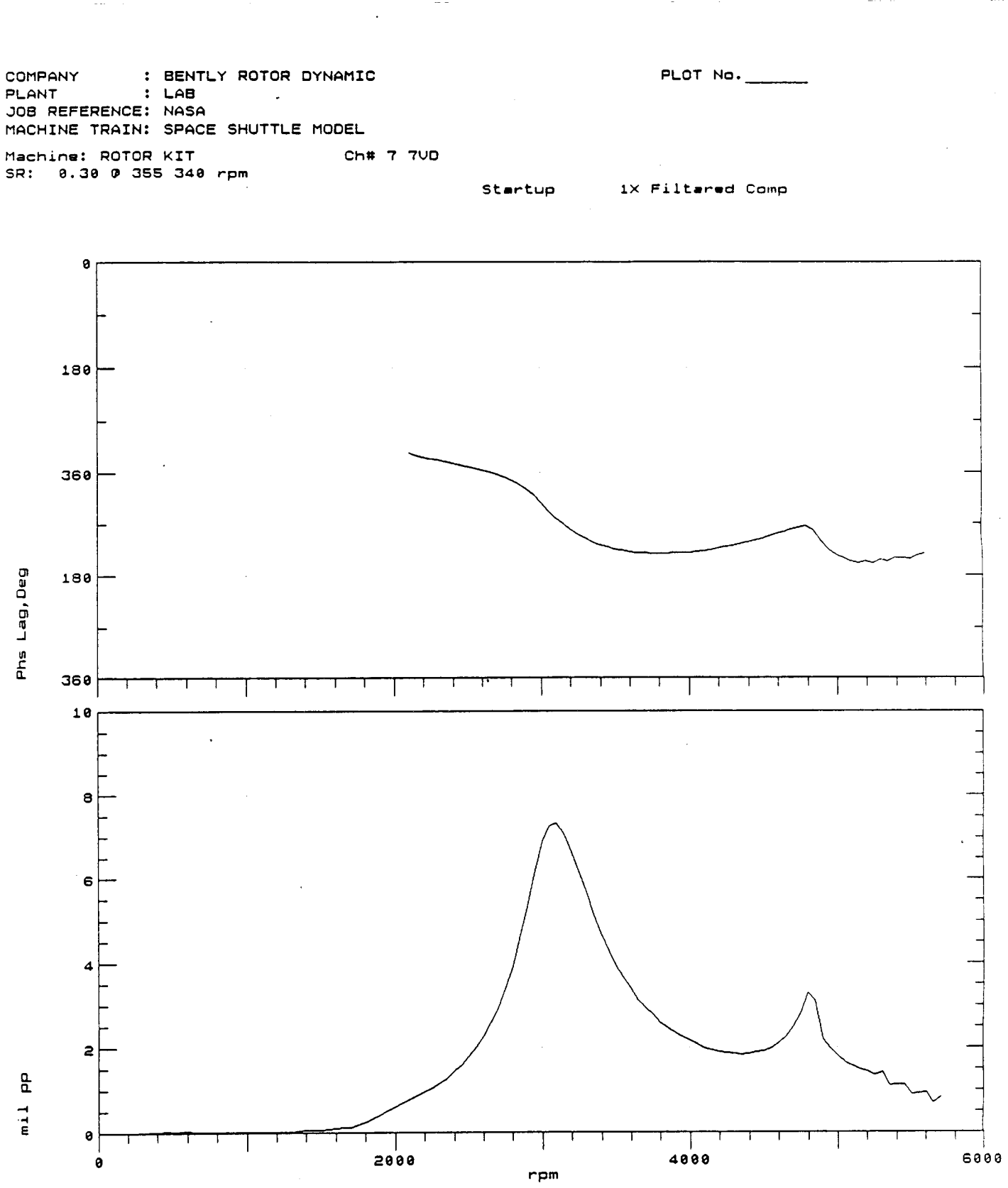

FIGURE 7.21 BODÉ PLOT OF ROTOR SYNCHRONOUS VIBRATION MEASURED AT CHANNEL #7. 5 PSI OIL PRESSURE AT SEAL SIMULATION BEARINGS. 0.0 INCH PRELOAD.

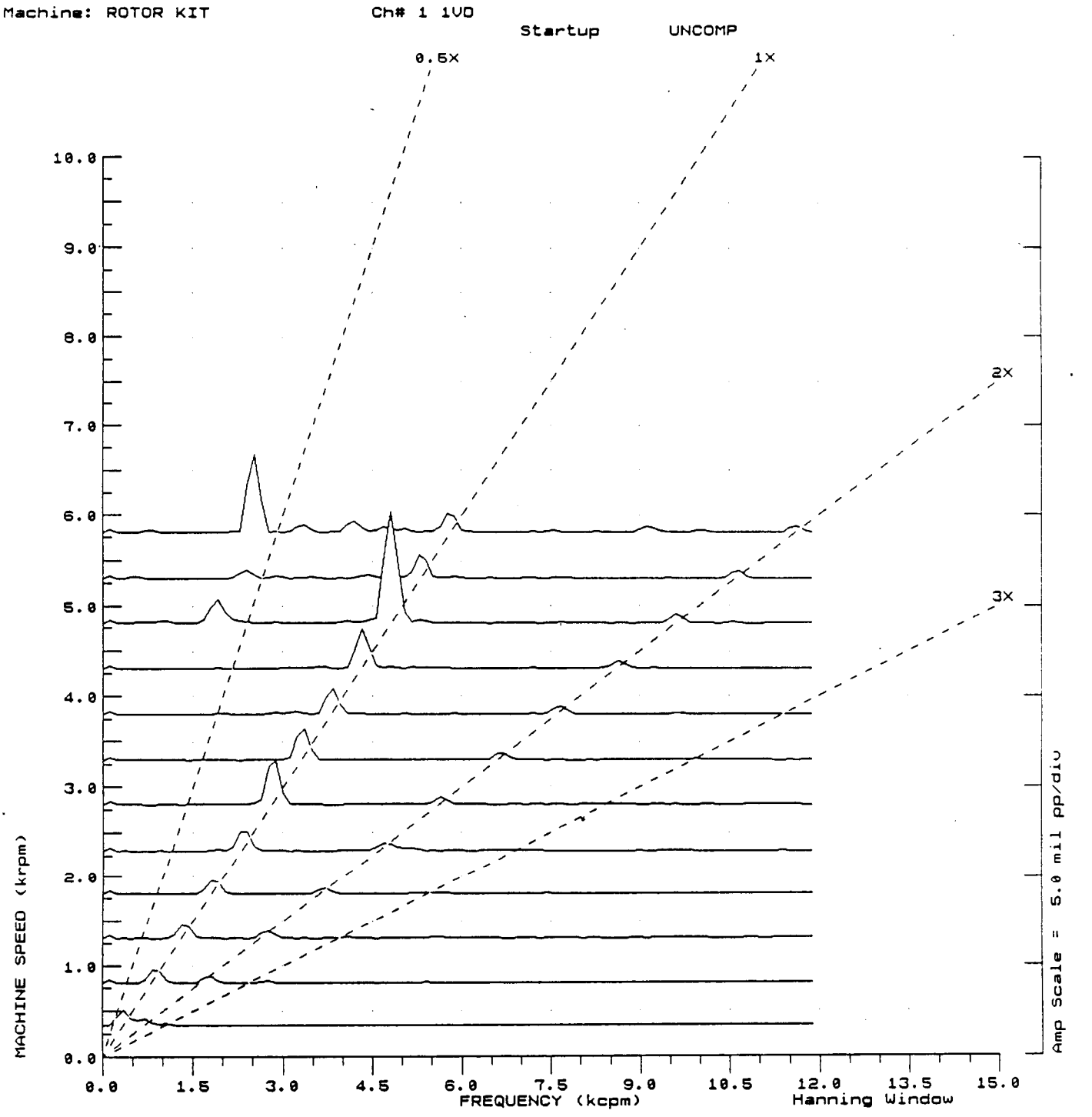

FIGURE 7.22 SPECTRUM CASCADE OF ROTOR VERTICAL VIBRATIONS DURING START–UP MEASURED AT CHANNEL #1. 5 PSI OIL PRESSURE AT SEAL SIMULATION BEARINGS. 0.0 INCH PRELOAD.

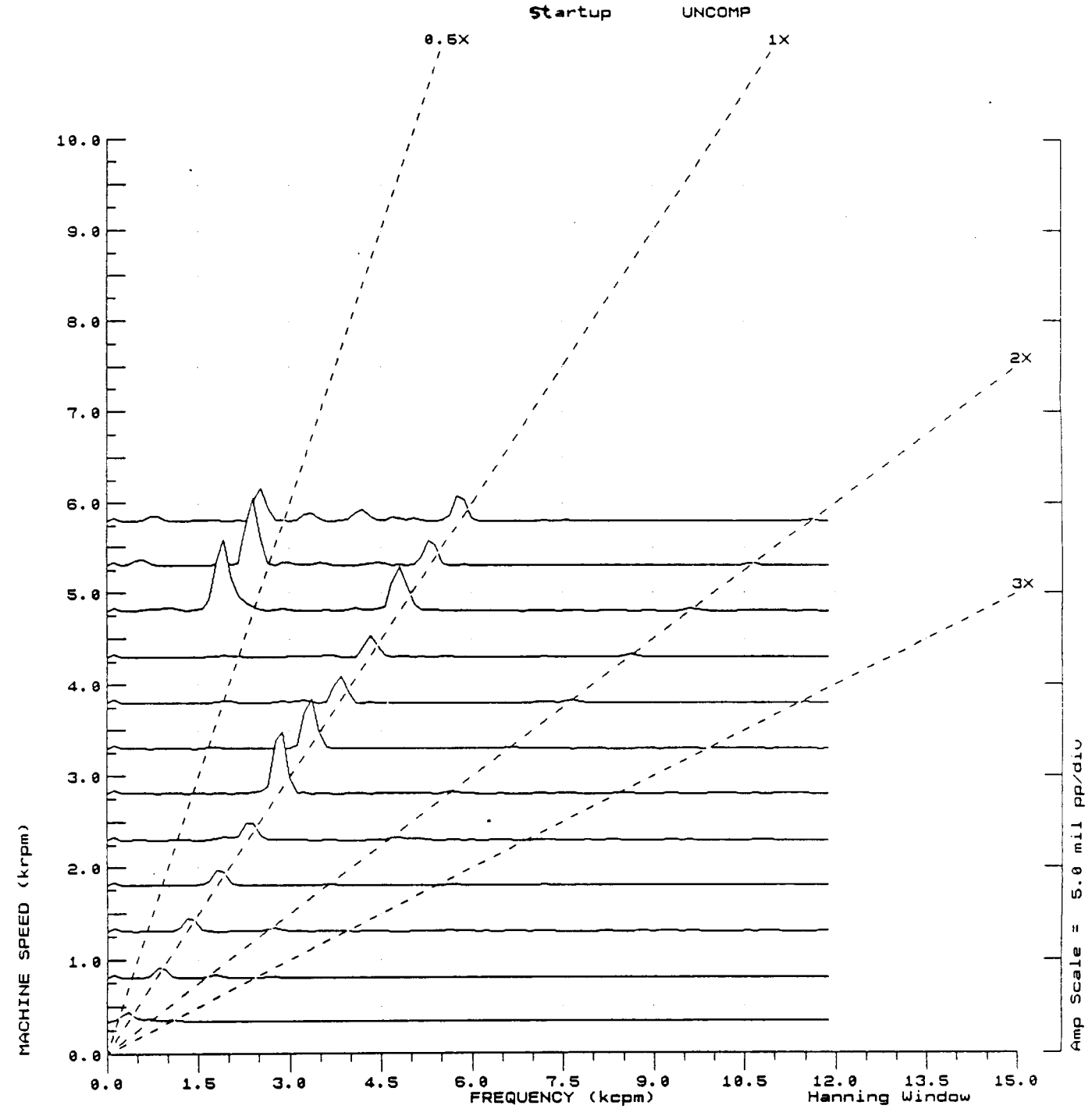

FIGURE 7.23 SPECTRUM CASCADE OF ROTOR VERTICAL VIBRATIONS DURING START–UP MEASURED AT CHANNEL #2. 5 PSI OIL PRESSURE AT SEAL SIMULATION BEARINGS. 0.0 INCH PRELOAD.

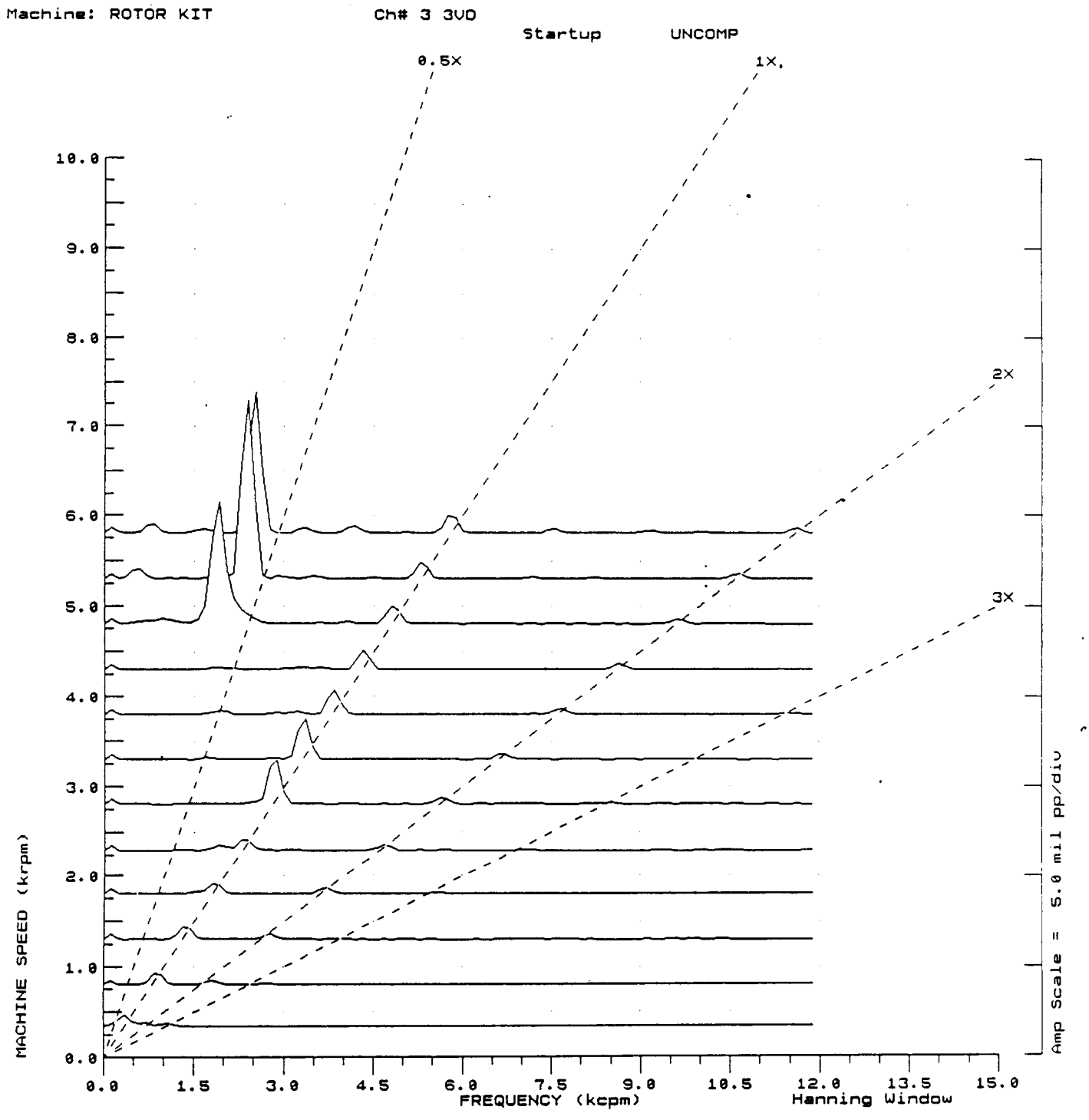

FIGURE 7.24 SPECTRUM CASCADE OF ROTOR VERTICAL VIBRATIONS DURING START–UP MEASURED AT CHANNEL #3. 5 PSI OIL PRESSURE AT SEAL SIMULATION BEARINGS. 0.0 INCH PRELOAD.

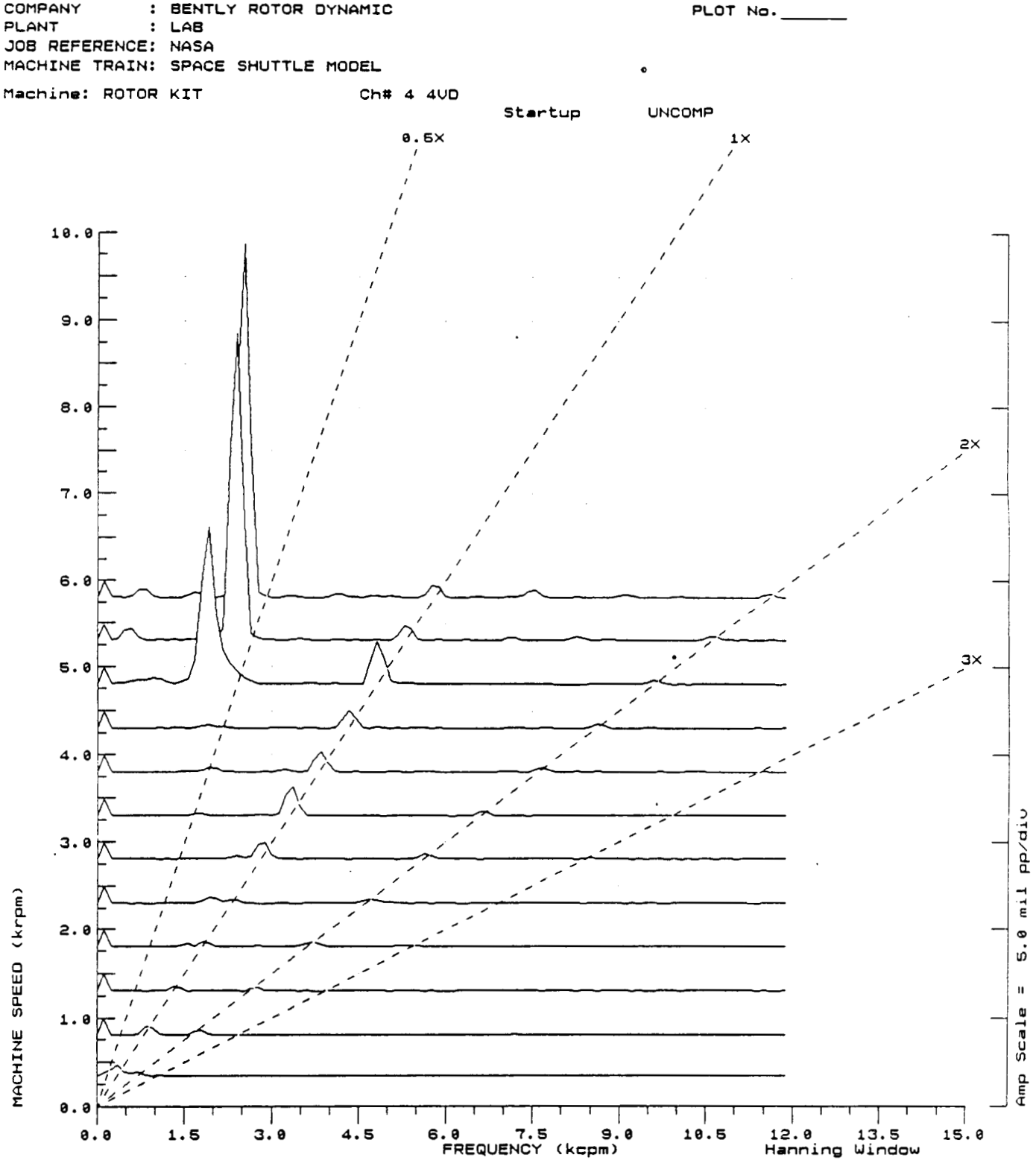

FIGURE 7.25 SPECTRUM CASCADE OF ROTOR VERTICAL VIBRATIONS DURING START–UP MEASURED AT CHANNEL #4. 5 PSI OIL PRESSURE AT SEAL SIMULATION BEARINGS. 0.0 INCH PRELOAD.

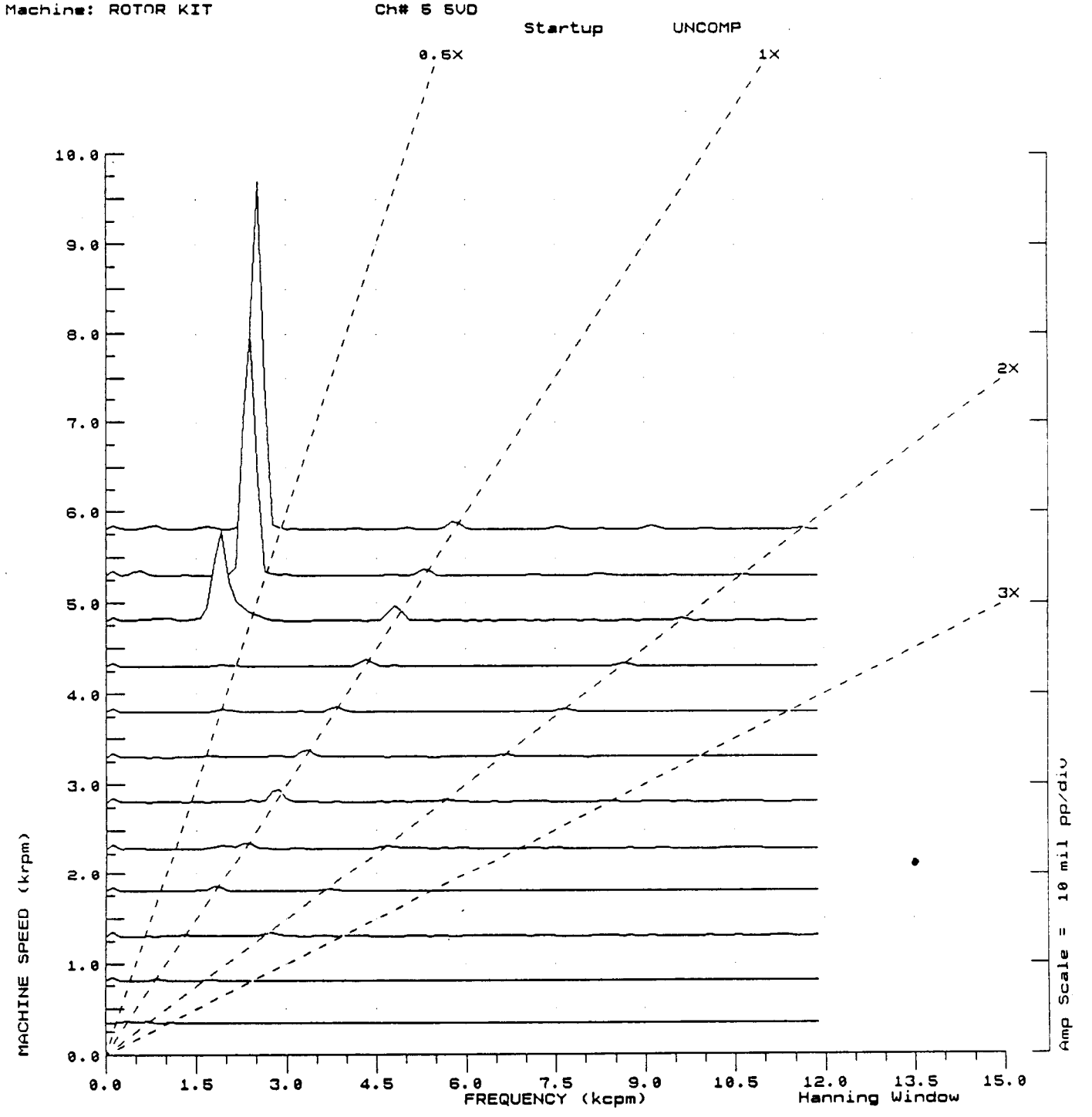

FIGURE 7.26 SPECTRUM CASCADE OF ROTOR VERTICAL VIBRATIONS DURING START-UP MEASURED AT CHANNEL #5. 5 PSI OIL PRESSURE AT SEAL SIMULATION BEARINGS. 0.0 INCH PRELOAD.

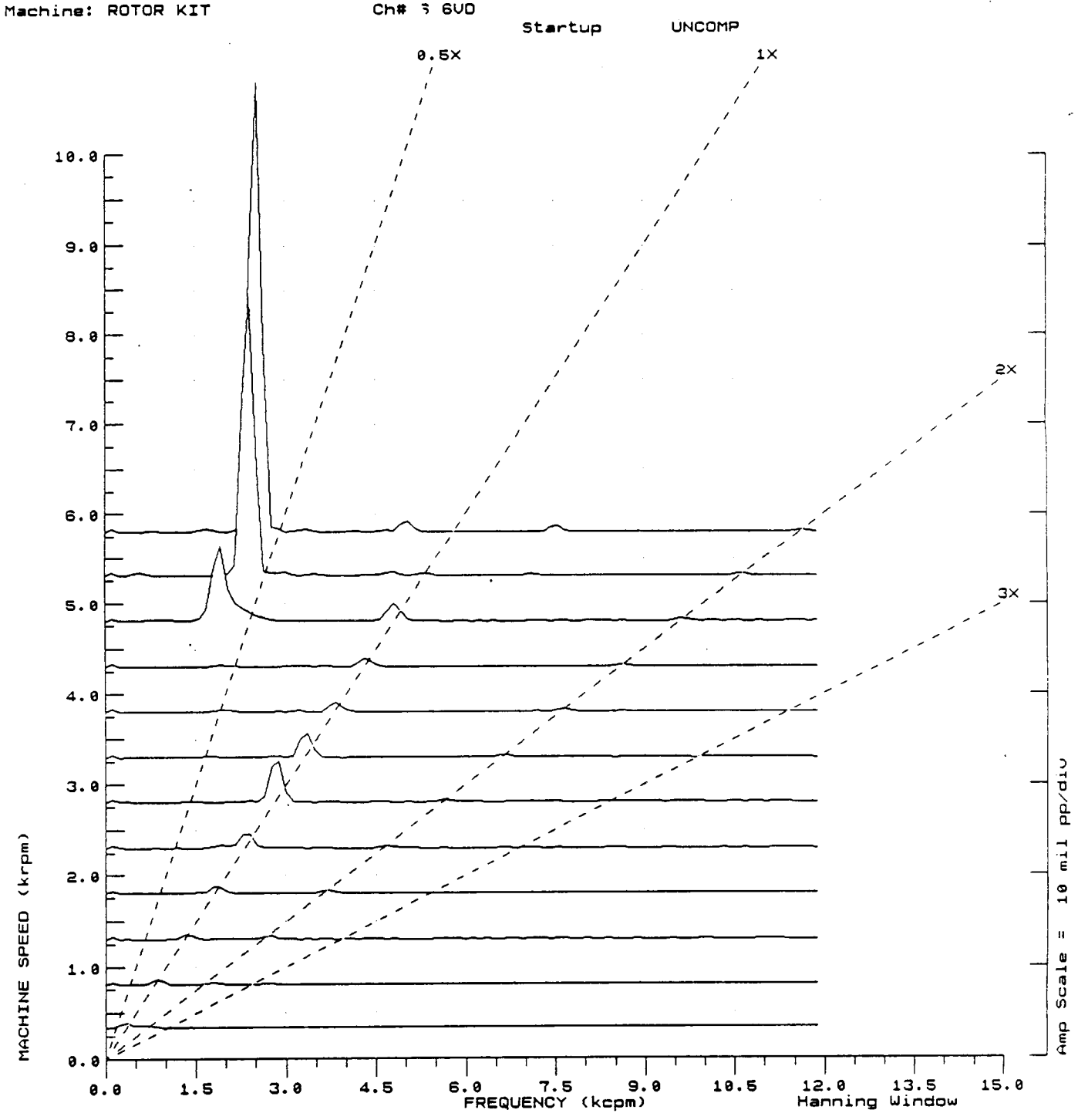

FIGURE 7.27 SPECTRUM CASCADE OF ROTOR VERTICAL VIBRATIONS DURING START-UP MEASURED AT CHANNEL #6. 5 PSI OIL PRESSURE AT SEAL SIMULATION BEARINGS. 0.0 INCH PRELOAD.

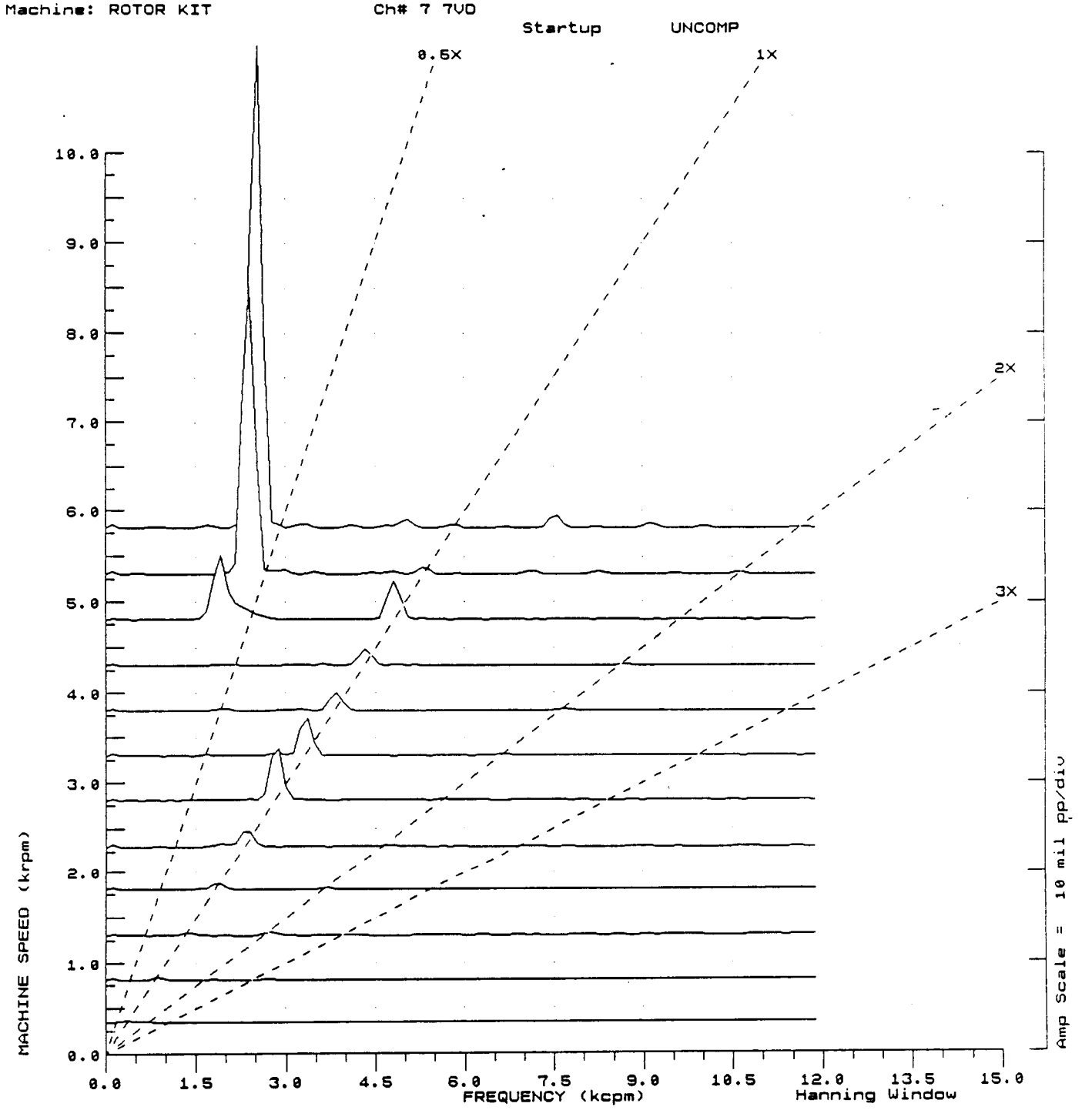

FIGURE 7.28 SPECTRUM CASCADE OF ROTOR VERTICAL VIBRATIONS DURING START–UP MEASURED AT CHANNEL #7. 5 PSI OIL PRESSURE AT SEAL SIMULATION BEARINGS. 0.0 INCH PRELOAD.

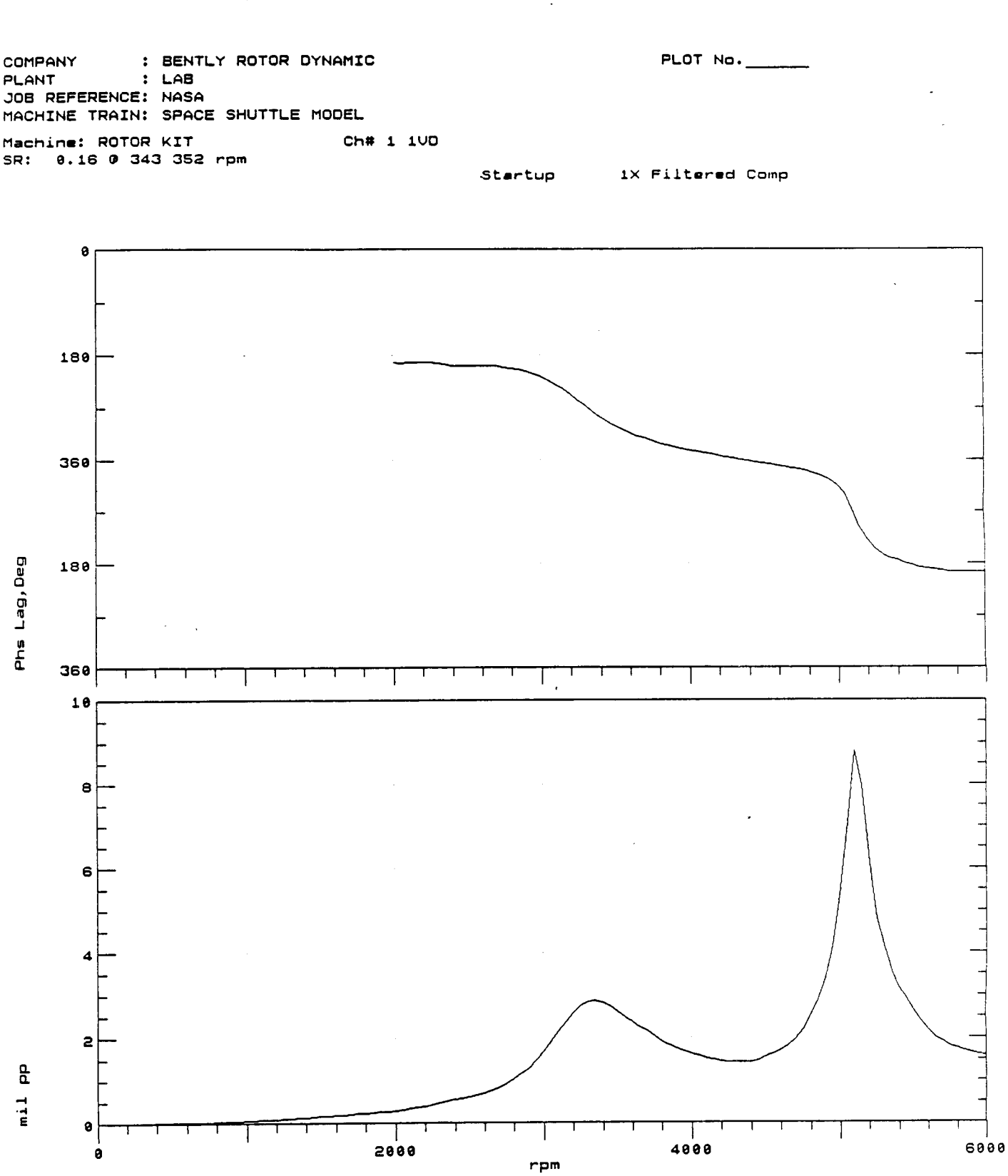

FIGURE 7.29 BODÉ PLOT OF ROTOR SYNCHRONOUS VIBRATION MEASURED AT CHANNEL #1. 10 PSI OIL PRESSURE AT SEAL SIMULATION BEARINGS. 0.0 INCH PRELOAD.

COMPANY : BENTLY ROTOR DYNAMIC PLOT No._____
PLANT : LAB
JOB REFERENCE: NASA
MACHINE TRAIN: SPACE SHUTTLE MODEL

Machine: ROTOR KIT Ch# 2 2VO
SR: 0.74 @ 230 352 rpm

Startup 1X Filtered Comp

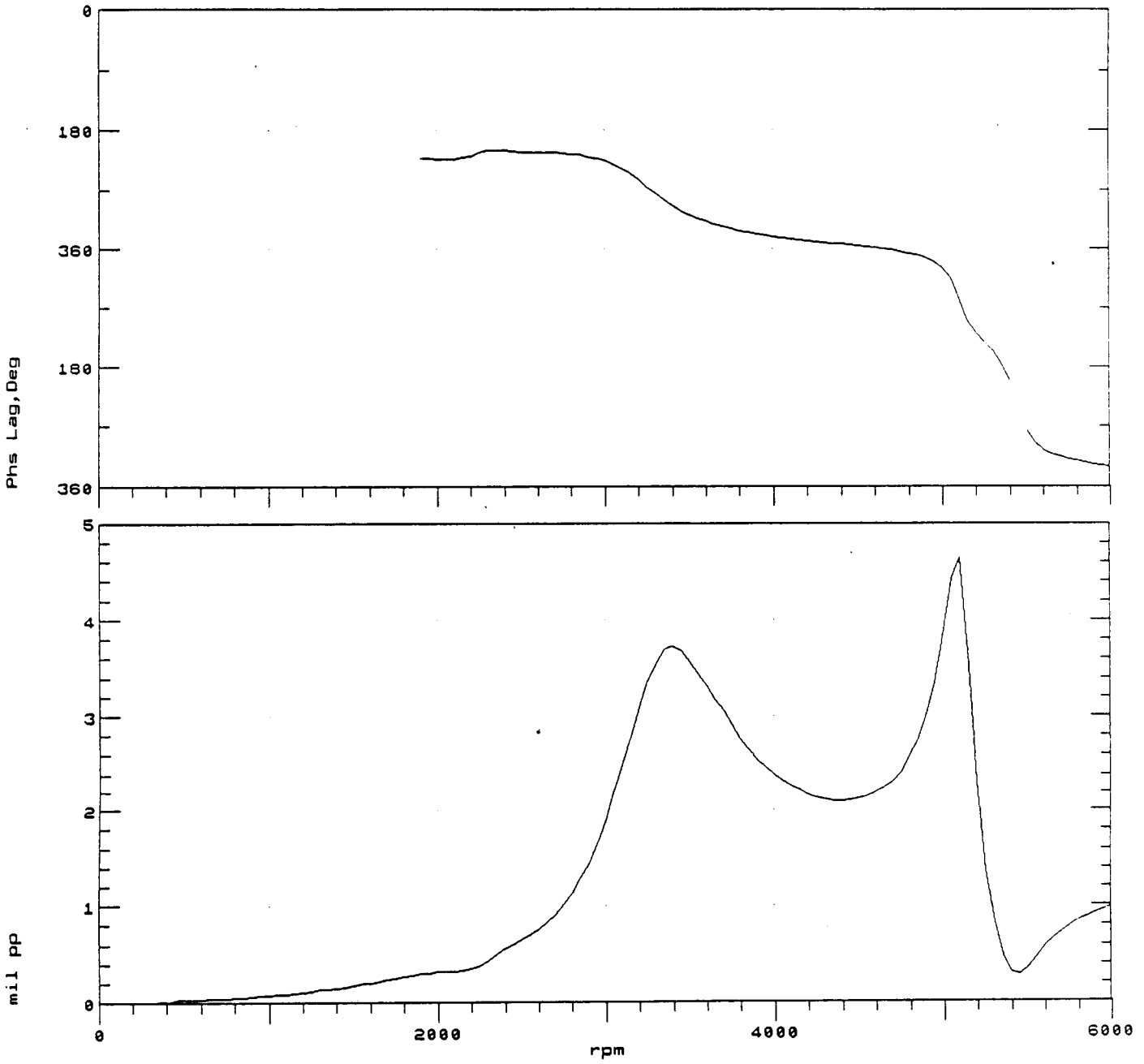

FIGURE 7.30 BODÉ PLOT OF ROTOR SYNCHRONOUS VIBRATION MEASURED AT CHANNEL #2. 10 PSI OIL PRESSURE AT SEAL SIMULATION BEARINGS. 0.0 INCH PRELOAD.

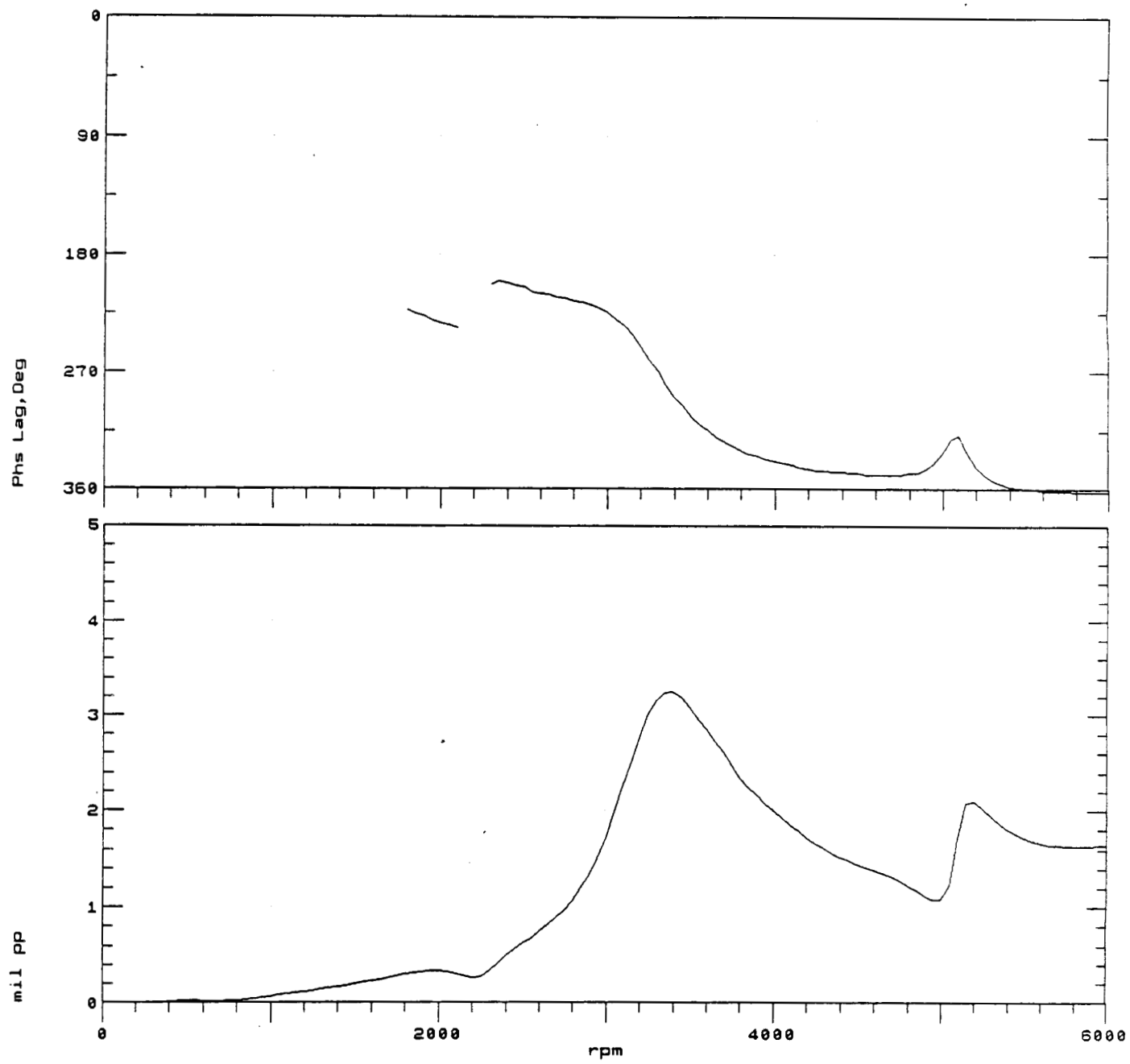

FIGURE 7.31 BODÉ PLOT OF ROTOR SYNCHRONOUS VIBRATION MEASURED AT CHANNEL #3. 10 PSI OIL PRESSURE AT SEAL SIMULATION BEARINGS. 0.0 INCH PRELOAD.

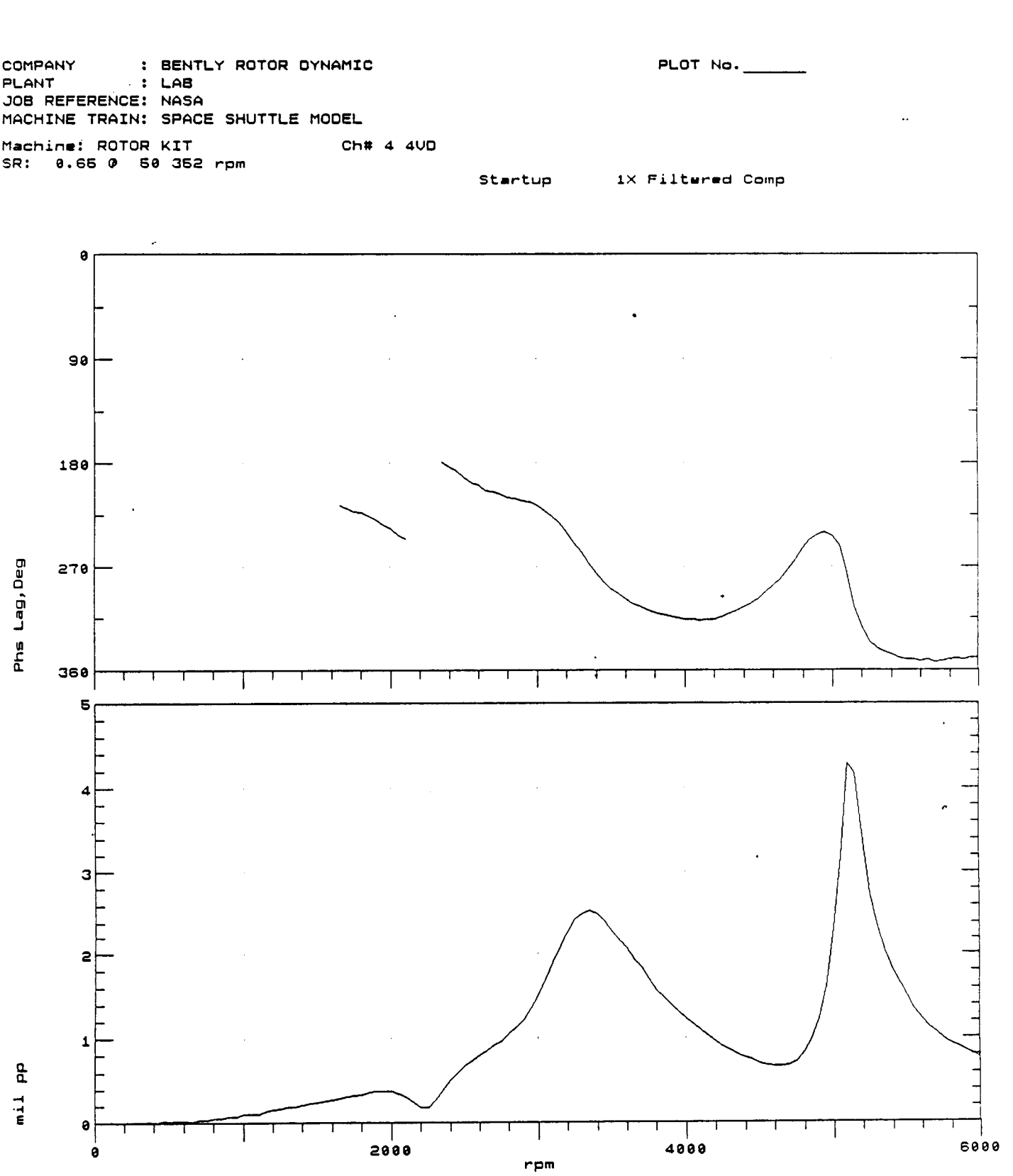

FIGURE 7.32 BODÉ PLOT OF ROTOR SYNCHRONOUS VIBRATION MEASURED AT CHANNEL #4. 10 PSI OIL PRESSURE AT SEAL SIMULATION BEARINGS. 0.0 INCH PRELOAD.

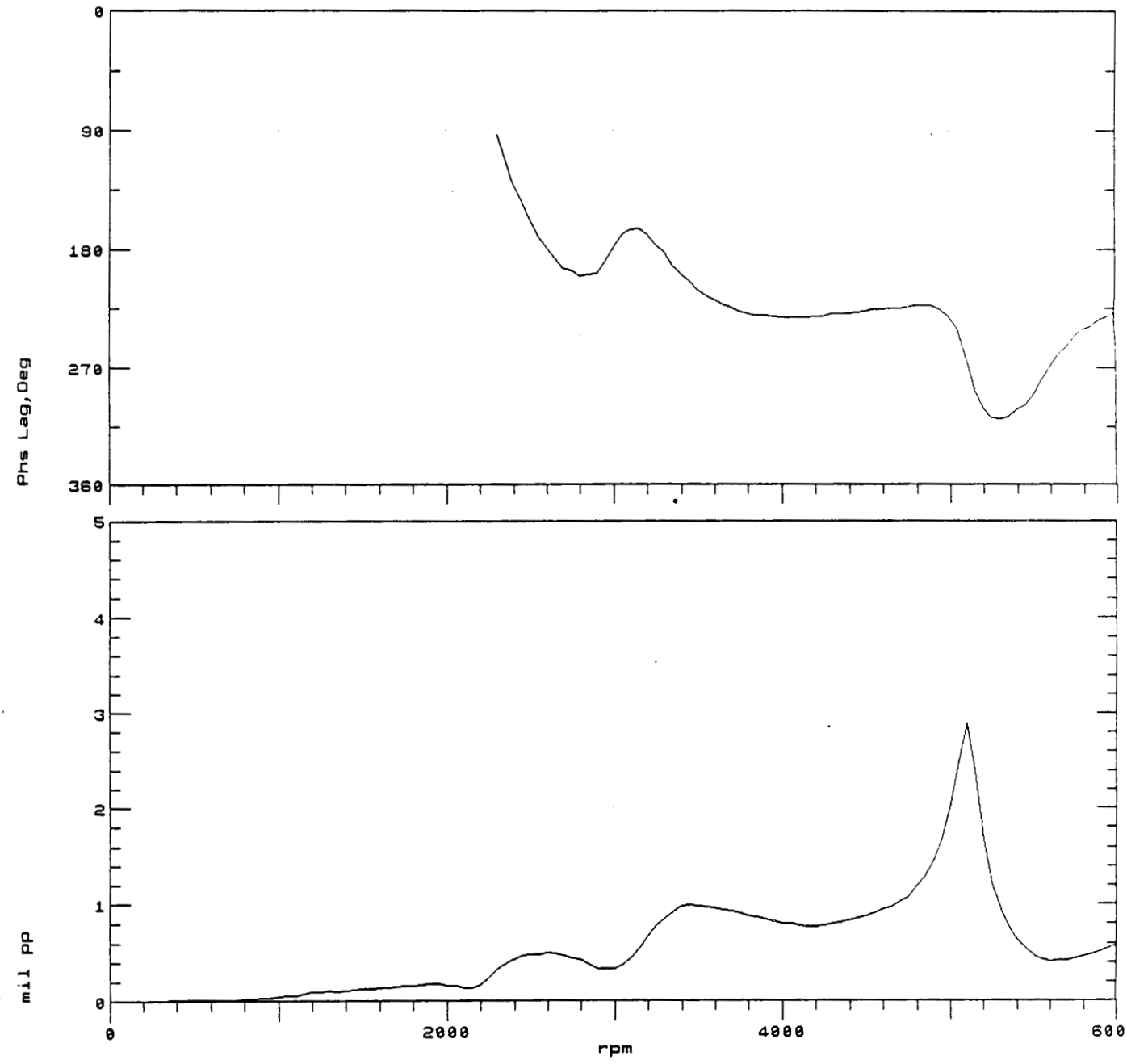

FIGURE 7.33 BODÉ PLOT OF ROTOR SYNCHRONOUS VIBRATION MEASURED AT CHANNEL #5. 10 PSI OIL PRESSURE AT SEAL SIMULATION BEARINGS. 0.0 INCH PRELOAD.

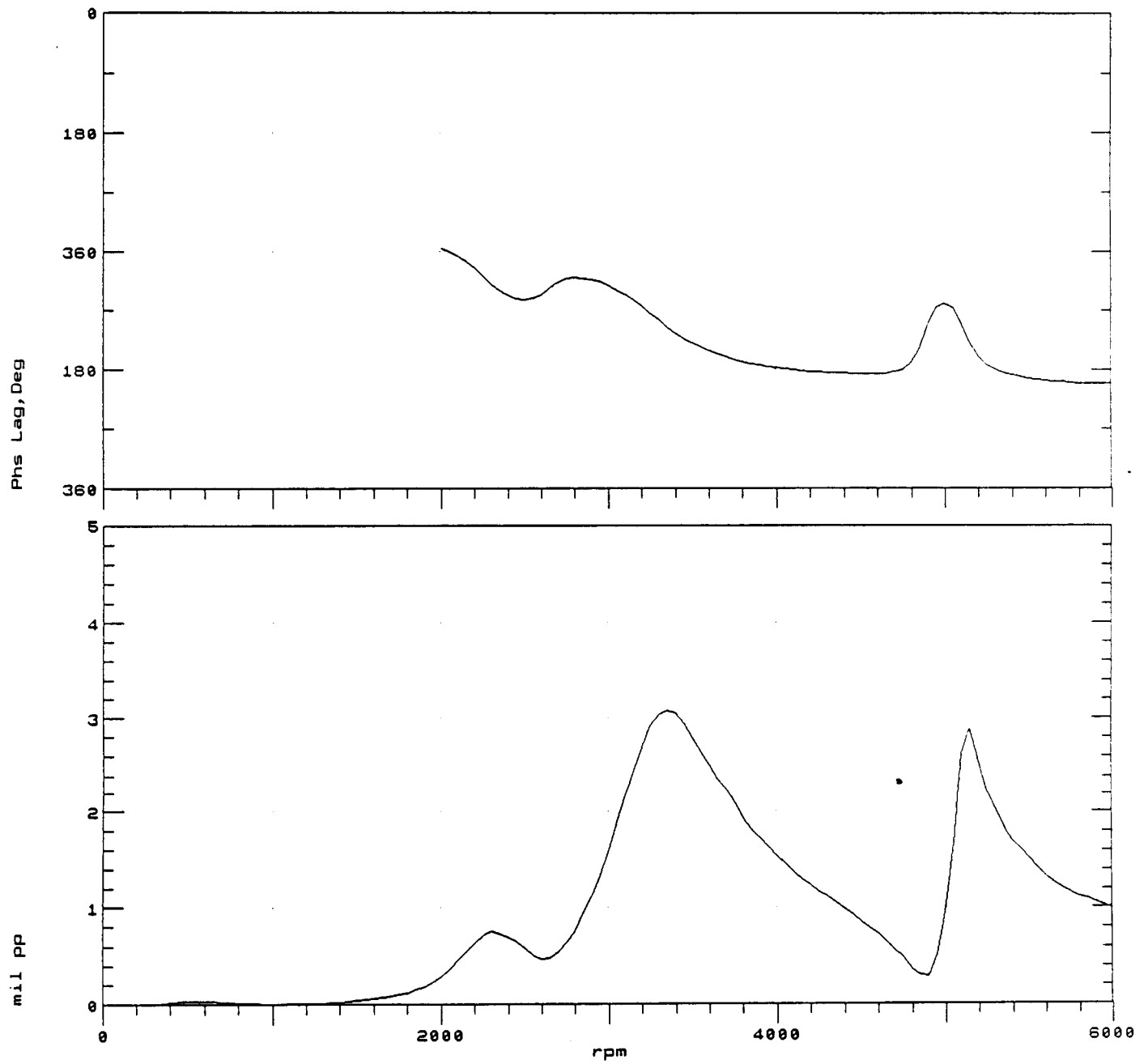

FIGURE 7.34 BODÉ PLOT OF ROTOR SYNCHRONOUS VIBRATION MEASURED AT CHANNEL #6. 10 PSI OIL PRESSURE AT SEAL SIMULATION BEARINGS. 0.0 INCH PRELOAD.

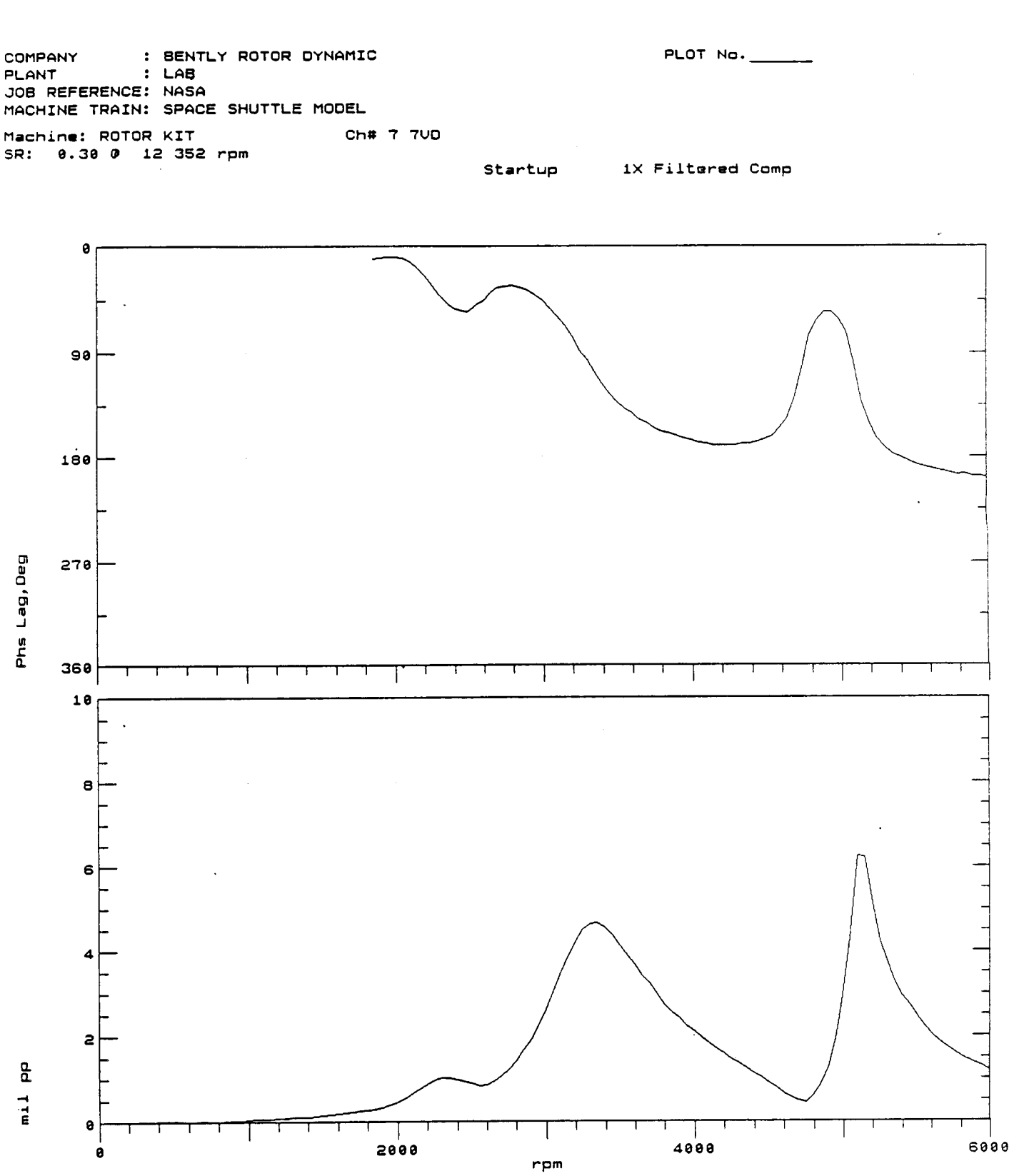

FIGURE 7.35 BODÉ PLOT OF ROTOR SYNCHRONOUS VIBRATION MEASURED AT CHANNEL #7. 10 PSI OIL PRESSURE AT SEAL SIMULATION BEARINGS. 0.0 INCH PRELOAD.

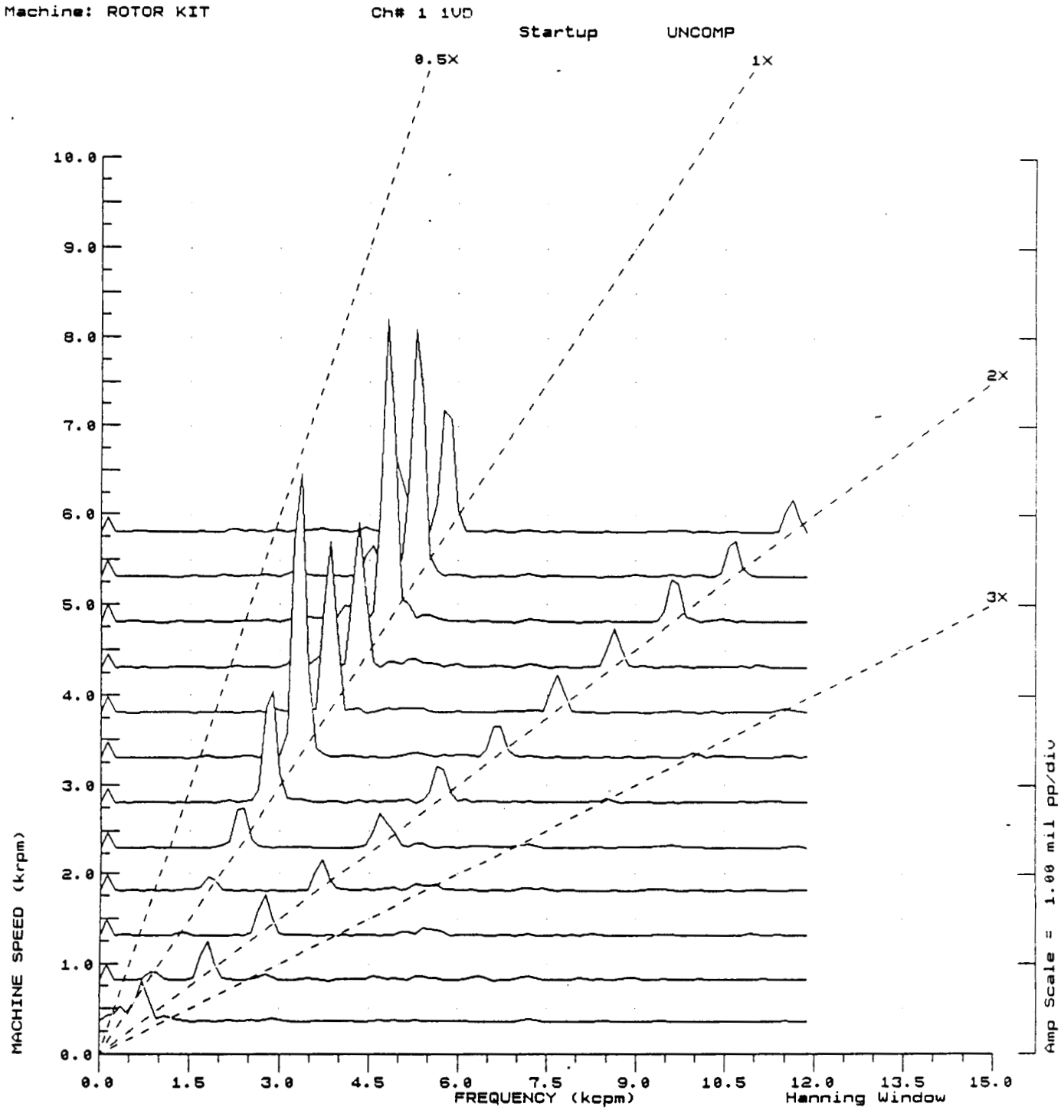

FIGURE 7.36 SPECTRUM CASCADE OF ROTOR VERTICAL VIBRATIONS DURING START–UP MEASURED AT CHANNEL #1. 10 PSI OIL PRESSURE AT SEAL SIMULATION BEARINGS. 0.0 INCH PRELOAD.

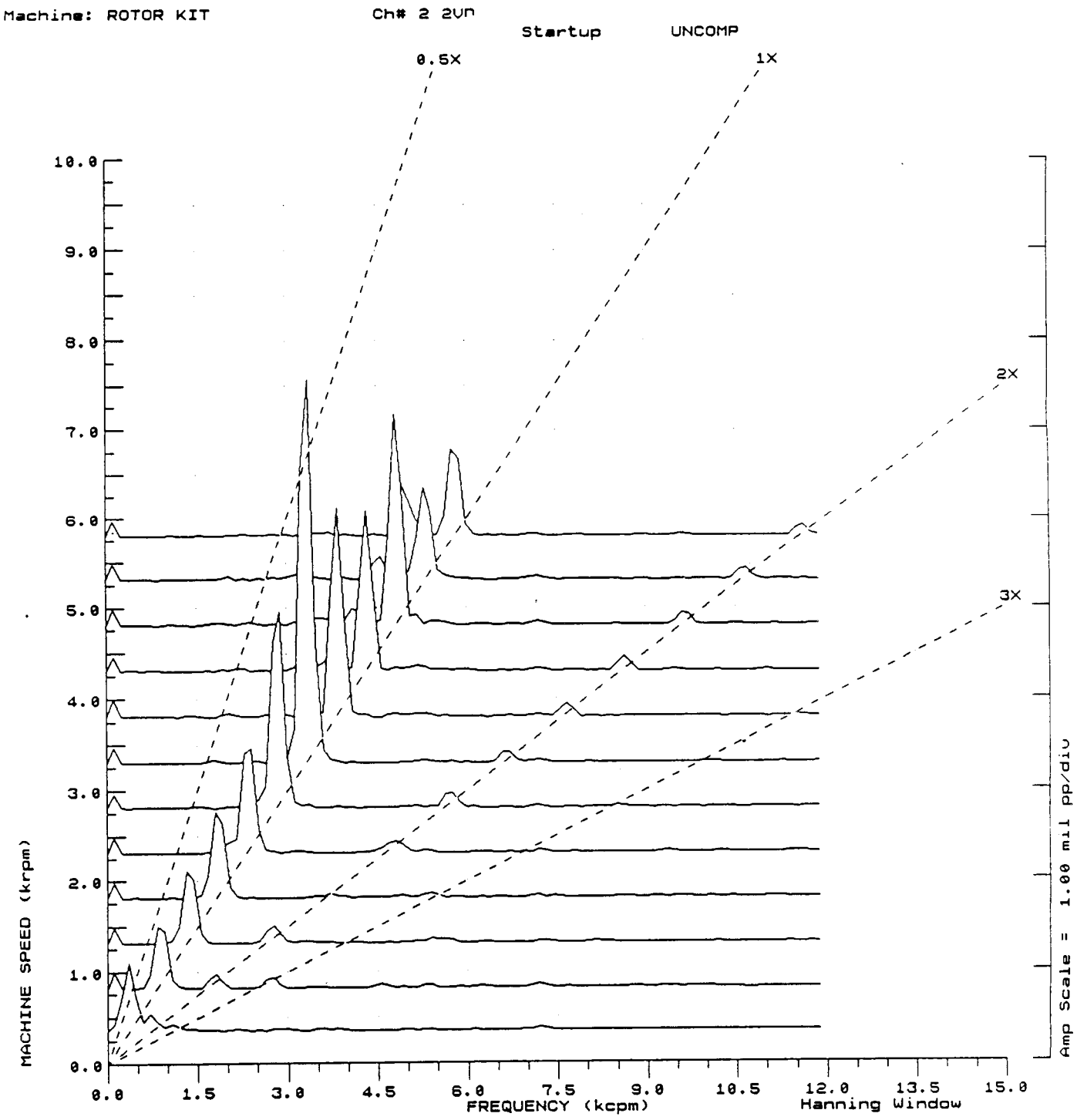

FIGURE 7.37 SPECTRUM CASCADE OF ROTOR VERTICAL VIBRATIONS DURING START-UP MEASURED AT CHANNEL #2. 10 PSI OIL PRESSURE AT SEAL SIMULATION BEARINGS. 0.0 INCH PRELOAD.

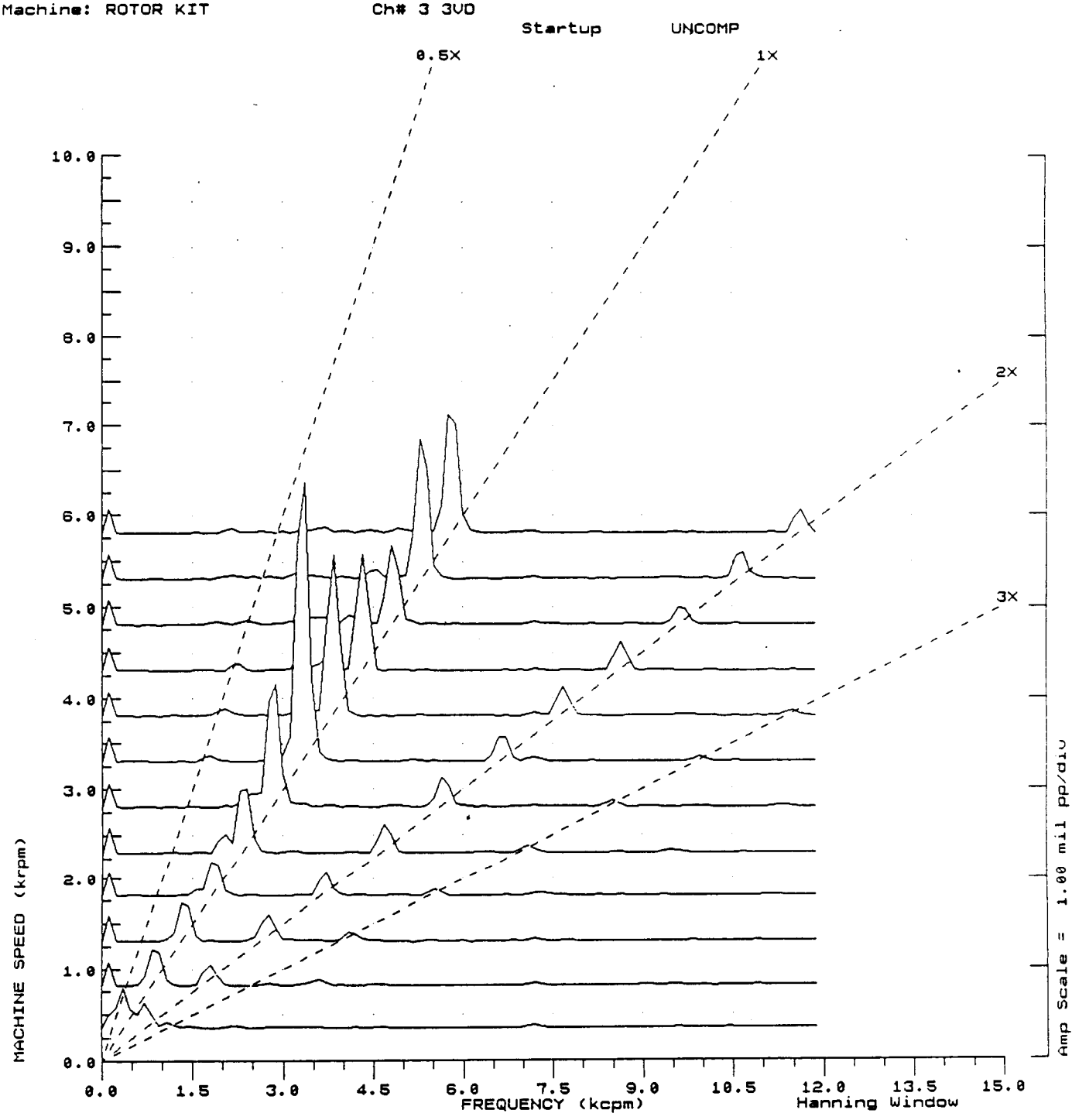

FIGURE 7.38 SPECTRUM CASCADE OF ROTOR VERTICAL VIBRATIONS DURING START–UP MEASURED AT CHANNEL #3. 10 PSI OIL PRESSURE AT SEAL SIMULATION BEARINGS. 0.0 INCH PRELOAD.

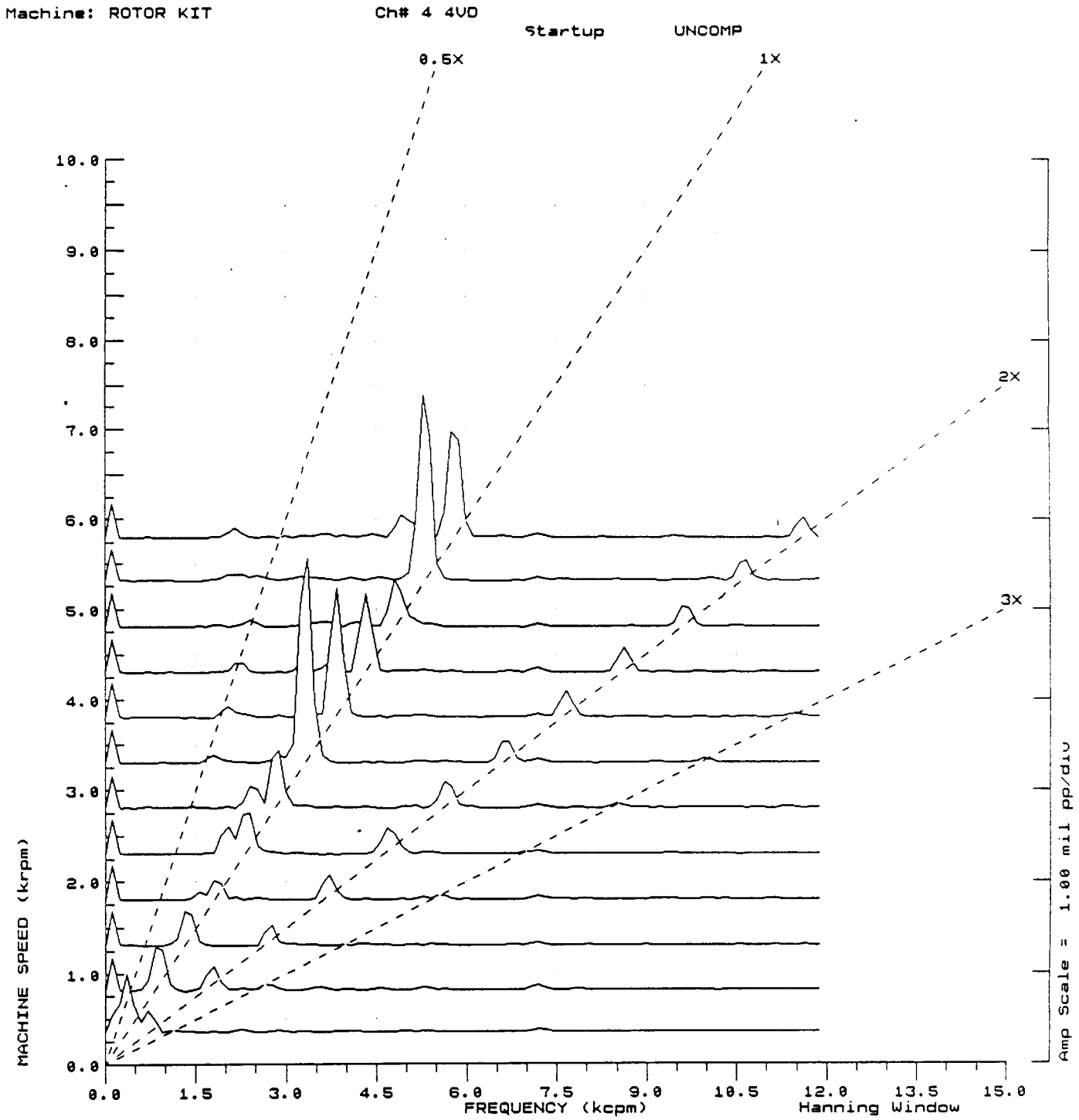

FIGURE 7.39 SPECTRUM CASCADE OF ROTOR VERTICAL VIBRATIONS DURING START–UP MEASURED AT CHANNEL #4. 10 PSI OIL PRESSURE AT SEAL SIMULATION BEARINGS. 0.0 INCH PRELOAD.

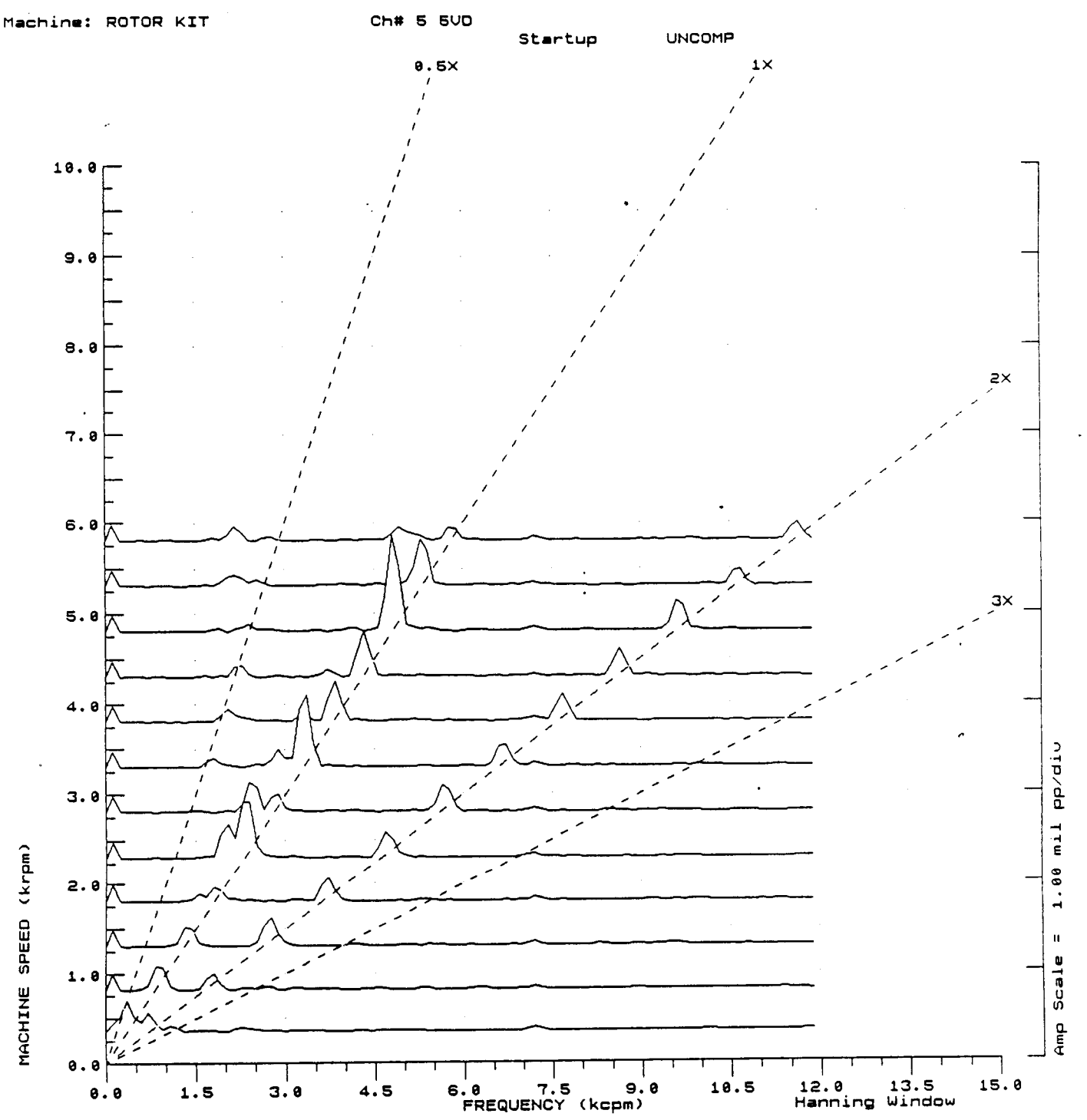

FIGURE 7.40 SPECTRUM CASCADE OF ROTOR VERTICAL VIBRATIONS DURING START–UP MEASURED AT CHANNEL #5. 10 PSI OIL PRESSURE AT SEAL SIMULATION BEARINGS. 0.0 INCH PRELOAD.

C-2

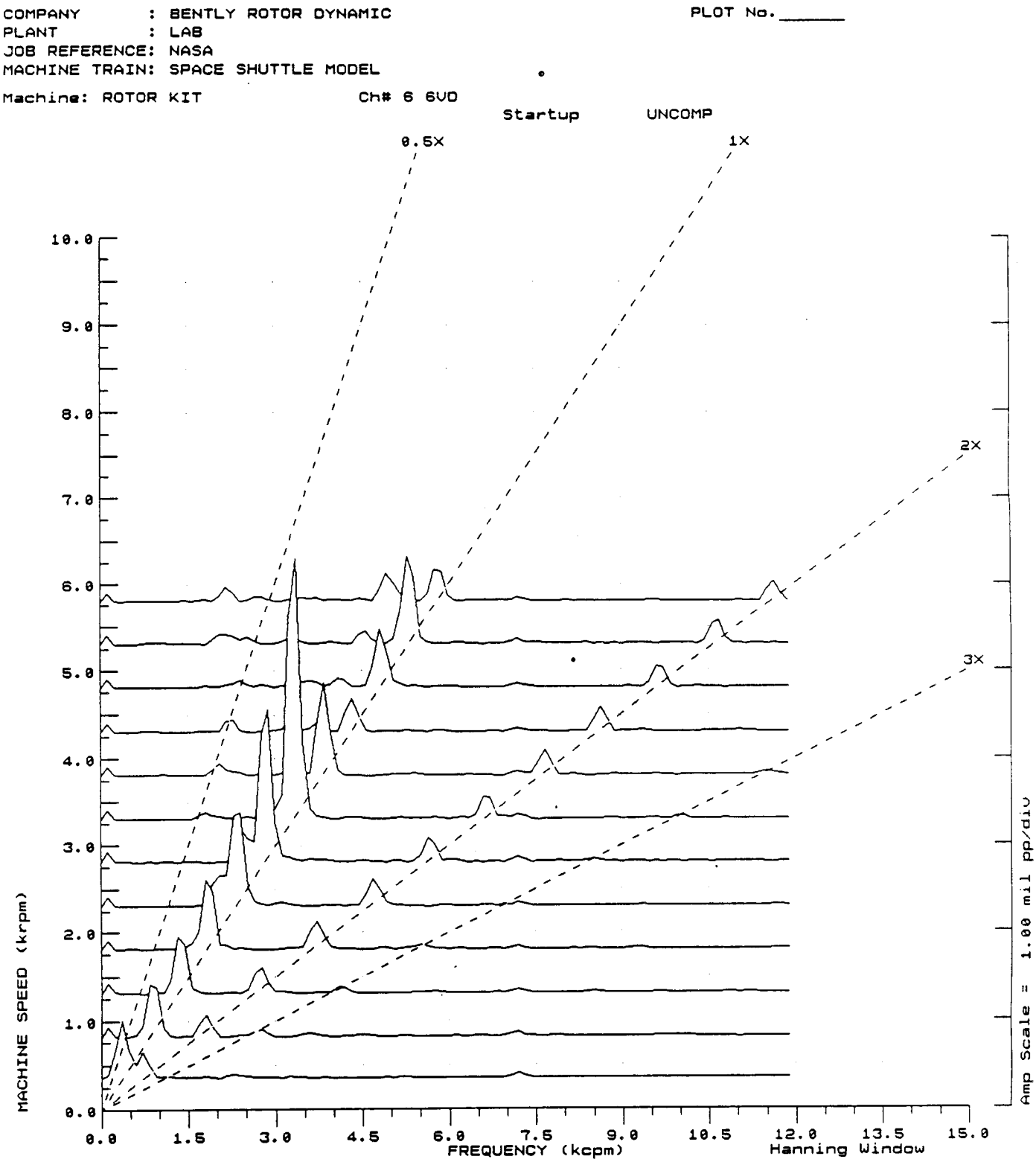

FIGURE 7.41 SPECTRUM CASCADE OF ROTOR VERTICAL VIBRATIONS DURING START–UP MEASURED AT CHANNEL #6. 10 PSI OIL PRESSURE AT SEAL SIMULATION BEARINGS. 0.0 INCH PRELOAD.

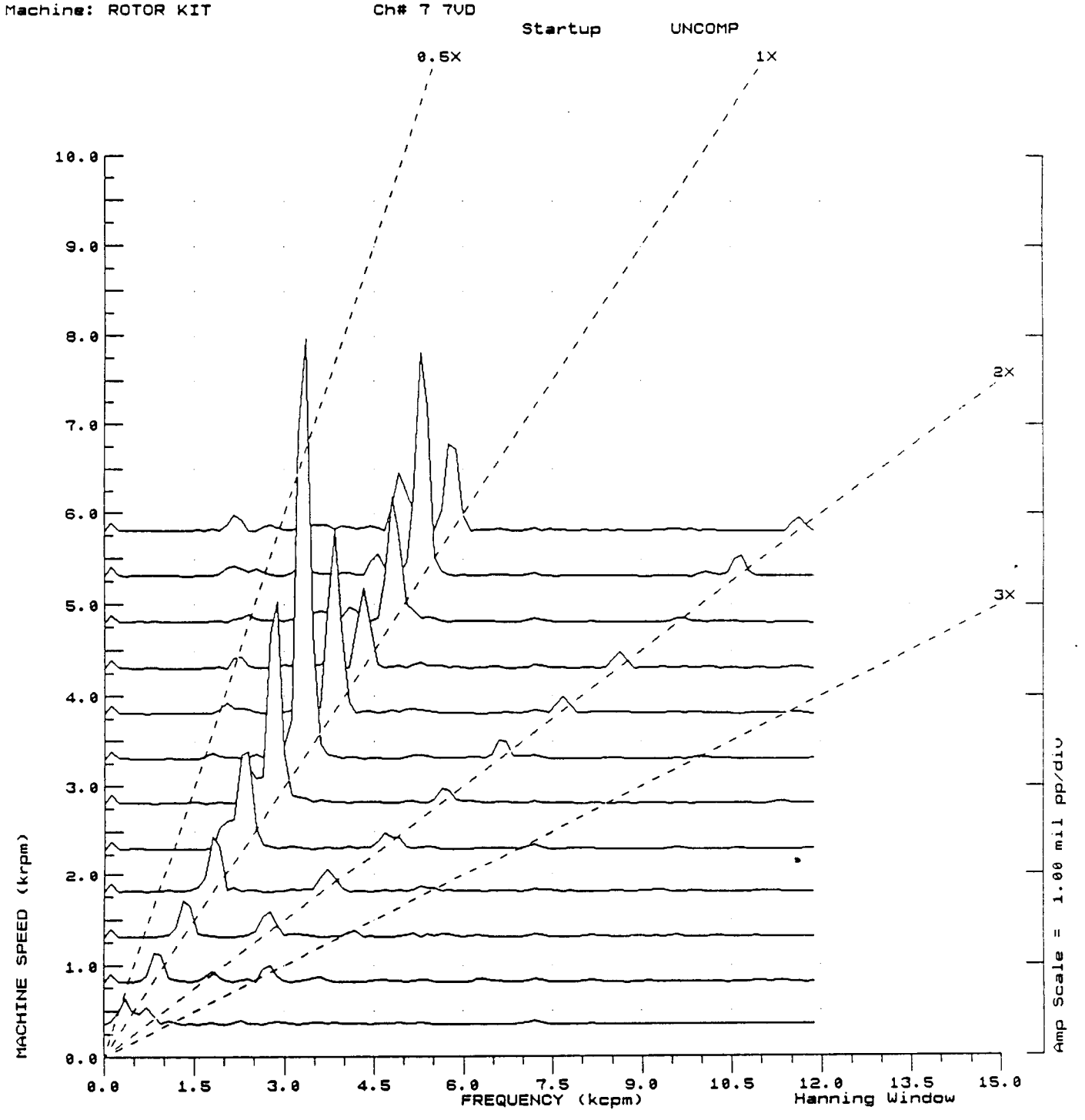

FIGURE 7.42 SPECTRUM CASCADE OF ROTOR VERTICAL VIBRATIONS DURING START–UP MEASURED AT CHANNEL #7. 10 PSI OIL PRESSURE AT SEAL SIMULATION BEARINGS. 0.0 INCH PRELOAD.

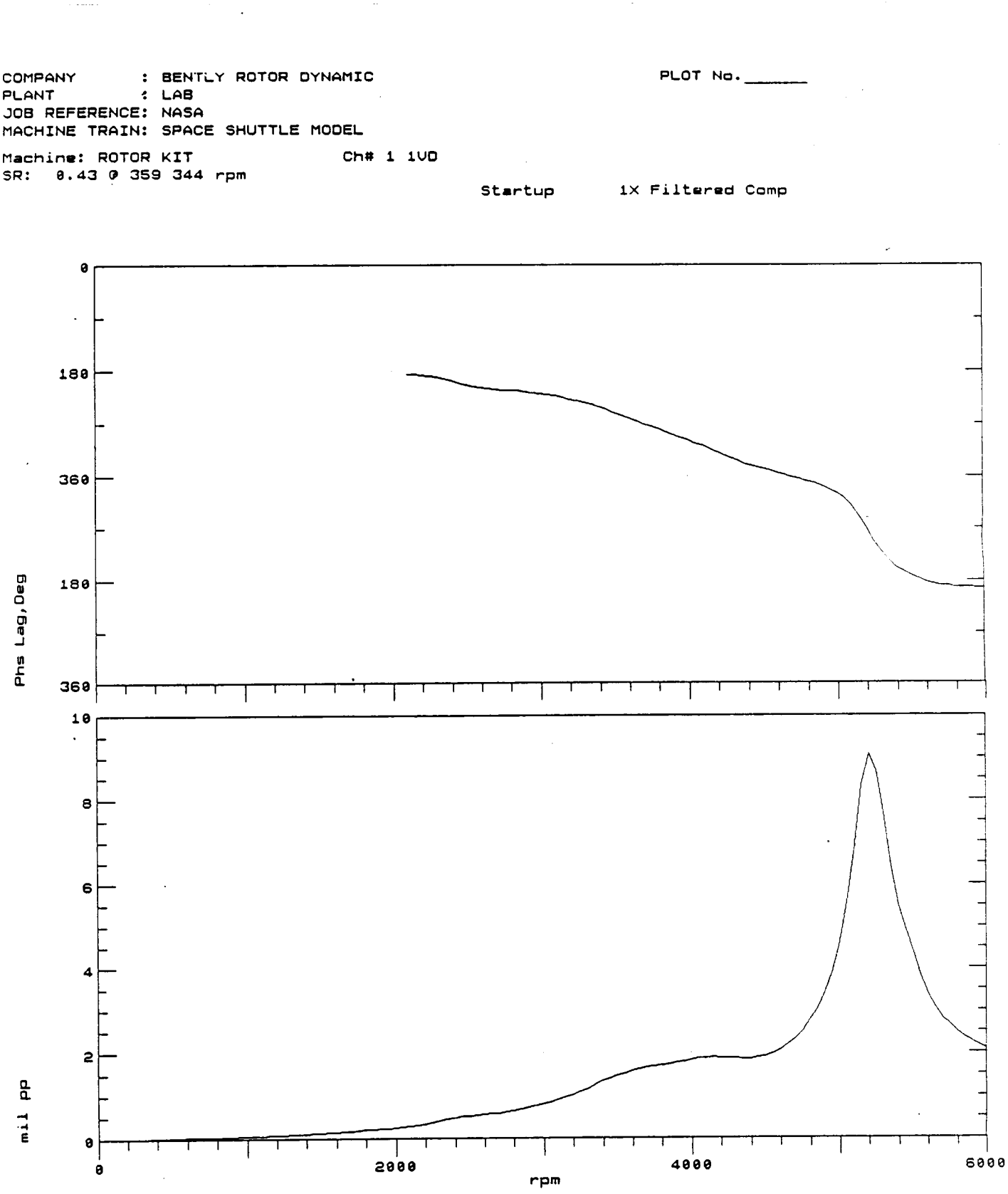

FIGURE 7.43 BODÉ PLOT OF ROTOR SYNCHRONOUS VIBRATION MEASURED AT CHANNEL #1. 15 PSI OIL PRESSURE AT SEAL SIMULATION BEARINGS. 0.0 INCH PRELOAD.

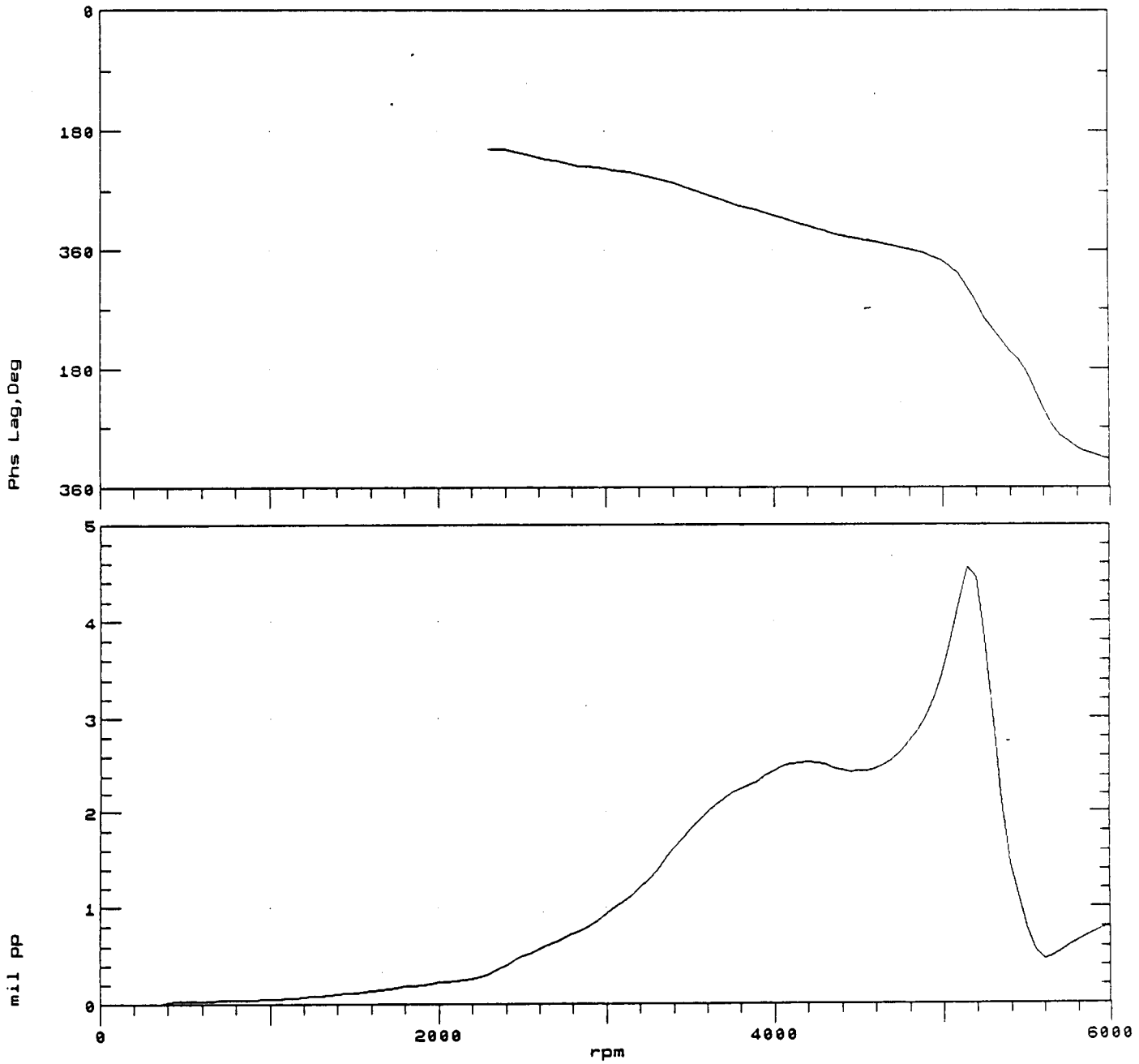

FIGURE 7.44 BODÉ PLOT OF ROTOR SYNCHRONOUS VIBRATION MEASURED AT CHANNEL #2. 15 PSI OIL PRESSURE AT SEAL SIMULATION BEARINGS. 0.0 INCH PRELOAD.

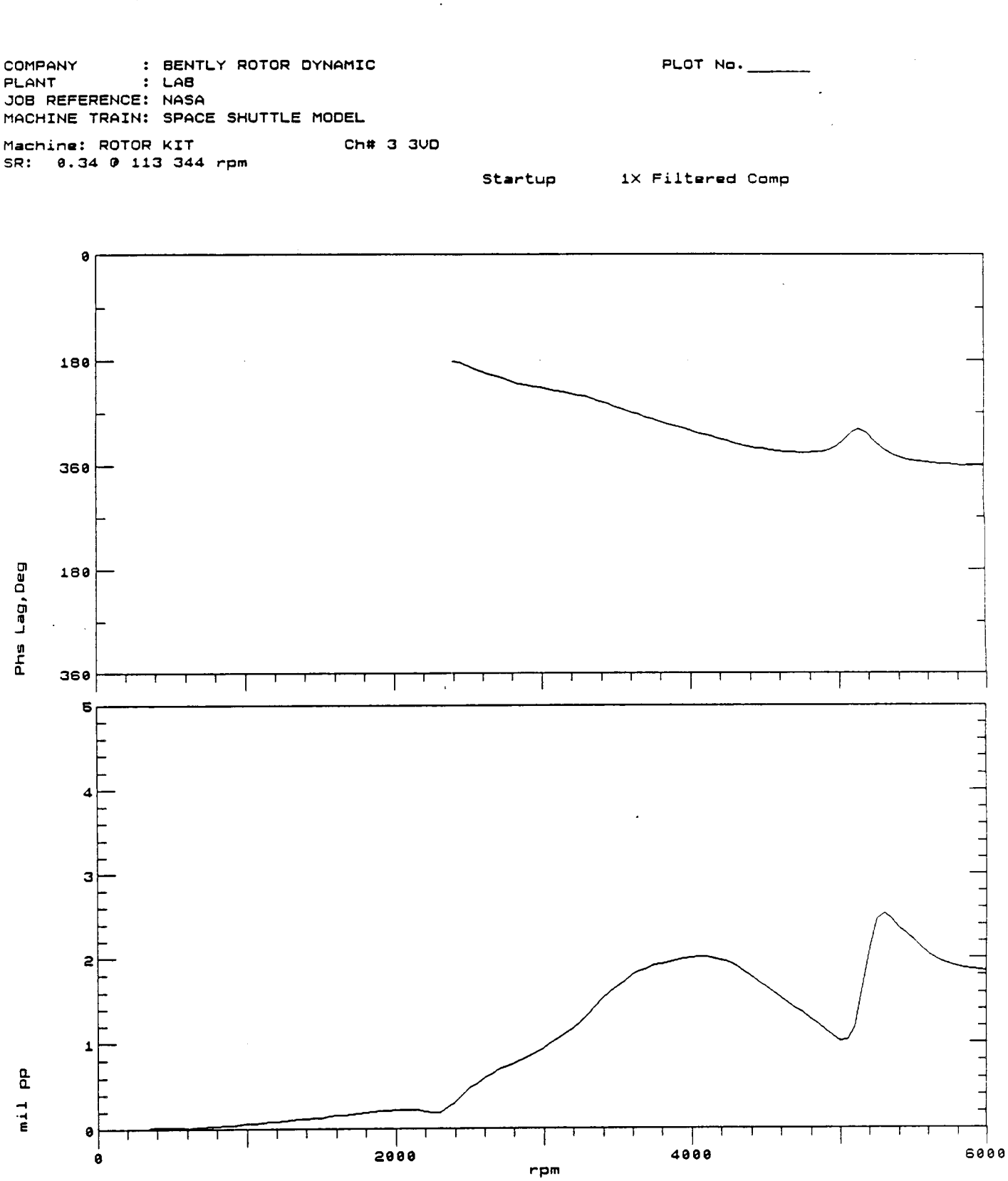

FIGURE 7.45 BODÉ PLOT OF ROTOR SYNCHRONOUS VIBRATION MEASURED AT CHANNEL #3. 15 PSI OIL PRESSURE AT SEAL SIMULATION BEARINGS. 0.0 INCH PRELOAD.

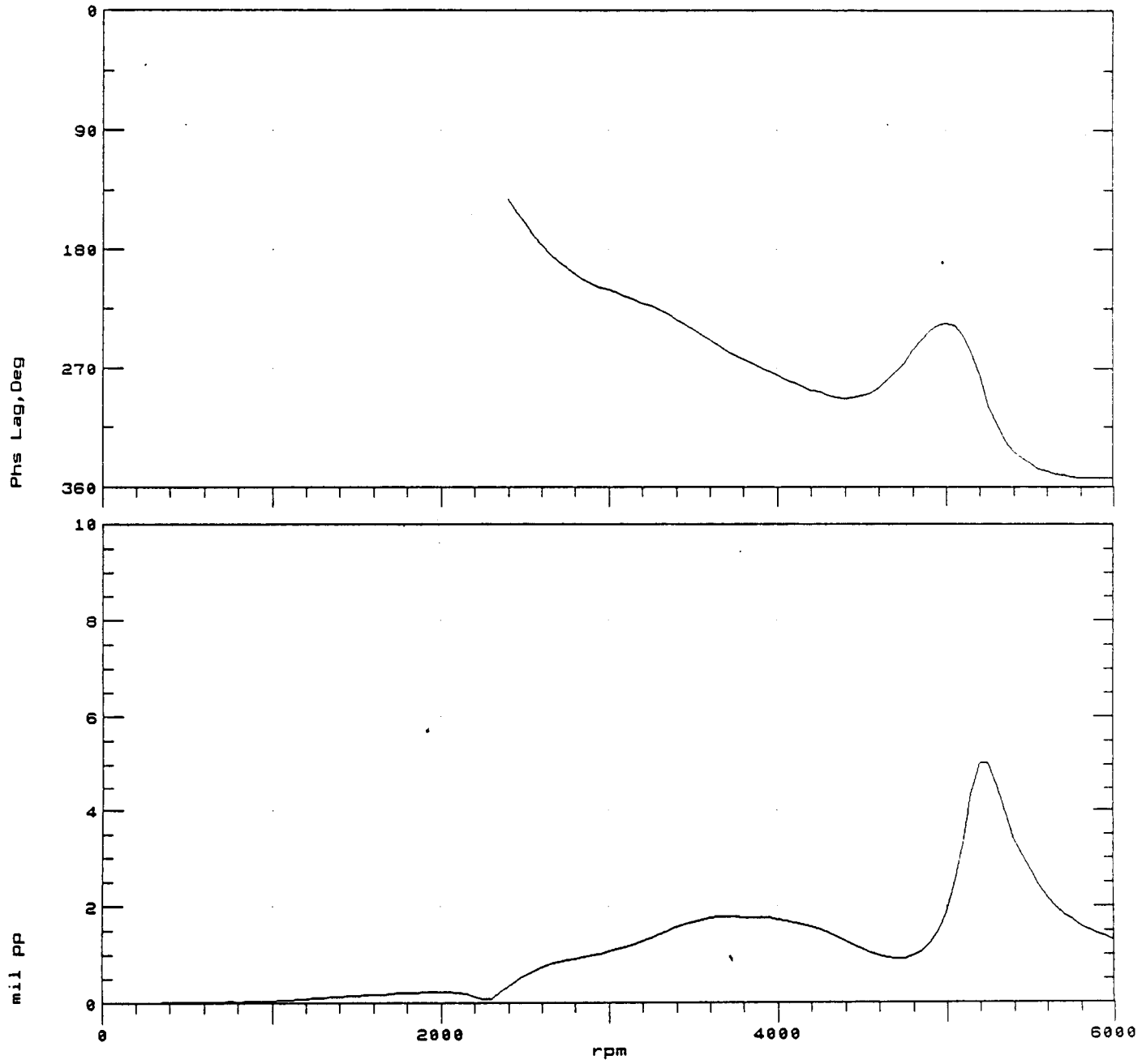

FIGURE 7.46 BODÉ PLOT OF ROTOR SYNCHRONOUS VIBRATION MEASURED AT CHANNEL #4. 15 PSI OIL PRESSURE AT SEAL SIMULATION BEARINGS. 0.0 INCH PRELOAD.

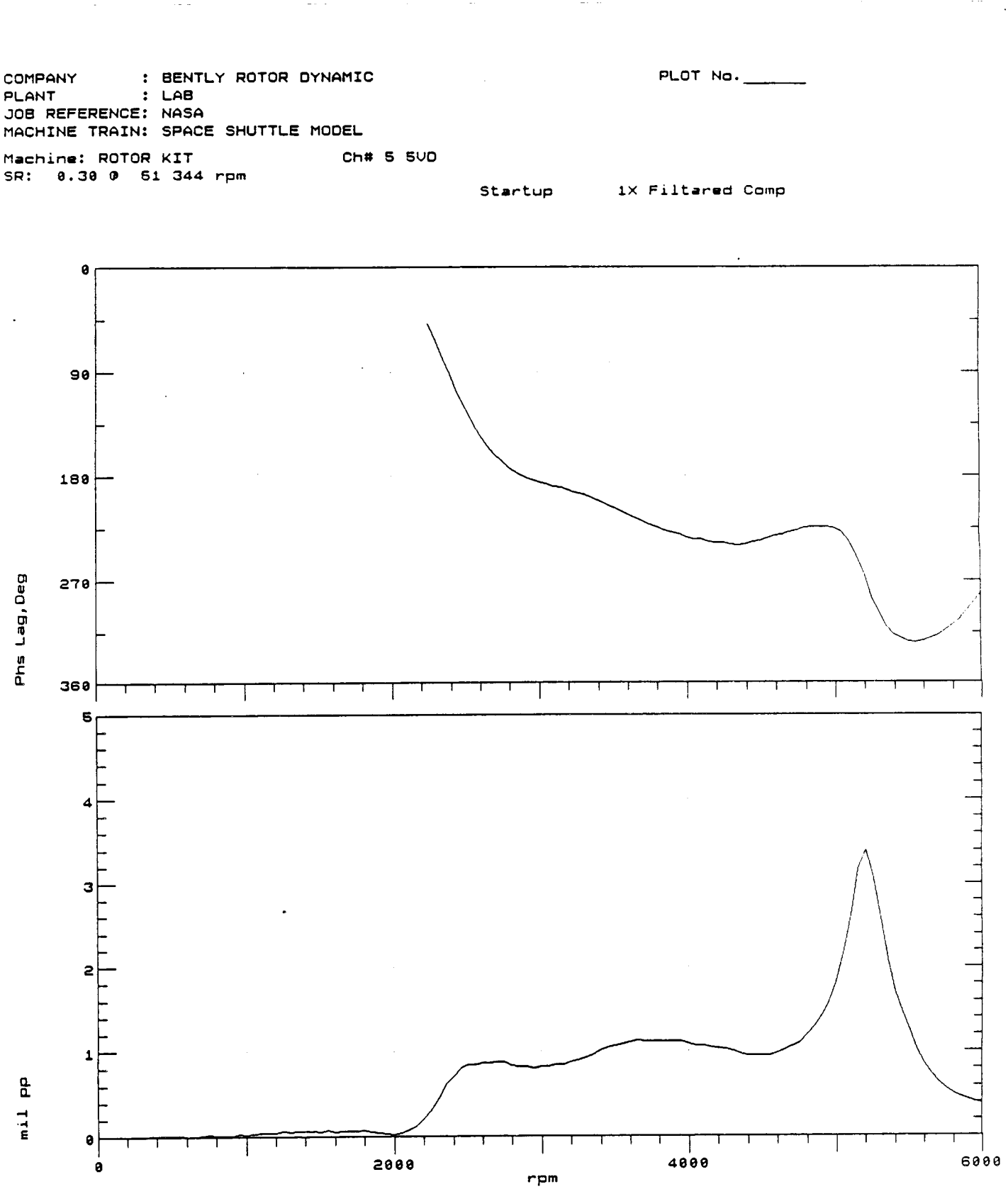

FIGURE 7.47 BODÉ PLOT OF ROTOR SYNCHRONOUS VIBRATION MEASURED AT CHANNEL #5. 15 PSI OIL PRESSURE AT SEAL SIMULATION BEARINGS. 0.0 INCH PRELOAD.

COMPANY : BENTLY ROTOR DYNAMIC PLOT No._____
PLANT : LAB
JOB REFERENCE: NASA
MACHINE TRAIN: SPACE SHUTTLE MODEL

Machine: ROTOR KIT Ch# 6 6VD
SR: 0.64 @ 16 344 rpm

Startup 1X Filtered Comp

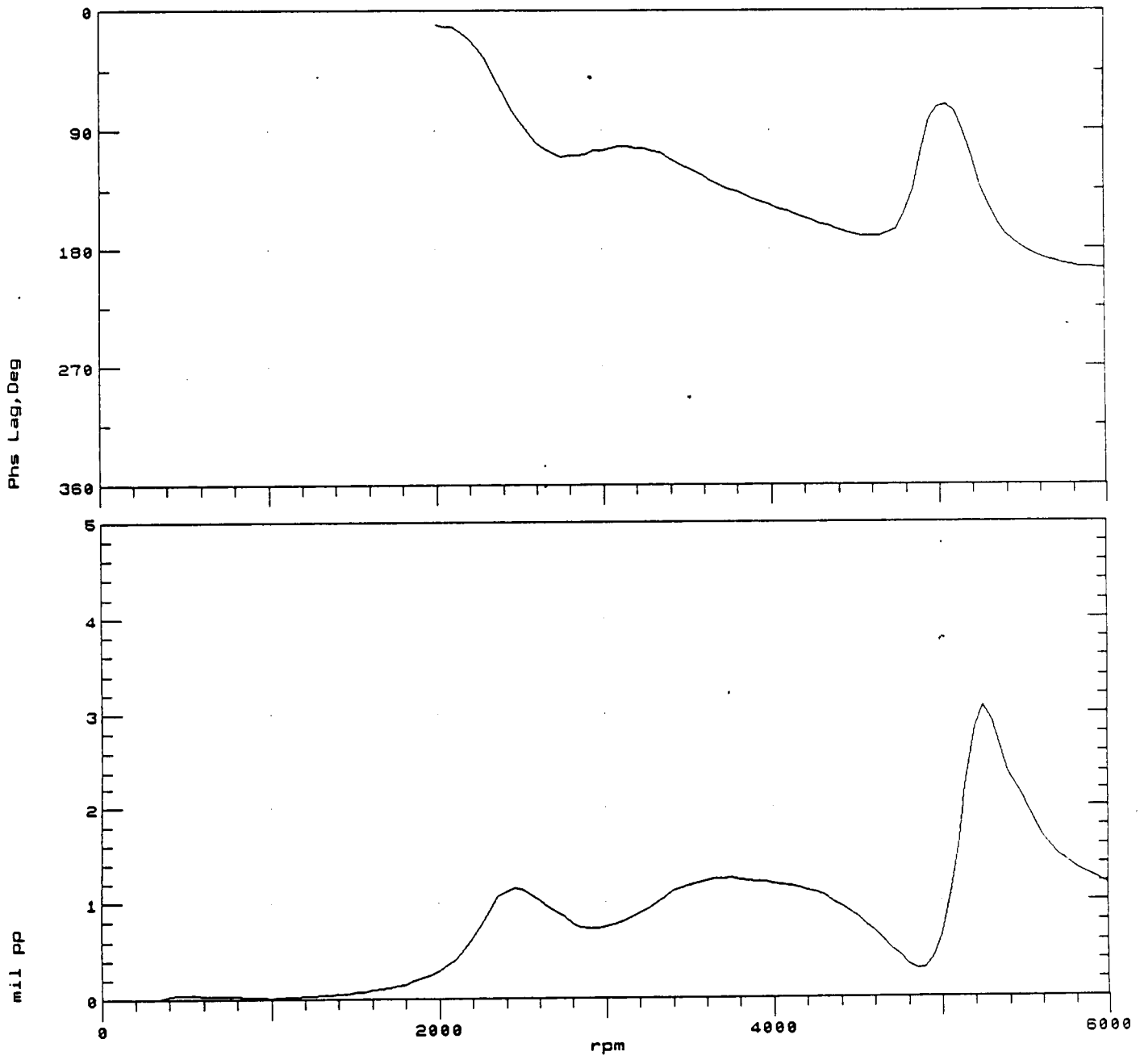

FIGURE 7.48 BODÉ PLOT OF ROTOR SYNCHRONOUS VIBRATION MEASURED AT CHANNEL #6. 15 PSI OIL PRESSURE AT SEAL SIMULATION BEARINGS. 0.0 INCH PRELOAD.

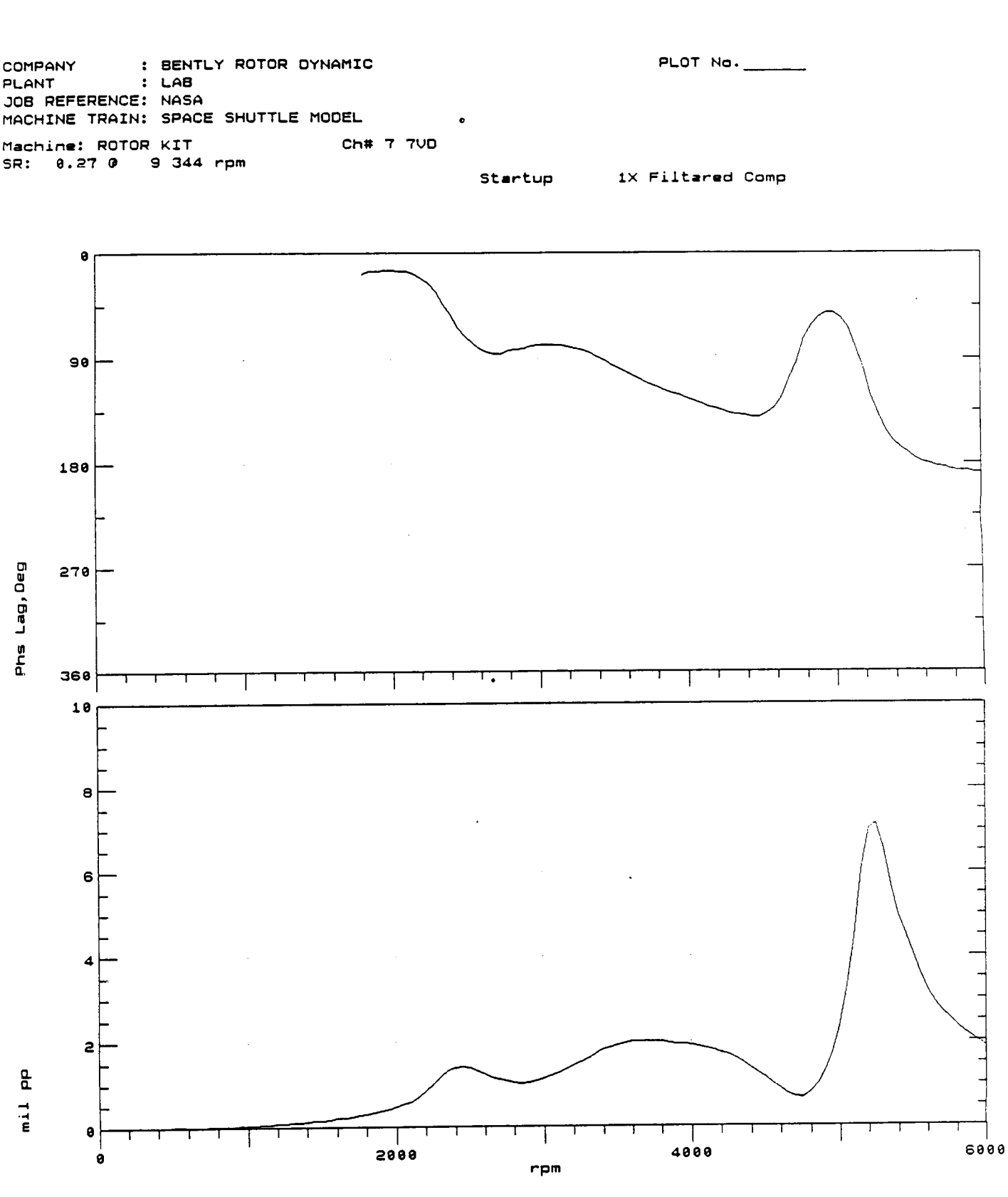

FIGURE 7.49 BODÉ PLOT OF ROTOR SYNCHRONOUS VIBRATION MEASURED AT CHANNEL #7. 15 PSI OIL PRESSURE AT SEAL SIMULATION BEARINGS. 0.0 INCH PRELOAD.

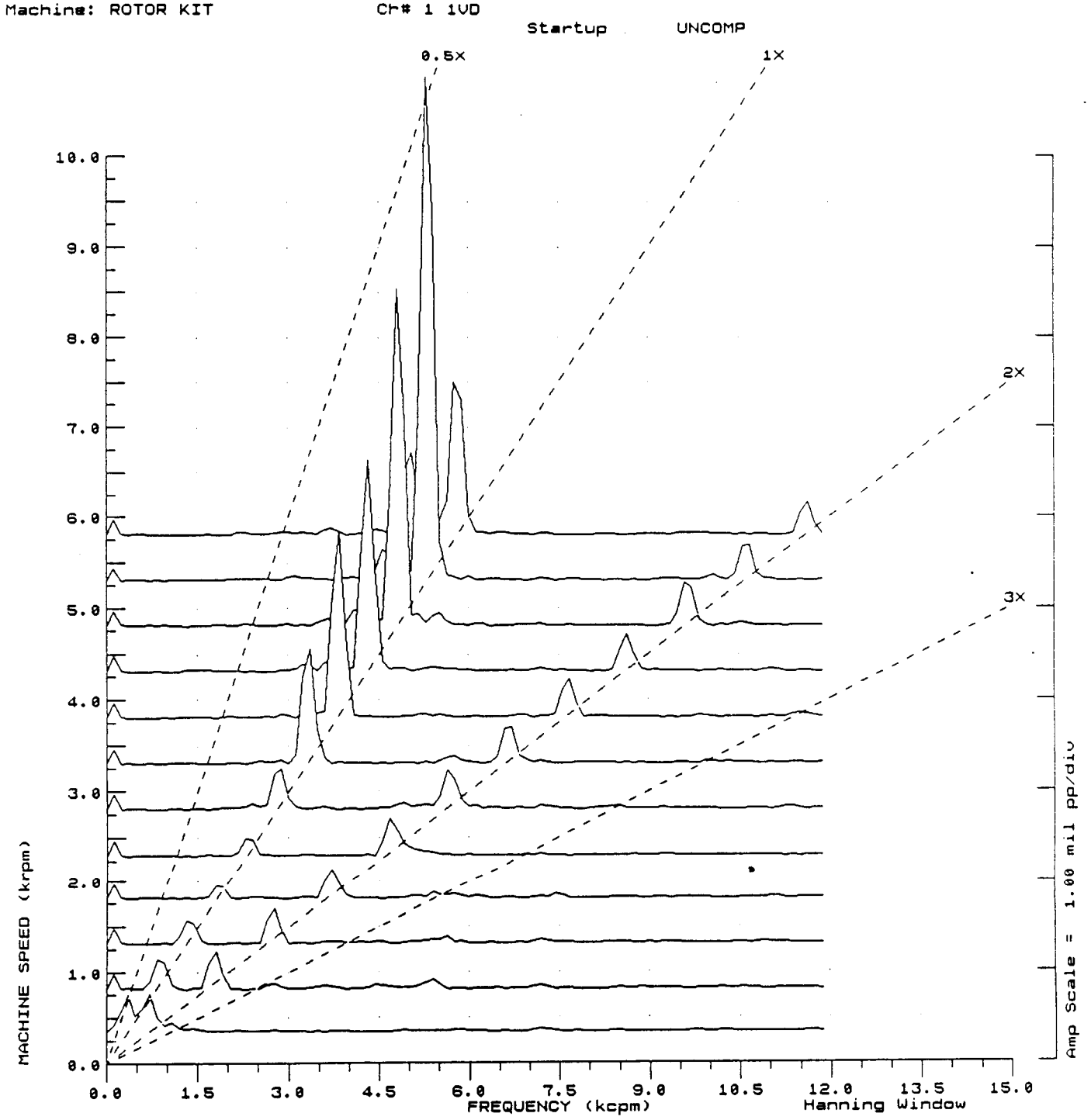

FIGURE 7.50 SPECTRUM CASCADE OF ROTOR VERTICAL VIBRATIONS DURING START–UP MEASURED AT CHANNEL #1. 15 PSI OIL PRESSURE AT SEAL SIMULATION BEARINGS. 0.0 INCH PRELOAD.

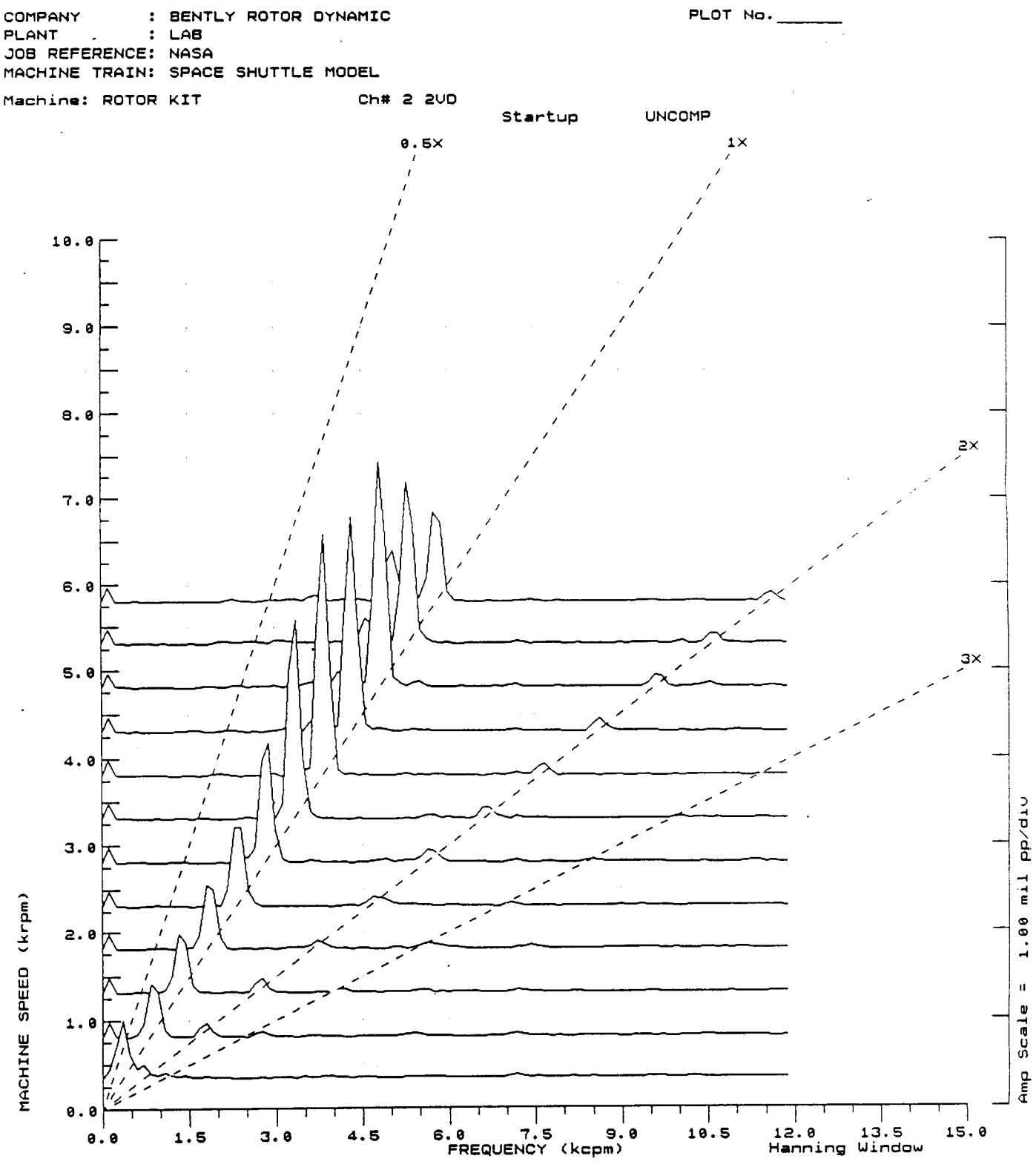

FIGURE 7.51 SPECTRUM CASCADE OF ROTOR VERTICAL VIBRATIONS DURING START–UP MEASURED AT CHANNEL #2. 15 PSI OIL PRESSURE AT SEAL SIMULATION BEARINGS. 0.0 INCH PRELOAD.

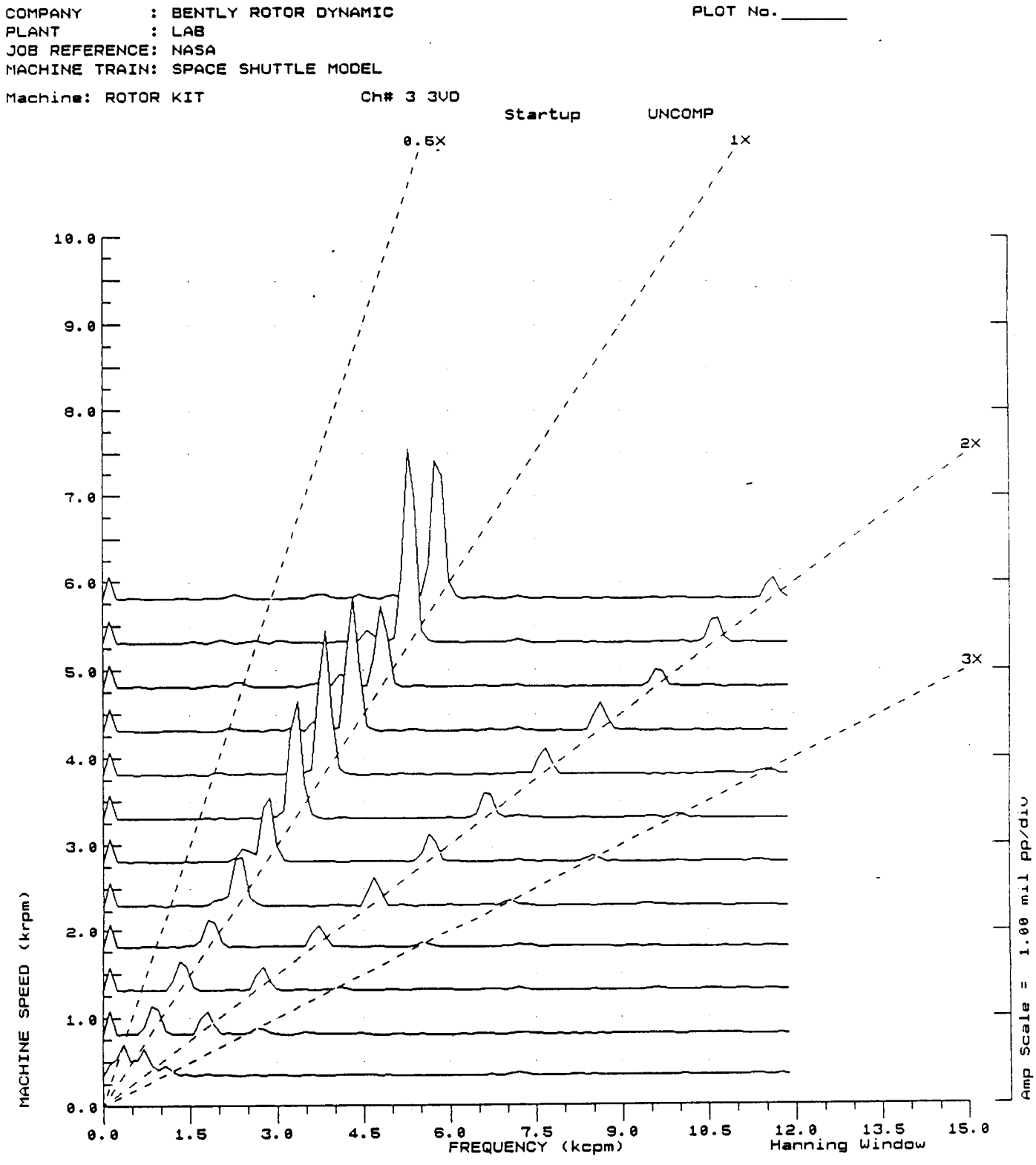

FIGURE 7.52 SPECTRUM CASCADE OF ROTOR VERTICAL VIBRATIONS DURING START–UP MEASURED AT CHANNEL #3. 15 PSI OIL PRESSURE AT SEAL SIMULATION BEARINGS. 0.0 INCH PRELOAD.

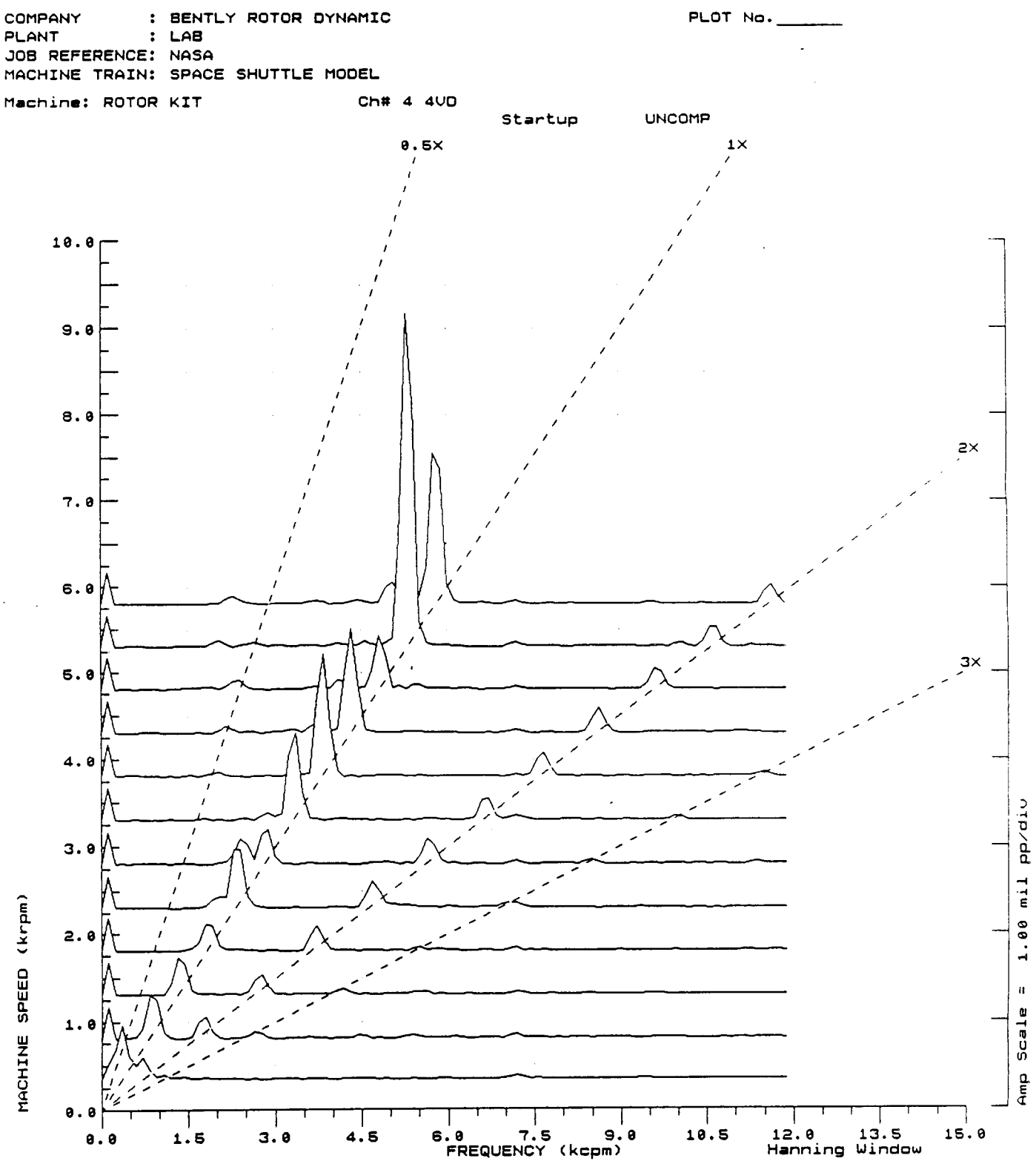

FIGURE 7.53 SPECTRUM CASCADE OF ROTOR VERTICAL VIBRATIONS DURING START–UP MEASURED AT CHANNEL #4. 15 PSI OIL PRESSURE AT SEAL SIMULATION BEARINGS. 0.0 INCH PRELOAD.

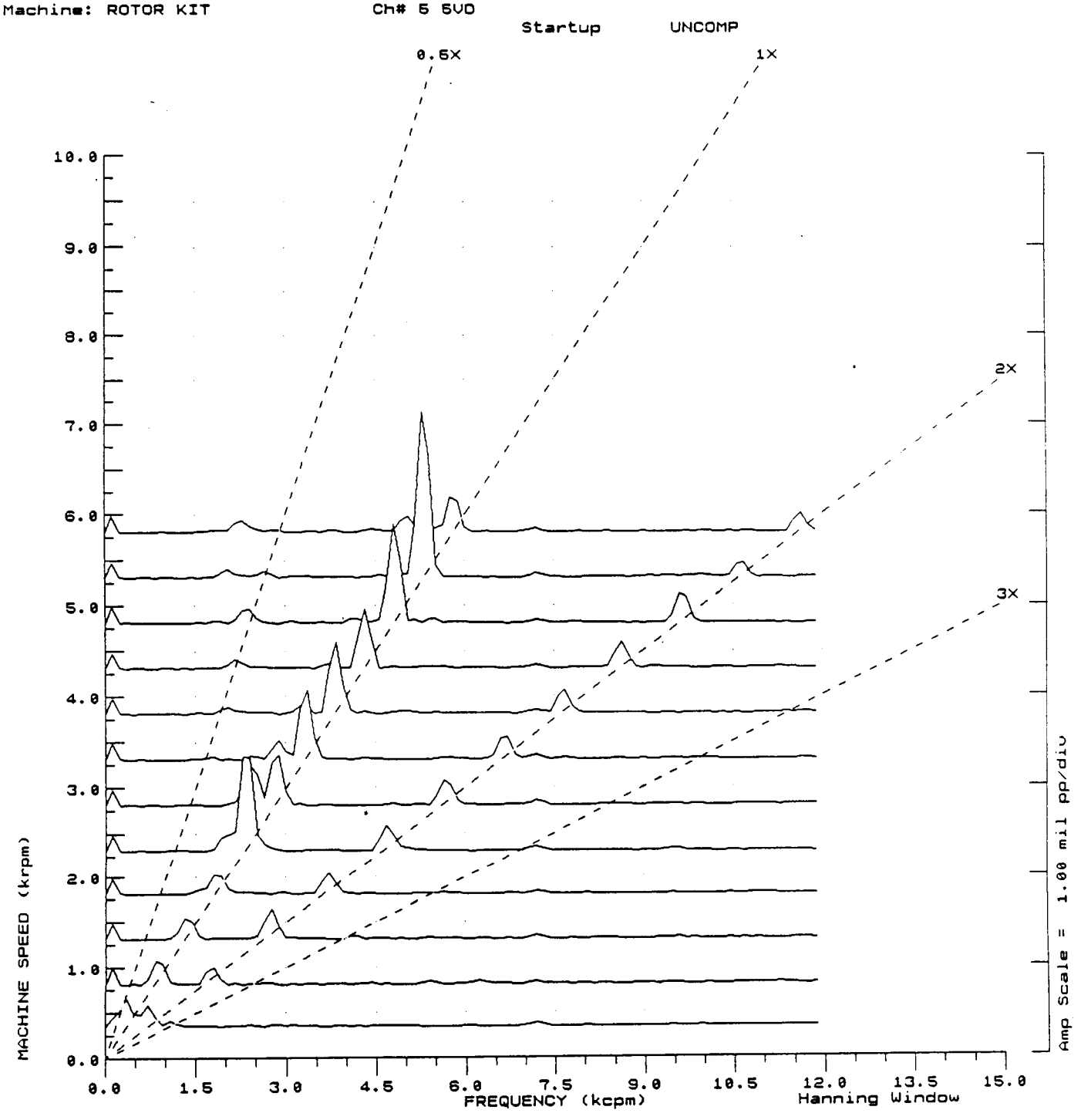

FIGURE 7.54 SPECTRUM CASCADE OF ROTOR VERTICAL VIBRATIONS DURING START–UP MEASURED AT CHANNEL #5. 15 PSI OIL PRESSURE AT SEAL SIMULATION BEARINGS. 0.0 INCH PRELOAD.

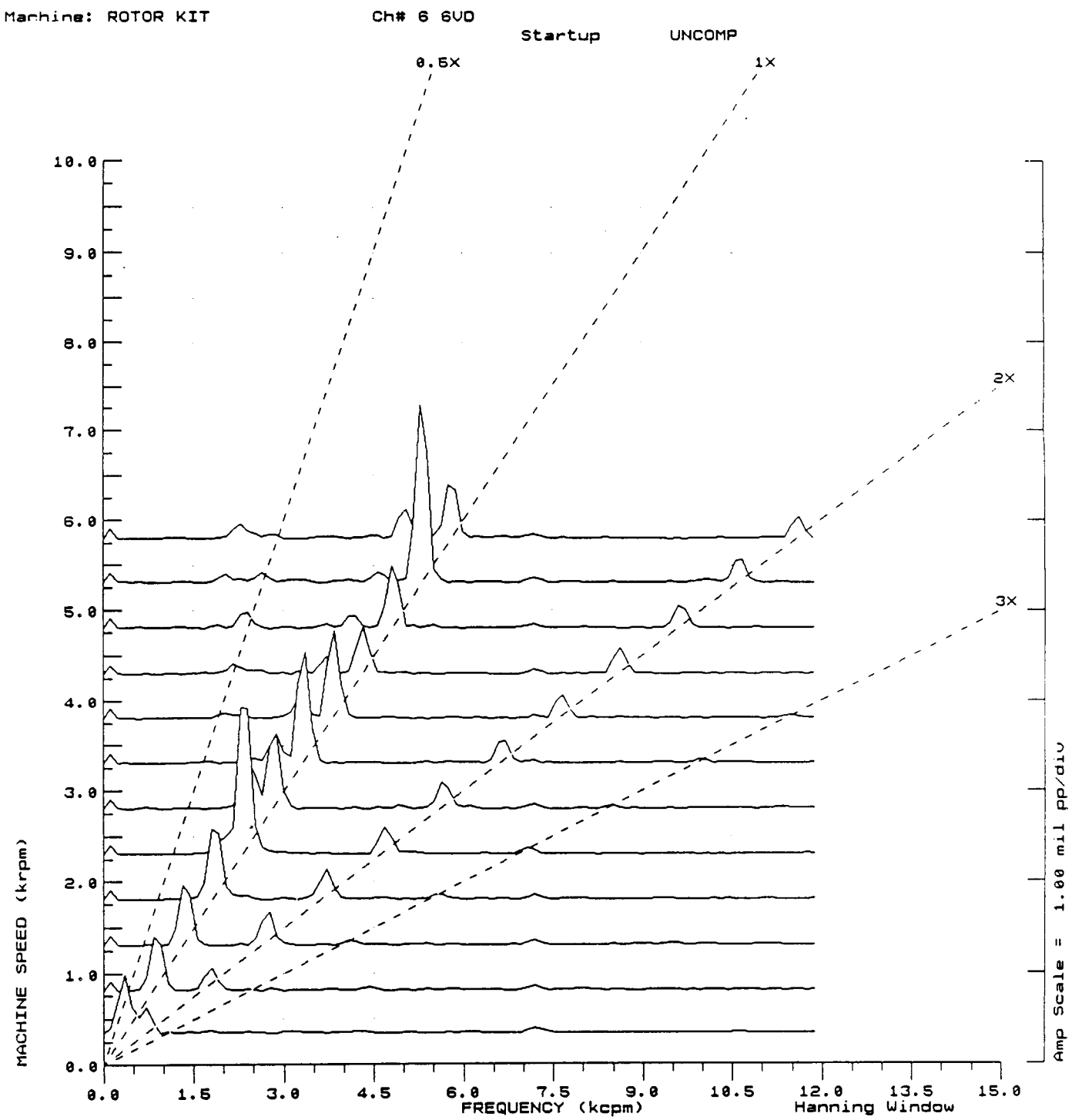

FIGURE 7.55 SPECTRUM CASCADE OF ROTOR VERTICAL VIBRATIONS DURING START–UP MEASURED AT CHANNEL #6. 15 PSI OIL PRESSURE AT SEAL SIMULATION BEARINGS. 0.0 INCH PRELOAD.

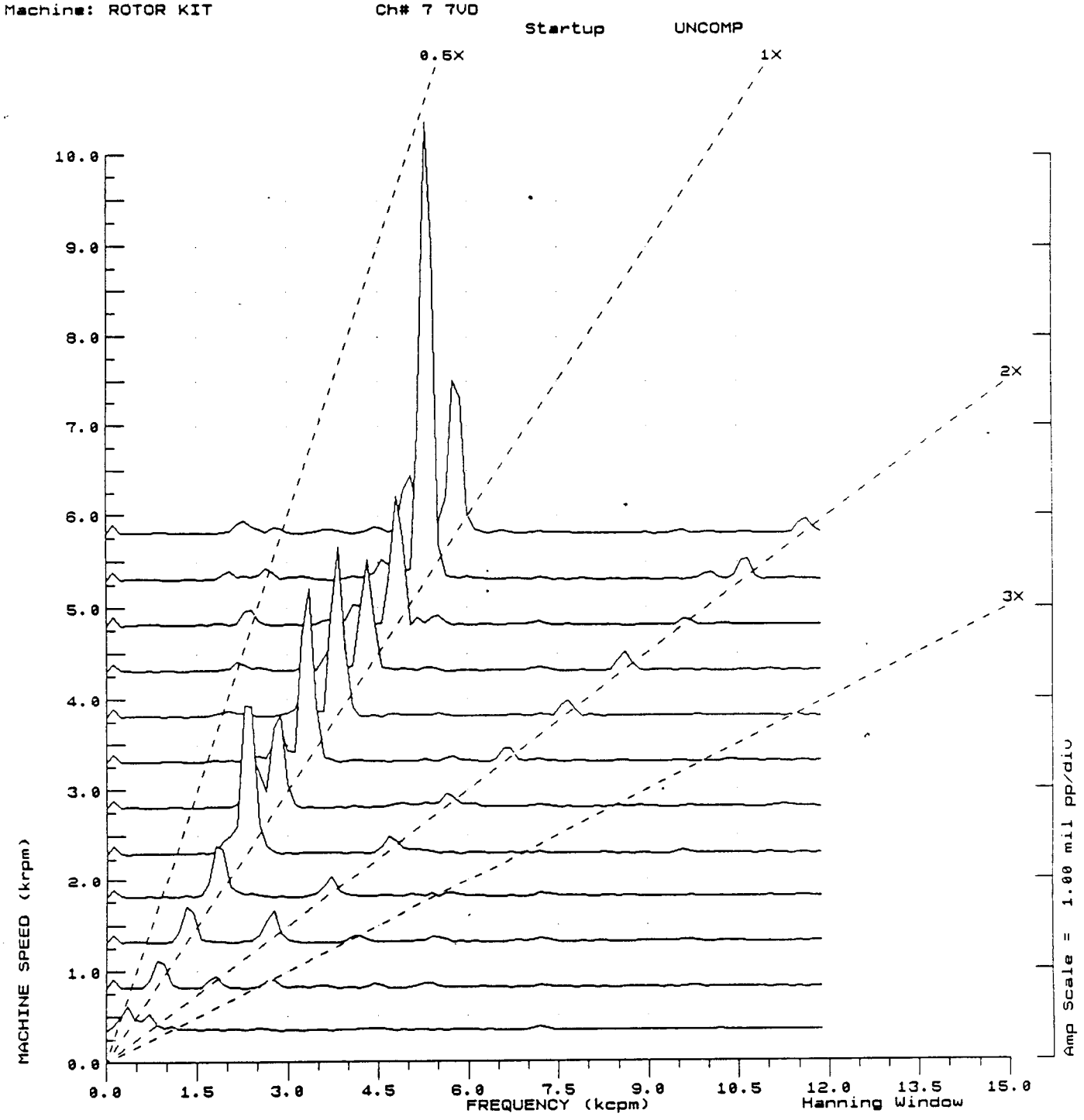

FIGURE 7.56 SPECTRUM CASCADE OF ROTOR VERTICAL VIBRATIONS DURING START–UP MEASURED AT CHANNEL #7. 15 PSI OIL PRESSURE AT SEAL SIMULATION BEARINGS. 0.0 INCH PRELOAD.

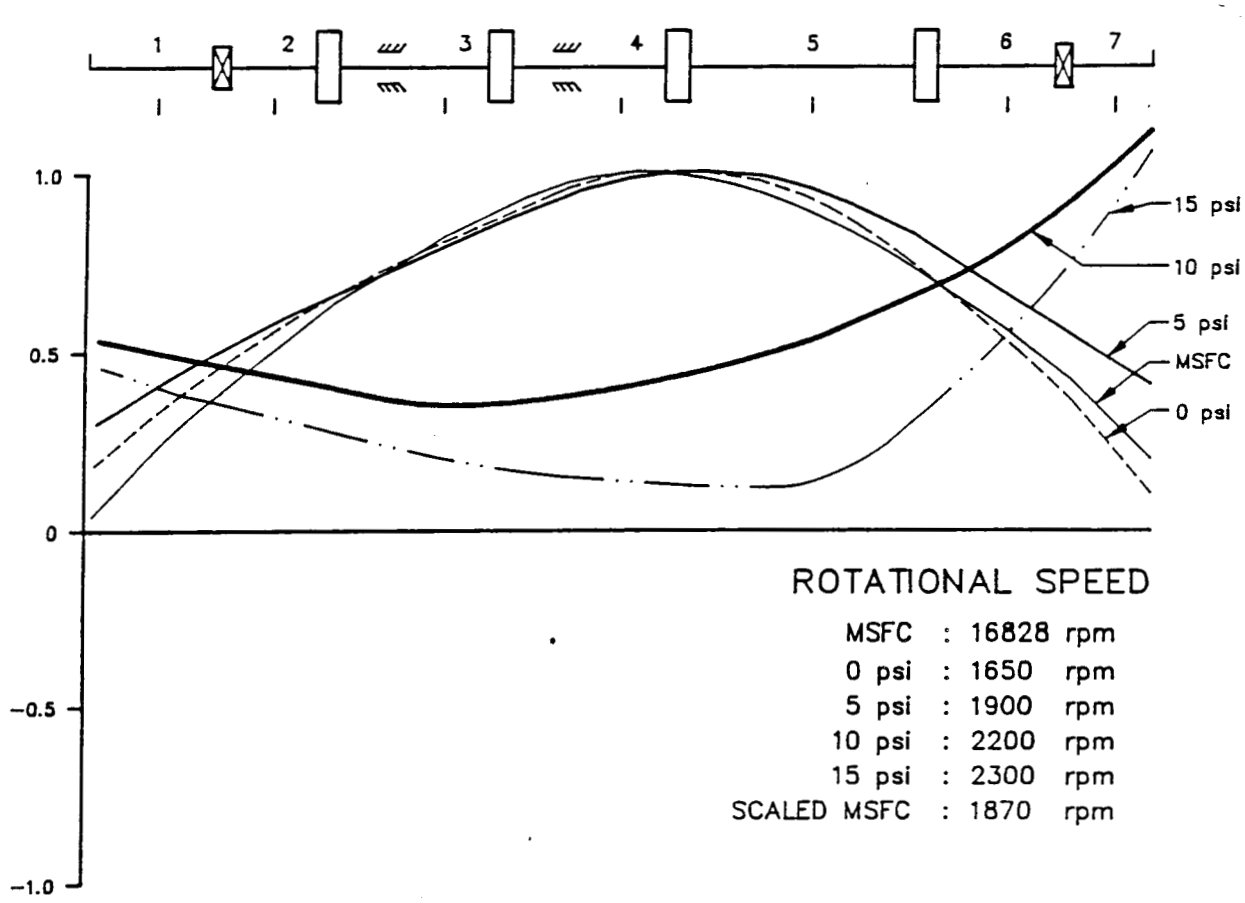

FIGURE 7.57 HPFTP SIMULATION ROTOR RIG 1ST MODE SHAPE VERSUS SEAL SIMULATING BEARING OIL PRESSURE REFERENCED TO HPFTP MODE SHAPE SUPPLIED BY NASA.

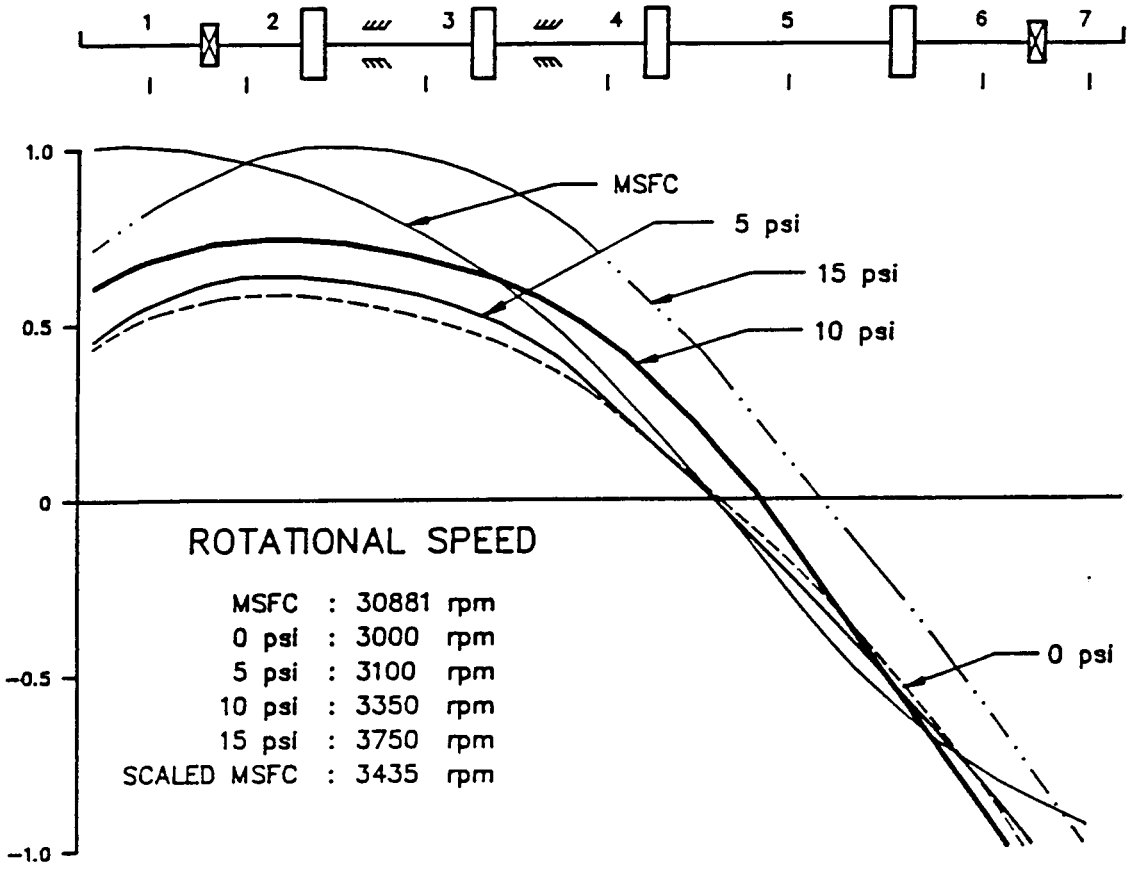

FIGURE 7.58 HPFTP SIMULATION ROTOR RIG 2ND MODE SHAPE VERSUS SEAL SIMULATING BEARING OIL PRESSURE REFERENCED TO HPFTP MODE SHAPE SUPPLIED BY NASA.

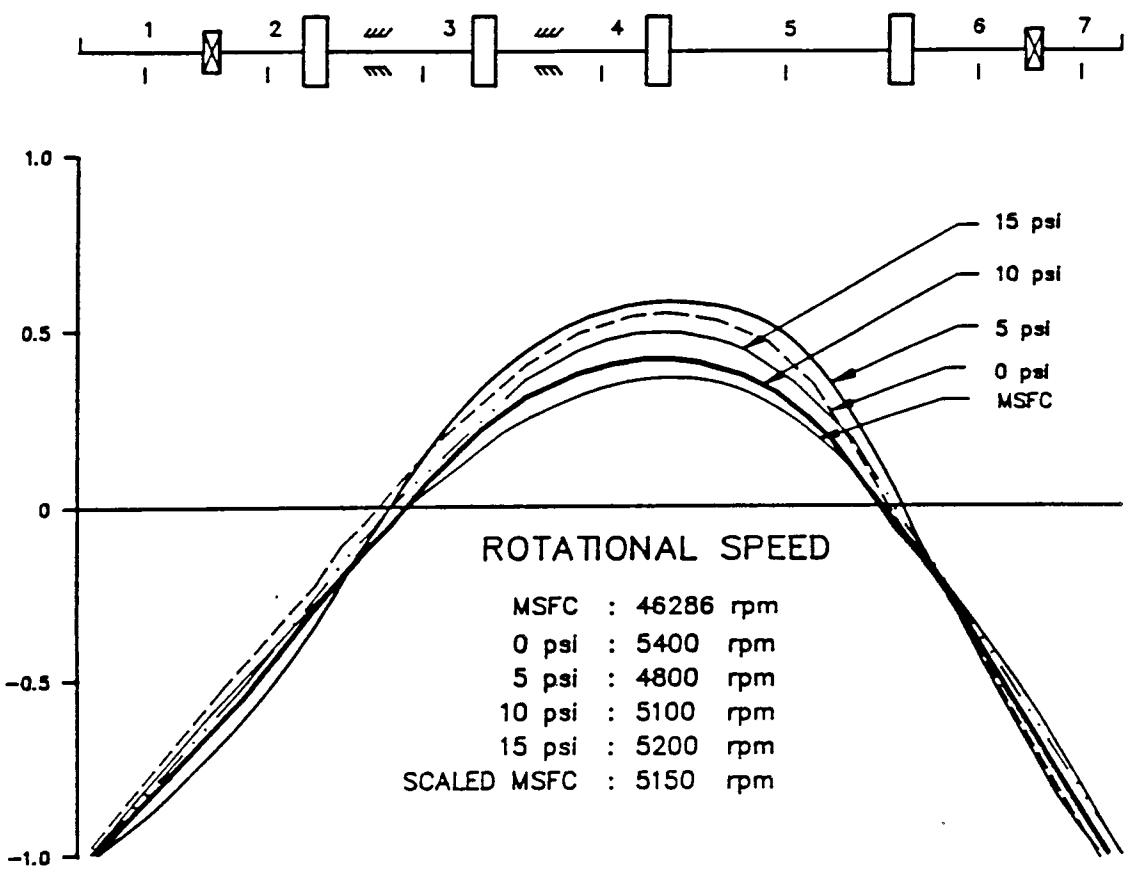

FIGURE 7.59 HPFTP SIMULATION ROTOR RIG 3RD MODE SHAPE VERSUS SEAL SIMULATING BEARING OIL PRESSURE REFERENCED TO HPFTP MODE SHAPE SUPPLIED BY NASA.

8. EFFECTS OF RUB ON ROTOR–AND–STATOR RUBBING SURFACES.

8.1 Objective of the Study

Friction plays an important role in rotor–to–stator rubbing. The objective of the first part of the study described in this chapter is to evaluate friction coefficient at the rubbing surfaces. Special blocks are designed to provide an easily replaceable rub surfaces for use in rotor/stator rub experiments. In order to explore the effects of surface finish and material contents, the blocks are constructed of different materials with varying surface finish qualities.

The objective of the second part of the study is to investigate the rub–related damage of the surfaces rubbing during a limited time.

8.2. Description of Rub Blocks for Surface Rub–Related Damage Study

The physical shape of the stator blocks is shown in Figure 8.1. Three types of stator simulating materials were used, namely 4140 steel, 2024 aluminum, and a free machining brass. The free machining brass varies from a standard "yellow brass" in that the alloy contains a small amount of lead. In all cases during the rotor–to–stator rub experiments, the rotor material was a tool steel drill rod (type 01).

The initial surface conditions of the rub blocks to be used in the rotor–to–stator rub tests were investigated by using a scanning electron microscope to photograph each of the surfaces. For reference, a series of photographs (Figs 8.2 to 8.7) presents two different surface finishes from the above–mentioned stator simulating materials prior to rubbing. The magnification was 200 times. The two surface finishes used are "as machined" and "polished." The polished surface is a 2–microinch RMS finish. The Table 8.1 lists some stator material properties of interest.

TABLE 8.1 Properties of Materials Used for Rub Blocks

Material	Modulus of Elast–icity	Density	Coefficient of Thermal Expansion	Thermal Conduct–ivity	Approx. Melting Temp.
	E, Mpsi	lb-sec^2/in^4	μ in/in-°F	BTU/hr-ft-°F	°F
Aluminum 2024	10.4	0.10	12.0	100	1200
Brass FM	15.5	0.31	10.5	45	1700
Steel 4140	30.0	0.28	6.3	22	2700

8.3 Friction Measurement Fixture and Coefficient of Friction Algorithm

The coefficient of friction test fixture (Fig. 8.8) when used with the rotor/measurement system shown in Figure 8.9 allows the determination of the coefficient of friction between the rub block and rotating shaft surfaces. The test fixture consists of a platform upon which the rub block under test is mounted. The rub block can be pressed against the rotating shaft by turning the normal force adjustment screw. By measuring the shaft deflection caused by the rub block pressing against the shaft with the fixture's eddy current

displacement probe, the normal force may be calculated by multiplying this displacement by the shaft's stiffness.

$$\text{Normal Force} = 2 \times (\text{shaft deflection}) \times \left[\frac{48\ EI}{1000\ L^3}\right] \tag{8.1}$$

where E = Young modulus; 3×10^7 [lb/in^2]

I = Shaft cross section moment of inertia; 9.7×10^{-4} [in^4]

L = Length of span between bearings; 12 [in]

The coefficient 1000 in the denominator corrects for units, allowing the shaft deflection to be measured in mils instead of inches. The additional multiplication factor of 2 is required because the bearing configuration creates two 12–inch shaft spans which must be deflected simultaneously, therefore doubling the stiffness. Combining constants, the formula (8.1) reduces to:

$$\text{Normal Force} = 1.62 \times (\text{shaft deflection}) \tag{8.2}$$

The tangential friction force can be determined by measuring the power of the motor and its rotational speed using the following formula:

$$\text{Friction Force} = V \times I \times (\text{Cos}\ (A)) \times \left[\frac{550}{746}\right] \times \left[\frac{1}{\omega}\right] \times \left[\frac{12}{0.187}\right] \times (0.85) \tag{8.3}$$

where V = Voltage across the motor [volts]

I = Current through the motor [amps]

A = Phase angle between V and I

(550/746) = Conversion factor from watts to ft·lbs/sec

ω = rotative speed [rad/sec]

(12/0.187) = Inverse of shaft radius [ft]

0.85 = Estimated motor efficiency factor

After combining the constants Eq. (8.3) reduces to the following:

$$\text{Friction Force} = \frac{40.21 \times V \times I \times (\text{Cos}\ (A))}{\omega}\ [\text{lbs}]$$

The coefficient of friction is then computed by dividing the friction force by the normal force, that is:

$$\text{Coefficient of Friction} = \frac{\text{Friction Force}}{\text{Normal Force}}$$

The rub experiments are performed using three different rub block materials each with two different surface finishes. This requires that the coefficient of friction be determined for each of the materials and surface finishes in order that the tangential force may be computed during the rub experiments. The experiments are performed at different rotative speeds. Therefore, this test system is also used to determine coefficient of friction sensitivity to rotative speed within the expected range of test speeds.

8.4 Results of Surface Friction Coefficient Measurements

The results of friction force versus normal force for the different rub block materials and the steel rotor are shown in Figure 8.10. As can be seen from the slope of the curves, the coefficient of friction is fairly constant in the range of applied forces. For aluminum/steel and brass/steel they are nearly the same and equal approximately 0.5, while the friction coefficient for steel/steel proved to be higher, at about 0.7.

8.5 Effects of Rotor–to–Stator Rub on Rubbing Surfaces

The rotor–to–stator rub causes rubbing surface damage due to friction, grinding, and wear. In this section the effects of rub on rubbing surface state are described. The results of the experimental testing are presented.

8.5.1 Test Procedure

A two–disk rotor rig was used to investigate the effect of material and surface properties during rotor–to–stator rub (Fig. 8.11). The operating speed of the rotor was held at 1000 rpm. With the rotor shaft diameter of 0.375 inches, this provides a surface velocity of 98.17 ft/min (0.499 m/s). The estimated normal force at rubbing surfaces during the test was 3 lbs. All testing was conducted at room temperature without any external source of lubrication (dry rub). The axial position of the rub block along with system geometry is given in Figure 8.12.

During experiments, the rotor was exposed to rub for two different durations of time. Actual rotor–to–stator contact was 15 and 60 seconds. Although arbitrarily selected, these time periods provided results with reasonable comparative values. Samples were then closely inspected and selected for further analysis via electron–microscopy (scanning electron microscope). Photographs of the individual stator simulating rub blocks and the corresponding rotor sections after rubbing experiments are presented in Figures 8.13 to 8.24.

8.5.2 Metallographic Analysis of Rub Surface Photographs

Initial inspection of the "polished" samples after rub proved to be inconclusive as surface conditions could not effectively be maintained for comparative purposes. The polished 2–microinch surface finish was corrupted so rapidly that further analysis was not considered practical. Testing of the different material types, run over the two rub durations, provided more conclusive results. Figures 8.13 to 8.24 illustrate the effects of rub for two time durations (15 sec. and 60 sec.) on each of the three stator–simulating materials (aluminum, brass, and steel). These photographs indicate a consistent pattern in the deformation process.

The stator–simulating material surfaces presented in Figures 8.13, 8.15, 8.17, 8.19, 8.21, and 8.23 (with the exception of Figure 8.17) are photographs of the rub zone trailing edge. The softer more ductile materials, namely aluminum and brass, indicate a significant "smearing" action taking place. The surfaces become more uniform with time. The

associated rotor shaft sections (Figures 8.14, 8.16, 8.18, 8.20, 8.22, and 8.24) show the build–up of stator–simulating materials on the shaft as time progresses. Figures 8.25 to 8.30 are full–view photographs of each of the rub blocks and the associated section of shaft. The areas of rub damages indicated by the arrows are plainly visible.

The purpose of the rotor–to–stator rub tests conducted with aluminum and brass was to investigate rub phenomena of dissimilar materials. "Dissimilarity" refers here to the different electrical, chemical, and mechanical properties of the materials at the atomic and macro levels. Electrical differences occur in the atoms' shell of valence electrons with the number of valence electrons controlling the bonding properties between atoms. At the macro level, chemical differences exist. Mechanical properties are largely determined by the amounts of the different elements present, as well as the crystal structure and grain structure induced by processes used to produce the final form of each material. To alter the form of a material requires an energy transfer of some type. In these experiments, rub provides the primary mode of energy transfer. Rub generates normal and tangential forces at the rotor–to–stator contact area initiating changes in rotor dynamic motion, as well as causing material surface deformation.

Figures 8.21 to 8.24 are photographs of the steel samples used for stator simulation and associated rotor shaft sections respectively. The surfaces appear less "smeared" and more abraded than those for aluminum and brass presented in previous photographs. During rub tests using the steel rub blocks with the steel rotor shaft, extreme, almost violent vibration, was experienced given enough time (2–3 minutes). This violent vibration was similar in nature to the rub phenomena known as "full annular rub." The violent vibration in this specific test exhibited rotor shaft backwards precessional motion, similar to that during a classical case of full annular rub. The apparatus used in these tests limited, however, the rotor motion to the 180–degree surface of the stator–simulating rub block. Lack of the restraint within the remaining 180–degree arc allows the shaft to vibrate freely with large amplitudes. Full annular rub restrains rotor motion within a full 360 degrees, limiting, therefore, the maximum vibration amplitude in the plane of rub to the available stator (bearing or seal) clearance.

8.5.3 Conclusions From Material Property Experiments

The results from the rotor–to–stator material property rub tests indicate that rub surfaces, as well as system vibrations, can vary based on the mechanical characteristics of the associated materials. The softer, more ductile stator–simulating materials are "smeared" during rub over the short period of time. Given longer periods of time, the stator–simulating materials build up on the shaft, generating a more uniform, yet roughened surface. The amount of material build–up during the rub process will, however, also be a function of the affinity of one material to another, as in the case with dissimilar materials, material temperatures, and rub contact normal forces.

The ductile stator–simulating materials may allow actual removal of material from the area of rub, thus increasing rotor–to–stator clearances leading to an alleviation of the rub condition, although perhaps only temporarily. Given enough time, the rub condition may transfer sufficient material from the stator to the rotor, for the rub interface to no longer act as that of dissimilar materials. This has a significant effect on the local coefficient of friction.

Inspection of the rotor on the HPFTP simulating rig after experiencing full annular rub within the aluminum seal revealed a heavy aluminum deposits on the rotor shaft at the contact surface. This deposit of aluminum on the steel rotor shaft is an example of material transfer. The violent vibration experienced during the rotor–to–stator rub tests on the two–mode rotor rig, as well as during previous tests with the HPFTP simulating rotor rig, led to similar, significant damage of the seal.

8.6 Summary

In this chapter the results of surface effects of rotor–to–stator rub were investigated. The specially designed fixture provided the values of the dry friction coefficients for materials used for the stator and rotor. The metallographic analysis of the rotor and stator surfaces after 15 seconds and 60 seconds of rotor–to–stator rubbing brought an insight on the effect of the dissimilarity of the rotor and stator initial surface finish on the rub–related damage.

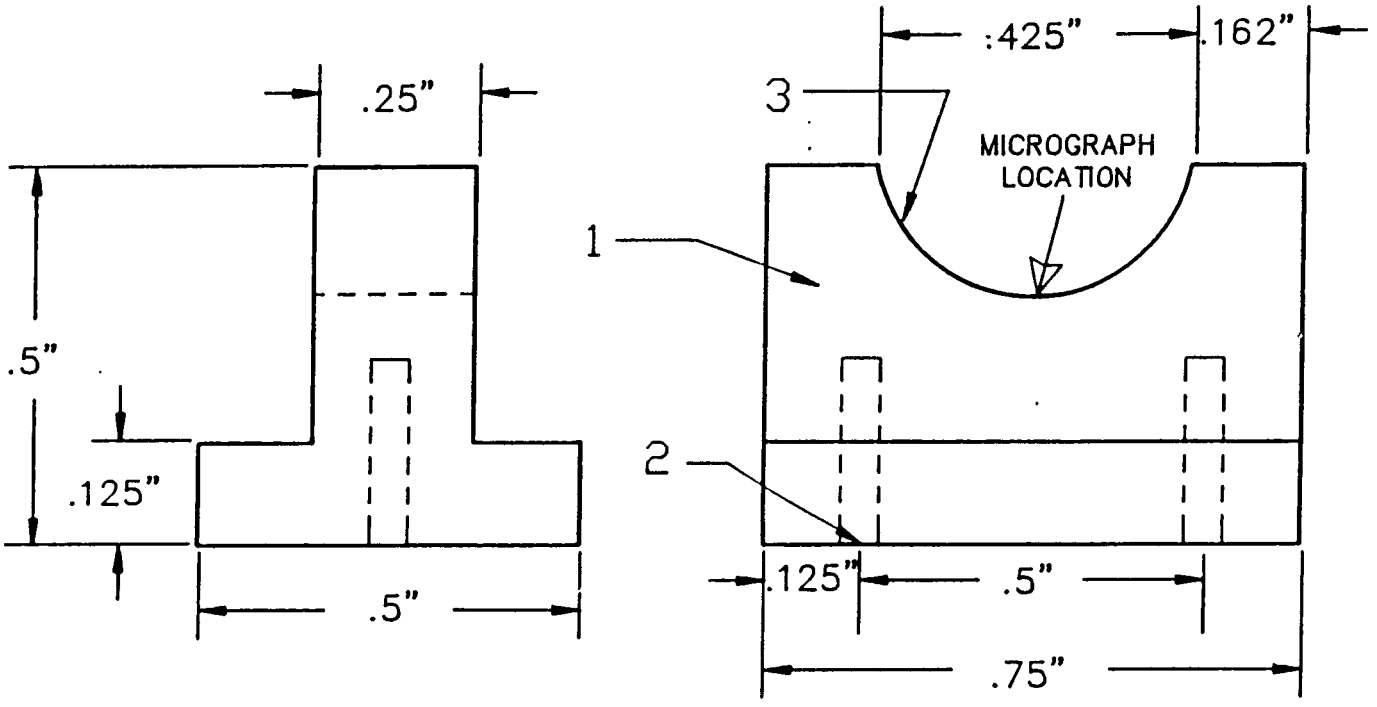

1. Rub Block Body
2. Tapped Mounting Holes (4–40)
3. Rub Surface

FIGURE 8.1 RUB BLOCK.

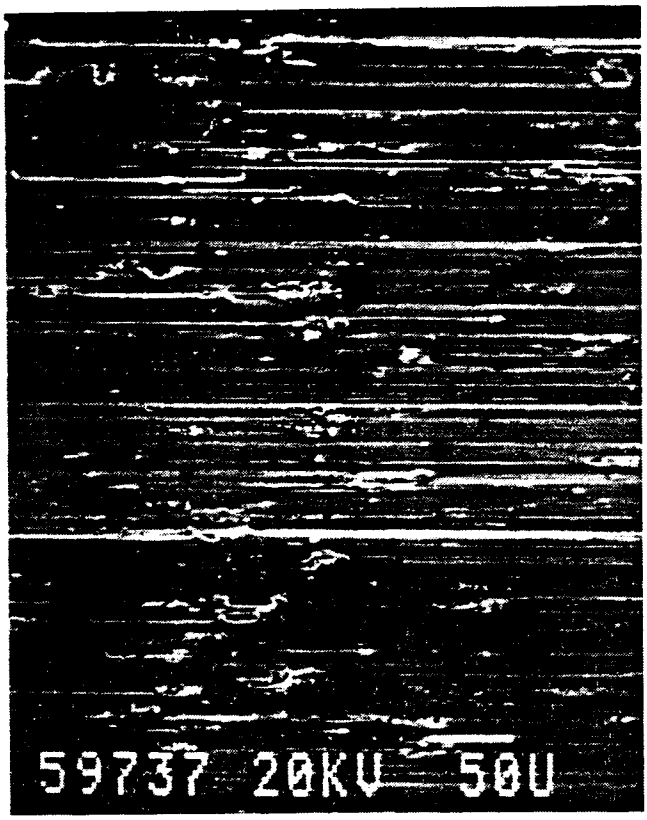

FIGURE 8.2 2024 ALUMINUM, AS MACHINED SURFACE FINISH MAGNIFIED 200 TIMES. PHOTO # 59737.

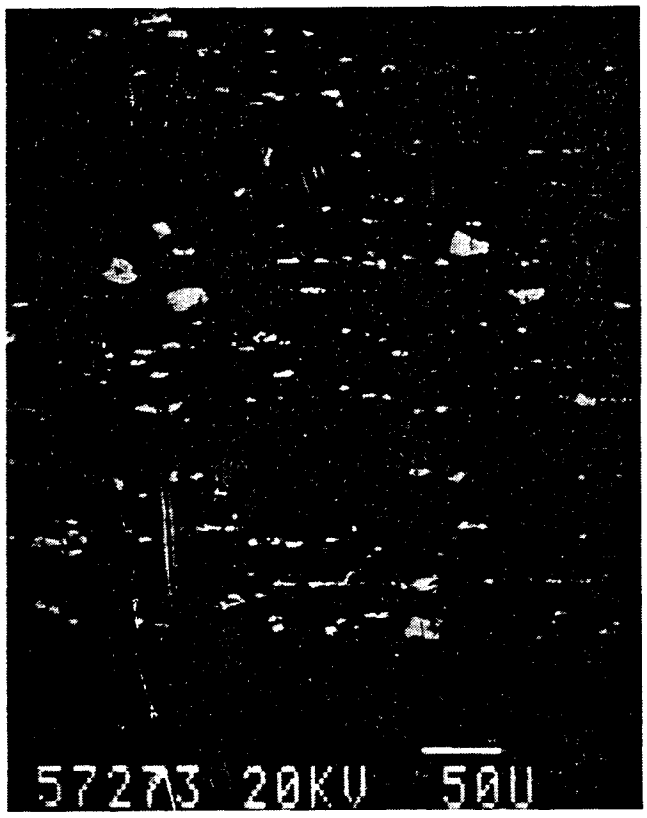

FIGURE 8.3 2024 ALUMINUM, POLISHED SURFACE FINISH MAGNIFIED 200 TIMES. PHOTO # 57273.

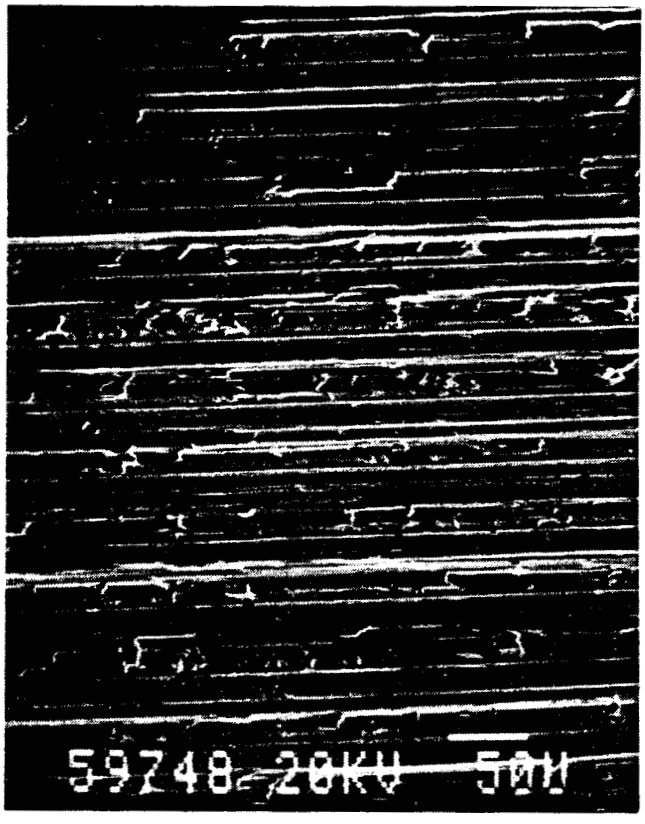

FIGURE 8.4 BRASS, AS MACHINED SURFACE FINISH MAGNIFIED 200 TIMES (FREE CUTTING, COLD DRAWN). PHOTO # 59748.

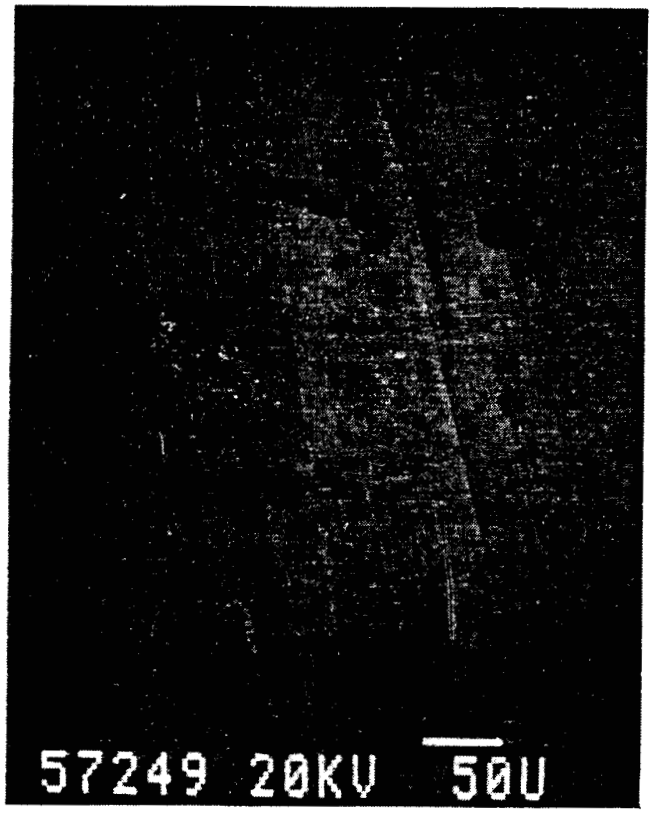

FIGURE 8.5 BRASS, POLISHED SURFACE FINISH MAGNIFIED 200 TIMES. (FREE CUTTING, COLD DRAWN). PHOTO # 59749.

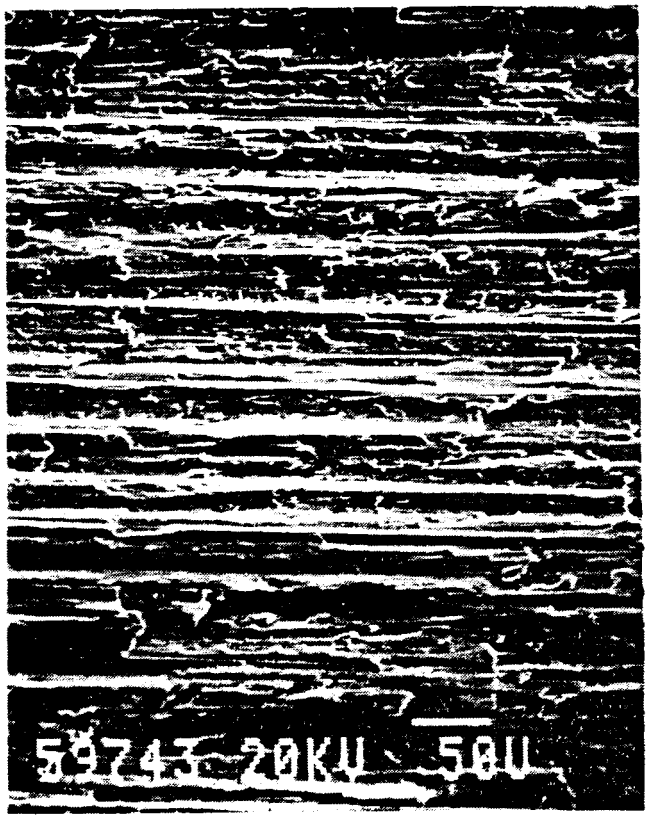

FIGURE 8.6 4140 STEEL, AS MACHINED SURFACE FINISH MAGNIFIED 200 TIMES. PHOTO # 59743.

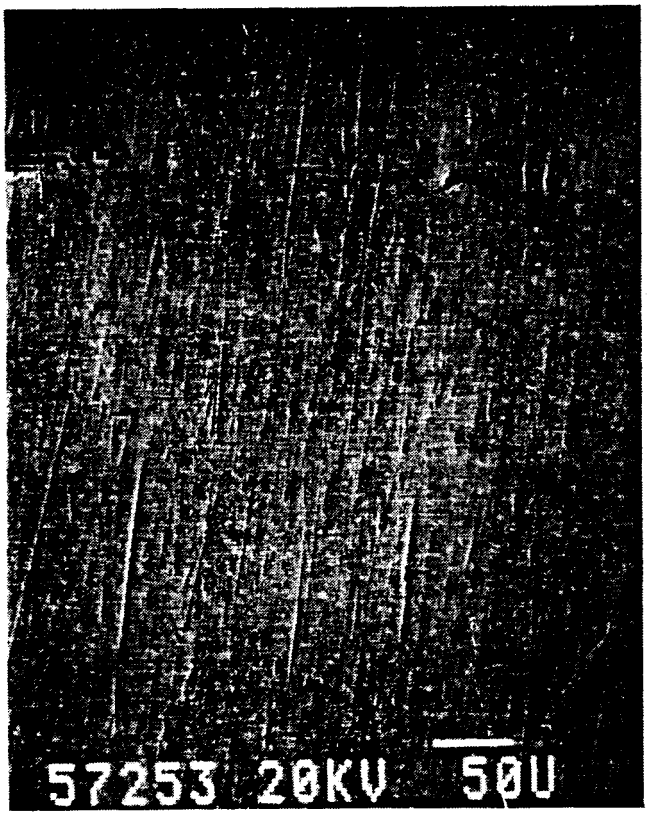

FIGURE 8.7 4140 STEEL, POLISHED SURFACE FINISH MAGNIFIED 200 TIMES. PHOTO # 59753.

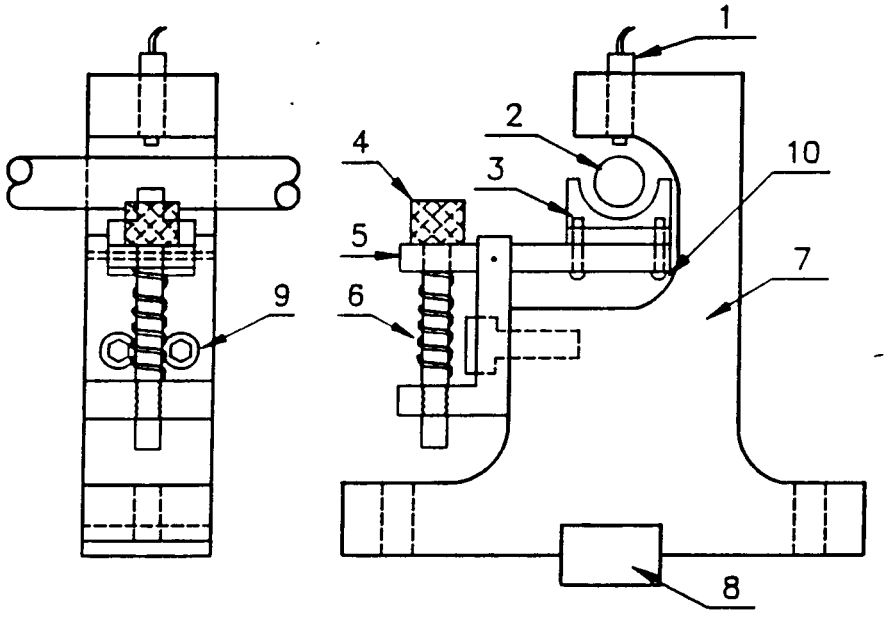

1. Eddy Current Displacement Probe
2. Test Shaft
3. Test Rub Block
4. Normal Force Adjustment Screw
5. Pivot Assembly
6. Return Spring
7. Probe Holder Body
8. Alignment Key
9. Pivot Assembly Mounting Bolts
10. Rub Block Mounting Screws

FIGURE 8.8 COEFFICIENT OF FRICTION TEST FIXTURE.

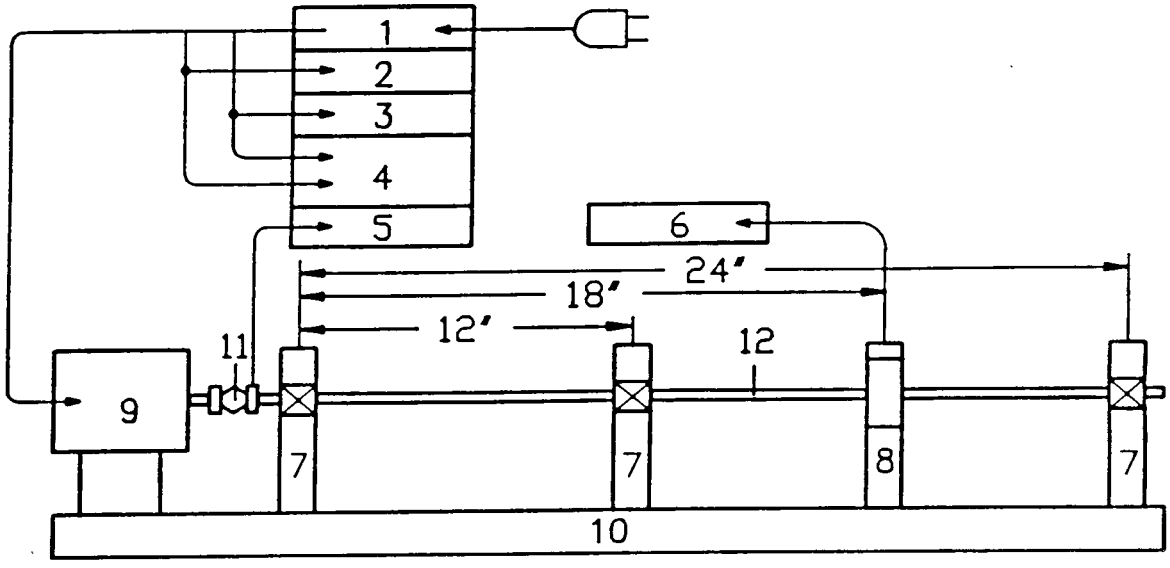

1. VARIAC
2. AC VOLTMETER
3. AC AMMETER
4. OSCILLOSCOPE
5. TACHOMETER
6. DC VOLTMETER
7. ROLLING ELEMENT BEARINGS
8. COEFFICIENT OF FRICTION TEST FIXTURE
9. ELECTRIC MOTOR
10. ROTOR BASE
11. FLEXIBLE COUPLING
12. TEST SHAFT

FIGURE 8.9 COEFFICIENT OF FRICTION TEST SYSTEM.

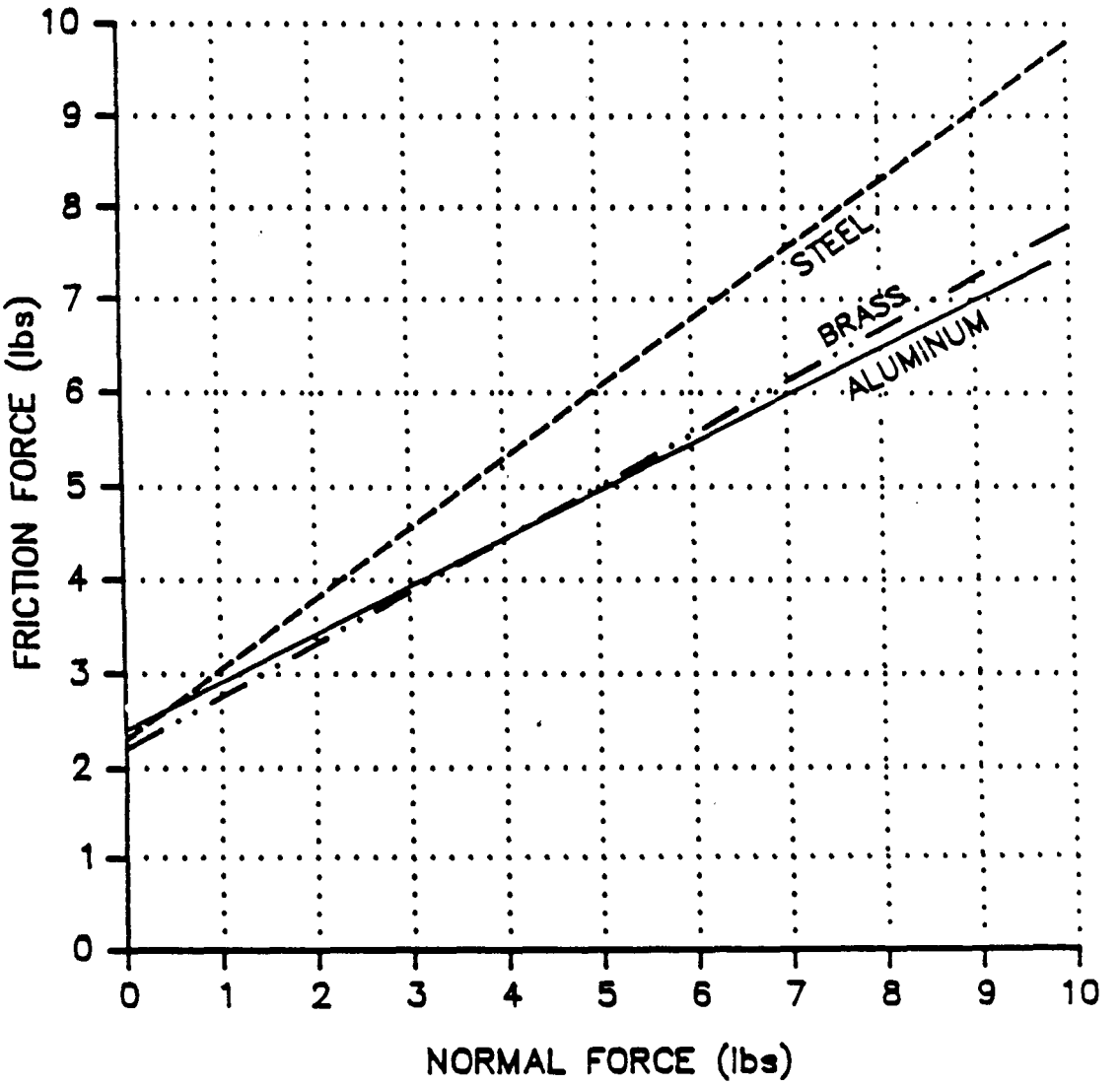

FIGURE 8.10 TEST RESULTS: FRICTION FORCE VERSUS NORMAL FORCE.

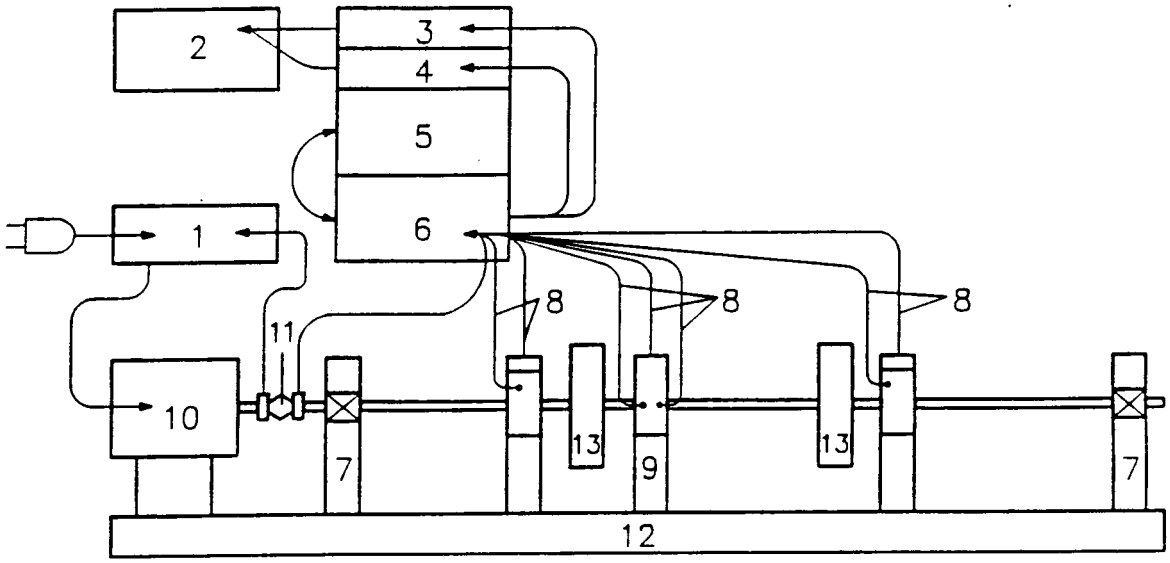

1. MOTOR SPEED CONTROL
2. COMPUTER
3. TRACKING FILTER
4. SPECTRUM ANALYZER
5. TAPE RECORDER
6. AMPLIFIER RACK
7. BRONZE BEARINGS
8. X–Y EDDY CURRENT DISPLACEMENT PROBES
9. RUB FIXTURE
10. ELECTRIC MOTOR
11. FLEXIBLE COUPLING
12. ROTOR BASE
13. 3 INCH DIAMETER DISCS

FIGURE 8.11 TWO–MODE–ROTOR RIG USED FOR RUBBING SURFACE EFFECT TESTS.

A – Electric Motor
B – Flexible Coupling
C – Inboard Bronze Bearing
D – Electrical Contact Device
E – Inboard X–Y Displacement Probe Mount
F – Inboard Mass
G – Rub Fixture/X–Y Displacement Probes
H – Outboard Mass
I – Outboard X–Y Displacement Probe Mount
J – Outboard Bronze Bearing
K – Rotor Shaft
L – Rotor Base

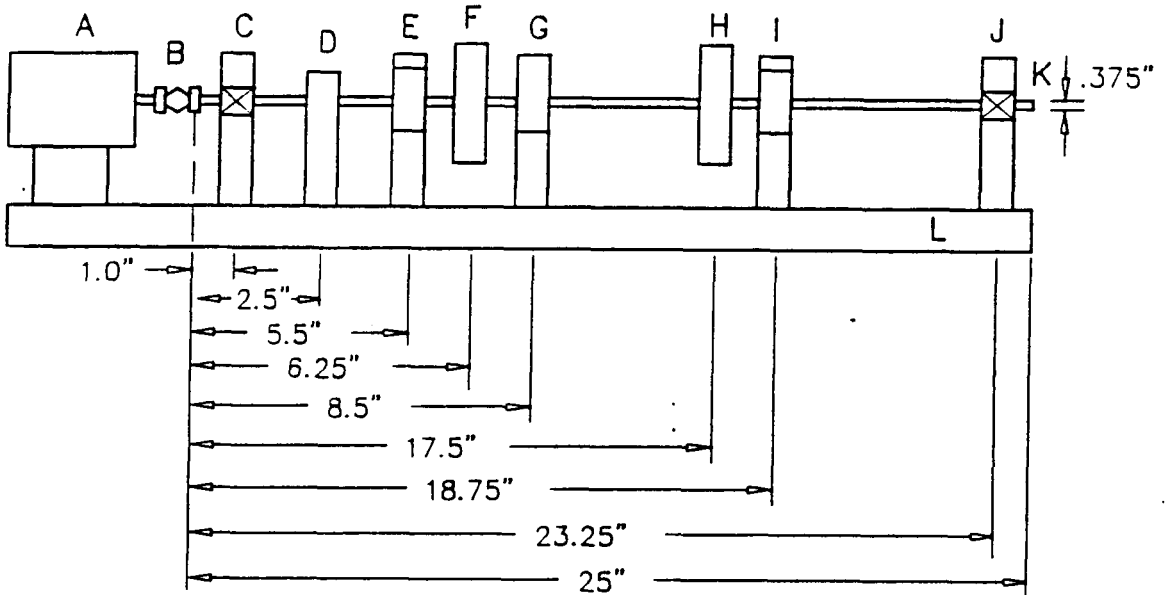

FIGURE 8.12 TWO–MODE–ROTOR RIG GEOMETRY.

FIGURE 8.13 2024 ALUMINUM, STATOR–SIMULATING RUB SURFACE AFTER 15 SECONDS OF RUB AGAINST THE STEEL SHAFT. MAGNIFICATION 50 TIMES. PHOTO # 50017.

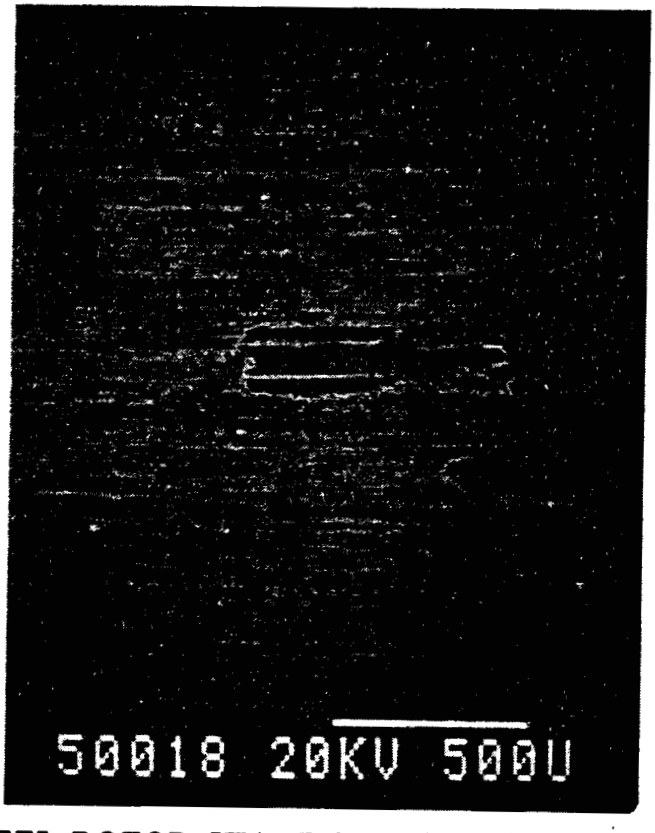

FIGURE 8.14 STEEL ROTOR SHAFT SURFACE AFTER 15 SECONDS OF RUB AGAINST ALUMINUM STATOR. MAGNIFICATION 50 TIMES. PHOTO # 50018.

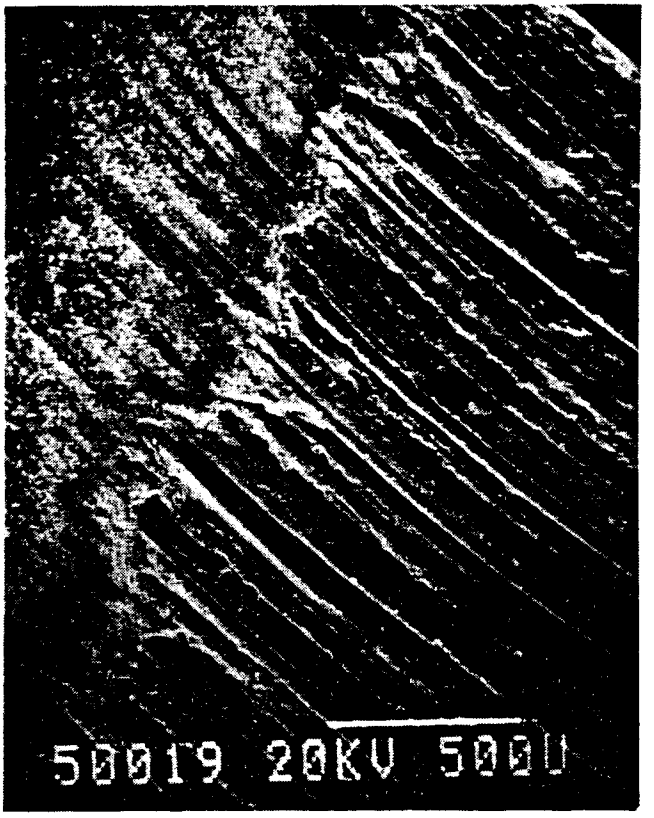

FIGURE 8.15 2024 ALUMINUM, STATOR–SIMULATING RUB SURFACE AFTER 60 SECONDS OF RUB AGAINST THE STEEL SHAFT. MAGNIFICATION: 50 TIMES. PHOTO # 50019.

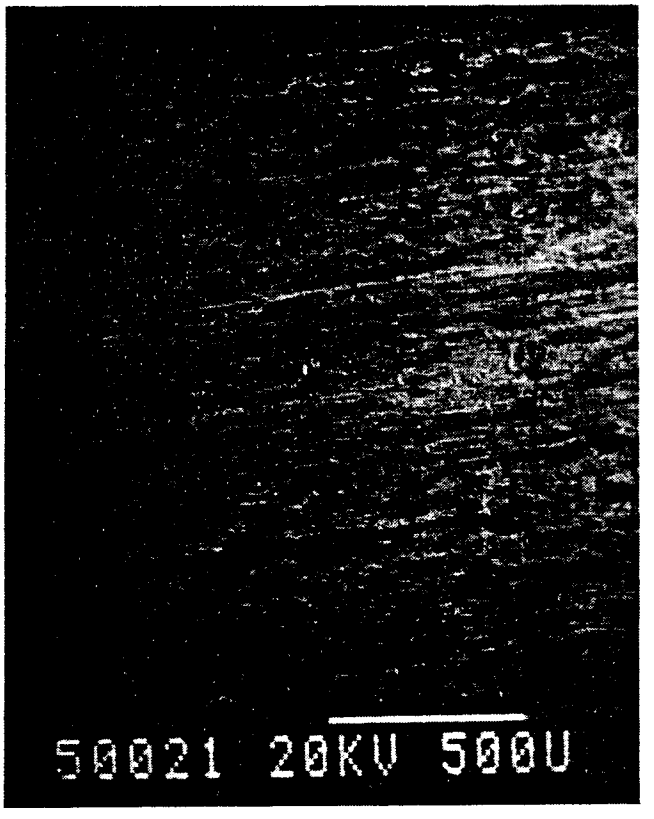

FIGURE 8.16 STEEL ROTOR SHAFT SURFACE AFTER 60 SECONDS OF RUB AGAINST ALUMINUM STATOR. MAGNIFICATION: 50 TIMES. PHOTO # 50021.

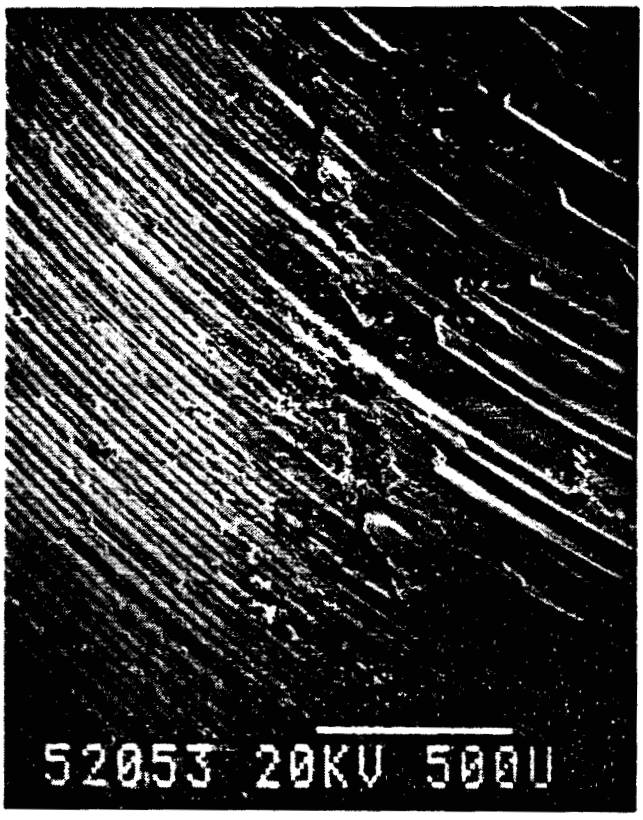

FIGURE 8.17 BRASS (FM), STATOR–SIMULATING RUB SURFACE AFTER 15 SECONDS OF RUB AGAINST THE STEEL SHAFT. MAGNIFICATION: 50 TIMES. PHOTO # 52053.

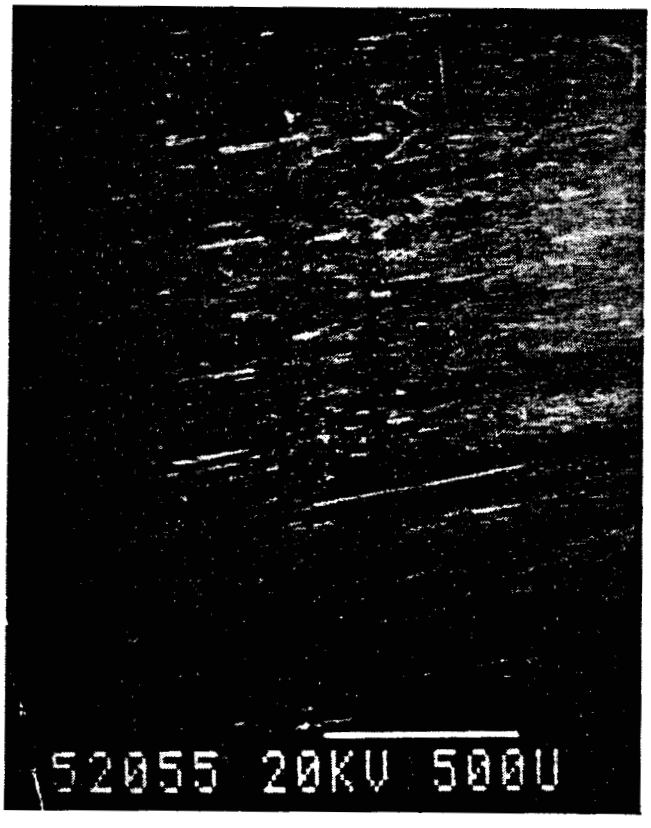

FIGURE 8.18 STEEL ROTOR SHAFT SURFACE AFTER 15 SECONDS OF RUB AGAINST BRASS STATOR. MAGNIFICATION: 50 TIMES. PHOTO # 52055.

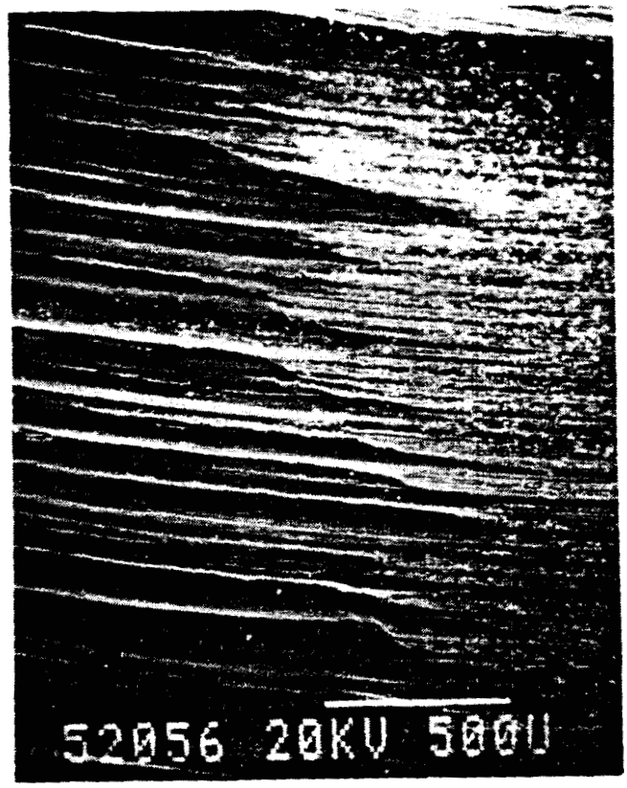

FIGURE 8.19 BRASS (FM), STATOR–SIMULATING RUB SURFACE AFTER 60 SECONDS OF RUB AGAINST THE STEEL SHAFT. MAGNIFICATION: 50 TIMES. PHOTO # 52056.

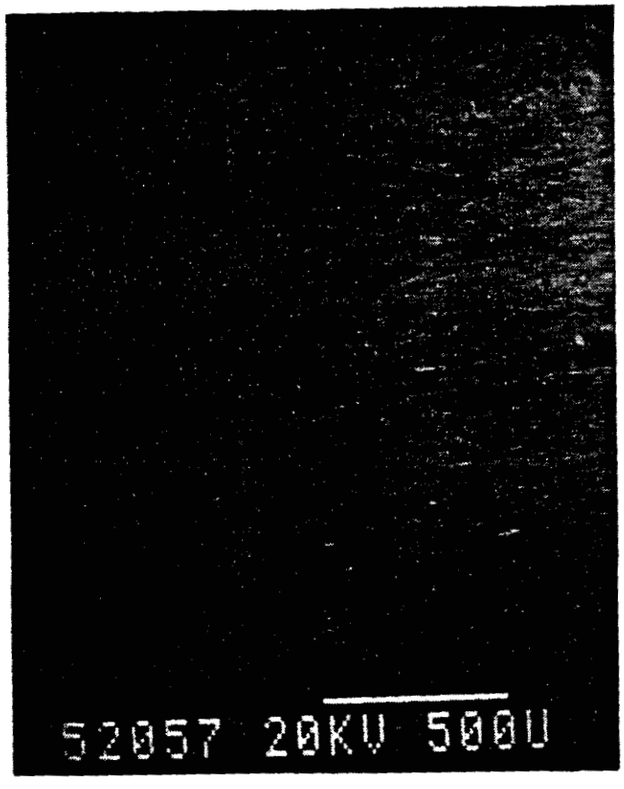

FIGURE 8.20 STEEL ROTOR SHAFT SURFACE AFTER 60 SECONDS OF RUB AGAINST BRASS STATOR. MAGNIFICATION: 50 TIMES. PHOTO # 52057.

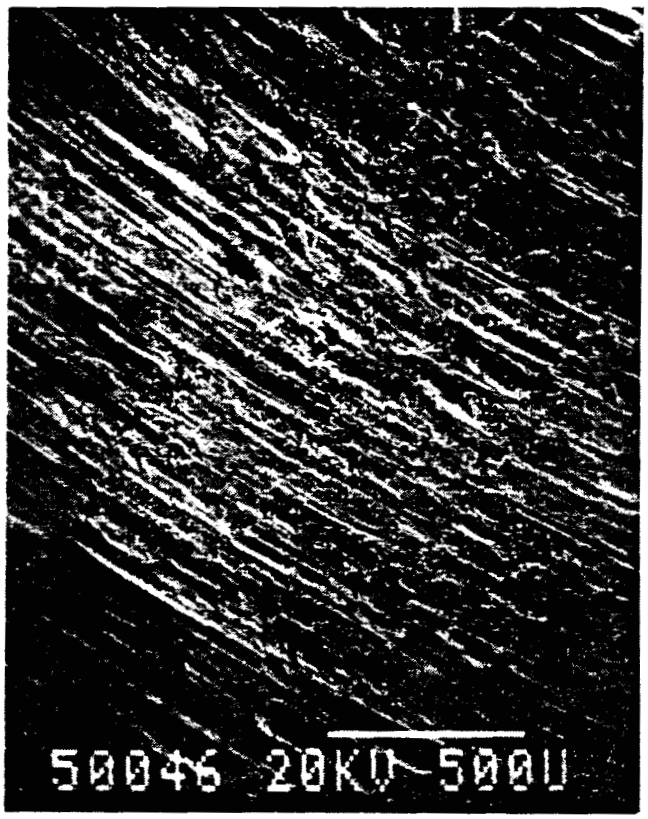

FIGURE 8.21 4140 STEEL, STATOR–SIMULATING RUB SURFACE AFTER 15 SECONDS OF RUB AGAINST THE STEEL SHAFT. MAGNIFICATION: 50 TIMES. PHOTO # 50046.

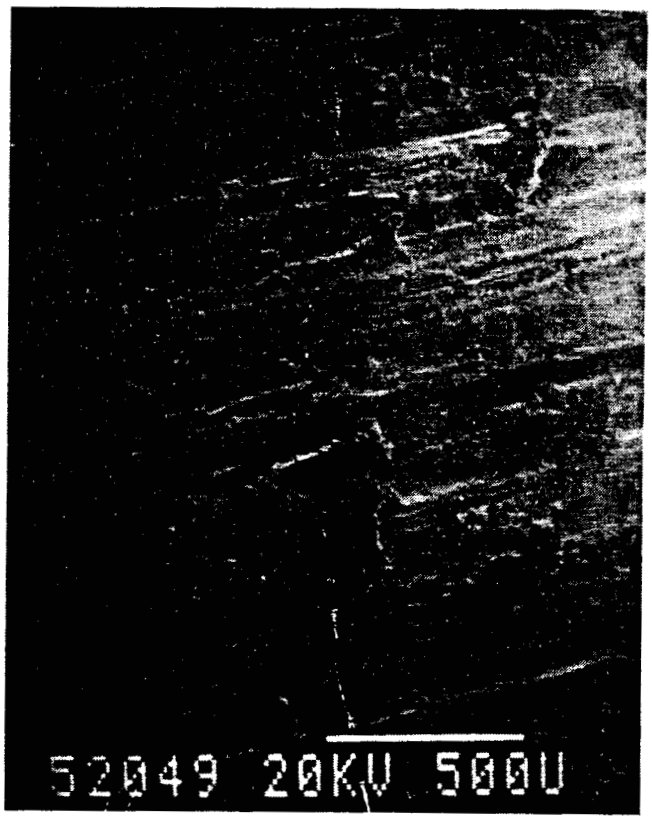

FIGURE 8.22 STEEL ROTOR SHAFT SURFACE AFTER 15 SECONDS OF RUB AGAINST STEEL STATOR. MAGNIFICATION: 50 TIMES. PHOTO # 52049.

FIGURE 8.23 4140 STEEL, STATOR–SIMULATING RUB SURFACE AFTER 60 SECONDS OF RUB AGAINST THE STEEL SHAFT. MAGNIFICATION: 50 TIMES. PHOTO # 52050.

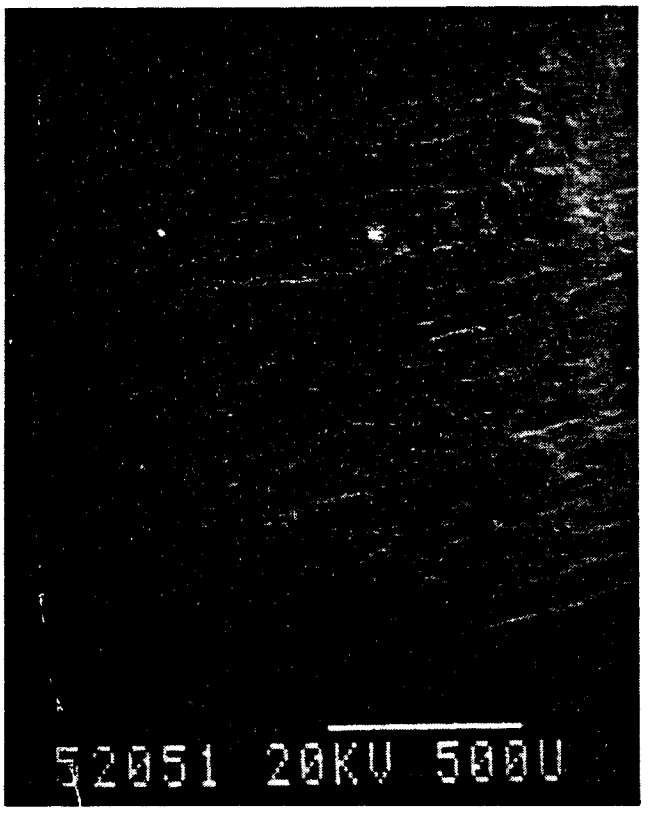

FIGURE 8.24 STEEL ROTOR SHAFT SURFACE AFTER 60 SECONDS OF RUB AGAINST STEEL STATOR. MAGNIFICATION: 50 TIMES. PHOTO # 52051.

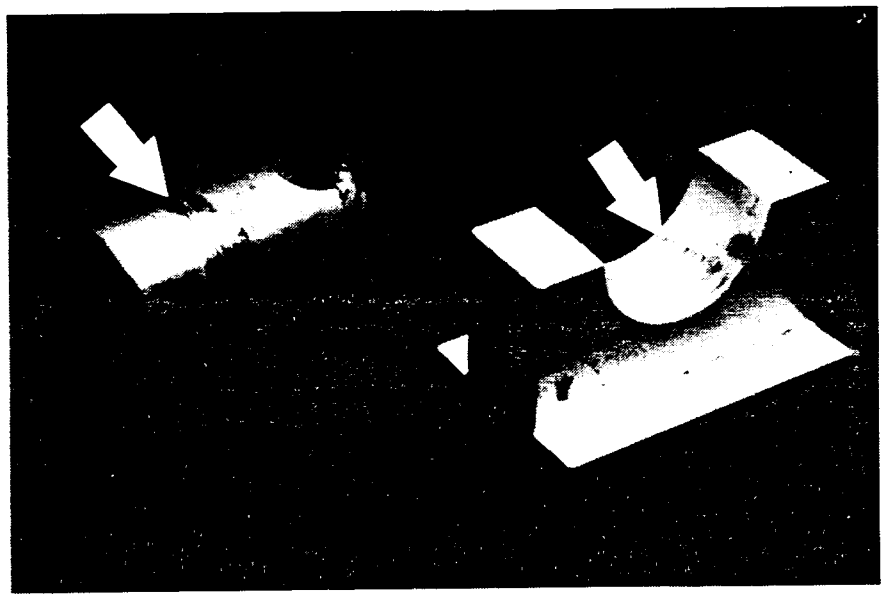

FIGURE 8.25 ALUMINUM RUB BLOCK AND CORRESPONDING SHAFT SECTION AFTER 15 SECONDS OF ROTOR–TO–STATOR RUBBING AT 1000 RPM. ARROWS INDICATE SURFACE DEFORMATION AND MATERIAL DEPOSIT ON STATOR SIMULATING RUB BLOCK AND SHAFT SECTION RESPECTIVELY. MICROPHOTOGRAPHS IN FIGURES 8.13 AND 8.14 SHOW THE DAMAGED SURFACES.

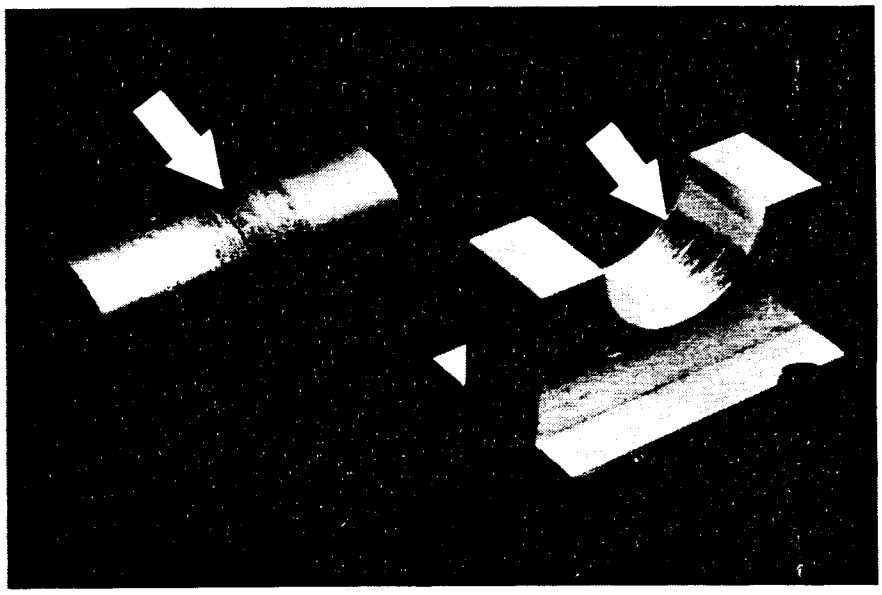

FIGURE 8.26 ALUMINUM RUB BLOCK AND CORRESPONDING SHAFT SECTION AFTER 60 SECONDS OF ROTOR–TO–STATOR RUBBING AT 100O RPM. ARROWS INDICATE SURFACE DEFORMATION AND MATERIAL DEPOSIT ON STATOR SIMULATING RUB BLOCK AND SHAFT SECTION RESPECTIVELY. MICROPHOTOGRAPHS IN FIGURES 8.15 AND 8.16 SHOW THE DAMAGED SURFACES.

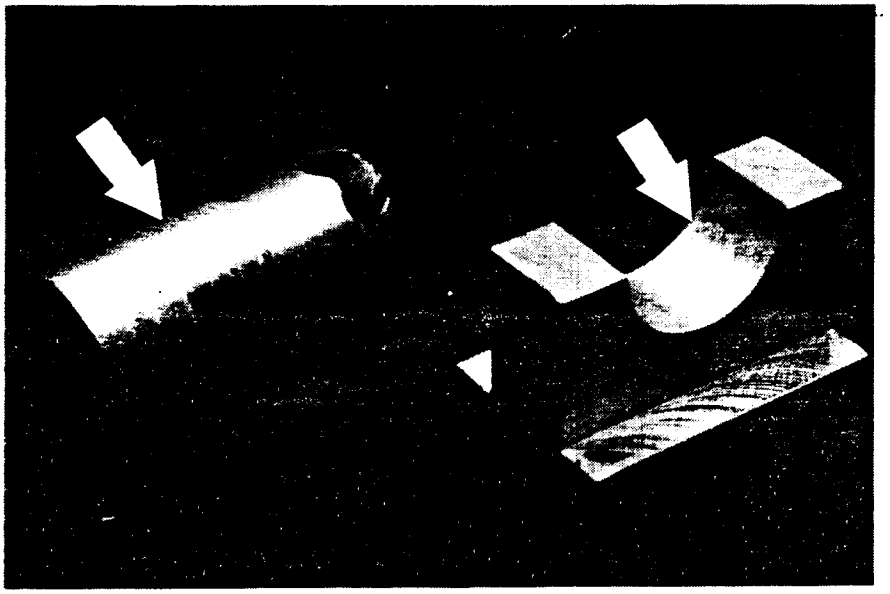

FIGURE 8.27 STEEL RUB BLOCK AND CORRESPONDING SHAFT SECTION AFTER 15 SECONDS OF ROTOR–TO–STATOR CONTACT. ARROWS INDICATE SURFACE DEFORMATION AND MATERIAL DEPOSIT ON STATOR SIMULATING RUB BLOCK AND SHAFT SECTION RESPECTIVELY. MICROPHOTOGRAPHS IN FIGURES 8.21 AND 8.22 SHOW THE DAMAGED SURFACES.

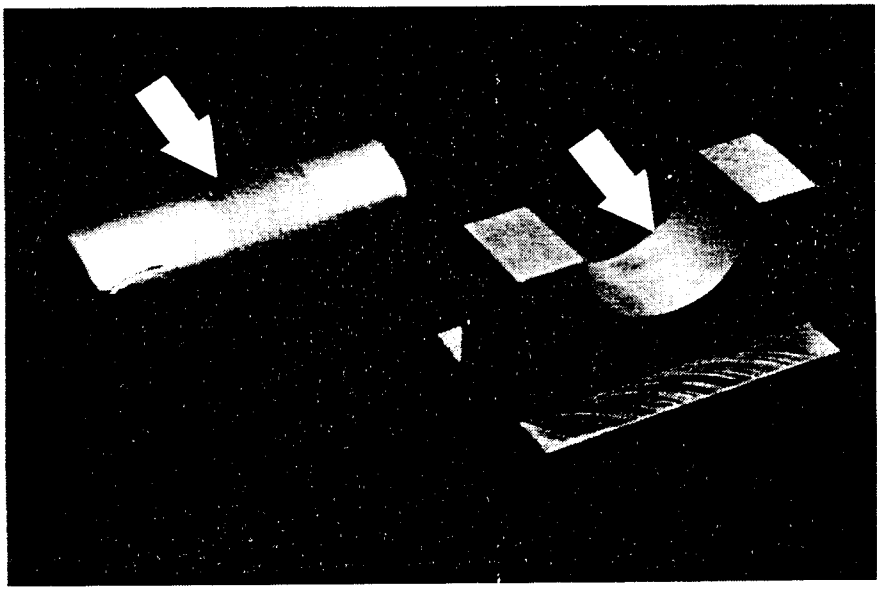

FIGURE 8.28 STEEL RUB BLOCK AND CORRESPONDING SHAFT SECTION AFTER 60 SECONDS OF ROTOR–TO–STATOR RUBBING AT 1000 RPM. ARROWS INDICATE SURFACE DEFORMATION AND MATERIAL DEPOSIT ON STATOR SIMULATING RUB BLOCK AND SHAFT SECTION RESPECTIVELY. MICROPHOTOGRAPHS IN FIGURES 8.23 AND 8.24 SHOW THE DAMAGED SURFACES.

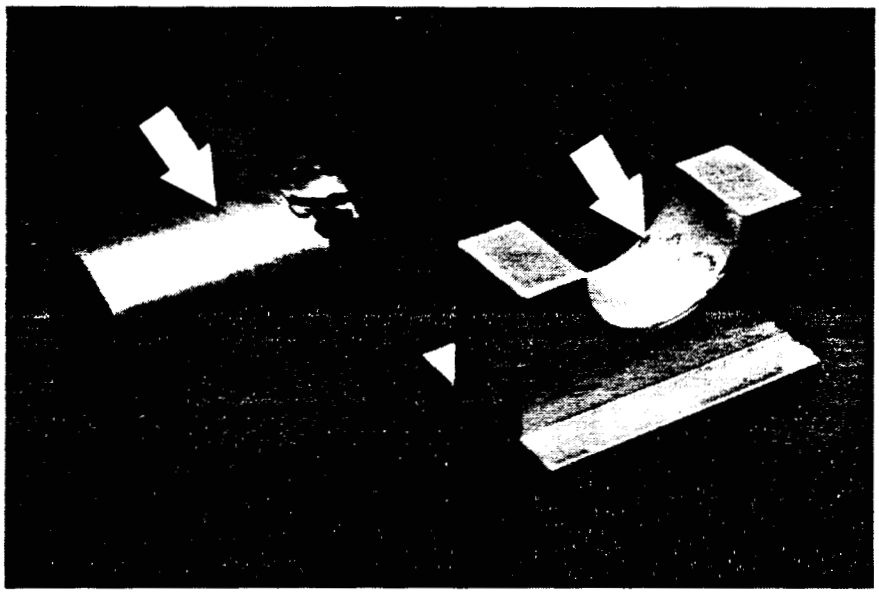

FIGURE 8.29 BRASS RUB BLOCK AND CORRESPONDING SHAFT SECTION AFTER 15 SECONDS OF ROTOR–TO–STATOR RUBBING AT 1000 RPM. ARROWS INDICATE SURFACE DEFORMATION AND MATERIAL DEPOSIT ON STATOR SIMULATING RUB BLOCK AND SHAFT SECTION RESPECTIVELY. MICROPHOTOGRAPHS IN FIGURES 8.17 AND 8.18 SHOW THE DAMAGED SURFACES.

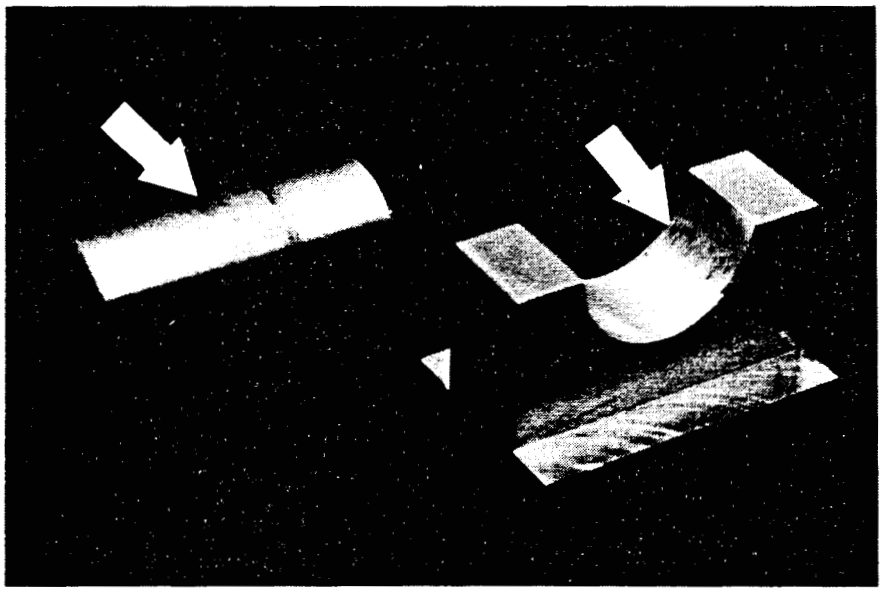

FIGURE 8.30 BRASS RUB BLOCK AND CORRESPONDING SHAFT SECTION AFTER 60 SECONDS OF ROTOR–TO–STATOR RUBBING AT 1000 RPM. ARROWS INDICATE SURFACE DEFORMATION AND MATERIAL DEPOSIT ON STATOR SIMULATING RUB BLOCK AND SHAFT SECTION RESPECTIVELY. MICROPHOTOGRAPHS IN FIGURES 8.19 AND 8.20 SHOW THE DAMAGED SURFACES.

9. TWO–BENDING–MODE RUBBING ROTOR RIG AND IDENTIFICATION OF ITS DYNAMIC CHARACTERISTICS.

9.1 Objective

The complexity of the HPFTP simulating rubbing rotor rig and involvement of many difficult–to–identify factors during experimental testing would prevent correct interpretation of the rub data. More generic study on rotor–to–stator rubs performed at a simpler rotor rig became a necessary prerequisite before the experimental testing of rubbing rotor on the HPFTP simulating rotor rig.

The results provide the relationship between the rubbing rotor dynamic response and the rotative speed, vibrational modes, rubbing material conditions, and stator compliance. It also gives an insight on the appropriate use of vibration measuring instrumentation.

9.2 Two–Bending–Mode Rubbing Rotor Experimental Rig

The rub test fixture (Fig. 9.1) which simulates the stator/casing when used in conjunction with the rotor system shown in Figures 9.2 and 9.3 allows the exploration of rotor response to partial rub[1] conditions. The fixture consists of a plunger supported in two linear bearings allowing for plunger axial horizontal motion when the shaft contacts the rub block. The rub block is mounted at the plunger end. The plunger is both positioned and restrained axially by a set of compression springs located in the body of the fixture. Adjustments to the spring assembly allow for axial position and spring preload adjustments to be made independently of one another. In addition to the on–line adjustments for stator modelling plunger position and preload, the shaft/stator rub normal force may be varied by replacing the compression springs with those of another stiffness value. There is an eddy current displacement probe mounted in the fixture to monitor the axial displacement of the plunger. The provided information, along with the spring stiffness, is used to determine the normal force between the shaft and rub block during the contact period. The normal force and the coefficient of friction between the shaft and rub block materials (determined in Chapter 8) allow the tangential force to be calculated. Shaft lateral vibration signals from X – Y proximity probes are collected at the rub fixture location and also at other axial locations along the shaft (Fig. 9.2). A sample calibration characteristic for Bently Nevada 3000 Series 190 transducer system is included in Figure 9.4. The curve indicates the wide range of linear operation characteristic of this type of Proximitor/probe system. The vibration information from the proximity probes is presented in shaft orbit or timebase formats and eventually processed through filters and an FFT analyzer to determine the frequency components contributing to the overall waveform. The information on lateral vibration from different axial locations of the shaft can be correlated to provide rotor mode shape. The tests were conducted with different rub blocks (made of different materials and with different surface finish), variable plunger support stiffnesses, and at different rotative speeds. The rotor–to–stator rubs can be initiated both by increasing the unbalance force with a fixed shaft/rub block clearance and setting a constant unbalance and changing the clearance by increasing the steady–state preload on the shaft. The results of the rotor–to–stator partial rubbing tests are presented in Chapter 10.

Enhancements were added to the rig as deemed necessary, including: an electrical contact device used to more accurately identify rub contact of the rotor and stator. Two high

---

[1]"Partial rub" signifies occasional rotor–to–stator contact during rotor precessional motion. See definitions in Chapters 2 and 3.

frequency accelerometers, one mounted on the plunger rub mechanism, the other on the rub fixture housing, completed the vibration measurement system.

Operation of the rotor rig required balancing and identification of the dynamic characteristics. The identification procedure is described in Section 9.4.

After achieving the desired balance state of the rotor, a controlled unbalance was introduced at the inboard plane, this unbalance being used to obtain a required level of the synchronous vibrations in order to initiate a rotor–to–stator rub.

9.2.1 High Frequency Accelerometer

Accelerometers are often used to provide information on the machine vibration level by measuring it on the outside casing. They are also applied for modal testing techniques on mechanical structures. Appropriate applications of accelerometers are necessary to obtain useful and interpretable vibration information. In particular, it is necessary to take into account that the accelerometers measure the casing vibrations, not the vibration main source, namely rotor vibrations. Thus the casing transmissibility being a function of its compliance plays a significant role in the results. In addition, the accelerometers do not have enough sensitivity to detect low frequency components and, therefore, high amplitude but low frequency, potentially destructive vibrations may not be apparent. On the other hand, the accelerometers provide useful information when looking at of higher frequency vibration components such as generated during rub. The amplitudes of higher frequency components increase with the severity of rub. This justifies the use of accelerometers for this application.

To detect and monitor the presence of higher order frequency vibration components, an accelerometer has been mounted in the plane of plunger movement (horizontal plane).

A second accelerometer has been mounted on the rub fixture housing. Information obtained from this location helps to detect the presence of vibrations transmitted to the rotor rig base from other areas of the apparatus, i.e., (bearing supports, couplings, and motor). Sensitivity/calibration information for the accelerometers used in the experiments is presented in Figure 9.4a.

9.2.2 Rub–Related Electrical Contact Device

This device has been incorporated onto the rotor rig to more accurately identify a rub condition. An extremely "light" rub may not be apparent by either vibration signals or a significantly altered shaft orbit shape. A 1–volt–dc potential is placed across the rotor shaft and rub block. The mechanical/electrical contact between the rotor shaft and rub block provides a circuit that can be monitored via oscilloscope with continuity position/timing correlated to the Keyphasor signal and plunger movement signal. This information is necessary to constructively analyze rotor vibration data.

9.3 Results of Stator Compliance Tests

The correct interpretation of the rotor–to–stator rub dynamic data requires the knowledge on the stator compliance. The static test was, therefore, performed to provide the necessary information. For a decreasing rub block plunger compliance (spring preload increasing), a larger normal force is necessary to overcome the spring resistance, and thus

produce movement. A graph of plunger force versus deflection for various spring preloads used in the experiments is presented in Figure 9.5. The spring stiffness is K = 107 lb/in. For the used amounts of force the range of deflections proved to be linear.

9.4. Identification of Rotor Rig Modal Parameters via Synchronous Dynamic Stiffness Testing

In order to identify dynamic parameters affecting the vibrational response of the rotor rig, the Synchronous Dynamic Stiffness testing has been conducted. Developing the identification technique for this relatively simple rig is necessary to aid in the identification of more complex systems such as the HPFTP simulation rig. Dynamic Stiffness testing is a technique used in Modal Analysis. It differs from the "Classical Modal Analysis" in the sense that focus is placed on the active rotor system lowest modes. The lowest modes of the system usually correspond to rotor modes, and are usually associated with high amplitude deformation of the shaft. These modes are easily excited by the unbalance force during start–ups and shutdowns, and are, therefore, of great interest.

Two approaches have been used to identify the rig synchronous modal parameters, namely a first mode technique and a two–mode technique. Both techniques employ a perturbation force to modify the dynamic equilibrium of the rotor system. The perturbation force, in this case a known unbalance attached to the rotor, results in a rotor vibrational response measured in the form of the shaft lateral displacements (perpendicular to the rotor axis). This type of synchronous perturbation technique provides a circular rotating force with a frequency equal to the shaft rotative speed. The resulting vibrational response filtered to the rotative speed frequency component is, therefore, referred to as "synchronous" vibration. Both tests (one– and two–mode identification) were run without rotor–to–stator rubbing to identify the system's "normal operation" synchronous modal parameters.

9.4.1 Mathematical Model of the Rotor at the First Lateral Mode

In mathematical modelling of the rotor fundamental synchronous response, the following assumptions hold:

- Rotor first lateral mode is considered only.
- Rotative speed is constant (or it varies very slowly so that transient motion can be neglected).
- Rotor/bearing/support system is linear (elastic force is proportional to lateral displacement, damping force is proportional to lateral velocity).
- Rotor/bearing/support system is laterally isotropic (has matched vertical and horizontal characteristics).
- Rotor/bearing/support system parameters are represented by generalized (modal) mass (M), stiffness (K), and damping (D) for the first lateral mode. (These parameters are sometimes called "effective," i.e., "effective mass," "effective stiffness," etc., of the first lateral mode).
- External damping has viscous character and is small (lower than critical). Internal damping is neglected.

- The steady–state response due to unbalance is considered only (transient free motion is neglected).

The mathematical model represents the balance of forces acting on the rotor:

$$M\ddot{x} + D\dot{x} + Kx = F\cos(\omega t + \phi) \qquad (9.1)$$

$$M\ddot{y} + D\dot{y} + Ky = F\sin(\omega t + \phi), \quad \cdot = \frac{d}{dt}, \quad \cdot\cdot = \frac{d}{dt^2} \qquad (9.2)$$

Inertia Force	+	Damping Force	+	Elastic Force	=	Exciting Force

where x(t), y(t) describe motion of the rotor in two orthogonal lateral directions (conventionally x – horizontal, y – vertical), t is time; $\dot{x}$, $\dot{y}$ are velocities, $\ddot{x}$, $\ddot{y}$ accelerations, t is time. Angle ϕ specifies the position of unbalance in the chosen coordinate system. In practical applications this coordinate system is correlated to the once–per–turn marker, the Keyphasor® system. ω is rotor rotative speed.

Eqs. (9.1), (9.2) can be conventionally transformed into one equation by using the complex number formalism.

Let Eq. (9.2) be multiplied by $j = \sqrt{-1}$ and then added to Eq. (9.1). By introducing a complex variable

$$z(t) = x(t) + jy(t)$$

Eqs. (9.1) and (9.2) can be presented in the following form:

$$M\ddot{z} + D\dot{z} + Kz = Fe^{j(\omega t+\phi)} \qquad (9.3)$$

Eq. (9.3) represents the mathematical model of an unbalanced symmetric rotor at its first lateral mode. Note that there is no assumption on whether the rotor and supports are "rigid" (hard) or "flexible" (soft). The model is entirely adequate for either case.

9.4.2 Synchronous Response

The forced solution of Eq. (9.3) yields the rotor fundamental response, synchronous with the rotative speed and unbalance force frequency ω:

$$z = Ae^{j(\omega t+\alpha)} \qquad (9.4)$$

Introducing (9.4) and its derivatives into Eq. (9.3) and eliminating the time–dependent harmonic function, $e^{j\omega t}$, the basic equation of the rotor fundamental response is obtained:

$$(K-M\omega^2+jD\omega)Ae^{j\alpha} = Fe^{j\phi} \quad \text{or} \quad \vec{\kappa}\, Ae^{j\alpha} = Fe^{j\phi} \quad \text{or}$$

$$(\kappa_D + j\kappa_Q)Ae^{j\alpha} = Fe^{j\phi} \tag{9.5}$$

where $K-M\omega^2+jD\omega = \vec{\kappa}$ is rotor Synchronous Complex Dynamic Stiffness (which is a vector with the direct part $\kappa_D=K-M\omega^2$ and the quadrature part $\kappa_Q=D\omega$).
The resulting Eq. (9.5) represents the Basic Equation for the Rotor Fundamental Synchronous Response. It contains three important components:

(i) Rotor Synchronous Complex Dynamic Stiffness $= K - M\omega^2 + jD\omega$ (9.6)

with

Direct Synchronous Dynamic Stiffness $= \kappa_D = K - M\omega^2$ (9.7)

and

Quadrature Synchronous Dynamic Stiffness $= \kappa_Q = D\omega$, (9.8)

(ii) Response Vector $= Ae^{j\alpha}$ (9.9)

as a complex number, with real part "A cos α," imaginary part "A sin α," phase α and length "A,"

(iii) Input Force Vector $= Fe^{j\phi}$.

From Eq. (9.5) the response vector and its amplitude and phase components can be calculated:

$$Ae^{j\alpha} = \frac{F}{K - M\omega^2 + jD\omega} e^{j\phi} \tag{9.10}$$

$$A = \frac{F}{\sqrt{(K - M\omega^2)^2 + (D\omega)^2}} \tag{9.11}$$

$$\alpha = \phi + \arctan\left(\frac{-D\omega}{K-M\omega^2}\right) \tag{9.12}$$

where the last term in (9.12) represents the net phase angle between the force vector and response vector.

9.4.3 The First Mode Identification of Rotor Parameters Using Synchronous Perturbation Testing

The flexible isotropic shaft carrying two disks and supported in relatively rigid isotropic bearings of the two–mode rig was run with low acceleration up to the speed 2500 rpm. After a preliminary balancing and achieving the satisfactory balance state of the rotor, the controlled unbalance of mr = 0.5 × 30.5 gram × mm was installed at ϕ=180° angular location of the inboard disk for the first run and at ϕ=0° location for the second run. The rotor was equipped with one Keyphasor® probe and twelve X–Y proximity probes at six axial locations of the shaft. The data was stored from the vertical probe only. The horizontal probe (X) signals were monitored on the oscilloscope. The information served for checking the lateral isotropy of the rotor system. The vertical probe located next to the inboard disk provided the data for the Dynamic Stiffness identification. The information from remaining vertical probes served for evaluation of the modal correction factor. The data acquisition and processing system consisted of a vector tracking filter (Bently Nevada Corporation DVF2) and the specially designed data acquisition and processing software for HP9836 computer. An oscilloscope and a spectrum analyzer completed the system, for additional reference checking.

For the above–mentioned two runs the filtered synchronous 1× response vectors $A_1e^{j\alpha_1}$, $A_2e^{j\alpha_2}$ measured by the inboard vertical probe were vectorially subtracted at each frequency step in the entire range of rotative speed:

$$Ae^{j\alpha} = A_1e^{j\alpha_1} - A_2e^{j\alpha_2} \tag{9.13}$$

This procedure eliminates any residual synchronous effects from sources other than the predetermined controlled unbalance.

The data measured at the inboard and outboard locations are presented in Figs. 9.6, 9.7, and 9.8.

The rotor synchronous dynamic stiffness (DS) components were calculated using Eq. (9.5) as follows:

$$\vec{\kappa} = \text{Complex DS} \quad = \beta \frac{2mr\omega^2 e^{180j}}{Ae^{j\alpha}} = K - M\omega^2 + jD\omega \tag{9.14}$$

$$\kappa_D = \text{Direct DS} \quad = -\beta \frac{2m\,r\,\omega^2}{A} \cos\alpha = K - M\omega^2 \tag{9.15}$$

$$\kappa_Q = \text{Quadrature DS} = \beta \frac{2m\,r\,\omega^2}{A} \sin\alpha = D\omega \tag{9.16}$$

where β is the modal correction factor, which takes into account the fact that the controlled unbalance (perturbation force) and the rotor displacement measuring probes are not at the same axial locations of the rotor, and in particular, not at the anti–nodal point. Using the information from remaining probes, the modal correction factor was estimated: $\beta = 0.94$.

From the rotor response data, the system synchronous dynamic stiffness is calculated for each rotative speed step and presented in the forms of "direct" and "quadrature" stiffnesses versus perturbation frequency, which in this case is the rotor operating speed. Figure 9.9 presents the raw data before the modal correction factor was introduced. According to Eqs. (9.15) and (9.16), the Direct Dynamic Stiffness versus perturbation frequency is a parabola where the intersection with the horizontal axis indicates the rotor system first natural frequency (Fig. 9.9a). Direct dynamic stiffness may also be presented versus perturbation frequency squared; this yields a straight–line relationship, the slope of the line being equal to the rotor modal mass and point of intersection with the horizontal axis indicating the modal stiffness/mass ratio (Fig. 9.9b). The modal stiffness can be read at the intersection of the straight line with the vertical axis. The Quadrature Stiffness versus perturbation frequency is a straight line relationship with the slope equal to the system modal damping coefficient (Fig. 9.9c). Except the low rotative speed range, the measured data was very close to analytically predicted.

From the Direct Dynamic Stiffness graph (Fig. 9.9b) the first mode stiffness and mass are obtained. With the modal correction factor taken into account the identified values are

First Mode Synchronous Stiffness = K = 280 lb/in

First Mode Synchronous Mass = M = 0.01 lb sec^2/in

The natural frequency of the system is $\omega_n = \sqrt{K/M} = \sqrt{280/0.01} = 167$ rad/s = 1598 rpm, which agrees with the resonant frequency at which the peak amplitude of forced vibration occurs (Fig. 9.7).

The Quadrature Dynamic Stiffness data (Fig. 9.9c) indicates the damping within the system is extremely low, approaching the instrumentation noise level. The dynamic stiffness method is, therefore, not the best evaluation technique for this case. It is possible, however, to calculate the modal damping factor using the classical Half Power Bandwidth method. The polar plot of the response (Fig. 9.6) directly provides the necessary information. Specifically, three frequencies are required: two of them, ω_1 and ω_2, corresponding to response vectors with the response phases $(\alpha - \phi)$ equal to -45 and -135 degrees, and the third, the resonant frequency (ω_n) when the magnitude of the response vector is at a maximum.

The Half Power Bandwidth method provides the modal damping factor ζ by the following equation:

$$\frac{\omega_2-\omega_1}{2\omega_n} = \frac{\omega_n(\sqrt{1+\zeta^2} + \zeta) - \omega_n(\sqrt{1+\zeta^2} - \zeta)}{2\omega_n} = \zeta. \tag{9.17}$$

The result for the first mode modal damping factor is as follows (Fig. 9.10):

$$\zeta = \frac{\omega_2-\omega_1}{2\omega_n} = \frac{1630 - 1535}{2(1580)} = .030 \tag{9.18}$$

The calculation of the modal damping is then quite simple. The relationship between the modal damping D and the modal damping factor ζ is as follows:

$$D = 2\zeta\sqrt{KM} \tag{9.19}$$

$$D = 2\sqrt{KM}\,\zeta = 2\sqrt{280\times0.01}\cdot\ 0.03 = 0.1 \text{ lb–sec/in.} \tag{9.20}$$

9.4.4 Mathematical Model of the Rotor With Two Lateral Modes

The mathematical model for two lateral modes may be developed by extending the one mode model. Included are the cross coupled spring and damping terms, as well as an additional tangential force acting at each mass ("cross–coupled" effect) (Fig. 9.11).

The set of equations describing the motion of a laterally isotropic rotor in two orthogonal lateral directions are as follows:

$$\begin{aligned}
&M_1\ddot{x}_1+(D_1+D_{12})\dot{x}_1-D_{12}\dot{x}_2+(K_1+K_{12})x_1-K_{12}x_2-K_{t_1}y_1 = F_1\cos(\omega t+\phi_1)\\
&M_1\ddot{y}_1+(D_1+D_{12})\dot{y}_1-D_{12}\dot{y}_2+(K_1+K_{12})y_1-K_{12}y_2+K_{t_1}x_1 = F_1\sin(\omega t+\phi_1)\\
&M_2\ddot{x}_2+(D_2+D_{21})\dot{x}_2-D_{21}\dot{x}_1+(K_2+K_{21})x_2-K_{21}x_1-K_{t_2}y_2 = F_2\cos(\omega t+\phi_2)\\
&M_2\ddot{y}_2+(D_2+D_{21})\dot{y}_2-D_{21}\dot{y}_1+(K_2+K_{21})y_2-K_{21}y_1+K_{t_2}x_2 = F_2\sin(\omega t+\phi_2)
\end{aligned} \tag{9.21}$$

In Eqs. (9.21) M_1, M_2 are modal masses of the rotor, K_1, K_2, $K_{12}=K_{21}$ are modal stiffnesses, D_1, D_2, $D_{12}=D_{21}$ are modal viscous damping coefficients, K_{t_1}, K_{t_2} are tangential force coefficients ("cross stiffnesses"), F_1, F_2 are amplitudes of the unbalance perturbation force, ϕ_1, ϕ_2 are the unbalance angular positions, x_1, x_2, y_1, y_2 are horizontal and vertical deflections of two axial positions ("inboard" and "outboard") of the rotor.

Assuming isotropy (symmetry) within the system (equal stiffnesses and dampings in both the x and y directions), introduction of the complex variable $j = \sqrt{-1}$ allows transformation of Eq. (9.21) into one equation for the motion of the shaft inboard and outboard sections (planes #1 and #2):

$$\begin{aligned}
&M_1\ddot{z}_1+(D_1+D_{12})\dot{z}_1-D_{12}\dot{z}_2+(K_1+K_{12})z_1-K_{12}z_2+jK_{t_1}z_1 = F_1e^{j(\omega t+\phi_1)}\\
&M_2\ddot{z}_2+(D_2+D_{21})\dot{z}_2-D_{21}\dot{z}_1+(K_2+K_{21})z_2-K_{21}z_1+jK_{t_2}z_2 = F_2e^{j(\omega t+\phi_2)}
\end{aligned} \tag{9.22}$$

where

$$z_1 = x_1 + jy_1 \quad \text{and} \quad z_2 = x_2 + jy_2 \tag{9.23}$$

Eqs. (9.22) represent a model of an unbalanced two–mass, two–mode rotor.

9.4.5 Forced Solution

The forced solution for Eqs. (9.22) yields the rotor synchronous response:

$$z_1 = A_1 e^{j(\omega t+\alpha_1)}$$
$$z_2 = A_2 e^{j(\omega t+\alpha_2)} \tag{9.23}$$

where A_1, A_2, and α_1, α_2 are response vector magnitudes (amplitudes) and phase angles respectively.

Introducing (9.23) and their derivatives into Eqs. (9.22), the complex algebraic equations are obtained:

$$[(K_1+K_{12})-M_1\omega^2]A_1e^{j(\omega t+\alpha_1)}+j[(D_1+D_{12})\omega+K_{t_1}]A_1e^{j(\omega t+\alpha_1)}-(K_{12}+jD_{12}\omega)A_2e^{j(\omega t+\alpha_2)}= = F_1e^{j(\omega t+\phi_1)}$$
$$[(K_2+K_{21})-M_2\omega^2]A_2e^{j(\omega t+\alpha_2)}+j[(D_2+D_{21})\omega+K_{t_2}]A_2e^{j(\omega t+\alpha_2)}-(K_{21}+jD_{21}\omega)A_1e^{j(\omega t+\alpha_1)}= = F_2e^{j(\omega t+\phi_2)} \tag{9.24}$$

In Eqs. (9.24) there are the rotor complex dynamic stiffness components, including "direct," "quadrature," and "coupled" terms. These terms may be separated as follows:

(i) Rotor Synchronous Complex Dynamic Stiffness components:

$$[(K_1+K_{12})-M_1\omega^2] + j[(D_1+D_{12})\omega+K_{t_1}] \equiv S_{11}$$
$$[(K_2+K_{21})-M_2\omega^2] + j[(D_2+D_{21})\omega+K_{t_2}] \equiv S_{22} \tag{9.25}$$

with Synchronous Direct Dynamic Stiffnesses

$$[(K_1+K_{12}) - M_1\omega^2] \ , \qquad [(K_2+K_{21}) - M_2\omega^2]$$

and Synchronous Quadrature Dynamic Stiffnesses

$$[(D_1+D_{12})\omega+K_{t_1}] \ , \qquad [(D_2+D_{21})\omega+K_{t_2}]$$

(ii) Synchronous Complex Coupled Dynamic Stiffnesses

$$[K_{12}+jD_{12}\omega] \equiv S_{12} \ , \qquad [K_{21}+jD_{21}\omega] \equiv S_{21} \tag{9.26}$$

With the notation introduced in (9.25) and (9.26), Eqs. (9.24) will read as follows:

$$S_{11}A_1e^{j(\omega t+\alpha_1)} - S_{12}A_2e^{j(\omega t+\alpha_2)} = F_1e^{j(\omega t+\phi_1)} \tag{9.27}$$

$$S_{22}A_2e^{j(\omega t+\alpha_2)} - S_{21}A_1e^{j(\omega t+\alpha_1)} = F_2e^{j(\omega t+\phi_2)} \tag{9.28}$$

Eqs. (9.27) and (9.28) are basic for the identification of dynamic stiffness components.

Placing an unbalance mass only at the inboard plane, as was the case for the first data run, essentially sets equation (9.28) equal to zero (F_2=0). Equations (9.27) and (9.28) will, therefore, model the response of the rotor at the plane #1 and #2 (inboard and outboard planes) due to a perturbation force only at plane #1. Using equations (9.27) and (9.28) again, the same methodology also holds true for an unbalance mass placed only in plane #2 (outboard plane), this time setting equation (9.27) equal to zero (F_1=0), as was the case for the second data run. This technique generates four equations, two for each data run. Since F_1, F_2 ϕ_1, ϕ_2 are known and A_1, A_2, α_1, α_2 are measured, solving for the four unknowns S_{11}, S_{12}, S_{21}, S_{22} (complex dynamic stiffness components) is then possible.

Equations (9.27) and (9.28) may also be solved in terms of response vectors for a single data run, i.e., for instance, when F_2=0:

$$A_1e^{j\alpha_1} = \frac{F_1e^{-j\phi_1}S_{22}}{(S_{22}S_{11}-S_{12}S_{21})}, \qquad A_2e^{j\alpha_2} = \frac{F_1e^{-j\phi_1}S_{21}}{(S_{22}S_{11}-S_{12}S_{21})} \tag{9.29}$$

For the identification purpose, however, Eqs. (9.27) and (9.28) are solved in terms of dynamic stiffnesses. The first run with force at plane #1 provides

$$S_{11}A_{11}e^{j\alpha_{11}} - S_{12}A_{21}e^{j\alpha_{21}} = F_1e^{j\phi_1}$$
$$S_{22}A_{21}e^{j\alpha_{21}} - S_{21}A_{11}e^{j\alpha_{11}} = 0 \tag{9.30}$$

The second run with force at plane #2 provides

$$S_{11}A_{12}e^{j\alpha_{12}} - S_{12}A_{22}e^{j\alpha_{22}} = 0$$
$$S_{22}A_{22}e^{j\alpha_{22}} - S_{21}A_{12}e^{j\alpha_{22}} = F_2e^{j\phi_2} \tag{9.31}$$

The time–dependent exponential function $e^{j\omega t}$ was eliminated from Eqs. (9.27) and (9.28).

The second subscript of amplitudes and phases in Eqs. (9.30) and (9.31) corresponds to the run number. From Eqs. (9.30) and (9.31) the dynamic stiffnesses are calculated:

$$S_{11} = \frac{F_1 e^{j\phi_1} A_{22} e^{j\alpha_{22}}}{A_{11} e^{j\alpha_{11}} A_{22} e^{j\alpha_{22}} - A_{12} e^{j\alpha_{12}} A_{21} e^{j\alpha_{21}}} \tag{9.32}$$

$$S_{12} = \frac{F_1 e^{j\phi_1} A_{12} e^{j\alpha_{12}}}{A_{11} e^{j\alpha_{11}} A_{22} e^{j\alpha_{22}} - A_{12} e^{j\alpha_{12}} A_{21} e^{j\alpha_{21}}} \tag{9.33}$$

$$S_{21} = \frac{F_2 e^{j\phi_2} A_{21} e^{j\alpha_{21}}}{A_{11} e^{j\alpha_{11}} A_{22} e^{j\alpha_{22}} - A_{12} e^{j\alpha_{12}} A_{21} e^{j\alpha_{21}}} \tag{9.34}$$

$$S_{22} = \frac{F_2 e^{j\phi_2} A_{11} e^{j\alpha_{11}}}{A_{11} e^{j\alpha_{11}} A_{22} e^{j\alpha_{22}} - A_{12} e^{j\alpha_{12}} A_{21} e^{j\alpha_{21}}} \tag{9.35}$$

The data acquisition and processing software uses Eqs. (9.32) to (9.35) to calculate the rotor Synchronous Dynamic Stiffness components at each frequency step within the two–mode range of the rotative speeds. The results of the two–mode identifcation tests are presented in the next section.

9.4.6 Two–Mode Identification of Rotor Parameters Using Synchronous Perturbation Testing

The same rotor rig as described in Section 9.4.3 and used for one–mode identification was now a subject of two–mode identification. The controlled unbalance mr = 30.5 gram × mm was installed first in the inboard disk, then in the outboard disk. The measurements were recorded each time at the inboard and outboard vertical locations.

The operating speed range for the two–mode identification ran from 275 rpm (slow roll speed) to approximately 6000 rpm. The method used to calculate the two–mode dynamic stiffness requires two sets of data, one from each rotor disk. This provides enough information to calculate the unknown dynamic stiffnesses, including the coupled terms. A controlled unbalance mass was placed first in the inboard rotor disk. Again vector subtraction of two controlled data runs with unbalance at 180° and then at 0° was used to eliminate any unwanted synchronous effects from sources other than the predetermined, controlled unbalance. With data recorded from the initial runs (Figs. 9.12, 9.13), the unbalance mass was then moved to the outboard disk, and the same procedure repeated (Figs. 9.14 and 9.15). Results were vectorially subtracted (Figs. 9.16 and 9.17) and eventually presented in the conventional "direct" and "quadrature" format of Dynamic Stiffness using Eqs. (9.32) to (9.35) (Fig. 9.18). The coupled terms (K_{12}, K_{21}, D_{12}, D_{21}) are presented independently (Fig. 9.19). (From the computer subroutine, they appear with conyentional negative signs). The Direct Dynamic Stiffness components are presented versus rotative speed squared. The remaining components are presented versus rotative speed.

The values of damping coefficients D_1, D_2, D_{12}, and D_{21} and cross–coupled stiffnesses K_{t_1}, K_{t_2} identified from the corresponding dynamic stiffness graphs were extremely small and fall into the instrumentation noise level. Similarly to the first mode damping factor (Eq.

9.17), the modal damping factor ζ_{II} for the second mode may be calculated applying the Half Power Bandwidth method using the polar plot (Fig. 9.20). The results from the second mode polar "circle" are as follows:

$$\zeta_{II} = \frac{\omega_2 - \omega_1}{2\omega_n} = \frac{4394 - 4120}{2(4225)} = .032$$

From direct dynamic stiffness and coupled dynamic stiffness graphs, the modal masses and stiffnesses are obtained:

Direct Stiffnesses

$$K_1 + K_{12} = 500 \text{ lb/in}$$
$$K_2 + K_{21} = 500 \text{ lb/in}$$

Coupled Stiffnesses

$$K_{12} = 375 \text{ lb/in} \quad \text{thus} \quad K_1 = 125 \text{ lb/in} \qquad (9.36)$$
$$K_{21} = 375 \text{ lb/in} \qquad K_2 = 125 \text{ lb/in}$$

Modal masses

$$M_1 = .0045 \text{ lb sec}^2/\text{in}$$
$$M_2 = .0045 \text{ lb sec}^2/\text{in}$$

The natural frequencies of the system are as follows:

$$\omega_{n_{1,2}} = \left\{ \frac{K_1+K_{12}}{2M_1} + \frac{K_2+K_{21}}{2M_2} \pm \sqrt{\left[\frac{K_1+K_{12}}{2M_1} - \frac{K_2+K_{21}}{2M_2}\right]^2 + \frac{K_{12}^2}{M_1M_2}} \right\}^{\frac{1}{2}} \qquad (9.37)$$

Taking the identified values (9.36) into consideration Eq. (9.37) yields

$$\omega_{n_1} = 167 \text{ rad/s} = 1591 \text{ rpm}$$
$$\omega_{n_2} = 441 \text{ rad/s} = 4211 \text{ rpm} \qquad (9.38)$$

These values agree with the system resonant frequencies at which the peak amplitudes of forced vibration occur (Fig. 9.17). Note that modal masses and modal stiffnesses identified using the first–mode method and the two–mode method differ. The first mode modal mass and stiffness for the identified values (9.36) is:

$$M = M_1+\phi_1^2M^2 = 0.0045(1+\phi_1^2)$$
$$K = K_1+K_{12}-2K_{12}\phi_1+(K_2+K_{21})\phi_1^2 = 500 - 750\phi_1 + 500\phi_1^2 \qquad (9.39)$$

where ϕ_1 is the modal function. Assuming $\phi_1 = 1$, as the system is nearly symmetric, Eqs. (9.39) yield

$M = 0.009$ lb sec^2/in

$K = 250$ lb/in

Comparing with the values identified by the first mode method (Section 9.4.3), there is about 10% discrepancy. This is due to the fact that modal functions were not precisely identified.

9.5 Summary

In this chapter the description of the two–bending mode rubbing rotor rig is given. In order to effectively run the rub testing and correctly interpret the results, the identification of the rig dynamic stiffness characteristics was necessary. The Synchronous Dynamic Stiffness Perturbation Method was used for this purpose.

The data and methodology presented for the first mode identification of the system dynamic stiffness yields rotor parameters for one mode. This first mode approach is limited; however, it provides a method which may be extended to more complex systems. The two–mode technique considers the coupling effects within a system having two complex degrees of freedom, and provides identification of the system parameters for two coupled modes. In either case, the knowledge of the dynamic stiffness parameters of a "normally" operating mechanical system is essential for efficient analysis and prediction of the system dynamic responses. An "active" structure (which is characterized by existence of internal energy, such as rotational energy) clearly has different mechanical characteristics than the "passive" structure. As in the case of the HPFTP, shaft rotational energy has a significant influence on rotor dynamic characteristics. In particular, rotating shaft natural frequencies differ from nonrotating shaft natural frequencies. Identification of parameters affected by fluid dynamic interaction within bearings/seals may also be accomplished using the Dynamic Stiffness Methodology and, in particular, the Nonsynchronous Perturbation Technique. It is appropriate to conclude that further analysis of the HPFTP utilizing this methodology would be quite useful.

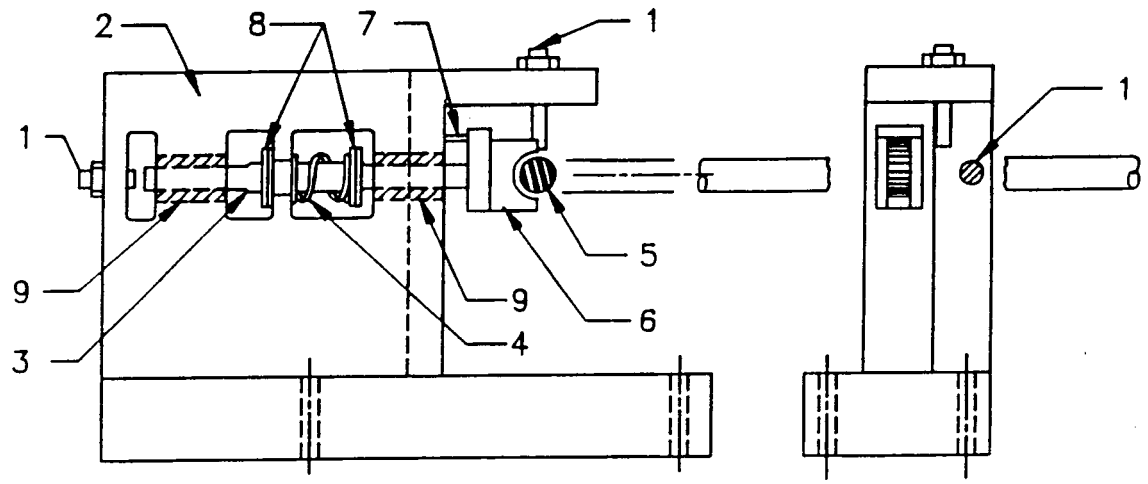

1. Eddy Current Displacement Probe
2. Fixture Body
3. Plunger Shaft
4. Compression Spring
5. Test Shaft
6. Test Rub Block
7. Alignment Pin
8. Position and Preload Adjusters
9. Linear Anti-friction Bearing

FIGURE 9.1 RUB FIXTURE.

A – Electric Motor
B – Flexible Coupling
C – Inboard Bronze Bearing
D – Electrical Contact Device
E – Inboard X-Y Displacement Probe Mount
F – Inboard Mass
G – Rub Fixture/X-Y Displacement Probes
H – Outboard Mass
I – Outboard X-Y Displacement Probe Mount
J – Outboard Bronze Bearing
K – Rotor Shaft
L – Rotor Base

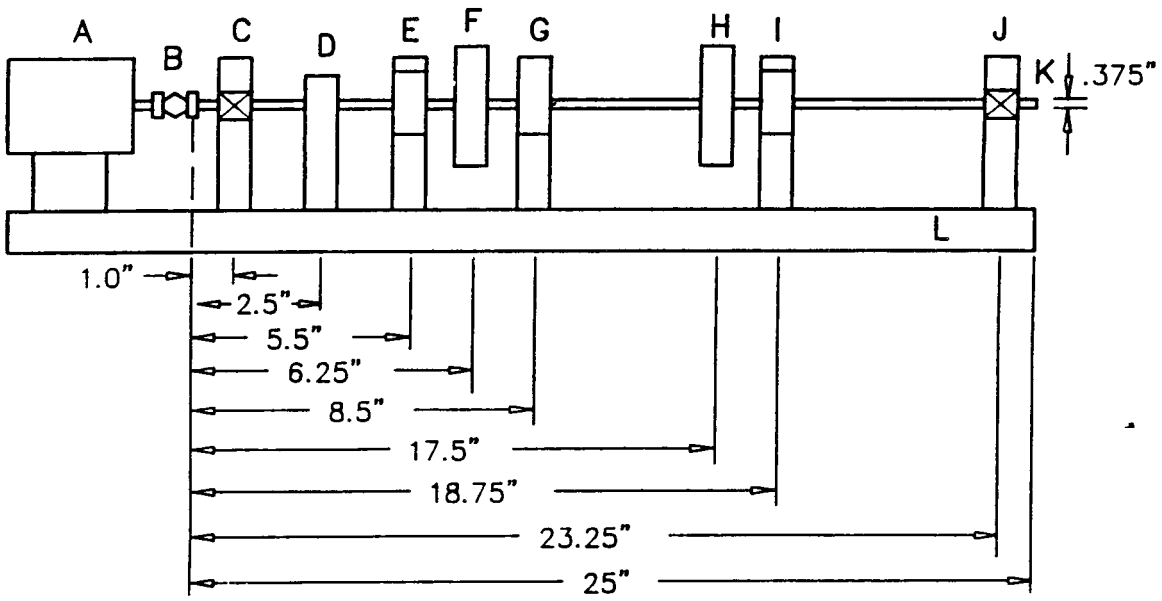

FIGURE 9.2 RUB TEST RIG.

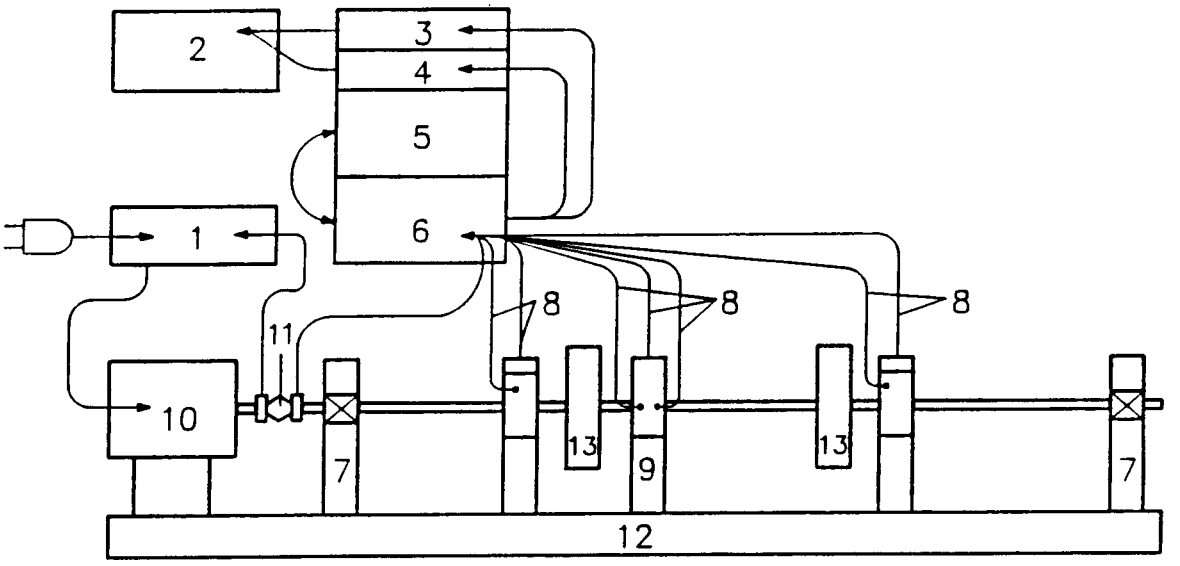

1. MOTOR SPEED CONTROL
2. COMPUTER
3. TRACKING FILTER
4. SPECTRUM ANALYZER
5. TAPE RECORDER
6. AMPLIFIER RACK
7. BRONZE BEARINGS
8. X-Y EDDY CURRENT DISPLACEMENT PROBES
9. RUB FIXTURE
10. ELECTRIC MOTOR
11. FLEXIBLE COUPLING
12. ROTOR BASE
13. 3 INCH DIAMETER DISKS

FIGURE 9.3 RUB TEST SYSTEM.

(a) BENTLY NEVADA

ACCELEROMETER CALIBRATION DATA

Model No. 2 4 : 4 7 =01 By wo
Serial No. 128 Date 8/28/87

P.O. Box 157
Minder, NV 89423
702-782-3611

SPECIFICATIONS

Basic Sensitivity 10.2 mv/g @ 100Hz (measured)
____ pc/g @ 100Hz (measured)
Frequency Response 2 Hz to 30 kHz +/-3db
Max Accel. w/o Clipping ____ g
Max Shock w/o Damage -- g
Bias Level 7.- volts Typ @ 2ma
Power Supply 9-15vdc 2.2ma

Resonant Frequency >55 kHz (typical)
Noise Floor .007 mv/rms (typical)
Transverse Sen. 3.0 % (measured
Time Constant — sec.
Temperature (Max.) 250 °F
Mounting Torque 10 in./lbs.
Accelerometer Capacitance -- pfc

Bently Nevada *calibration data is traceable to NBS at selected frequencies from 2 Hz to 10 KHz and conforms to MIL-STD 45662*

NBS Project No. 732/237849-86 Calibration Level 1 g. (nominal)

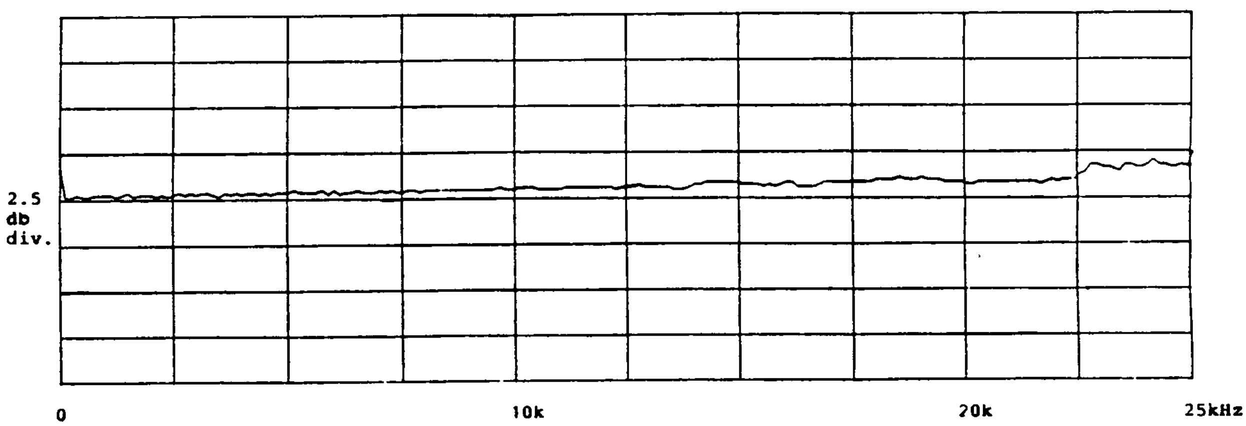

(b)

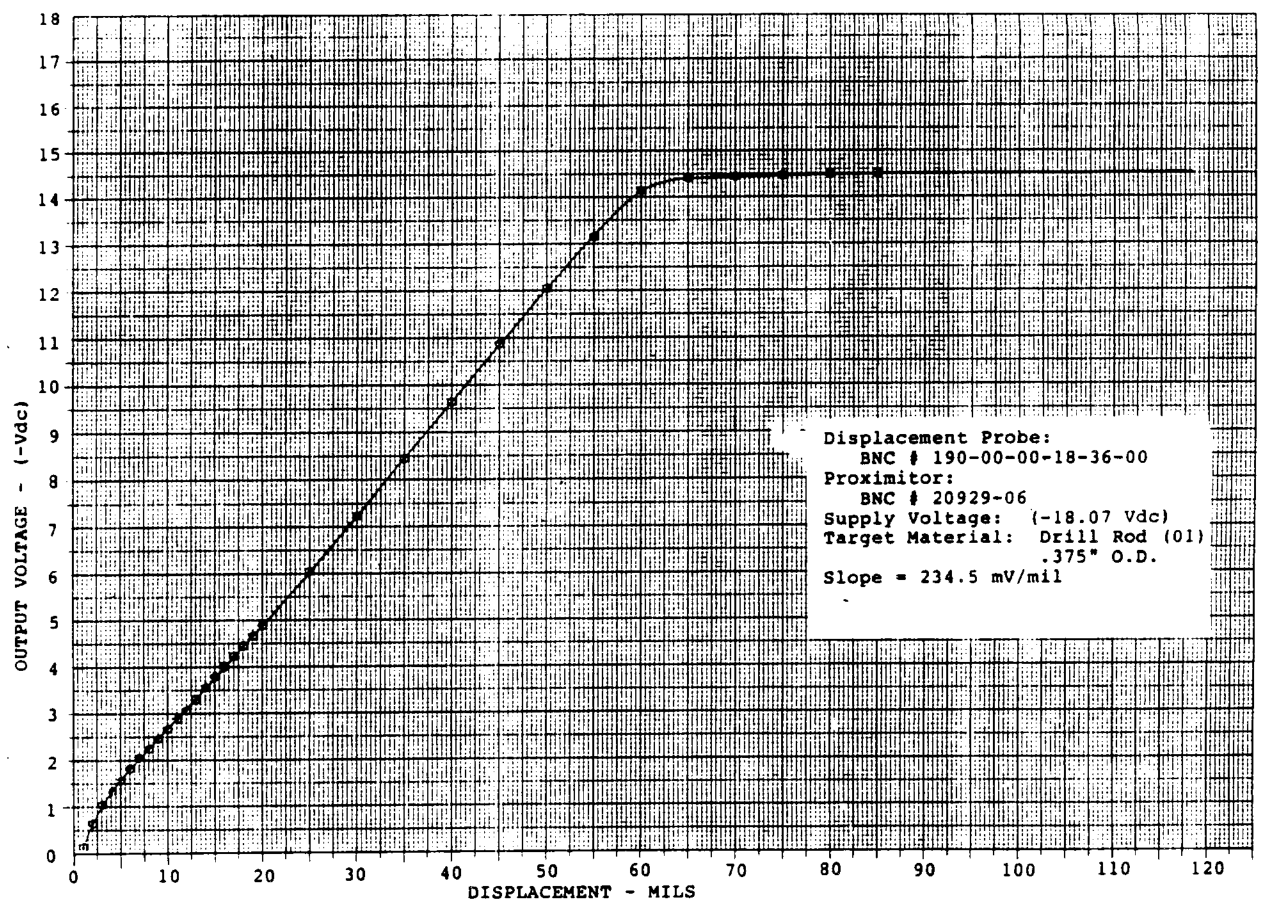

FIGURE 9.4 (a) ACCELEROMETER CHARACTERISTICS (b) TYPICAL CALIBRATION CURVE FOR BENTLY NEVADA 3000 SERIES 190 PROXIMITY TRANSDUCER SYSTEM.

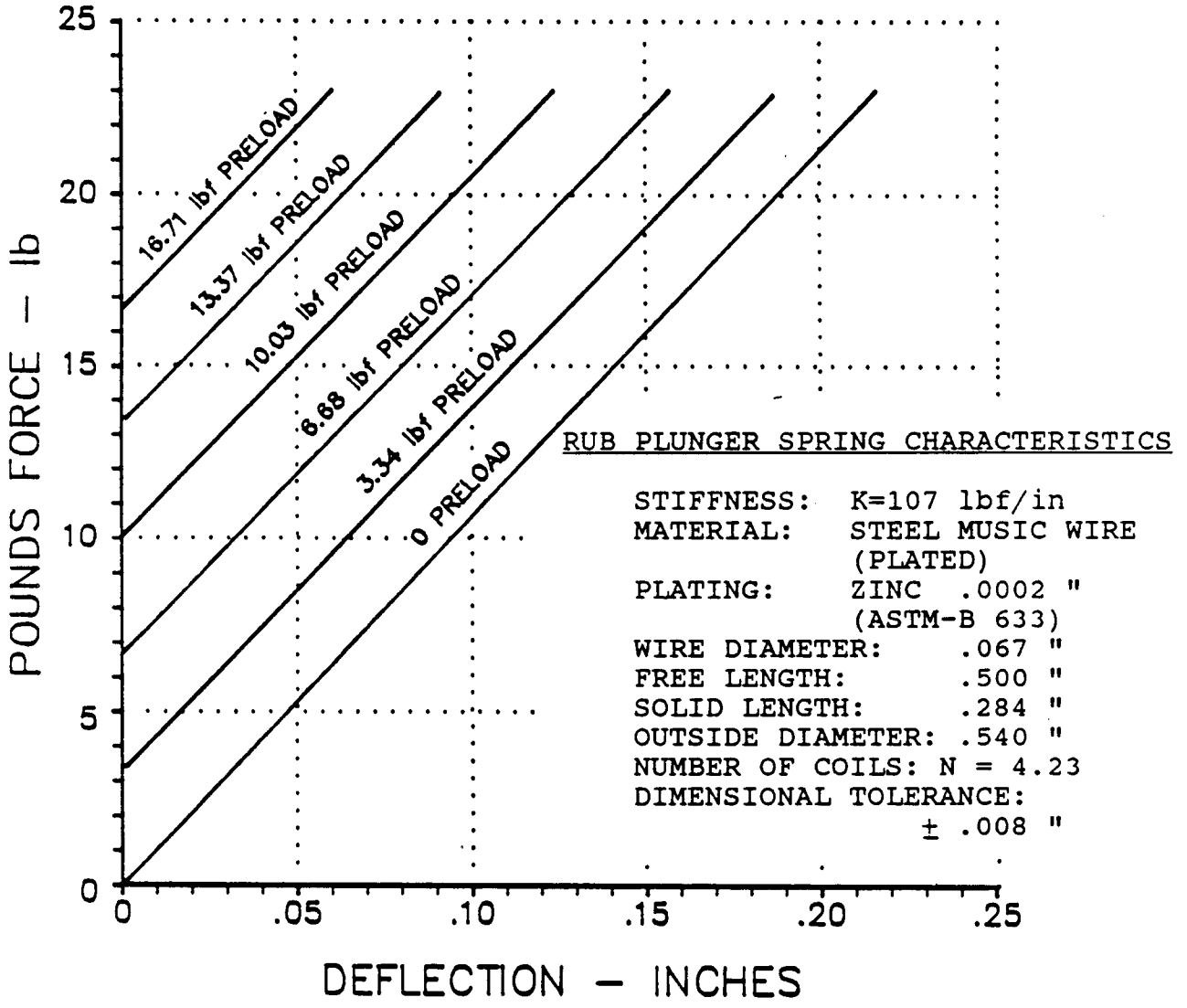

FIGURE 9.5 STATOR COMPLIANCE TEST RESULTS.

(a)

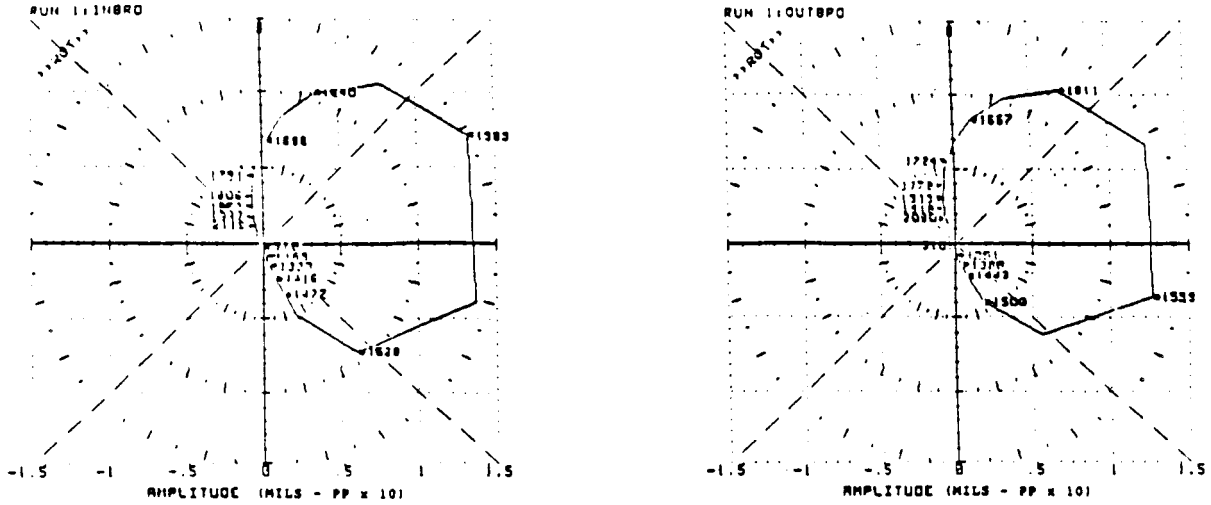

RUN 1 -- UNBALANCE: .5 GRAMS, 180 DEGREES, RADIUS = 1.2 IN, INBOARD.

(b)

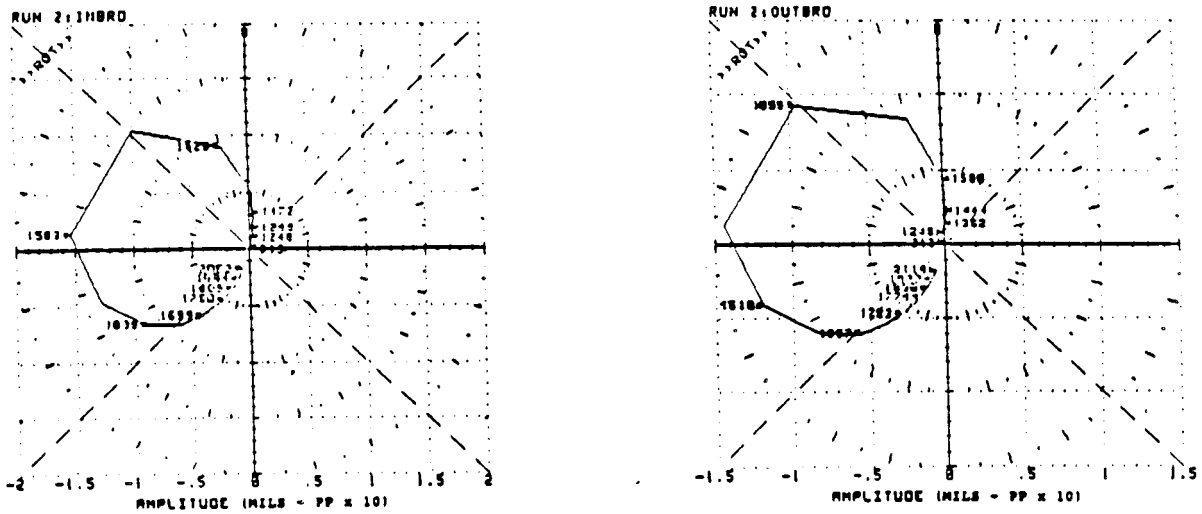

RUN 2 -- UNBALANCE: .5 GRAMS, 0 DEGREES RADIUS, = 1.2 IN, INBOARD.

(c)

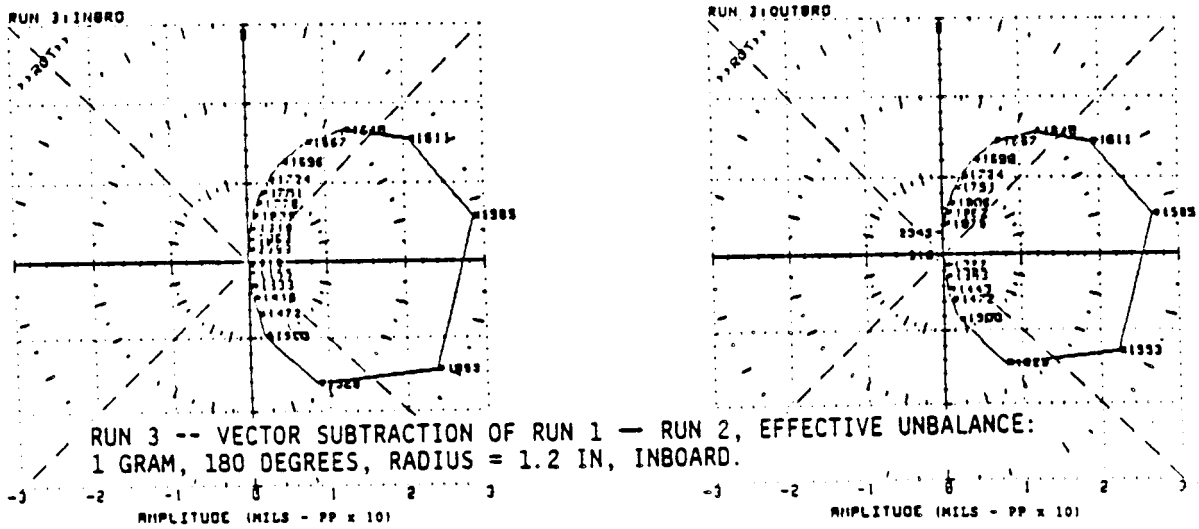

RUN 3 -- VECTOR SUBTRACTION OF RUN 1 — RUN 2, EFFECTIVE UNBALANCE: 1 GRAM, 180 DEGREES, RADIUS = 1.2 IN, INBOARD.

FIGURE 9.6 POLAR PLOTS OF ROTOR SYNCHRONOUS RESPONSE TO THE CORRESPONDING CONTROLLED UNBALANCE COVERING THE FIRST LATERAL MODE.

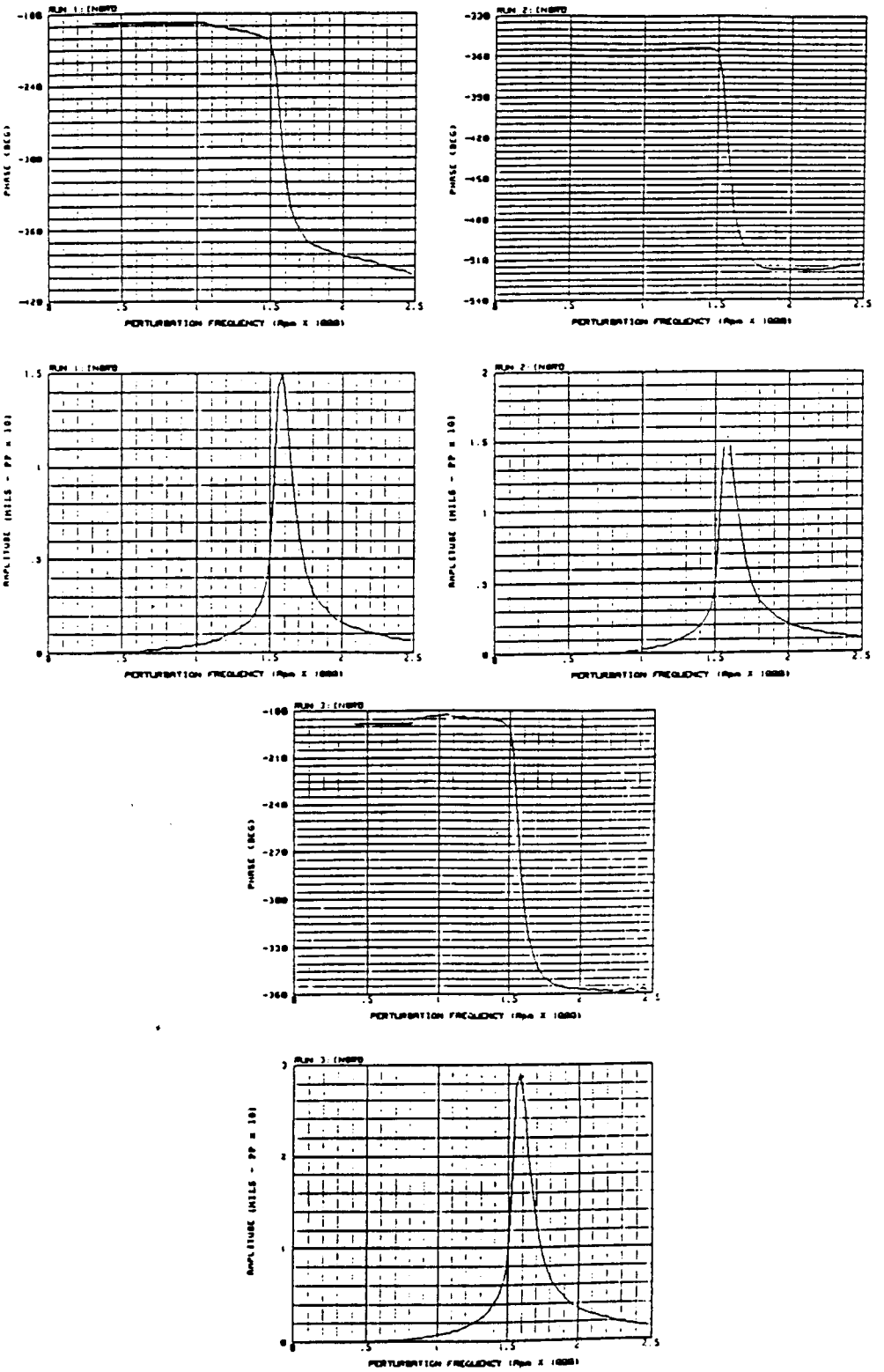

FIGURE 9.7 BODÉ PLOTS OF ROTOR SYNCHRONOUS RESPONSE TO THE CORRESPONDING CONTROLLED UNBALANCE FOR FIRST LATERAL MODE (INBOARD DISK ONLY). RUN 1 — UNBALANCE: .5 GRAMS, 180 DEGREES, RADIUS = 1.2 IN, INBOARD. RUN 2 — UNBALANCE: .5 GRAMS, 0 DEGREES RADIUS, = 1.2 IN, INBOARD. RUN 3 — VECTOR SUBTRACTION OF RUN 1 MINUS RUN 2, EFFECTIVE UNBALANCE: 1 GRAM, 180 DEGREES, RADIUS = 1.2 IN, INBOARD.

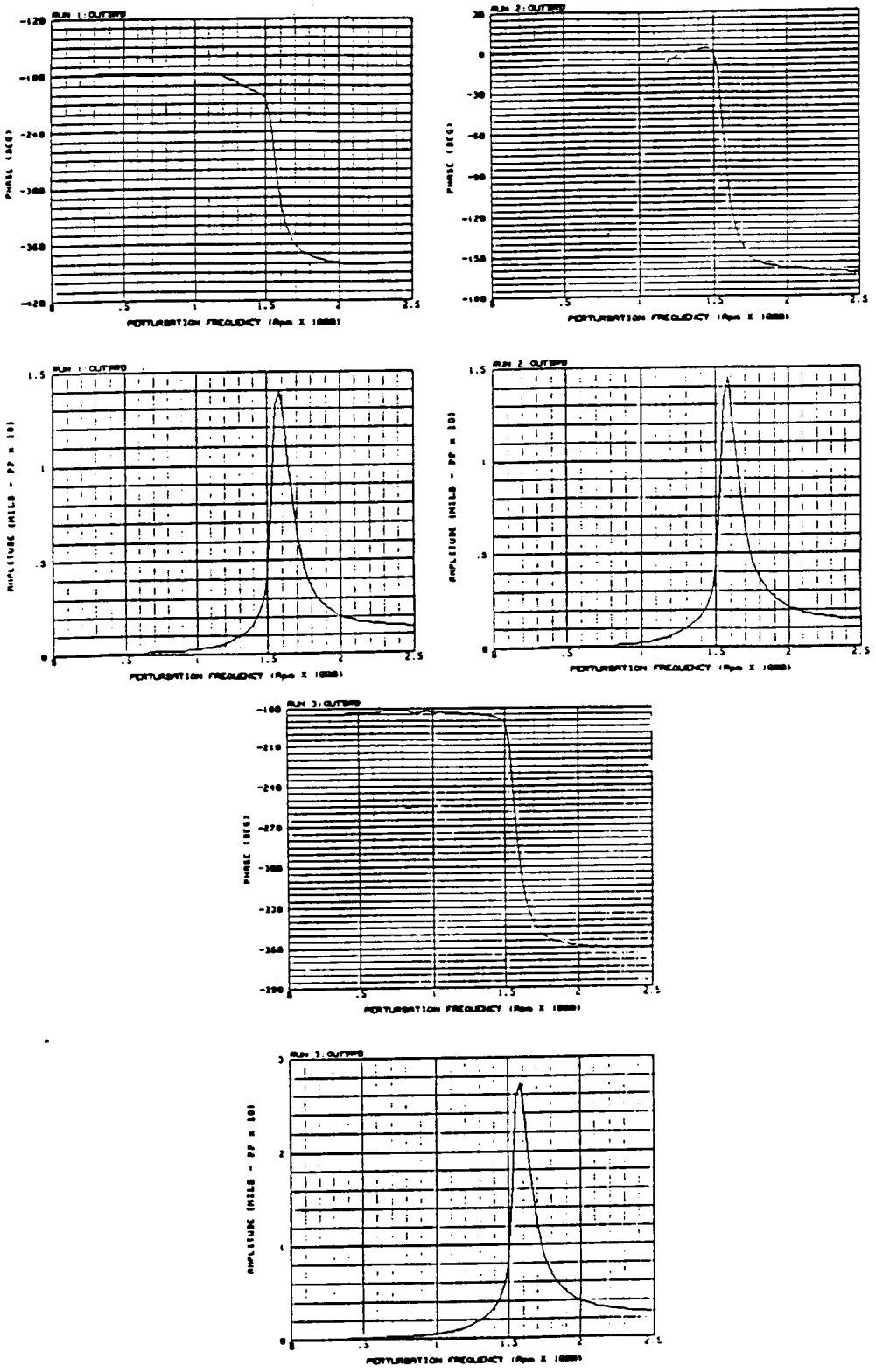

FIGURE 9.8 BODÉ PLOTS OF ROTOR SYNCHRONOUS RESPONSE TO THE CORRESPONDING CONTROLLED UNBALANCE FOR FIRST LATERAL MODE (OUTBOARD DISK ONLY). RUN 1 — UNBALANCE: .5 GRAMS, 180 DEGREES, RADIUS = 1.2 IN, INBOARD. RUN 2 — UNBALANCE: .5 GRAMS, 0 DEGREES RADIUS, = 1.2 IN, INBOARD. RUN 3 — VECTOR SUBTRACTION OF RUN 1 — RUN 2, EFFECTIVE UNBALANCE: 1 GRAM, 180 DEGREES, RADIUS – 1.2 IN, INBOARD.

(a)

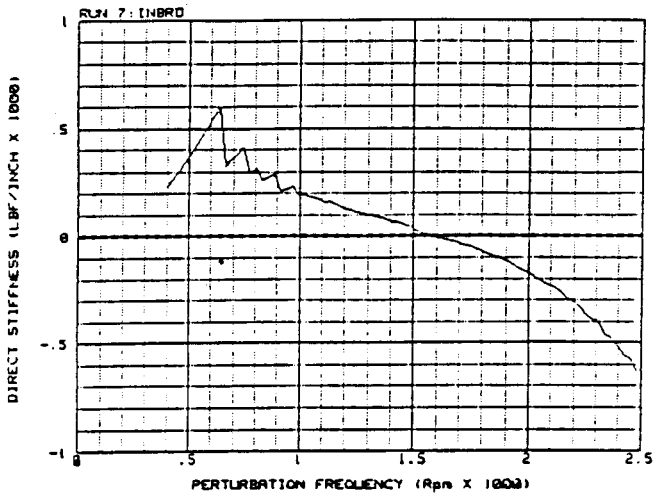

(b)

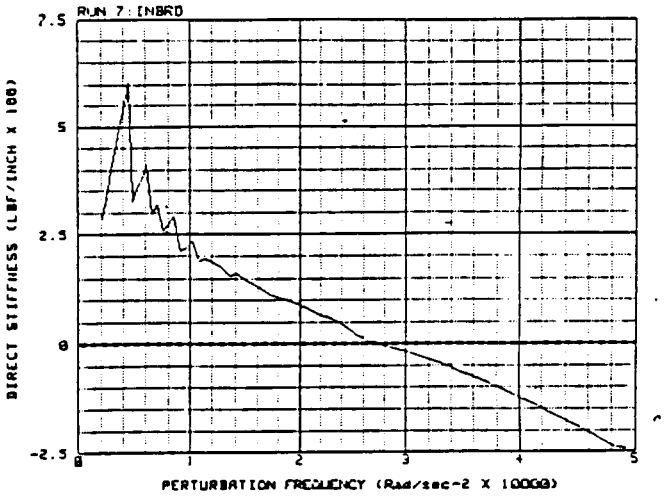

(c)

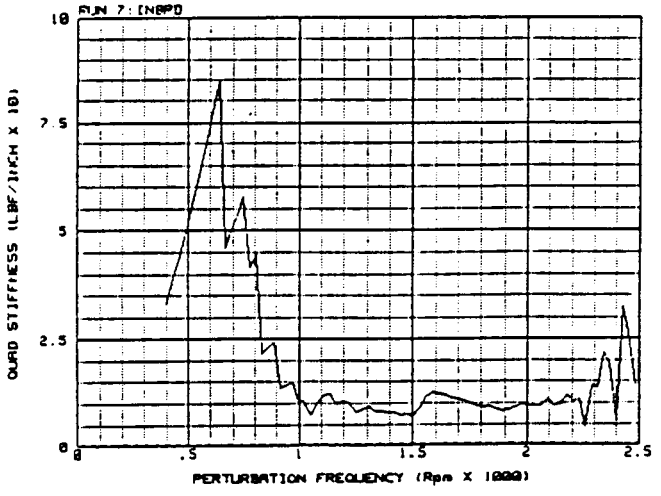

FIGURE 9.9 ROTOR DYNAMIC STIFFNESS COMPONENTS FOR FIRST LATERAL MODE, CALCULATED USING EQS. (9.15) AND (9.16) (EFFECTIVE UNBALANCE: 1 GRAM, 180 DEGREES, RADIUS = 1.2 IN, INBOARD).

ORIGINAL PAGE IS
OF POOR QUALITY

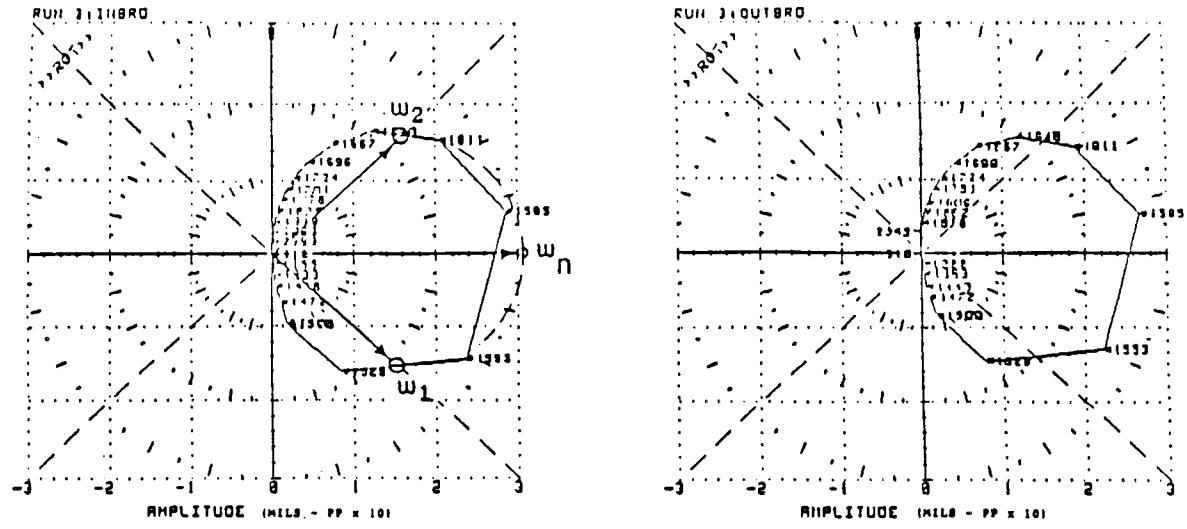

FIRST MODE

$$\frac{\omega_2-\omega_1}{2\omega_n} = \frac{\omega_n(\sqrt{1+\zeta^2}+\zeta) - \omega_n(\sqrt{1+\zeta^2}-\zeta)}{2\omega_n} = \zeta \qquad \frac{1630-1535}{2(1580)} = .030 = \zeta$$

FIGURE 9.10 CALCULATION OF MODAL DAMPING FACTOR FOR THE FIRST MODE (THE SAME PLOTS AS IN FIG. 9.6 c).

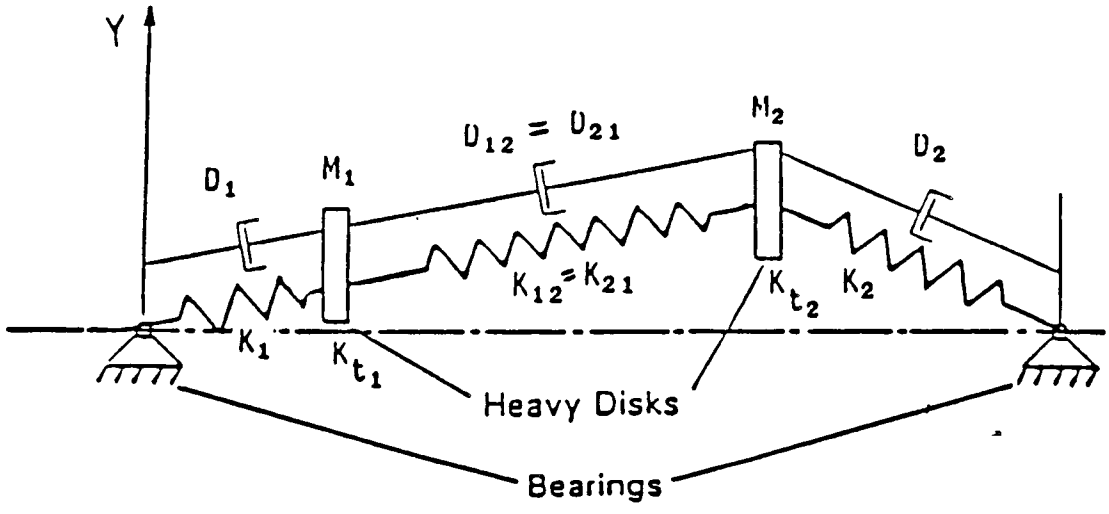

FIGURE 9.11 TWO DEGREE OF FREEDOM ROTOR MODEL.

(a)

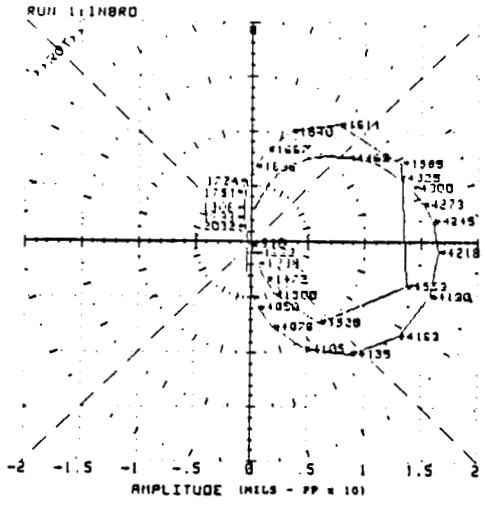

(b)

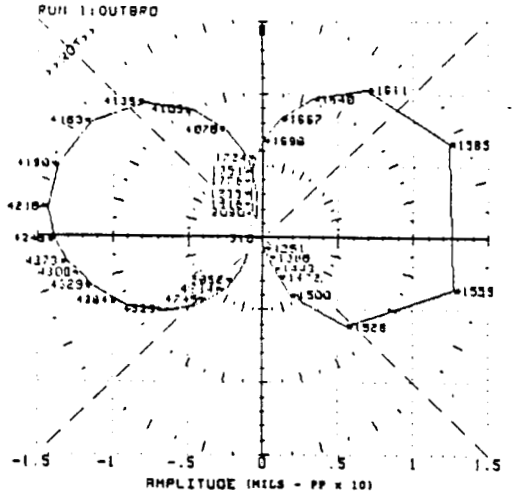

RUN 1 -- UNBALANCE: .5 GRAMS, 180 DEGREES, RADIUS = 1.2 IN, INBOARD.

(c)

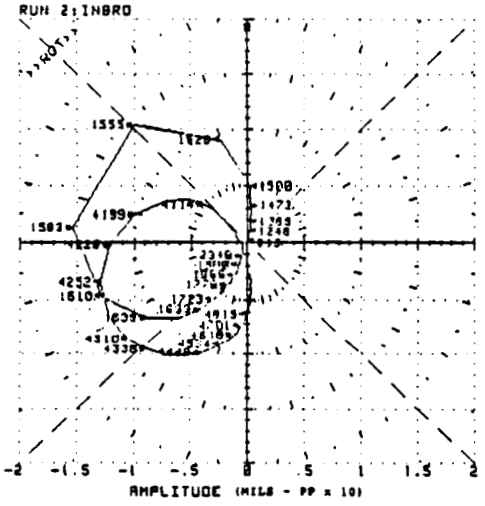

(d)

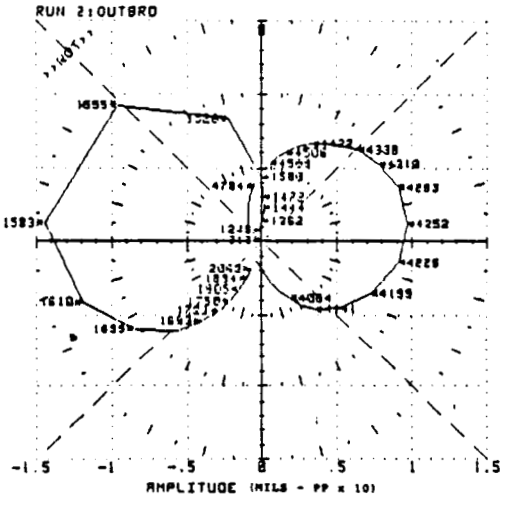

RUN 2 -- UNBALANCE: .5 GRAMS, 0 DEGREES RADIUS, = 1.2 IN, INBOARD.

FIGURE 9.12 POLAR PLOTS OF ROTOR SYNCHRONOUS RESPONSE AT THE INBOARD ((a) AND (c)) AND OUTBOARD ((b) AND (d)) LOCATIONS WHEN THE CONTROLLED UNBALANCE WAS IN THE INBOARD PLANE AT 180° ((a) AND (b)) AND 0° ((c) AND (d)).

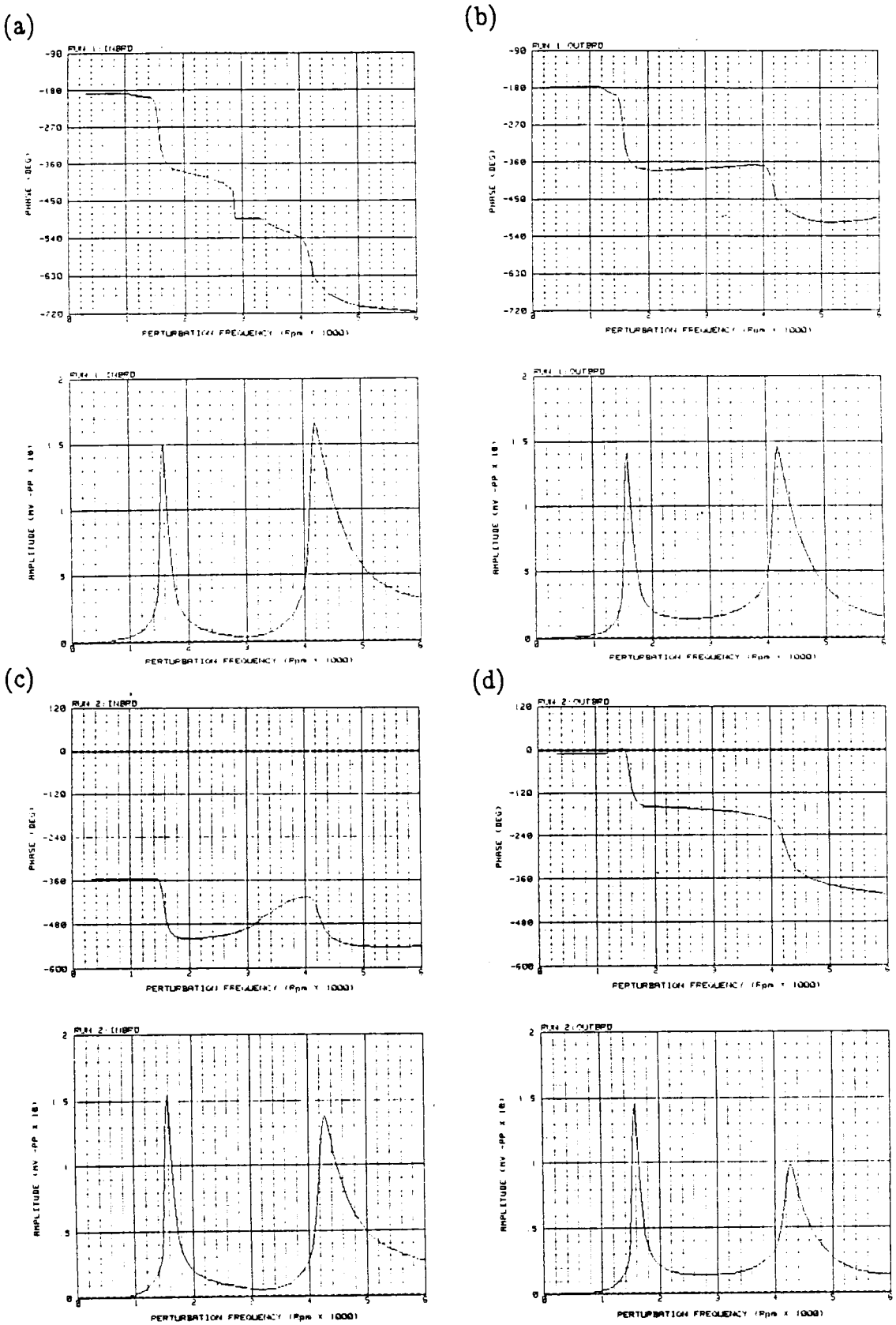

FIGURE 9.13 BODÉ PLOTS OF ROTOR SYNCHRONOUS RESPONSE AT THE INBOARD ((a) AND (c)) AND OUTBOARD ((b) AND (d)) LOCATIONS WHEN THE CONTROLLED UNBALANCE WAS IN THE INBOARD PLANE AT 180° ((a) AND (b)) AND 0° ((c) AND (d)).

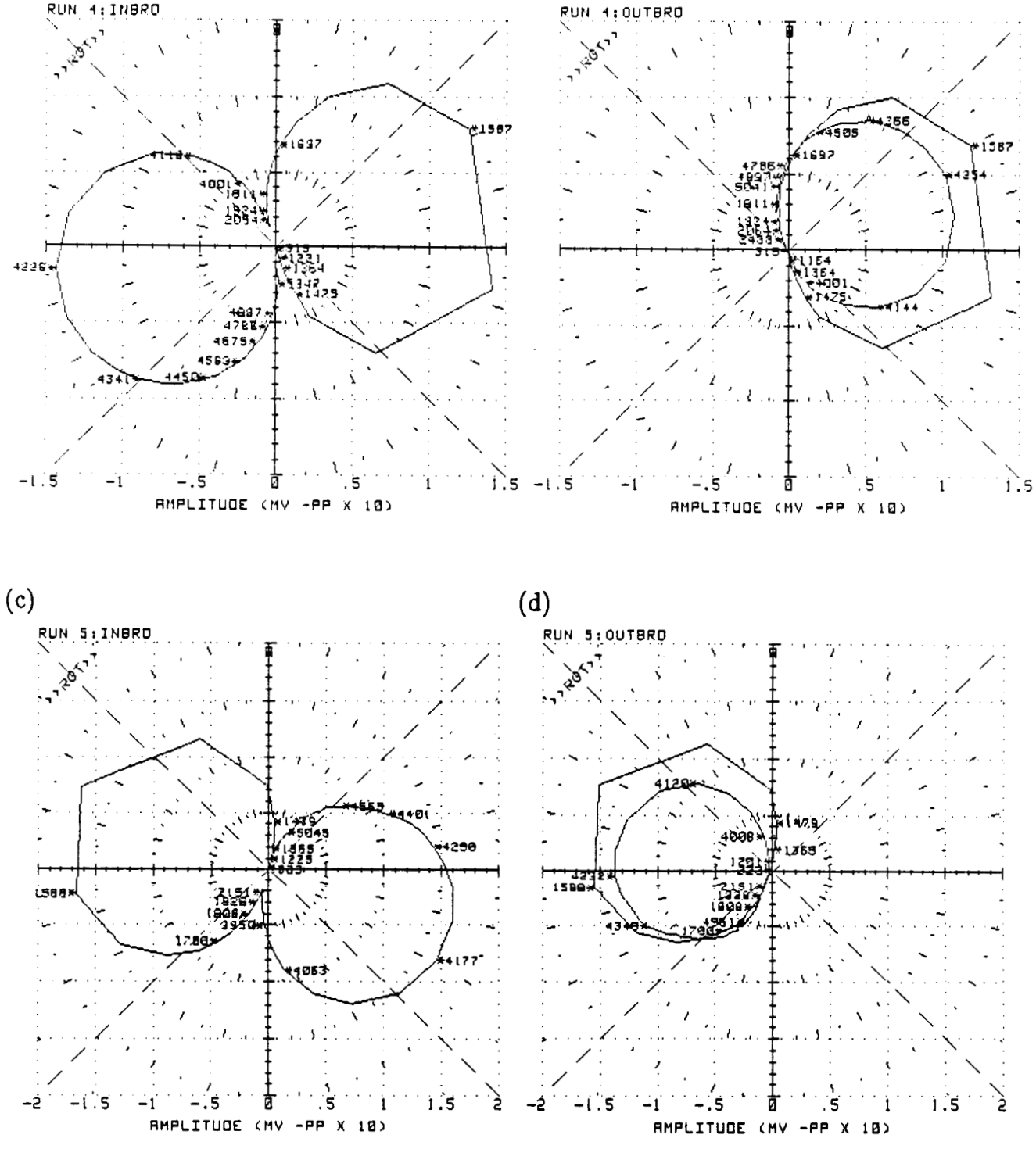

FIGURE 9.14 POLAR PLOTS OF ROTOR SYNCHRONOUS RESPONSE AT THE INBOARD ((a) AND (c)) AND OUTBOARD ((b) AND (d)) LOCATIONS WHEN THE CONTROLLED UNBALANCE WAS IN THE OUTBOARD PLANE 180° ((a) AND (b)) AND 0° ((c) AND (d)).

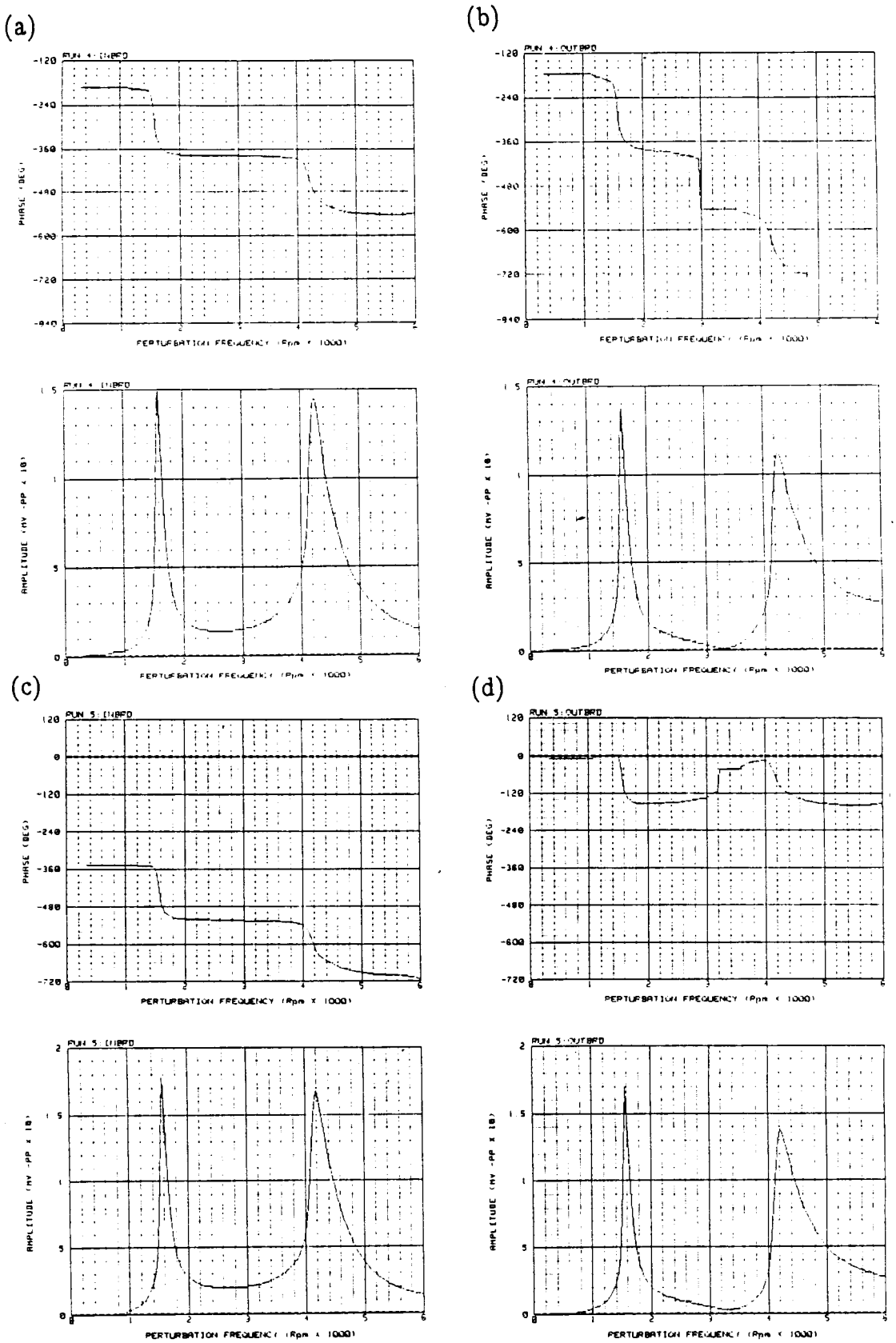

FIGURE 9.15 BODÉ PLOTS OF ROTOR SYNCHRONOUS RESPONSE AT THE INBOARD ((a) AND (c)) AND OUTBOARD ((b) AND ((d)) LOCATIONS WHEN THE CONTROLLED UNBALANCE WAS IN THE OUTBOARD PLANE 180° ((a) AND (b)) AND 0° ((c) AND (d)).

(a)

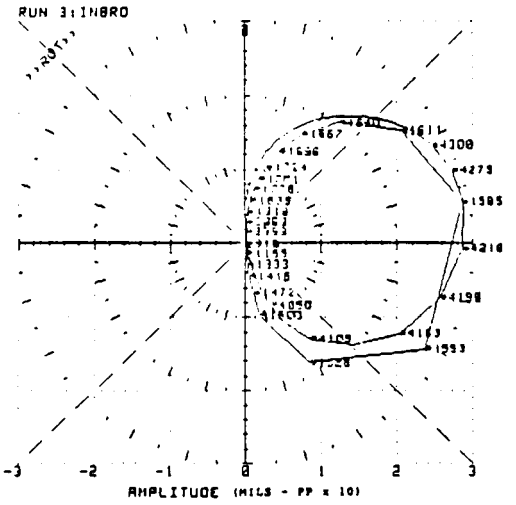

(b)

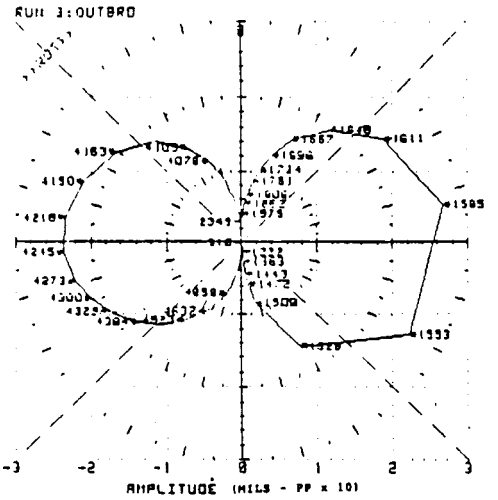

RUN 3 -- VECTOR SUBTRACTION OF RUN 1 — RUN 2, EFFECTIVE UNBALANCE:
1 GRAM, 180 DEGREES, RADIUS = 1.2 IN, INBOARD.

(c)

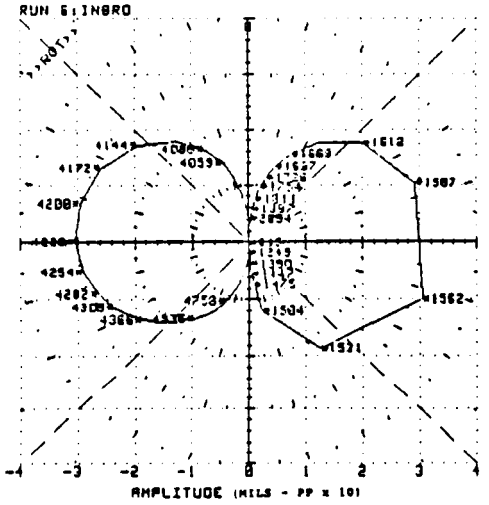

(d)

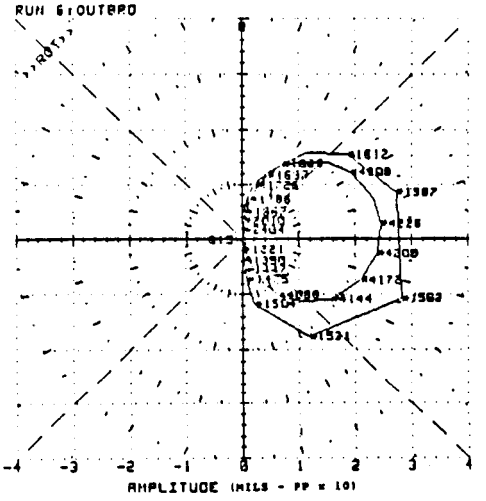

RUN 6 -- VECTOR SUBTRACTION OF RUN 4 — RUN 5 SECOND DATA
RUN REQUIRED FOR TWO DEGREES OF FREEDOM SYSTEM. EFFECTIVE UNBALANCE:
1 GRAM, 180 DEGREES, RADIUS = 1.2 IN, OUTBOARD.

FIGURE 9.16 POLAR PLOTS OF THE VECTORIALLY SUBTRACTED DATA PRESENTED IN FIGURES 9.12 AND 9.14: THE MATRIX OF POLAR PLOTS OF THE ROTOR NET RESPONSES AT THE INBOARD ((a) AND (c)) AND OUTBOARD ((b) AND (d)) LOCATIONS TO CONTROLLED UNBALANCES AT THE INBOARD ((a) AND (b)) AND OUTBOARD ((c) AND (d)) PLANES CORRESPONDINGLY.

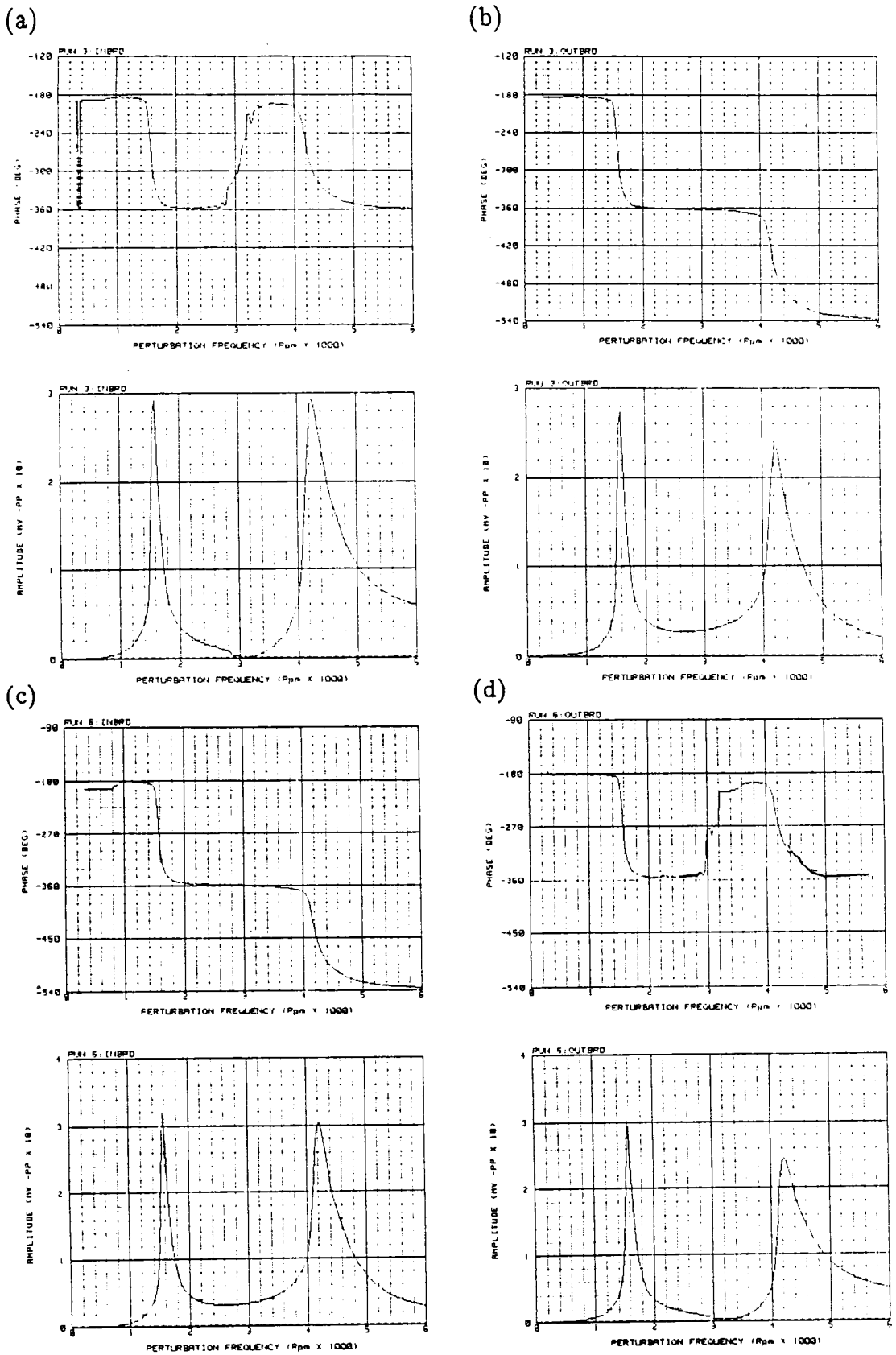

FIGURE 9.17 BODÉ PLOTS OF THE VECTORIALLY SUBTRACTED DATA PRESENTED IN FIGURES 9.13 AND 9.15: THE BODÉ MATRIX OF NET THE ROTOR RESPONSE AT THE INBOARD ((a) AND (c)) AND OUTBOARD ((b) AND (d)) LOCATIONS TO CONTROLLED UNBALANCES AT THE INBOARD ((a) AND (b)) AND OUTBOARD ((c) AND (d)) PLANES CORRESPONDINGLY.

ORIGINAL PAGE IS
OF POOR QUALITY

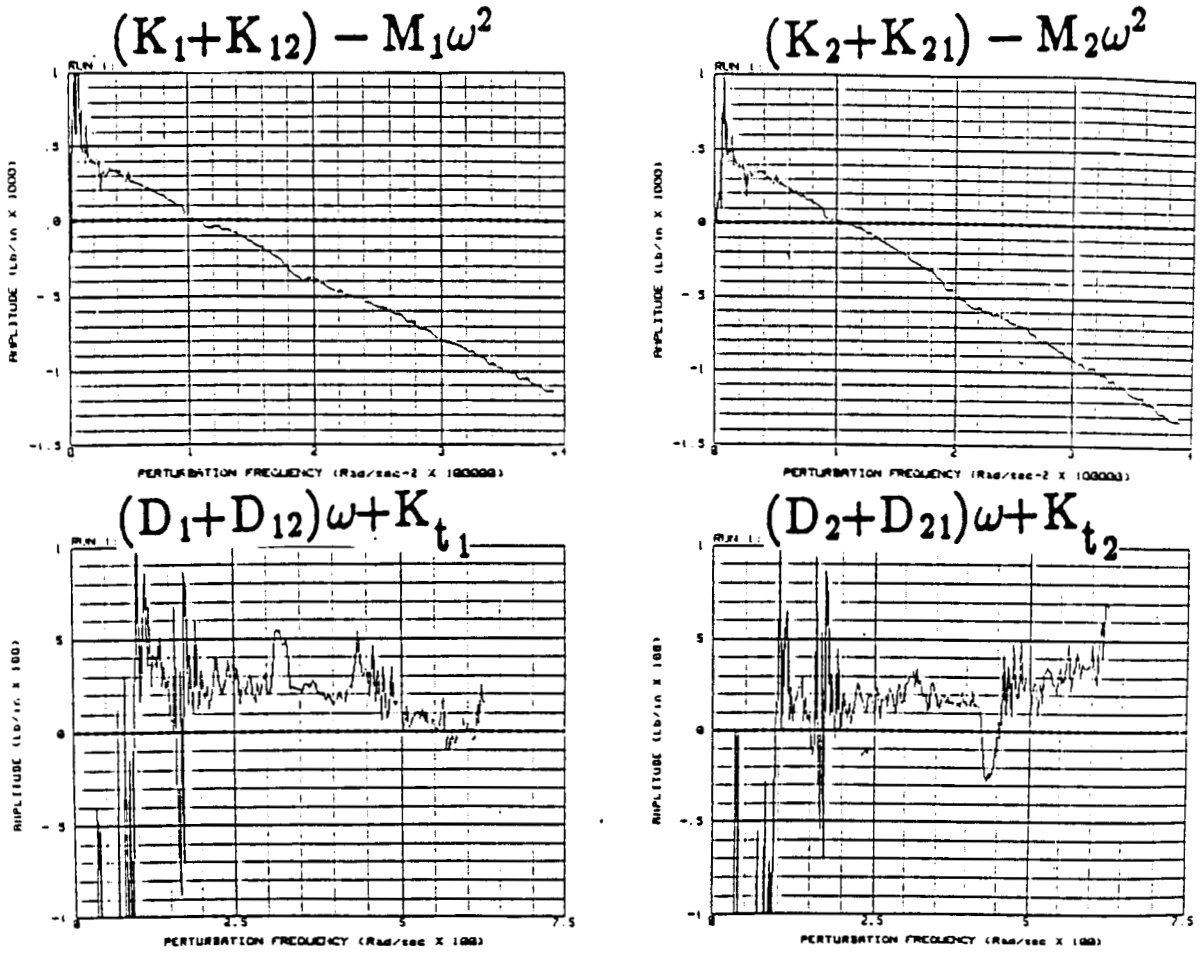

FIGURE 9.18 DIRECT AND QUADRATURE DYNAMIC STIFFNESS COMPONENTS.

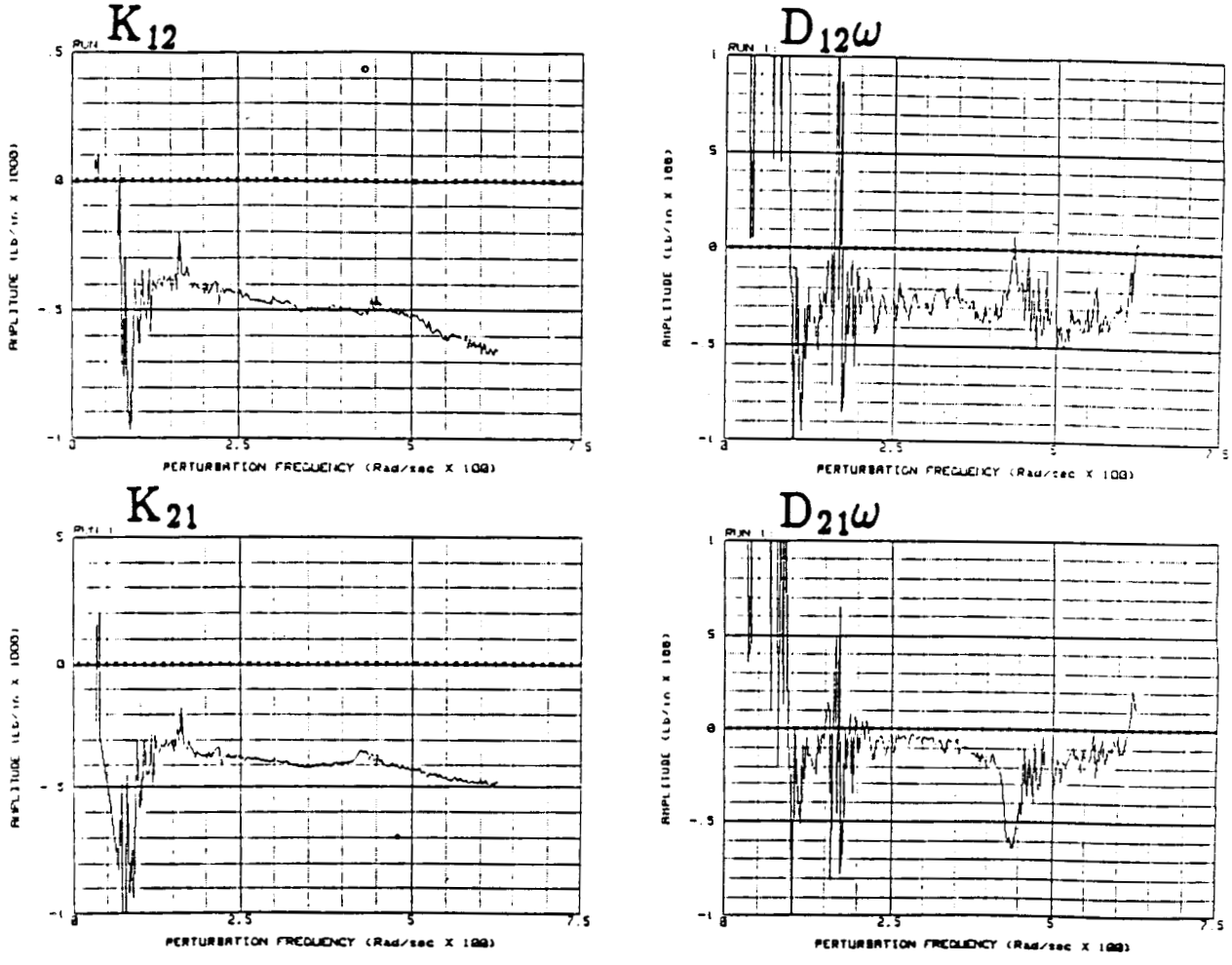

FIGURE 9.19 COUPLED DYNAMIC STIFFNESS COMPONENTS.

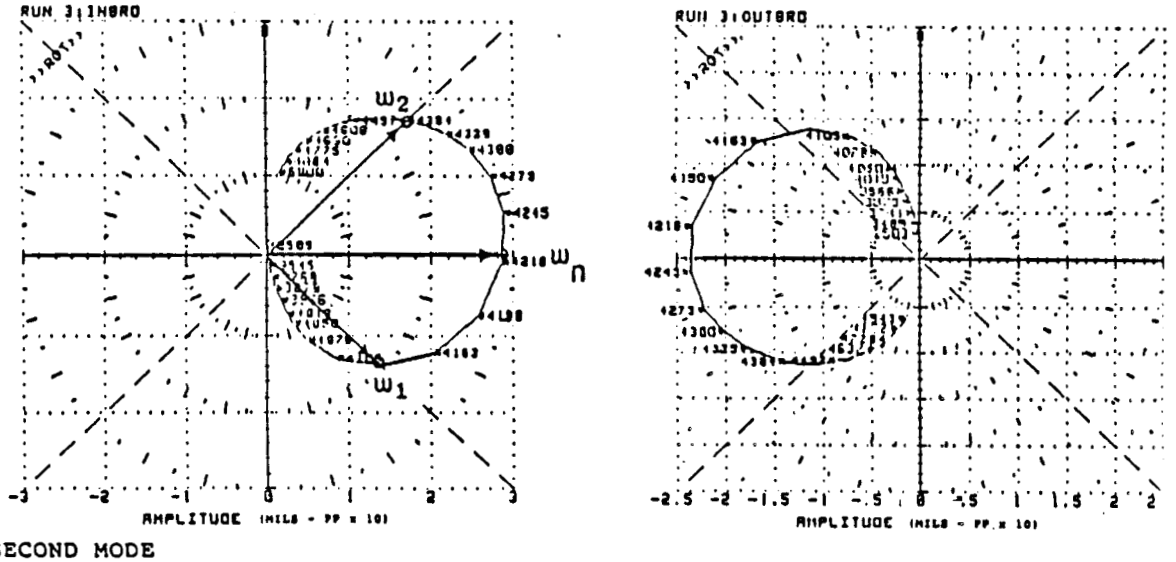

SECOND MODE

$$\frac{\omega_2-\omega_1}{2\omega_n} = \frac{\omega_n(\sqrt{1+\zeta^2}+\zeta) - \omega_n(\sqrt{1+\zeta^2}-\zeta)}{2\omega_n} = \zeta \qquad \frac{4394-4120}{2(4225)} = .032 = \zeta$$

FIGURE 9.20 CALCULATION OF THE SECOND MODE DAMPING FACTOR USING HALF–POWER BANDWIDTH METHOD.

10. RESULTS OF PARTIAL ROTOR–TO–STATOR RUB EXPERIMENTS ON TWO–MODE ROTOR RIG.

10.1 Introduction

Partial rotor–to–stator rub is the condition when the rotor occasionally touches the stator during its precessional (orbital) motion and maintains contact with the stator for a short time, a fraction of the precessional period. The partial rotor–to–stator rub conditions usually occur when the rotor vibrates (precesses) around an eccentric position within the rotor/stator clearance, and the vibration amplitudes are high enough to exceed the available clearance. Described in Chapter 9, the two–mode rotor rig with the adjustable stiffness plunger mechanism simulating the stator is used to generate the rotor–to–stator partial rub. In the test there was no radial force applied to the shaft. Rubbing occurred due to rotor unbalance–related high amplitude vibrations around the neutral centerline.

10.2 Test Procedure

The description of the rig is given in Section 9.2. Using the controlled unbalance–generated rotating force introduced at the inboard plane to achieve the required level of the synchronous vibrations in order to initiate a rotor–to–stator rub, both transient (during start–ups and shutdowns) and steady–state data (at constant rotative speed) have been acquired through noncontacting proximity probes and accelerometers. In this Chapter the transient data (run–up) are presented in polar, Bodé, and spectral formats (cascade plots). Steady–state data are presented in orbit and timebase formats. Both transient as well as steady–state data have been captured using a variety of plunger spring preloads, i.e., for various stator/casing compliances. Operating speeds (for data recording) range from 300 to 10,000 rpm, running well above the second balance resonance speed for this rotor rig in its present configuration (Fig. 9.2).

10.3 No–Rub Test

For this test the rub block was removed from the rig. The rotor was then run, and it exhibited a considerable amount of unbalance. The balancing procedure was then performed. Transient data representing both unbalanced and balanced states is presented in Figs. 10.1 to 10.21. This data clearly shows the first and second balance resonances which occur at about 1600 and 4300 rpm respectively.

Spectrum Cascade plots indicate dominance of synchronous (1×) component typically generated by unbalance forces. Accelerometer data indicated the lack of lower frequency components (below 250 Hz) with maximum amplitudes for higher order harmonic components (in the range from 250 Hz to 1 KHz) being only .42 g's for both balanced and unbalanced states. Such small amplitudes provide little information as the accelerometer signal levels fall within noise levels.

10.4 Results From Rub Tests

The controlled unbalance weight to generate rotor–to–stator rub was located in the inboard disk. Its amount was 0.48 grams at 0 degrees related to the Keyphasor® notch. The slow roll amplitude was maintained less than .5 mils at all times. This means that the shaft was maintained straight (not bent) and other mechanical and electrical glitches minimized. For the series of data presented in this chapter, all runs were with the unbalance located at the inboard plane.

The aluminum rub block was installed on the rig. An example of the shaft vibrational, orbital (precessional) motion due to rub against the rub block is shown in Figure 10.22. Note that the orbit in this figure is magnified, while the rub block and the shaft sizes are reduced, so the picture represents the shaft actual behavior in qualitative terms only. The orbit very clearly indicates the rebounding effect of the rotor shaft caused by the rub.

The plunger preload was varied from zero through 3.34 lbs. and 6.68 lbs. to 10.03 lbs. The test parameters are given in Table 10.1.

TABLE 10.1 Partial Rub Test Parameters

Plunger Preload Force [lbs]	Rotative Speeds for Steady–State Data [rpm]	Data Presented in Figures
0	1600 3866	10.23 to 10.28
3.34	1573 1603 1915 3919 5652	10.29 to 10.41 and 10.74 to 10.77
6.68	1565 1614 1936 3924 5211 5637 7037	10.42 to 10.59 and 10.78 to 10.83
10.03	1581 1613 1930 3989 5836	10.60 to 10.73

Transient rub data from displacement probes show the presence of both subsynchronous and supersynchronous vibration components. The spectrum cascade plots of the displacement probe signals indicate high amplitude subsynchronous components with frequencies 1/2×, 1/3×, and 1/4× rotative speed with significantly high amplitudes at rotative speeds equal a multiple of the first balance resonance speed (Figs. 10.23, 10.29, 10.30, 10.42, 10.43, 10.60, and 10.61). Data from the horizontal accelerometer mounted on the plunger shows highly defined, well ordered higher harmonic components. However, the prevalence of these components diminish with increasing preload (simulating a decreasing stator compliance) of the plunger mechanism (Figs. 10.24, 10.31, 10.44, 10.45, 10.62, and 10.63).

Plunger movement caused by a rub is monitored via a displacement probe mounted axially at the far end of the rub fixture. Plunger movement data is presented with data from the electrical contact device (Figs. 10.26, 10.28, 10.33, 10.35, 10.37, 10.39, 10.41, 10.47, 10.49, 10.51, 10.53, 10.55, 10.57, 10.59, 10.65, 10.67, 10.69, 10.71, and 10.73). This provides a correlation between the onset of rub and actual plunger movement. As previously mentioned, the rub does not necessitate plunger movement. Only when the horizontal component (parallel with the plunger axis) of the rub force exceeds the plunger preload will movement occur.

When the stator compliance is large, the plunger shows significant motion during rub (Figs. 10.26, 10.28). This motion gradually decreases with increasing stator stiffness (Figs. 10.39, 10.41, 10.55, 10.57, and 10.73). When the stator stiffness is high enough, and the rotor–to–stator rub normal force is relatively small, the plunger does not move (Figs. 10.33, 10.35, 10.37, 10.47, 10.49, 10.51, 10.53, 10.59, 10.65, 10.67, 10.69, and 10.71). This indicates that in these cases the horizontal component of the rotor/stator normal force is lower than the corresponding plunger preload force.

The contact device provides the indication whether and when in the vibrational period the physical contact of the rotor–to–stator occurs. It indicates that sometimes the rotor rubs only once per precessional period (Figs. 10.26, 10.28, 10.37, 10.39, 10.51, 10.53, 10.65, 10.69 for 1× rub, Figs. 10.41 and 10.71 for 1/2× rub, Figs. 10.55 and 10.73 for 1/3× rub, and Fig. 10.57 for 1/4× rub). Sometimes the rotor rubs twice (Figs. 10.35, 10.47, 10.67) or three times (Fig. 10.49) per precessional period. Sometimes the rubbing contact is quite irregular (Fig. 10.33).

Steady–state data from the rubbing rotor presented in orbit/timebase formats also indicate the presence of both subsynchronous and supersynchronous vibration components (Figs. 10.25, 10.27, 10.32, 10.34, 10.36, 10.38, 10.40, 10.46, 10.48, 10.50, 10.52, 10.54, 10.56, 10.58, 10.64, 10.66, 10.68, 10.70, and 10.72). The stator compliance has an effect on the rotor response orbital motion (compare Figs. 10.25, 10.34, and 10.66; Figs. 10.27, 10.38, 10.52, and 10.70; Figs. 10.36, 10.50, and 10.68; Figs. 10.40 and 10.72). To better represent the relationship between rub and the shaft motion, orbit plots at the location of rub from a variety of rub cases can be overlayed with a sketch of the rub block surface (Figs. 10.74 to 10.83).

From the rub data presented, it becomes apparent that the actual rotative speed and the casing/stator simulating plunger rub mechanism compliance play a significant role in the rotor vibrational response. Figure 10.84 presents a summarizing table of rotor orbits for several rotative speeds and several values of stator compliance.

10.5 Results Obtained From Displacement Probes Versus Results Obtained From Accelerometers

With less preload on the plunger mechanism (higher casing/stator compliance), accelerometer data from the plunger indicates significant excitation of higher frequency components (from 5 Kcpm to 15 Kcpm, i.e., 83.3–250 Hz), with displacement probes showing only a short period of 1/2× vibration. As plunger compliance decreases, accelerometer data indicates decreasing excitation of higher frequency components while displacement probes show greater excitation of subsynchronous vibration components (i.e., 1/4×, 1/3×, 1/2×). Accelerometers measure casing vibrations transmitted from the rotor, while displacement probes measure rotor vibrations directly at the source. Relatively speaking, lower frequency vibrations correspond to large displacements. As plunger

preload and stiffness increases, its displacement range must decrease, provided external forces remain constant. This results in the progressive lack of lower frequency components in the accelerometer readings. The accelerometer, through the casing, measures the indirect vibrations transmitted from its source, i.e., from the rotor through the casing. The accelerometer reading is also significantly affected by the casing transmissibility: in general a soft casing would transmit higher level of vibration; a rigid casing would exhibit only very low level. The transmissibility is also a function of casing geometry. In practical application of accelerometer casing measurements this fact should be taken into consideration. Since the casing transmissibility is generally not known, a caution should be applied if the accelerometer measurements do not indicate any vibrations. It is well known that accelerometers are sensitive to higher frequency vibrations, as the acceleration amplitudes are proportional to frequency squared, thus become significantly magnified in high frequency range. Accelerometers are practically useless in low frequency vibration measurements. Low frequency acceleration amplitudes usually do not exceed accelerometer sensitivity level. The proximity probes measuring rotor displacement relative to the stator are the most convenient transducers for rotating machines. They not only measure the direct source of machine vibrations, i.e., the rotor actual motion, but also they are sensitive in low frequency range of vibration (including rotor static position). The rotor low frequency vibrations (especially those in subsynchronous region) usually exhibit the highest amplitudes, and they are the most dangerous for the machine integrity.

The successively increasing amplitudes of subsynchronous vibrations from about 1.5 to 2.5 pp mils at ~4000 rpm (Figs. 10.23 and 10.61), as indicated by the displacement probes are correlated to increasing plunger preload. The increase in plunger preload effectively increases the stator/casing rigidity and the coefficient of restitution, thus the velocity of the rotor shaft after impact, and resultant displacement are accordingly higher.

10.6 Investigation of Multiple Partial Rub With Full 360 Degree Rub Fixture

The two–mode rubbing rotor rig assembled to aid in the study of rub incorporated a half cylinder rub fixture described in Chapter 9, (Fig. 9.1). It limited the occurrence of rub to a 180 degree surface while allowing motion of the plunger mechanism, simulating the casing, only along a horizontal axis.

To help further investigate the phenomena of rub, as they occur in seals of the HPFTP simulation rig, a prototype rub fixture was built. This rub fixture is referred to as the "360 degree rub fixture". The 360 degree rub fixture incorporates a ring suspended by four tension springs, allowing for its motion in the X–Y plane and its steady state position to be adjustable. This feature may be used to simulate misalignment or rotor shaft preload. Both rotor shaft and fixture ring X–Y motion are monitored via displacement probes. A sketch of the 360 degree rub fixture is given in figure 10.85. The rotor rig test system with the 360 degree rub fixture are given in Figure 10.86.

As expected, initial testing of the rubbing rotor response provided different results from those obtained while using the 180 degree type rub fixture. The full 360 degree restraint of the rotor shaft provides a very significant rebounding effect. Initiated due to unbalance, the rub–related orbit represents a "star–like" motion shown in Figure 10.87 (a). The strong subsynchronous backward component indicated in Figure 10.87 (b) is due to excitation of the system first balance resonance, (28 Hz = 1680 RPM), slightly above that of the system first balance resonance without rub, (26.33 Hz = 1580 RPM). The rub coupling of the rotor and stator modifies the system stiffness, increasing it slightly, thus causing the higher first balance resonance. The occurrence of this "star–like" orbit represents a potentially destructive phenomenon by introducing large amplitude backward components in the rotor response.

After preliminary testing this series of experiments was however discontinued, due to lack of time.

10.7 Summary

The results of partial rotor–to–stator rubbing experiments performed on the two–mode rotor rig are presented in this chapter. For four values of the stator stiffness simulated by the plunger preload, the general features of the obtained results can be summarized as follows:

- Rotor–to–stator partial rub causes significant changes in rotor vibration responses in frequency content, in amplitudes and orbital shapes of the rotor motion.
- The light partial rub causes a steady–state rotor response which can be maintained during a considerable, but limited, time.
- When the rotor rotative speed is lower than twice first balance resonance speed (first natural frequency of the rotor bending mode), then the lowest component in the rotor vibration spectrum is 1× synchronous vibration. When the rotative speed ω is equal to or higher than twice first balance resonance speed (ω_r), the subsynchronous components appear in the vibrational spectrum: In the range $2\omega_r < \omega < 3\omega_r$ the 1/2× vibration components are generated. In the range $3\omega_r < \omega < 4\omega_r$ the 1/3× vibration components are generated.. This rule also extends for higher rotative speeds.
- When the rub conditions change (for instance, due to surface wear), the partial rub may stop, and with a transient response, the rotor comes back to the original 1× response due to the residual unbalance. This transient response has the frequency equal to the first natural frequency of the rotor. Due to uneven wear of the surfaces, the transient responses may appear occasionally in the vibrational spectrum.
- Since the stator was simulated by a half of a ring, the partial rub occurred at either one spot or at several spots of the stator ("multiple partial rub"). It was, however, difficult to predict.
- The stator compliance has a significant effect on rubbing rotor responses. Stator large compliance (low rigidity) results in the stator plunger motion, thus rotor vibration amplitudes are lower in comparison to the case of low compliance, when entire energy goes into the rotor motion, resulting in rotor higher vibration amplitudes. The stator compliance has also an effect on shape of the resulting orbital motion of the rotor.
- The same experimental data captured by the displacement proximity probes and the accelerometer mounted on the rotor casing differ considerably. The proximity probes provide distinct vibrations in low frequency range. Their readings reproduce the rotor motion in its orbital shape. The accelerometer provides only high frequency components in the vibrational spectrum. When rub occurs and causes high amplitude, low frequency vibration, the accelerometer shows the appearance of a wide range of high frequency components (measured up to 1 kHz). The accelerometer readings are affected by the stator compliance, however, vibration components with "relatively high" amplitudes may still be generated when the stator rigidity is large and vibration frequencies are high.

The experimental results on the rotor–to–stator partial rub with only two variable parameters, namely, the rotative speed and the stator compliance provided a manifold matrix of results, proving that rub has very rich occurrences. Preliminary results on rotor rubbing against a 360 degree seal–simulating rub fixture show that the boundary geometry plays an important role in the rotor rub–affected response.

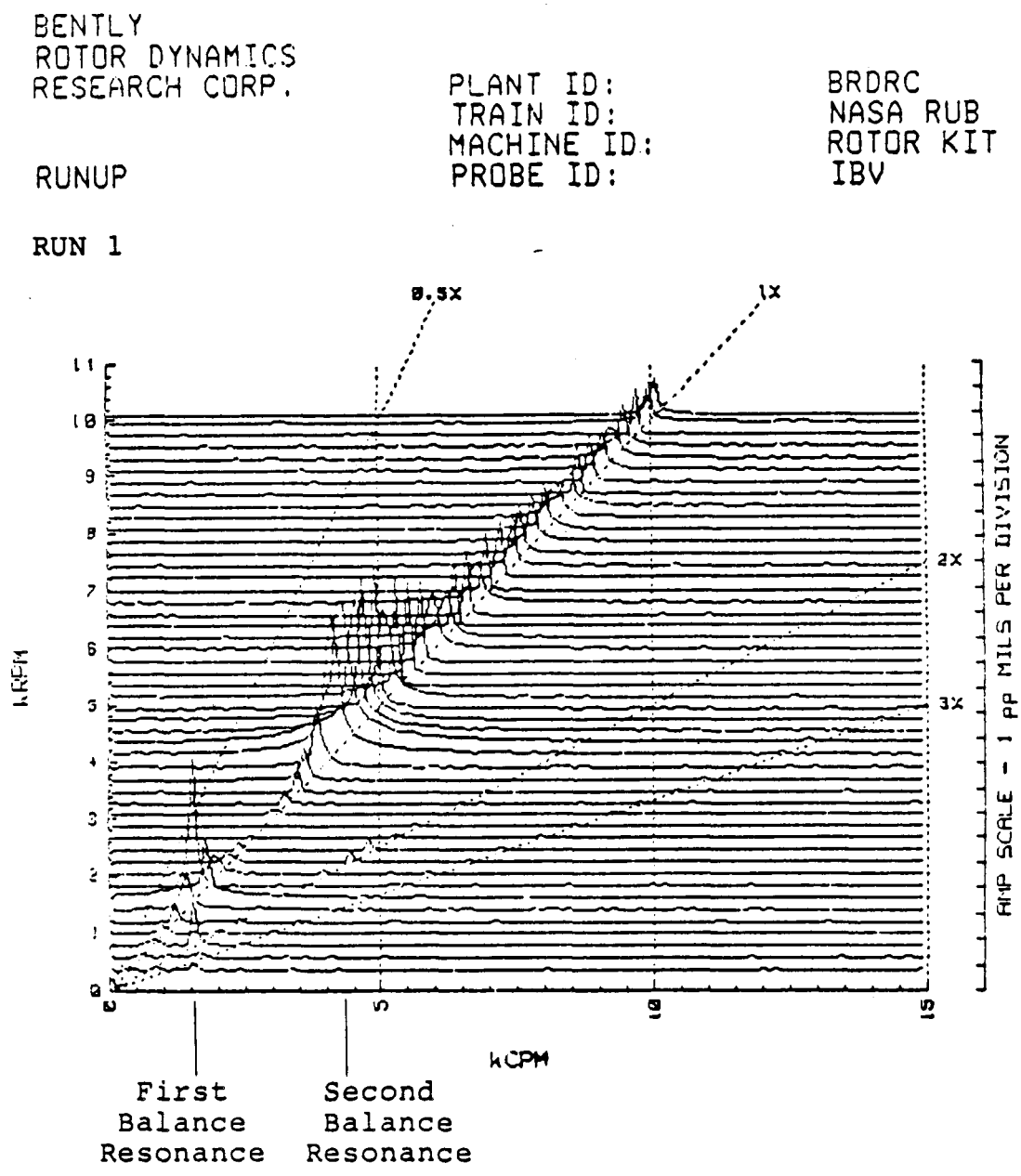

FIGURE 10.1 SPECTRUM CASCADE PLOT OF THE ROTOR VIBRATION DURING RUN–UP AS SEEN BY INBOARD VERTICAL DISPLACEMENT PROBE. NOTE DOMINANT 1X (SYNCHRONOUS) RESPONSE (UNBALANCED, NO RUB).

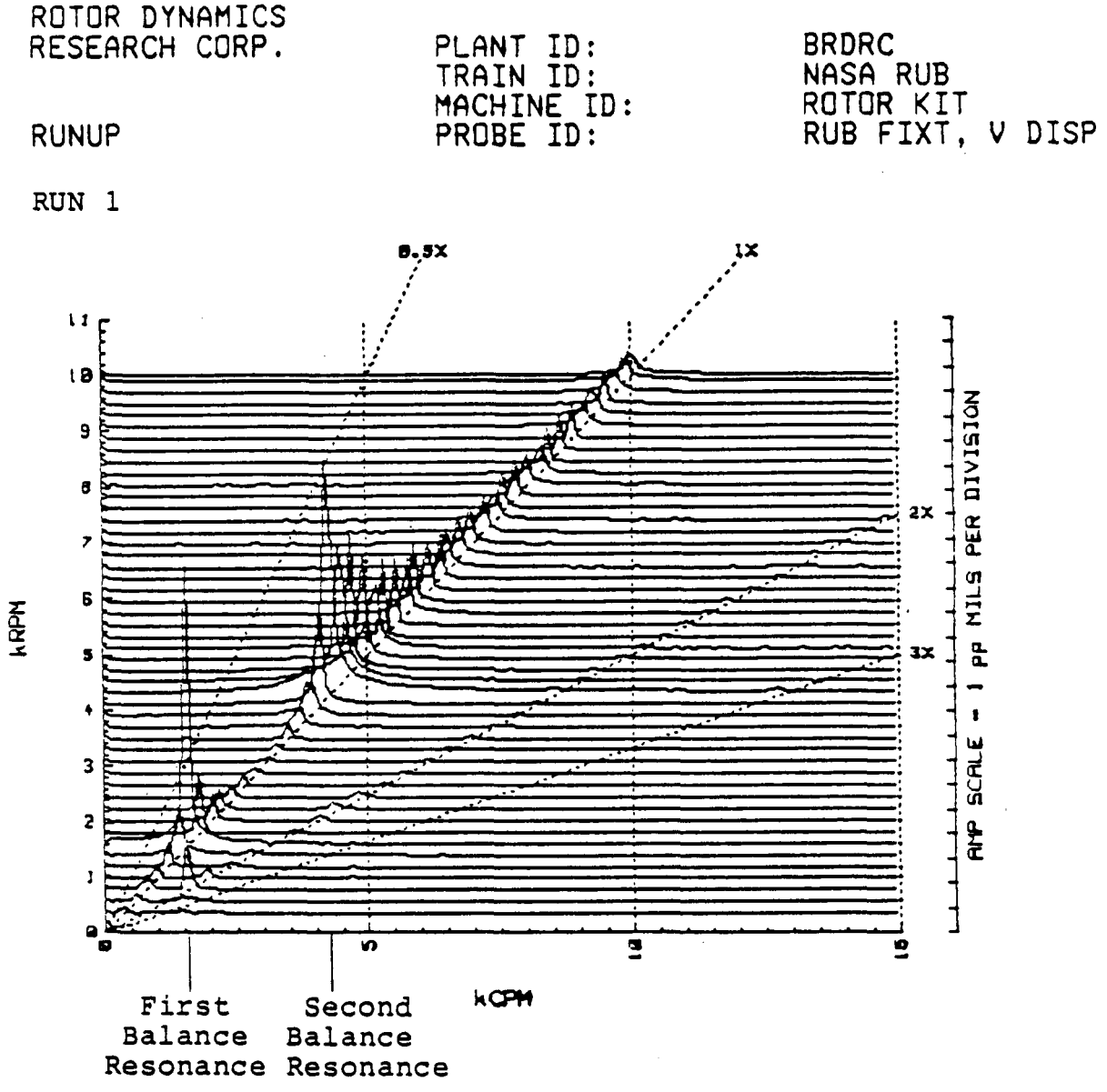

FIGURE 10.2 SPECTRUM CASCADE PLOT OF THE ROTOR VIBRATION DURING RUN–UP AS SEEN BY RUB FIXTURE VERTICAL DISPLACEMENT PROBE. NOTE DOMINANT 1X (SYNCHRONOUS) RESPONSE (UNBALANCED, NO RUB).

ORIGINAL PAGE IS
OF POOR QUALITY

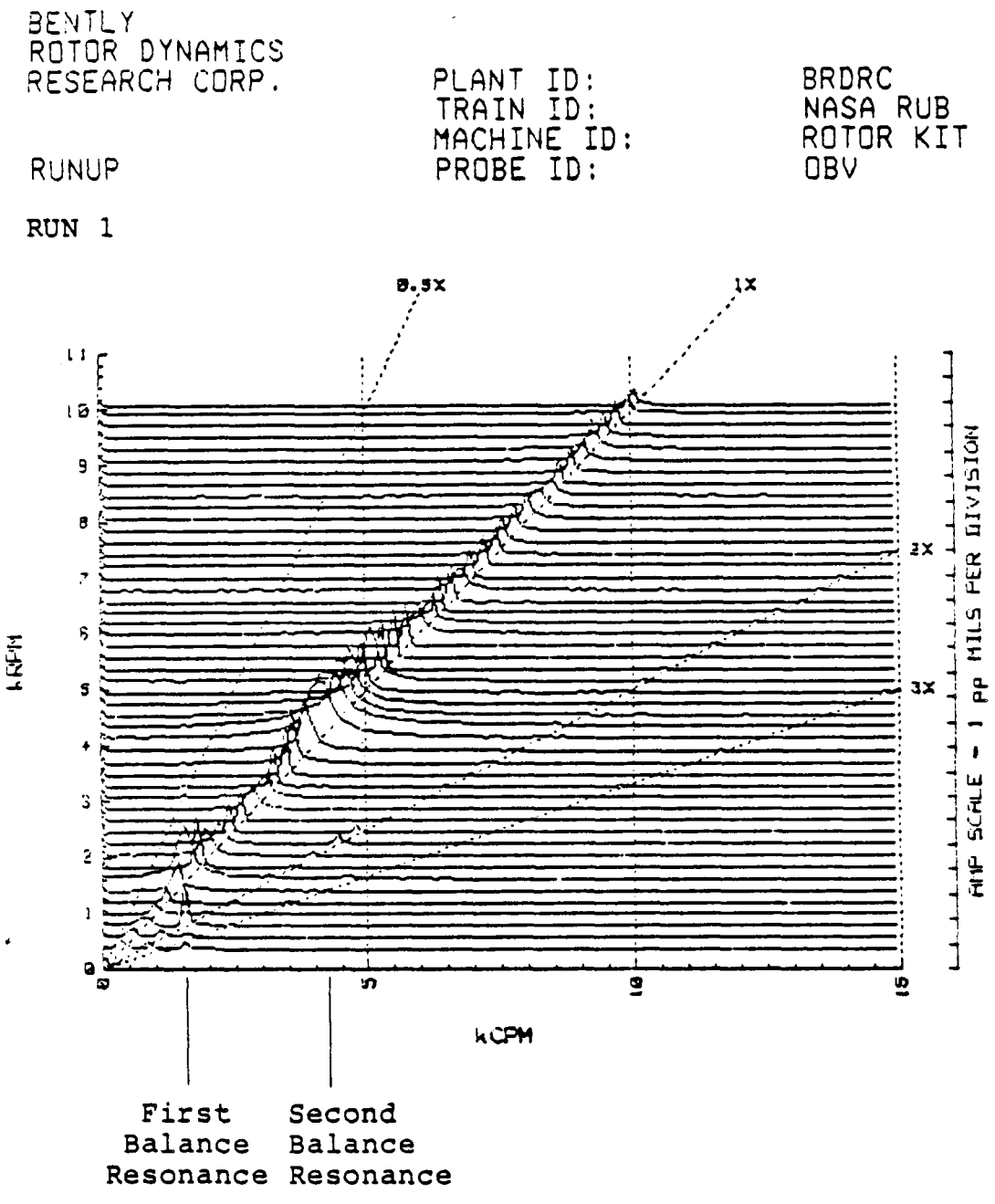

FIGURE 10.3 SPECTRUM CASCADE PLOT OF THE ROTOR VIBRATION DURING RUN–UP AS SEEN BY OUTBOARD VERTICAL DISPLACEMENT PROBE. NOTE DOMINANT 1X (SYNCHRONOUS) RESPONSE (UNBALANCED, NO RUB).

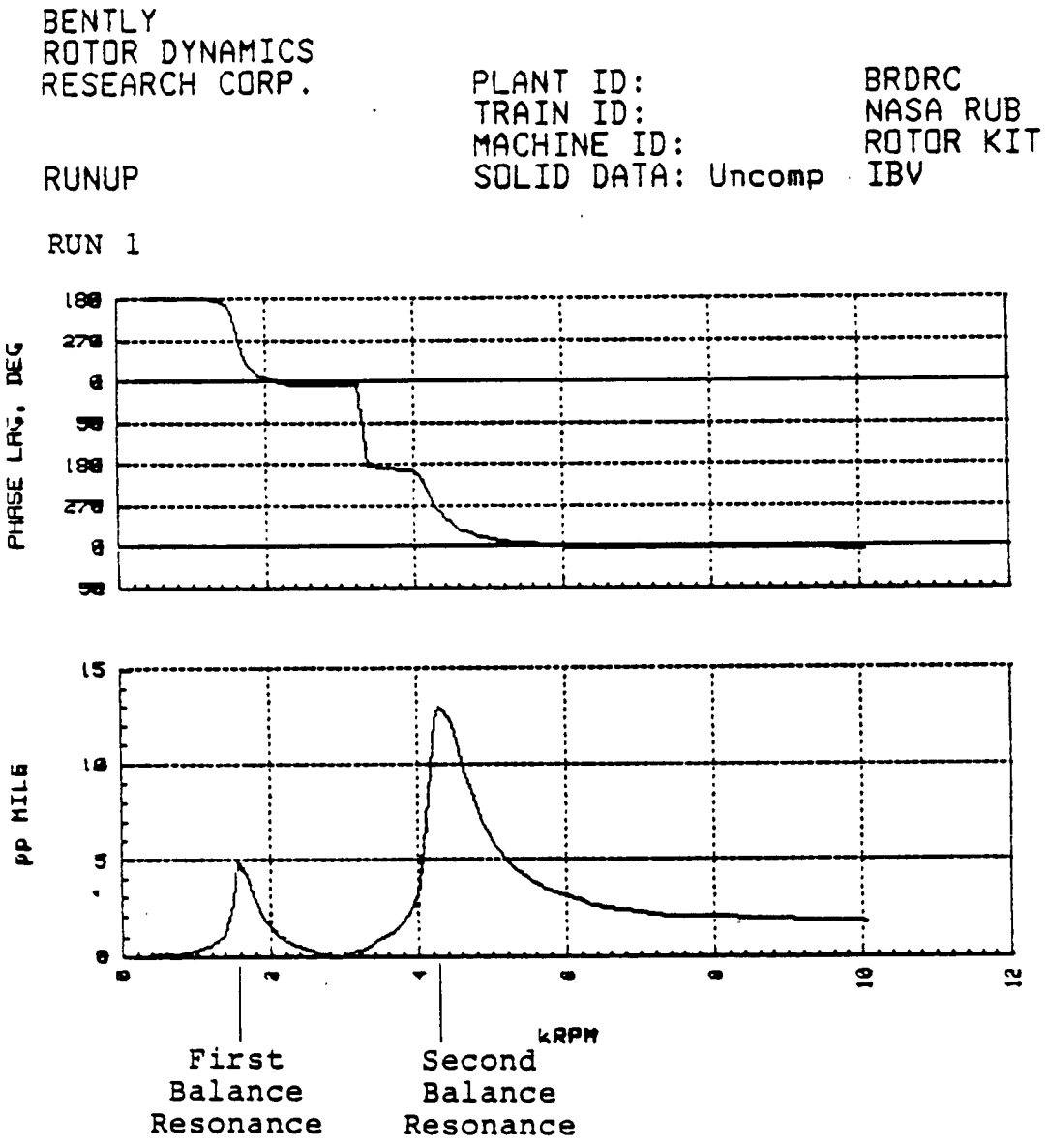

FIGURE 10.4 BODÉ PLOT OF THE ROTOR FILTERED SYNCHRONOUS VIBRATION RESPONSE DURING RUN–UP AS SEEN BY THE INBOARD VERTICAL DISPLACEMENT PROBE (UNBALANCED, NO RUB).

BENTLY
ROTOR DYNAMICS
RESEARCH CORP.

PLANT ID: BRDRC
TRAIN ID: NASA RUB
MACHINE ID: ROTOR KIT
SOLID DATA: Uncomp IBV

RUNUP
RUN 1

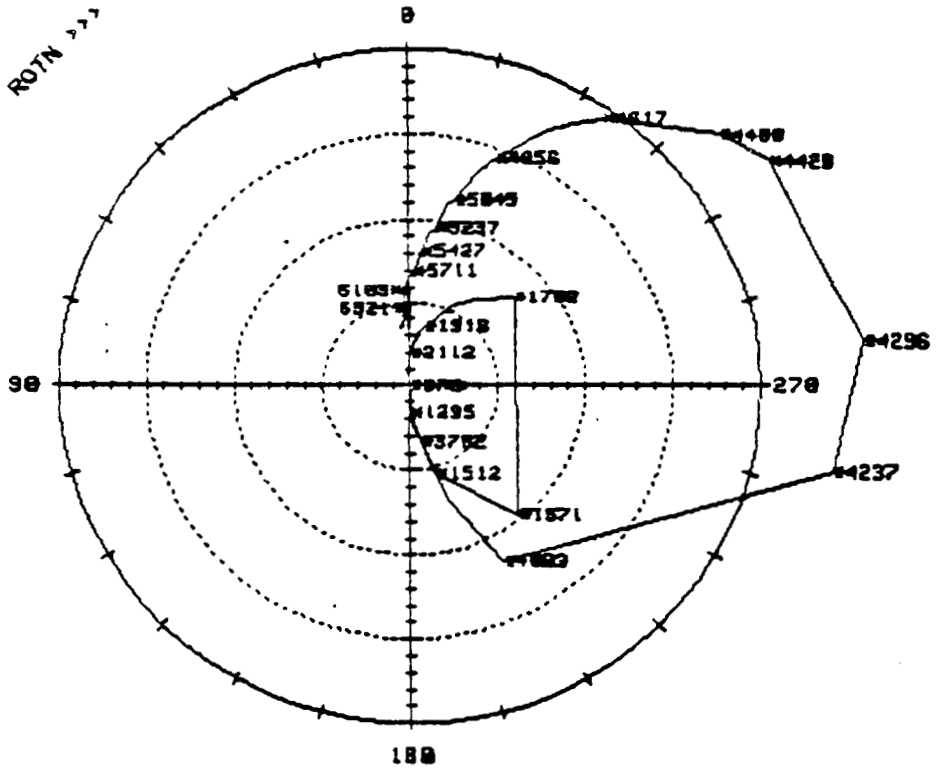

FULL SCALE AMP = 10 pp MILS AMP PER DIV = .5 pp MILS

FIGURE 10.5 POLAR PLOT OF THE ROTOR FILTERED SYNCHRONOUS VIBRATION RESPONSE DURING RUN–UP AS SEEN BY THE INBOARD VERTICAL DISPLACEMENT PROBE (UNBALANCED, NO RUB).

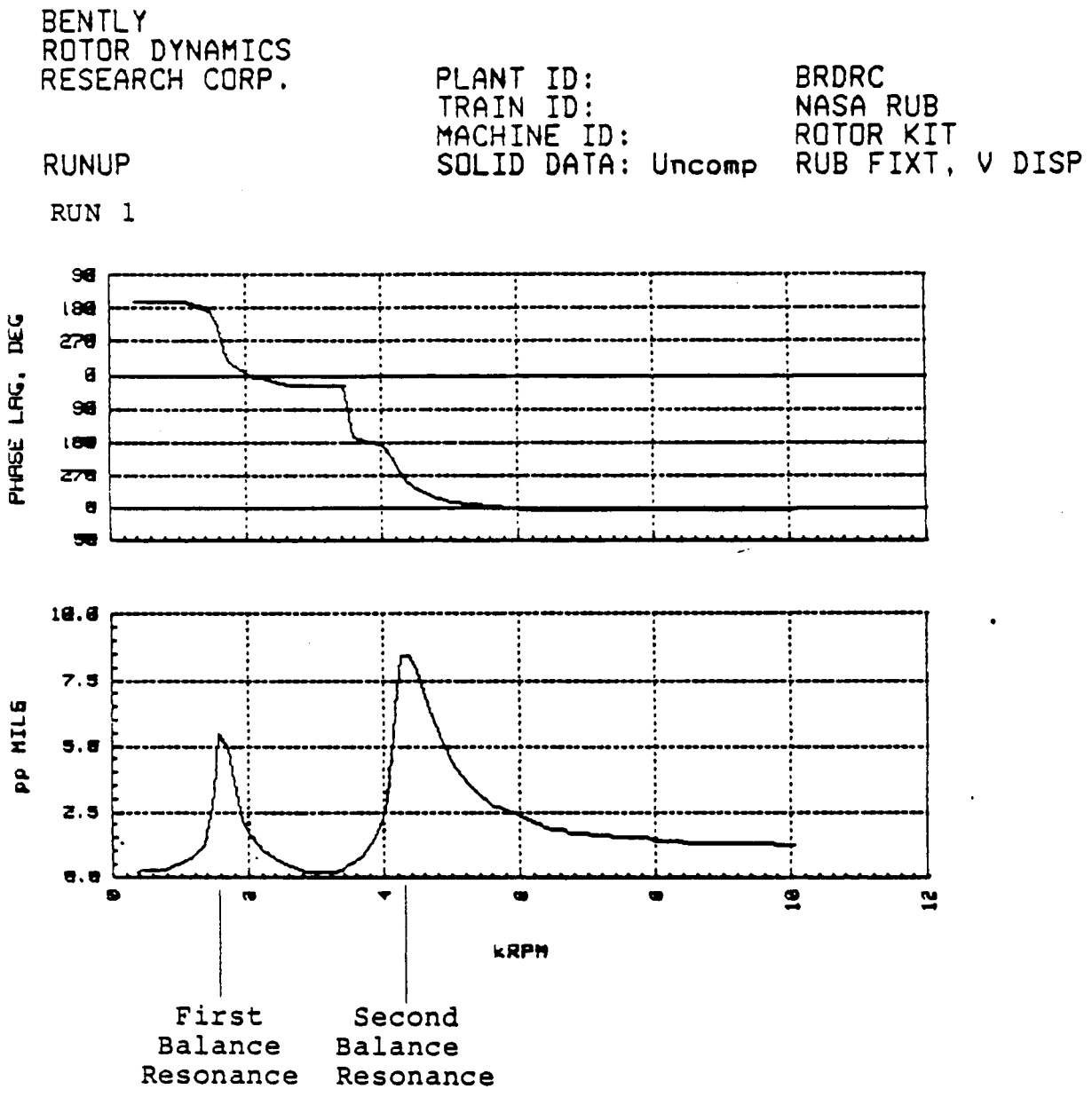

FIGURE 10.6 BODÉ PLOT OF THE ROTOR FILTERED SYNCHRONOUS VIBRATION RESPONSE DURING RUN–UP AS SEEN BY THE RUB FIXTURE VERTICAL DISPLACEMENT PROBE (UNBALANCED, NO RUB).

BENTLY
ROTOR DYNAMICS
RESEARCH CORP.

PLANT ID: BRDRC
TRAIN ID: NASA RUB
MACHINE ID: ROTOR KIT
SOLID DATA: Uncomp RUB FIXT, V DISP

RUNUP

RUN 1

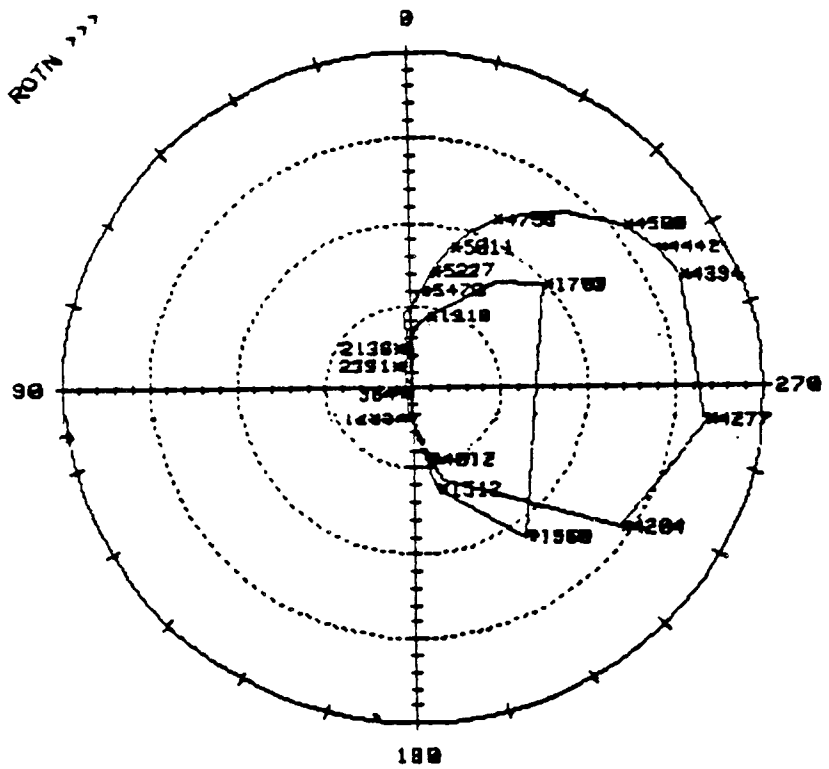

FULL SCALE AMP = 10 pp MILS AMP PER DIV = .5 pp MILS

FIGURE 10.7 POLAR PLOT OF THE ROTOR FILTERED SYNCHRONOUS VIBRATION RESPONSE DURING RUN–UP AS SEEN BY THE RUB FIXTURE VERTICAL DISPLACEMENT PROBE (UNBALANCED, NO RUB).

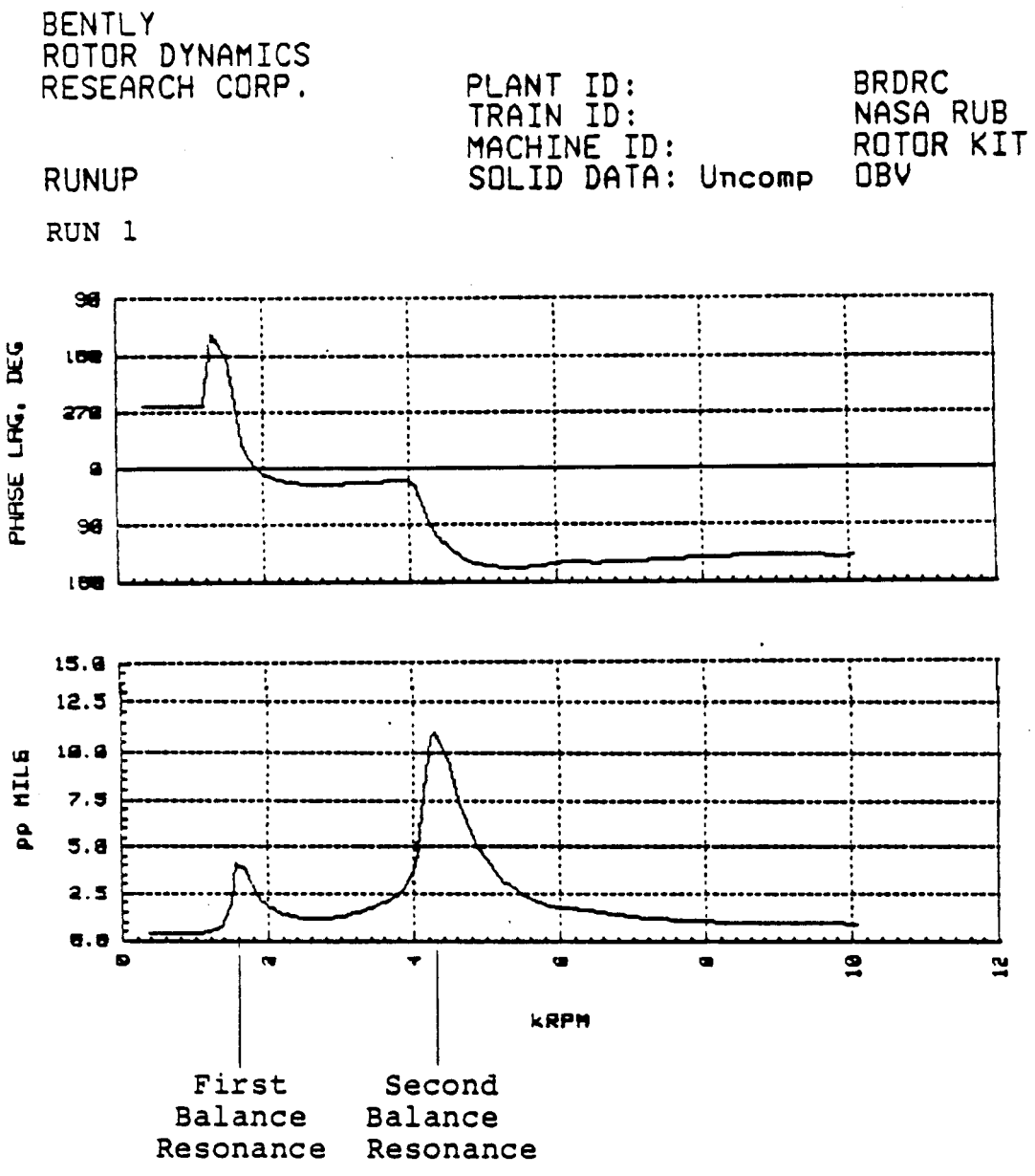

FIGURE 10.8 BODÉ PLOT OF THE ROTOR FILTERED SYNCHRONOUS VIBRATION RESPONSE DURING RUN–UP AS SEEN BY THE OUTBOARD VERTICAL DISPLACEMENT PROBE (UNBALANCED, NO RUB).

ORIGINAL PAGE IS
OF POOR QUALITY

BENTLY
ROTOR DYNAMICS
RESEARCH CORP.

PLANT ID: BRDRC
TRAIN ID: NASA RUB
MACHINE ID: ROTOR KIT
SOLID DATA: Uncomp OBV

RUNUP

RUN 1

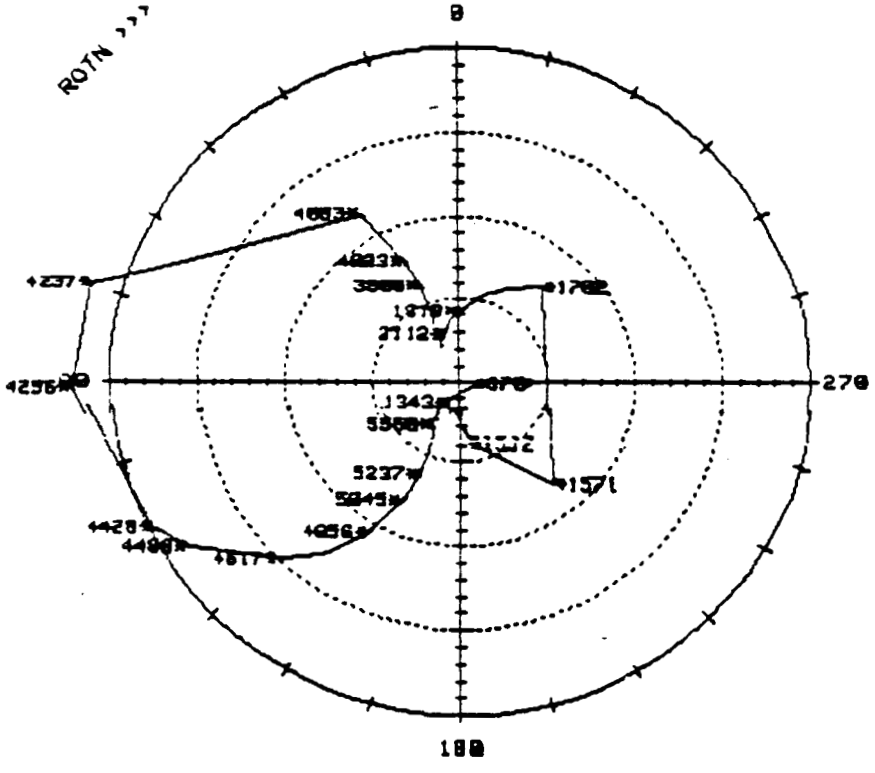

FULL SCALE AMP = 10 pp MILS AMP PER DIV = .5 pp MILS

FIGURE 10.9 POLAR PLOT OF THE ROTOR FILTERED SYNCHRONOUS VIBRATION RESPONSE DURING RUN–UP AS SEEN BY THE OUTBOARD VERTICAL DISPLACEMENT PROBE (UNBALANCED, NO RUB).

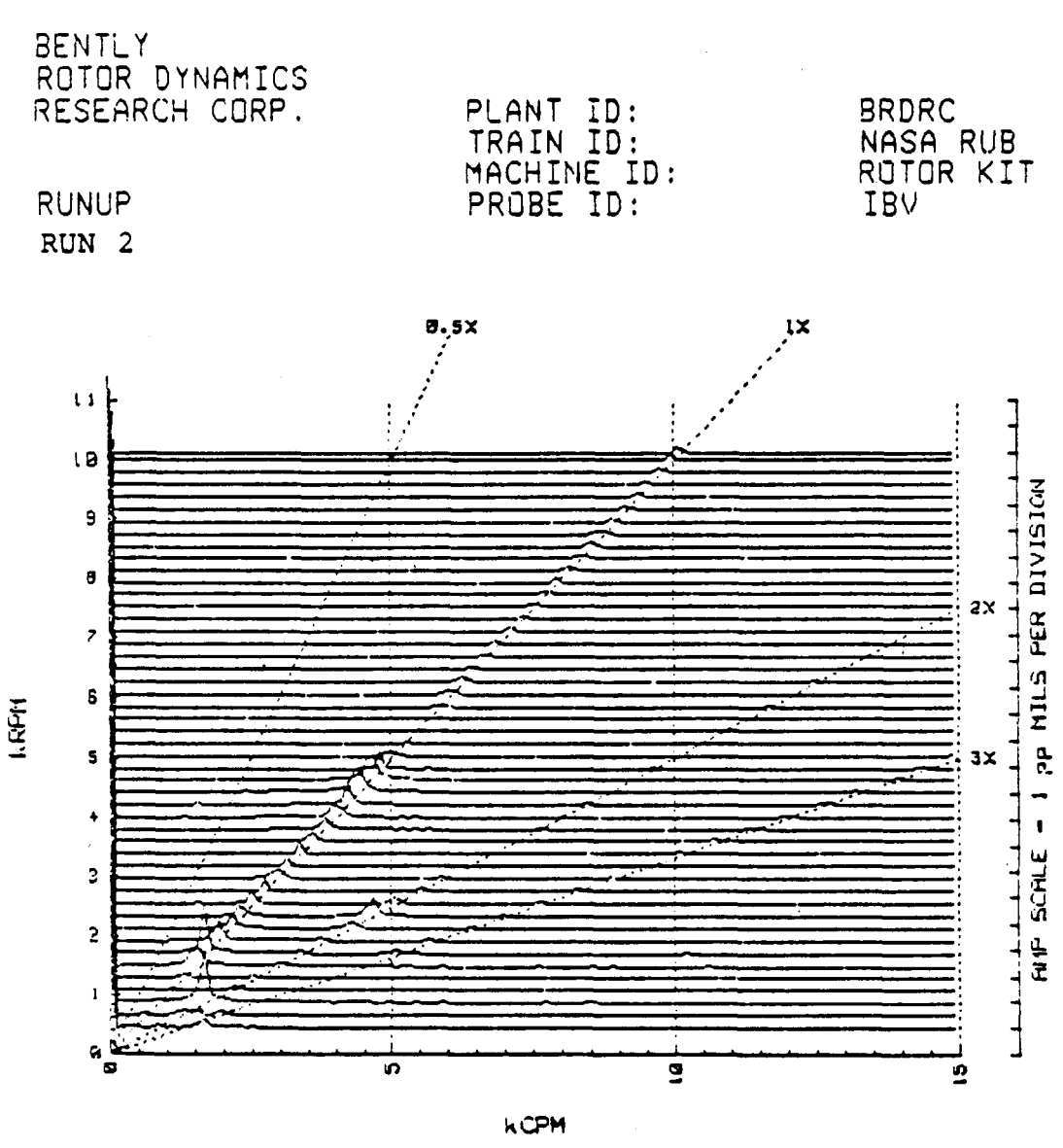

FIGURE 10.10 SPECTRUM CASCADE PLOT OF THE ROTOR VIBRATION DURING RUN–UP AS SEEN BY THE INBOARD VERTICAL DISPLACEMENT PROBE (BALANCED, NO RUB).

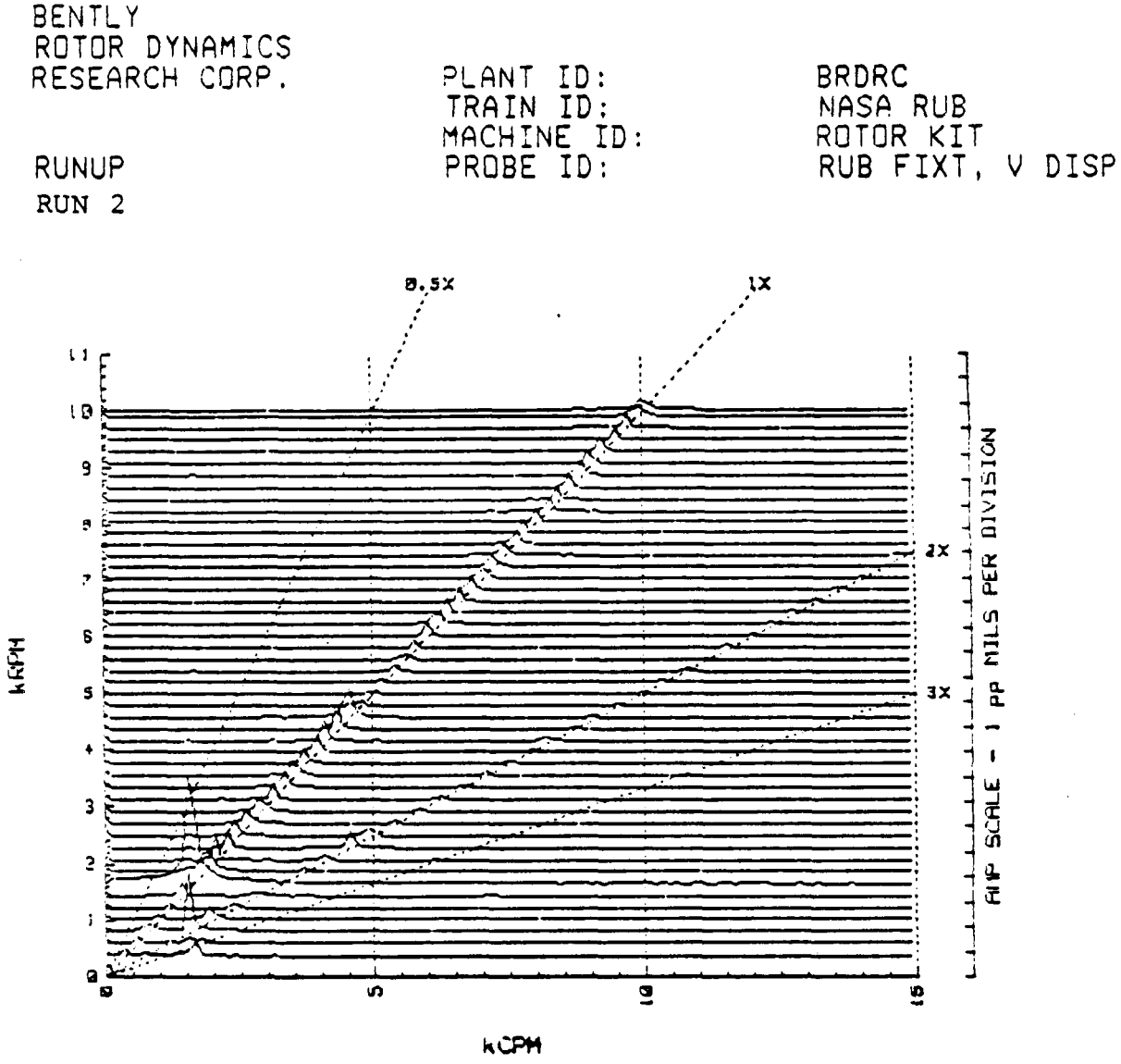

FIGURE 10.11 SPECTRUM CASCADE PLOT OF THE ROTOR VIBRATION RESPONSE DURING RUN–UP AS SEEN BY THE RUB FIXTURE VERTICAL DISPLACEMENT PROBE (BALANCED, NO RUB).

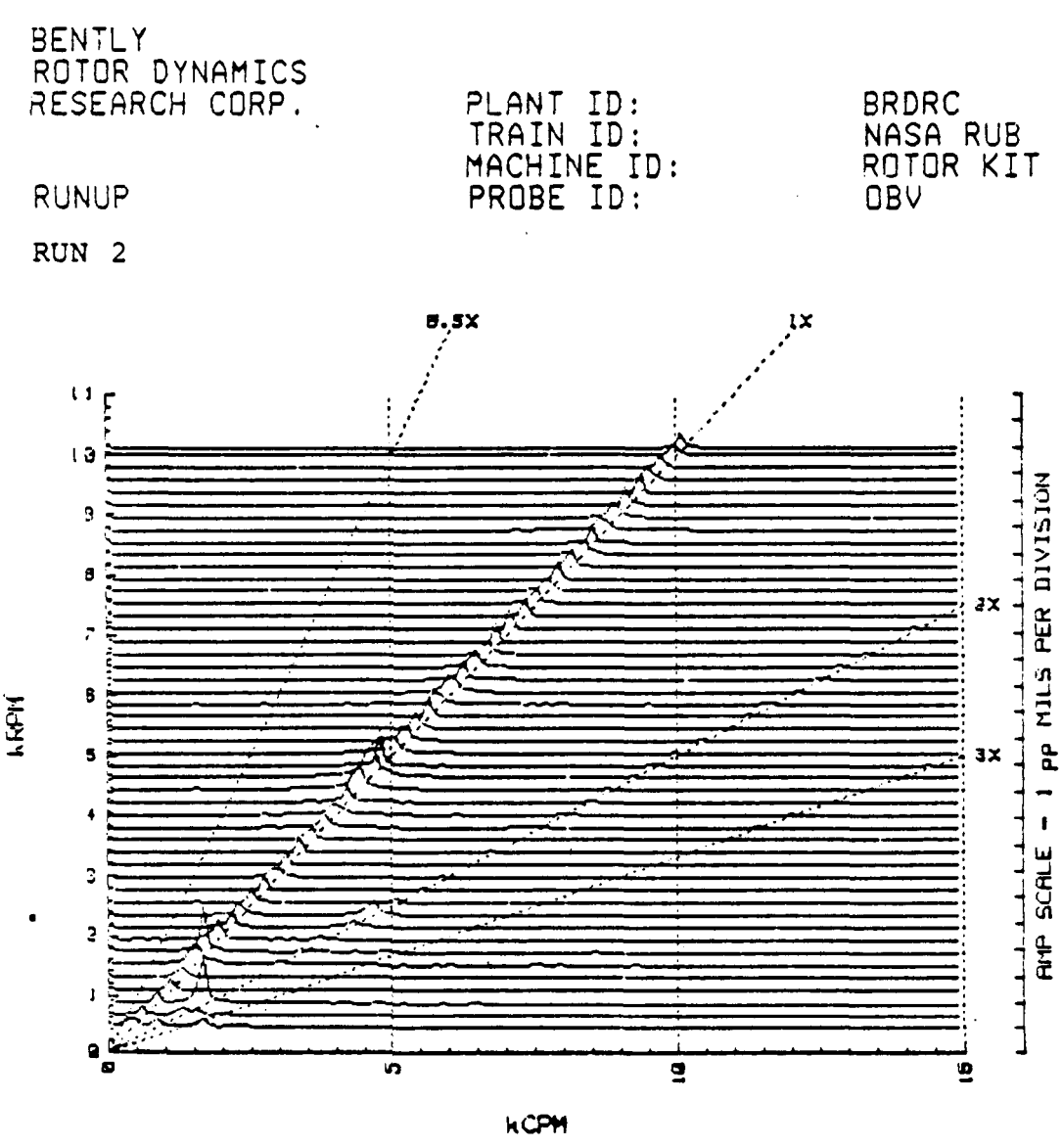

FIGURE 10.12 SPECTRUM CASCADE PLOT OF THE ROTOR VIBRATION RESPONSE DURING RUN–UP AS SEEN BY THE OUTBOARD VERTICAL DISPLACEMENT PROBE (BALANCED, NO RUB).

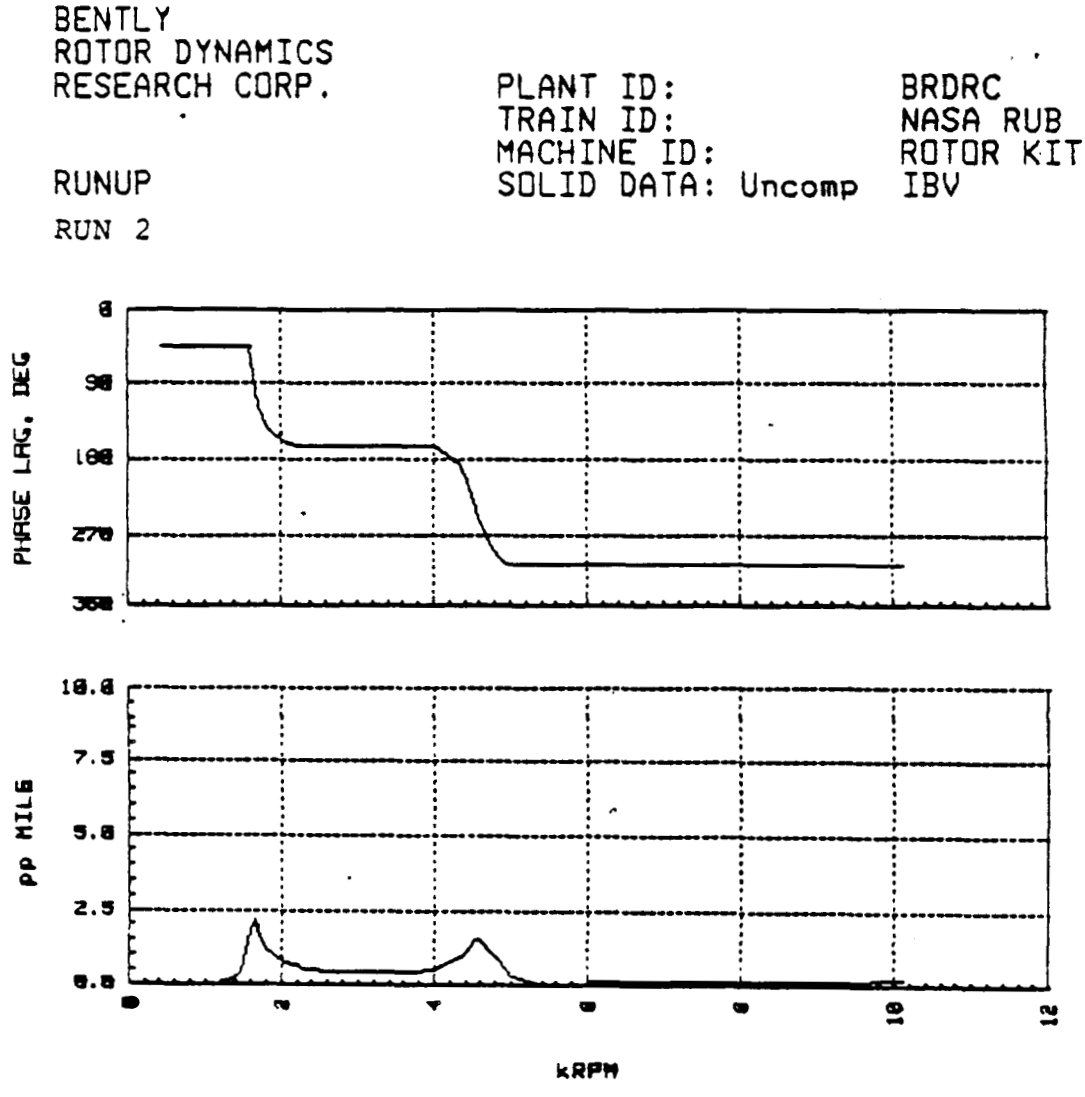

FIGURE 10.13 BODÉ PLOT OF THE ROTOR FILTERED SYNCHRONOUS VIBRATION RESPONSE DURING RUN–UP AS SEEN BY THE INBOARD VERTICAL DISPLACEMENT PROBE (BALANCED, NO RUB).

BENTLY
ROTOR DYNAMICS
RESEARCH CORP.

RUNUP
RUN 2

PLANT ID: BRDRC
TRAIN ID: NASA RUB
MACHINE ID: ROTOR KIT
SOLID DATA: Uncomp IBV

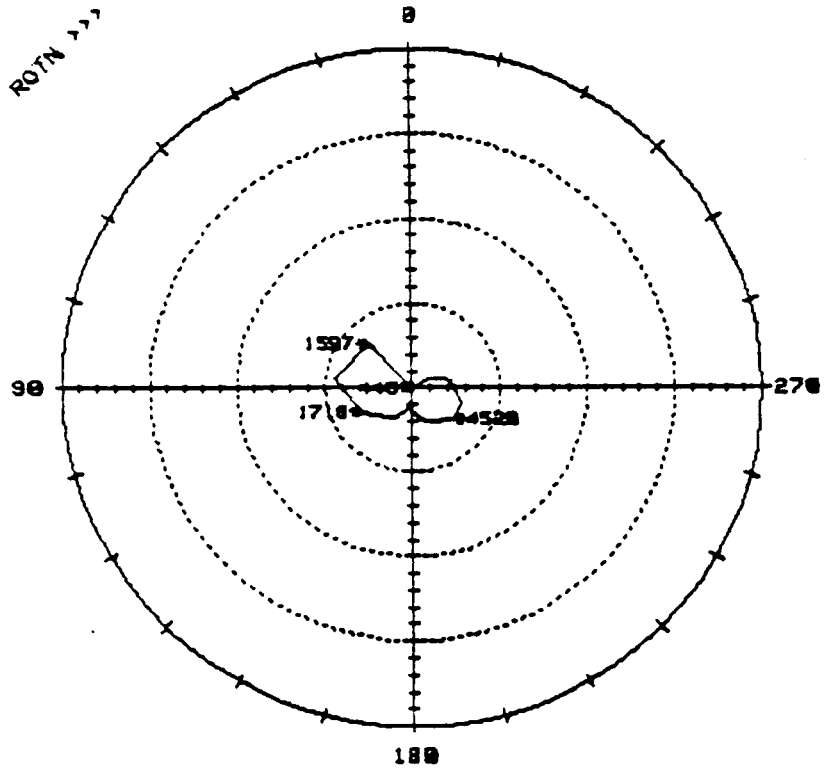

FULL SCALE AMP = 10 pp MILS AMP PER DIV = .5 pp MILS

FIGURE 10.14 POLAR PLOT OF THE ROTOR FILTERED SYNCHRONOUS VIBRATION RESPONSE DURING RUN–UP AS SEEN BY THE INBOARD VERTICAL DISPLACEMENT PROBE (BALANCED, NO RUB).

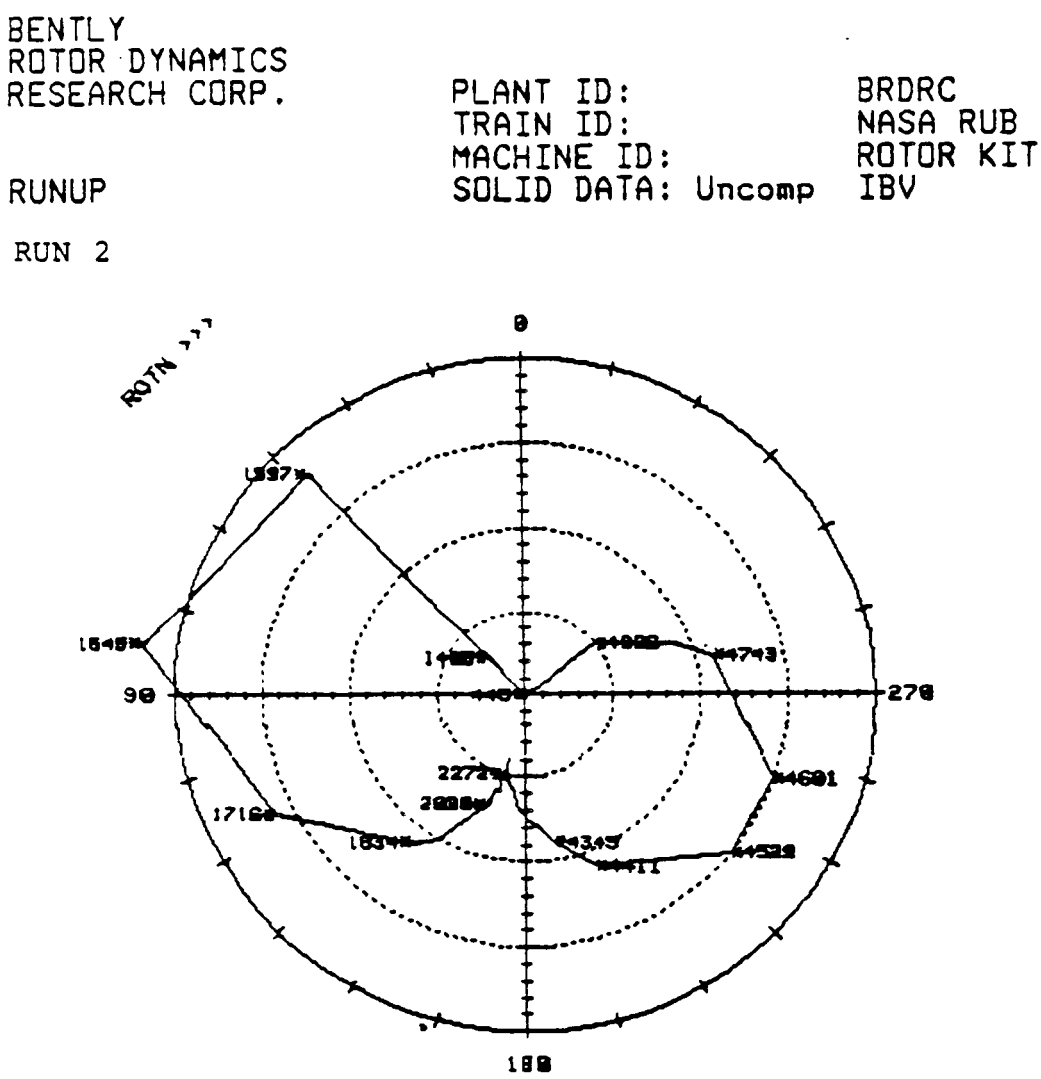

FIGURE 10.15 POLAR PLOT OF THE ROTOR FILTERED SYNCHRONOUS VIBRATION RESPONSE DURING RUN–UP AS SEEN BY THE INBOARD VERTICAL DISPLACEMENT PROBE. NOTE: THIS DATA IS THE SAME AS FIGURE 10.14 WITH DIFFERENCE SCALING (BALANCED, NO RUB).

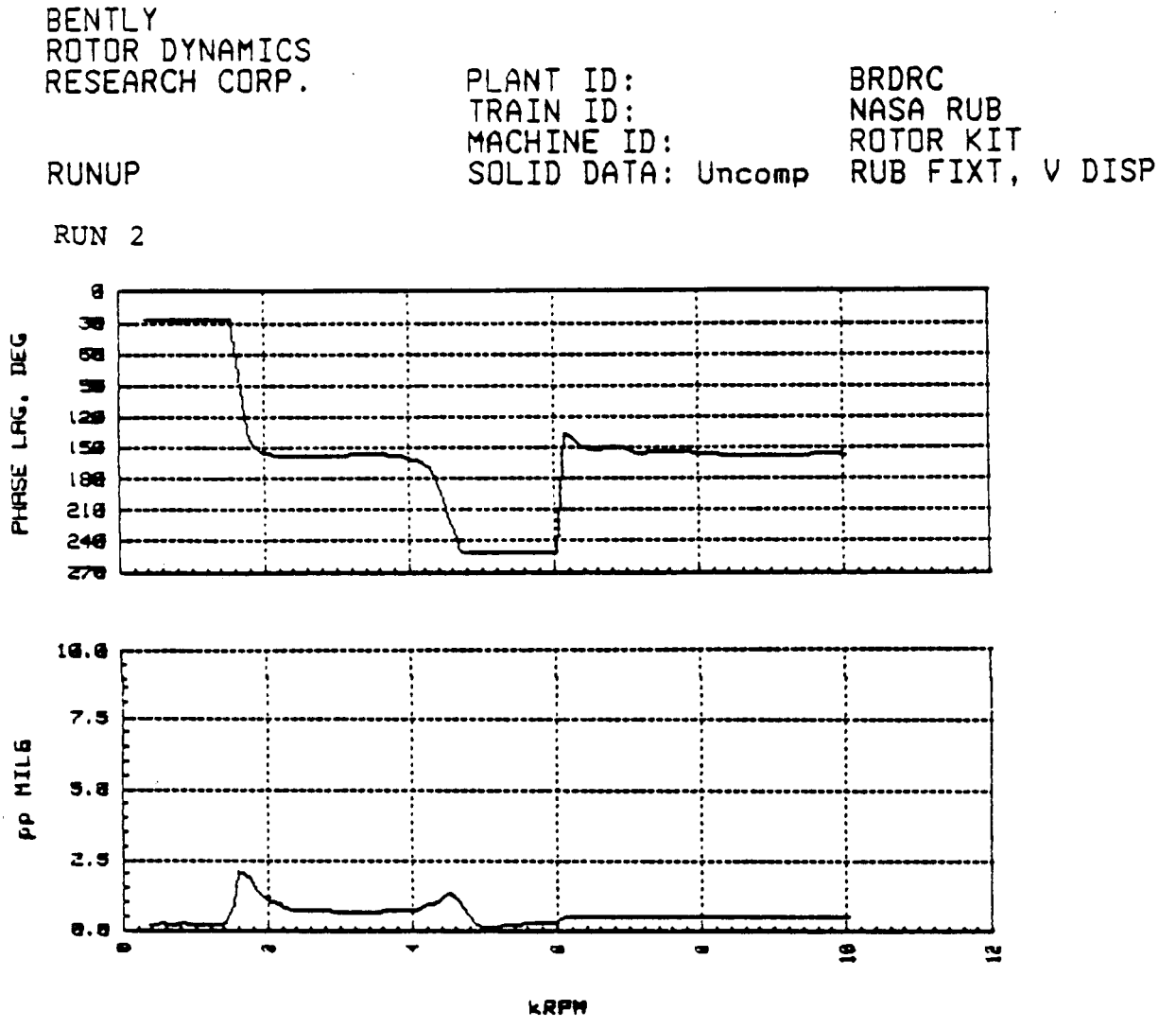

FIGURE 10.16 BODÉ PLOT OF THE ROTOR FILTERED SYNCHRONOUS VIBRATION RESPONSE DURING RUN–UP AS SEEN BY THE RUB FIXTURE VERTICAL DISPLACEMENT PROBE (BALANCED, NO RUB).

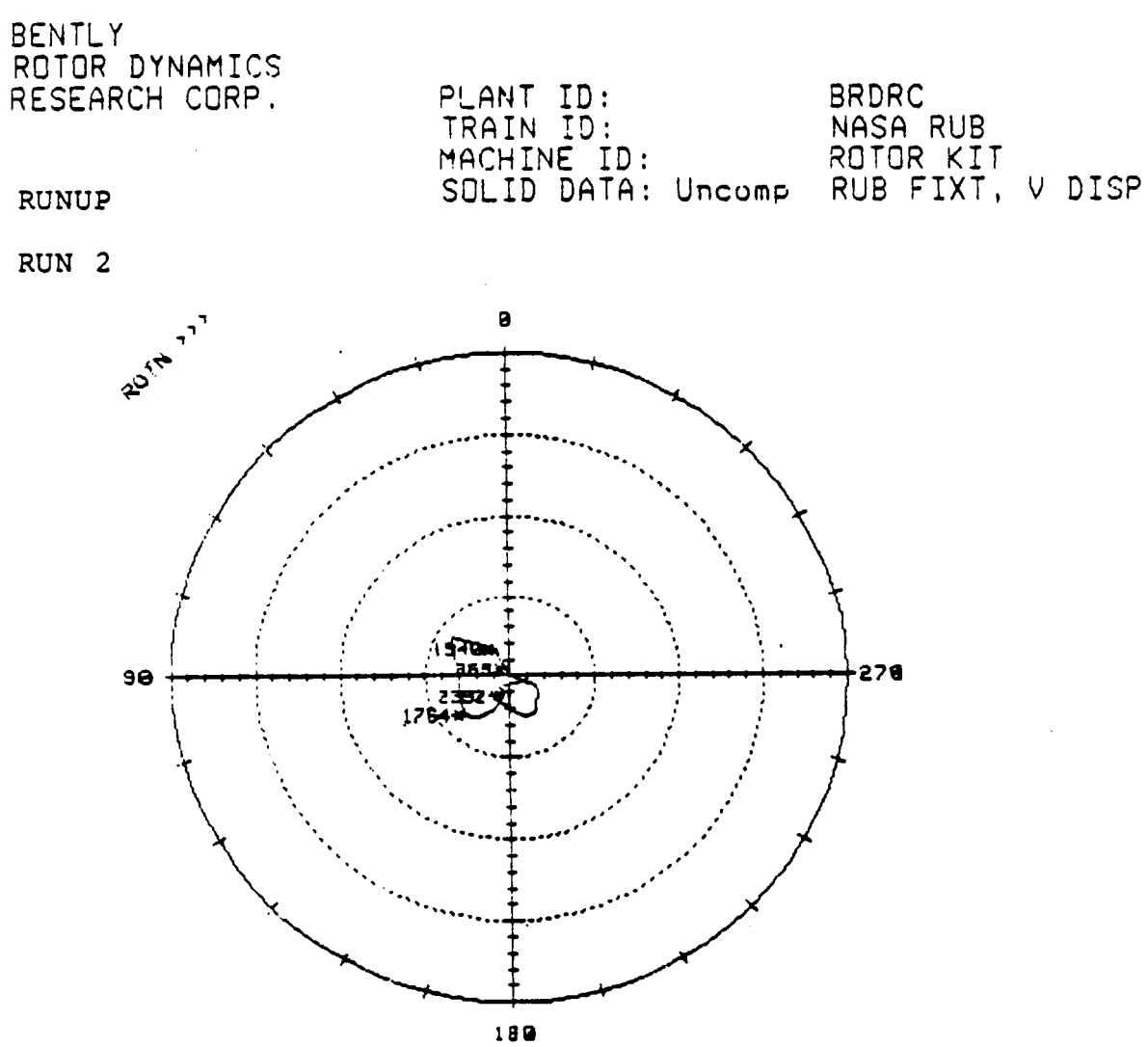

FIGURE 10.17 POLAR PLOT OF ROTOR FILTERED SYNCHRONOUS VIBRATION RESPONSE DURING RUN–UP AS SEEN BY THE RUB FIXTURE VERTICAL DISPLACEMENT PROBE (BALANCED, NO RUB).

ORIGINAL PAGE IS
OF POOR QUALITY

BENTLY
ROTOR DYNAMICS
RESEARCH CORP.

PLANT ID: BRDRC
TRAIN ID: NASA RUB
MACHINE ID: ROTOR KIT
SOLID DATA: Uncomp. RUB FIXT, V DISP

RUNUP

RUN 2

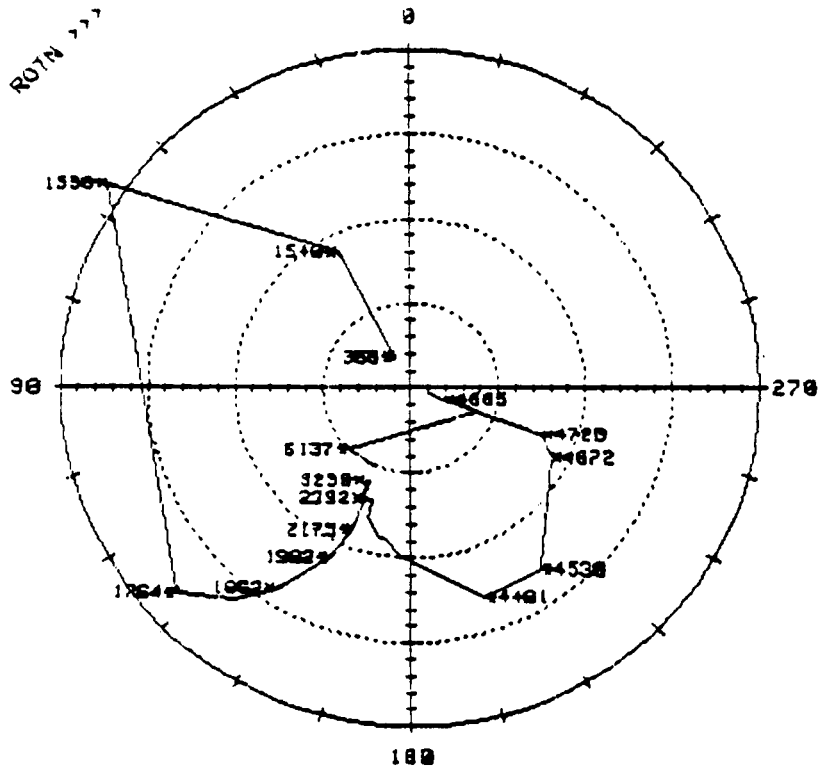

FULL SCALE AMP = 2 pp MILS AMP PER DIV = .1 pp MILS

FIGURE 10.18 POLAR PLOT OF THE ROTOR FILTERED SYNCHRONOUS VIBRATION RESPONSE DURING RUN–UP AS SEEN BY THE RUB FIXTURE VERTICAL DISPLACEMENT PROBE. NOTE: THIS DATA IS THE SAME AS FIGURE 10.17 WITH DIFFERENT SCALING (BALANCED, NO RUB).

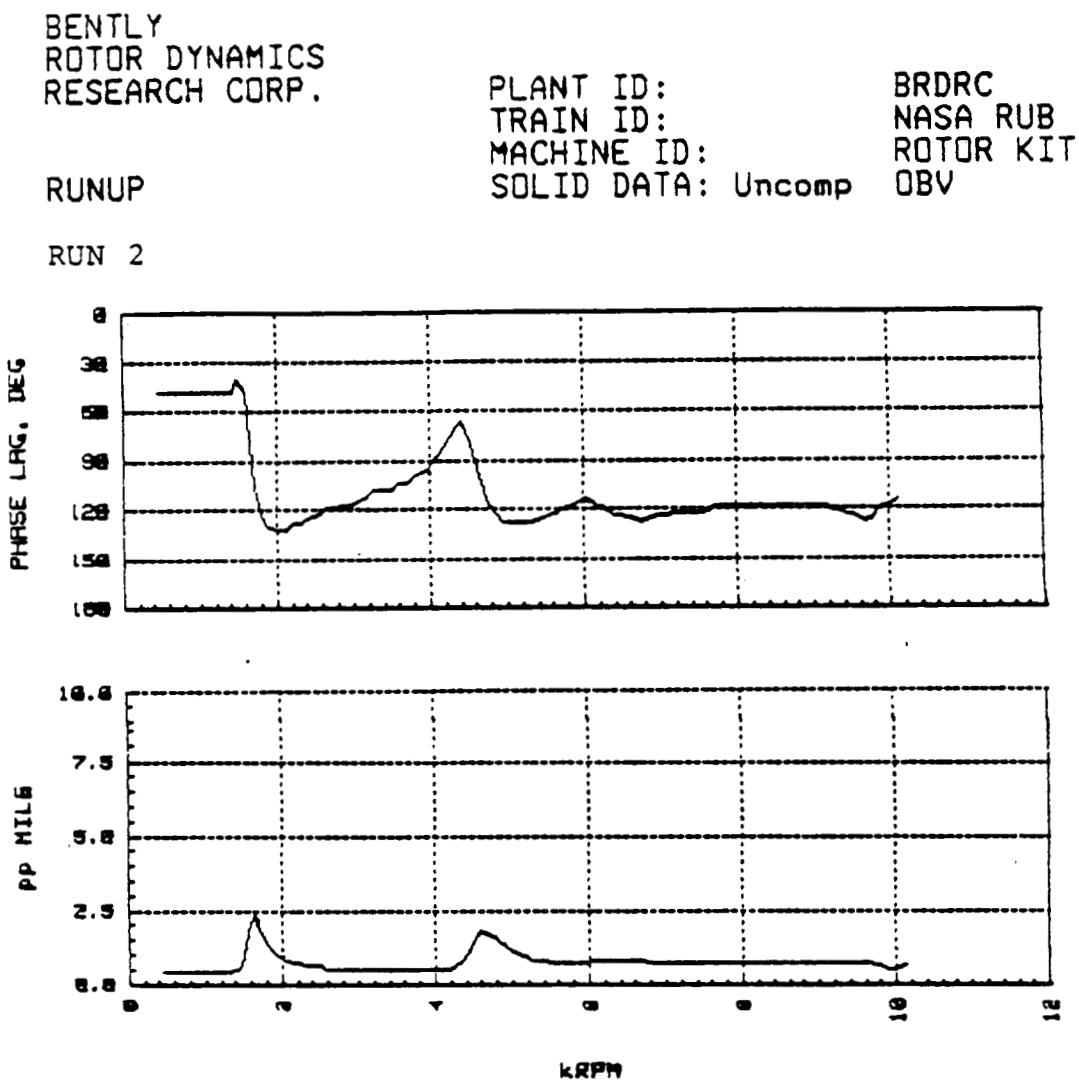

FIGURE 10.19 BODÉ PLOT OF THE ROTOR FILTERED SYNCHRONOUS VIBRATION RESPONSE DURING RUN–UP AS SEEN BY THE OUTBOARD VERTICAL DISPLACEMENT PROBE (BALANCED, NO RUB).

BENTLY
ROTOR DYNAMICS
RESEARCH CORP.

RUNUP

RUN 2

PLANT ID: BRDRC
TRAIN ID: NASA RUB
MACHINE ID: ROTOR KIT
SOLID DATA: Uncomp OBV

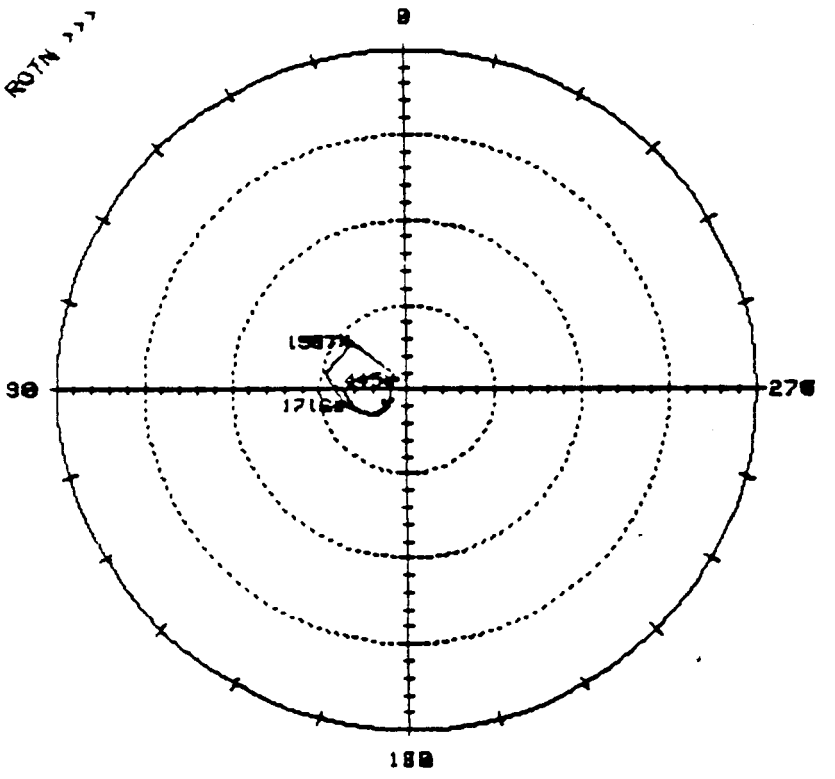

FULL SCALE AMP = 10 pp MILS AMP PER DIV = .5 pp MILS

FIGURE 10.20 POLAR PLOT OF THE ROTOR FILTERED SYNCHRONOUS VIBRATION RESPONSE DURING RUN–UP AS SEEN BY THE OUTBOARD VERTICAL DISPLACEMENT PROBE (BALANCED, NO RUB).

BENTLY
ROTOR DYNAMICS
RESEARCH CORP.

RUNUP

PLANT ID:	BRDRC
TRAIN ID:	NASA RUB
MACHINE ID:	ROTOR KIT
SOLID DATA: Uncomp	OBV

RUN 2

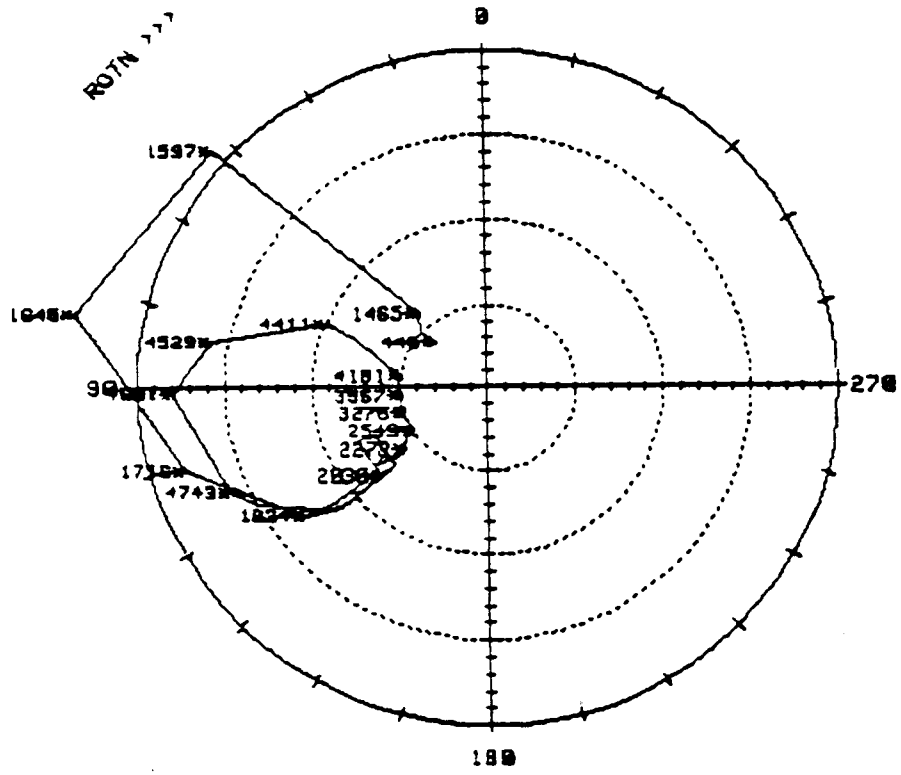

FULL SCALE AMP = 2 pp MILS AMP PER DIV = .1 pp MILS

FIGURE 10.21 POLAR PLOT OF THE ROTOR FILTERED SYNCHRONOUS VIBRATION RESPONSE DURING RUN-UP AS SEEN BY THE OUTBOARD VERTICAL DISPLACEMENT PROBE. NOTE: THIS DATA IS THE SAME AS FIGURE 10.20 WITH DIFFERENT SCALING.

C-3

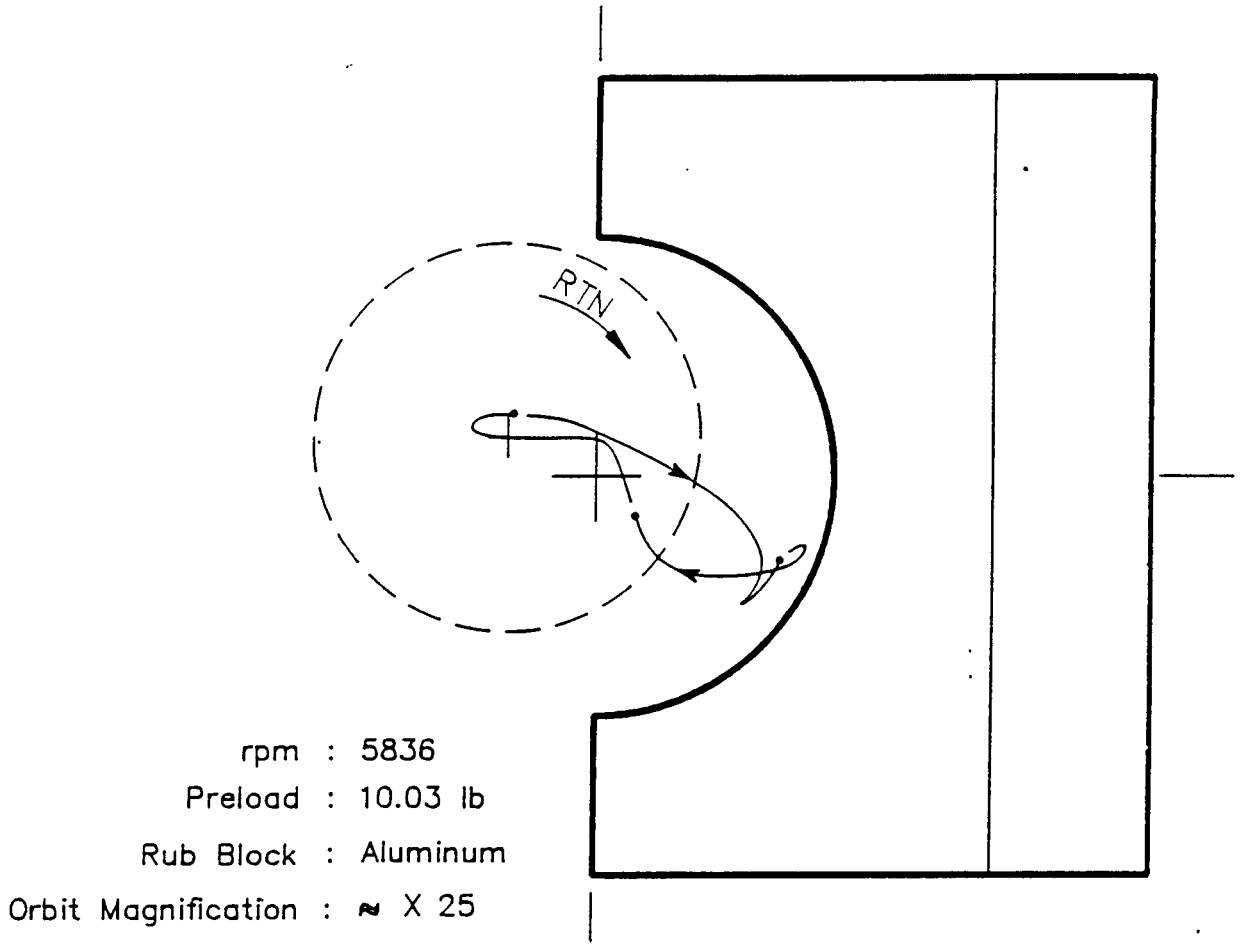

FIGURE 10.22 ORBIT OF THE SHAFT RUBBING AGAINST THE STATIONARY RUB BLOCK. QUALITATIVE EXAMPLE.

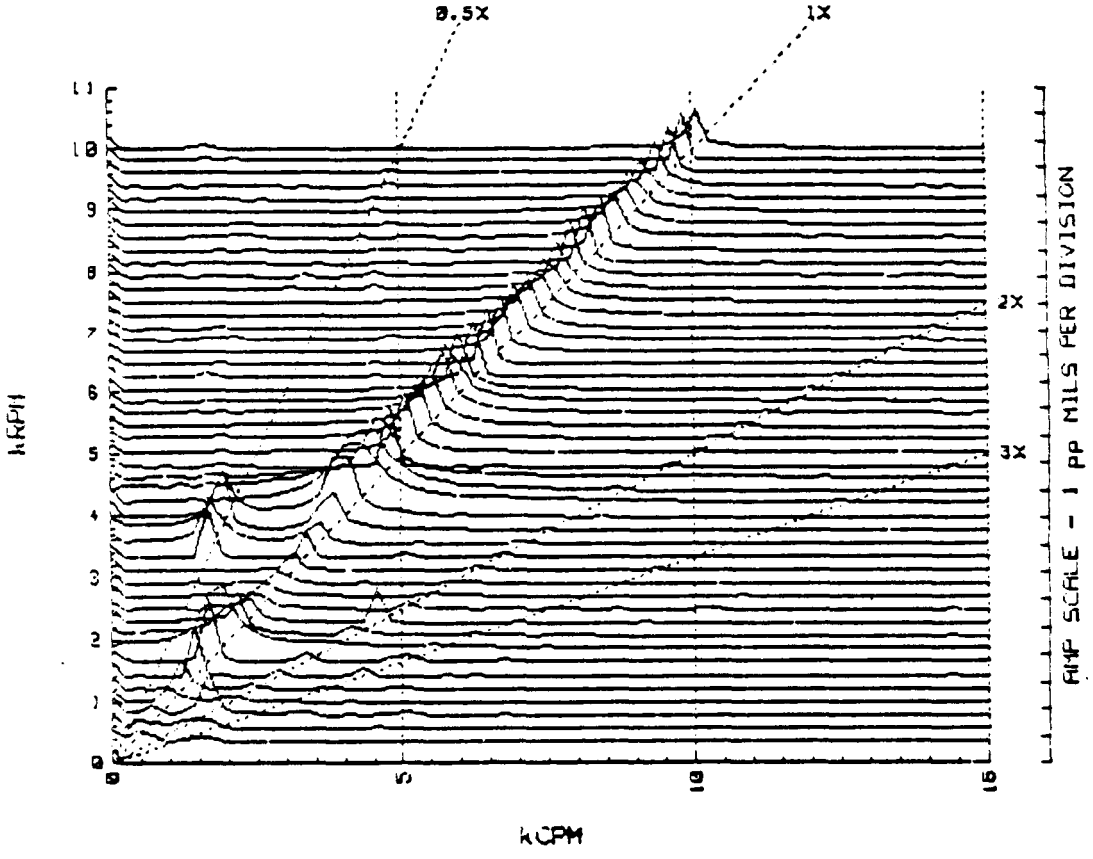

FIGURE 10.23 CASCADE PLOT OF ROTOR VIBRATION RESPONSE DURING RUN–UP AS SEEN BY THE RUB FIXTURE HORIZONTAL DISPLACEMENT PROBE. NOTE 1/2X COMPONENT GENERATED BY RUB (0.0 PRELOAD, INBOARD UNBALANCE: .48 GRAMS AT 0. DEGREES AND RADIUS = 1.2 IN.).

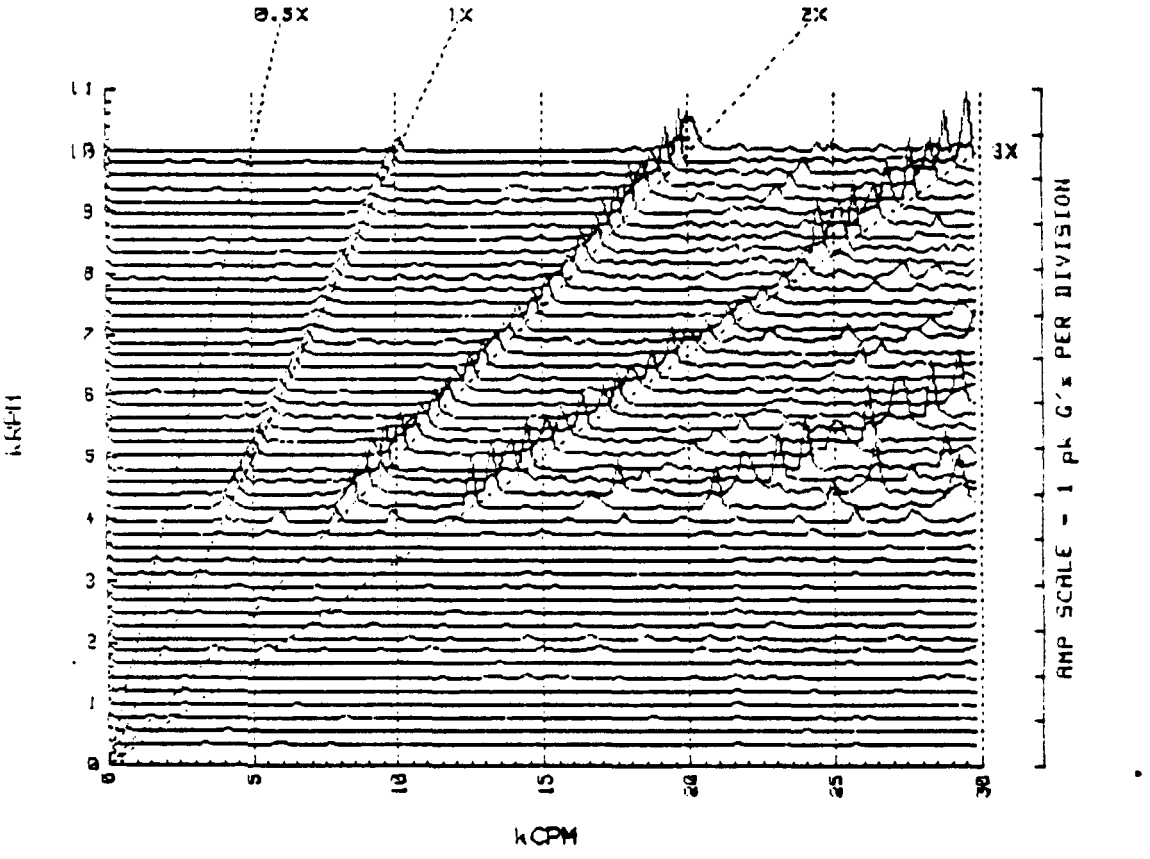

FIGURE 10.24 CASCADE PLOT OF ROTOR VIBRATION RESPONSE DURING RUN–UP AS SEEN BY ACCELEROMETER MOUNTED ON PLUNGER MECHANISM. NOTE WELL–DEFINED 2X, 3X, 4X, AND HIGHER COMPONENTS. THE SAME RUN AS IN FIGURE 10.23. NOTE LACK OF LOW FREQUENCY COMPONENTS (0.0 PRELOAD, INBOARD UNBALANCE: .48 GRAMS AT 0 DEGREES AND RADIUS = 1.2 IN.).

BENTLY
NEVADA
CORP.

PLANT ID: B.R.D.R.C
TRAIN ID: NASA RUB RIG
MACHINE ID: RUB ORBITS

RUN 3

PROBE #1 ID: RUB FIXTURE VERT
1X FILTERED
ORIENTATION= 90 DEG
1X VECTOR= 13.30 MILS PK-PK @-329

PROBE #2 ID: RUB FIXTURE HOR
1X FILTERED
ORIENTATION= 0 DEG
1X VECTOR= 2.60 MILS PK-PK @-333

ROTATION: CW
RPM(START)= 1600 RPM(END)= 1600

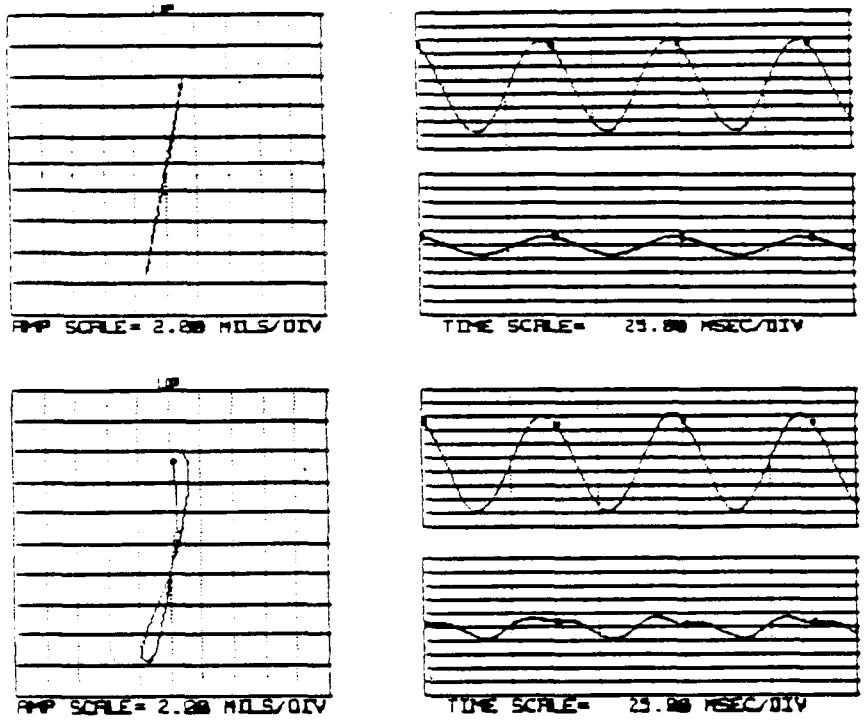

RUN 3

PROBE #1 ID: RUB FIXTURE VERT
UNFILTERED
ORIENTATION= 90 DEG
MAX AMP= 14.20 MILS PK-PK

PROBE #2 ID: RUB FIXTURE HOR
UNFILTERED
ORIENTATION= 0 DEG
MAX AMP= 3.20 MILS PK-PK

ROTATION: CW
RPM(START)= 1600 RPM(END)= 1600

FIGURE 10.25 STEADY-STATE ORBIT/TIMEBASE WAVE OF THE ROTOR VIBRATIONAL RESPONSE AT 1600 RPM AS SEEN BY RUB FIXTURE VERTICAL AND HORIZONTAL DISPLACEMENT PROBES. 1X RUB. TOP: 1X FILTERED SIGNAL, BOTTOM: UNFILTERED SIGNAL. (0.0 PRELOAD, INBOARD UNBALANCE: .48 GRAMS AT 0 DEGREES AND RADIUS = 1.2 IN.).

BENTLY
NEVADA
CORP.

PLANT ID: B.R.D.R.C
TRAIN ID: NASA RUB
MACHINE ID: ELEC CONTACT REF.

RUN 3

PROBE #1 ID: RUB PLUNGER
UNFILTERED

ORIENTATION= 0 DEG
MAX AMP= 3.30 MILS PK-PK

PROBE #2 ID: RUB ELEC. CONTACT
UNFILTERED

ORIENTATION= 0 DEG
MAX AMP= 5.70 MILS PK-PK

ROTATION: CW
RPM(START)= 1587 RPM(END)= 1584

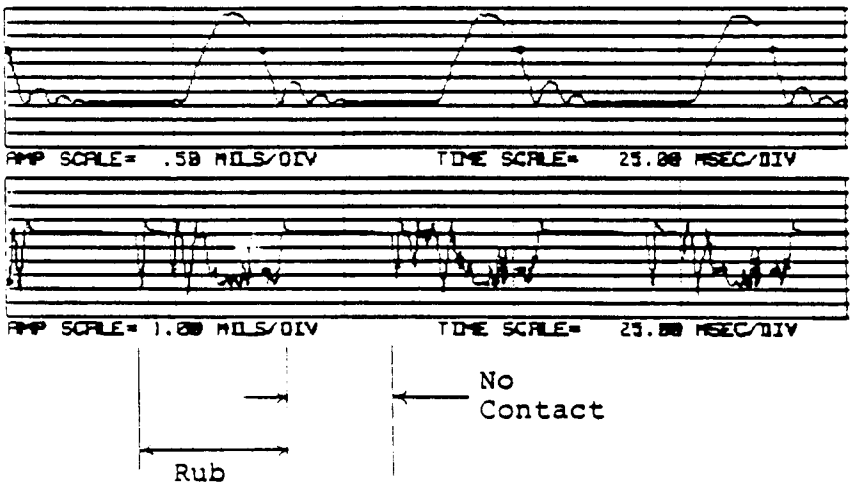

FIGURE 10.26 TIMEBASE WAVE PRESENTATION OF 1X RUB VIBRATION SIGNALS. TOP: PLUNGER MOTION, BOTTOM: ELECTRICAL SIGNAL OF ROTOR–TO–STATOR CONTACT (RUB–RELATED). NOTE STICK/SLIP /REBOUNDING MOTION OF THE SHAFT AT 1X RUB (0.0 PRELOAD, INBOARD UNBALANCE: .48 GRAMS AT 0 DEGREES AND RADIUS = 1.2 IN.).

BENTLY
NEVADA
CORP.

PLANT ID: B.R.D.R.C
TRAIN ID: NASA RUB RIG
MACHINE ID: RUB ORBITS

RUN 3

PROBE #1 ID: RUB FIXTURE VERT
1X FILTERED

ORIENTATION= 90 DEG
1X VECTOR= 1.90 MILS PK-PK @-188

PROBE #2 ID: RUB FIXTURE HOR
1X FILTERED

ORIENTATION= 0 DEG
1X VECTOR= 3.00 MILS PK-PK @-276

ROTATION: CW
RPM(START)= 3866 RPM(END)= 3867

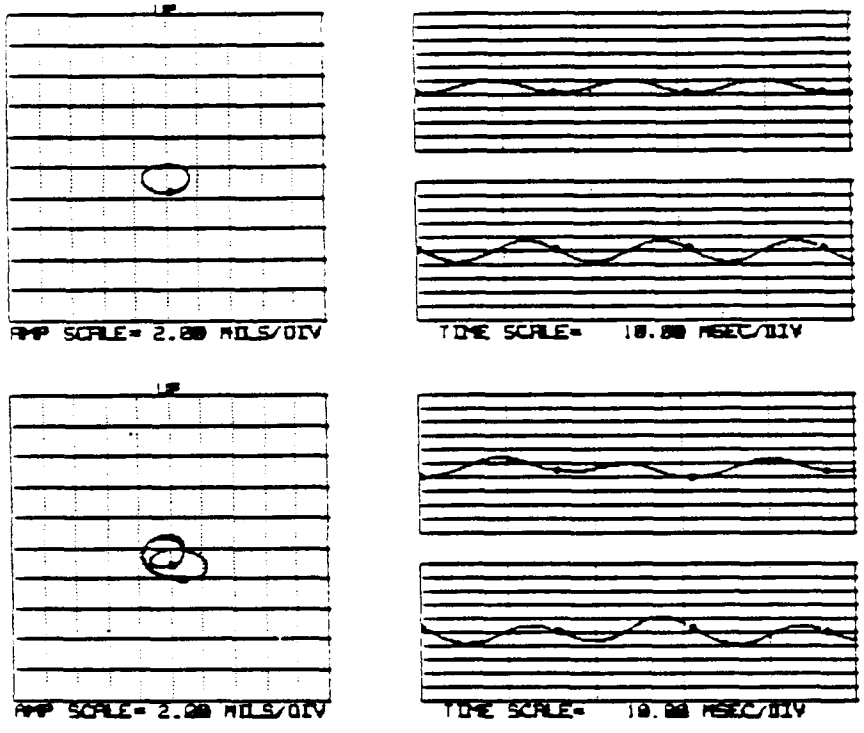

RUN 3

PROBE #1 ID: RUB FIXTURE VERT
UNFILTERED

ORIENTATION= 90 DEG
MAX AMP= 3.00 MILS PK-PK

PROBE #2 ID: RUB FIXTURE HOR
UNFILTERED

ORIENTATION= 0 DEG
MAX AMP= 4.10 MILS PK-PK

ROTATION: CW
RPM(START)= 3867 RPM(END)= 3869

FIGURE 10.27 STEADY-STATE ORBIT/TIMEBASE WAVE OF ROTOR VIBRATIONAL RESPONSE AT 3867 RPM AS SEEN BY RUB FIXTURE VERTICAL AND HORIZONTAL DISPLACEMENT PROBES. 1/2X RUB. TOP: 1X FILTERED SIGNAL, BOTTOM: UNFILTERED SIGNAL. (0.0 PRELOAD, INBOARD UNBALANCE: .48 GRAMS AT 0 DEGREES AND RADIUS = 1.2 IN.).

BENTLY
NEVADA
CORP.

PLANT ID: B.R.D.R.C
TRAIN ID: NASA RUB
MACHINE ID: ELEC CONTACT REF.

RUN 3

PROBE #1 ID: RUB PLUNGER
UNFILTERED
ORIENTATION= 0 DEG
MAX AMP= 1.00 MILS PK-PK

PROBE #2 ID: RUB ELEC. CONTACT
UNFILTERED
ORIENTATION= 0 DEG
MAX AMP= 5.60 MILS PK-PK

ROTATION: CW
RPM(START)= 4712 RPM(END)= 4712

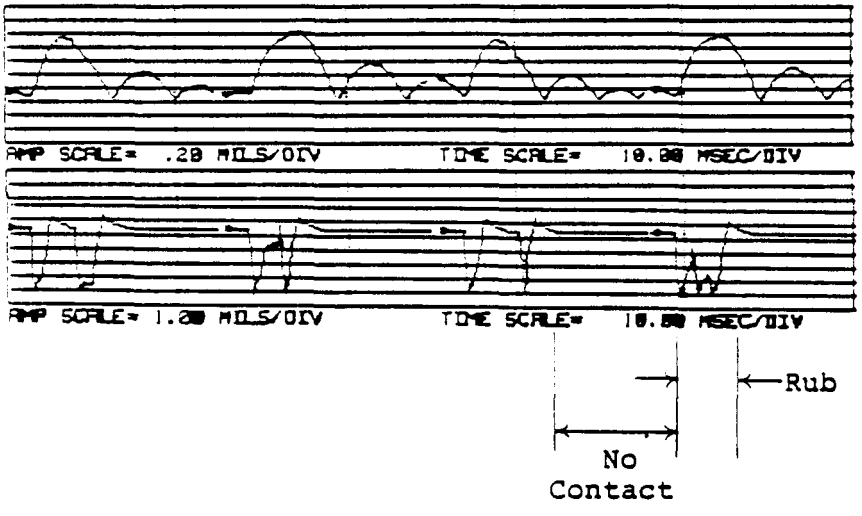

FIGURE 10.28 TIMEBASE WAVE PRESENTATION OF 1X RUB VIBRATION SIGNALS. TOP: PLUNGER MOTION, BOTTOM: ELECTRICAL SIGNAL OF ROTOR–TO–STATOR CONTACT (RUB–RELATED). (0.0 PRELOAD, INBOARD UNBALANCE: .48 GRAMS AT 0 DEGREES AND RADIUS = 1.2 IN.).

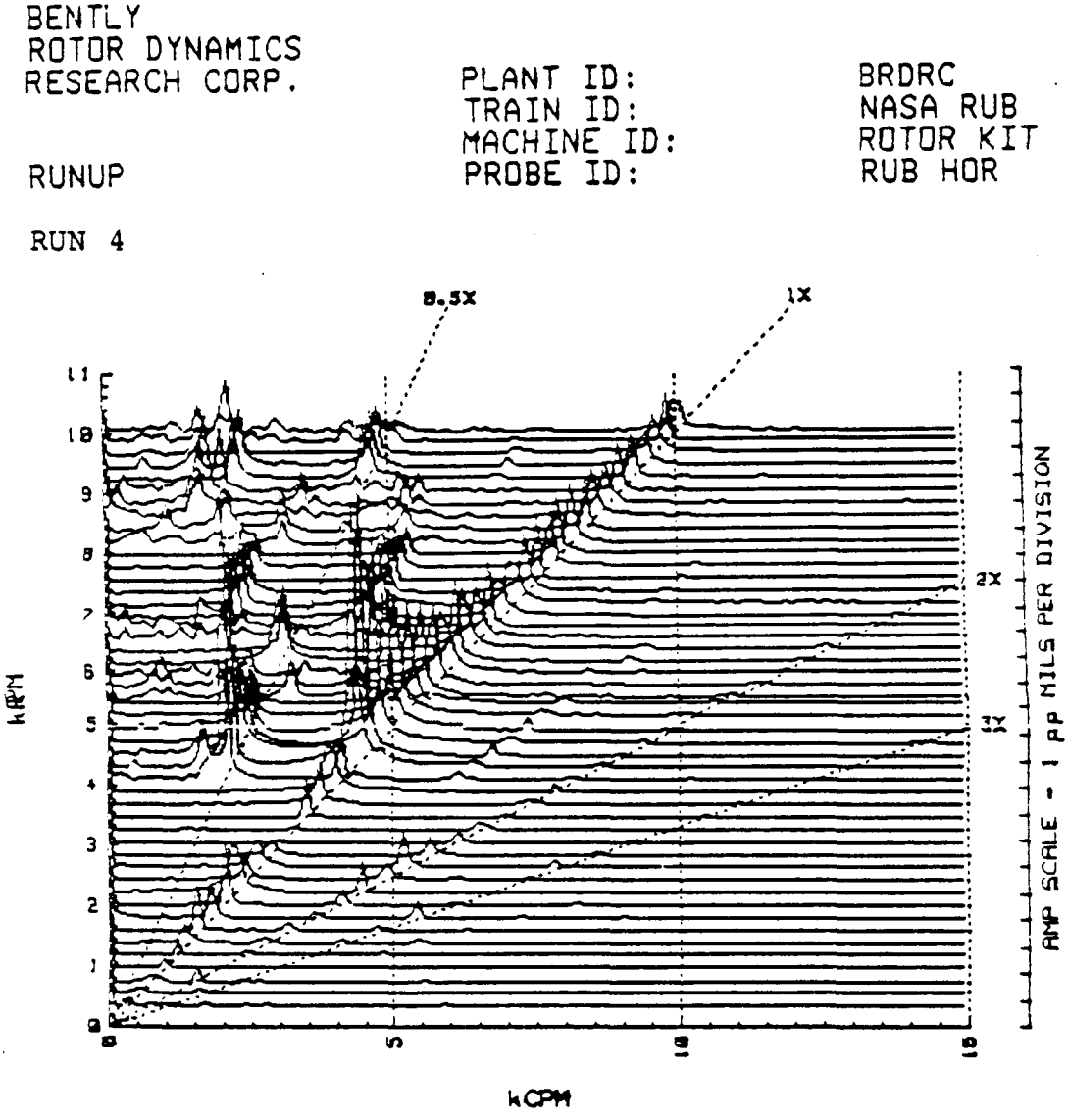

FIGURE 10.29 CASCADE PLOT OF ROTOR VIBRATION RESPONSE DURING RUN–UP AS SEEN BY RUB FIXTURE HORIZONTAL DISPLACEMENT PROBE. NOTE SIGNIFICANT EXCITATION OF SUBSYNCHRONOUS COMPONENTS WITH FREQUENCIES 1/2X, 1/3X, AND 1/4X. COMPARE WITH FIGURE 10.23 (3.34 LB PRELOAD, INBOARD UNBALANCE: .48 GRAMS AT 0 DEGREES AND RADIUS = 1.2 IN.).

BENTLY
ROTOR DYNAMICS
RESEARCH CORP.

RUNUP

PLANT ID: BRDRC
TRAIN ID: NASA RUB
MACHINE ID: ROTOR KIT
PROBE ID: RUB HOR

RUN 4

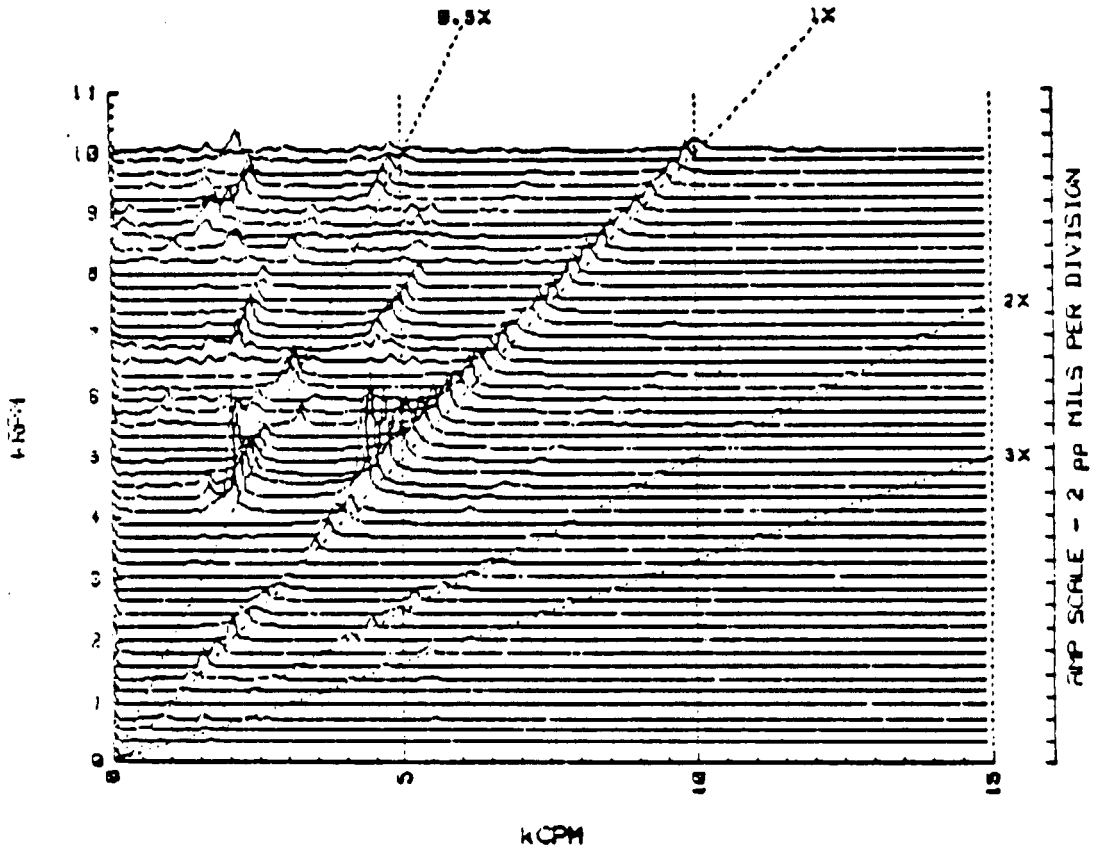

FIGURE 10.30 CASCADE PLOT OF ROTOR VIBRATION RESPONSE DURING RUN–UP. NOTE: THIS IS THE SAME DATA AS IN FIGURE 10.29 WITH DIFFERENT SCALING (3.34 LB PRELOAD, INBOARD UNBALANCE: .48 GRAMS AT 0 DEGREES AND RADIUS = 1.2 IN.).

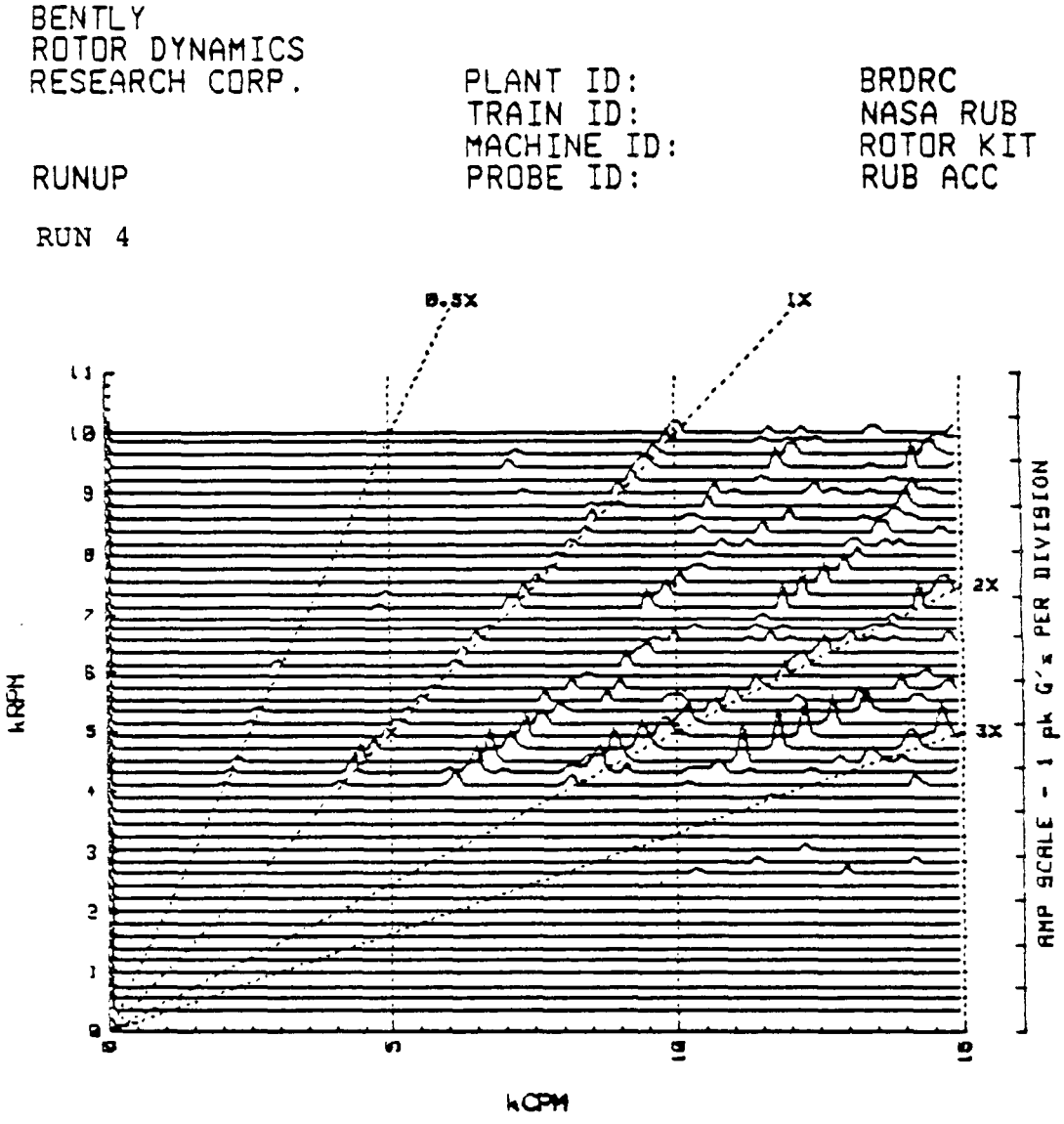

FIGURE 10.31 CASCADE PLOT OF ROTOR VIBRATION RESPONSE DURING RUN–UP AS SEEN BY ACCELEROMETER MOUNTED ON PLUNGER MECHANISM. NOTE: COMPONENTS ARE LESS PROMINENT THAN THESE FROM THE SYSTEM WITH 0.0 PRELOAD (FIGURE 10.24) (3.34 LB PRELOAD, INBOARD UNBALANCE: .48 GRAMS AT 0 DEGREES AND RADIUS = 1.2 IN.).

RUN 4

PROBE #1 ID: RUB FIXTURE VERT — ORIENTATION= 90 DEG
UNFILTERED — MAX AMP= 12.00 MILS PK-PK

PROBE #2 ID: RUB FIXTURE HOR — ORIENTATION= 0 DEG
UNFILTERED — MAX AMP= 6.10 MILS PK-PK

ROTATION: CW
RPM(START)= 1573 RPM(END)= 1574

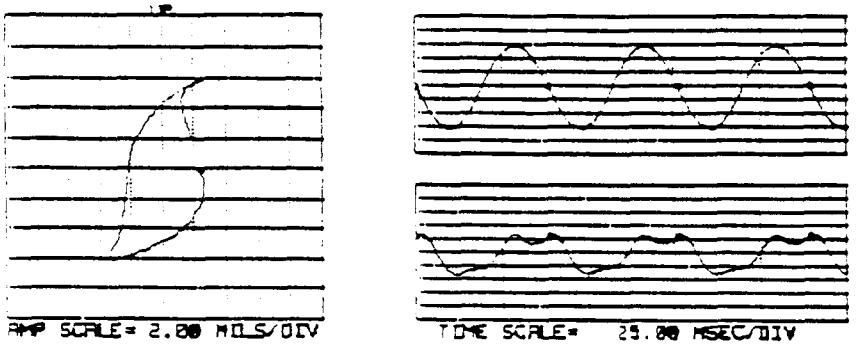

ORIGINAL PAGE IS
OF POOR QUALITY

FIGURE 10.32 STEADY–STATE ORBIT/TIMEBASE WAVE OF THE ROTOR VIBRATIONAL RESPONSE AT 1574 RPM, AS SEEN BY RUB FIXTURE VERTICAL AND HORIZONTAL DISPLACEMENT PROBES. UNFILTERED ORBIT INDICATES ONSET OF 2X COMPONENT. 1X RUB (3.34 LB. PRELOAD, INBOARD UNBALANCE: 0.48 GRAMS AT 0 DEGREES AND RADIUS = 1.2 IN.).

PROBE #1 ID: RUB PLUNGER — ORIENTATION= 0 DEG
UNFILTERED — MAX AMP= 0.00 MILS PK-PK

PROBE #2 ID: RUB ELEC. CONTACT — ORIENTATION= 0 DEG
UNFILTERED — MAX AMP= 4.60 MILS PK-PK

ROTATION: CW
RPM(START)= 1573 RPM(END)= 1574

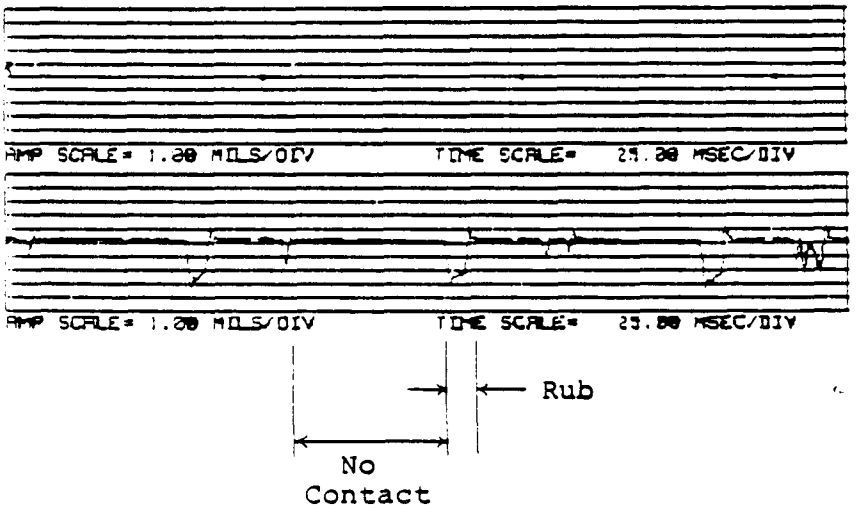

FIGURE 10.33 TIMEBASE WAVE PRESENTATION OF 1X RUB VIBRATION SIGNALS. TOP: PLUNGER MOTION, BOTTOM: ELECTRICAL SIGNAL OF ROTOR–TO–STATOR CONTACT (RUB–RELATED). NOTE: NO INDICATION OF PLUNGER MOTION, SMALL 2X COMPONENT RECORDED BY ELECTRICAL CONTACT SIGNAL (3.34 LB PRELOAD, INBOARD UNBALANCE: .48 GRAMS AT 0 DEGREES AND RADIUS = 1.2 IN.).

RUN 4

PROBE #1 ID: RUB FIXTURE VERT — ORIENTATION= 90 DEG
UNFILTERED — MAX AMP= 13.20 MILS PK-PK

PROBE #2 ID: RUB FIXTURE HOR — ORIENTATION= 0 DEG
UNFILTERED — MAX AMP= 3.00 MILS PK-PK

ROTATION: CW
RPM(START)= 1604 RPM(END)= 1603

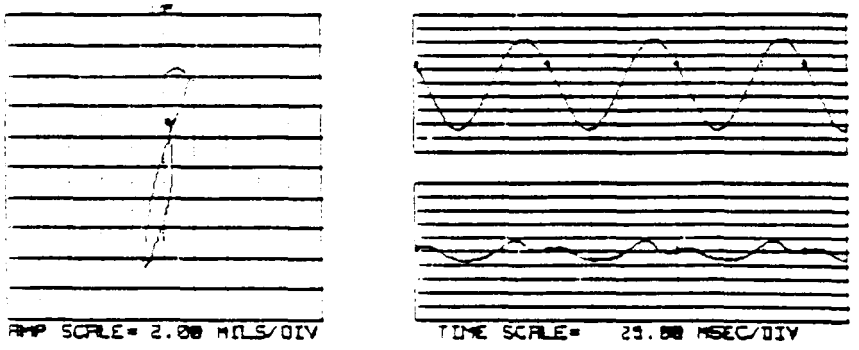

FIGURE 10.34 STEADY–STATE ORBIT/TIMEBASE WAVE OF ROTOR VIBRATIONAL RESPONSE AT 1603 RPM AS SEEN BY RUB FIXTURE VERTICAL AND HORIZONTAL DISPLACEMENT PROBES. UNFILTERED ORBIT INDICATES EXISTENCE OF A 2X COMPONENT. 1X RUB (3.34 LB. PRELOAD, INBOARD UNBALANCE: 0.48 GRAMS AT 0 DEGREES AND RADIUS = 1.2 IN.).

PROBE #1 ID: RUB PLUNGER — ORIENTATION= 0 DEG
UNFILTERED — MAX AMP= 0.00 MILS PK-PK

PROBE #2 ID: RUB ELEC. CONTACT — ORIENTATION= 0 DEG
UNFILTERED — MAX AMP= 4.70 MILS PK-PK

ROTATION: CW
RPM(START)= 1600 RPM(END)= 1600

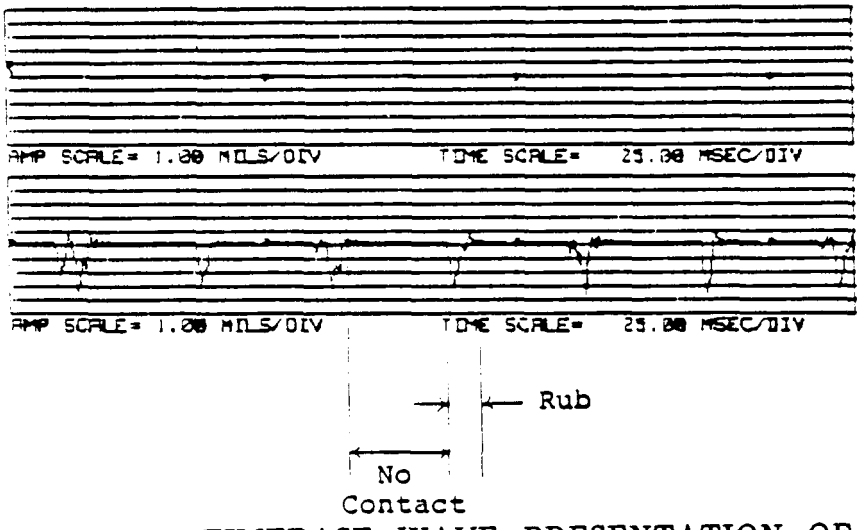

ORIGINAL PAGE IS OF POOR QUALITY

FIGURE 10.35 TIMEBASE WAVE PRESENTATION OF 1X RUB VIBRATION SIGNALS. TOP: PLUNGER MOTION, BOTTOM: ELECTRICAL SIGNAL OF ROTOR–TO–STATOR CONTACT (RUB–RELATED). NOTE: ELECTRICAL SIGNAL SHOWS 2X COMPONENT (3.34 LB PRELOAD, INBOARD UNBALANCE: .48 GRAMS AT 0 DEGREES AND RADIUS = 1.2 IN.).

RUN 4

PROBE #1 ID: RUB FIXTURE VERT — ORIENTATION= 90 DEG
UNFILTERED — MAX AMP= 2.50 MILS PK-PK

PROBE #2 ID: RUB FIXTURE HOR — ORIENTATION= 0 DEG
UNFILTERED — MAX AMP= 6.90 MILS PK-PK

ROTATION: CW
RPM(START)= 1915 RPM(END)= 1915

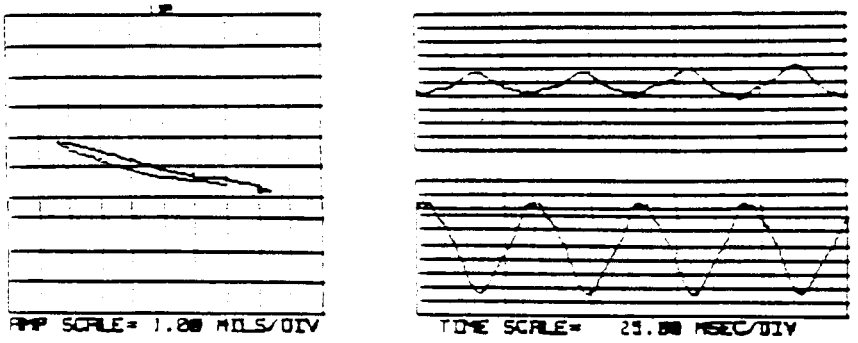

ORIGINAL PAGE IS
OF POOR QUALITY

FIGURE 10.36 STEADY-STATE ORBIT/TIMEBASE WAVE OF ROTOR VIBRATIONAL RESPONSE AT 1915 RPM AS SEEN BY RUB FIXTURE VERTICAL AND HORIZONTAL DISPLACEMENT PROBES. UNFILTERED ORBIT SHOWS SIGNIFICANT LATERAL MOTION OF ROTOR SHAFT. 1X RUB (3.34 LB. PRELOAD, INBOARD UNBALANCE: 0.48 GRAMS AT 0 DEGREES AND RADIUS = 1.2 IN.).

PROBE #1 ID: RUB PLUNGER — ORIENTATION= 0 DEG
UNFILTERED — MAX AMP= .20 MILS PK-PK

PROBE #2 ID: RUB ELEC. CONTACT — ORIENTATION= 0 DEG
UNFILTERED — MAX AMP= 4.40 MILS PK-PK

ROTATION: CW
RPM(START)= 1913 RPM(END)= 1916

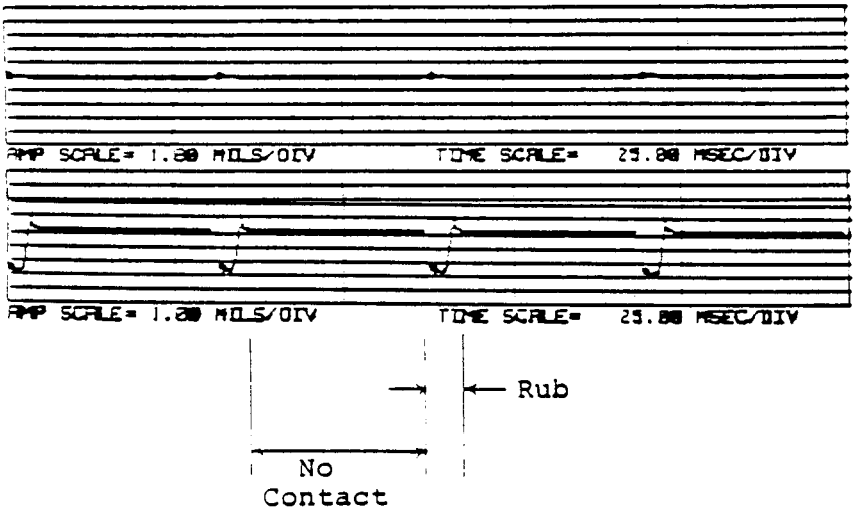

FIGURE 10.37 TIMEBASE WAVE PRESENTATION OF 1X RUB VIBRATION SIGNALS. TOP: PLUNGER MOTION, BOTTOM: ELECTRICAL SIGNAL OF ROTOR-TO-STATOR CONTACT (RUB-RELATED). NOTE: PLUNGER MOTION EXTREMELY SMALL (3.34 LB. PRELOAD, INBOARD UNBALANCE: 0.48 GRAMS AT 0 DEGREES AND RADIUS = 1.2 IN.).

PROBE #1 ID: RUB FIXTURE VERT ORIENTATION= 90 DEG
UNFILTERED MAX AMP= 7.00 MILS PK-PK

PROBE #2 ID: RUB FIXTURE HOR ORIENTATION= 0 DEG
UNFILTERED MAX AMP= 9.00 MILS PK-PK

ROTATION: CW
RPM(START)= 3919 RPM(END)= 3918

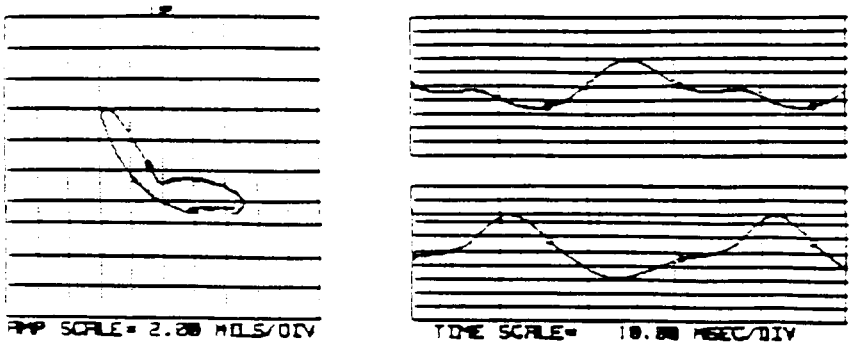

FIGURE 10.38 STEADY-STATE ORBIT/TIMEBASE WAVE OF ROTOR VIBRATIONAL RESPONSE AT 3918 RPM AS SEEN BY RUB FIXTURE VERTICAL AND HORIZONTAL DISPLACEMENT PROBES. NOTE: UNFILTERED ORBIT NOW INDICATES THE PRESENCE OF A 1/2X COMPONENT (3.34 LB. PRELOAD, INBOARD UNBALANCE: 0.48 GRAMS AT 0 DEGREES AND RADIUS = 1.2 IN.).

PROBE #1 ID: RUB PLUNGER ORIENTATION= 0 DEG
UNFILTERED MAX AMP= 1.10 MILS PK-PK

PROBE #2 ID: RUB ELEC. CONTACT ORIENTATION= 0 DEG
UNFILTERED MAX AMP= 5.80 MILS PK-PK

ROTATION: CW
RPM(START)= 3916 RPM(END)= 3916

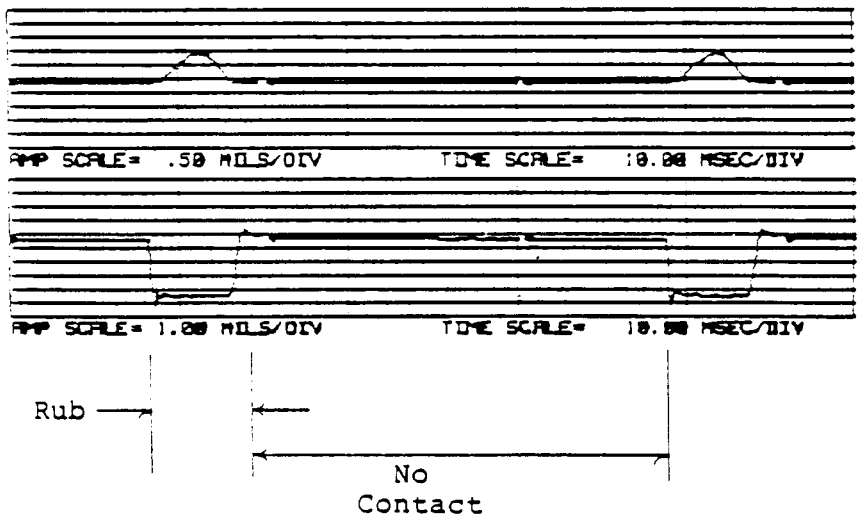

ORIGINAL PAGE IS
OF POOR QUALITY

FIGURE 10.39 TIMEBASE WAVE PRESENTATION OF 1/2X RUB VIBRATION SIGNALS. TOP: PLUNGER MOTION, BOTTOM: ELECTRICAL SIGNAL OF ROTOR-TO-STATOR CONTACT (RUB-RELATED). NOTE: SIGNIFICANT PLUNGER MOTION, LONG PERIOD OF CONTACT, 1/2X COMPONENT (3.34 LB. PRELOAD, INBOARD UNBALANCE: 0.48 GRAMS AT 0 DEGREES AND RADIUS = 1.2 IN.).

RUN 4

PROBE #1 ID: RUB FIXTURE VERT — ORIENTATION= 90 DEG
UNFILTERED — MAX AMP= 9.20 MILS PK-PK

PROBE #2 ID: RUB FIXTURE HOR — ORIENTATION= 0 DEG
UNFILTERED — MAX AMP= 10.60 MILS PK-PK

ROTATION: CW
RPM(START)= 5652 RPM(END)= 5652

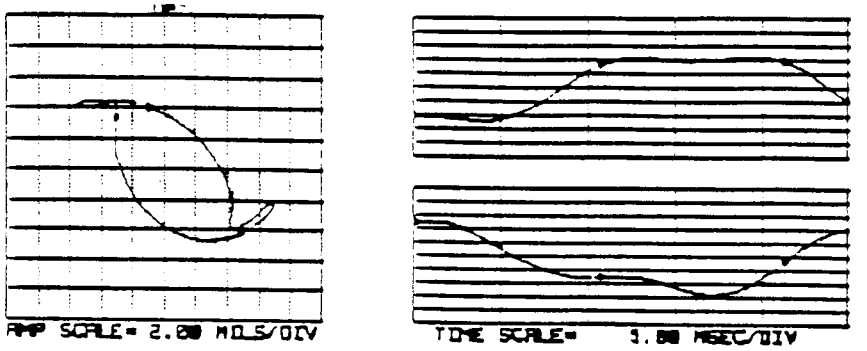

FIGURE 10.40 STEADY-STATE ORBIT/TIMEBASE WAVE OF ROTOR VIBRATIONAL RESPONSE AT 5652 RPM AS SEEN BY RUB FIXTURE VERTICAL AND HORIZONTAL DISPLACEMENT PROBES. NOTE: UNFILTERED ORBIT INDICATES EXISTENCE OF A 1/3X COMPONENT (3.34 LB. PRELOAD, INBOARD UNBALANCE: 0.48 GRAMS AT 0 DEGREES AND RADIUS = 1.2 IN.).

PROBE #1 ID: RUB PLUNGER — ORIENTATION= 0 DEG
UNFILTERED — MAX AMP= 1.70 MILS PK-PK

PROBE #2 ID: RUB ELEC. CONTACT — ORIENTATION= 0 DEG
UNFILTERED — MAX AMP= 5.80 MILS PK-PK

ROTATION: CW
RPM(START)= 5648 RPM(END)= 5649

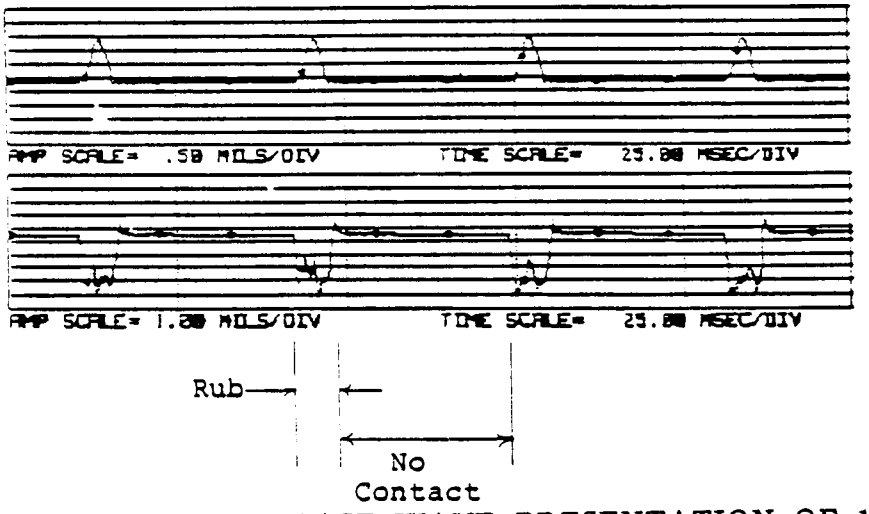

FIGURE 10.41 TIMEBASE WAVE PRESENTATION OF 1/3X RUB VIBRATION SIGNALS. TOP: PLUNGER MOTION, BOTTOM: ELECTRICAL SIGNAL OF ROTOR-TO-STATOR CONTACT (RUB-RELATED). NOTE: BOTH SIGNALS INDICATE THE PRESENCE OF A 1/3X COMPONENT AS SEEN IN FIGURE 10.40 (3.34 LB PRELOAD, INBOARD UNBALANCE: .48 GRAMS AT 0 DEGREES AND RADIUS = 1.2 IN.).

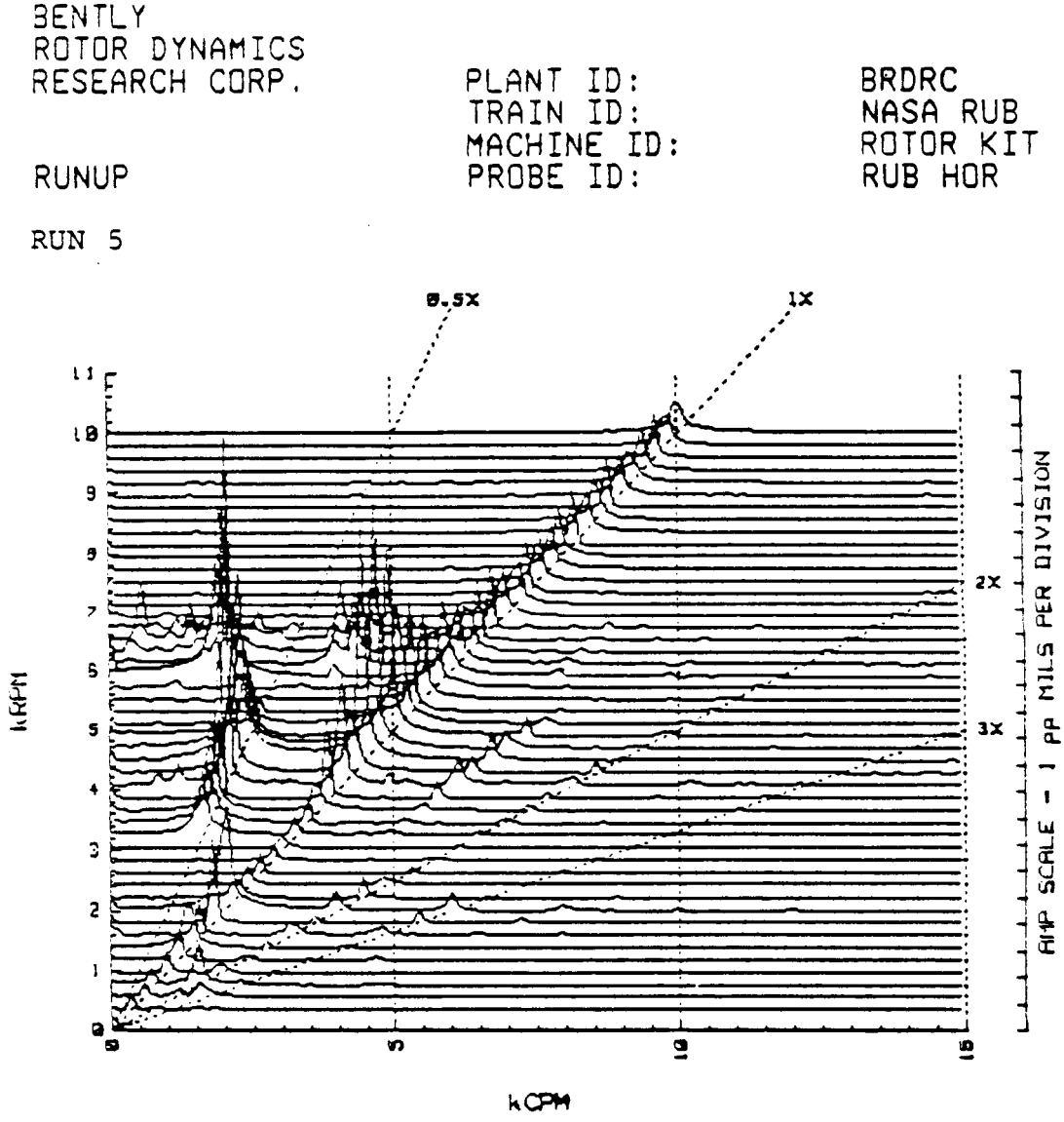

FIGURE 10.42 SPECTRUM CASCADE PLOT OF ROTOR VIBRATION DURING RUN–UP AS SEEN BY RUB FIXTURE HORIZONTAL DISPLACEMENT PROBE. NOTE: EXCITATION OF SUBSYNCHRONOUS, MAINLY 1/2X COMPONENTS (6.68 LB PRELOAD, INBOARD UNBALANCE: .48 GRAMS AT 0 DEGREES AND RADIUS = 1.2 IN.).

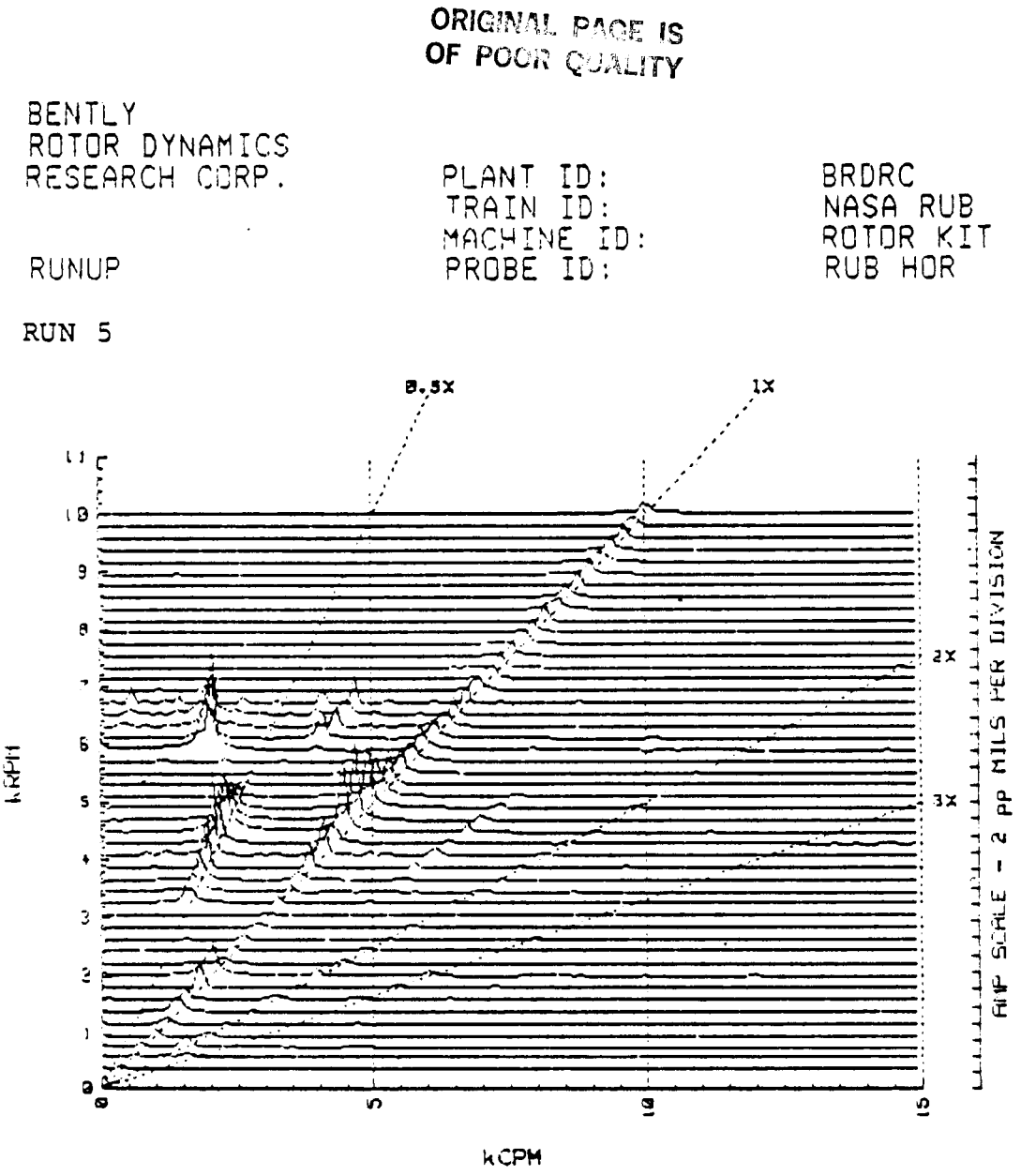

FIGURE 10.43 SPECTRUM CASCADE PLOT OF ROTOR VIBRATION DURING RUN–UP AS SEEN BY RUB FIXTURE HORIZONTAL DISPLACEMENT PROBE. NOTE: THIS IS THE SAME DATA WITH DIFFERENT SCALING AS FIGURE 10.42.

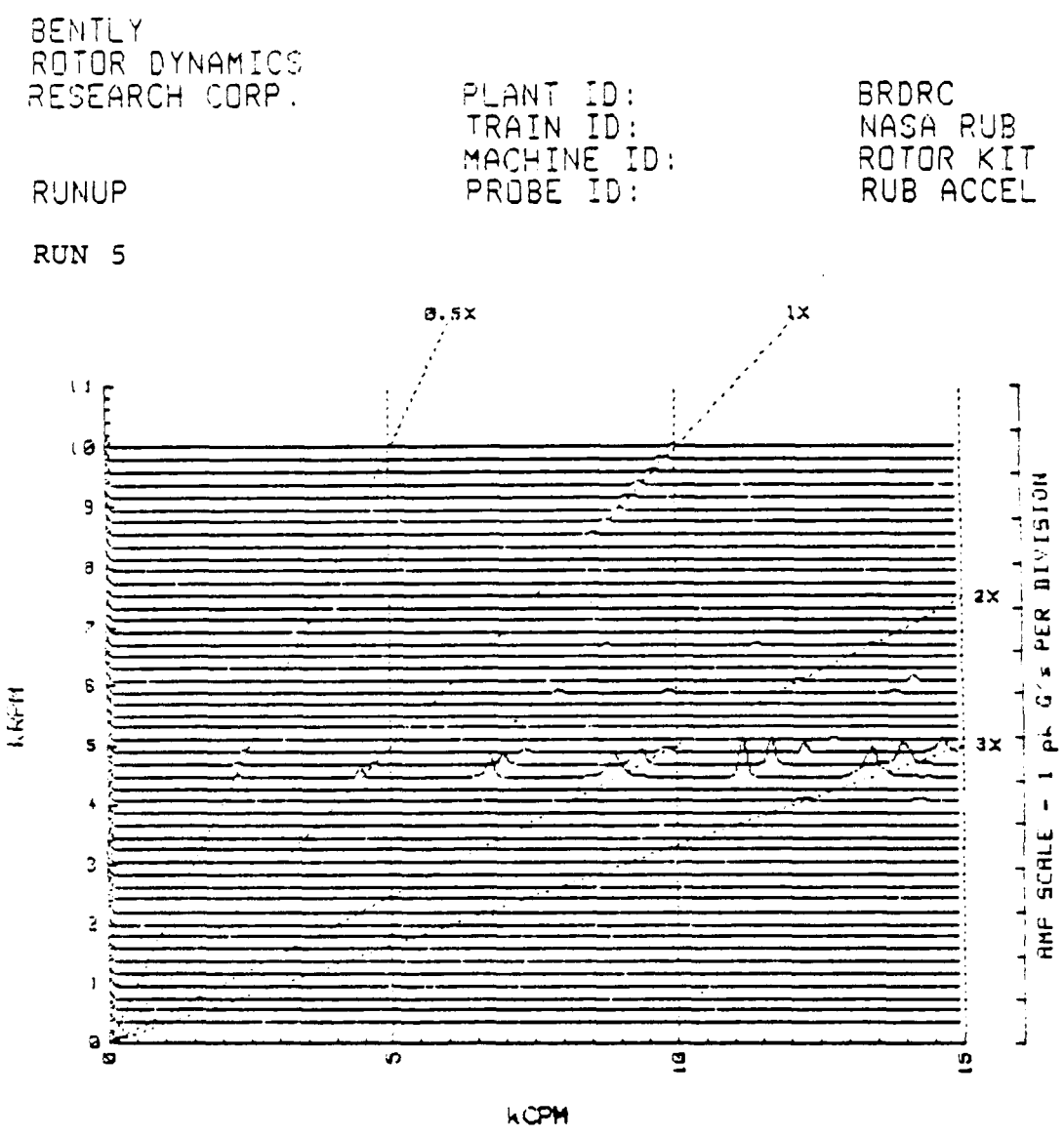

FIGURE 10.44 SPECTRUM CASCADE PLOT OF ROTOR VIBRATION DURING RUN–UP AS SEEN BY THE ACCELEROMETER MOUNTED ON THE RUB FIXTURE PLUNGER MECHANISM. THIS IS THE SAME TYPE OF DATA AS IN FIGURES 10.42 AND 10.43. NOTE SUPERSYNCHRONOUS COMPONENTS ONLY WHEN 1/2X AND 1X COMPONENTS ARE SIGNIFICANT. COMPARE WITH FIGURE 10.42 (6.68 LB PRELOAD, INBOARD UNBALANCE: .48 GRAMS AT 0 DEGREES AND RADIUS = 1.2 IN.).

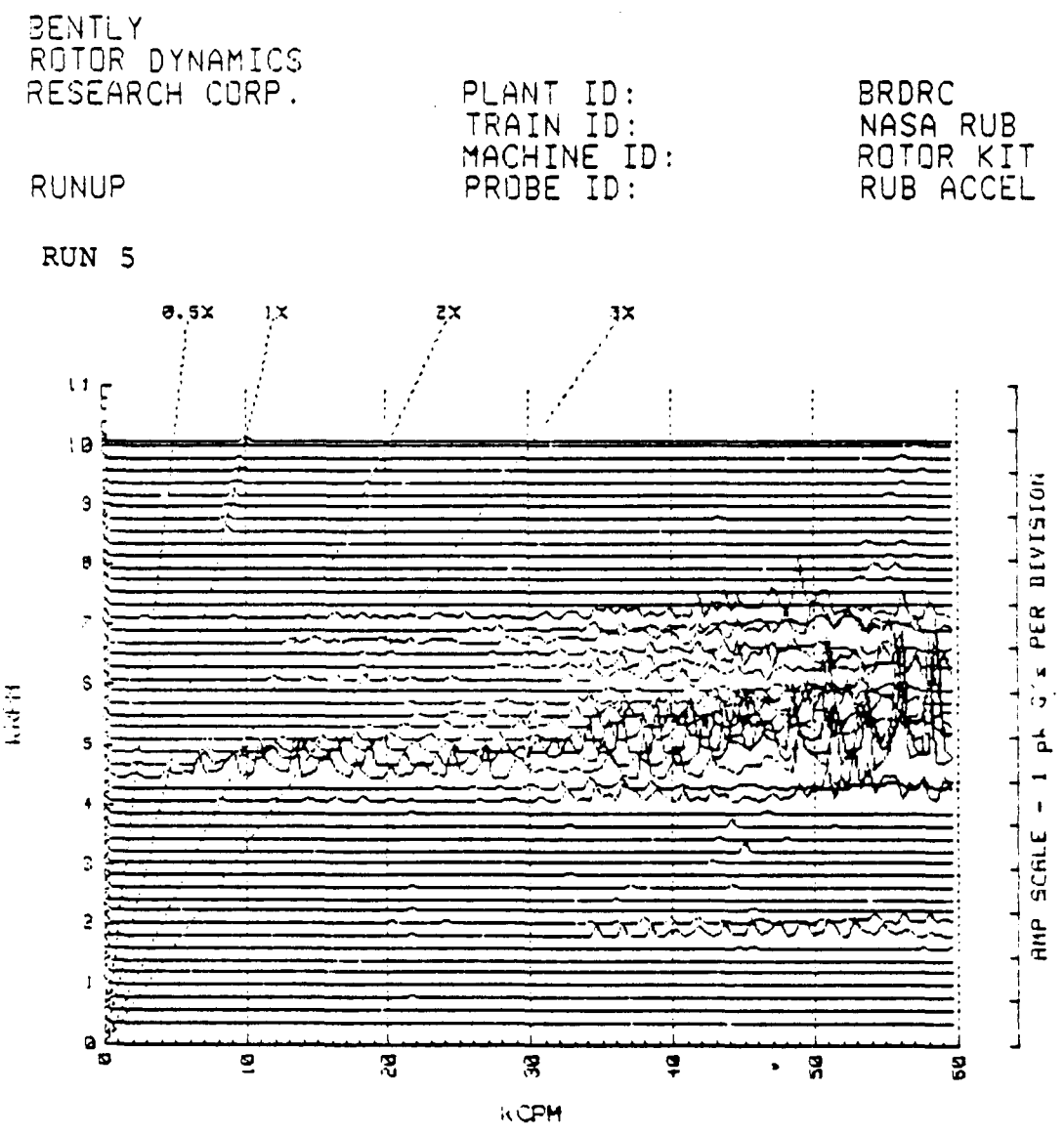

FIGURE 10.45 SPECTRUM CASCADE PLOT OF ROTOR VIBRATION DURING RUN–UP AS SEEN BY THE ACCELEROMETER MOUNTED ON THE RUB FIXTURE PLUNGER MECHANISM. THE SAME DATA AS IN FIG. 10.44 BUT WIDER FREQUENCY RANGE. NOTE EXCITATION OF HIGHER ORDER COMPONENTS. COMPARE WITH FIGURES 10.42 THROUGH 10.44 (6.68 LB. PRELOAD, INBOARD UNBALANCE: 0.48 GRAMS AT 0 DEGREES AND RADIUS = 1.2 IN.).

BENTLY
NEVADA
CORP.

PLANT ID: B.R.D.R.C
TRAIN ID: NASA RUB RIG
MACHINE ID: RUB ORBITS

RUN 5

PROBE #1 ID: RUB FIXTURE VERT
UNFILTERED

ORIENTATION= 90 DEG
MAX AMP= 13.60 MILS PK-PK

PROBE #2 ID: RUB FIXTURE HOR
UNFILTERED

ORIENTATION= 0 DEG
MAX AMP= 2.30 MILS PK-PK

ROTATION: CW
RPM(START)= 1565 RPM(END)= 1564

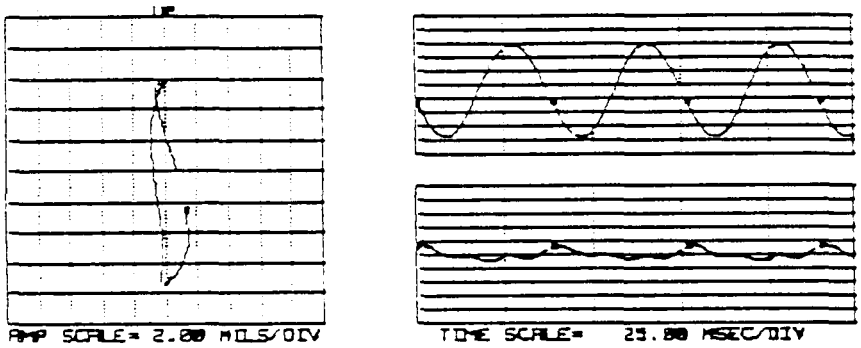

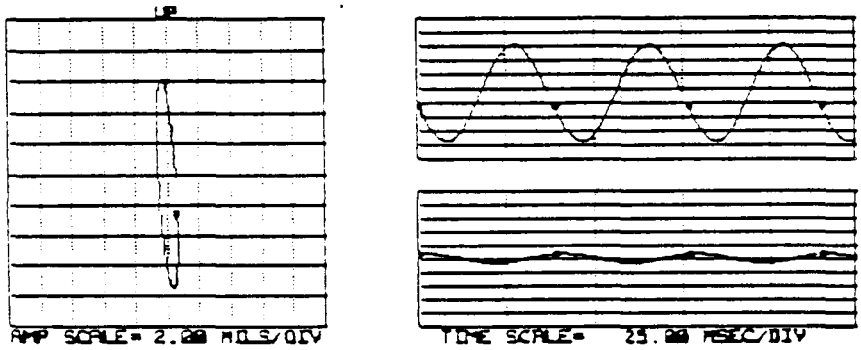

RUN 5

PROBE #1 ID: RUB FIXTURE VERT
1X FILTERED

ORIENTATION= 90 DEG
1X VECTOR= 13.70 MILS PK-PK @-250

PROBE #2 ID: RUB FIXTURE HOR
1X FILTERED

ORIENTATION= 0 DEG
1X VECTOR= 1.30 MILS PK-PK @-12

ROTATION: CW
RPM(START)= 1565 RPM(END)= 1565

FIGURE 10.46 STEADY–STATE ORBIT/TIMEBASE WAVE OF ROTOR VIBRATIONAL RESPONSE AT 1564 RPM AS SEEN BY RUB FIXTURE VERTICAL AND HORIZONTAL DISPLACEMENT PROBES. TOP: UNFILTERED 1X RUB SIGNAL, BOTTOM: 1X FILTERED SIGNAL. (6.68 LB PRELOAD, INBOARD UNBALANCE: .48 GRAMS AT 0 DEGREES AND RADIUS = 1.2 IN.).

BENTLY
NEVADA
CORP.

PLANT ID: B.R.D.R.C
TRAIN ID: NASA RUB
MACHINE ID: ELEC CONTACT REF.

RUN 5

PROBE #1 ID: RUB PLUNGER
UNFILTERED

ORIENTATION= 0 DEG
MAX AMP= 0.00 MILS PK-PK

PROBE #2 ID: RUB ELEC. CONTACT
UNFILTERED

ORIENTATION= 0 DEG
MAX AMP= 5.50 MILS PK-PK

ROTATION: CW
RPM(START)= 1569 RPM(END)= 1570

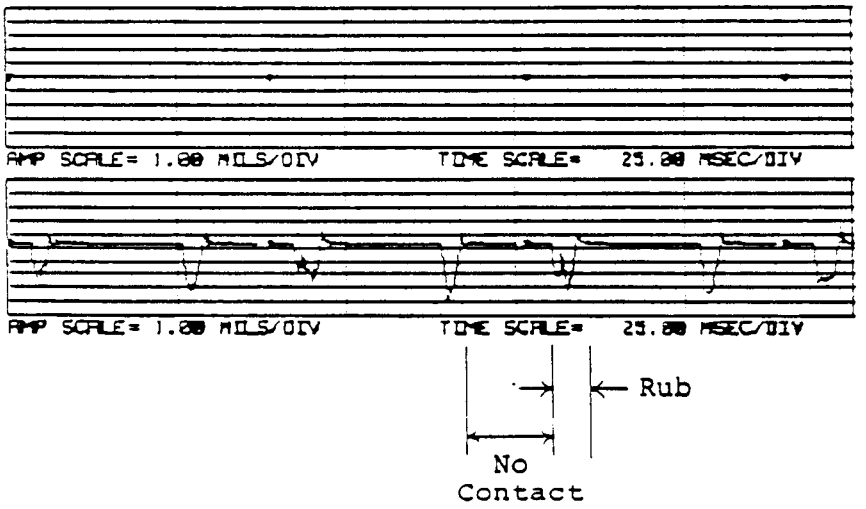

FIGURE 10.47 TIMEBASE WAVE PRESENTATION OF 1X RUB VIBRATION SIGNALS. TOP: PLUNGER MOTION, BOTTOM: ELECTRICAL SIGNAL OF ROTOR–TO–STATOR CONTACT (RUB–RELATED). (6.68 LB PRELOAD, INBOARD UNBALANCE: .48 GRAMS AT 0 DEGREES AND RADIUS = 1.2 IN.).

BENTLY
NEVADA
CORP.

PLANT ID: B.R.D.R.C
TRAIN ID: NASA RUB RIG
MACHINE ID: RUB ORBITS

RUN 5

PROBE #1 ID: RUB FIXTURE VERT
UNFILTERED

ORIENTATION= 90 DEG
MAX AMP= 15.80 MILS PK-PK

PROBE #2 ID: RUB FIXTURE HOR
UNFILTERED

ORIENTATION= 0 DEG
MAX AMP= 3.20 MILS PK-PK

ROTATION: CW
RPM(START)= 1614 RPM(END)= 1612

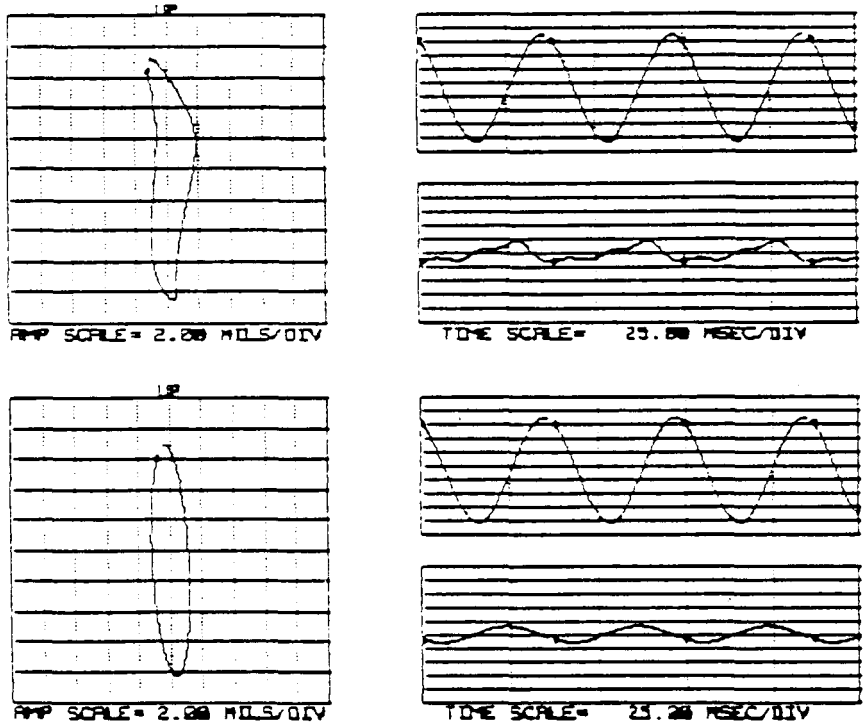

RUN 5

PROBE #1 ID: RUB FIXTURE VERT
1X FILTERED

ORIENTATION= 90 DEG
1X VECTOR= 15.20 MILS PK-PK @-328

PROBE #2 ID: RUB FIXTURE HOR
1X FILTERED

ORIENTATION= 0 DEG
1X VECTOR= 2.40 MILS PK-PK @-221

ROTATION: CW
RPM(START)= 1612 RPM(END)= 1615

FIGURE 10.48 STEADY–STATE ORBIT/TIMEBASE WAVE OF ROTOR VIBRATIONAL RESPONSE AT 1612 RPM AS SEEN BY RUB FIXTURE VERTICAL AND HORIZONTAL DISPLACEMENT PROBES. TOP: UNFILTERED 1X RUB SIGNAL, BOTTOM: 1X FILTERED SIGNAL. (6.68 LB PRELOAD, INBOARD UNBALANCE: .48 GRAMS AT 0 DEGREES AND RADIUS = 1.2 IN.).

BENTLY
NEVADA
CORP.

PLANT ID: B.R.D.R.C
TRAIN ID: NASA RUB
MACHINE ID: ELEC CONTACT REF.

RUN 5

PROBE #1 ID: RUB PLUNGER
UNFILTERED

ORIENTATION= 0 DEG
MAX AMP= 0.00 MILS PK-PK

PROBE #2 ID: RUB ELEC. CONTACT
UNFILTERED

ORIENTATION= 0 DEG
MAX AMP= 5.70 MILS PK-PK

ROTATION: CW
RPM(START)= 1614 RPM(END)= 1614

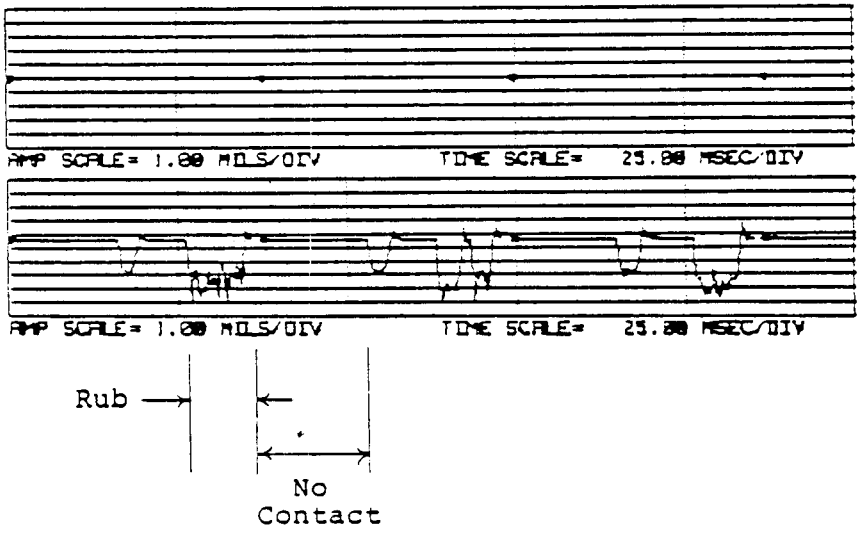

FIGURE 10.49 TIMEBASE WAVE PRESENTATION OF 1X RUB VIBRATION SIGNALS. TOP: PLUNGER MOTION, BOTTOM: ELECTRICAL SIGNAL OF ROTOR–TO–STATOR CONTACT (RUB–RELATED). (6.68 LB PRELOAD, INBOARD UNBALANCE: .48 GRAMS AT 0 DEGREES AND RADIUS = 1.2 IN.).

BENTLY
NEVADA
CORP.

PLANT ID: B.R.D.R.C
TRAIN ID: NASA RUB RIG
MACHINE ID: RUB ORBITS

RUN 5

PROBE #1 ID: RUB FIXTURE VERT
UNFILTERED

ORIENTATION= 90 DEG
MAX AMP= .80 MILS PK-PK

PROBE #2 ID: RUB FIXTURE HOR
UNFILTERED

ORIENTATION= 0 DEG
MAX AMP= 6.10 MILS PK-PK

ROTATION: CW
RPM(START)= 1936 RPM(END)= 1936

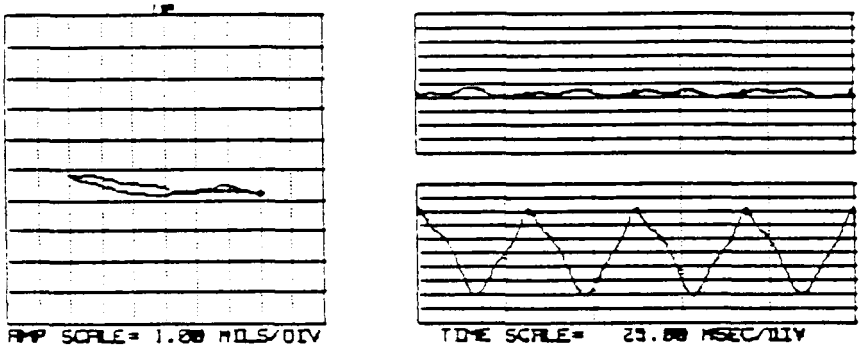

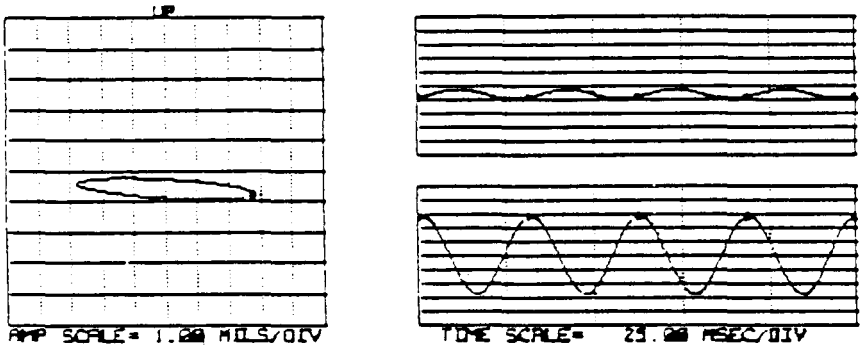

RUN 5

PROBE #1 ID: RUB FIXTURE VERT
1X FILTERED

ORIENTATION= 90 DEG
1X VECTOR= .70 MILS PK-PK @-117

PROBE #2 ID: RUB FIXTURE HOR
1X FILTERED

ORIENTATION= 0 DEG
1X VECTOR= 5.60 MILS PK-PK @-2

ROTATION: CW
RPM(START)= 1936 RPM(END)= 1935

FIGURE 10.50 STEADY–STATE ORBIT/TIMEBASE WAVE OF ROTOR VIBRATIONAL RESPONSE AT 1936 AS SEEN BY RUB FIXTURE VERTICAL AND HORIZONTAL DISPLACEMENT PROBES. TOP: UNFILTERED 1X RUB SIGNAL, BOTTOM: 1X FILTERED SIGNAL. (6.68 LB PRELOAD, INBOARD UNBALANCE: .48 GRAMS AT 0 DEGREES AND RADIUS = 1.2 IN.).

BENTLY
NEVADA
CORP.

PLANT ID: B.R.D.R.C
TRAIN ID: NASA RUB
MACHINE ID: ELEC CONTACT REF.

RUN 5

PROBE #1 ID: RUB PLUNGER
UNFILTERED

ORIENTATION= 0 DEG
MAX AMP= 0.00 MILS PK-PK

PROBE #2 ID: RUB ELEC. CONTACT
UNFILTERED

ORIENTATION= 0 DEG
MAX AMP= 5.60 MILS PK-PK

ROTATION: CW
RPM(START)= 1926 RPM(END)= 1922

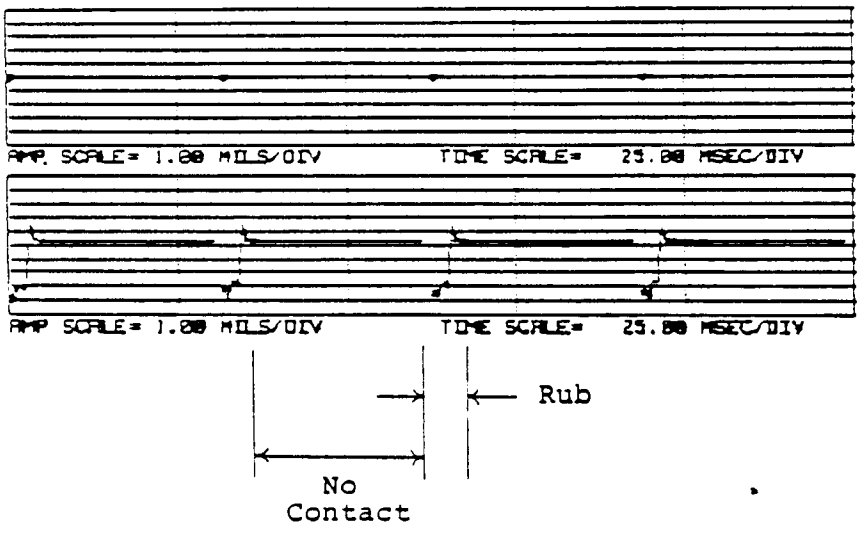

FIGURE 10.51 TIMEBASE WAVE PRESENTATION OF 1X RUB VIBRATION SIGNALS. TOP: PLUNGER MOTION, BOTTOM: ELECTRICAL SIGNAL OF ROTOR–TO–STATOR CONTACT (RUB–RELATED). (6.68 LB PRELOAD, INBOARD UNBALANCE: .48 GRAMS AT 0 DEGREES AND RADIUS = 1.2 IN.).

BENTLY
NEVADA
CORP.

PLANT ID: B.R.D.R.C
TRAIN ID: NASA RUB RIG
MACHINE ID: RUB ORBITS

RUN 5

PROBE #1 ID: RUB FIXTURE VERT
UNFILTERED

ORIENTATION= 90 DEG
MAX AMP= 6.40 MILS PK-PK

PROBE #2 ID: RUB FIXTURE HOR
UNFILTERED

ORIENTATION= 0 DEG
MAX AMP= 12.40 MILS PK-PK

ROTATION: CW
RPM(START)= 3924 RPM(END)= 3924

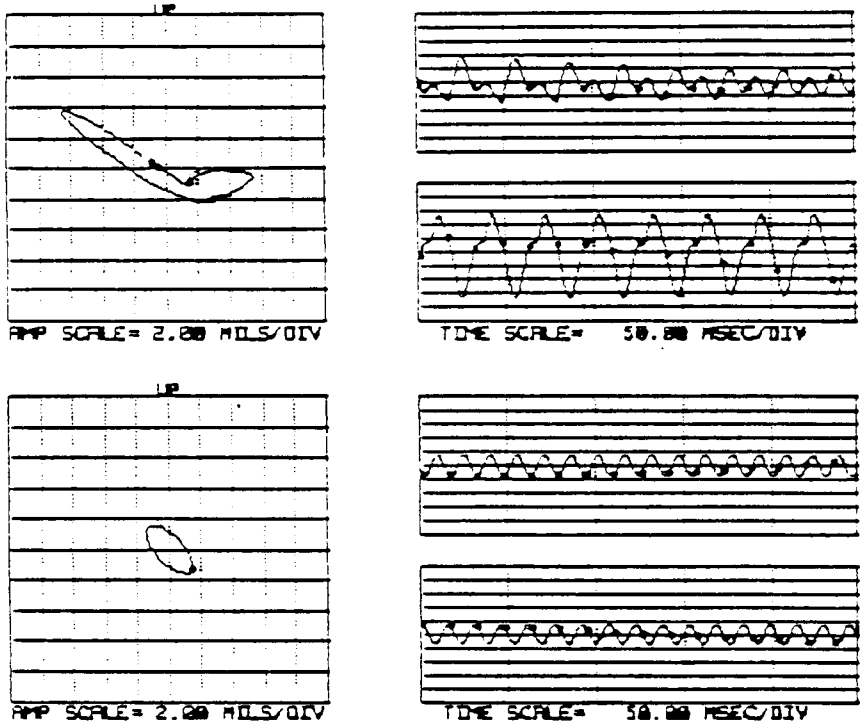

RUN 5

PROBE #1 ID: RUB FIXTURE VERT
1X FILTERED

ORIENTATION= 90 DEG
1X VECTOR= 3.10 MILS PK-PK @-194

PROBE #2 ID: RUB FIXTURE HOR
1X FILTERED

ORIENTATION= 0 DEG
1X VECTOR= 2.90 MILS PK-PK @-327

ROTATION: CW
RPM(START)= 3924 RPM(END)= 3924

FIGURE 10.52 STEADY–STATE ORBIT/TIMEBASE WAVE OF ROTOR VIBRATIONAL RESPONSE AT 3924 RPM AS SEEN BY RUB FIXTURE VERTICAL AND HORIZONTAL DISPLACEMENT PROBES. NOTE 1/2X COMPONENT IN TOP ORBIT. TOP: UNFILTERED SIGNAL, BOTTOM: 1X FILTERED SIGNAL. (6.68 LB PRELOAD, INBOARD UNBALANCE: .48 GRAMS AT 0 DEGREES AND RADIUS = 1.2 IN.).

BENTLY
NEVADA
CORP.

PLANT ID: B.R.D.R.C
TRAIN ID: NASA RUB
MACHINE ID: ELEC CONTACT REF.

RUN 5

PROBE #1 ID: RUB PLUNGER
UNFILTERED

ORIENTATION= 0 DEG
MAX AMP= .40 MILS PK-PK

PROBE #2 ID: RUB ELEC. CONTACT
UNFILTERED

ORIENTATION= 0 DEG
MAX AMP= 5.80 MILS PK-PK

ROTATION: CW
RPM(START)= 3920 RPM(END)= 3919

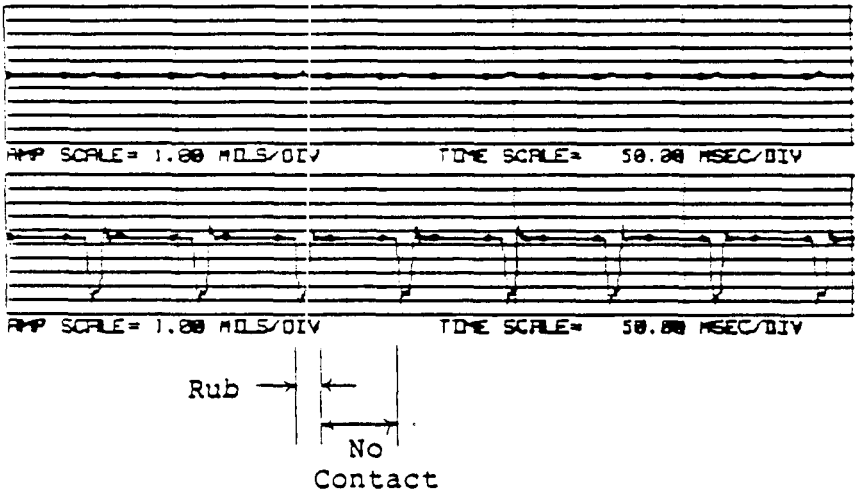

FIGURE 10.53 TIMEBASE WAVE PRESENTATION OF 1/2X RUB VIBRATION SIGNALS. TOP: PLUNGER MOTION, BOTTOM: ELECTRICAL SIGNAL OF ROTOR–TO–STATOR CONTACT (RUB–RELATED). NOTE: SMALL PLUNGER MOTION AND 1/2X RUB INDICATED BY ELECTRICAL CONTACT (6.68 LB INBOARD PRELOAD, UNBALANCE: .48 GRAMS AT 0 DEGREES AND RADIUS = 1.2 IN.).

BENTLY
NEVADA
CORP.

PLANT ID: B.R.D.R.C
TRAIN ID: NASA RUB RIG
MACHINE ID: RUB ORBITS

RUN 5

PROBE #1 ID: RUB FIXTURE VERT
UNFILTERED

ORIENTATION= 90 DEG
MAX AMP= 5.00 MILS PK-PK

PROBE #2 ID: RUB FIXTURE HOR
UNFILTERED

ORIENTATION= 0 DEG
MAX AMP= 13.00 MILS PK-PK

ROTATION: CW
RPM(START)= 5211 RPM(END)= 5211

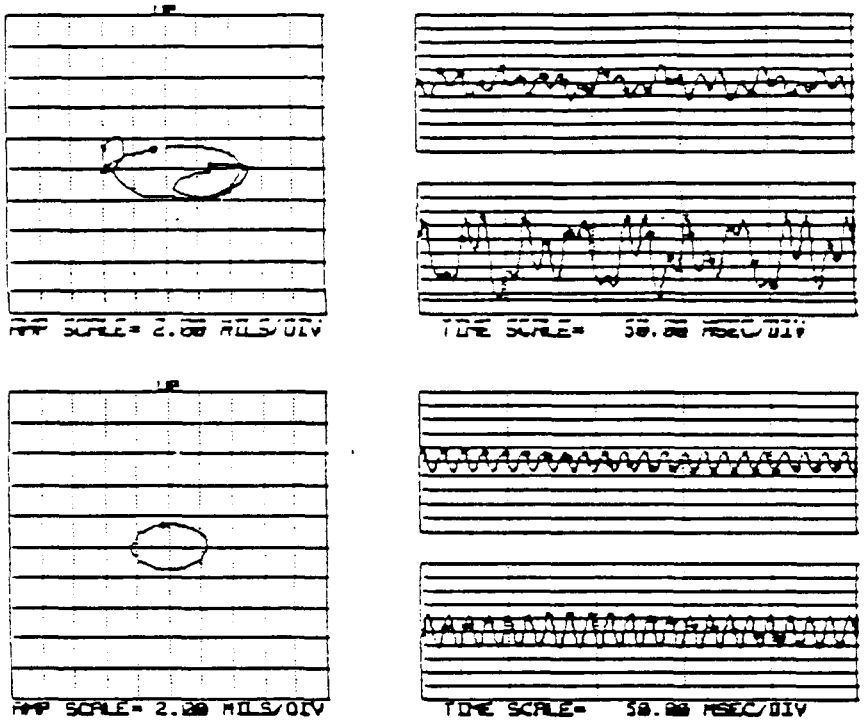

RUN 5

PROBE #1 ID: RUB FIXTURE VERT
1X FILTERED

ORIENTATION= 90 DEG
1X VECTOR= 3.00 MILS PK-PK @-350

PROBE #2 ID: RUB FIXTURE HOR
1X FILTERED

ORIENTATION= 0 DEG
1X VECTOR= 4.80 MILS PK-PK @-76

ROTATION: CW
RPM(START)= 5212 RPM(END)= 5213

FIGURE 10.54 STEADY-STATE ORBIT/TIMEBASE WAVE OF ROTOR VIBRATIONAL RESPONSE AT 5211 RPM AS SEEN BY RUB FIXTURE VERTICAL AND HORIZONTAL DISPLACEMENT PROBES. TOP: UNFILTERED 1/3X RUB SIGNAL, BOTTOM: 1X FILTERED SIGNAL. NOTE COMPLEX TOP ORBIT SHAPE (6.68 LB PRELOAD, INBOARD UNBALANCE: .48 GRAMS AT 0 DEGREES AND RADIUS = 1.2 IN.).

BENTLY NEVADA CORP.

PLANT ID: B.R.D.R.C
TRAIN ID: NASA RUB
MACHINE ID: ELEC CONTACT REF.

RUN 5

PROBE #1 ID: RUB PLUNGER
UNFILTERED
ORIENTATION= 0 DEG
MAX AMP= .20 MILS PK-PK

PROBE #2 ID: RUB ELEC. CONTACT
UNFILTERED
ORIENTATION= 0 DEG
MAX AMP= 6.00 MILS PK-PK

ROTATION: CW
RPM(START)= 5212 RPM(END)= 5212

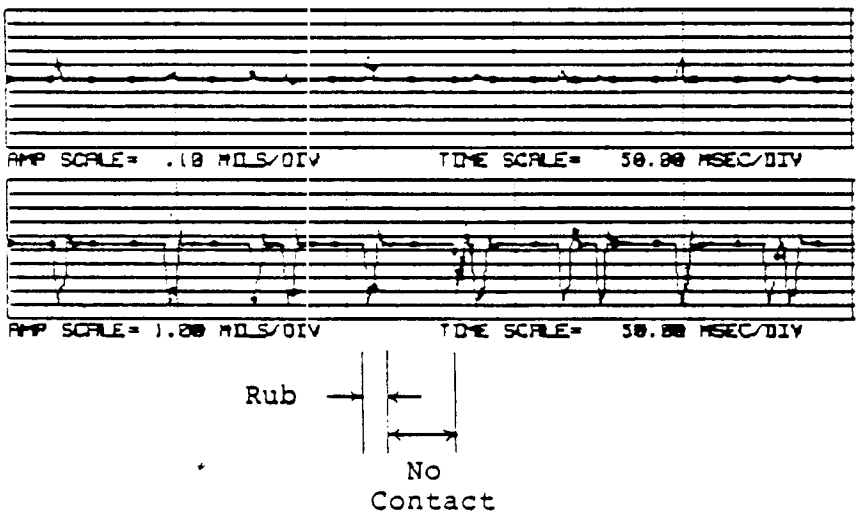

FIGURE 10.55 TIMEBASE WAVE PRESENTATION OF 1/3X RUB VIBRATION SIGNALS. TOP: PLUNGER MOTION, BOTTOM: ELECTRICAL SIGNAL OF ROTOR–TO–STATOR CONTACT (RUB–RELATED). NOTE: COMPLEX ELECTRICAL CONTACT SIGNAL (6.68 LB PRELOAD, INBOARD UNBALANCE: .48 GRAMS AT 0 DEGREES AND RADIUS = 1.2 IN.).

BENTLY
NEVADA
CORP.

PLANT ID: B.R.D.R.C
TRAIN ID: NASA RUB RIG
MACHINE ID: RUB ORBITS

RUN 5

PROBE #1 ID: RUB FIXTURE VERT
UNFILTERED

ORIENTATION= 90 DEG
MAX AMP= 6.60 MILS PK-PK

PROBE #2 ID: RUB FIXTURE HOR
UNFILTERED

ORIENTATION= 0 DEG
MAX AMP= 10.80 MILS PK-PK

ROTATION: CW
RPM(START)= 5637 RPM(END)= 5636

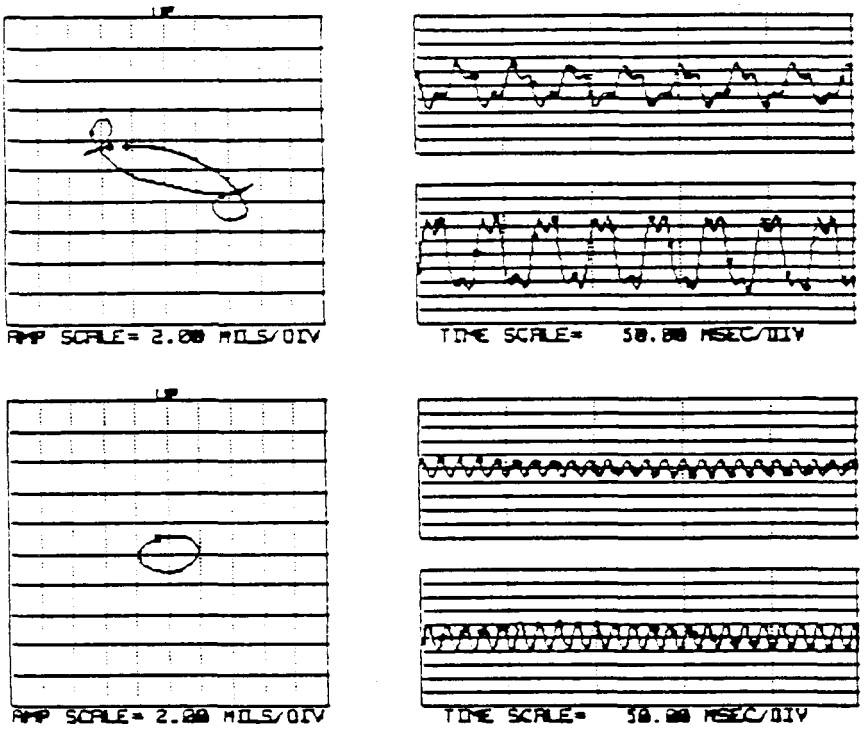

RUN 5

PROBE #1 ID: RUB FIXTURE VERT
1X FILTERED

ORIENTATION= 90 DEG
1X VECTOR= 2.40 MILS PK-PK @-357

PROBE #2 ID: RUB FIXTURE HOR
1X FILTERED

ORIENTATION= 0 DEG
1X VECTOR= 3.70 MILS PK-PK @-82

ROTATION: CW
RPM(START)= 5639 RPM(END)= 5637

FIGURE 10.56 STEADY–STATE ORBIT/TIMEBASE WAVE OF ROTOR VIBRATIONAL RESPONSE AT 5636 RPM AS SEEN BY RUB FIXTURE VERTICAL AND HORIZONTAL DISPLACEMENT PROBES. TOP: UNFILTERED 1/4X RUB SIGNAL, BOTTOM: 1X FILTERED SIGNAL. NOTE: COMPLEX TOP ORBIT SHAPE (6.68 LB PRELOAD, INBOARD UNBALANCE: .48 GRAMS AT 0 DEGREES AND RADIUS = 1.2 IN.).

BENTLY
NEVADA
CORP.

PLANT ID: B.R.D.R.C
TRAIN ID: NASA RUB
MACHINE ID: ELEC CONTACT REF.

RUN 5

PROBE #1 ID: RUB PLUNGER
UNFILTERED

ORIENTATION= 0 DEG
MAX AMP= .10 MILS PK-PK

PROBE #2 ID: RUB ELEC. CONTACT
UNFILTERED

ORIENTATION= 0 DEG
MAX AMP= 5.80 MILS PK-PK

ROTATION: CW
RPM(START)= 5635 RPM(END)= 5637

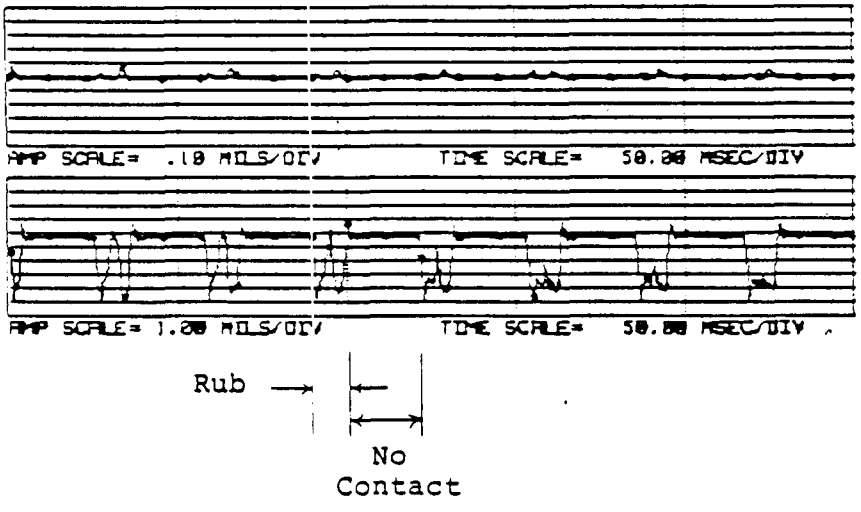

FIGURE 10.57 TIMEBASE WAVE PRESENTATION OF 1/4X RUB VIBRATION SIGNALS. TOP: PLUNGER MOTION, BOTTOM: ELECTRICAL CONTACT SIGNAL OF ROTOR–TO–STATOR (RUB–RELATED). NOTE: COMPLEX ELECTRICAL CONTACT SIGNAL (6.68 LB PRELOAD, INBOARD UNBALANCE: .48 GRAMS AT 0 DEGREES AND RADIUS = 1.2 IN.).

BENTLY
NEVADA
CORP.

PLANT ID: B.R.D.R.C
TRAIN ID: NASA RUB RIG
MACHINE ID: RUB ORBITS

RUN 5

PROBE #1 ID: RUB FIXTURE VERT
UNFILTERED

ORIENTATION= 90 DEG
MAX AMP= 1.60 MILS PK-PK

PROBE #2 ID: RUB FIXTURE HOR
UNFILTERED

ORIENTATION= 0 DEG
MAX AMP= 2.30 MILS PK-PK

ROTATION: CW
RPM(START)= 7037 RPM(END)= 7036

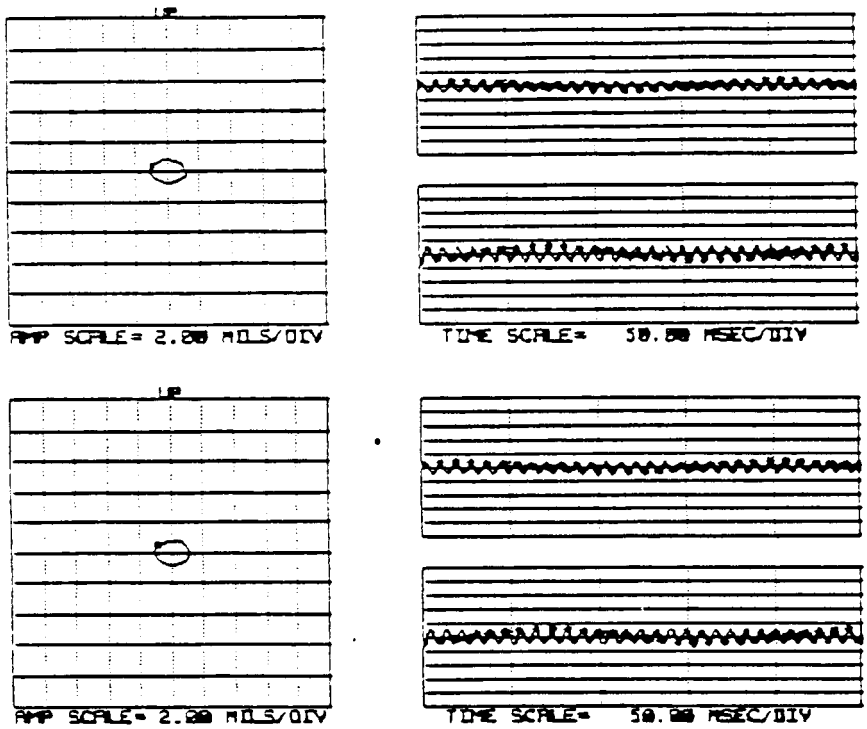

RUN 5

PROBE #1 ID: RUB FIXTURE VERT
1X FILTERED

ORIENTATION= 90 DEG
1X VECTOR= 1.60 MILS PK-PK @-7

PROBE #2 ID: RUB FIXTURE HOR
1X FILTERED

ORIENTATION= 0 DEG
1X VECTOR= 2.20 MILS PK-PK @-100

ROTATION: CW
RPM(START)= 7037 RPM(END)= 7038

FIGURE 10.58 STEADY–STATE ORBIT/TIMEBASE WAVE OF ROTOR VIBRATIONAL RESPONSE AT 7036 RPM AS SEEN BY RUB FIXTURE VERTICAL AND HORIZONTAL DISPLACEMENT PROBES. TOP: UNFILTERED 1X SIGNAL, BOTTOM: 1X FILTERED SIGNAL. NOTE: NO RUB, 1X UNBALANCE RESPONSE ONLY (6.68 LB PRELOAD, INBOARD UNBALANCE: .48 GRAMS AT 0 DEGREES AND RADIUS = 1.2 IN.).

BENTLY
NEVADA
CORP.

PLANT ID: B.R.D.R.C
TRAIN ID: NASA RUB
MACHINE ID: ELEC CONTACT REF.

RUN 5

PROBE #1 ID: RUB PLUNGER
UNFILTERED

ORIENTATION= 0 DEG
MAX AMP= 0.00 MILS PK-PK

PROBE #2 ID: RUB ELEC. CONTACT
UNFILTERED

ORIENTATION= 0 DEG
MAX AMP= 0.00 MILS PK-PK

ROTATION: CW
RPM(START)= 7029 RPM(END)= 7027

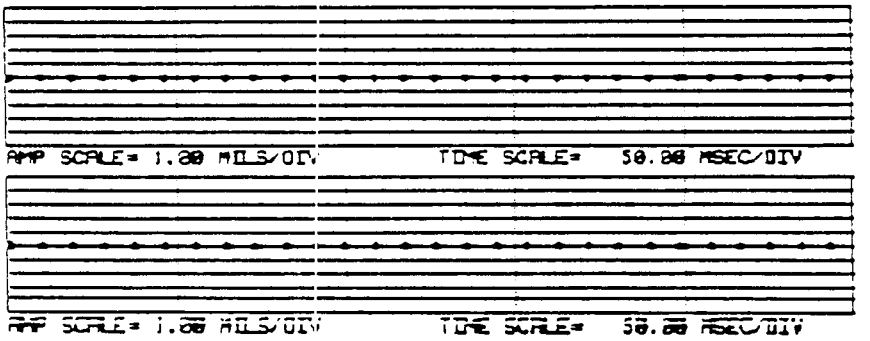

No
Contact

FIGURE 10.59 TIMEBASE WAVE PRESENTATION OF VIBRATION SIGNALS. TOP: PLUNGER MOTION, BOTTOM: ELECTRICAL SIGNAL OF ROTOR–TO–STATOR CONTACT (RUB–RELATED). NOTE: NO PLUNGER MOTION, NO ELECTRICAL CONTACT (RUB) (6.68 LB PRELOAD, INBOARD UNBALANCE: .48 GRAMS AT 0 DEGREES AND RADIUS = 1.2 IN.).

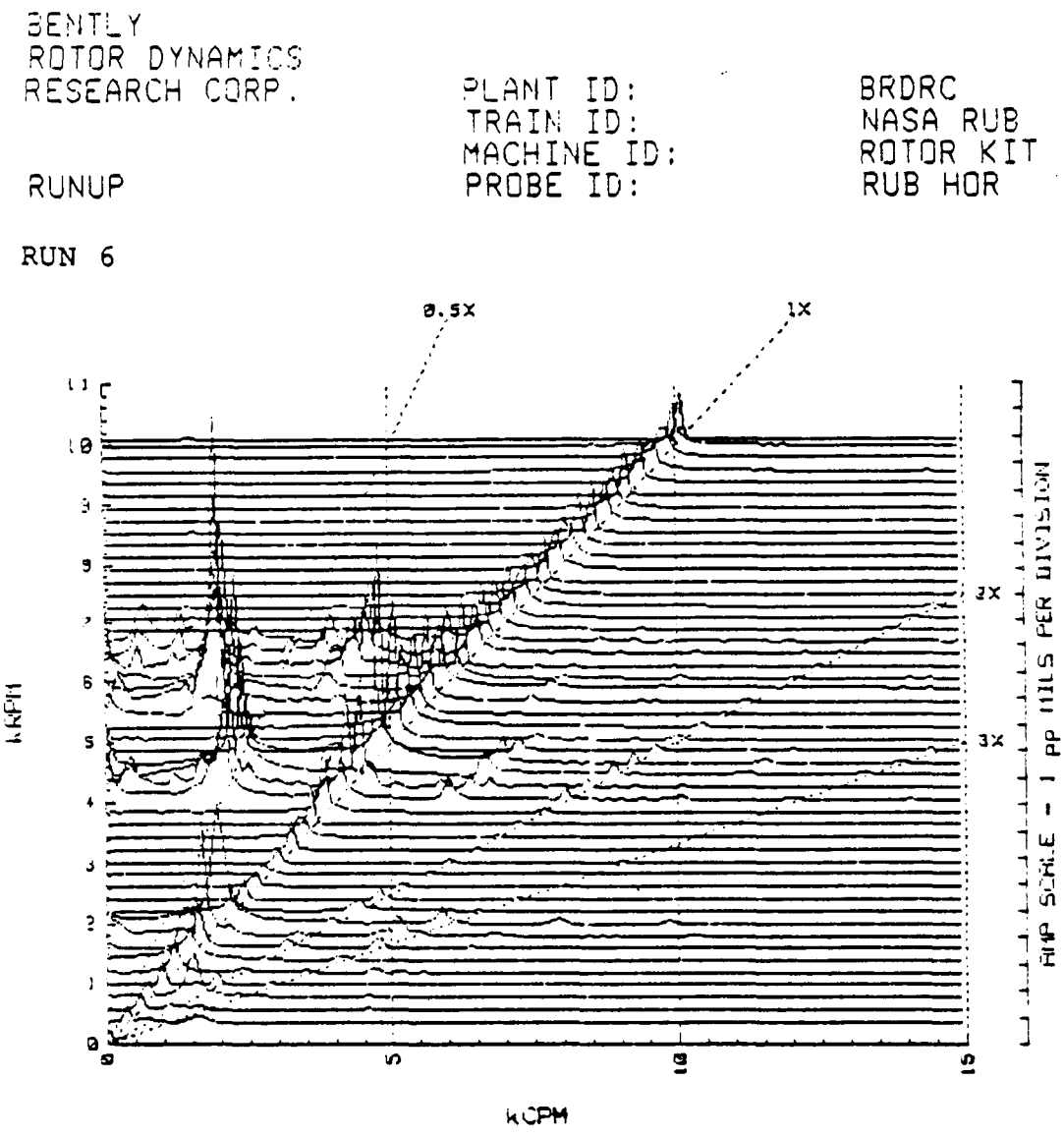

FIGURE 10.60 CASCADE PLOT OF ROTOR VIBRATION RESPONSE DURING RUN–UP AS SEEN BY RUB FIXTURE HORIZONTAL DISPLACEMENT PROBE. NOTE SIGNIFICANT EXCITATION OF SUB-SYNCHRONOUS COMPONENTS GENERATED BY RUB (10.03 LB PRELOAD, INBOARD UNBALANCE: .48 GRAMS AT 0 DEGREES AND RADIUS = 1.2 IN.).

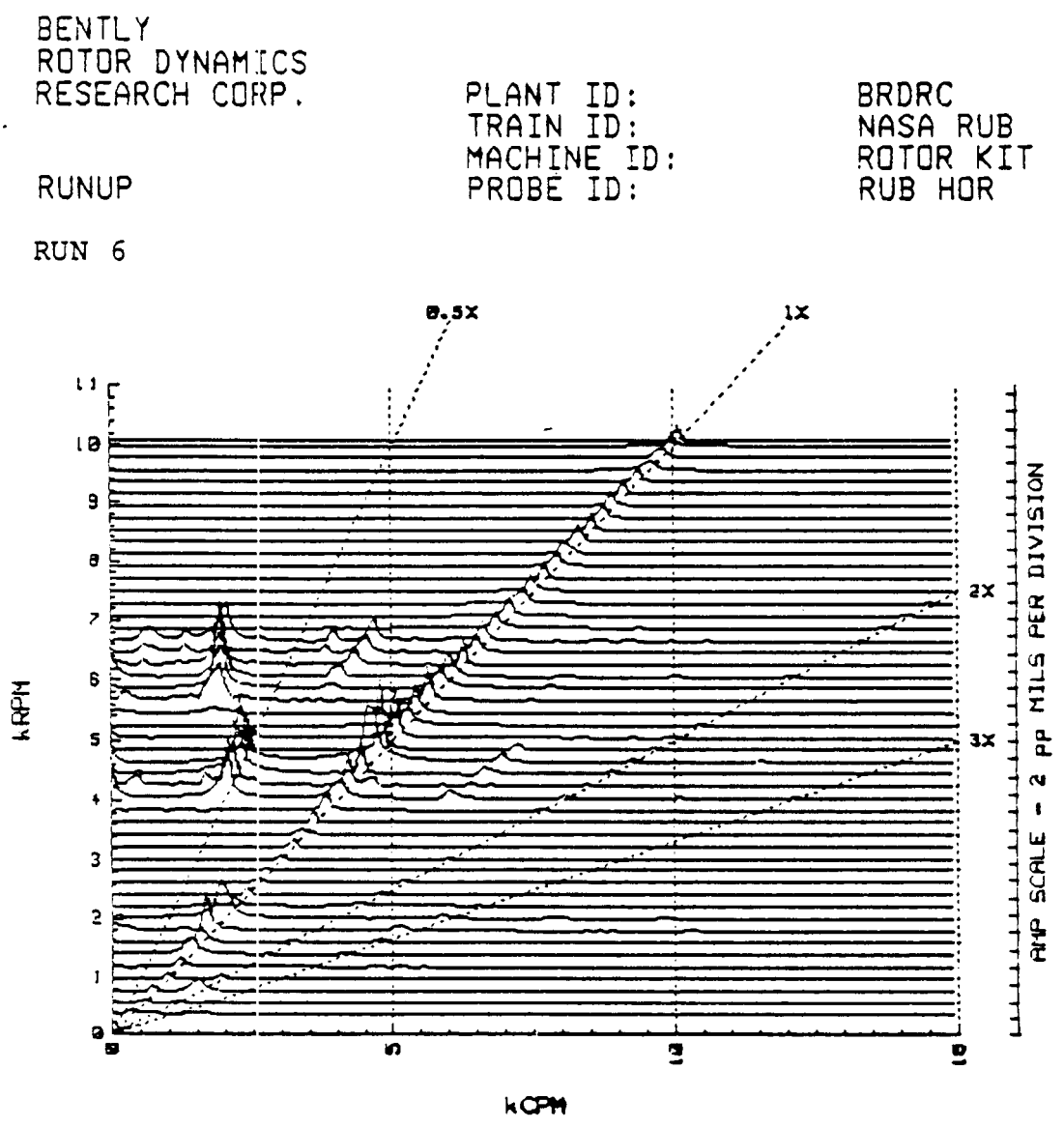

FIGURE 10.61 CASCADE PLOT OF ROTOR VIBRATION RESPONSE DURING RUN–UP AS SEEN BY RUB FIXTURE HORIZONTAL DISPLACEMENT PROBE. NOTE: THIS IS THE SAME DATA AS IN FIGURE 10.60 WITH DIFFERENT SCALING. 1/2X AND 1/3X COMPONENTS ARE EVIDENT.

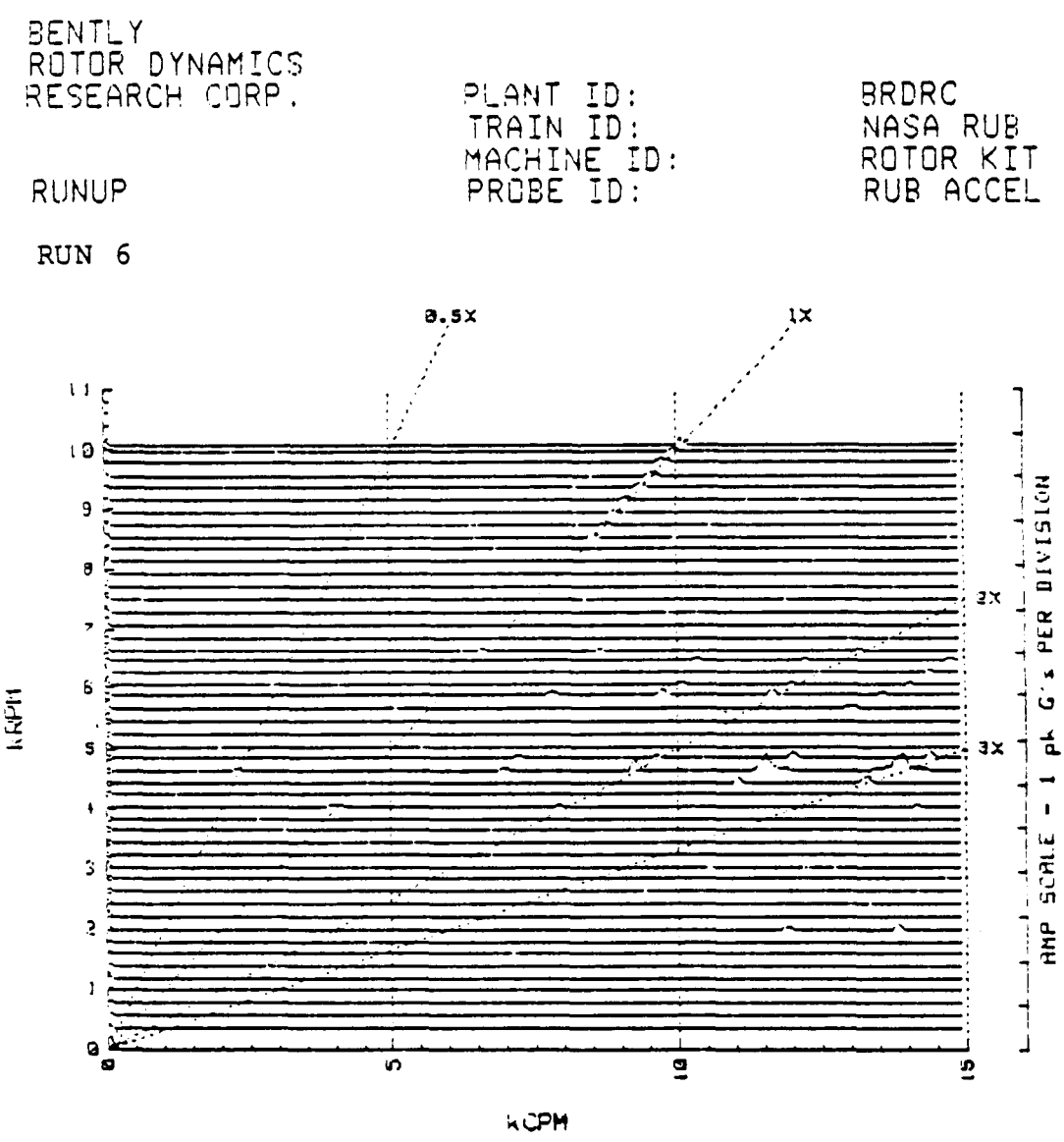

FIGURE 10.62 CASCADE PLOT OF ROTOR VIBRATION RESPONSE DURING RUN–UP AS SEEN BY ACCELEROMETER MOUNTED ON PLUNGER MECHANISM. NOTE: PROGRESSIVE LACK OF COMPONENTS AND VERY SMALL AMPLITUDES ABOVE 10 KCPM (10.03 LB PRELOAD, INBOARD UNBALANCE: .48 GRAMS AT 0 DEGREES AND RADIUS = 1.2 IN.).

ORIGINAL PAGE IS
OF POOR QUALITY

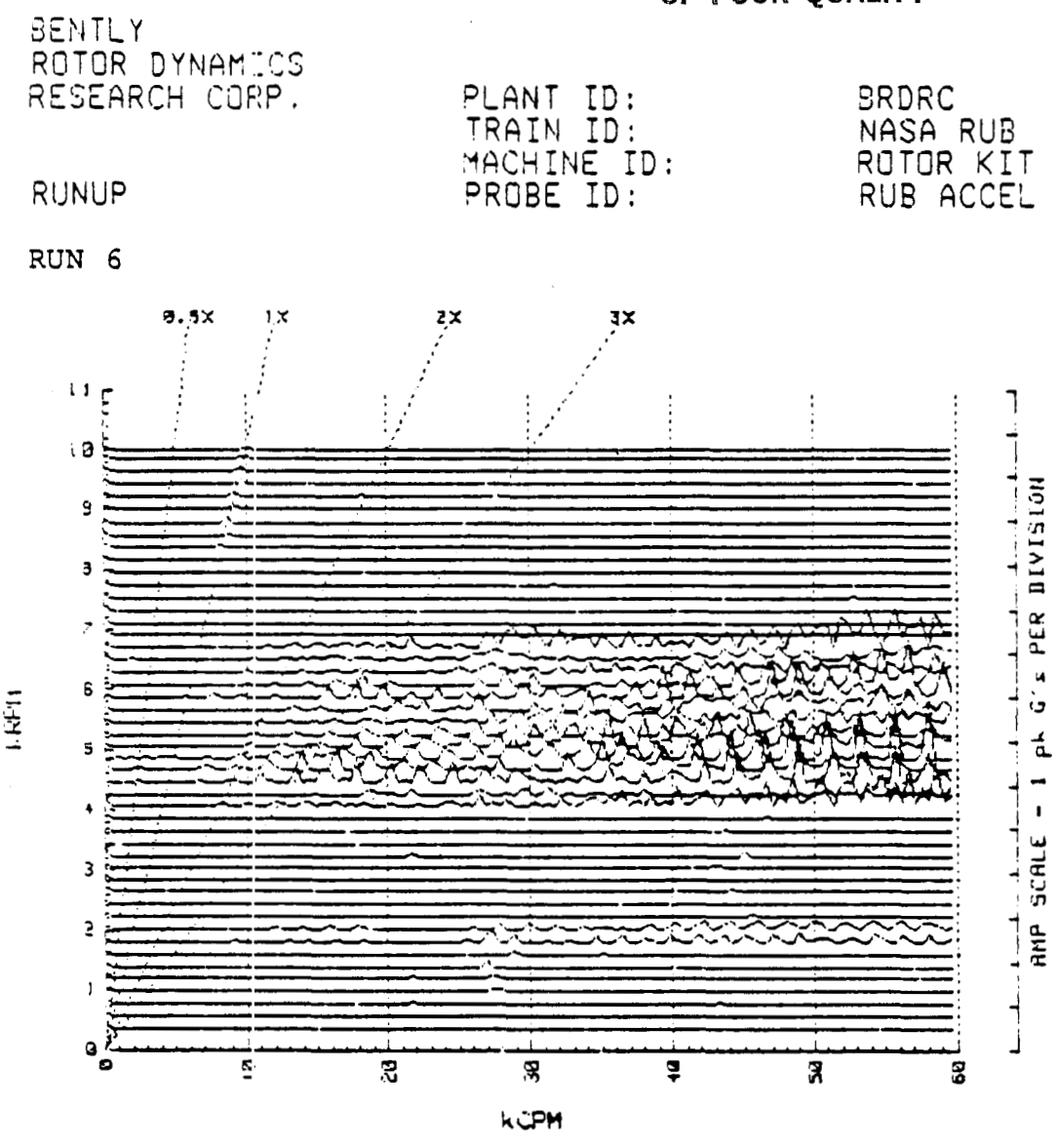

FIGURE 10.63 CASCADE PLOT OF ROTOR VIBRATION RESPONSE DURING RUN–UP AS SEEN BY ACCELEROMETER MOUNTED ON PLUNGER MECHANISM. DATA IS FROM THE SAME RUN AS FIGURE 10.62 WITH WIDER FREQUENCY RANGE. NOTE: PRESENCE OF HIGHER ORDER COMPONENTS (10.03 LB PRELOAD, INBOARD UNBALANCE: .48 GRAMS AT 0 DEGREES AND RADIUS = 1.2 IN.).

BENTLY NEVADA CORP.

PLANT ID: B.R.D.R.C
TRAIN ID: NASA RUB RIG
MACHINE ID: RUB ORBITS

RUN 6

PROBE #1 ID: RUB FIXTURE VERT
UNFILTERED

ORIENTATION= 90 DEG
MAX AMP= 12.50 MILS PK-PK

PROBE #2 ID: RUB FIXTURE HOR
UNFILTERED

ORIENTATION= 0 DEG
MAX AMP= 1.60 MILS PK-PK

ROTATION: CW
RPM(START)= 1581 RPM(END)= 1582

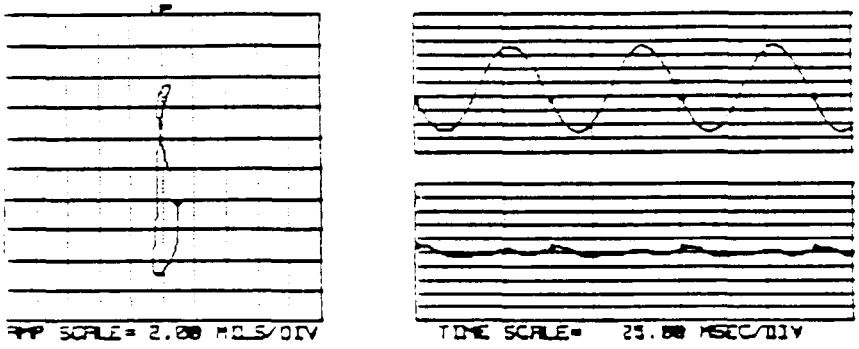

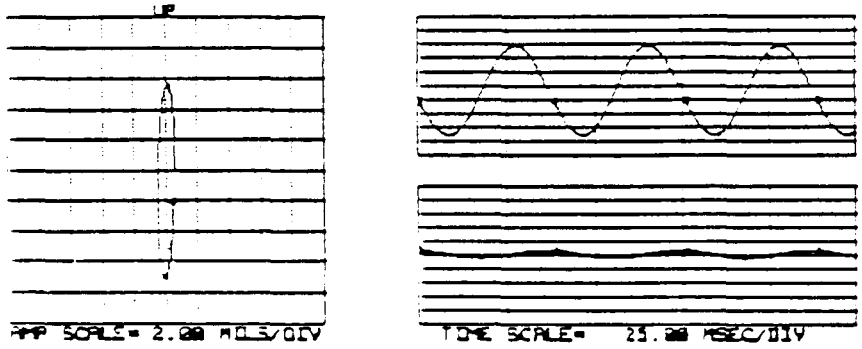

PROBE #1 ID: RUB FIXTURE VERT
1X FILTERED

ORIENTATION= 90 DEG
1X VECTOR= 12.90 MILS PK-PK @-254

PROBE #2 ID: RUB FIXTURE HOR
1X FILTERED

ORIENTATION= 0 DEG
1X VECTOR= 1.10 MILS PK-PK @-331

ROTATION: CW
RPM(START)= 1581 RPM(END)= 1582

FIGURE 10.64 STEADY–STATE ORBIT/TIMEBASE WAVE OF ROTOR VIBRATIONAL RESPONSE AT 1582 RPM AS SEEN BY RUB FIXTURE VERTICAL AND HORIZONTAL DISPLACEMENT PROBES. TOP: UNFILTERED 1X RUB SIGNAL, BOTTOM: 1X FILTERED SIGNAL. NOTE: UNFILTERED ORBIT SHOWS SMALL 2X COMPONENT, MOTION OF ROTOR SHAFT IS PRIMARILY IN THE VERTICAL PLANE (10.03 LB PRELOAD, INBOARD UNBALANCE: .48 GRAMS AT 0 DEGREES AND RADIUS = 1.2 IN.).

ORIGINAL PAGE IS
OF POOR QUALITY

BENTLY
NEVADA
CORP.

PLANT ID: B.R.D.R.C
TRAIN ID: NASA RUB
MACHINE ID: ELEC CONTACT REF.

RUN 6

PROBE #1 ID: RUB PLUNGER
UNFILTERED

ORIENTATION= 0 DEG
MAX AMP= 0.00 MILS PK-PK

PROBE #2 ID: RUB ELEC. CONTACT
UNFILTERED

ORIENTATION= 0 DEG
MAX AMP= 5.60 MILS PK-PK

ROTATION: CW
RPM(START)= 1587 RPM(END)= 1588

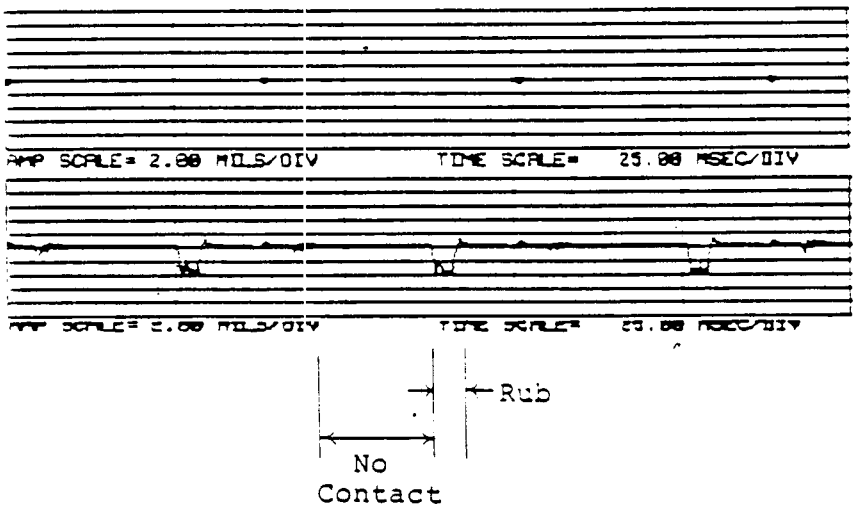

FIGURE 10.65 TIMEBASE WAVE PRESENTATION OF 1X RUB VIBRATION SIGNAL. TOP: PLUNGER MOTION, BOTTOM: ELECTRICAL SIGNAL OF ROTOR–TO–STATOR CONTACT (RUB–RELATED). NOTE: NO DETECTION OF PLUNGER MOTION, SMALL 2X COMPONENT SHOWN BY ELECTRICAL CONTACT SIGNAL (10.03 LB PRELOAD, INBOARD UNBALANCE: .48 GRAMS AT 0 DEGREES AND RADIUS = 1.2 IN.).

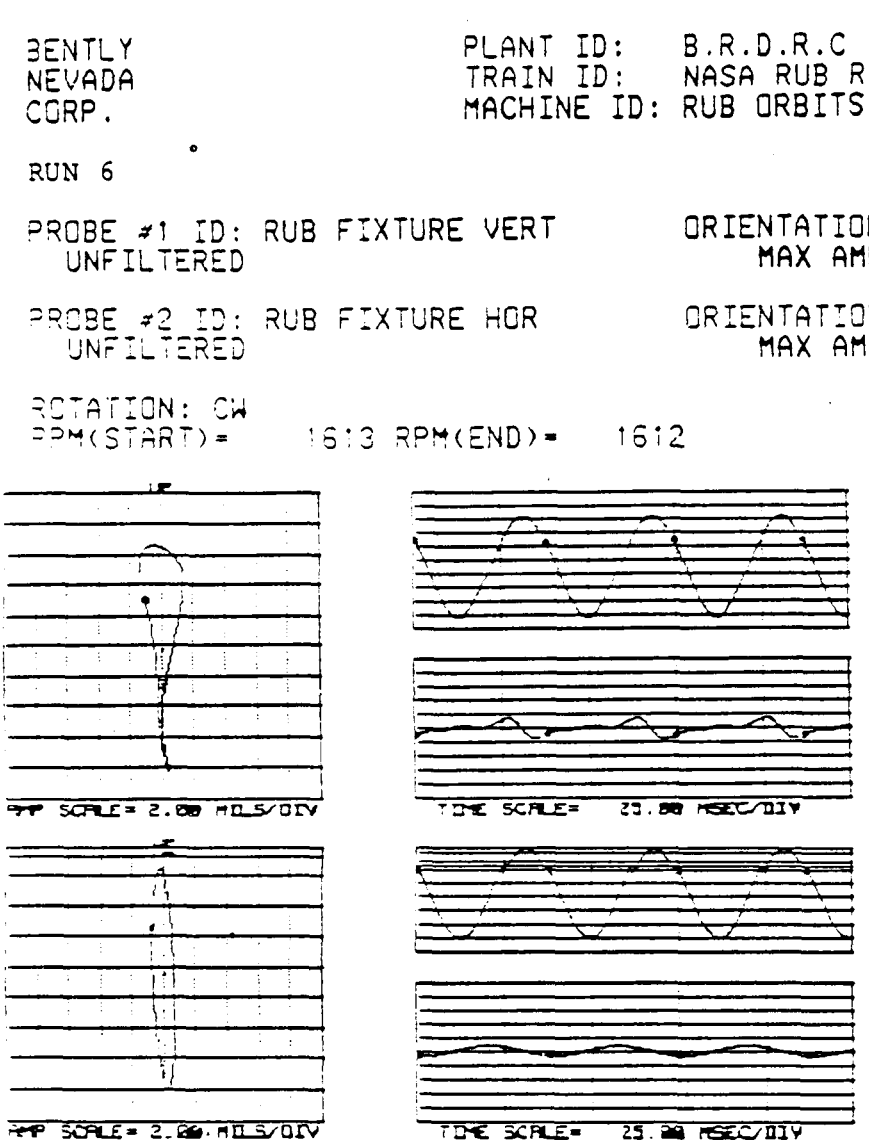

FIGURE 10.66 STEADY–STATE ORBIT/TIMEBASE WAVE OF ROTOR VIBRATIONAL RESPONSE AT 1612 RPM AS SEEN BY RUB FIXTURE VERTICAL AND HORIZONTAL DISPLACEMENT PROBES. TOP: UNFILTERED 1X RUB SIGNAL, BOTTOM: 1X FILTERED SIGNAL. NOTE: PRIMARILY VERTICAL ROTOR SHAFT MOTION AND 180 DEGREE PHASE CHANGE FROM THE ORBIT IN FIGURE 10.64 (10.03 LB PRELOAD, INBOARD UNBALANCE: .48 GRAMS AT 0 DEGREES AND RADIUS = 1.2 IN.).

BENTLY
NEVADA
CORP.

PLANT ID: B.R.D.R.C
TRAIN ID: NASA RUB
MACHINE ID: ELEC CONTACT REF.

RUN 6

PROBE #1 ID: RUB PLUNGER
UNFILTERED

ORIENTATION= 0 DEG
MAX AMP= 0.00 MILS PK-PK

PROBE #2 ID: RUB ELEC. CONTACT
UNFILTERED

ORIENTATION= 0 DEG
MAX AMP= 5.60 MILS PK-PK

ROTATION: CW
RPM(START)= 1607 RPM(END)= 1609

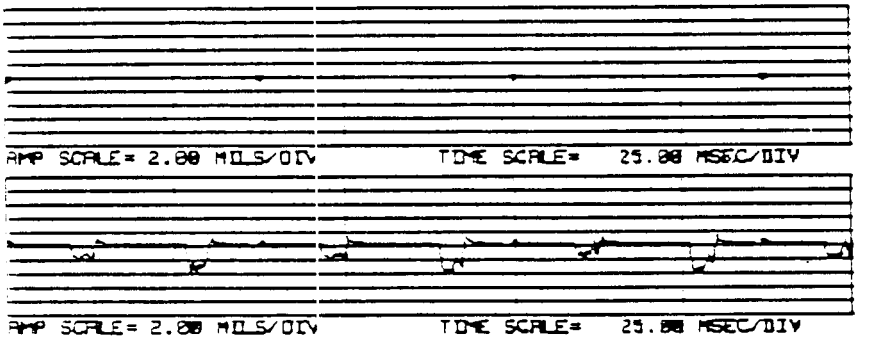

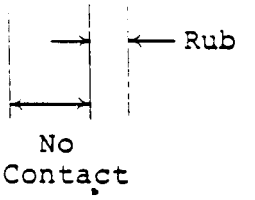

FIGURE 10.67 TIMEBASE WAVE PRESENTATION OF 1X RUB VIBRATION SIGNALS. TOP: PLUNGER MOTION, BOTTOM: ELECTRICAL SIGNAL OF ROTOR–TO–STATOR CONTACT (RUB–RELATED). NOTE: NO DETECTION OF PLUNGER MOTION, 2X COMPONENT SHOWN BY ELECTRICAL CONTACT SIGNAL (10.03 LB PRELOAD, INBOARD UNBALANCE: .48 GRAMS AT 0 DEGREES AND RADIUS = 1.2 IN.).

BENTLY
NEVADA
CORP.

PLANT ID: B.R.D.R.C
TRAIN ID: NASA RUB RIG
MACHINE ID: RUB ORBITS

RUN 6

PROBE #1 ID: RUB FIXTURE VERT
UNFILTERED

ORIENTATION= 90 DEG
MAX AMP= .90 MILS PK-PK

PROBE #2 ID: RUB FIXTURE HOR
UNFILTERED

ORIENTATION= 0 DEG
MAX AMP= 6.40 MILS PK-PK

ROTATION: CW
RPM(START)= 1930 RPM(END)= 1930

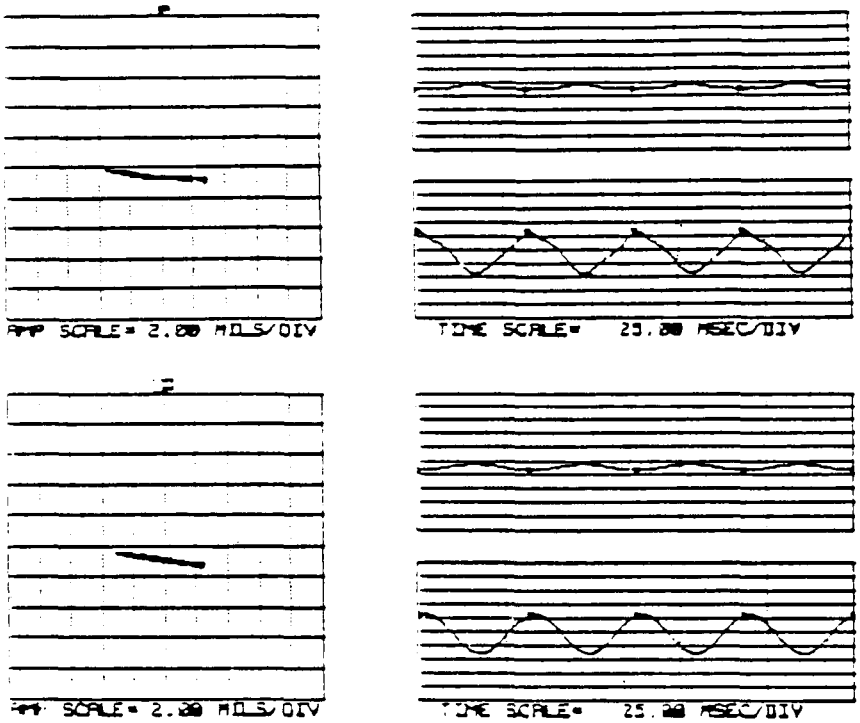

ORIGINAL PAGE IS
OF POOR QUALITY

RUN 6

PROBE #1 ID: RUB FIXTURE VERT
1X FILTERED

ORIENTATION= 90 DEG
1X VECTOR= .90 MILS PK-PK @-175

PROBE #2 ID: RUB FIXTURE HOR
1X FILTERED

ORIENTATION= 0 DEG
1X VECTOR= 5.70 MILS PK-PK @-13

ROTATION: CW
RPM(START)= 1932 RPM(END)= 1932

FIGURE 10.68 STEADY–STATE ORBIT/TIMEBASE WAVE OF ROTOR VIBRATIONAL RESPONSE AT 1930 RPM AS SEEN BY RUB FIXTURE VERTICAL AND HORIZONTAL DISPLACEMENT PROBES. TOP: UNFILTERED 1X RUB SIGNAL, BOTTOM: 1X FILTERED SIGNAL. NOTE: PREDOMINANT 1X COMPONENT WITH ROTOR SHAFT MOTION PRIMARILY IN HORIZONTAL PLANE (10.03 LB PRELOAD, INBOARD UNBALANCE: .48 GRAMS AT 0 DEGREES AND RADIUS = 1.2 IN.).

BENTLY
NEVADA
CORP.

PLANT ID: B.R.D.R.C
TRAIN ID: NASA RUB
MACHINE ID: ELEC CONTACT REF.

RUN 6

PROBE #1 ID: RUB PLUNGER
UNFILTERED
ORIENTATION= 0 DEG
MAX AMP= .10 MILS PK-PK

PROBE #2 ID: RUB ELEC. CONTACT
UNFILTERED
ORIENTATION= 0 DEG
MAX AMP= 4.90 MILS PK-PK

ROTATION: CW
RPM(START)= 1937 RPM(END)= 1938

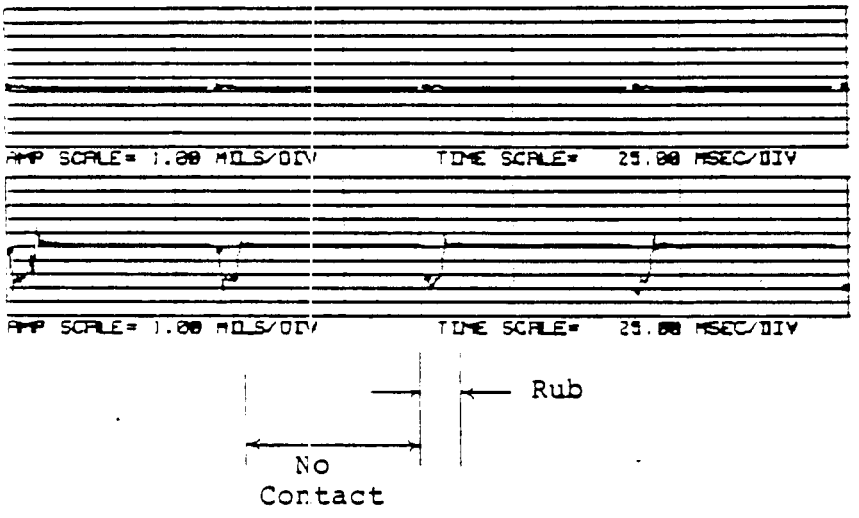

FIGURE 10.69 TIMEBASE WAVE PRESENTATION OF 1X RUB VIBRATION SIGNALS. TOP: PLUNGER MOTION, BOTTOM: ELECTRICAL SIGNAL OF ROTOR–TO–STATOR CONTACT (RUB–RELATED). NOTE: VERY SMALL PLUNGER MOTION, ELECTRICAL CONTACT SIGNAL SHOWS 1X COMPONENT (10.03 LB PRELOAD, INBOARD UNBALANCE: .48 GRAMS AT 0 DEGREES AND RADIUS = 1.2 IN.).

BENTLY
NEVADA
CORP.

PLANT ID: B.R.D.R.C
TRAIN ID: NASA RUB RIG
MACHINE ID: RUB ORBITS

RUN 6

PROBE #1 ID: RUB FIXTURE VERT
UNFILTERED

ORIENTATION= 90 DEG
MAX AMP= 5.50 MILS PK-PK

PROBE #2 ID: RUB FIXTURE HOR
UNFILTERED

ORIENTATION= 0 DEG
MAX AMP= 11.50 MILS PK-PK

ROTATION: CW
RPM(START)= 3989 RPM(END)= 3990

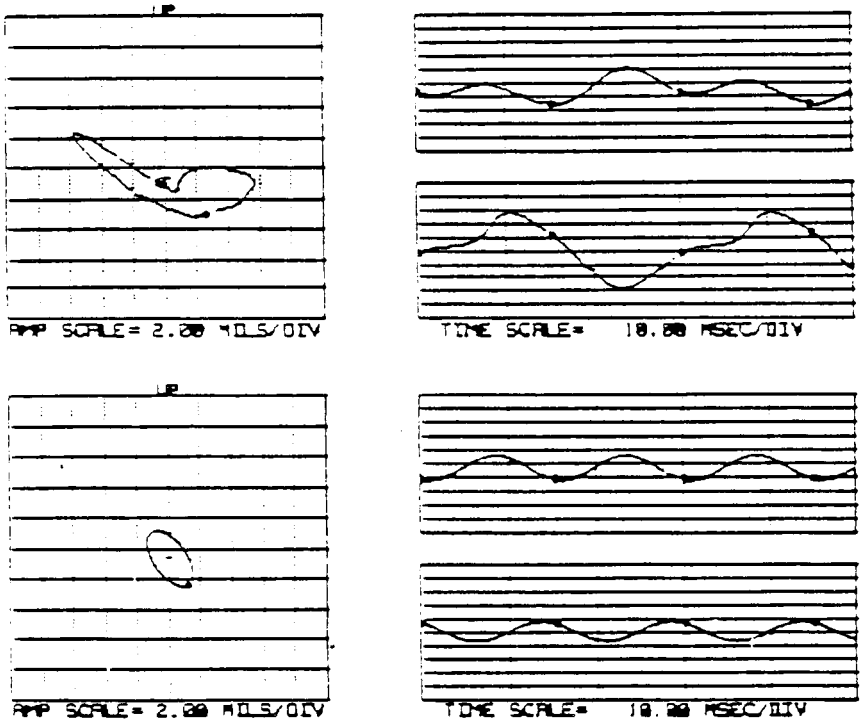

RUN 6

PROBE #1 ID: RUB FIXTURE VERT
1X FILTERED

ORIENTATION= 90 DEG
1X VECTOR= 3.60 MILS PK-PK @-197

PROBE #2 ID: RUB FIXTURE HOR
1X FILTERED

ORIENTATION= 0 DEG
1X VECTOR= 2.90 MILS PK-PK @-321

ROTATION: CW
RPM(START)= 3988 RPM(END)= 3990

FIGURE 10.70 STEADY-STATE ORBIT/TIMEBASE WAVE OF ROTOR VIBRATIONAL RESPONSE AT 3990 RPM AS SEEN BY RUB FIXTURE VERTICAL AND HORIZONTAL DISPLACEMENT PROBES. TOP: UNFILTERED 1/2X RUB SIGNAL, BOTTOM: 1X FILTERED SIGNAL. NOTE: UNFILTERED ORBIT SHOWS STRONG 1/2X COMPONENT (10.03 LB PRELOAD, INBOARD UNBALANCE: .48 GRAMS AT 0 DEGREES AND RADIUS = 1.2 IN.).

BENTLY NEVADA CORP.

PLANT ID: B.R.D.R.C
TRAIN ID: NASA RUB
MACHINE ID: ELEC CONTACT REF.

RUN 6

PROBE #1 ID: RUB PLUNGER
UNFILTERED
ORIENTATION= 0 DEG
MAX AMP= .10 MILS PK-PK

PROBE #2 ID: RUB ELEC. CONTACT
UNFILTERED
ORIENTATION= 0 DEG
MAX AMP= 5.80 MILS PK-PK

ROTATION: CW
RPM(START)= 3996 RPM(END)= 3995

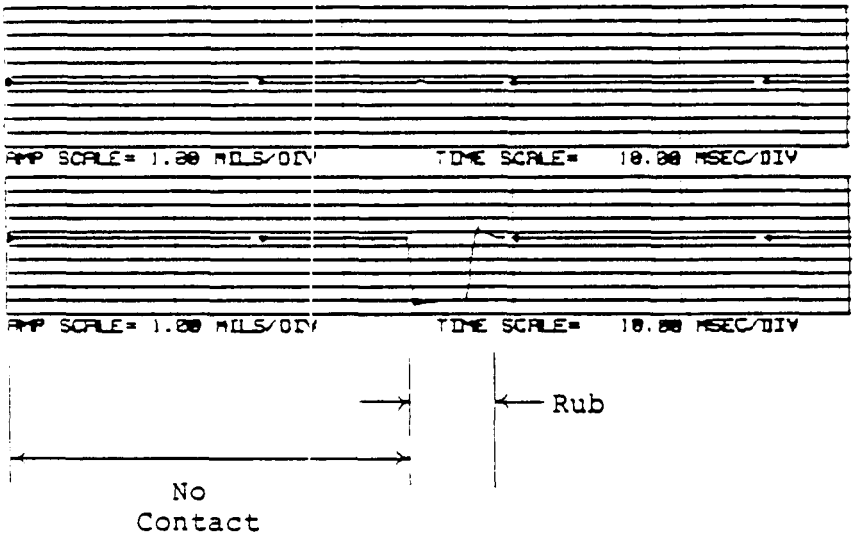

FIGURE 10.71 TIMEBASE WAVE PRESENTATION OF 1/2X RUB VIBRATION SIGNALS. TOP: PLUNGER MOTION, BOTTOM: ELECTRICAL SIGNAL OF ROTOR–TO–STATOR CONTACT (RUB–RELATED). NOTE: ELECTRICAL CONTACT SIGNAL SHOWS STRONG 1/2X COMPONENT WITH A LONG PERIOD OF RUB (10.03 LB PRE-LOAD, INBOARD UNBALANCE: .48 GRAMS AT 0 DEGREES AND RADIUS = 1.2 IN.).

BENTLY
NEVADA
CORP.

PLANT ID: B.R.D.R.C
TRAIN ID: NASA RUB RIG
MACHINE ID: RUB ORBITS

RUN 6

PROBE #1 ID: RUB FIXTURE VERT
UNFILTERED

ORIENTATION= 90 DEG
MAX AMP= 5.10 MILS PK-PK

PROBE #2 ID: RUB FIXTURE HOR
UNFILTERED

ORIENTATION= 0 DEG
MAX AMP= 13.40 MILS PK-PK

ROTATION: CW
RPM(START)= 5836 RPM(END)= 5836

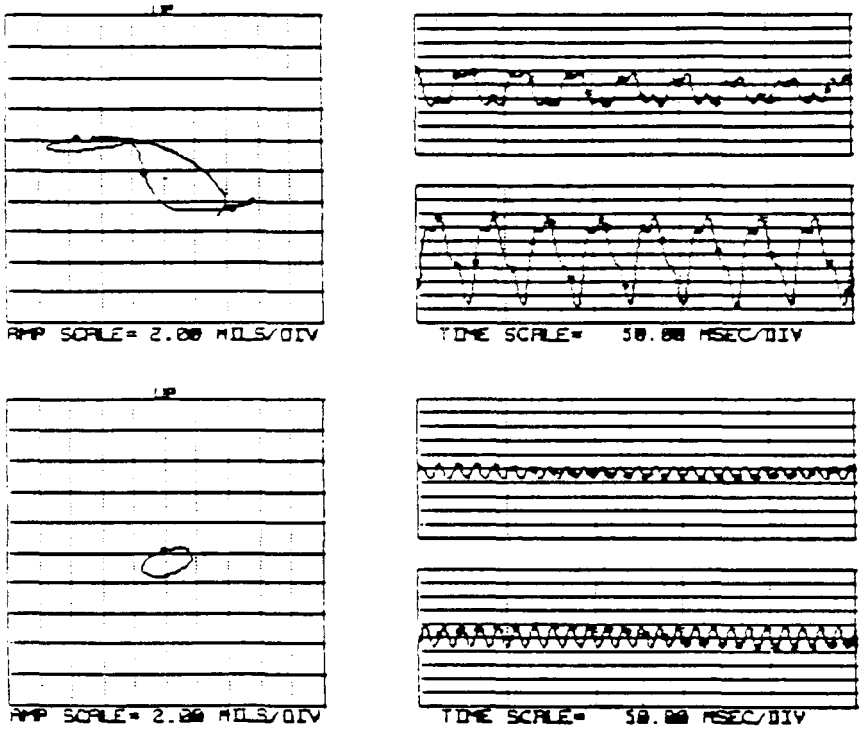

RUN 6

PROBE #1 ID: RUB FIXTURE VERT
1X FILTERED

ORIENTATION= 90 DEG
1X VECTOR= 1.90 MILS PK-PK @-8

PROBE #2 ID: RUB FIXTURE HOR
1X FILTERED

ORIENTATION= 0 DEG
1X VECTOR= 3.20 MILS PK-PK @-71

ROTATION: CW
RPM(START)= 5840 RPM(END)= 5839

FIGURE 10.72 STEADY-STATE ORBIT/TIMEBASE WAVE OF ROTOR VIBRATIONAL RESPONSE AT 5836 RPM AS SEEN BY RUB FIXTURE VERTICAL AND HORIZONTAL DISPLACEMENT PROBES. TOP: UNFILTERED 1/3X RUB SIGNAL, BOTTOM: 1X FILTERED SIGNAL. NOTE: UNFILTERED ORBIT INDICATES STRONG 1/3X COMPONENT (10.03 LB PRELOAD, INBOARD UNBALANCE: .48 GRAMS AT 0 DEGREES AND RADIUS = 1.2 IN.).

BENTLY NEVADA CORP.

PLANT ID: B.R.D.R.C
TRAIN ID: NASA RUB
MACHINE ID: ELEC CONTACT REF.

RUN 6

PROBE #1 ID: RUB PLUNGER
UNFILTERED
ORIENTATION= 0 DEG
MAX AMP= .40 MILS PK-PK

PROBE #2 ID: RUB ELEC. CONTACT
UNFILTERED
ORIENTATION= 0 DEG
MAX AMP= 5.70 MILS PK-PK

ROTATION: CW
RPM(START)= 5849 RPM(END)= 5850.

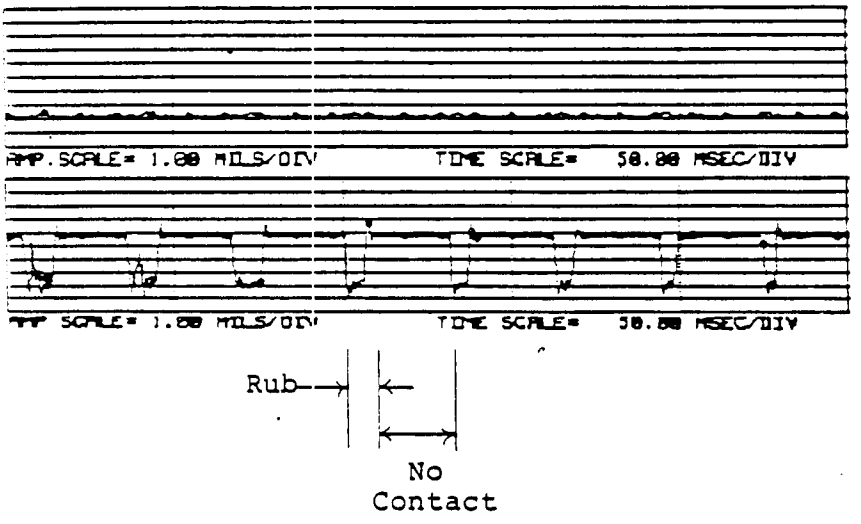

FIGURE 10.73 TIMEBASE PRESENTATION 1/3X RUB VIBRATION SIGNALS. TOP: PLUNGER MOTION, BOTTOM: ELECTRICAL SIGNAL OF ROTOR–TO–STATOR CONTACT (RUB–RELATED). NOTE: PLUNGER MOTION STILL QUITE SMALL, ELECTRICAL CONTACT SIGNAL INDICATES 1/3X COMPONENT AS SEEN IN FIGURE 10.72 (10.03 LB PRELOAD, INBOARD UNBALANCE: .48 GRAMS AT 0 DEGREES AND RADIUS = 1.2 IN.).

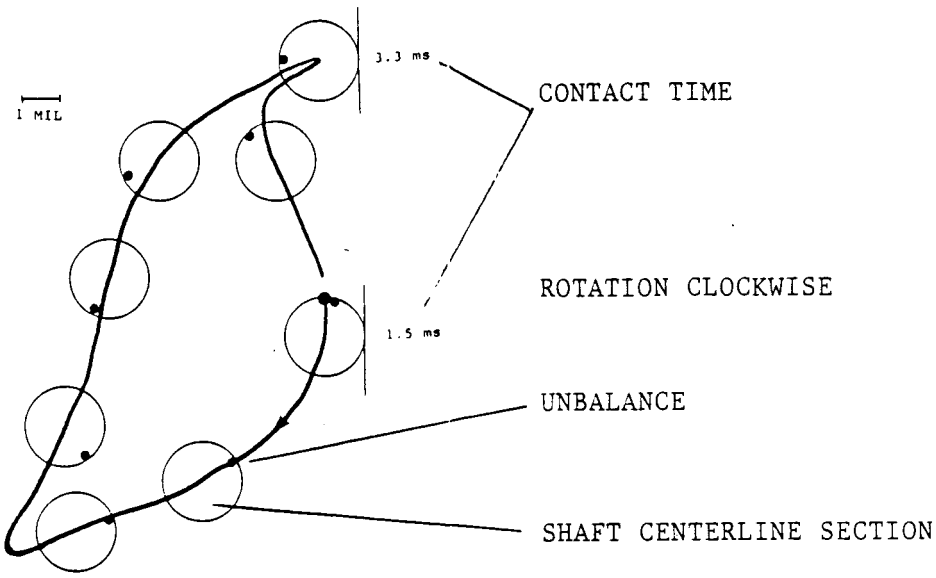

FIGURE 10.74 STEADY–STATE UNFILTERED ORBIT OF THE ROTOR VIBRATIONAL RESPONSE AT 1574 RPM AS SEEN BY THE RUB FIXTURE VERTICAL AND HORIZONTAL DISPLACEMENT PROBES. THE SAME ORBIT AS IN FIG. 10.32. RUB CONTACT (~15% OF ROTATIONAL PERIOD) AND UNBALANCE POSITIONS ARE INDICATED. 1× RUB. THE ORBIT IS REVERSED AND SIGNIFICANTLY MODIFIED FROM THE ORIGINAL CIRCULAR SHAPE (3.34 LB. PLUNGER PRELOAD, UNBALANCE: 0.48 GRAMS, 0 DEGREES, INBOARD, RADIUS = 1.2 IN.).

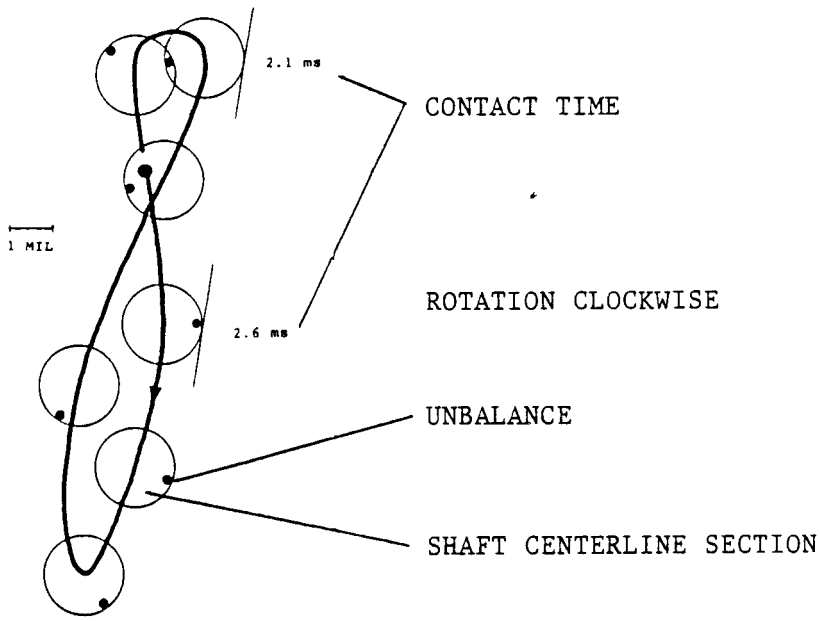

FIGURE 10.75 STEADY–STATE UNFILTERED ORBIT OF THE ROTOR VIBRATIONAL RESPONSE AT 1604 RPM AS SEEN BY THE RUB FIXTURE VERTICAL AND HORIZONTAL DISPLACEMENT PROBES. THE SAME ORBIT AS IN FIG. 10.34. RUB CONTACT (~13% OF ROTATIONAL PERIOD) AND UNBALANCE POSITIONS ARE INDICATED. 1× RUB. THE ORBIT HAS AN EXTERNAL LOOP (3.34 LB. PRELOAD, UNBALANCE: 0.48 GRAMS, 0 DEGREES, INBOARD, RADIUS = 1.2 IN.).

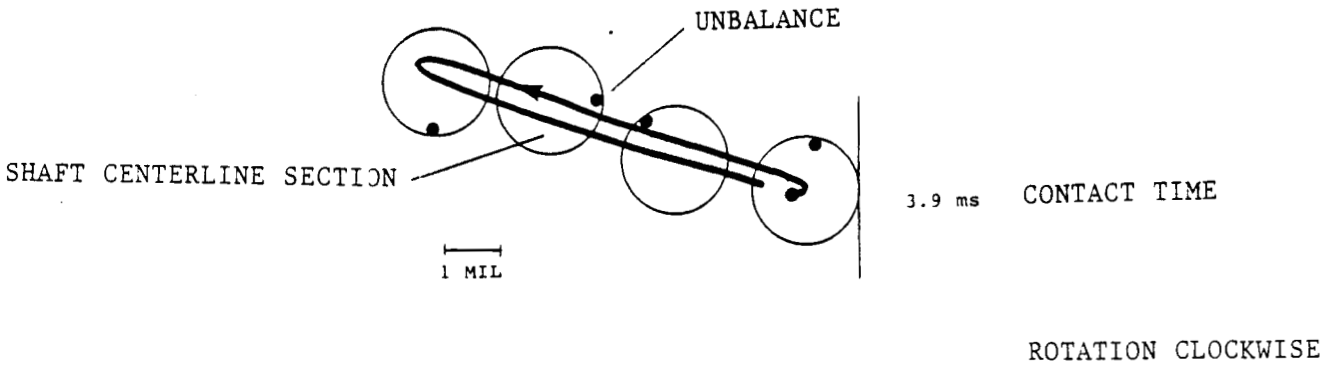

FIGURE 10.76 STEADY-STATE UNFILTERED ORBIT OF THE ROTOR VIBRATIONAL RESPONSE AT 1915 RPM AS SEEN BY THE RUB FIXTURE VERTICAL AND HORIZONTAL DISPLACEMENT PROBES. THE SAME ORBIT AS IN FIG. 10.36. RUB CONTACT (~12% OF ROTATIONAL PERIOD) AND UNBALANCE POSITIONS ARE INDICATED. 1× RUB. THE ORBIT IS REVERSE (3.34 LB. PLUNGER PRELOAD, UNBALANCE: 0.48 GRAMS, 0 DEGREES, INBOARD, RADIUS = 1.2 IN.).

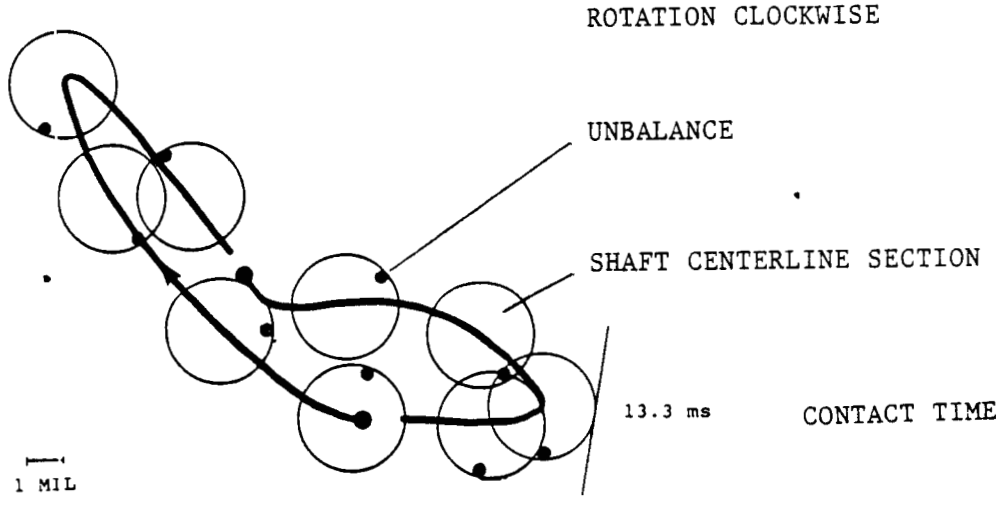

FIGURE 10.77 STEADY-STATE UNFILTERED ORBIT OF THE ROTOR VIBRATIONAL RESPONSE AT 3918 RPM AS SEEN BY THE RUB FIXTURE VERTICAL AND HORIZONTAL DISPLACEMENT PROBES. THE SAME ORBIT AS IN FIG. 10.38. RUB CONTACT (~87% OF ROTATIONAL PERIOD) AND UNBALANCE POSITIONS ARE INDICATED. 1× RUB. ORBIT FORWARD (3.34 LB. PLUNGER PRELOAD, UNBALANCE: 0.48 GRAMS, 0 DEGREES, INBOARD, RADIUS = 1.2 IN.).

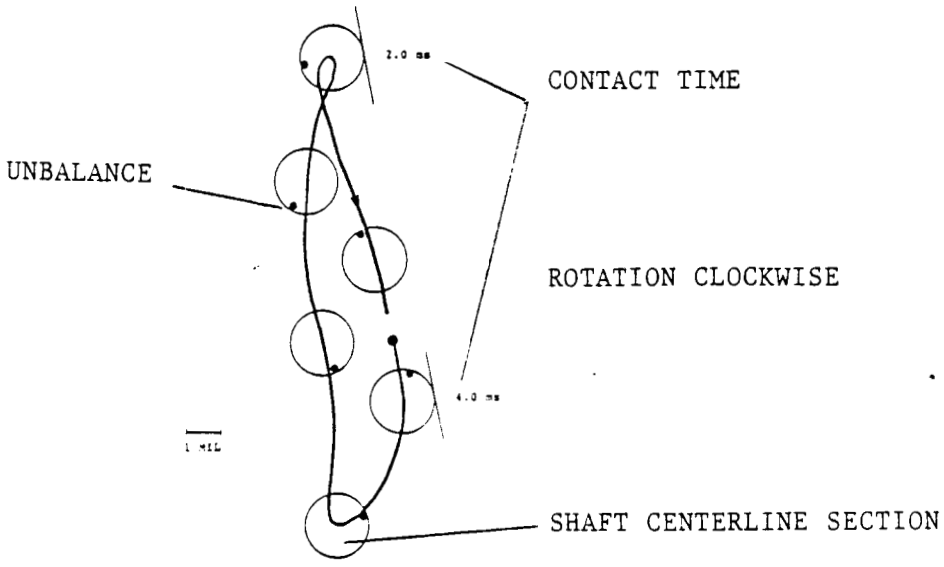

FIGURE 10.78 STEADY–STATE UNFILTERED ORBIT OF THE ROTOR VIBRATIONAL RESPONSE AT 1564 RPM AS SEEN BY THE RUB FIXTURE VERTICAL AND HORIZONTAL DISPLACEMENT PROBES. THE SAME ORBIT AS IN FIG. 10.46. THE SAME ORBIT AS IN FIG. 10.46. RUB CONTACT (~16% OF ROTATIONAL PERIOD) AND UNBALANCE POSITIONS ARE INDICATED. 1× RUB. ORBIT HAS AN EXTERNAL LOOP (6.68 LB. PLUNGER PRELOAD, UNBALANCE: 0.48 GRAMS, 0 DEGREES, INBOARD, RADIUS = 1.2 IN.). COMPARE WITH FIGURE 10.74.

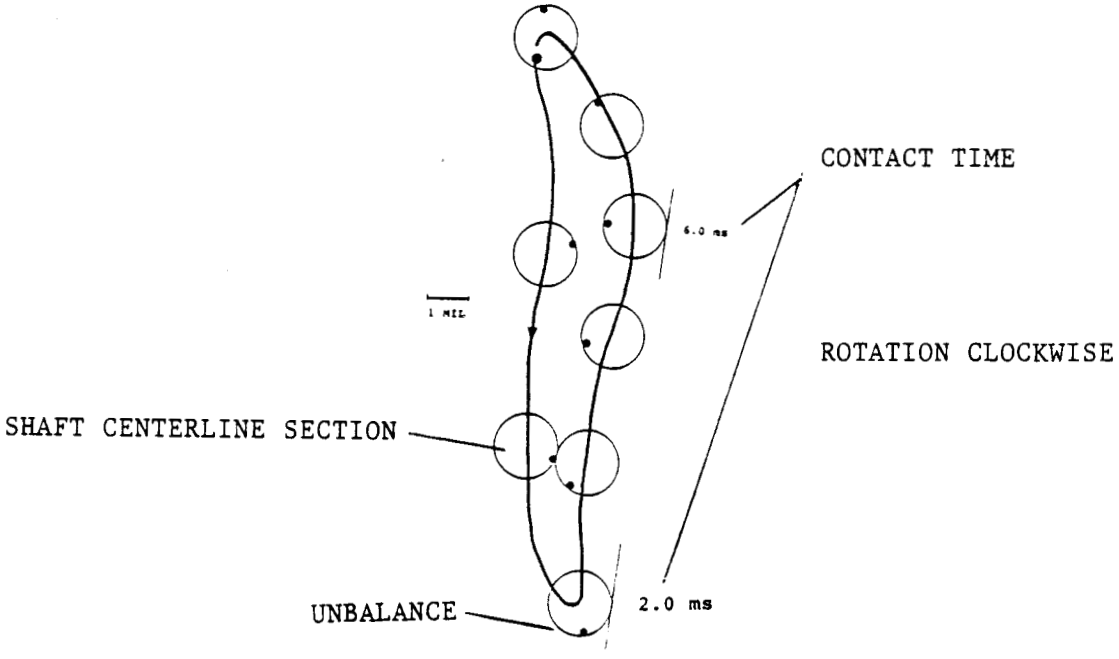

FIGURE 10.79 STEADY–STATE UNFILTERED ORBIT OF THE ROTOR VIBRATIONAL RESPONSE AT 1612 RPM AS SEEN BY THE RUB FIXTURE VERTICAL AND HORIZONTAL DISPLACEMENT PROBES. THE SAME ORBIT AS IN FIG. 10.48. RUB CONTACT (~21% OF ROTATIONAL PERIOD) AND UNBALANCE POSITIONS ARE INDICATED. 1× RUB. ORBIT REVERSE (6.68 LB. PLUNGER PRELOAD, UNBALANCE: 0.48 GRAMS, 0 DEGREES, INBOARD, RADIUS = 1.2 IN.). COMPARE WITH FIGURE 10.75.

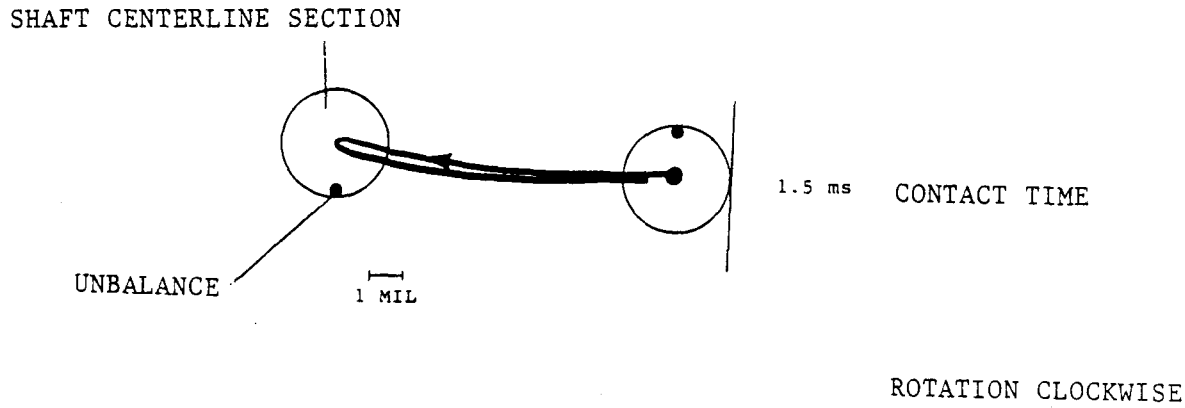

FIGURE 10.80 STEADY–STATE UNFILTERED ORBIT OF THE ROTOR VIBRATIONAL RESPONSE AT 1936 RPM AS SEEN BY THE RUB FIXTURE VERTICAL AND HORIZONTAL DISPLACEMENT PROBES. THE SAME ORBIT AS IN FIG. 10.50. RUB CONTACT (~5% OF ROTATIONAL PERIOD) AND UNBALANCE POSITIONS ARE INDICATED. 1× RUB. ORBIT REVERSE (6.68 LB. PLUNGER PRELOAD, UNBALANCE: 0.48 GRAMS, 0 DEGREES, INBOARD, RADIUS = 1.2 IN.). COMPARE WITH FIGURE 10.76.

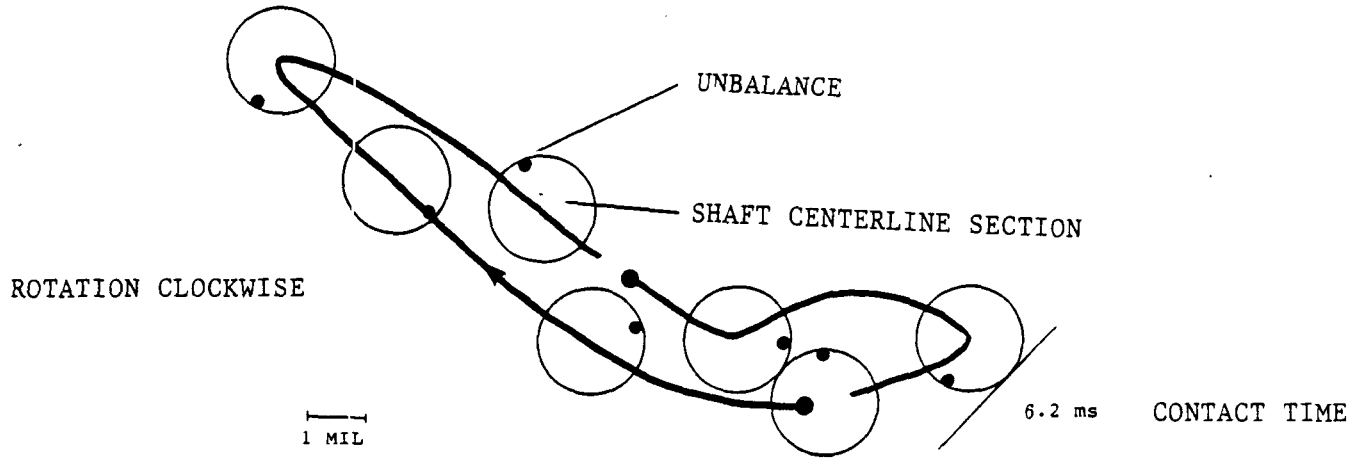

FIGURE 10.81 STEADY–STATE UNFILTERED ORBIT OF THE ROTOR VIBRATIONAL RESPONSE AT 3924 RPM AS SEEN BY THE RUB FIXTURE VERTICAL AND HORIZONTAL DISPLACEMENT PROBES. THE SAME ORBIT AS IN FIG. 10.52. RUB CONTACT (~41% OF ROTATIONAL PERIOD) AND UNBALANCE POSITIONS ARE INDICATED. 1/2 RUB. ORBIT FORWARD (6.681B PLUNGER PRELOAD, UNBALANCE: 0.48 GRAMS, 0 DEGREES, INBOARD, RADIUS = 1.2 IN.). COMPARE WITH FIGURE 10.77.

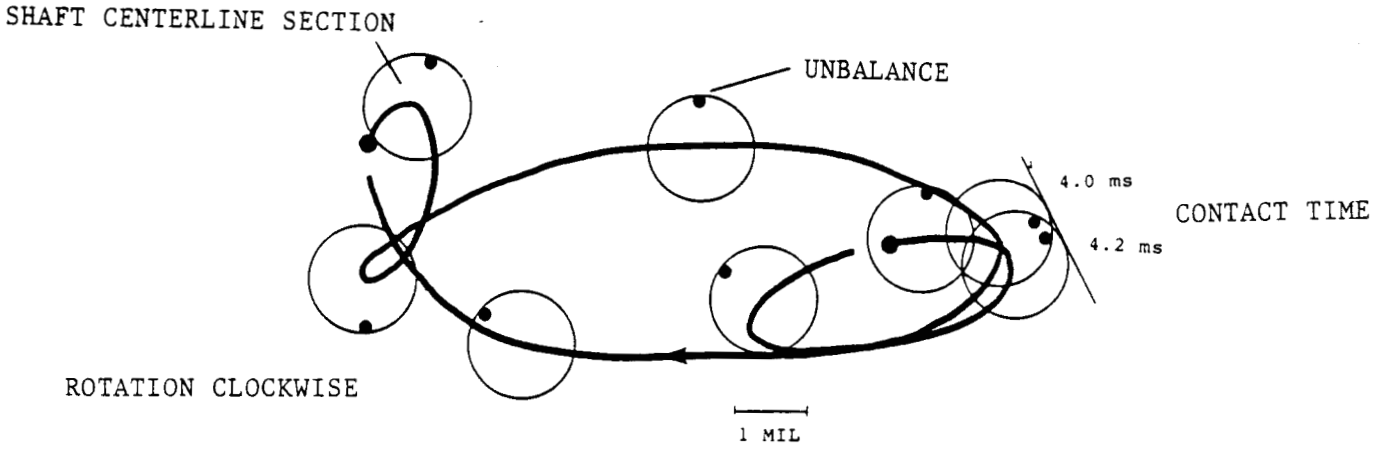

FIGURE 10.82 STEADY–STATE UNFILTERED ORBIT OF THE ROTOR VIBRATIONAL RESPONSE AT 5212 RPM AS SEEN BY THE RUB FIXTURE VERTICAL AND HORIZONTAL DISPLACEMENT PROBES. THE SAME ORBIT AS IN FIG. 10.54. RUB CONTACT (~35% OF ROTATIONAL PERIOD) AND UNBALANCE POSITIONS ARE INDICATED. 1/3 RUB. FORWARD LOOPS ON THE ORBIT (6.68 LB. PLUNGER PRELOAD, UNBALANCE: 0.48 GRAMS, 0 DEGREES, INBOARD, RADIUS = 1.2 IN.).

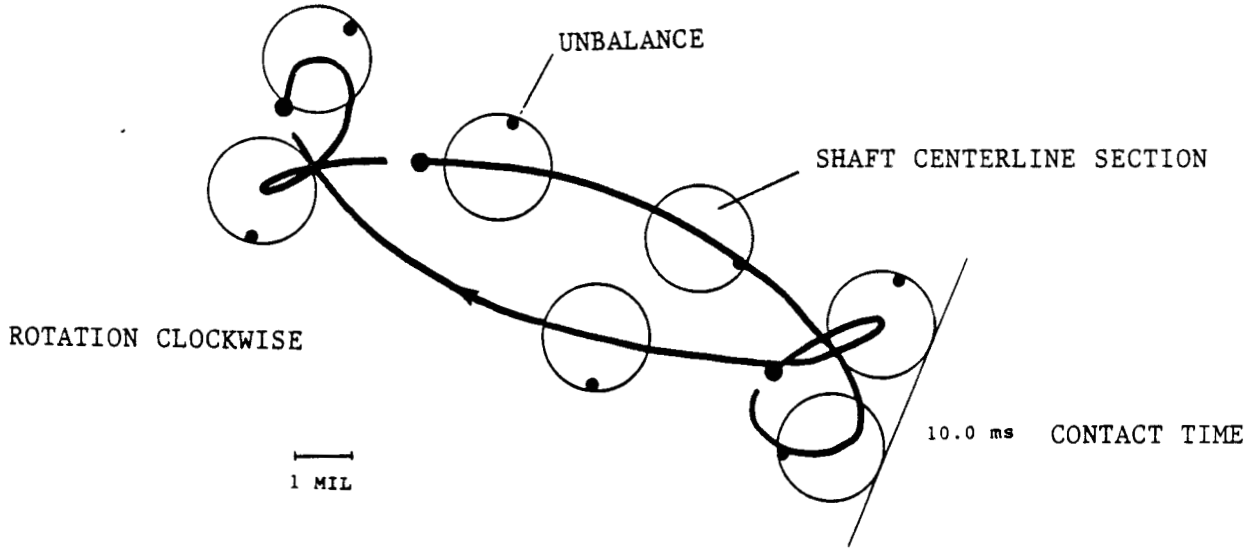

FIGURE 10.83 STEADY–STATE UNFILTERED ORBIT OF THE ROTOR VIBRATIONAL RESPONSE AT 5636 RPM AS SEEN BY THE RUB FIXTURE VERTICAL AND HORIZONTAL DISPLACEMENT PROBES. THE SAME ORBIT AS IN FIG. 10.56. RUB CONTACT (~94% OF ROTATIONAL PERIOD) AND UNBALANCE POSITIONS ARE INDICATED. 1/3 RUB. FORWARD LOOPS ON THE ORBIT (6.68 LB. PLUNGER PRELOAD, UNBALANCE: 0.48 GRAMS, 0 DEGREES, INBOARD, RADIUS = 1.2 IN.).

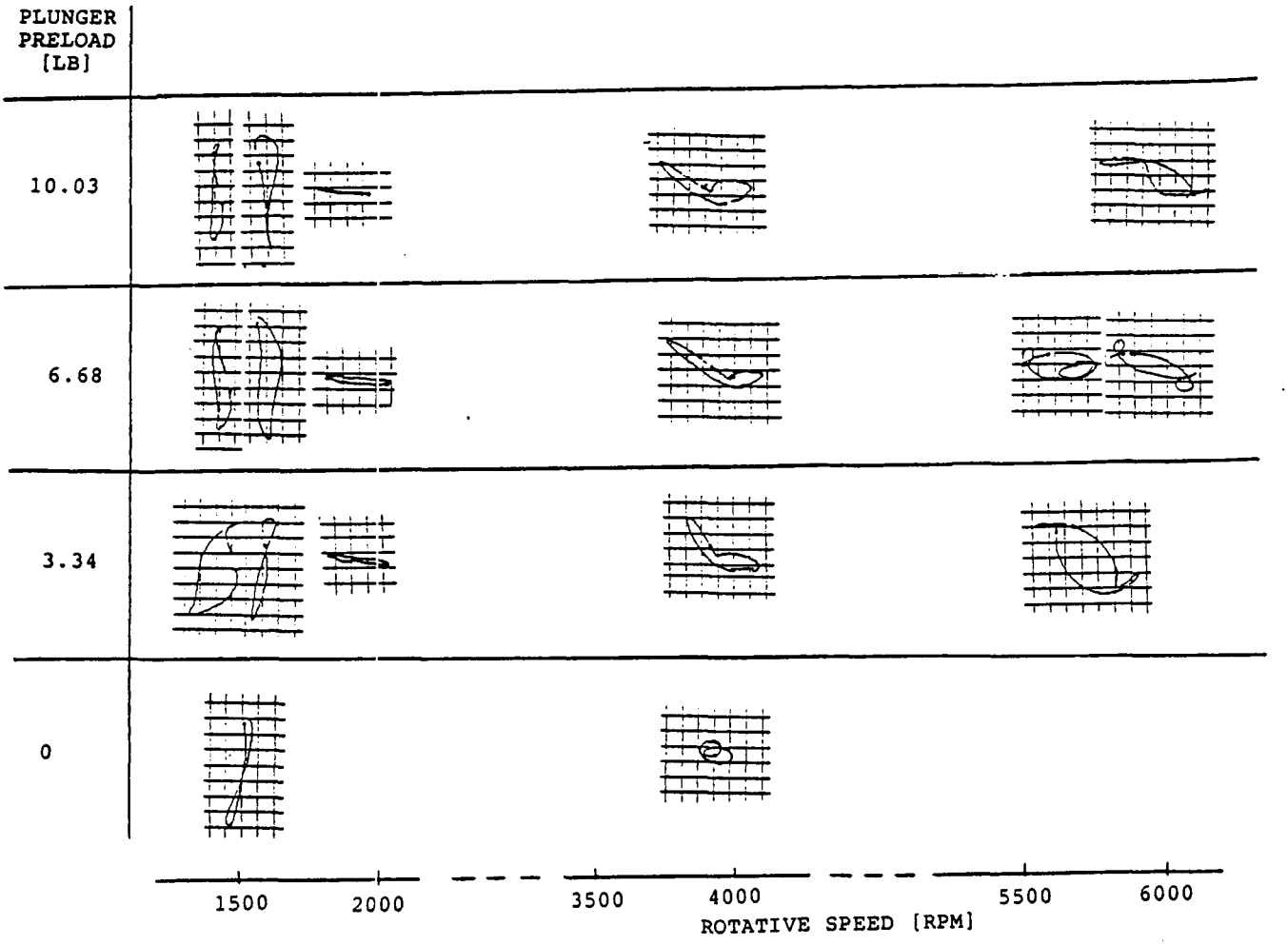

FIGURE 10.84 SHAFT RESPONSE ORBITS FOR VARIOUS ROTATIVE SPEEDS AND PLUNGER PRELOADS (STATOR COMPLIANCE). DATA FROM RUN 3 TO 6 PRESENTED IN FIGURES 10.25 TO 10.72. ORBIT AMPLITUDE SCALE: 2 MILS PER DIVISION.

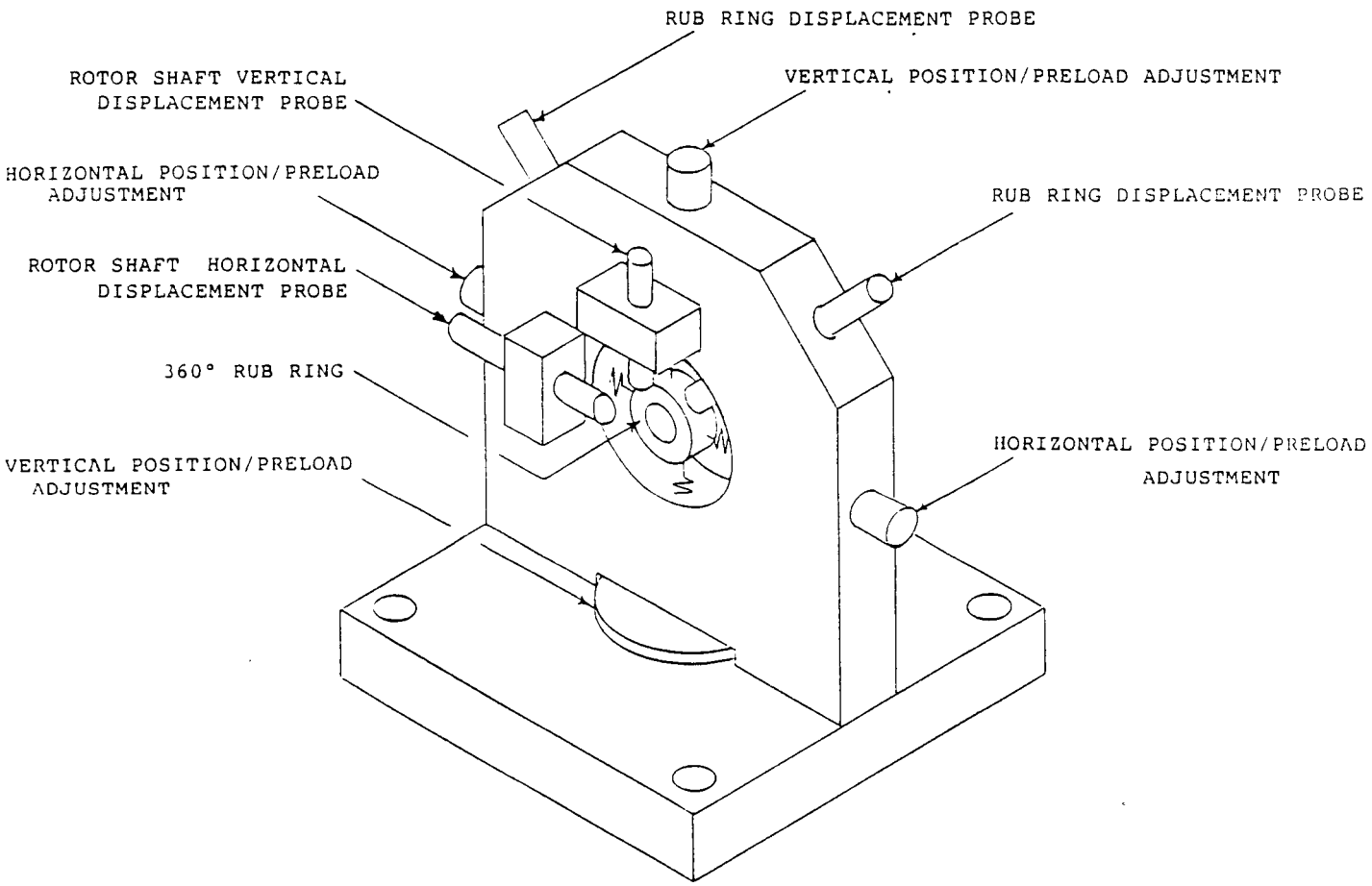

FIGURE 10.85 360 DEGREE MULTIPLE PARTIAL RUB TEST FIXTURE

A – Electric Motor
B – Flexible Coupling
C – Inboard Bronze Bearing
D – Electrical Contact Device
E – Inboard X – Y Displacement Probe Mount
F – Inboard Mass
G – Outboard X – Y Displacement Probe Mount
H – Outboard Mass
I – 360° Rub Fixture/X – Y Displacement Probes
J – Outboard Bronze Bearing
K – Rotor Shaft
L – Rotor Base

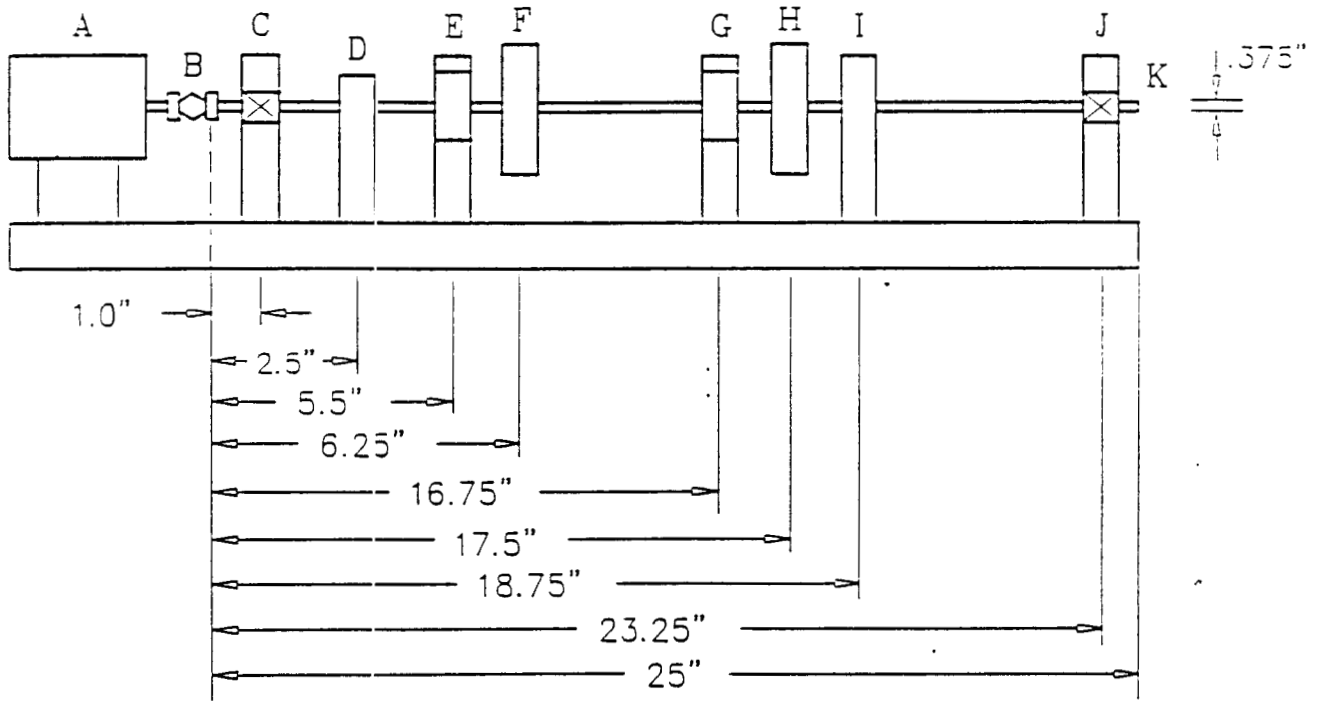

FIGURE 10.86 MULTIPLE PARTIAL RUB TEST SYSTEM WITH 360 DEGREE RUB FIXTURE

(a)

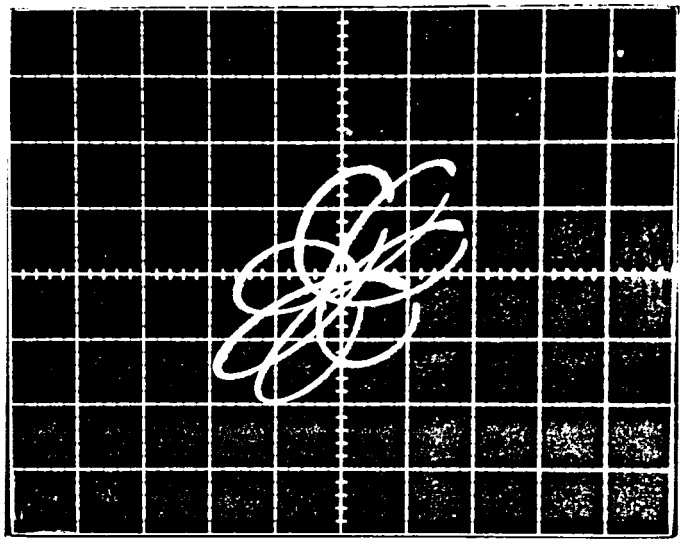

1.0 VOLT/DIV

0.2 VOLT/MIL

7.5 MIL RADIAL CLEARANCE

UNFILTERED ORBIT OF RUBBING ROTOR IN 360° FIXTURE AS OBSERVED BY THE OUTBOARD X-Y DISPLACEMENT PROBES, 4128 RPM, SHAFT ROTATION CLOCKWISE.

(b)

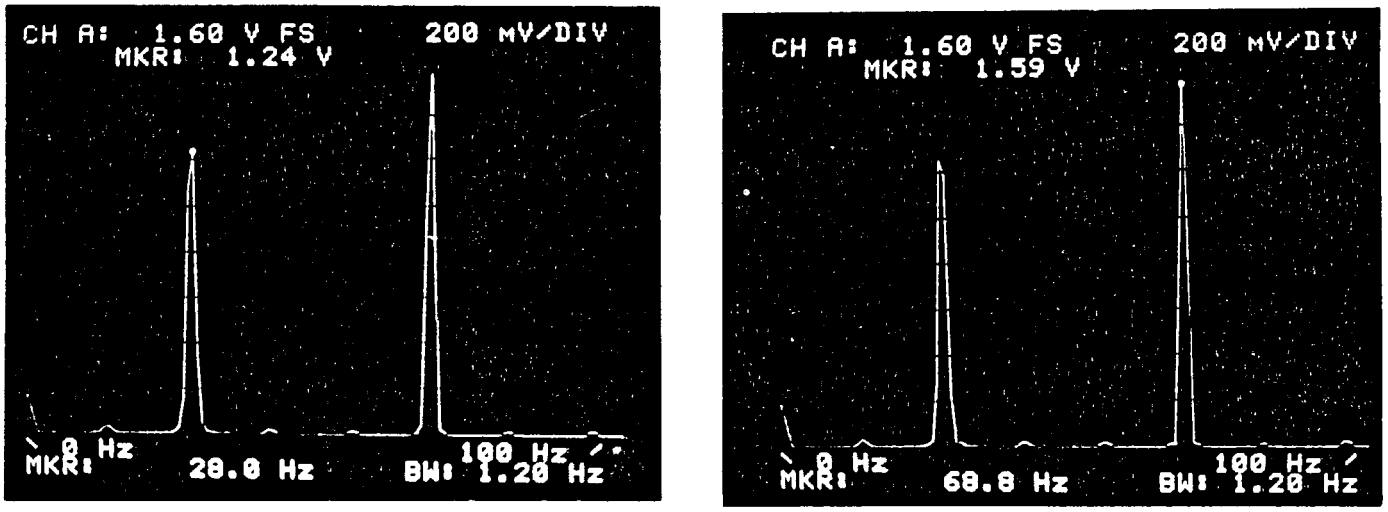

28.0 Hz | 1680 RPM | 0.41x

68.8 Hz | 4128 RPM | RUNNING SPEED | 1x

14.4 Hz | 40.8 Hz | 54.4 Hz | 81.6 Hz | 96.0 Hz

FIRST BALANCE RESONANCE OF THE SYSTEM WITHOUT RUB = 1590 RPM

SECOND BALANCE RESONANCE OF THE SYSTEM WITHOUT RUB = 4220 RPM

(BOTH SPECTRA ARE THE SAME DATA WITH DIFFERENT MARKER POSITION)

FIGURE 10.87 (a) UNFILTERED ORBIT OF RUBBING ROTOR AS OBSERVED BY THE OUTBOARD X-Y DISPLACEMENT PROBES AT 4128 RPM. CLOCKWISE SHAFT ROTATION. UNBALANCE: .5 GRAMS AT 225 DEGREES, RADIUS = 1.2", OUTBOARD. (b) STEADY STATE SPECTRUM OF RUBBING ROTOR RESPONSE AT 4128 RPM. NOTE LARGE SUBSYNCHRONOUS COMPONENT DUE TO EXCITATION OF SYSTEM FIRST BALANCE RESONANCE.

11. MATHEMATICAL MODEL OF THE RUBBING ROTOR MECHANICAL SYSTEM.

11.1 Initial Assumptions

In the mathematical modelling of the rubbing rotor the modal concept is applied. The rotor model is limited to the first three lateral modes. At the first approximation, the rotor is considered laterally symmetric (isotropic). Four axial point locations of rotor–to–stator rub are considered in the model. Since rub most probably occurs at the seal locations, the additional flow–related forces are introduced in the model. The rub forces included in the model describe the main physical phenomena taking place when rotor–to–stator rub occurs, namely friction, system stiffness modifications, and impacting. The rub forces are expressed in an "averaged" sense, explained below.

The physical model of the rotor is presented in Figure 11.1. Since three lateral modes are taken into consideration, the model contains three modal masses (M_1, M_2, M_3). $K_1,\ldots,K_7$ are rotor modal stiffnesses. Note that the model does not correspond to the classical modal model. The classical modal approach would have each mode uncoupled from the others, with only one modal mass and one stiffness for each mode. The model considered here is more complex, however limited to three coupled modes. The modal masses and stiffnesses can be obtained from the numerical analysis (using transfer matrix or finite element methods, followed by reduction to three modes), and/or identified from the experiment, using the dynamic stiffness concept outlined in Chapter 5.

11.2 Mathematical Model

The equations representing the balance of forces at the mass locations z_1, z_2, z_3 and at the locations where rub potentially occurs, $\tilde{z}_1$, $\tilde{z}_2$, $\tilde{z}_3$, $\tilde{z}_4$ (see Fig. 11.1) are as follows:

$$M_1\ddot{z}_1 + K_1(z_1-\tilde{z}_1) + K_2(z_1-\tilde{z}_2) + D_{s_1}\dot{z}_1 = m_1r_1\omega^2e^{j(\omega t+\varepsilon_1)} + P_1e^{j\gamma_1} \tag{11.1}$$

$$M_2\ddot{z}_2 + K_3(z_2-\tilde{z}_2) + K_4(z_2-\tilde{z}_3) + D_{s_2}\dot{z}_2 = m_2r_2\omega^2e^{j(\omega t+\varepsilon_2)} + P_2e^{j\gamma_2} \tag{11.2}$$

$$M_3\ddot{z}_3 + K_5(z_3-\tilde{z}_3) + K_6(z_3-\tilde{z}_4) + D_{s_3}\dot{z}_3 = m_3r_3\omega^2e^{j(\omega t+\varepsilon_3)} + P_3e^{j\gamma_3} \tag{11.3}$$

$$K_1(\tilde{z}_1-z_1) + F_1 = 0 \tag{11.4}$$

$$K_2(\tilde{z}_2-z_1) + K_3(\tilde{z}_2-z_2) + F_2 = 0 \tag{11.5}$$

$$K_4(\tilde{z}_3-z_2) + K_5(\tilde{z}_3-z_3) + F_3 = 0 \tag{11.6}$$

$$K_6(\tilde{z}_4-z_3) + K_7\tilde{z}_4 + F_4 = 0 \tag{11.7}$$

where

$$z_i = x_i + jy_i\,, \quad \tilde{z}_i = \tilde{x}_i + j\tilde{y}_i\,, \quad j = \sqrt{-1}\,, \quad i = 1,2,3$$

are radial (lateral) displacements of the shaft centerline at corresponding axial locations (x – horizontal, y – vertical), consolidated in one complex variable. D_{si}, i = 1,2,3 are modal damping coefficients; $m_i r_i e^{j\varepsilon_i}$ are modal unbalance vectors(m_i, r_i, ε_i are masses, radiuses and unbalance angular locations respectively), ω is rotative speed, $P_i e^{j\gamma_i}$ are constant radial force vectors (P_i are amplitudes, γ_i are angular positions).

The rub and fluid forces are described by the functions F_i, and impact velocity relationships:

$$F_i = f_i\,[K_{ri}(|\tilde{z}_i| - C_i)(1+j\mu_i)]e^{j\delta_i} + D_i(\dot{\tilde{z}}_i/\kappa_i - j\lambda_i\omega\tilde{z}_i) + K_{bi}\tilde{z}_i, \qquad (11.8)$$

$$i = 1, 2, 3, 4$$

where C_i, is the rotor/stator radial clearance. The functions f_i describe the timing of "contact" ($f_i = 1$ for $|\tilde{z}_i| \geq C_i$) versus "no contact" ($f_i = 0$ for $|\tilde{z}_i| < C_i$). The function $K_{ri}(|\tilde{z}_i| - C_i)$ describes the radially applied additional stiffness force due to contact with the stationary part. It also represents the rotor/stator normal force. K_{ri} is the stator stiffness. μ_i are friction coefficients at rubbing surfaces. The function $K_{ri}(|\tilde{z}_i| - C_i)j\mu_i$ models the tangentially directed friction force. The angles δ_i indicate rub angular location (Figs. 11.2 and 11.3):

$$\delta_i = \arctan\,(\tilde{y}_i/\tilde{x}_i), \qquad i = 1, 2, 3, 4.$$

It is assumed that the rubbing spot occurs at the extension of the rotor and stator center lines.

The coefficients D_i, K_{bi}, and λ_i represent the fluid dynamic forces in bearings and seals. They are fluid film radial dampings, stiffnesses, and average circumferential velocity ratios respectively. D_i, K_{bi}, and λ_i are nonlinear functions of the shaft radial deflections $|\tilde{z}_i| = \sqrt{\tilde{x}^2 + \tilde{y}^2}$. Eq. (11.8) describes also the impacting condition when rotor–to–stator contact occurs; κ is the coefficient of restitution quantifying the irreversible energy losses due to impacting. (For more advanced models, due to rotation–related high tangential velocity component the restitution coefficient κ might acquire more complex functional form, than a constant value, such as in the straight impact case).

An explanation of the impact model in Eq. (11.8) is given below.

When Eq. (11.8) for i = 1 is substituted into Eq. (11.4) it results in

$$D_1(\dot{\tilde{z}}_1/\kappa_1 - j\lambda_1\omega\tilde{z}_1) + (K_{b1}+K_1)z_1 - K_1\tilde{z}_1 + f_1K_{r_1}(|\tilde{z}_1| - C_1)(1 + j\mu_1) = 0 \qquad (11.9)$$

Before the rotor–to–stator contact occurs, i.e., for

$|\tilde{z}_1| - C_1 < 0$ there is $f_1 = 0$ and $\kappa_1 = 1$, thus

$$D_1(\dot{\tilde{z}}_{1(-)} - j\lambda_1\omega\tilde{z}_1) + (K_{b_1} + K_1)z_1 - K_1\tilde{z}_1 = 0 \qquad (11.10)$$

where the subscript $_{(-)}$ next to velocity $\dot{\tilde{z}}_1$ indicates the "before collision" situation. Following the classical impact theory, during collision only velocities are instantaneously affected. Displacements remain the same.

Just after collision, i.e., for

$|\tilde{z}_1| - C_1 \geq O$ there is $f_1 = 1$ and $\kappa < 1$, thus

$$D_1(\dot{\tilde{z}}_{1(+)}/\kappa_1 - j\lambda_1\omega\tilde{z}_1) + (K_{b1}+K_1)z_1 - K_1\tilde{z}_1 + K_{r_1}(|\tilde{z}_1| - C_1)(1+j\mu_1) = 0 \qquad (11.11)$$

where the subscript $_{(+)}$ next to velocity $\dot{\tilde{z}}_1$ indicates the "after collision" situation. Taking into account Eqs. (11.10) and (11.11) the coefficient of restitution κ_1 is defined as follows:

$$\kappa_1 = \frac{\dot{\tilde{z}}_{1(+)}}{\dot{\tilde{z}}_{1(-)} - K_{r_1}(|\tilde{z}_1| - C_1)(1 + j\mu_1)/D_1} \qquad (11.12)$$

Note that there are differences in this definition, as compared to the classical straight impact theory. In Eq. (11.12) both velocities $\dot{\tilde{z}}_{1(-)}$ and $\dot{\tilde{z}}_{1(+)}$ have the same sign. There is no justification to assume that in the rotor planar motion the impact against a compliant stator causes complex velocities to reverse immediately. The second difference is the addition of the stator stiffness–related normal and tangential forces, modifying the "after collision" velocity, the last term of the following equation:

$$\dot{\tilde{z}}_{1(+)} = \kappa_1[\dot{\tilde{z}}_{1(-)} - K_{r_1}(|\tilde{z}_1| - C_1)(1 + j\mu_1)/D_1] \qquad (11.13)$$

When the stator stiffness is low the after collision motion continues in the same direction until, due to an increase of displacement $\tilde{z}_1$, a balance occurs, and $\dot{\tilde{z}}_{1(+)} = 0$. At this moment the motion is reversed.

The similar impact situations take place for all rub locations i = 1, 2, 3, 4.

Eqs. (11.1) to (11.7) can be simplified by eliminating displacements $\tilde{z}_1$ to $\tilde{z}_4$ from Eqs. (11.1), (11.2), (11.3). In a compact form the mathematical model of the rubbing rotor is as follows:

$$M_i\ddot{z}_i + \alpha_i K_{2i-2}(z_i - z_{i-1}) + \alpha_{i+1}K_{2i}(z_i - z_{i+1}) + D_{si}\dot{z}_i + \alpha_i F_i + \alpha_{i+1}\beta_{2i}F_{i+1} = \tag{11.14}$$

$$= m_i r_i \omega^2 e^{j(\omega t+\varepsilon_i)} + P_i e^{j\gamma_i}, \quad i = 1,2,3, \quad z_i = x_i + jy_i, \quad j = \sqrt{-1}$$

$$\tilde{z}_i = \frac{K_{2i-2}z_{i-1} + K_{2i-1}z_i - F_i}{K_{2i-2} + K_{2i-1}}, \qquad i = 1,2,3,4$$

or

$$\tilde{z}_i = \alpha_i(\beta_{2i-2}z_{i-1} + z_i - F_i/K_{2i-1})$$

where

$$\alpha_i = \frac{1}{1+\beta_{2i-2}}, \qquad \beta_{2i} = \frac{K_{2i}}{K_{2i+1}} \qquad K_o = z_o = z_4 = 0. \tag{11.15}$$

Eqs. (11.8) to (11.15) represent the mathematical model of the rubbing isotropic rotor.

Note that the model contains three destabilizing factors: dry friction tangential forces, represented by the friction coefficients μ_i, fluid–related tangential forces, represented by the fluid circumferential velocity ratios λ_i, and impact conditions, represented by the coefficient (or function) of restitution, κ_i. The model includes also the system stiffening effect (through radial stiffness forces $K_{ri}(|\tilde{z}_i| - C_i)$). The relative significance of each factor determines the final result, i.e., rotor response.

11.3 Calculation of the Rotor–to–Stator Rub Contact Normal Force

The contact between rotor and stator occurs when either rotor is pushed to the side by a radial preload, and rotates around its centerline displaced from the neutral position, or the rotor vibration amplitude (due to residual unbalance or other sources) exceeds the available clearance. Most often these two events occur simultaneously: rotating shaft vibrates around a displaced position.

In this section an average normal force at the rotor/stator contacting surfaces is calculated. The stator is assumed rigid. Its circular shape with radius "R" models a seal, where contact with rotor usually occurs. It is assumed that the shaft of radius "r" is displaced from its neutral position due to a constant radial force. Its eccentricity is denoted "e." Rotor lateral vibrations are supposed harmonic, and result in a circular orbit with the amplitude "A." Figure 11.4 illustrates the situation when the shaft eccentricity plus vibration amplitude "BO_1" exceed the available clearance (R–r). The difference (BO_1 – (R–r)) = BC multiplied by the shaft stiffness "K" represents the normal force at the contacting surfaces. It is assumed that the stator is rigid.

During its vibrational motion around the eccentric position O_2 (variable angle ε), the shaft enters into the contact with the seal at certain angle ε_0. At this angle BC = 0 and the normal force is zero. When the shaft proceeds in its orbital motion, the value "BC" increases till its maximum (e+A+r–R) when $\varepsilon = 0$. The second part of the vibrational cycle is symmetric: The shaft leaves the stator at the angle "$-\varepsilon_0$" and vibrates freely until the contact occurs again at the angle ε_0, during the next vibrational cycle.

Taking into consideration the trigonometric relationships, the distance "BC" is calculated as follows:

$$BC = O_1B–O_1C = O_1B–R = DB+O_1D–R = r + O_1D–R$$

From the triangle O_1O_2D results $O_1D = \sqrt{e^2+A^2+2eA\ \cos\ \varepsilon}$, thus

$$BC = r–R + \sqrt{e^2+A^2--2eA\ \cos\ \varepsilon} \tag{11.16}$$

The value "BC" depends on the angle ε. "BC" equals zero for the "just to touch" contact at ε_0:

$$0 = r–R + \sqrt{e^2+A^2+2eA\ \cos\ \varepsilon_0}$$

from which the angle ε_0 can be calculated:

$$\varepsilon_0 = \text{arc cos}\ \frac{(R–r)^2\ –\ e^2\ –\ A^2}{2eA} \tag{11.17}$$

The value "BC" reaches its maximum (r–R+e+A) when $\varepsilon = 0$.

Since "BC", and consequently the normal force N = (BC)K vary with ε during the shaft vibrational cycle, it is reasonable to calculate their average values.

The average of cosine function (cos ε) in limits ($-\varepsilon_0$, + ε_0) based on equality of areas is

$$\frac{1}{2\varepsilon_0}\int_{-\varepsilon_0}^{\varepsilon_0} \cos\ \varepsilon\ d\varepsilon = \frac{\sin\ \varepsilon_0}{\varepsilon_0} \tag{11.18}$$

With Eq. (11.18) taken into account the average value of the shaft/stator normal force at the contact during one cycle of shaft vibration is as follows:

$$N_{av} = (BC)_{av}K = \left[r–R+\sqrt{\ e^2+A^2+2eA\ \frac{\sin\ \varepsilon_0}{\varepsilon_0}}\right]K \tag{11.19}$$

where K is shaft stiffness and ε_0 can be calculated from Eq. (11.17).

Figure 11.5 illustrates the maximum and average normal force–to–shaft stiffness and average clearance ratio $\left[\frac{N_{av}}{K(R–r)}\right]$ versus vibration amplitude–to–clearance ratio for a few values of eccentricity--to–clearance ratios. The relation between the average force and the clearance is linear. The average force versus either A or e is almost linear.

Figure 11.5 shows also the corresponding angles ε_0, i.e., the half–arcs of the rotor–to–stator rubbing contact. Figure 11.6 illustrates the average normal force ratio versus the half arc contact angle ε_0. As can be seen, the normal force as a function of the arc angle depends on the relationship of the shaft eccentricity versus vibrational amplitude. For low eccentricities the graph of the normal force versus angle ε_0 is flat; the relationship is close to proportional. For high eccentricities the force versus contact angle has more pronounced parabolic shape.

Since the rotor–to–stator contact normal force is responsible for the friction force, a simple contact arc angle is not an appropriate representative measure of the severity of rub. For a single value of the contact arc (for instance, at $\varepsilon_0 = 60°$) the normal force ratio may vary from 0.04 to almost 0.10 depending on the relationship between shaft eccentricity "e" and vibration amplitude "A." The highest force ratio for a given arc results when "e" and "A" are of the same magnitude.

11.4 Rub–related Impact Model

There are two effects of the impact of a rotating shaft against a rigid stationary element: straight impact and superball effect. Mathematical models of these effects are discussed in this section.

Just before the collision the shaft incoming precessional velocity components are $\dot{x}$ and $\dot{y}$. The rotor collides with the stator at angle φ with velocity v_0 (Fig. 11.7):

$$v_0 = \sqrt{\dot{x}^2 + \dot{y}^2} \qquad \varphi = 90° - \arctan(\dot{y}/\dot{x}) \tag{11.20}$$

Similarly to the straight impact theory it is assumed that the rebound motion has the velocity v_1 proportional to the incoming one, with the coefficient of restitution κ, and has "symmetrical" (mirror image) direction (Fig. 11.7):

$$v_1 = \sqrt{\dot{x}_1^2 + \dot{y}_1^2} = \kappa v_0 \tag{11.21}$$

The components of the velocity v_1 are as follows:

$$\dot{x}_1 = -\kappa(\dot{x}\cos 2\beta + \dot{y}\sin 2\beta)$$

$$\dot{y}_1 = -\kappa(\dot{x}\sin 2\beta - \dot{y}\cos 2\beta) \tag{11.22}$$

where

$$\beta = \arctan(y/x) \tag{11.23}$$

describes the location where the impact occurs (Fig. 11.7).

In the superball impact effect the components of the after impact velocity are modeled as follows (Fig. 11.8):

$$\dot{x}_2 = \kappa_s\, \omega r \sin\beta$$

$$\dot{y}_2 = -\kappa_s\, \omega r \cos\beta \tag{11.24}$$

where ω and r are shaft rotative speed and radius respectively, thus ωr is the shaft surface velocity. The coefficient κ_s describes the superball effect–related loss of energy.

The total after impact velocity components including both effects modeled by Eqs. (11.22) and (11.24) are:

$$\dot{x}(+) = -\kappa\,(\dot{x}\cos 2\beta + \dot{y}\sin 2\beta) + \kappa_s\,\omega r \sin\beta$$

$$\dot{y}(+) = -\kappa\,(\dot{x}\sin 2\beta - \dot{y}\cos 2\beta) - \kappa_s\,\omega r \cos\beta$$

where the subscript $(+)$ denotes the after impact situation.

Note that this model does not include stator compliance.

11.4 Summary

The rubbing rotor/stator mathematical model is developed in this chapter. The model based on modal characteristics for the rotor includes its three lateral modes. The rub phenomenon due to rotor–to–stator contact may occur at four axial locations of the rotor. The rub model includes friction, impacting, and a system stiffening effect.

The local rotor/stator normal force is calculated as function of radial clearance, shaft eccentricity, and shaft vibrational amplitude. It is shown that the simple arc of rotor–to–stator contact is not an adequate measure of severity of rub.

A simple model of rotor impacting a rigid stator is also given in this chapter.

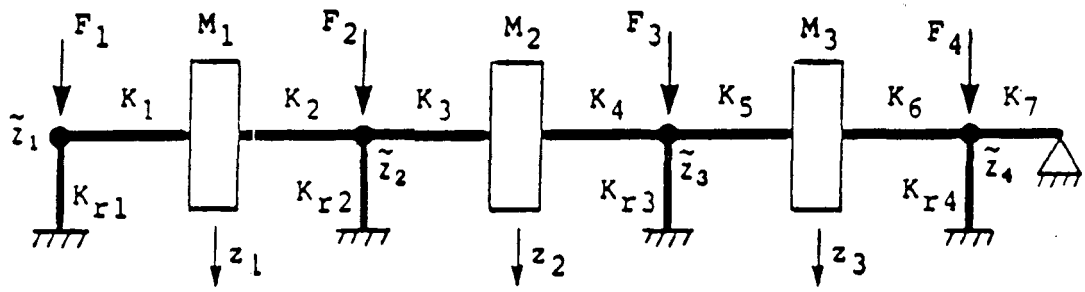

FIG. 11.1 MODEL OF THE RUBBING ROTOR

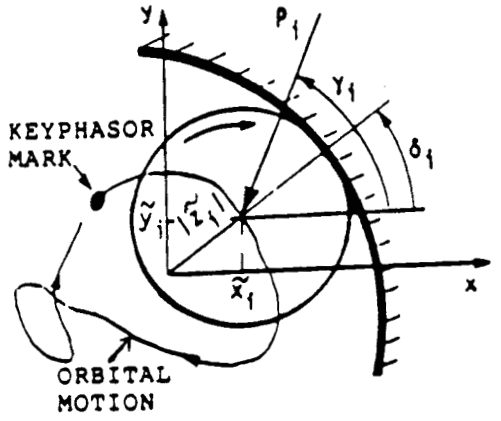

FIG. 11.2 SHAFT RUBBING AGAINST THE STATOR OR A SEAL

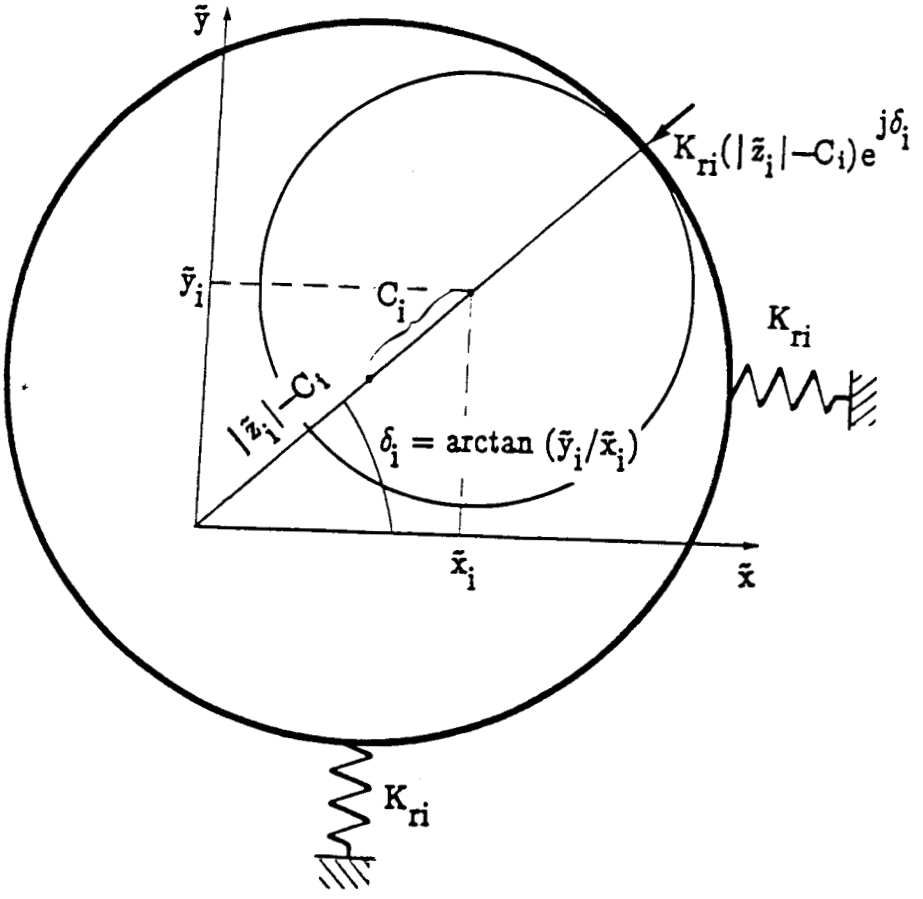

FIGURE 11.3 RUBBING ROTOR INSIDE A SEAL

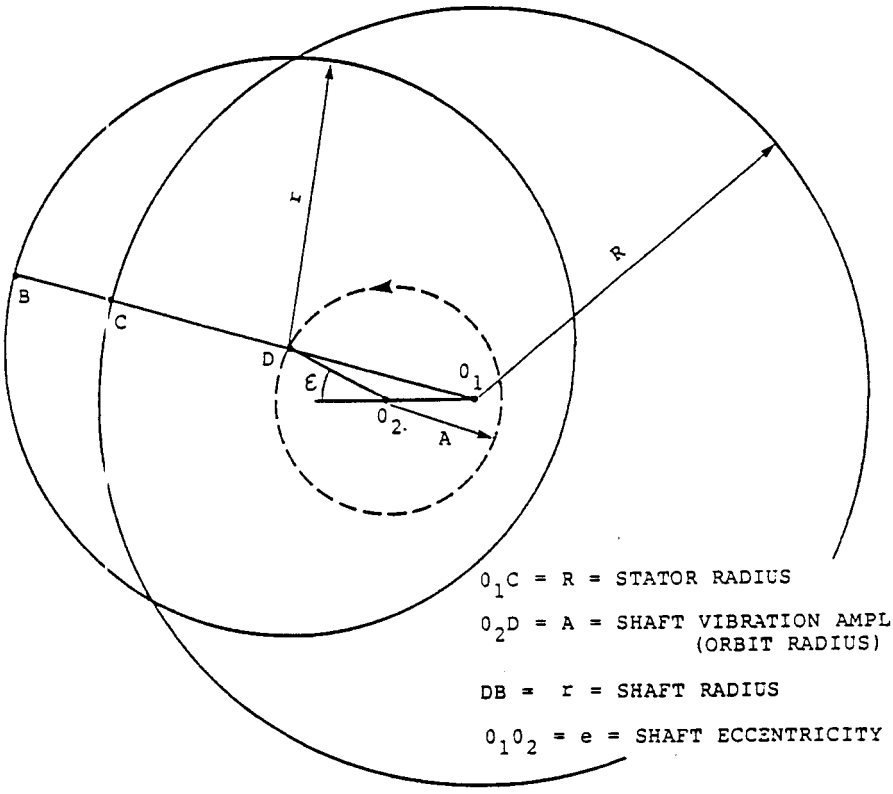

FIGURE 11.4 ROTOR AND STATOR (OR SEAL) CONTACT GEOMETRY

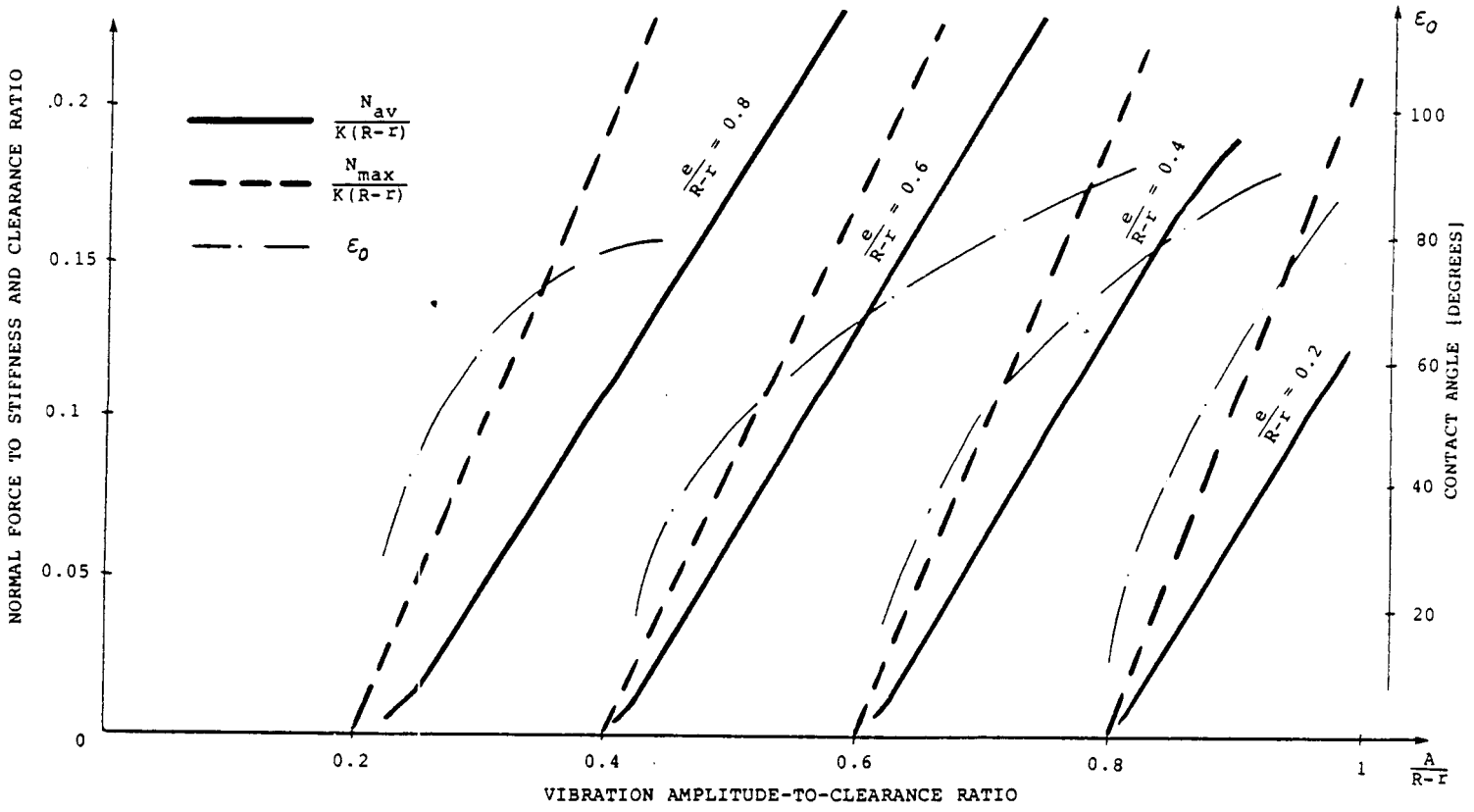

FIGURE 11.5 MAXIMUM AND AVERAGE NORMAL FORCE RATIO AND CONTACT ANGLE VERSUS VIBRATION AMPLITUDE–TO–ECCENTRICITY RATIO.

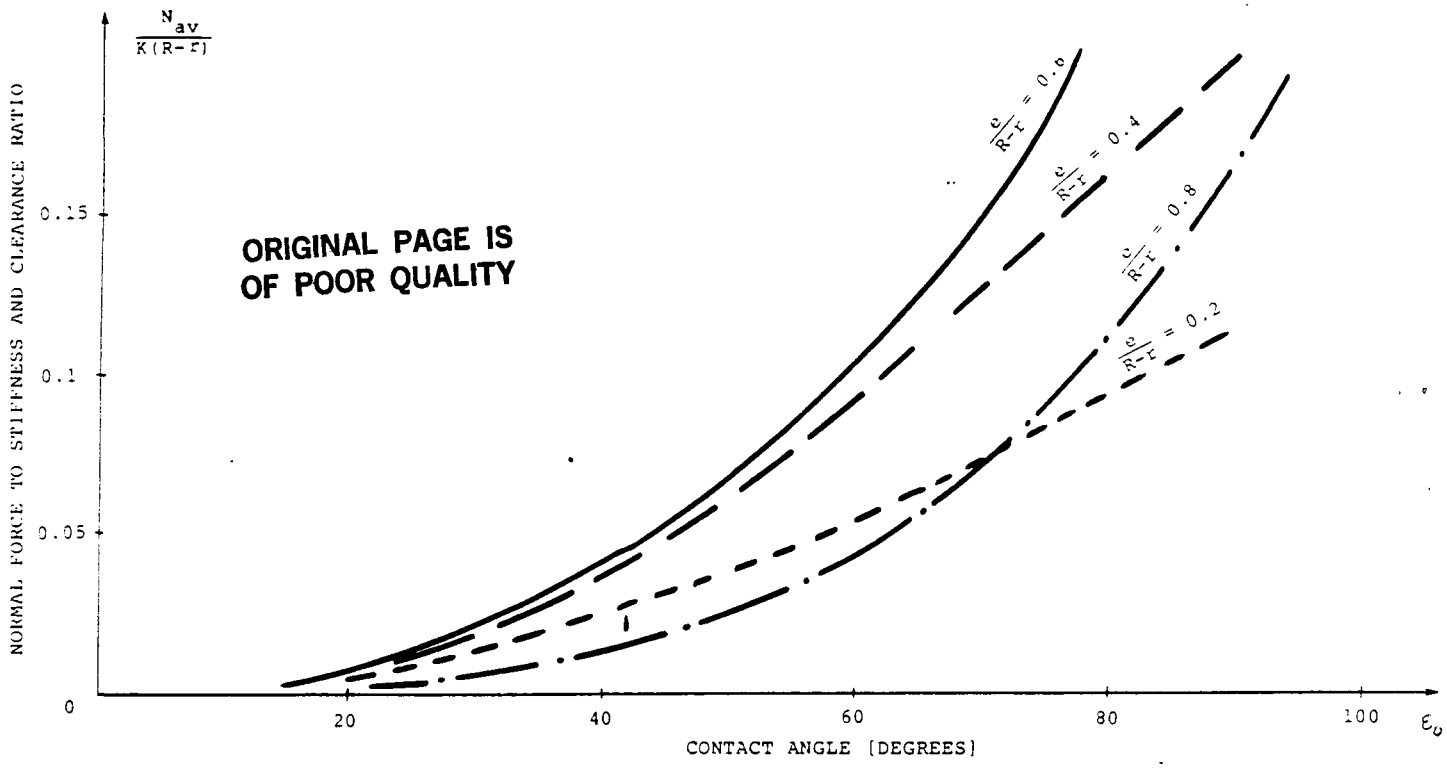

FIGURE 11.6 AVERAGE NORMAL FORCE VERSUS CONTACT ANGLE FOR DIFFERENT VALUES OF SHAFT ECCENTRICITY.

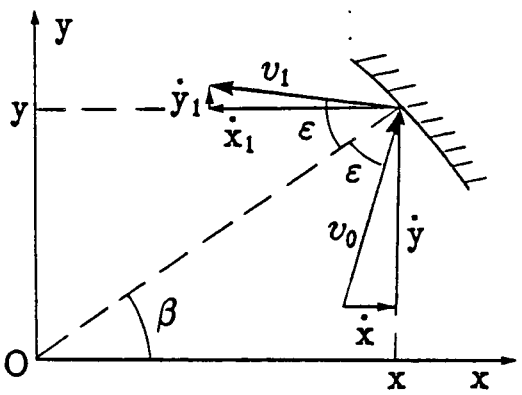

FIGURE 11.7 STRAIGHT IMPACT MODEL

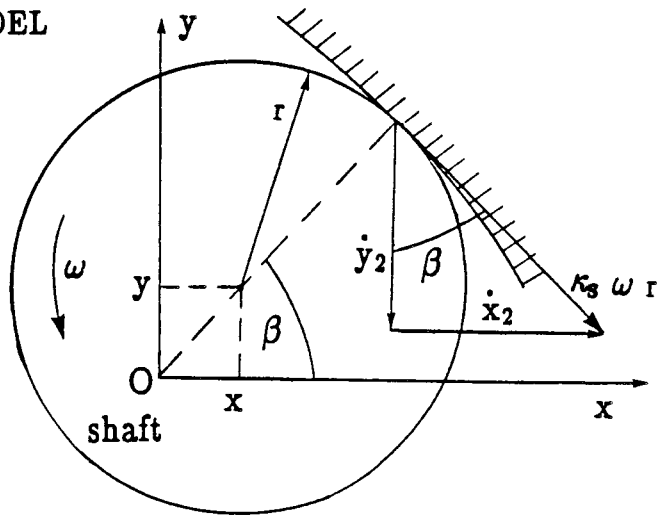

FIGURE 11.8 SUPERBALL IMPACT MODEL

12. RESULTS OF ROTOR–TO–STATOR RUBBING EXPERIMENTAL TESTING OF THE HPFTP–SIMULATING ROTOR RIG.

12.1 Introduction

In order to determine the vibration response patterns of the HPFTP–simulating rotor rig, with and without rub, two major experiments were performed. The first experiment explored the normal and rub–induced vibration responses of the rotor with an axial unbalance distribution which excited predominantly the first and second mode responses, while the second experiment used an unbalance distribution to predominantly excite the first and third mode responses. A description of the test sequences and the resultant data is presented in this chapter.

12.2 Experiment With Mass Unbalance in Turbine Disk

This set of tests consisted of placing a 0.8 inch-gram unbalance in the turbine disk of the HPFTP–simulating rig (see Fig. 12.1) at zero degrees and running the rotor at a constant speed of 4000 rpm, which corresponds to the scaled HPFTP operating speed. This produces a once–per–turn vibration pattern axially along the rotor comprised of mainly first and second mode responses. In addition to the once–per–turn unbalance–related forcing function, a static radial force is applied to the rotor by a spring with adjustable preload. The spring is attached to the rotor through a rolling element bearing mounted between the third pump impeller and the turbine disk. This radial force simulates the preload on the HPFTP rotor produced by the pumped working fluid at the discharge section. Since the once–per–turn response is not large enough to cause rub by itself, the rub is initiated, and its severity controlled by the static preload force. This dictated a base test sequence in which the static preload force was incrementally increased and the vibration responses at different axial locations along the shaft recorded for each static preload level. In order to determine the effect of the varying stiffness introduced by the pump interstage seals, this base test sequence was performed with incrementally stepped oil pressures in the seal simulation bearings. Figures 12.2 to 12.6 illustrate rotor static deflections at the operating speed 4000 rpm and for different radial preload forces and different oil pressures.

The HPFTP–simulating rig was equipped with electrical contact devices (such as described in Section 9.2.2), indicating the physical contact between the rotor and stationary part.

The orbit, timebase, and spectral content at each axial probe location, plus the timebase and spectral content of the shaft/seal or shaft/rub block contact, was acquired using an ADRE® III Data Acquisition System. The data are presented in Figures 12.7 to 12.161. Each segment of figures is preceded by a corresponding mode shape of the rotor for the specific oil pressure. The spectral content and timebase information on rub from the two seal simulation bearings, for conditions in which the seal clearance area is fully oil–lubricated, could not be presented (Figures 12.57, 12.58, 12.88, 12.89, 12.119, 12.120, 12.150, 12.151), as the oil effectively prevents the actual metal–to–metal contact required for the sensing system. The omission of this data is not intended to infer that the nonlinear radial bearing characteristics of the seal do not produce forces on the shaft similar to the ones generated during rub.

The cascade spectra for the shaft–to–rub block contact signals indicate the occurrence of metal–to–metal contact, and the frequency of the rotor/stationary part physical contact occurrence for the lowest frequency component. The shape of the electrical waveform used to detect contact occurrence generates higher harmonics of the fundamental rub frequency. It is seen on the cascade plots (for example the second harmonics are in Figs. 12.35, 12.36,

12.37). The existence of these higher harmonics is caused by the on–off contact waveform, and does not mean that rub occurs with these higher frequencies.

The data shows changes in the orbit, timebase, and spectral content of the vibration signals with increases in the preload force. With no preload the shaft is centered within the seals and the rub block, producing a rub–free vibration response. The orbit is primarily circular, and the spectral content is predominantly once per turn (synchronous response). As the preload is increased, first a light contact between elements occurs. This results in a "figure eight"–shaped orbit due to the appearance of the 0.5× vibrational component. Transient responses with the system natural frequencies also appear in the rotor response spectrum. As the preload is increased and the rotor eccentricity increased, the orbit becomes smaller and more elliptically deformed, while the spectral content shifts from predominantly 0.5× to predominantly 1×, 2×, and system natural frequency components. This is the effect of stiffness nonlinearity. Increasing the oil pressure at the seal locations basically increases the system stiffness, allowing less radial motion of the rotor for a given preload. It results in delaying the onset of the rubbing phenomena with a given preload force, but does not change the vibration patterns generated once the rub condition is achieved.

12.3 Experiment With Mass Unbalance in Third Pump Impeller Disk

This set of tests was performed similarly to those described in Section 12.2, the only change being the unbalance mass distribution. Instead of placing the unbalance mass in the turbine disk, as was done in the previous case, the unbalance mass for these tests was located in the third pump impeller disk. This produces a once–per–turn vibration response which is predominantly comprised of the first and third mode responses. The experimental data is presented in Figures 12.162 to 12.316.

The changes in the vibrational responses with increasing preload were also similar to those obtained from the tests described in Section 12.2. The preload for rub inception was higher than for the previous case, since the rub locations fall near the 1× nodal points. Since the maximum amplitude is the summation of the static eccentricity and 1× vibration amplitudes, a larger static deflection is required to compensate for the smaller 1× vibration amplitudes at the potential rub locations to produce resultant rotor motion greater than the allowable clearance. Therefore, larger static preload forces are required to initiate rub. The progression of synchronous responses for no rubbing, moving to 0.5× components at light rub, to 1×, 2×, and the appearance of transient components with system natural frequencies for heavy rubs described for the previous test was also observed during the present tests. Varying seal simulation bearing oil pressures again had only minor effects on the vibration patterns.

12.4 Summary

The HPFTP–simulating rig rotor vibration responses caused by rotor–to–stator rubbing and their changes from normal no–rub responses were explored for two different rotor unbalance mass distributions: one predominantly for the first and a second mode, the other predominantly for the first and third mode. The rotor speed was constant 4000 rpm. The inception and severity of the rub were controlled by varying a static radial preload applied to the rotor between the third pump impeller and turbine disks. The effects of additional stiffness at the seals between the pump impellers were also investigated. This additional stiffness was achieved by varying oil pressure at the seal–simulating bearings. The similar patterns of rotor vibrations were observed for all tests. When no rub occurs, the 1× synchronous response due to the unbalance is dominant. With the initiation of light rub, a large 0.5× component appears in the vibrational response. This component gradually disappears as the rub severity increases (radial load increases). As the 0.5× component disappears, more rub–related changes in 1× responses as well as appearance of significant

higher harmonic components are noted. Some transient vibrational responses with frequencies corresponding to the system natural frequencies also appear in the spectrum. The additional stiffness at the seal locations modified the point of inception for the rub, but did not change the vibrational patterns significantly.

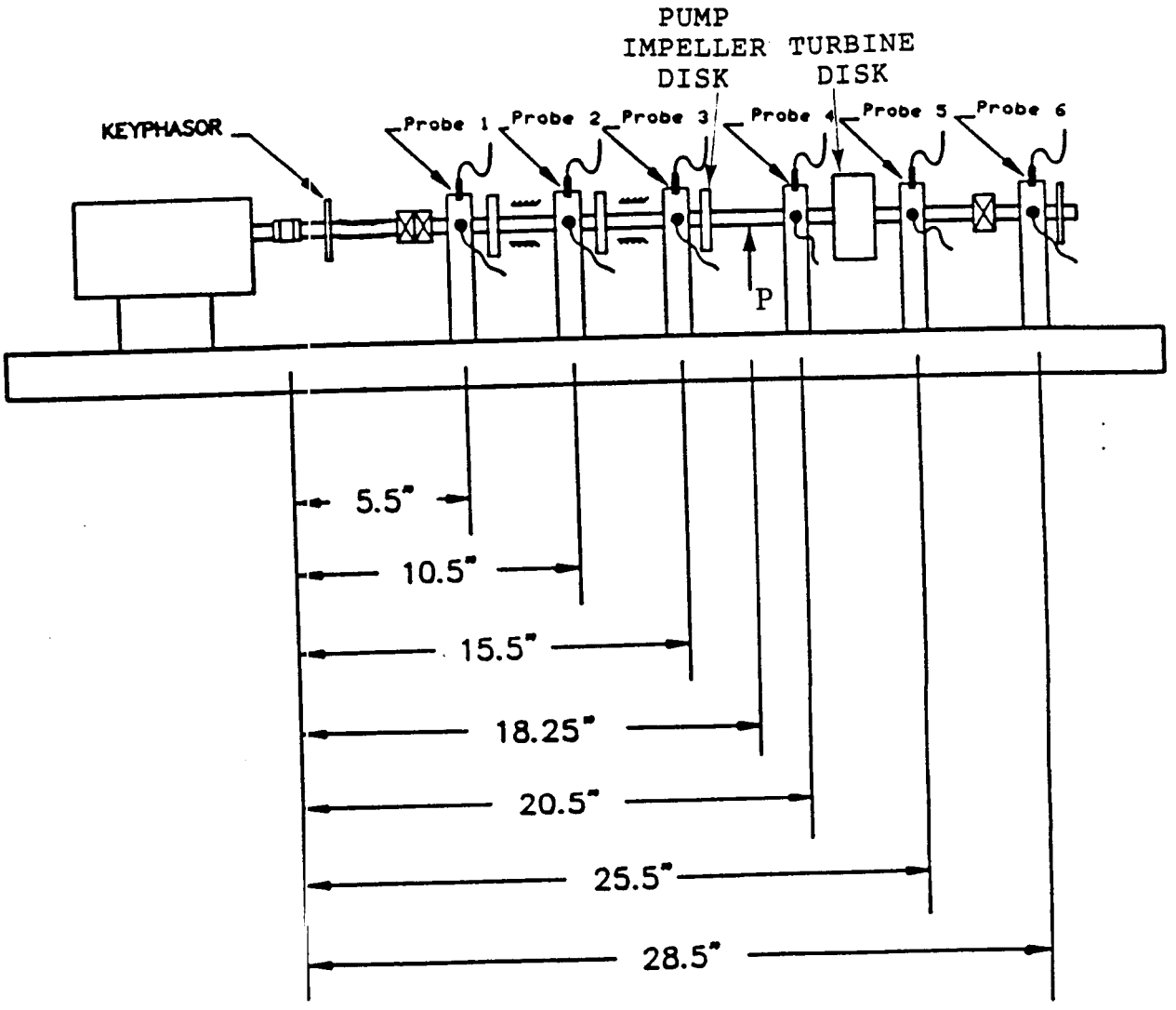

FIGURE 12.1 ROTOR CONFIGURATION.

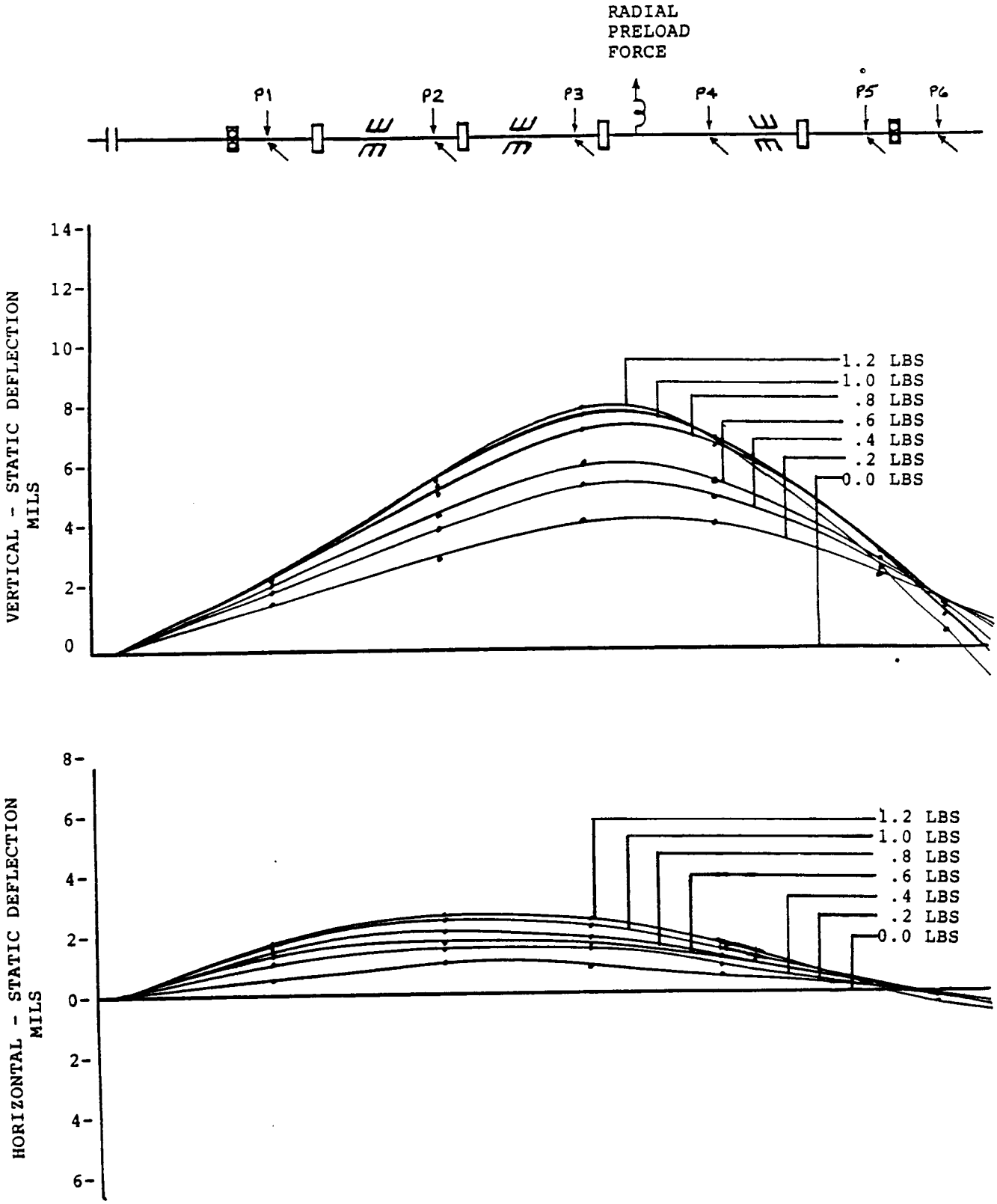

FIGURE 12.2 ROTOR STATIC DEFLECTIONS AT 4000 RPM, (0 PSI SEAL OIL PRESSURE)DUE TO INCREASING STATIC PRELOAD FORCES.

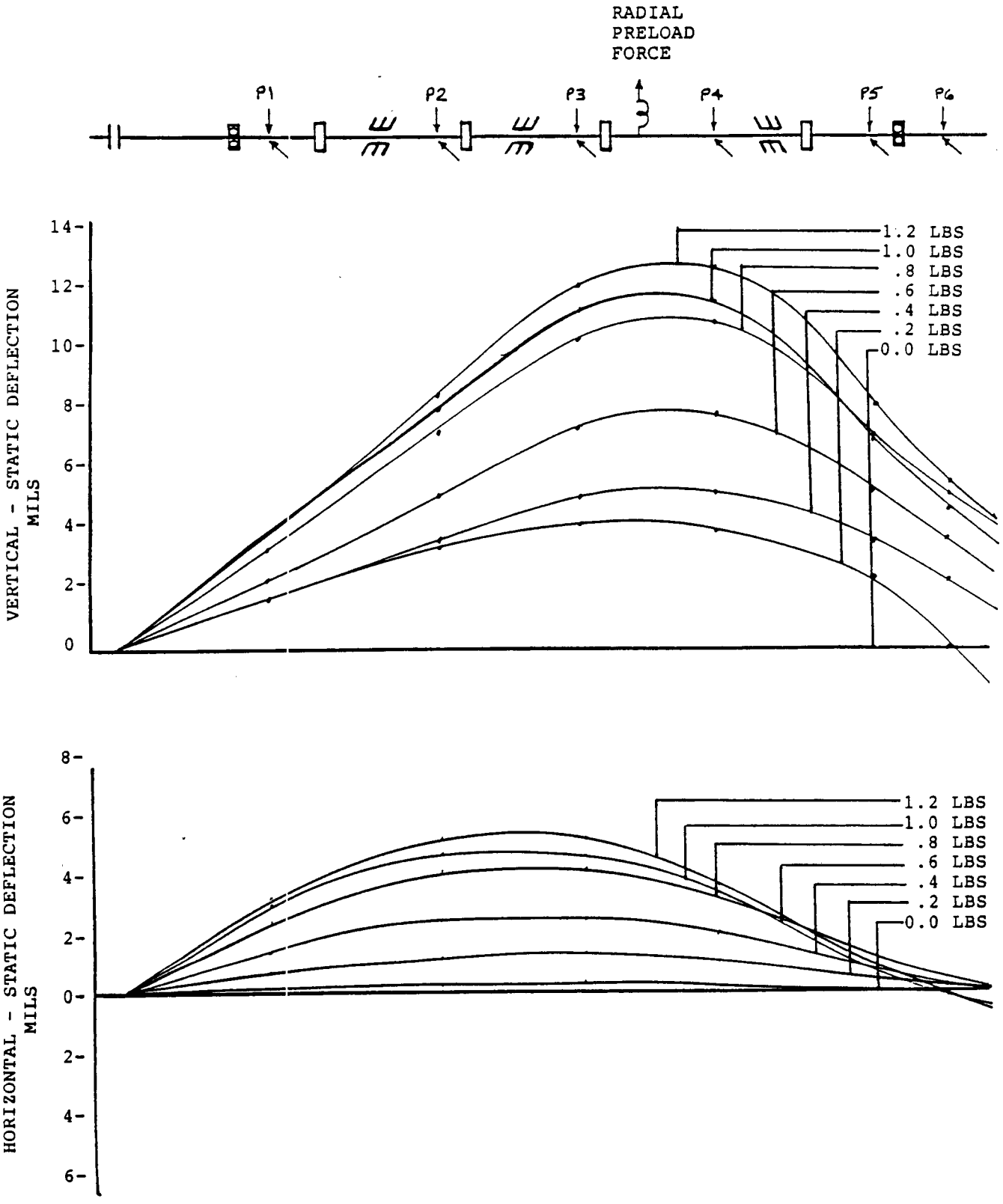

FIGURE 12.3 ROTOR STATIC DEFLECTIONS AT 4000 RPM, (2.5 PSI SEAL OIL PRESSURE) DUE TO INCREASING STATIC PRELOAD FORCES.

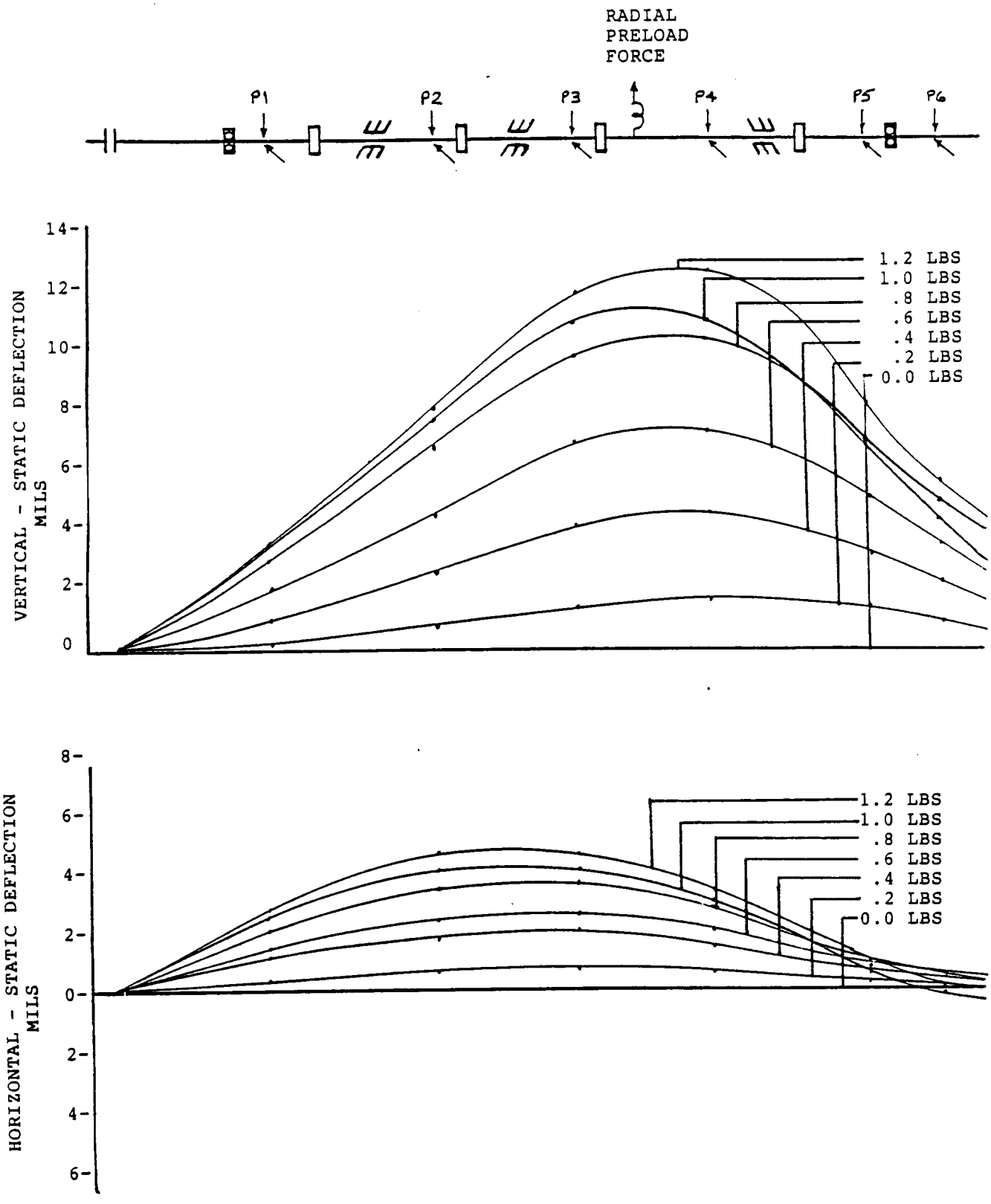

FIGURE 12.4 ROTOR STATIC DEFLECTIONS AT 4000 RPM,(5.0 PSI SEAL OIL PRESSURE)DUE TO INCREASING STATIC PRELOAD FORCES.

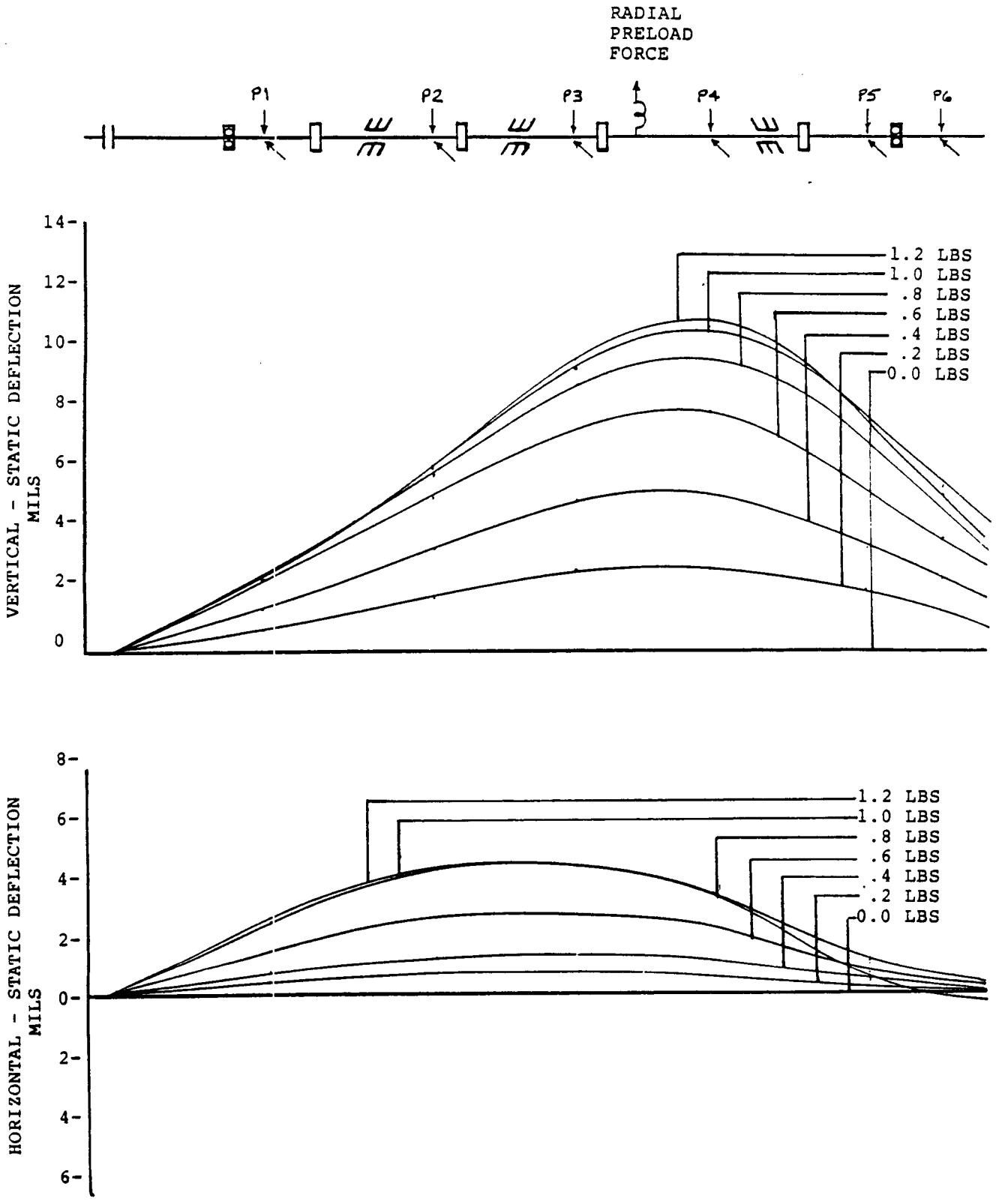

FIGURE 12.5 ROTOR ROTOR STATIC DEFLECTIONS AT 4000 RPM,(7.5 PSI SEAL OIL PRESSURE)DUE TO INCREASING STATIC PRELOAD FORCES.

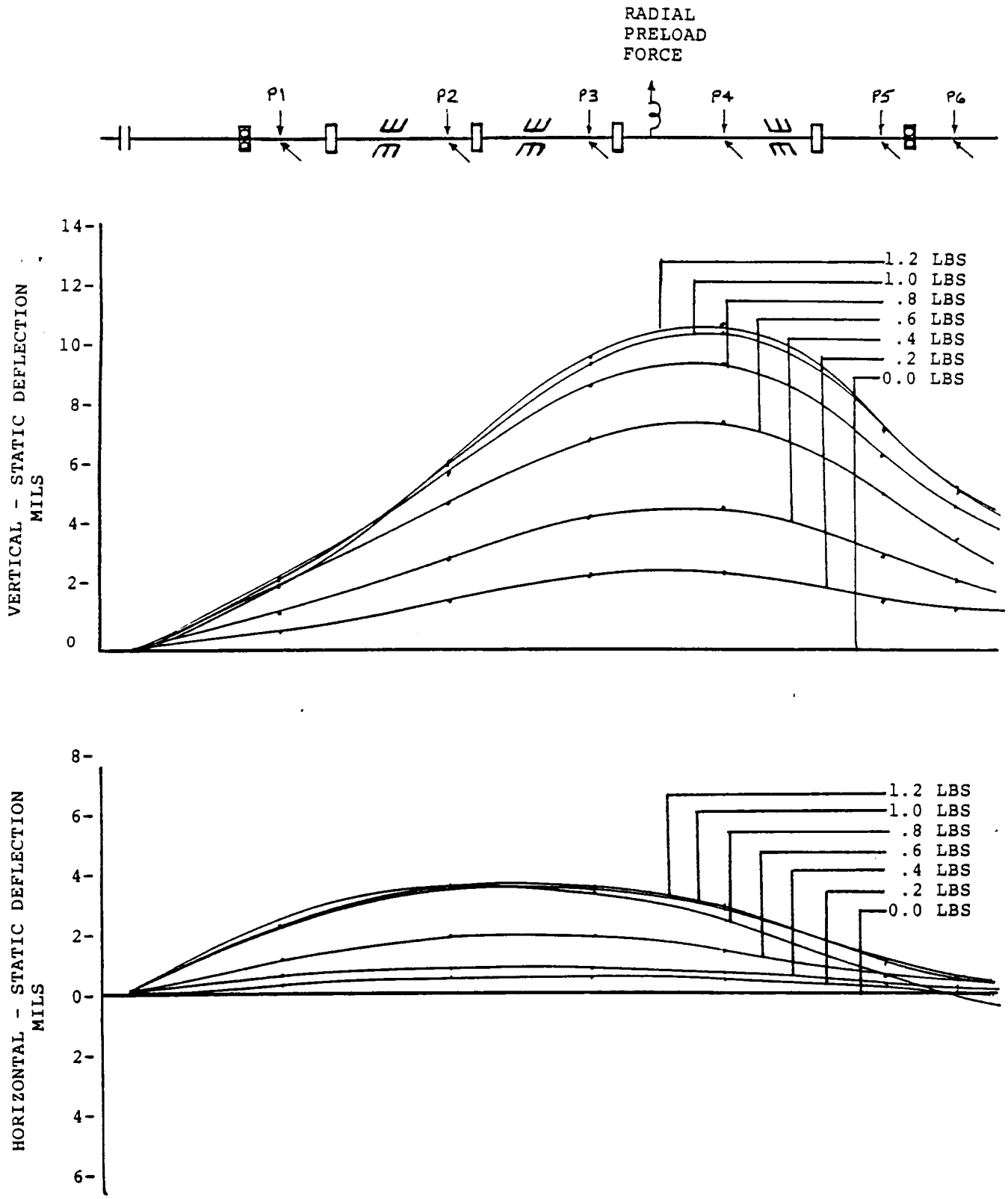

FIGURE 12.6 ROTOR STATIC DEFLECTIONS AT 4000 RPM, (10.0 PSI SEAL OIL PRESSURE) DUE TO INCREASING STATIC PRELOAD FORCES.

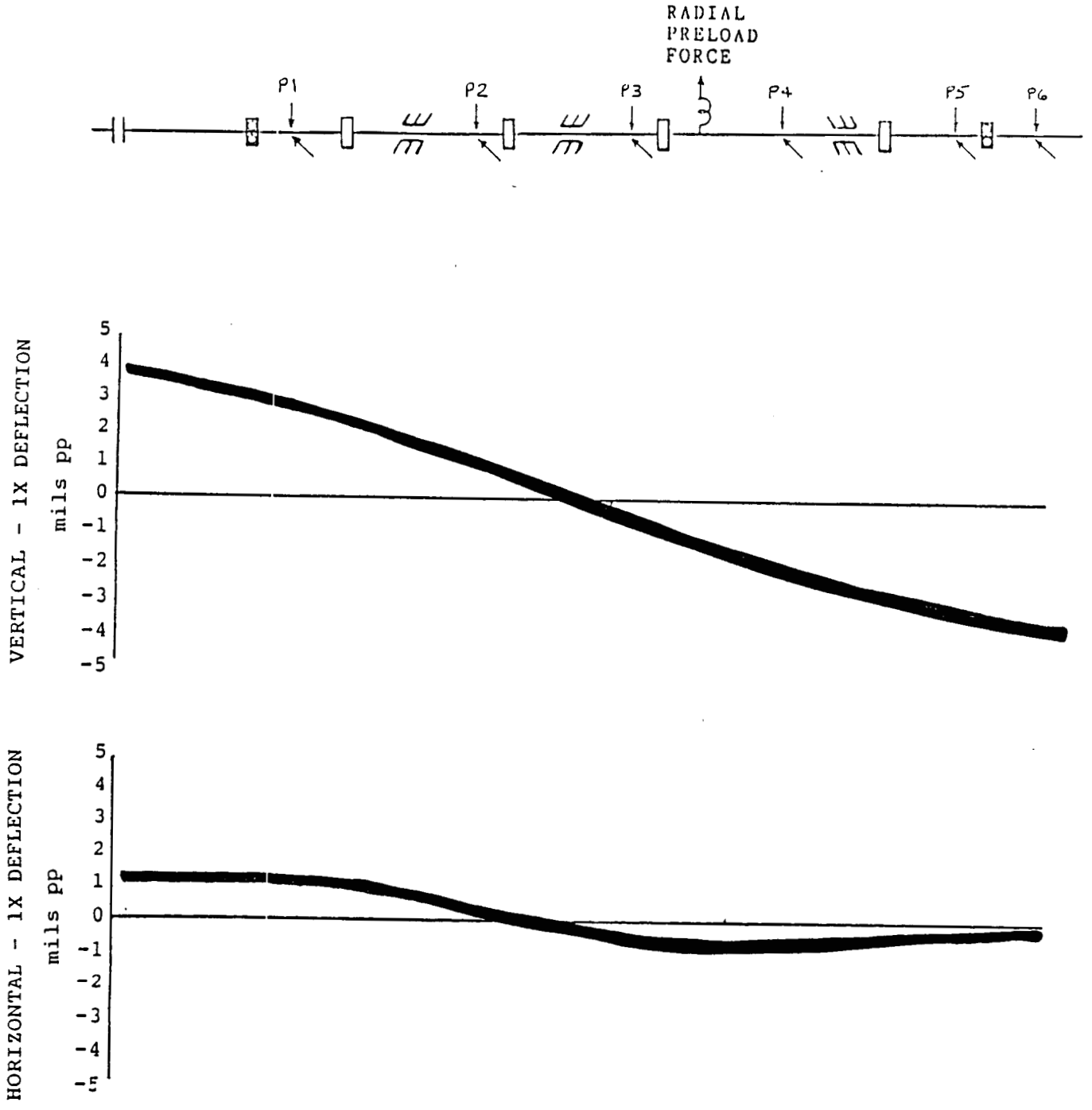

FIGURE 12.7 ROTOR MODE SHAPE AT 4000 RPM,(0 PSI SEAL OIL PRESSURE) DUE TO 0.8 IN-GRAM UNBALANCE LOCATED IN THE TURBINE DISK.

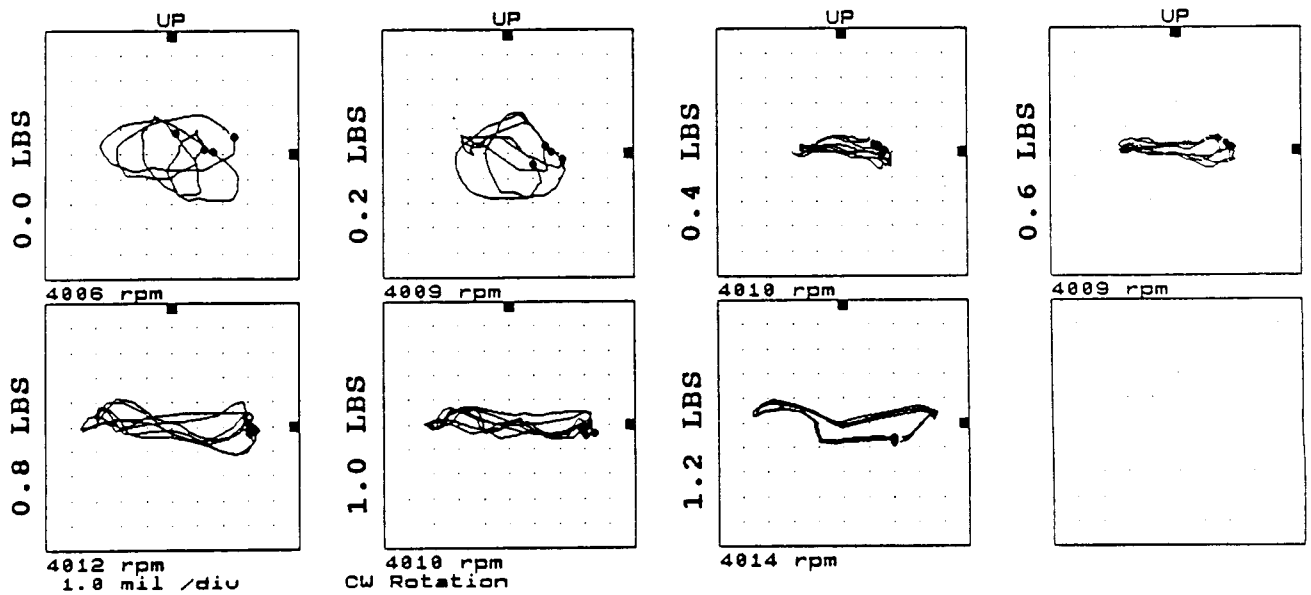

FIGURE 12.8 ORBITS AT PROBE LOCATION 1 AT 4000 RPM, 0 PSI SEAL OIL PRESSURE, 0.8 IN–GRAM UNBALANCE LOCATED IN THE TURBINE DISK, FOR INCREASING STATIC PRELOAD FORCES.

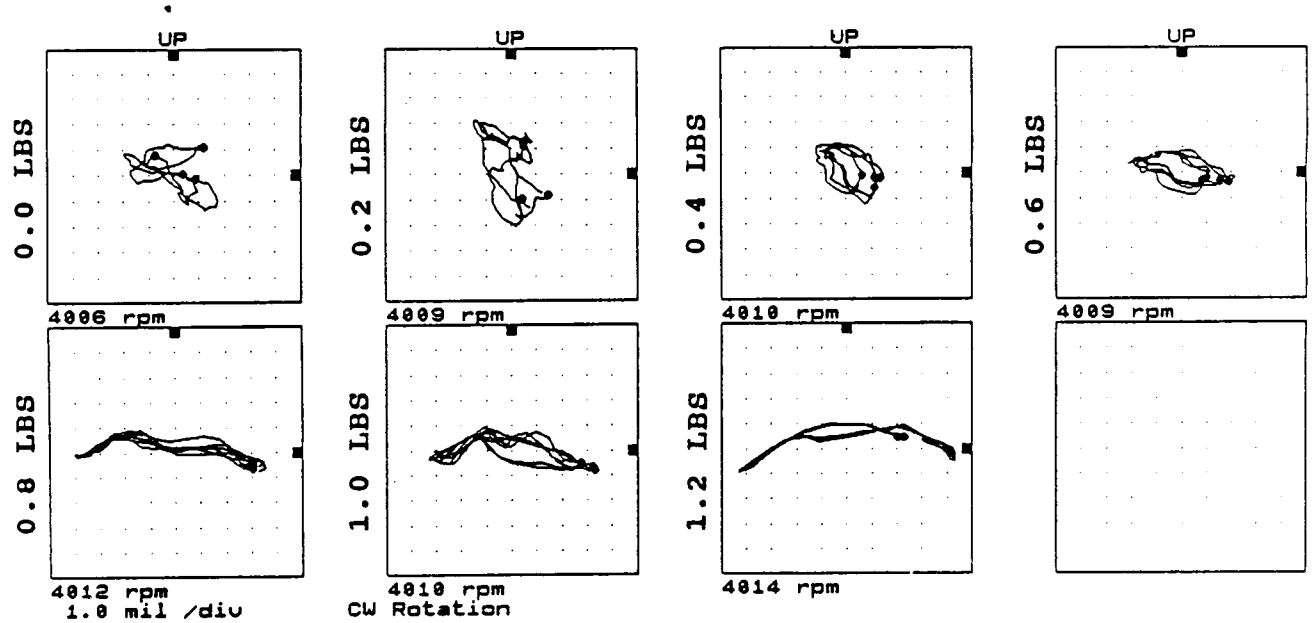

FIGURE 12.9 ORBITS AT PROBE LOCATION 2 AT 4000 RPM, 0 PSI SEAL OIL PRESSURE, 0.8 IN–GRAM UNBALANCE LOCATED IN THE TURBINE DISK, FOR INCREASING STATIC PRELOAD FORCES.

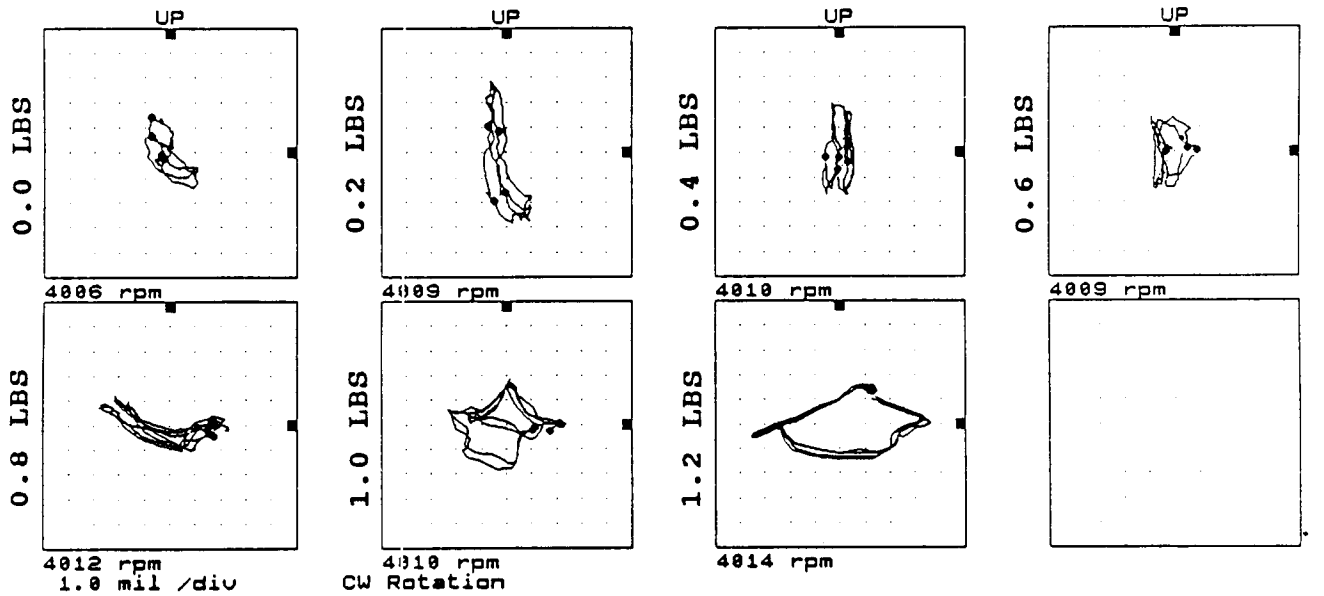

FIGURE 12.10 ORBITS AT PROBE LOCATION 3 AT 4000 RPM, 0 PSI SEAL OIL PRESSURE, 0.8 IN–GRAM UNBALANCE LOCATED IN THE TURBINE DISK, FOR INCREASING STATIC PRELOAD FORCES.

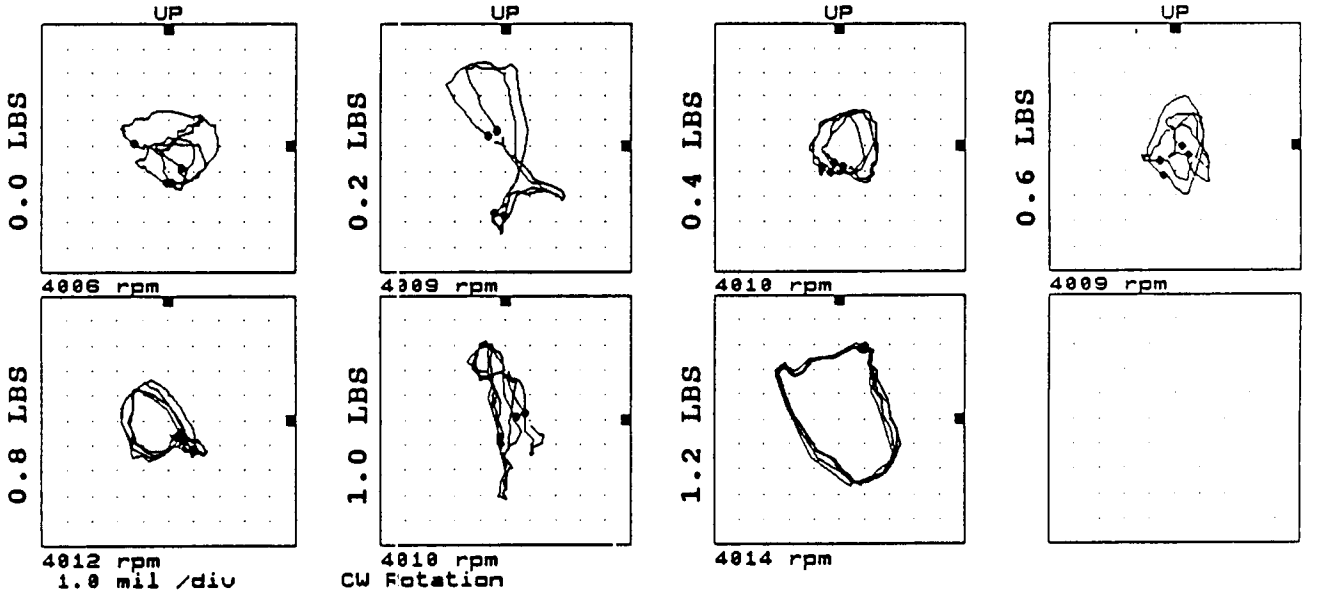

FIGURE 12.11 ORBITS AT PROBE LOCATION 4 AT 4000 RPM, 0 PSI SEAL OIL PRESSURE, 0.8 IN–GRAM UNBALANCE LOCATED IN THE TURBINE DISK, FOR INCREASING STATIC PRELOAD FORCES.

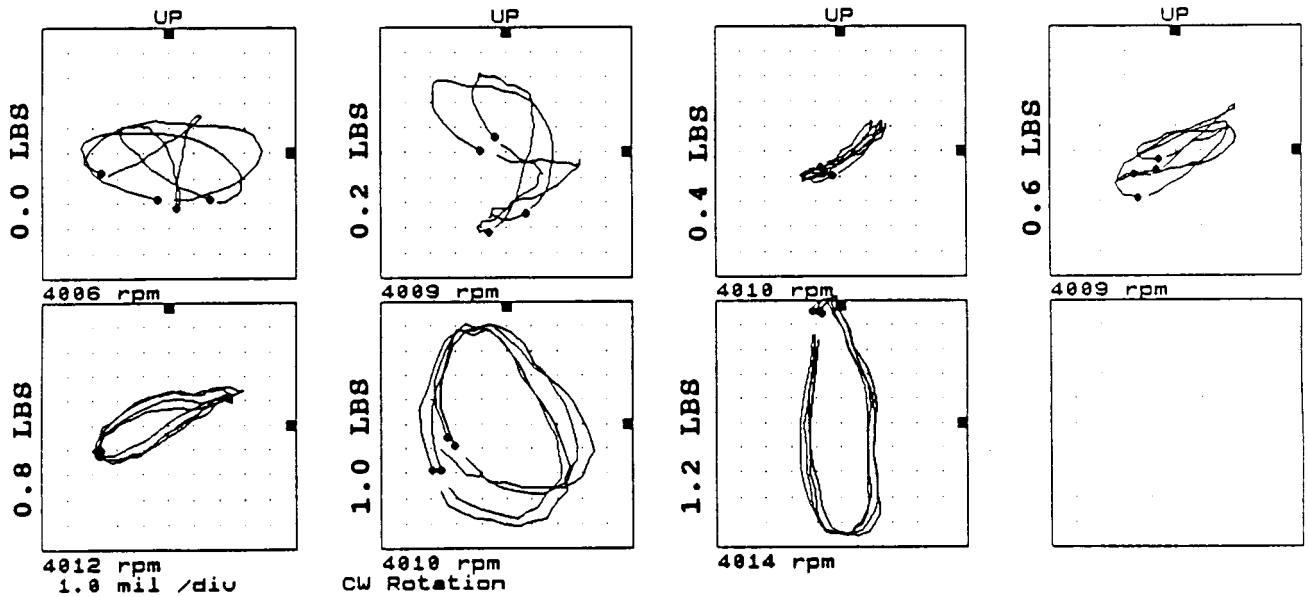

FIGURE 12.12 ORBITS AT PROBE LOCATION 5 AT 4000 RPM, 0 PSI SEAL OIL PRESSURE, 0.8 IN–GRAM UNBALANCE LOCATED IN THE TURBINE DISK, FOR INCREASING STATIC PRELOAD FORCES.

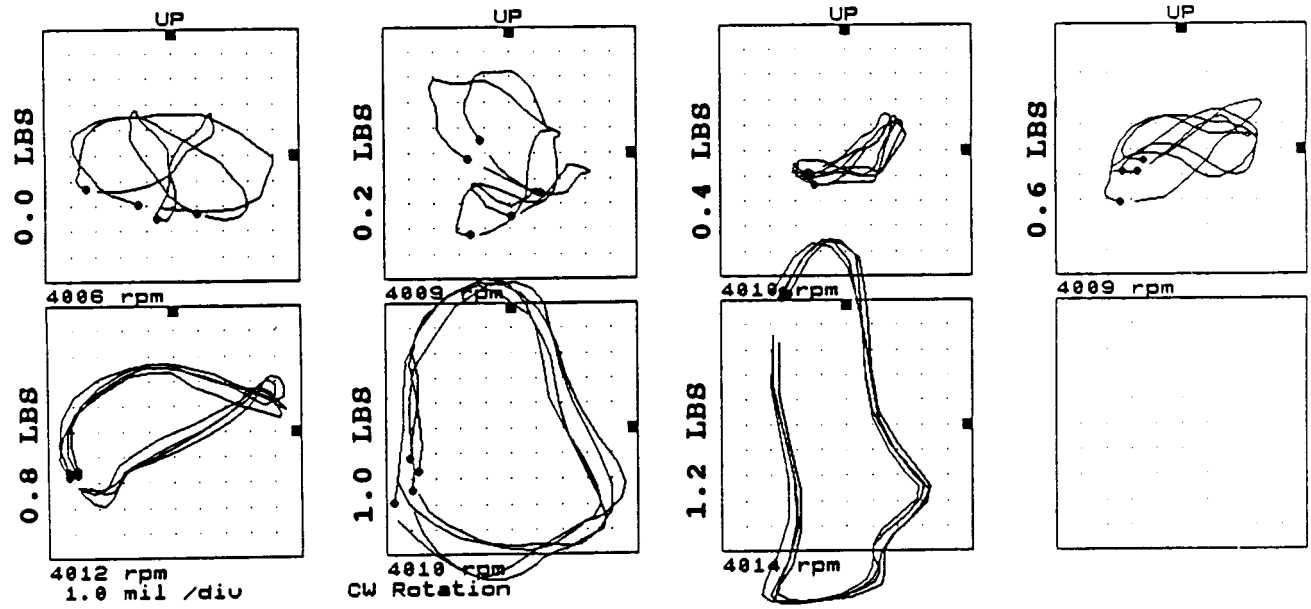

FIGURE 12.13 ORBITS AT PROBE LOCATION 6 AT 4000 RPM, 0 PSI SEAL OIL PRESSURE, 0.8 IN–GRAM UNBALANCE LOCATED IN THE TURBINE DISK, FOR INCREASING STATIC PRELOAD FORCES.

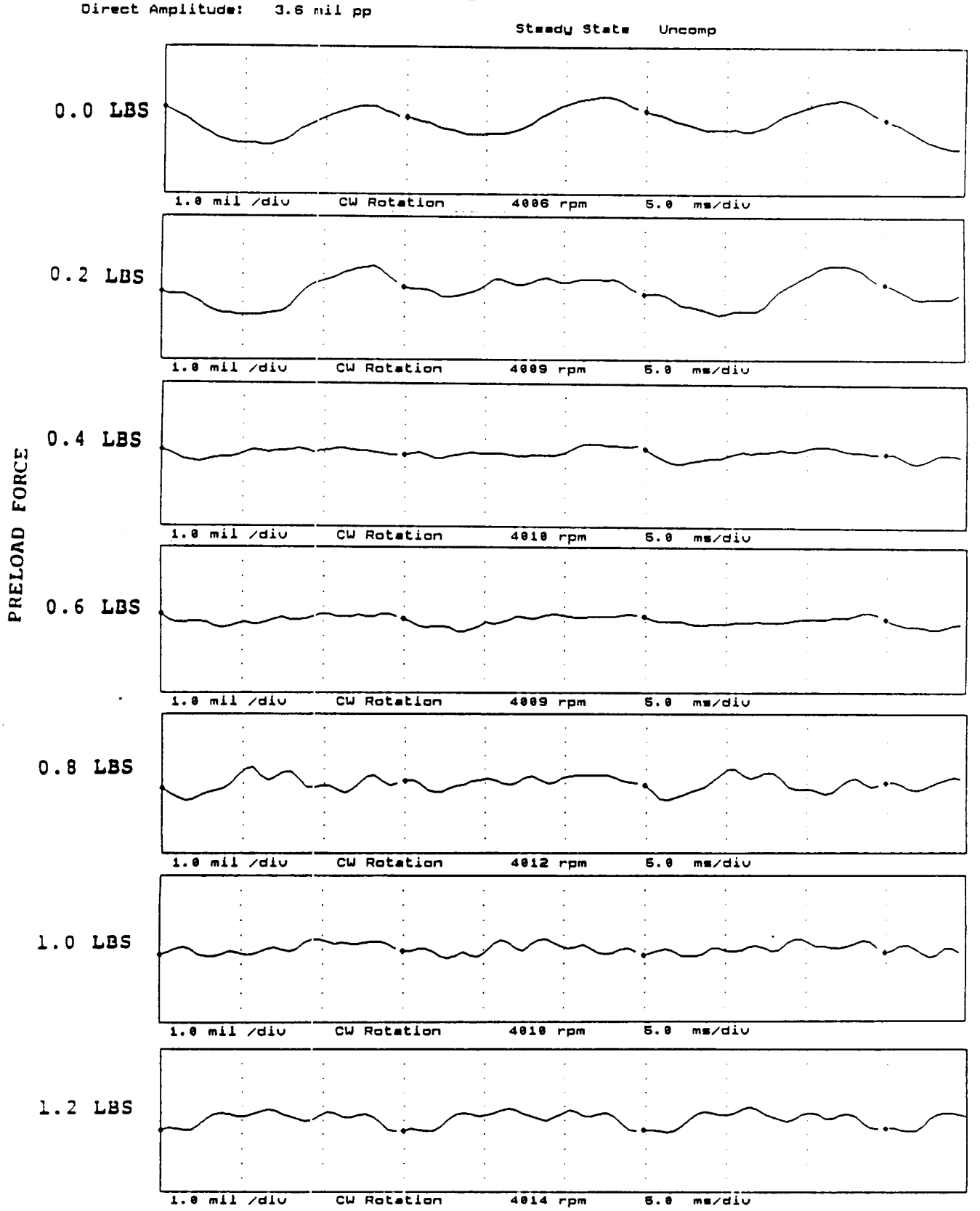

FIGURE 12.14 TIMEBASE FOR VERTICAL PROBE AT LOCATION 1 AT 4000 RPM, 0 PSI SEAL OIL PRESSURE, 0.8 IN–GRAM UNBALANCE LOCATED IN THE TURBINE DISK, FOR INCREASING STATIC PRELOADS.

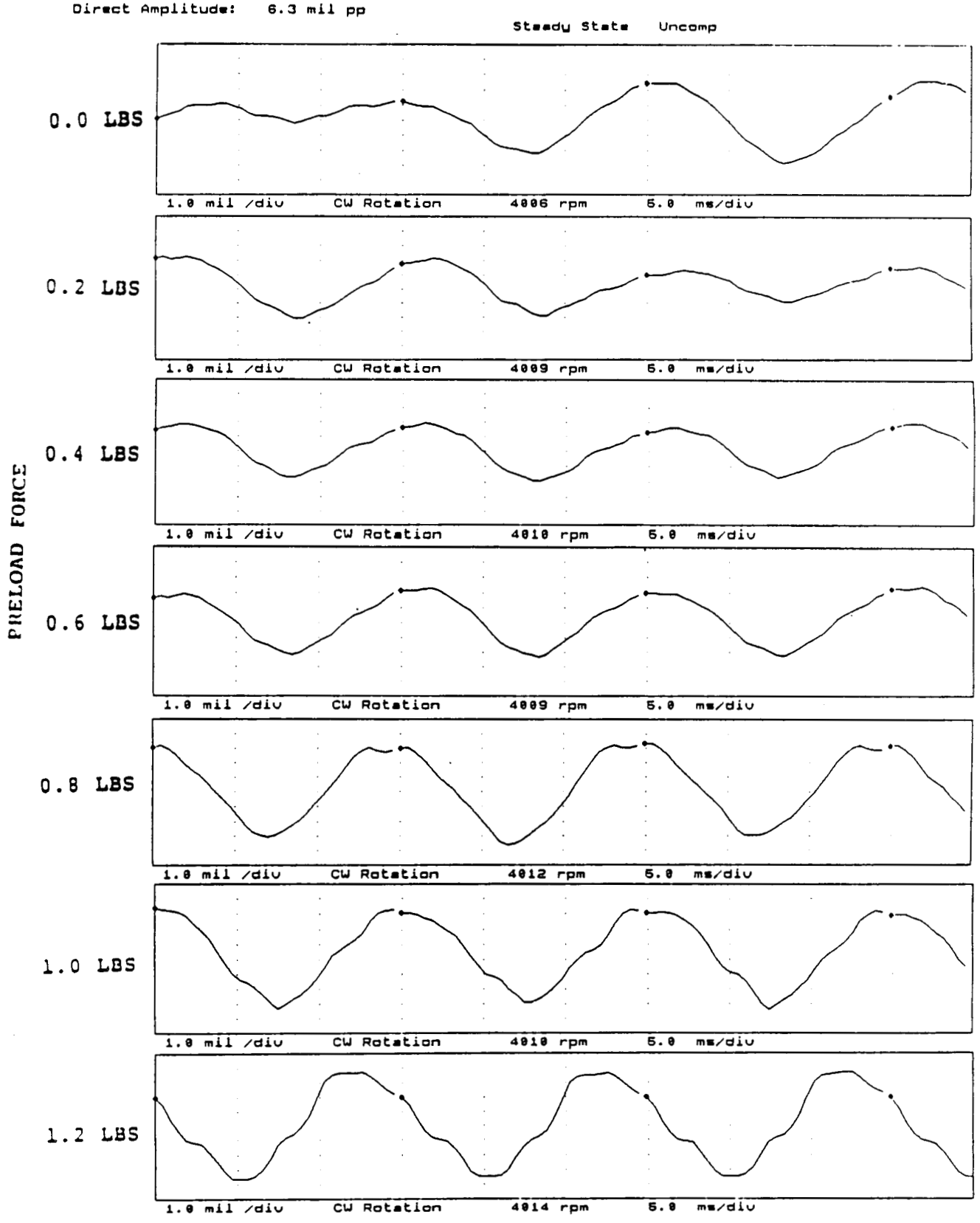

FIGURE 12.15 TIMEBASE FOR HORIZONTAL PROBE AT LOCATION 1 AT 4000 RPM, 0 PSI SEAL OIL PRESSURE, 0.8 IN–GRAM UNBALANCE LOCATED IN THE TURBINE DISK, FOR INCREASING STATIC PRELOADS.

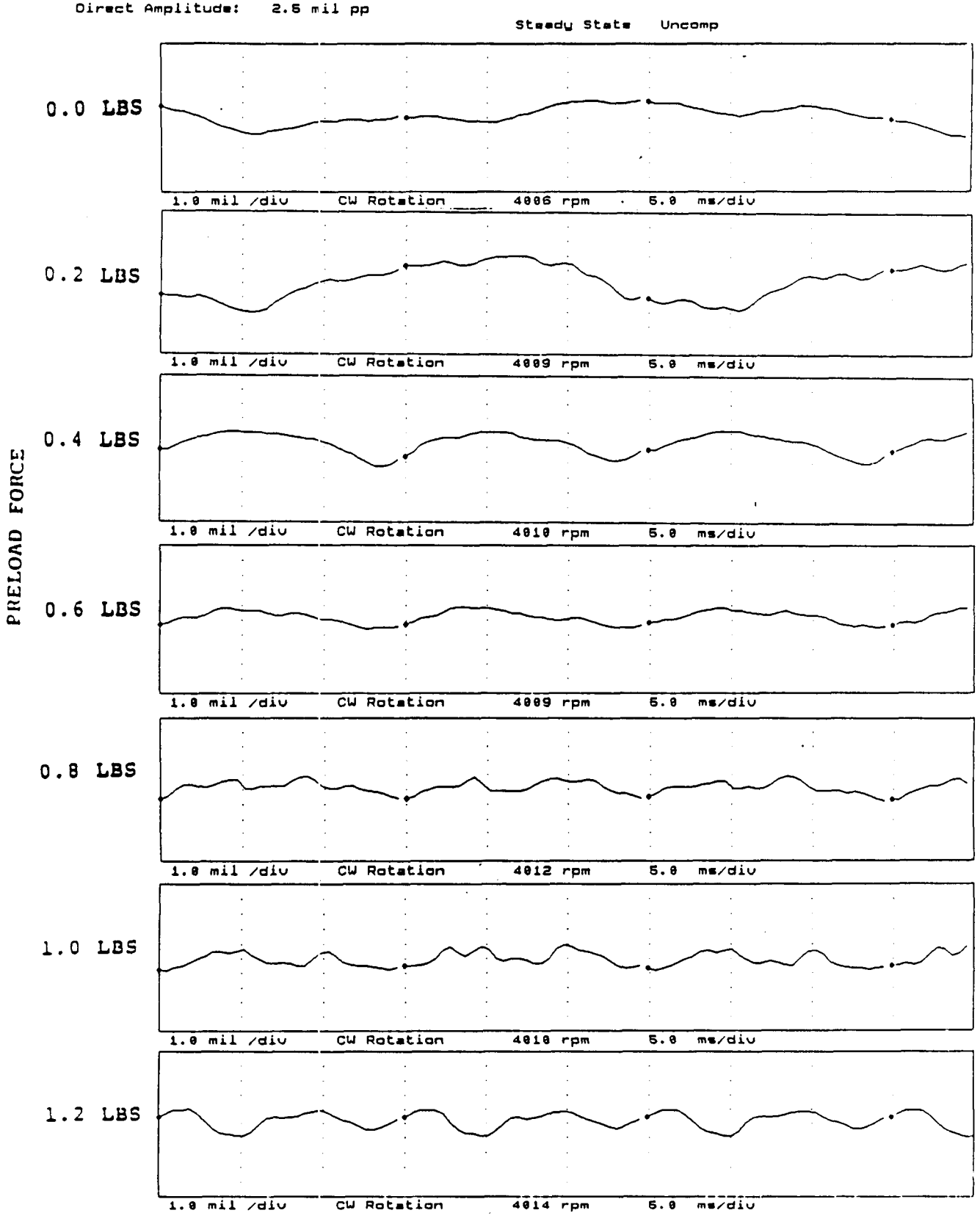

FIGURE 12.16 TIMEBASE FOR VERTICAL PROBE AT LOCATION 2 AT 4000 RPM, 0 PSI SEAL OIL PRESSURE, 0.8 IN–GRAM UNBALANCE LOCATED IN THE TURBINE DISK, FOR INCREASING STATIC PRELOADS.

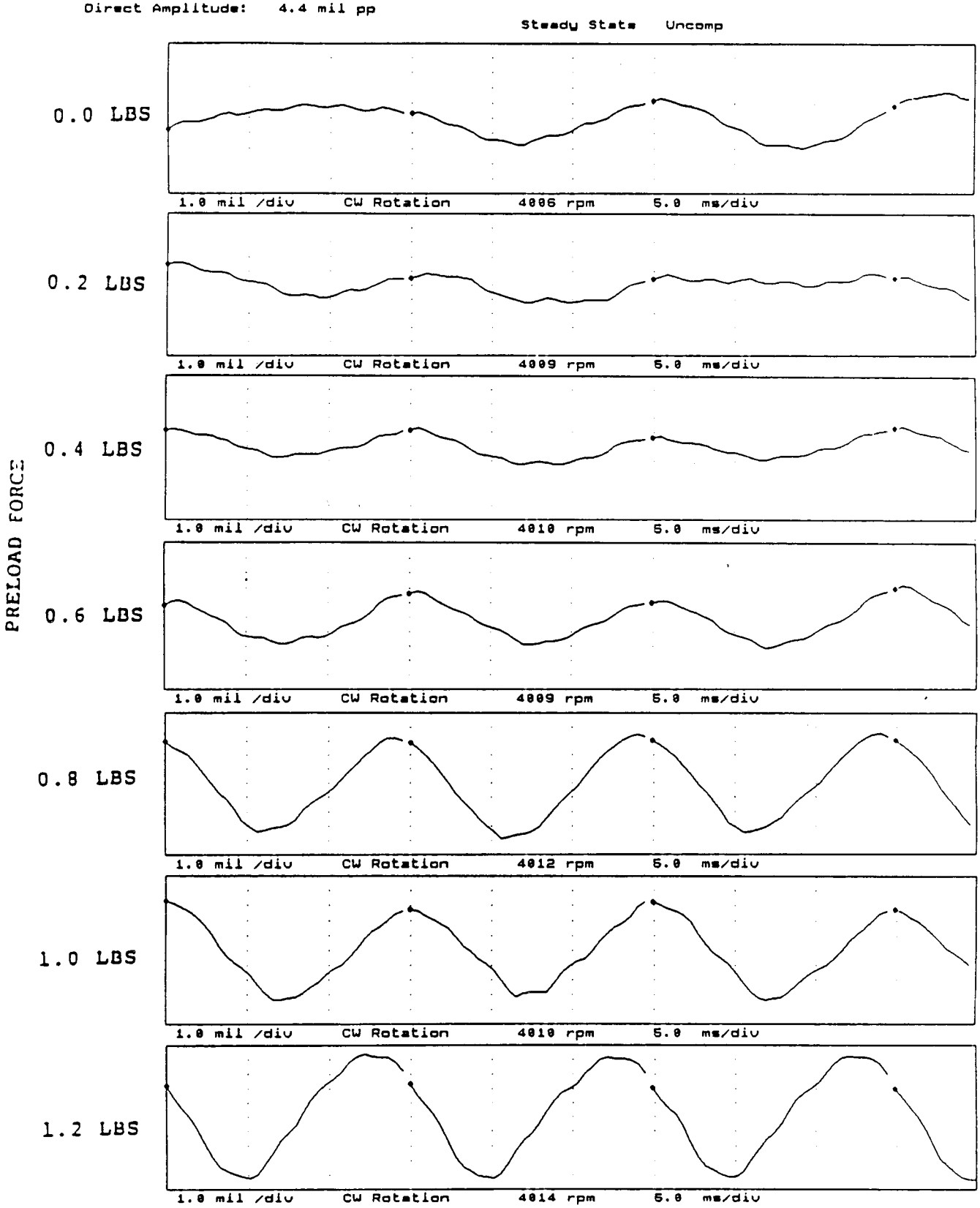

FIGURE 12.17 TIMEBASE FOR HORIZONTAL PROBE AT LOCATION 2 AT 4000 RPM, 0 PSI SEAL OIL PRESSURE, 0.8 IN–GRAM UNBALANCE LOCATED IN THE TURBINE DISK, FOR INCREASING STATIC PRELOADS.

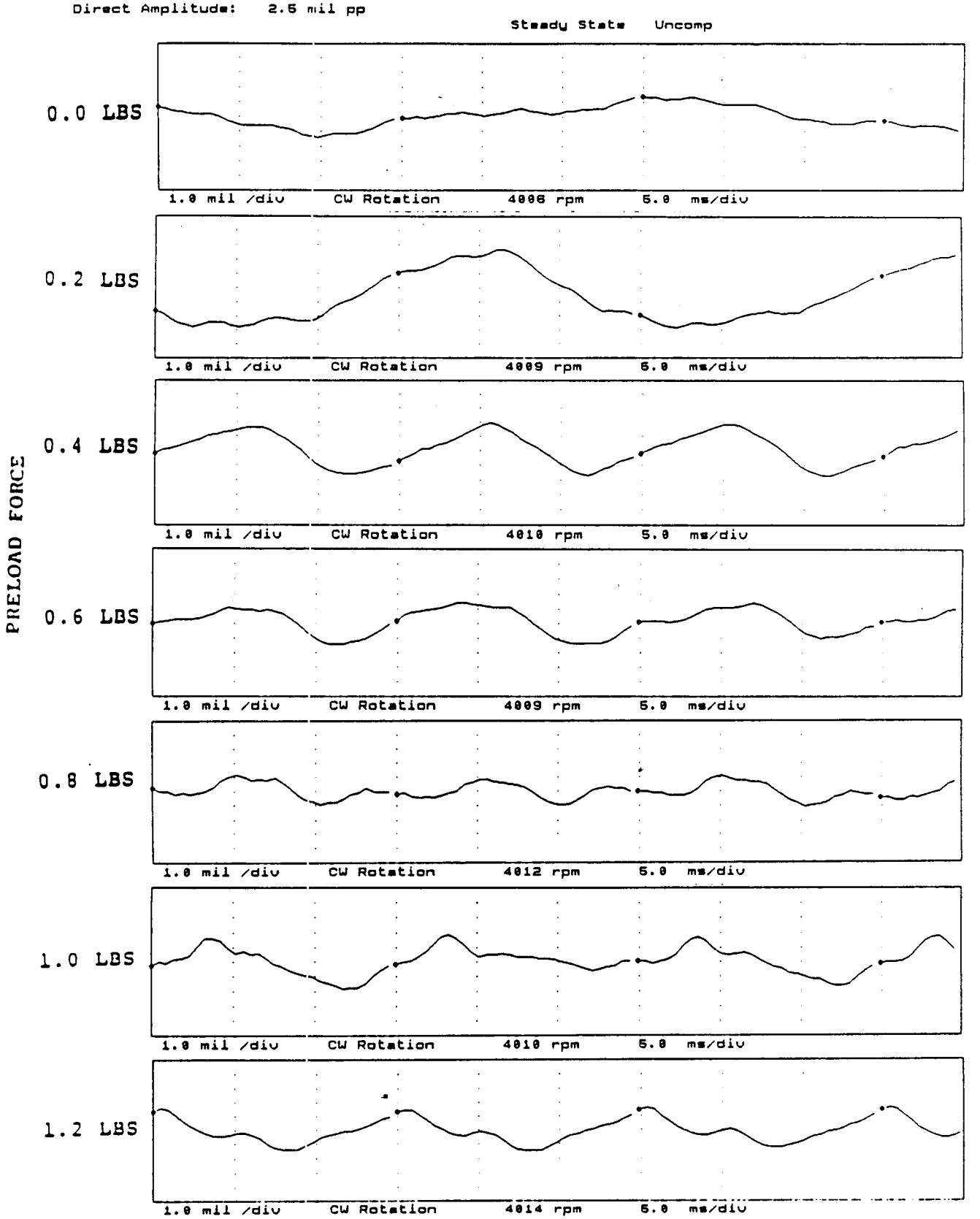

FIGURE 12.18 TIMEBASE FOR VERTICAL PROBE AT LOCATION 3 AT 4000 RPM, 0 PSI SEAL OIL PRESSURE, 0.8 IN–GRAM UNBALANCE LOCATED IN THE TURBINE DISK, FOR INCREASING STATIC PRELOADS.

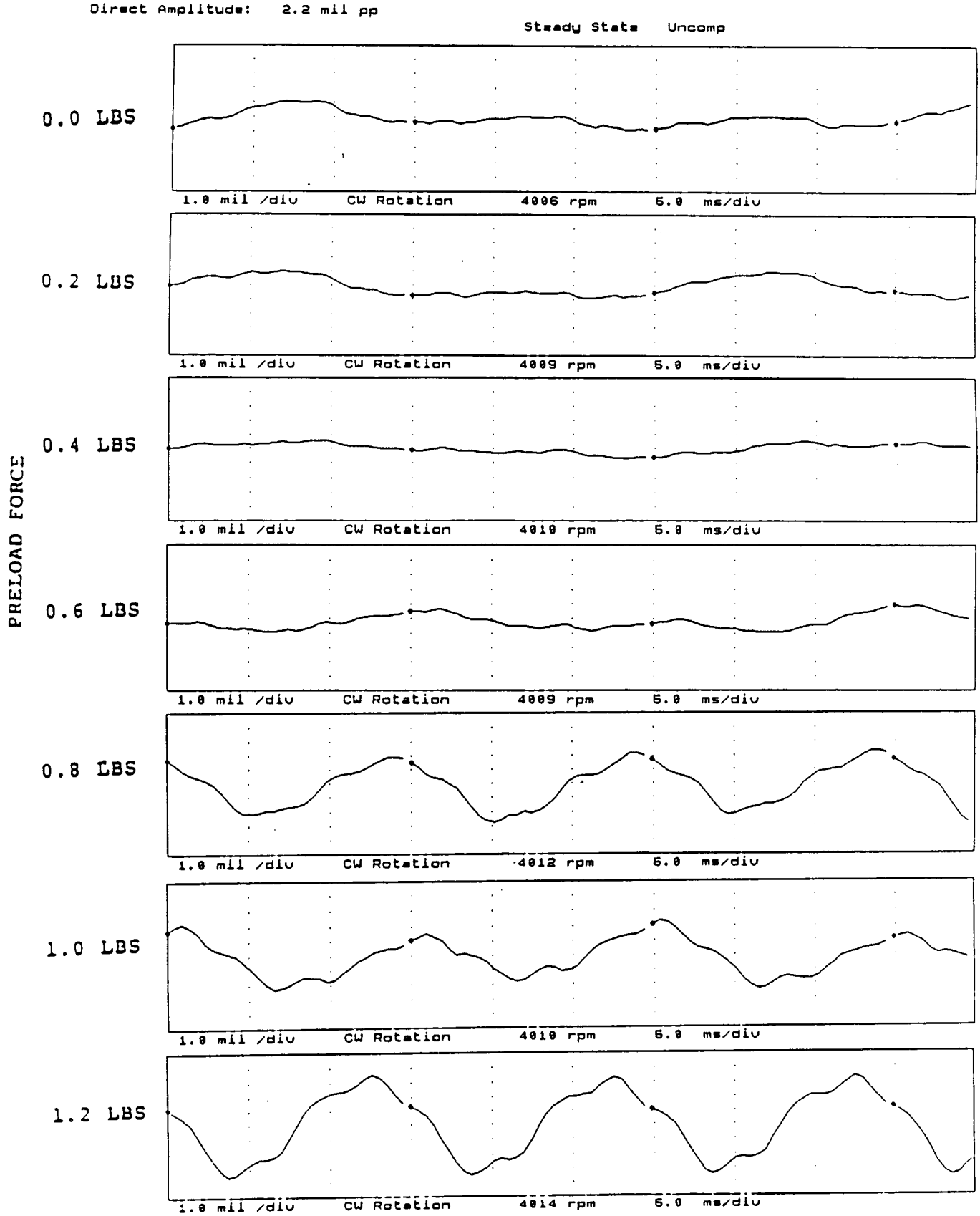

FIGURE 12.19 TIMEBASE FOR HORIZONTAL PROBE AT LOCATION 3 AT 4000 RPM, 0 PSI SEAL OIL PRESSURE, 0.8 IN–GRAM UNBALANCE LOCATED IN THE TURBINE DISK, FOR INCREASING STATIC PRELOADS.

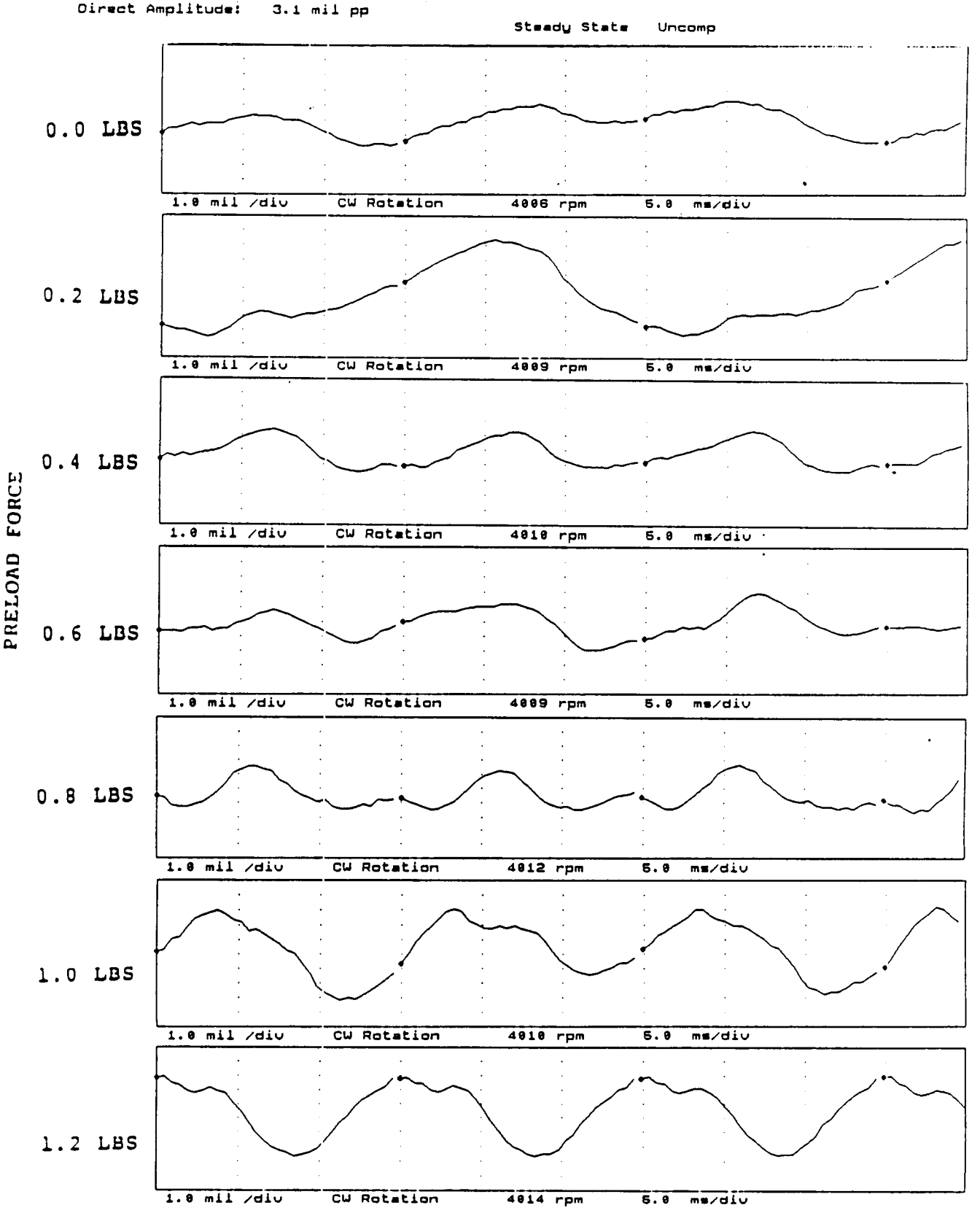

FIGURE 12.20 TIMEBASE FOR VERTICAL PROBE AT LOCATION 4 AT 4000 RPM, 0 PSI SEAL OIL PRESSURE, 0.8 IN–GRAM UNBALANCE LOCATED IN THE TURBINE DISK, FOR INCREASING STATIC PRELOADS.

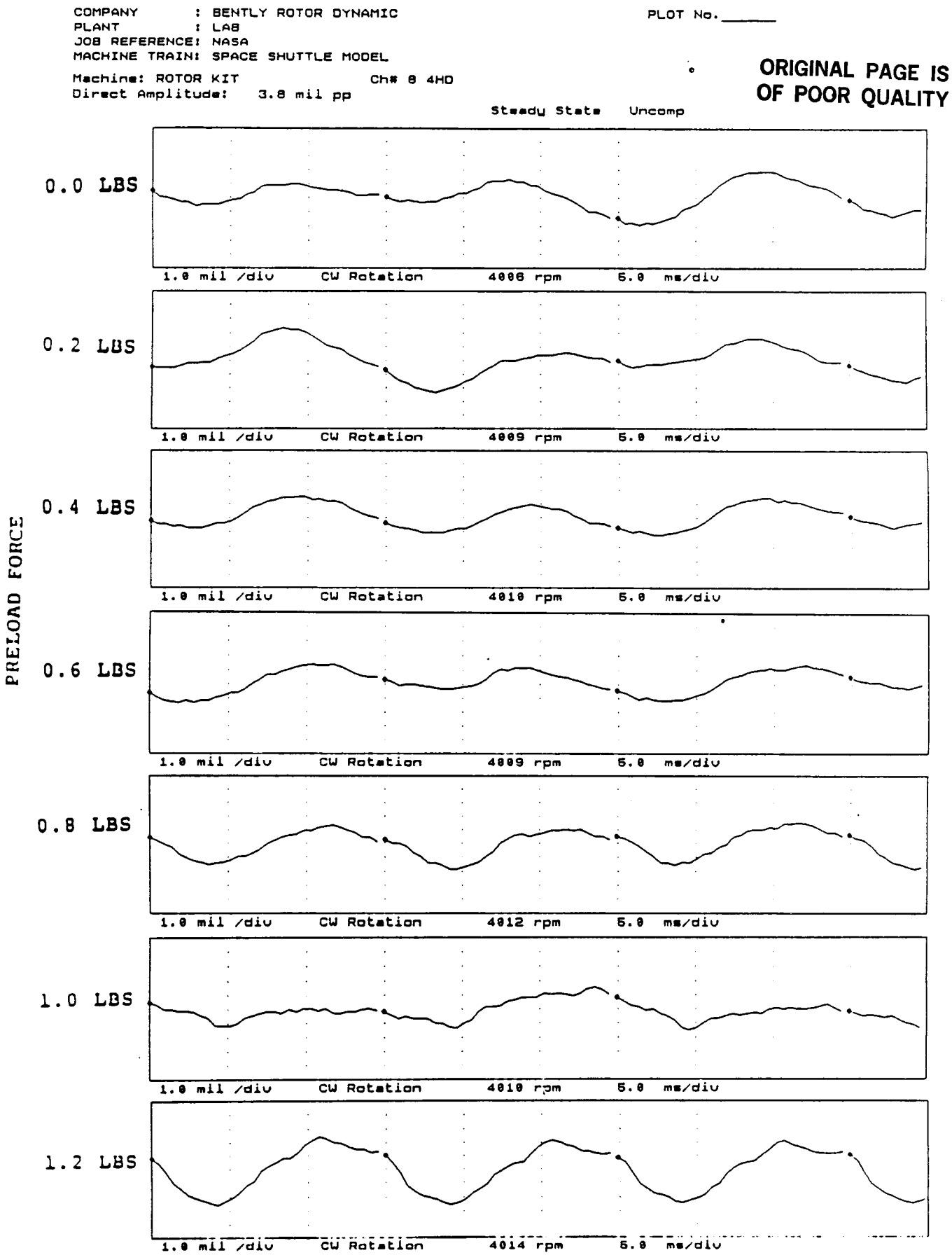

FIGURE 12.21 TIMEBASE FOR HORIZONTAL PROBE AT LOCATION 4 AT 4000 RPM, 0 PSI SEAL OIL PRESSURE, 0.8 IN–GRAM UNBALANCE LOCATED IN THE TURBINE DISK, FOR INCREASING STATIC PRELOADS.

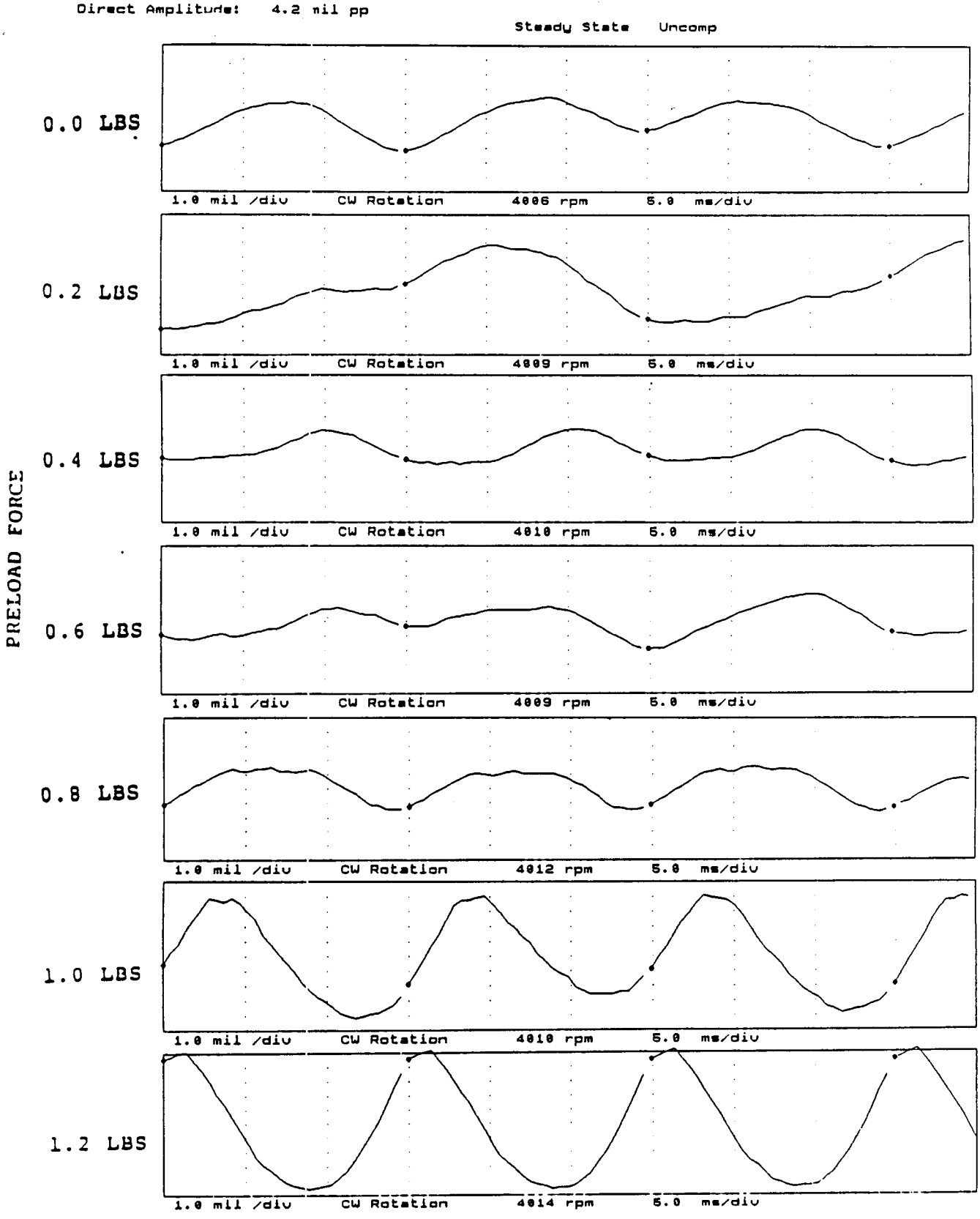

FIGURE 12.22 TIMEBASE FOR VERTICAL PROBE AT LOCATION 5 AT 4000 RPM, 0 PSI SEAL OIL PRESSURE, 0.8 IN–GRAM UNBALANCE LOCATED IN THE TURBINE DISK, FOR INCREASING STATIC PRELOADS.

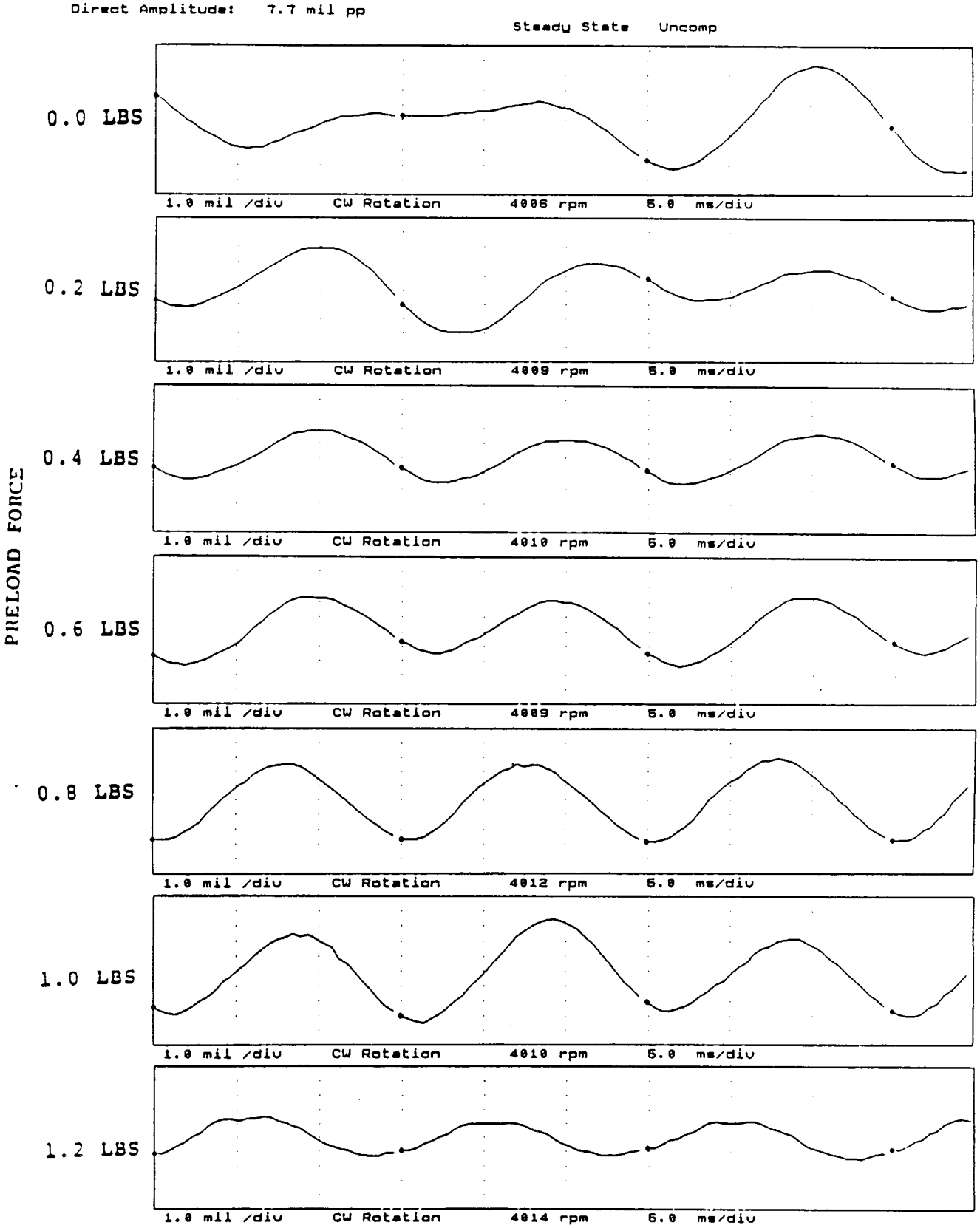

FIGURE 12.23 TIMEBASE FOR HORIZONTAL PROBE AT LOCATION 5 AT 4000 RPM, 0 PSI SEAL OIL PRESSURE, 0.8 IN–GRAM UNBALANCE LOCATED IN THE TURBINE DISK, FOR INCREASING STATIC PRELOADS.

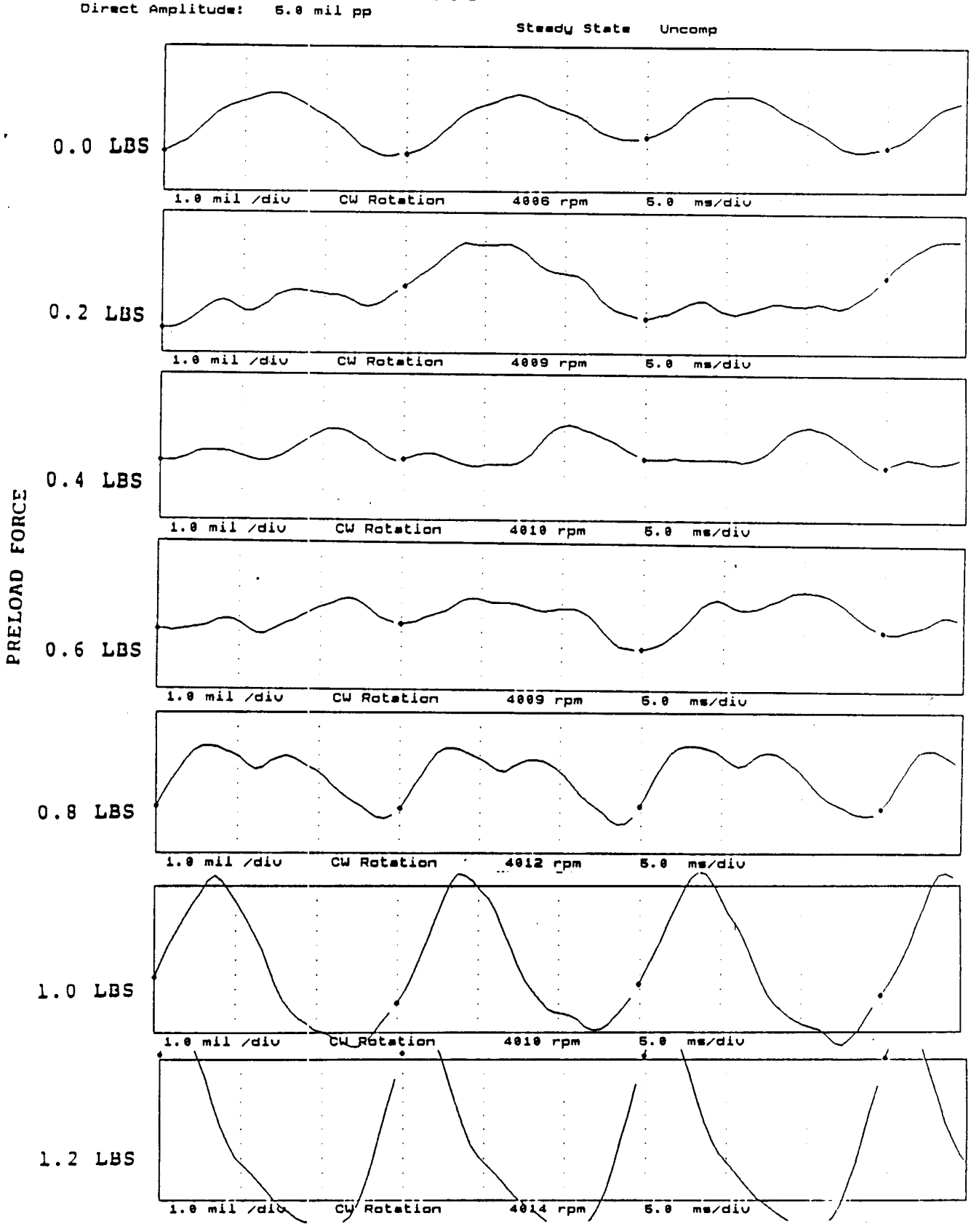

FIGURE 12.24 TIMEBASE FOR VERTICAL PROBE AT LOCATION 6 AT 4000 RPM, 0 PSI SEAL OIL PRESSURE, 0.8 IN–GRAM UNBALANCE LOCATED IN THE TURBINE DISK, FOR INCREASING STATIC PRELOADS.

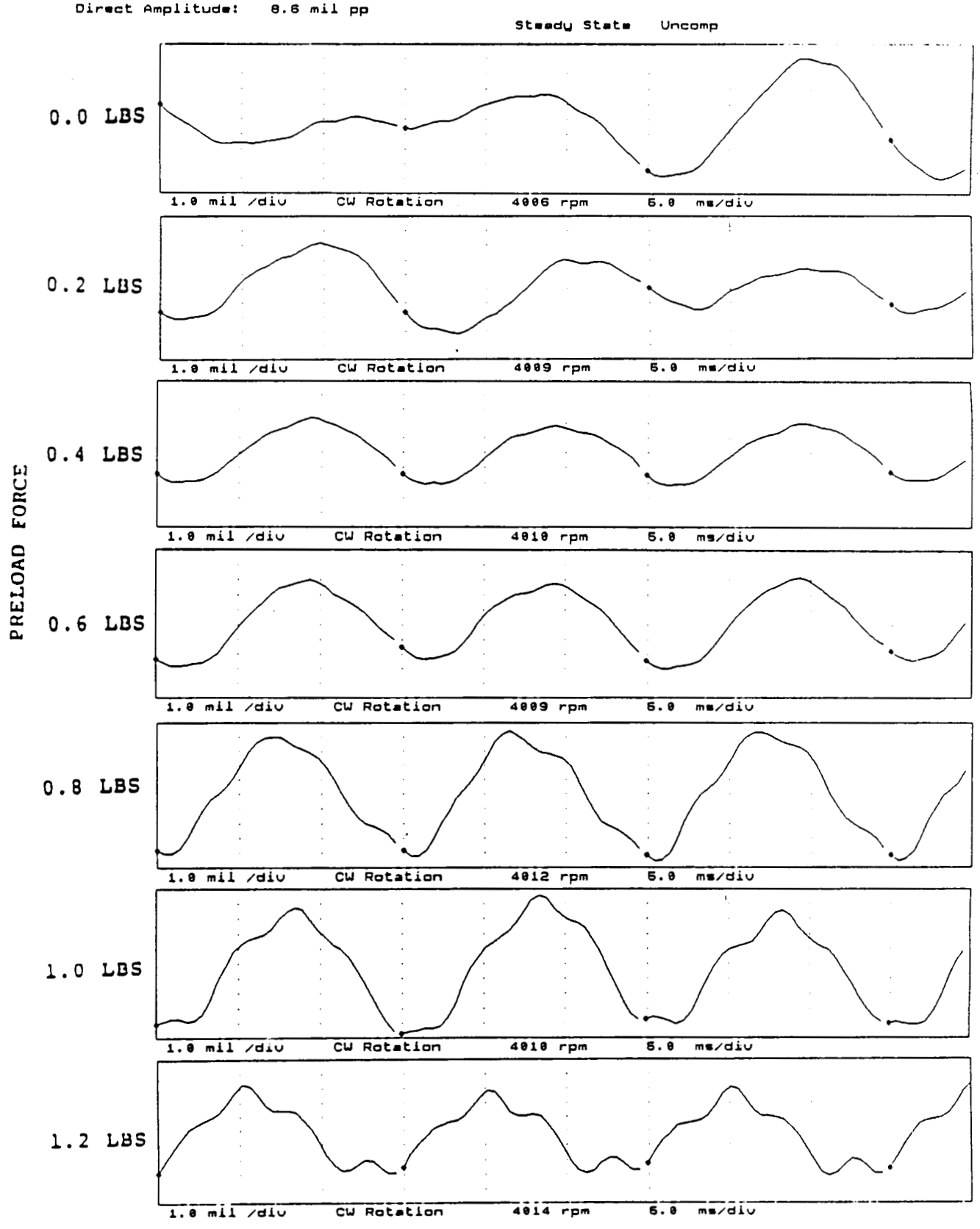

FIGURE 12.25 TIMEBASE FOR HORIZONTAL PROBE AT LOCATION 6 AT 4000 RPM, 0 PSI SEAL OIL PRESSURE, 0.8 IN–GRAM UNBALANCE LOCATED IN THE TURBINE DISK, FOR INCREASING STATIC PRELOADS.

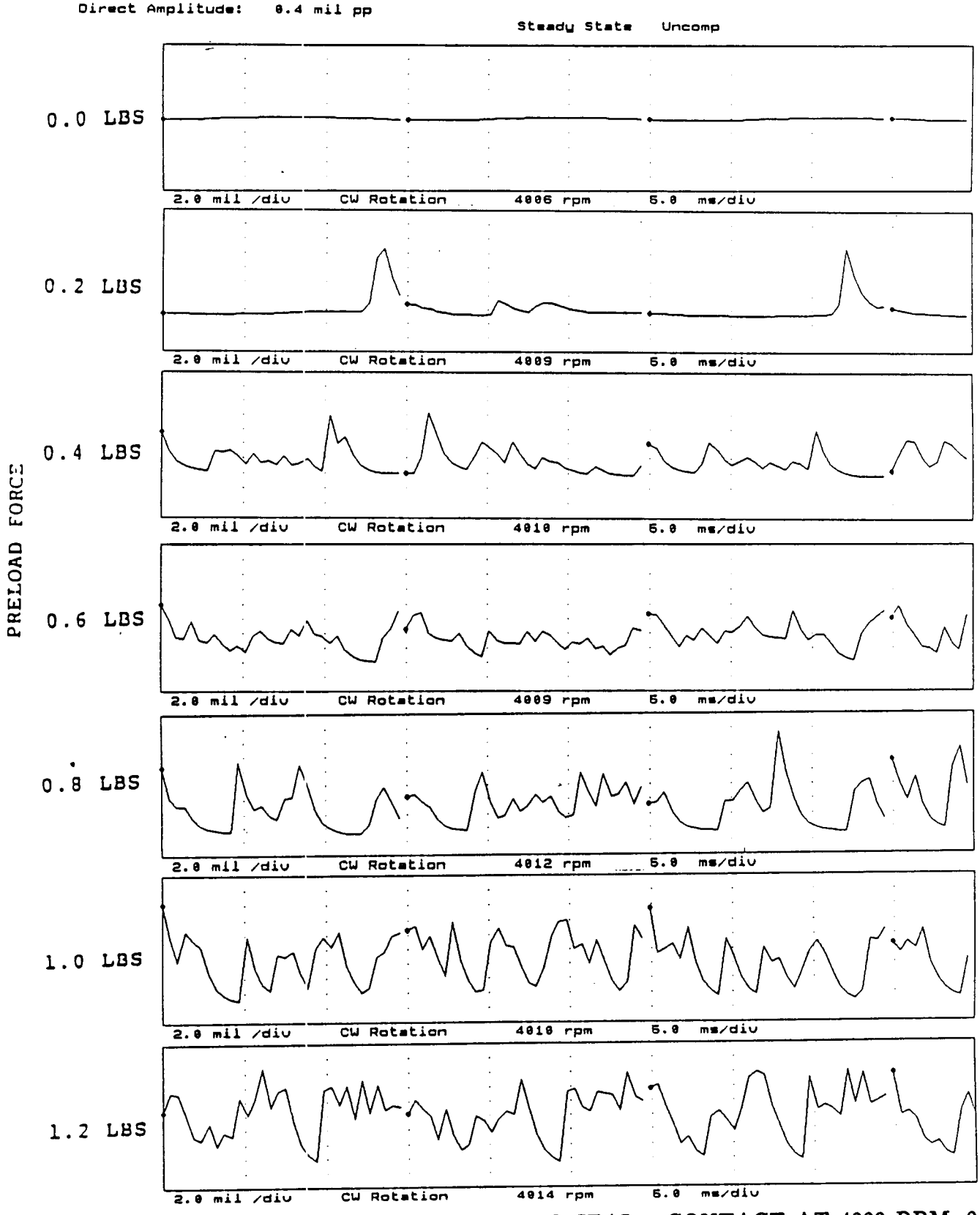

FIGURE 12.26 TIMEBASE FOR SHAFT TO SEAL 1 CONTACT AT 4000 RPM, 0 PSI SEAL OIL PRESSURE, 0.8 IN–GRAM UNBALANCE LOCATED IN THE TURBINE DISK, FOR INCREASING STATIC PRELOADS.

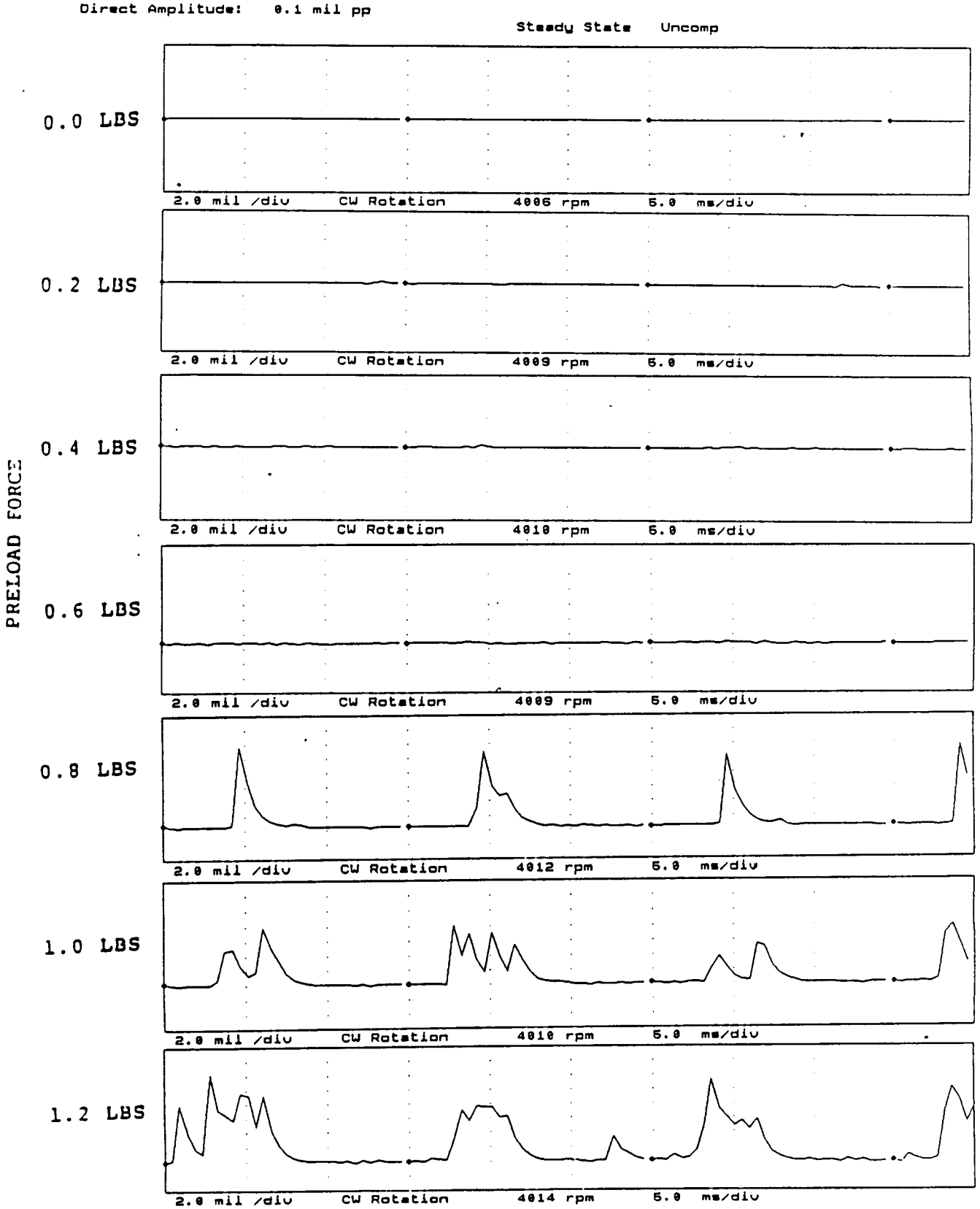

FIGURE 12.27 TIMEBASE FOR SHAFT TO SEAL 2 CONTACT AT 4000 RPM, 0 PSI SEAL OIL PRESSURE, 0.8 IN–GRAM UNBALANCE LOCATED IN THE TURBINE DISK, FOR INCREASING STATIC PRELOADS.

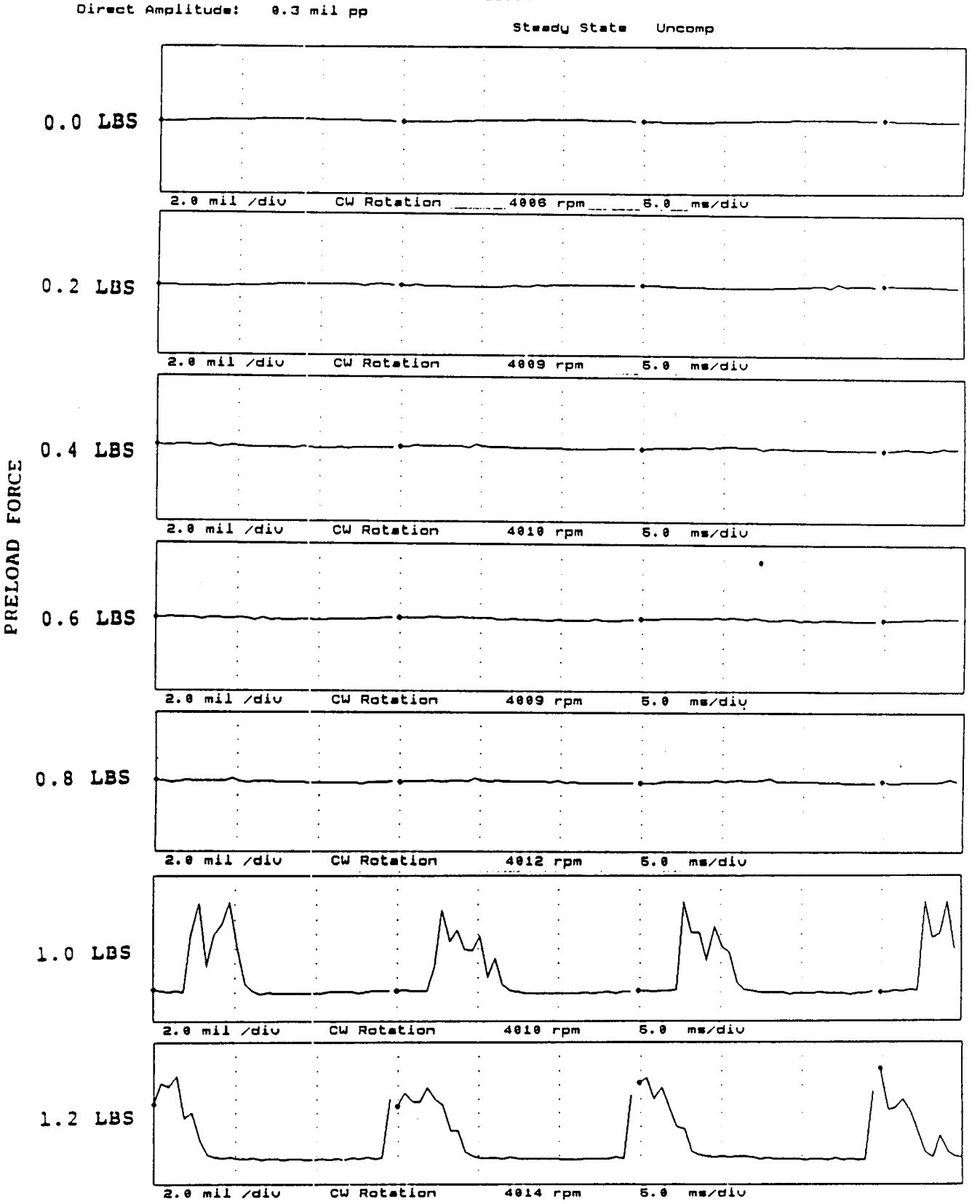

FIGURE 12.28 TIMEBASE FOR SHAFT TO RUB BLOCK CONTACT AT 4000 RPM, 0 PSI SEAL OIL PRESSURE, 0.8 IN–GRAM UNBALANCE LOCATED IN THE TURBINE DISK, FOR INCREASING STATIC PRELOADS.

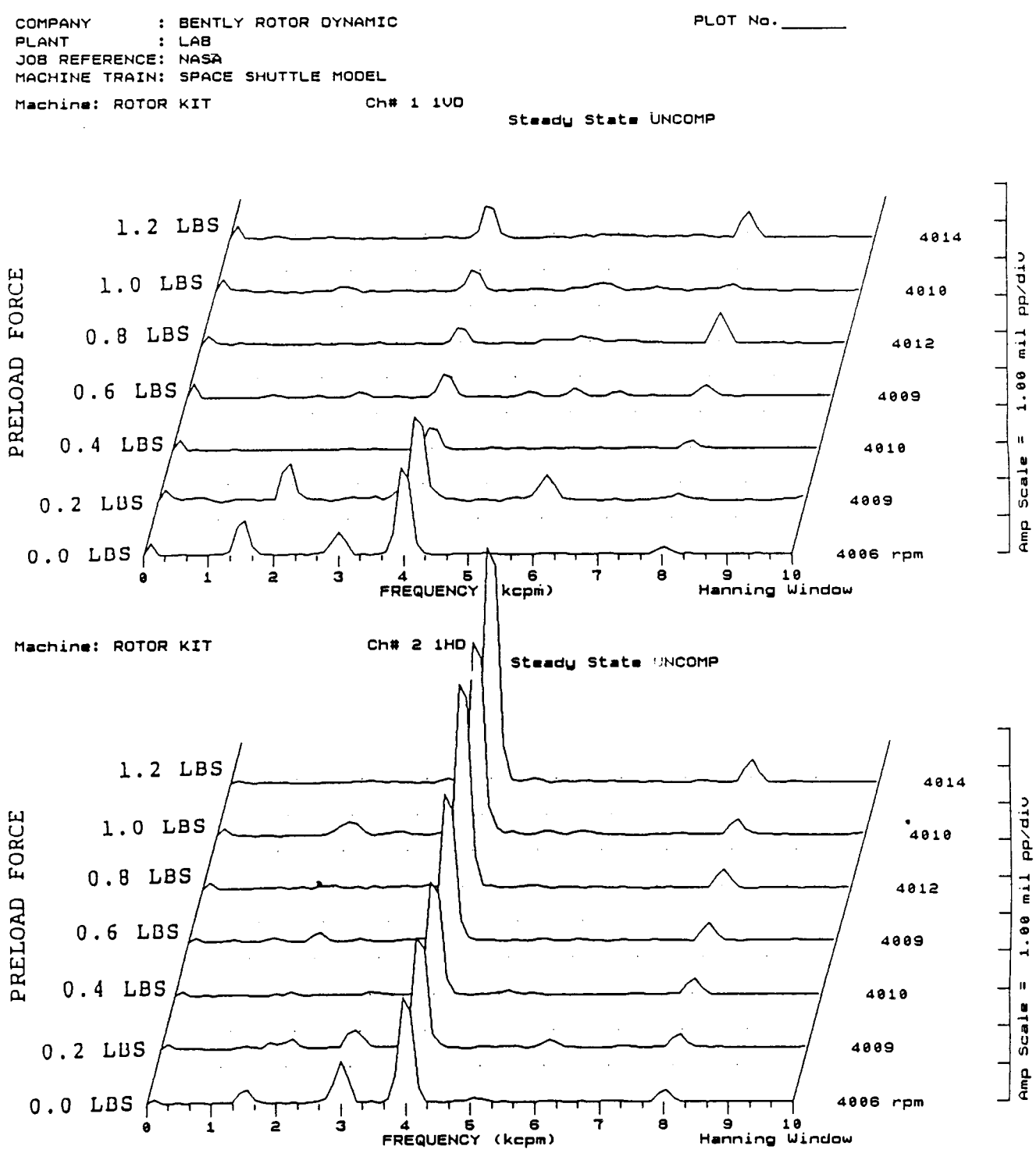

FIGURE 12.29 SPECTRAL CONTENT AT PROBE LOCATION 1 AT 4000 RPM, 0 PSI SEAL OIL PRESSURE, 0.8 IN–GRAM UNBALANCE LOCATED IN THE TURBINE DISK, FOR INCREASING STATIC PRELOADS.

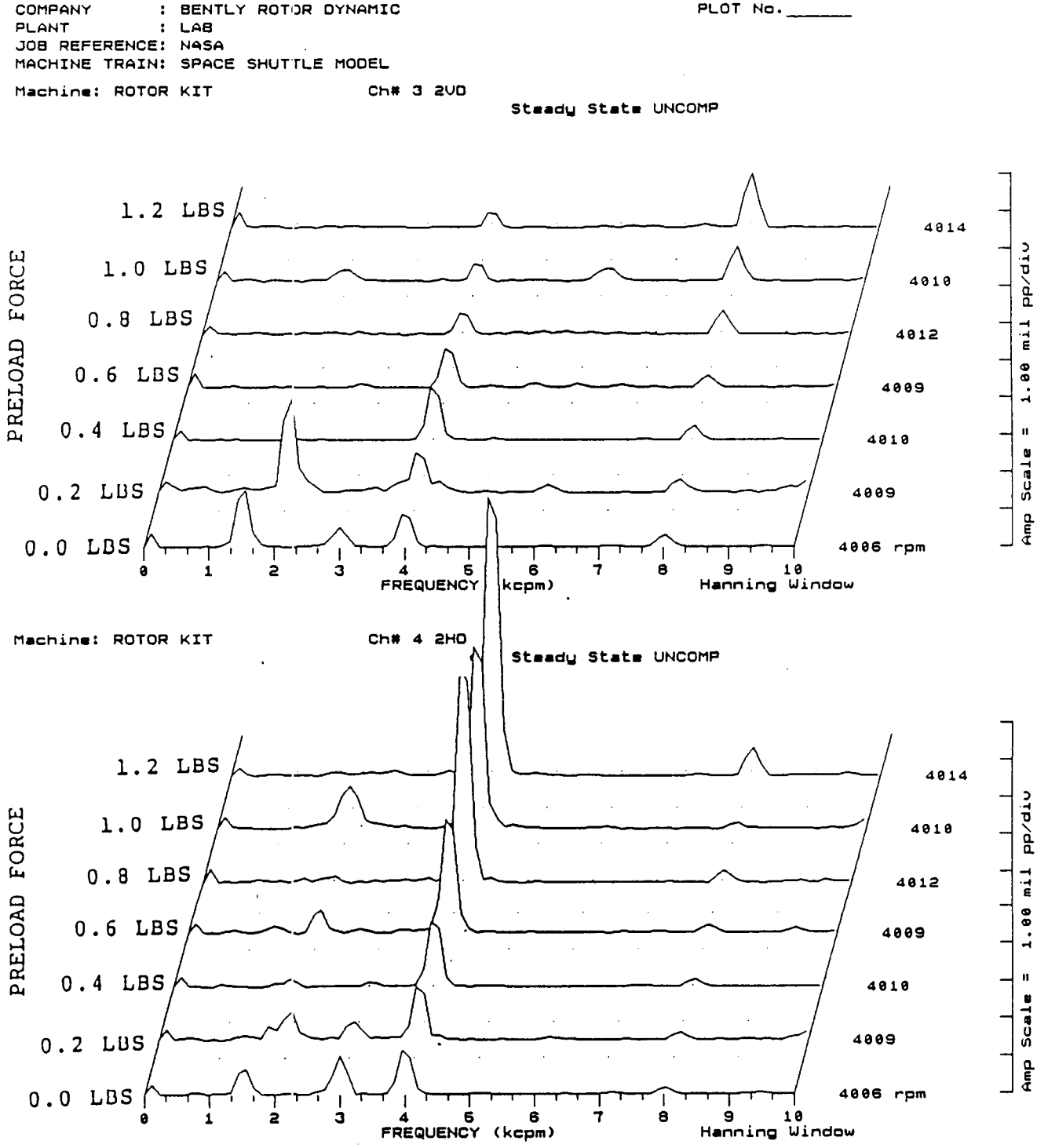

FIGURE 12.30 SPECTRAL CONTENT AT PROBE LOCATION 2 AT 4000 RPM, 0 PSI SEAL OIL PRESSURE, 0.8 IN–GRAM UNBALANCE LOCATED IN THE TURBINE DISK, FOR INCREASING STATIC PRELOADS.

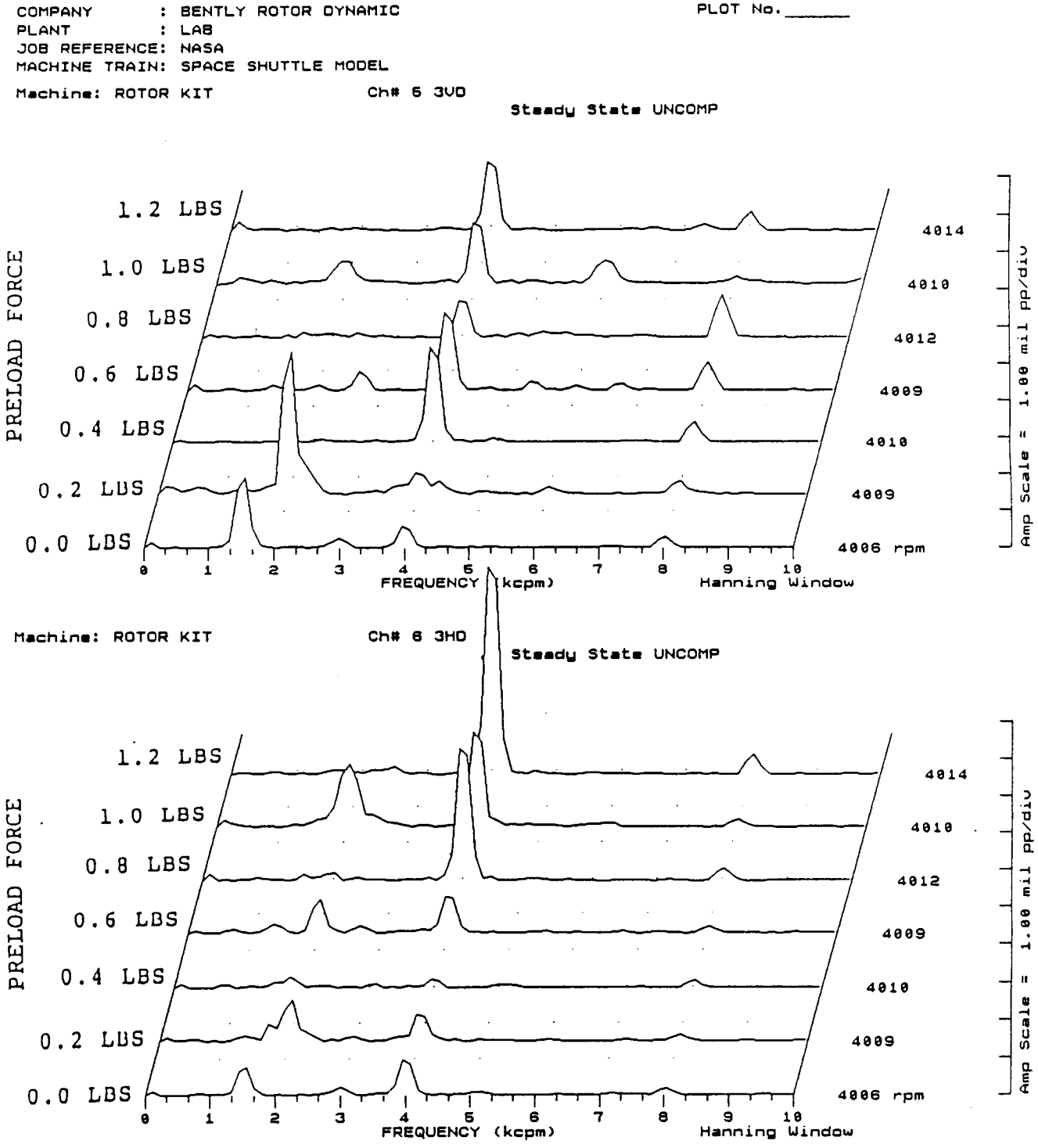

FIGURE 12.31 SPECTRAL CONTENT AT PROBE LOCATION 3 AT 4000 RPM, 0 PSI SEAL OIL PRESSURE, 0.8 IN–GRAM UNBALANCE LOCATED IN THE TURBINE DISK, FOR INCREASING STATIC PRELOADS.

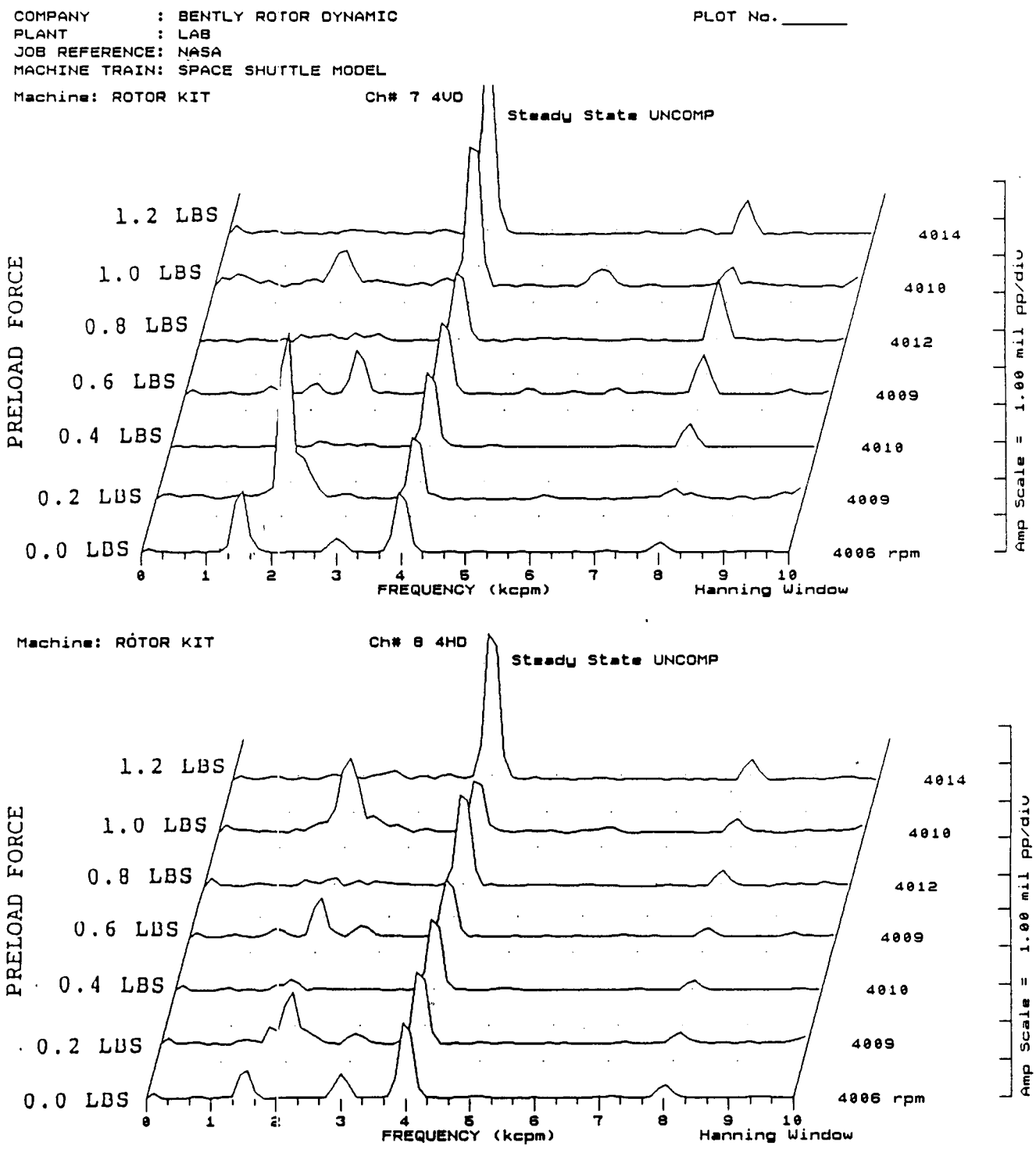

FIGURE 12.32 SPECTRAL CONTENT AT PROBE LOCATION 4 AT 4000 RPM, 0 PSI SEAL OIL PRESSURE, 0.8 IN–GRAM UNBALANCE LOCATED IN THE TURBINE DISK, FOR INCREASING STATIC PRELOADS.

C-4

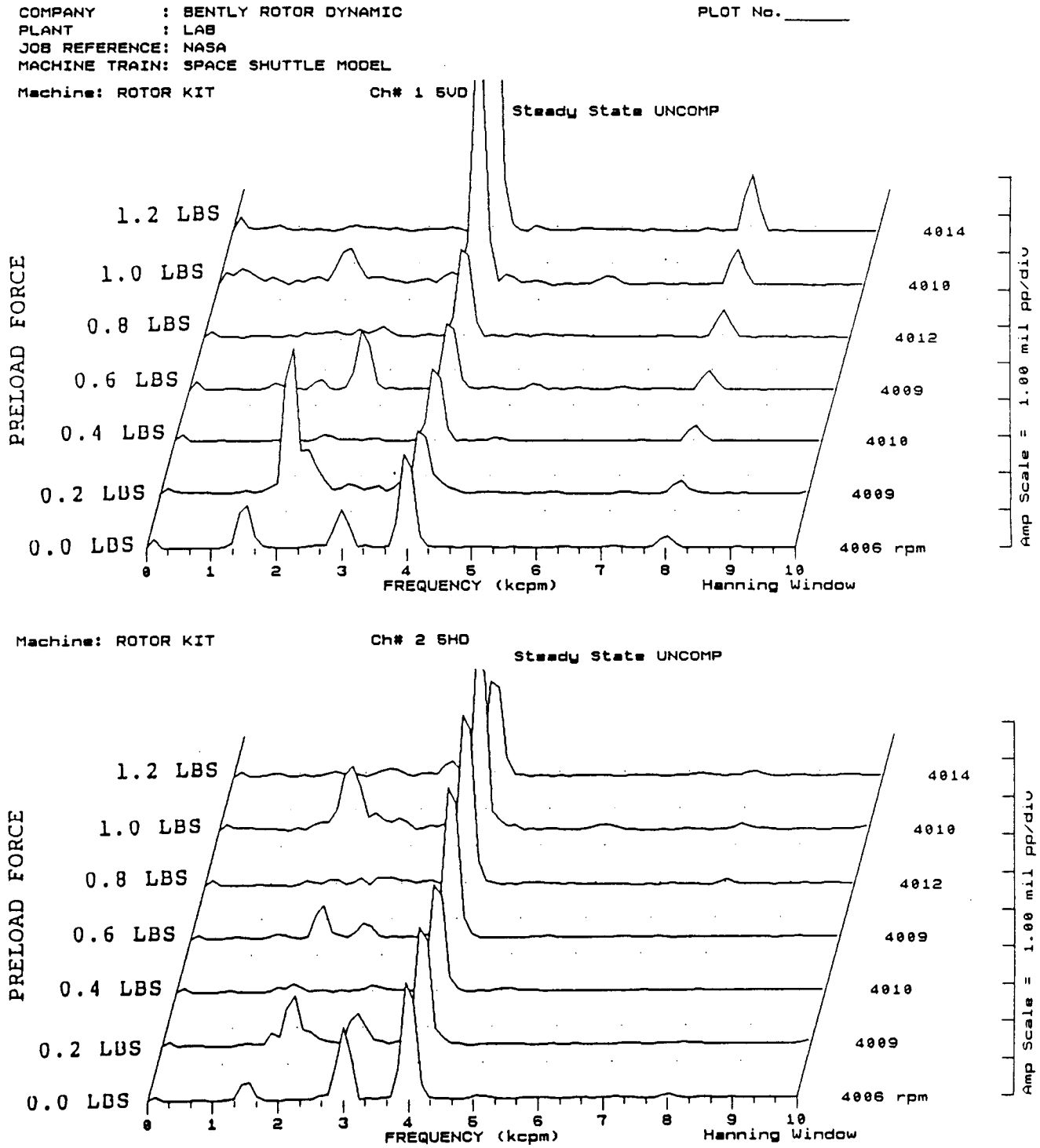

FIGURE 12.33 SPECTRAL CONTENT AT PROBE LOCATION 5 AT 4000 RPM, 0 PSI SEAL OIL PRESSURE, 0.8 IN–GRAM UNBALANCE LOCATED IN THE TURBINE DISK, FOR INCREASING STATIC PRELOADS.

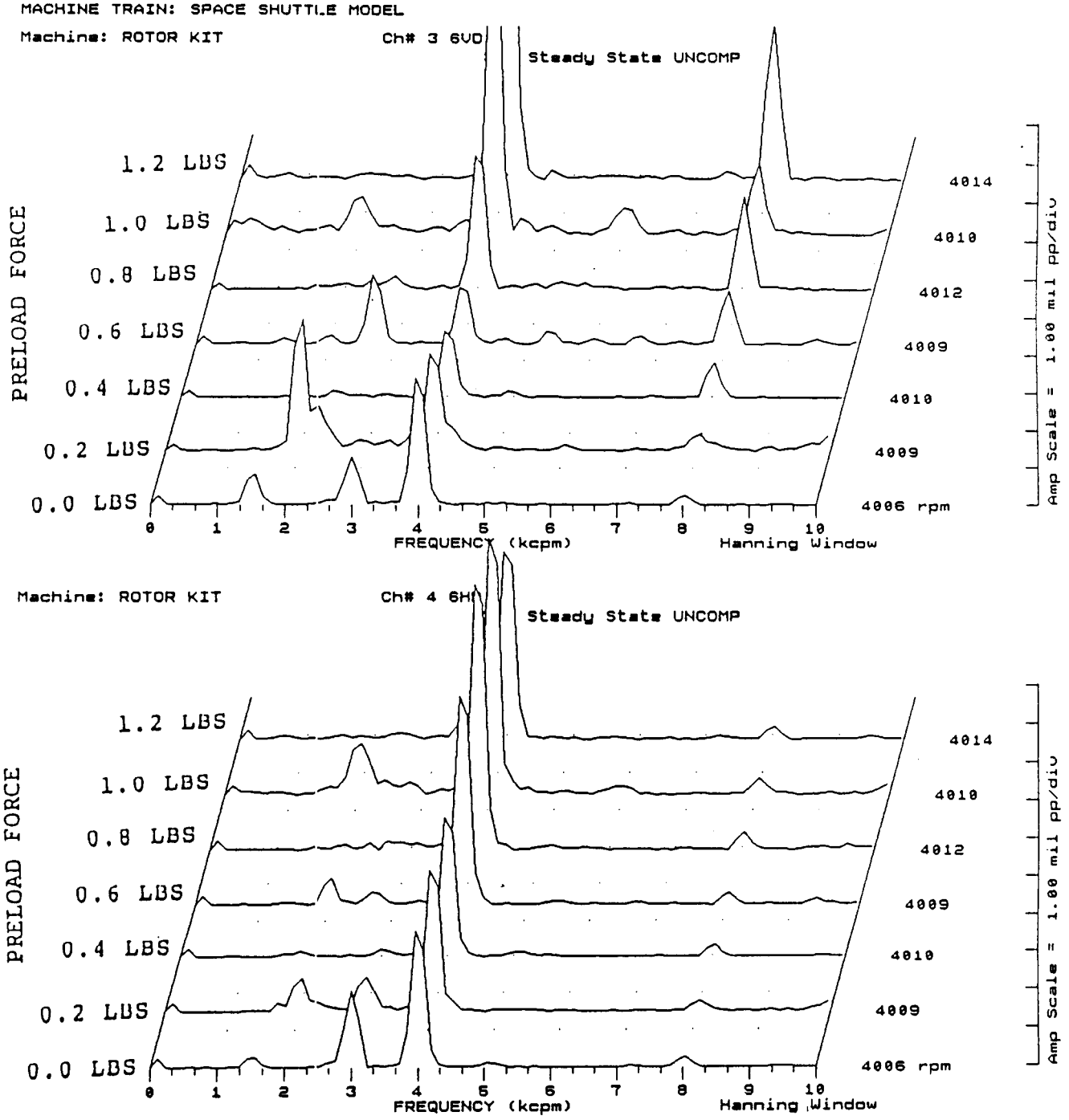

FIGURE 12.34 SPECTRAL CONTENT AT PROBE LOCATION 6 AT 4000 RPM, 0 PSI SEAL OIL PRESSURE, 0.8 IN–GRAM UNBALANCE LOCATED IN THE TURBINE DISK, FOR INCREASING STATIC PRELOADS.

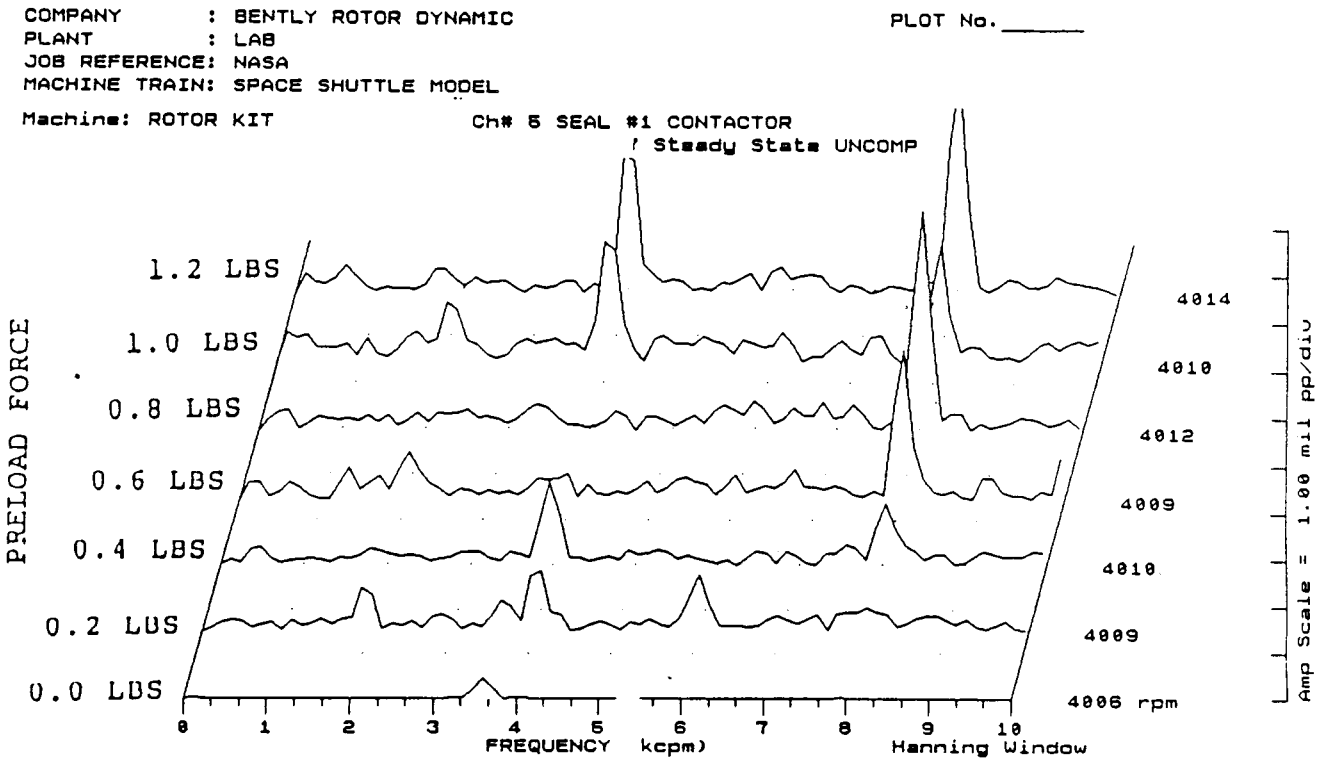

FIGURE 12.35 SPECTRAL CONTENT FOR SHAFT TO SEAL 1 CONTACT AT 4000 RPM, 0 PSI SEAL OIL PRESSURE, 0.8 IN–GRAM UNBALANCE LOCATED IN THE TURBINE DISK, FOR INCREASING STATIC PRELOADS.

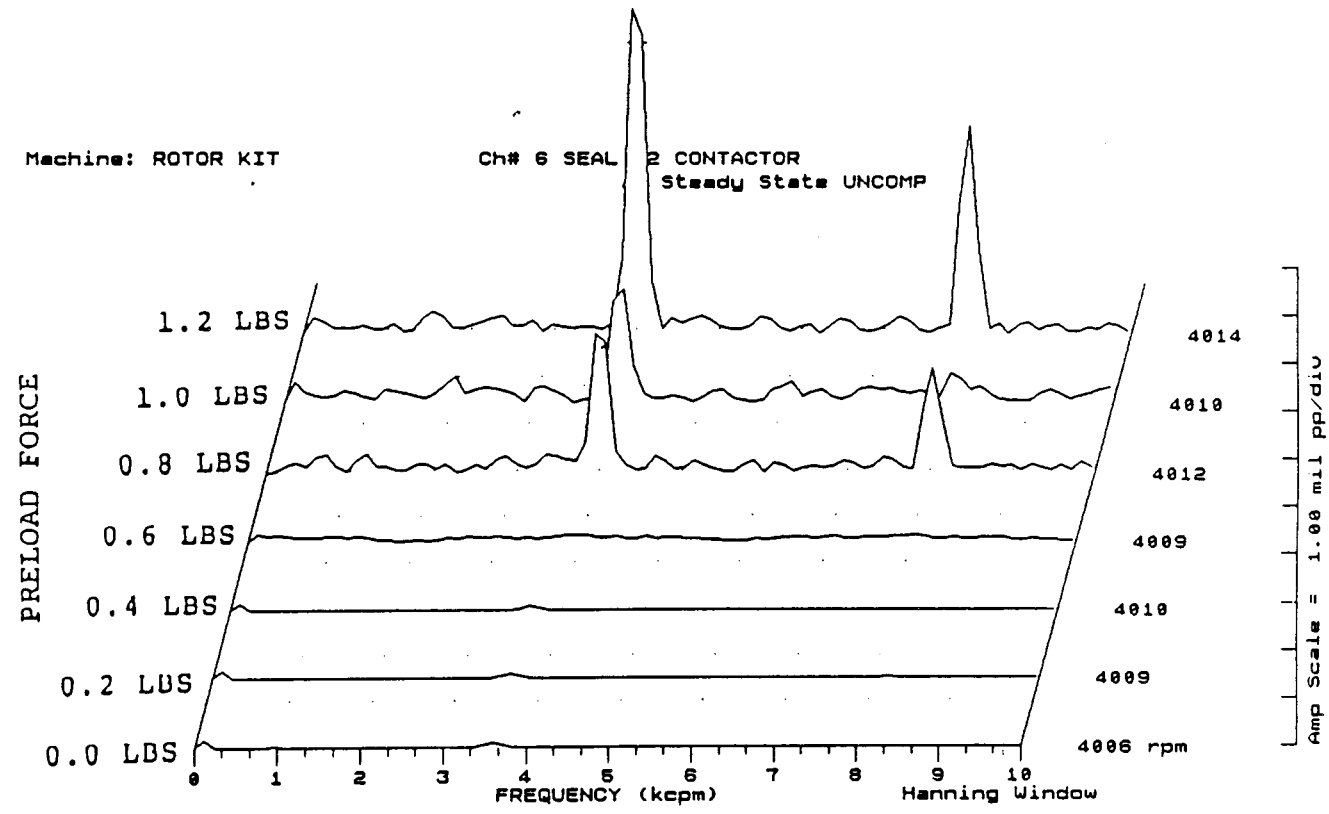

FIGURE 12.36 SPECTRAL CONTENT FOR SHAFT TO SEAL 2 CONTACT AT 4000 RPM, 0 PSI SEAL OIL PRESSURE, 0.8 IN–GRAM UNBALANCE LOCATED IN THE TURBINE DISK, FOR INCREASING STATIC PRELOADS.

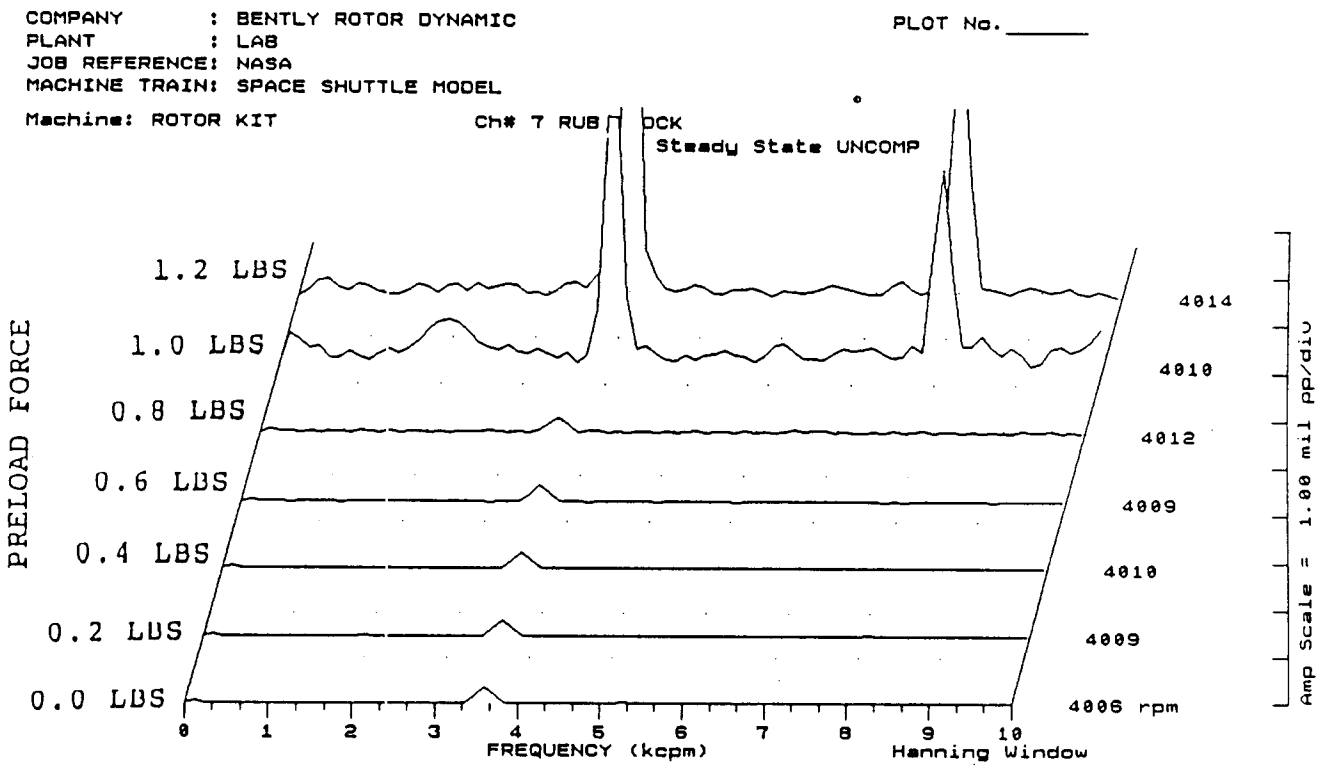

FIGURE 12.37 SPECTRAL CONTENT FOR SHAFT TO RUB BLOCK CONTACT AT 4000 RPM, 0 PSI SEAL OIL PRESSURE, 0.8 IN–GRAM UNBALANCE LOCATED IN THE . TURBINE DISK, FOR INCREASING STATIC PRELOADS.

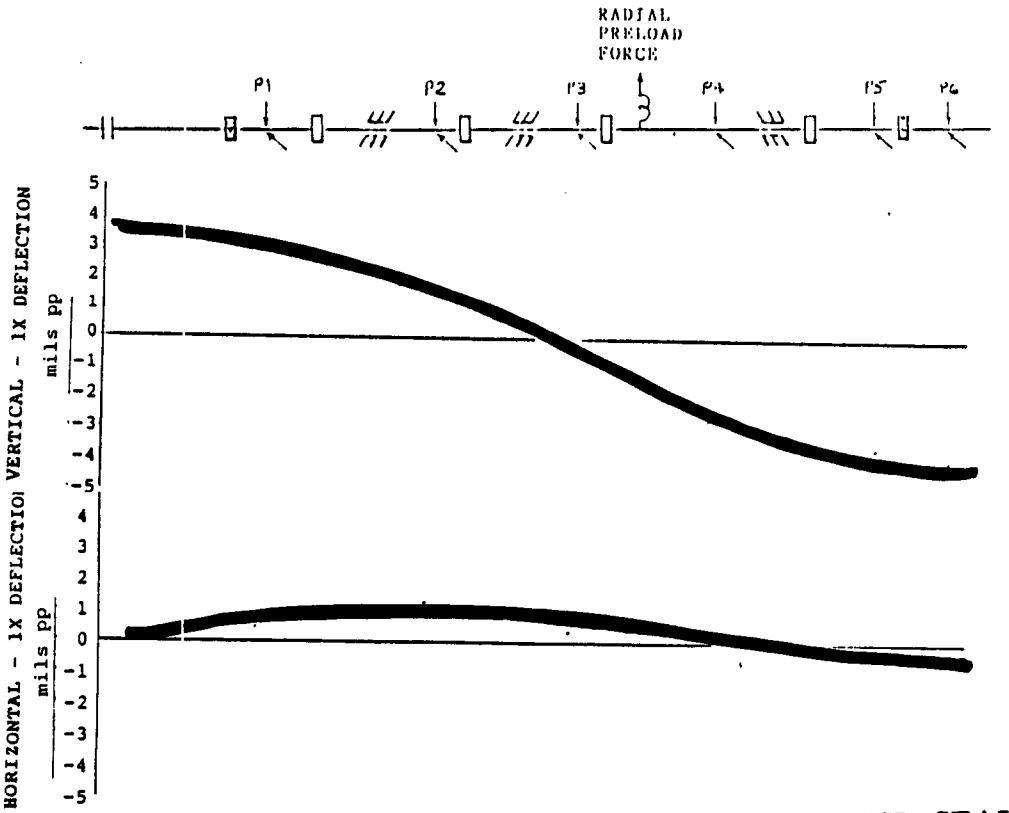

FIGURE 12.38 ROTOR MODE SHAPE AT 4000 RPM, 2.5 PSI SEAL OIL PRESSURE DUE TO 0.8 IN–GRAM UNBALANCE LOCATED IN THE TURBINE DISK.

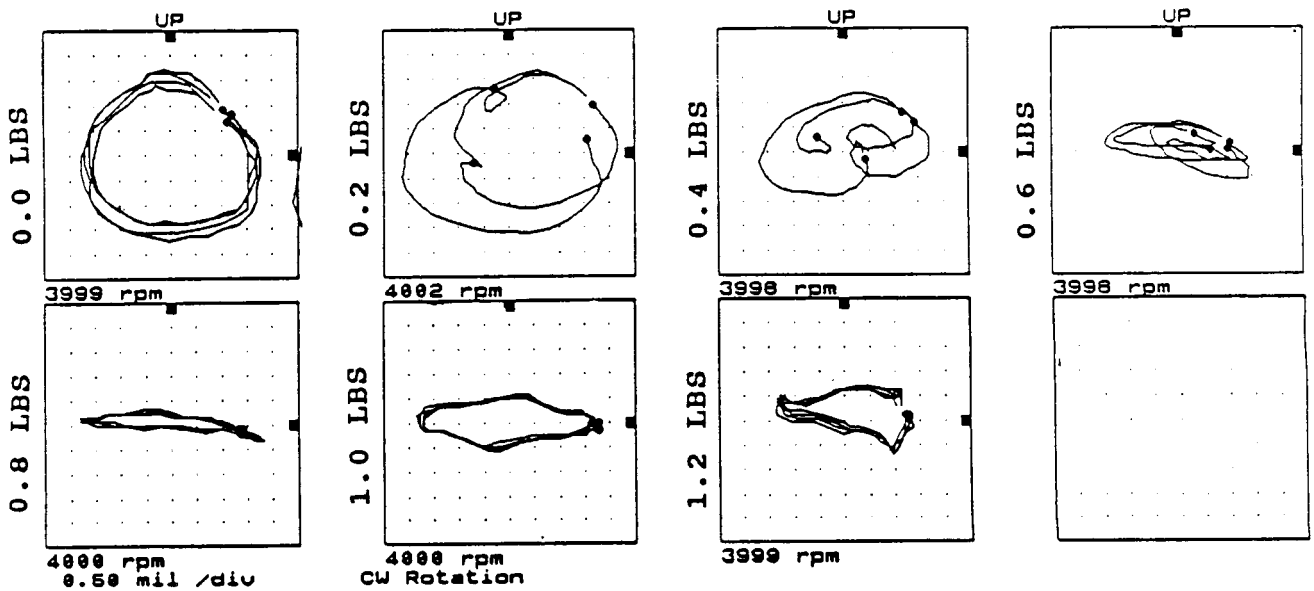

FIGURE 12.39 ORBITS AT PROBE LOCATION 1 AT 4000 RPM, 2.5 PSI SEAL OIL PRESSURE, 0.8 IN–GRAM UNBALANCE LOCATED IN THE TURBINE DISK, FOR INCREASING STATIC PRELOAD FORCES.

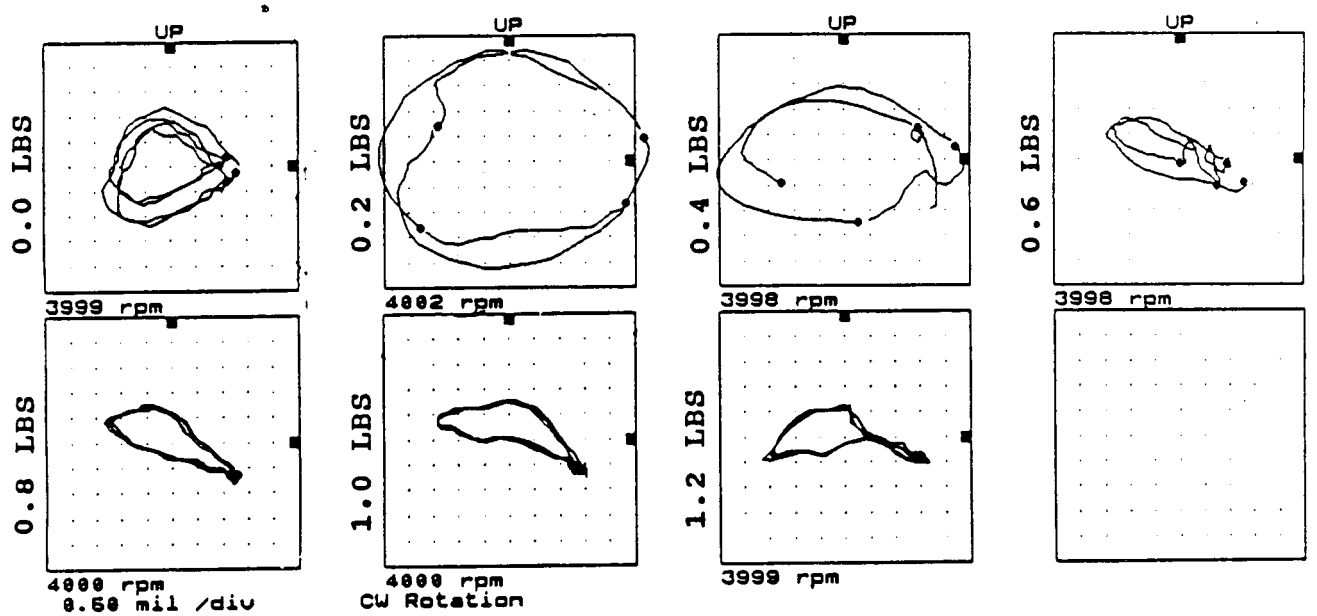

FIGURE 12.40 ORBITS AT PROBE LOCATION 2 AT 4000 RPM, 2.5 PSI SEAL OIL PRESSURE, 0.8 IN–GRAM UNBALANCE LOCATED IN THE TURBINE DISK, FOR INCREASING STATIC PRELOAD FORCES.

COMPANY : BENTLY ROTOR DYNAMIC PLOT No._____
PLANT : LAB
JOB REFERENCE: NASA
MACHINE TRAIN: SPACE SHUTTLE MODEL

Machine: ROTOR KIT Ch# 5 3VD 0 deg.
Machine: ROTOR KIT Ch# 6 3HD 270 deg.
Steady State Uncomp

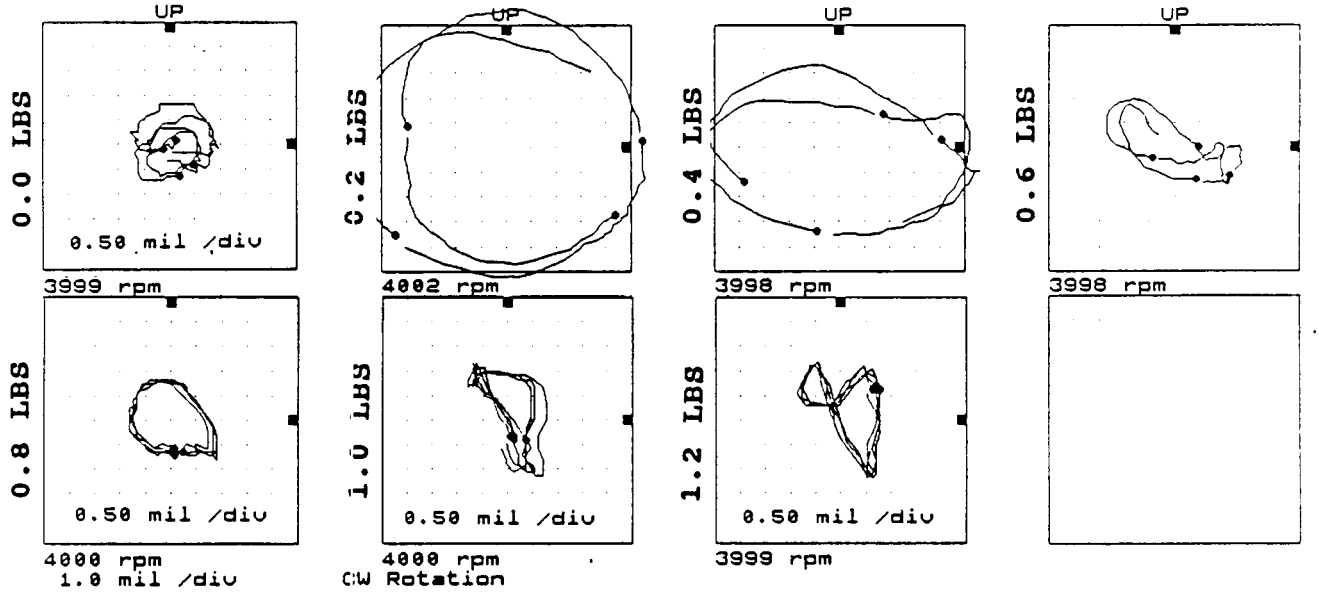

FIGURE 12.41 ORBITS AT PROBE LOCATION 3 AT 4000 RPM, 2.5 PSI SEAL OIL PRESSURE, 0.8 IN–GRAM UNBALANCE LOCATED IN THE TURBINE DISK, FOR INCREASING STATIC PRELOAD FORCES.

Machine: ROTOR KIT Ch# 7 4VD 0 deg.
Machine: ROTOR KIT Ch# 8 4HD 270 deg.
Steady State Uncomp

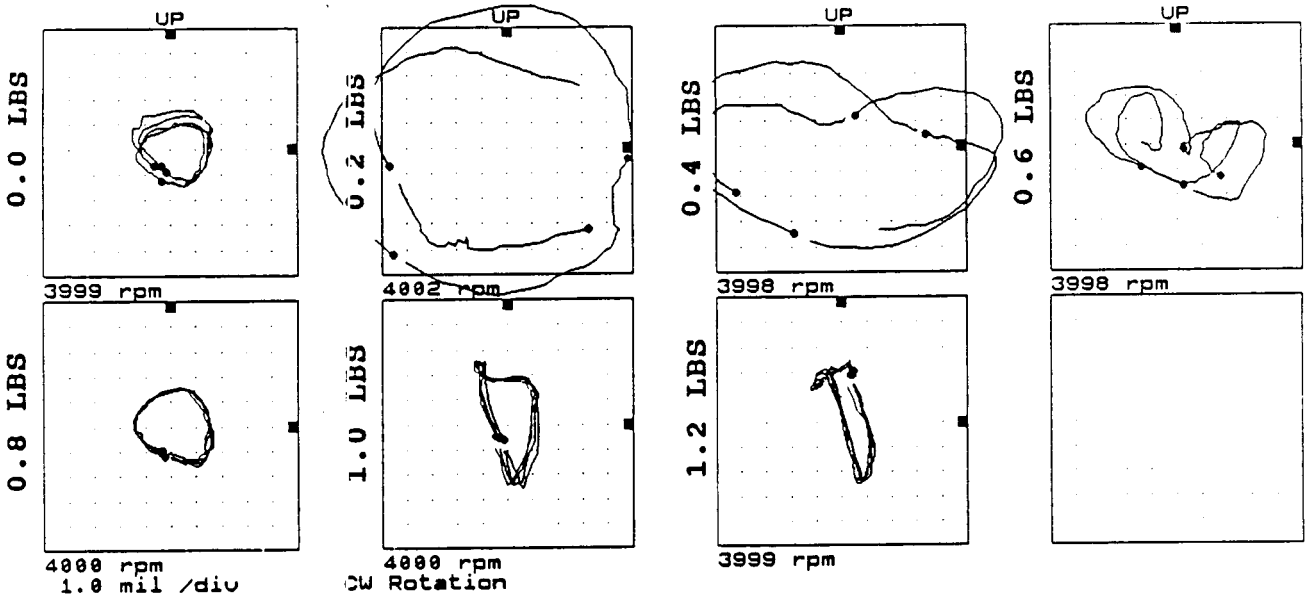

FIGURE 12.42 ORBITS AT PROBE LOCATION 4 AT 4000 RPM, 2.5 PSI SEAL OIL PRESSURE, 0.8 IN–GRAM UNBALANCE LOCATED IN THE TURBINE DISK, FOR INCREASING STATIC PRELOAD FORCES.

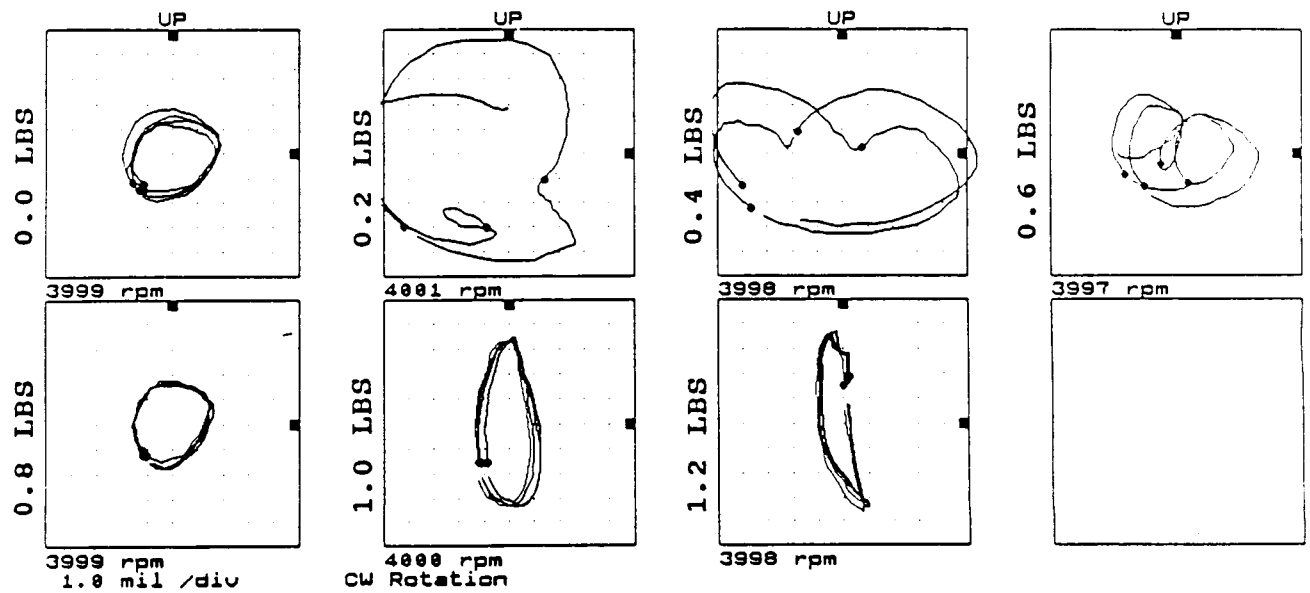

FIGURE 12.43 ORBITS AT PROBE LOCATION 5 AT 4000 RPM, 2.5 PSI SEAL OIL PRESSURE, 0.8 IN–GRAM UNBALANCE LOCATED IN THE TURBINE DISK, FOR INCREASING STATIC PRELOAD FORCES.

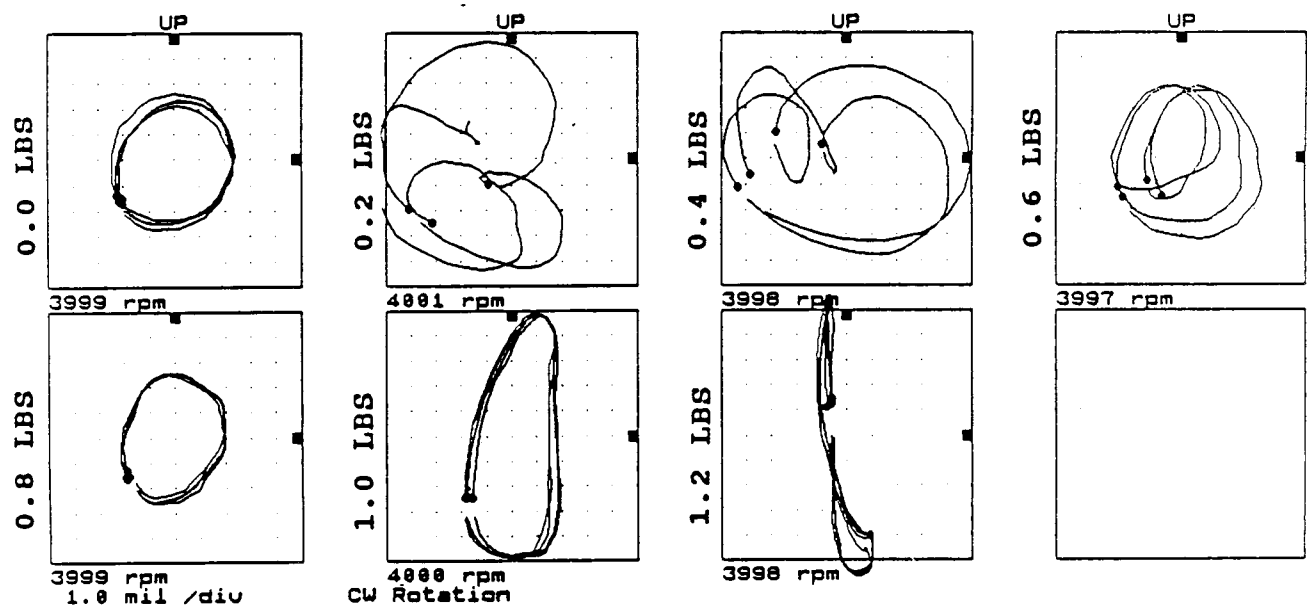

FIGURE 12.44 ORBITS AT PROBE LOCATION 6 AT 4000 RPM, 2.5 PSI SEAL OIL PRESSURE, 0.8 IN–GRAM UNBALANCE LOCATED IN THE TURBINE DISK, FOR INCREASING STATIC PRELOAD FORCES.

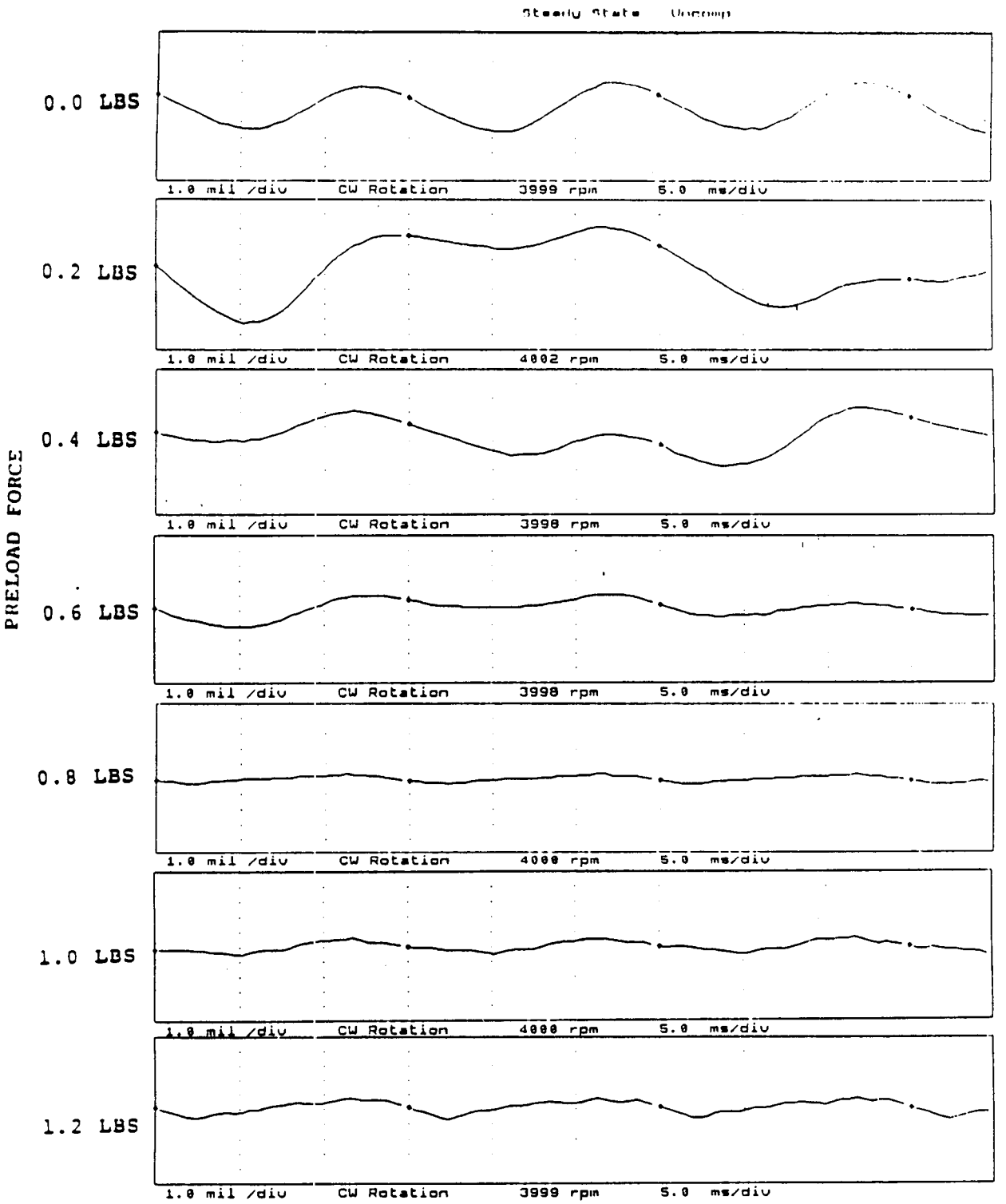

FIGURE 12.45 TIMEBASE FOR VERTICAL PROBE AT LOCATION 1 AT 4000 RPM, 2.5 PSI SEAL OIL PRESSURE, 0.8 IN–GRAM UNBALANCE LOCATED IN THE TURBINE DISK, FOR INCREASING STATIC PRELOADS.

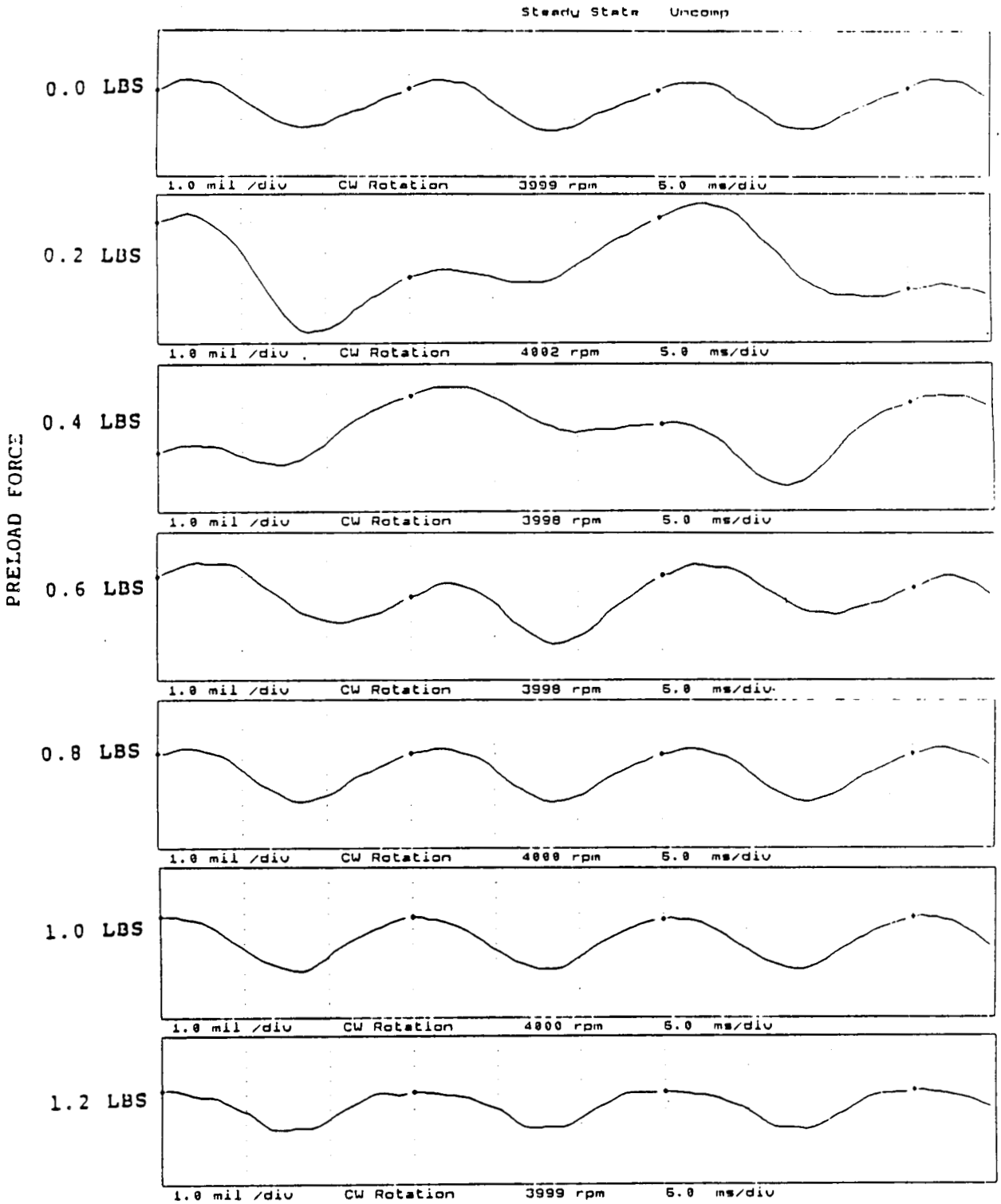

FIGURE 12.46 TIMEBASE FOR HORIZONTAL PROBE AT LOCATION 1 AT 4000 RPM, 2.5 PSI SEAL OIL PRESSURE, 0.8 IN–GRAM UNBALANCE LOCATED IN THE TURBINE DISK, FOR INCREASING STATIC PRELOADS.

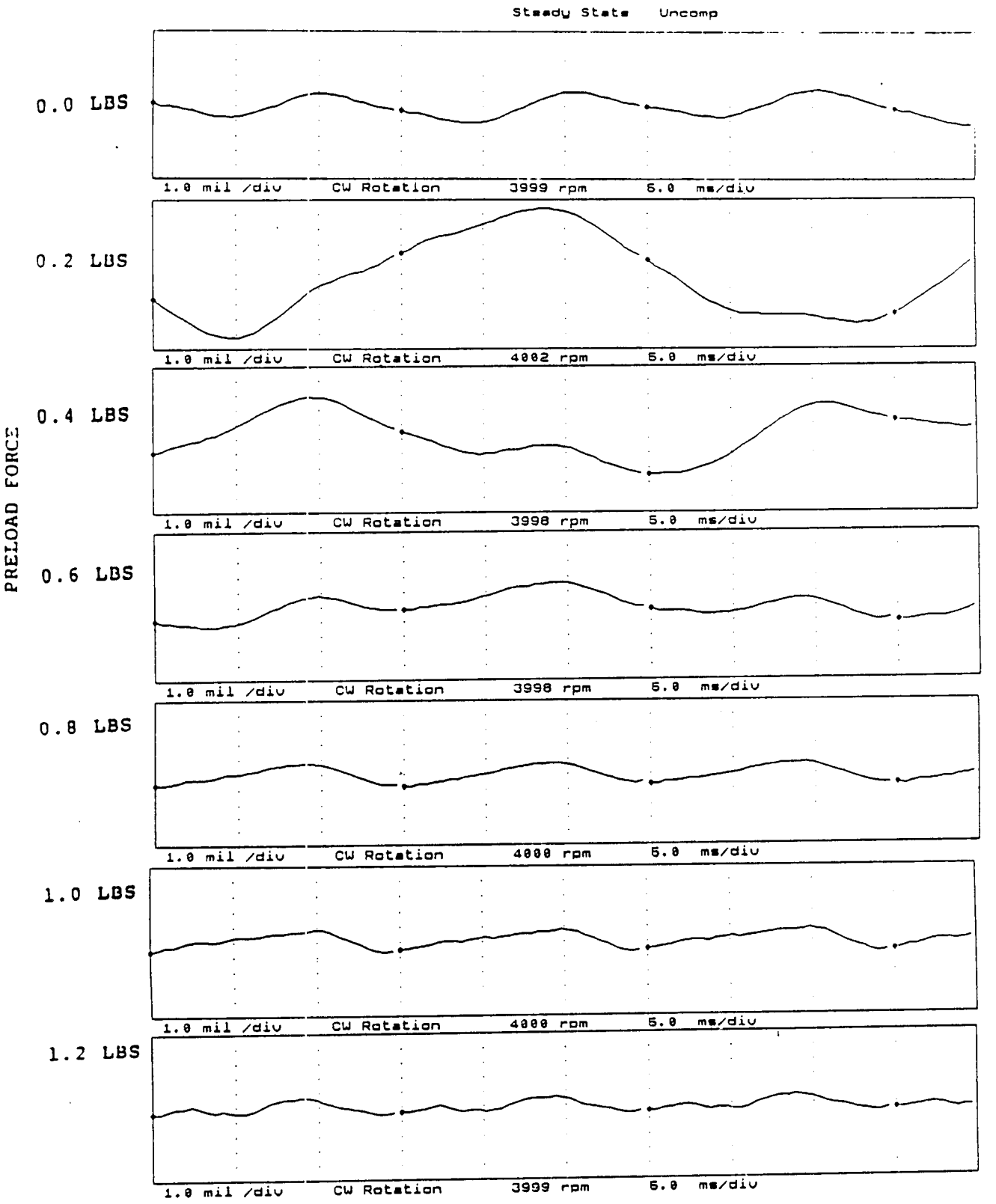

FIGURE 12.47 TIMEBASE FOR VERTICAL PROBE AT LOCATION 2 AT 4000 RPM, 2.5 PSI SEAL OIL PRESSURE, 0.8 IN–GRAM UNBALANCE LOCATED IN THE TURBINE DISK, FOR INCREASING STATIC PRELOADS.

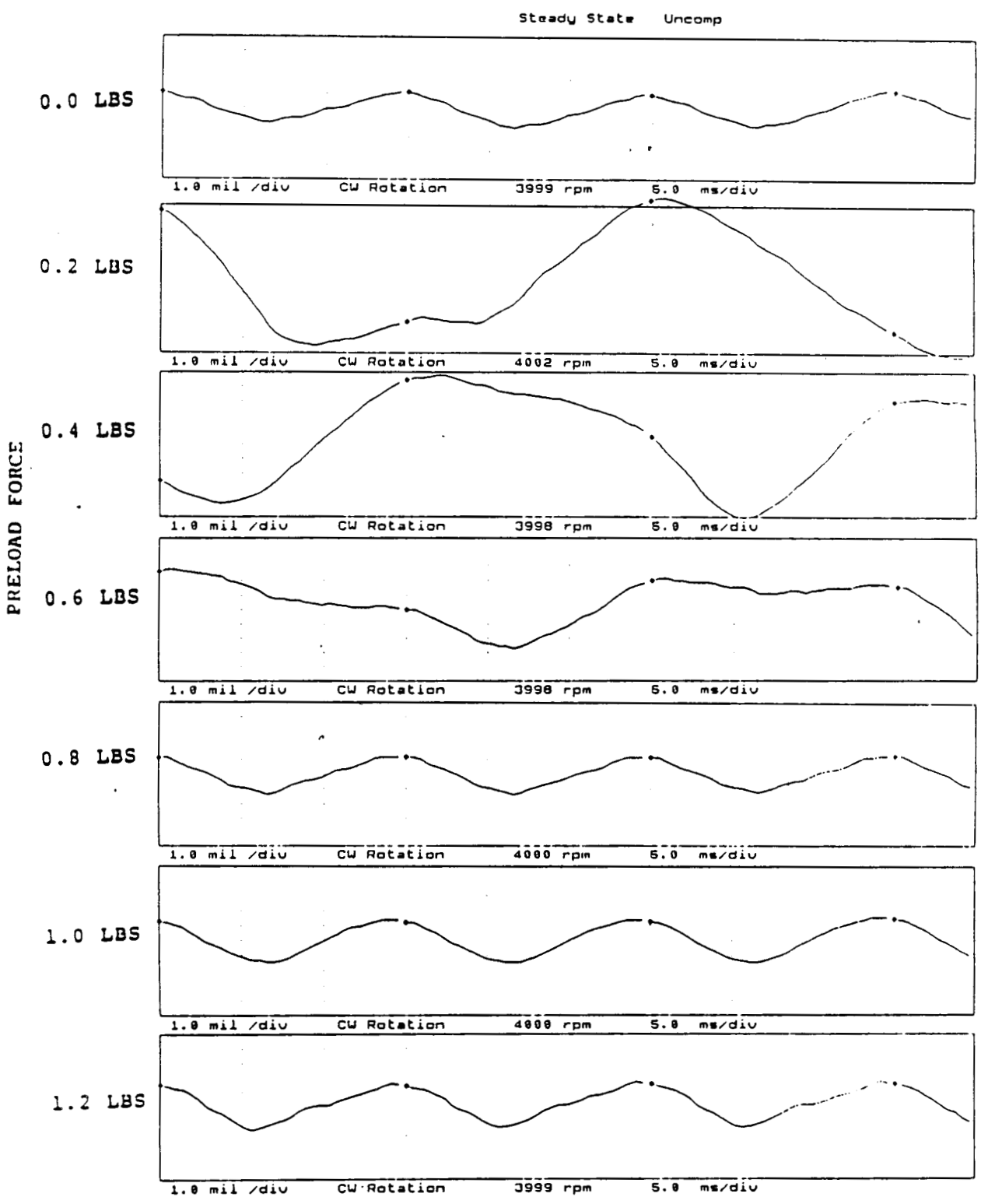

FIGURE 12.48 TIMEBASE FOR HORIZONTAL PROBE AT LOCATION 2 AT 4000 RPM, 2.5 PSI SEAL OIL PRESSURE, 0.8 IN–GRAM UNBALANCE LOCATED IN THE TURBINE DISK, FOR INCREASING STATIC PRELOADS.

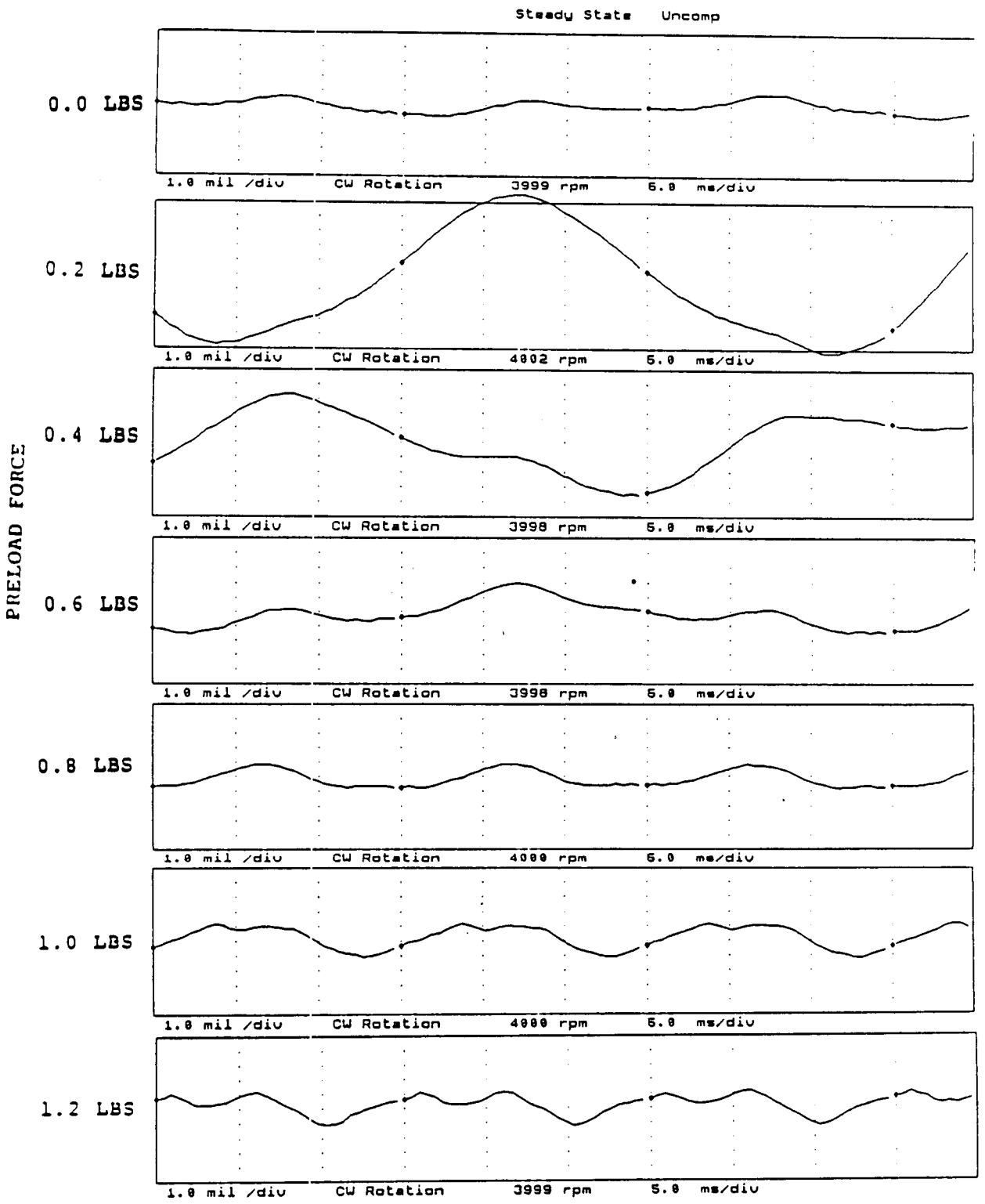

FIGURE 12.49 TIMEBASE FOR VERTICAL PROBE AT LOCATION 3 AT 4000 RPM, 2.5 PSI SEAL OIL PRESSURE, 0.8 IN–GRAM UNBALANCE LOCATED IN THE TURBINE DISK, FOR INCREASING STATIC PRELOADS.

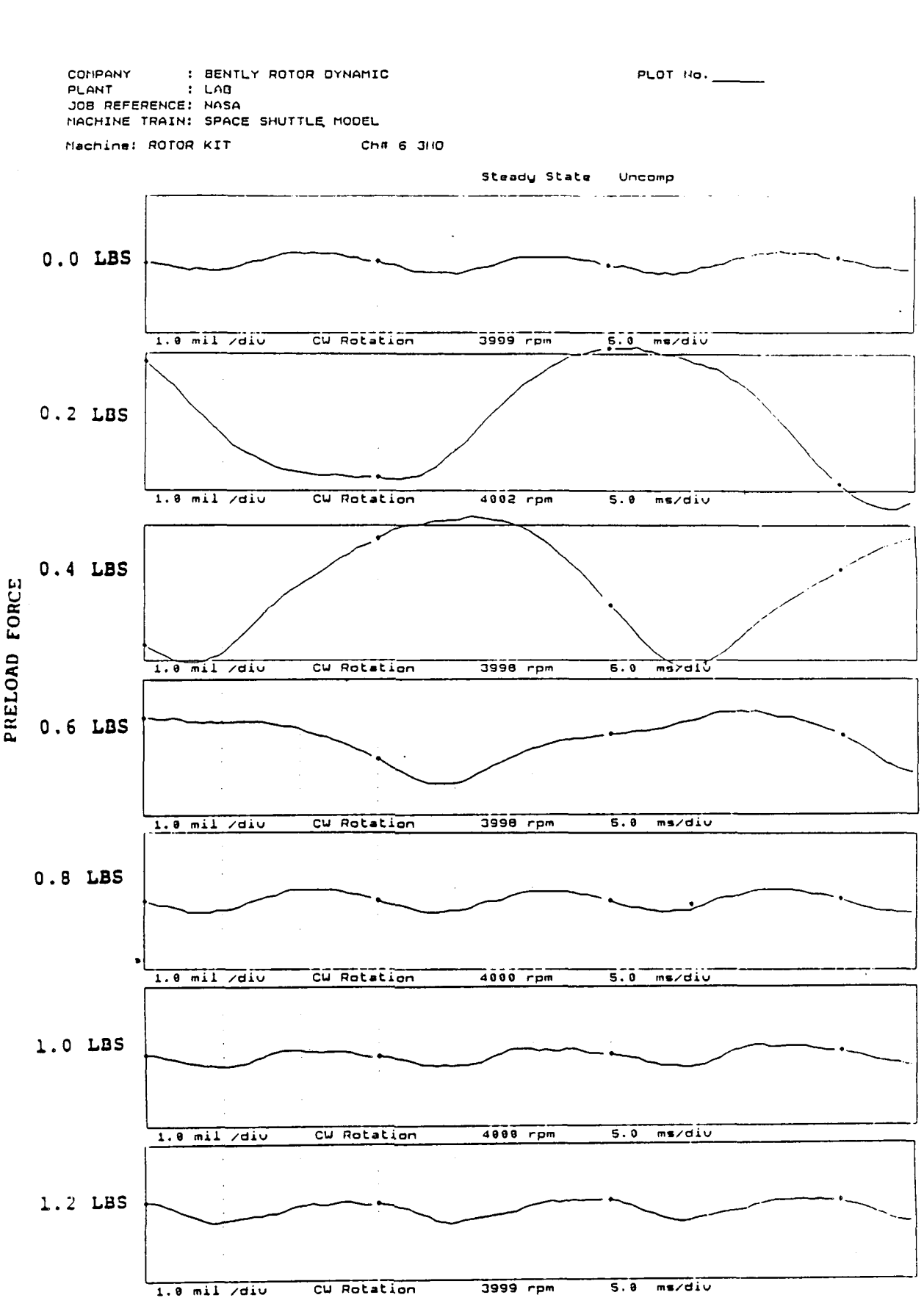

FIGURE 12.50 TIMEBASE FOR HORIZONTAL PROBE AT LOCATION 3 AT 4000 RPM, 2.5 PSI SEAL OIL PRESSURE, 0.8 IN–GRAM UNBALANCE LOCATED IN THE TURBINE DISK, FOR INCREASING STATIC PRELOADS.

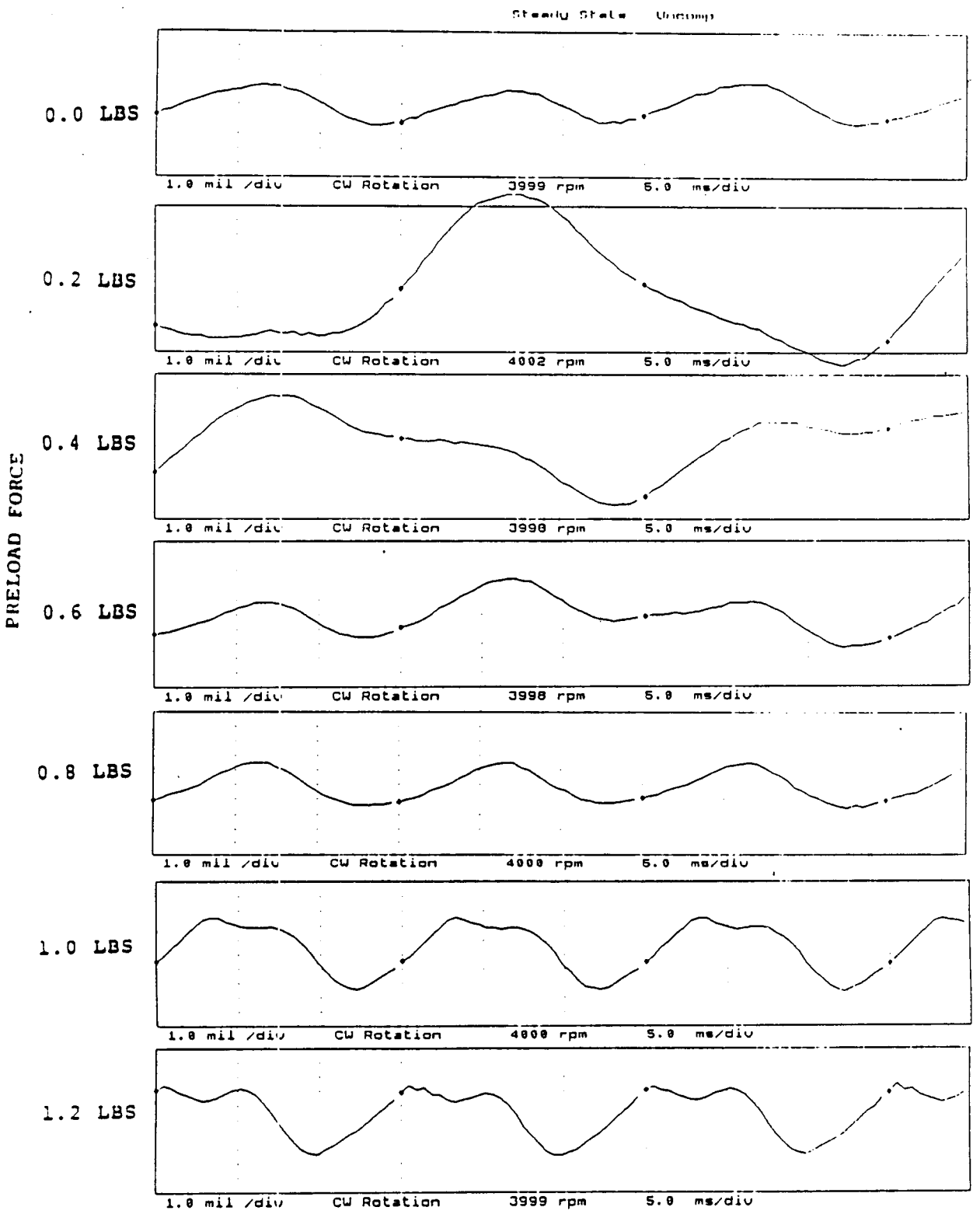

FIGURE 12.51 TIMEBASE FOR VERTICAL PROBE AT LOCATION 4 AT 4000 RPM. 2.5 PSI SEAL OIL PRESSURE, 0.8 IN–GRAM UNBALANCE LOCATED IN THE TURBINE DISK, FOR INCREASING STATIC PRELOADS.

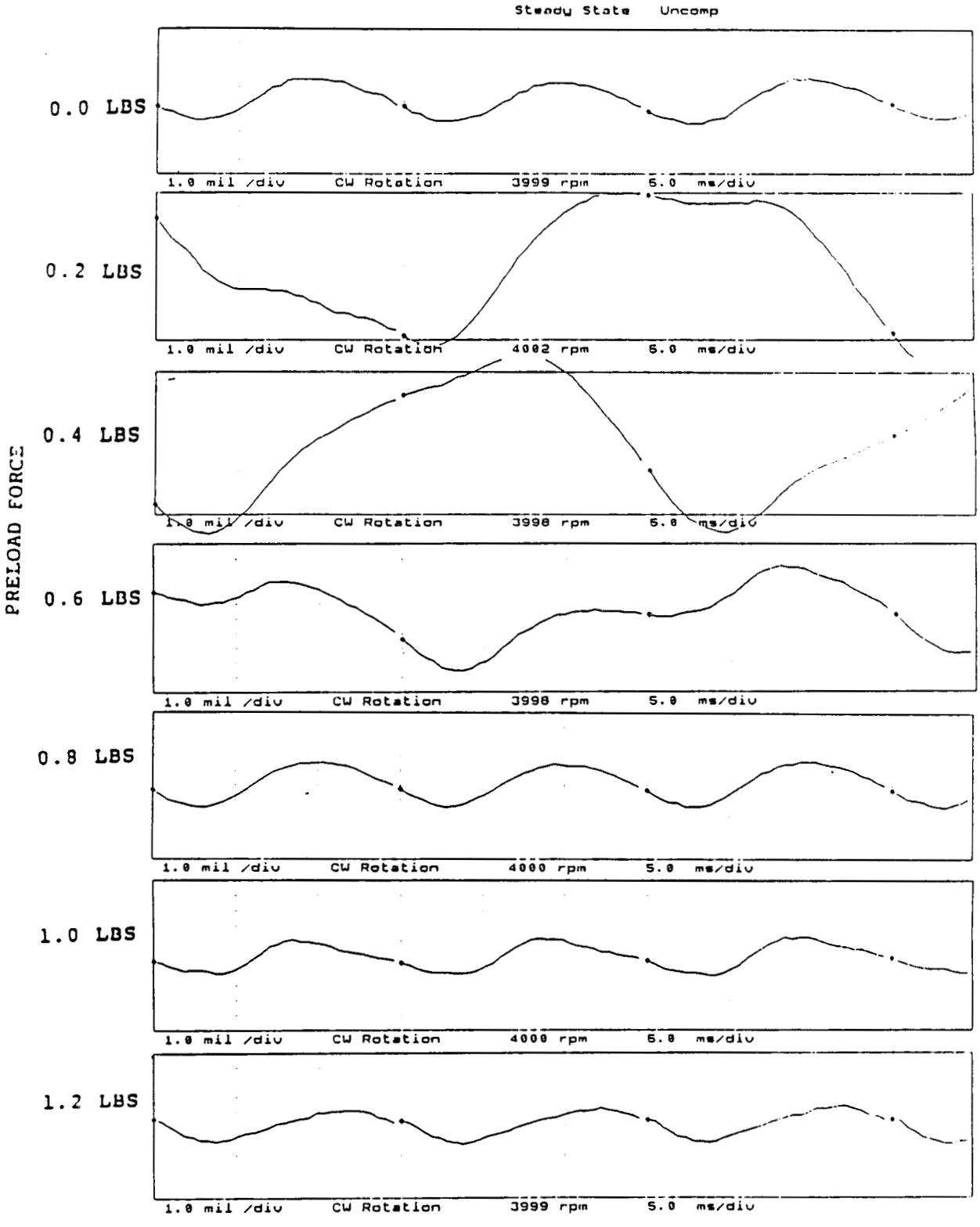

FIGURE 12.52 TIMEBASE FOR HORIZONTAL PROBE AT LOCATION 4 AT 4000 RPM, 2.5 PSI SEAL OIL PRESSURE, 0.8 IN–GRAM UNBALANCE LOCATED IN THE TURBINE DISK, FOR INCREASING STATIC PRELOADS.

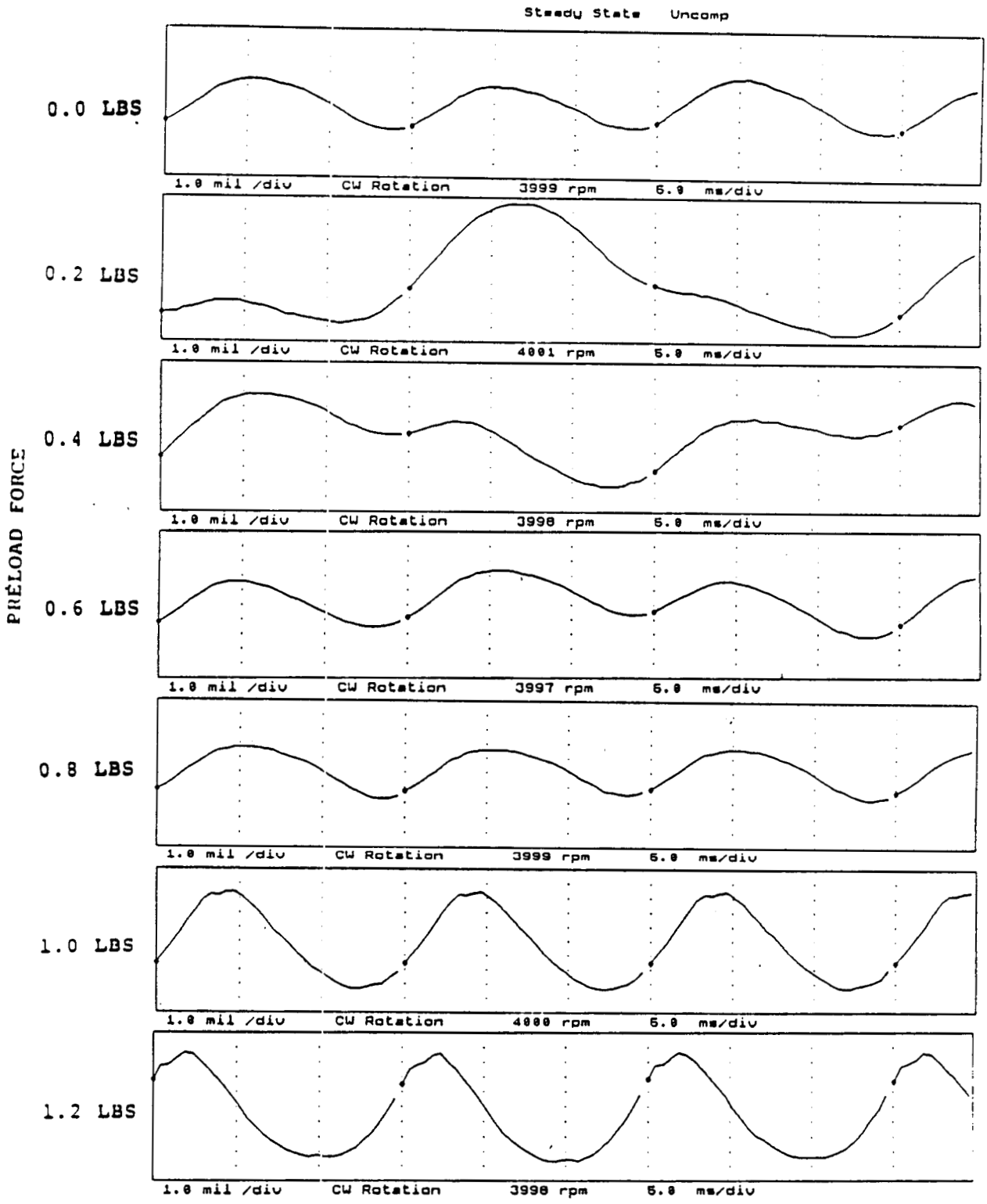

FIGURE 12.53 TIMEBASE FOR VERTICAL PROBE AT LOCATION 5 AT 4000 RPM, 2.5 PSI SEAL OIL PRESSURE, 0.8 IN–GRAM UNBALANCE LOCATED IN THE TURBINE DISK, FOR INCREASING STATIC PRELOADS.

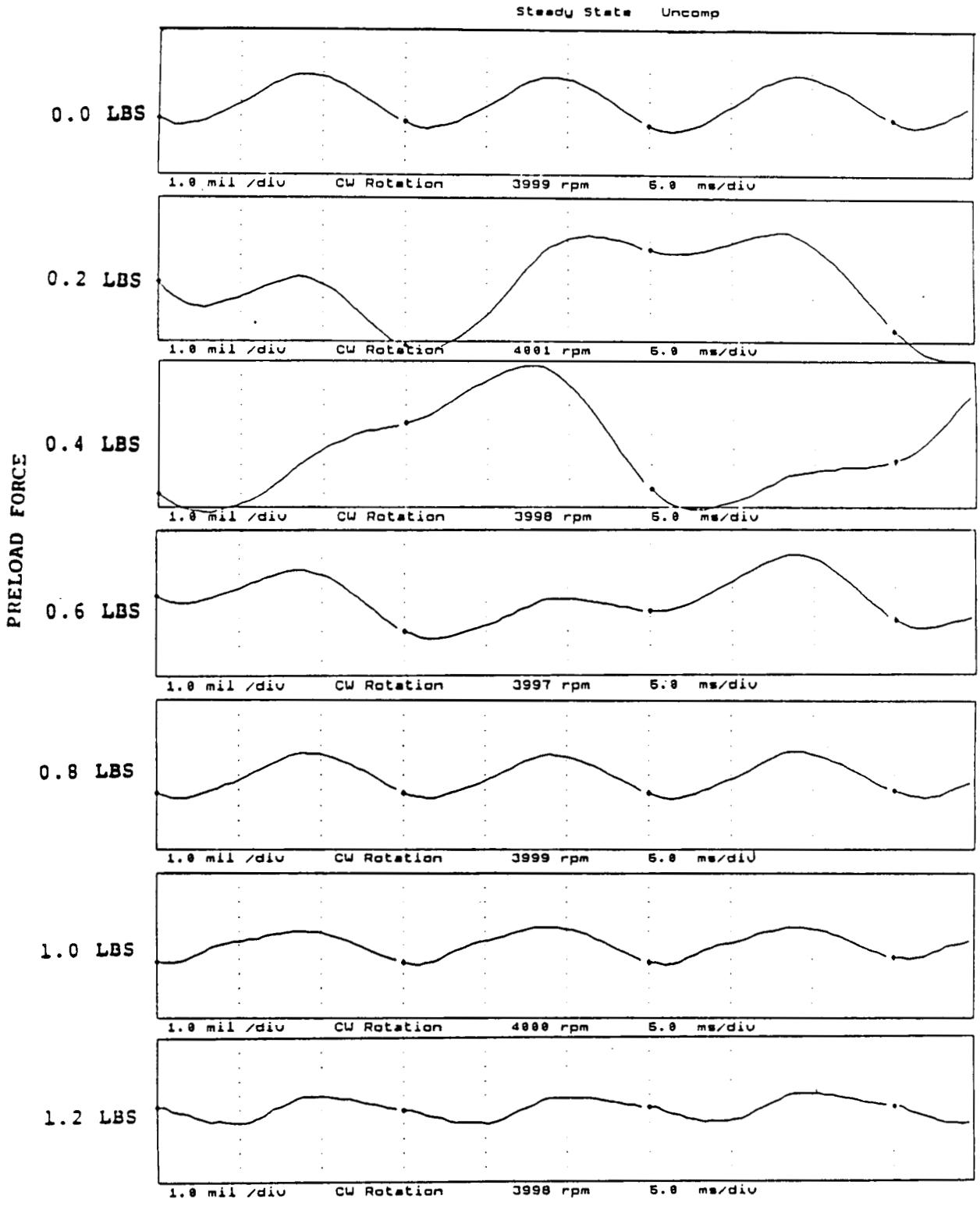

FIGURE 12.54 TIMEBASE FOR HORIZONTAL PROBE AT LOCATION 5 AT 4000 RPM, 2.5 PSI SEAL OIL PRESSURE, 0.8 IN–GRAM UNBALANCE LOCATED IN THE TURBINE DISK, FOR INCREASING STATIC PRELOADS.

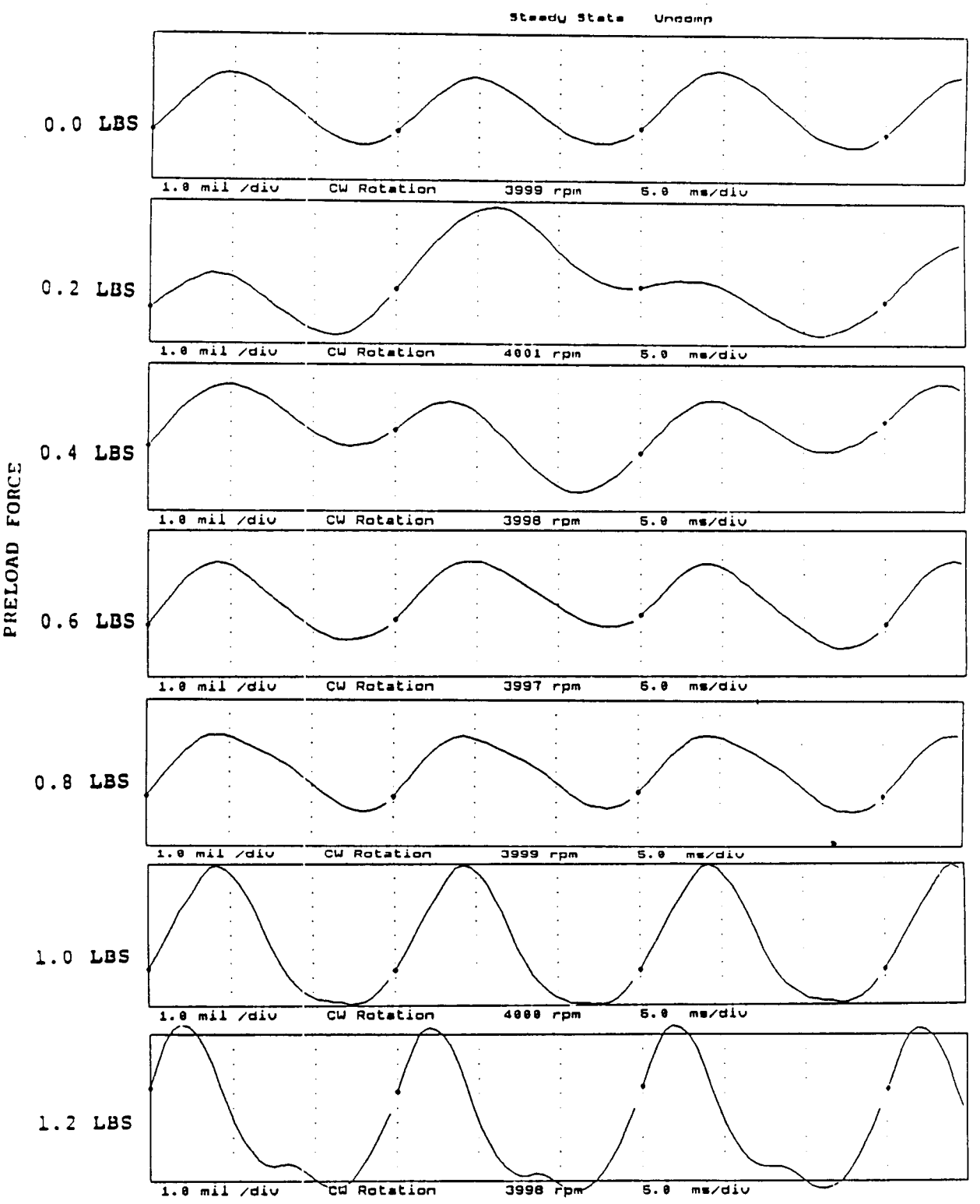

FIGURE 12.55 TIMEBASE FOR VERTICAL PROBE AT LOCATION 6 AT 4000 RPM, 2.5 PSI SEAL OIL PRESSURE, 0.8 IN–GRAM UNBALANCE LOCATED IN THE TURBINE DISK, FOR INCREASING STATIC PRELOADS.

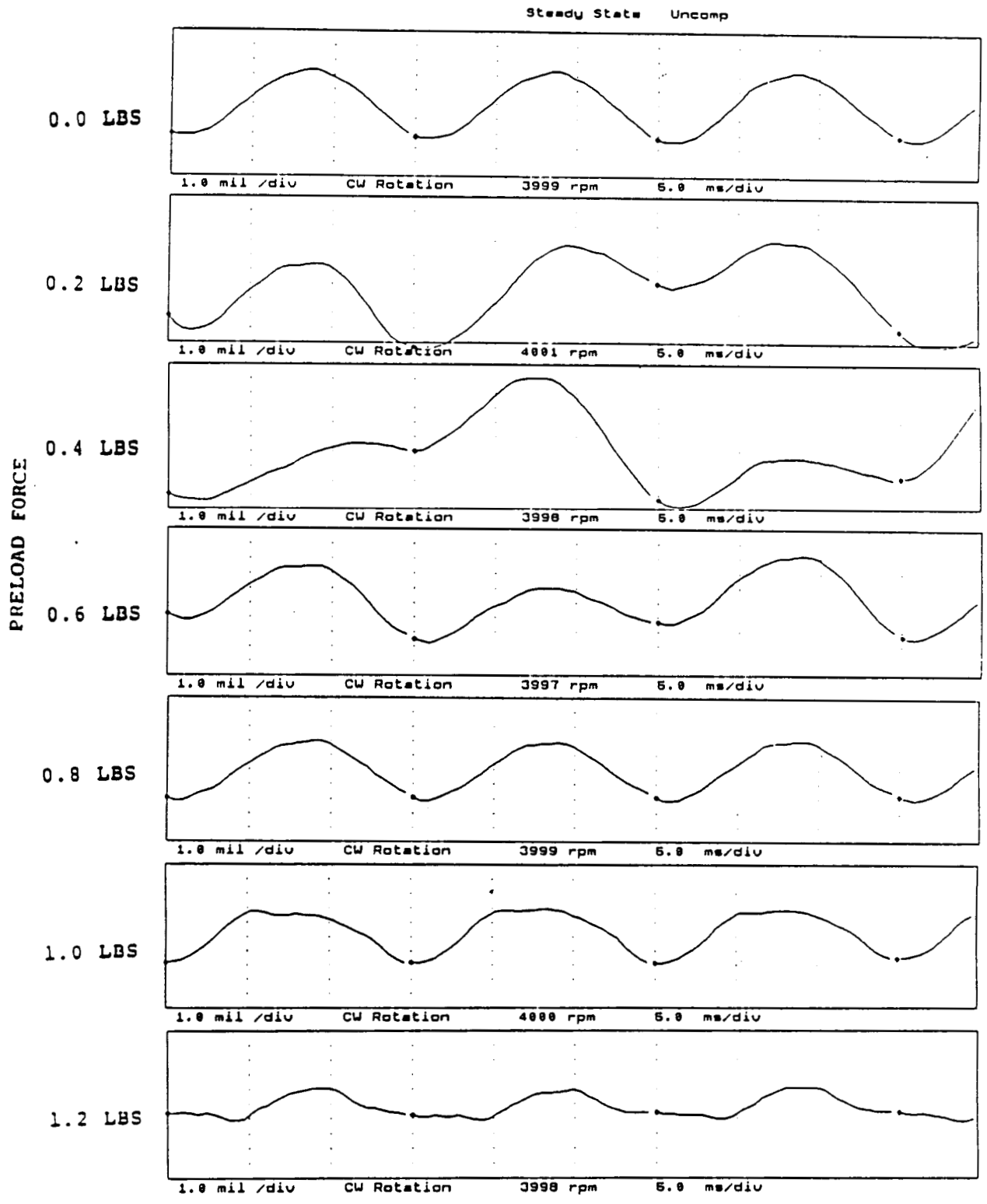

FIGURE 12.56 TIMEBASE FOR HORIZONTAL PROBE AT LOCATION 6 AT 4000 RPM, 2.5 PSI SEAL OIL PRESSURE, 0.8 IN–GRAM UNBALANCE LOCATED IN THE TURBINE DISK, FOR INCREASING STATIC PRELOADS.

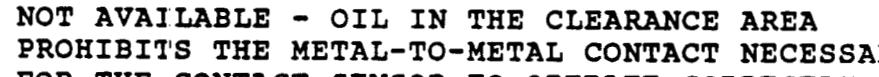

FIGURE 12.57 TIMEBASE FOR SHAFT TO SEAL 1 CONTACT AT 4000 RPM, 2.5 PSI SEAL OIL PRESSURE, 0.8 IN–GRAM UNBALANCE LOCATED IN THE TURBINE DISK, FOR INCREASING STATIC PRELOADS.

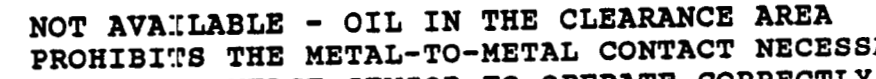

FIGURE 12.58 TIMEBASE FOR SHAFT TO SEAL 2 CONTACT AT 4000 RPM, 2.5 PSI SEAL OIL PRESSURE, 0.8 IN–GRAM UNBALANCE LOCATED IN THE TURBINE DISK, FOR INCREASING STATIC PRELOADS.

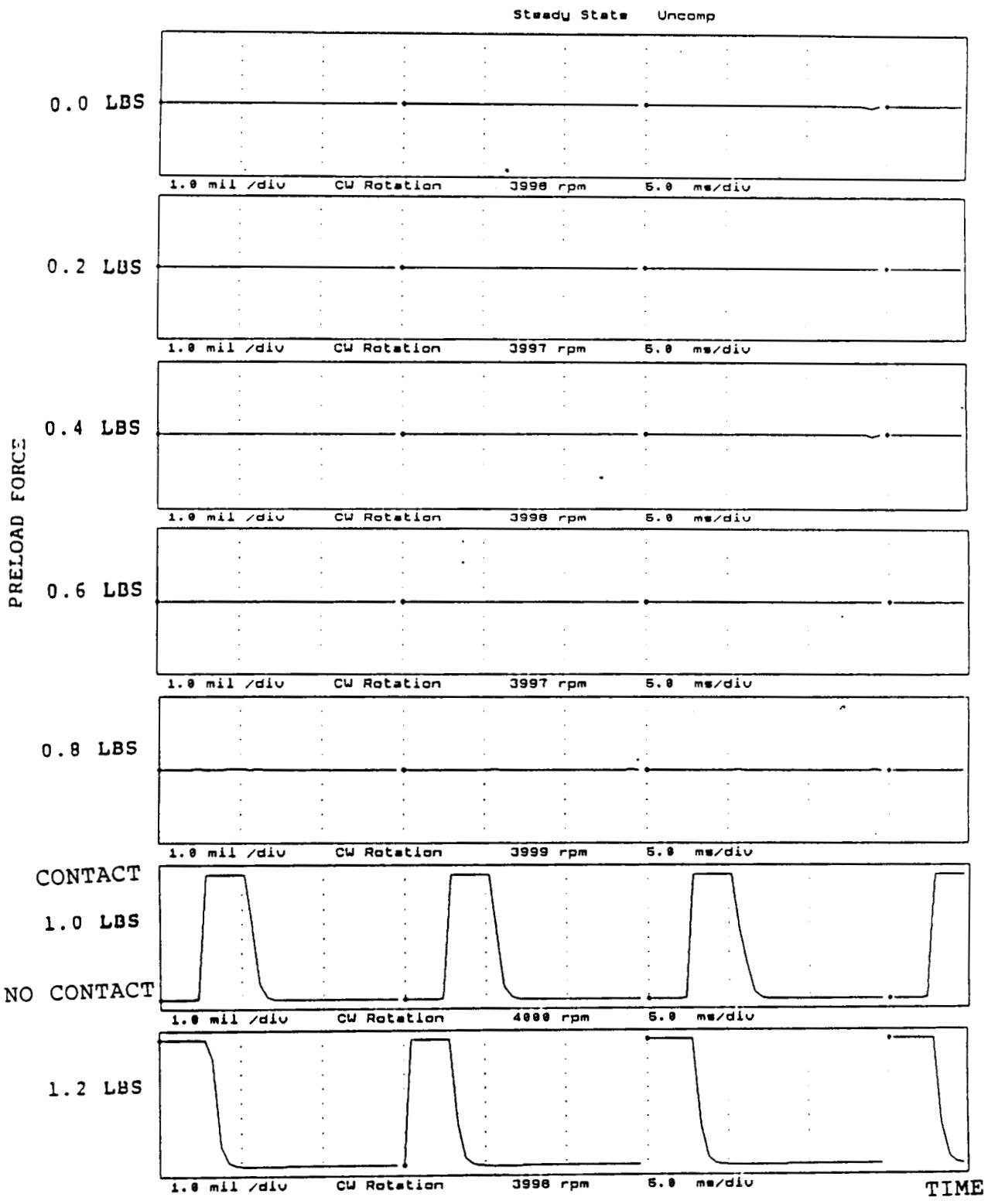

FIGURE 12.59 TIMEBASE FOR SHAFT TO RUB BLOCK CONTACT AT 4000 RPM, 2.5 PSI SEAL OIL PRESSURE, 0.8 IN–GRAM UNBALANCE LOCATED IN THE TURBINE DISK, FOR INCREASING STATIC PRELOADS.

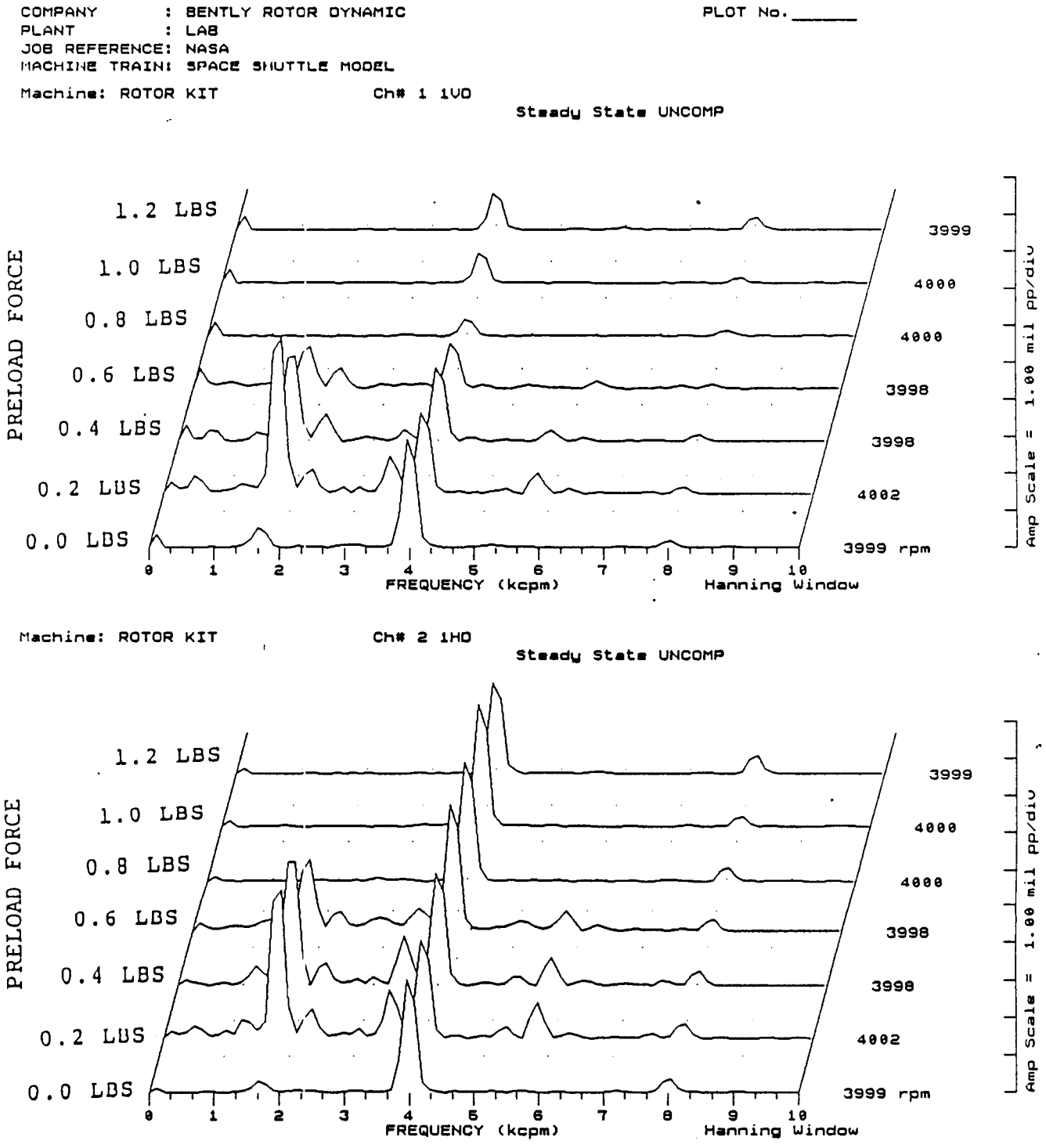

FIGURE 12.60 SPECTRAL CONTENT AT PROBE LOCATION 1 AT 4000 RPM, 2.5 PSI SEAL OIL PRESSURE, 0.8 IN–GRAM UNBALANCE LOCATED IN THE TURBINE DISK, FOR INCREASING STATIC PRELOADS.

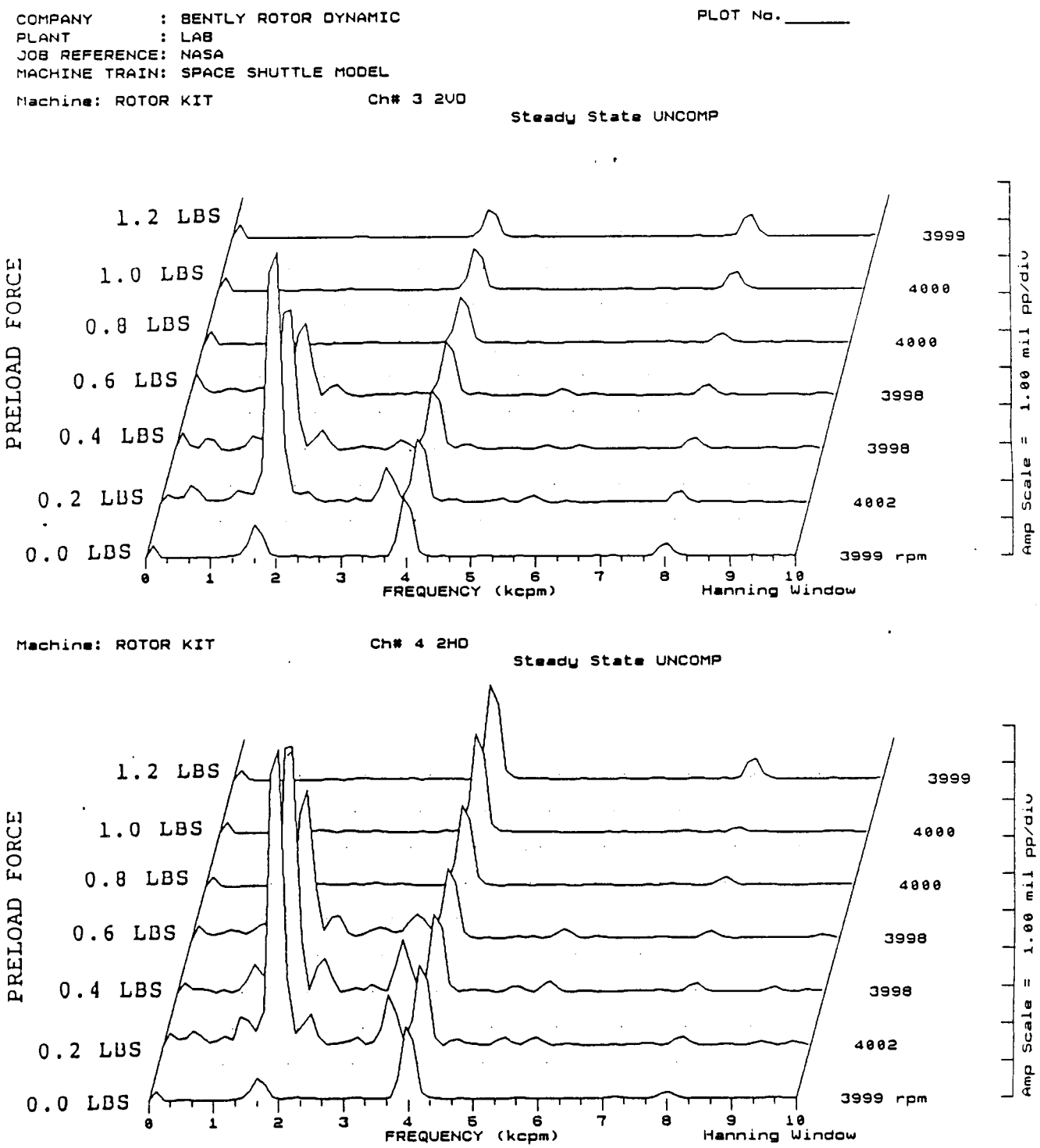

FIGURE 12.61 SPECTRAL CONTENT AT PROBE LOCATION 2 AT 4000 RPM, 2.5 PSI SEAL OIL PRESSURE, 0.8 IN–GRAM UNBALANCE LOCATED IN THE TURBINE DISK, FOR INCREASING STATIC PRELOADS.

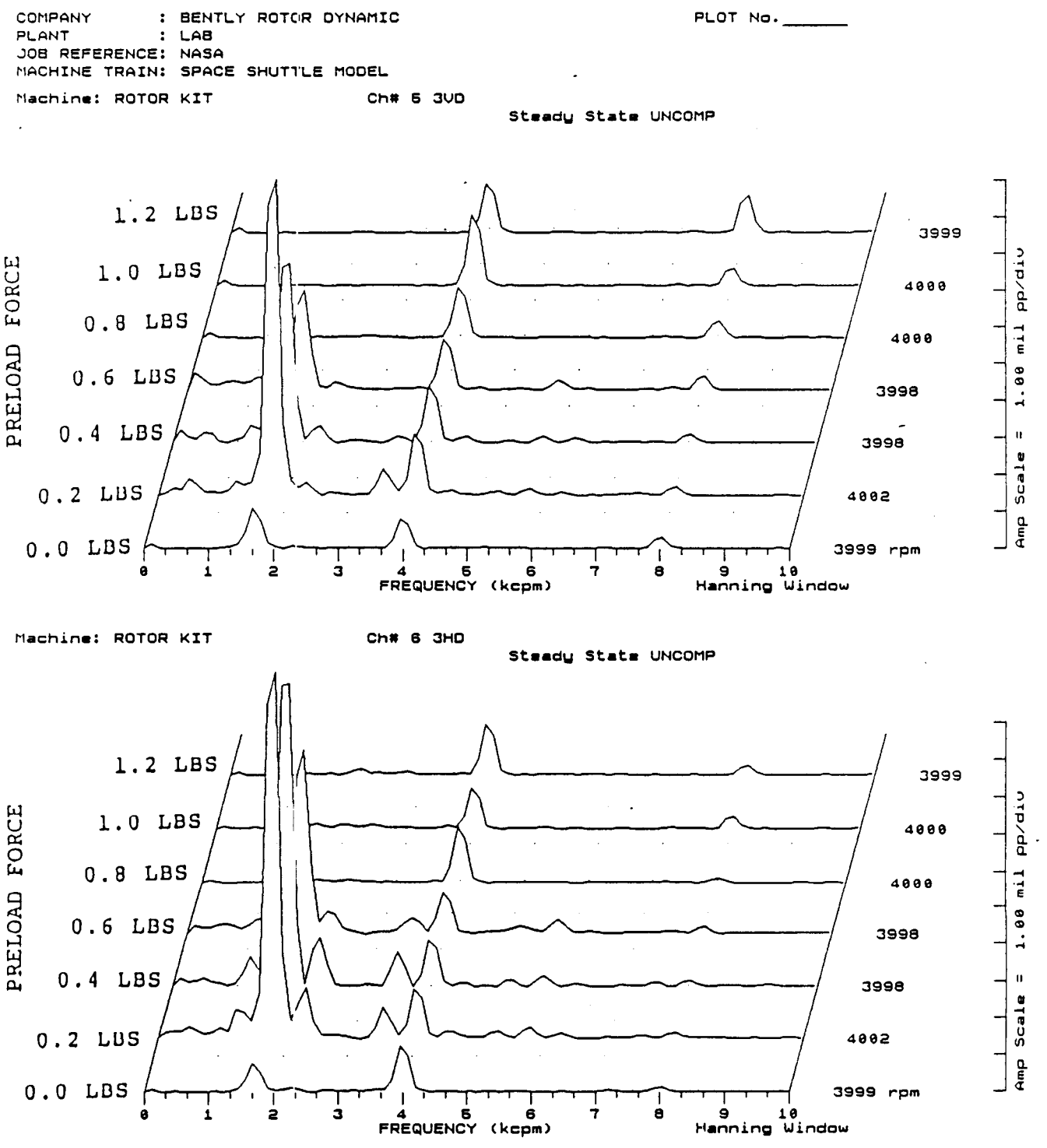

FIGURE 12.62 SPECTRAL CONTENT AT PROBE LOCATION 3 AT 4000 RPM, 2.5 PSI SEAL OIL PRESSURE, 0.8 IN–GRAM UNBALANCE LOCATED IN THE TURBINE DISK, FOR INCREASING STATIC PRELOADS.

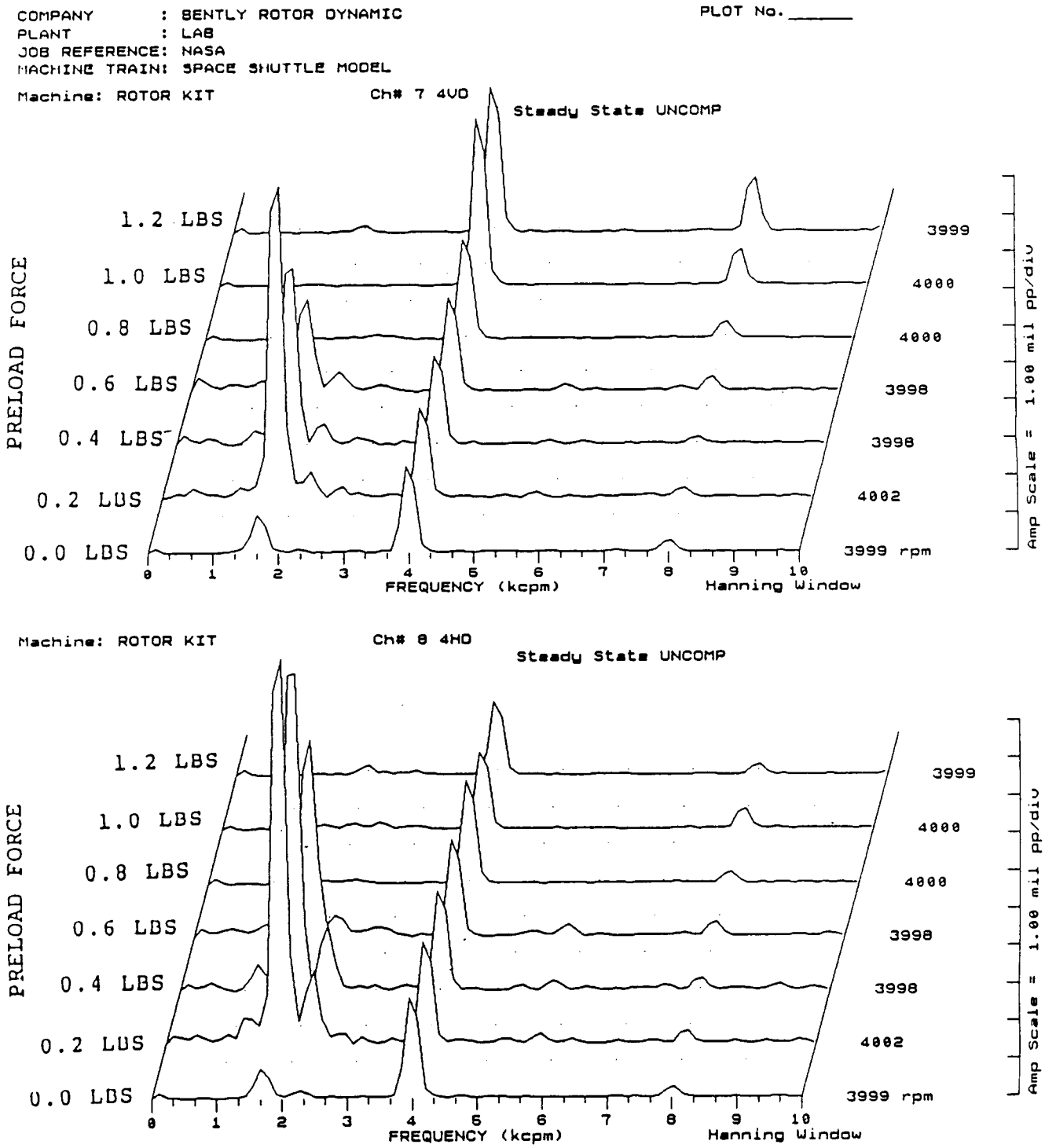

FIGURE 12.63 SPECTRAL CONTENT AT PROBE LOCATION 4 AT 4000 RPM, 2.5 PSI SEAL OIL PRESSURE, 0.8 IN–GRAM UNBALANCE LOCATED IN THE TURBINE DISK, FOR INCREASING STATIC PRELOADS.

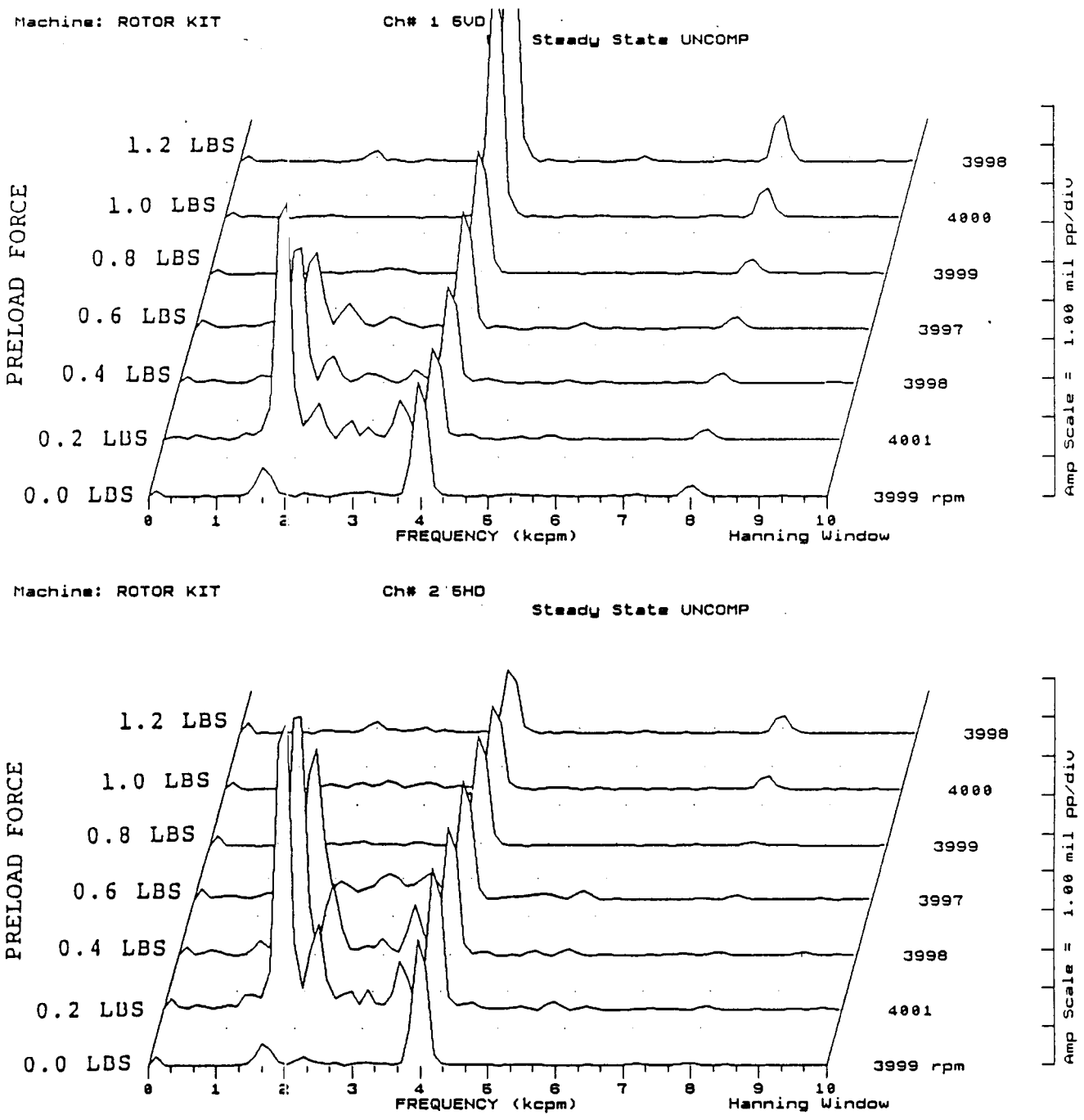

FIGURE 12.64 - SPECTRAL CONTENT AT PROBE LOCATION 5 AT 4000 RPM, 2.5 PSI SEAL OIL PRESSURE, 0.8 IN–GRAM UNBALANCE LOCATED IN THE TURBINE DISK, FOR INCREASING STATIC PRELOADS.

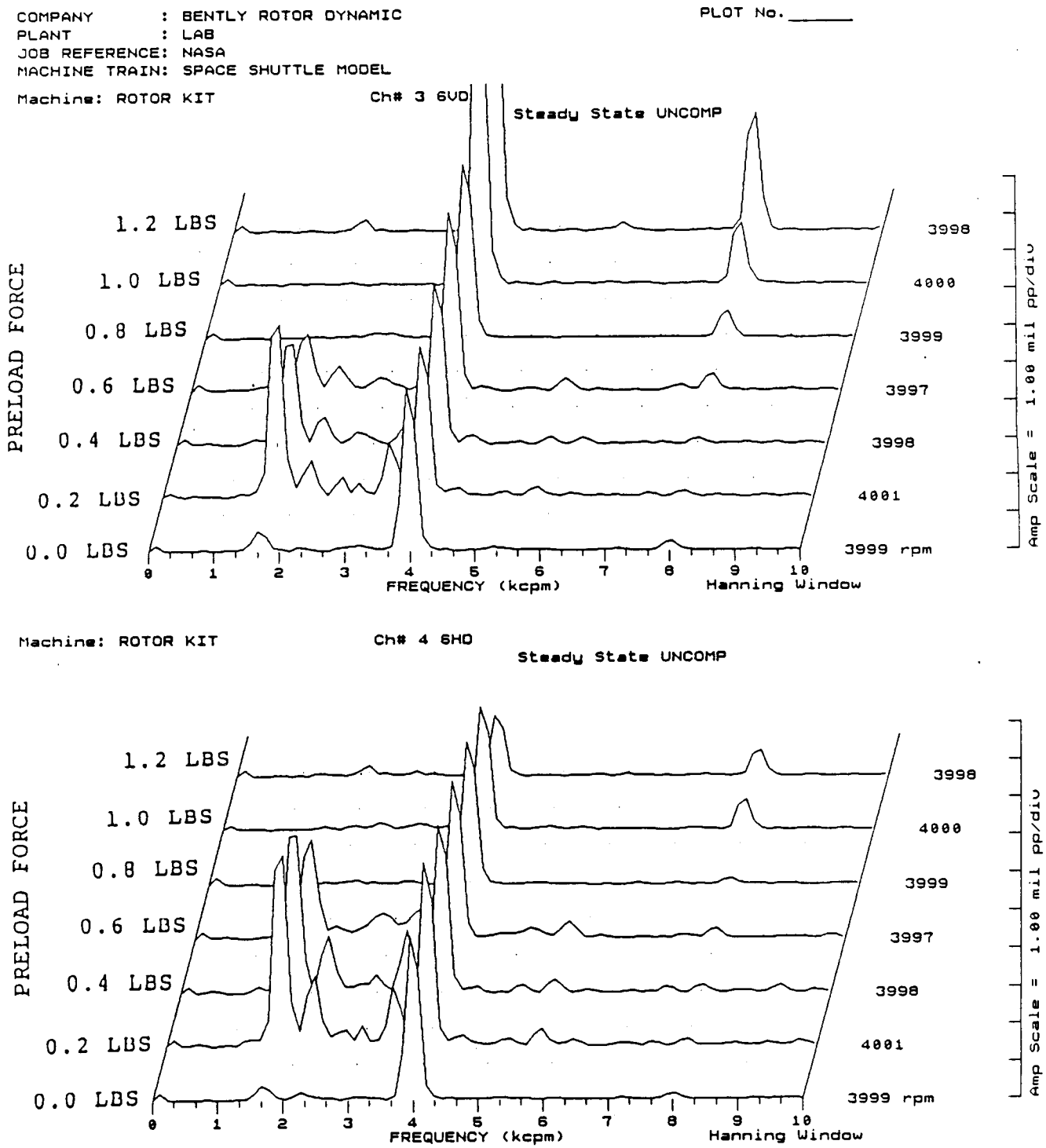

FIGURE 12.65 SPECTRAL CONTENT AT PROBE LOCATION 6 AT 4000 RPM, 2.5 PSI SEAL OIL PRESSURE, 0.8 IN–GRAM UNBALANCE LOCATED IN THE TURBINE DISK, FOR INCREASING STATIC PRELOADS.

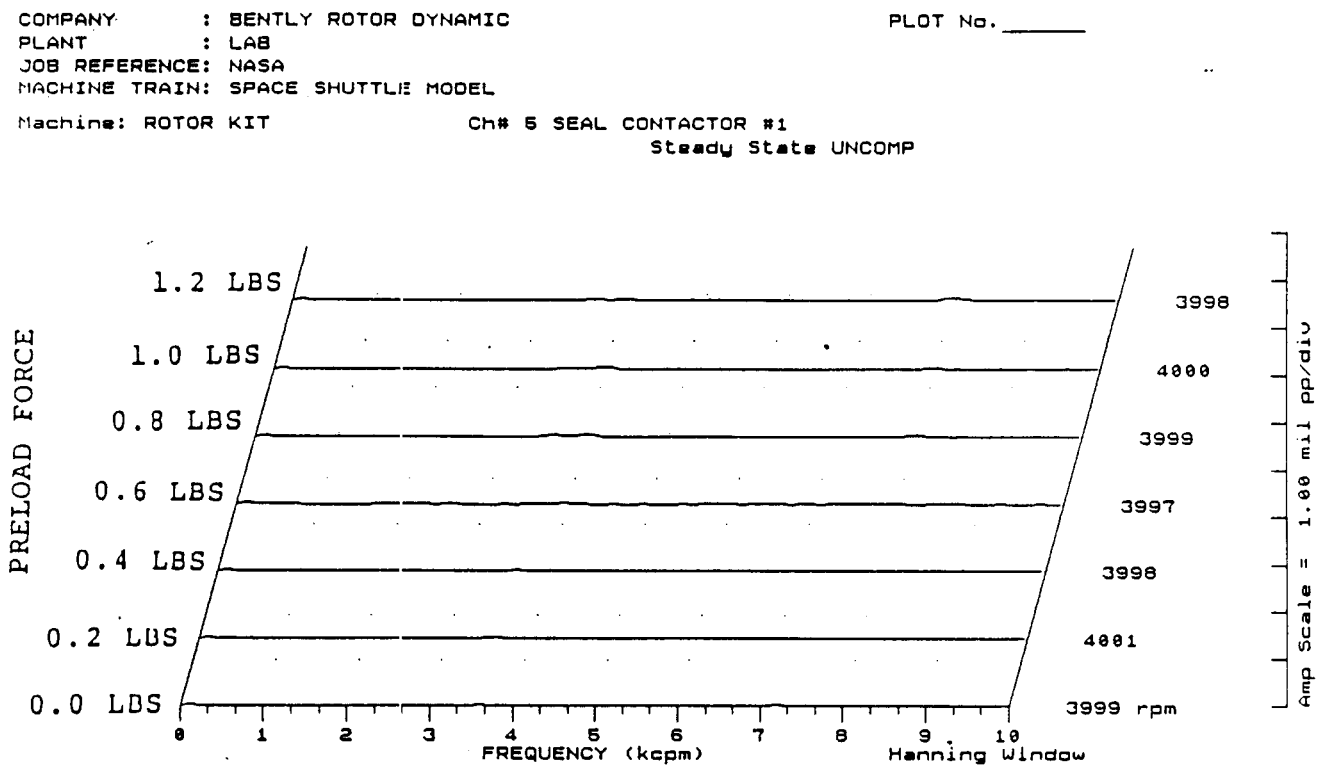

FIGURE 12.66 SPECTRAL CONTENT FOR SHAFT TO SEAL 1 CONTACT AT 4000 RPM, 2.5 PSI SEAL OIL PRESSURE, 0.8 IN–GRAM UNBALANCE LOCATED IN THE TURBINE DISK, FOR INCREASING STATIC PRELOADS.

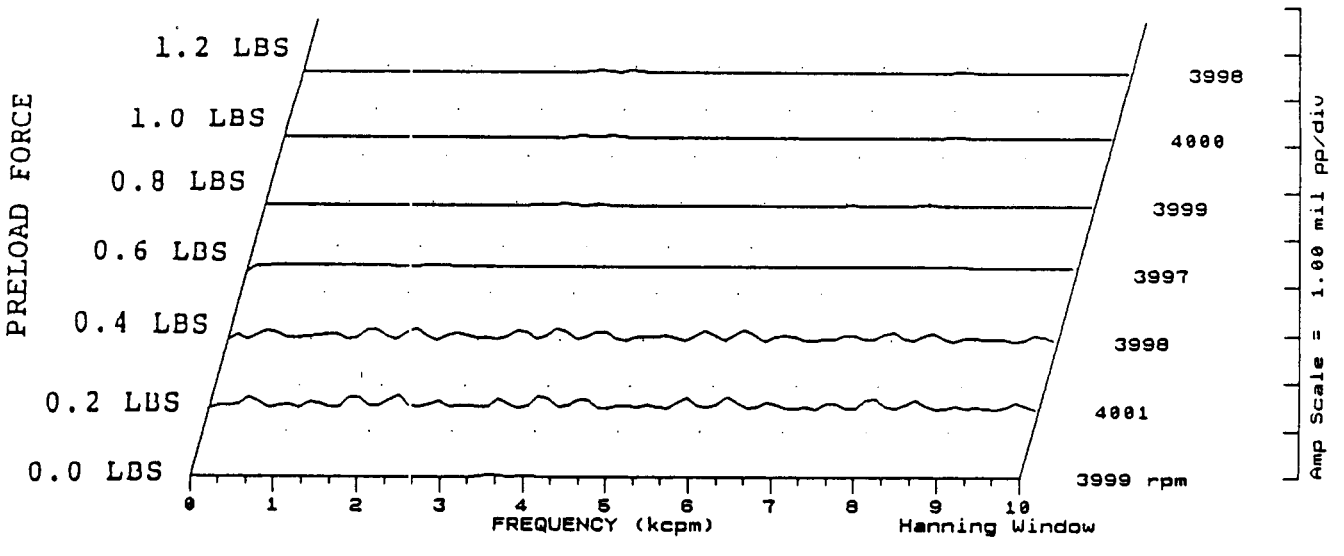

FIGURE 12.67 SPECTRAL CONTENT FOR SHAFT TO SEAL 2 CONTACT AT 4000 RPM, 2.5 PSI SEAL OIL PRESSURE, 0.8 IN–GRAM UNBALANCE LOCATED IN THE TURBINE DISK, FOR INCREASING STATIC PRELOADS.

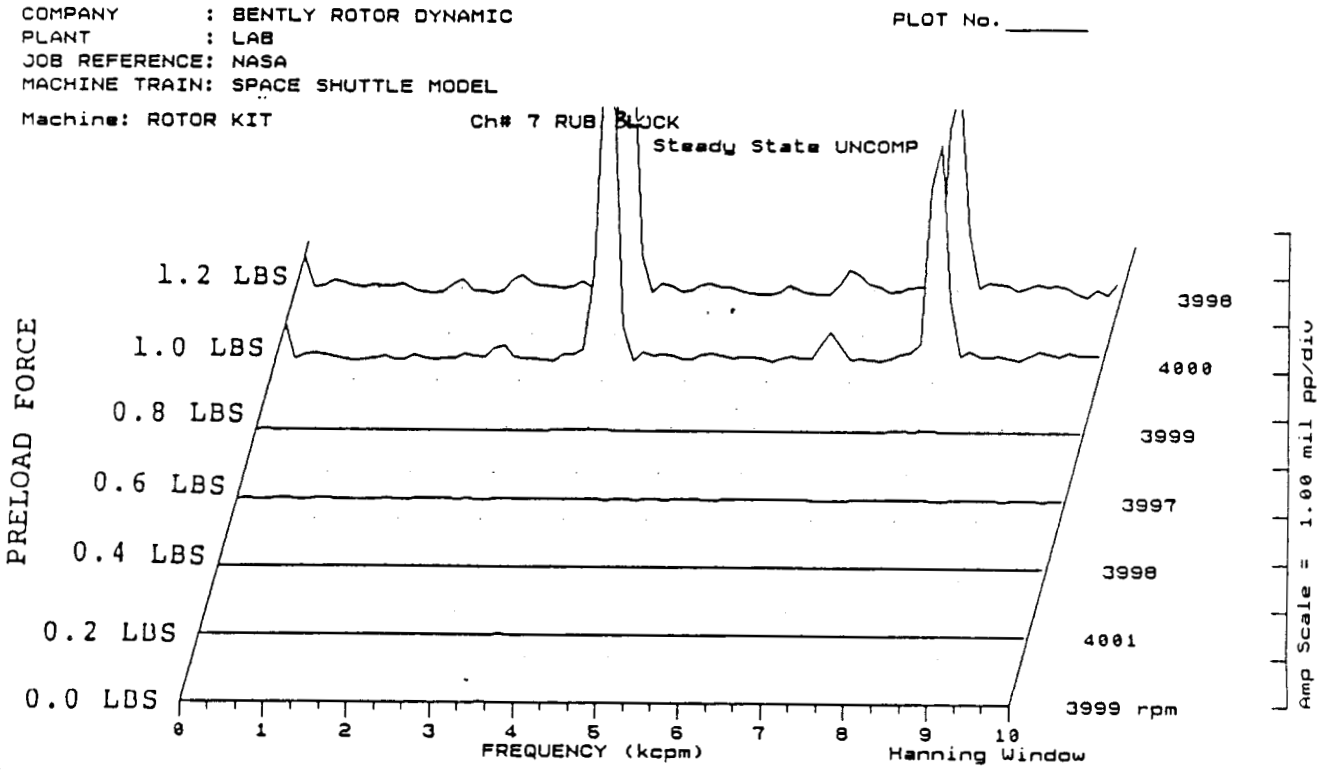

FIGURE 12.68 SPECTRAL CONTENT FOR SHAFT TO RUB BLOCK CONTACT AT 4000 RPM, 2.5 PSI SEAL OIL PRESSURE, 0.8 IN–GRAM UNBALANCE LOCATED IN THE TURBINE DISK, FOR INCREASING STATIC PRELOADS.

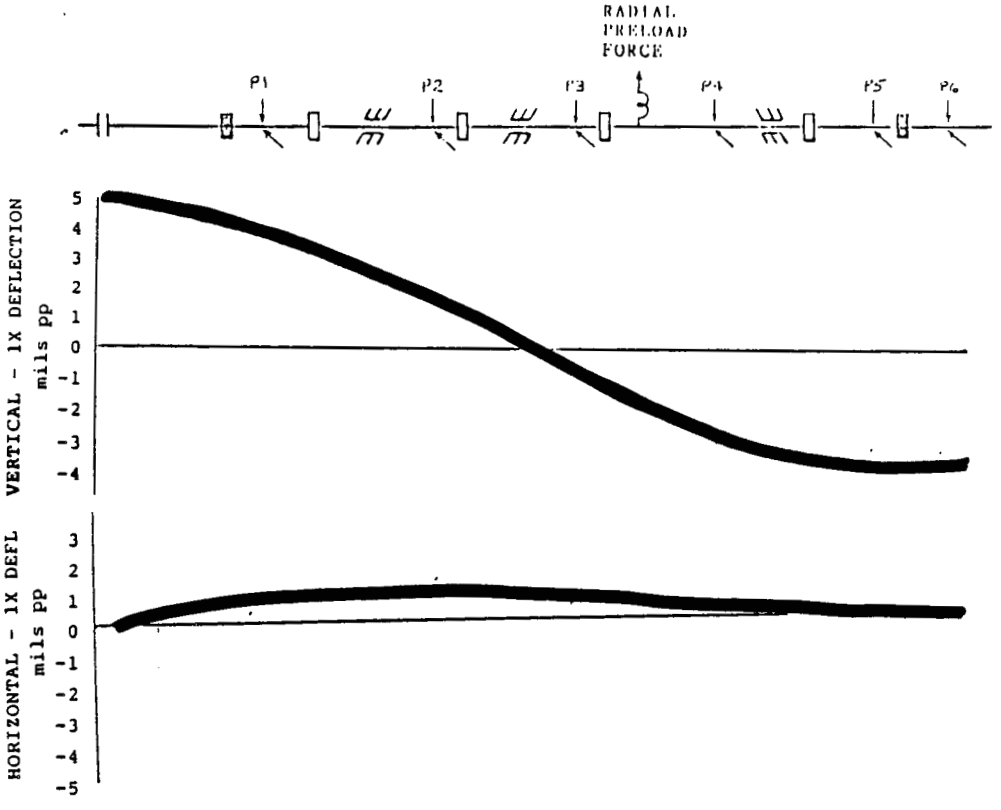

FIGURE 12.69 ROTOR MODE SHAPE AT 4000 RPM, 5.0 PSI SEAL OIL PRESSURE DUE TO 0.8 IN–GRAM UNBALANCE LOCATED IN THE TURBINE DISK.

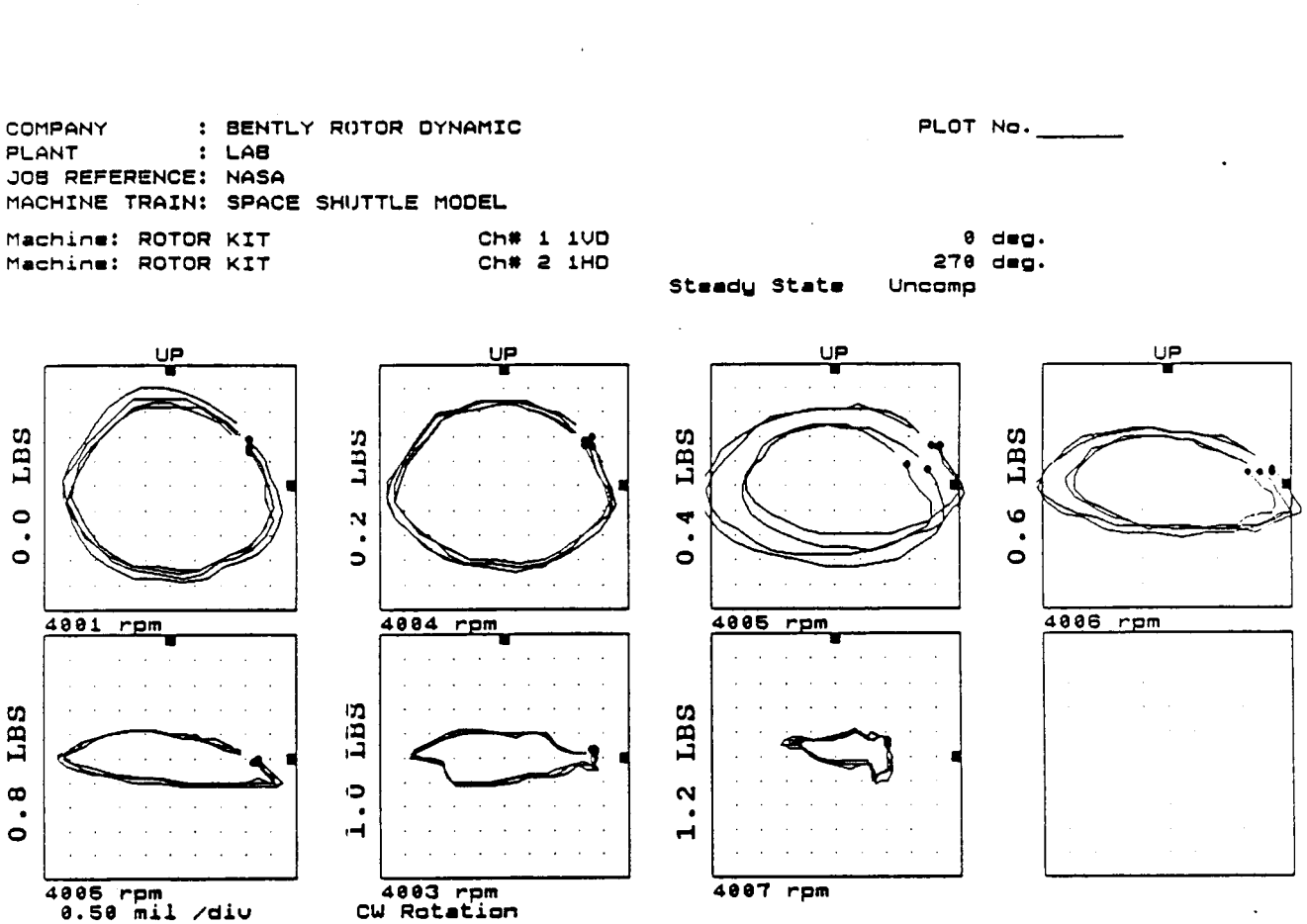

FIGURE 12.70 ORBITS AT PROBE LOCATION 1 AT 4000 RPM, 5.0 PSI SEAL OIL PRESSURE, 0.8 IN–GRAM UNBALANCE LOCATED IN THE TURBINE DISK, FOR INCREASING STATIC PRELOAD FORCES.

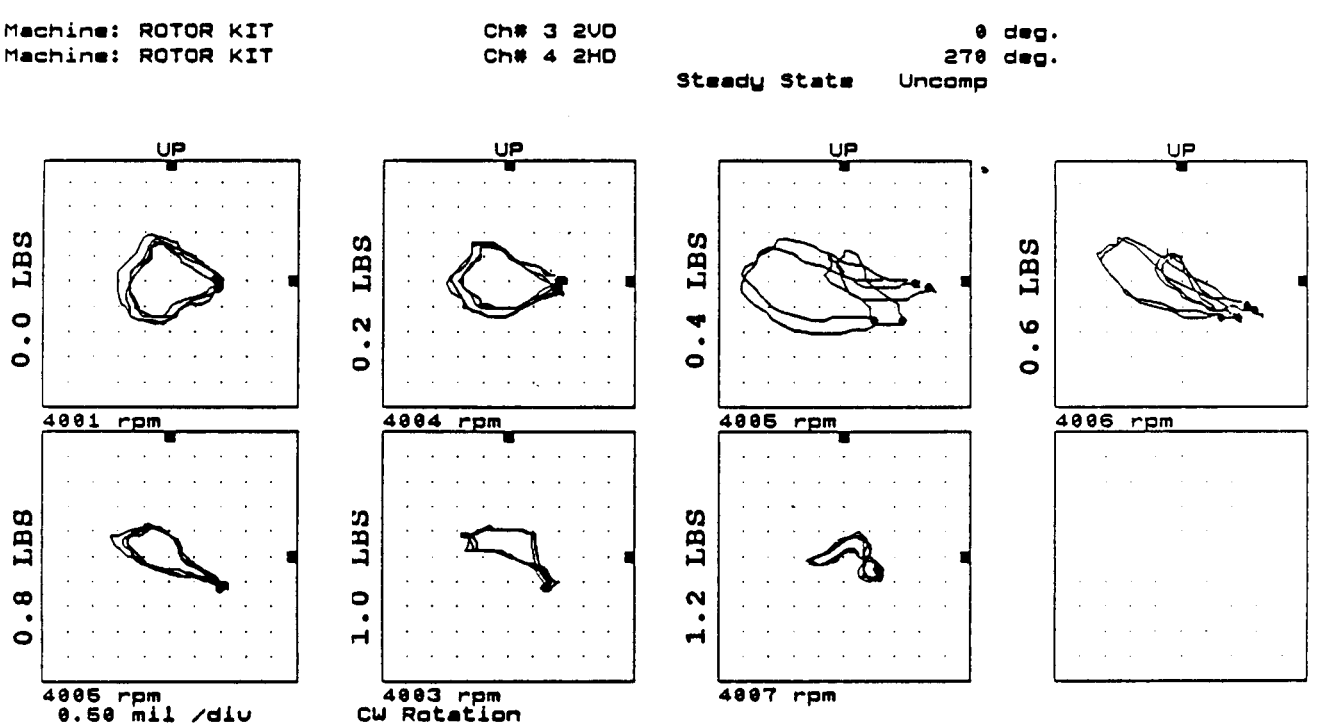

FIGURE 12.71 ORBITS AT PROBE LOCATION 2 AT 4000 RPM, 5.0 PSI SEAL OIL PRESSURE, 0.8 IN–GRAM UNBALANCE LOCATED IN THE TURBINE DISK, FOR INCREASING STATIC PRELOAD FORCES.

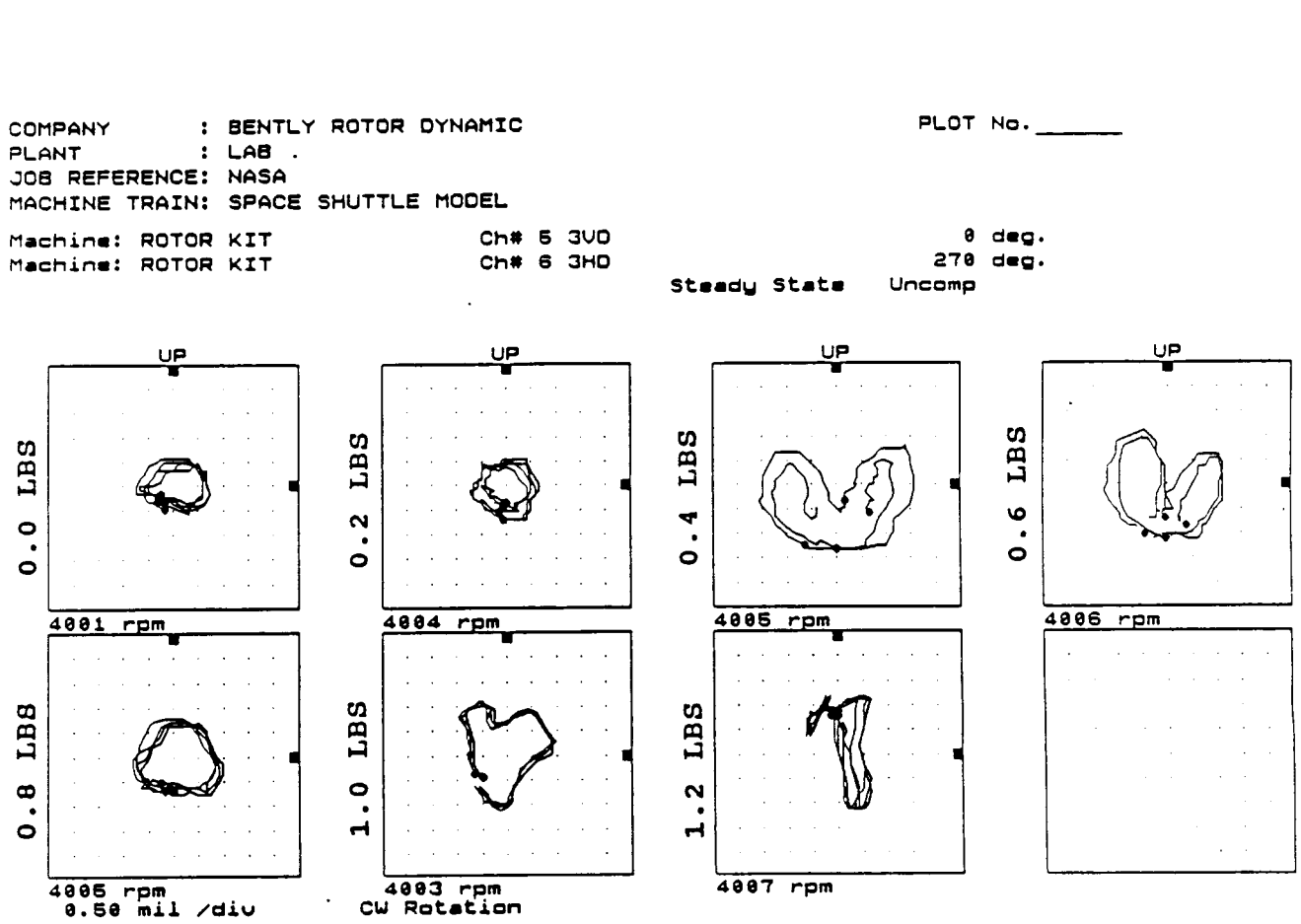

FIGURE 12.72 ORBITS AT PROBE LOCATION 3 AT 4000 RPM, 5.0 PSI SEAL OIL PRESSURE, 0.8 IN–GRAM UNBALANCE LOCATED IN THE TURBINE DISK, FOR INCREASING STATIC PRELOAD FORCES.

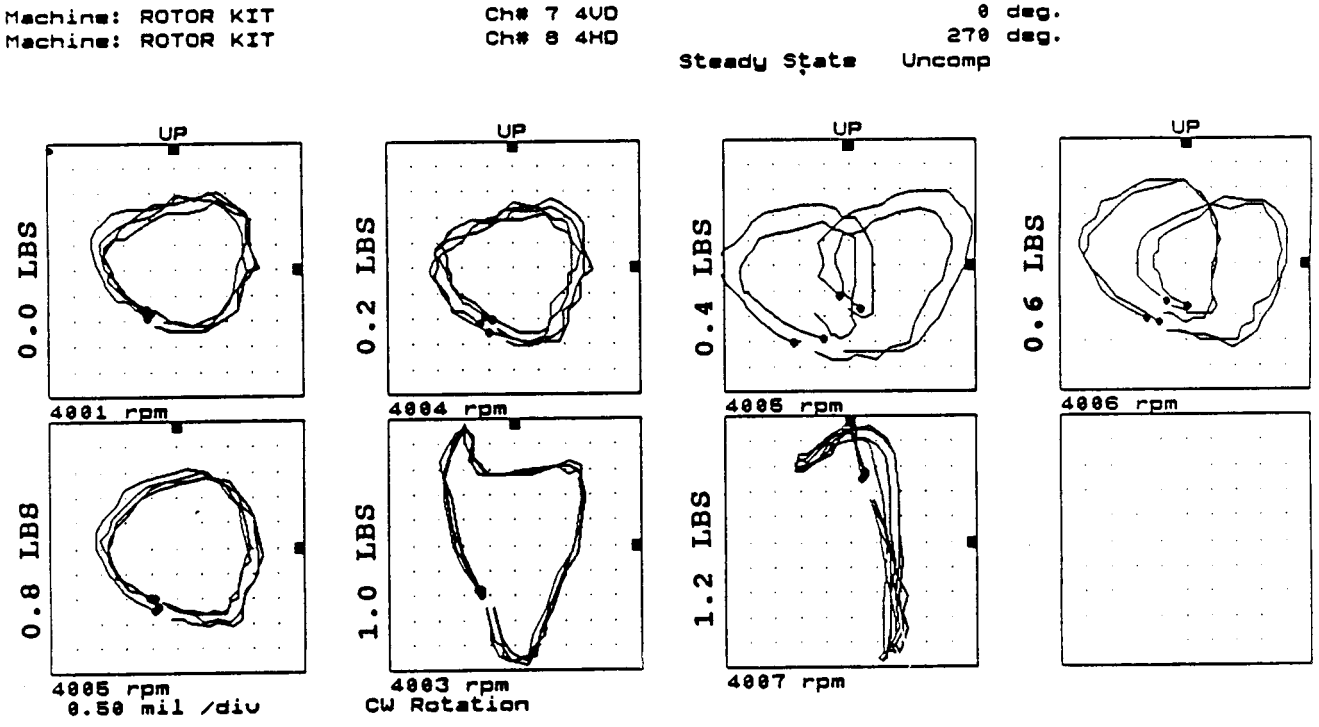

FIGURE 12.73 ORBITS AT PROBE LOCATION 4 AT 4000 RPM, 5.0 PSI SEAL OIL PRESSURE, 0.8 IN–GRAM UNBALANCE LOCATED IN THE TURBINE DISK, FOR INCREASING STATIC PRELOAD FORCES.

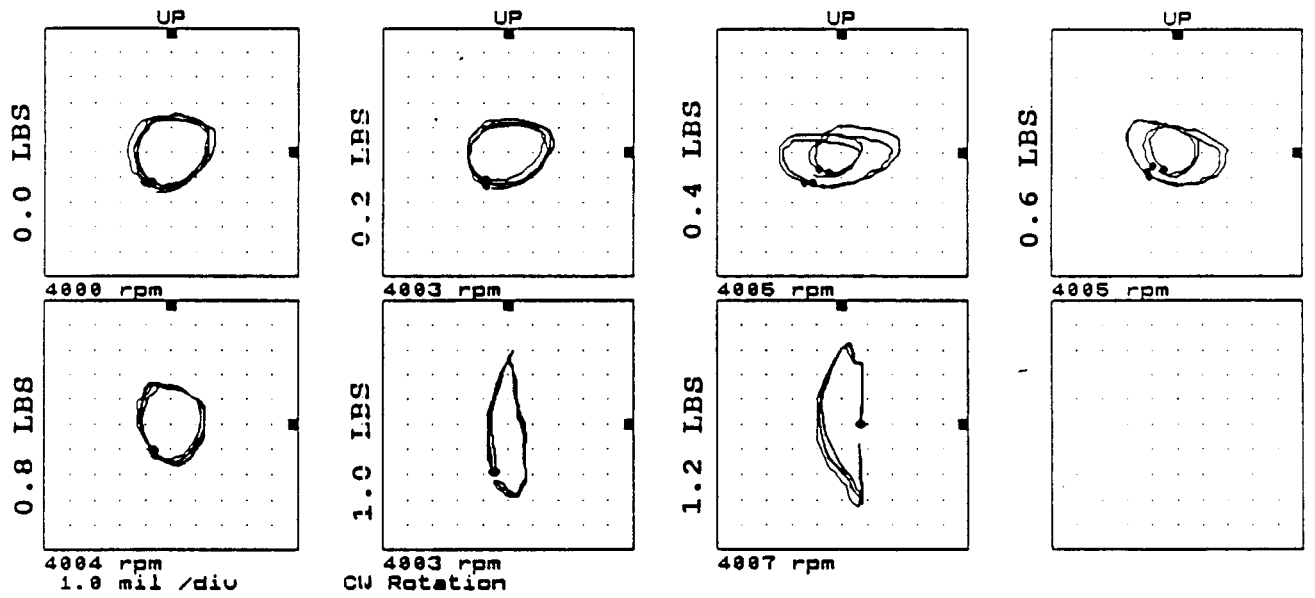

FIGURE 12.74 ORBITS AT PROBE LOCATION 5 AT 4000 RPM, 5.0 PSI SEAL OIL PRESSURE, 0.8 IN–GRAM UNBALANCE LOCATED IN THE TURBINE DISK, FOR INCREASING STATIC PRELOAD FORCES.

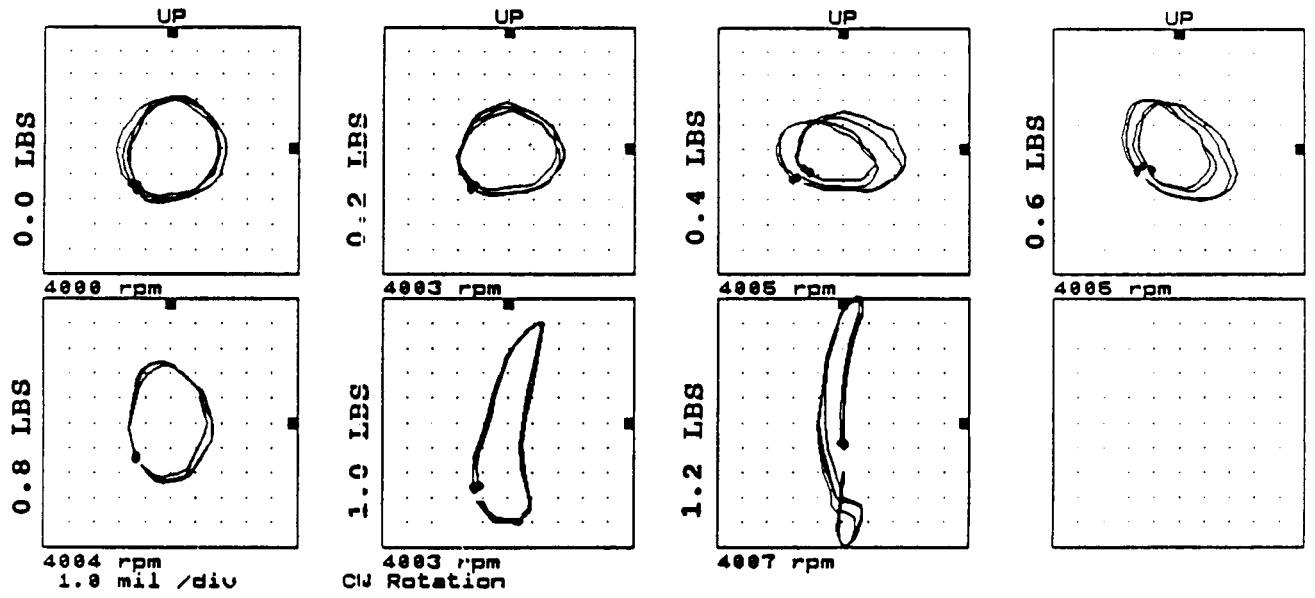

FIGURE 12.75 ORBITS AT PROBE LOCATION 6 AT 4000 RPM, 5.0 PSI SEAL OIL PRESSURE, 0.8 IN–GRAM UNBALANCE LOCATED IN THE TURBINE DISK, FOR INCREASING STATIC PRELOAD FORCES.

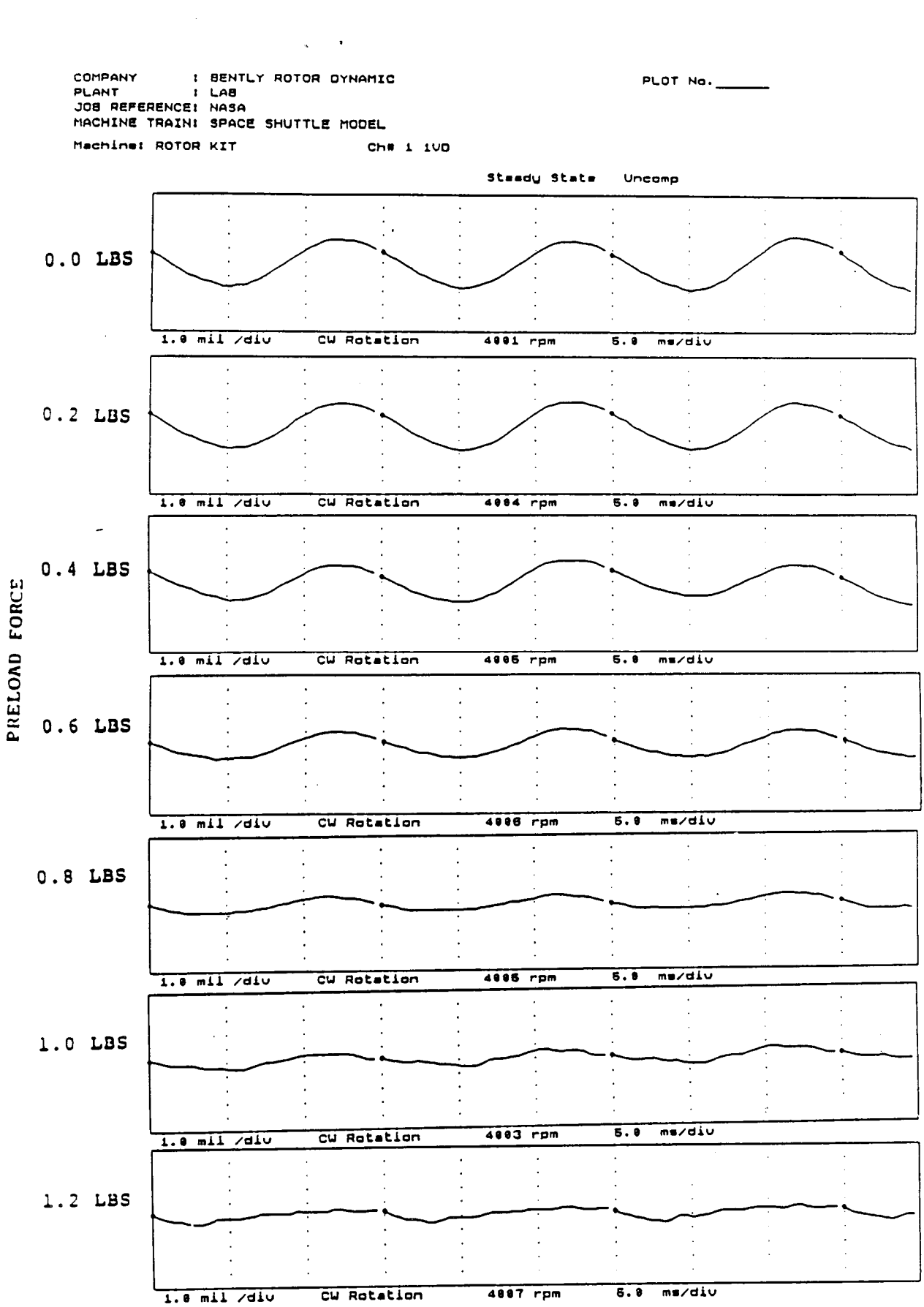

FIGURE 12.76 TIMEBASE FOR VERTICAL PROBE AT LOCATION 1 AT 4000 RPM, 5.0 PSI SEAL OIL PRESSURE, 0.8 IN–GRAM UNBALANCE LOCATED IN THE TURBINE DISK, FOR INCREASING STATIC PRELOADS.

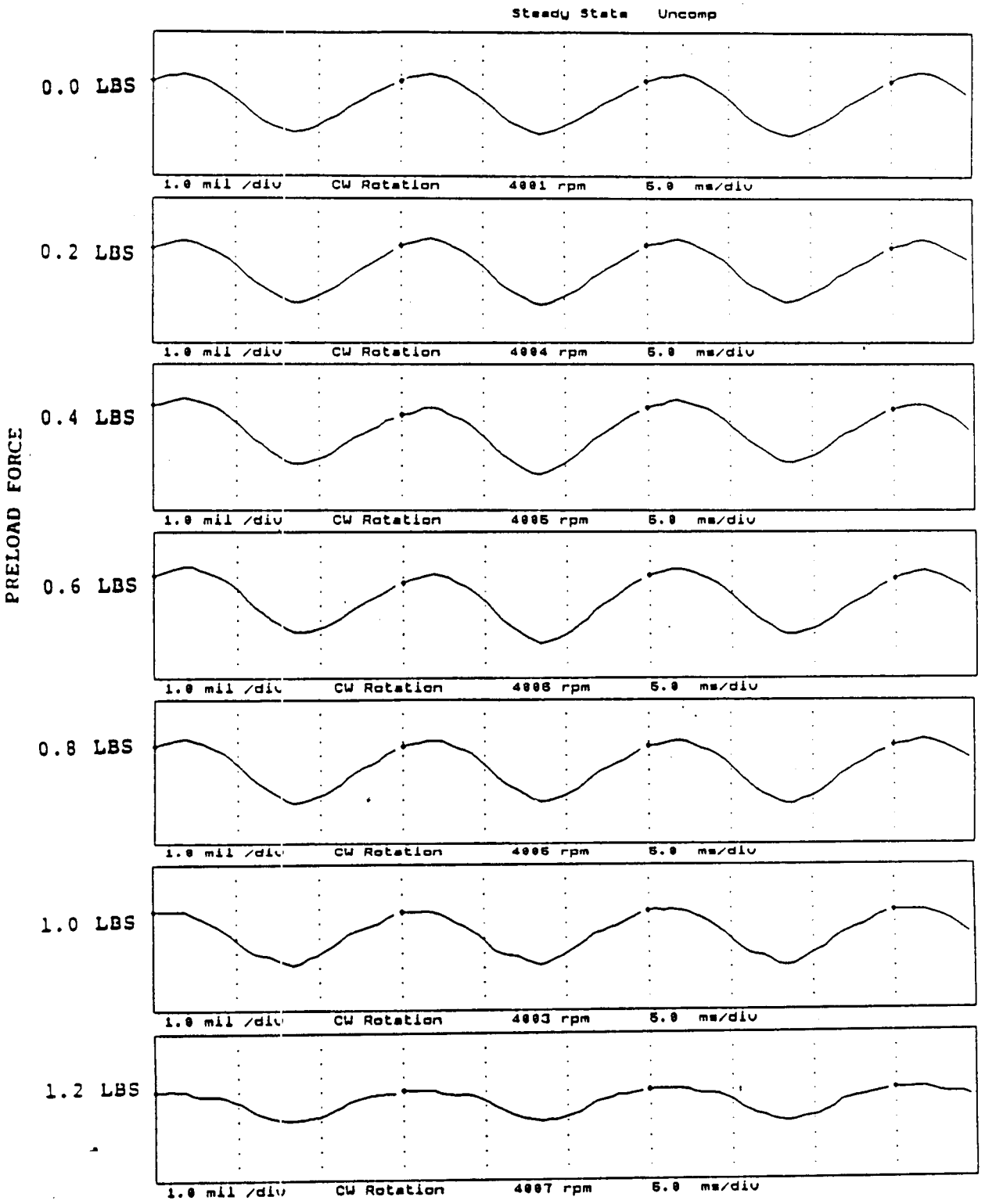

FIGURE 12.77 TIMEBASE FOR HORIZONTAL PROBE AT LOCATION 1 AT 4000 RPM, 5.0 PSI SEAL OIL PRESSURE, 0.8 IN–GRAM UNBALANCE LOCATED IN THE TURBINE DISK, FOR INCREASING STATIC PRELOADS.

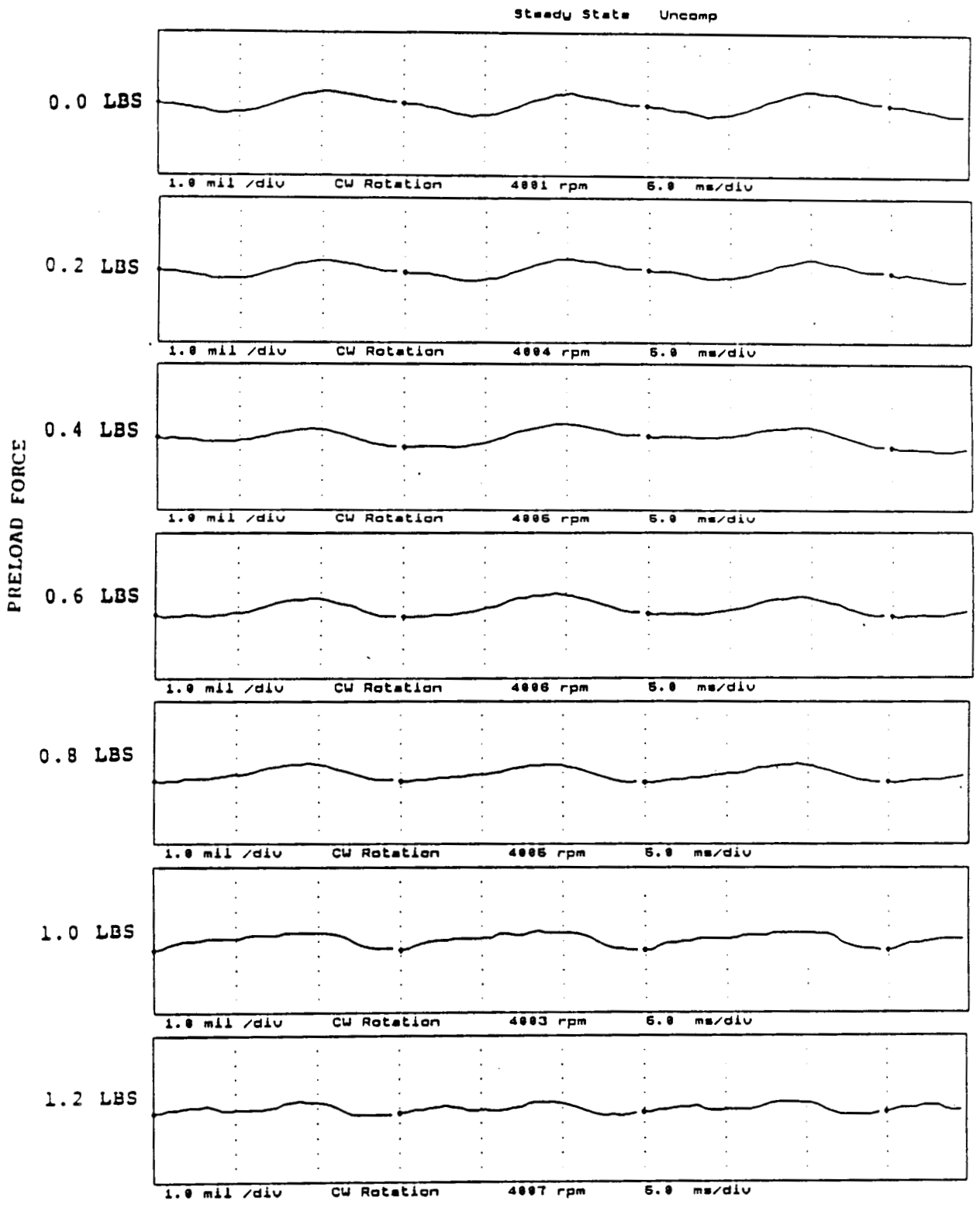

FIGURE 12.78 TIMEBASE FOR VERTICAL PROBE AT LOCATION 2 AT 4000 RPM, 5.0 PSI SEAL OIL PRESSURE, 0.8 IN–GRAM UNBALANCE LOCATED IN THE TURBINE DISK, FOR INCREASING STATIC PRELOADS.

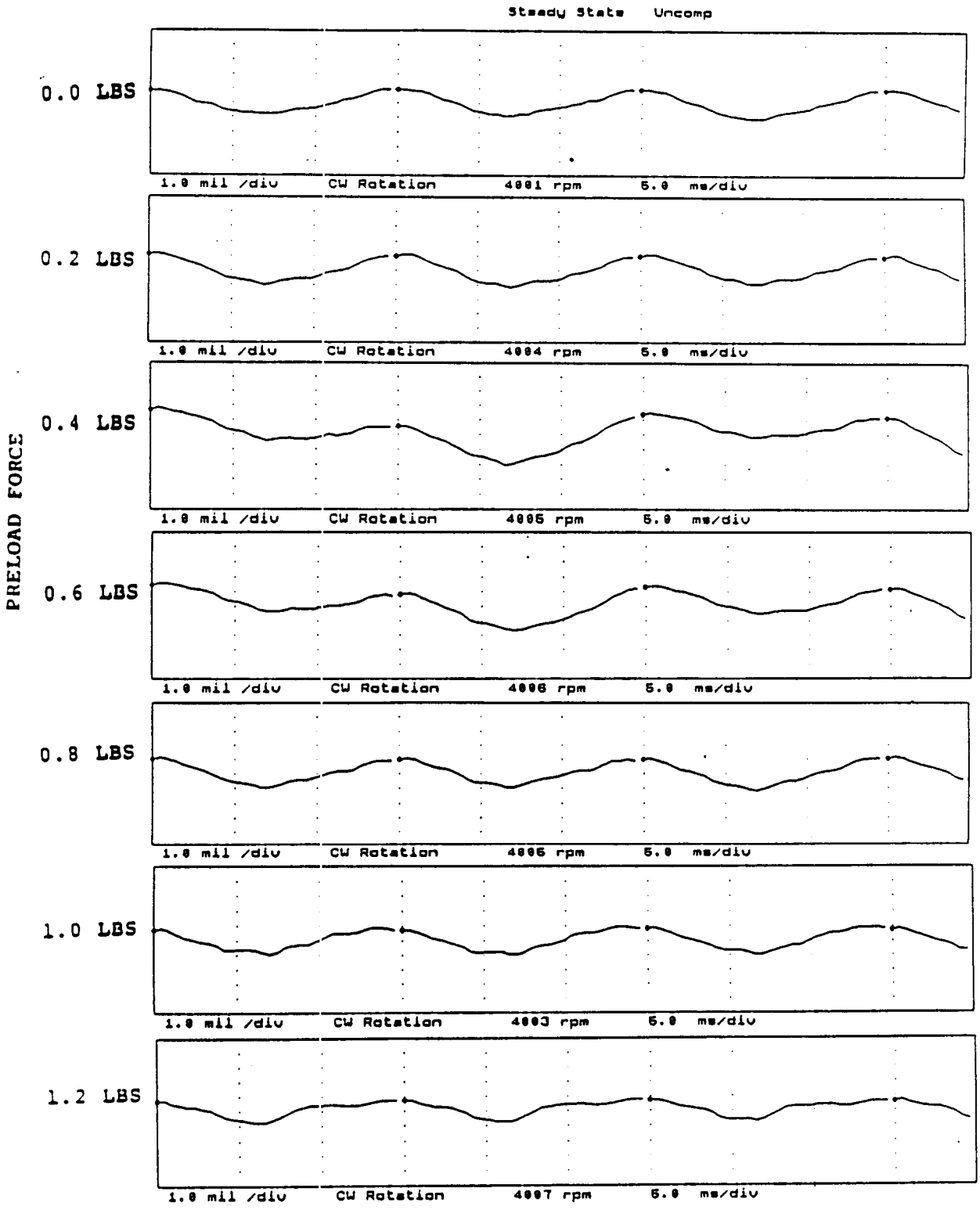

FIGURE 12.79 TIMEBASE FOR HORIZONTAL PROBE AT LOCATION 2 AT 4000 RPM, 5.0 PSI SEAL OIL PRESSURE, 0.8 IN–GRAM UNBALANCE LOCATED IN THE TURBINE DISK, FOR INCREASING STATIC PRELOADS.

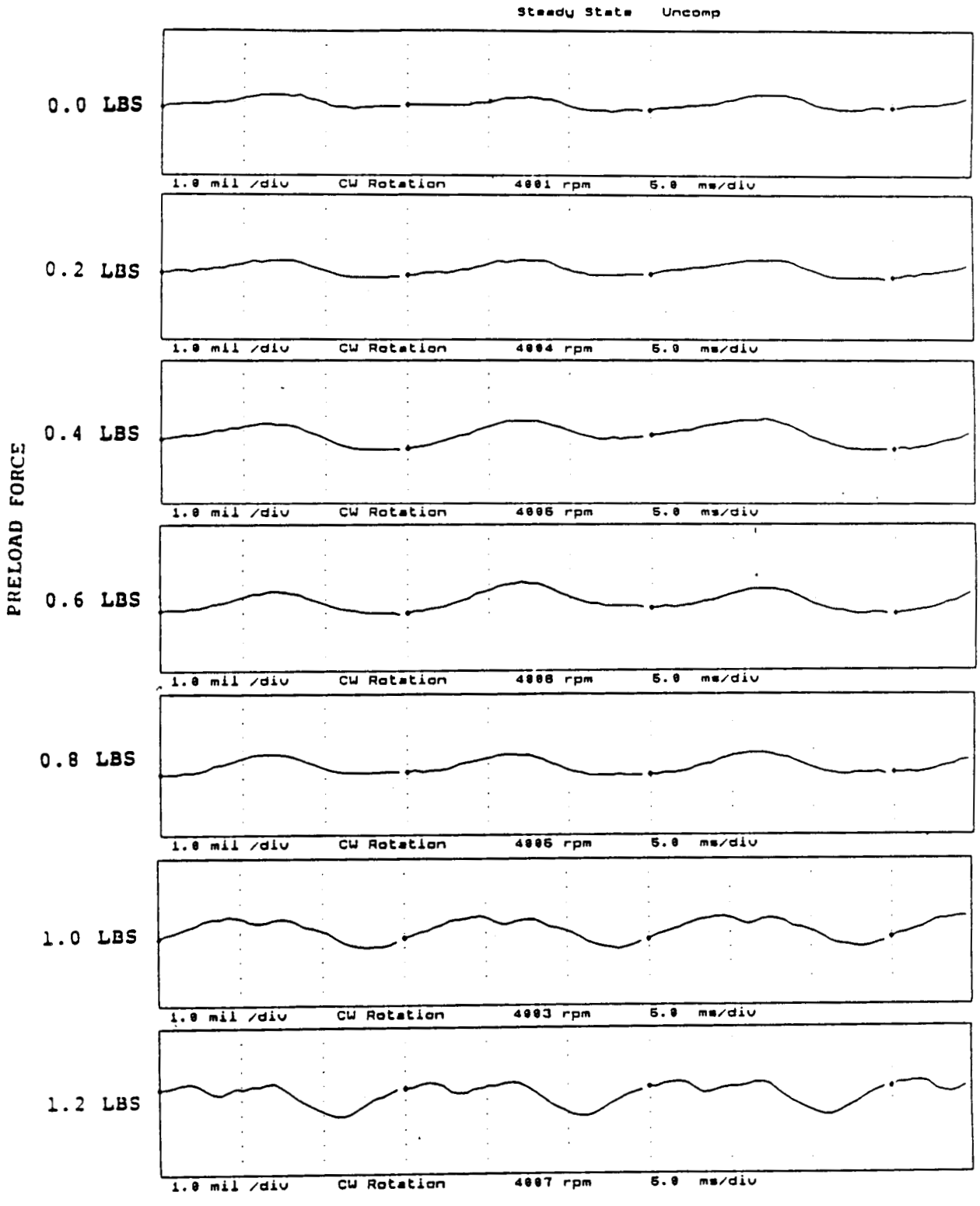

FIGURE 12.80 TIMEBASE FOR VERTICAL PROBE AT LOCATION 3 AT 4000 RPM, 5.0 PSI SEAL OIL PRESSURE, 0.8 IN–GRAM UNBALANCE LOCATED IN THE TURBINE DISK, FOR INCREASING STATIC PRELOADS.

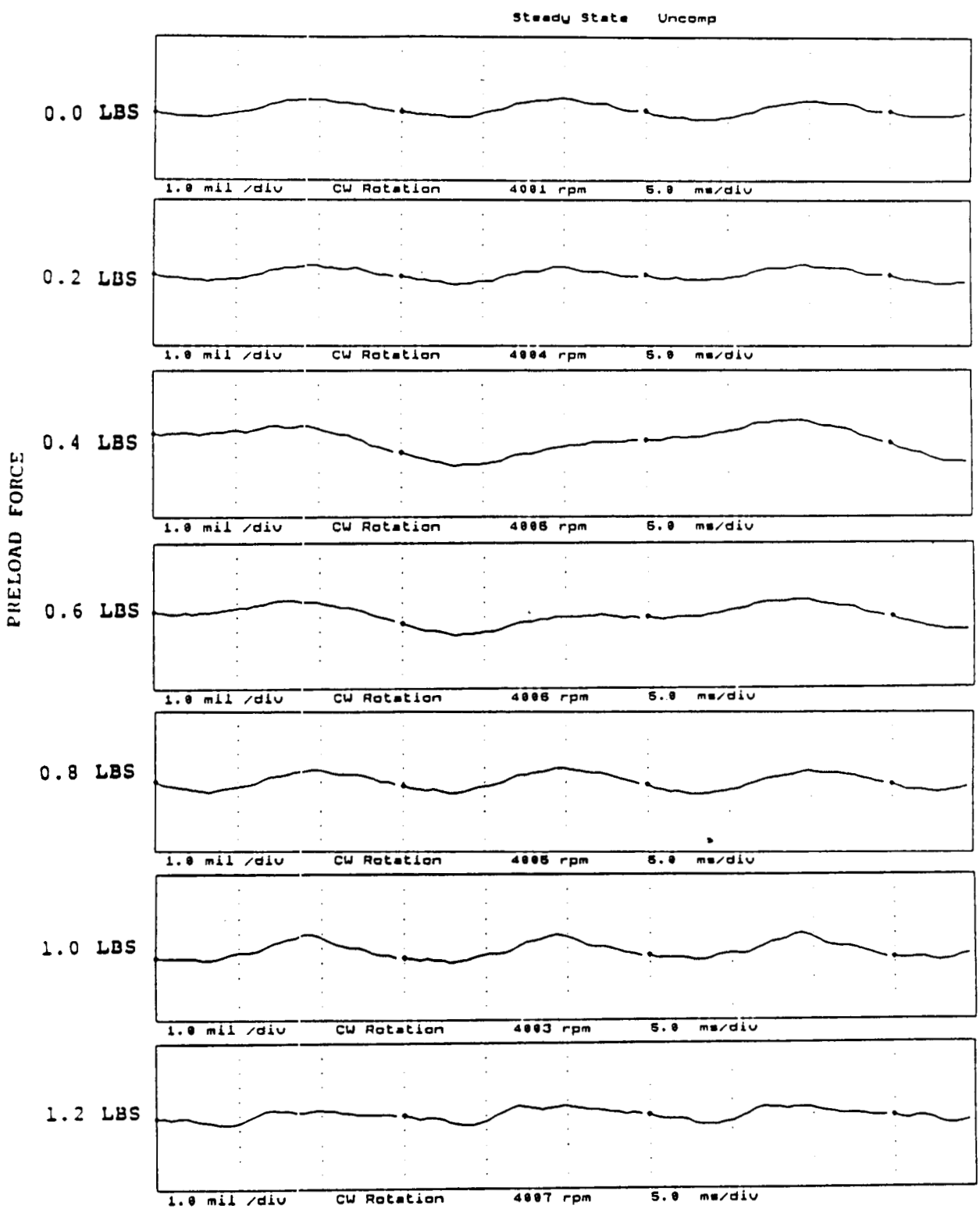

FIGURE 12.81 TIMEBASE FOR HORIZONTAL PROBE AT LOCATION 3 AT 4000 RPM, 5.0 PSI SEAL OIL PRESSURE, 0.8 IN–GRAM UNBALANCE LOCATED IN THE TURBINE DISK, FOR INCREASING STATIC PRELOADS.

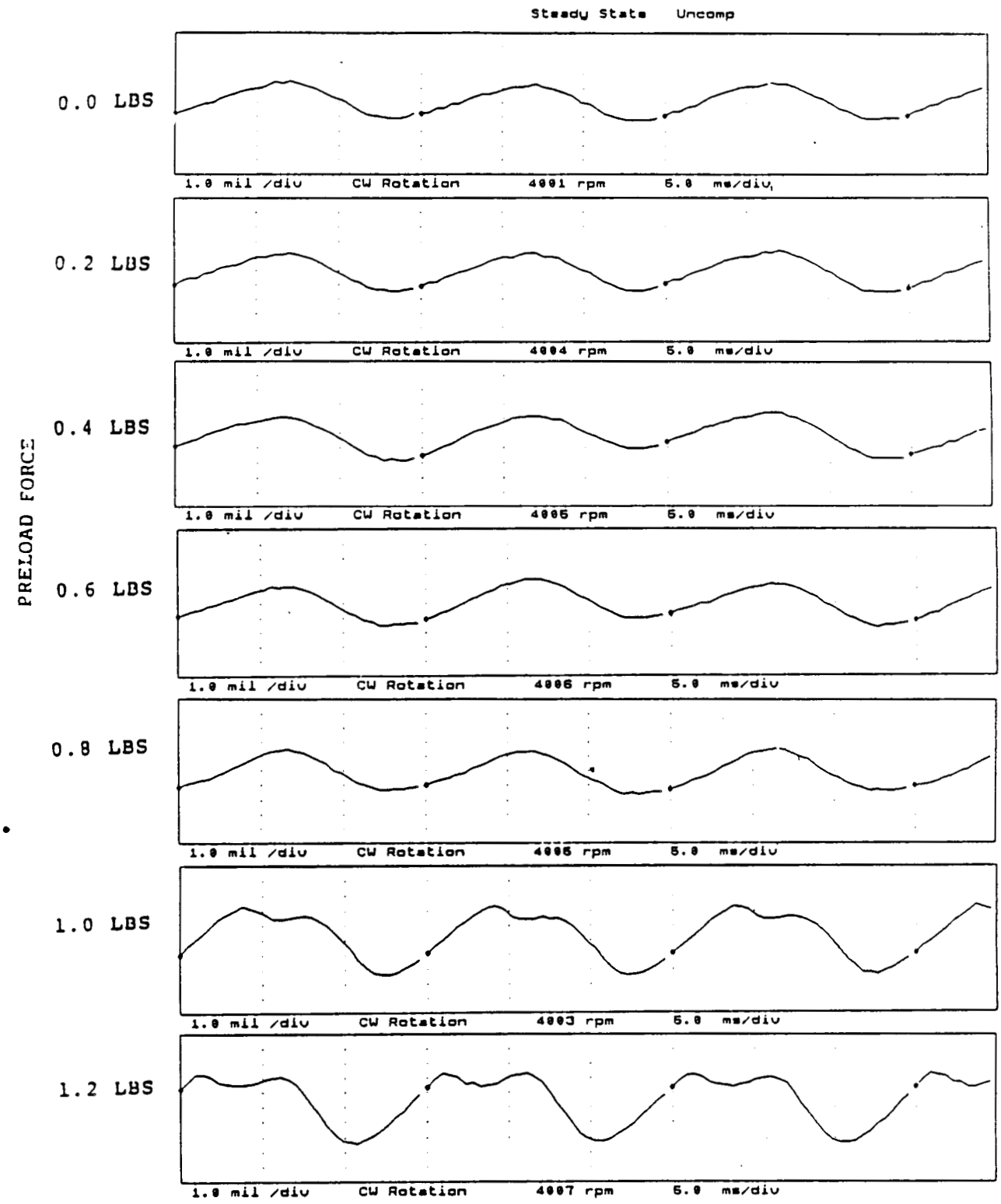

FIGURE 12.82 TIMEBASE FOR VERTICAL PROBE AT LOCATION 4 AT 4000 RPM, 5.0 PSI SEAL OIL PRESSURE, 0.8 IN–GRAM UNBALANCE LOCATED IN THE TURBINE DISK, FOR INCREASING STATIC PRELOADS.

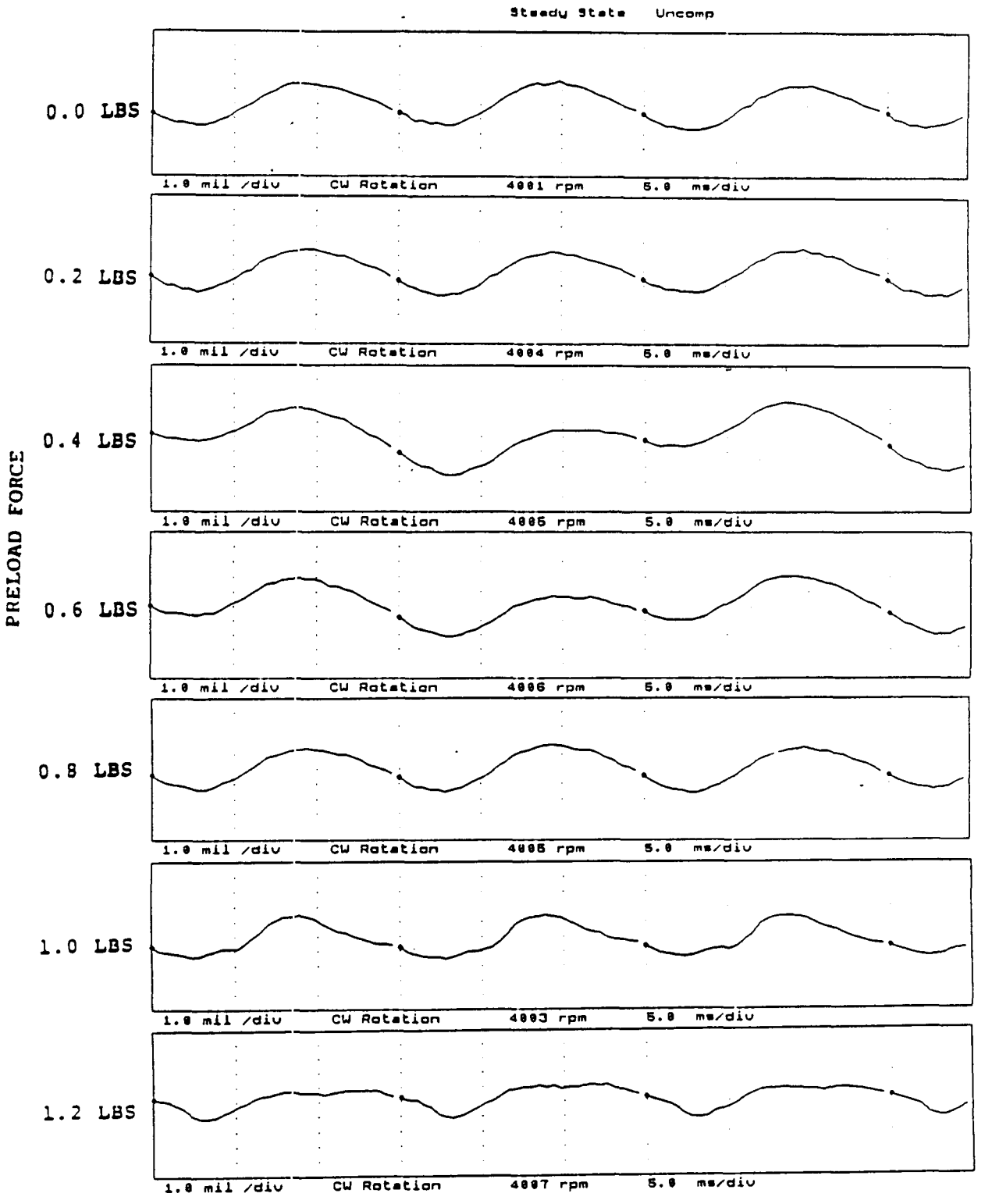

FIGURE 12.83 TIMEBASE FOR HORIZONTAL PROBE AT LOCATION 4 AT 4000 RPM, 5.0 PSI SEAL OIL PRESSURE, 0.8 IN–GRAM UNBALANCE LOCATED IN THE TURBINE DISK, FOR INCREASING STATIC PRELOADS.

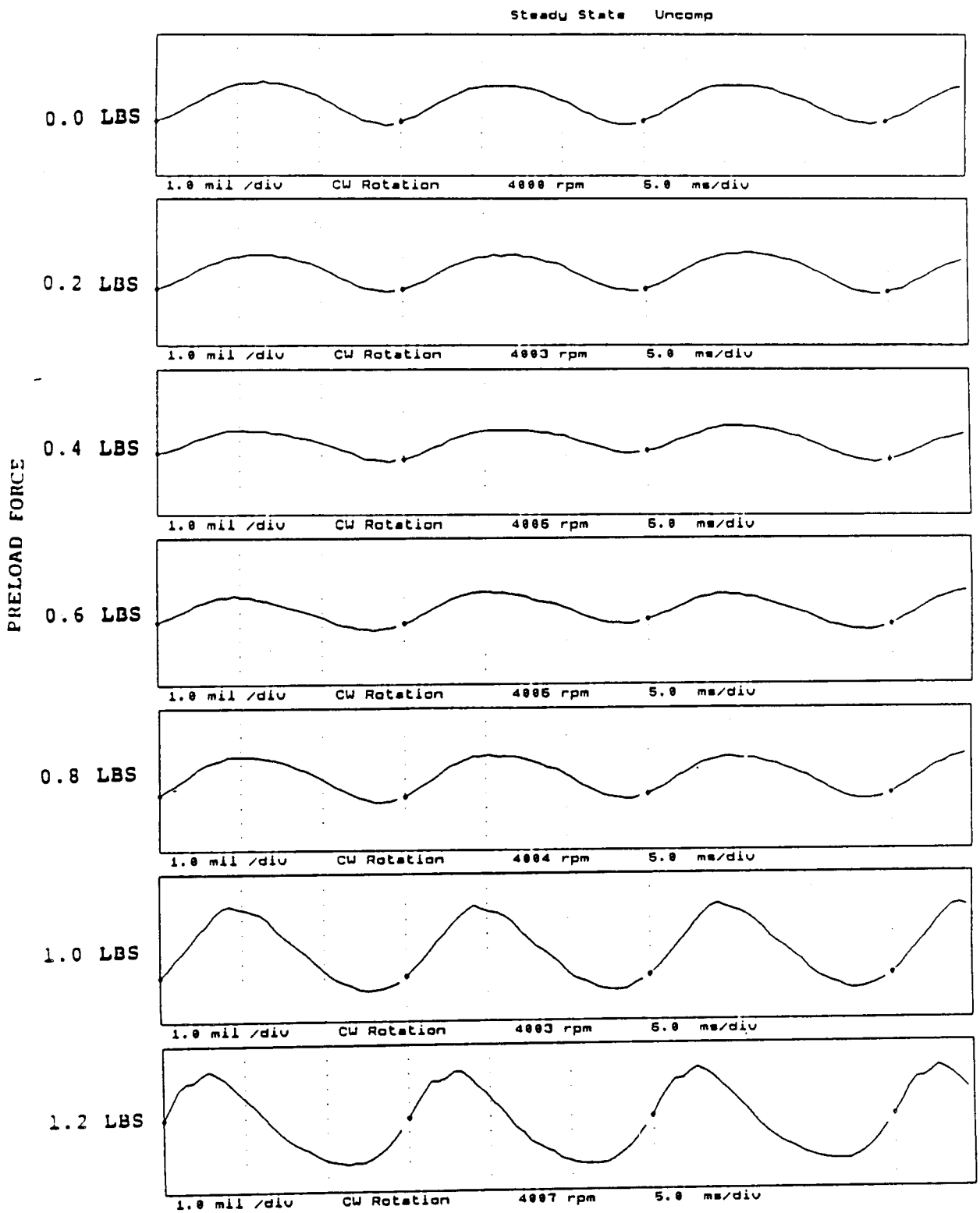

FIGURE 12.84 TIMEBASE FOR VERTICAL PROBE AT LOCATION 5 AT 4000 RPM, 5.0 PSI SEAL OIL PRESSURE, 0.8 IN–GRAM UNBALANCE LOCATED IN THE TURBINE DISK, FOR INCREASING STATIC PRELOADS.

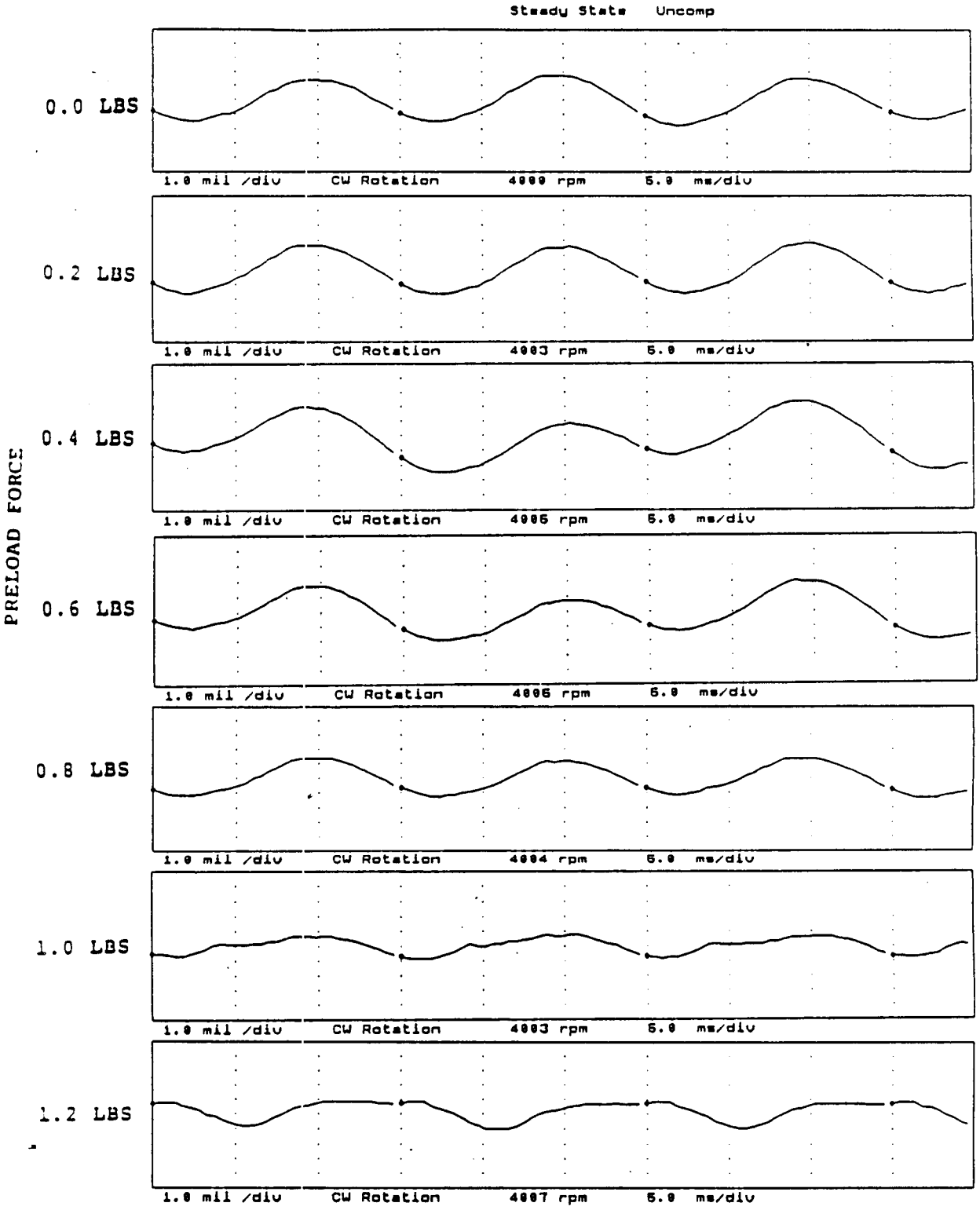

FIGURE 12.85 TIMEBASE FOR HORIZONTAL PROBE AT LOCATION 5 AT 4000 RPM, 5.0 PSI SEAL OIL PRESSURE, 0.8 IN–GRAM UNBALANCE LOCATED IN THE TURBINE DISK, FOR INCREASING STATIC PRELOADS.

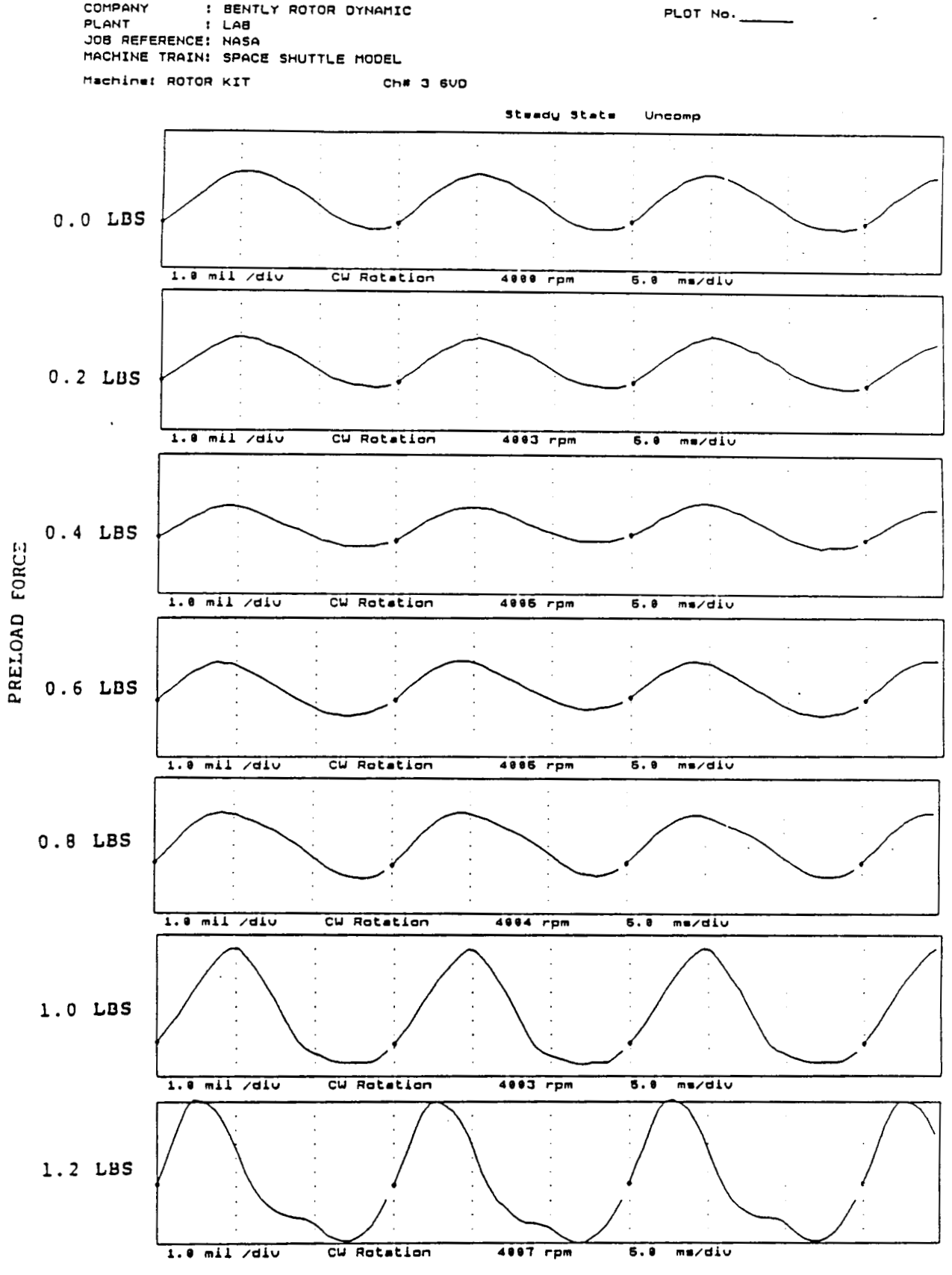

FIGURE 12.86 TIMEBASE FOR VERTICAL PROBE AT LOCATION 6 AT 4000 RPM, 5.0 PSI SEAL OIL PRESSURE, 0.8 IN–GRAM UNBALANCE LOCATED IN THE TURBINE DISK, FOR INCREASING STATIC PRELOADS.

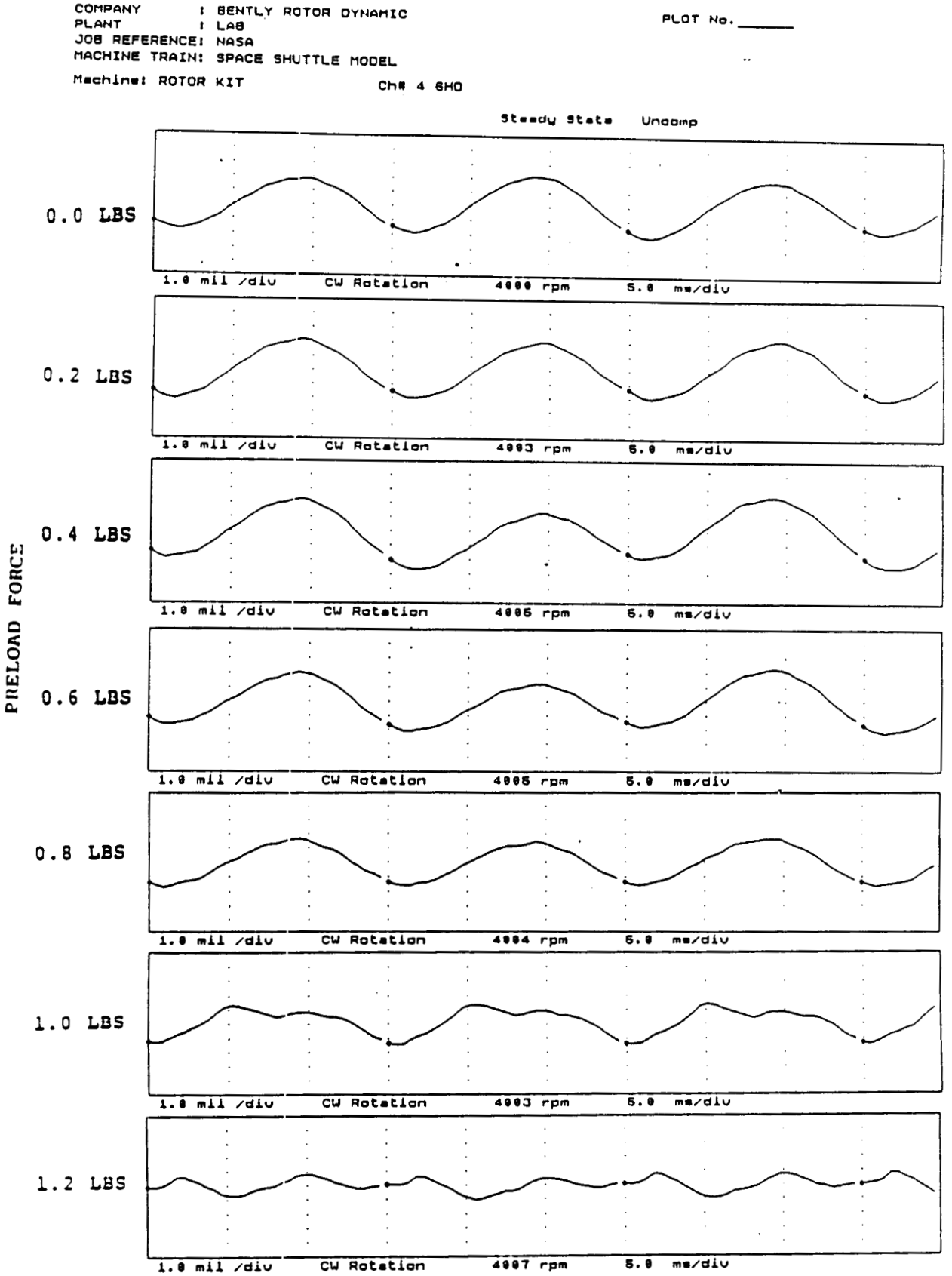

FIGURE 12.87 TIMEBASE FOR HORIZONTAL PROBE AT LOCATION 6 AT 4000 RPM, 5.0 PSI SEAL OIL PRESSURE, 0.8 IN–GRAM UNBALANCE LOCATED IN THE TURBINE DISK, FOR INCREASING STATIC PRELOADS.

NOT AVAILABLE - OIL IN THE CLEARANCE AREA
PROHIBITS THE METAL-TO-METAL CONTACT NECESSARY
FOR THE CONTACT SENSOR TO OPERATE CORRECTLY.

FIGURE 12.88 TIMEBASE FOR SHAFT TO SEAL 1 CONTACT AT 4000 RPM, 5.0 PSI SEAL OIL PRESSURE, 0.8 IN–GRAM UNBALANCE LOCATED IN THE TURBINE DISK, FOR INCREASING STATIC PRELOADS.

NOT AVAILABLE - OIL IN THE CLEARANCE AREA
PROHIBITS THE METAL-TO-METAL CONTACT NECESSARY
FOR THE CONTACT SENSOR TO OPERATE CORRECTLY.

FIGURE 12.89 TIMEBASE FOR SHAFT TO SEAL 2 CONTACT AT 4000 RPM, 5.0 PSI SEAL OIL PRESSURE, 0.8 IN–GRAM UNBALANCE LOCATED IN THE TURBINE DISK, FOR INCREASING STATIC PRELOADS.

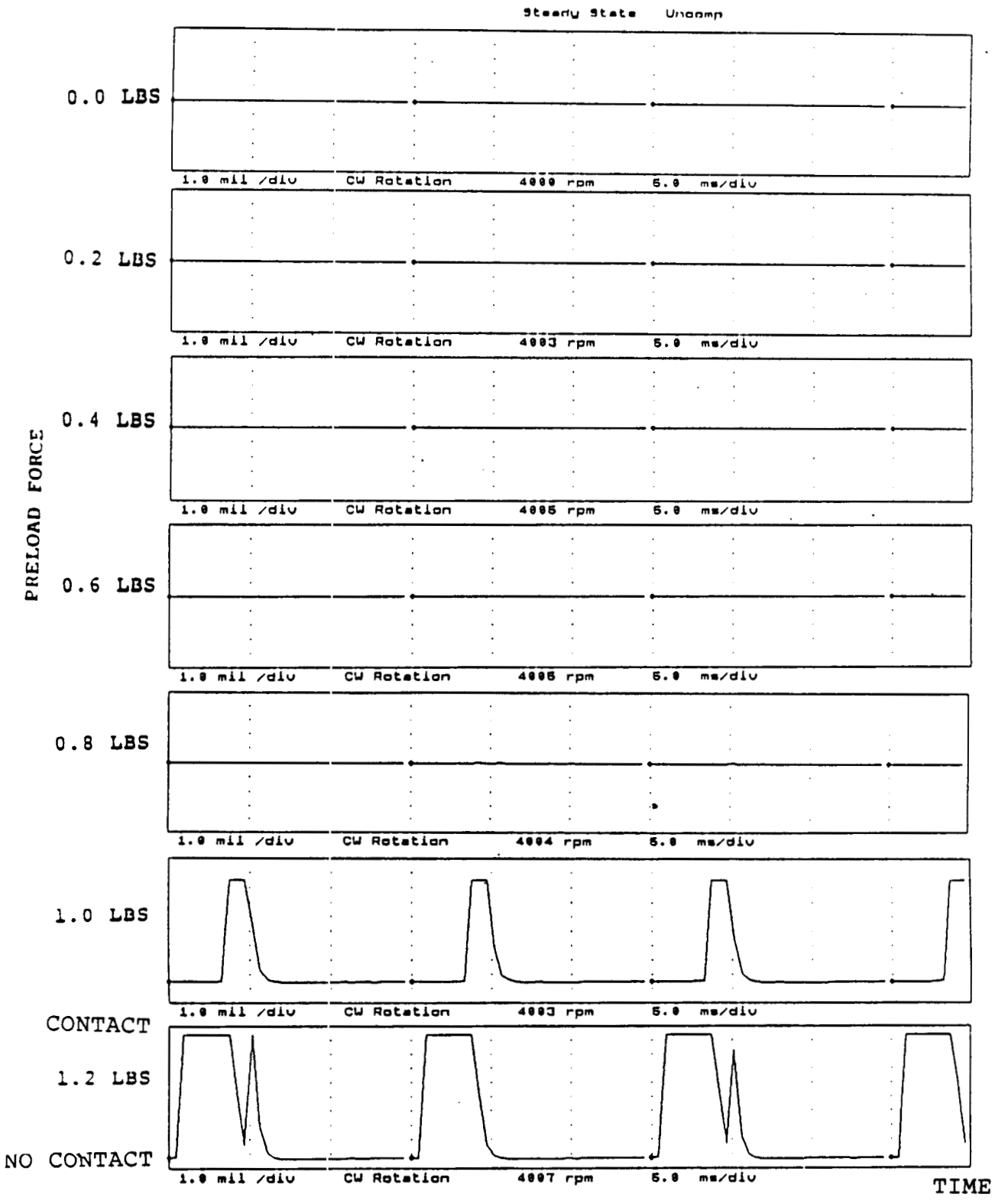

FIGURE 12.90 TIMEBASE FOR SHAFT TO RUB BLOCK CONTACT AT 4000 RPM, 5.0 PSI SEAL OIL PRESSURE, 0.8 IN–GRAM UNBALANCE LOCATED IN THE TURBINE DISK, FOR INCREASING STATIC PRELOADS.

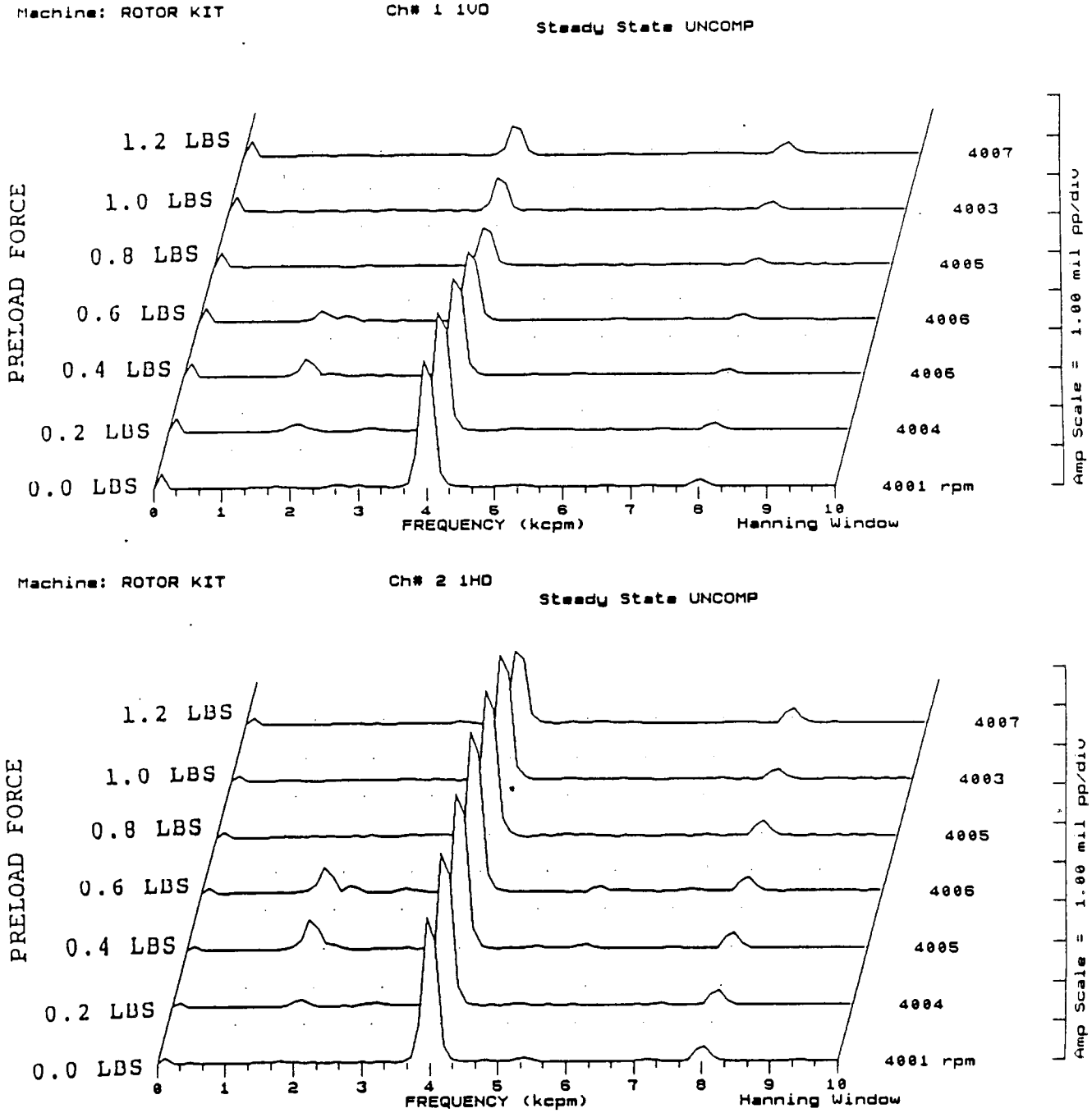

FIGURE 12.91 SPECTRAL CONTENT AT PROBE LOCATION 1 AT 4000 RPM, 5.0 PSI SEAL OIL PRESSURE, 0.8 IN–GRAM UNBALANCE LOCATED IN THE TURBINE DISK, FOR INCREASING STATIC PRELOADS.

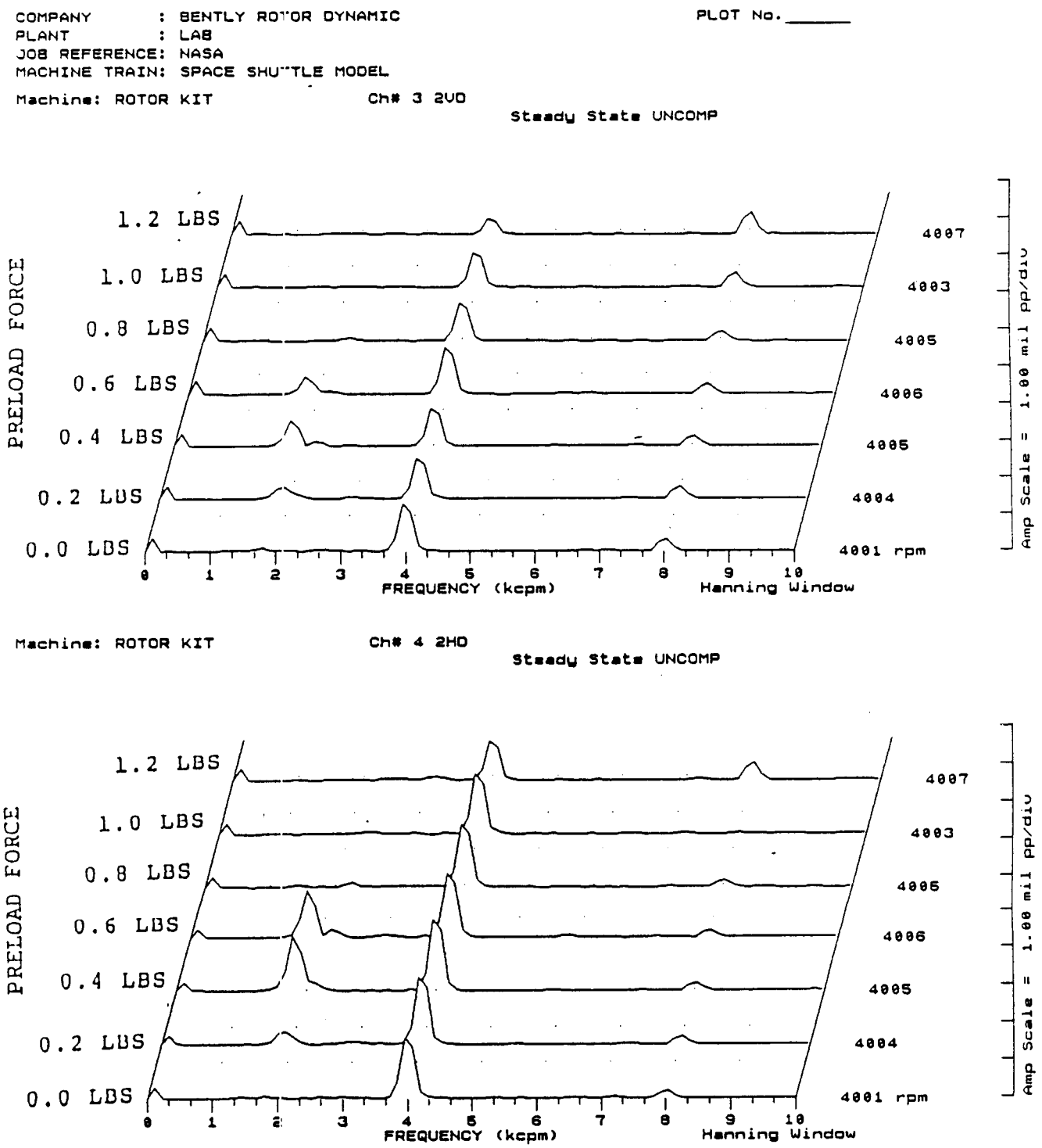

FIGURE 12.92 SPECTRAL CONTENT AT PROBE LOCATION 2 AT 4000 RPM, 5.0 PSI SEAL OIL PRESSURE, 0.8 IN–GRAM UNBALANCE LOCATED IN THE TURBINE DISK, FOR INCREASING STATIC PRELOADS.

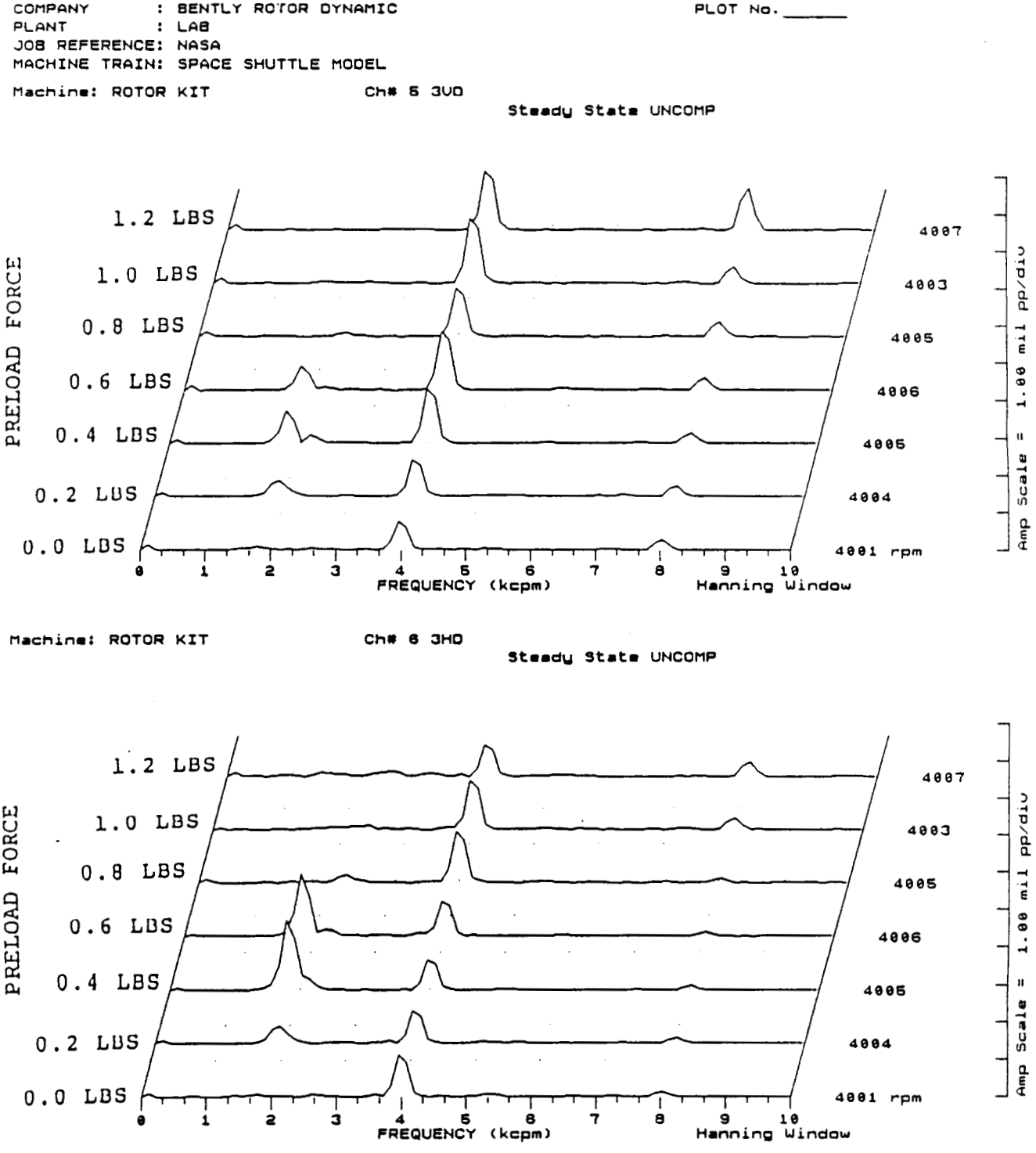

FIGURE 12.93 SPECTRAL CONTENT AT PROBE LOCATION 3 AT 4000 RPM, 5.0 PSI SEAL OIL PRESSURE, 0.8 IN–GRAM UNBALANCE LOCATED IN THE TURBINE DISK, FOR INCREASING STATIC PRELOADS.

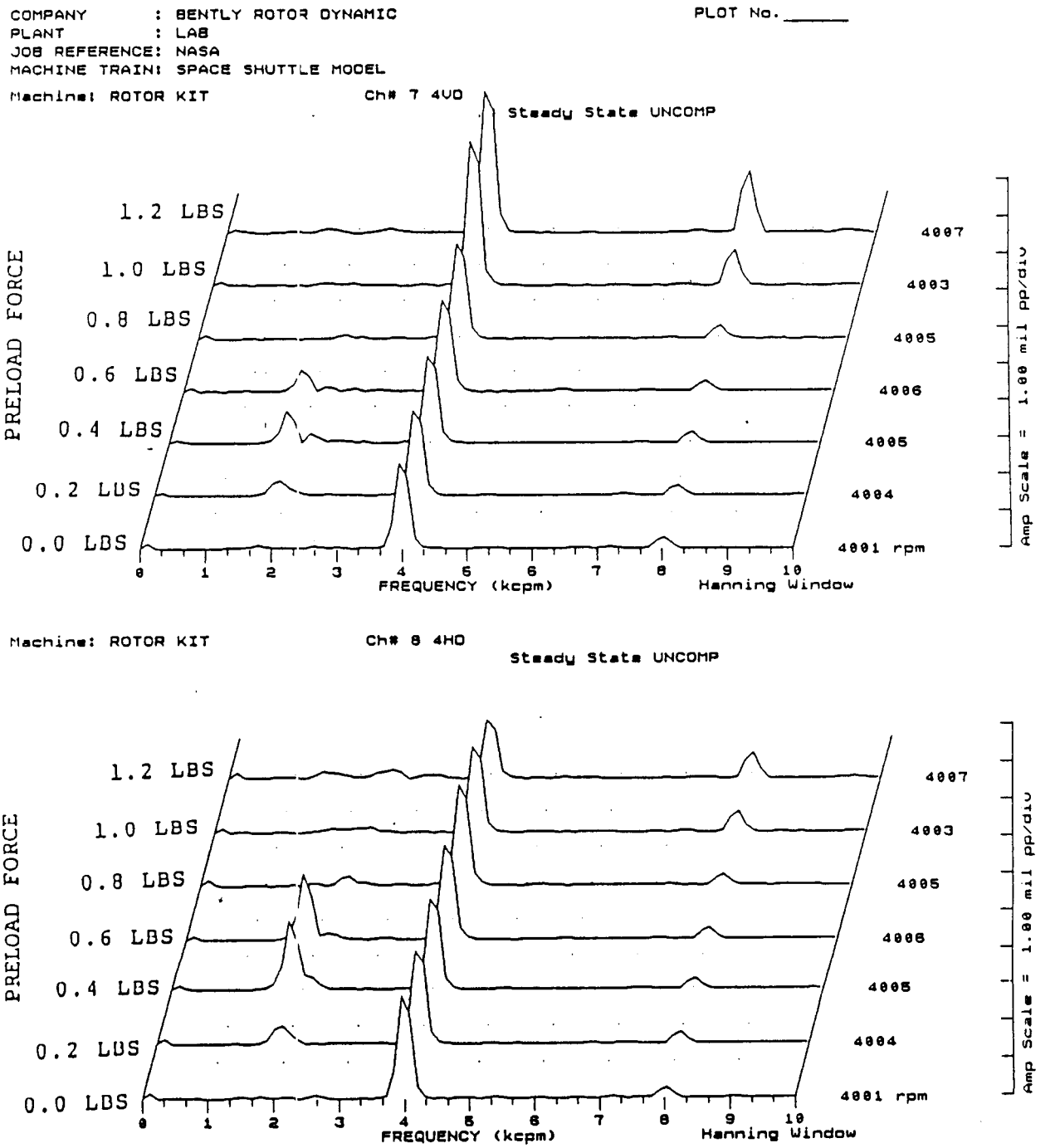

FIGURE 12.94 SPECTRAL CONTENT AT PROBE LOCATION 4 AT 4000 RPM, SEAL OIL PRESSURE, 0.8 IN–GRAM UNBALANCE LOCATED IN THE TURBINE DISK, FOR INCREASING STATIC PRELOADS.

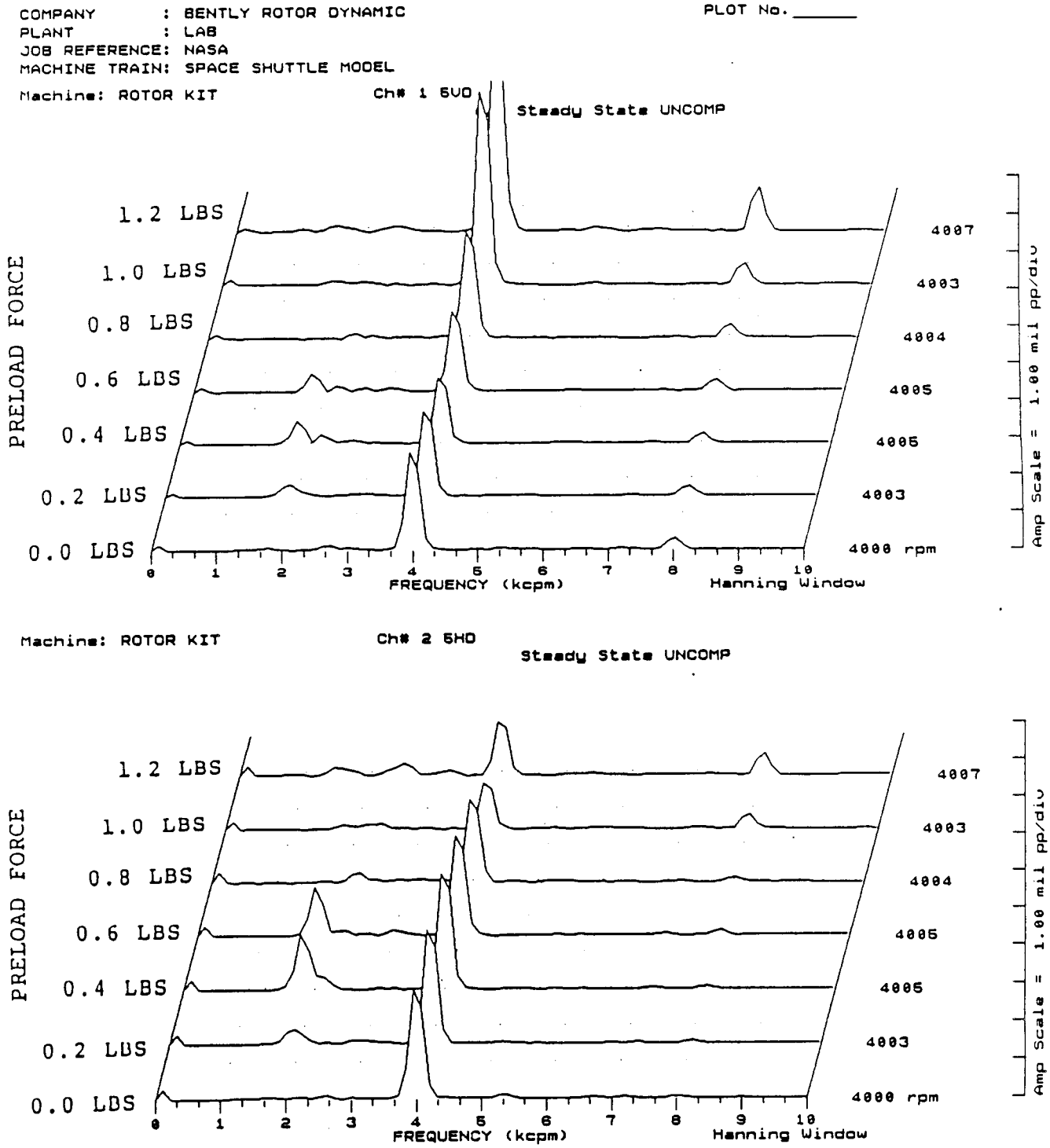

FIGURE 12.95 SPECTRAL CONTENT AT PROBE LOCATION 5 AT 4000 RPM, 5.0 PSI SEAL OIL PRESSURE, 0.8 IN–GRAM UNBALANCE LOCATED IN THE TURBINE DISK, FOR INCREASING STATIC PRELOADS.

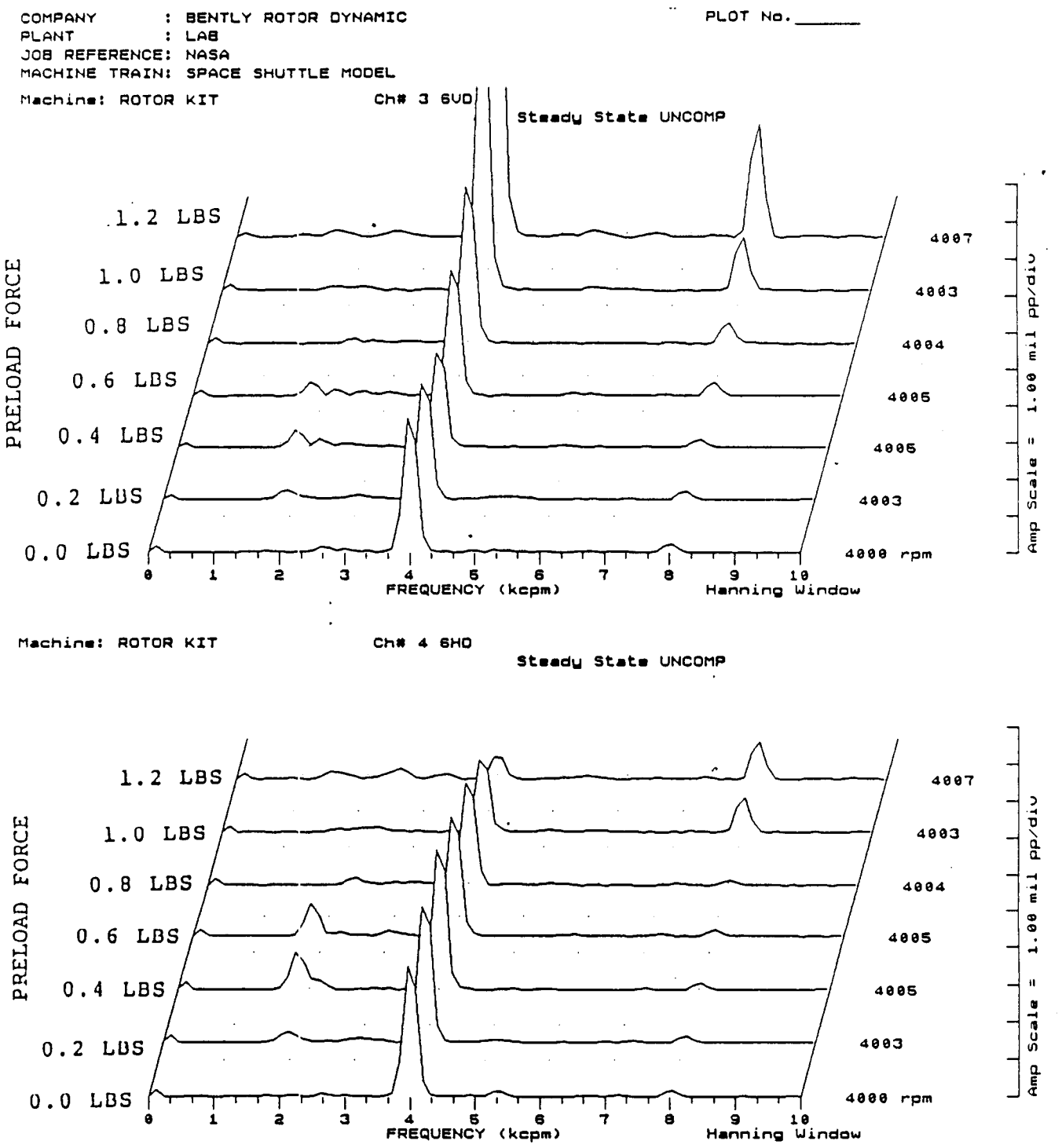

FIGURE 12.96 SPECTRAL CONTENT AT PROBE LOCATION 6 AT 4000 RPM, 5.0 PSI SEAL OIL PRESSURE, 0.8 IN–GRAM UNBALANCE LOCATED IN THE TURBINE DISK, FOR INCREASING STATIC PRELOADS.

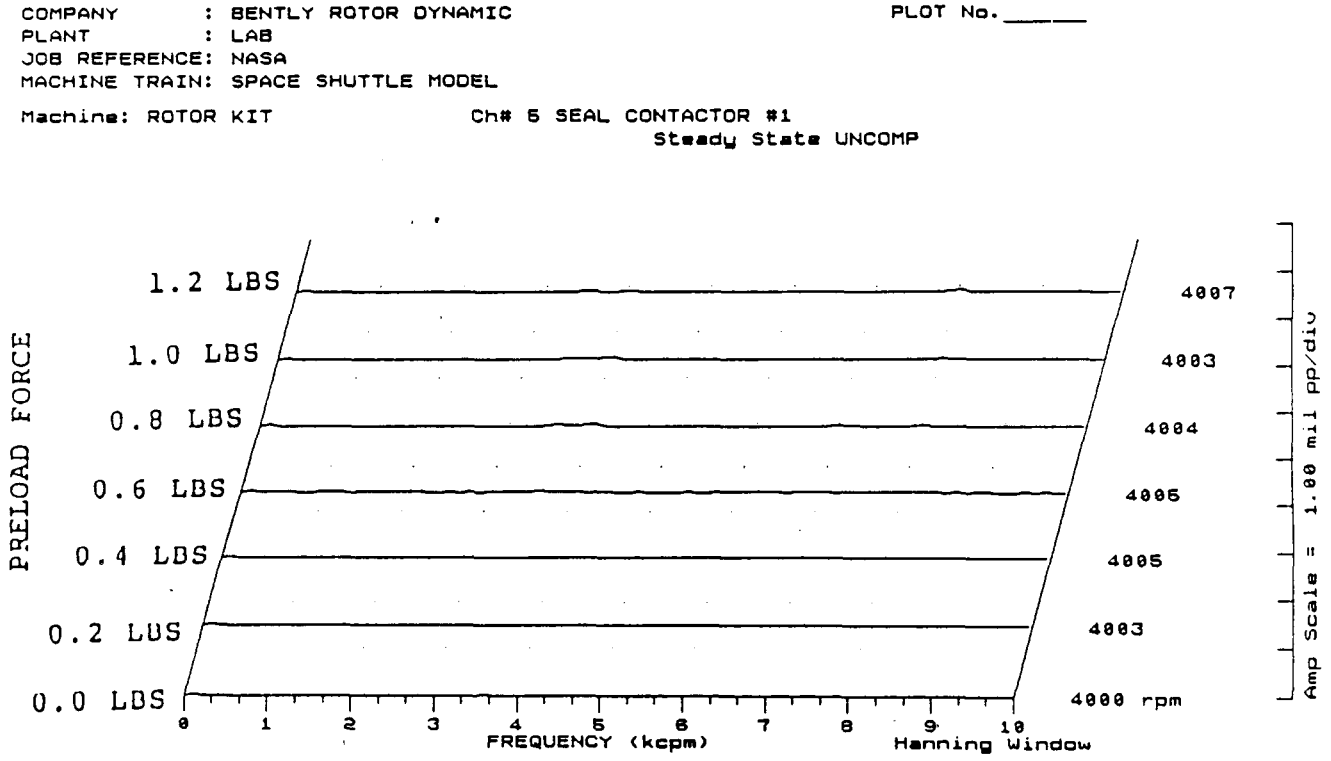

FIGURE 12.97 SPECTRAL CONTENT FOR SHAFT TO SEAL 1 CONTACT AT 4000 RPM, 5.0 PSI SEAL OIL PRESSURE, 0.8 IN–GRAM UNBALANCE LOCATED IN THE TURBINE DISK, FOR INCREASING STATIC PRELOADS.

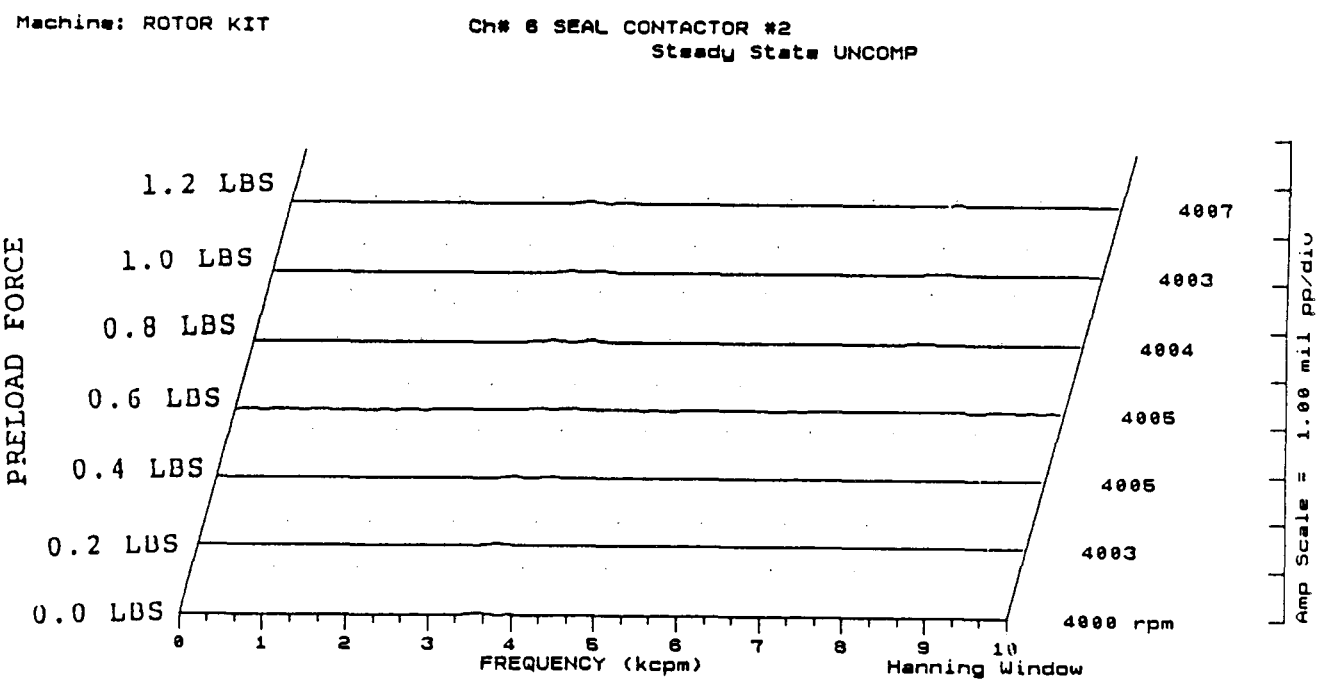

FIGURE 12.98 SPECTRAL CONTENT FOR SHAFT TO SEAL 2 CONTACT AT 4000 RPM, 5.0 PSI SEAL OIL PRESSURE, 0.8 IN–GRAM UNBALANCE LOCATED IN THE TURBINE DISK, FOR INCREASING STATIC PRELOADS.

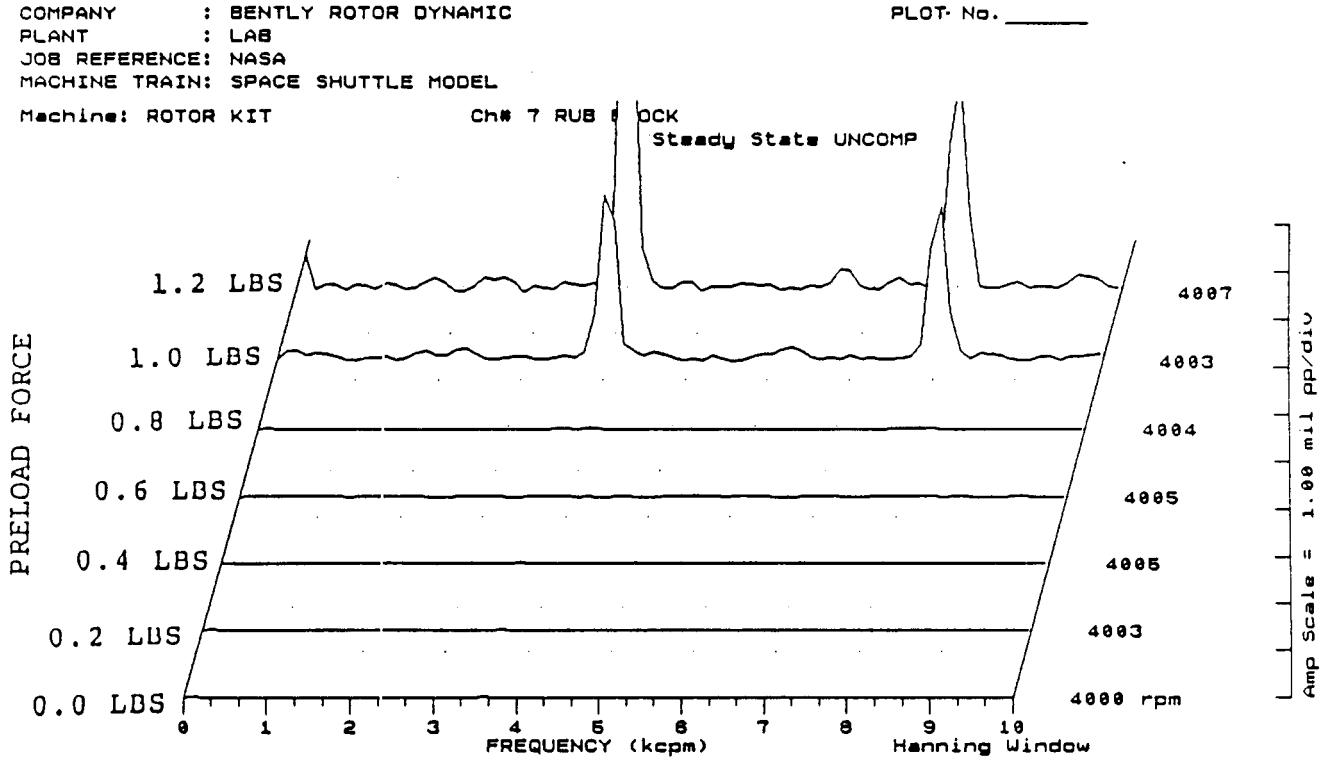

FIGURE 12.99 SPECTRAL CONTENT FOR SHAFT TO RUB BLOCK CONTACT AT 4000 RPM, 5.0 PSI SEAL OIL PRESSURE, 0.8 IN–GRAM UNBALANCE LOCATED IN THE TURBINE DISK, FOR INCREASING STATIC PRELOADS.

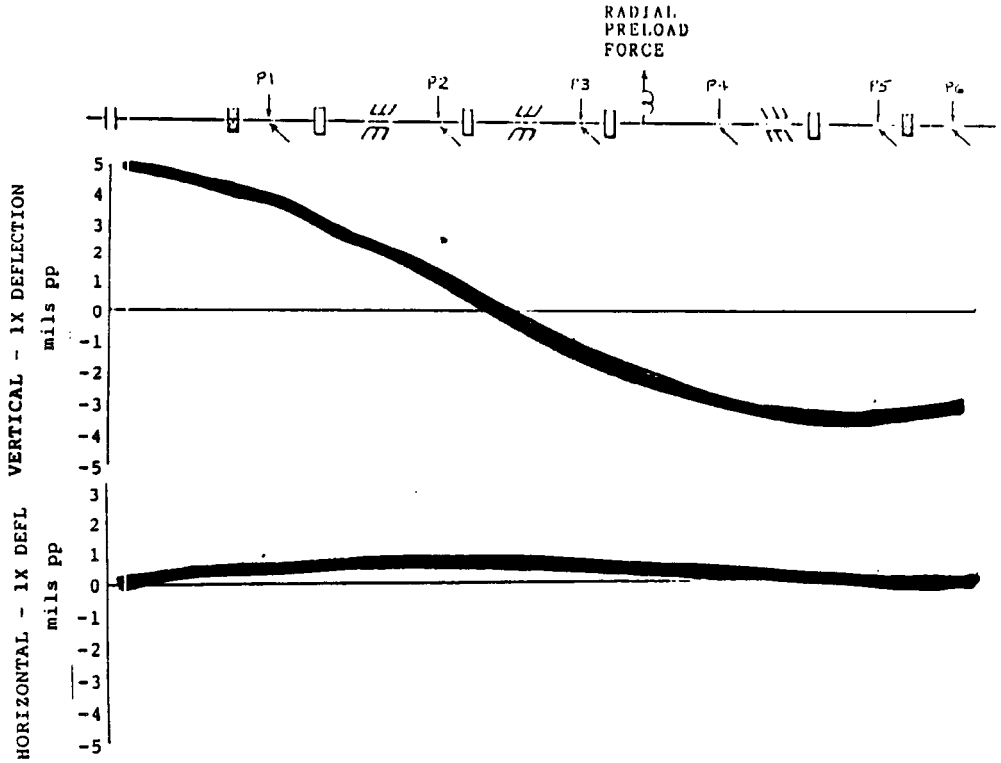

FIGURE 12.100 ROTOR MODE SHAPE AT 4000 RPM, 7.5 PSI SEAL OIL PRESSURE DUE TO 0.8 IN–GRAM UNBALANCE LOCATED IN THE TURBINE DISK.

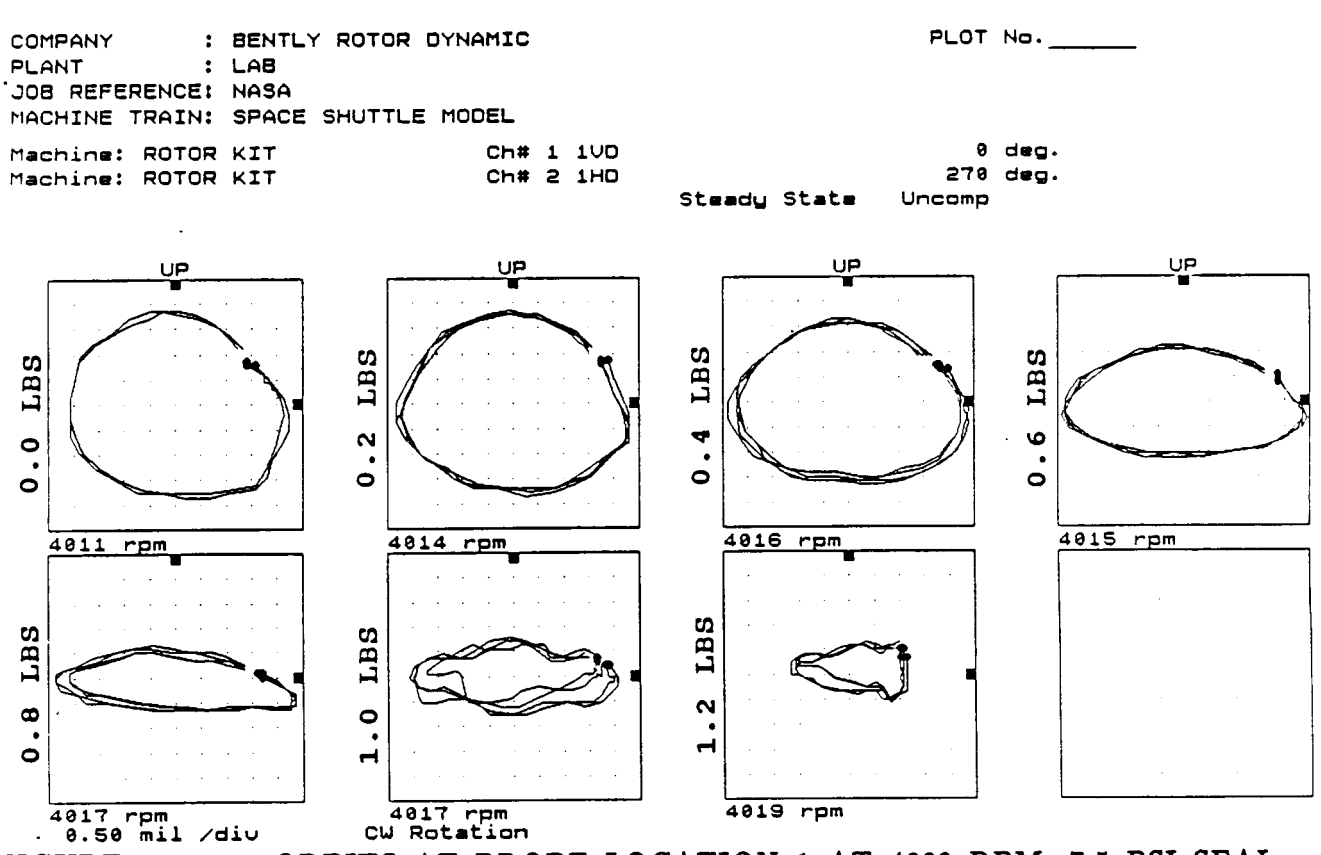

FIGURE 12.101 ORBITS AT PROBE LOCATION 1 AT 4000 RPM, 7.5 PSI SEAL OIL PRESSURE, 0.8 IN–GRAM UNBALANCE LOCATED IN THE TURBINE DISK, FOR INCREASING STATIC PRELOAD FORCES.

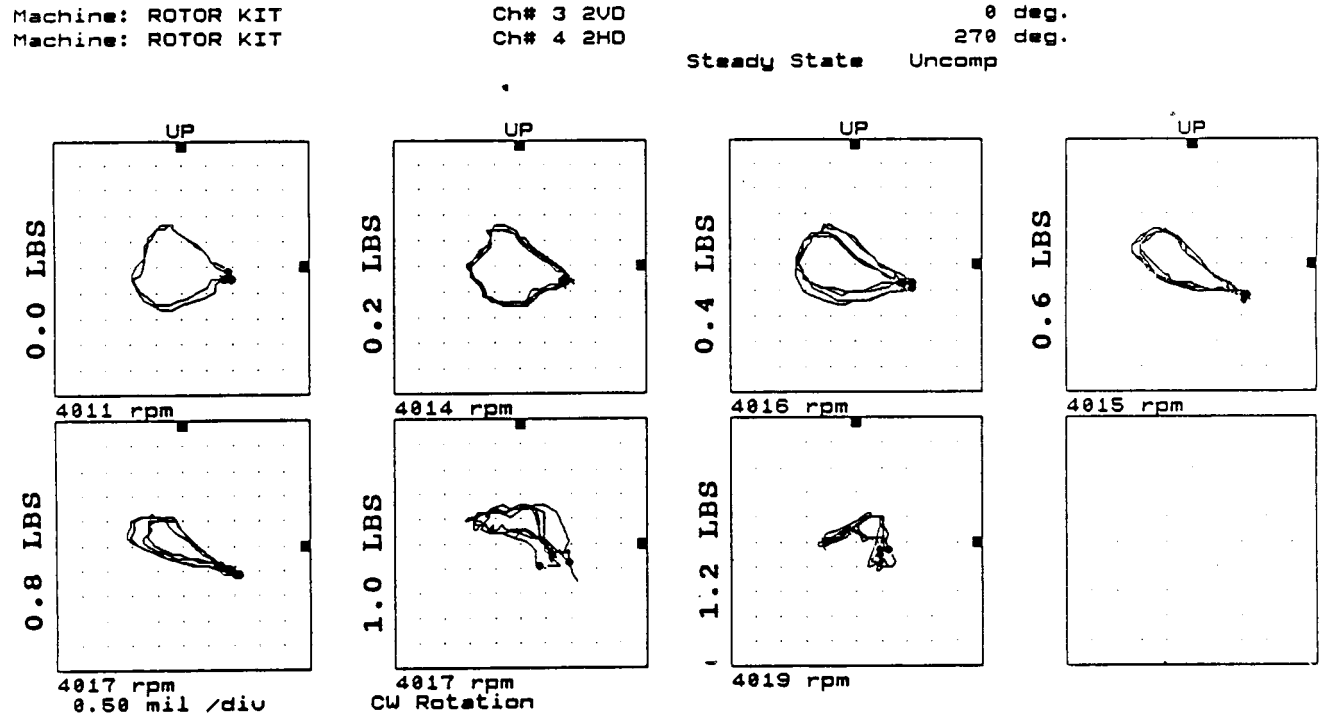

FIGURE 12.102 ORBITS AT PROBE LOCATION 2 AT 4000 RPM, 7.5 PSI SEAL OIL PRESSURE, 0.8 IN–GRAM UNBALANCE LOCATED IN THE TURBINE DISK, FOR INCREASING STATIC PRELOAD FORCES.

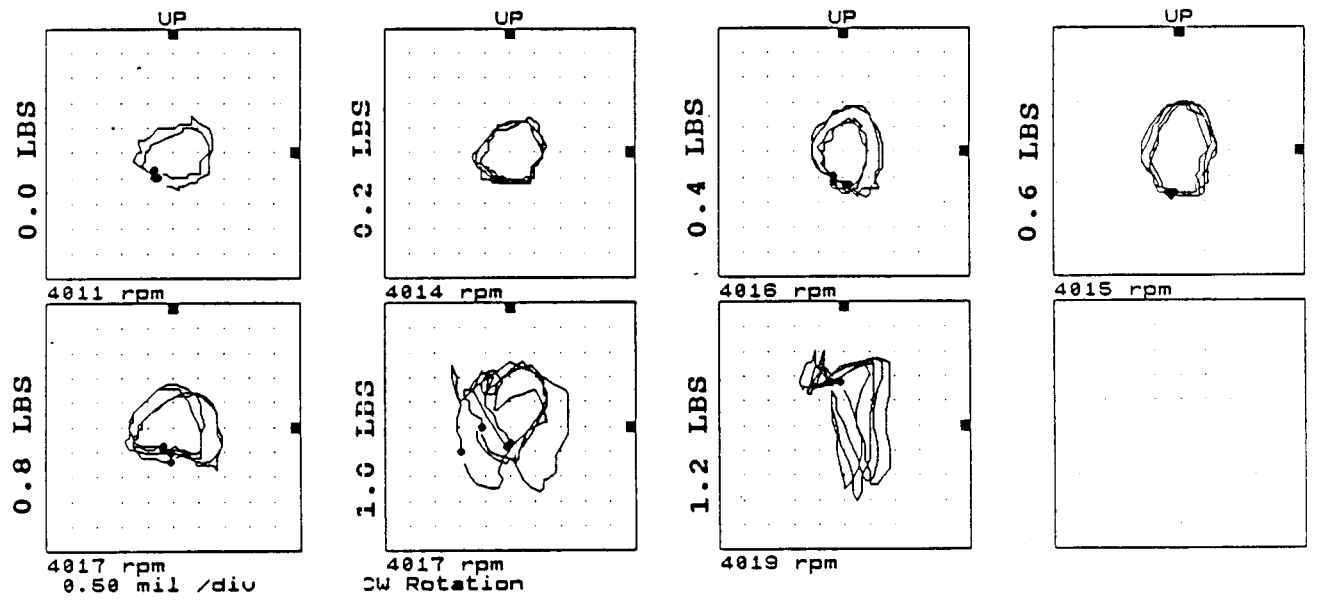

FIGURE 12.103 ORBITS AT PROBE LOCATION 3 AT 4000 RPM, 7.5 PSI SEAL OIL PRESSURE, 0.8 IN–GRAM UNBALANCE LOCATED IN THE TURBINE DISK, FOR INCREASING STATIC PRELOAD FORCES.

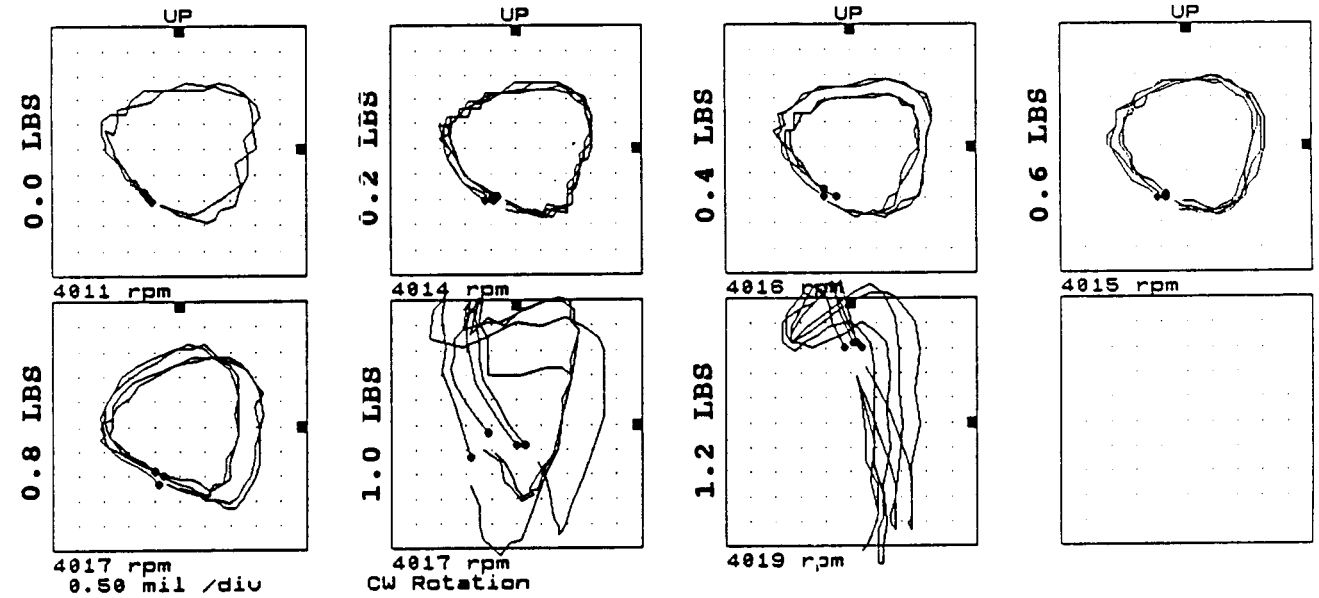

FIGURE 12.104 ORBITS AT PROBE LOCATION 4 AT 4000 RPM, 7.5 PSI SEAL OIL PRESSURE, 0.8 IN–GRAM UNBALANCE LOCATED IN THE TURBINE DISK, FOR INCREASING STATIC PRELOAD FORCES.

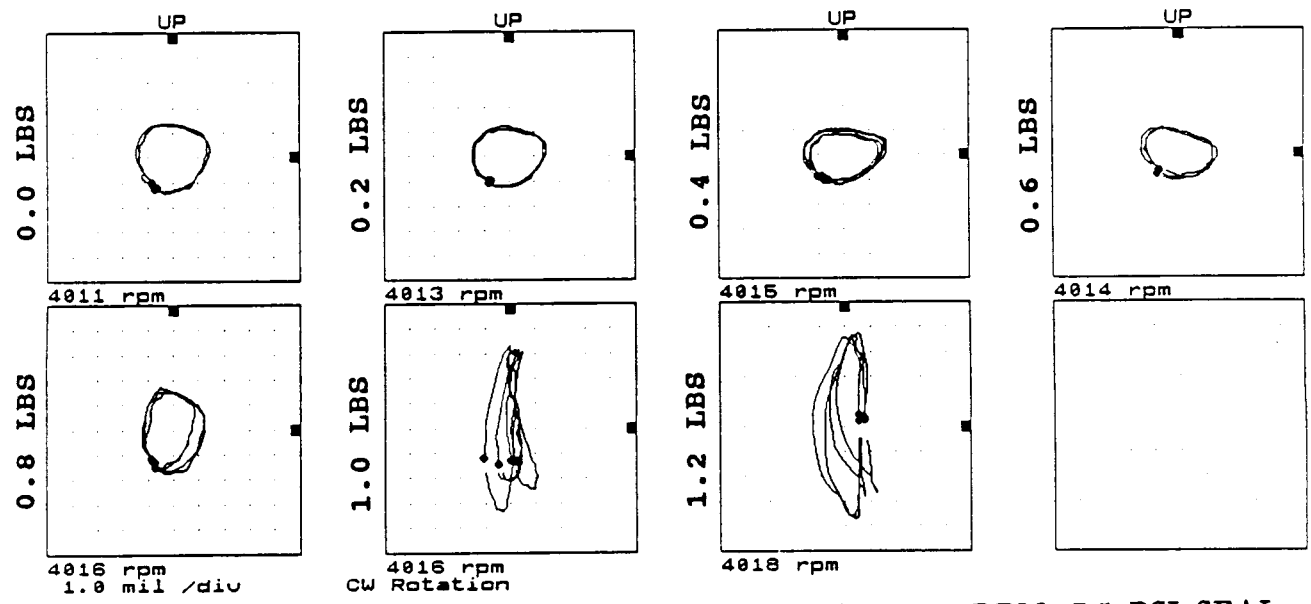

FIGURE 12.105 ORBITS AT PROBE LOCATION 5 AT 4000 RPM, 7.5 PSI SEAL OIL PRESSURE, 0.8 IN–GRAM UNBALANCE LOCATED IN THE TURBINE DISK, FOR INCREASING STATIC PRELOAD FORCES.

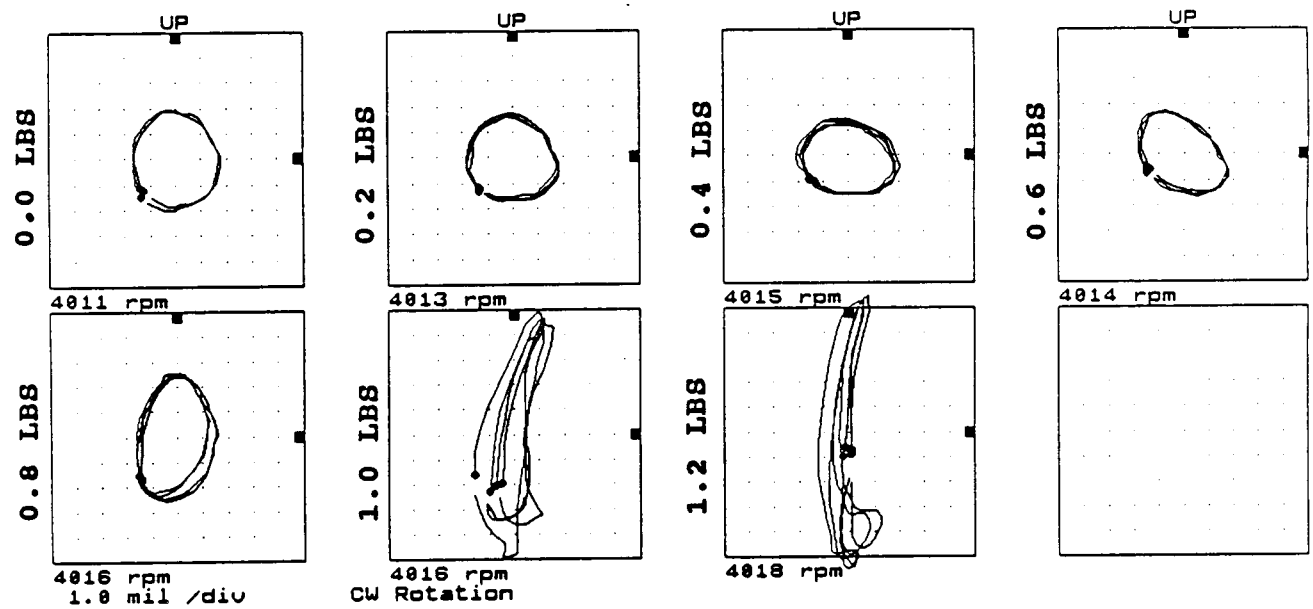

FIGURE 12.106 ORBITS AT PROBE LOCATION 6 AT 4000 RPM, 7.5 PSI SEAL OIL PRESSURE, 0.8 IN–GRAM UNBALANCE LOCATED IN THE TURBINE DISK, FOR INCREASING STATIC PRELOAD FORCES.

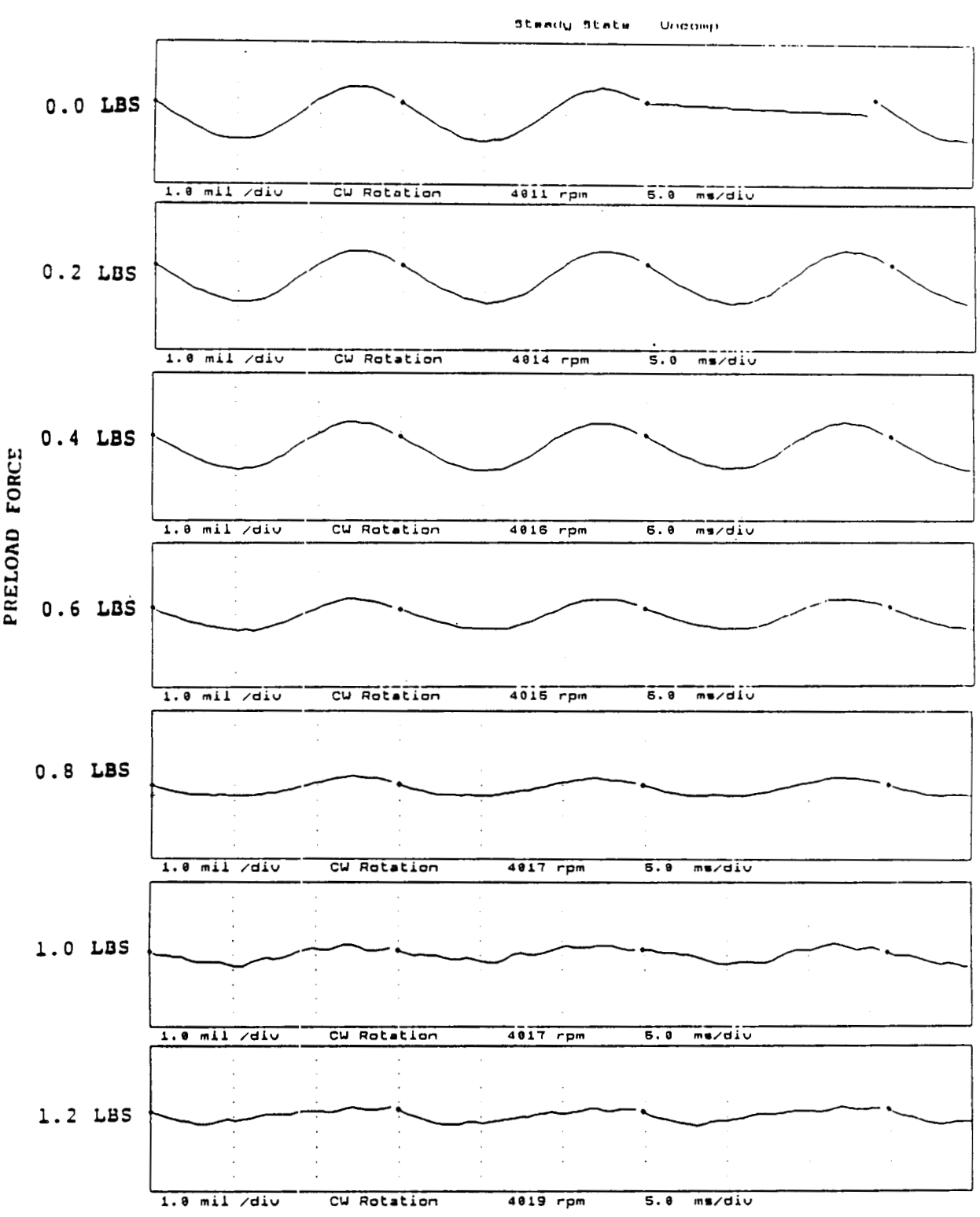

FIGURE 12.107 TIMEBASE FOR VERTICAL PROBE AT LOCATION 1 AT 4000 RPM, 7.5 PSI SEAL OIL PRESSURE, 0.8 IN–GRAM UNBALANCE LOCATED IN THE TURBINE DISK, FOR INCREASING STATIC PRELOADS.

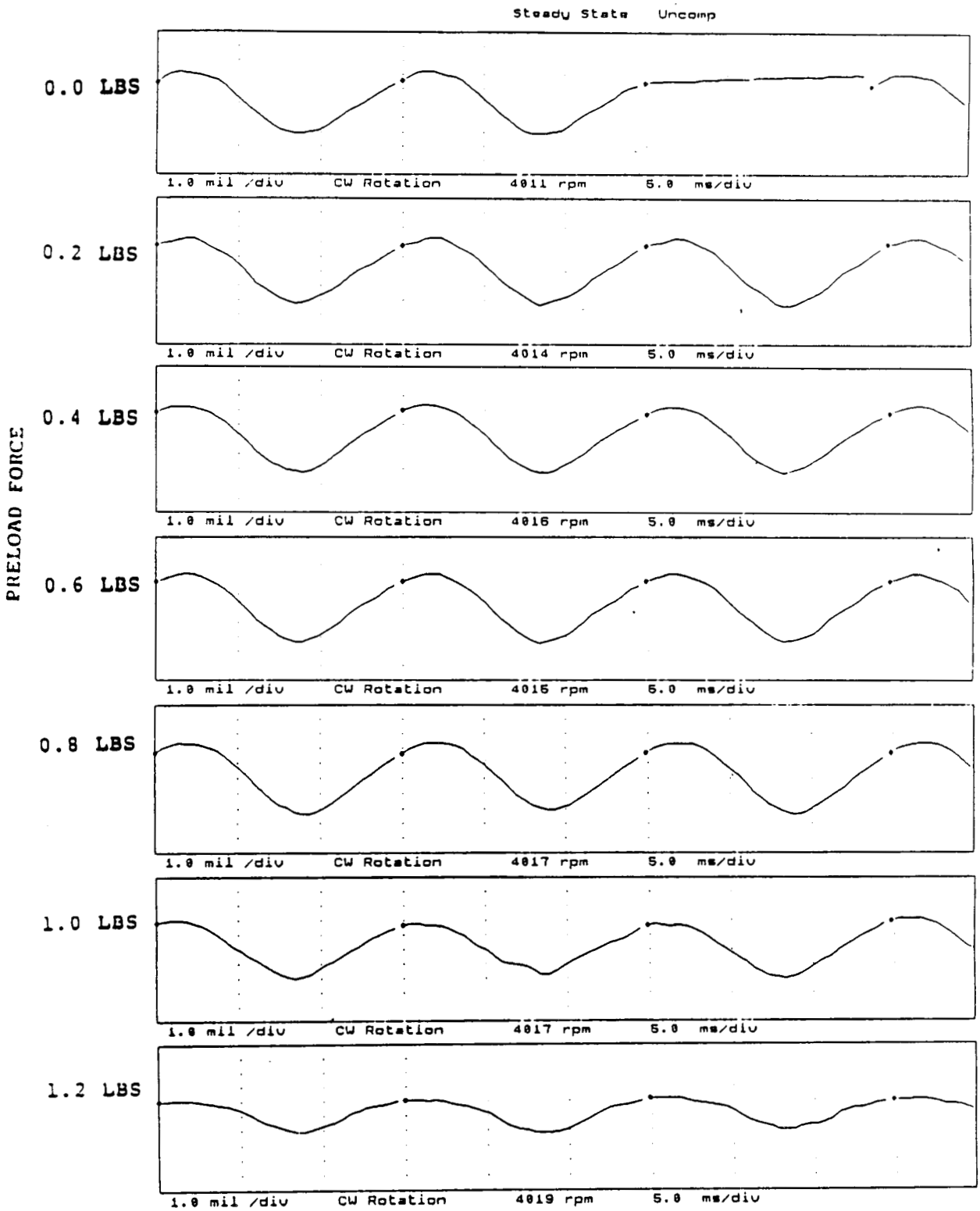

FIGURE 12.108 TIMEBASE FOR HORIZONTAL PROBE AT LOCATION 1 AT 4000 RPM, 7.5 PSI SEAL OIL PRESSURE, 0.8 IN–GRAM UNBALANCE LOCATED IN THE TURBINE DISK, FOR INCREASING STATIC PRELOADS.

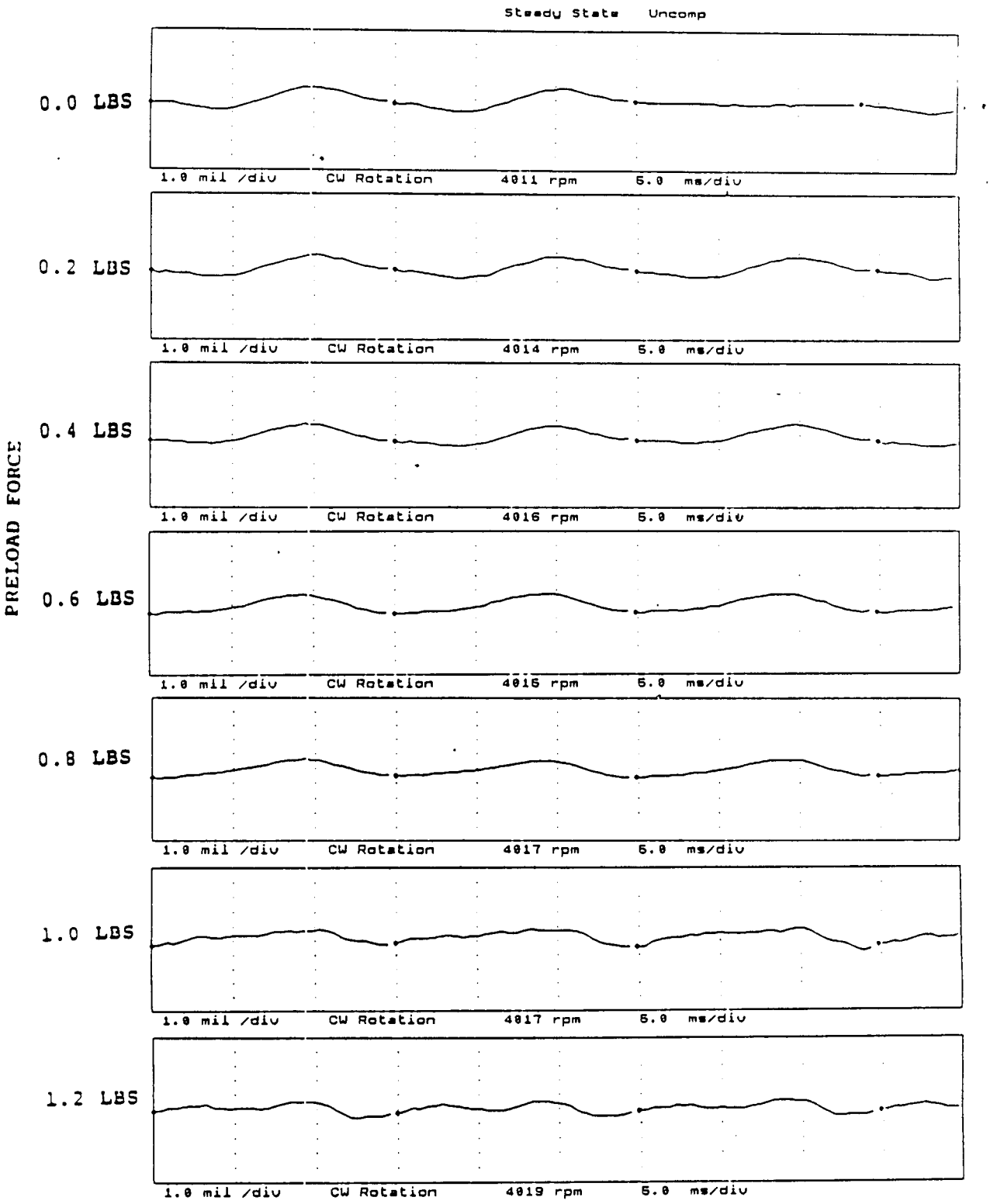

FIGURE 12.109 TIMEBASE FOR VERTICAL PROBE AT LOCATION 2 AT 4000 RPM, 7.5 PSI SEAL OIL PRESSURE, 0.8 IN–GRAM UNBALANCE LOCATED IN THE TURBINE DISK, FOR INCREASING STATIC PRELOADS.

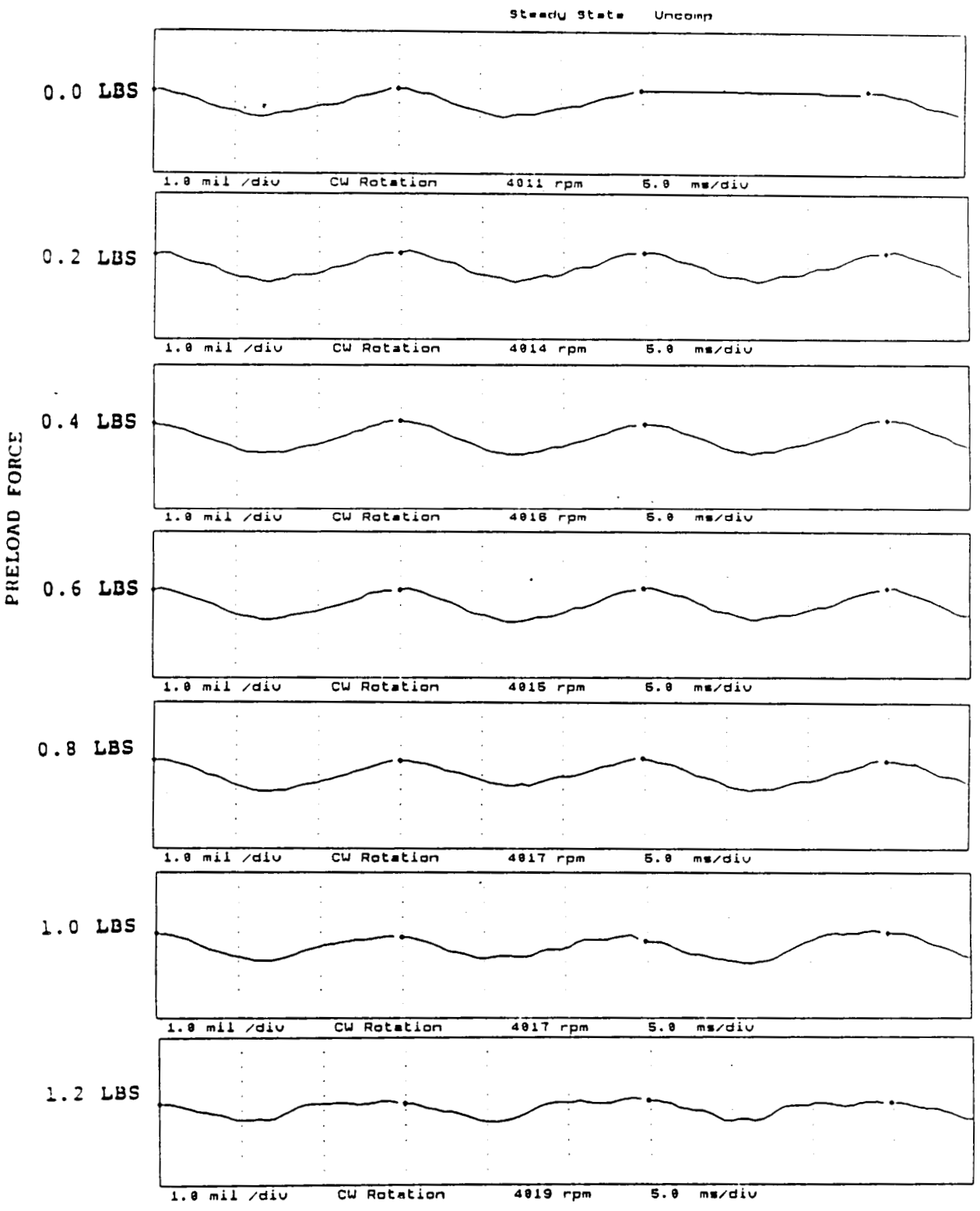

FIGURE 12.110 TIMEBASE FOR HORIZONTAL PROBE AT LOCATION 2 AT 4000 RPM, 7.5 PSI SEAL OIL PRESSURE, 0.8 IN–GRAM UNBALANCE LOCATED IN THE TURBINE DISK, FOR INCREASING STATIC PRELOADS.

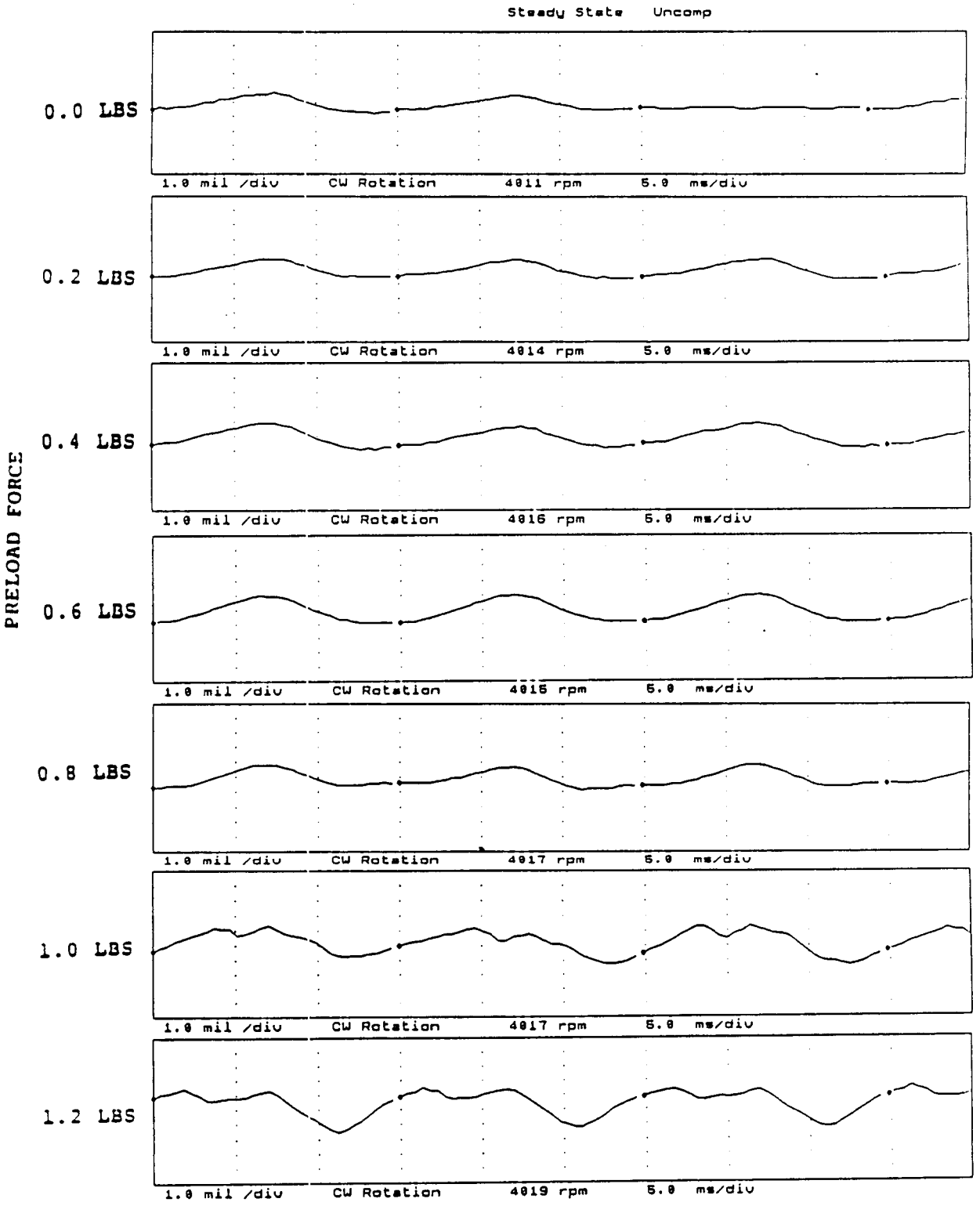

FIGURE 12.111 TIMEBASE FOR VERTICAL PROBE AT LOCATION 3 AT 4000 RPM, 7.5 PSI SEAL OIL PRESSURE, 0.8 IN–GRAM UNBALANCE LOCATED IN THE TURBINE DISK, FOR INCREASING STATIC PRELOADS.

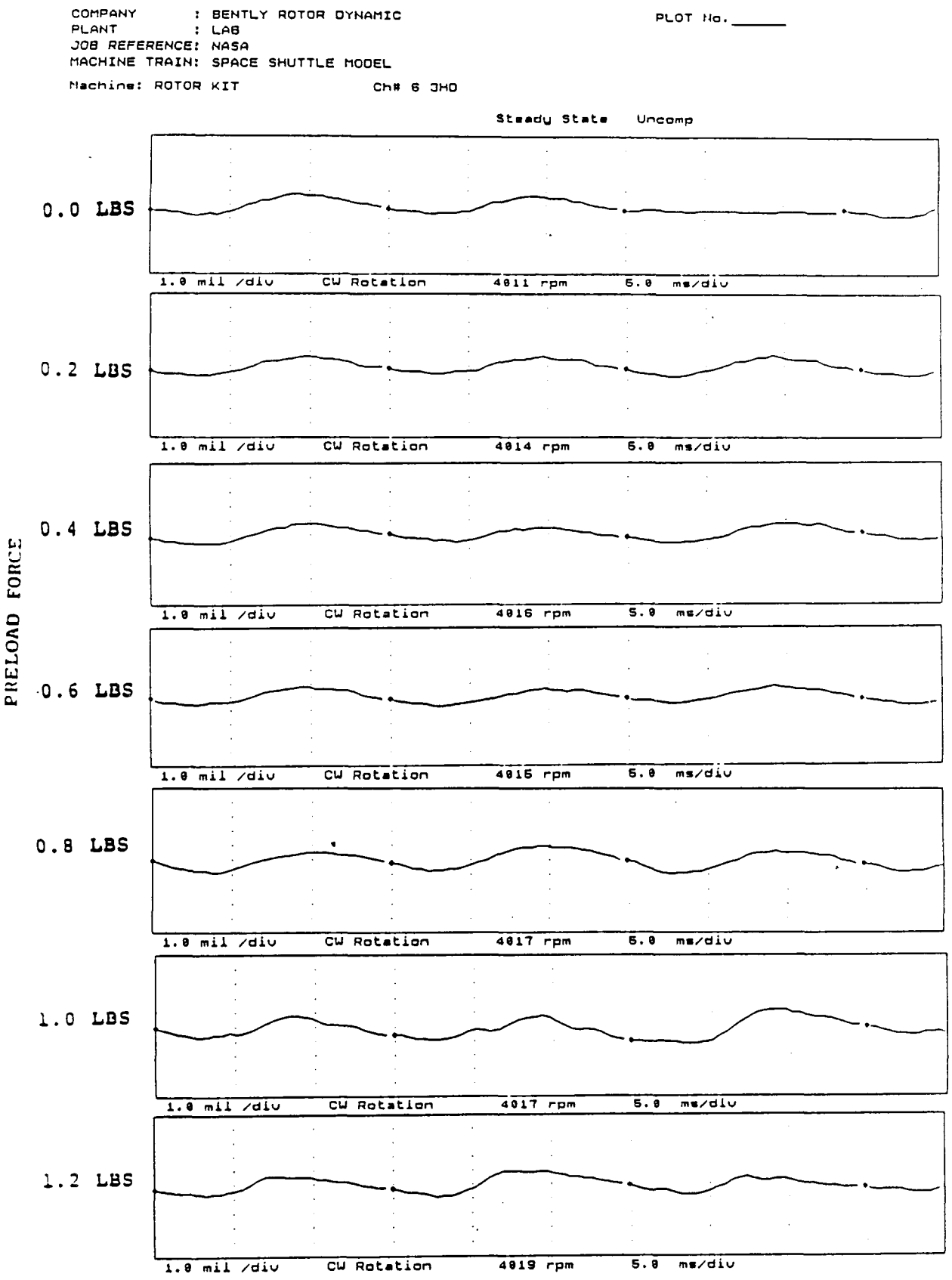

FIGURE 12.112 TIMEBASE FOR HORIZONTAL PROBE AT LOCATION 3 AT 4000 RPM, 7.5 PSI SEAL OIL PRESSURE, 0.8 IN–GRAM UNBALANCE LOCATED IN THE TURBINE DISK, FOR INCREASING STATIC PRELOADS.

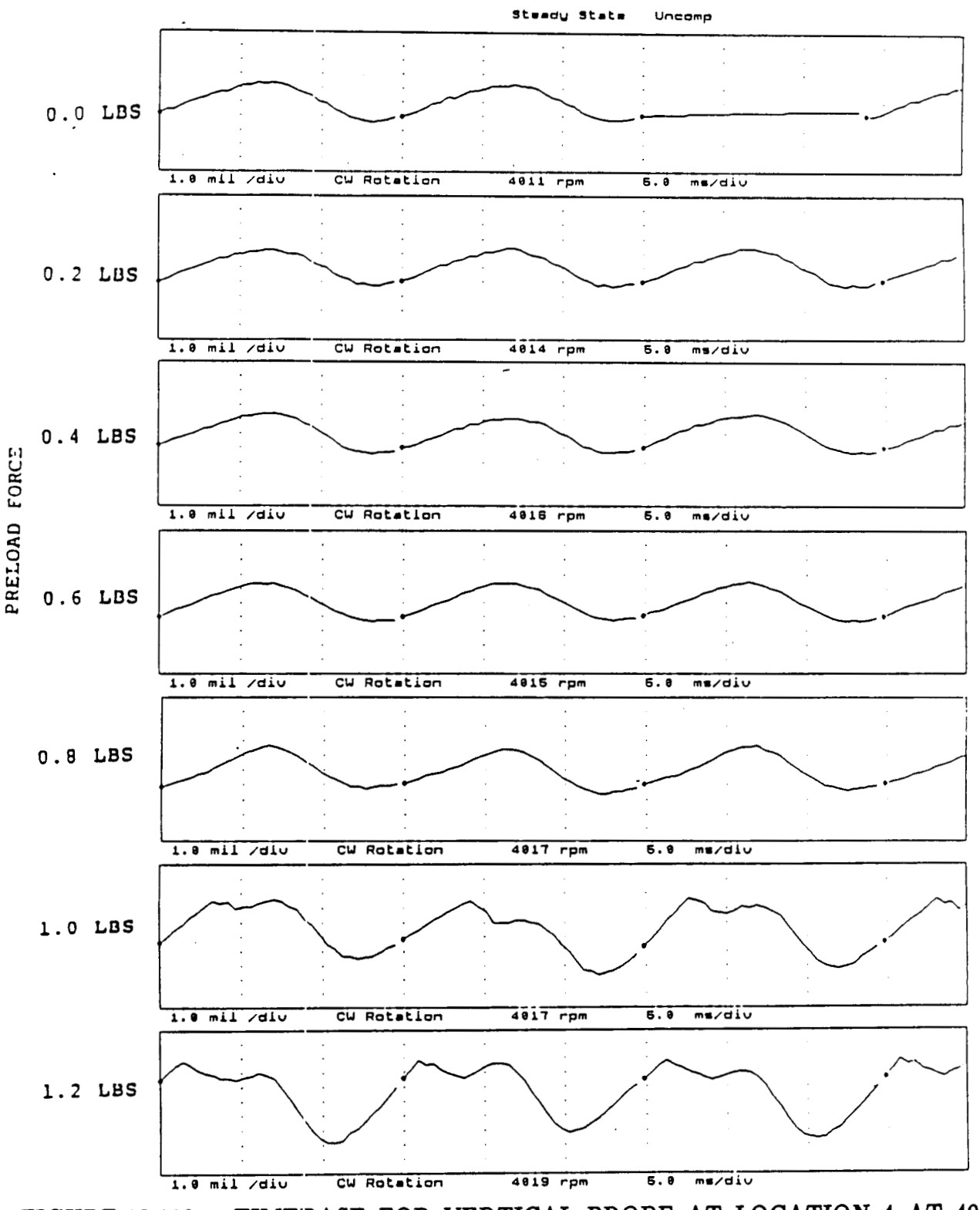

FIGURE 12.113 TIMEBASE FOR VERTICAL PROBE AT LOCATION 4 AT 4000 RPM, 7.5 PSI SEAL OIL PRESSURE, 0.8 IN–GRAM UNBALANCE LOCATED IN THE TURBINE DISK, FOR INCREASING STATIC PRELOADS.

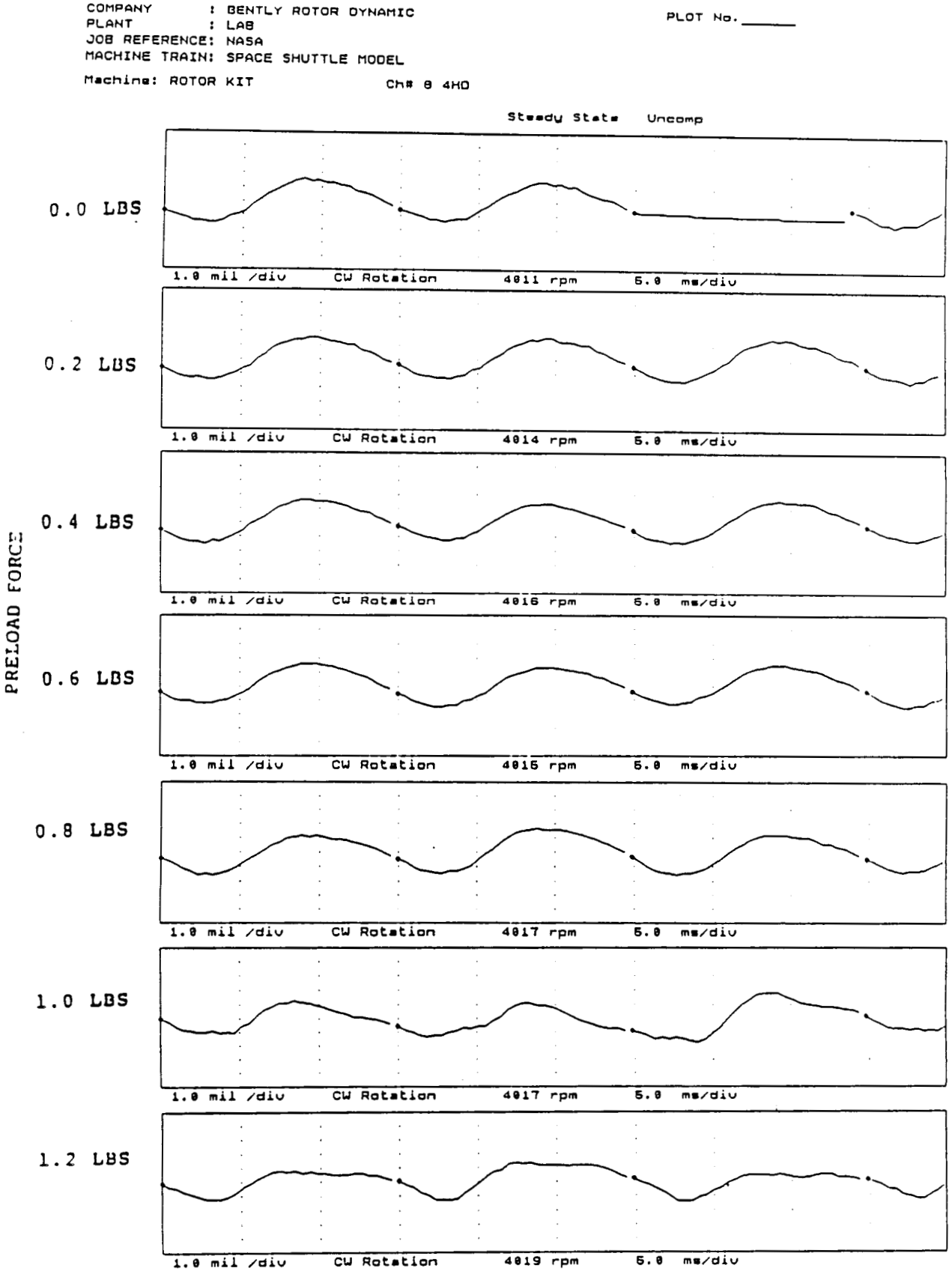

FIGURE 12.114 TIMEBASE FOR HORIZONTAL PROBE AT LOCATION 4 AT 4000 RPM, 7.5 PSI SEAL OIL PRESSURE, 0.8 IN–GRAM UNBALANCE LOCATED IN THE TURBINE DISK, FOR INCREASING STATIC PRELOADS.

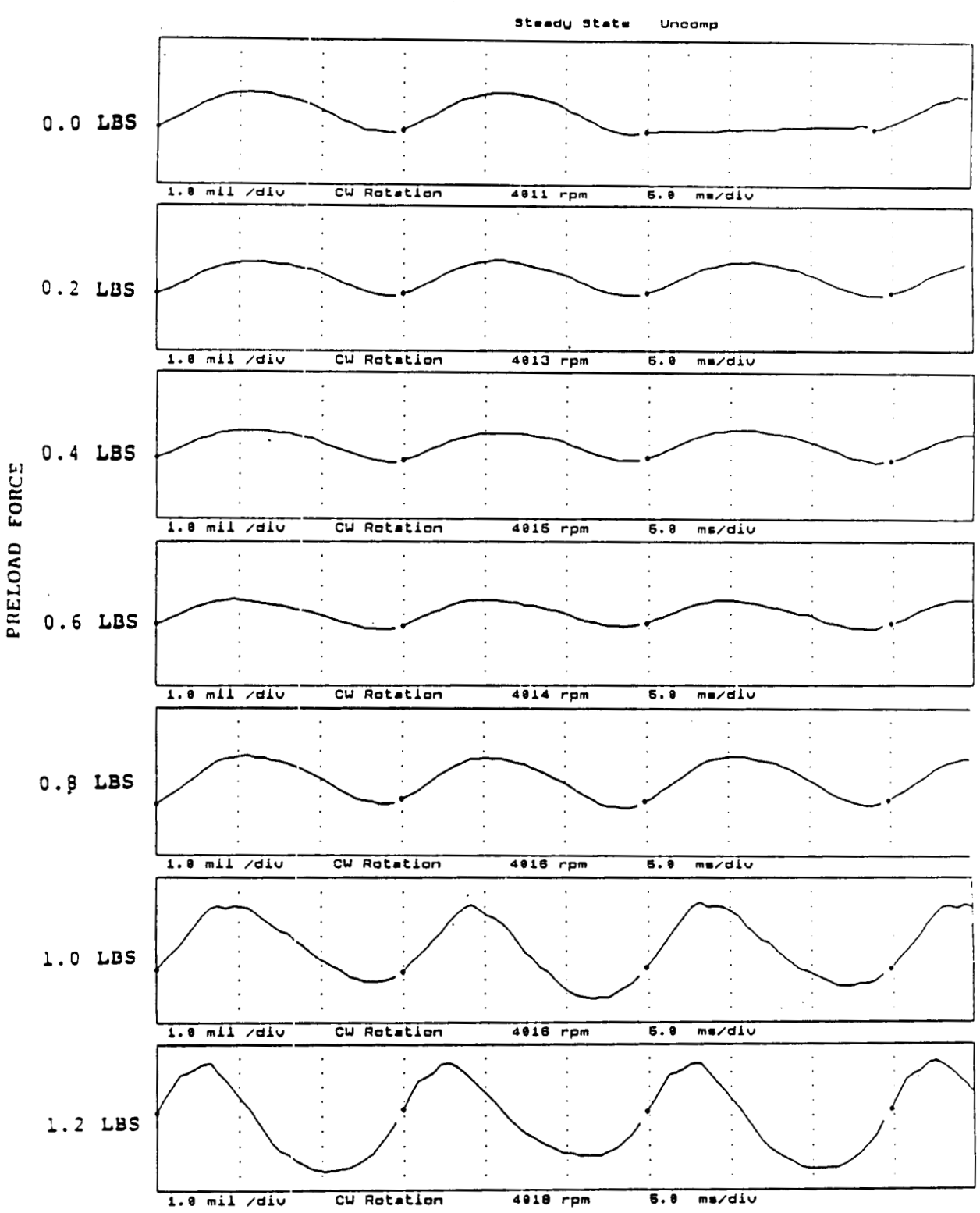

FIGURE 12.115 TIMEBASE FOR VERTICAL PROBE AT LOCATION 5 AT 4000 RPM, 7.5 PSI SEAL OIL PRESSURE, 0.8 IN–GRAM UNBALANCE LOCATED IN THE TURBINE DISK, FOR INCREASING STATIC PRELOADS.

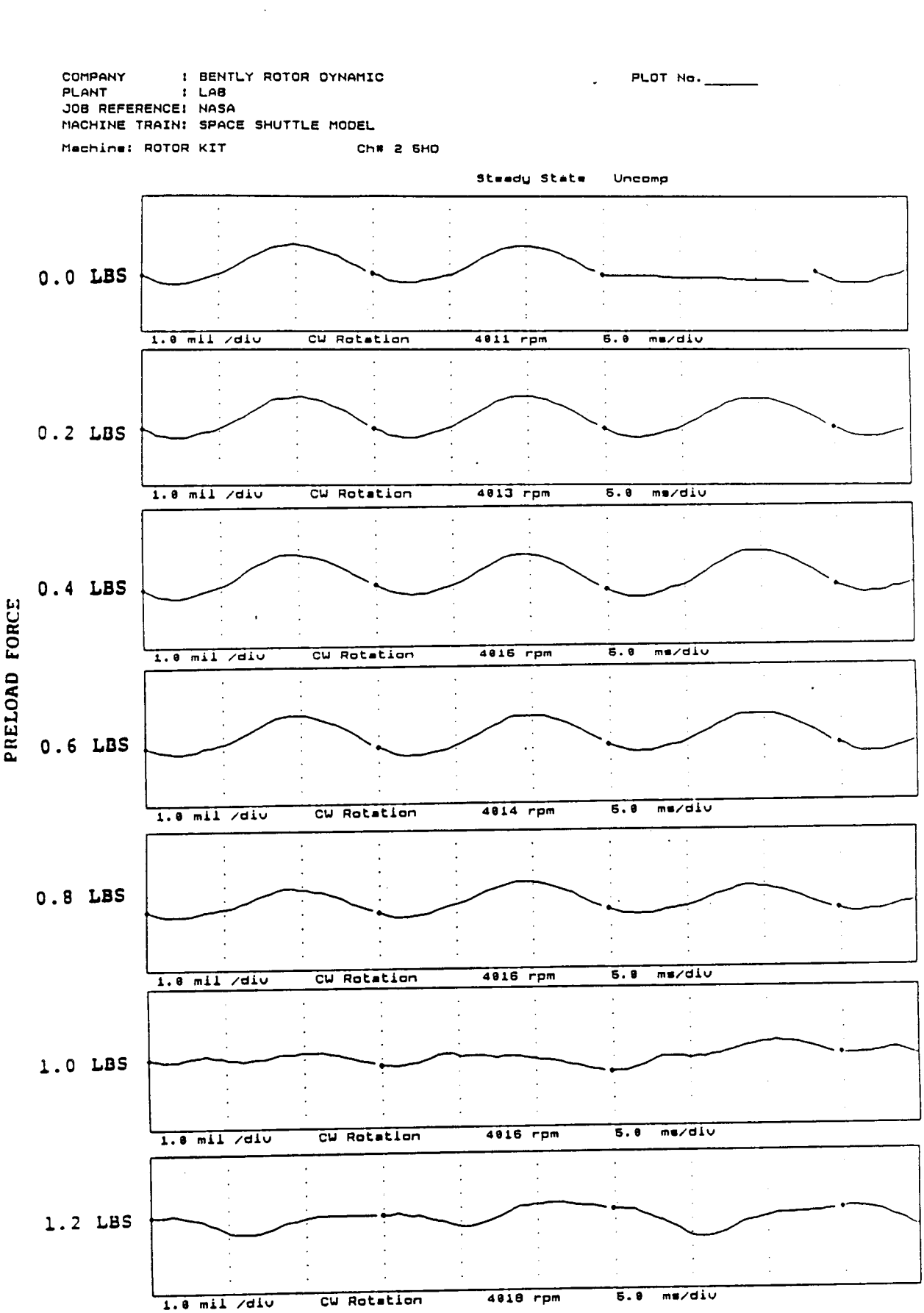

FIGURE 12.116 TIMEBASE FOR HORIZONTAL PROBE AT LOCATION 5 AT 4000 RPM, 7.5 PSI SEAL OIL PRESSURE, 0.8 IN–GRAM UNBALANCE LOCATED IN THE TURBINE DISK, FOR INCREASING STATIC PRELOADS.

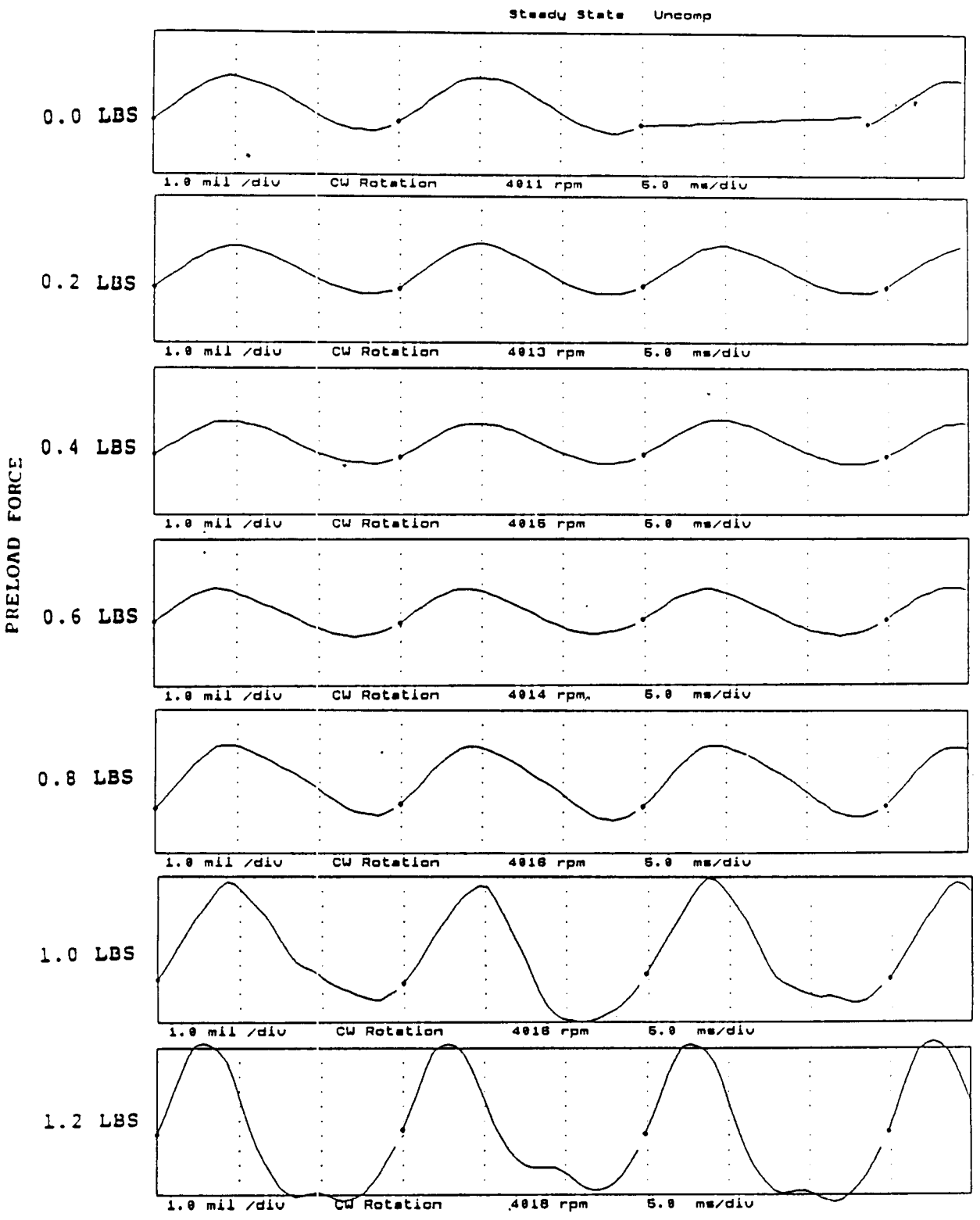

FIGURE 12.117 TIMEBASE FOR VERTICAL PROBE AT LOCATION 6 AT 4000 RPM, 7.5 PSI SEAL OIL PRESSURE, 0.8 IN–GRAM UNBALANCE LOCATED IN THE TURBINE DISK, FOR INCREASING STATIC PRELOADS.

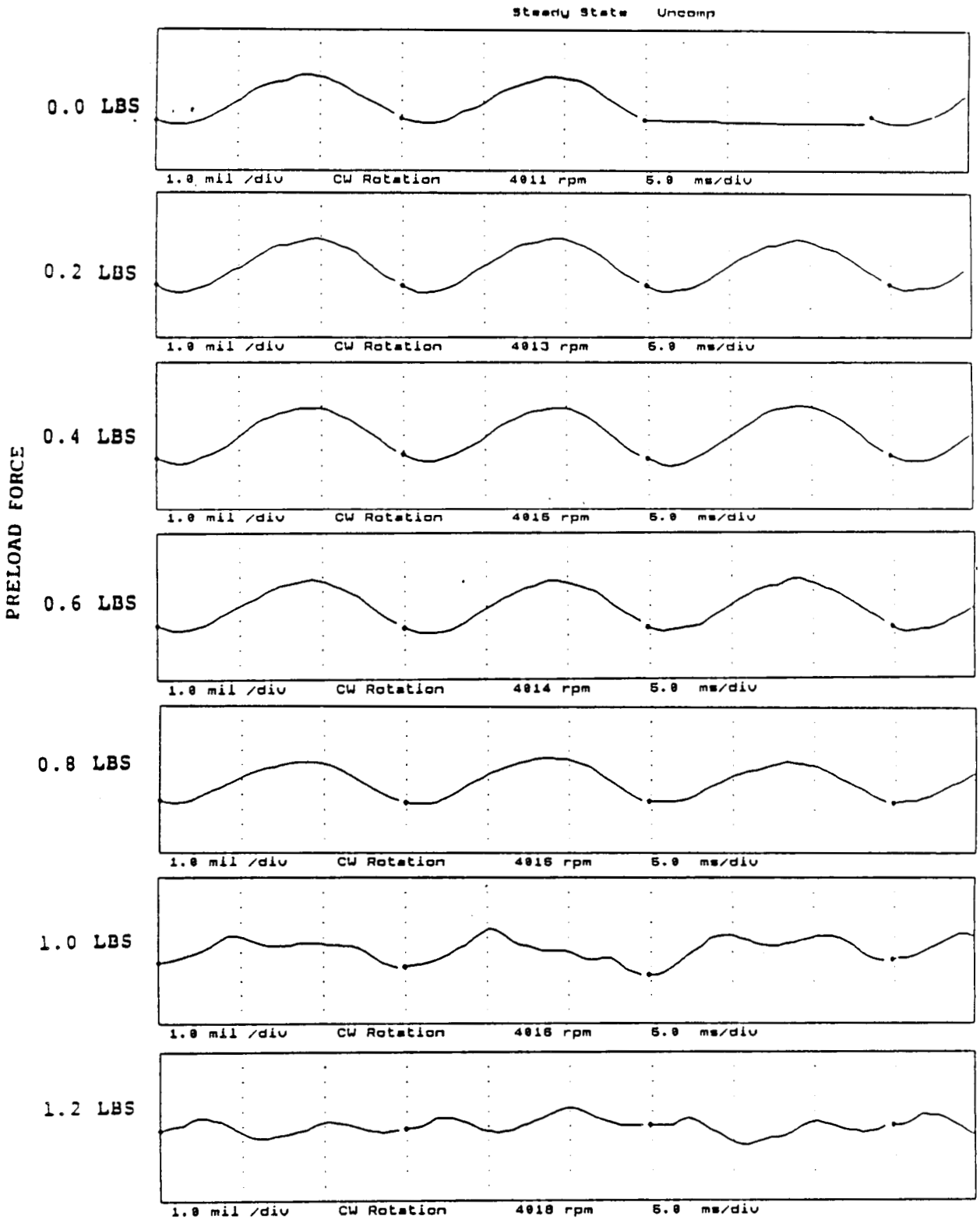

FIGURE 12.118 TIMEBASE FOR HORIZONTAL PROBE AT LOCATION 6 AT 4000 RPM, 7.5 PSI SEAL OIL PRESSURE, 0.8 IN–GRAM UNBALANCE LOCATED IN THE TURBINE DISK, FOR INCREASING STATIC PRELOADS.

NOT AVAILABLE - OIL IN THE CLEARANCE AREA
PROHIBITS THE METAL-TO-METAL CONTACT NECESSARY
FOR THE CONTACT SENSOR TO OPERATE CORRECTLY.

FIGURE 12.119 TIMEBASE FOR SHAFT TO SEAL 1 CONTACT AT 4000 RPM, 7.5 PSI SEAL OIL PRESSURE, 0.8 IN–GRAM UNBALANCE LOCATED IN THE TURBINE DISK, FOR INCREASING STATIC PRELOADS.

NOT AVAILABLE - OIL IN THE CLEARANCE AREA
PROHIBITS THE METAL-TO-METAL CONTACT NECESSARY
FOR THE CONTACT SENSOR TO OPERATE CORRECTLY.

FIGURE 12.120 TIMEBASE FOR SHAFT TO SEAL 2 CONTACT AT 4000 RPM, 7.5 PSI SEAL OIL PRESSURE, 0.8 IN–GRAM UNBALANCE LOCATED IN THE TURBINE DISK, FOR INCREASING STATIC PRELOADS.

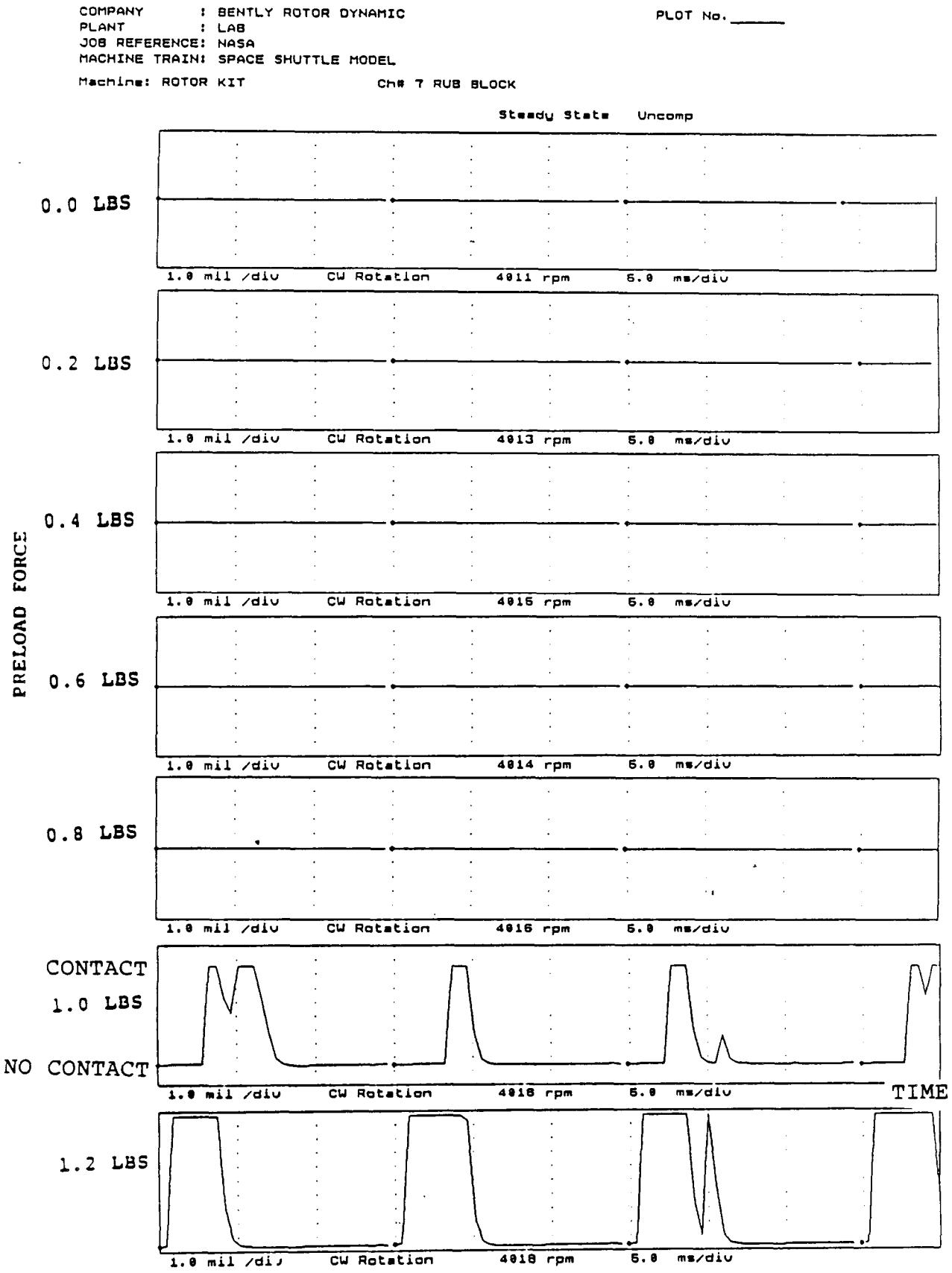

FIGURE 12.121 TIMEBASE FOR SHAFT TO RUB BLOCK CONTACT AT 4000 RPM, 7.5 PSI SEAL OIL PRESSURE, 0.8 IN–GRAM UNBALANCE LOCATED IN THE TURBINE DISK, FOR INCREASING STATIC PRELOADS.

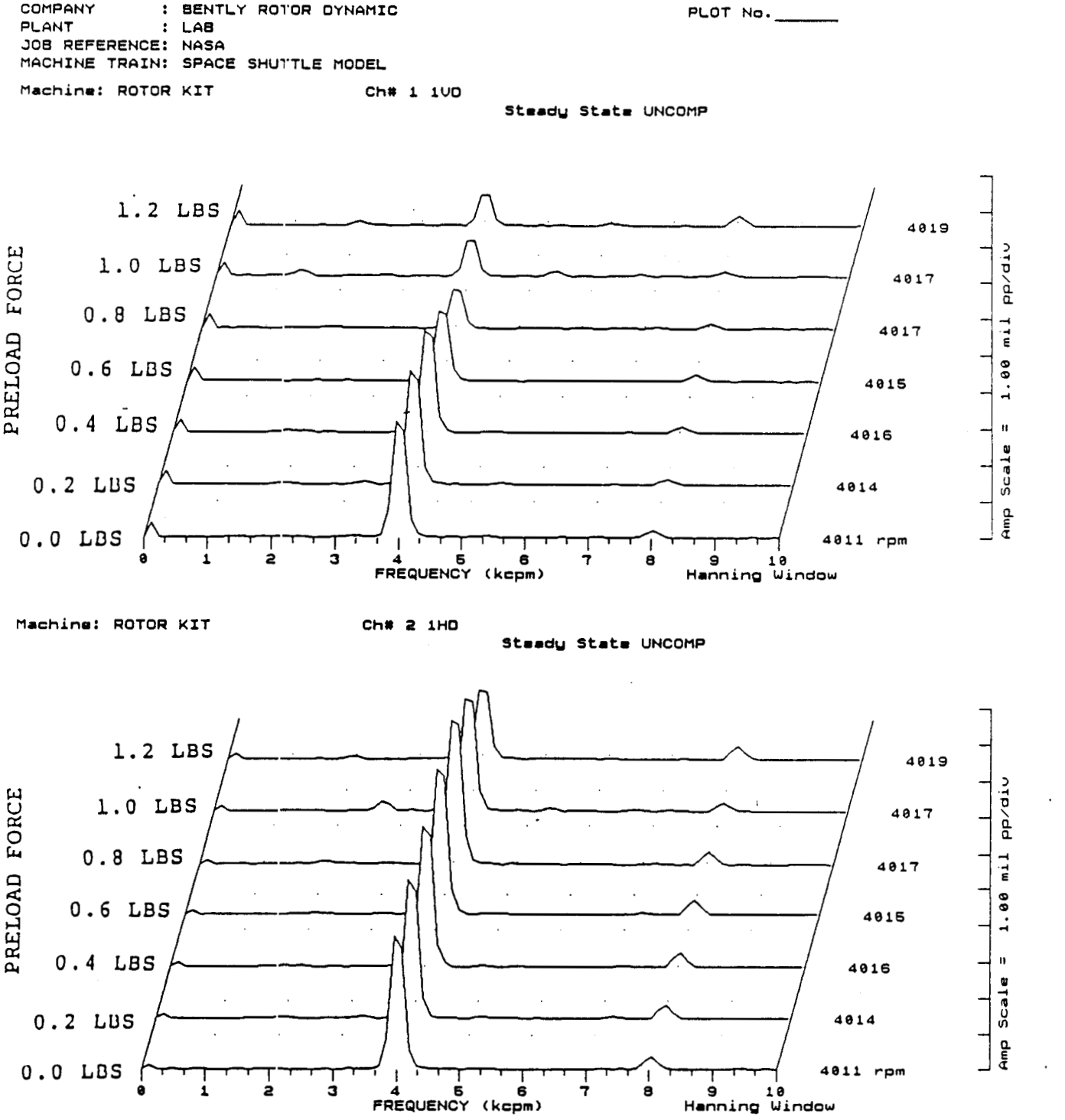

FIGURE 12.122 SPECTRAL CONTENT AT PROBE LOCATION 1 AT 4000 RPM, 7.5 PSI SEAL OIL PRESSURE, 0.8 IN–GRAM UNBALANCE LOCATED IN THE TURBINE DISK, FOR INCREASING STATIC PRELOADS.

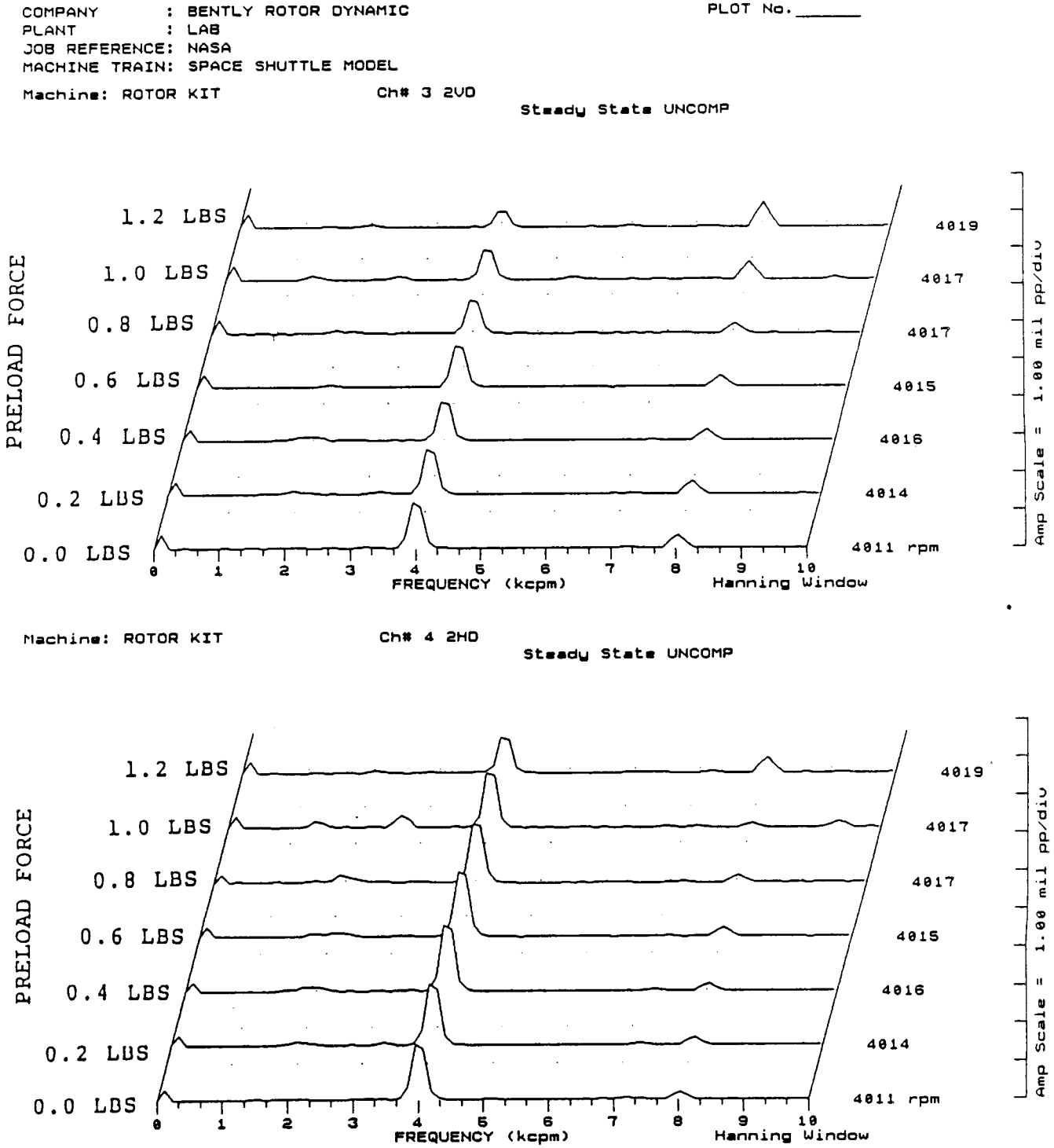

FIGURE 12.123 SPECTRAL CONTENT AT PROBE LOCATION 2 AT 4000 RPM, 7.5 PSI SEAL OIL PRESSURE, 0.8 IN–GRAM UNBALANCE LOCATED IN THE TURBINE DISK, FOR INCREASING STATIC PRELOADS.

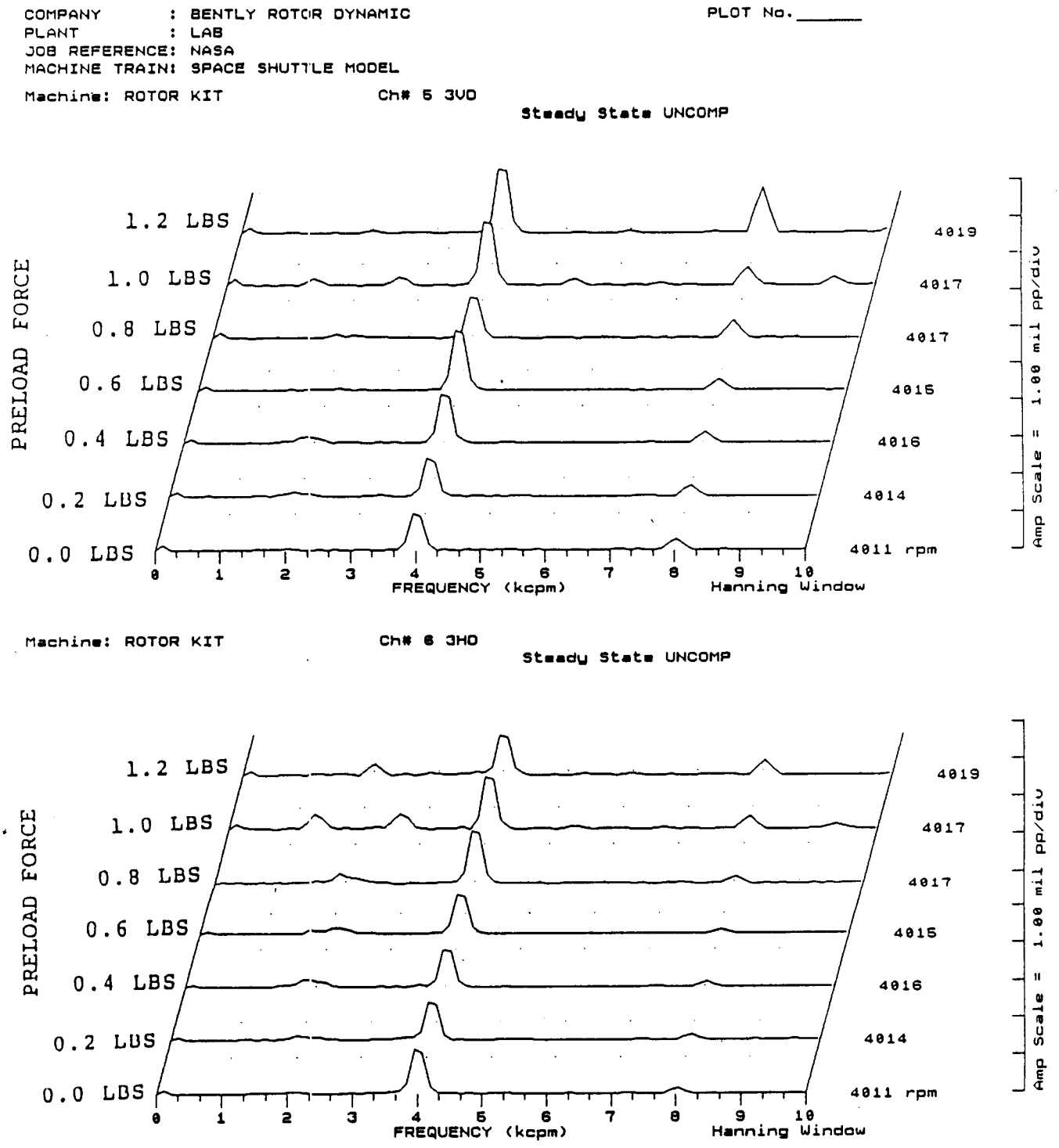

FIGURE 12.124 SPECTRAL CONTENT AT PROBE LOCATION 3 AT 4000 RPM, 7.5 PSI SEAL OIL PRESSURE, 0.8 IN–GRAM UNBALANCE LOCATED IN THE TURBINE DISK, FOR INCREASING STATIC PRELOADS.

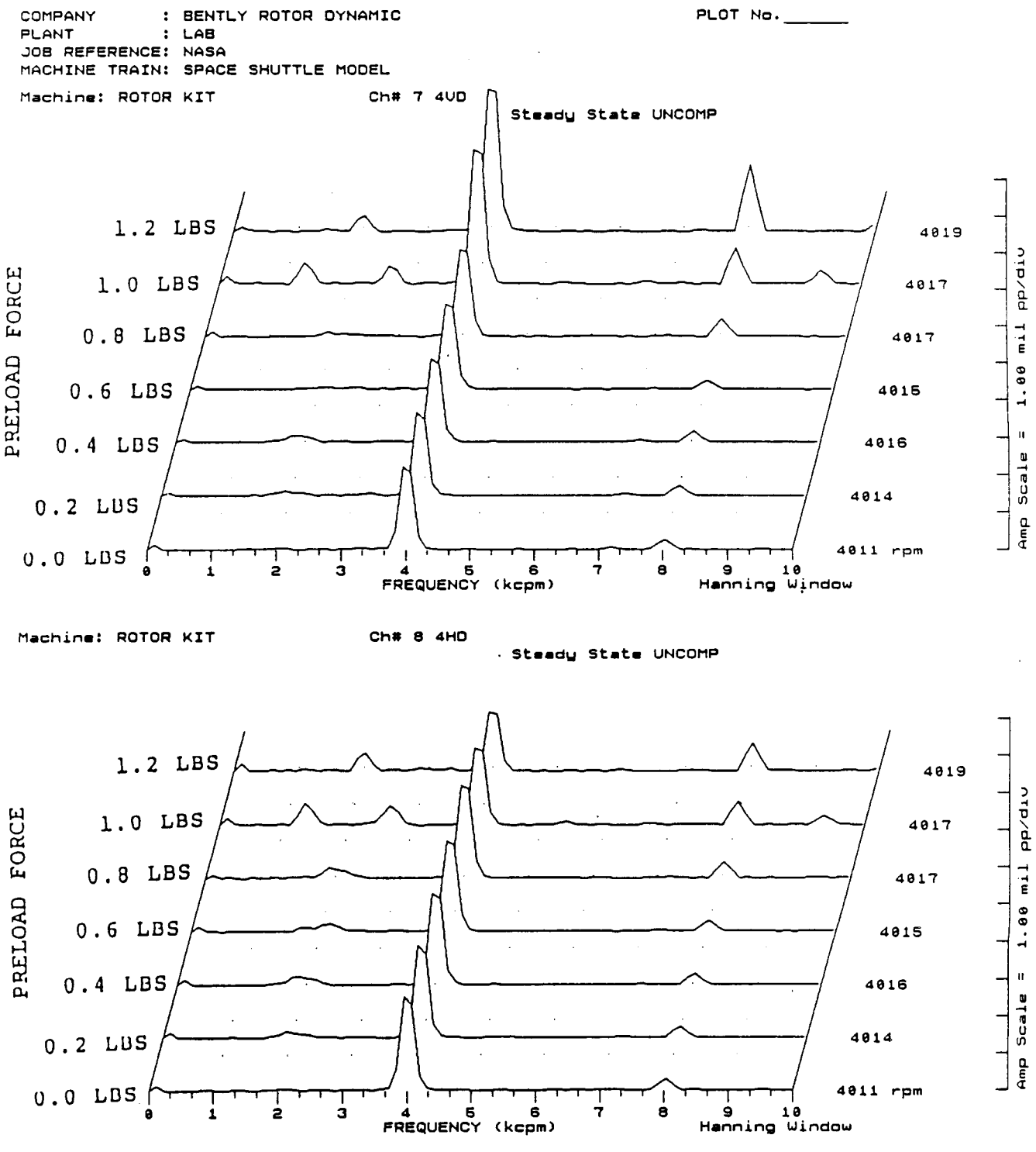

FIGURE 12.125 SPECTRAL CONTENT AT PROBE LOCATION 4 AT 4000 RPM, 7.5 PSI SEAL OIL PRESSURE, 0.8 IN–GRAM UNBALANCE LOCATED IN THE TURBINE DISK, FOR INCREASING STATIC PRELOADS.

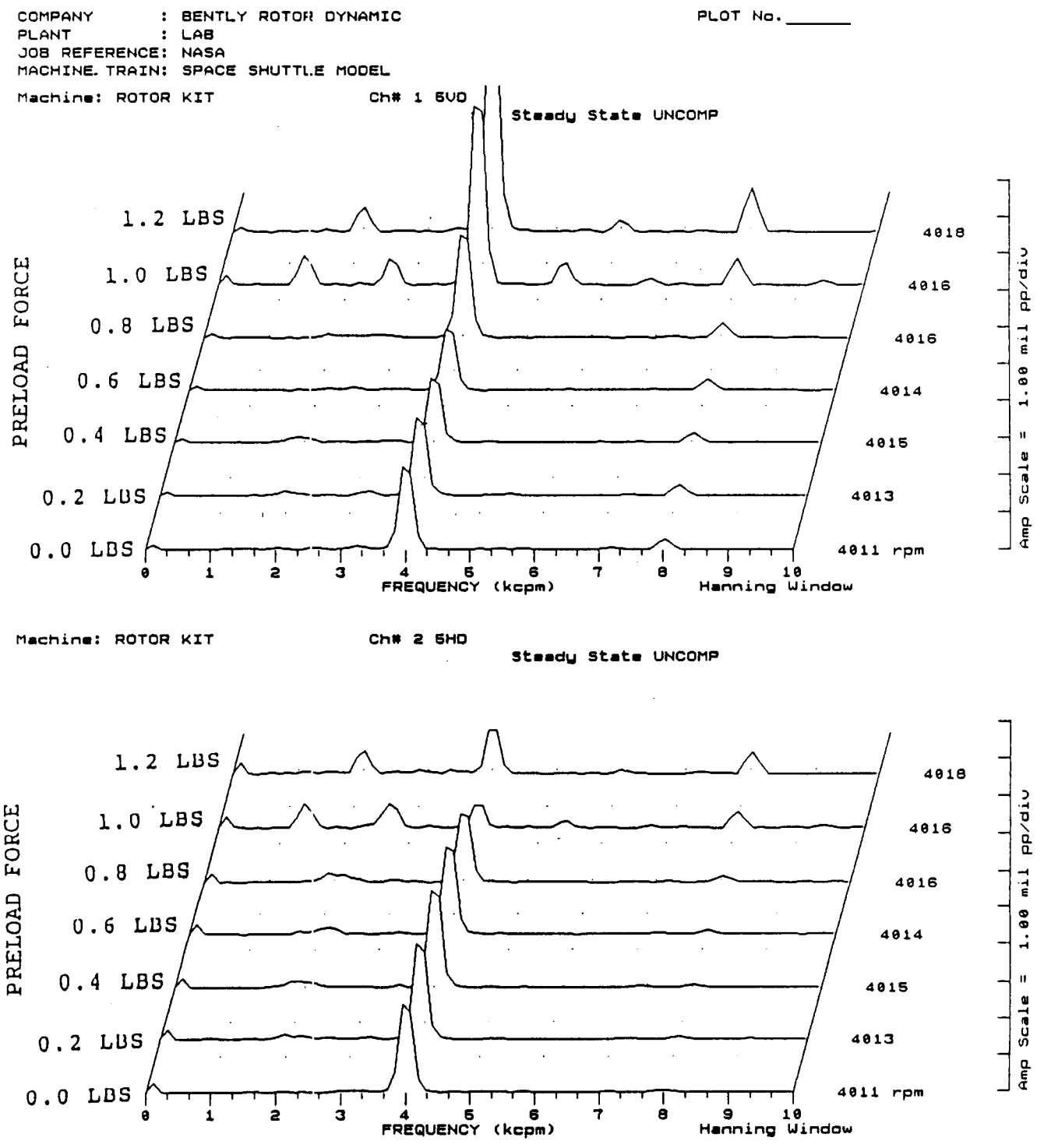

FIGURE 12.126 SPECTRAL CONTENT AT PROBE LOCATION 5 AT 4000 RPM, 7.5 PSI SEAL OIL PRESSURE, 0.8 IN–GRAM UNBALANCE LOCATED IN THE TURBINE DISK, FOR INCREASING STATIC PRELOADS.

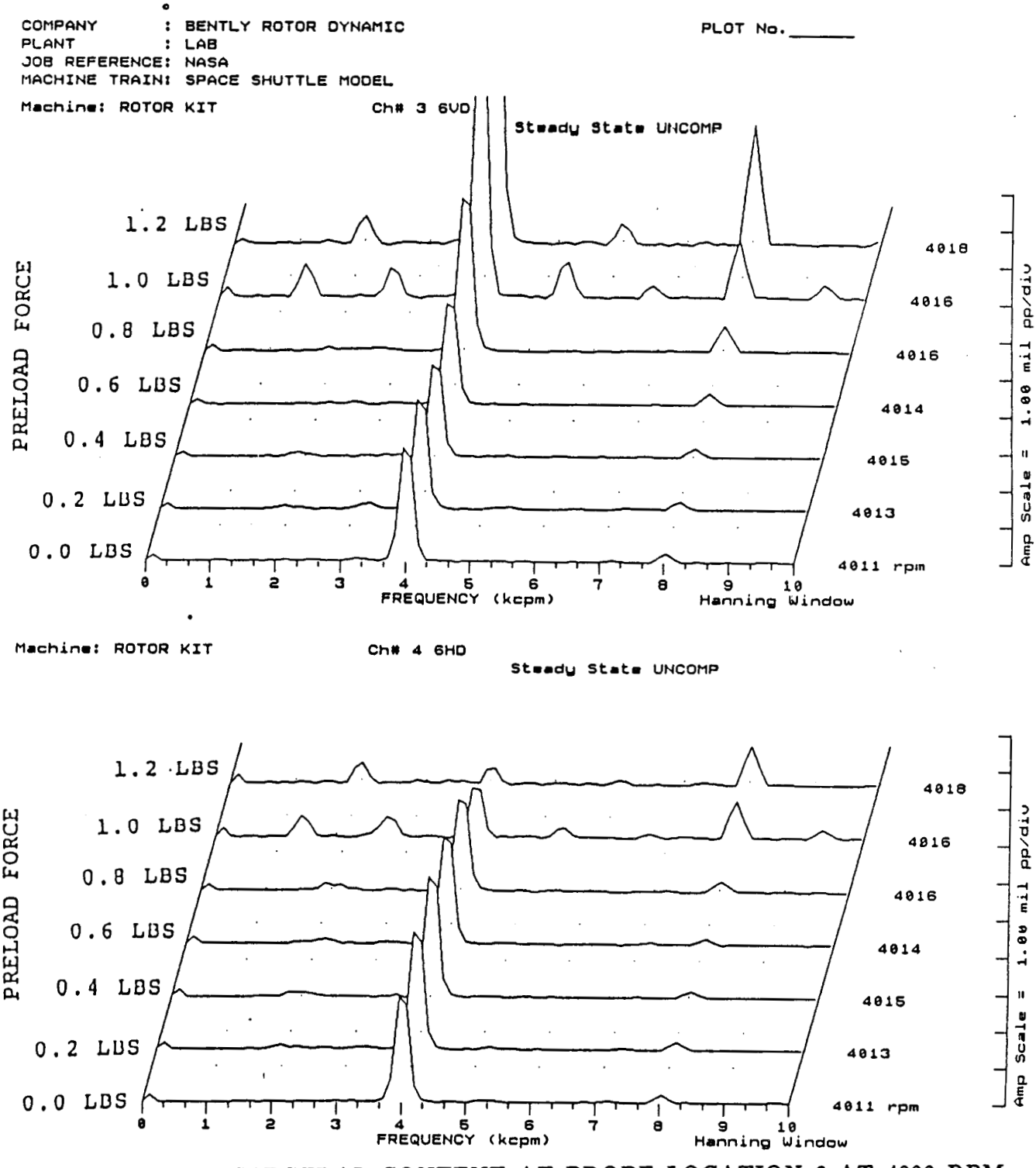

FIGURE 12.127 SPECTRAL CONTENT AT PROBE LOCATION 6 AT 4000 RPM, 7.5 PSI SEAL OIL PRESSURE, 0.8 IN–GRAM UNBALANCE LOCATED IN THE TURBINE DISK, FOR INCREASING STATIC PRELOADS.

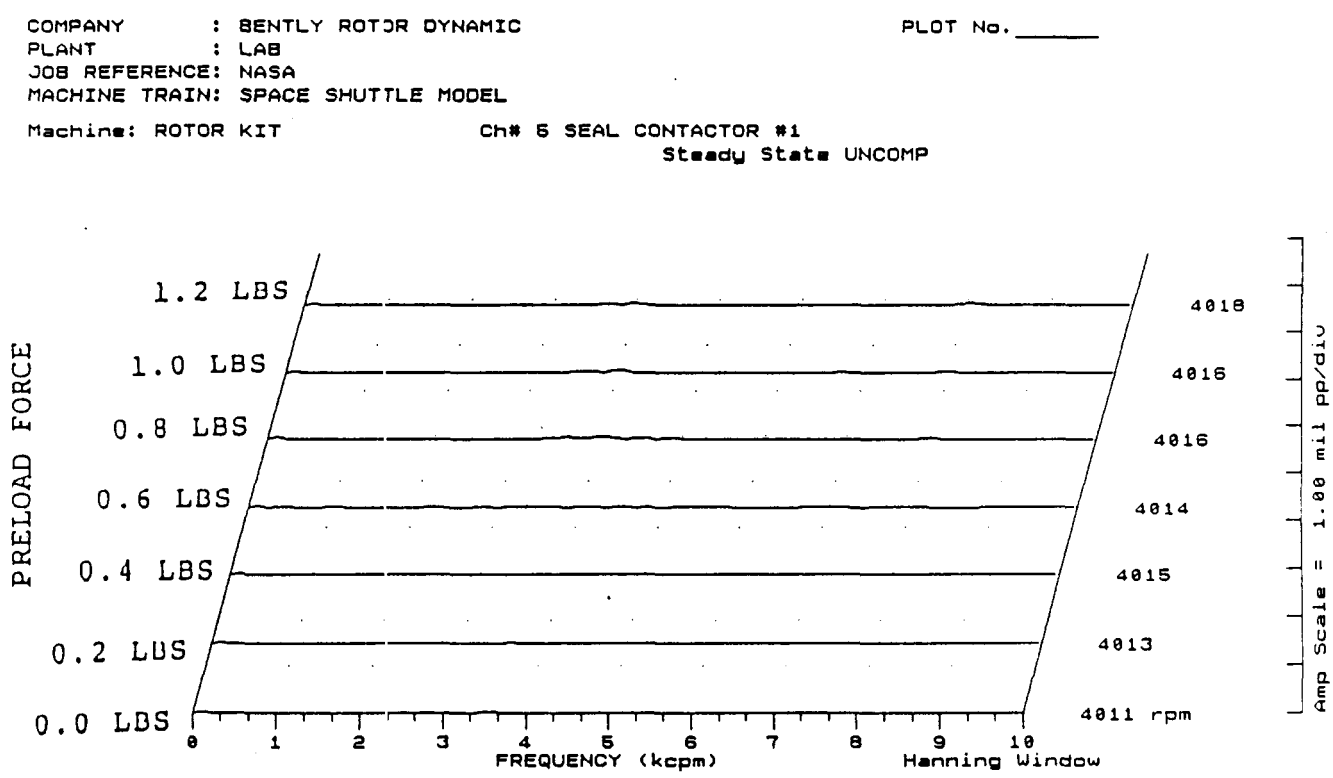

FIGURE 12.128 SPECTRAL CONTENT FOR SHAFT TO SEAL 1 CONTACT AT 4000 RPM, 7.5 PSI SEAL OIL PRESSURE, 0.8 IN–GRAM UNBALANCE LOCATED IN THE TURBINE DISK, FOR INCREASING STATIC PRELOADS.

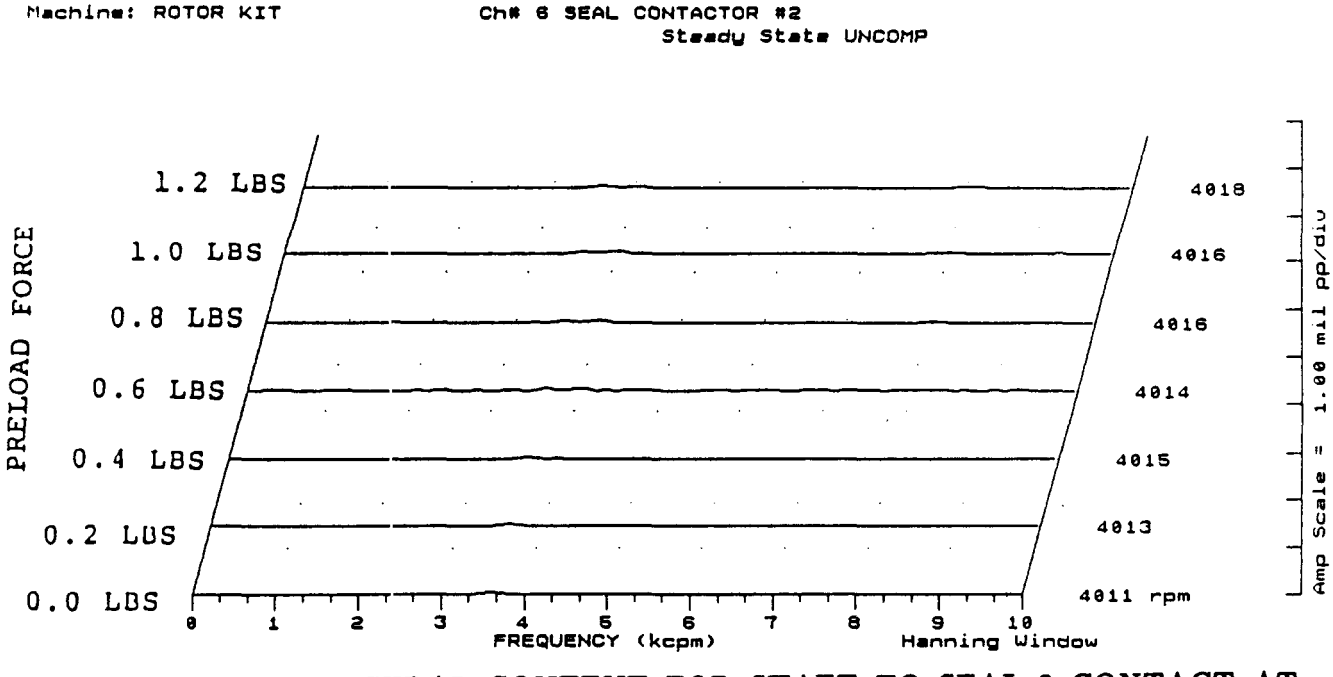

FIGURE 12.129 SPECTRAL CONTENT FOR SHAFT TO SEAL 2 CONTACT AT 4000 RPM, 7.5 PSI SEAL OIL PRESSURE, 0.8 IN–GRAM UNBALANCE LOCATED IN THE TURBINE DISK, FOR INCREASING STATIC PRELOADS.

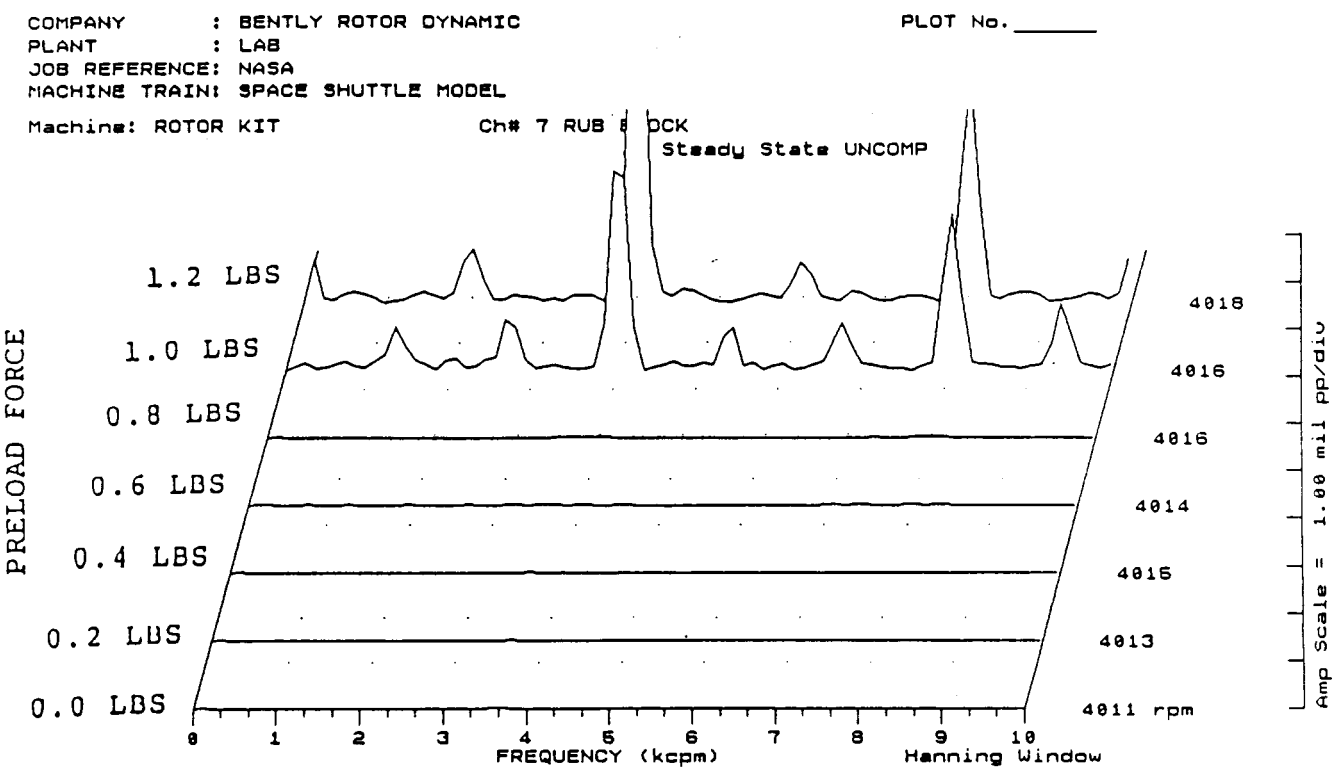

FIGURE 12.130 SPECTRAL CONTENT FOR SHAFT TO RUB BLOCK CONTACT AT 4000 RPM, 7.5 PSI SEAL OIL PRESSURE, 0.8 IN–GRAM UNBALANCE LOCATED IN THE TURBINE DISK, FOR INCREASING STATIC PRELOADS.

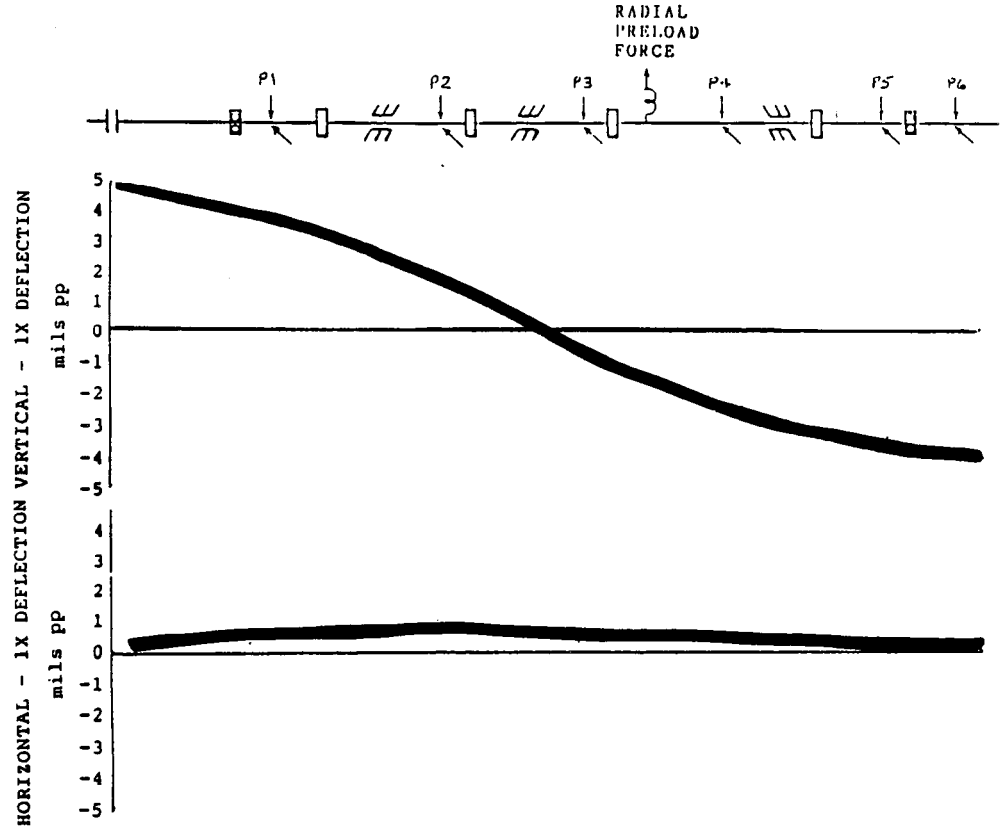

FIGURE 12.131 ROTOR MODE SHAPE AT 4000 RPM, 10.0 PSI SEAL OIL PRESSURE DUE TO 0.8 IN–GRAM UNBALANCE LOCATED IN THE TURBINE DISK.

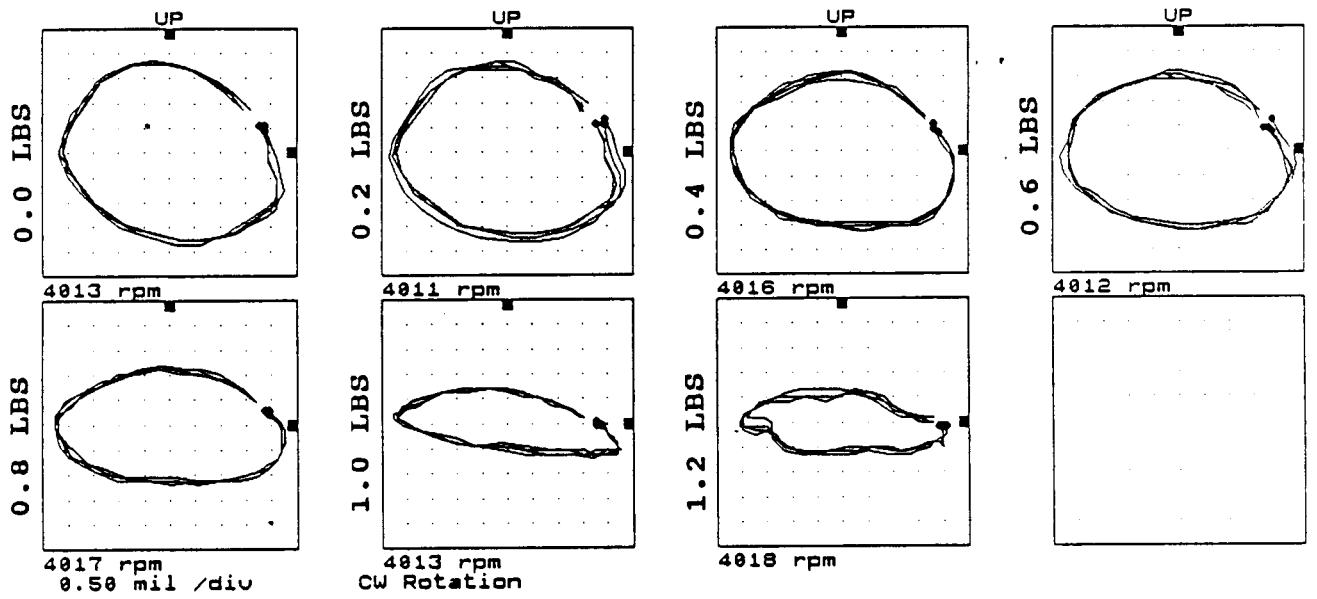

FIGURE 12.132 ORBITS AT PROBE LOCATION 1 AT 4000 RPM, 10.0 PSI SEAL OIL PRESSURE, 0.8 IN–GRAM UNBALANCE LOCATED IN THE TURBINE DISK, FOR INCREASING STATIC PRELOAD FORCES.

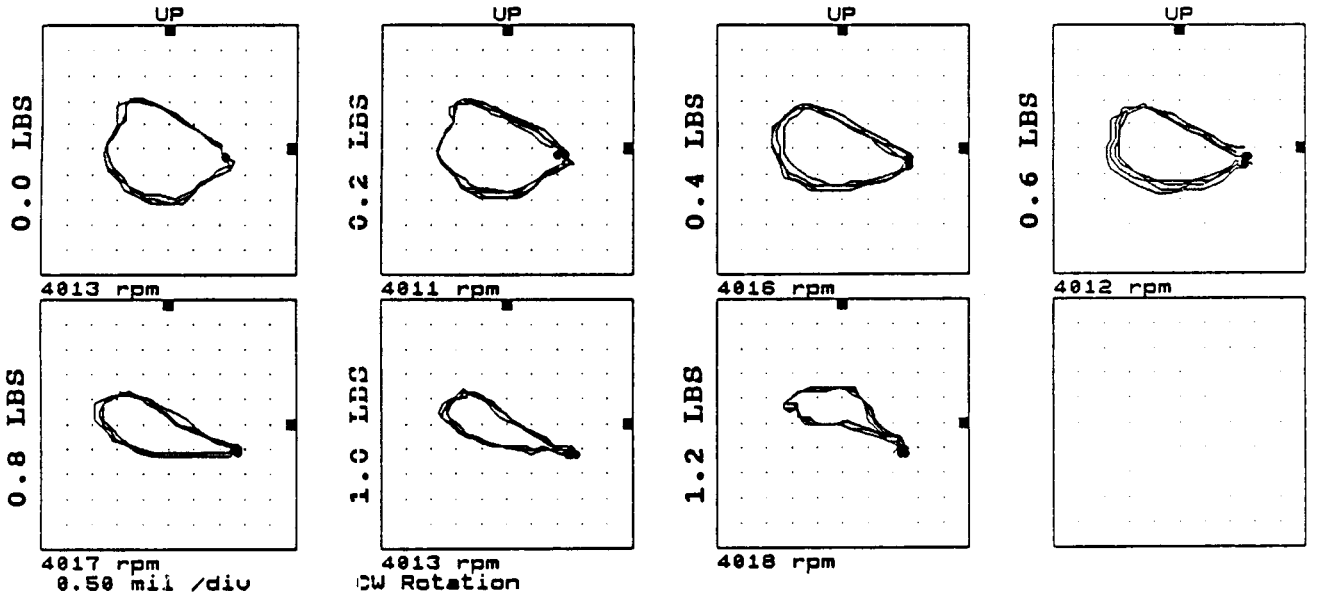

FIGURE 12.133 ORBITS AT PROBE LOCATION 2 AT 4000 RPM, 10.0 PSI SEAL OIL PRESSURE, 0.8 IN–GRAM UNBALANCE LOCATED IN THE TURBINE DISK, FOR INCREASING STATIC PRELOAD FORCES.

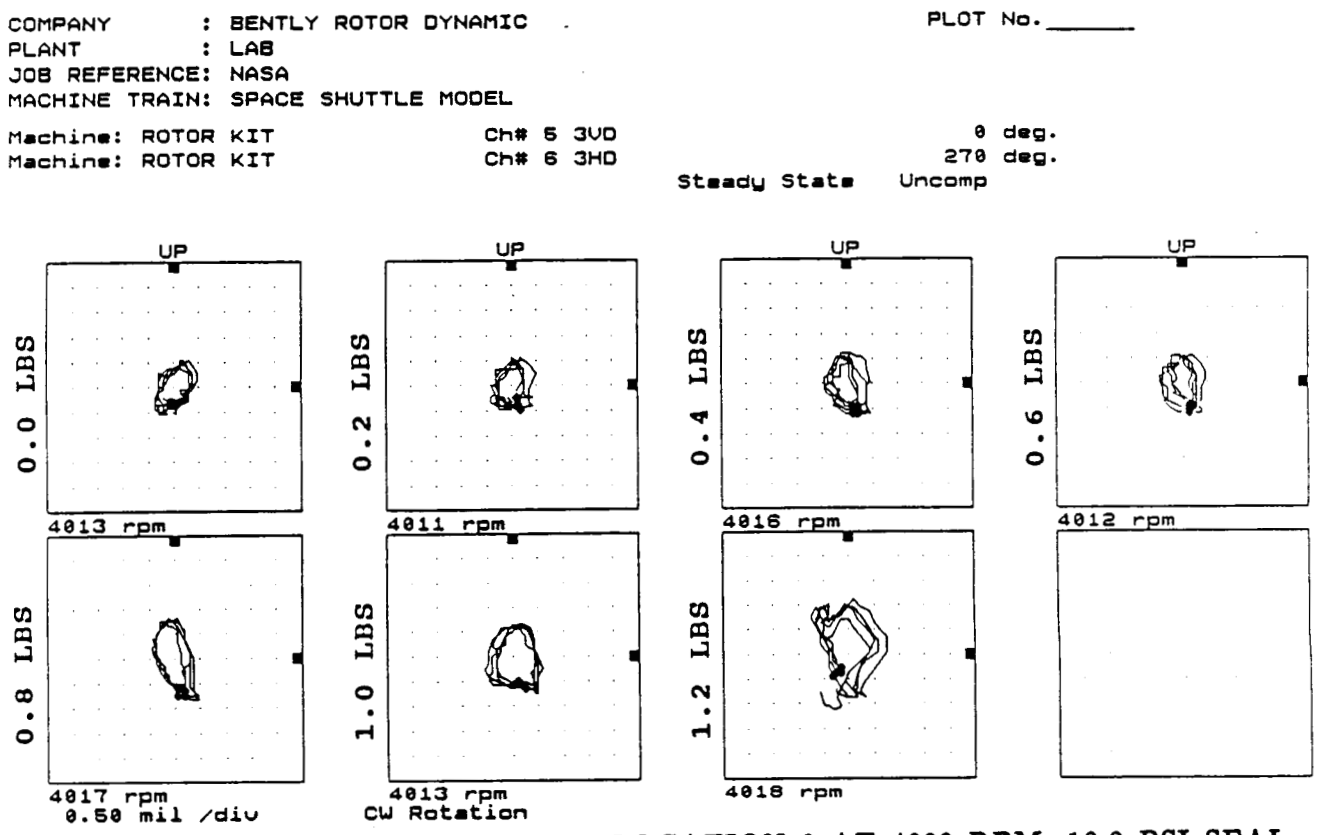

FIGURE 12.134 ORBITS AT PROBE LOCATION 3 AT 4000 RPM, 10.0 PSI SEAL OIL PRESSURE, 0.8 IN–GRAM UNBALANCE LOCATED IN THE TURBINE DISK, FOR INCREASING STATIC PRELOAD FORCES.

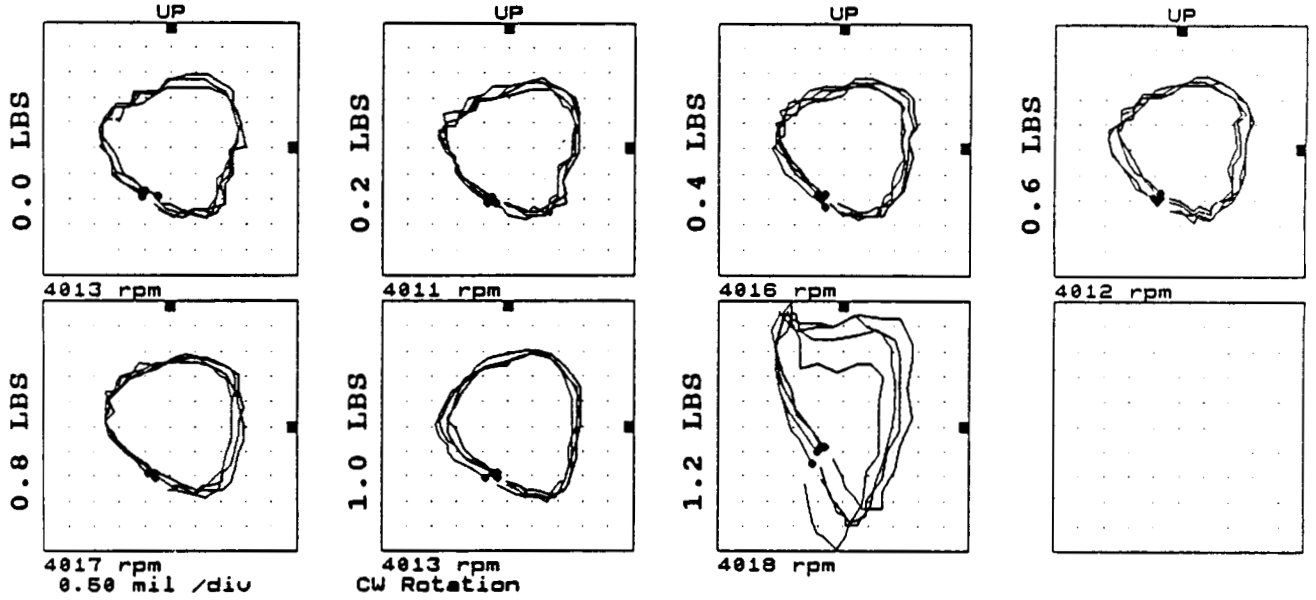

FIGURE 12.135 ORBITS AT PROBE LOCATION 4 AT 4000 RPM, 10.0 PSI SEAL OIL PRESSURE, 0.8 IN–GRAM UNBALANCE LOCATED IN THE TURBINE DISK, FOR INCREASING STATIC PRELOAD FORCES.

COMPANY : BENTLY ROTOR DYNAMIC PLOT No._____
PLANT : LAB
JOB REFERENCE: NASA
MACHINE TRAIN: SPACE SHUTTLE MODEL

Machine: ROTOR KIT Ch# 1 6VD 0 deg.
Machine: ROTOR KIT Ch# 2 6HD 270 deg.
Steady State Uncomp

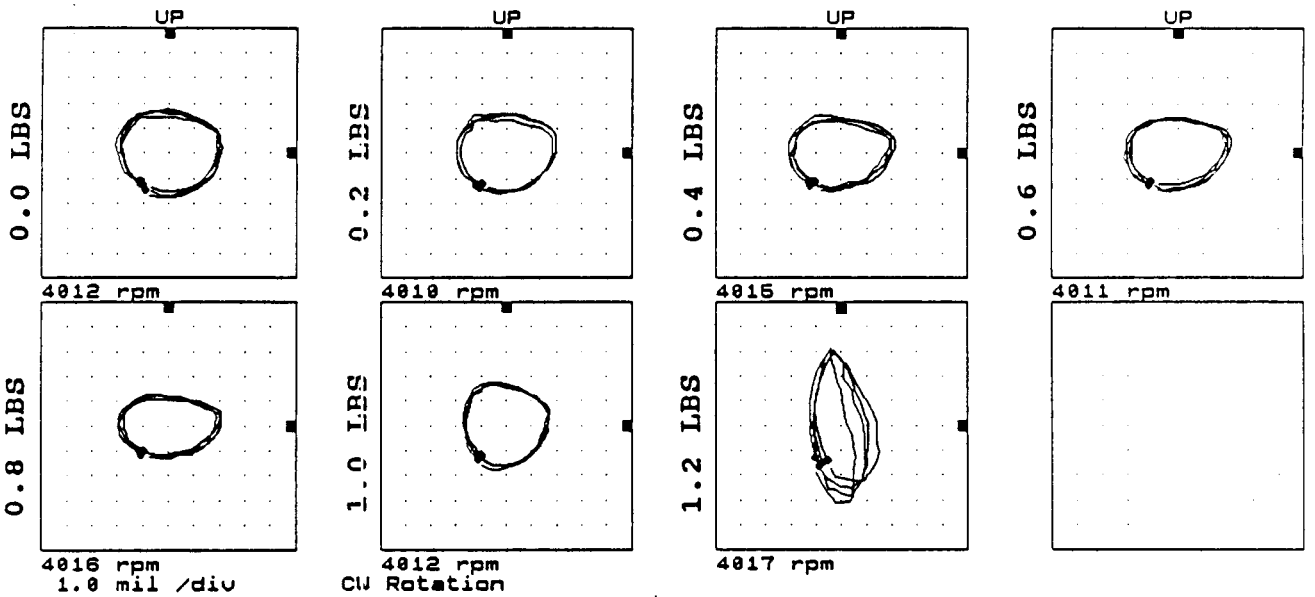

FIGURE 12.136 ORBITS AT PROBE LOCATION 5 AT 4000 RPM, 10.0 PSI SEAL OIL PRESSURE, 0.8 IN–GRAM UNBALANCE LOCATED IN THE TURBINE DISK, FOR INCREASING STATIC PRELOAD FORCES.

Machine: ROTOR KIT Ch# 3 6VD 0 deg.
Machine: ROTOR KIT Ch# 4 6HD 270 deg.
Steady State Uncomp

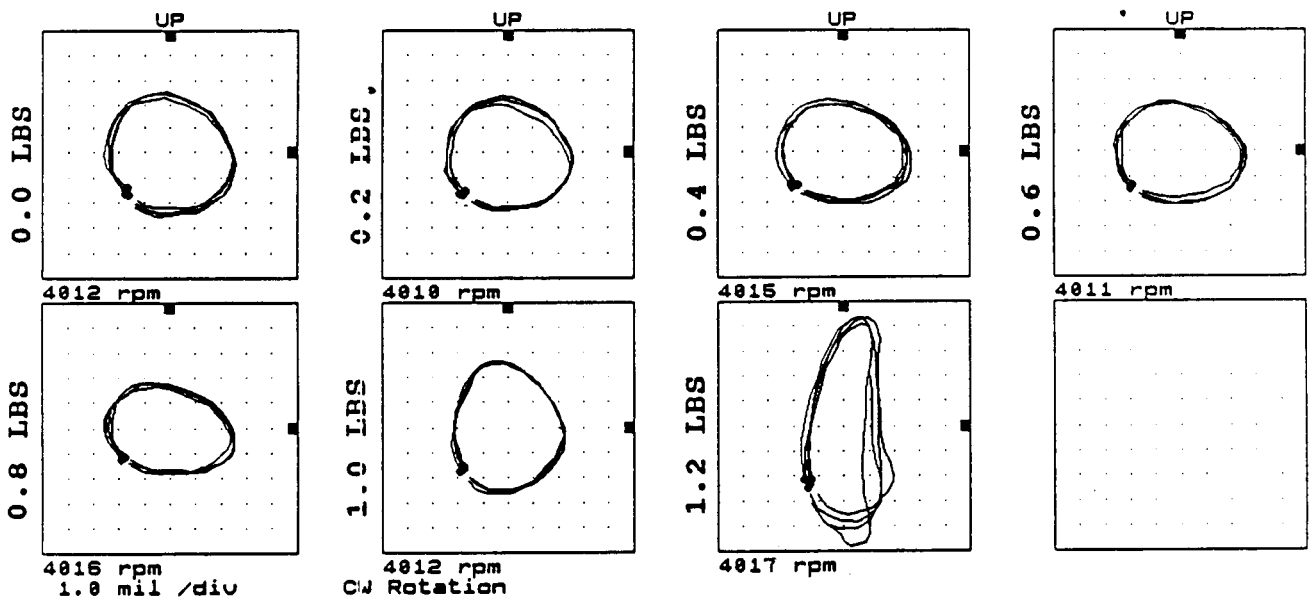

FIGURE 12.137 ORBITS AT PROBE LOCATION 6 AT 4000 RPM, 10.0 PSI SEAL OIL PRESSURE, 0.8 IN–GRAM UNBALANCE LOCATED IN THE TURBINE DISK, FOR INCREASING STATIC PRELOAD FORCES.

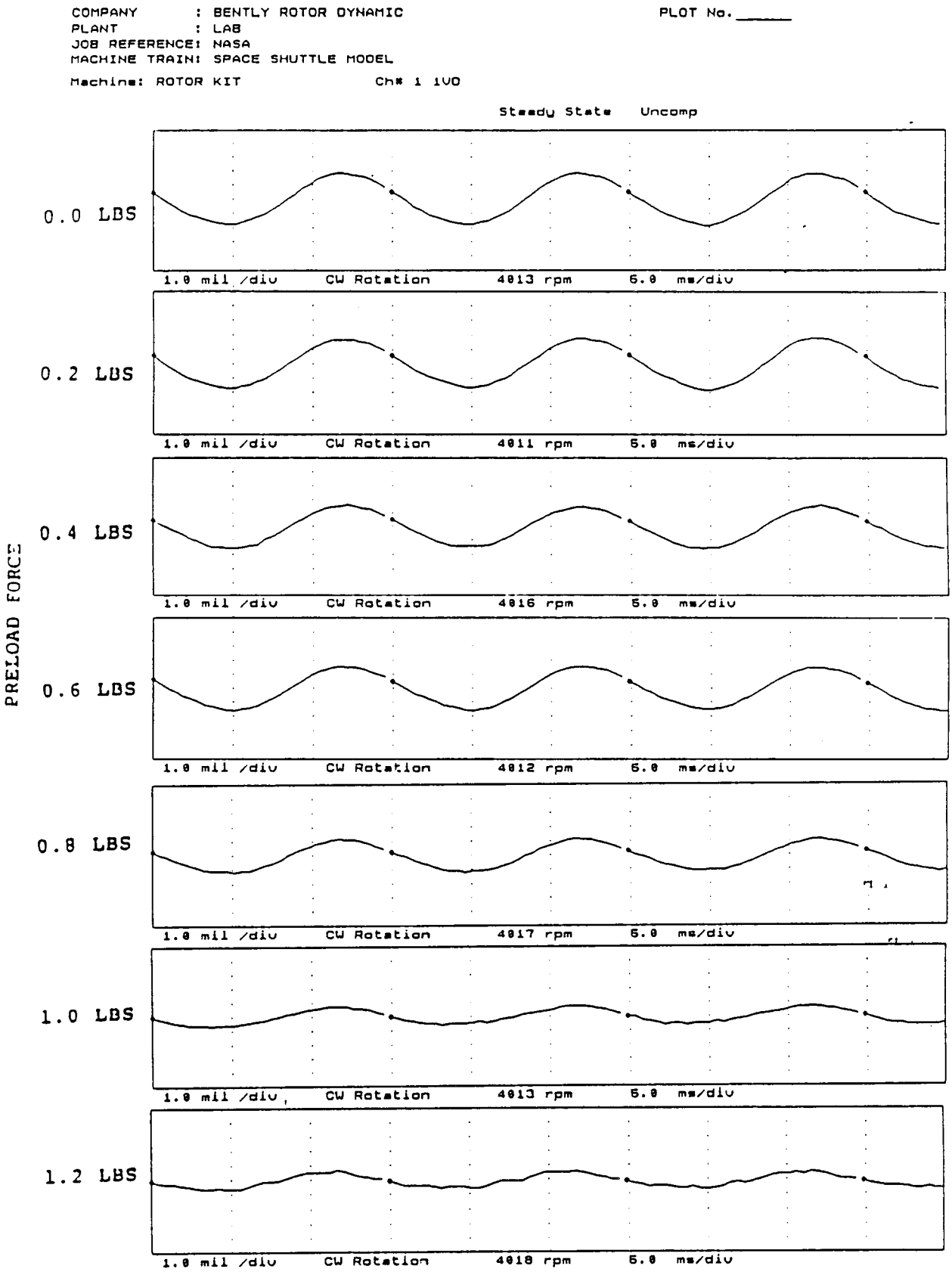

FIGURE 12.138 TIMEBASE FOR VERTICAL PROBE AT LOCATION 1 AT 4000 RPM, 10.0 PSI SEAL OIL PRESSURE, 0.8 IN–GRAM UNBALANCE LOCATED IN THE TURBINE DISK, FOR INCREASING STATIC PRELOADS.

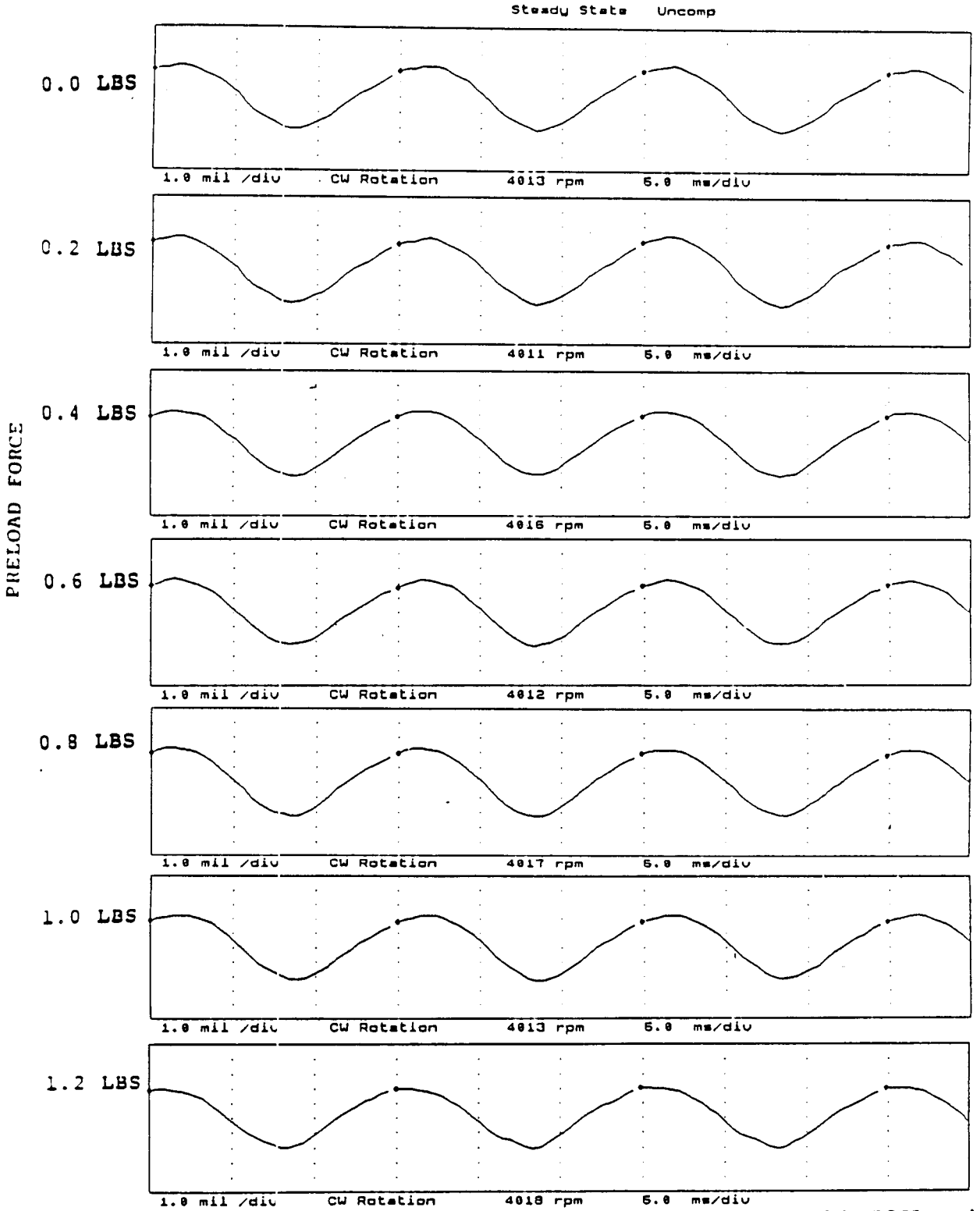

FIGURE 12.139 TIMEBASE FOR HORIZONTAL PROBE AT LOCATION 1 AT 4000 RPM, 10.0 PSI SEAL OIL PRESSURE, 0.8 IN–GRAM UNBALANCE LOCATED IN THE TURBINE DISK, FOR INCREASING STATIC PRELOADS.

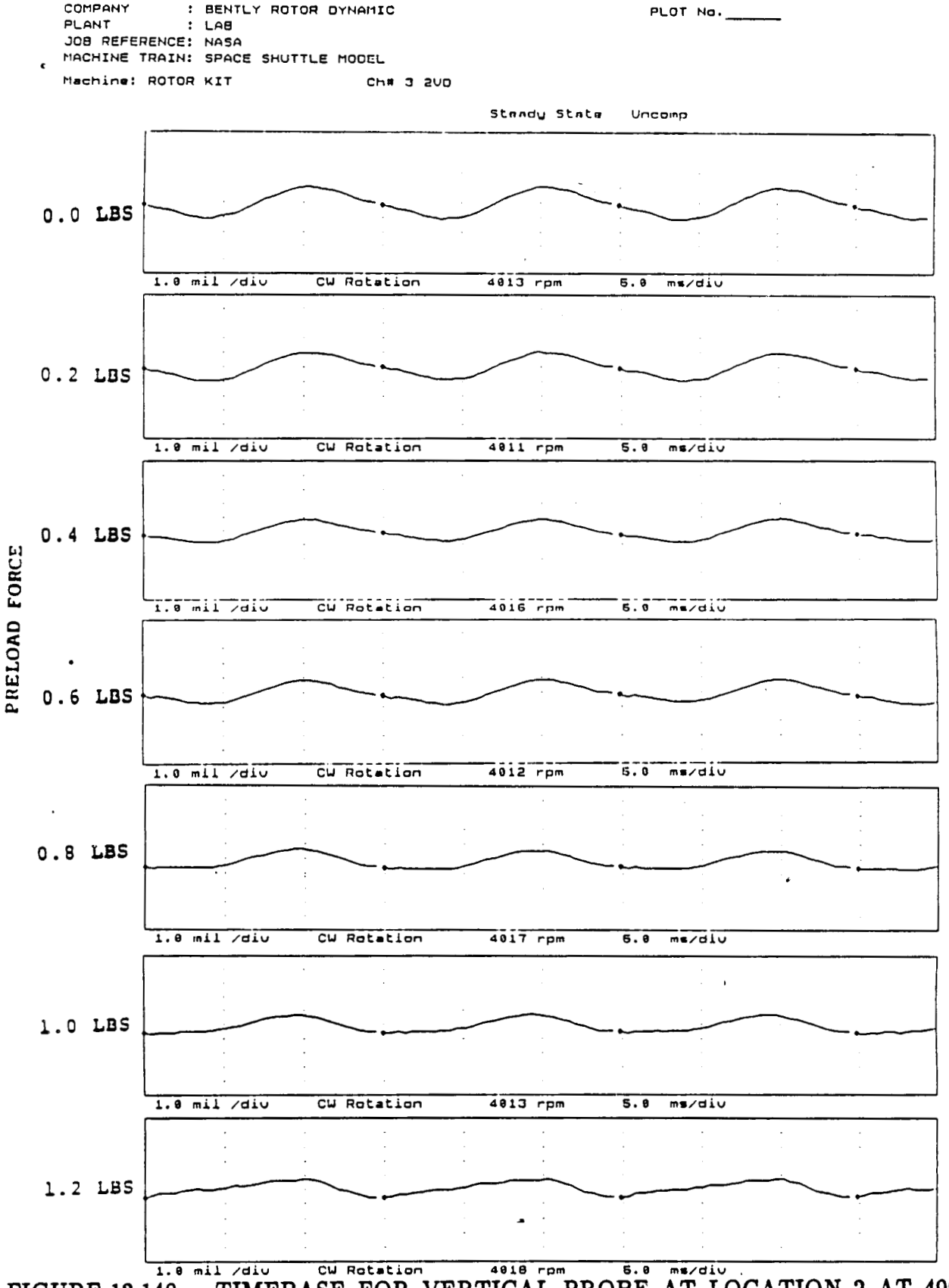

FIGURE 12.140 TIMEBASE FOR VERTICAL PROBE AT LOCATION 2 AT 4000 RPM, 10.0 PSI SEAL OIL PRESSURE, 0.8 IN–GRAM UNBALANCE LOCATED IN THE TURBINE DISK, FOR INCREASING STATIC PRELOADS.

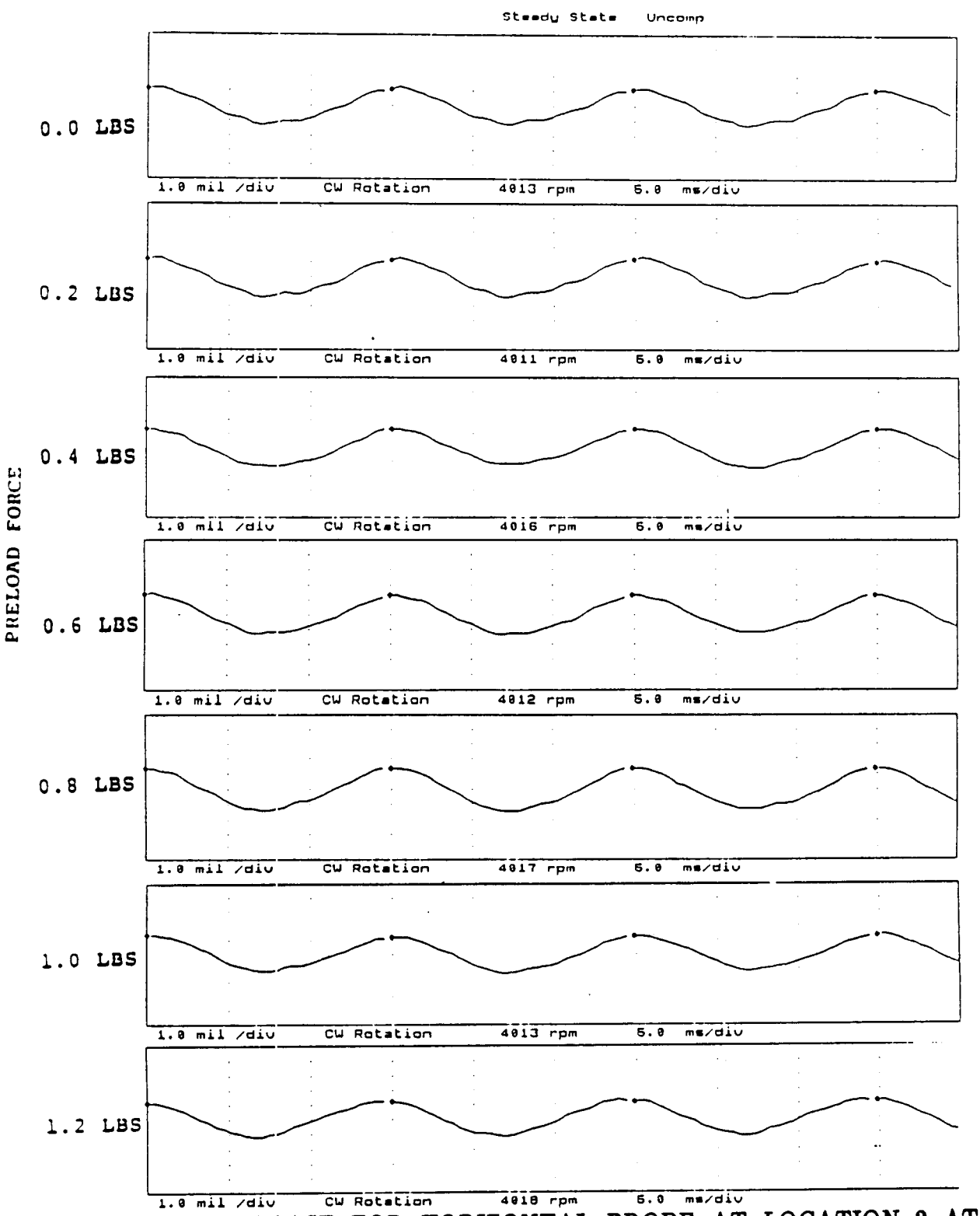

FIGURE 12.141 TIMEBASE FOR HORIZONTAL PROBE AT LOCATION 2 AT 4000 RPM, 10.0 PSI SEAL OIL PRESSURE, 0.8 IN–GRAM UNBALANCE LOCATED IN THE TURBINE DISK, FOR INCREASING STATIC PRELOADS.

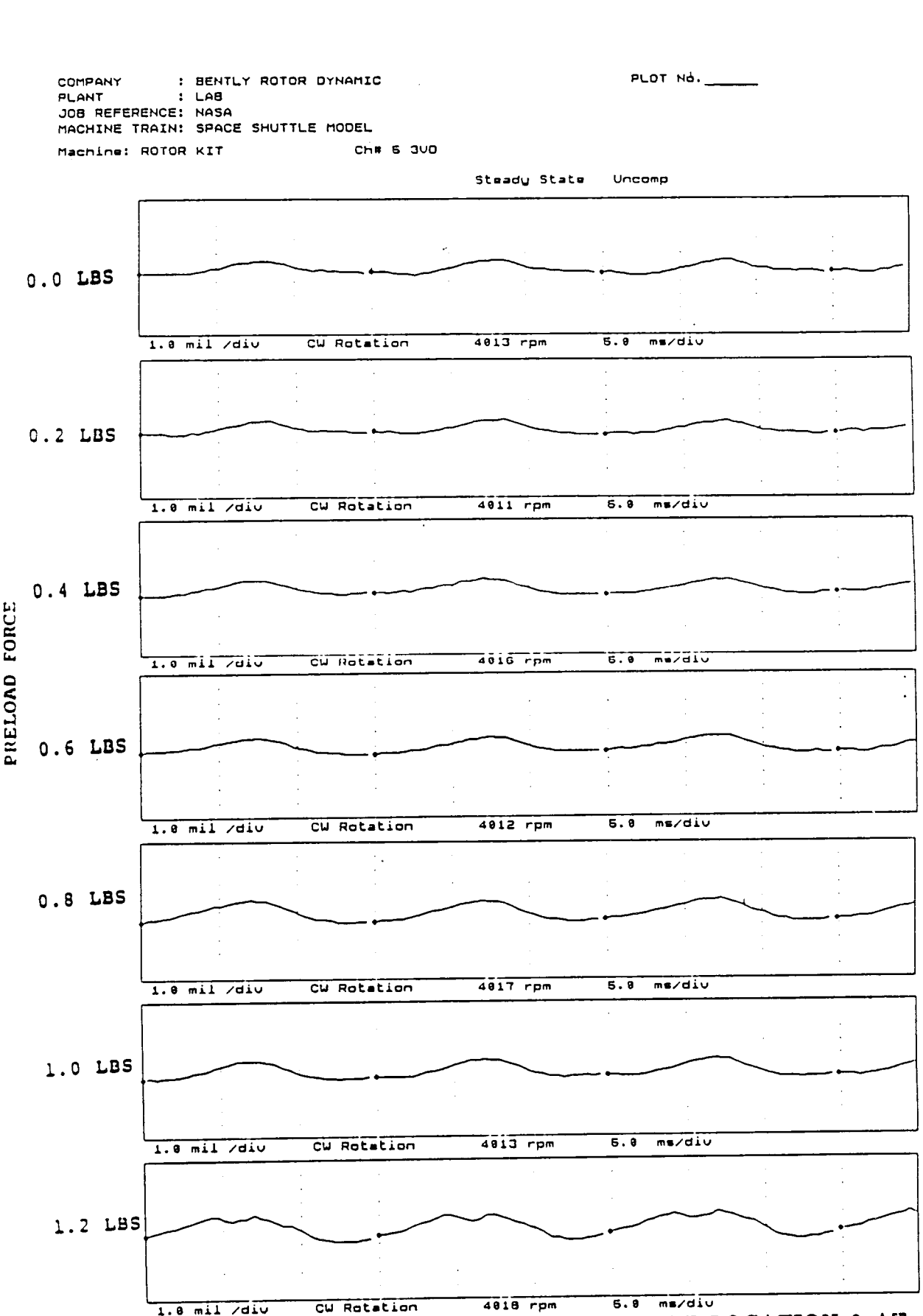

FIGURE 12.142 TIMEBASE FOR VERTICAL PROBE AT LOCATION 3 AT 4000 RPM, 10.0 PSI SEAL OIL PRESSURE, 0.8 IN–GRAM UNBALANCE LOCATED IN THE TURBINE DISK, FOR INCREASING STATIC PRELOADS.

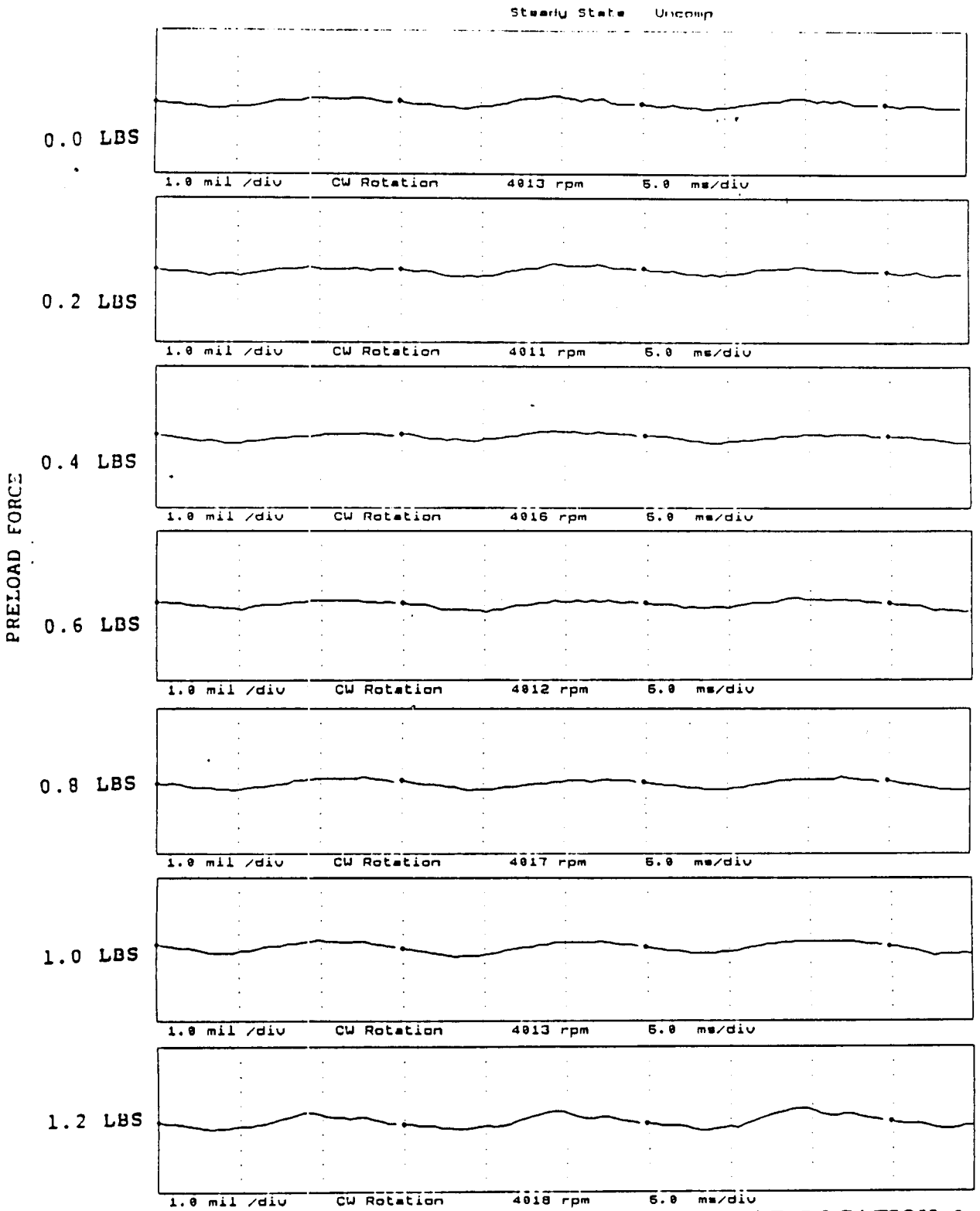

FIGURE 12.143 TIMEBASE FOR HORIZONTAL PROBE AT LOCATION 3 AT 4000 RPM, 10.0 PSI SEAL OIL PRESSURE, 0.8 IN–GRAM UNBALANCE LOCATED IN THE TURBINE DISK, FOR INCREASING STATIC PRELOADS.

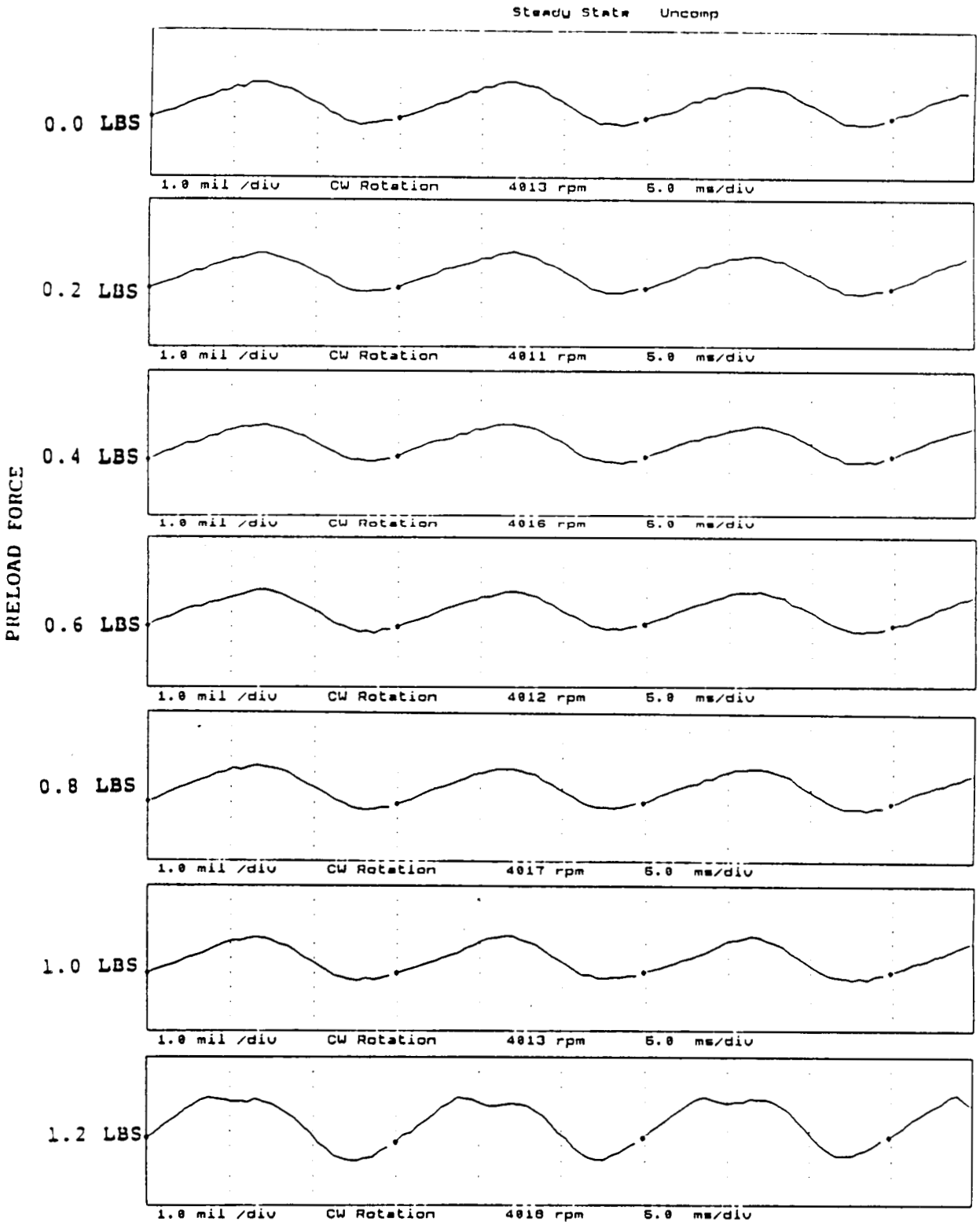

FIGURE 12.144 TIMEBASE FOR VERTICAL PROBE AT LOCATION 4 AT 4000 RPM, 10.0 PSI SEAL OIL PRESSURE, 0.8 IN–GRAM UNBALANCE LOCATED IN THE TURBINE DISK, FOR INCREASING STATIC PRELOADS.

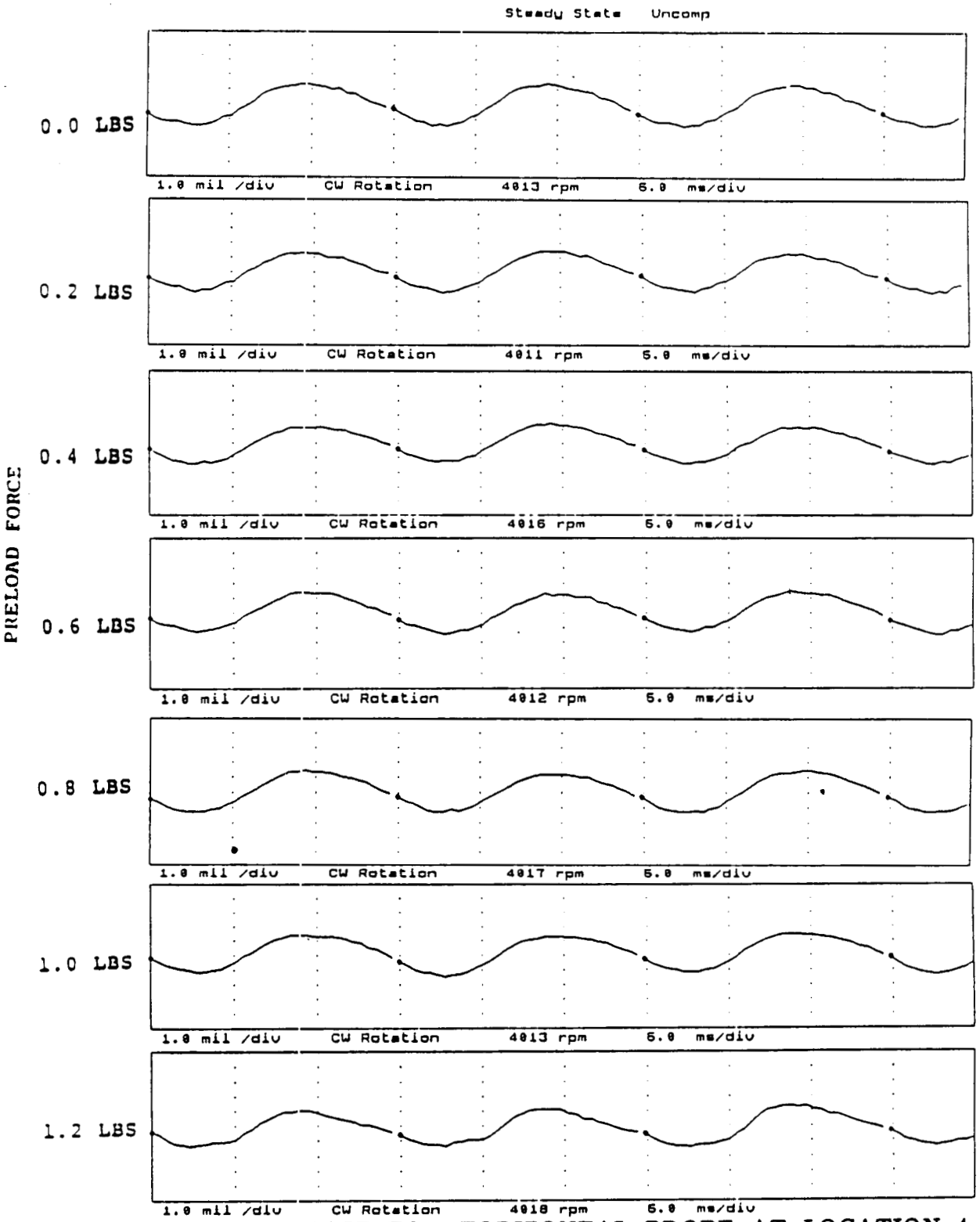

FIGURE 12.145 TIMEBASE FOR HORIZONTAL PROBE AT LOCATION 4 AT 4000 RPM, 10.0 PSI SEAL OIL PRESSURE, 0.8 IN–GRAM UNBALANCE LOCATED IN THE TURBINE DISK, FOR INCREASING STATIC PRELOADS.

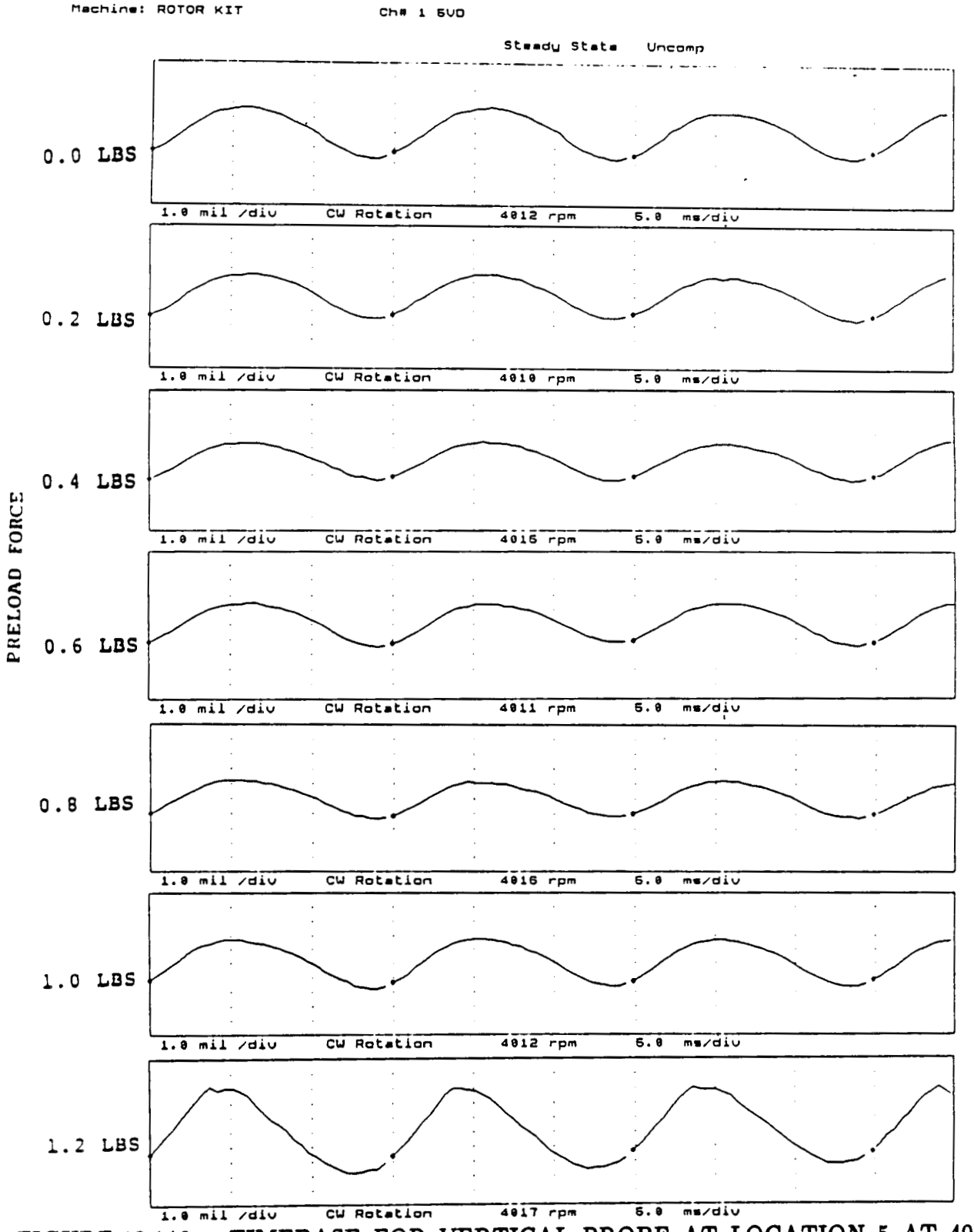

FIGURE 12.146 TIMEBASE FOR VERTICAL PROBE AT LOCATION 5 AT 4000 RPM, 10.0 PSI SEAL OIL PRESSURE, 0.8 IN–GRAM UNBALANCE LOCATED IN THE TURBINE DISK, FOR INCREASING STATIC PRELOADS.

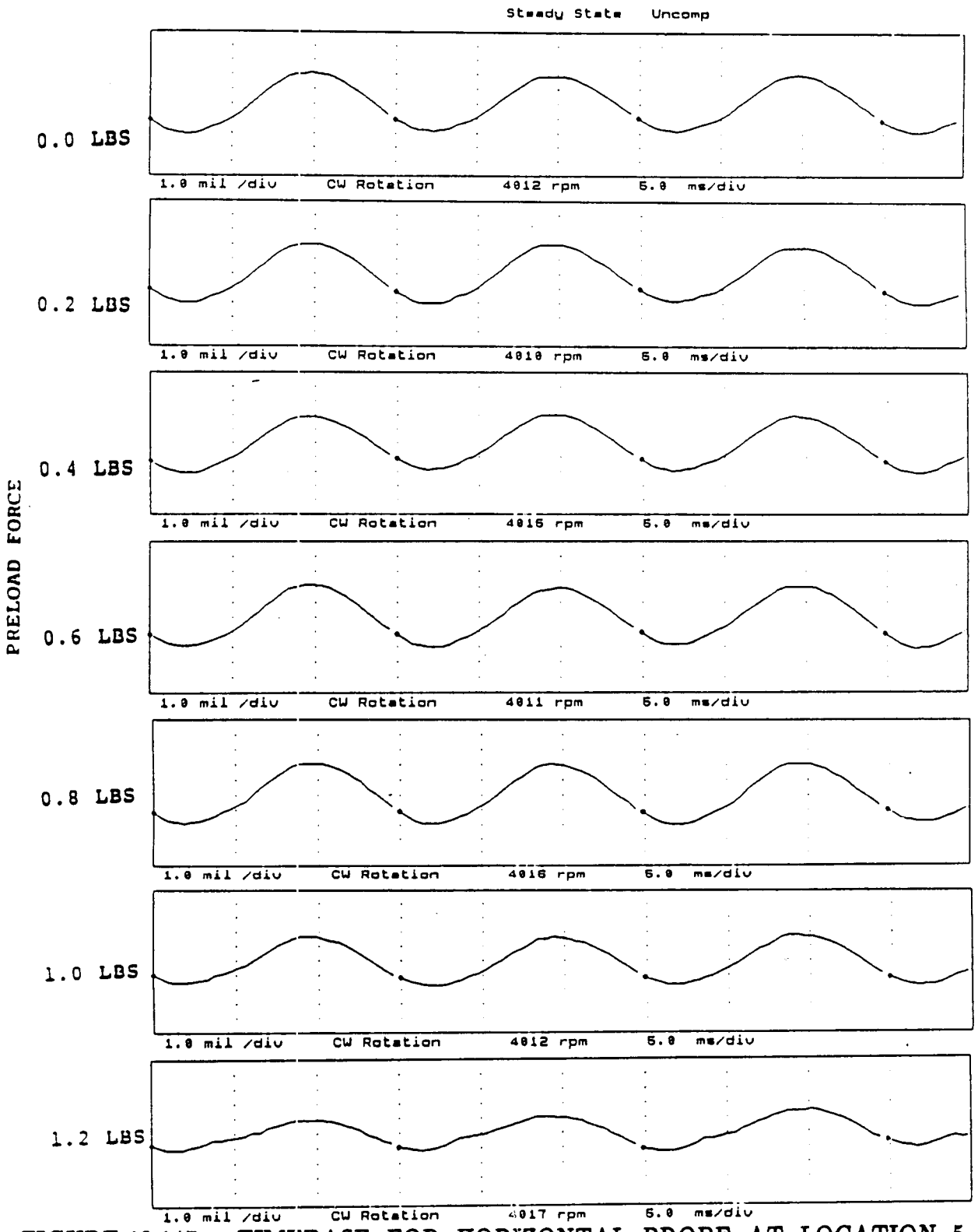

FIGURE 12.147 TIMEBASE FOR HORIZONTAL PROBE AT LOCATION 5 AT 4000 RPM, 10.0 PSI SEAL OIL PRESSURE, 0.8 IN–GRAM UNBALANCE LOCATED IN THE TURBINE DISK, FOR INCREASING STATIC PRELOADS.

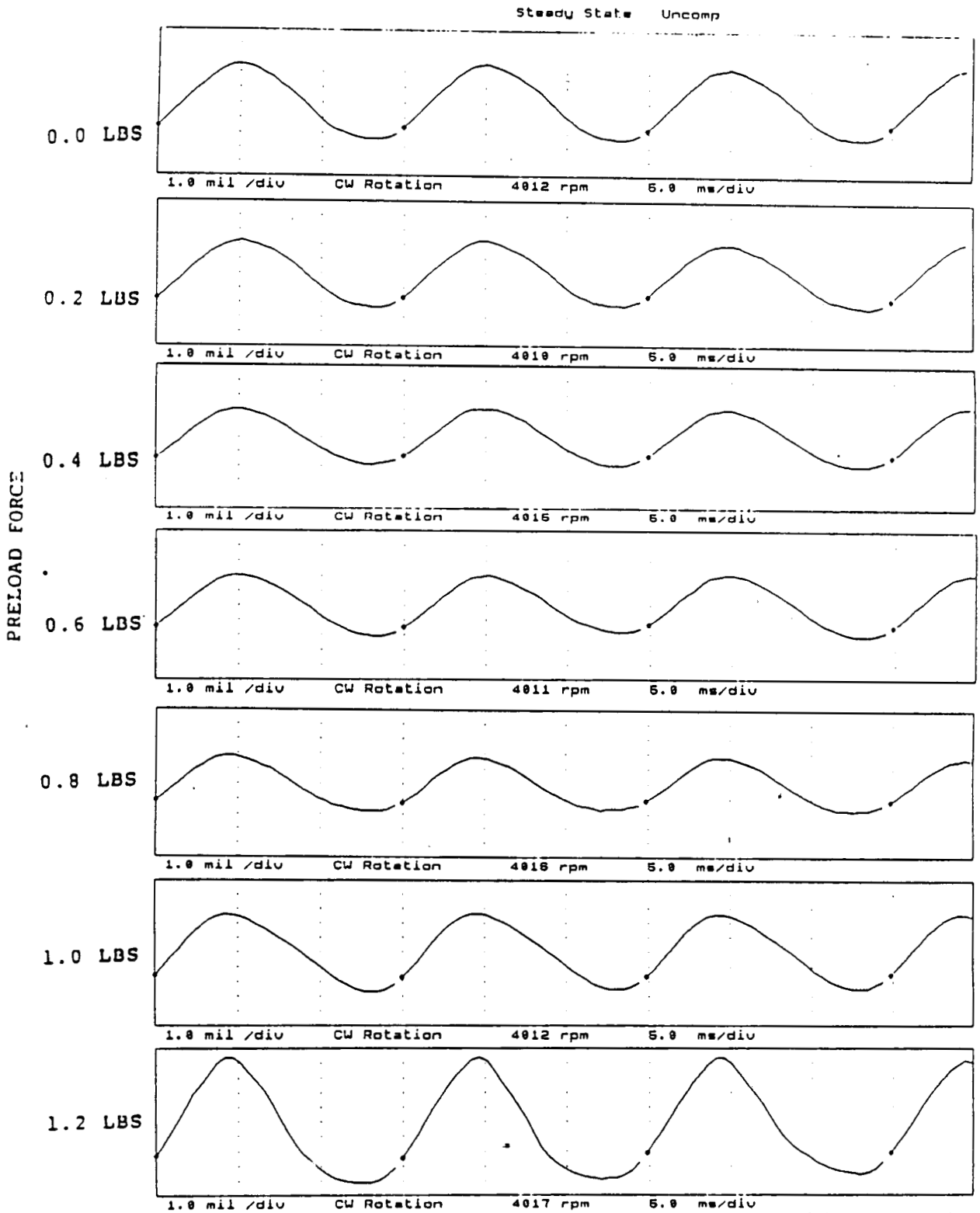

FIGURE 12.148 TIMEBASE FOR VERTICAL PROBE AT LOCATION 6 AT 400 RPM, 10.0 PSI SEAL OIL PRESSURE, 0.8 IN–GRAM UNBALANCE LOCATED IN THE TURBINE DISK, FOR INCREASING STATIC PRELOADS.

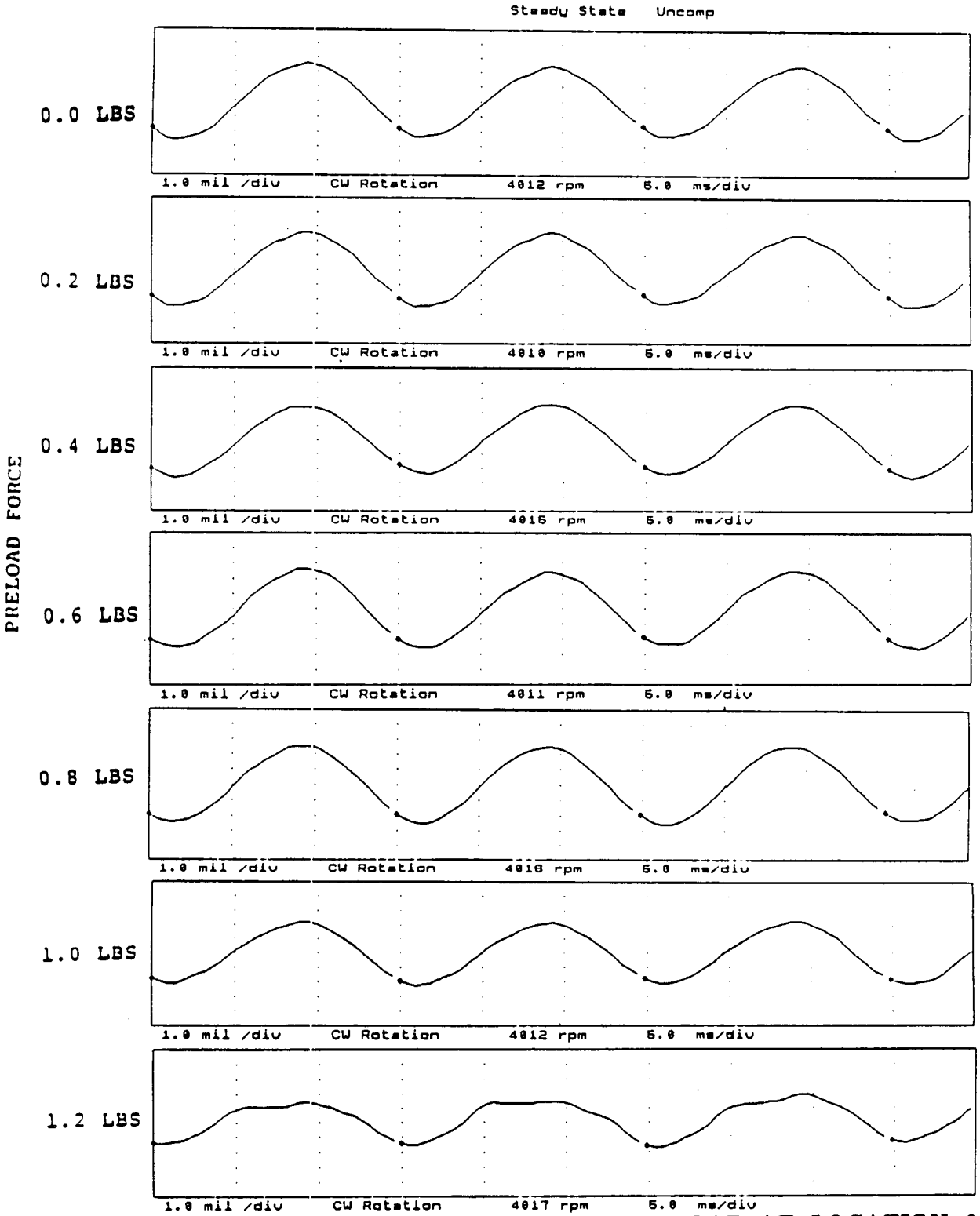

FIGURE 12.149 TIMEBASE FOR HORIZONTAL PROBE AT LOCATION 6 AT 4000 RPM, 10.0 PSI SEAL OIL PRESSURE, 0.8 IN–GRAM UNBALANCE LOCATED IN THE TURBINE DISK, FOR INCREASING STATIC PRELOADS.

NOT AVAILABLE - OIL IN THE CLEARANCE AREA
PROHIBITS THE METAL-TO-METAL CONTACT NECESSARY
FOR THE CONTACT SENSOR TO OPERATE CORRECTLY.

FIGURE 12.150 TIMEBASE FOR SHAFT TO SEAL 1 CONTACT AT 4000 RPM, 10.0 PSI SEAL OIL PRESSURE, 0.8 IN–GRAM UNBALANCE LOCATED IN THE TURBINE DISK, FOR INCREASING STATIC PRELOADS.

NOT AVAILABLE - OIL IN THE CLEARANCE AREA
PROHIBITS THE METAL-TO-METAL CONTACT NECESSARY
FOR THE CONTACT SENSOR TO OPERATE CORRECTLY.

FIGURE 12.151 TIMEBASE FOR SHAFT TO SEAL 2 CONTACT AT 4000 RPM, 10.0 PSI SEAL OIL PRESSURE, 0.8 IN–GRAM UNBALANCE LOCATED IN THE TURBINE DISK, FOR INCREASING STATIC PRELOADS.

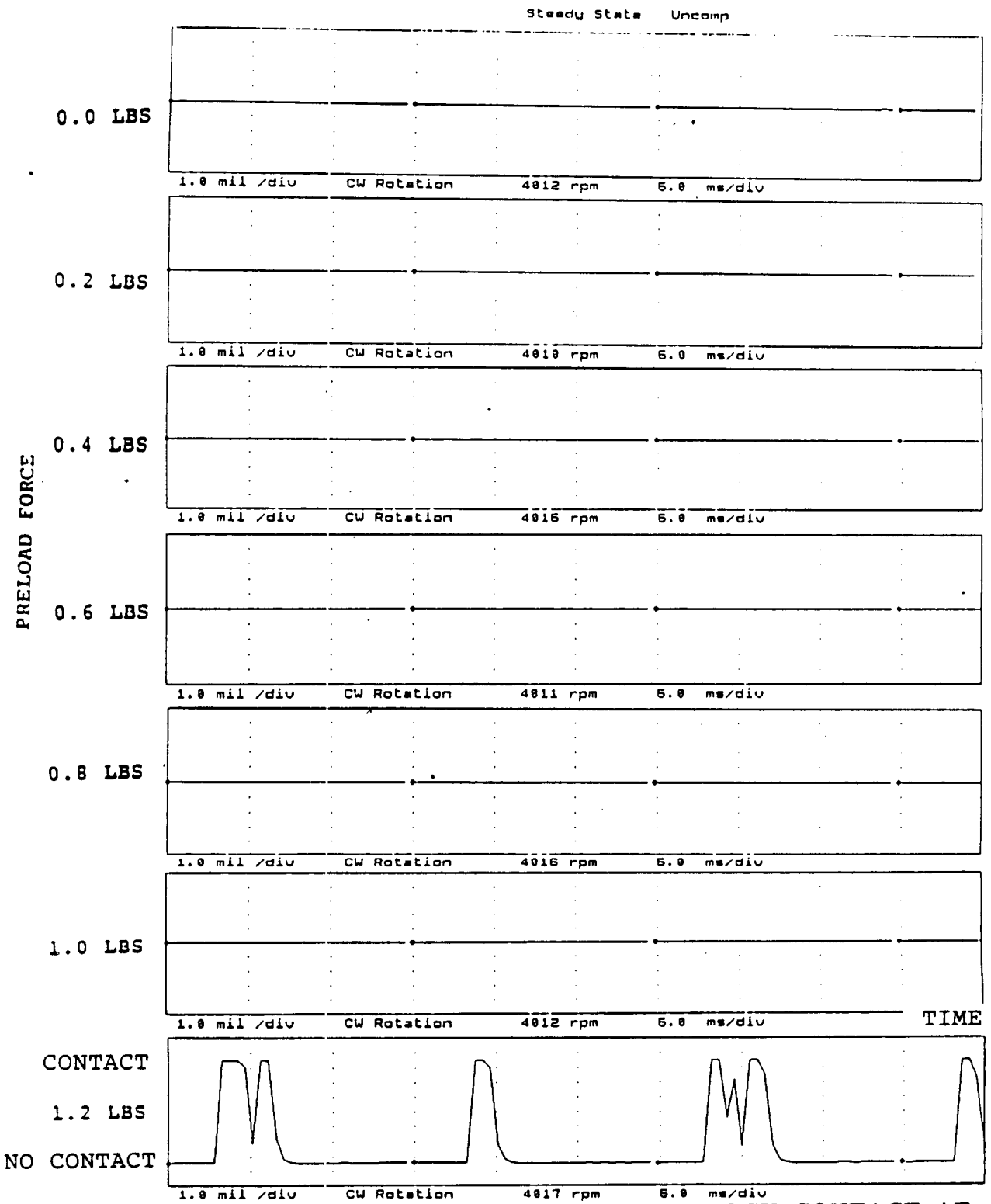

FIGURE 12.152 TIMEBASE FOR SHAFT TO RUB BLOCK CONTACT AT 4000 RPM, 10.0 PSI SEAL OIL PRESSURE, 0.8 IN–GRAM UNBALANCE LOCATED IN THE TURBINE DISK, FOR INCREASING STATIC PRELOADS.

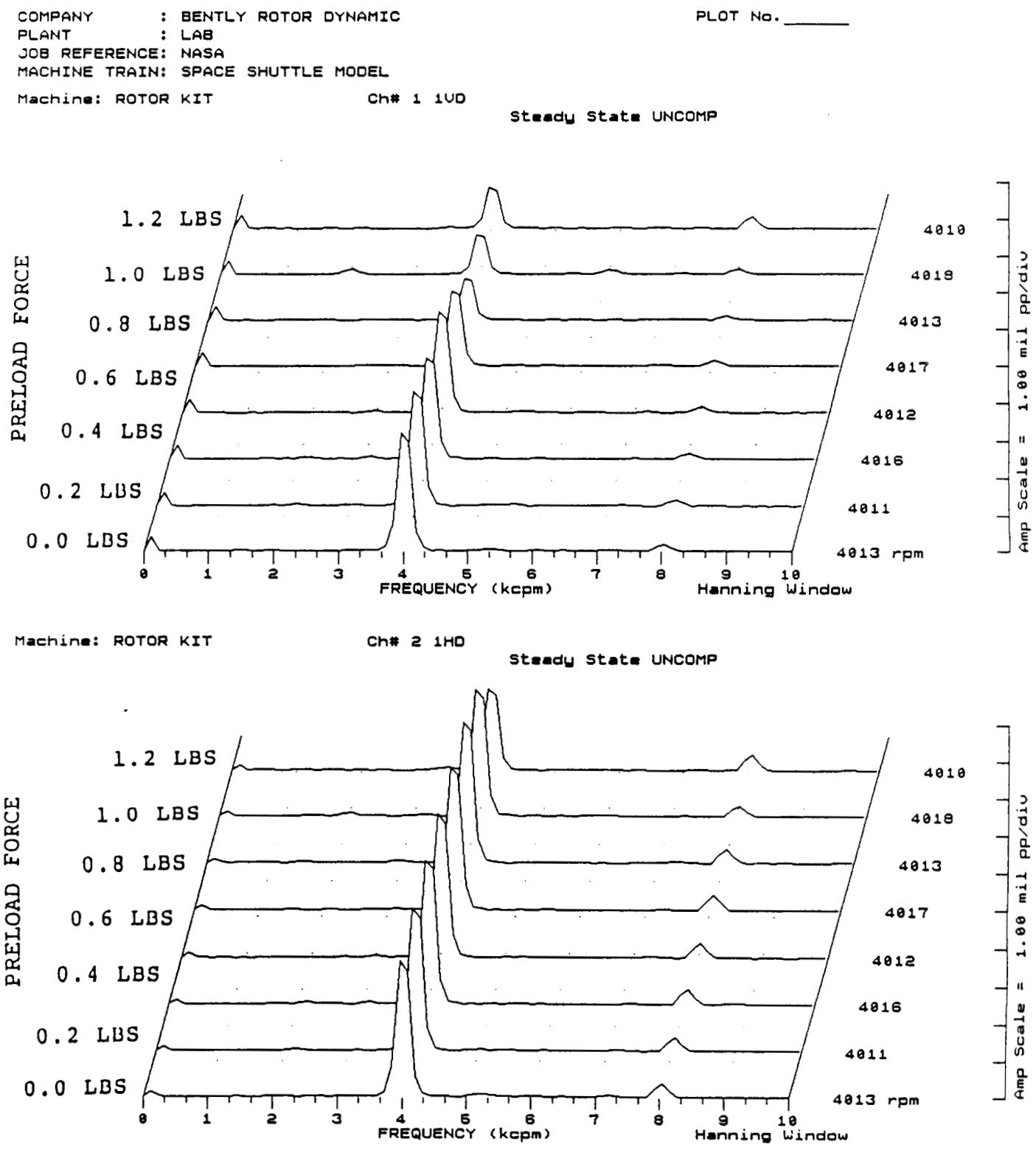

FIGURE 12.153 SPECTRAL CONTENT AT PROBE LOCATION 1 AT 4000 RPM, 10.0 PSI SEAL OIL PRESSURE, 0.8 IN–GRAM UNBALANCE LOCATED IN THE TURBINE DISK, FOR INCREASING STATIC PRELOADS.

C.5

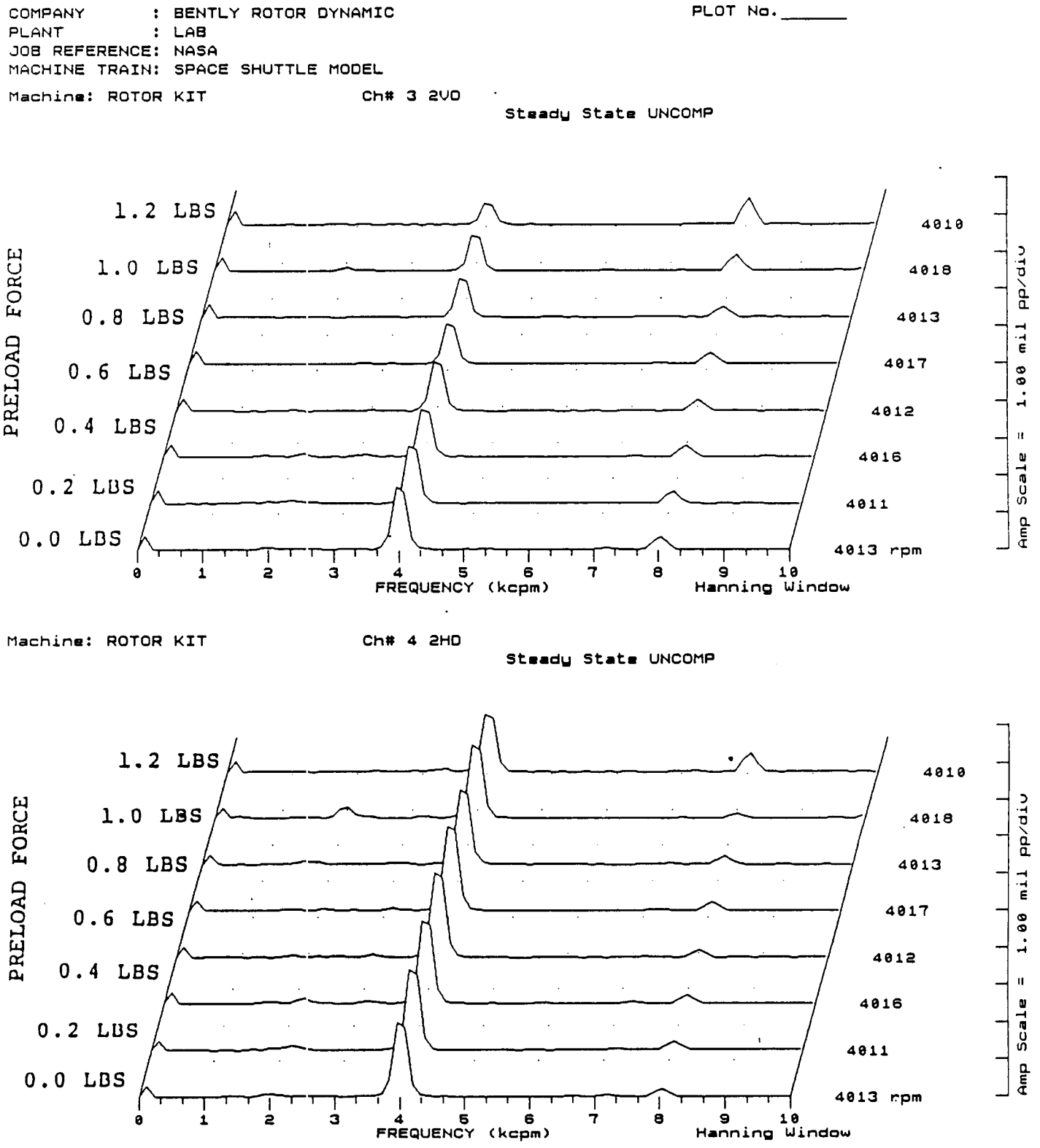

FIGURE 12.154 SPECTRAL CONTENT AT PROBE LOCATION 2 AT 4000 RPM, 10.0 PSI SEAL OIL PRESSURE, 0.8 IN–GRAM UNBALANCE LOCATED IN THE TURBINE DISK, FOR INCREASING STATIC PRELOADS.

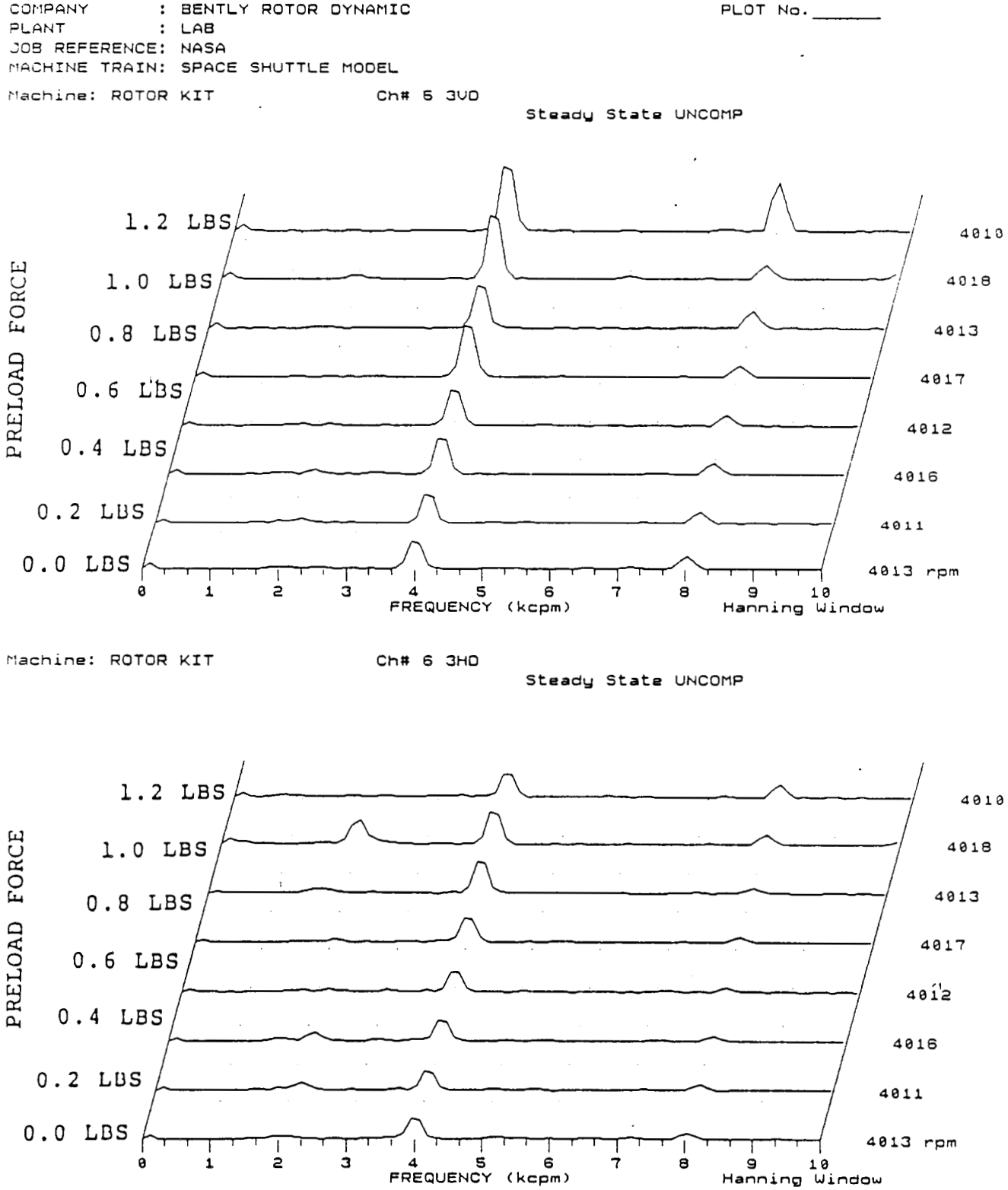

FIGURE 12.155 SPECTRAL CONTENT AT PROBE LOCATION 3 AT 4000 RPM, 10.0 PSI SEAL OIL PRESSURE, 0.8 IN–GRAM UNBALANCE LOCATED IN THE TURBINE DISK, FOR INCREASING STATIC PRELOADS.

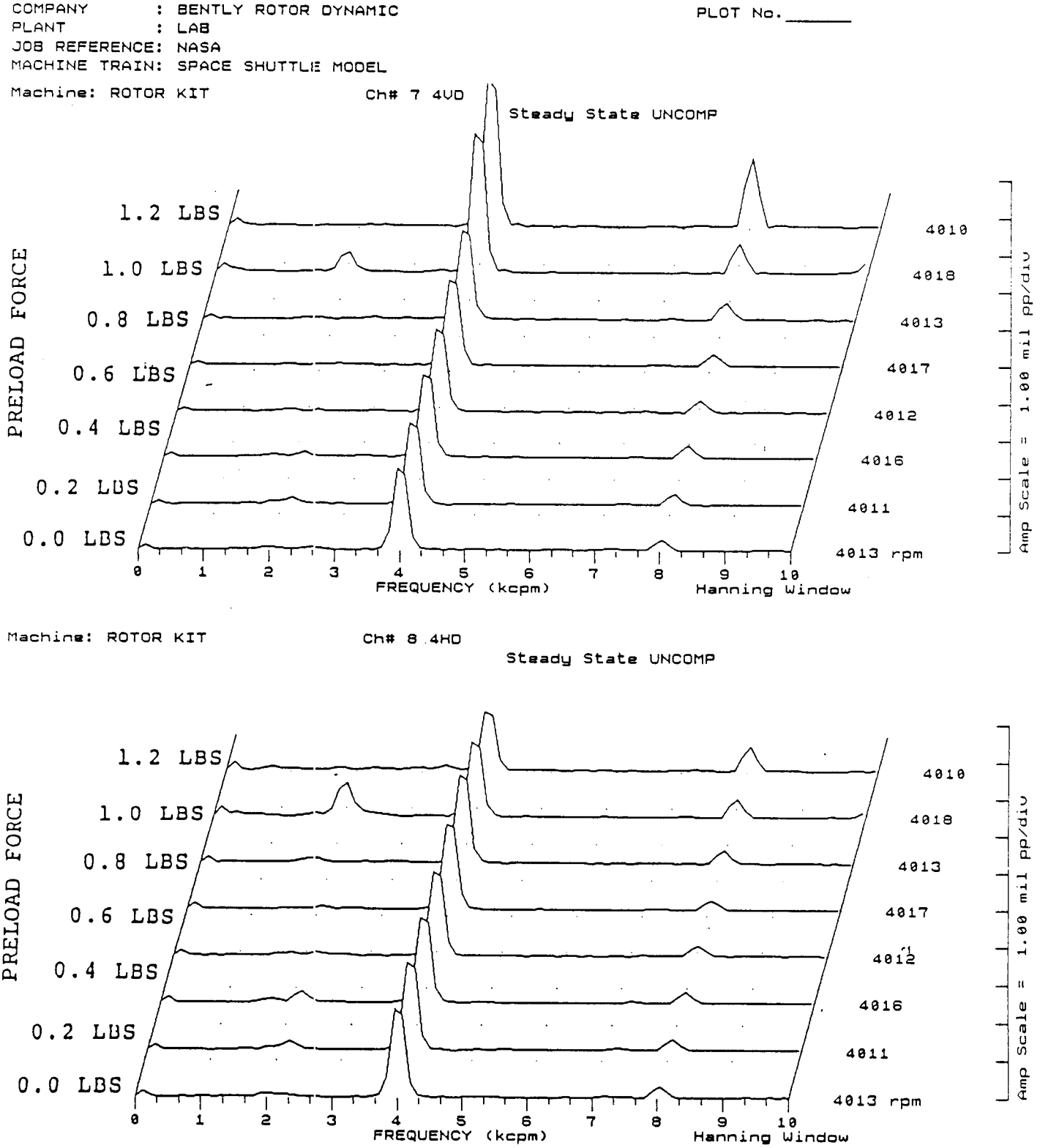

FIGURE 12.156 SPECTRAL CONTENT AT PROBE LOCATION 4 AT 4000 RPM, 10.0 PSI SEAL OIL PRESSURE, 0.8 IN–GRAM UNBALANCE LOCATED IN THE TURBINE DISK, FOR INCREASING STATIC PRELOADS.

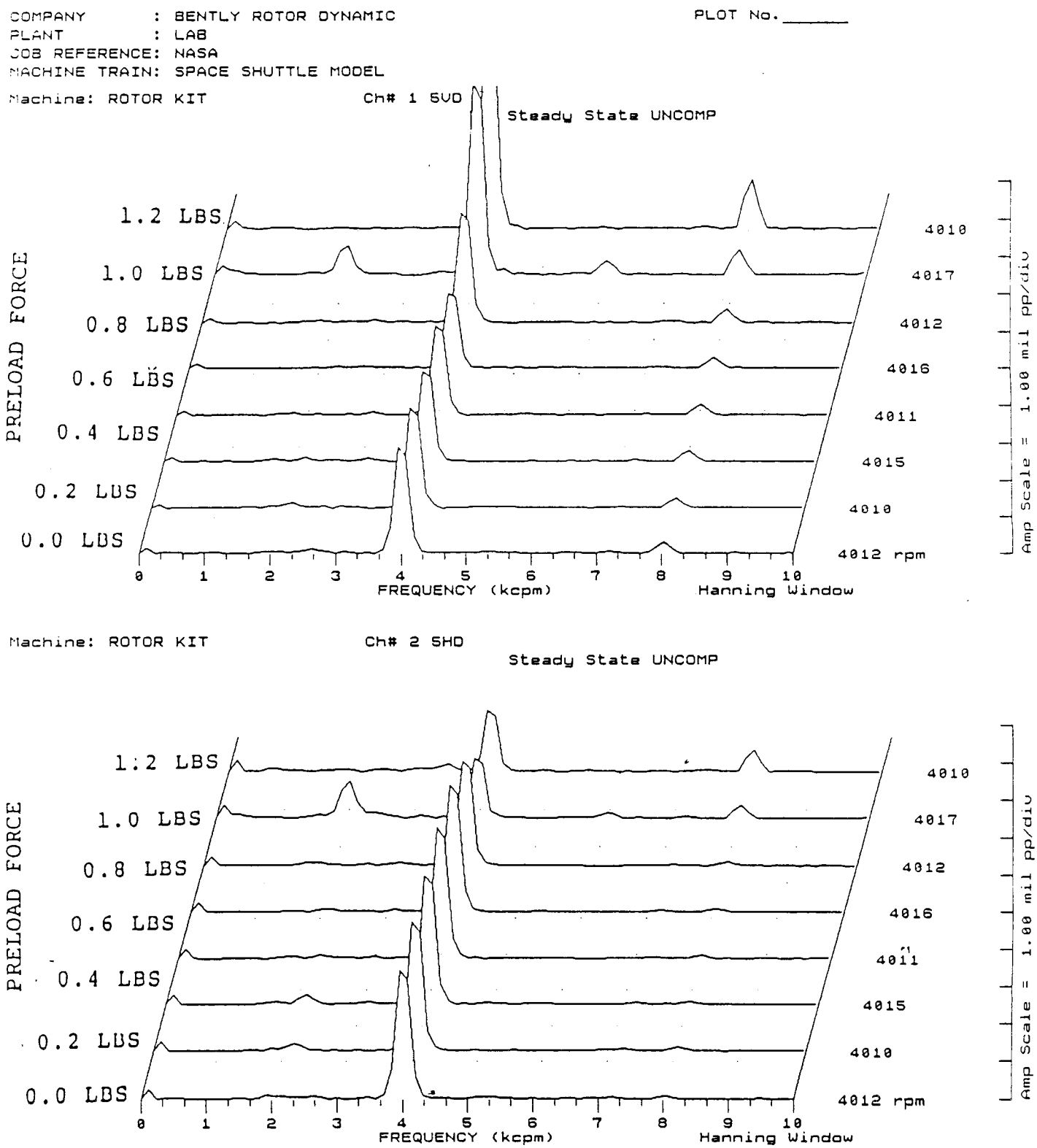

FIGURE 12.157 SPECTRAL CONTENT AT PROBE LOCATION 5 AT 4000 RPM, 10.0 PSI SEAL OIL PRESSURE, 0.8 IN-GRAM UNBALANCE LOCATED IN THE TURBINE DISK, FOR INCREASING STATIC PRELOADS.

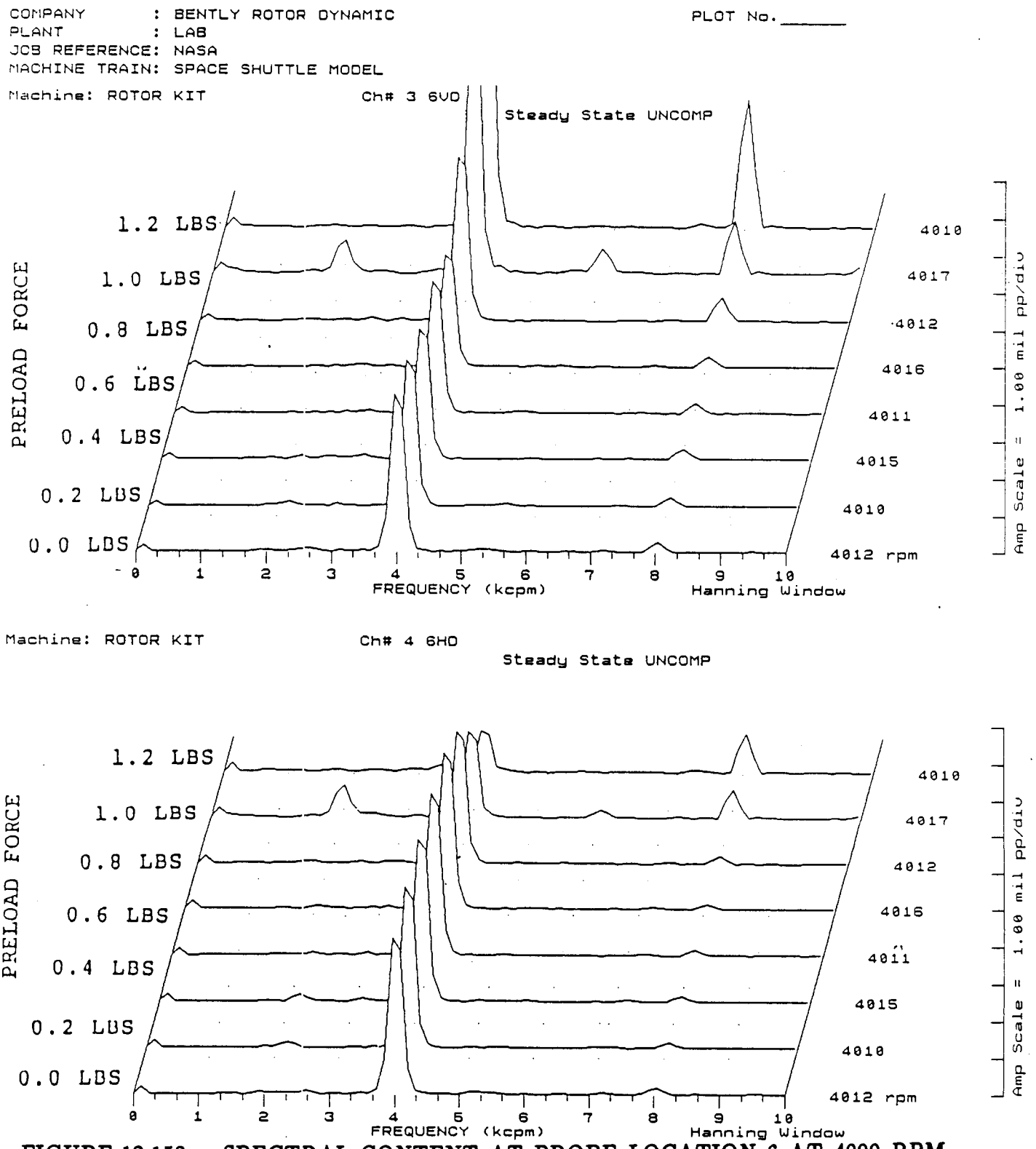

FIGURE 12.158 SPECTRAL CONTENT AT PROBE LOCATION 6 AT 4000 RPM, 10.0 PSI SEAL OIL PRESSURE, 0.8 IN–GRAM UNBALANCE LOCATED IN THE TURBINE DISK, FOR INCREASING STATIC PRELOADS.

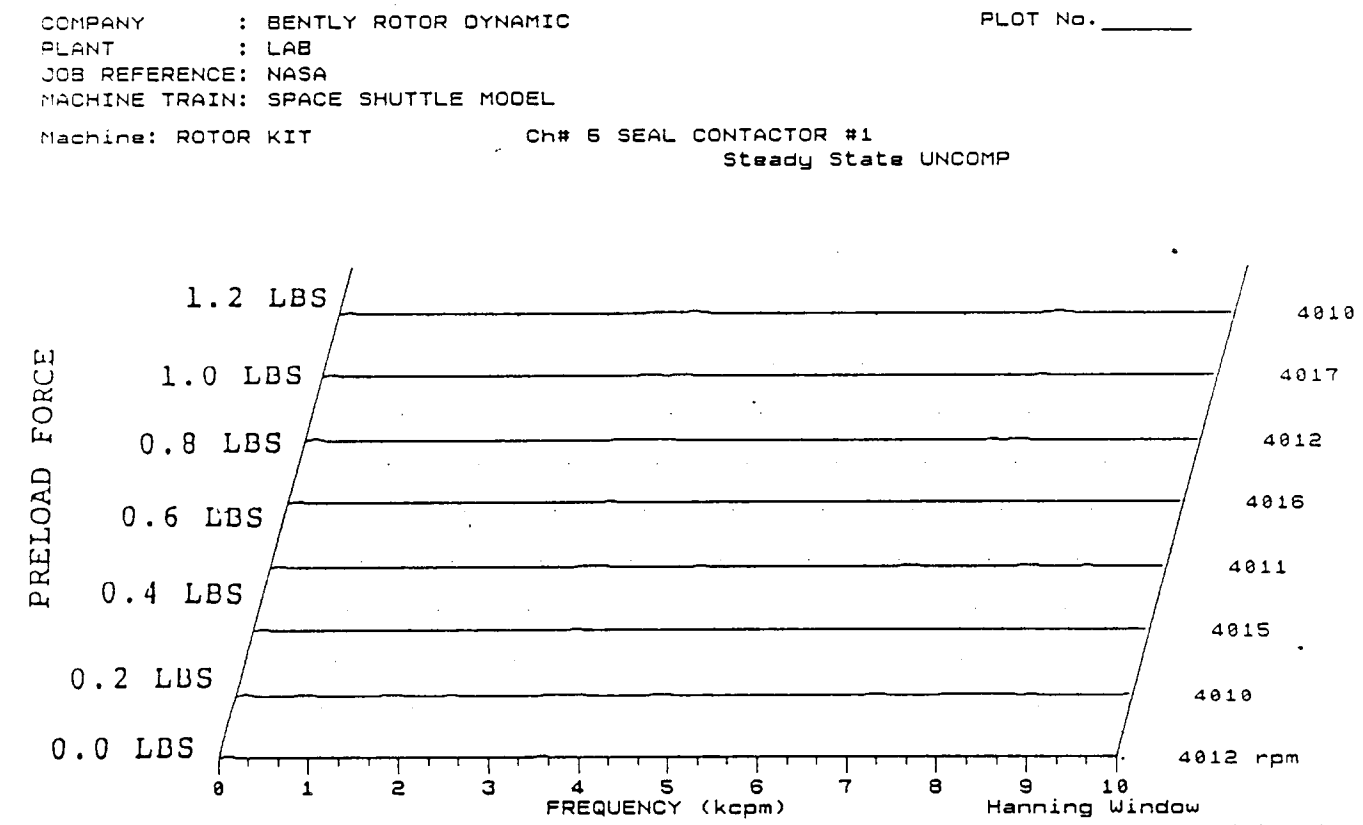

FIGURE 12.159 SPECTRAL CONTENT FOR SHAFT TO SEAL 1 CONTACT AT 4000 RPM, 10.0 PSI SEAL OIL PRESSURE, 0.8 IN–GRAM UNBALANCE LOCATED IN THE TURBINE DISK, FOR INCREASING STATIC PRELOADS.

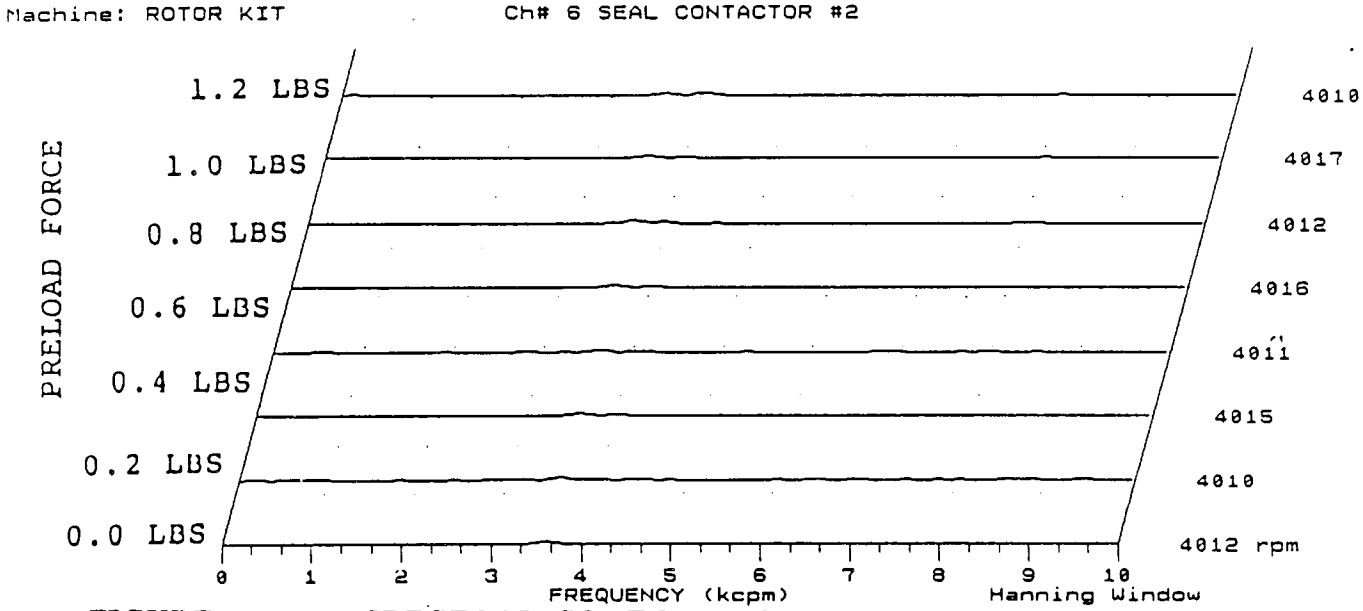

FIGURE 12.160 SPECTRAL CONTENT FOR SHAFT TO SEAL 2 CONTACT AT 4000 RPM, 10.0 PSI SEAL OIL PRESSURE, 0.8 IN–GRAM UNBALANCE LOCATED IN THE TURBINE DISK, FOR INCREASING STATIC PRELOADS.

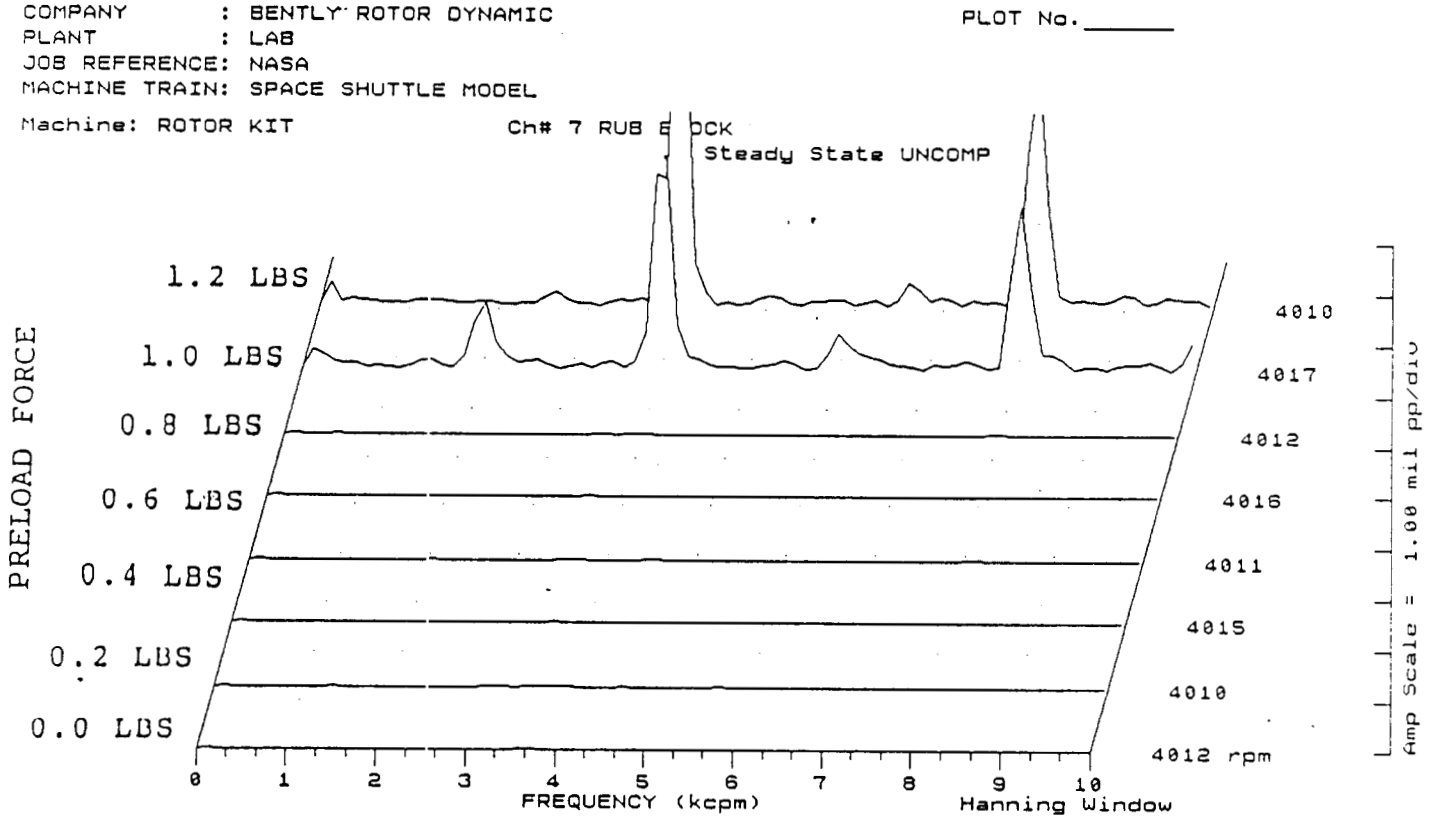

FIGURE 12.161 SPECTRAL CONTENT FOR SHAFT TO RUB BLOCK CONTACT AT 4000 RPM, 10.0 PSI SEAL OIL PRESSURE, 0.8 IN–GRAM UNBALANCE LOCATED IN THE TURBINE DISK, FOR INCREASING STATIC PRELOADS.

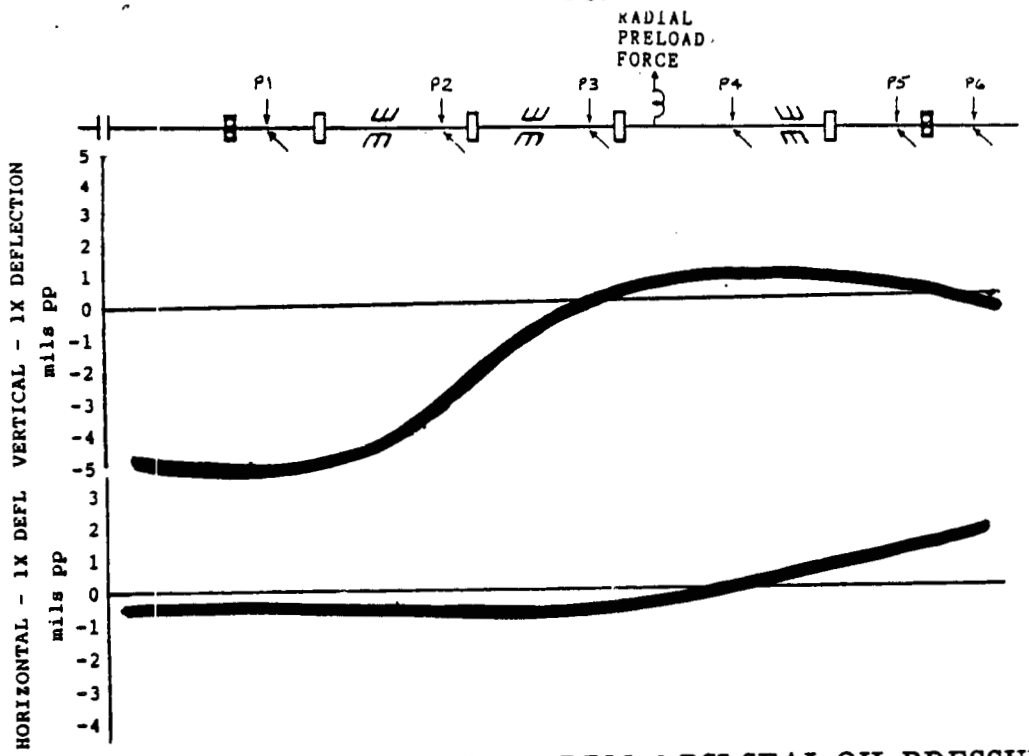

FIGURE 12.162 ROTOR MODE SHAPE AT 4000 RPM, 0 PSI SEAL OIL PRESSURE DUE TO 0.8 IN–GRAM UNBALANCE LOCATED IN THE THIRD PUMP IMPELLER DISK.

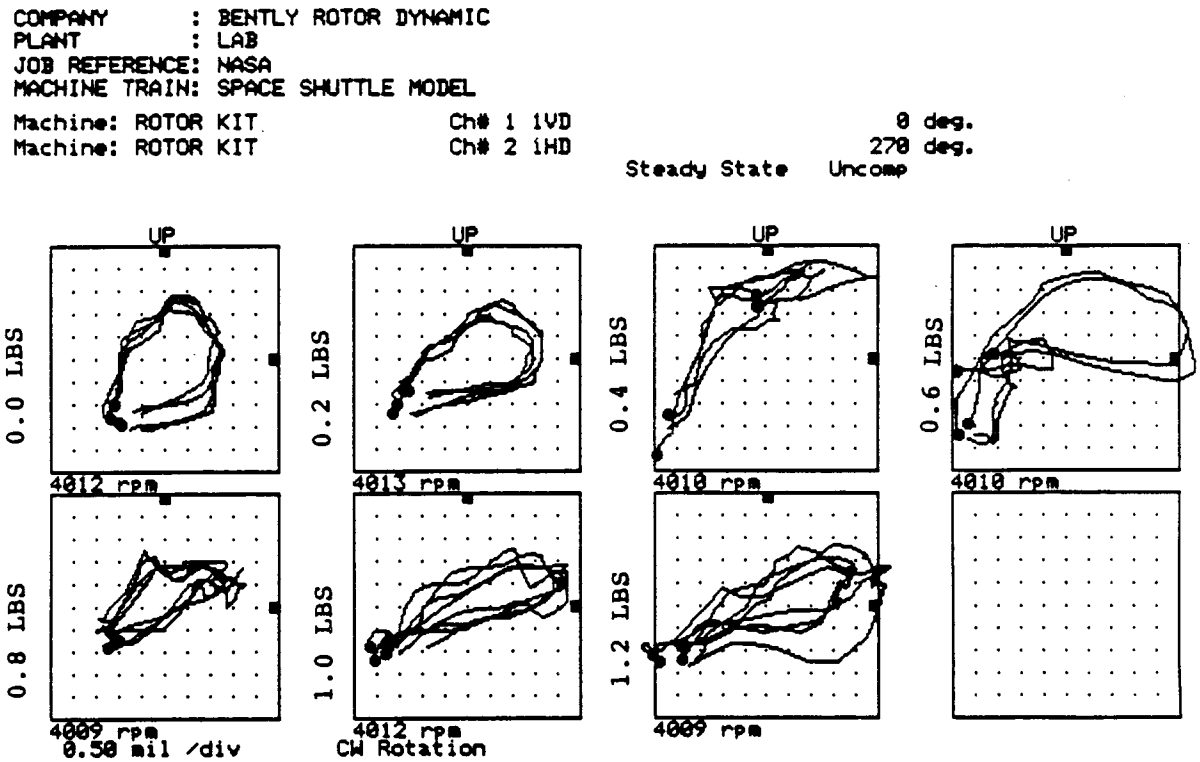

FIGURE 12.163 ORBITS AT PROBE LOCATION 1 AT 4000 RPM, 0 PSI SEAL OIL PRESSURE, 0.8 IN–GRAM UNBALANCE LOCATED IN THE THIRD PUMP IMPELLER DISK, FOR INCREASING STATIC PRELOAD FORCES.

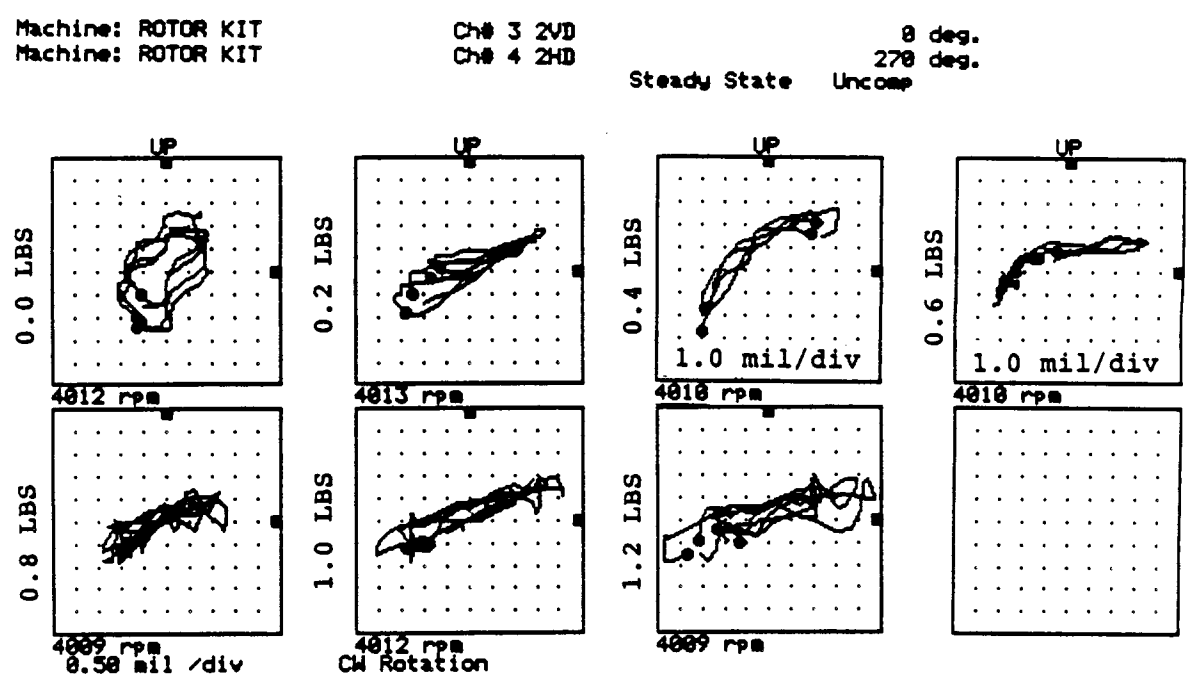

FIGURE 12.164 ORBITS AT PROBE LOCATION 2 AT 4000 RPM, 0 PSI SEAL OIL PRESSURE, 0.8 IN–GRAM UNBALANCE LOCATED IN THE THIRD PUMP IMPELLER DISK, FOR INCREASING STATIC PRELOAD FORCES.

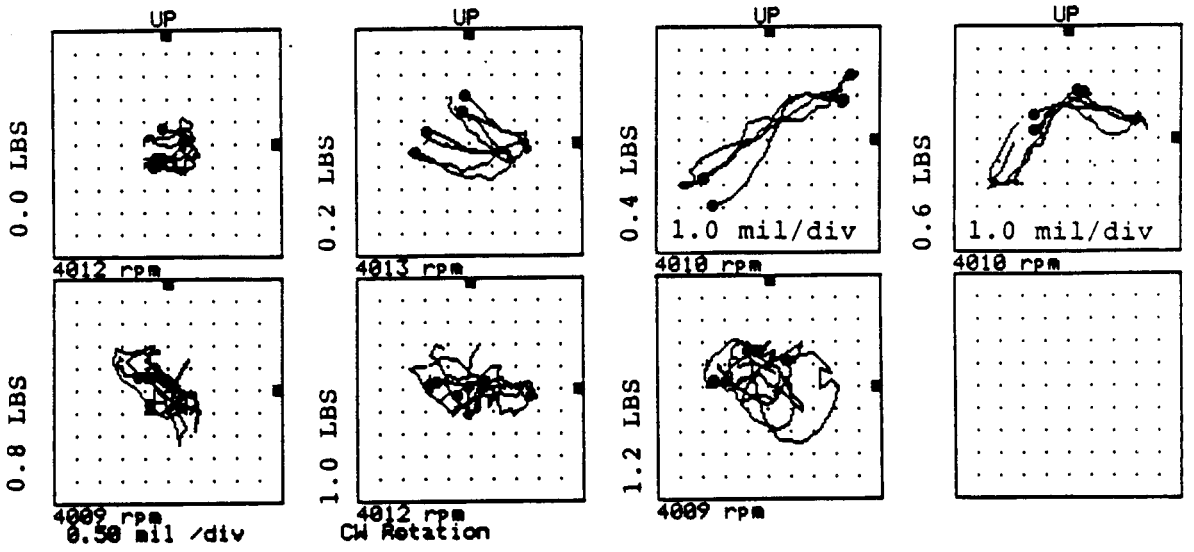

FIGURE 12.165 ORBITS AT PROBE LOCATION 3 AT 4000 RPM, 0 PSI SEAL OIL PRESSURE, 0.8 IN–GRAM UNBALANCE LOCATED IN THE THIRD PUMP IMPELLER DISK, FOR INCREASING STATIC PRELOAD FORCES.

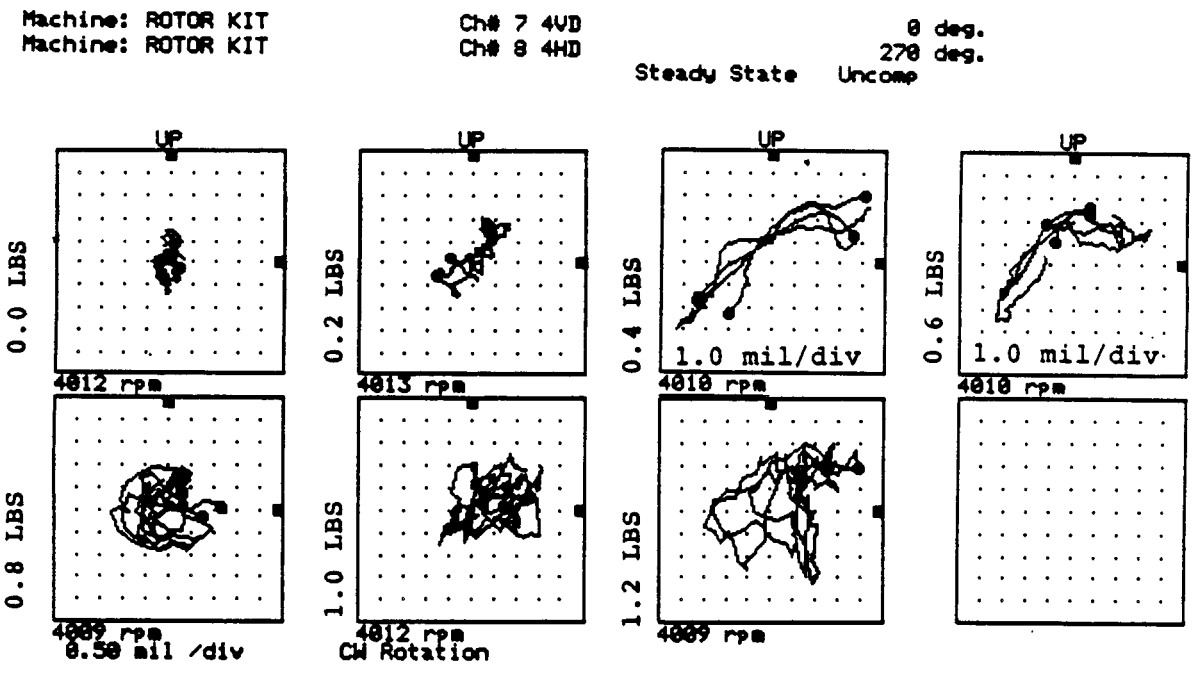

FIGURE 12.166 ORBITS AT PROBE LOCATION 4 AT 4000 RPM, 0 PSI SEAL OIL PRESSURE, 0.8 IN–GRAM UNBALANCE LOCATED IN THE THIRD PUMP IMPELLER DISK, FOR INCREASING STATIC PRELOAD FORCES.

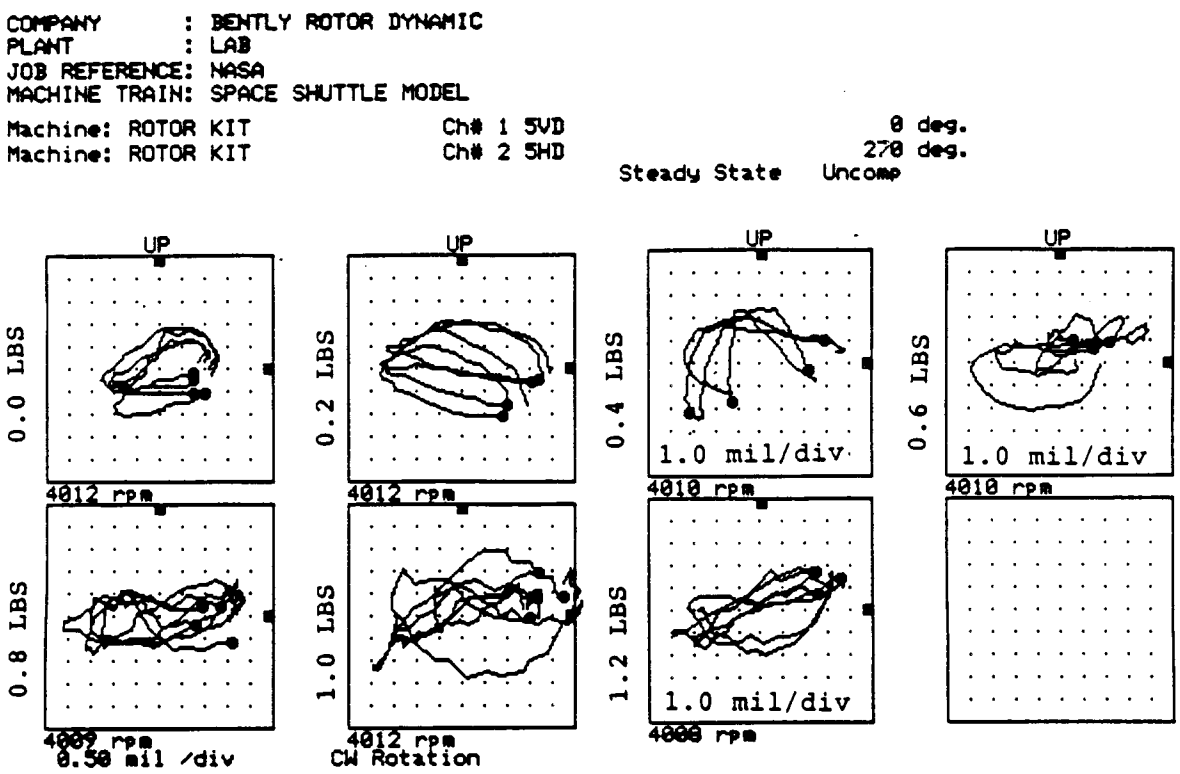

FIGURE 12.167 ORBITS AT PROBE LOCATION 5 AT 4000 RPM, 0 PSI SEAL OIL PRESSURE, 0.8 IN–GRAM UNBALANCE LOCATED IN THE THIRD PUMP IMPELLER DISK, FOR INCREASING STATIC PRELOAD FORCES.

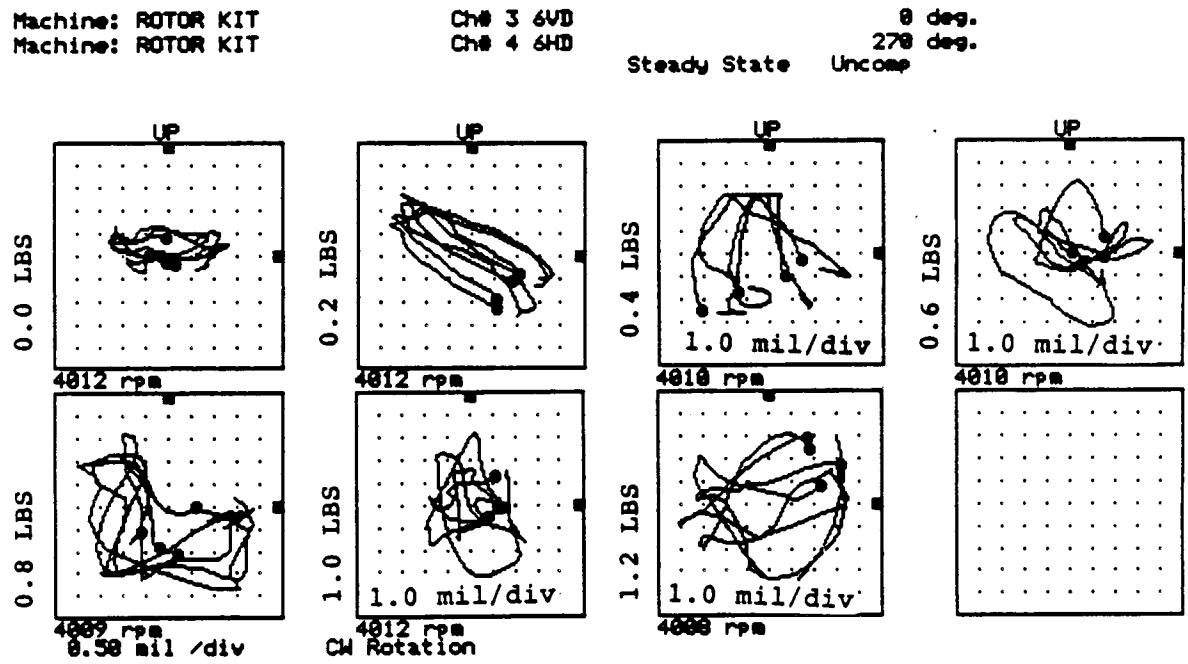

FIGURE 12.168 ORBITS AT PROBE LOCATION 6 AT 4000 RPM, 0 PSI SEAL OIL PRESSURE, 0.8 IN–GRAM UNBALANCE LOCATED IN THE THIRD PUMP IMPELLER DISK, FOR INCREASING STATIC PRELOAD FORCES.

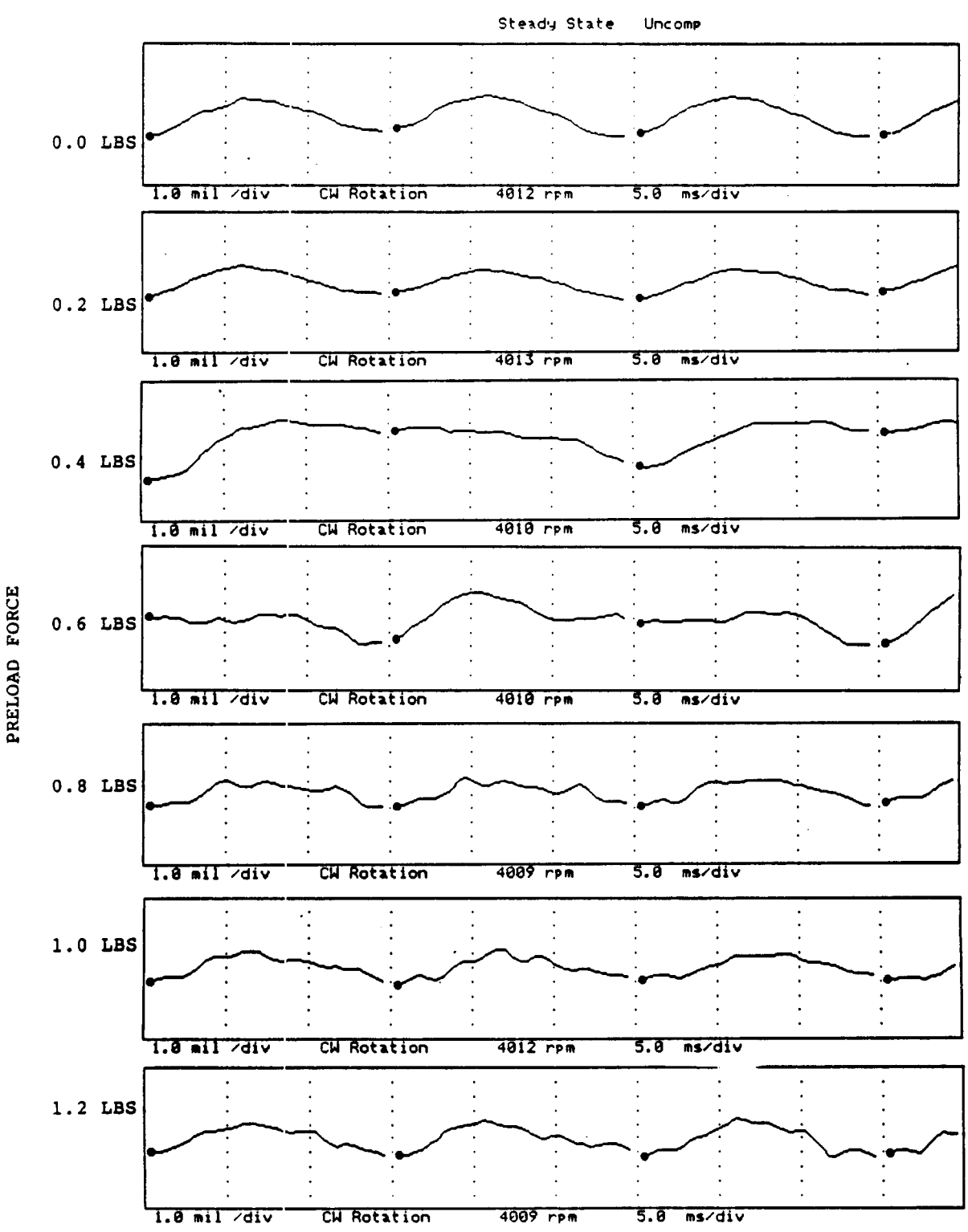

FIGURE 12.169 TIMEBASE FOR VERTICAL PROBE AT LOCATION 1 AT 4000 RPM, 0 PSI SEAL OIL PRESSURE, 0.8 IN–GRAM UNBALANCE LOCATED IN THE THIRD PUMP IMPELLER DISK, FOR INCREASING STATIC PRELOADS.

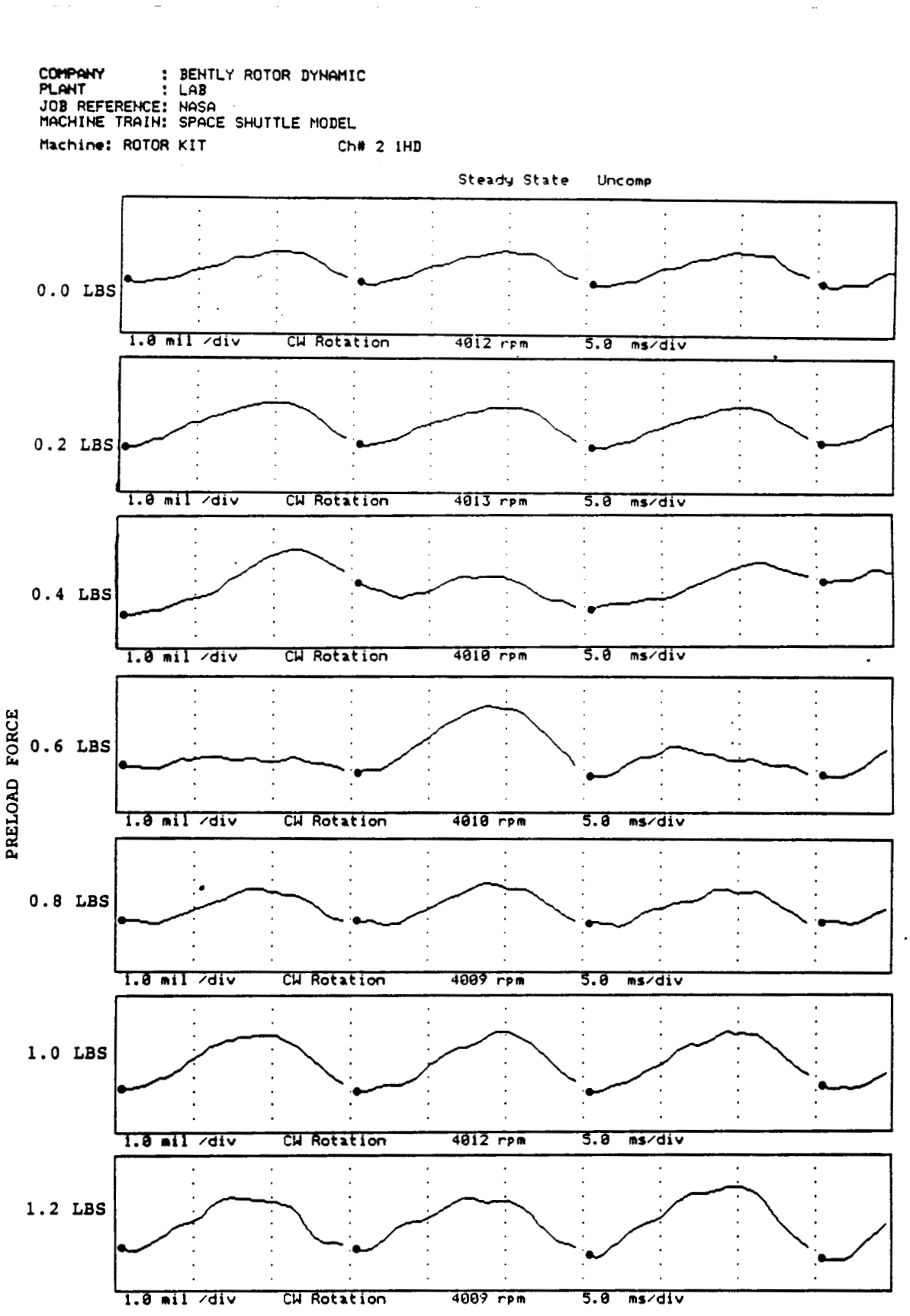

FIGURE 12.170 TIMEBASE FOR HORIZONTAL PROBE AT LOCATION 1 AT 4000 RPM, 0 PSI SEAL OIL PRESSURE, 0.8 IN–GRAM UNBALANCE LOCATED IN THE THIRD PUMP IMPELLER DISK, FOR INCREASING STATIC PRELOADS.

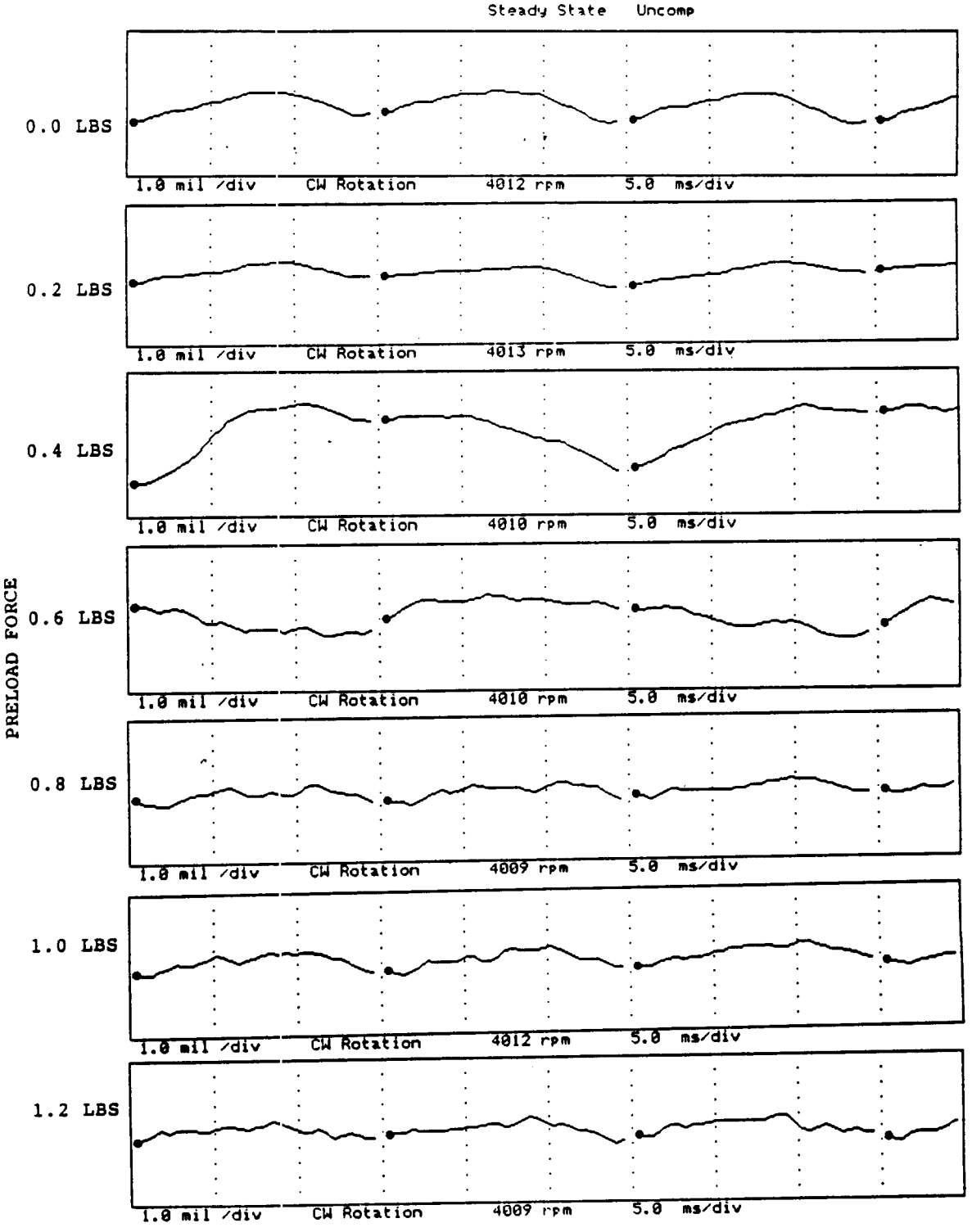

FIGURE 12.171 TIMEBASE FOR VERTICAL PROBE AT LOCATION 2 AT 4000 RPM, 0 PSI SEAL OIL PRESSURE, 0.8 IN–GRAM UNBALANCE LOCATED IN THE THIRD PUMP IMPELLER DISK, FOR INCREASING STATIC PRELOADS.

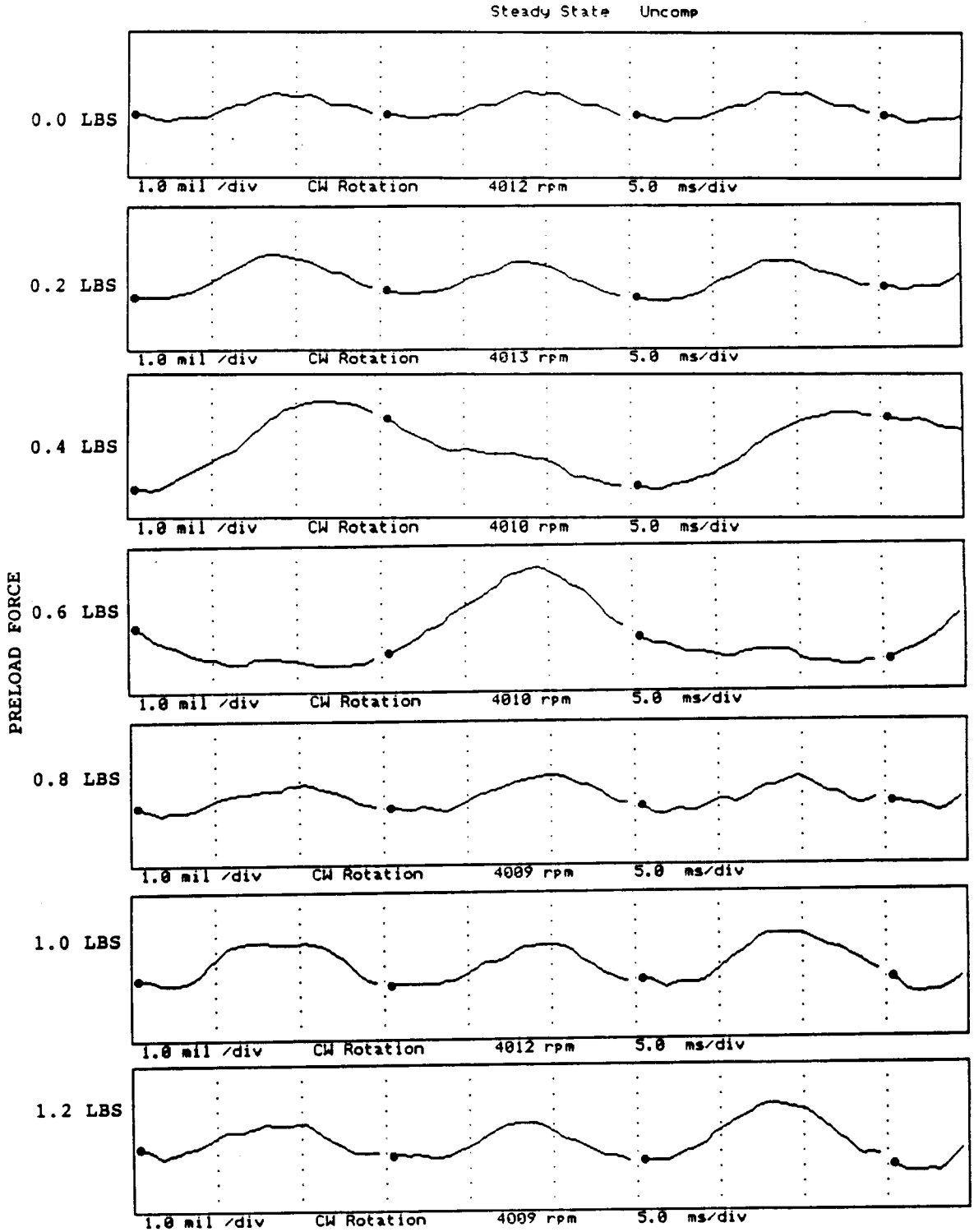

FIGURE 12.172 TIMEBASE FOR HORIZONTAL PROBE AT LOCATION 2 AT 4000 RPM, 0 PSI SEAL OIL PRESSURE, 0.8 IN–GRAM UNBALANCE LOCATED IN THE THIRD PUMP IMPELLER DISK, FOR INCREASING STATIC PRELOADS.

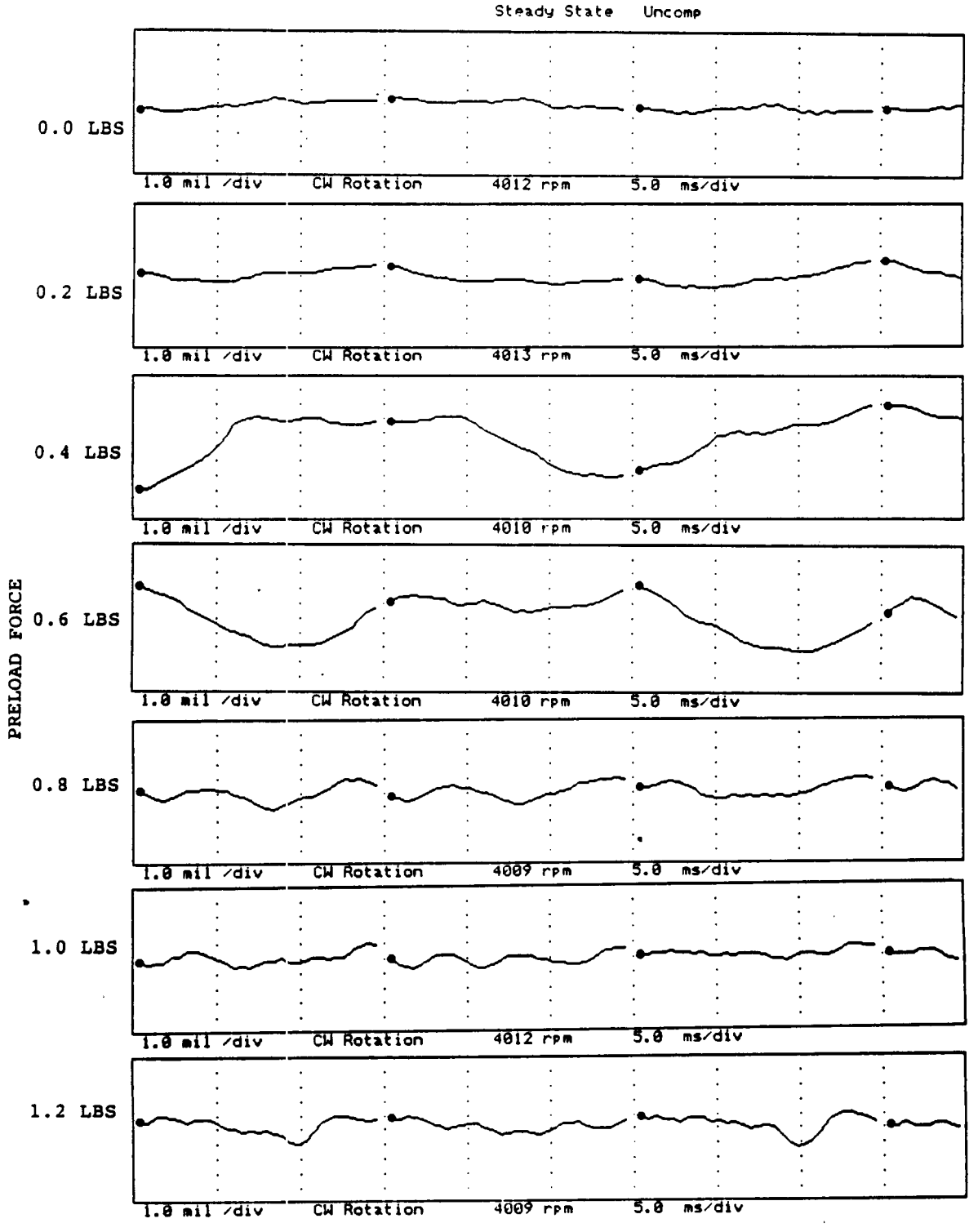

FIGURE 12.173 TIMEBASE FOR VERTICAL PROBE AT LOCATION 3 AT 4000 RPM, 0 PSI SEAL OIL PRESSURE, 0.8 IN–GRAM UNBALANCE LOCATED IN THE THIRD PUMP IMPELLER DISK, FOR INCREASING STATIC PRELOADS.

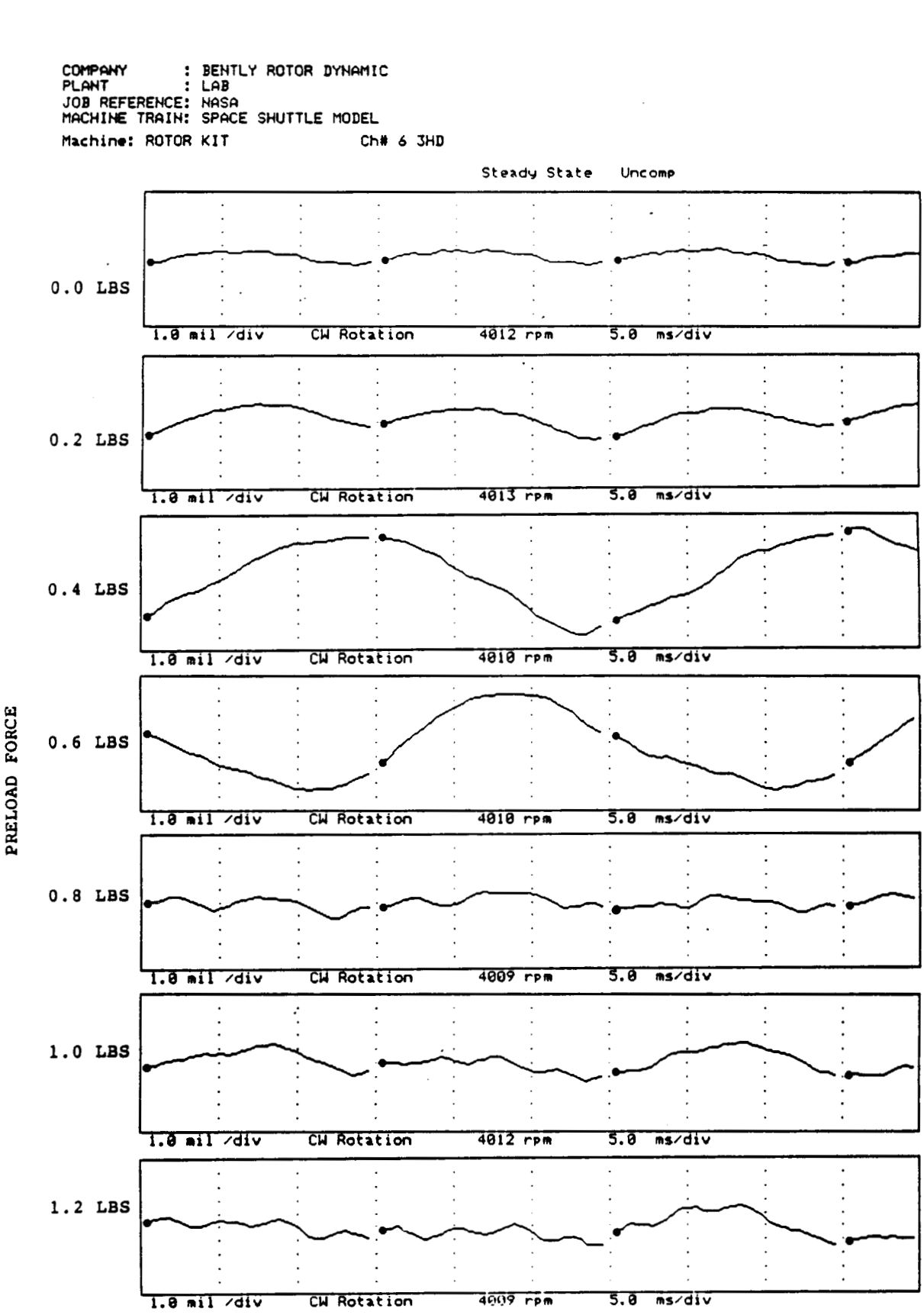

FIGURE 12.174 TIMEBASE FOR HORIZONTAL PROBE AT LOCATION 3 AT 4000 RPM, 0 PSI SEAL OIL PRESSURE, 0.8 IN–GRAM UNBALANCE LOCATED IN THE THIRD PUMP IMPELLER DISK, FOR INCREASING STATIC PRELOADS.

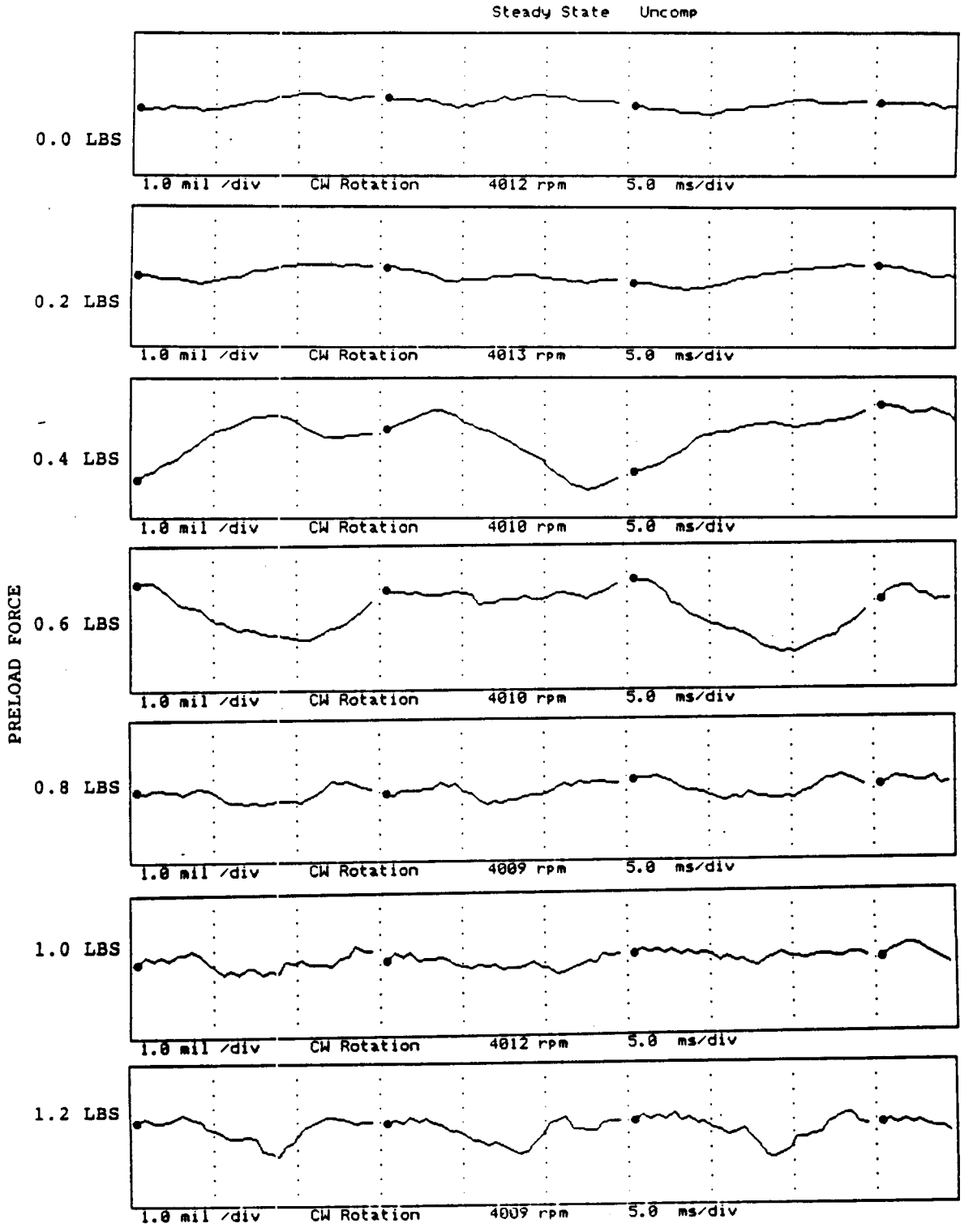

FIGURE 12.175 TIMEBASE FOR VERTICAL PROBE AT LOCATION 4 AT 4000 RPM, 0 PSI SEAL OIL PRESSURE, 0.8 IN–GRAM UNBALANCE LOCATED IN THE THIRD PUMP IMPELLER DISK, FOR INCREASING STATIC PRELOADS.

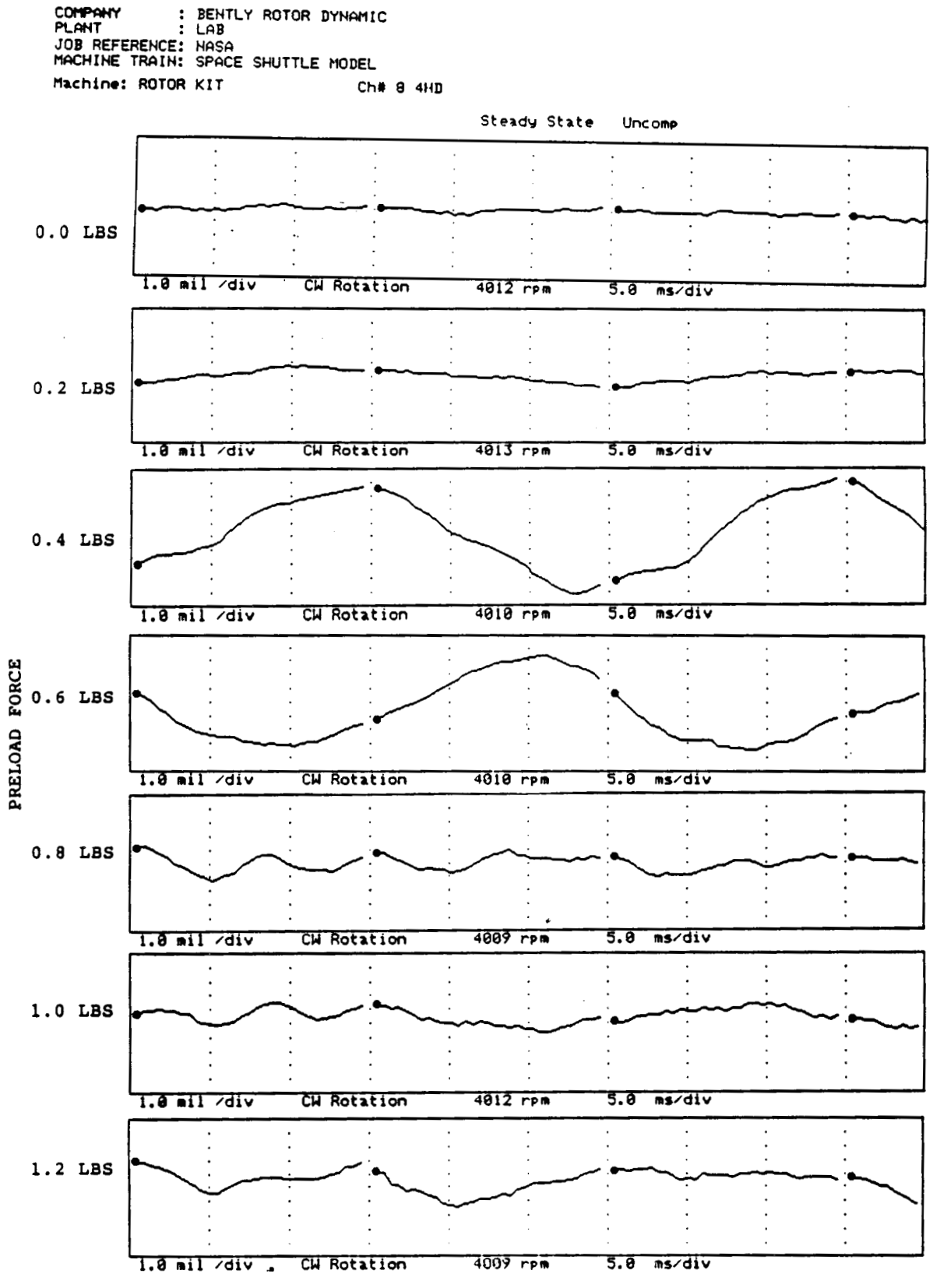

FIGURE 12.176 TIMEBASE FOR HORIZONTAL PROBE AT LOCATION 4 AT 4000 RPM, 0 PSI SEAL OIL PRESSURE, 0.8 IN–GRAM UNBALANCE LOCATED IN THE THIRD PUMP IMPELLER DISK, FOR INCREASING STATIC PRELOADS.

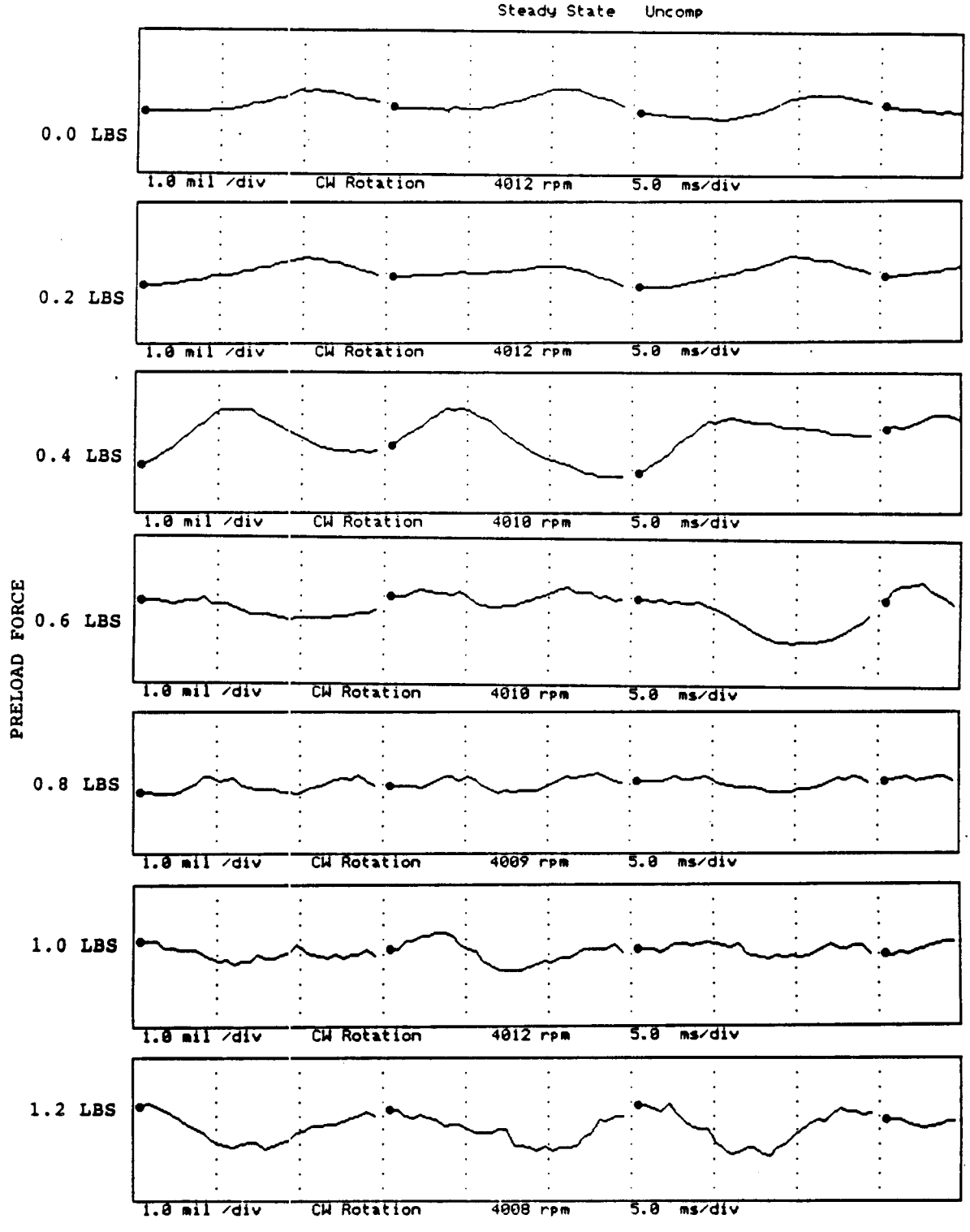

FIGURE 12.177 TIMEBASE FOR VERTICAL PROBE AT LOCATION 5 AT 4000 RPM, 0 PSI SEAL OIL PRESSURE, 0.8 IN–GRAM UNBALANCE LOCATED IN THE THIRD PUMP IMPELLER DISK, FOR INCREASING STATIC PRELOADS.

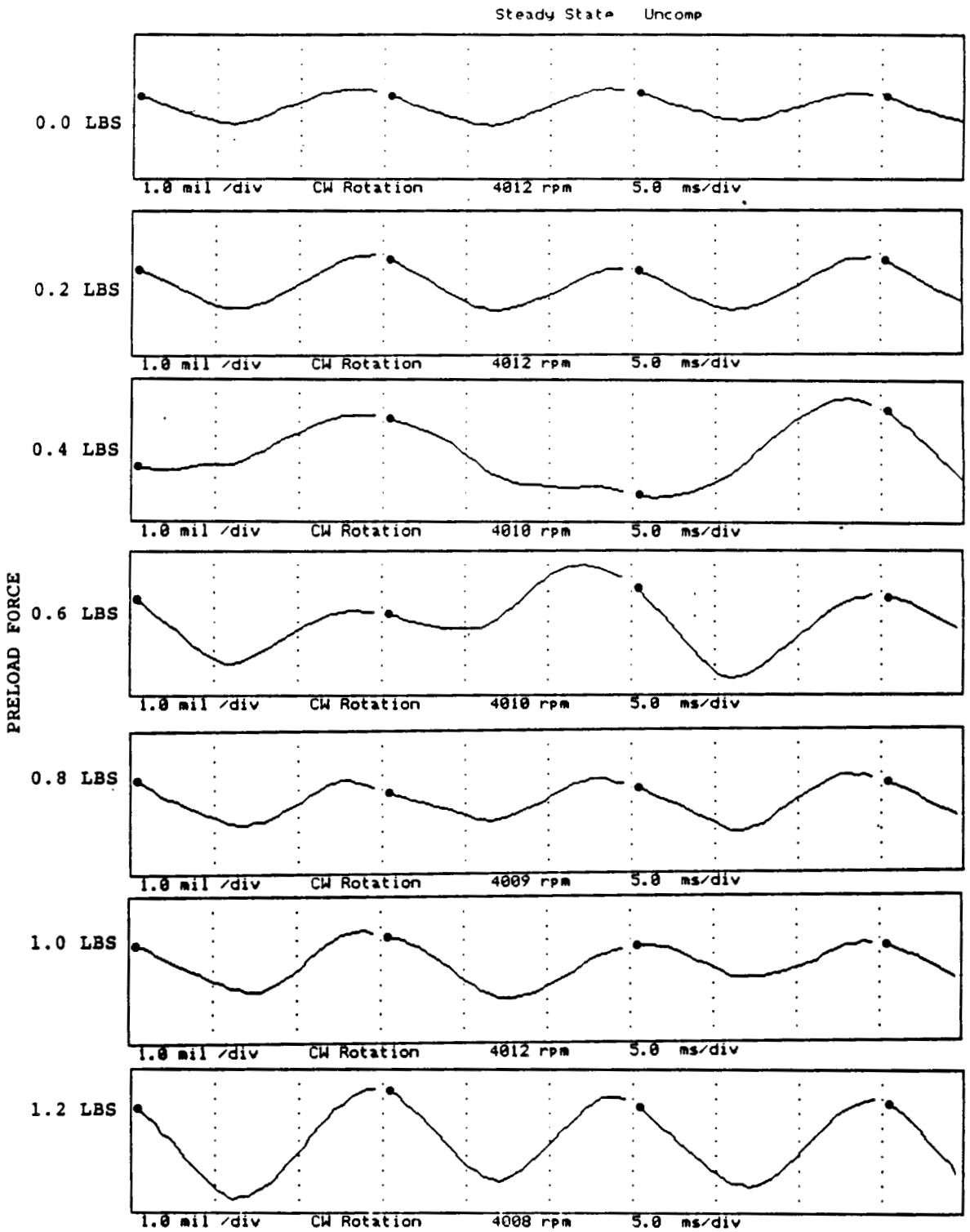

FIGURE 12.178 TIMEBASE FOR HORIZONTAL PROBE AT LOCATION 5 AT 4000 RPM, 0 PSI SEAL OIL PRESSURE, 0.8 IN–GRAM UNBALANCE LOCATED IN THE THIRD PUMP IMPELLER DISK, FOR INCREASING STATIC PRELOADS.

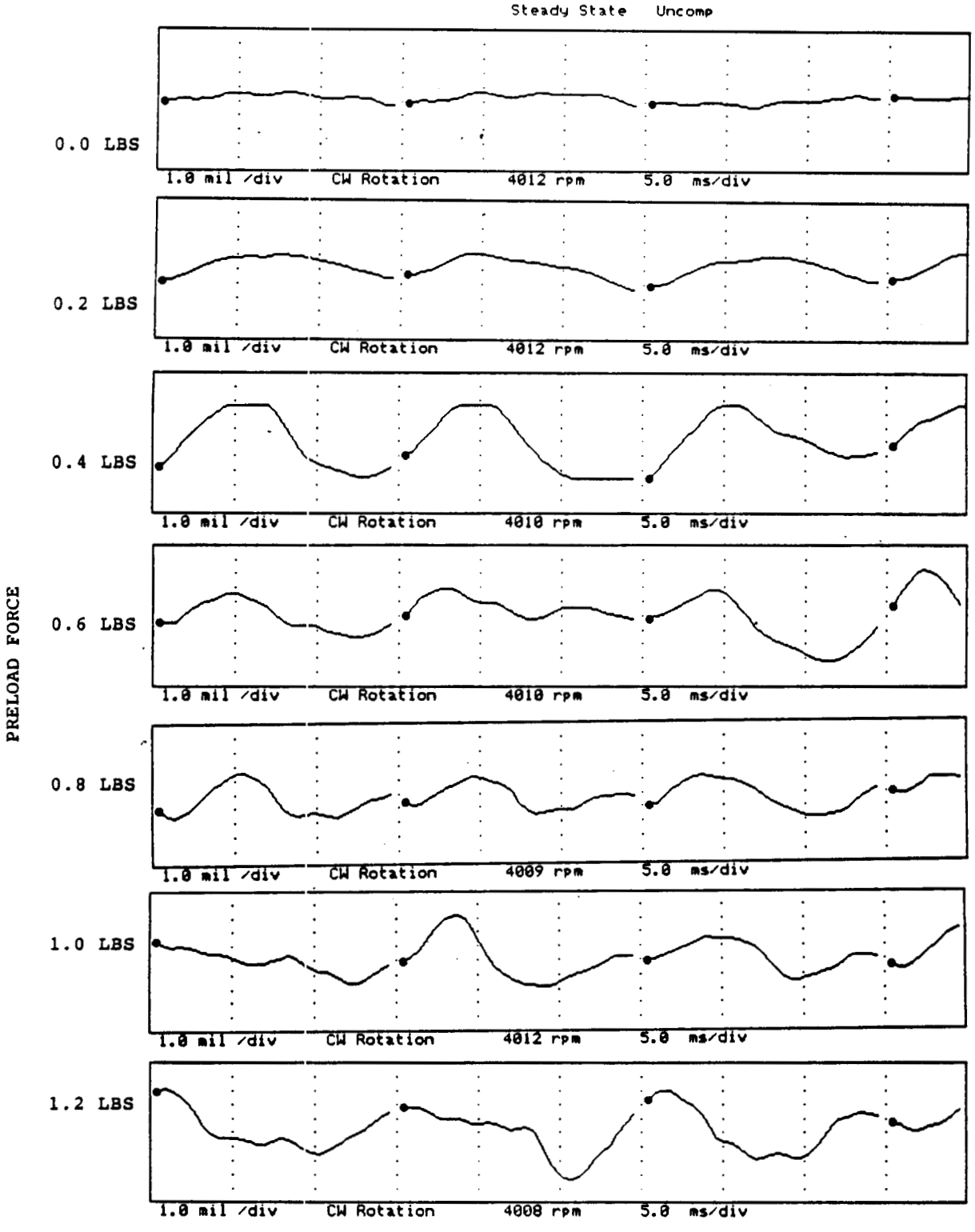

FIGURE 12.179 TIMEBASE FOR VERTICAL PROBE AT LOCATION 6 AT 4000 RPM, 0 PSI SEAL OIL PRESSURE, 0.8 IN–GRAM UNBALANCE LOCATED IN THE THIRD PUMP IMPELLER DISK, FOR INCREASING STATIC PRELOADS.

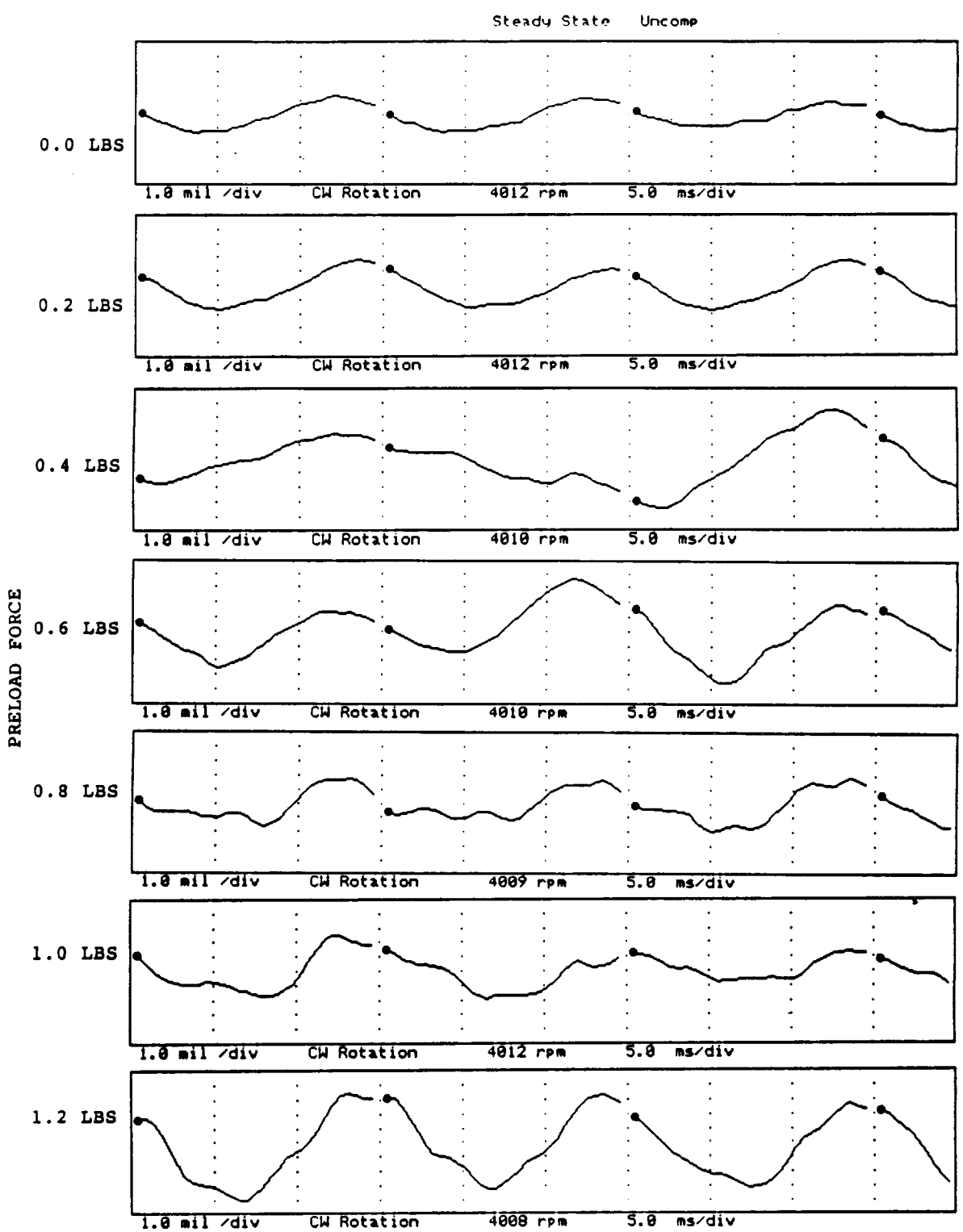

FIGURE 12.180 TIMEBASE FOR HORIZONTAL PROBE AT LOCATION 6 AT 4000 RPM, 0 PSI SEAL OIL PRESSURE, 0.8 IN–GRAM UNBALANCE LOCATED IN THE THIRD PUMP IMPELLER DISK, FOR INCREASING STATIC PRELOADS.

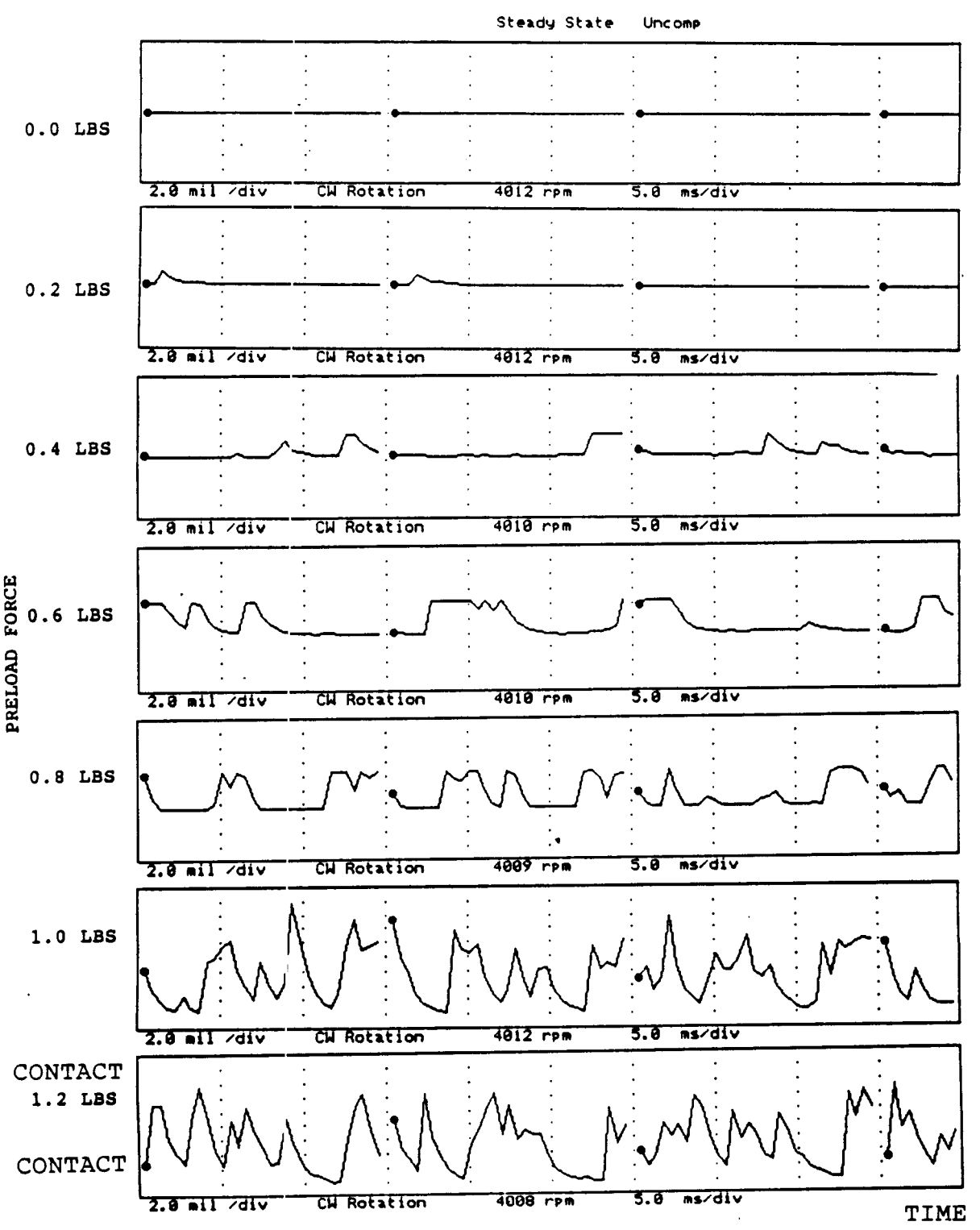

FIGURE 12.181 TIMEBASE FOR SHAFT TO SEAL 1 CONTACT AT 4000 RPM, 0 PSI SEAL OIL PRESSURE, 0.8 IN–GRAM UNBALANCE LOCATED IN THE THIRD PUMP IMPELLER DISK, FOR INCREASING STATIC PRELOADS.

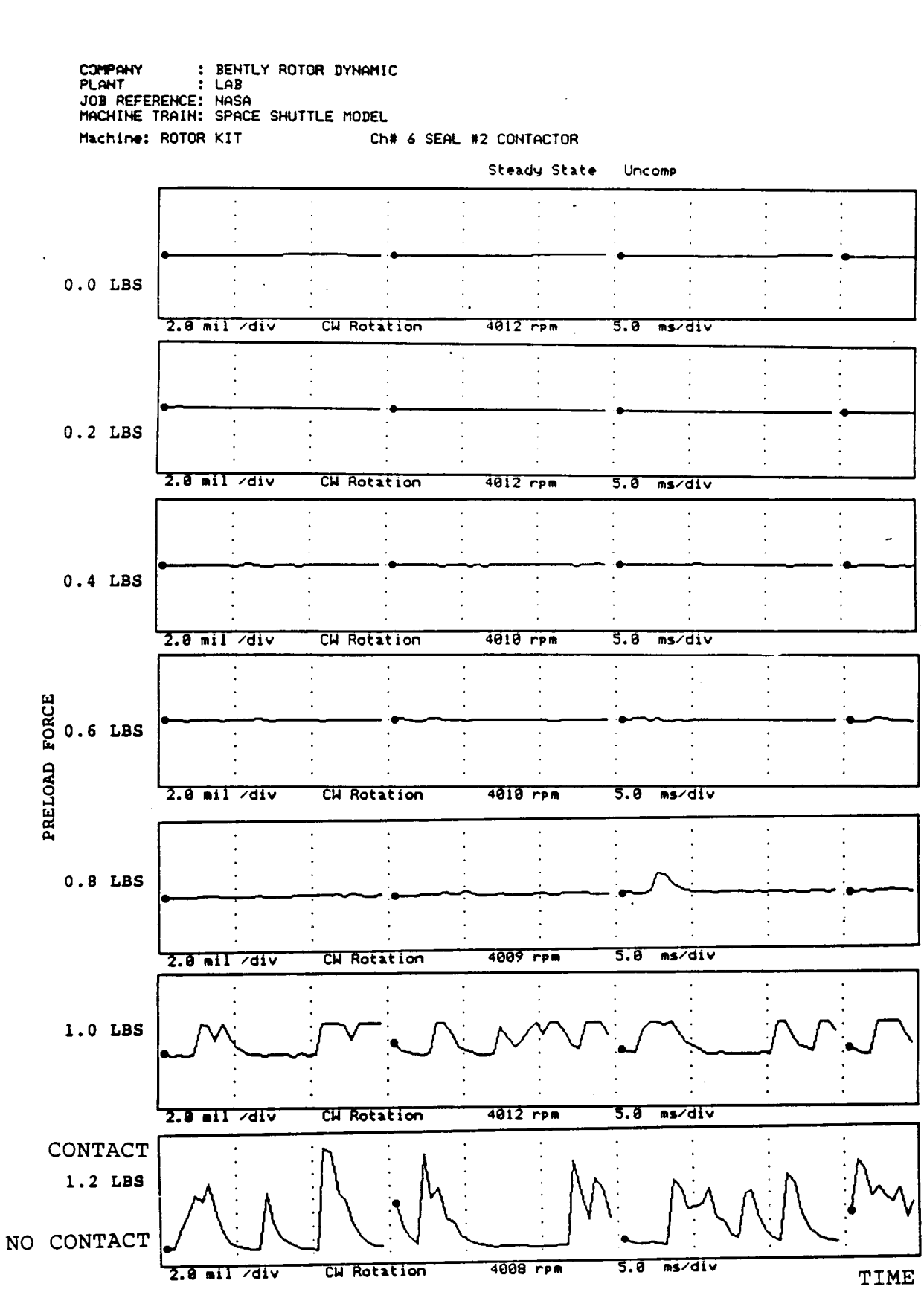

FIGURE 12.182 TIMEBASE FOR SHAFT TO SEAL 2 CONTACT AT 4000 RPM, 0 PSI SEAL OIL PRESSURE, 0.8 IN–GRAM UNBALANCE LOCATED IN THE THIRD PUMP IMPELLER DISK, FOR INCREASING STATIC PRELOADS.

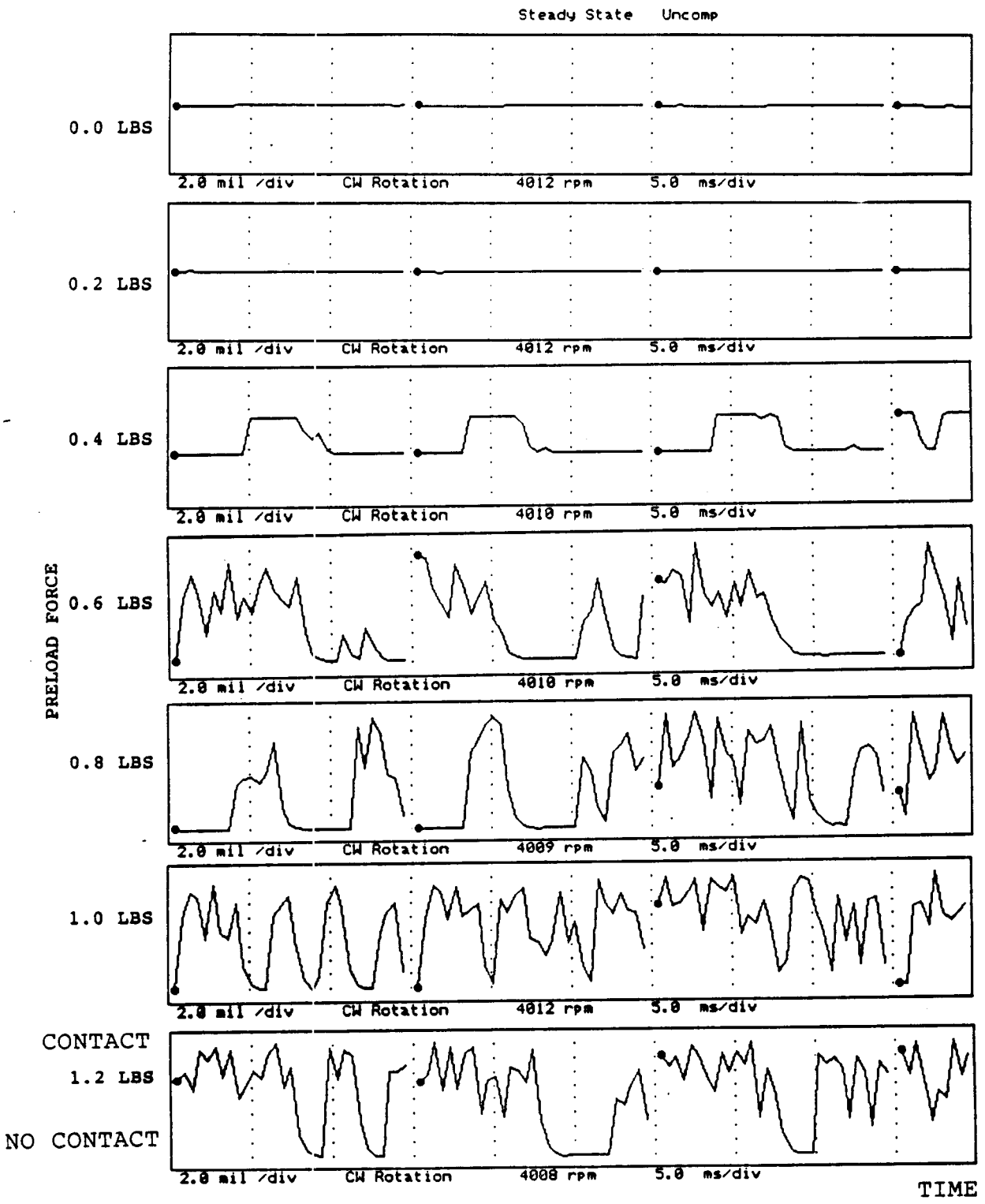

FIGURE 12.183 TIMEBASE FOR SHAFT TO RUB BLOCK CONTACT AT 4000 RPM, 0 PSI SEAL OIL PRESSURE, 0.8 IN–GRAM UNBALANCE LOCATED IN THE THIRD PUMP IMPELLER DISK, FOR INCREASING STATIC PRELOADS.

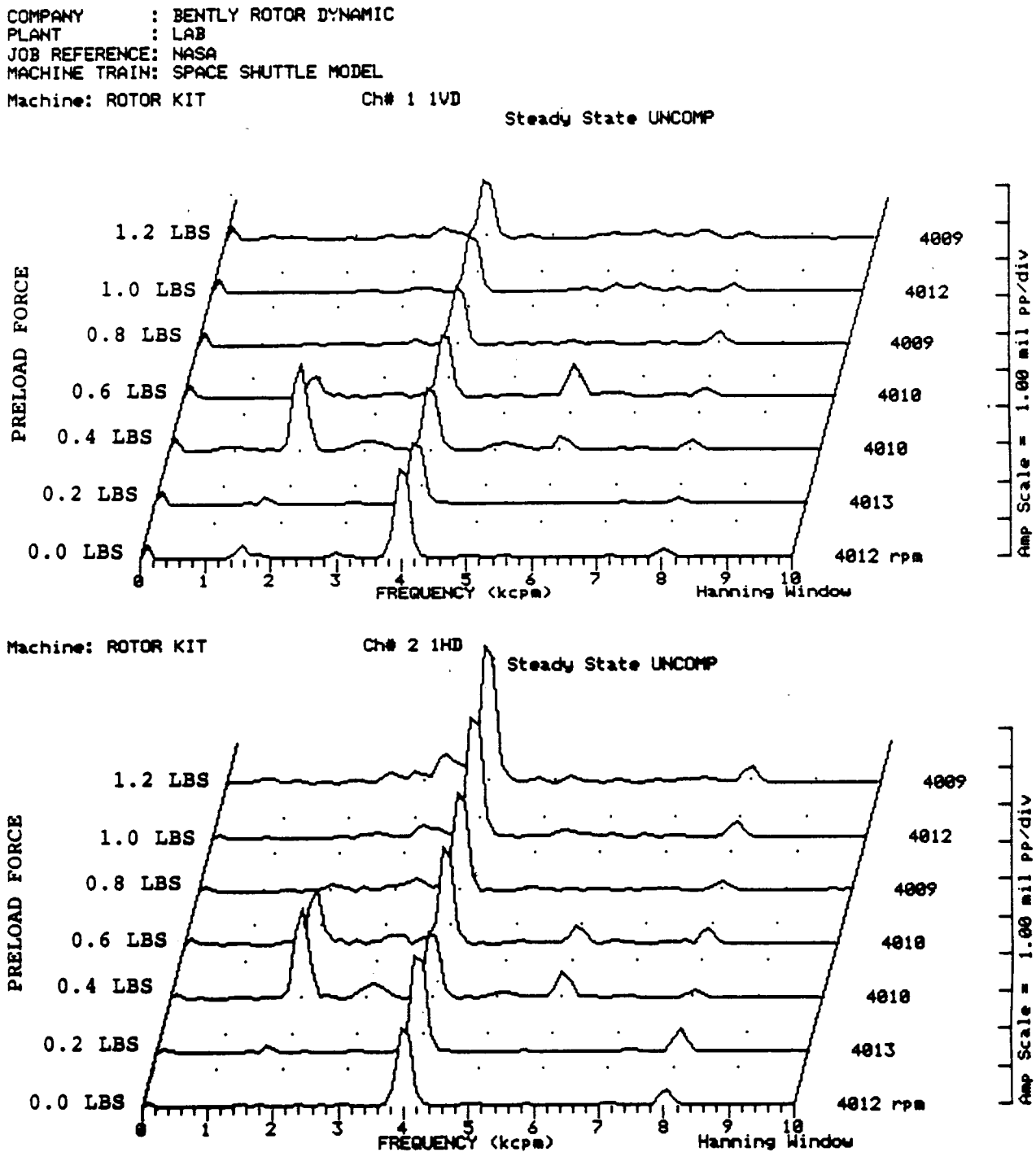

FIGURE 12.184 SPECTRAL CONTENT AT PROBE LOCATION 1 AT 4000 RPM, 0 PSI SEAL OIL PRESSURE, 0.8 IN–GRAM UNBALANCE LOCATED IN THE THIRD PUMP IMPELLER DISK, FOR INCREASING STATIC PRELOADS.

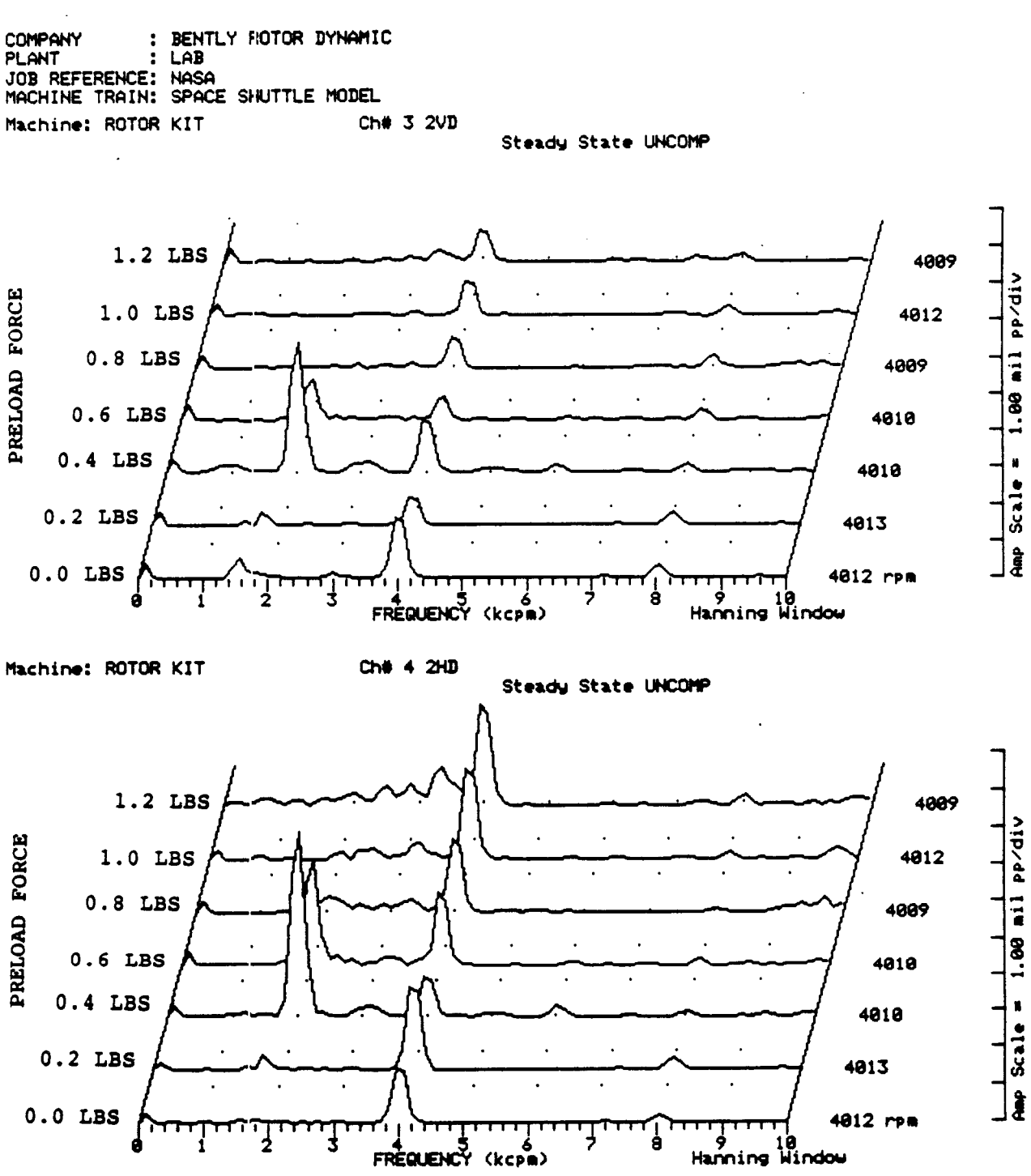

FIGURE 12.185 SPECTRAL CONTENT AT PROBE LOCATION 2 AT 4000 RPM, 0 PSI SEAL OIL PRESSURE, 0.8 IN–GRAM UNBALANCE LOCATED IN THE THIRD PUMP IMPELLER DISK, FOR INCREASING STATIC PRELOADS.

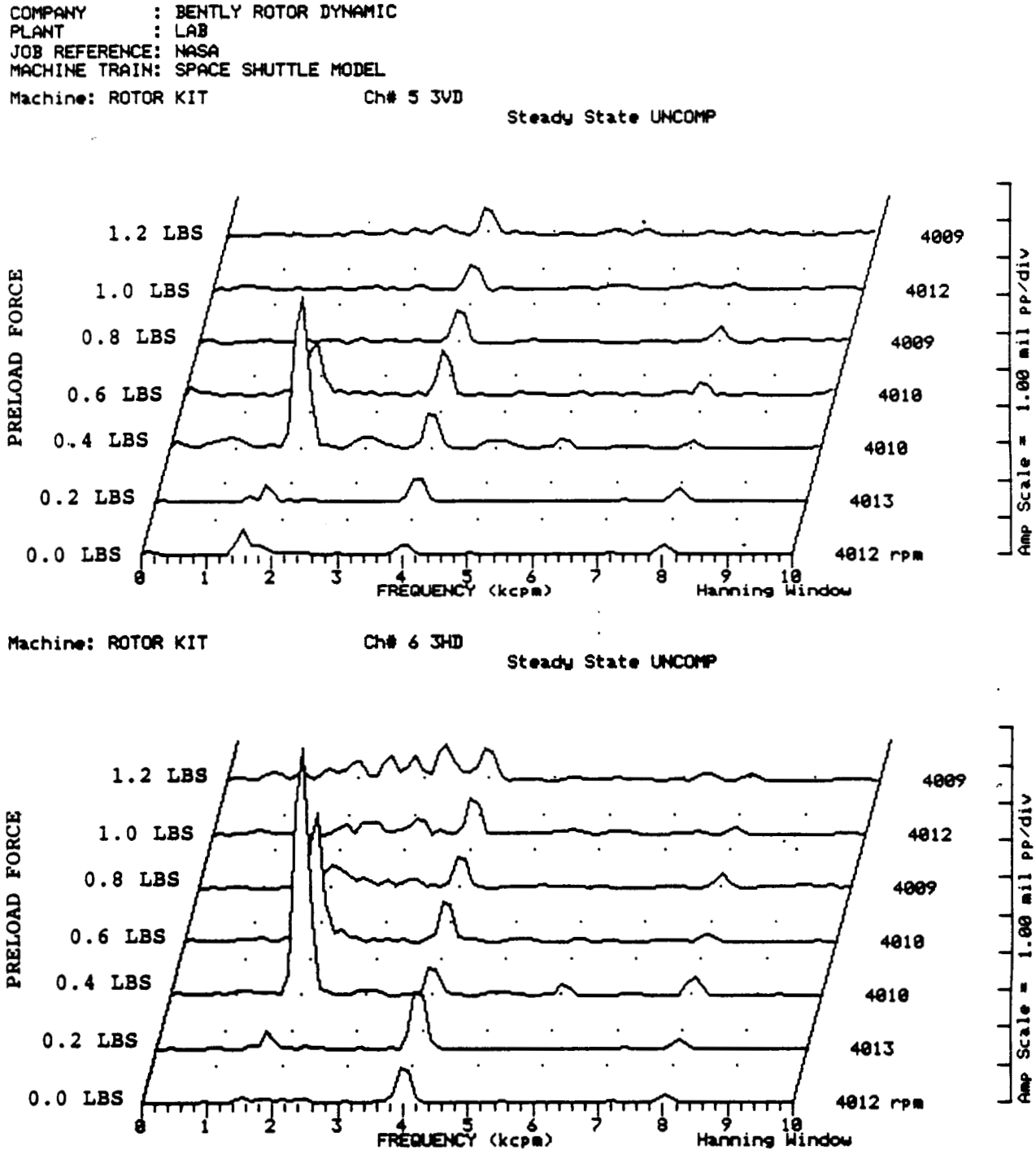

FIGURE 12.186 SPECTRAL CONTENT AT PROBE LOCATION 3 AT 4000 RPM, 0 PSI SEAL OIL PRESSURE, 0.8 IN–GRAM UNBALANCE LOCATED IN THE THIRD PUMP IMPELLER DISK, FOR INCREASING STATIC PRELOADS.

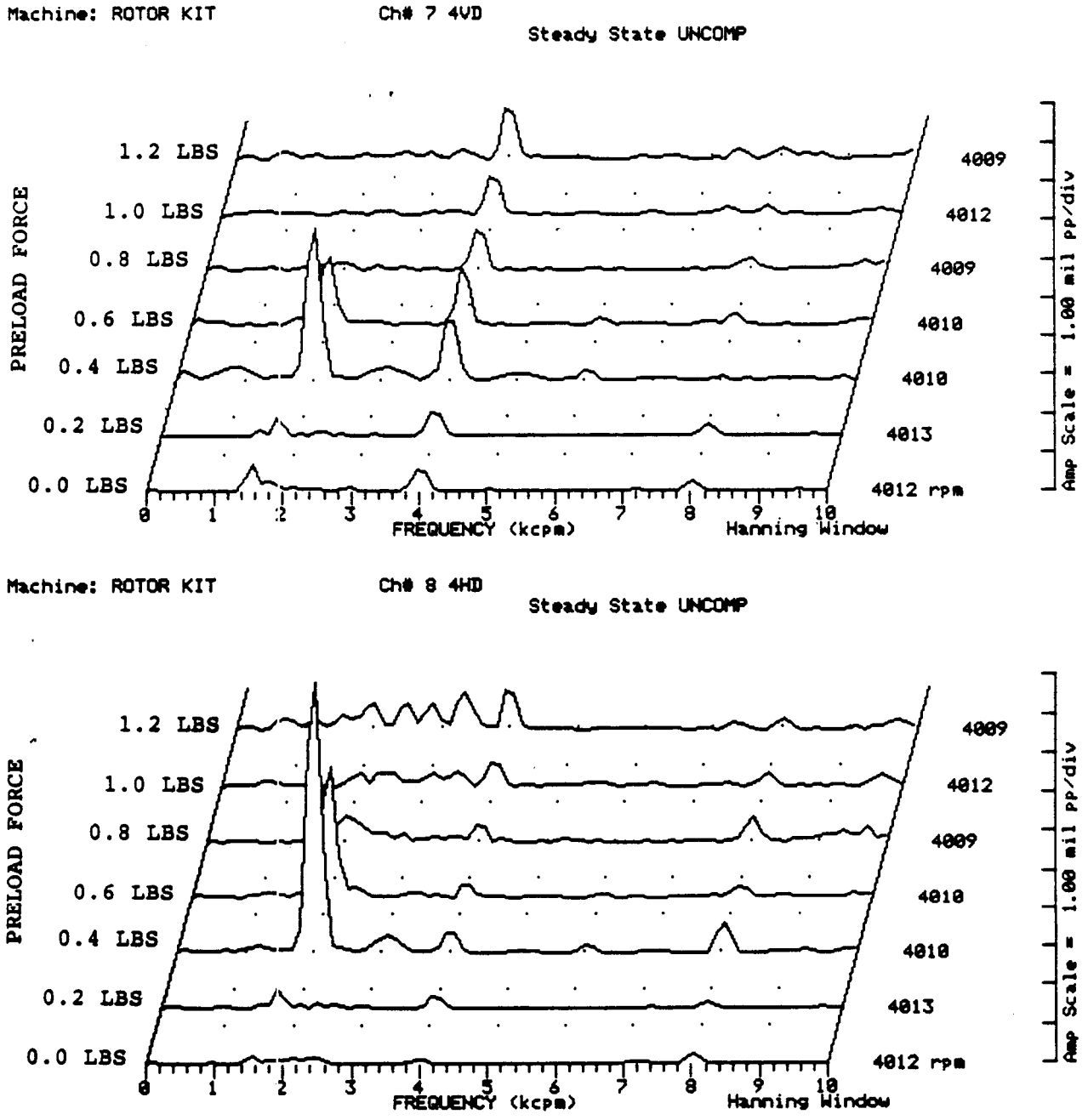

FIGURE 12.187 SPECTRAL CONTENT AT PROBE LOCATION 4 AT 4000 RPM, 0 PSI SEAL OIL PRESSURE, 0.8 IN–GRAM UNBALANCE LOCATED IN THE THIRD PUMP IMPELLER DISK, FOR INCREASING STATIC PRELOADS.

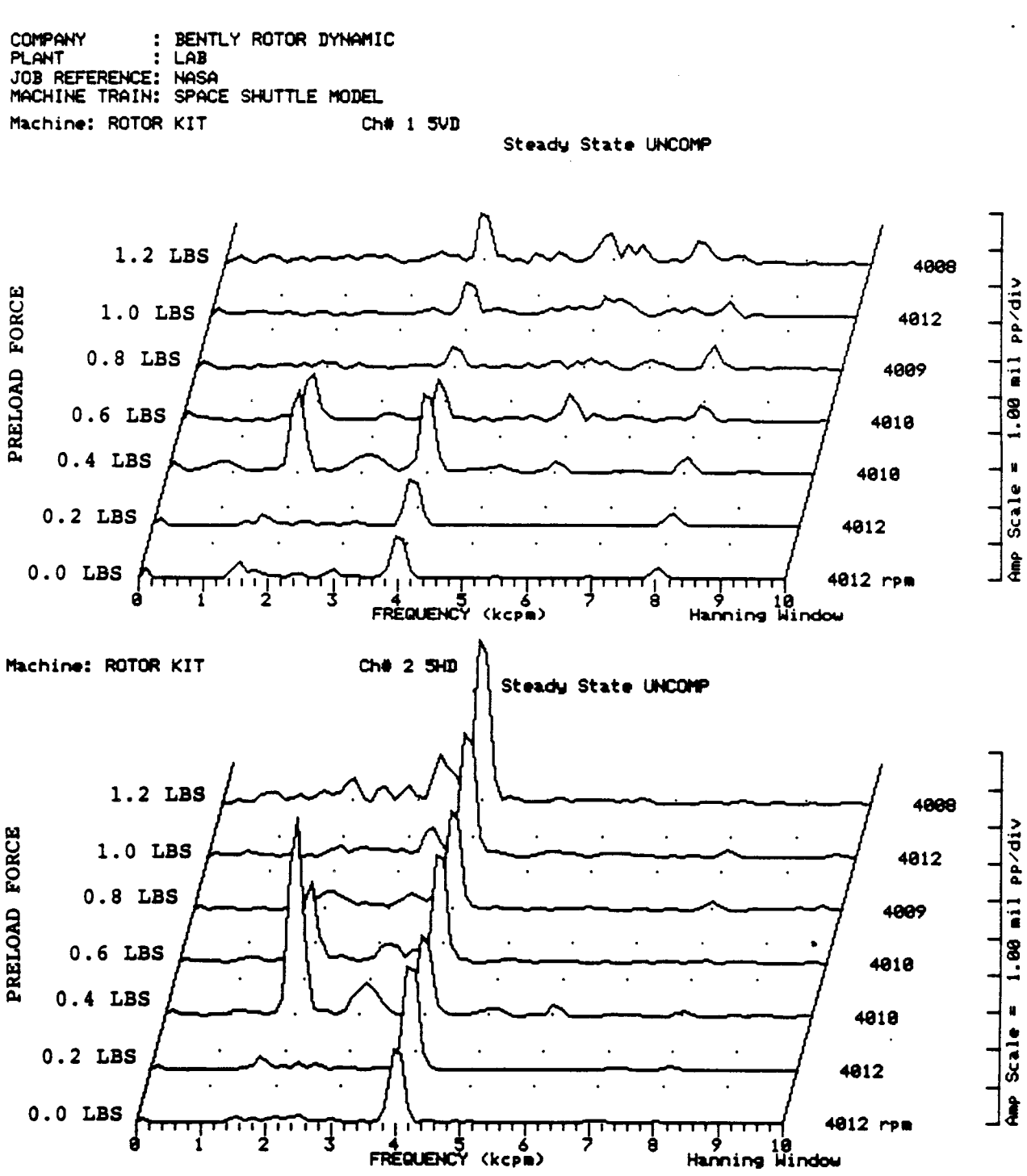

FIGURE 12.188 SPECTRAL CONTENT AT PROBE LOCATION 5 AT 4000 RPM, 0 PSI SEAL OIL PRESSURE, 0.8 IN–GRAM UNBALANCE LOCATED IN THE THIRD PUMP IMPELLER DISK, FOR INCREASING STATIC PRELOADS.

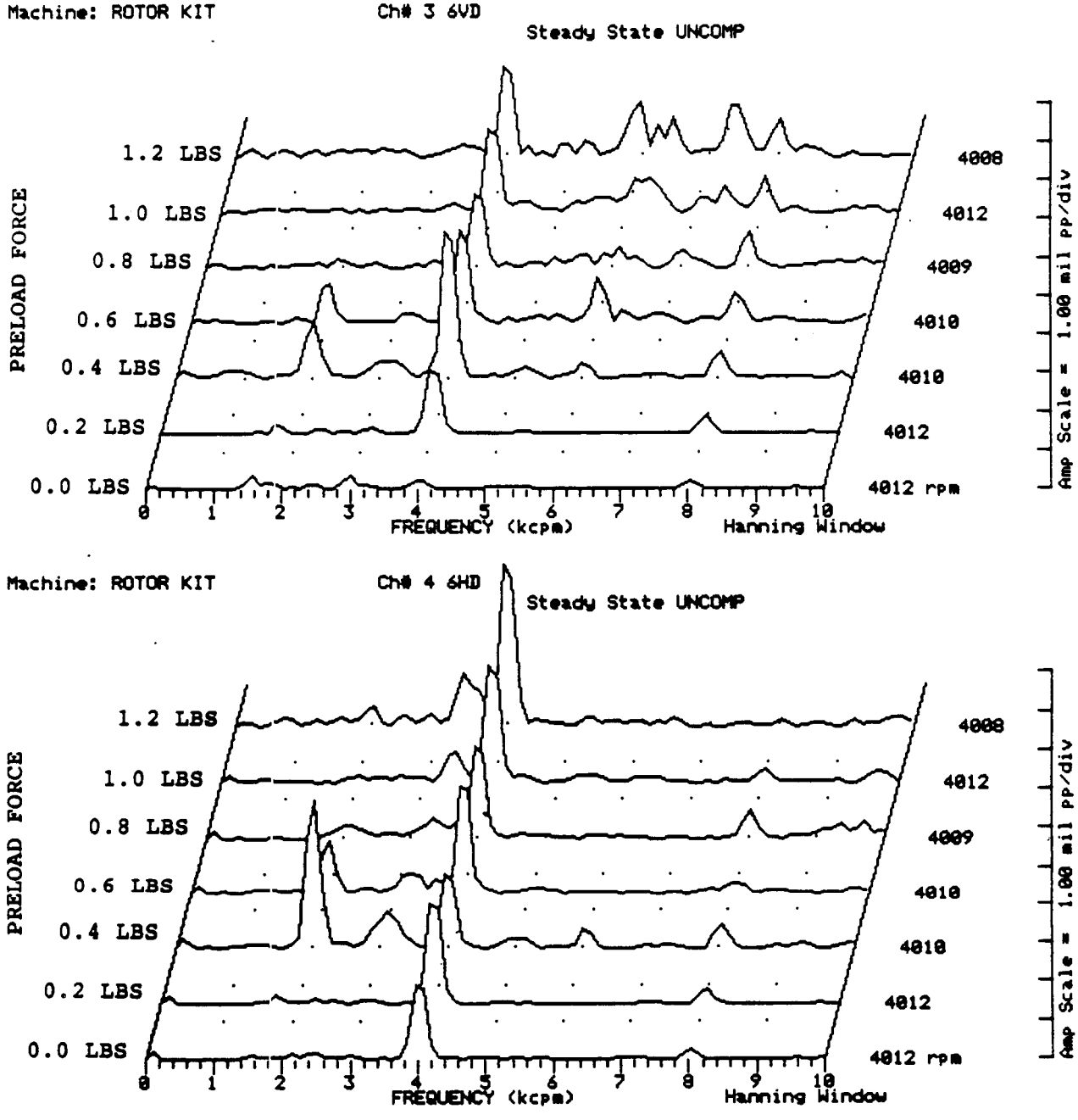

FIGURE 12.189 SPECTRAL CONTENT AT PROBE LOCATION 6 AT 4000 RPM, 0 PSI SEAL OIL PRESSURE, 0.8 IN–GRAM UNBALANCE LOCATED IN THE THIRD PUMP IMPELLER DISK, FOR INCREASING STATIC PRELOADS.

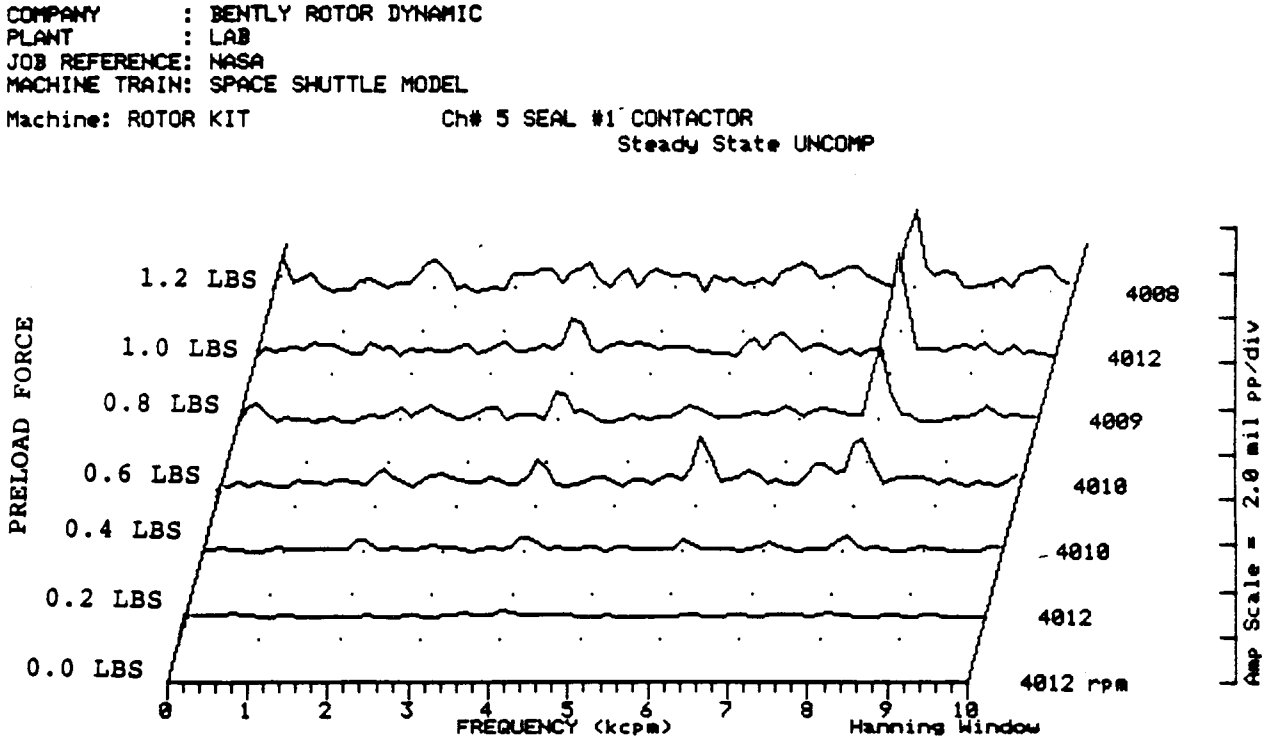

FIGURE 12.190 SPECTRAL CONTENT FOR SHAFT TO SEAL 1 CONTACT AT 4000 RPM, 0 PSI SEAL OIL PRESSURE, 0.8 IN–GRAM UNBALANCE LOCATED IN THE THIRD PUMP IMPELLER DISK, FOR INCREASING STATIC PRELOADS.

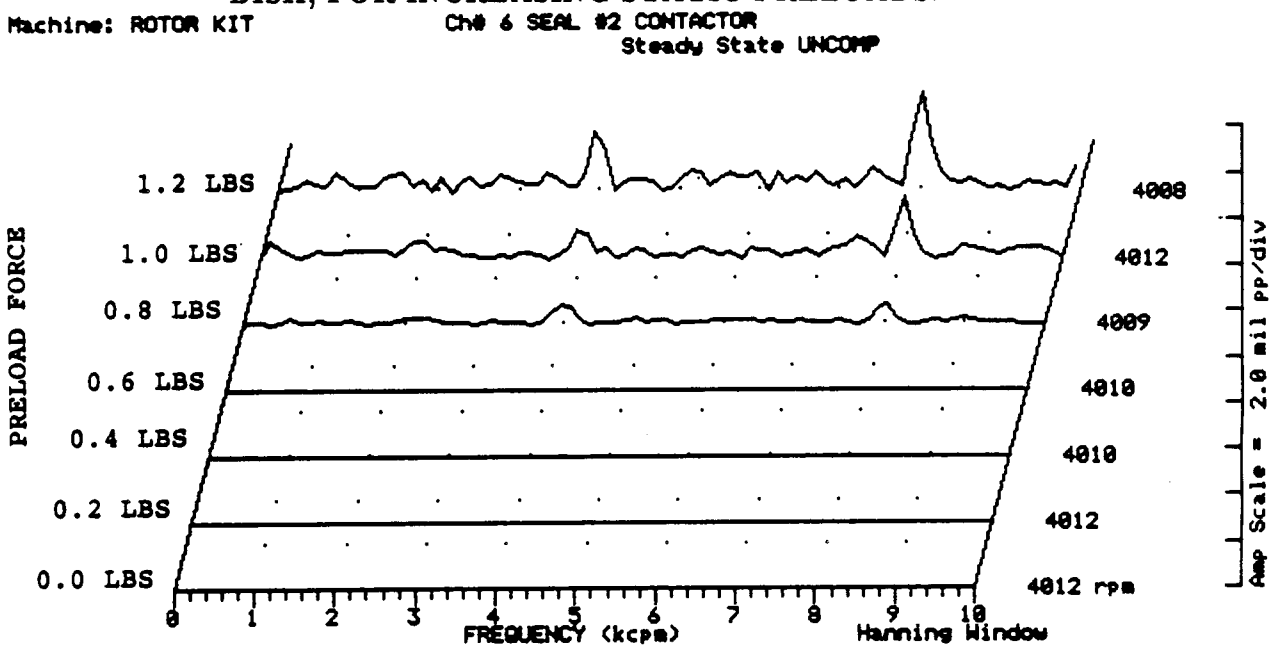

FIGURE 12.191 SPECTRAL CONTENT FOR SHAFT TO SEAL 2 CONTACT AT 4000 RPM, 0 PSI SEAL OIL PRESSURE, 0.8 IN–GRAM UNBALANCE LOCATED IN THE THIRD PUMP IMPELLER DISK, FOR INCREASING STATIC PRELOADS.

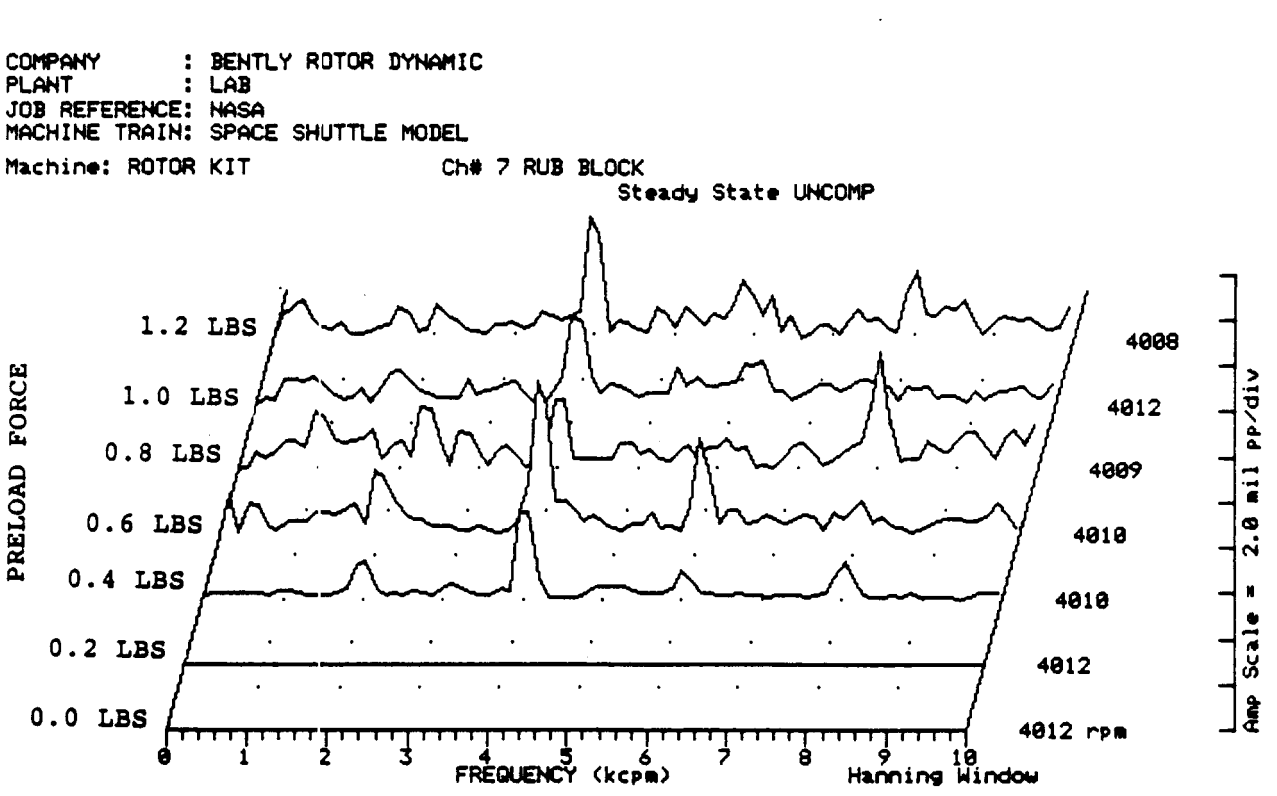

FIGURE 12.192 SPECTRAL CONTENT FOR SHAFT TO RUB BLOCK CONTACT AT 4000 RPM, 0 PSI SEAL OIL PRESSURE, 0.8 IN–GRAM UNBALANCE LOCATED IN THE THIRD PUMP IMPELLER DISK, FOR INCREASING STATIC PRELOADS.

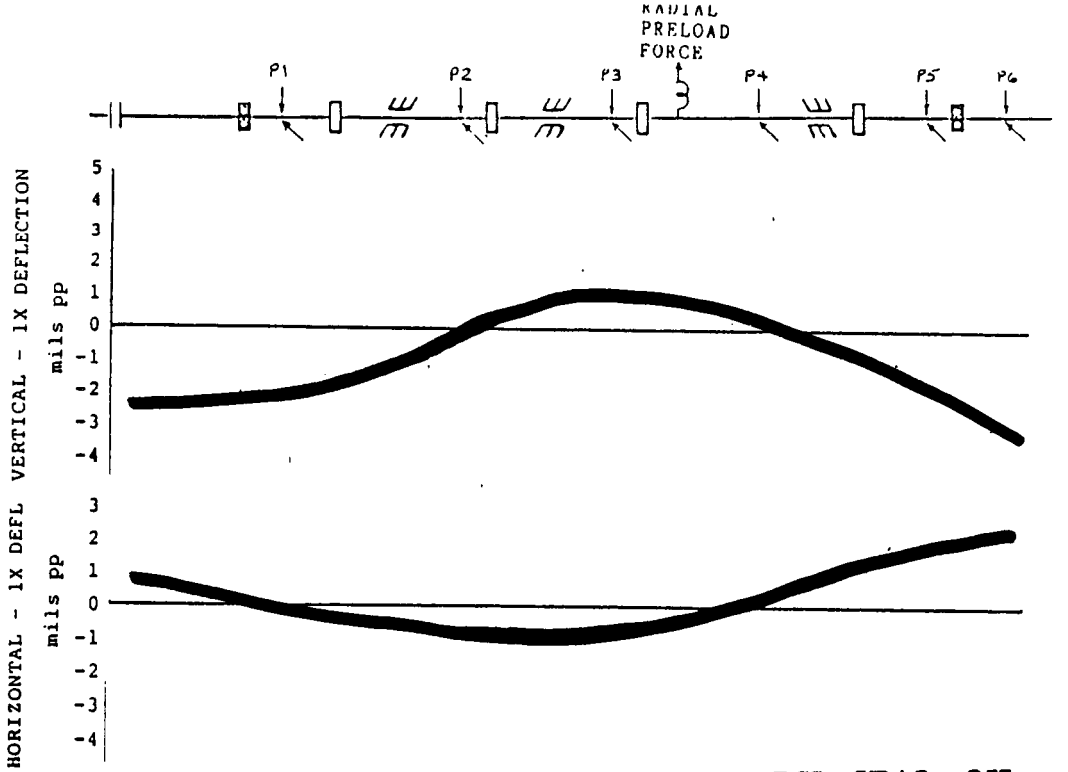

FIGURE 12.193 ROTOR MODE SHAPE AT 4000 RPM, 2.5 PSI SEAL OIL PRESSURE DUE TO 0.8 IN–GRAM UNBALANCE LOCATED IN THE THIRD PUMP IMPELLER DISK.

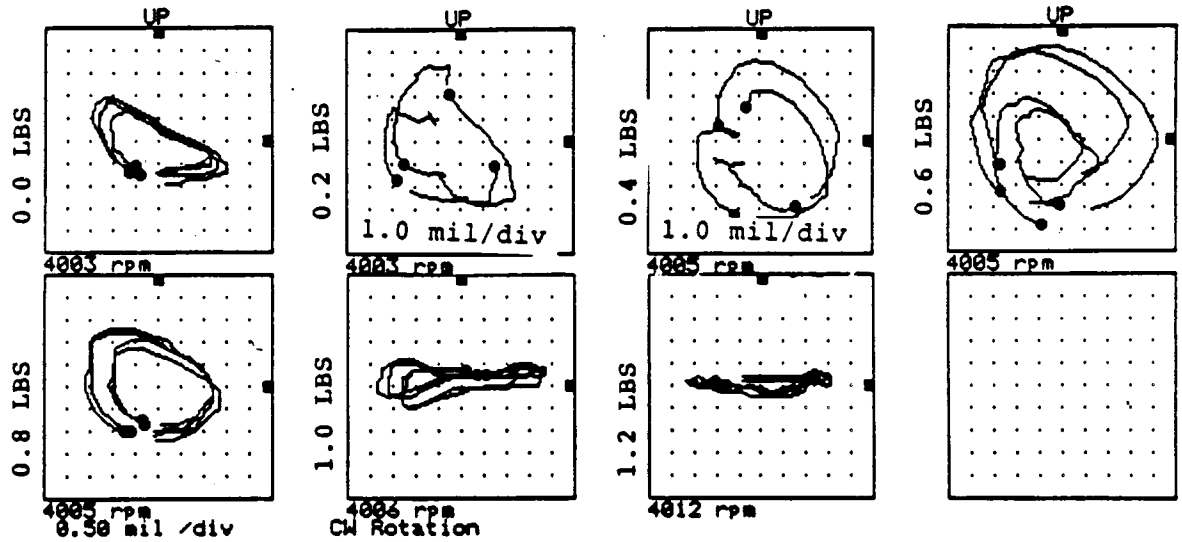

FIGURE 12.194 ORBITS AT PROBE LOCATION 1 AT 4000 RPM, 2.5 PSI SEAL OIL PRESSURE, 0.8 IN–GRAM UNBALANCE LOCATED IN THE THIRD PUMP IMPELLER DISK, FOR INCREASING STATIC PRELOAD FORCES.

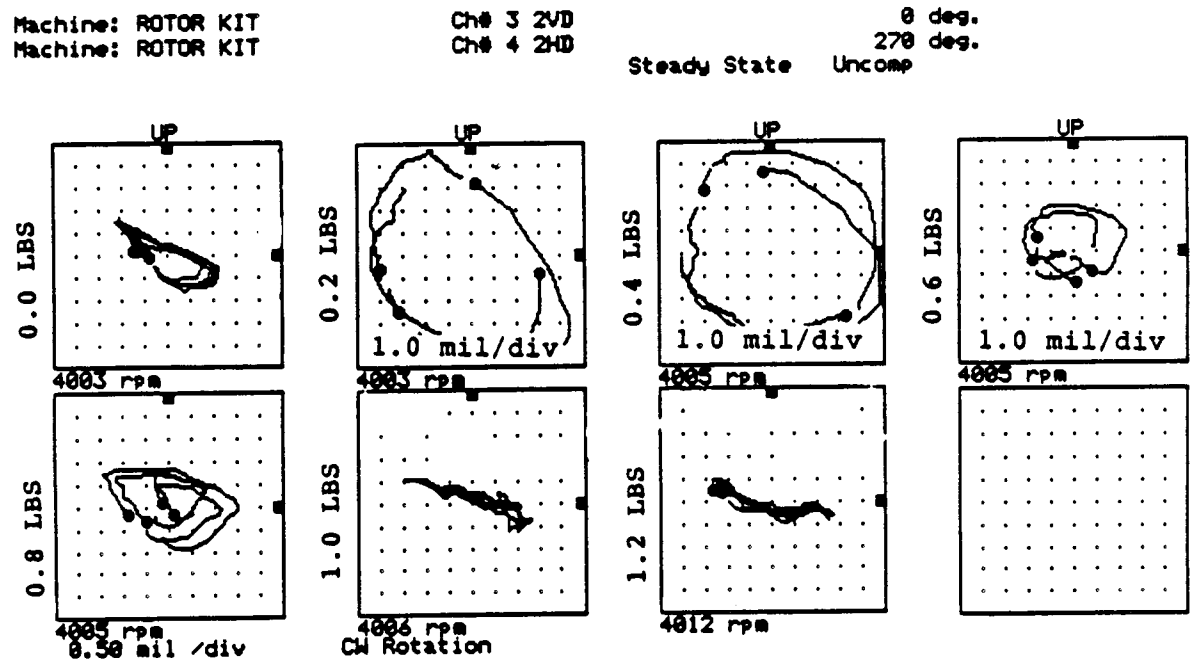

FIGURE 12.195 ORBITS AT PROBE LOCATION 2 AT 4000 RPM, 2.5 PSI SEAL OIL PRESSURE, 0.8 IN–GRAM UNBALANCE LOCATED IN THE THIRD PUMP IMPELLER DISK, FOR INCREASING STATIC PRELOAD.

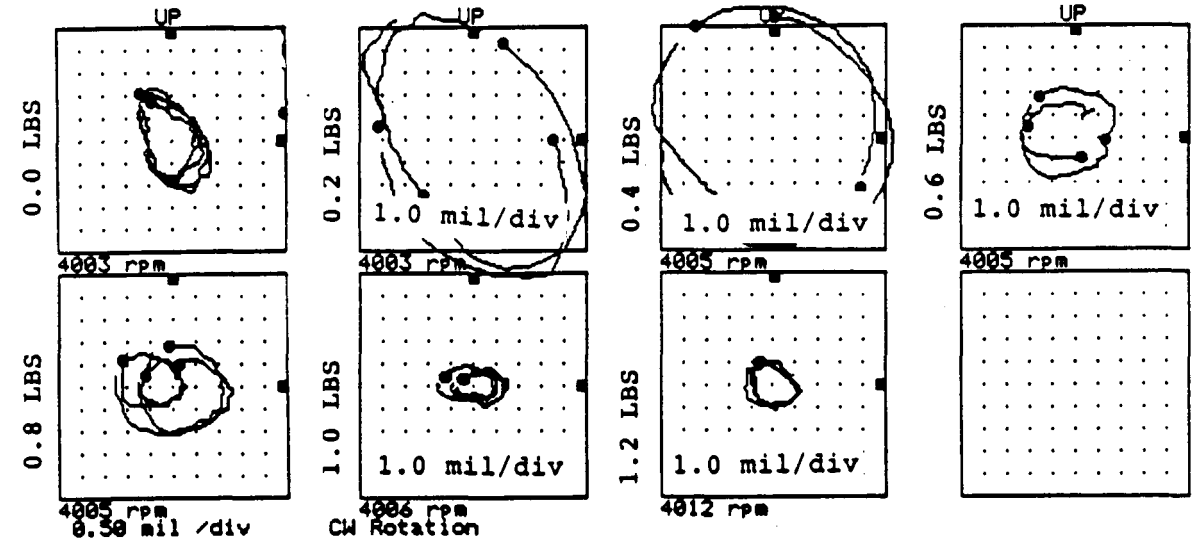

FIGURE 12.196 ORBITS AT PROBE LOCATION 3 AT 4000 RPM, 2.5 PSI SEAL OIL PRESSURE, 0.8 IN–GRAM UNBALANCE LOCATED IN THE THIRD PUMP IMPELLER DISK, FOR INCREASING STATIC PRELOAD FORCES.

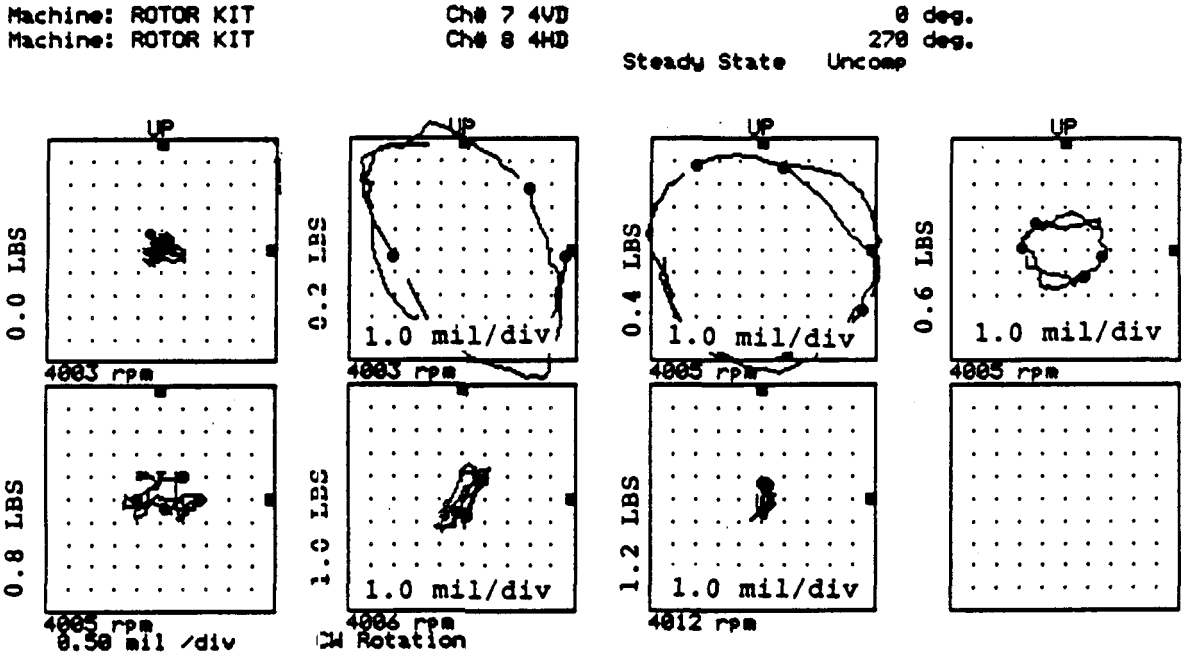

FIGURE 12.197 ORBITS AT PROBE LOCATION 4 AT 4000 RPM, 2.5 PSI SEAL OIL PRESSURE, 0.8 IN–GRAM UNBALANCE LOCATED IN THE THIRD PUMP IMPELLER DISK, FOR INCREASING STATIC PRELOAD FORCES.

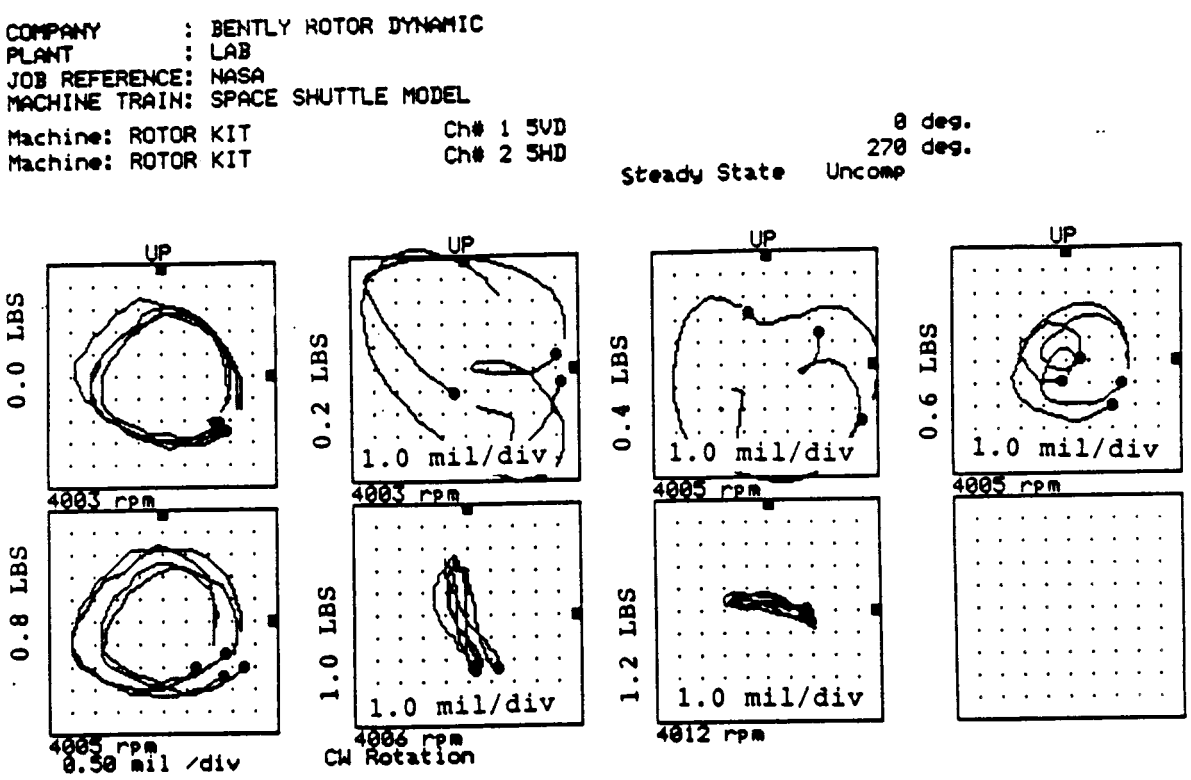

FIGURE 12.198 ORBITS AT PROBE LOCATION 5 AT 4000 RPM, 2.5 PSI SEAL OIL PRESSURE, 0.8 IN–GRAM UNBALANCE LOCATED IN THE THIRD PUMP IMPELLER DISK, FOR INCREASING STATIC PRELOAD FORCES.

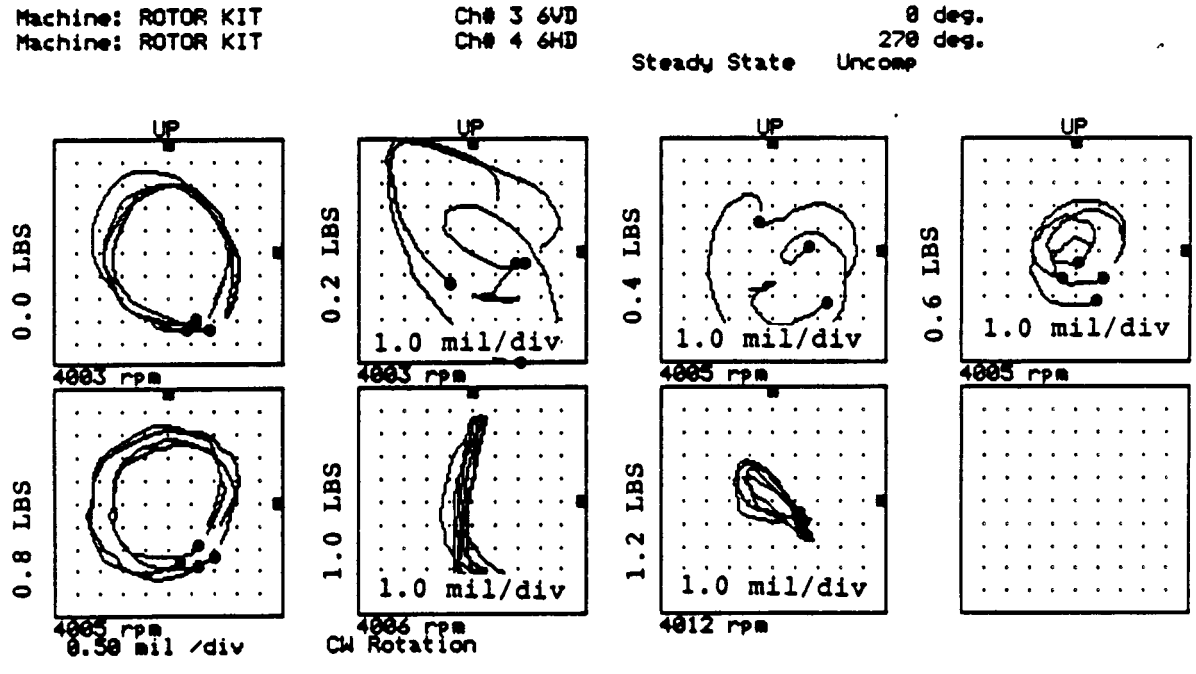

FIGURE 12.199 ORBITS AT PROBE LOCATION 6 AT 4000 RPM, 2.5 PSI SEAL OIL PRESSURE, 0.8 IN–GRAM UNBALANCE LOCATED IN THE THIRD PUMP IMPELLER DISK, FOR INCREASING STATIC PRELOAD FORCES.

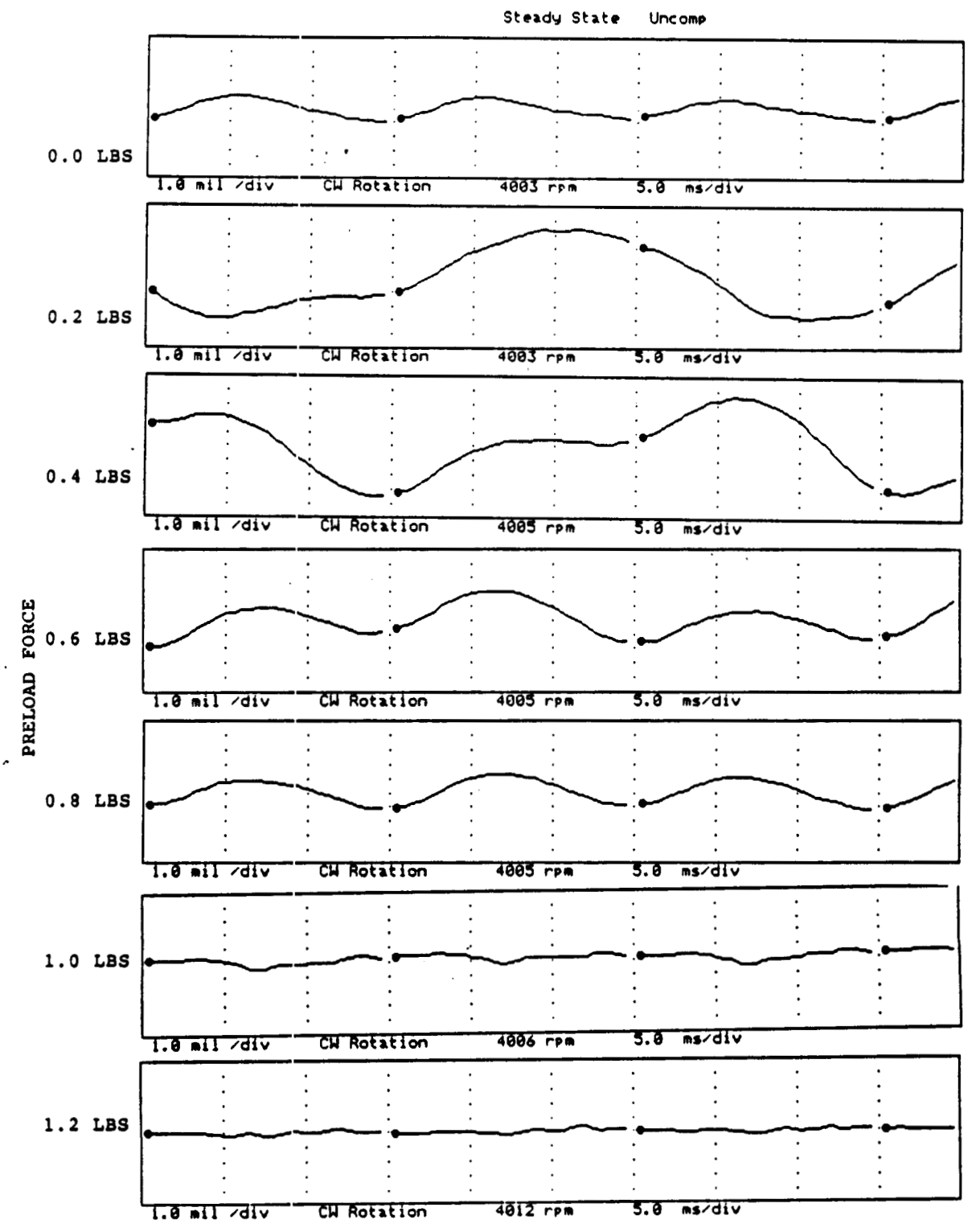

FIGURE 12.200 TIMEBASE FOR VERTICAL PROBE AT LOCATION 1 AT 4000 RPM, 2.5 PSI SEAL OIL PRESSURE, 0.8 IN–GRAM UNBALANCE LOCATED IN THE THIRD PUMP IMPELLER DISK, FOR INCREASING STATIC PRELOADS.

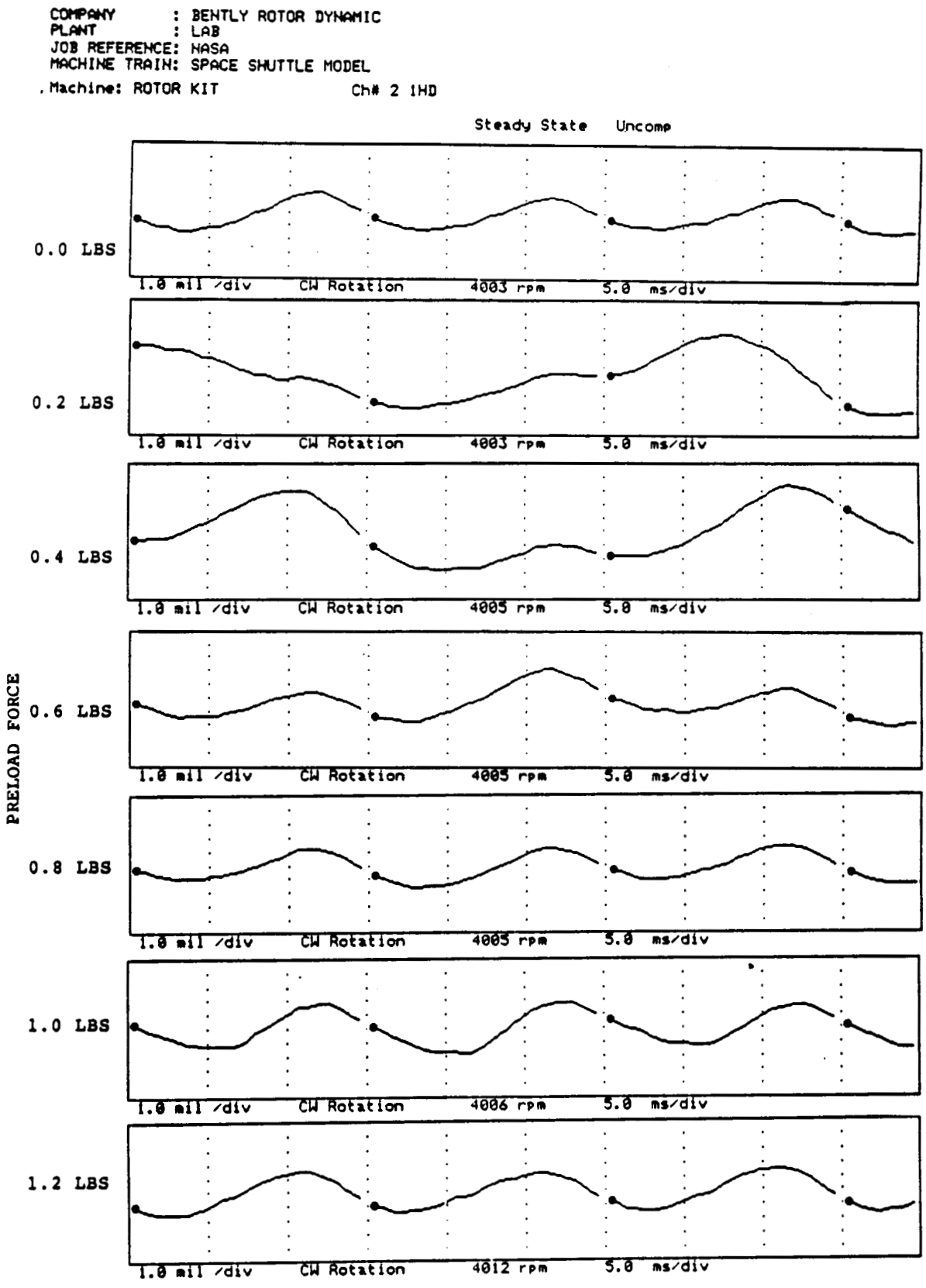

FIGURE 12.201 TIMEBASE FOR HORIZONTAL PROBE AT LOCATION 1 AT 4000 RPM, 2.5 PSI SEAL OIL PRESSURE, 0.8 IN–GRAM UNBALANCE LOCATED IN THE THIRD PUMP IMPELLER DISK, FOR INCREASING STATIC PRELOADS.

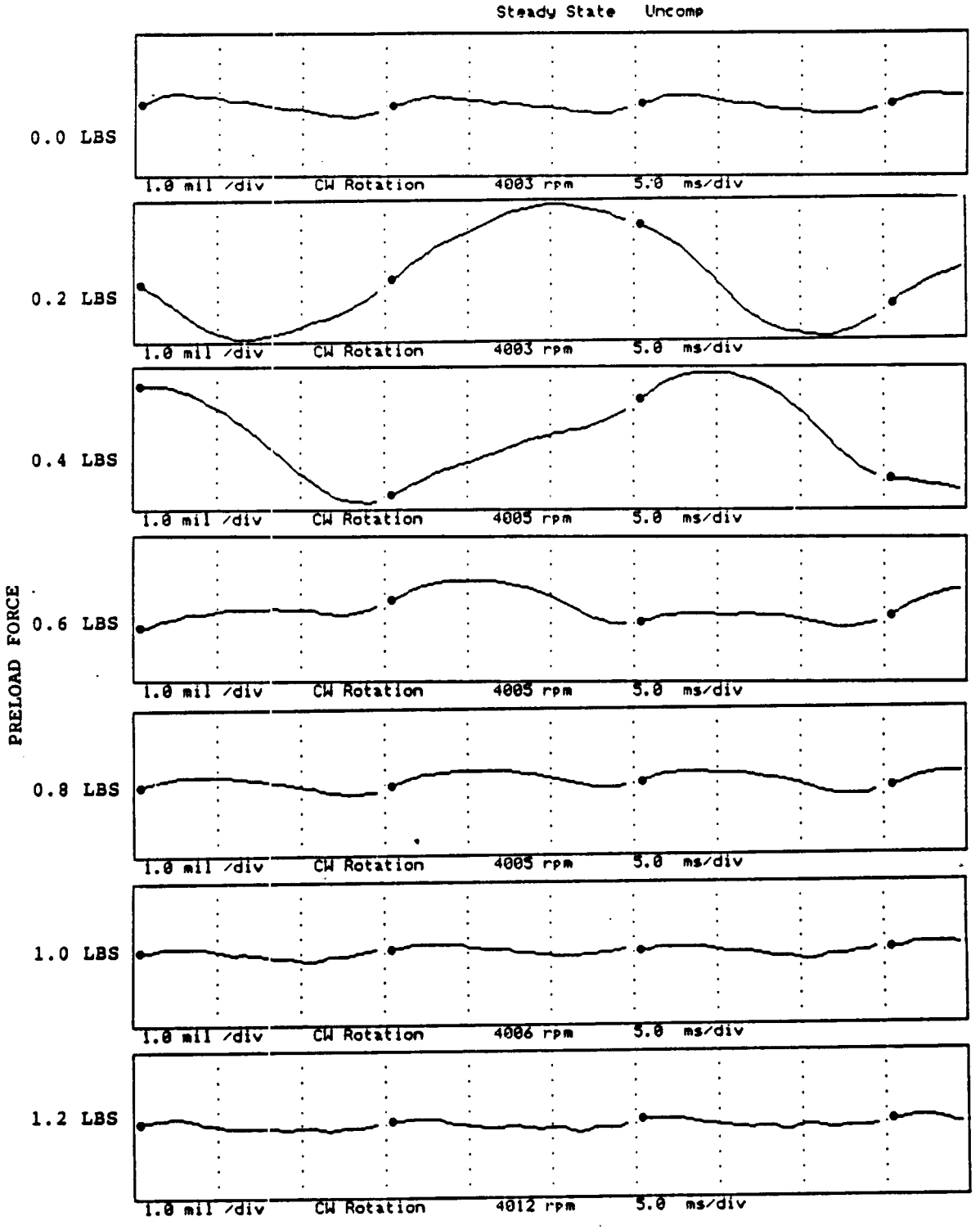

FIGURE 12.202 TIMEBASE FOR VERTICAL PROBE AT LOCATION 2 AT 4000 RPM., 2.5 PSI SEAL OIL PRESSURE, 0.8 IN–GRAM UNBALANCE LOCATED IN THE THIRD PUMP IMPELLER DISK, FOR INCREASING STATIC PRELOADS.

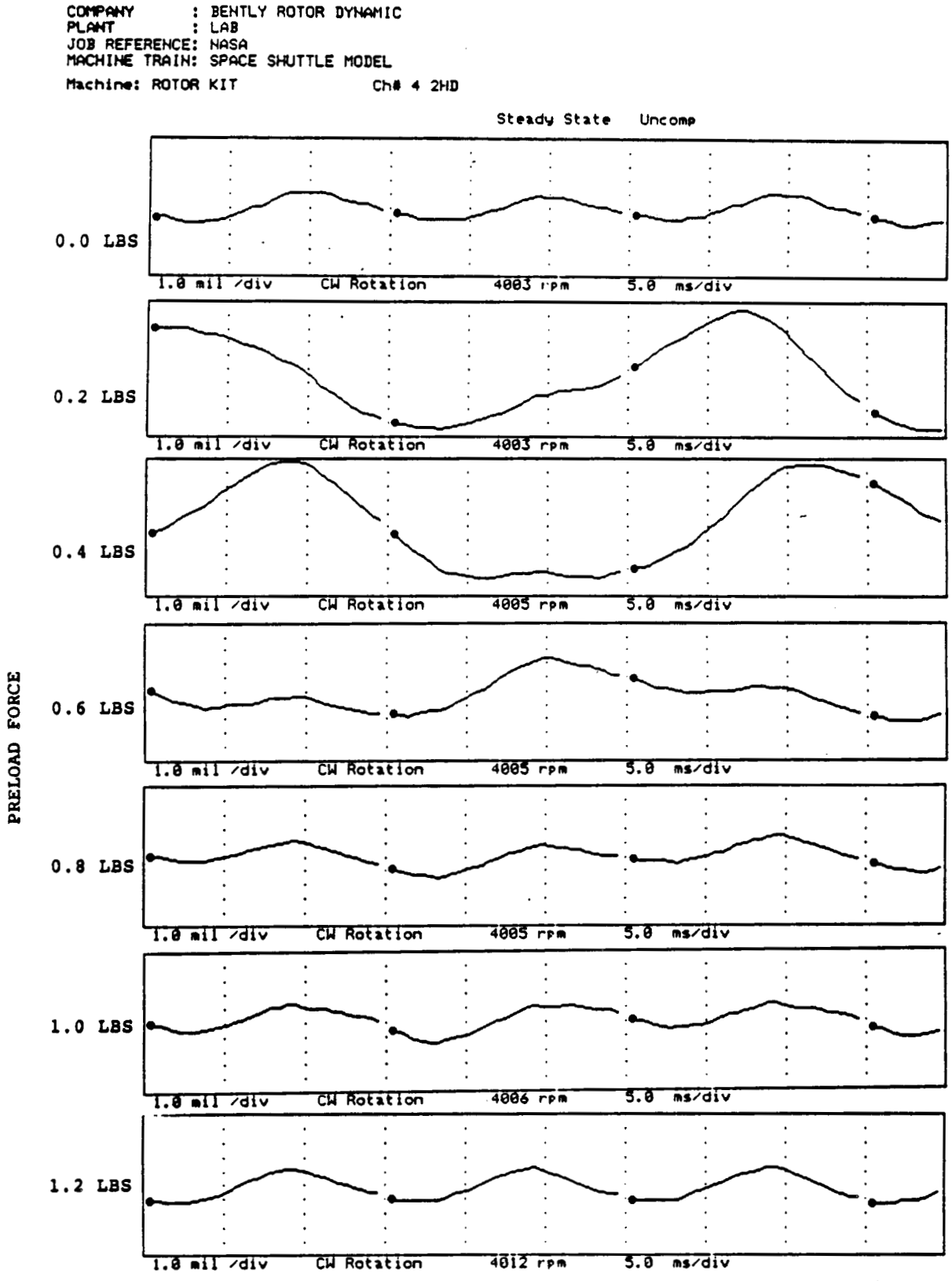

FIGURE 12.203 TIMEBASE FOR HORIZONTAL PROBE AT LOCATION 2 AT 4000 RPM, 2.5 PSI SEAL OIL PRESSURE, 0.8 IN–GRAM UNBALANCE LOCATED IN THE THIRD PUMP IMPELLER DISK, FOR INCREASING STATIC PRELOADS.

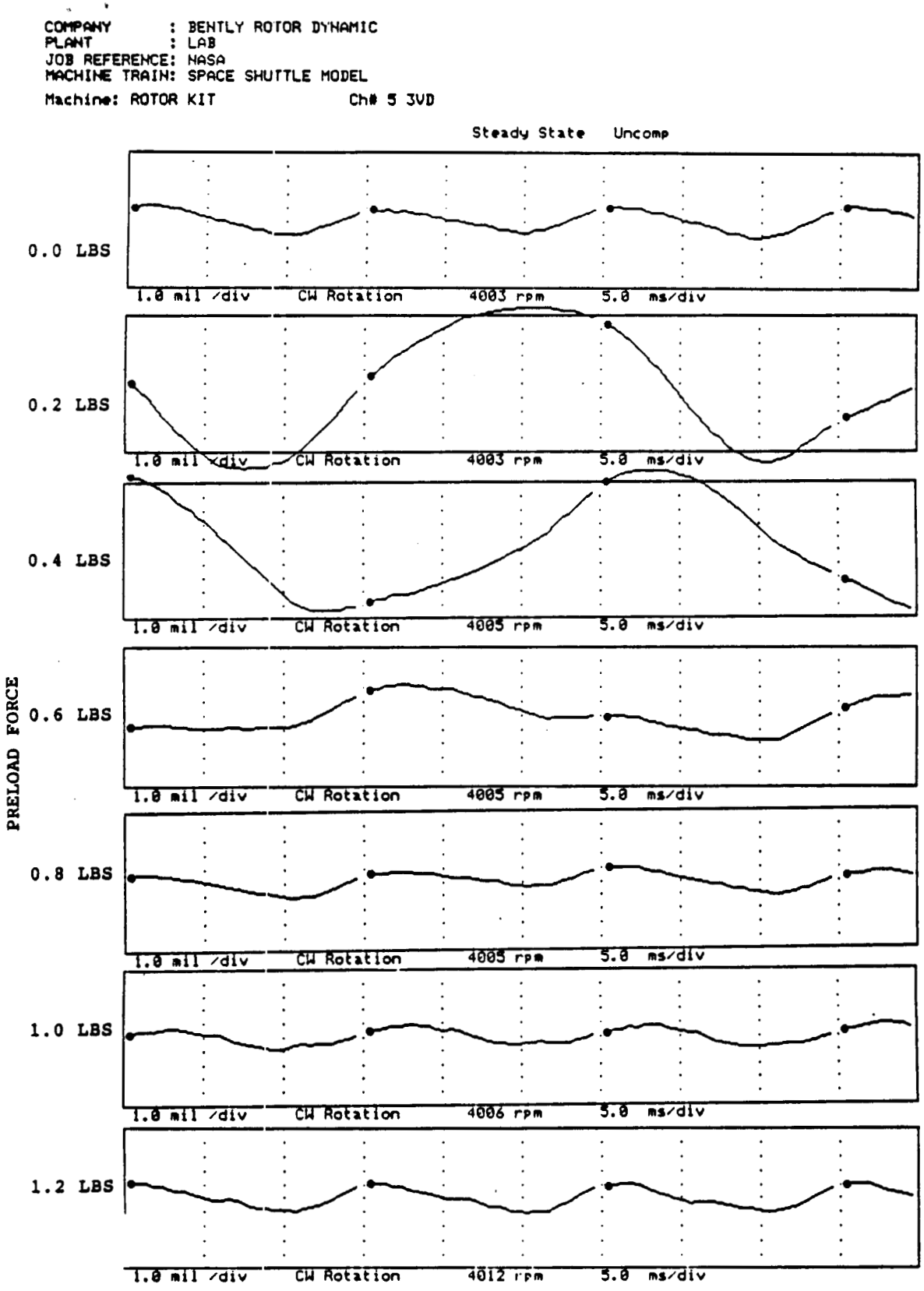

FIGURE 12.204 TIMEBASE FOR VERTICAL PROBE AT LOCATION 3 AT 4000 RPM, 2.5 PSI SEAL OIL PRESSURE, 0.8 IN–GRAM UNBALANCE LOCATED IN THE THIRD PUMP IMPELLER DISK, FOR INCREASING STATIC PRELOADS.

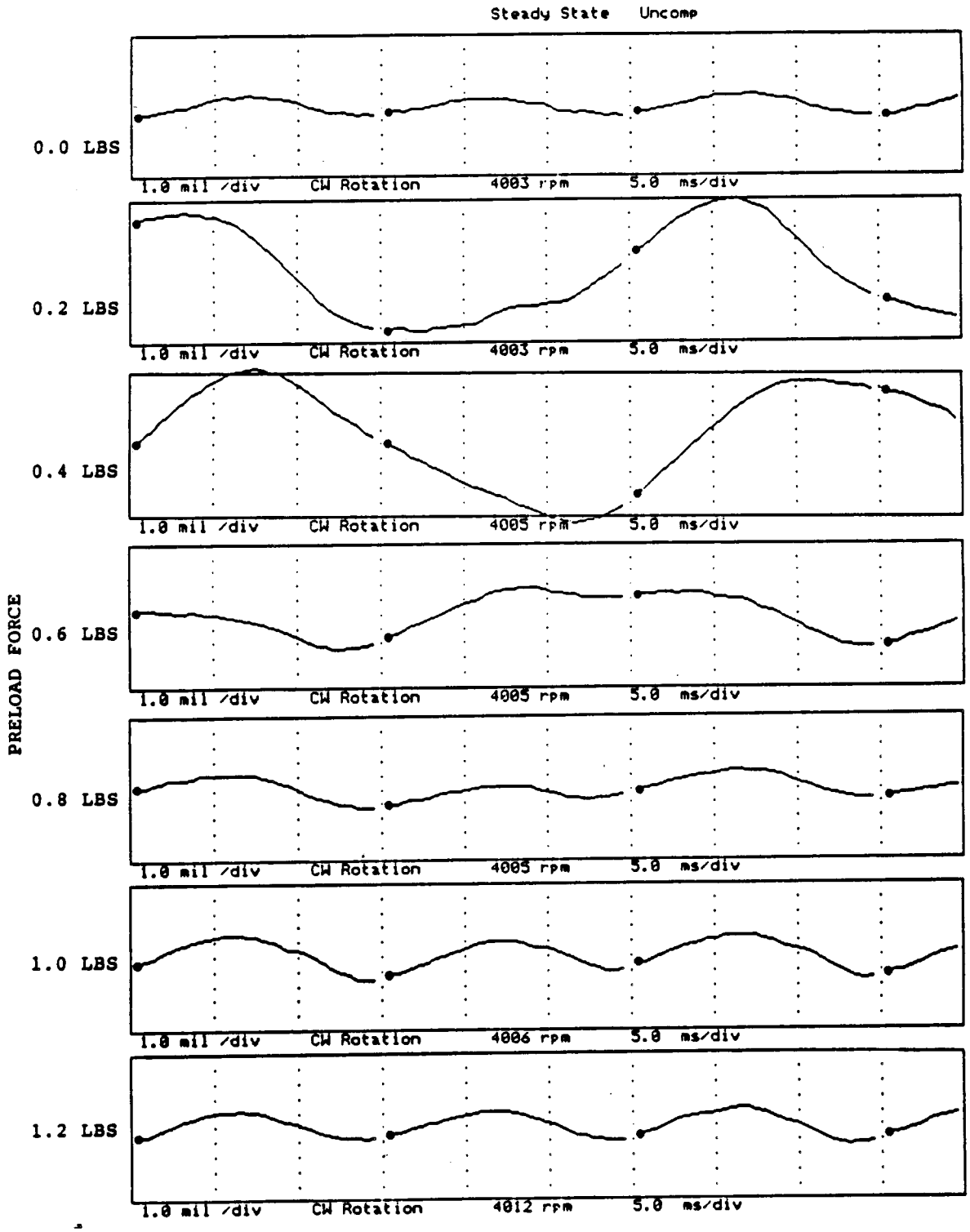

FIGURE 12.205 TIMEBASE FOR HORIZONTAL PROBE AT LOCATION 3 AT 4000 RPM, 2.5 PSI SEAL OIL PRESSURE, 0.8 IN–GRAM UNBALANCE LOCATED IN THE THIRD PUMP IMPELLER DISK, FOR INCREASING STATIC PRELOADS.

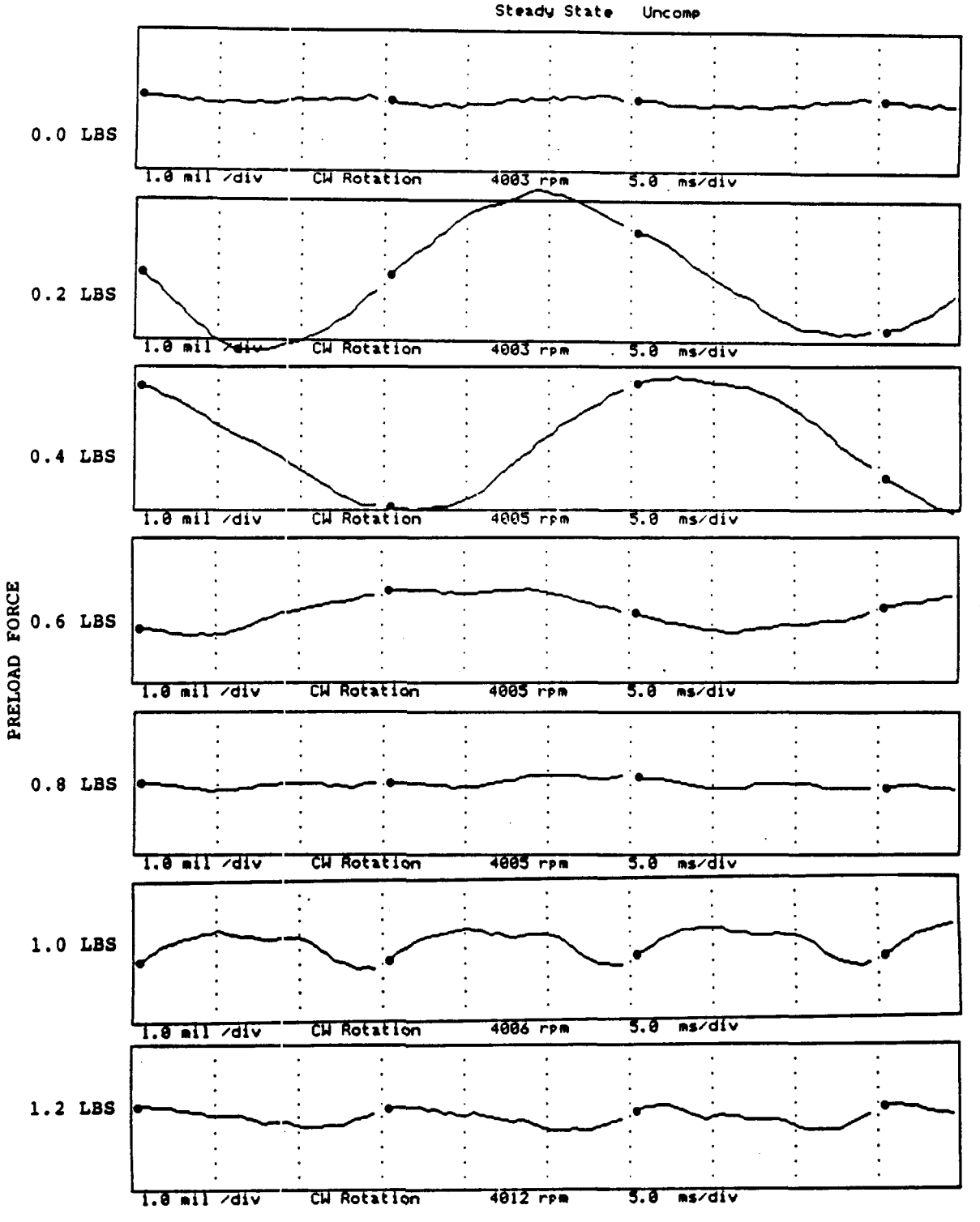

FIGURE 12.206 TIMEBASE FOR VERTICAL PROBE AT LOCATION 4 AT 4000 RPM, 2.5 PSI SEAL OIL PRESSURE, 0.8 IN–GRAM UNBALANCE LOCATED IN THE THIRD PUMP IMPELLER DISK, FOR INCREASING STATIC PRELOADS.

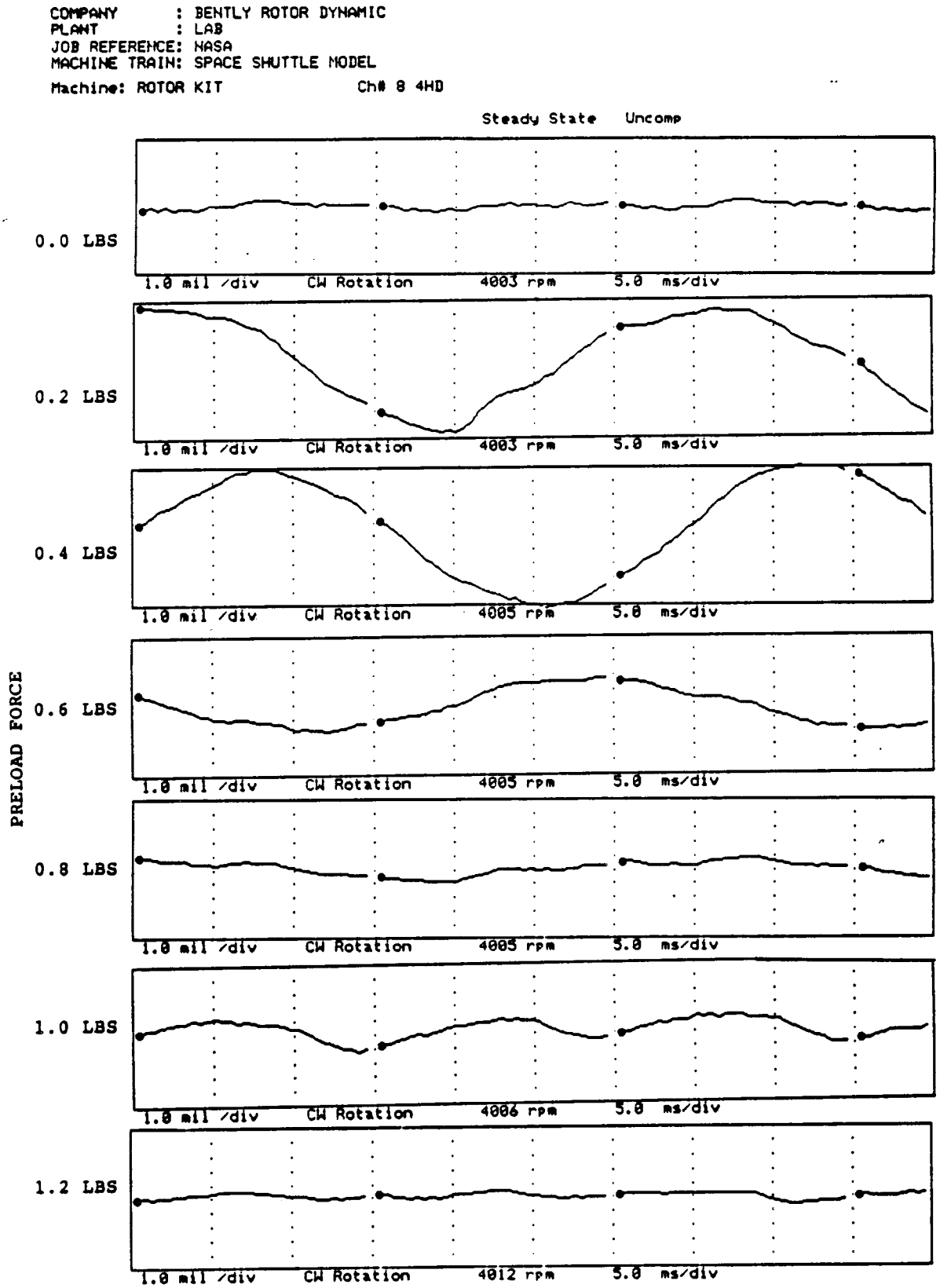

FIGURE 12.207 TIMEBASE FOR HORIZONTAL PROBE AT LOCATION 4 AT 4000 RPM, 2.5 PSI SEAL OIL PRESSURE, 0.8 IN–GRAM UNBALANCE LOCATED IN THE THIRD PUMP IMPELLER DISK, FOR INCREASING STATIC PRELOADS.

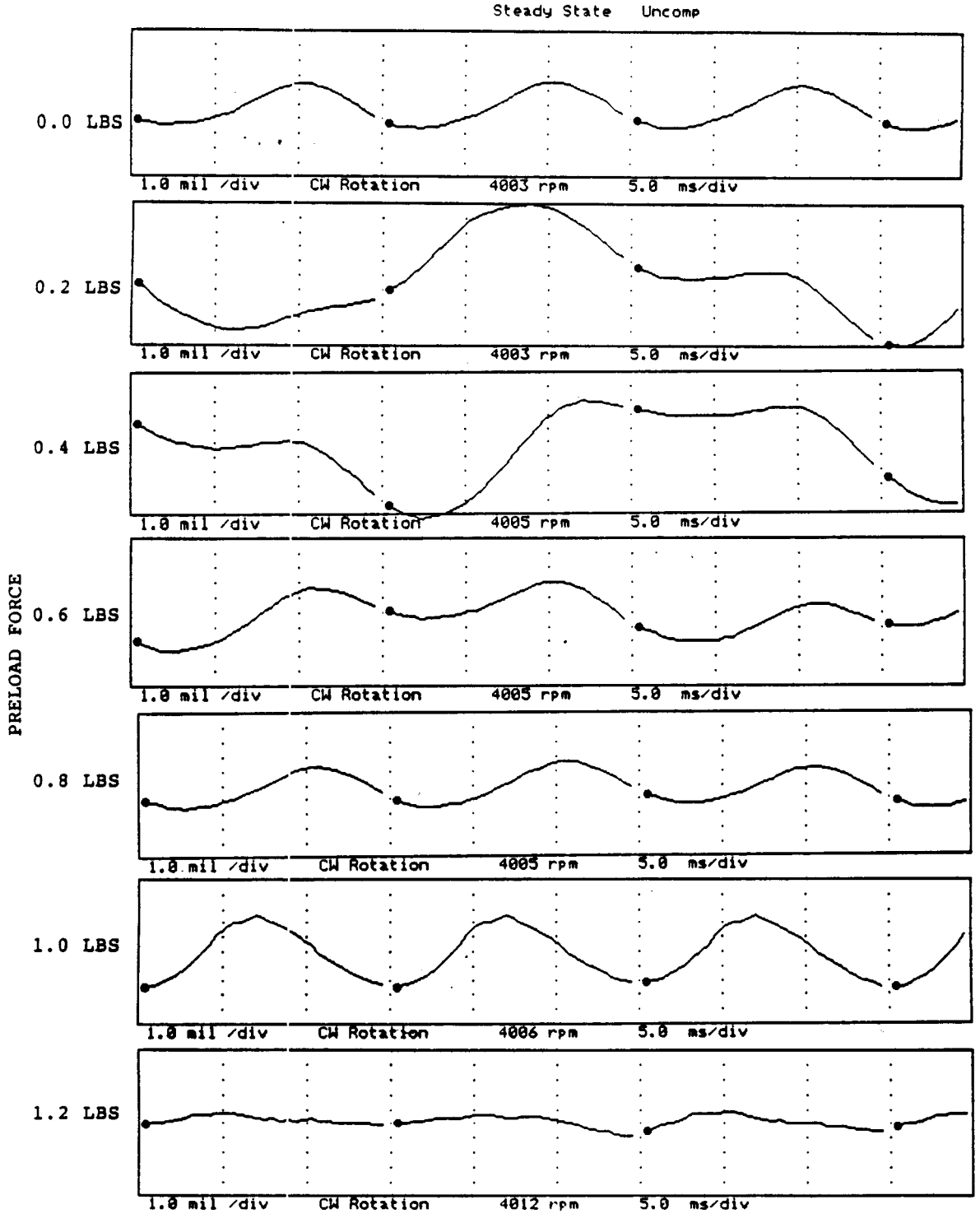

FIGURE 12.208 TIMEBASE FOR VERTICAL PROBE AT LOCATION 5 AT 4000 RPM, 2.5 PSI SEAL OIL PRESSURE, 0.8 IN–GRAM UNBALANCE LOCATED IN THE THIRD PUMP IMPELLER DISK, FOR INCREASING STATIC PRELOADS.

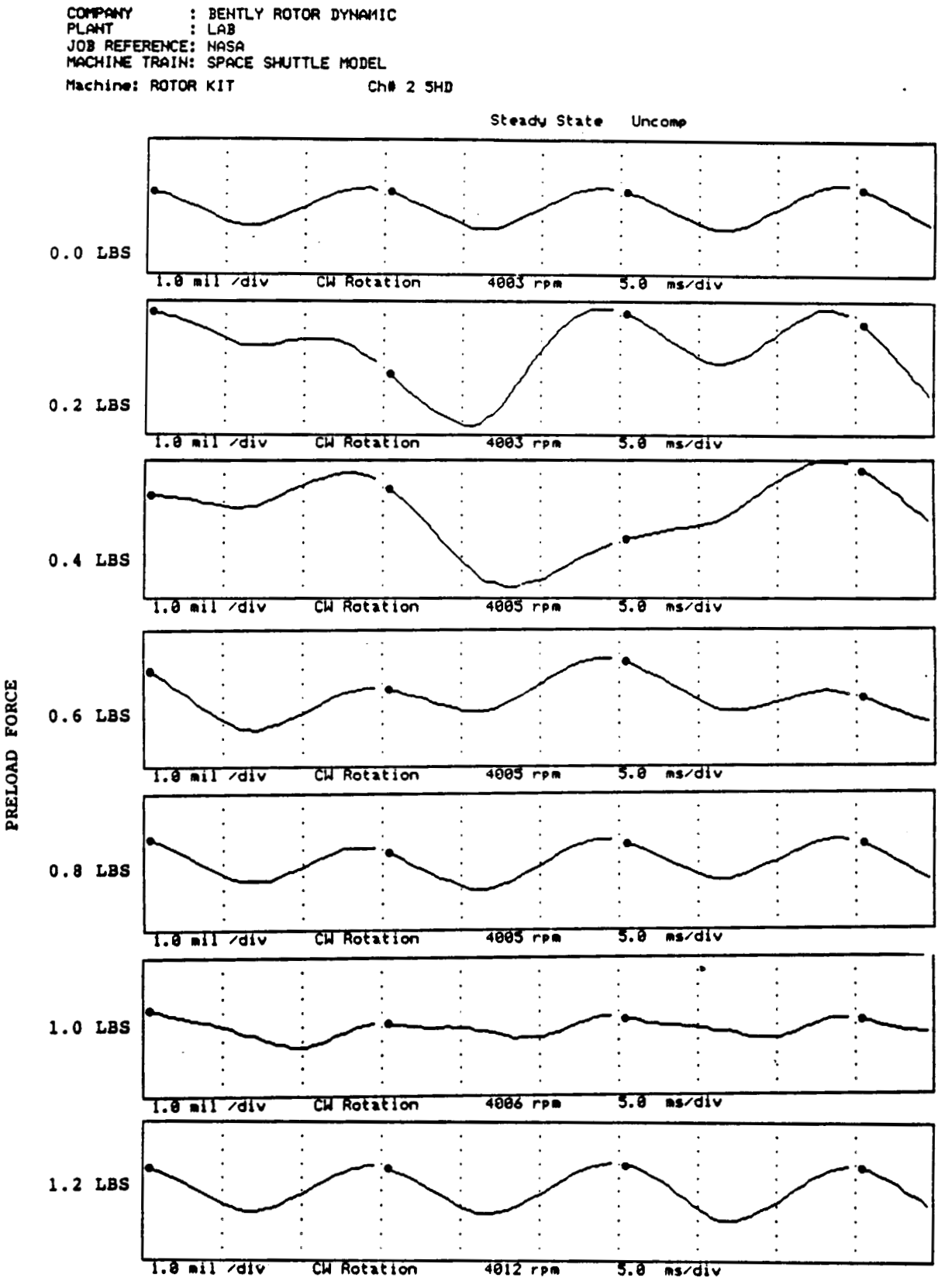

FIGURE 12.209 TIMEBASE FOR HORIZONTAL PROBE AT LOCATION 5 AT 4000 RPM, 2.5 PSI SEAL OIL PRESSURE, 0.8 IN–GRAM UNBALANCE LOCATED IN THE THIRD PUMP IMPELLER DISK, FOR INCREASING STATIC PRELOADS.

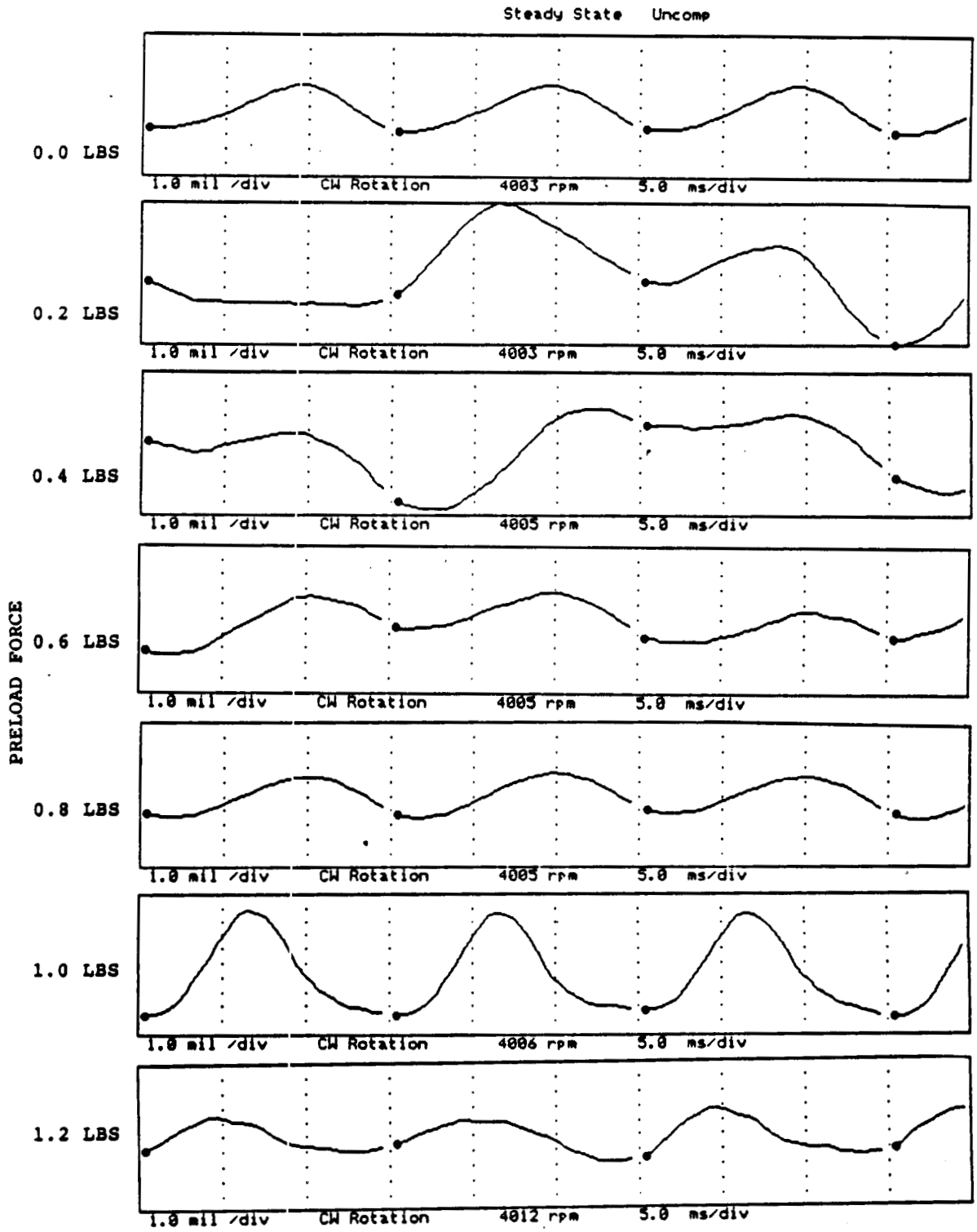

FIGURE 12.210 TIMEBASE FOR VERTICAL PROBE AT LOCATION 6 AT 4000 RPM, 2.5 PSI SEAL OIL PRESSURE, 0.8 IN–GRAM UNBALANCE LOCATED IN THE THIRD PUMP IMPELLER DISK, FOR INCREASING STATIC PRELOADS.

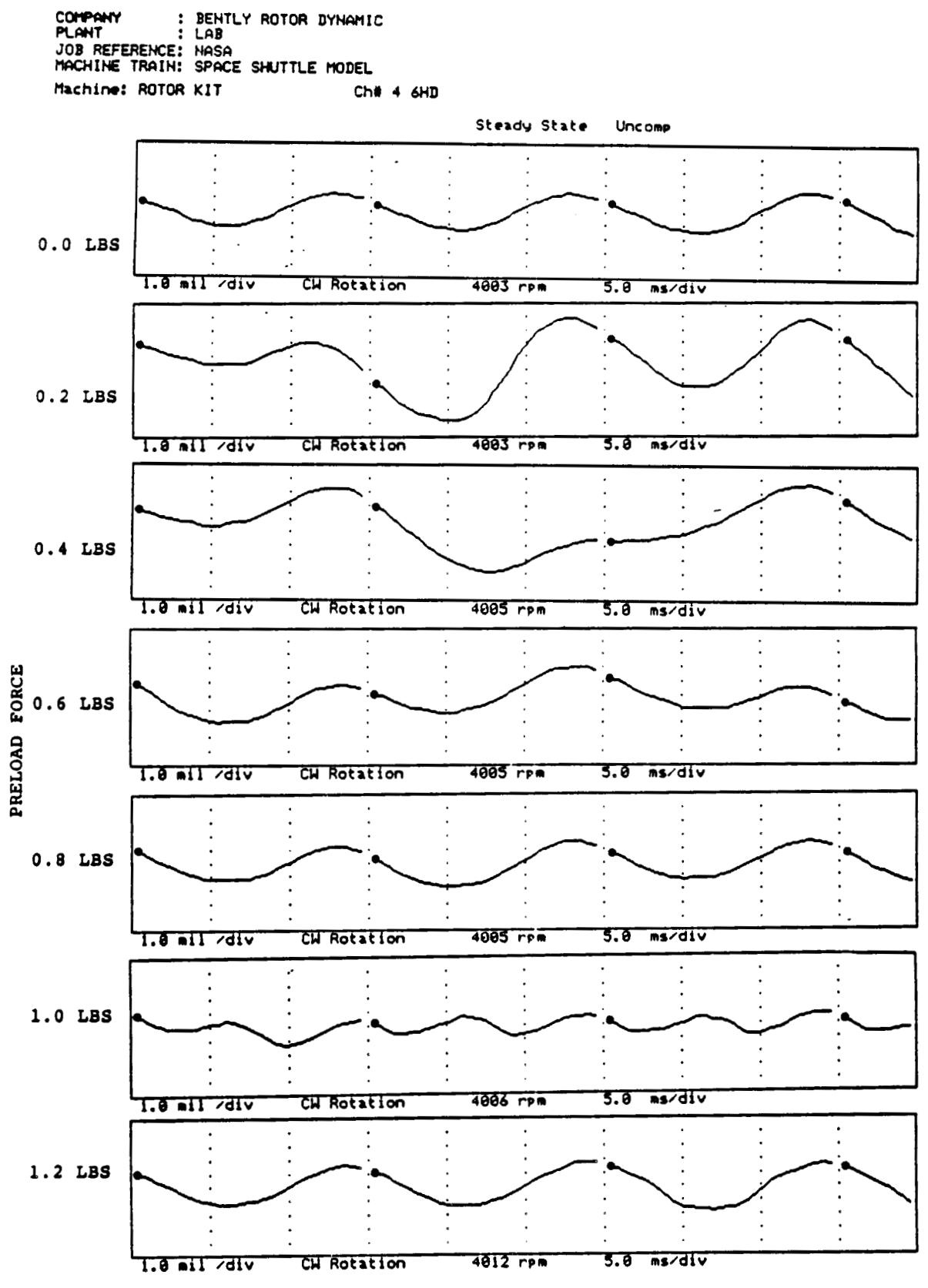

FIGURE 12.211 TIMEBASE FOR HORIZONTAL PROBE AT LOCATION 6 AT 4000 RPM, 2.5 PSI SEAL OIL PRESSURE, 0.8 IN–GRAM UNBALANCE LOCATED IN THE THIRD PUMP IMPELLER DISK, FOR INCREASING STATIC PRELOADS.

NOT AVAILABLE - OIL IN THE CLEARANCE AREA PROHIBITS THE METAL-TO-METAL CONTACT NECESSARY FOR THE CONTACT SENSOR TO OPERATE CORRECTLY.

FIGURE 12.212 TIMEBASE FOR SHAFT TO SEAL 1 CONTACT AT 4000 RPM, 2.5 PSI SEAL OIL PRESSURE, 0.8 IN–GRAM UNBALANCE LOCATED IN THE THIRD PUMP IMPELLER DISK, FOR INCREASING STATIC PRELOADS.

NOT AVAILABLE - OIL IN THE CLEARANCE AREA PROHIBITS THE METAL-TO-METAL CONTACT NECESSARY FOR THE CONTACT SENSOR TO OPERATE CORRECTLY.

FIGURE 12.213 TIMEBASE FOR SHAFT TO SEAL 2 CONTACT AT 4000 RPM 2.5 PSI SEAL OIL PRESSURE, 0.8 IN–GRAM UNBALANCE LOCATED IN THE THIRD PUMP IMPELLER DISK, FOR INCREASING STATIC PRELOADS.

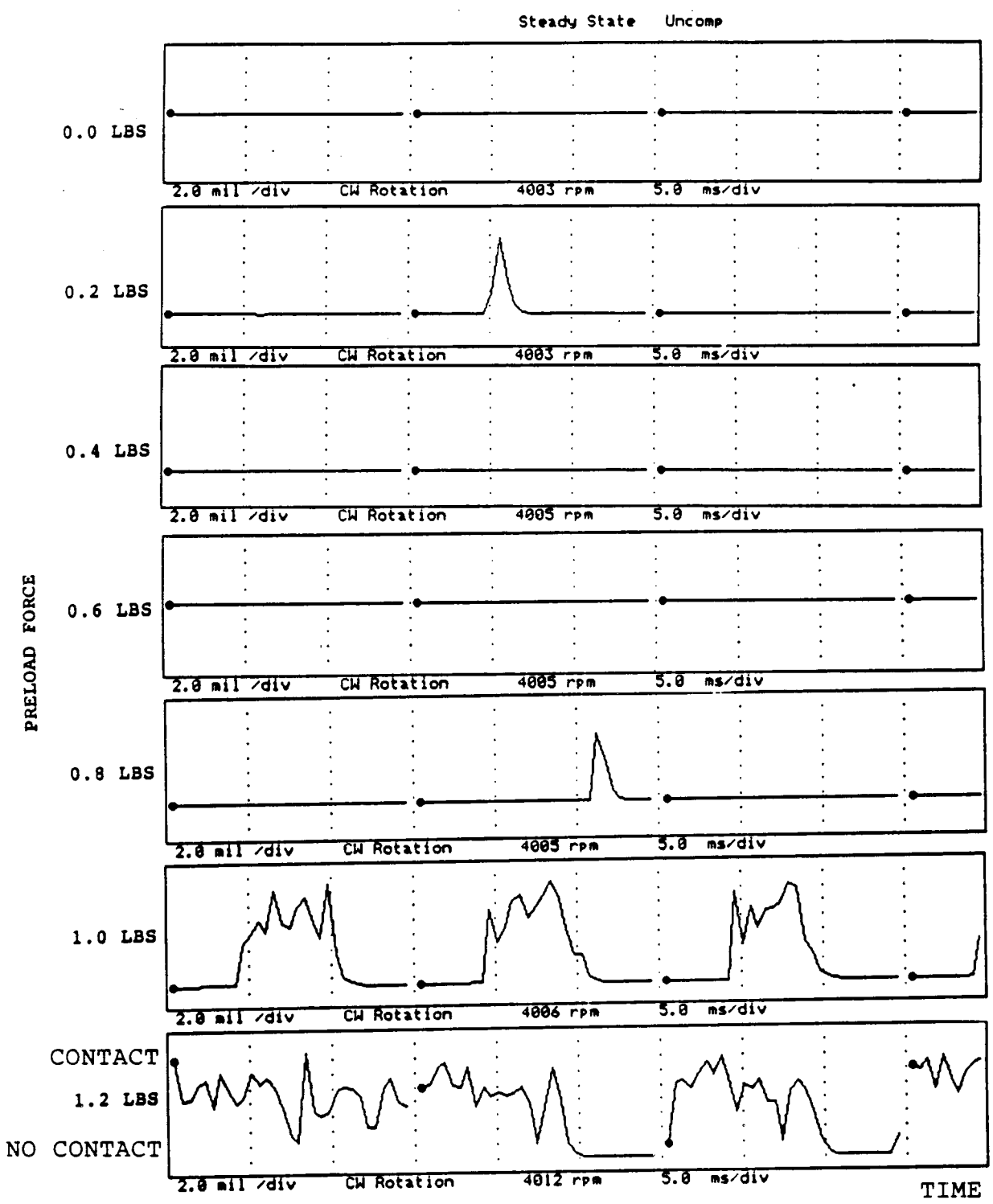

FIGURE 12.214 TIMEBASE FOR SHAFT TO RUB BLOCK CONTACT AT 4000 RPM, 2.5 PSI SEAL OIL PRESSURE, 0.8 IN–GRAM UNBALANCE LOCATED IN THE THIRD PUMP IMPELLER DISK, FOR INCREASING STATIC PRELOADS.

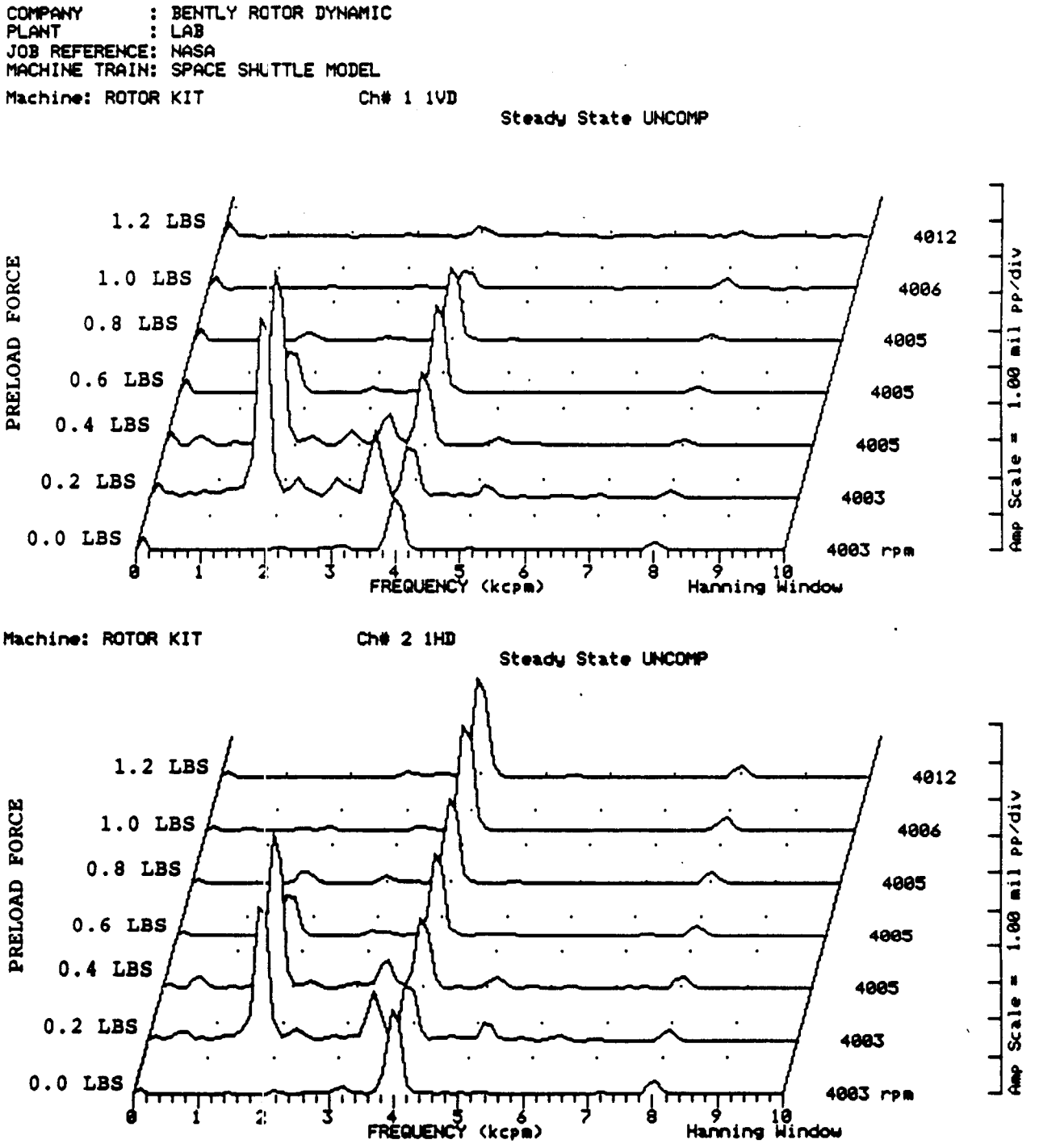

FIGURE 12.215 SPECTRAL CONTENT AT PROBE LOCATION 1 AT 4000 RPM, 2.5 PSI SEAL OIL PRESSURE, 0.8 IN–GRAM UNBALANCE LOCATED IN THE THIRD PUMP IMPELLER DISK, FOR INCREASING STATIC PRELOADS.

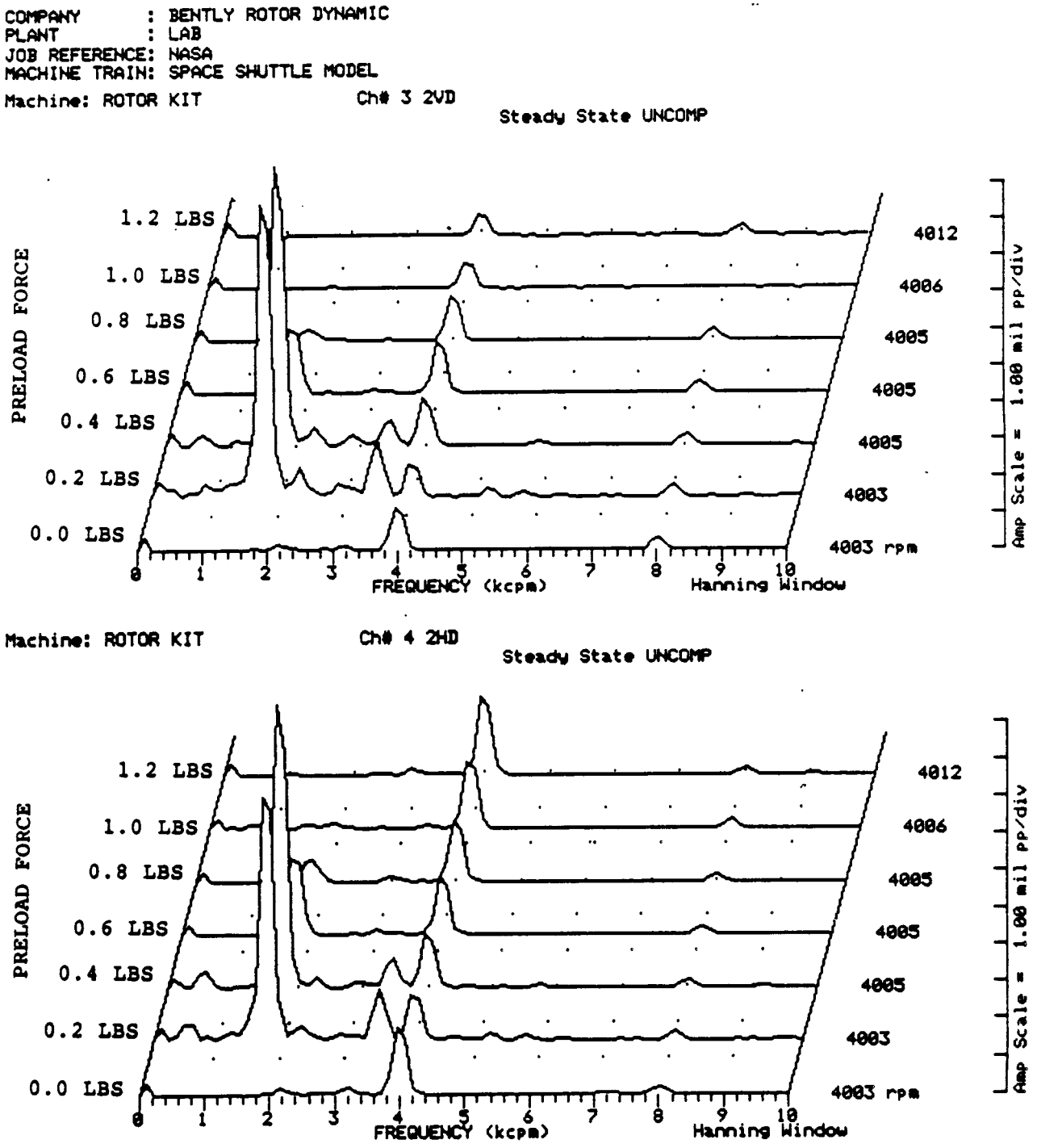

FIGURE 12.216 SPECTRAL CONTENT AT PROBE LOCATION 2 AT 4000 RPM, 2.5 PSI SEAL OIL PRESSURE, 0.8 IN–GRAM UNBALANCE LOCATED IN THE THIRD PUMP IMPELLER DISK, FOR INCREASING STATIC PRELOADS.

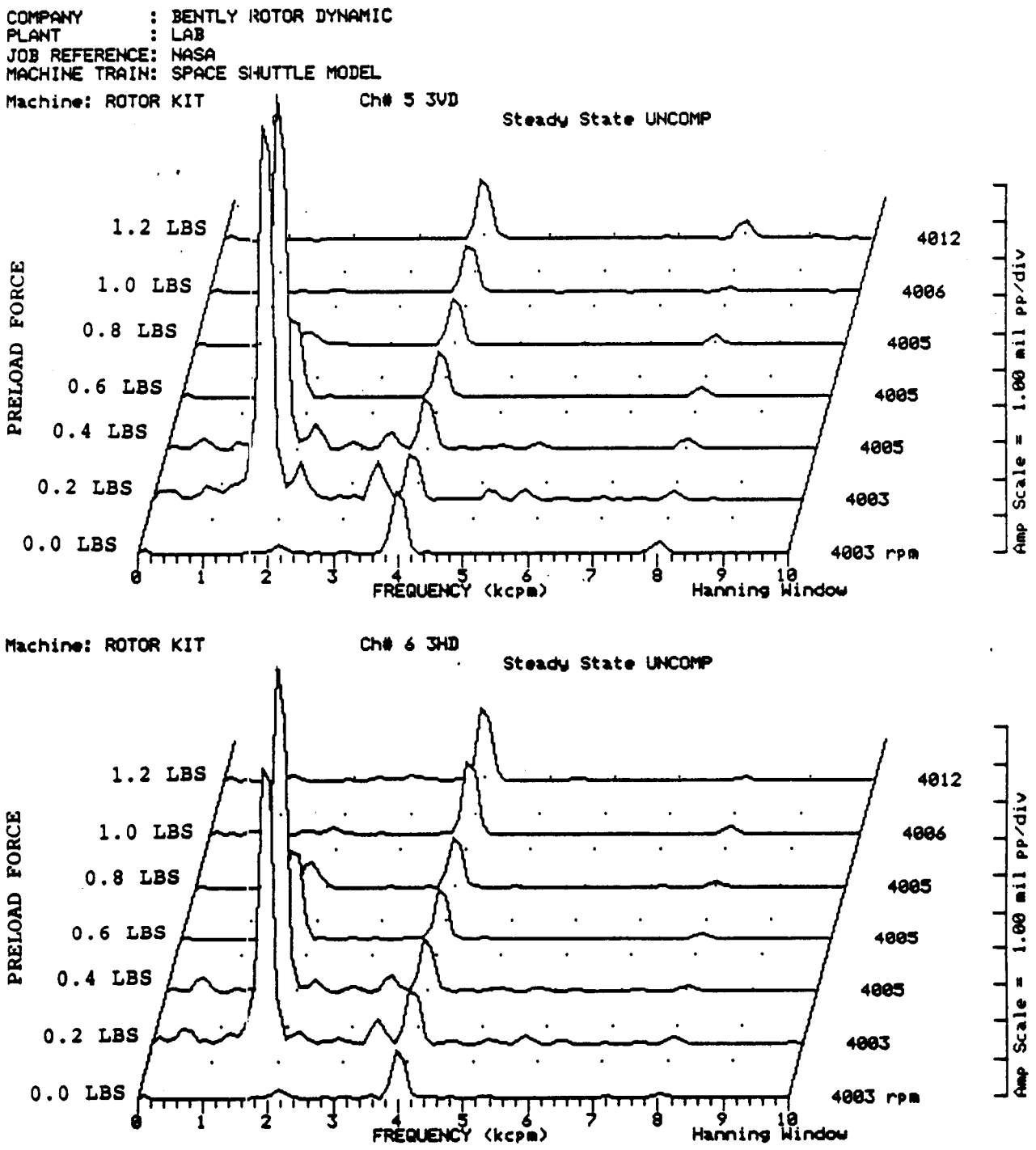

FIGURE 12.217 SPECTRAL CONTENT AT PROBE LOCATION 3 AT 4000 RPM, 2.5 PSI SEAL OIL PRESSURE, 0.8 IN–GRAM UNBALANCE LOCATED IN THE THIRD PUMP IMPELLER DISK, FOR INCREASING STATIC PRELOADS.

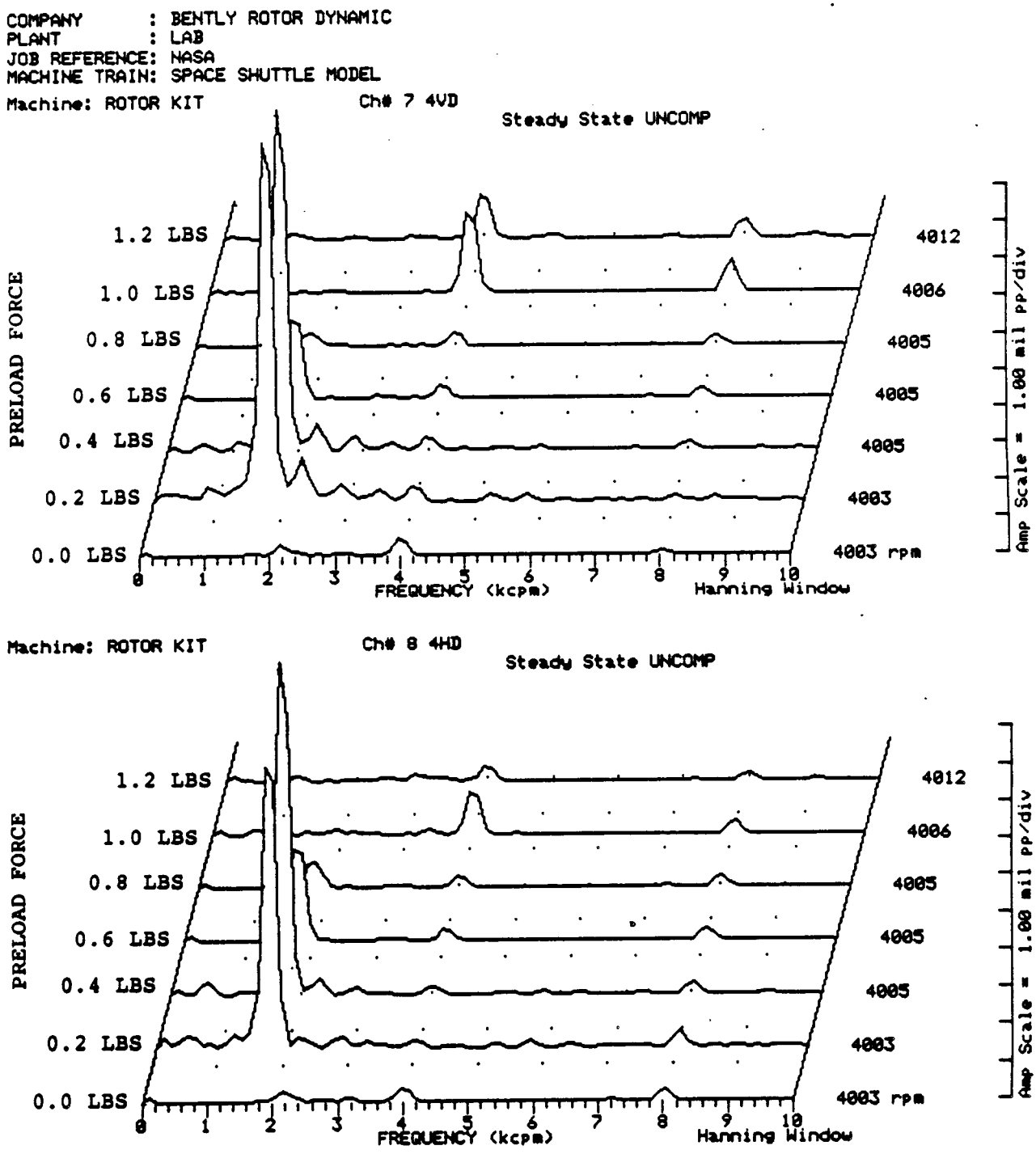

FIGURE 12.218 SPECTRAL CONTENT AT PROBE LOCATION 4 AT 4000 RPM, 2.5 PSI SEAL OIL PRESSURE, 0.8 IN–GRAM UNBALANCE LOCATED IN THE THIRD PUMP IMPELLER DISK, FOR INCREASING STATIC PRELOADS.

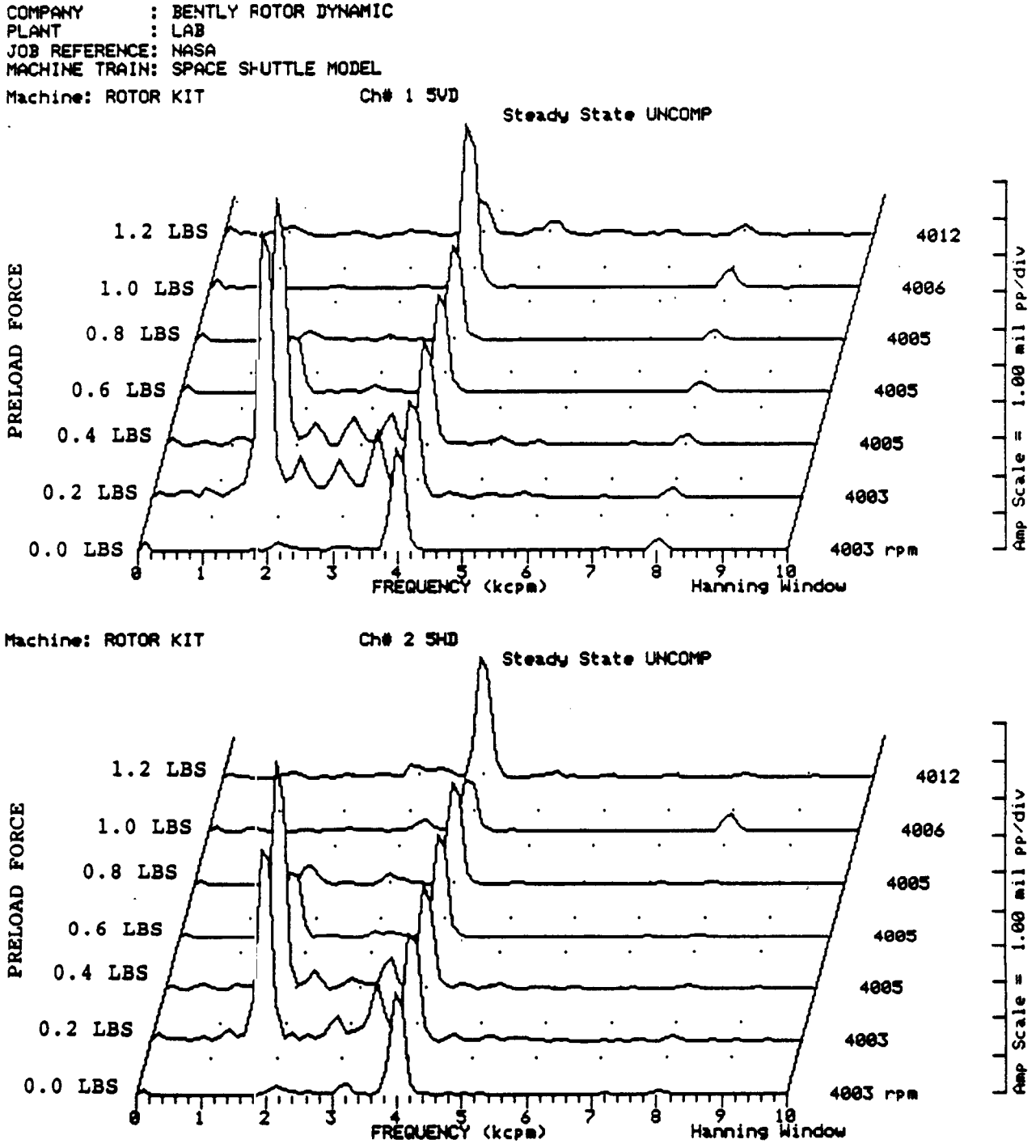

FIGURE 12.219 SPECTRAL CONTENT AT PROBE LOCATION 5 AT 4000 RPM, 2.5 PSI SEAL OIL PRESSURE, 0.8 IN–GRAM UNBALANCE LOCATED IN THE THIRD PUMP IMPELLER DISK, FOR INCREASING STATIC PRELOADS.

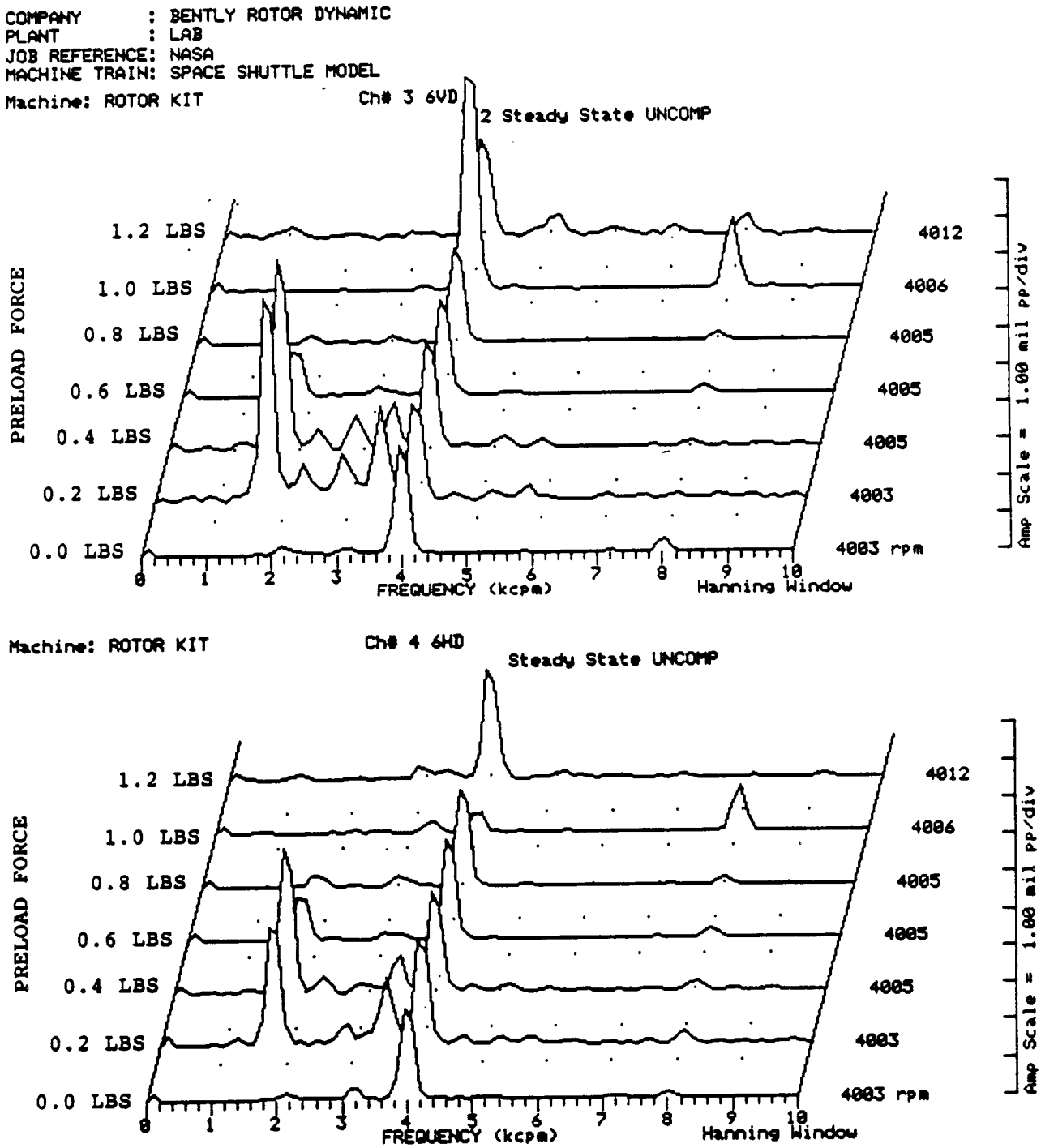

FIGURE 12.220 SPECTRAL CONTENT AT PROBE LOCATION 6 AT 4000 RPM, 2.5 PSI SEAL OIL PRESSURE, 0.8 IN–GRAM UNBALANCE LOCATED IN THE THIRD PUMP IMPELLER DISK, FOR INCREASING STATIC PRELOADS.

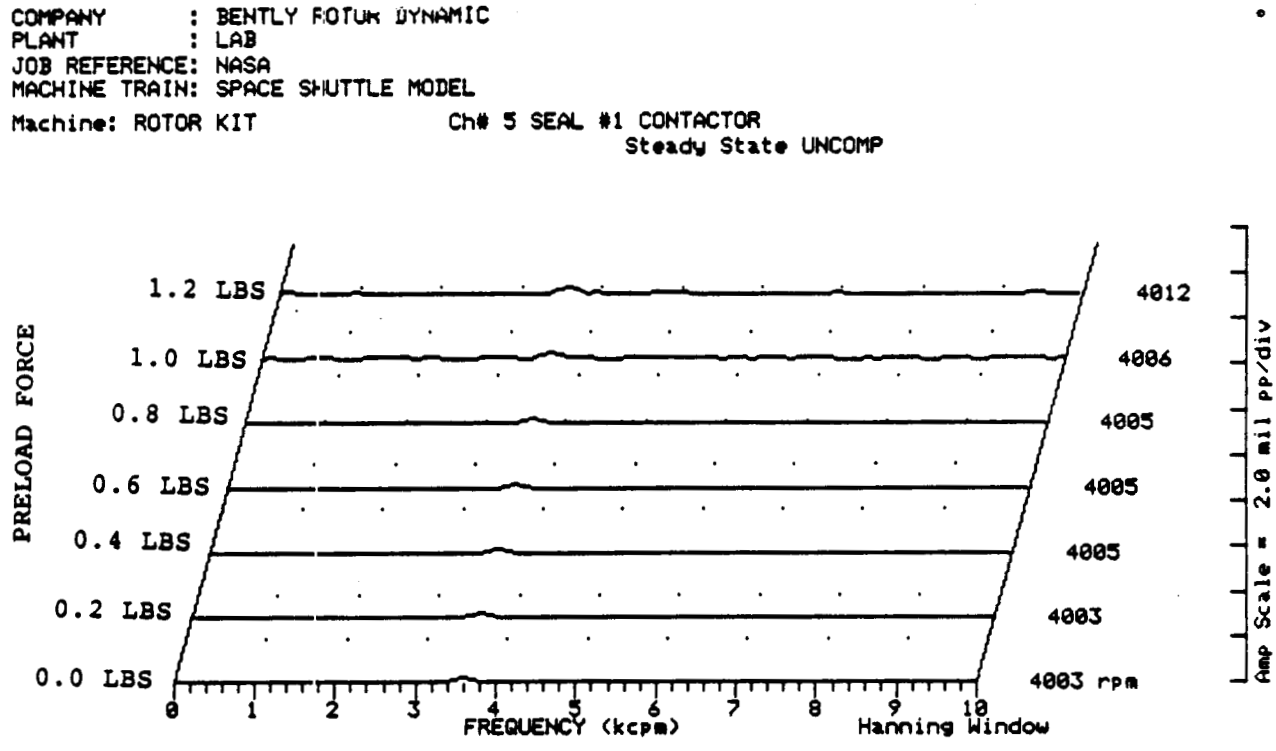

FIGURE 12.221 SPECTRAL CONTENT FOR SHAFT TO SEAL 1 CONTACT AT 4000 RPM, 2.5 PSI SEAL OIL PRESSURE, 0.8 IN–GRAM UNBALANCE LOCATED IN THE THIRD PUMP IMPELLER DISK, FOR INCREASING STATIC PRELOADS.

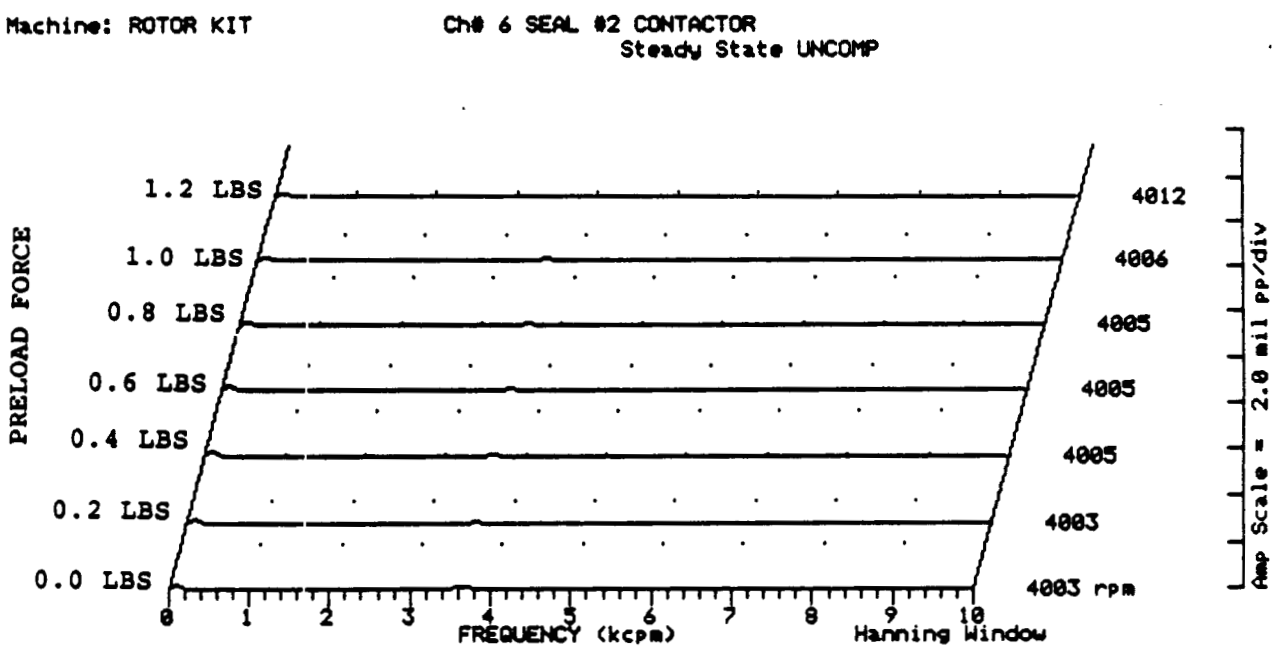

FIGURE 12.222 SPECTRAL CONTENT FOR SHAFT TO SEAL 2 CONTACT AT 4000 RPM, 2.5 PSI SEAL OIL PRESSURE, 0.8 IN–GRAM UNBALANCE LOCATED IN THE THIRD PUMP IMPELLER DISK, FOR INCREASING STATIC PRELOADS.

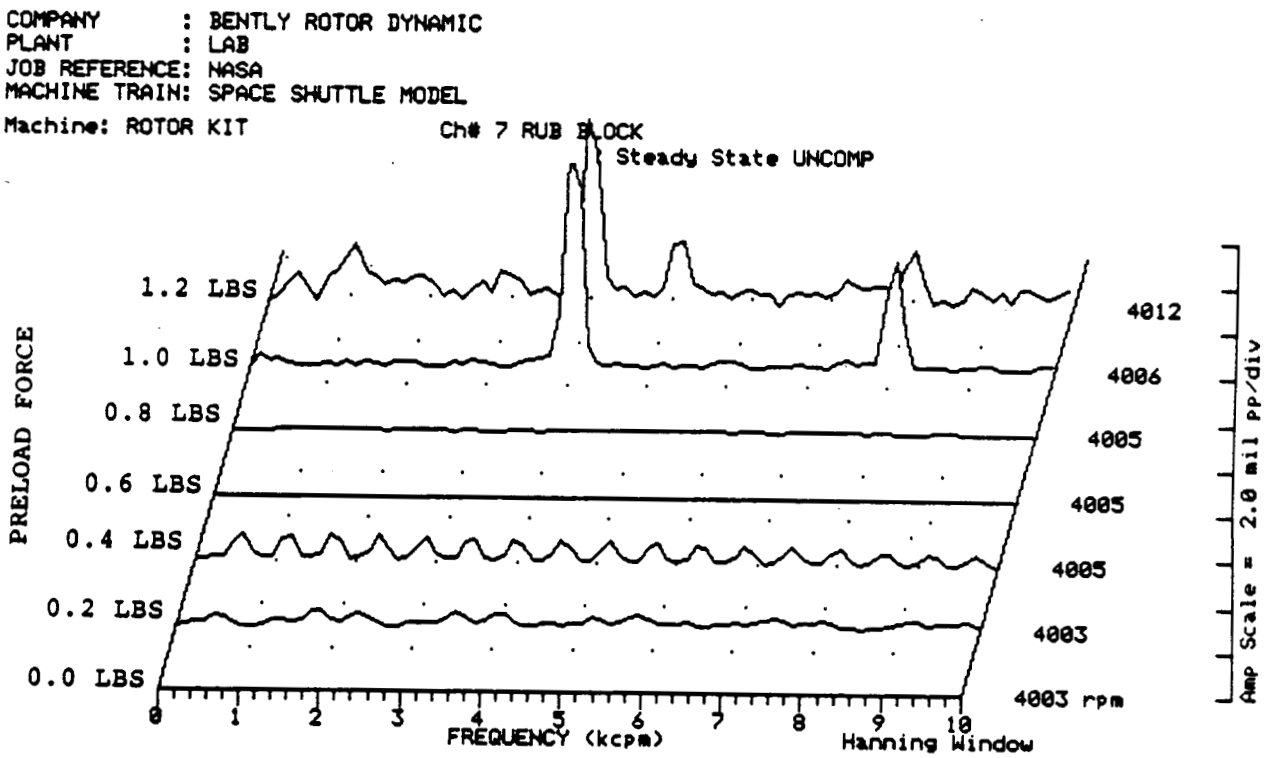

FIGURE 12.223 SPECTRAL CONTENT FOR SHAFT TO RUB BLOCK CONTACT AT 4000 RPM, 2.5 PSI SEAL OIL PRESSURE, 0.8 IN–GRAM UNBALANCE LOCATED IN THE THIRD PUMP IMPELLER DISK, FOR INCREASING STATIC PRELOADS.

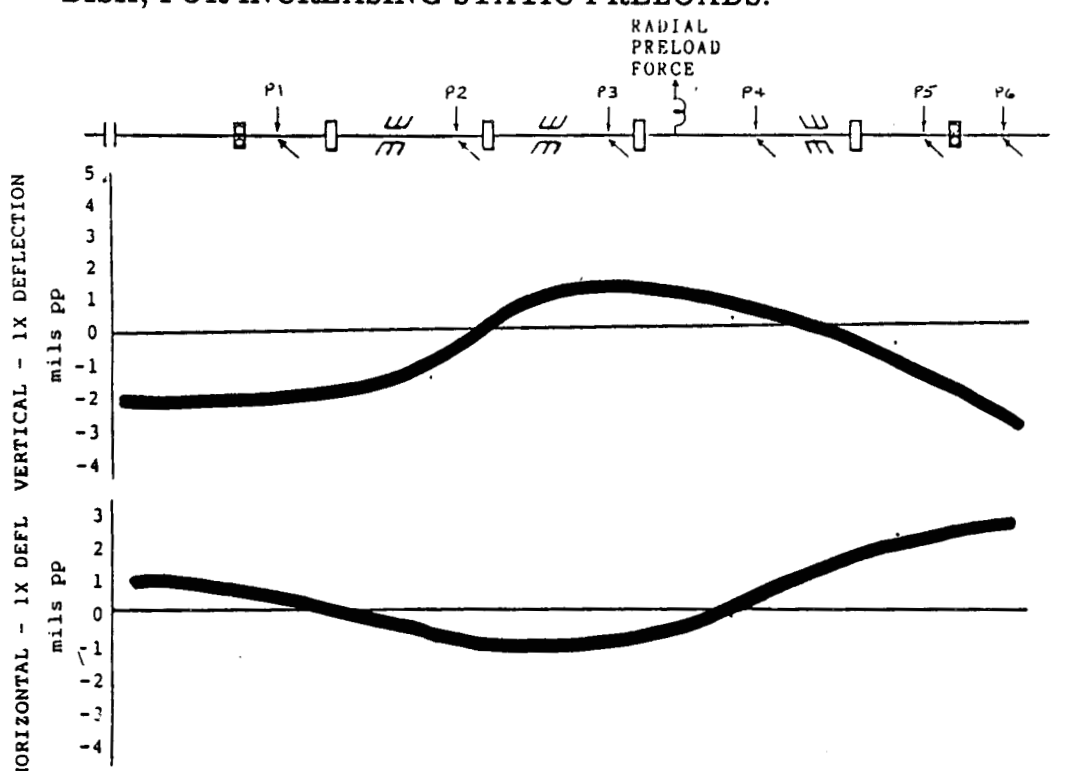

FIGURE 12.224 ROTOR MODE SHAPE AT 4000 RPM, 5.0 PSI SEAL OIL PRESSURE DUE TO 0.8 IN–GRAM UNBALANCE LOCATED IN THE THIRD PUMP IMPELLER DISK.

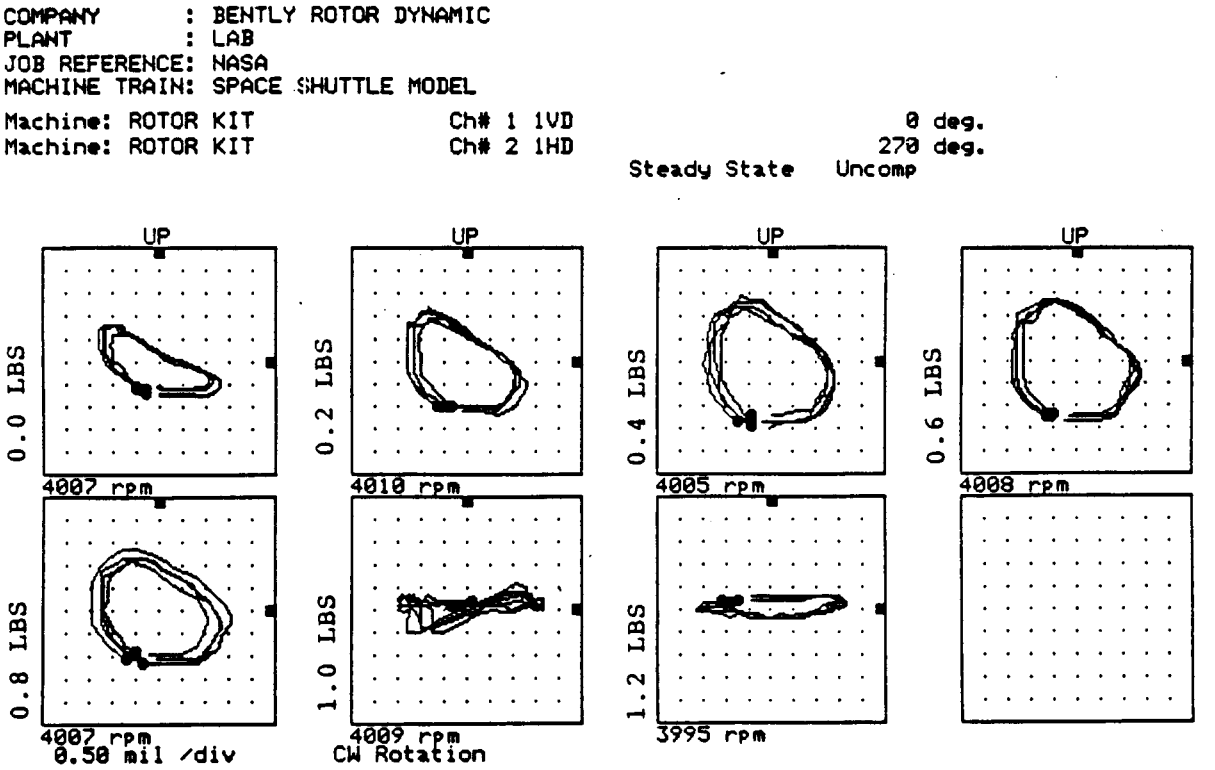

FIGURE 12.225 ORBITS AT PROBE LOCATION 1 AT 4000 RPM, 5.0 PSI SEAL OIL PRESSURE, 0.8 IN–GRAM UNBALANCE LOCATED IN THE THIRD PUMP IMPELLER DISK, FOR INCREASING STATIC PRELOAD FORCES.

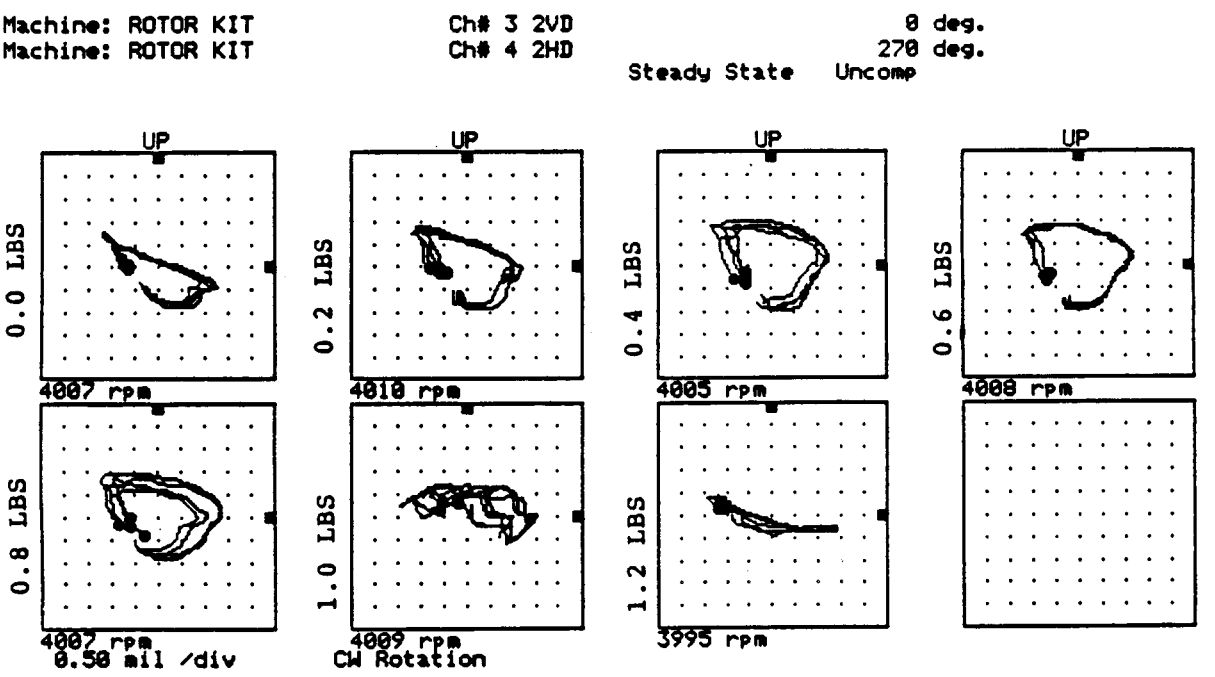

FIGURE 12.226 ORBITS AT PROBE LOCATION 2 AT 4000 RPM, 5.0 PSI SEAL OIL PRESSURE, 0.8 IN–GRAM UNBALANCE LOCATED IN THE THIRD PUMP IMPELLER DISK, FOR INCREASING STATIC PRELOAD FORCES.

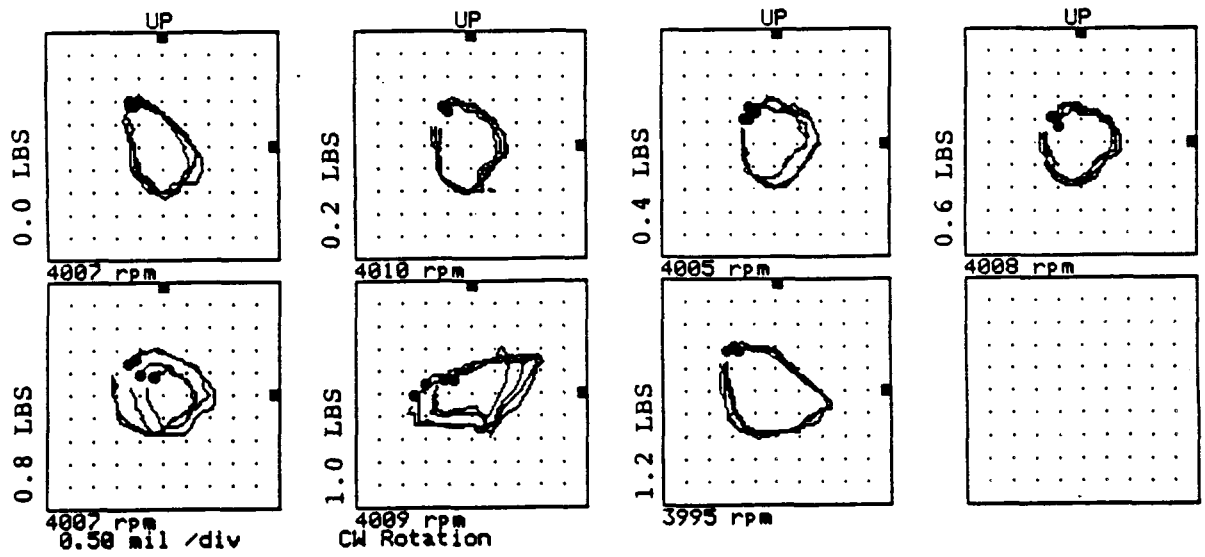

FIGURE 12.227 ORBITS AT PROBE LOCATION 3 AT 4000 RPM, 5.0 PSI SEAL OIL PRESSURE, 0.8 IN–GRAM UNBALANCE LOCATED IN THE THIRD PUMP IMPELLER DISK, FOR INCREASING STATIC PRELOAD FORCES.

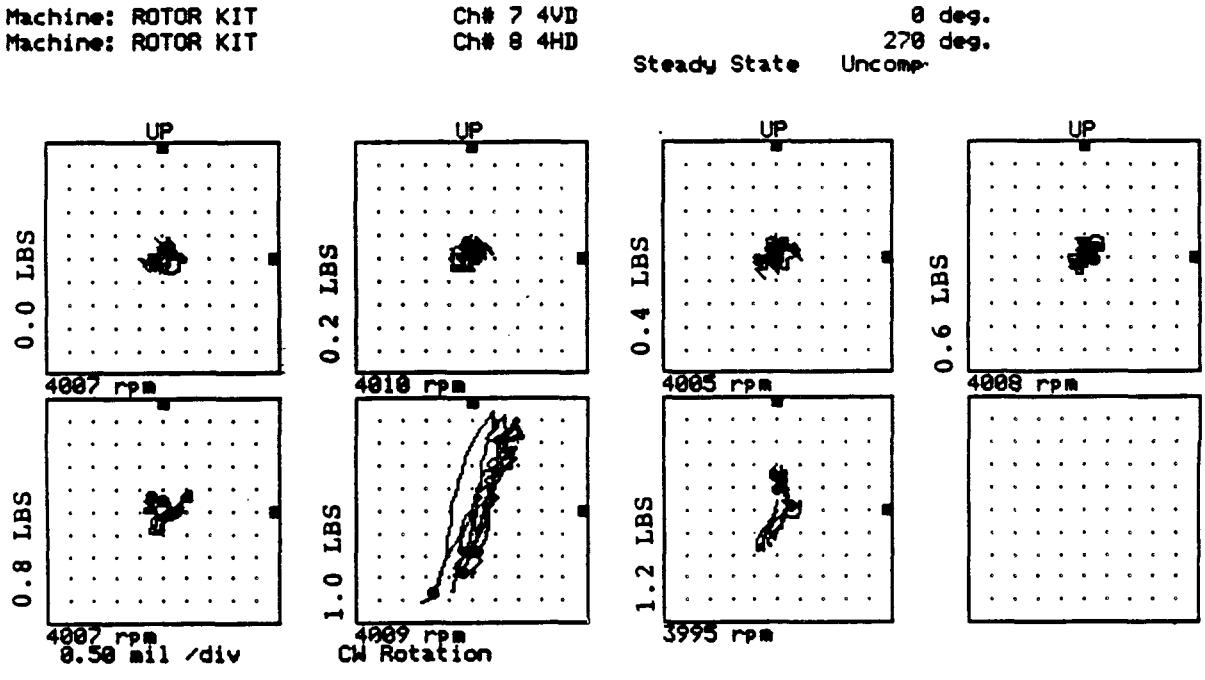

FIGURE 12.228 ORBITS AT PROBE LOCATION 4 AT 4000 RPM, 5.0 PSI SEAL OIL PRESSURE, 0.8 IN–GRAM UNBALANCE LOCATED IN THE THIRD PUMP IMPELLER DISK, FOR INCREASING STATIC PRELOAD FORCES.

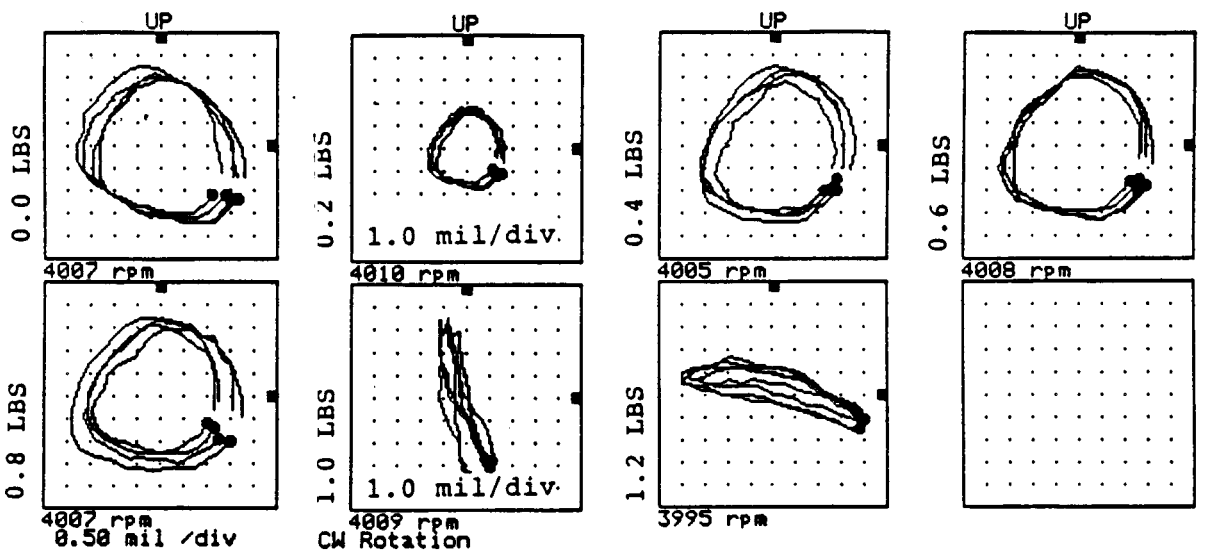

FIGURE 12.229 ORBITS AT PROBE LOCATION 5 AT 4000 RPM, 5.0 PSI SEAL OIL PRESSURE, 0.8 IN–GRAM UNBALANCE LOCATED IN THE THIRD PUMP IMPELLER DISK, FOR INCREASING STATIC PRELOAD FORCES.

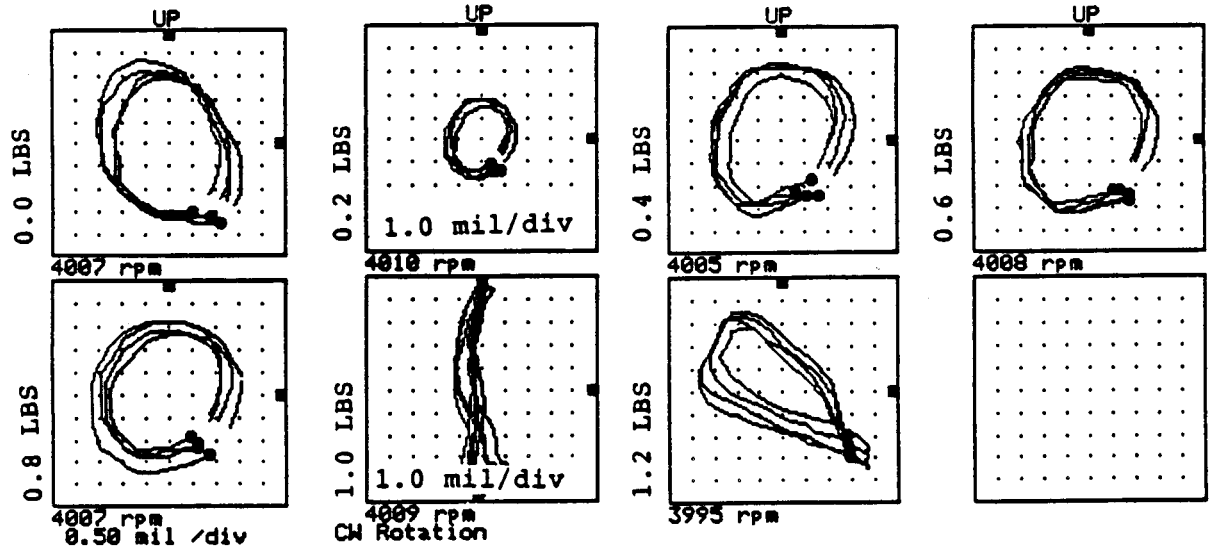

FIGURE 12.230 ORBITS AT PROBE LOCATION 6 AT 4000 RPM, 5.0 PSI SEAL OIL PRESSURE, 0.8 IN–GRAM UNBALANCE LOCATED IN THE THIRD PUMP IMPELLER DISK, FOR INCREASING STATIC PRELOAD FORCES.

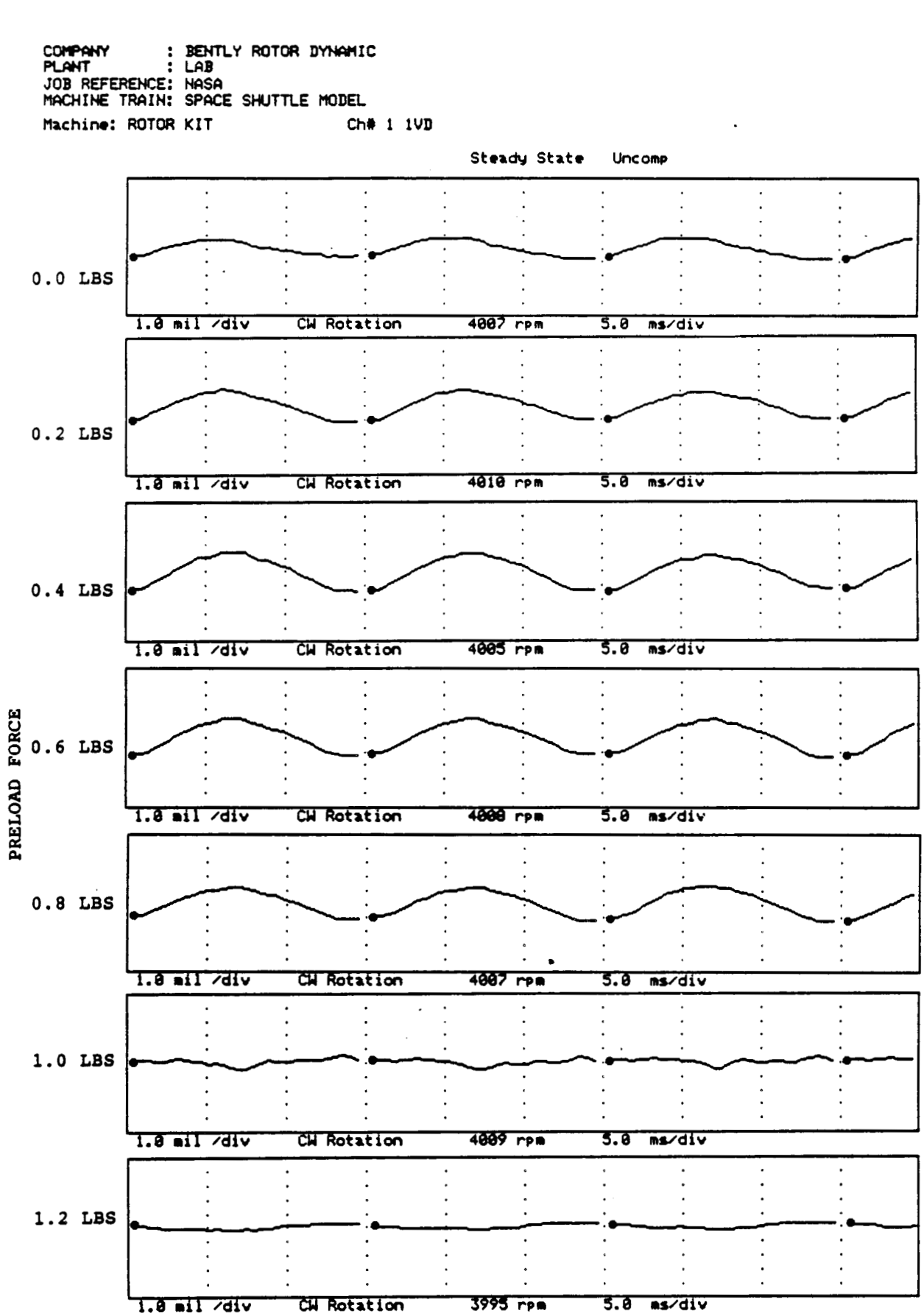

FIGURE 12.231 TIMEBASE FOR VERTICAL PROBE AT LOCATION 1 AT 4000 RPM, 5.0 PSI SEAL OIL PRESSURE, 0.8 IN–GRAM UNBALANCE LOCATED IN THE THIRD PUMP IMPELLER DISK, FOR INCREASING STATIC PRELOADS.

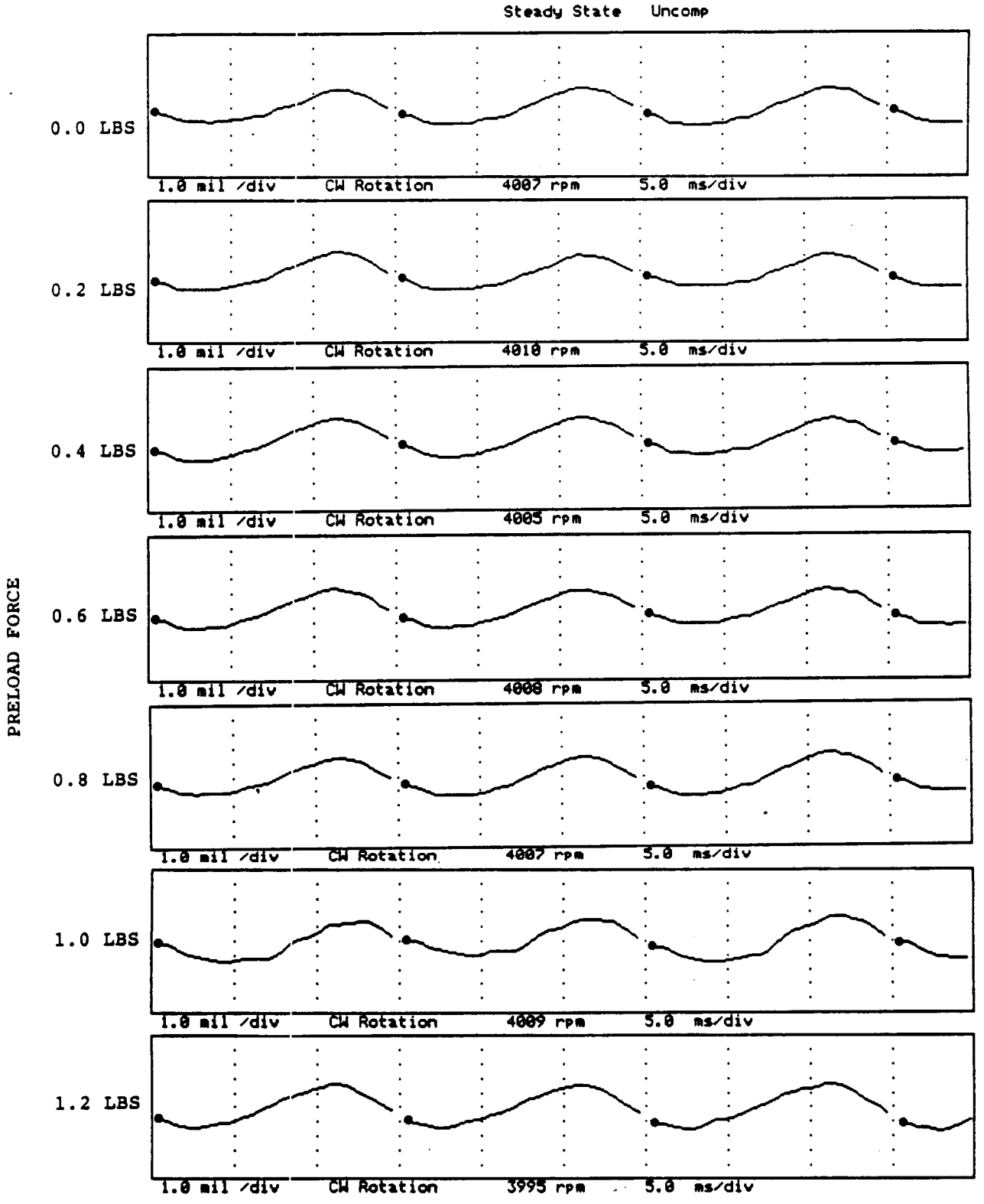

FIGURE 12.232 TIMEBASE FOR HORIZONTAL PROBE AT LOCATION 1 AT 4000 RPM, 5.0 PSI SEAL OIL PRESSURE, 0.8 IN–GRAM UNBALANCE LOCATED IN THE THIRD PUMP IMPELLER DISK, FOR INCREASING STATIC PRELOADS.

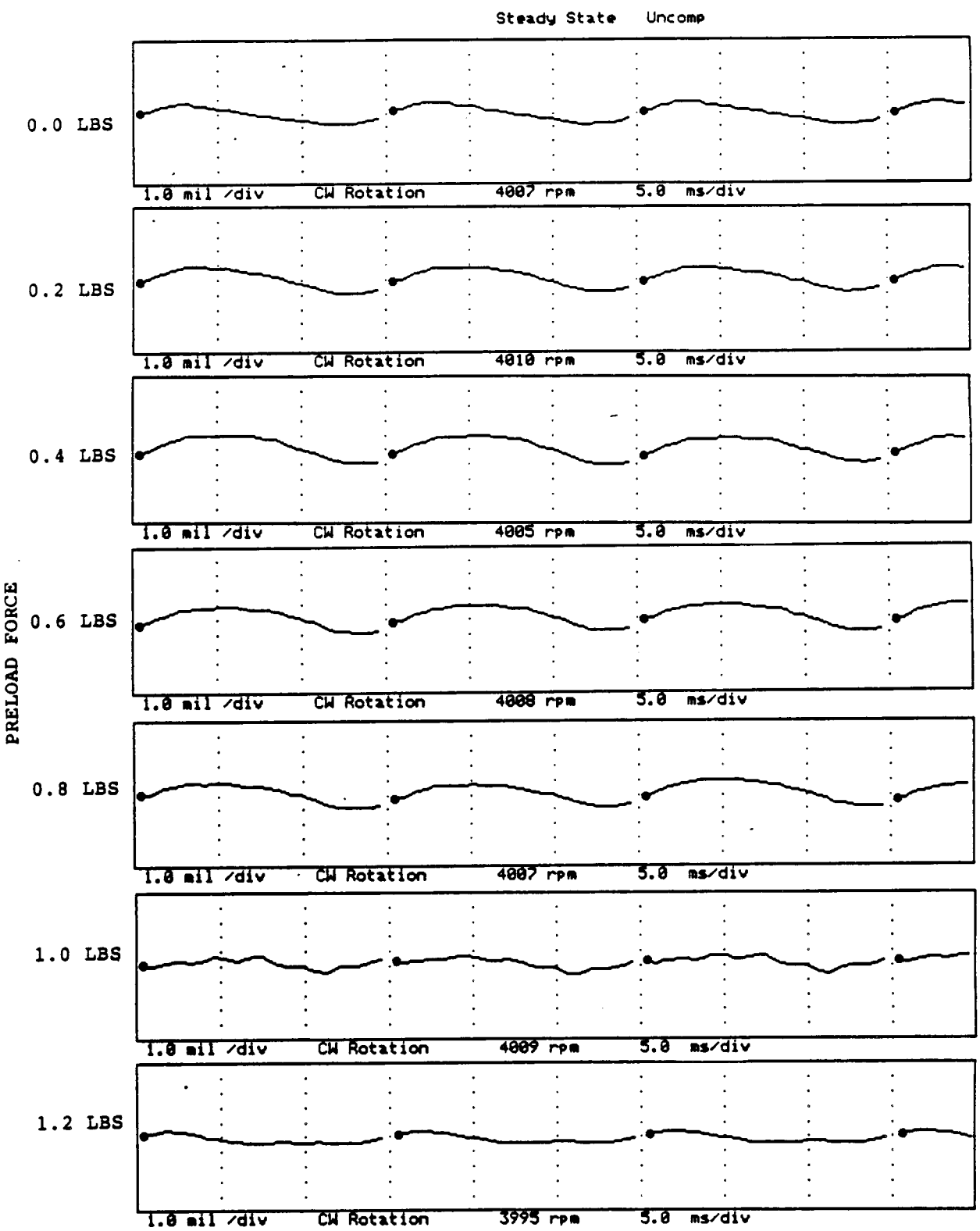

FIGURE 12.233 TIMEBASE FOR VERTICAL PROBE AT LOCATION 2 AT 4000 RPM, 5.0 PSI SEAL OIL PRESSURE, 0.8 IN–GRAM UNBALANCE LOCATED IN THE THIRD PUMP IMPELLER DISK, FOR INCREASING STATIC PRELOADS.

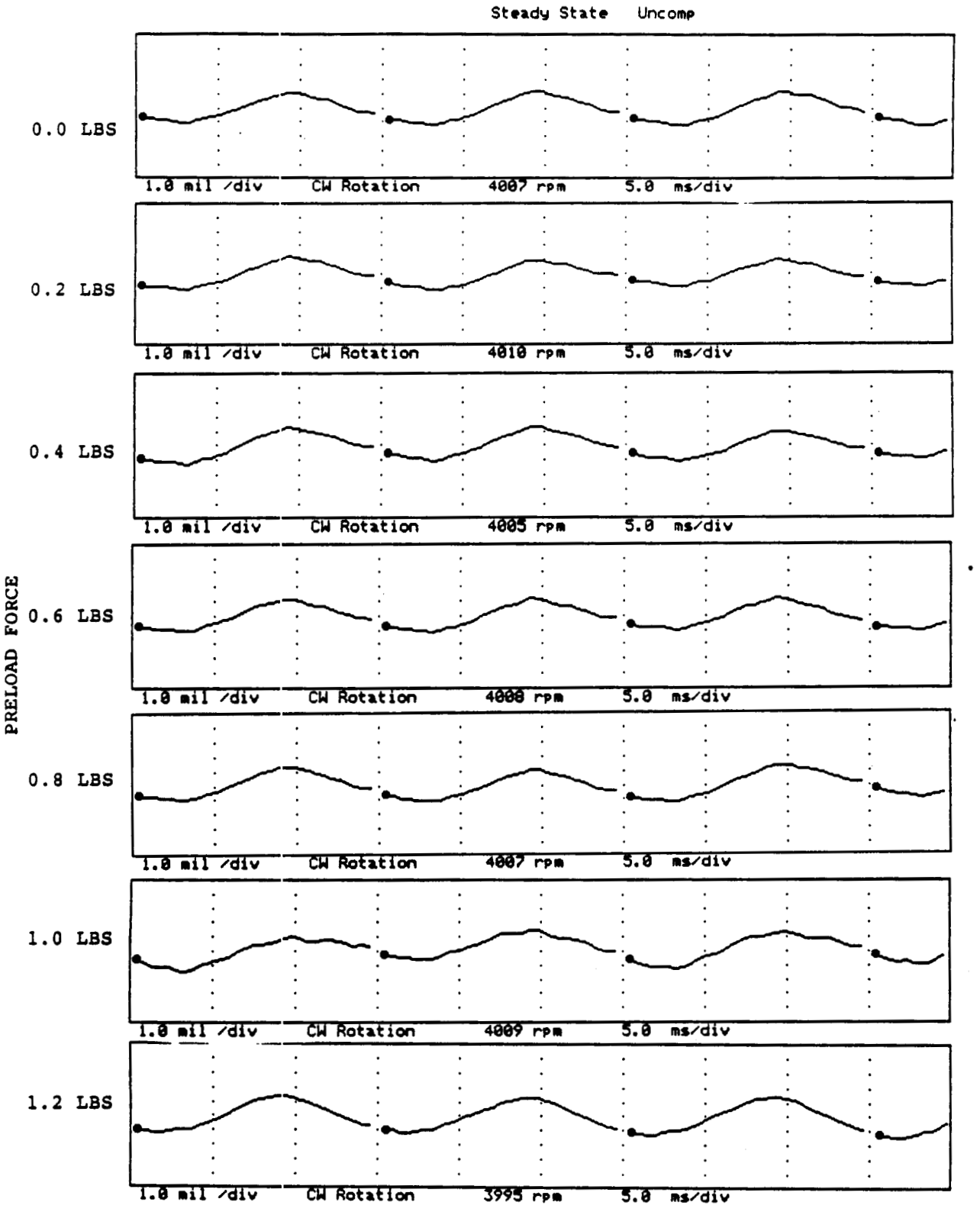

FIGURE 12.234 TIMEBASE FOR HORIZONTAL PROBE AT LOCATION 2 AT 4000 RPM, 5.0 PSI SEAL OIL PRESSURE, 0.8 IN–GRAM UNBALANCE LOCATED IN THE THIRD PUMP IMPELLER DISK, FOR INCREASING STATIC PRELOADS.

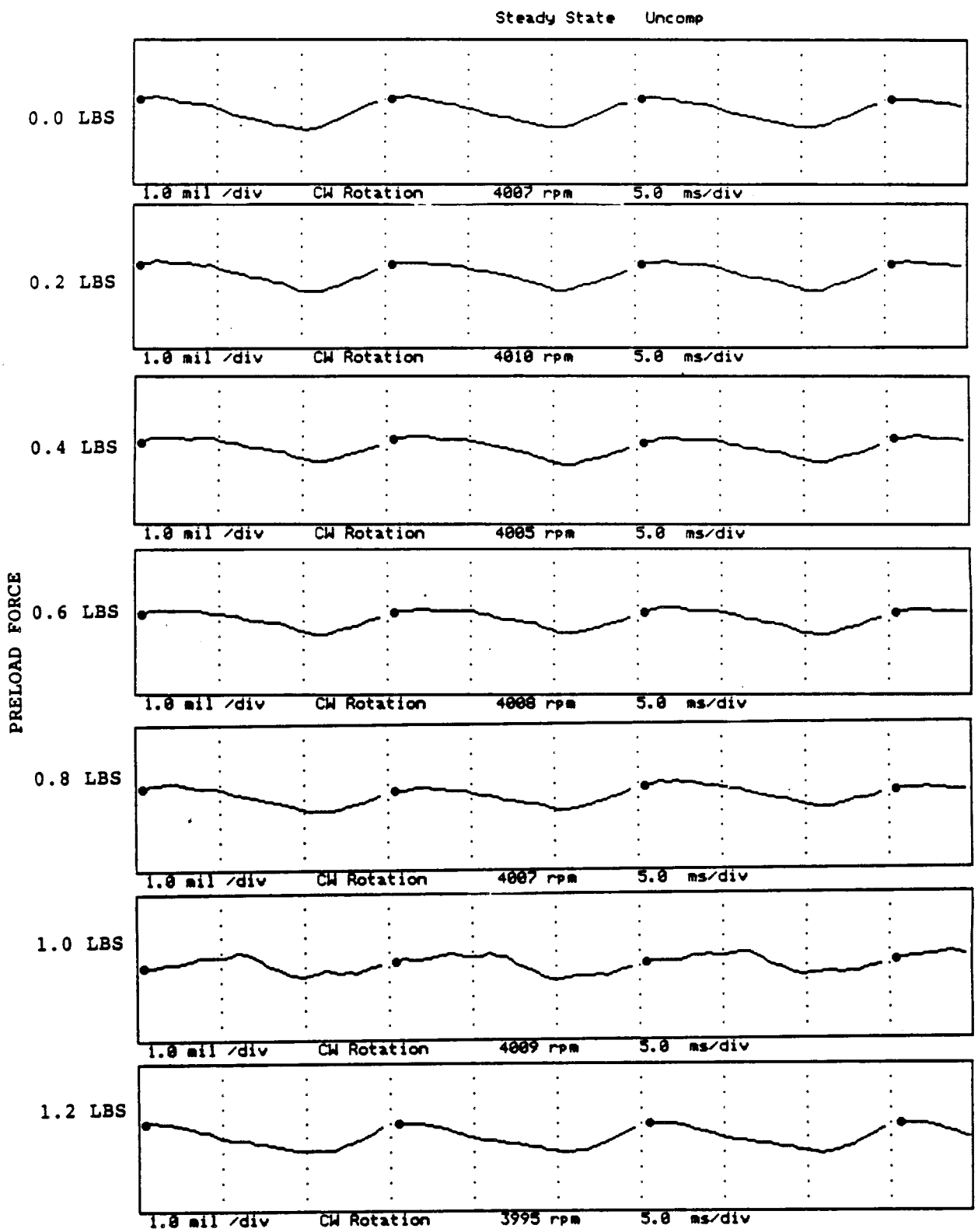

FIGURE 12.235 TIMEBASE FOR VERTICAL PROBE AT LOCATION 3 AT 4000 RPM, 5.0 PSI SEAL OIL PRESSURE, 0.8 IN–GRAM UNBALANCE LOCATED IN THE THIRD PUMP IMPELLER DISK, FOR INCREASING STATIC PRELOADS.

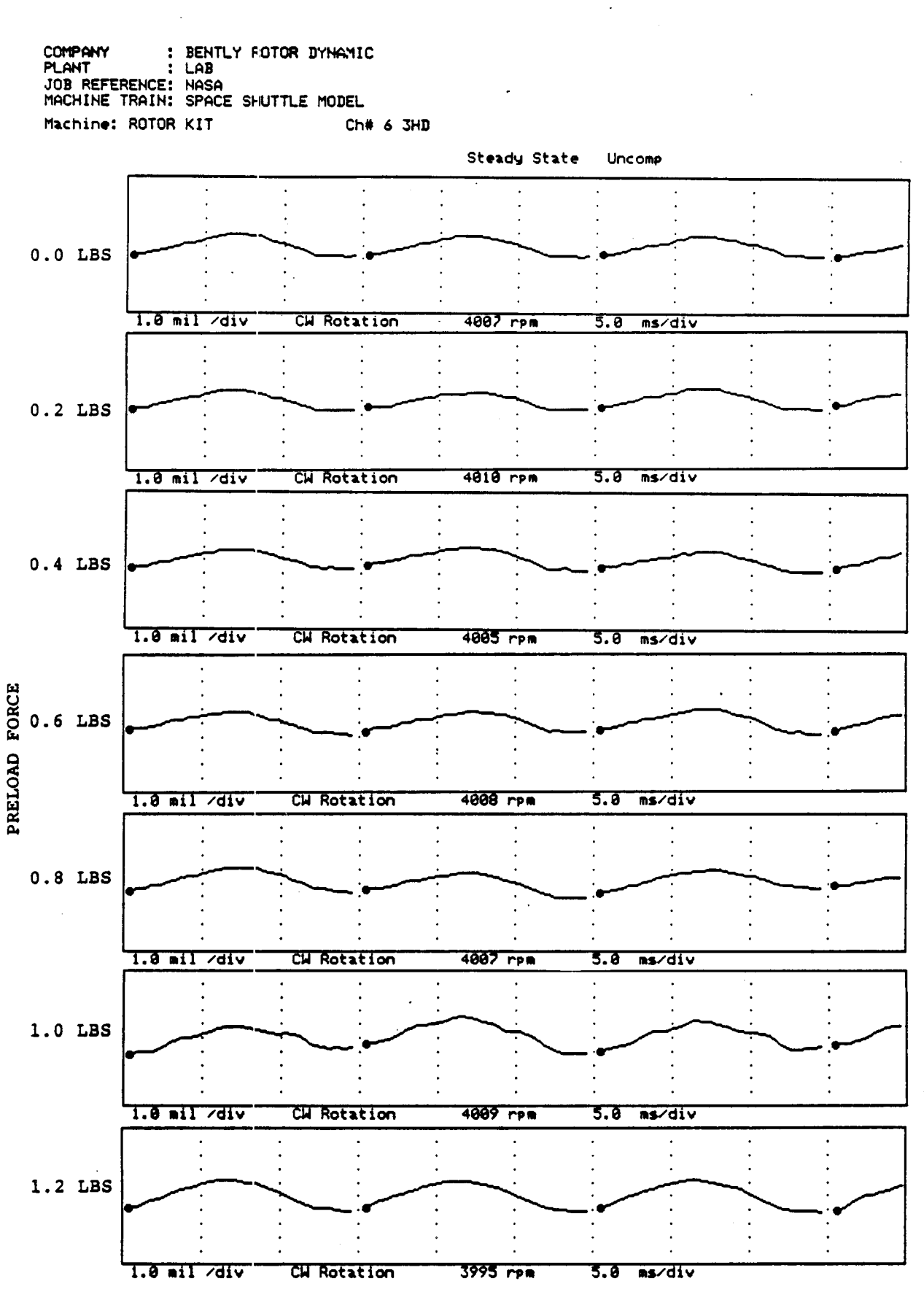

FIGURE 12.236 TIMEBASE FOR HORIZONTAL PROBE AT LOCATION 3 AT 4000 RPM, 5.0 PSI SEAL OIL PRESSURE, 0.8 IN–GRAM UNBALANCE LOCATED IN THE THIRD PUMP IMPELLER DISK, FOR INCREASING STATIC PRELOADS.

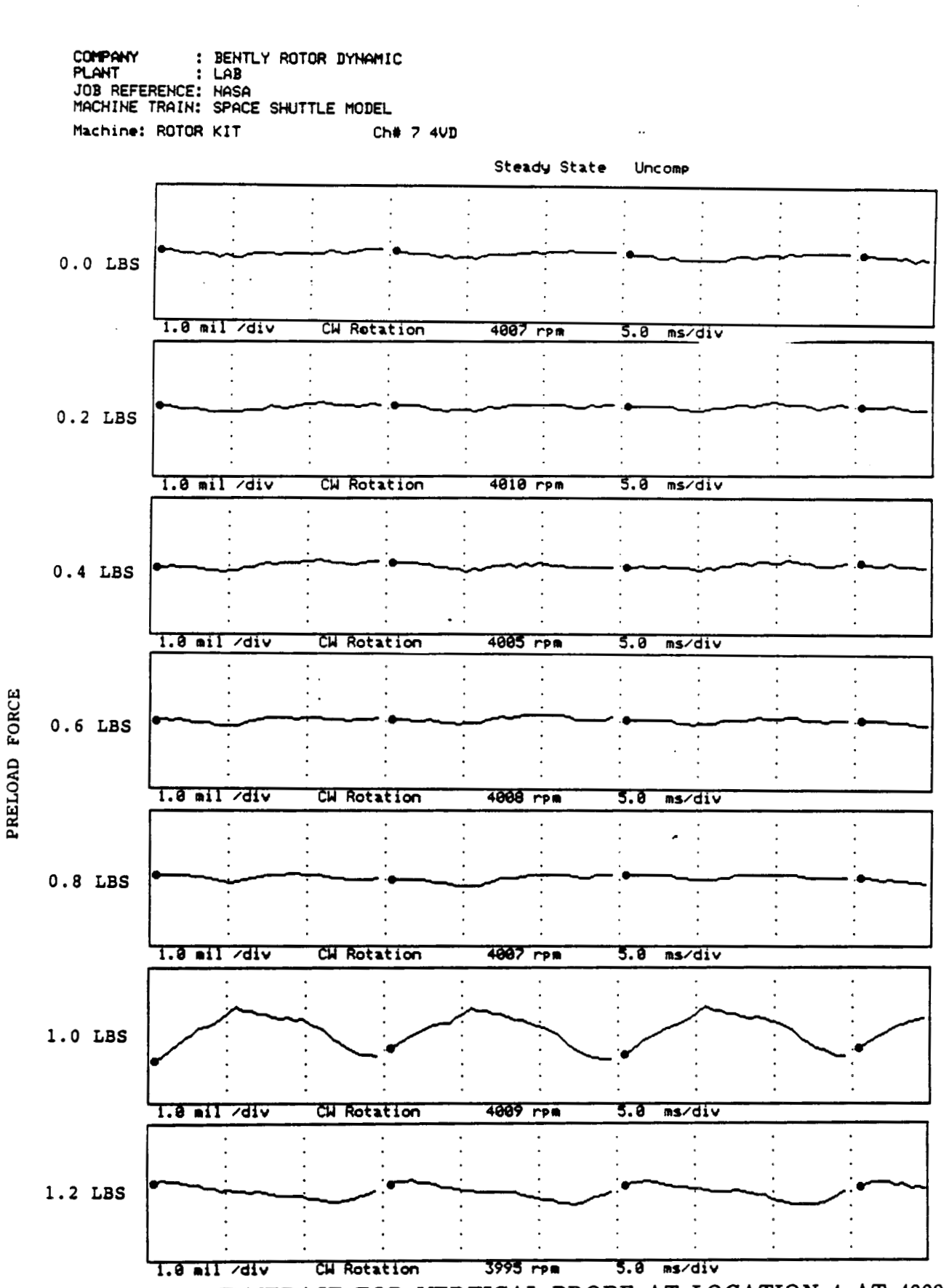

FIGURE 12.237 TIMEBASE FOR VERTICAL PROBE AT LOCATION 4 AT 4000 RPM, 5.0 PSI SEAL OIL PRESSURE, 0.8 IN–GRAM UNBALANCE LOCATED IN THE THIRD PUMP IMPELLER DISK, FOR INCREASING STATIC PRELOADS.

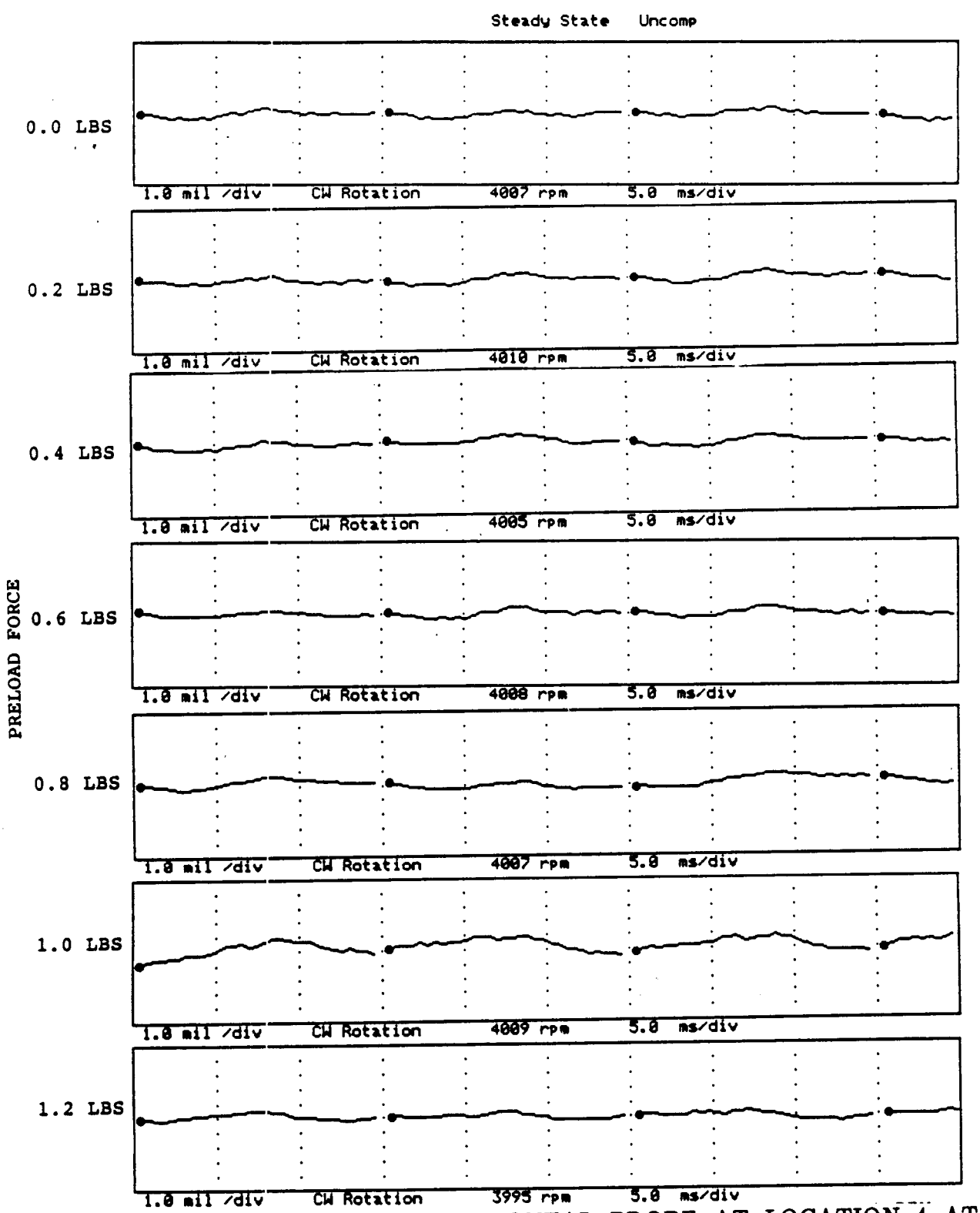

FIGURE 12.238 TIMEBASE FOR HORIZONTAL PROBE AT LOCATION 4 AT 4000 RPM, 5.0 PSI SEAL OIL PRESSURE, 0.8 IN–GRAM UNBALANCE LOCATED IN THE THIRD PUMP IMPELLER DISK, FOR INCREASING STATIC PRELOADS.

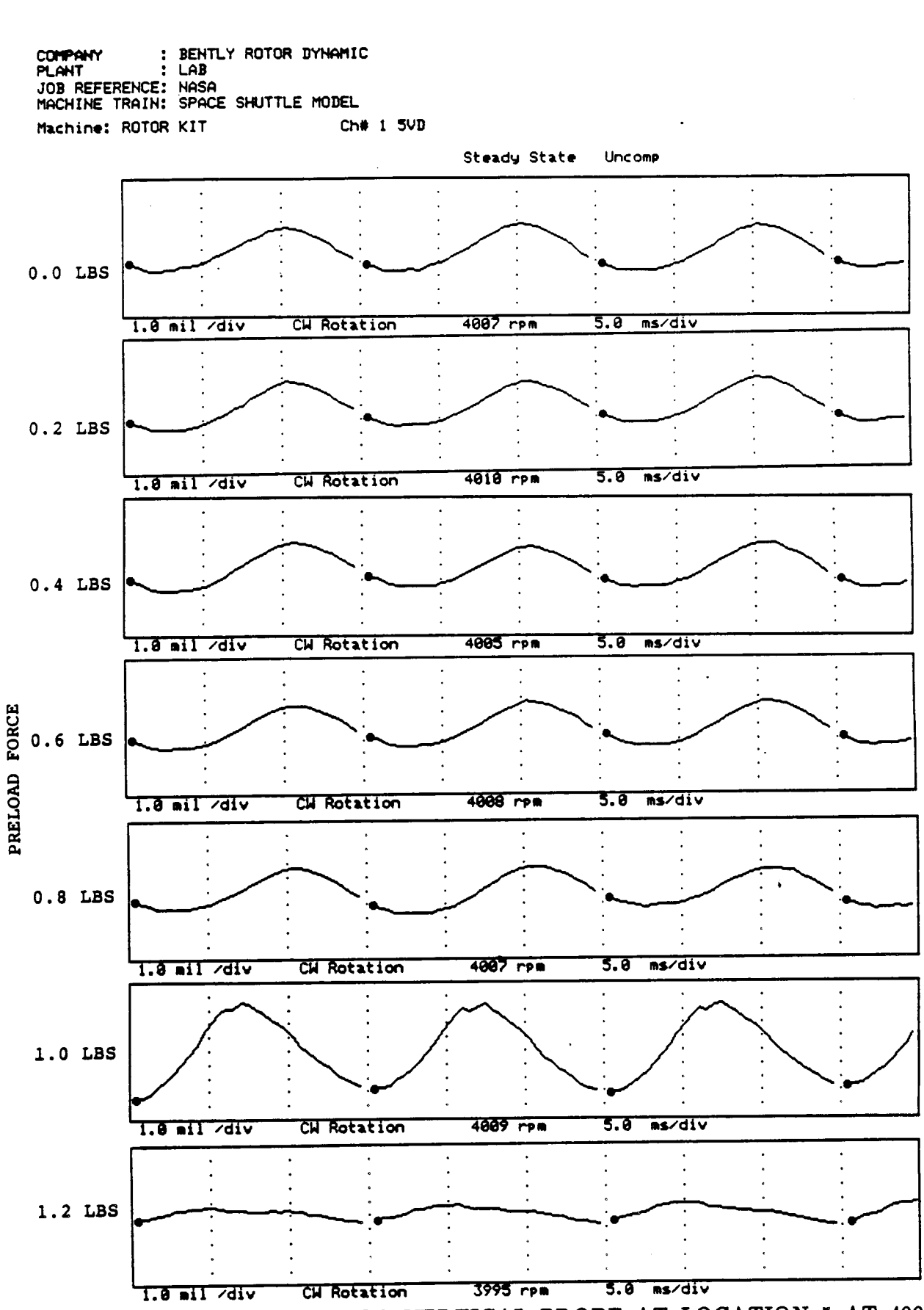

FIGURE 12.239 TIMEBASE FOR VERTICAL PROBE AT LOCATION 5 AT 4000 RPM, 5.0 PSI SEAL OIL PRESSURE, 0.8 IN–GRAM UNBALANCE LOCATED IN THE THIRD PUMP IMPELLER DISK, FOR INCREASING STATIC PRELOADS.

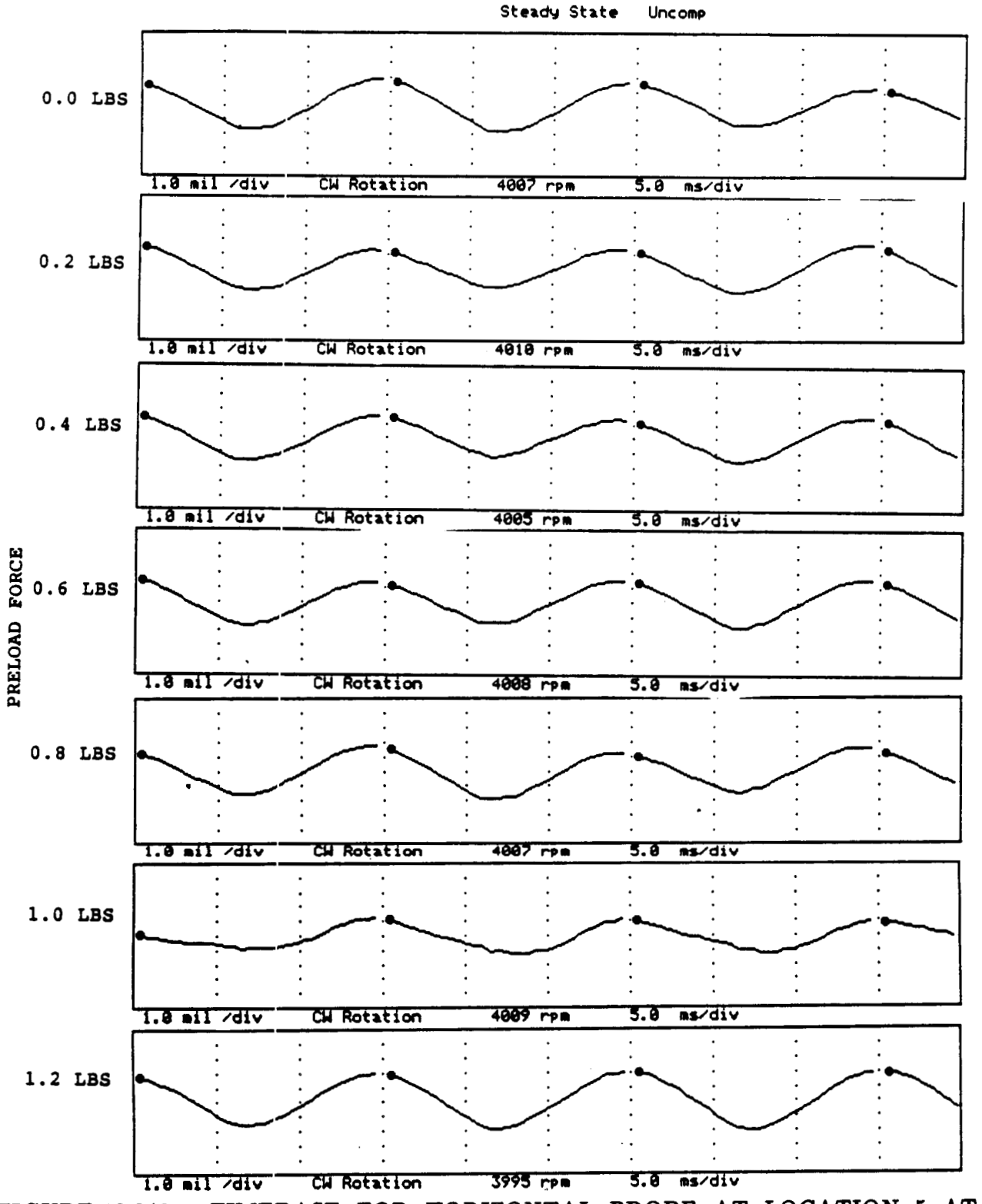

FIGURE 12.240 TIMEBASE FOR HORIZONTAL PROBE AT LOCATION 5 AT 4000 RPM, 5.0 PSI SEAL OIL PRESSURE, 0.8 IN–GRAM UNBALANCE LOCATED IN THE THIRD PUMP IMPELLER DISK, FOR INCREASING STATIC PRELOADS.

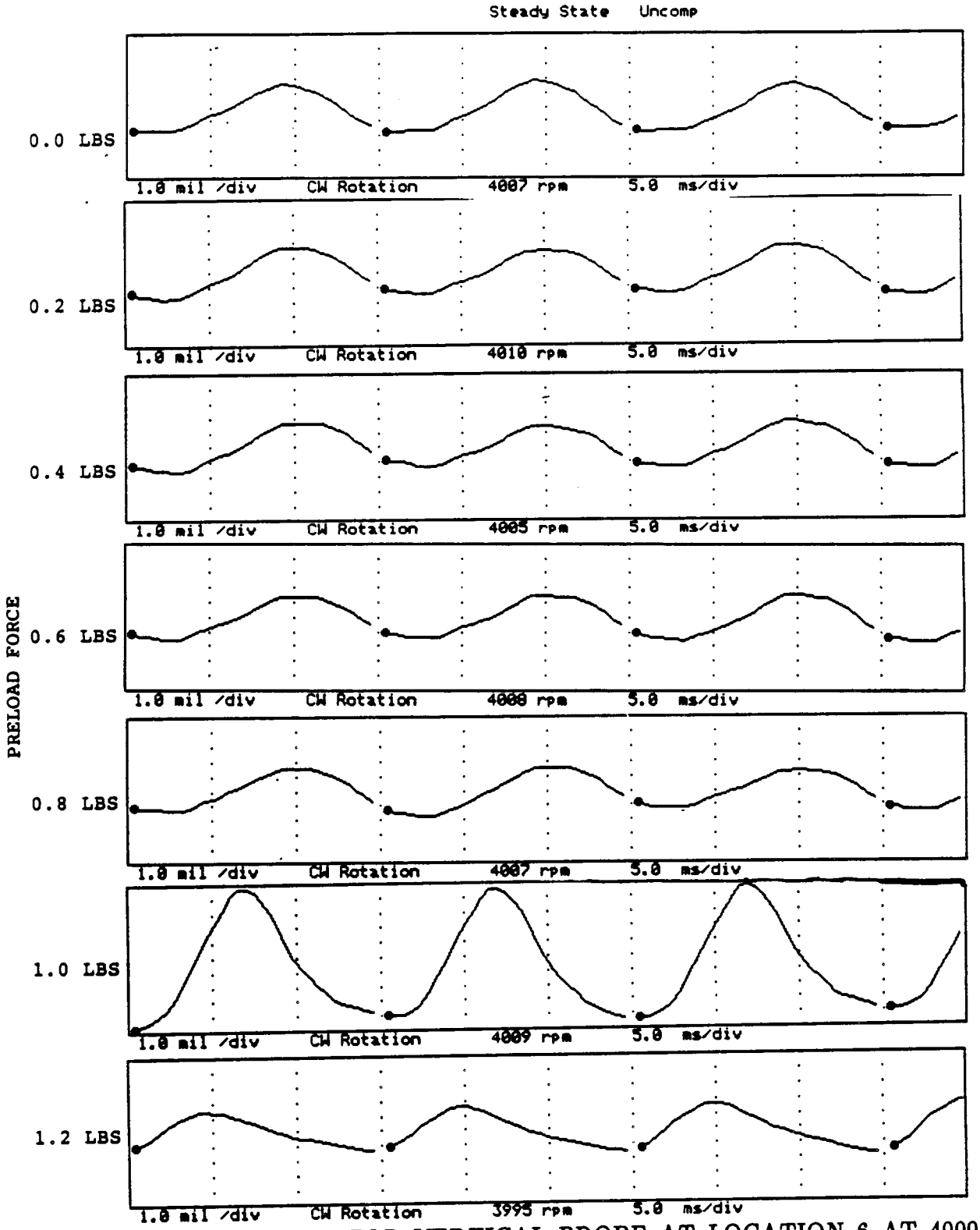

FIGURE 12.241 TIMEBASE FOR VERTICAL PROBE AT LOCATION 6 AT 4000 RPM, 5.0 PSI SEAL OIL PRESSURE, 0.8 IN–GRAM UNBALANCE LOCATED IN THE THIRD PUMP IMPELLER DISK, FOR INCREASING STATIC PRELOADS.

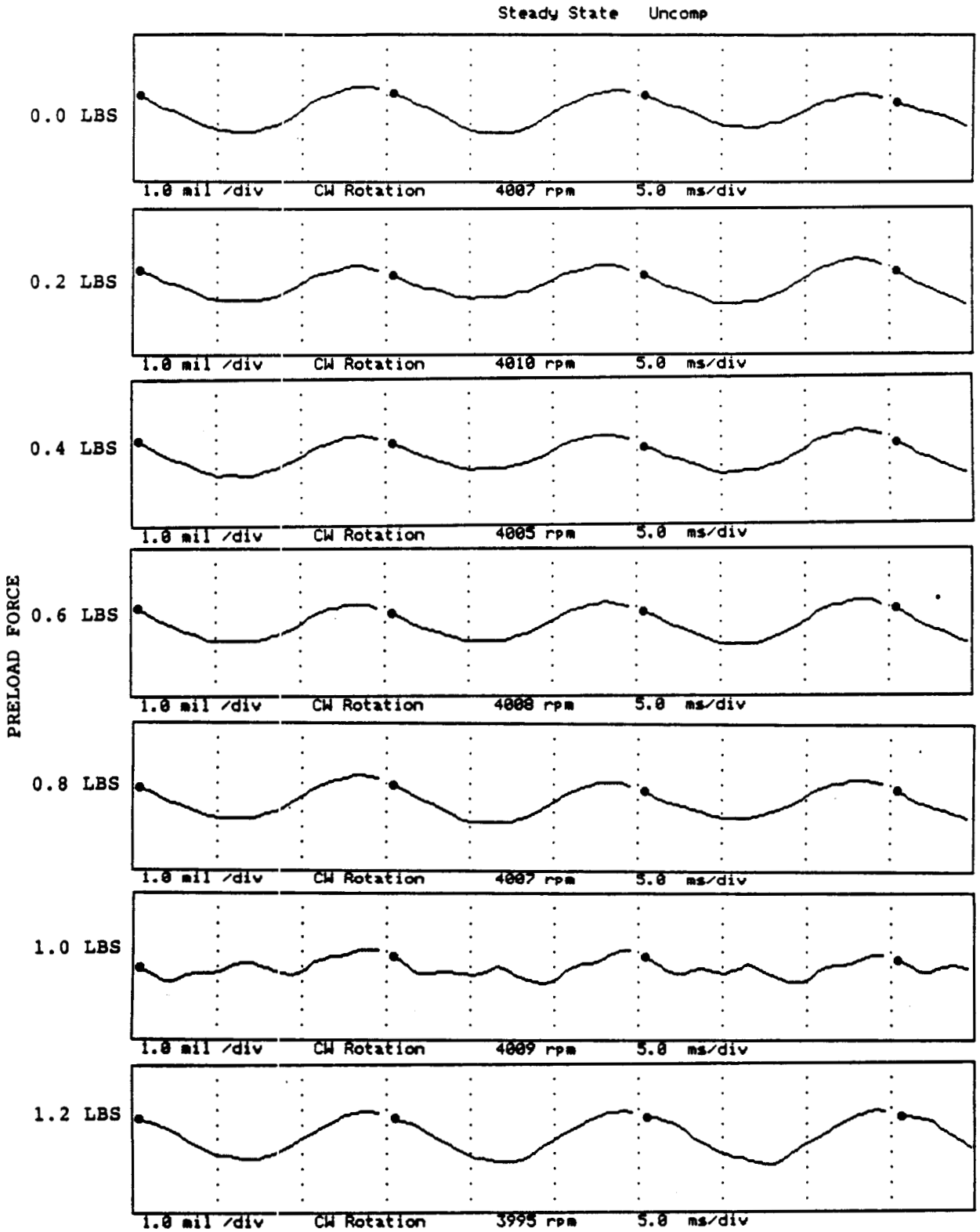

FIGURE 12.242 TIMEBASE FOR HORIZONTAL PROBE AT LOCATION 6 AT 4000 RPM, 5.0 PSI SEAL OIL PRESSURE, 0.8 IN–GRAM UNBALANCE LOCATED IN THE THIRD PUMP IMPELLER DISK, FOR INCREASING STATIC PRELOADS.

NOT AVAILABLE - OIL IN THE CLEARANCE AREA PROHIBITS THE METAL-TO-METAL CONTACT NECESSARY FOR THE CONTACT SENSOR TO OPERATE CORRECTLY.

FIGURE 12.243 TIMEBASE FOR SHAFT TO SEAL 1 CONTACT AT 4000 RPM, 5.0 PSI SEAL OIL PRESSURE, 0.8 IN–GRAM UNBALANCE LOCATED IN THE THIRD PUMP IMPELLER DISK, FOR INCREASING STATIC PRELOADS.

NOT AVAILABLE - OIL IN THE CLEARANCE AREA PROHIBITS THE METAL-TO-METAL CONTACT NECESSARY FOR THE CONTACT SENSOR TO OPERATE CORRECTLY.

FIGURE 12.244 TIMEBASE FOR SHAFT TO SEAL 2 CONTACT AT 4000 RPM, 5.0 PSI SEAL OIL PRESSURE, 0.8 IN–GRAM UNBALANCE LOCATED IN THE THIRD PUMP IMPELLER DISK, FOR INCREASING STATIC PRELOADS.

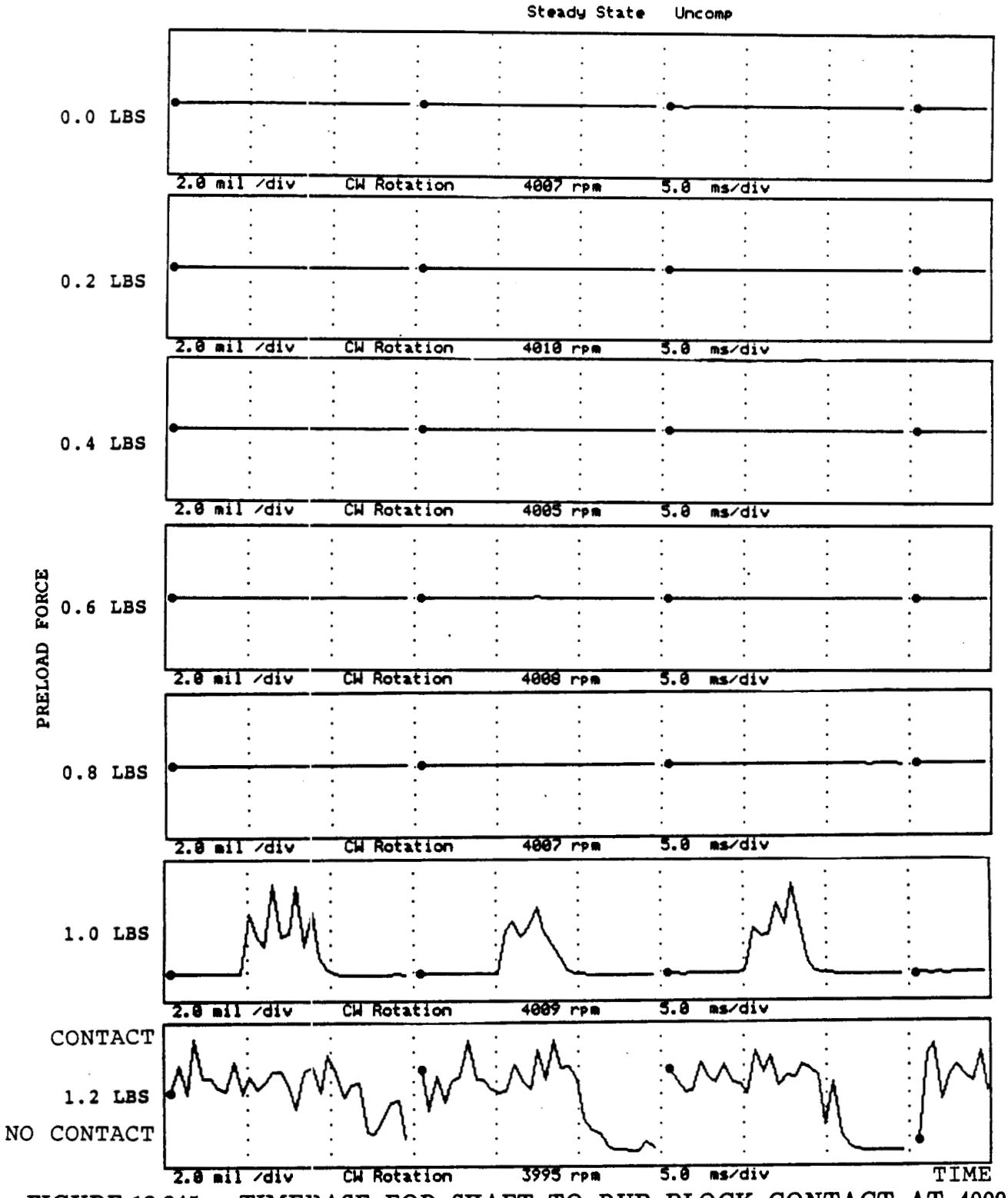

FIGURE 12.245 TIMEBASE FOR SHAFT TO RUB BLOCK CONTACT AT 4000 RPM, 5.0 PSI SEAL OIL PRESSURE, 0.8 IN–GRAM UNBALANCE LOCATED IN THE THIRD PUMP IMPELLER DISK, FOR INCREASING STATIC PRELOADS.

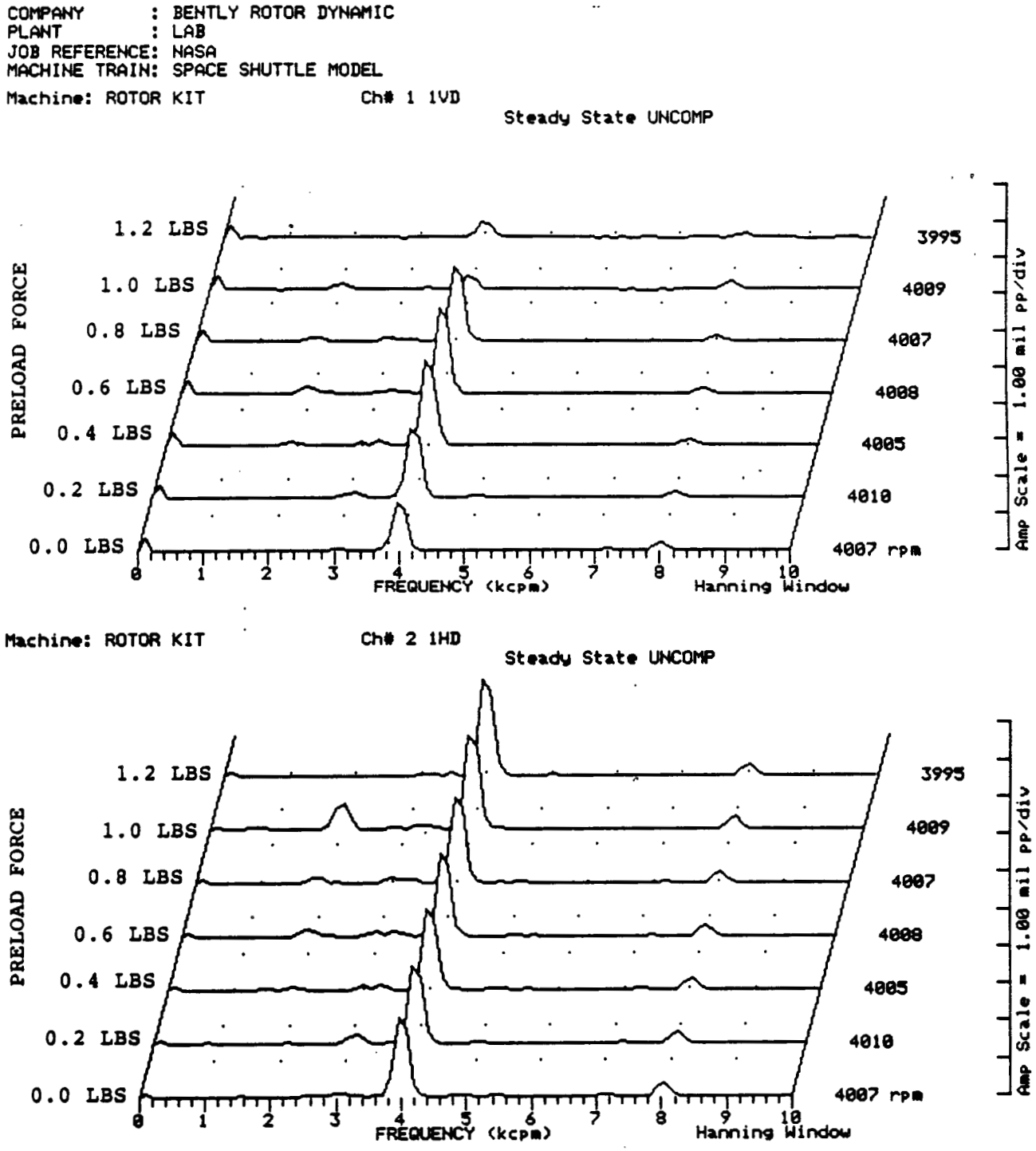

FIGURE 12.246 SPECTRAL CONTENT AT PROBE LOCATION 1 AT 4000 RPM, 5.0 PSI SEAL OIL PRESSURE, 0.8 IN–GRAM UNBALANCE LOCATED IN THE THIRD PUMP IMPELLER DISK, FOR INCREASING STATIC PRELOAD.

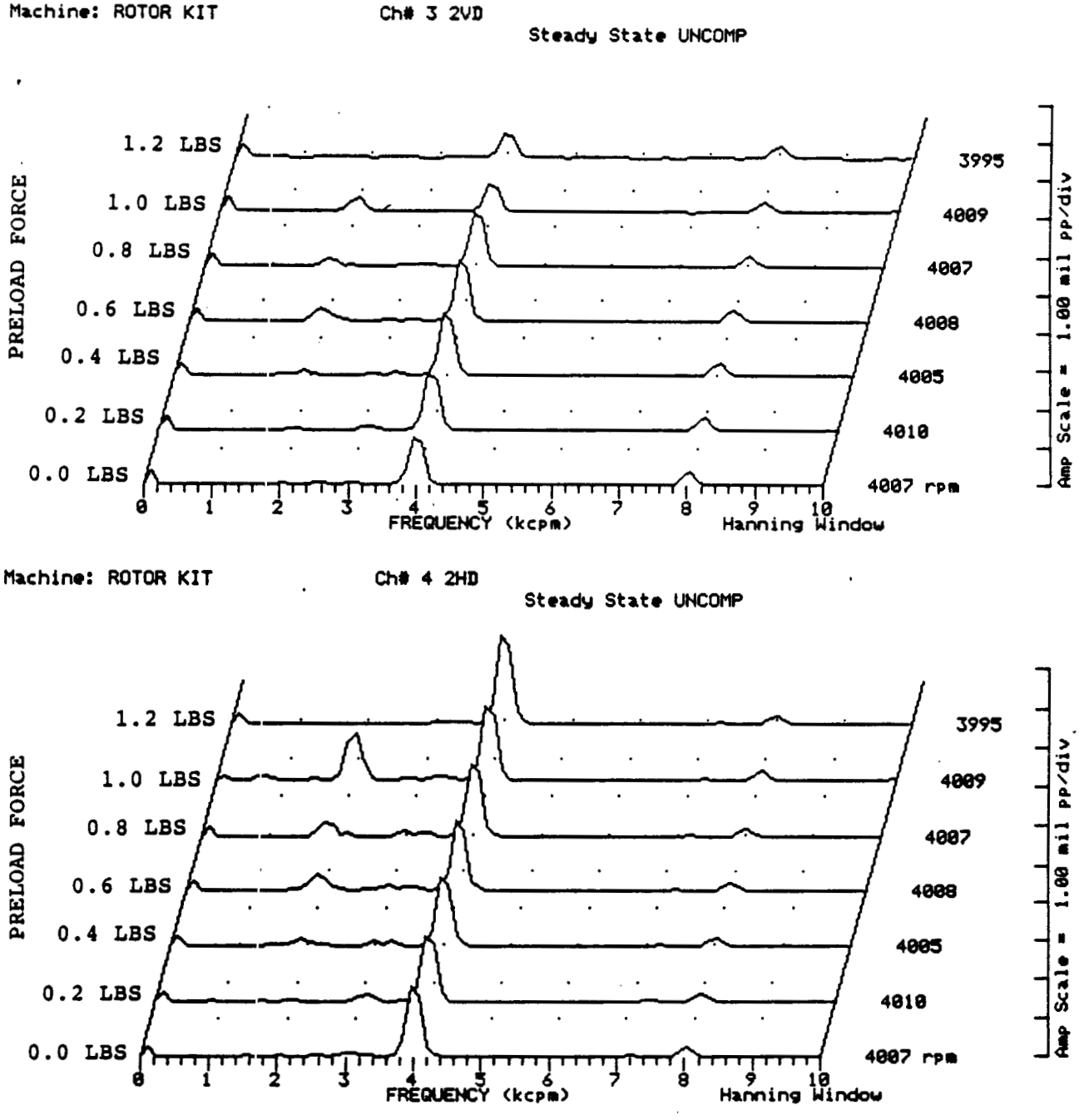

FIGURE 12.247 SPECTRAL CONTENT AT PROBE LOCATION 2 AT 4000 RPM, 5.0 PSI SEAL OIL PRESSURE, 0.8 IN–GRAM UNBALANCE LOCATED IN THE THIRD PUMP IMPELLER DISK, FOR INCREASING STATIC PRELOADS.

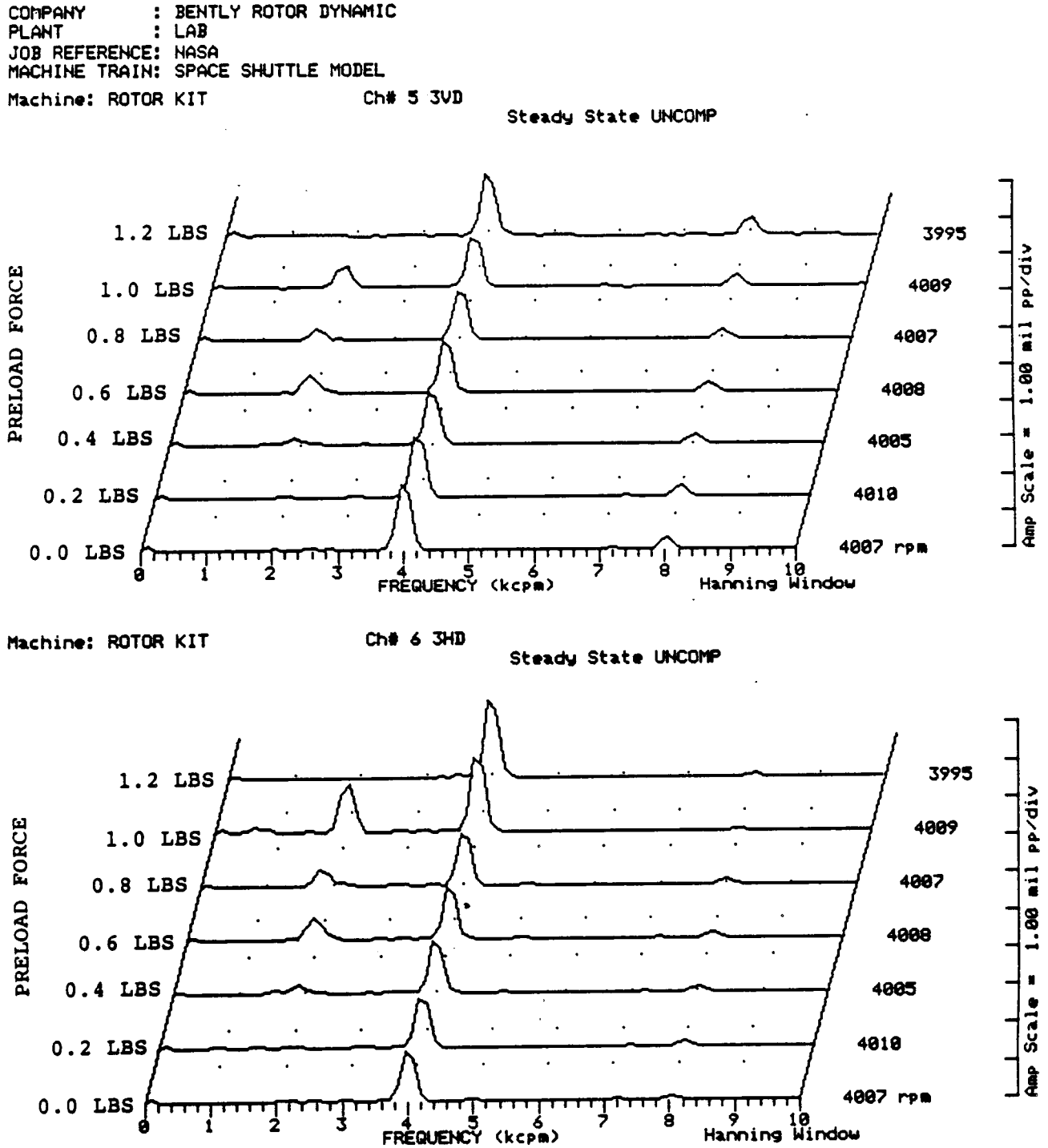

FIGURE 12.248 SPECTRAL CONTENT AT PROBE LOCATION 3 AT 4000 RPM, 5.0 PSI SEAL OIL PRESSURE, 0.8 IN–GRAM UNBALANCE LOCATED IN THE THIRD PUMP IMPELLER DISK, FOR INCREASING STATIC PRELOADS.

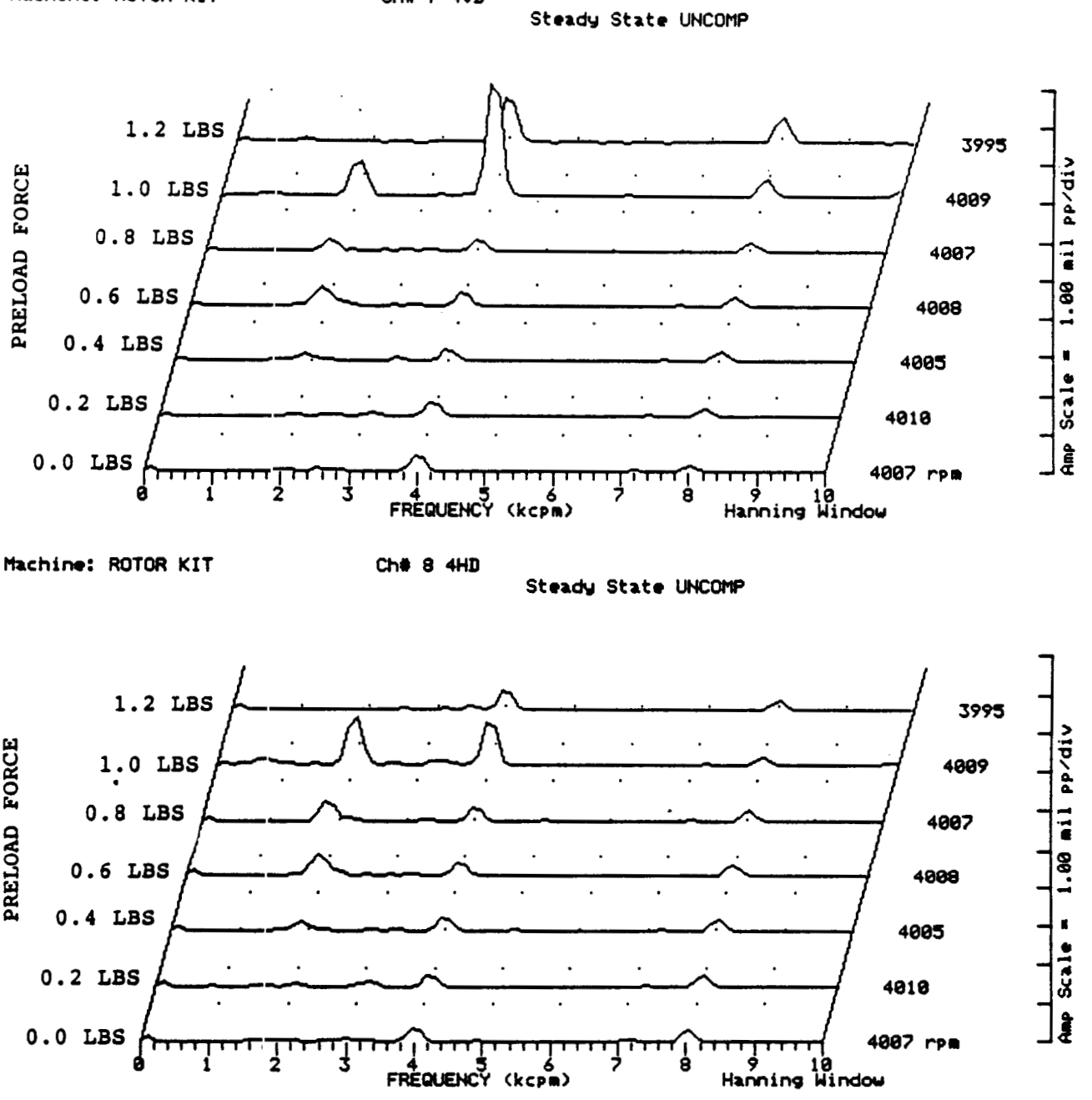

FIGURE 12.249 SPECTRAL CONTENT AT PROBE LOCATION 4 AT 4000 RPM, 5.0 PSI SEAL OIL PRESSURE, 0.8 IN–GRAM UNBALANCE LOCATED IN THE THIRD PUMP IMPELLER DISK, FOR INCREASING STATIC PRELOADS.

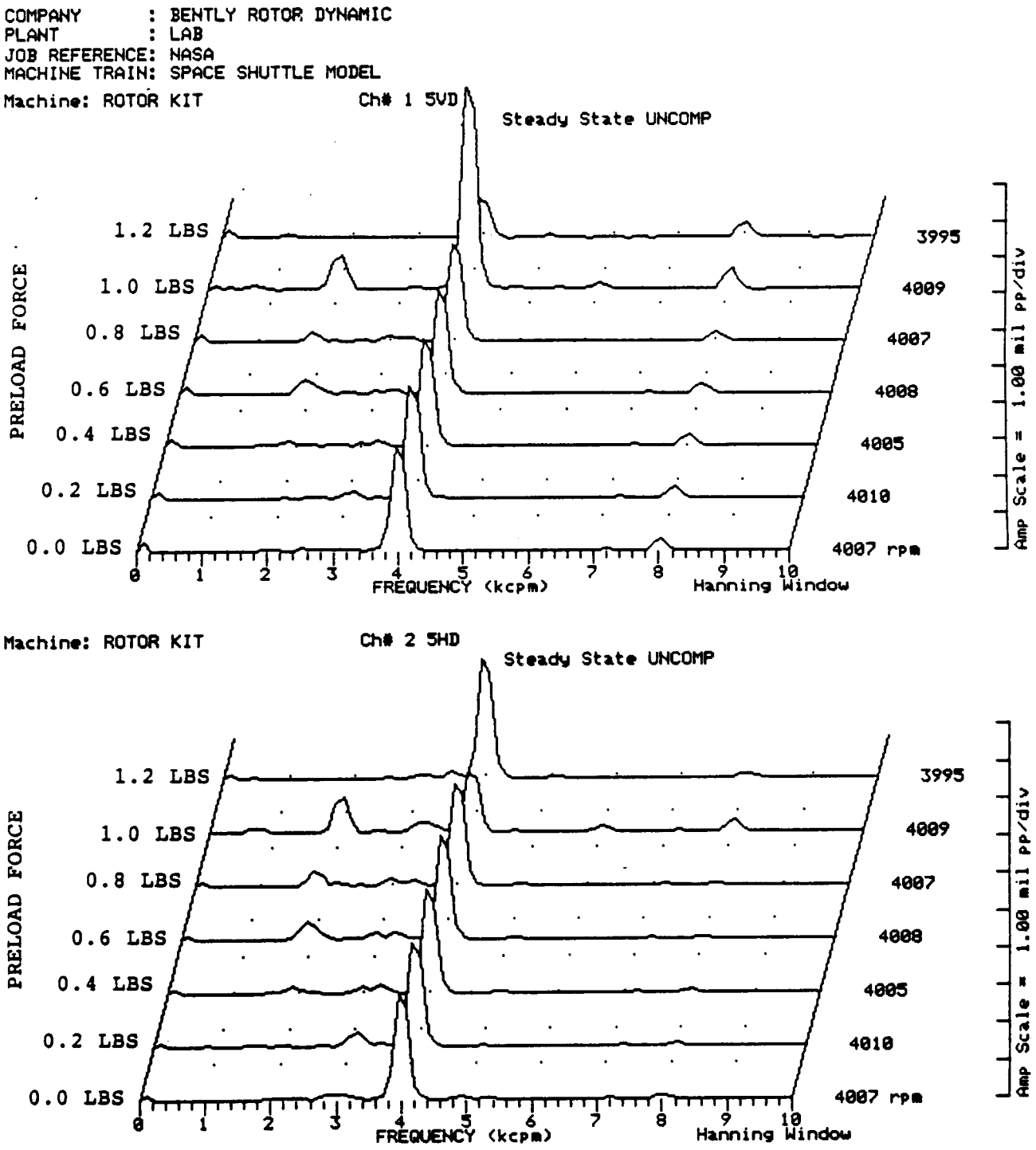

FIGURE 12.250 SPECTRAL CONTENT AT PROBE LOCATION 5 AT 4000 RPM, 5.0 PSI SEAL OIL PRESSURE, 0.8 IN–GRAM UNBALANCE LOCATED IN THE THIRD PUMP IMPELLER DISK, FOR INCREASING STATIC PRELOADS.

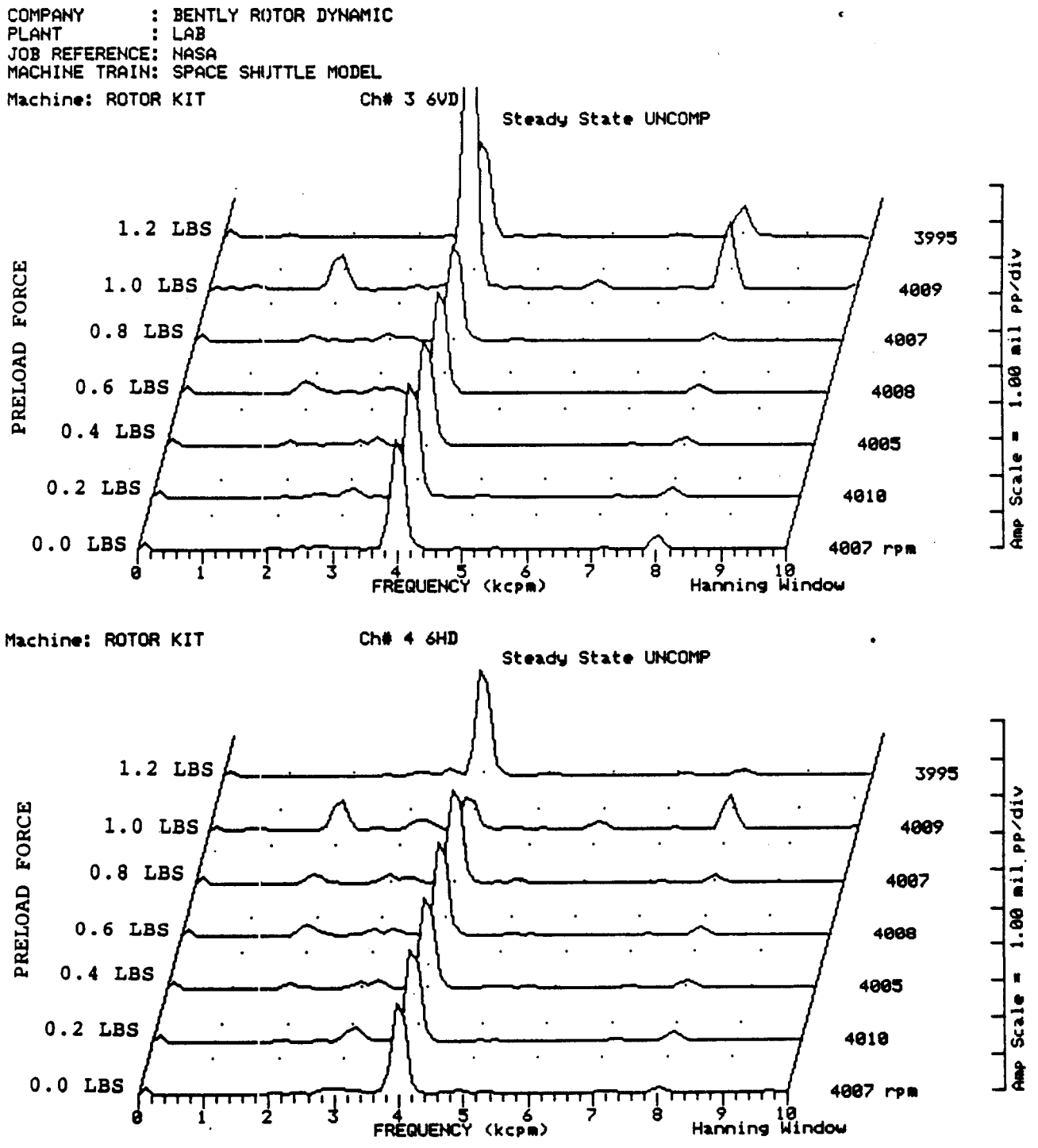

FIGURE 12.251 SPECTRAL CONTENT AT PROBE LOCATION 6 AT 4000 RPM, 5.0 PSI SEAL OIL PRESSURE, 0.8 IN–GRAM UNBALANCE LOCATED IN THE THIRD PUMP IMPELLER DISK, FOR INCREASING STATIC PRELOADS.

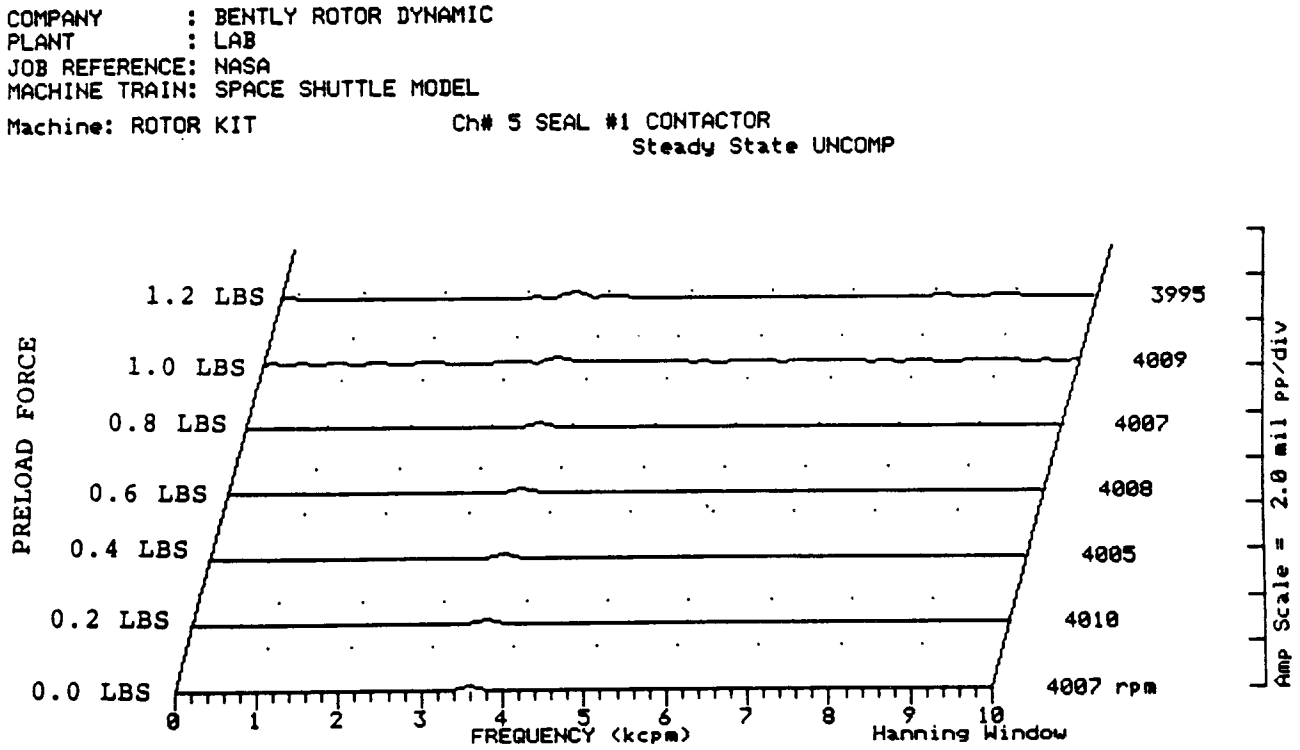

FIGURE 12.252 SPECTRAL CONTENT FOR SHAFT TO SEAL 1 CONTACT AT 4000 RPM, 5.0 PSI SEAL OIL PRESSURE, 0.8 IN–GRAM UNBALANCE LOCATED IN THE THIRD PUMP IMPELLER DISK, FOR INCREASING STATIC PRELOADS.

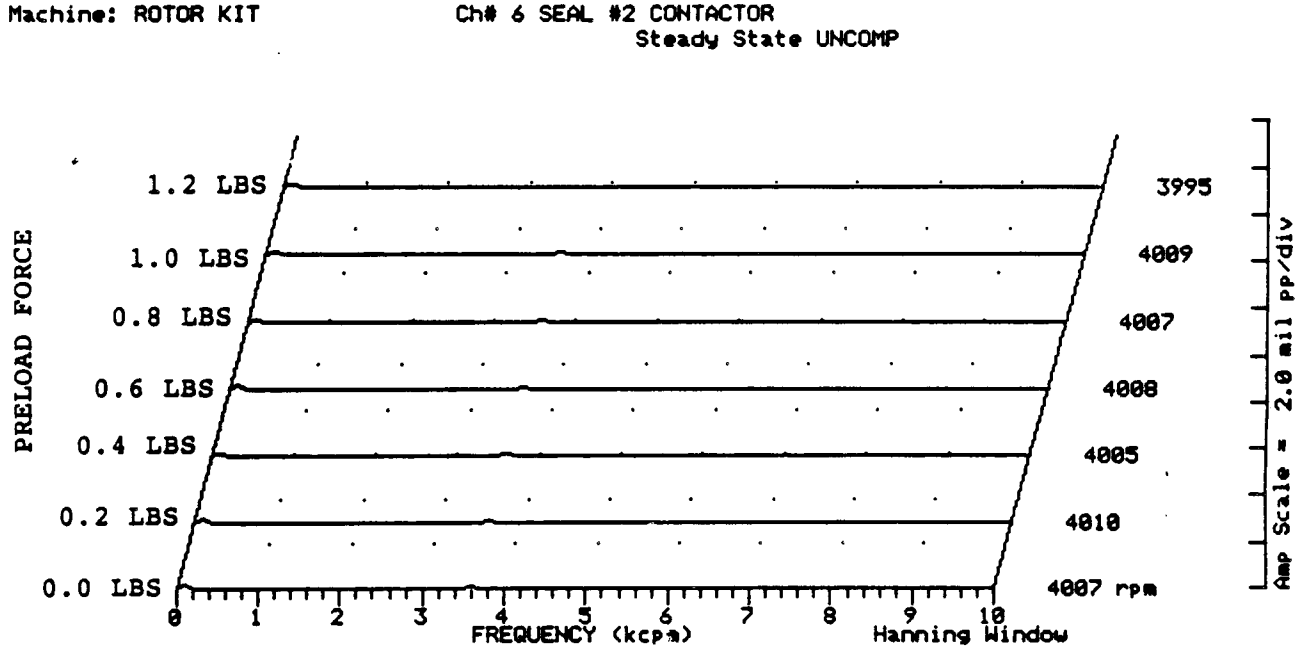

FIGURE 12.253 SPECTRAL CONTENT FOR SHAFT TO SEAL 2 CONTACT AT 4000 RPM, 5.0 PSI SEAL OIL PRESSURE, 0.8 IN–GRAM UNBALANCE LOCATED IN THE THIRD PUMP IMPELLER DISK, FOR INCREASING STATIC PRELOADS.

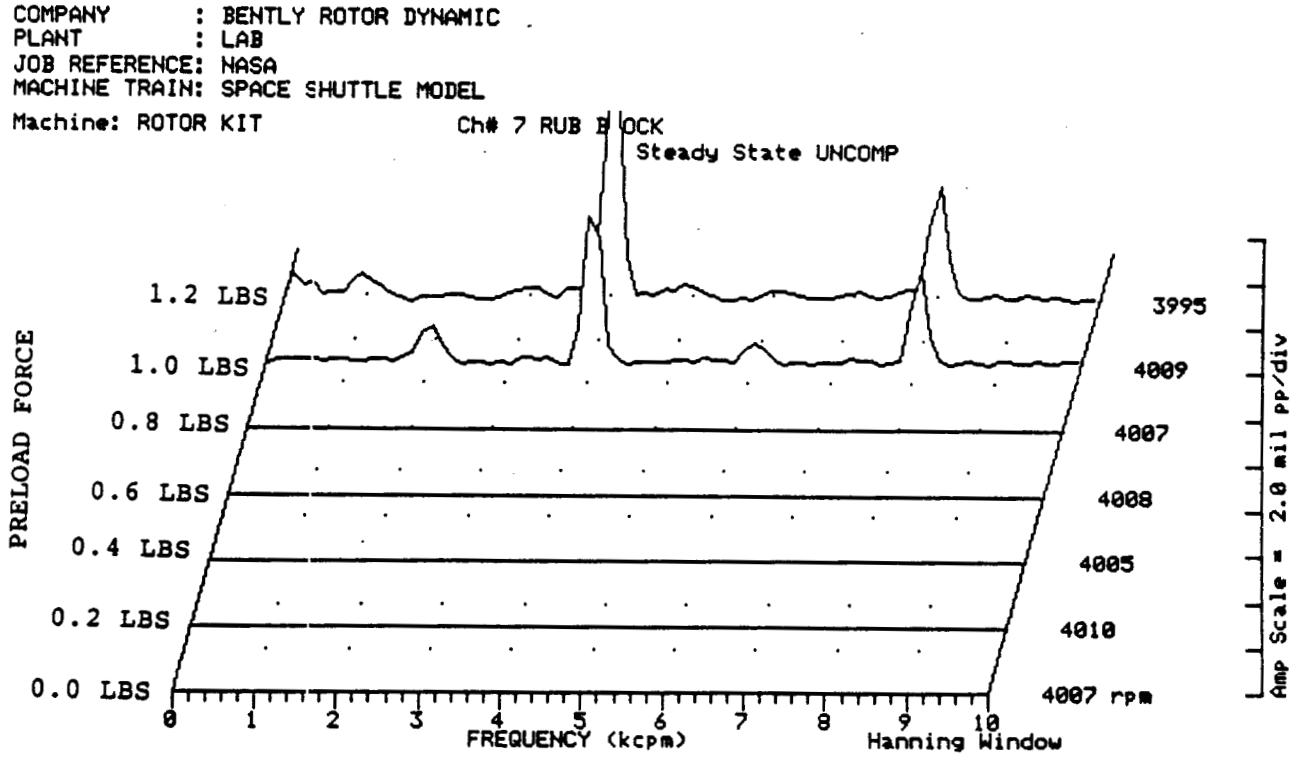

FIGURE 12.254 SPECTRAL CONTENT FOR SHAFT TO RUB BLOCK CONTACT AT 4000 RPM, 5.0 PSI SEAL OIL PRESSURE, 0.8 IN–GRAM UNBALANCE LOCATED IN THE THIRD PUMP IMPELLER DISK, FOR INCREASING STATIC PRELOADS.

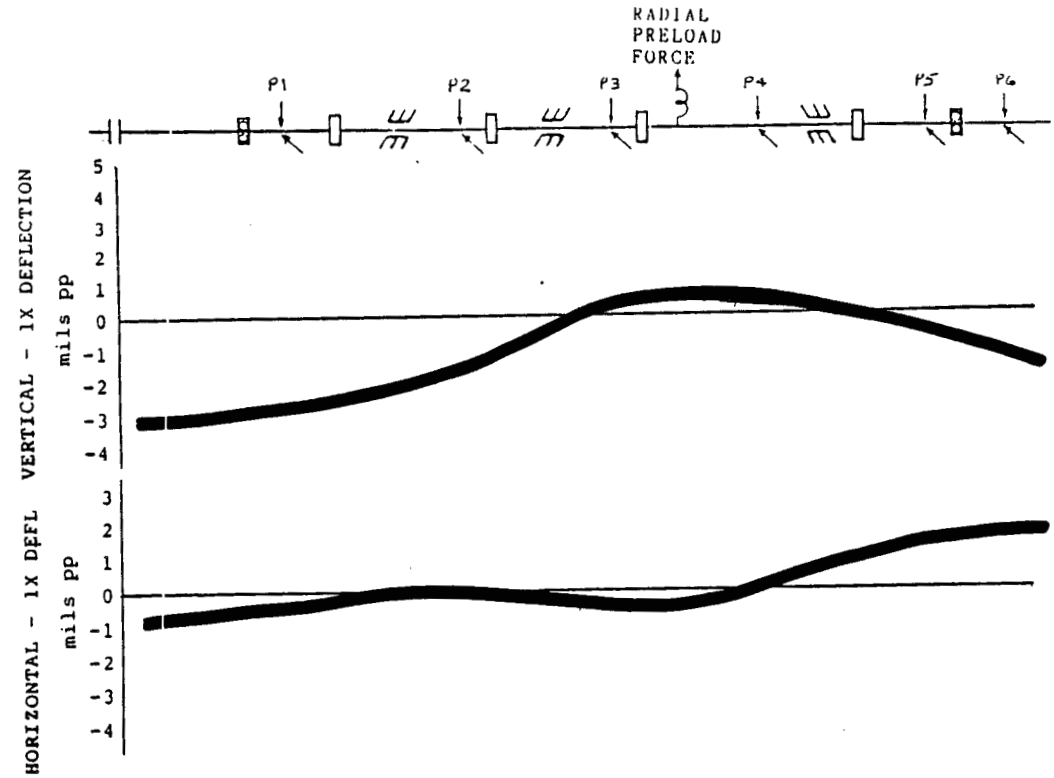

FIGURE 12.255 ROTOR MODE SHAPE AT 4000 RPM, 7.5 PSI SEAL OIL PRESSURE DUE TO 0.8 IN–GRAM UNBALANCE LOCATED IN THE THIRD PUMP IMPELLER DISK.

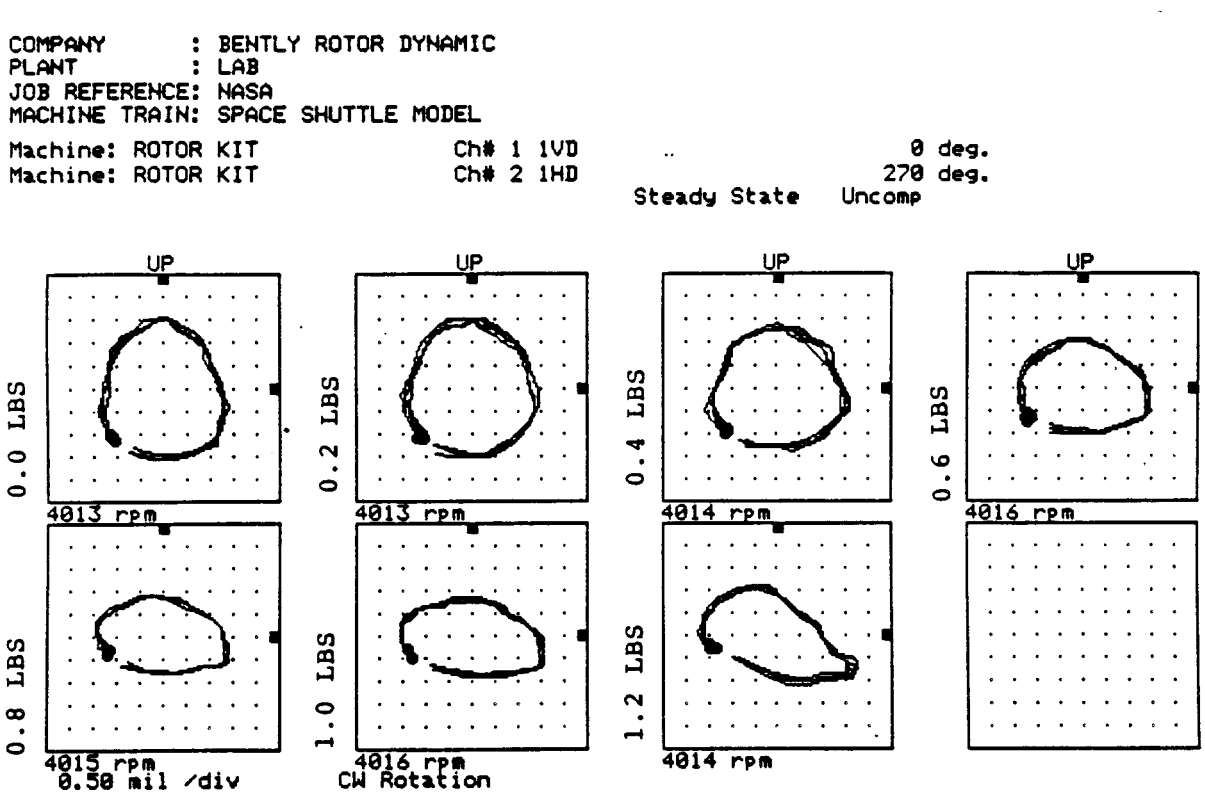

FIGURE 12.256 ORBITS AT PROBE LOCATION 1 AT 4000 RPM, 7.5 PSI SEAL OIL PRESSURE, 0.8 IN–GRAM UNBALANCE LOCATED IN THE THIRD PUMP IMPELLER DISK, FOR INCREASING STATIC PRELOAD FORCES.

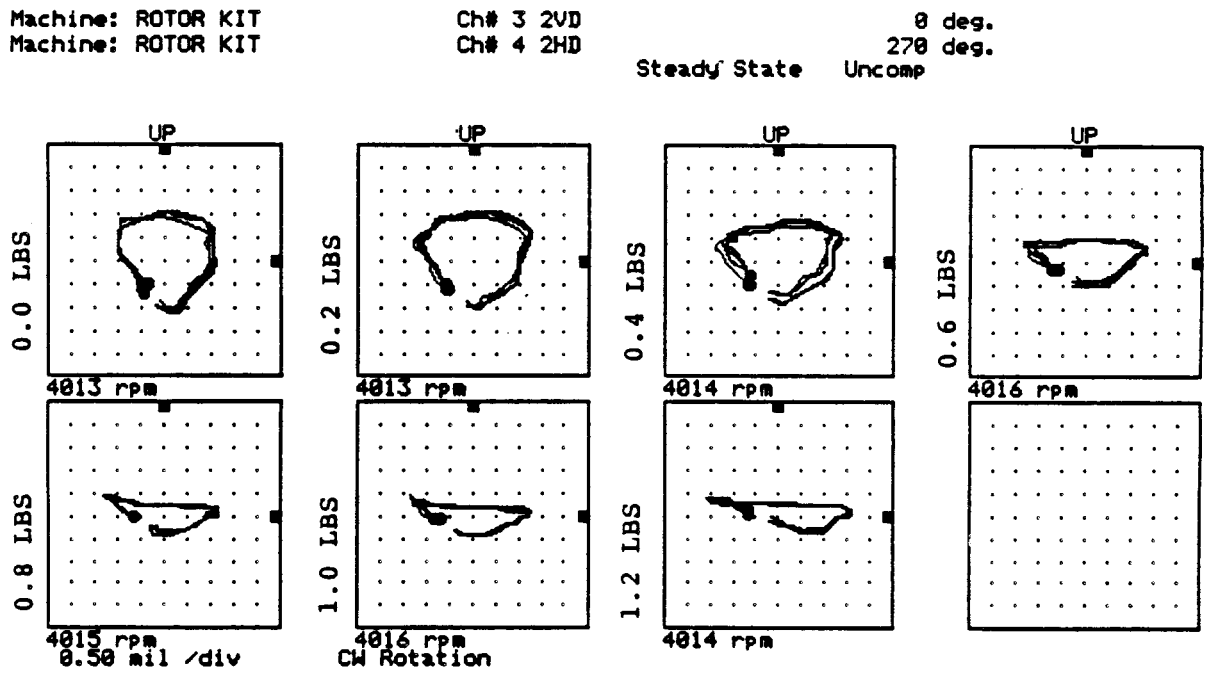

FIGURE 12.257 ORBITS AT PROBE LOCATION 2 AT 4000 RPM, 7.5 PSI SEAL OIL PRESSURE, 0.8 IN–GRAM UNBALANCE LOCATED IN THE THIRD PUMP IMPELLER DISK, FOR INCREASING STATIC PRELOAD FORCES.

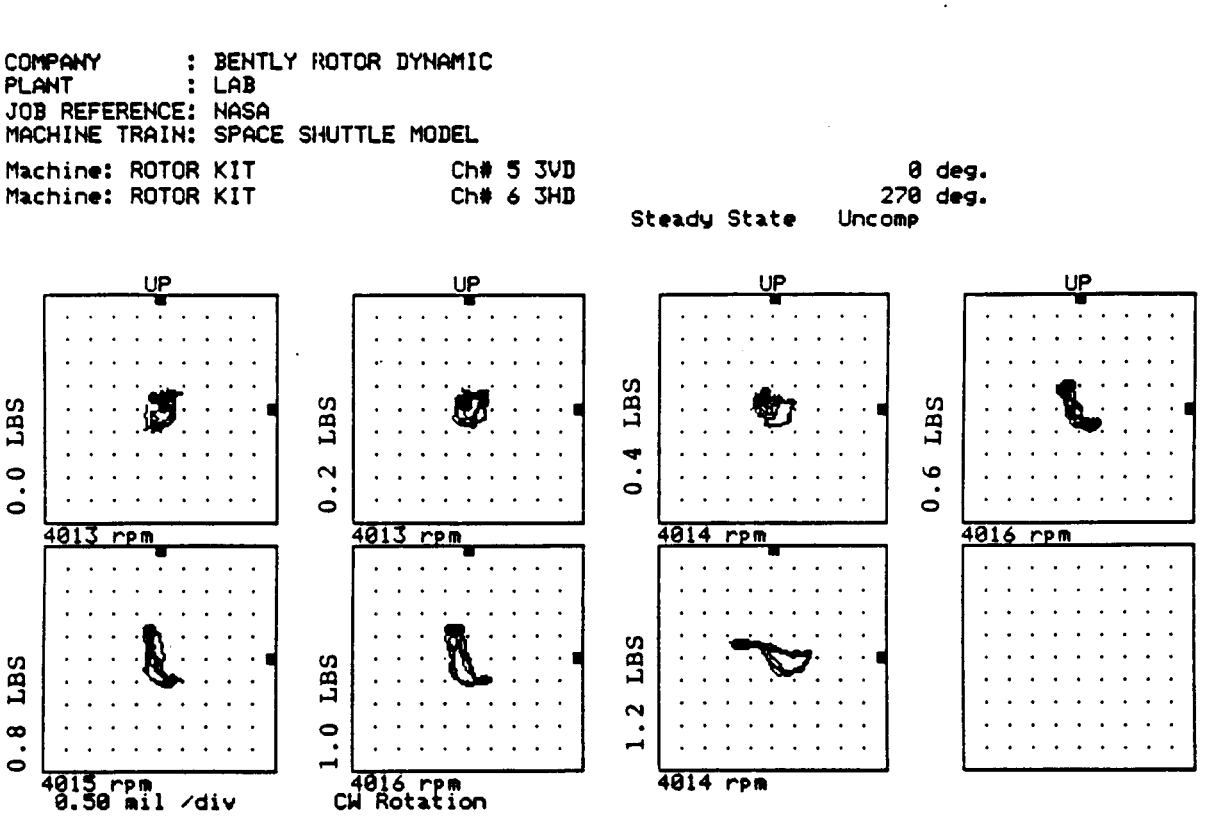

FIGURE 12.258 ORBITS AT PROBE LOCATION 3 AT 4000 RPM, 7.5 PSI SEAL OIL PRESSURE, 0.8 IN–GRAM UNBALANCE LOCATED IN THE THIRD PUMP IMPELLER DISK, FOR INCREASING STATIC PRELOAD FORCES.

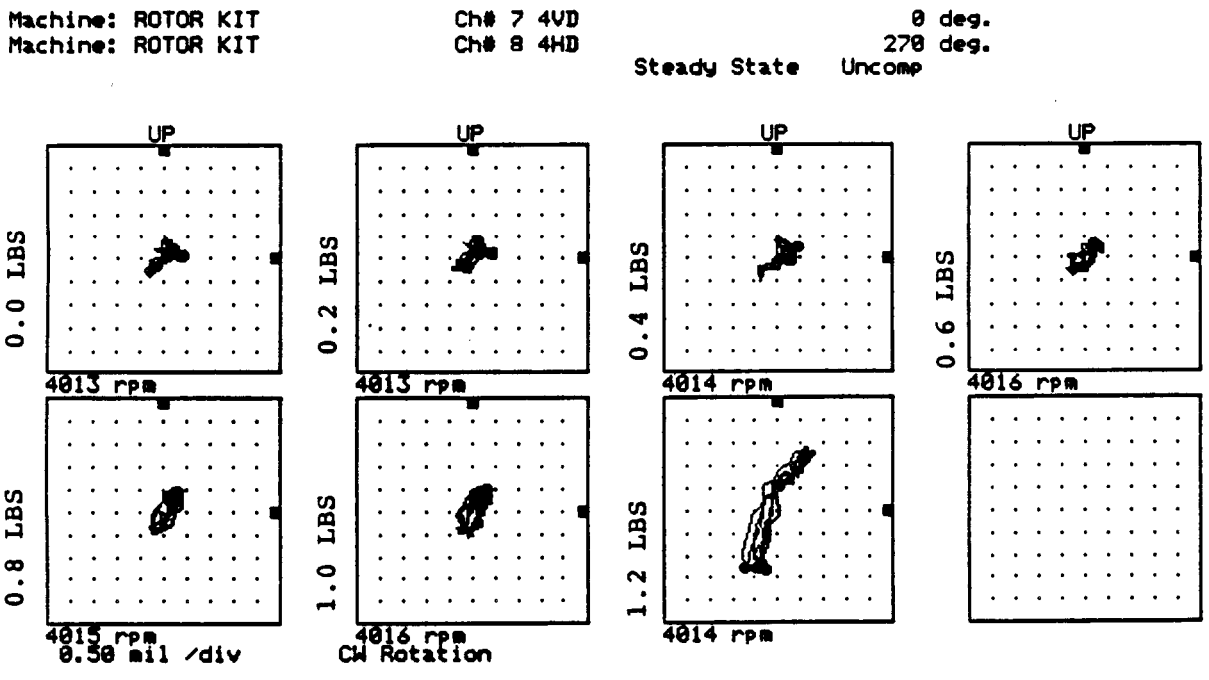

FIGURE 12.259 ORBITS AT PROBE LOCATION 4 AT 4000 RPM, 7.5 PSI SEAL OIL PRESSURE, 0.8 IN–GRAM UNBALANCE LOCATED IN THE THIRD PUMP IMPELLER DISK, FOR INCREASING STATIC PRELOAD FORCES.

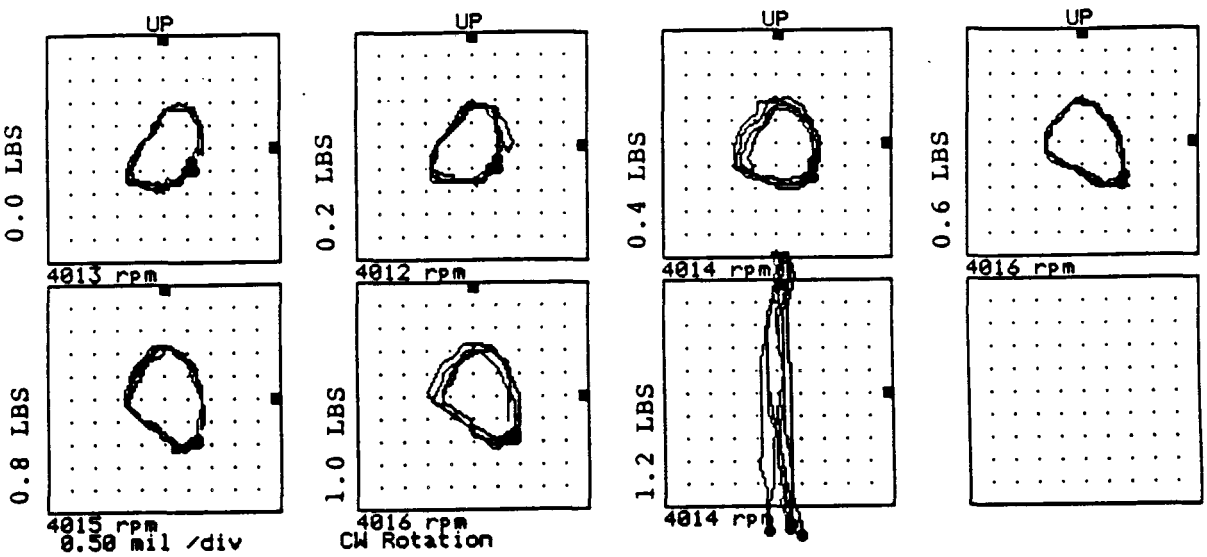

FIGURE 12.260 ORBITS AT PROBE LOCATION 5 AT 4000 RPM, 7.5 PSI SEAL OIL PRESSURE, 0.8 IN–GRAM UNBALANCE LOCATED IN THE THIRD PUMP IMPELLER DISK, FOR INCREASING STATIC PRELOAD FORCES.

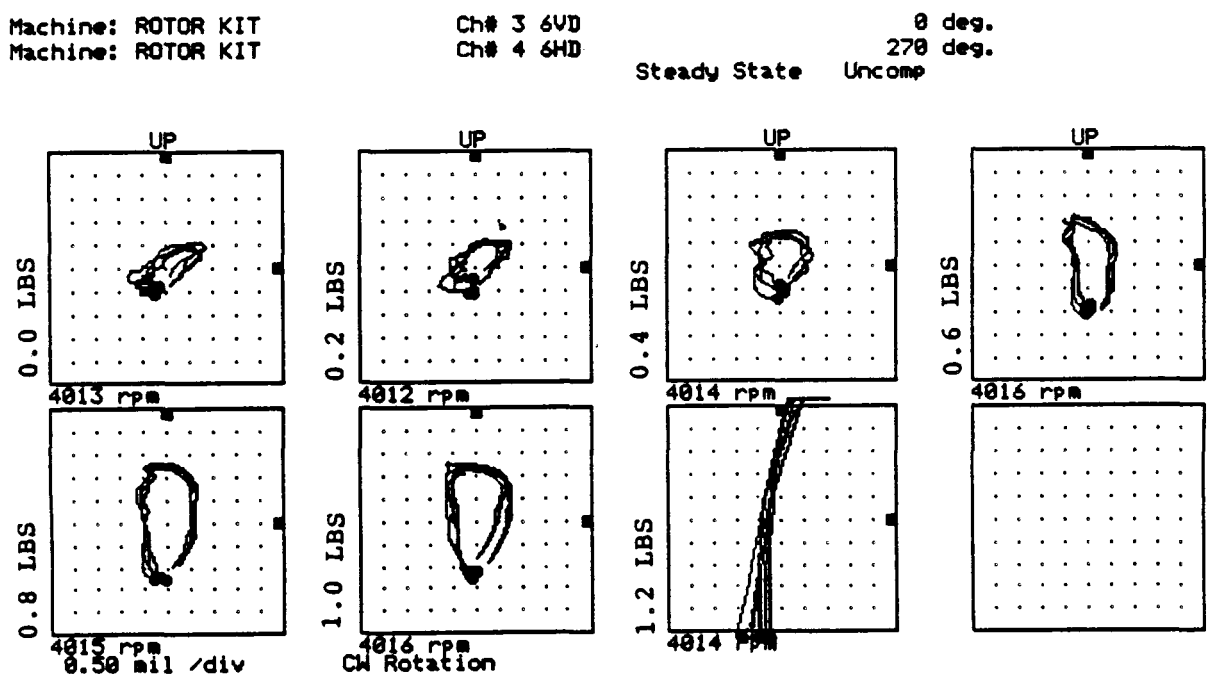

FIGURE 12.261 ORBITS AT PROBE LOCATION 6 AT 4000 RPM, 7.5 PSI SEAL OIL PRESSURE, 0.8 IN–GRAM UNBALANCE LOCATED IN THE THIRD PUMP IMPELLER DISK, FOR INCREASING STATIC PRELOAD FORCES.

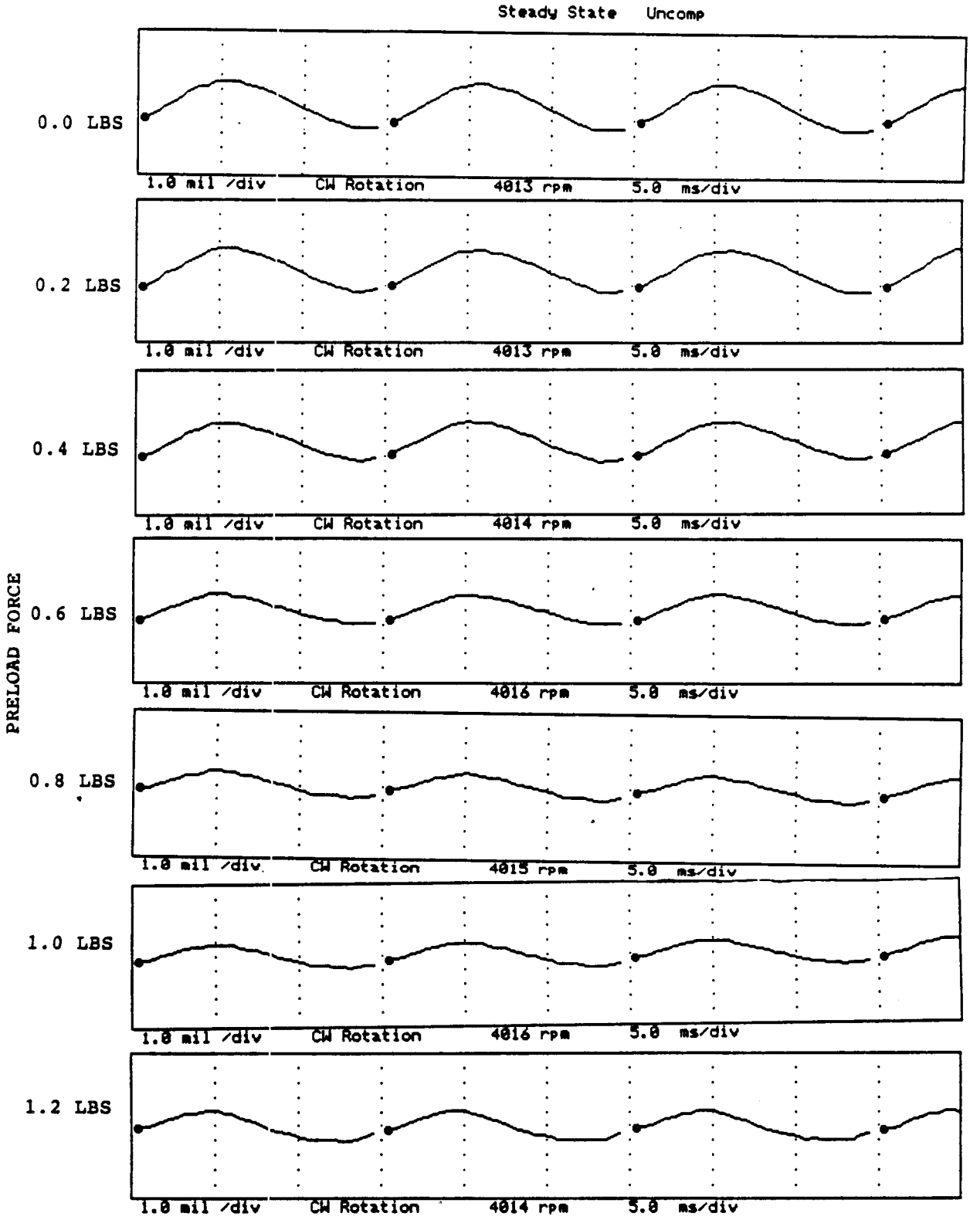

FIGURE 12.262 TIMEBASE FOR VERTICAL PROBE AT LOCATION 1 AT 4000 RPM, 7.5 PSI SEAL OIL PRESSURE, 0.8 IN–GRAM UNBALANCE LOCATED IN THE THIRD PUMP IMPELLER DISK, FOR INCREASING STATIC PRELOADS.

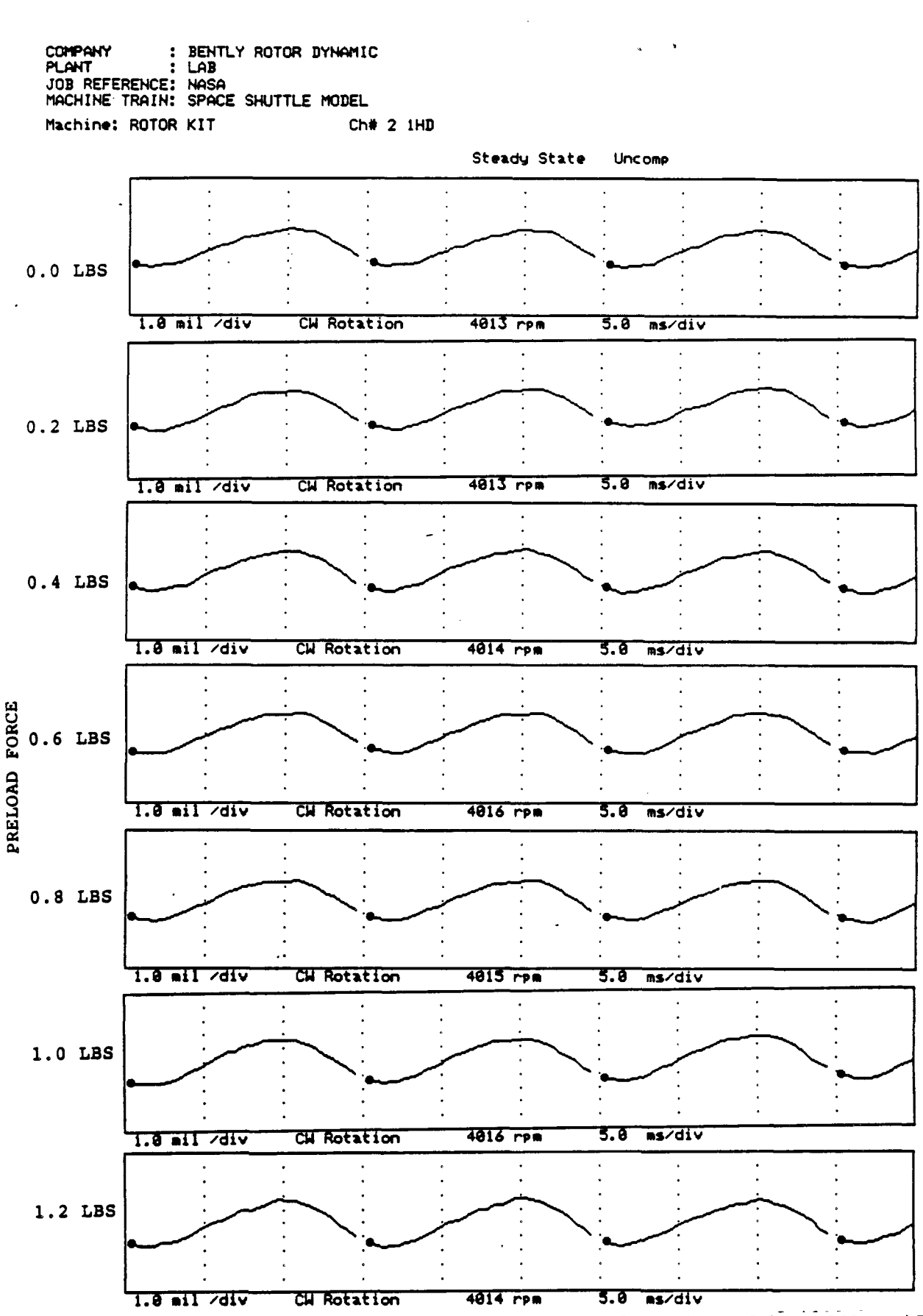

FIGURE 12.263 TIMEBASE FOR HORIZONTAL PROBE AT LOCATION 1 AT 4000 RPM, 7.5 PSI SEAL OIL PRESSURE, 0.8 IN–GRAM UNBALANCE LOCATED IN THE THIRD PUMP IMPELLER DISK, FOR INCREASING STATIC PRELOADS.

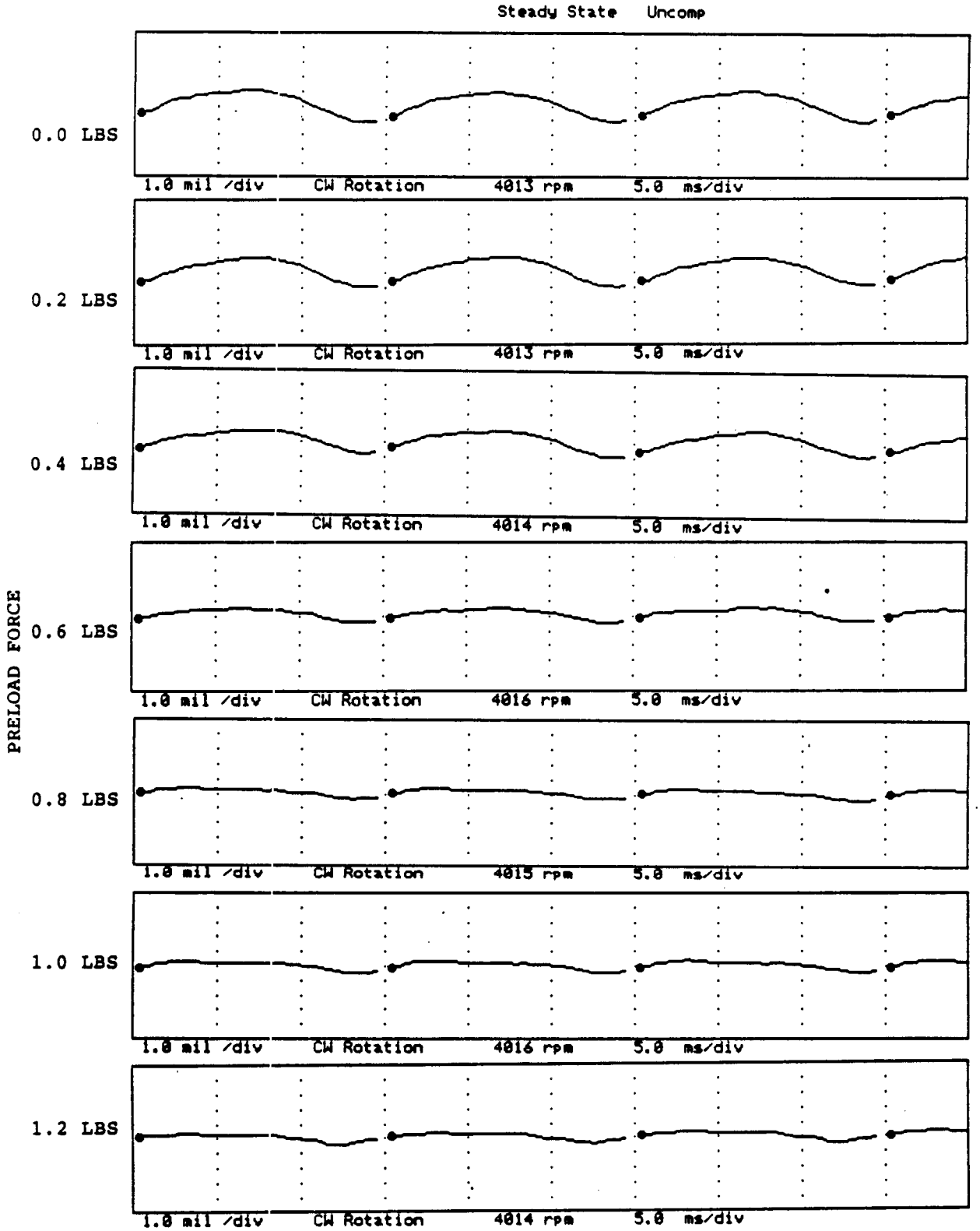

FIGURE 12.264 TIMEBASE FOR VERTICAL PROBE AT LOCATION 2 AT 4000 RPM, 7.5 PSI SEAL OIL PRESSURE, 0.8 IN–GRAM UNBALANCE LOCATED IN THE THIRD PUMP IMPELLER DISK, FOR INCREASING STATIC PRELOADS.

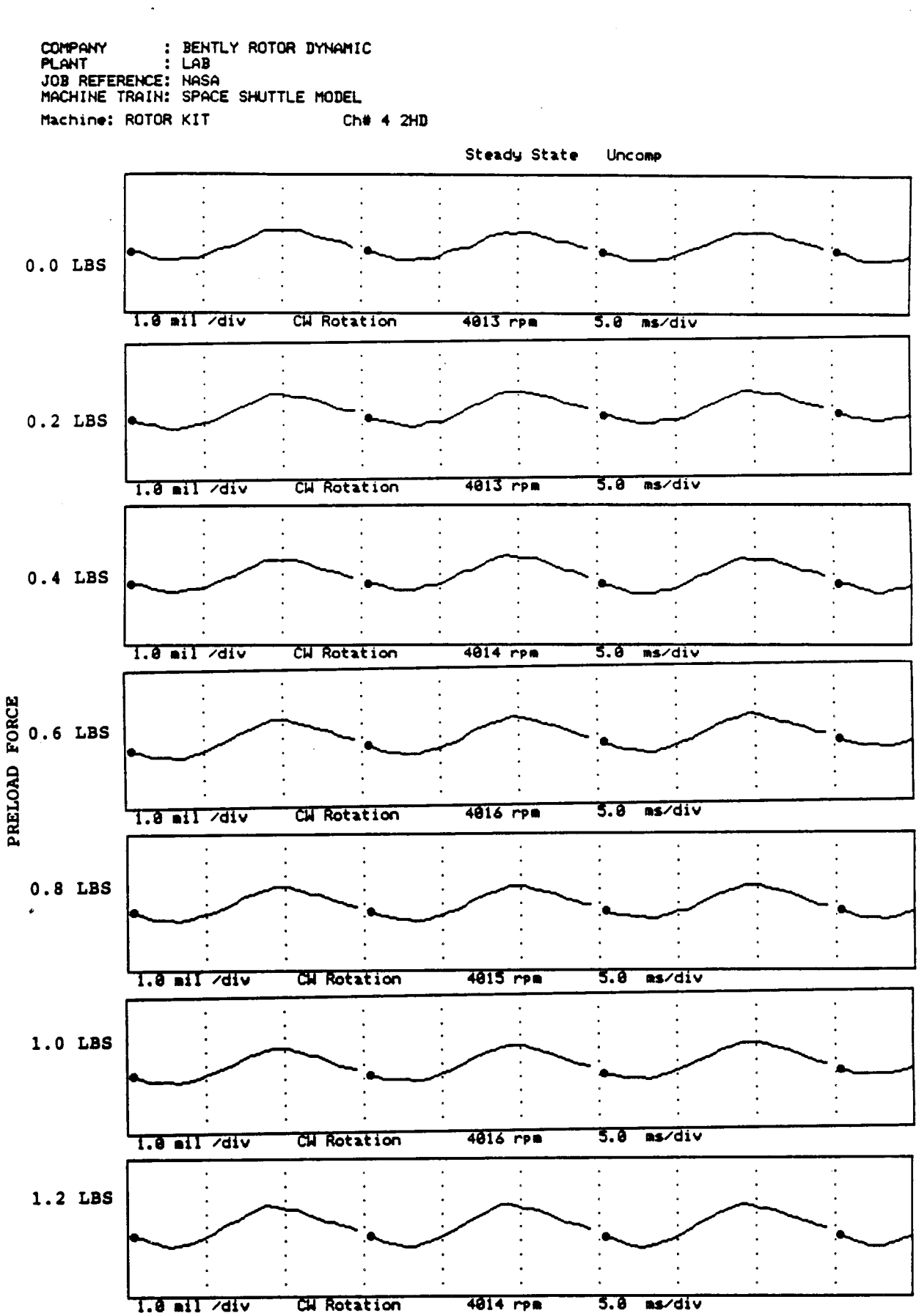

FIGURE 12.265 TIMEBASE FOR HORIZONTAL PROBE AT LOCATION 2 AT 4000 RPM, 7.5 PSI SEAL OIL PRESSURE, 0.8 IN–GRAM UNBALANCE LOCATED IN THE THIRD PUMP IMPELLER DISK, FOR INCREASING STATIC PRELOADS.

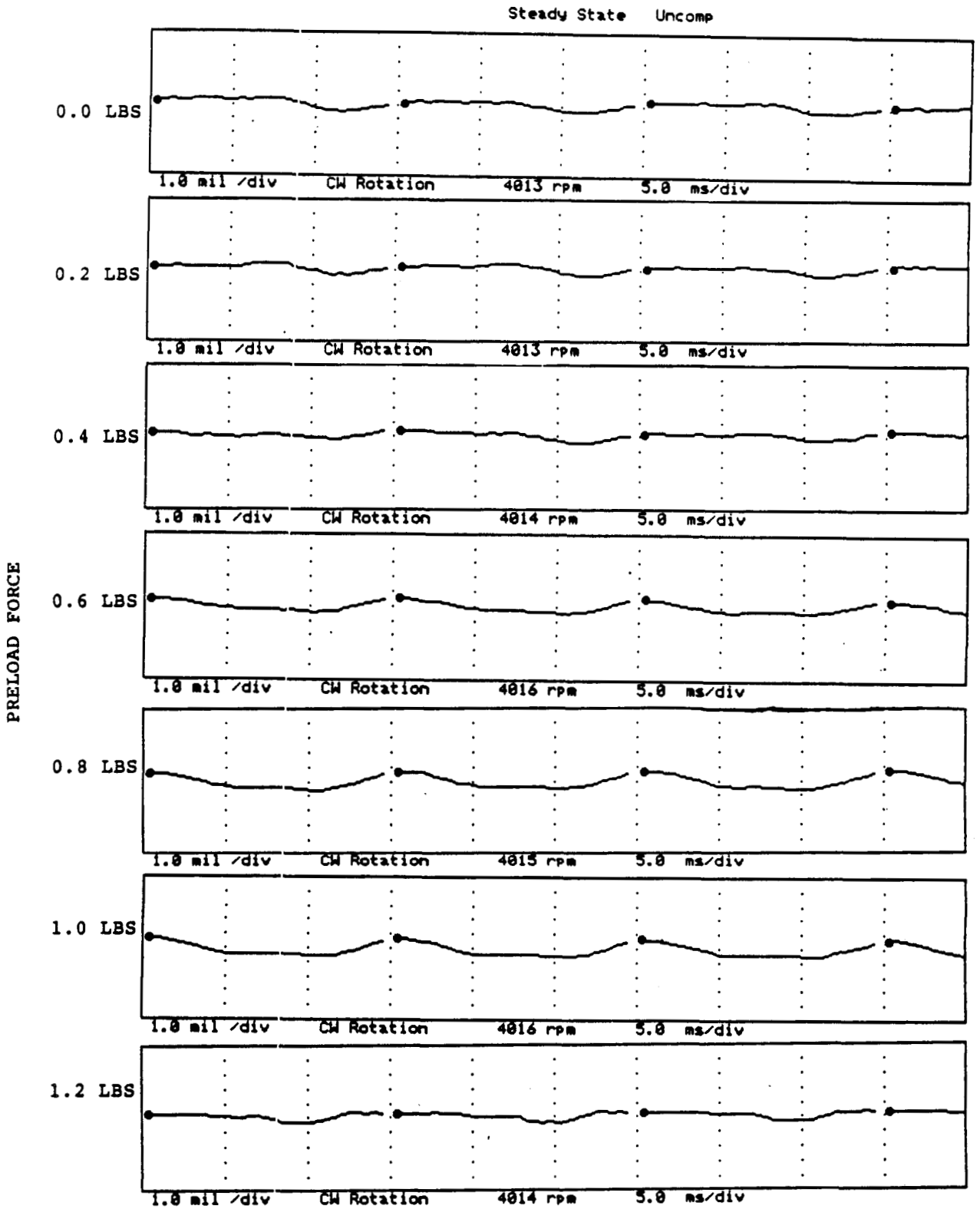

FIGURE 12.266 TIMEBASE FOR VERTICAL PROBE AT LOCATION 3 AT 4000 RPM, 7.5 PSI SEAL OIL PRESSURE, 0.8 IN–GRAM UNBALANCE LOCATED IN THE THIRD PUMP IMPELLER DISK, FOR INCREASING STATIC PRELOADS.

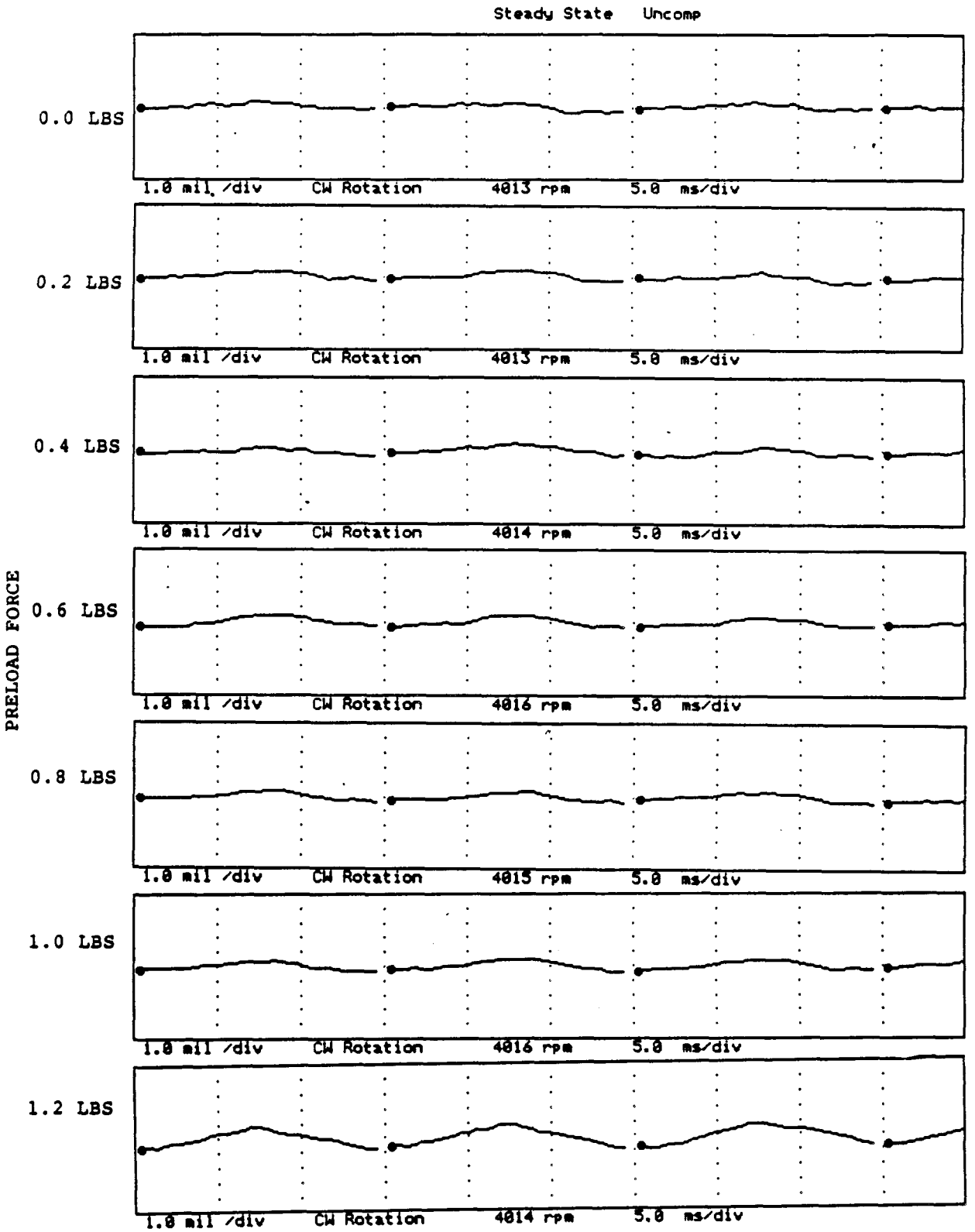

FIGURE 12.267 TIMEBASE FOR HORIZONTAL PROBE AT LOCATION 3 AT 4000 RPM, 7.5 PSI SEAL OIL PRESSURE, 0.8 IN–GRAM UNBALANCE LOCATED IN THE THIRD PUMP IMPELLER DISK, FOR INCREASING STATIC PRELOADS.

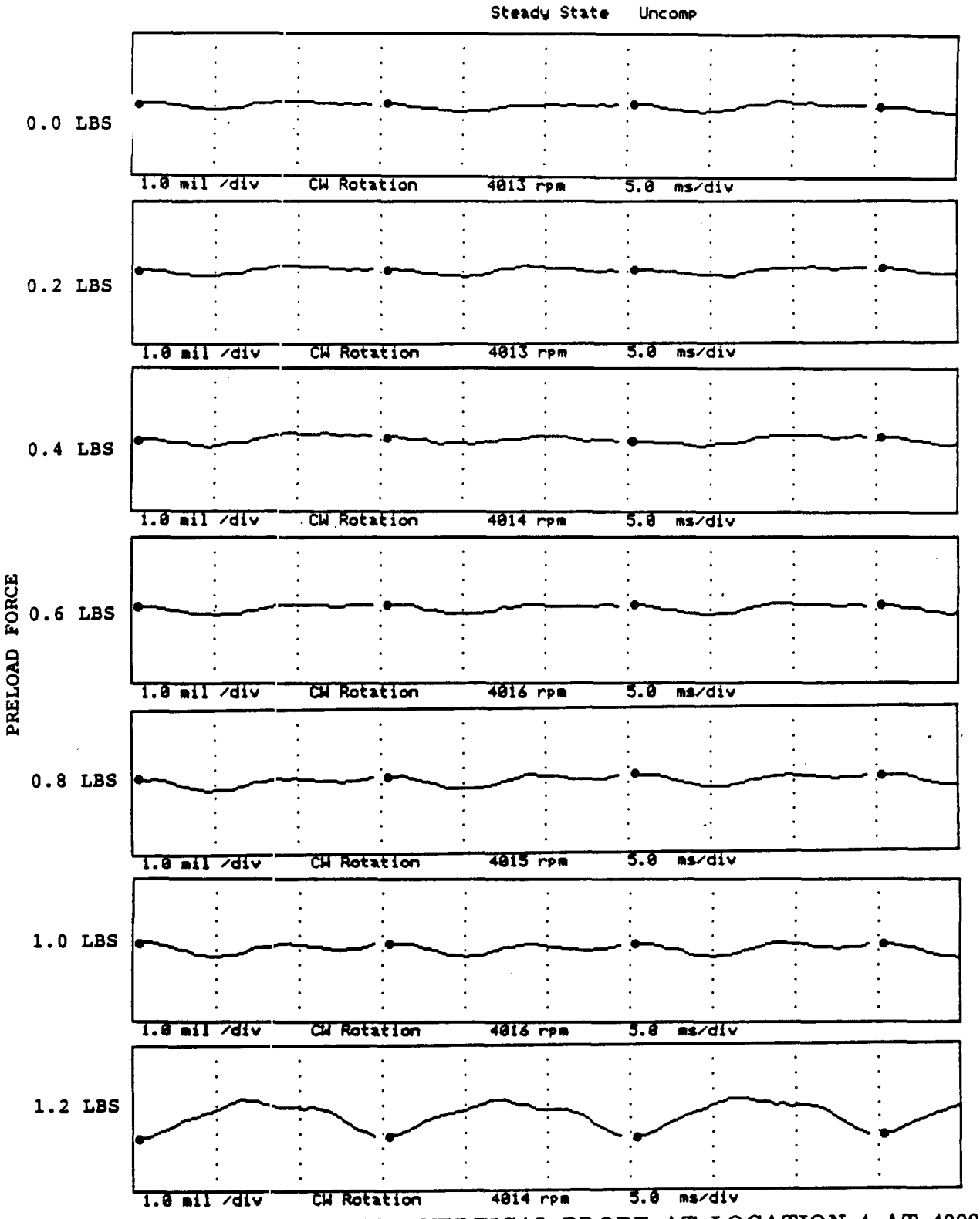

FIGURE 12.268 TIMEBASE FOR VERTICAL PROBE AT LOCATION 4 AT 4000 RPM, 7.5 PSI SEAL OIL PRESSURE, 0.8 IN–GRAM UNBALANCE LOCATED IN THE THIRD PUMP IMPELLER DISK, FOR INCREASING STATIC PRELOADS.

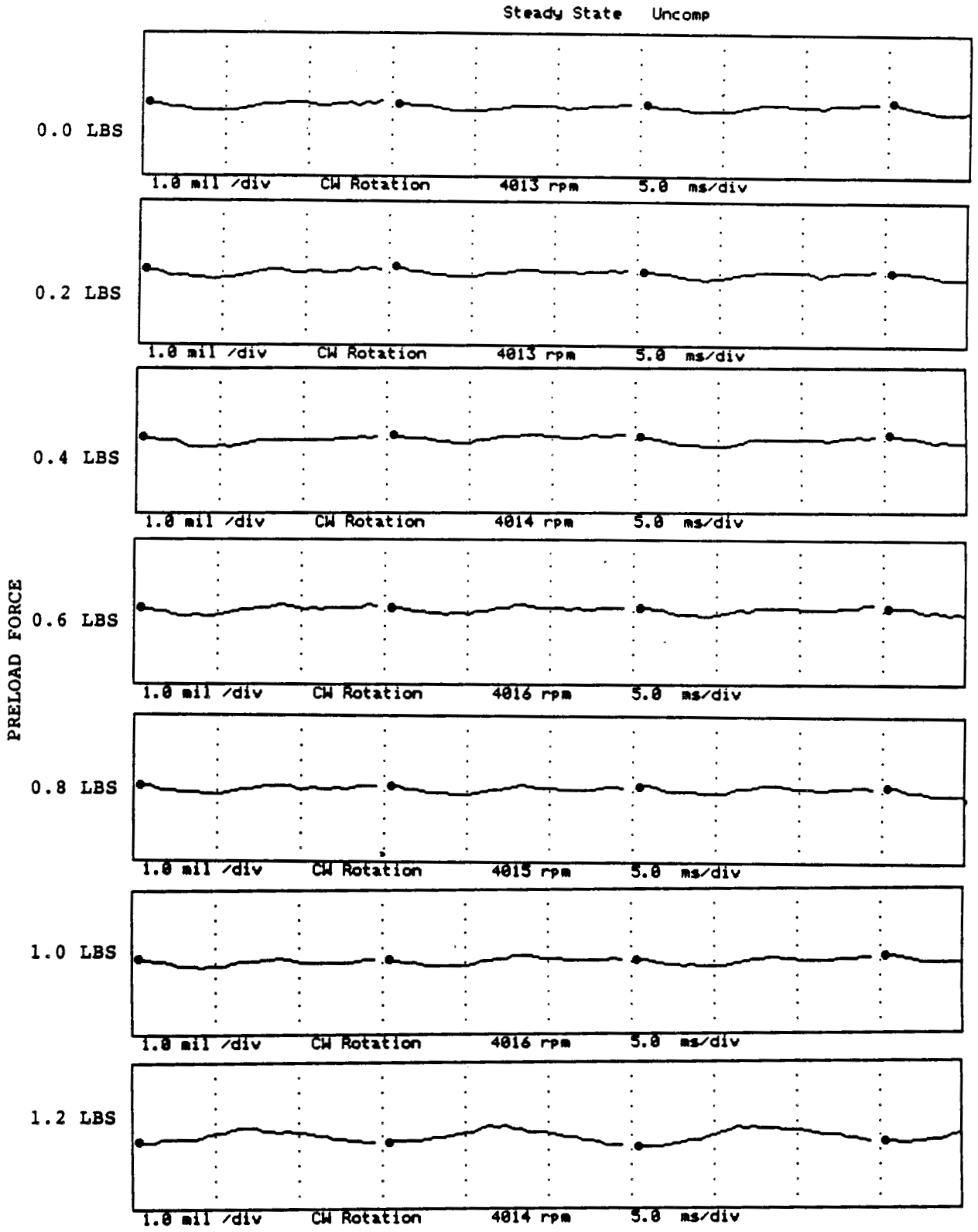

FIGURE 12.269 TIMEBASE FOR HORIZONTAL PROBE AT LOCATION 4 AT 4000 RPM, 7.5 PSI SEAL OIL PRESSURE, 0.8 IN–GRAM UNBALANCE LOCATED IN THE THIRD PUMP IMPELLER DISK, FOR INCREASING STATIC PRELOADS.

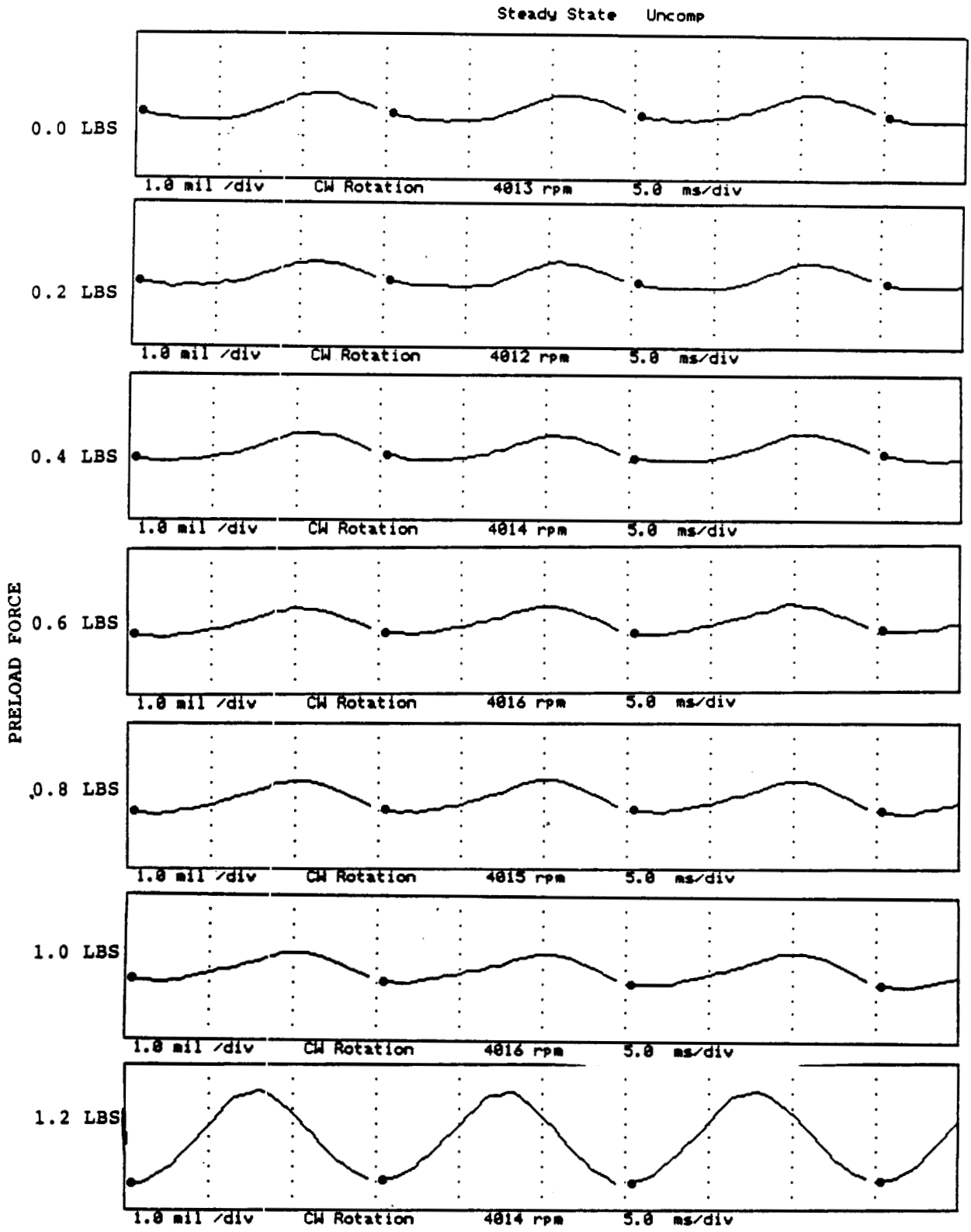

FIGURE 12.270 TIMEBASE FOR VERTICAL PROBE AT LOCATION 5 AT 4000 RPM, 7.5 PSI SEAL OIL PRESSURE, 0.8 IN–GRAM UNBALANCE LOCATED IN THE THIRD PUMP IMPELLER DISK, FOR INCREASING STATIC PRELOADS.

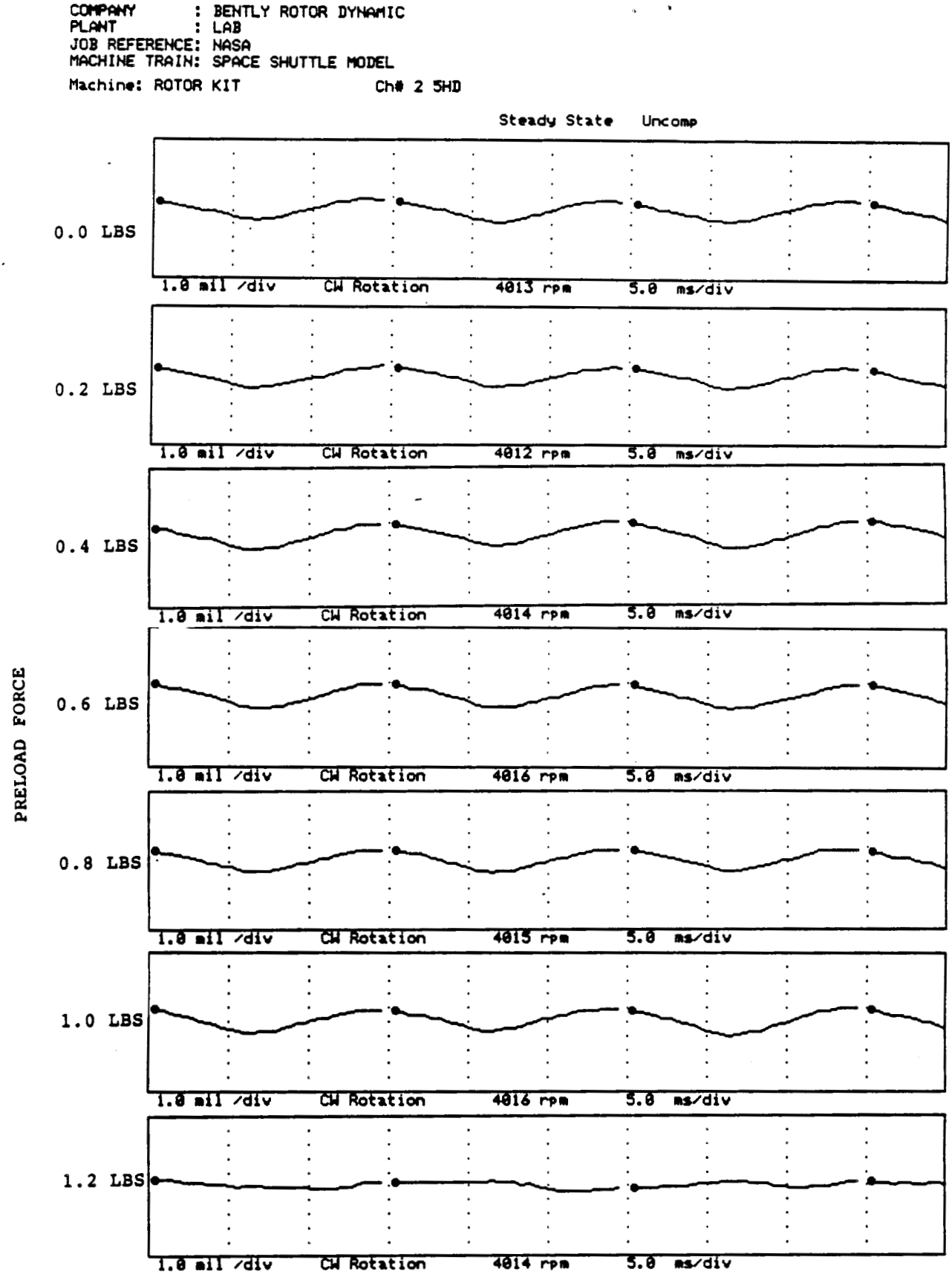

FIGURE 12.271 TIMEBASE FOR HORIZONTAL PROBE AT LOCATION 5 AT 4000 RPM, 7.5 PSI SEAL OIL PRESSURE, 0.8 IN–GRAM UNBALANCE LOCATED IN THE THIRD PUMP IMPELLER DISK, FOR INCREASING STATIC PRELOADS.

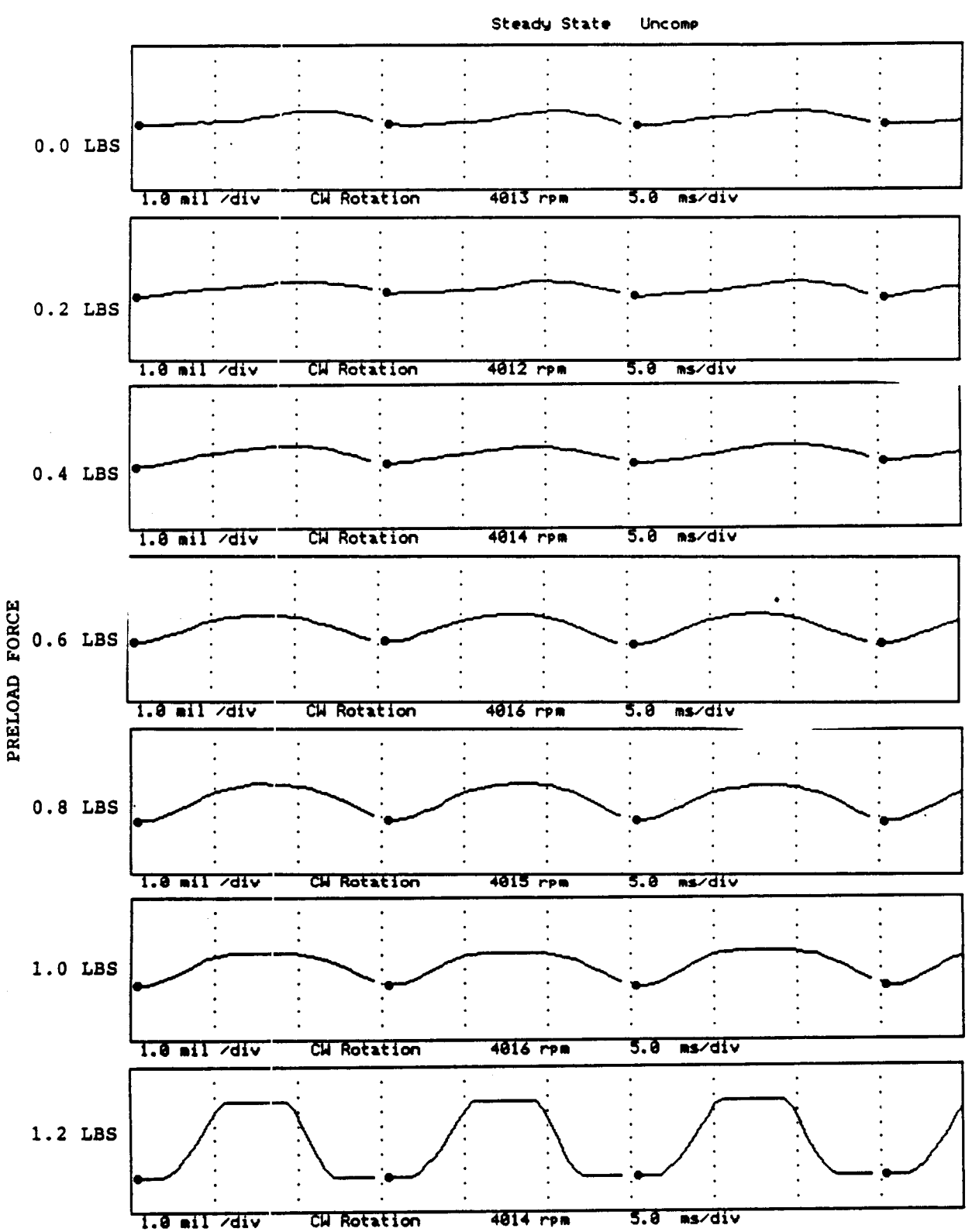

FIGURE 12.272 TIMEBASE FOR VERTICAL PROBE AT LOCATION 6 AT 4000 RPM, 7.5 PSI SEAL OIL PRESSURE, 0.8 IN–GRAM UNBALANCE LOCATED IN THE THIRD PUMP IMPELLER DISK, FOR INCREASING STATIC PRELOADS.

C-6

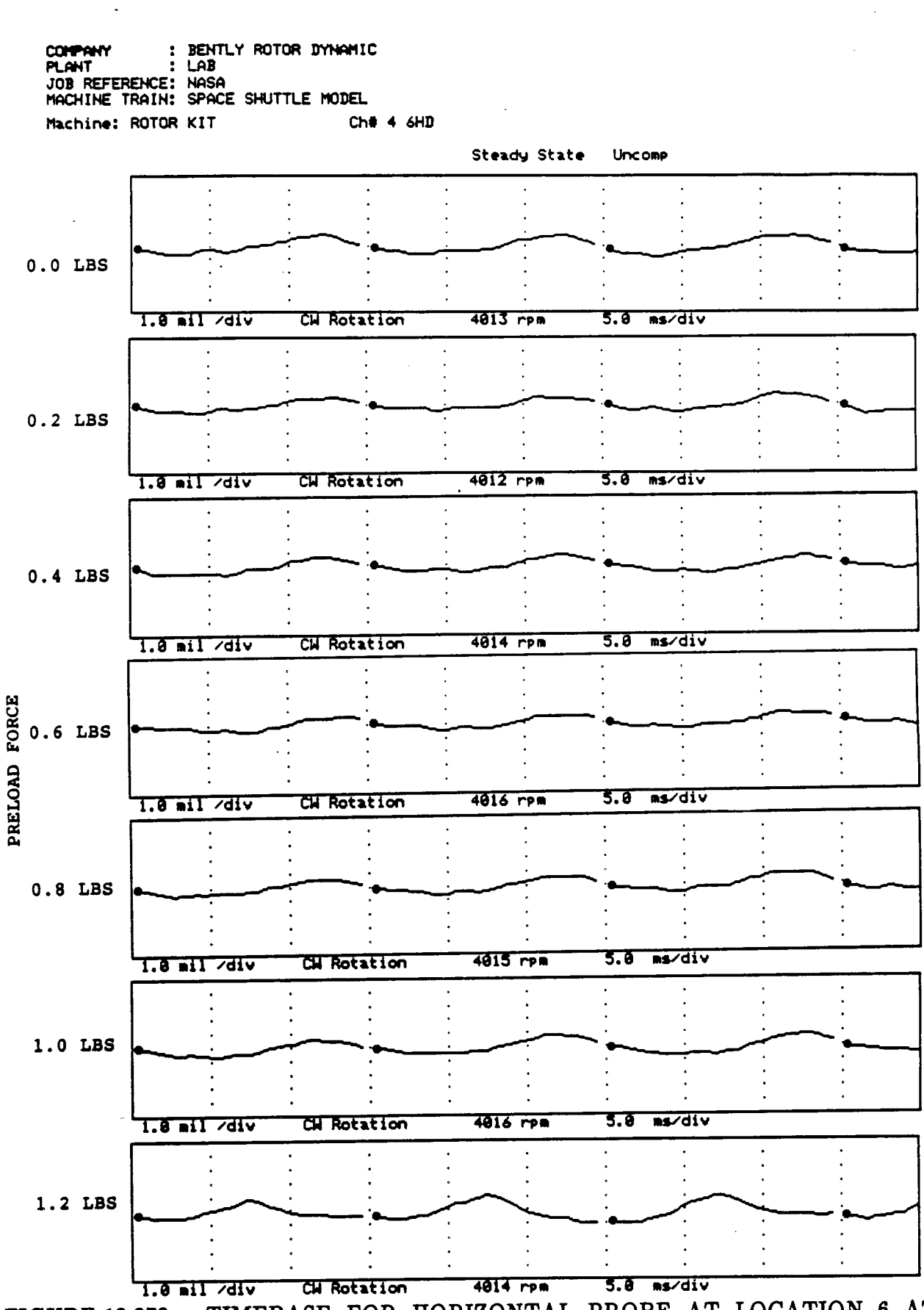

FIGURE 12.273 TIMEBASE FOR HORIZONTAL PROBE AT LOCATION 6 AT 4000 RPM, 7.5 PSI SEAL OIL PRESSURE, 0.8 IN–GRAM UNBALANCE LOCATED IN THE THIRD PUMP IMPELLER DISK, FOR INCREASING STATIC PRELOADS.

NOT AVAILABLE - OIL IN THE CLEARANCE AREA PROHIBITS THE METAL-TO-METAL CONTACT NECESSARY FOR THE CONTACT SENSOR TO OPERATE CORRECTLY.

FIGURE 12.274 TIMEBASE FOR SHAFT TO SEAL 1 CONTACT AT 4000 RPM, 7.5 PSI SEAL OIL PRESSURE, 0.8 IN–GRAM UNBALANCE LOCATED IN THE THIRD PUMP IMPELLER DISK, FOR INCREASING STATIC PRELOADS.

NOT AVAILABLE - OIL IN THE CLEARANCE AREA PROHIBITS THE METAL-TO-METAL CONTACT NECESSARY FOR THE CONTACT SENSOR TO OPERATE CORRECTLY.

FIGURE 12.275 TIMEBASE FOR SHAFT TO SEAL 1 CONTACT AT 4000 RPM, 7.5 PSI SEAL OIL PRESSURE, 0.8 IN–GRAM UNBALANCE LOCATED IN THE THIRD PUMP IMPELLER DISK, FOR INCREASING STATIC PRELOADS.

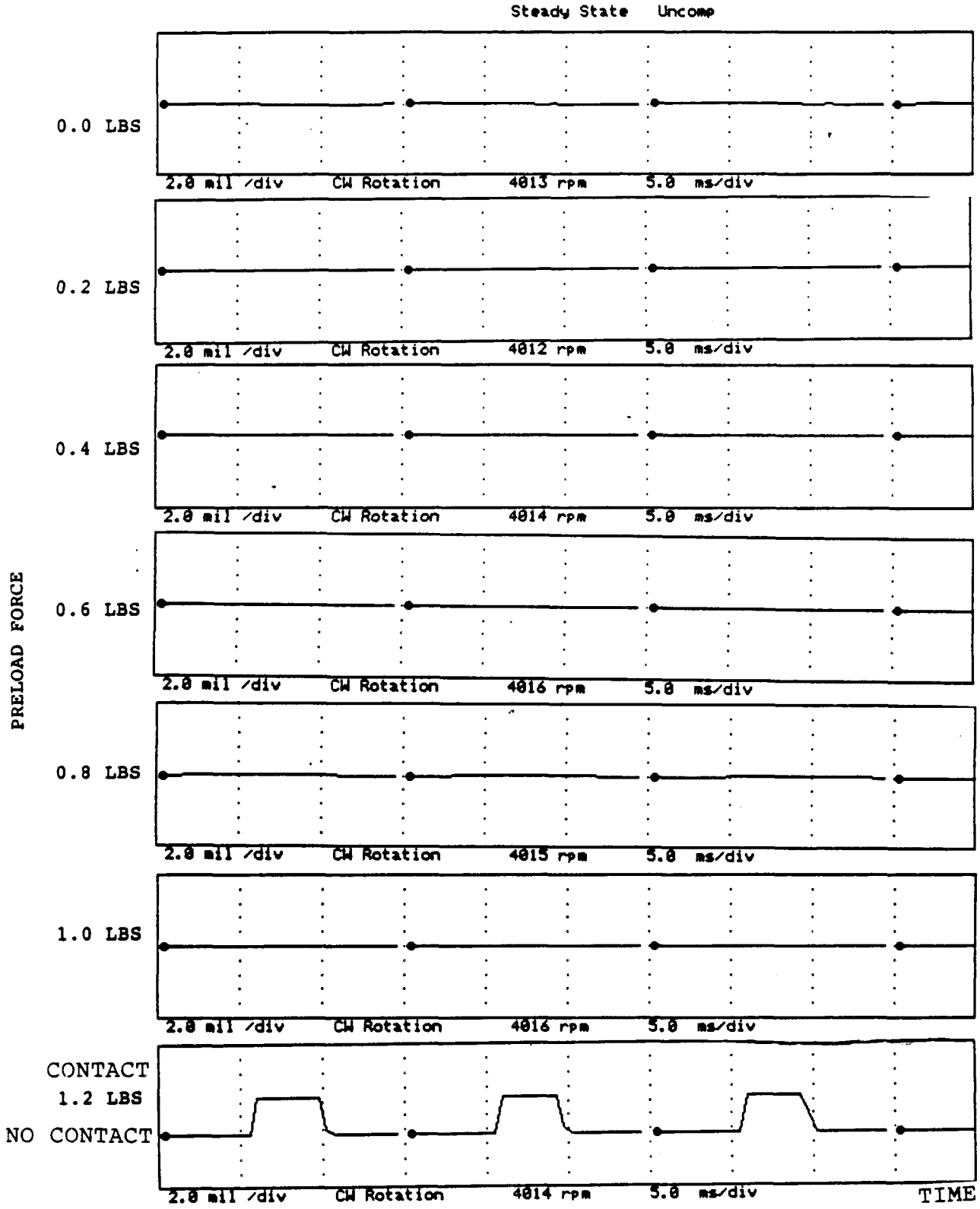

FIGURE 12.276 TIMEBASE FOR SHAFT TO RUB BLOCK CONTACT AT 4000 RPM, 7.5 PSI SEAL OIL PRESSURE, 0.8 IN–GRAM UNBALANCE LOCATED IN THE THIRD PUMP IMPELLER DISK, FOR INCREASING STATIC PRELOADS.

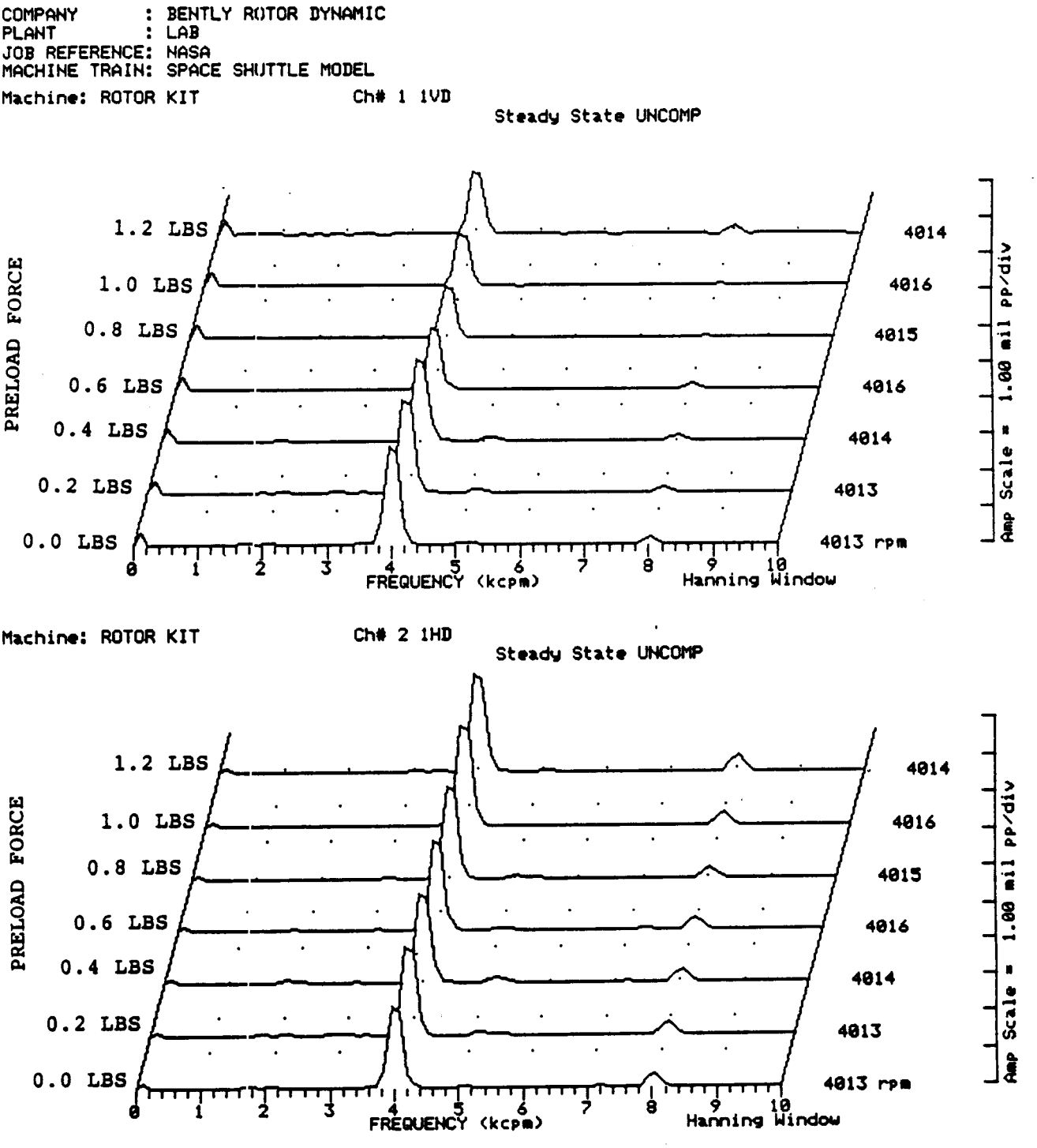

FIGURE 12.277 SPECTRAL CONTENT AT PROBE LOCATION 1 AT 4000 RPM, 7.5 PSI SEAL OIL PRESSURE, 0.8 IN–GRAM UNBALANCE LOCATED IN THE THIRD PUMP IMPELLER DISK, FOR INCREASING STATIC PRELOADS.

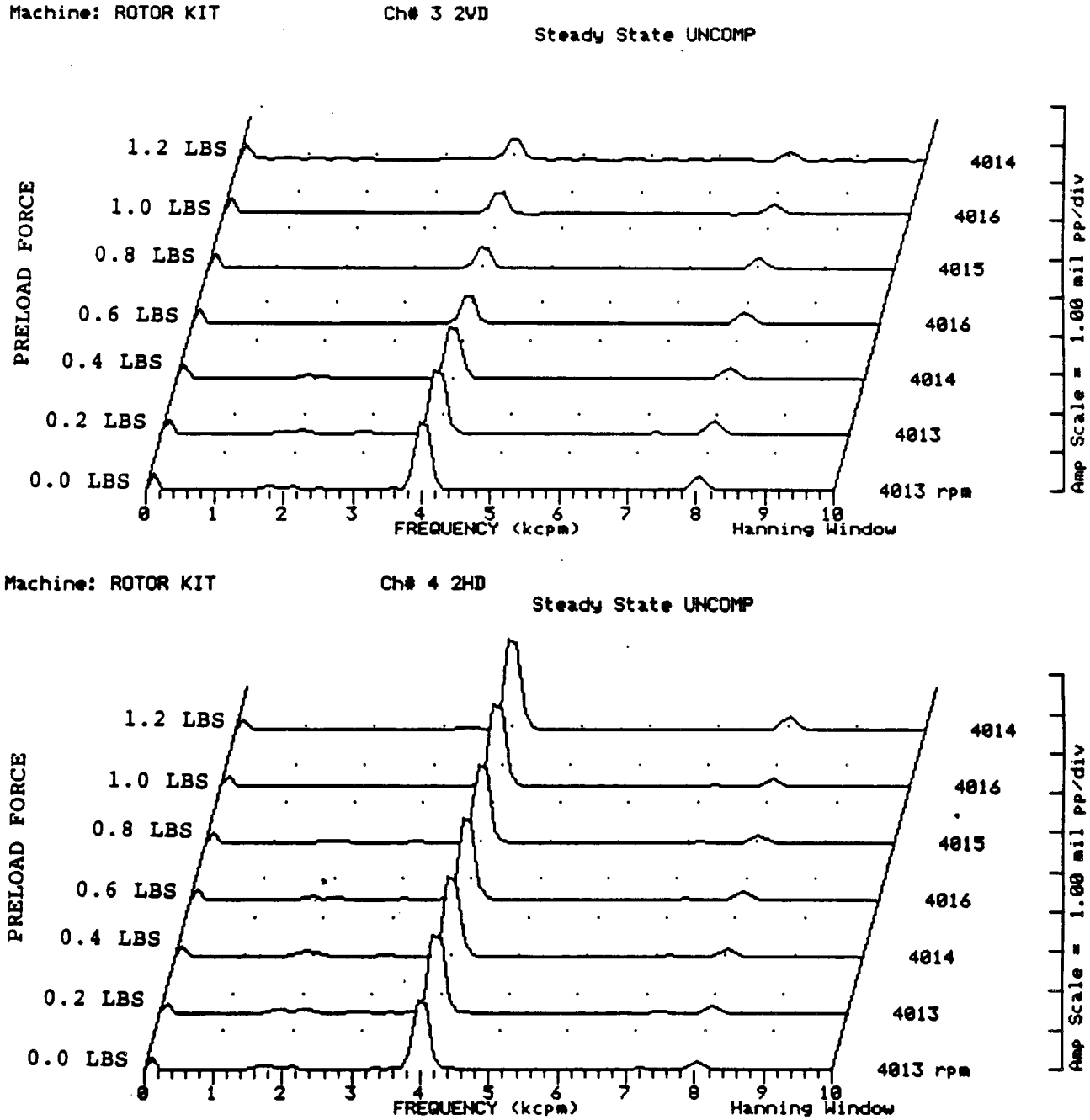

FIGURE 12.278 SPECTRAL CONTENT AT PROBE LOCATION 2 AT 4000 RPM, 7.5 PSI SEAL OIL PRESSURE, 0.8 IN–GRAM UNBALANCE LOCATED IN THE THIRD PUMP IMPELLER DISK, FOR INCREASING STATIC PRELOADS.

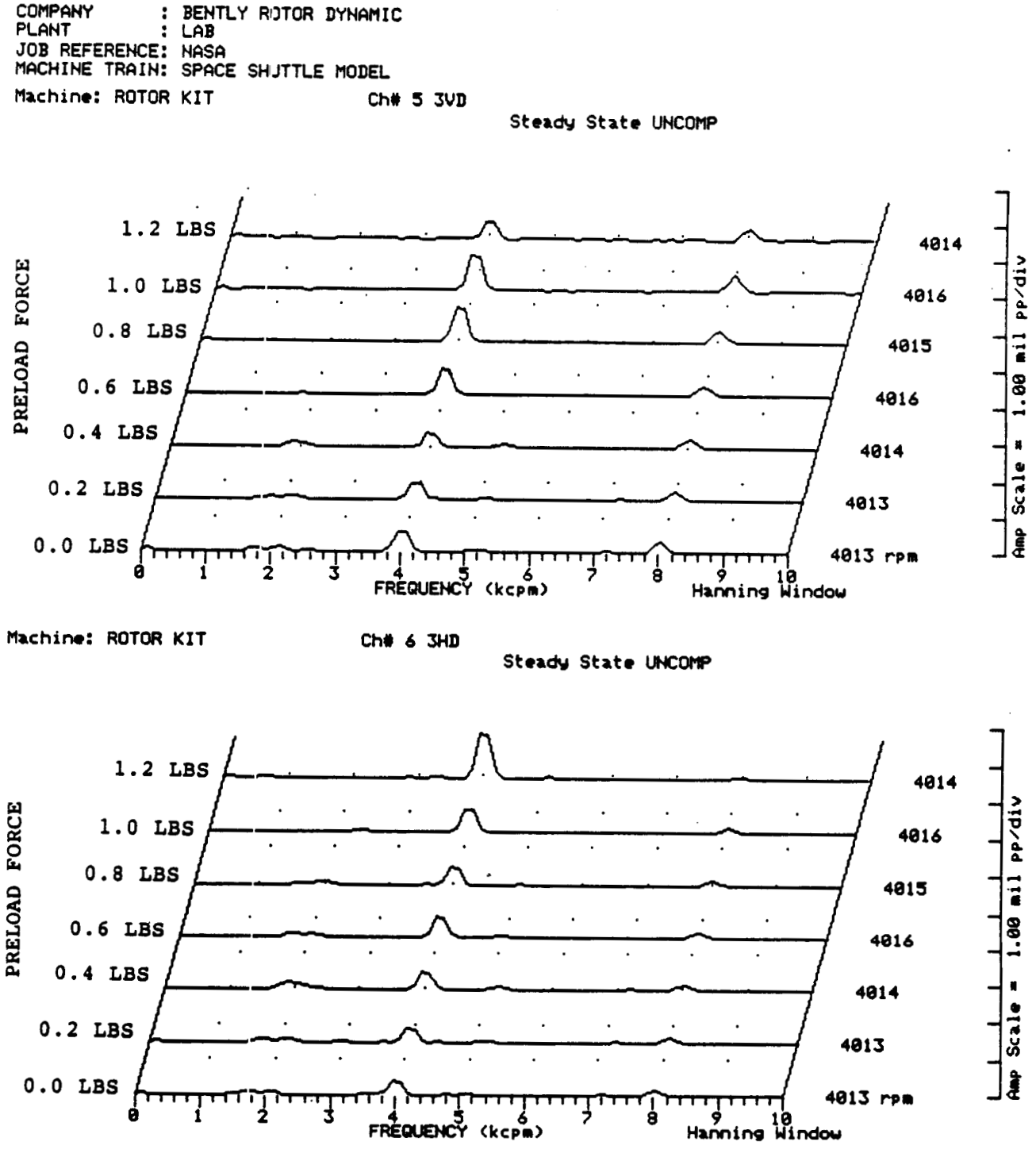

FIGURE 12.279 SPECTRAL CONTENT AT PROBE LOCATION 3 AT 4000 RPM, 7.5 PSI SEAL OIL PRESSURE, 0.8 IN–GRAM UNBALANCE LOCATED IN THE THIRD PUMP IMPELLER DISK, FOR INCREASING STATIC PRELOADS.

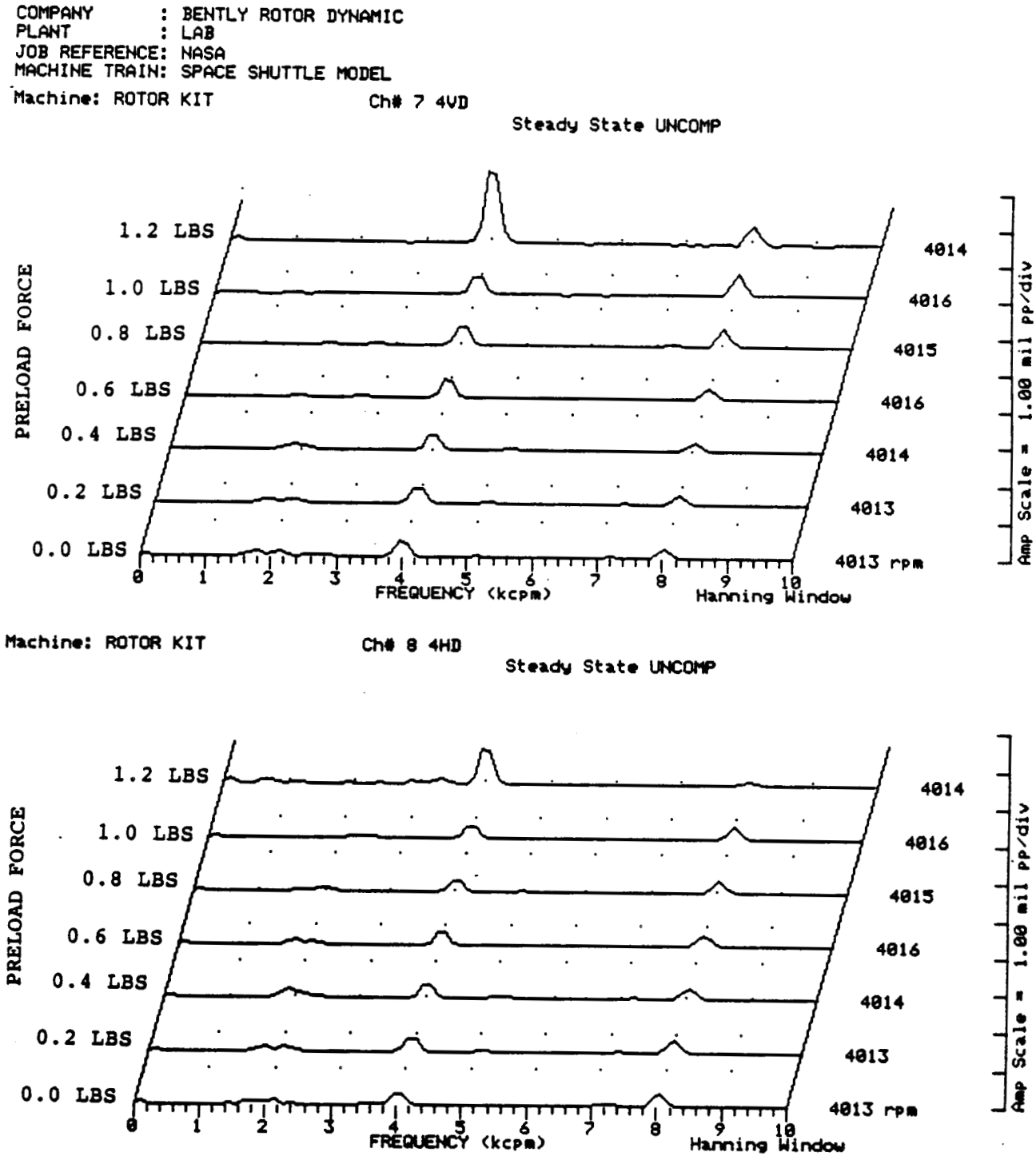

FIGURE 12.280 SPECTRAL CONTENT AT PROBE LOCATION 4 AT 4000 RPM, 7.5 PSI SEAL OIL PRESSURE, 0.8 IN–GRAM UNBALANCE LOCATED IN THE THIRD PUMP IMPELLER DISK, FOR INCREASING STATIC PRELOADS.

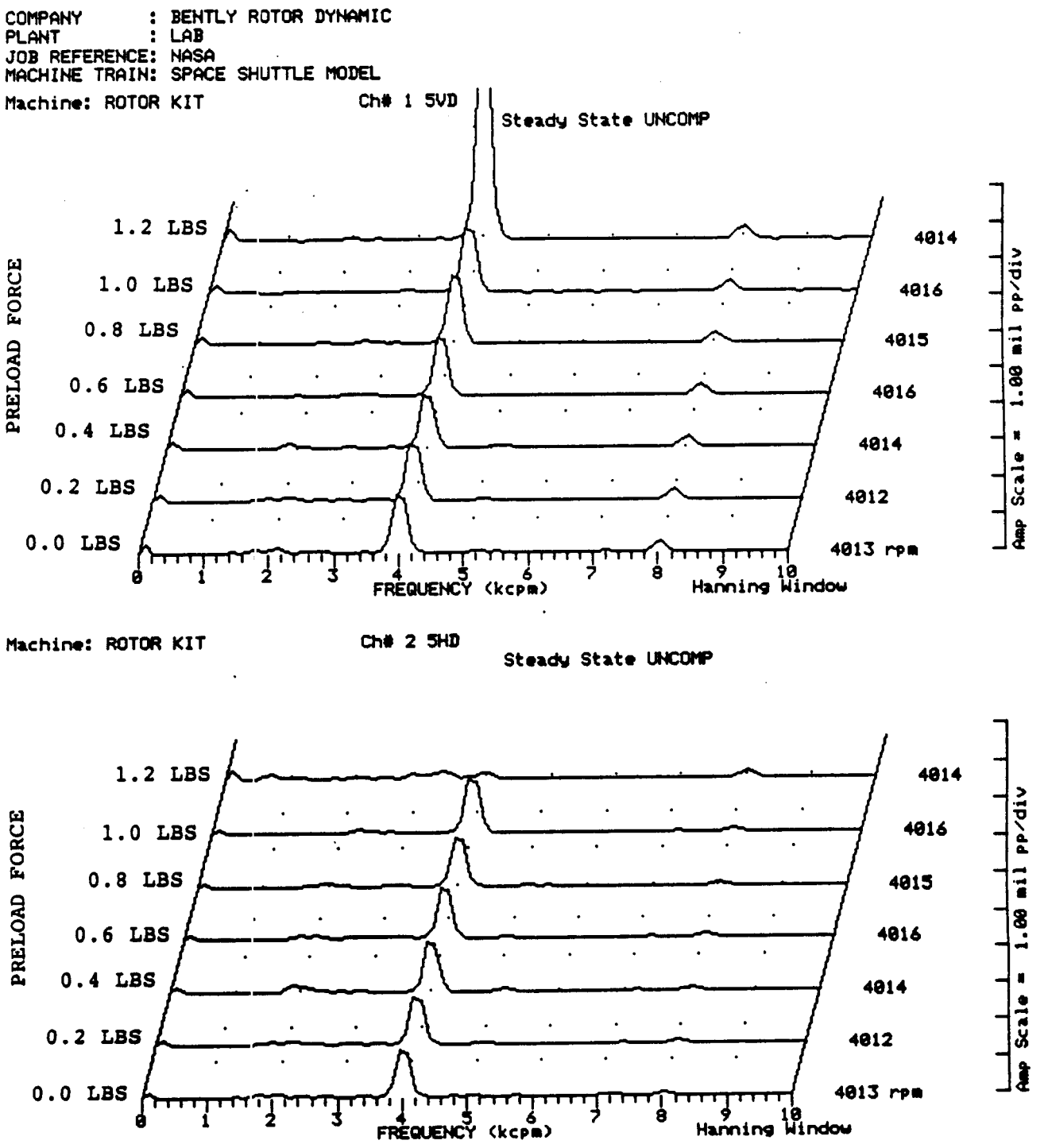

FIGURE 12.281 SPECTRAL CONTENT AT PROBE LOCATION 5 AT 4000 RPM, 7.5 PSI SEAL OIL PRESSURE, 0.8 IN–GRAM UNBALANCE LOCATED IN THE THIRD PUMP IMPELLER DISK, FOR INCREASING STATIC PRELOADS.

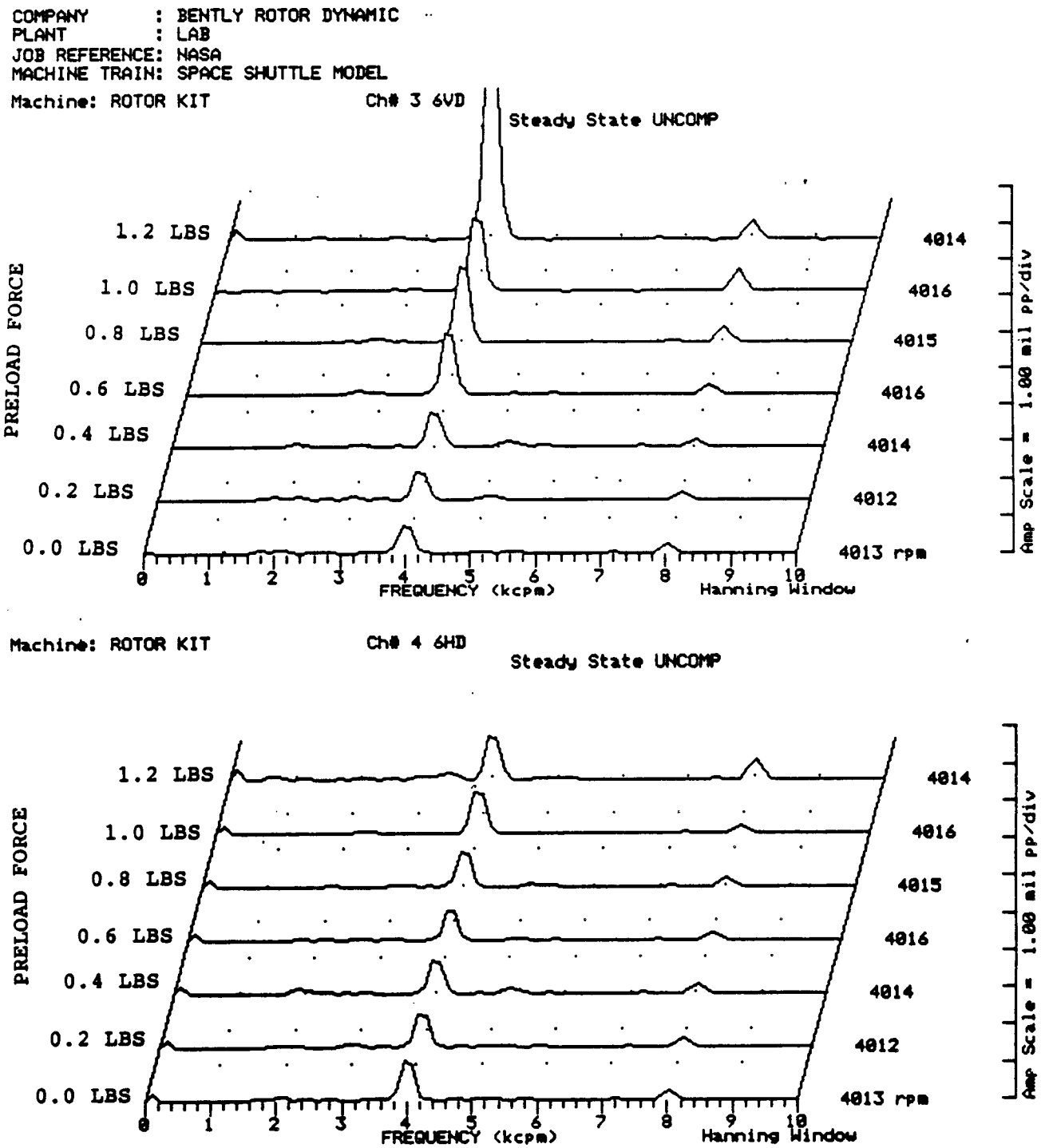

FIGURE 12.282 SPECTRAL CONTENT AT PROBE LOCATION 6 AT 4000 RPM, 7.5 PSI SEAL OIL PRESSURE, 0.8 IN–GRAM UNBALANCE LOCATED IN THE THIRD PUMP IMPELLER DISK, FOR INCREASING STATIC PRELOADS.

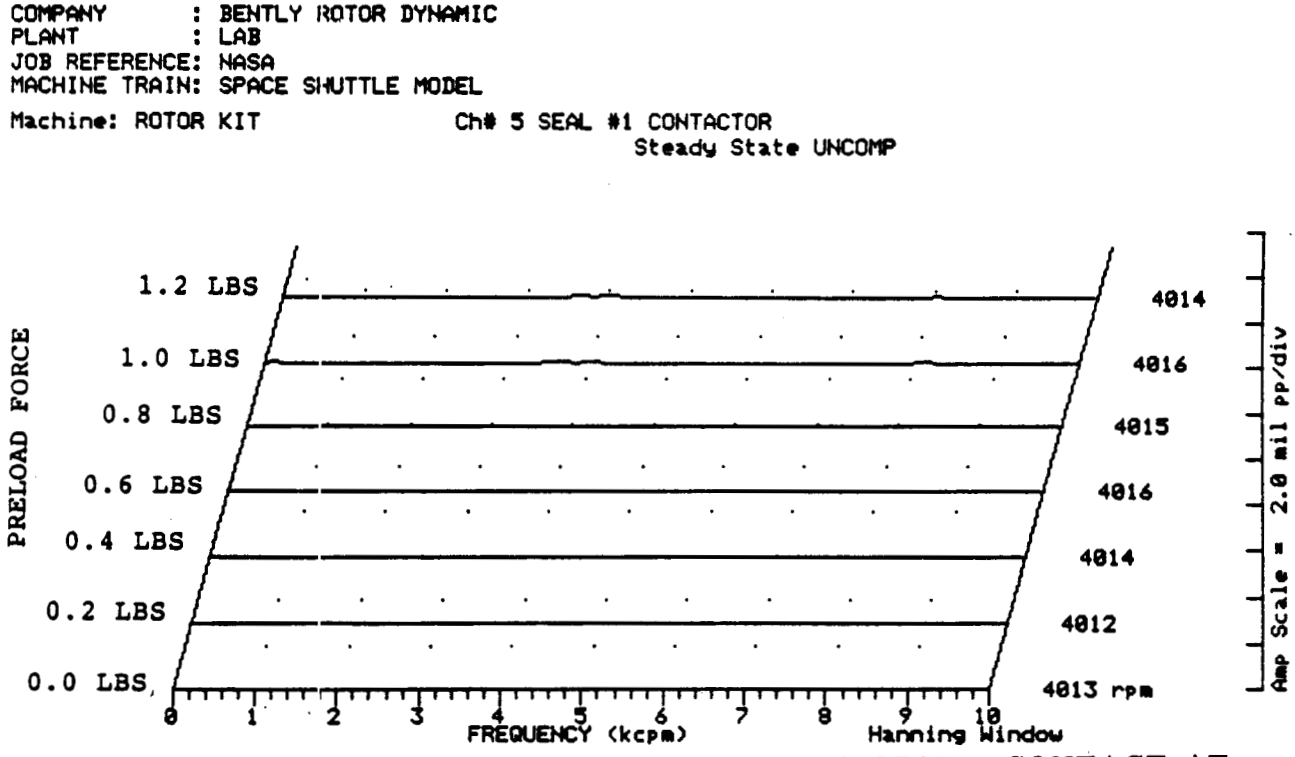

FIGURE 12.283 SPECTRAL CONTENT FOR SHAFT TO SEAL 1 CONTACT AT 4000 RPM, 7.5 PSI SEAL OIL PRESSURE, 0.8 IN–GRAM UNBALANCE LOCATED IN THE THIRD PUMP IMPELLER DISK, FOR INCREASING STATIC PRELOADS.

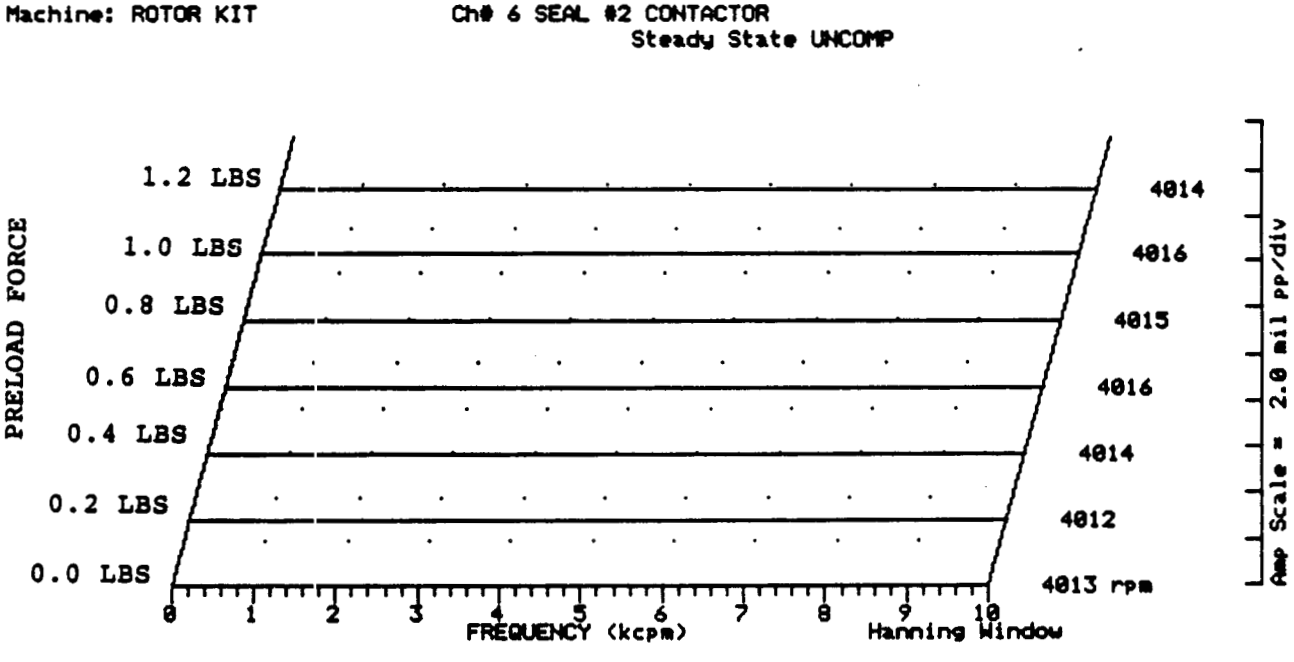

FIGURE 12.284 SPECTRAL CONTENT FOR SHAFT TO SEAL 2 CONTACT AT 4000 RPM, 7.5 PSI SEAL OIL PRESSURE, 0.8 IN–GRAM UNBALANCE LOCATED IN THE THIRD PUMP IMPELLER DISK, FOR INCREASING STATIC PRELOADS.

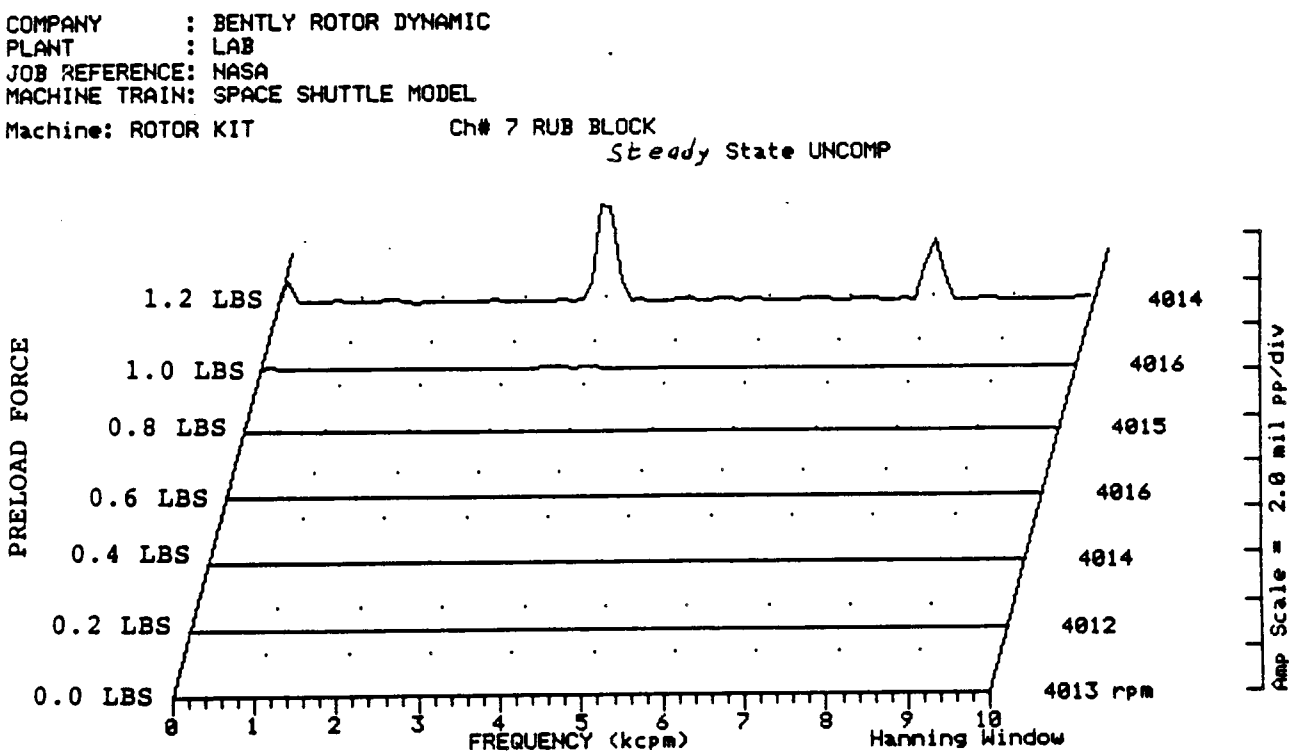

FIGURE 12.285 SPECTRAL CONTENT FOR SHAFT TO RUB BLOCK CONTACT AT 4000 RPM, 7.5 PSI SEAL OIL PRESSURE, 0.8 IN–GRAM UNBALANCE LOCATED IN THE THIRD PUMP IMPELLER DISK, FOR INCREASING STATIC PRELOADS.

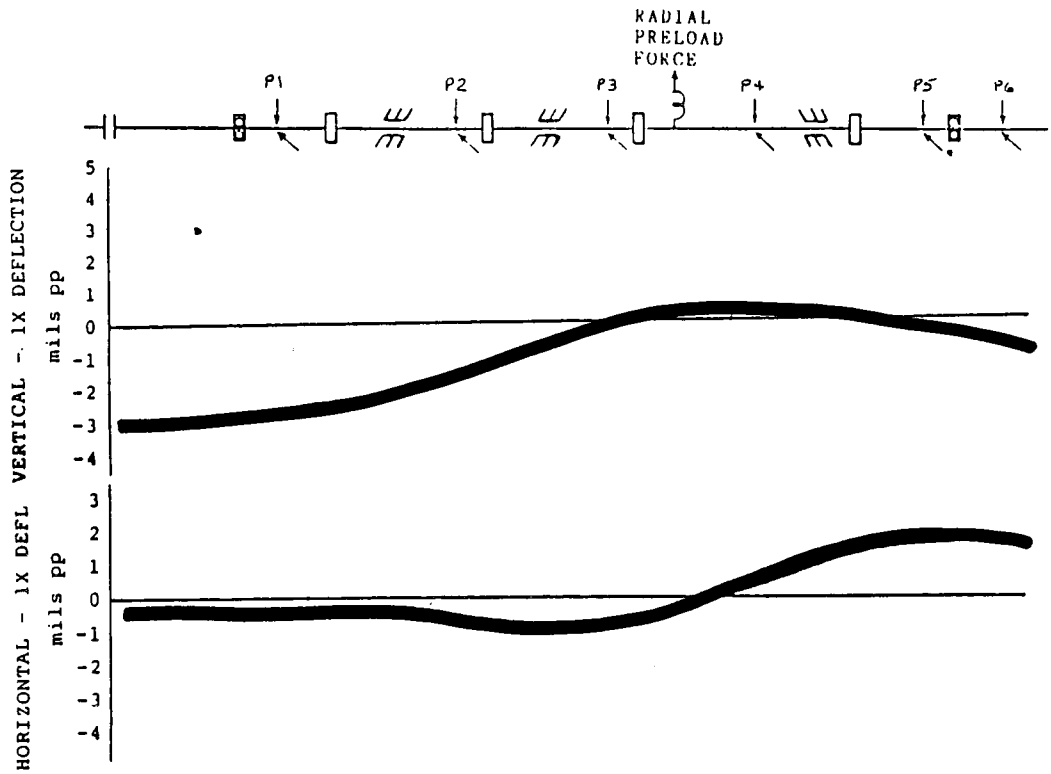

FIGURE 12.286 ROTOR MODE SHAPE AT 4000 RPM, 10.0 PSI SEAL OIL PRESSURE DUE TO 0.8 IN–GRAM UNBALANCE LOCATED IN THE THIRD PUMP IMPELLER DISK.

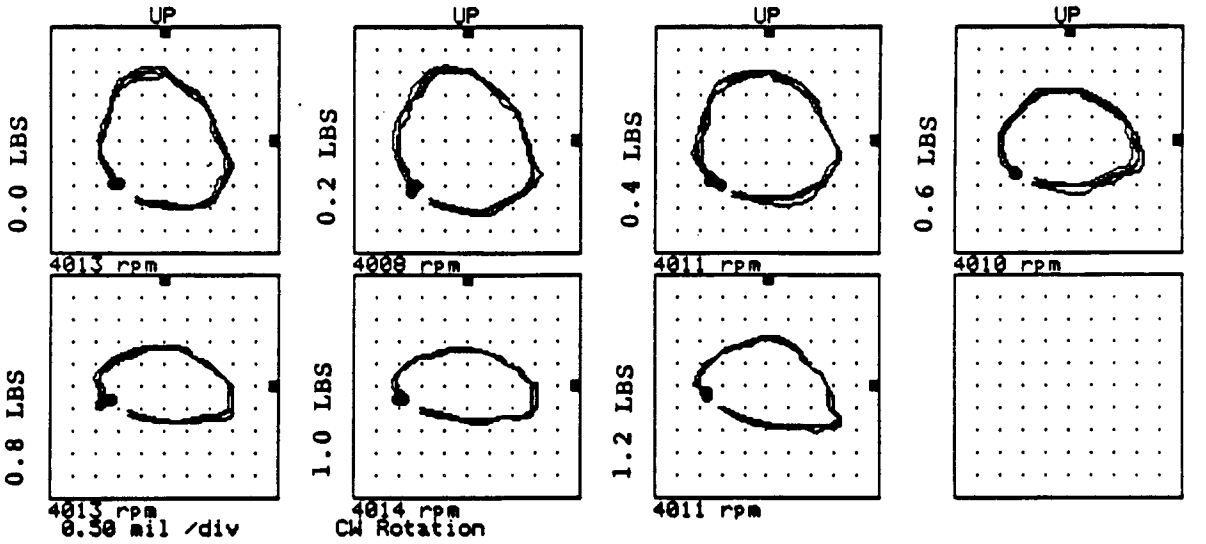

FIGURE 12.287 ORBITS AT PROBE LOCATION 1 AT 4000 RPM, 10.0 PSI SEAL OIL PRESSURE, 0.8 IN–GRAM UNBALANCE LOCATED IN THE THIRD PUMP IMPELLER DISK, FOR INCREASING STATIC PRELOAD FORCES.

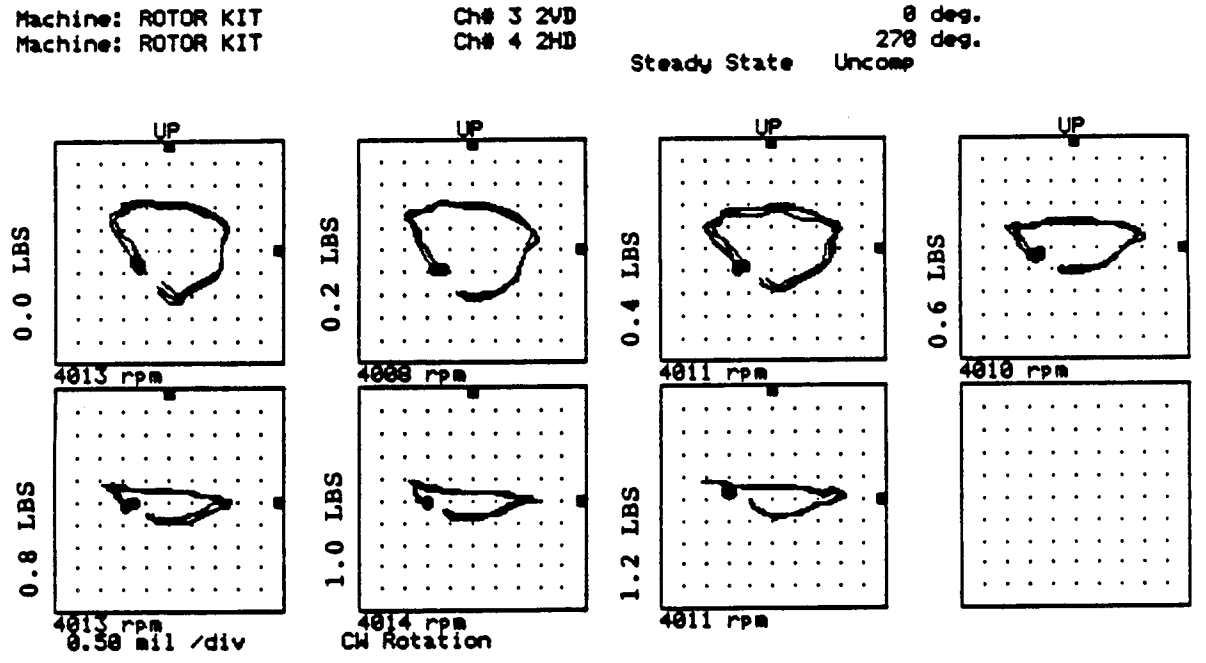

FIGURE 12.288 ORBITS AT PROBE LOCATION 2 AT 4000 RPM, 10.0 PSI SEAL OIL PRESSURE, 0.8 IN–GRAM UNBALANCE LOCATED IN THE THIRD PUMP IMPELLER DISK, FOR INCREASING STATIC PRELOAD FORCES.

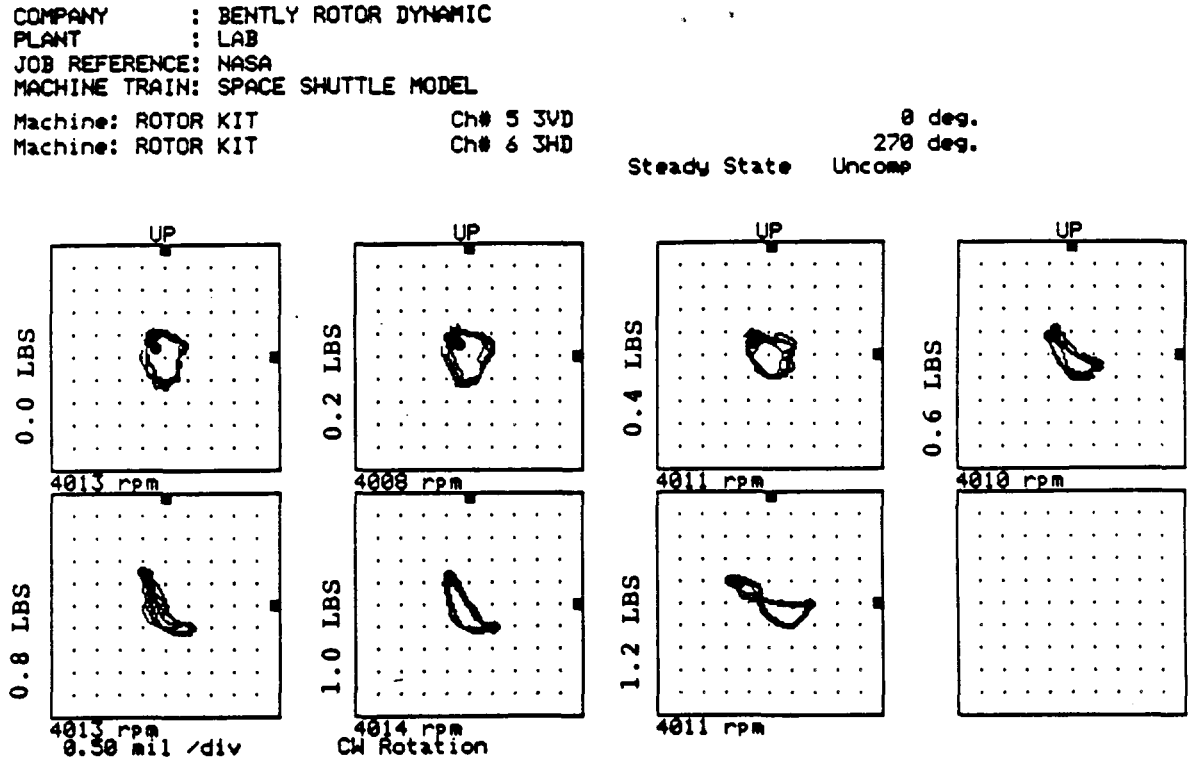

FIGURE 12.289 ORBITS AT PROBE LOCATION 3 AT 4000 RPM, 10.0 PSI SEAL OIL PRESSURE, 0.8 IN–GRAM UNBALANCE LOCATED IN THE THIRD PUMP IMPELLER DISK, FOR INCREASING STATIC PRELOAD FORCES.

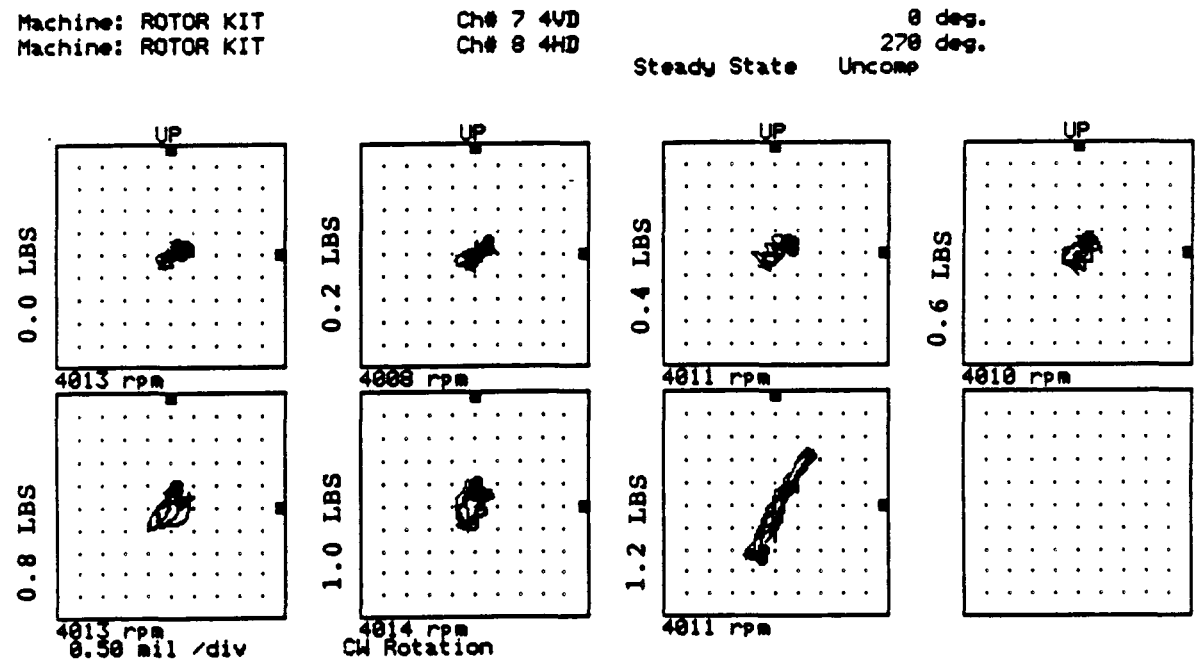

FIGURE 12.290 ORBITS AT PROBE LOCATION 4 AT 4000 RPM, 10.0 PSI SEAL OIL PRESSURE, 0.8 IN–GRAM UNBALANCE LOCATED IN THE THIRD PUMP IMPELLER DISK, FOR INCREASING STATIC PRELOAD FORCES.

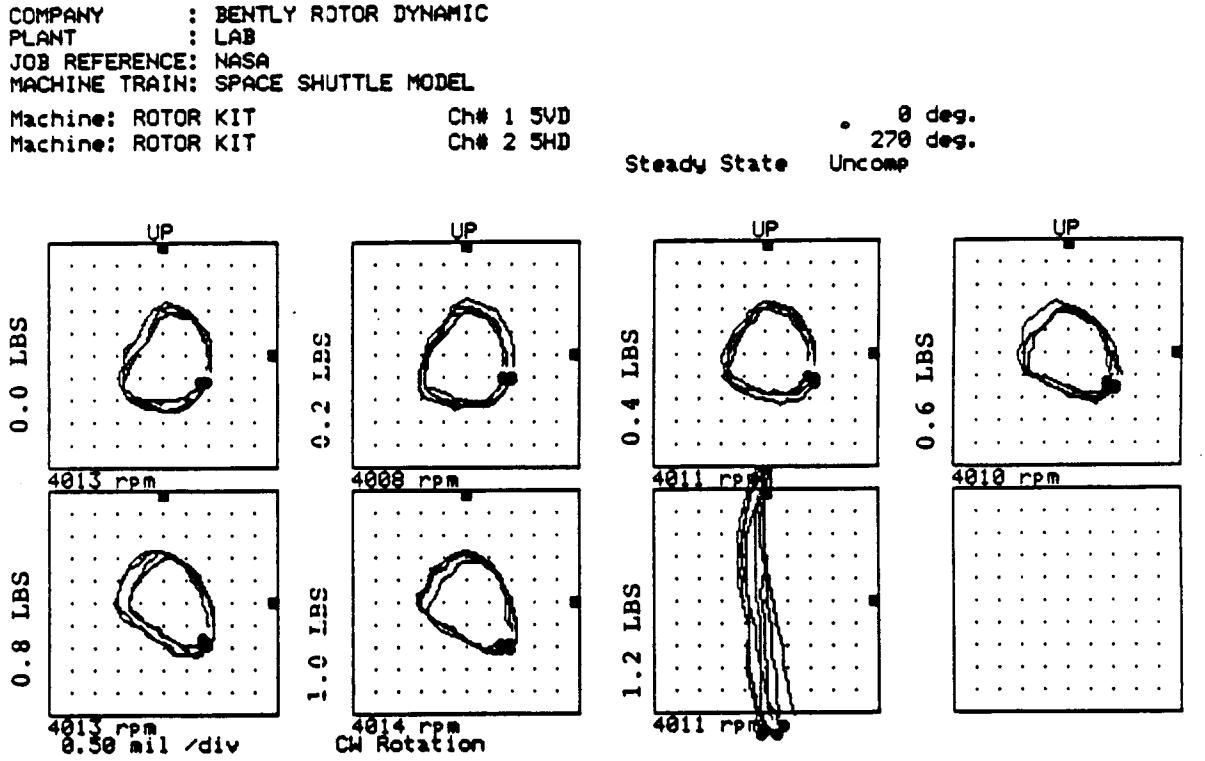

FIGURE 12.291 ORBITS AT PROBE LOCATION 5 AT 4000 RPM, 10.0 PSI SEAL OIL PRESSURE, 0.8 IN–GRAM UNBALANCE LOCATED IN THE THIRD PUMP IMPELLER DISK, FOR INCREASING STATIC PRELOAD FORCES.

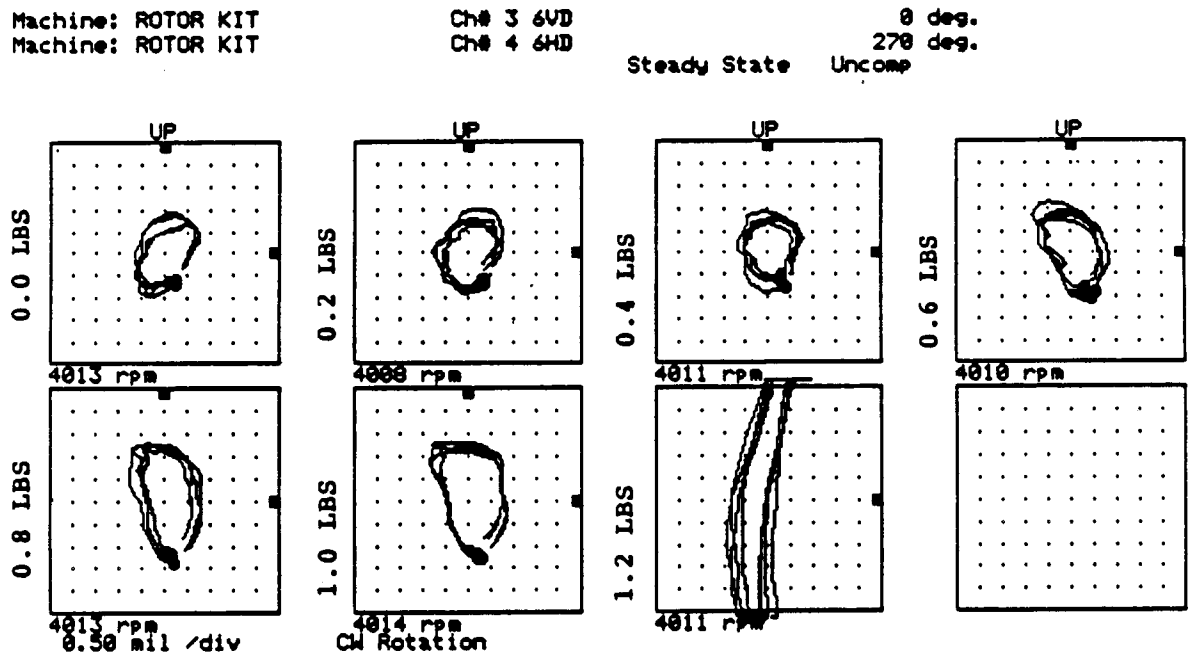

FIGURE 12.292 ORBITS AT PROBE LOCATION 6 AT 4000 RPM, 10.0 PSI SEAL OIL PRESSURE, 0.8 IN–GRAM UNBALANCE LOCATED IN THE THIRD PUMP IMPELLER DISK, FOR INCREASING STATIC PRELOAD FORCES.

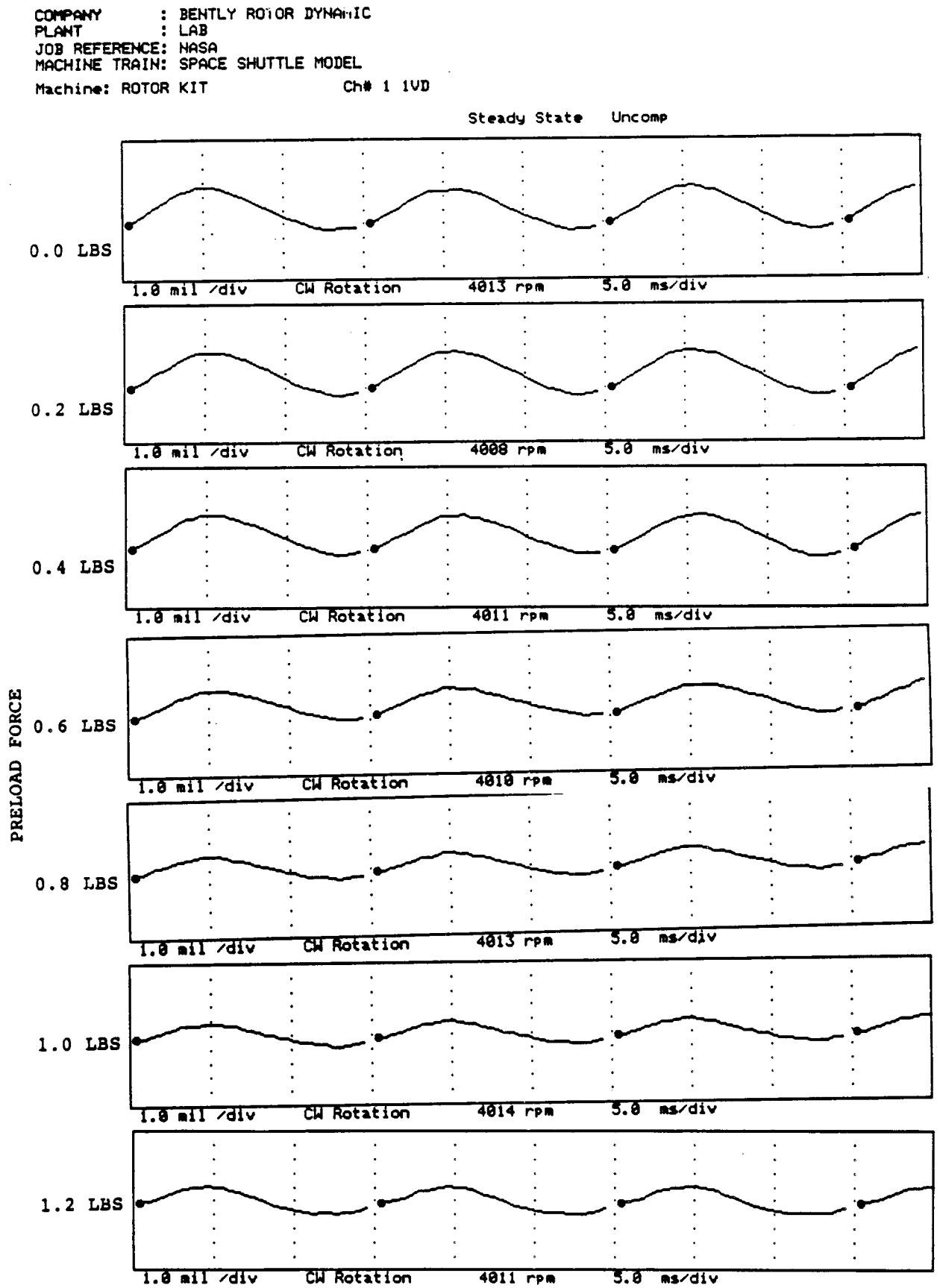

FIGURE 12.293 TIMEBASE FOR VERTICAL PROBE AT LOCATION 1 AT 4000 RPM, 10.0 PSI SEAL OIL PRESSURE, 0.8 IN–GRAM UNBALANCE LOCATED IN THE THIRD PUMP IMPELLER DISK, FOR INCREASING STATIC PRELOADS.

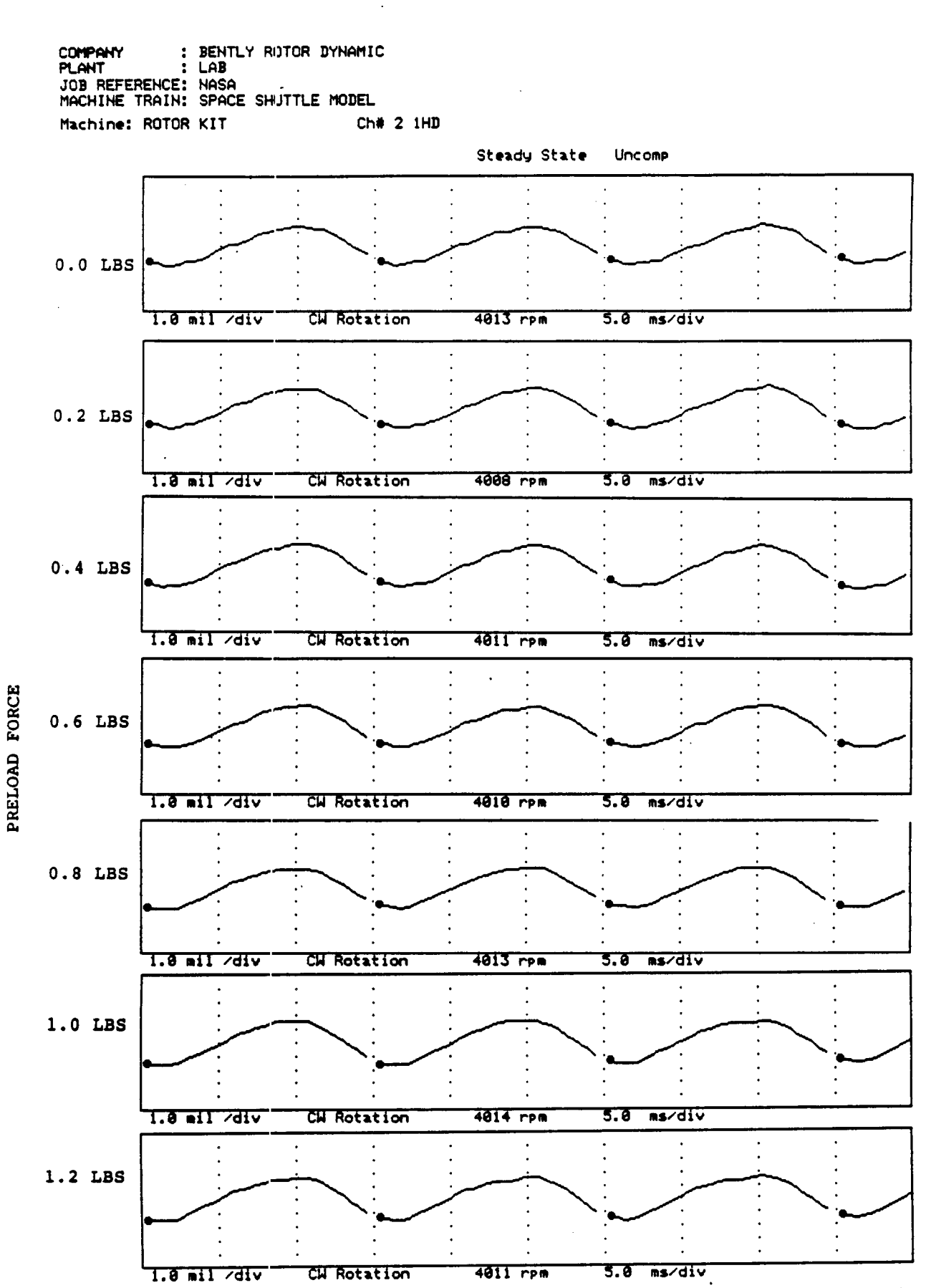

FIGURE 12.294 TIMEBASE FOR HORIZONTAL PROBE AT LOCATION 1 AT 4000 RPM, 10.0 PSI SEAL OIL PRESSURE, 0.8 IN–GRAM UNBALANCE LOCATED IN THE THIRD PUMP IMPELLER DISK, FOR INCREASING STATIC PRELOADS.

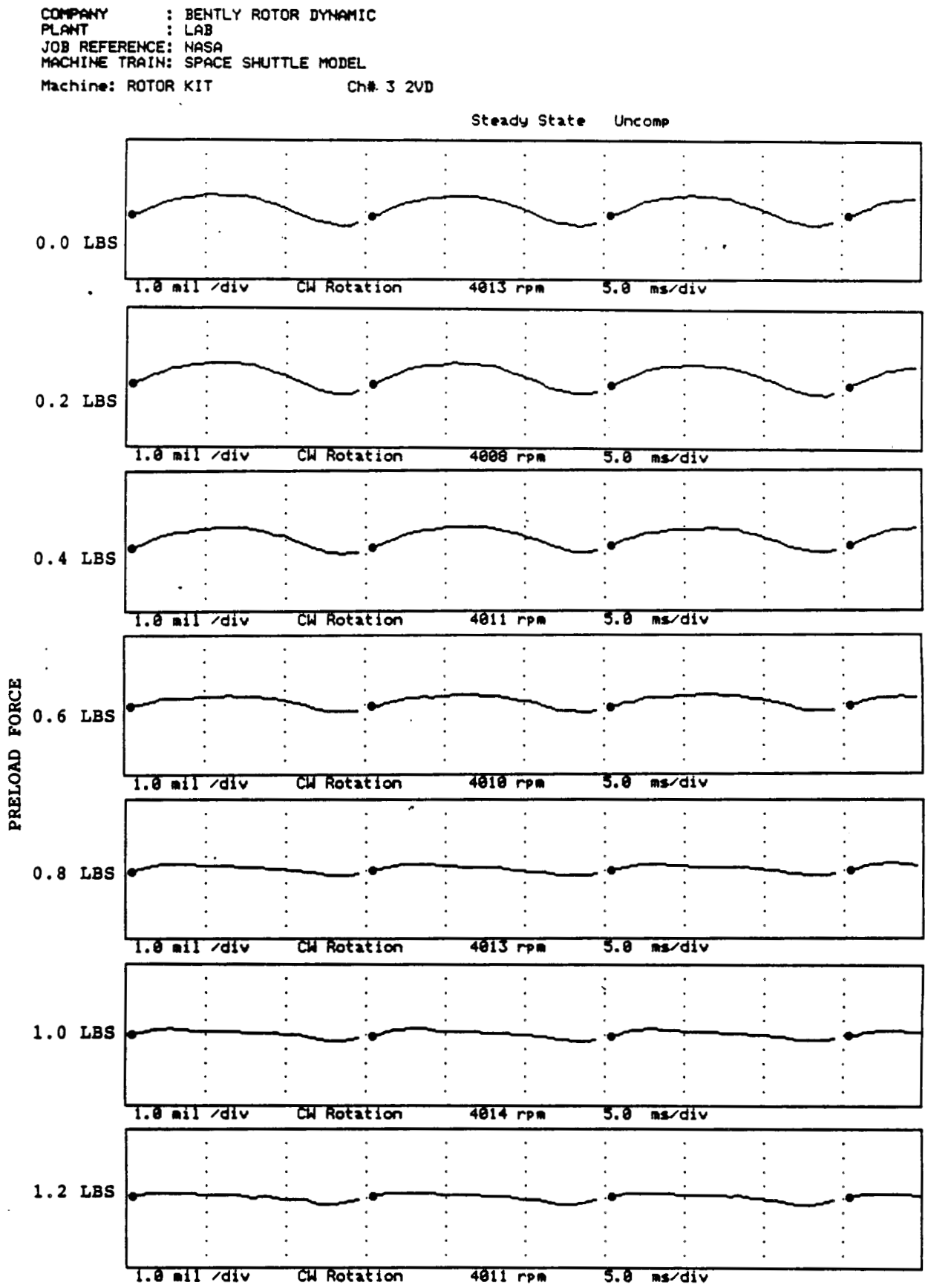

FIGURE 12.295 TIMEBASE FOR VERTICAL PROBE AT LOCATION 2 AT 4000 RPM, 10.0 PSI SEAL OIL PRESSURE, 0.8 IN–GRAM UNBALANCE LOCATED IN THE THIRD PUMP IMPELLER DISK, FOR INCREASING STATIC PRELOADS.

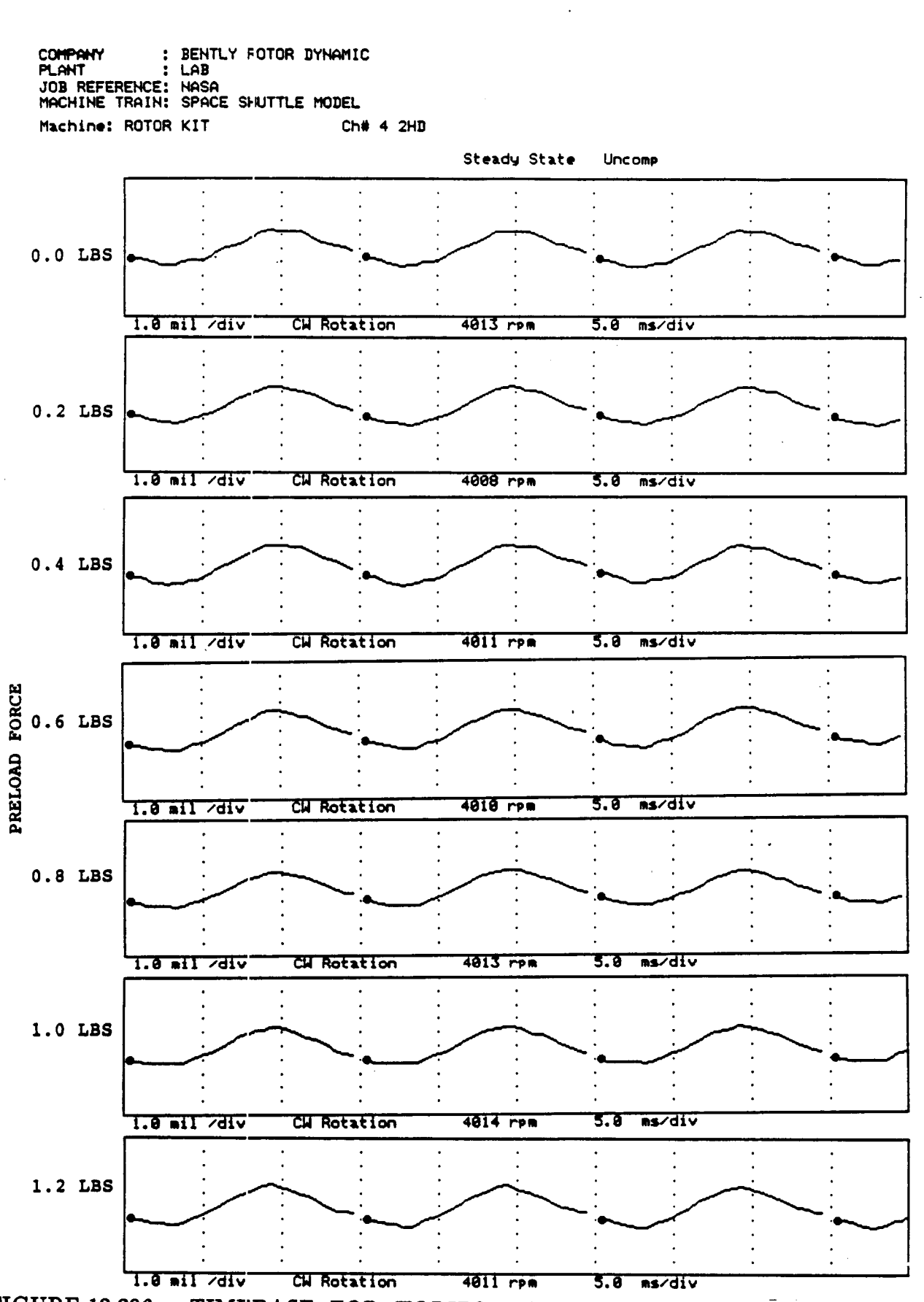

FIGURE 12.296 TIMEBASE FOR HORIZONTAL PROBE AT LOCATION 2 AT 4000 RPM, 10.0 PSI SEAL OIL PRESSURE, 0.8 IN–GRAM UNBALANCE LOCATED IN THE THIRD PUMP IMPELLER DISK, FOR INCREASING STATIC PRELOADS.

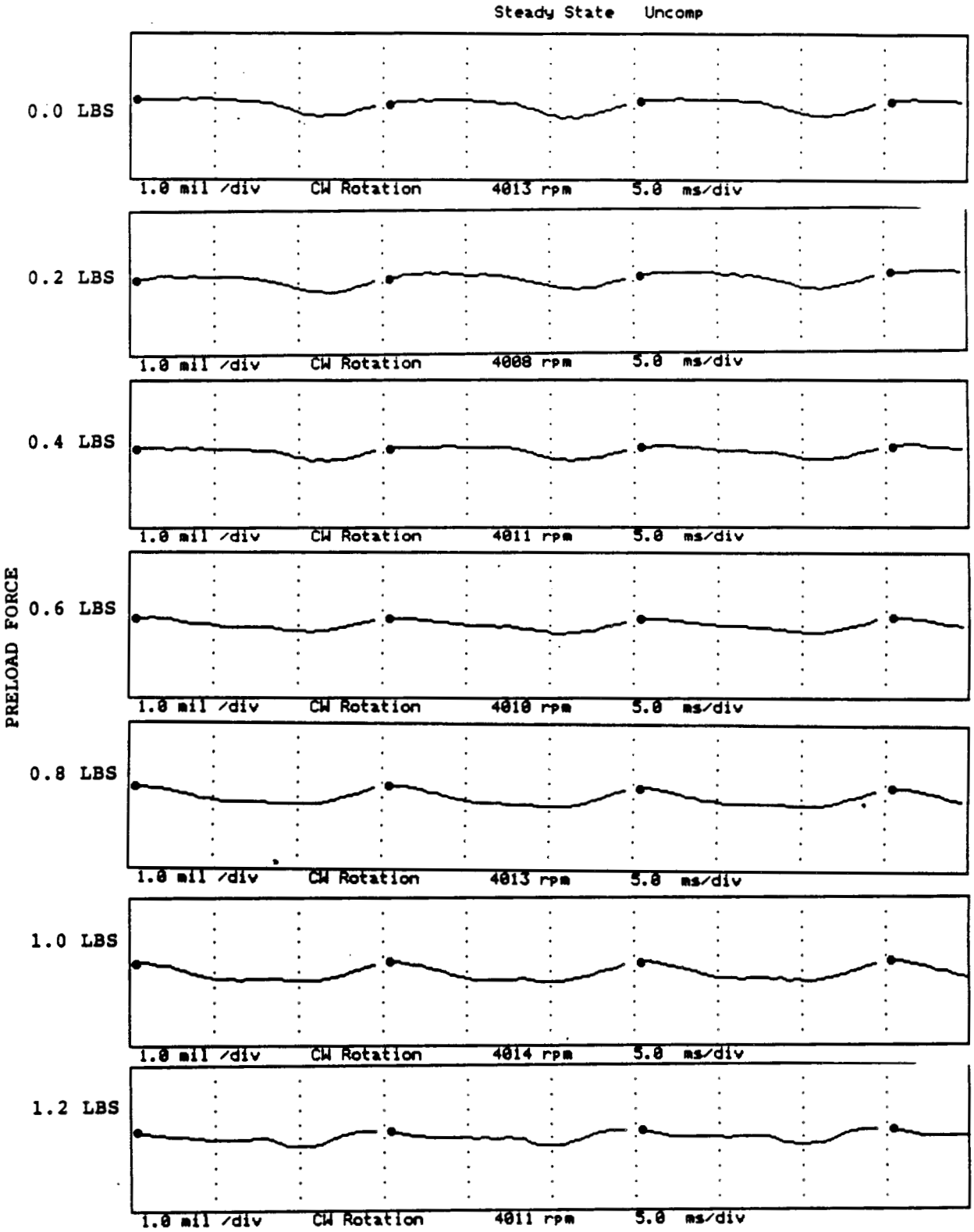

FIGURE 12.297 TIMEBASE FOR VERTICAL PROBE AT LOCATION 3 AT 4000 RPM, 10.0 PSI SEAL OIL PRESSURE, 0.8 IN–GRAM UNBALANCE LOCATED IN THE THIRD PUMP IMPELLER DISK, FOR INCREASING STATIC PRELOADS.

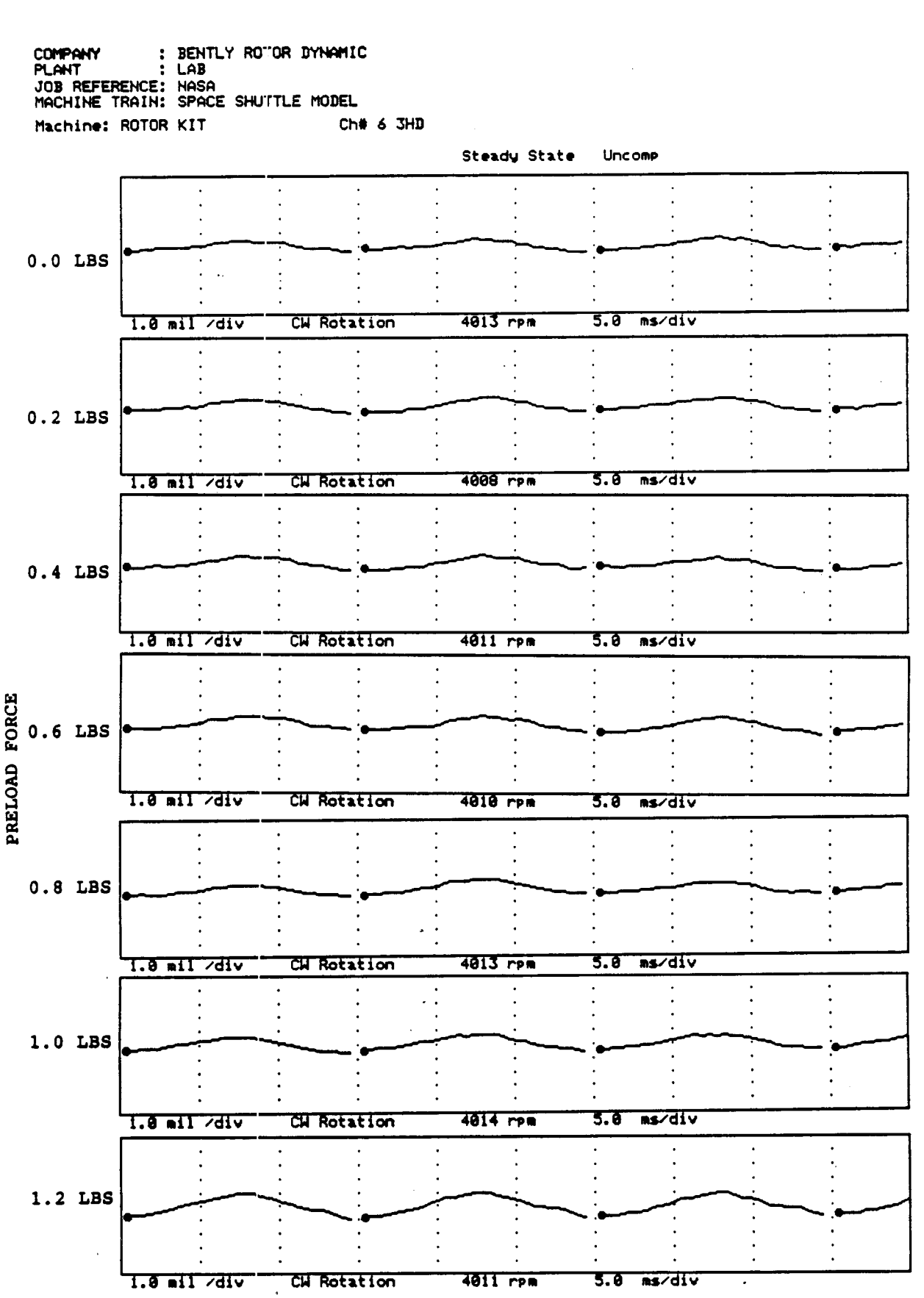

FIGURE 12.298 TIMEBASE FOR HORIZONTAL PROBE AT LOCATION 3 AT 4000 RPM, 10.0 PSI SEAL OIL PRESSURE, 0.8 IN–GRAM UNBALANCE LOCATED IN THE THIRD PUMP IMPELLER DISK, FOR INCREASING STATIC PRELOADS.

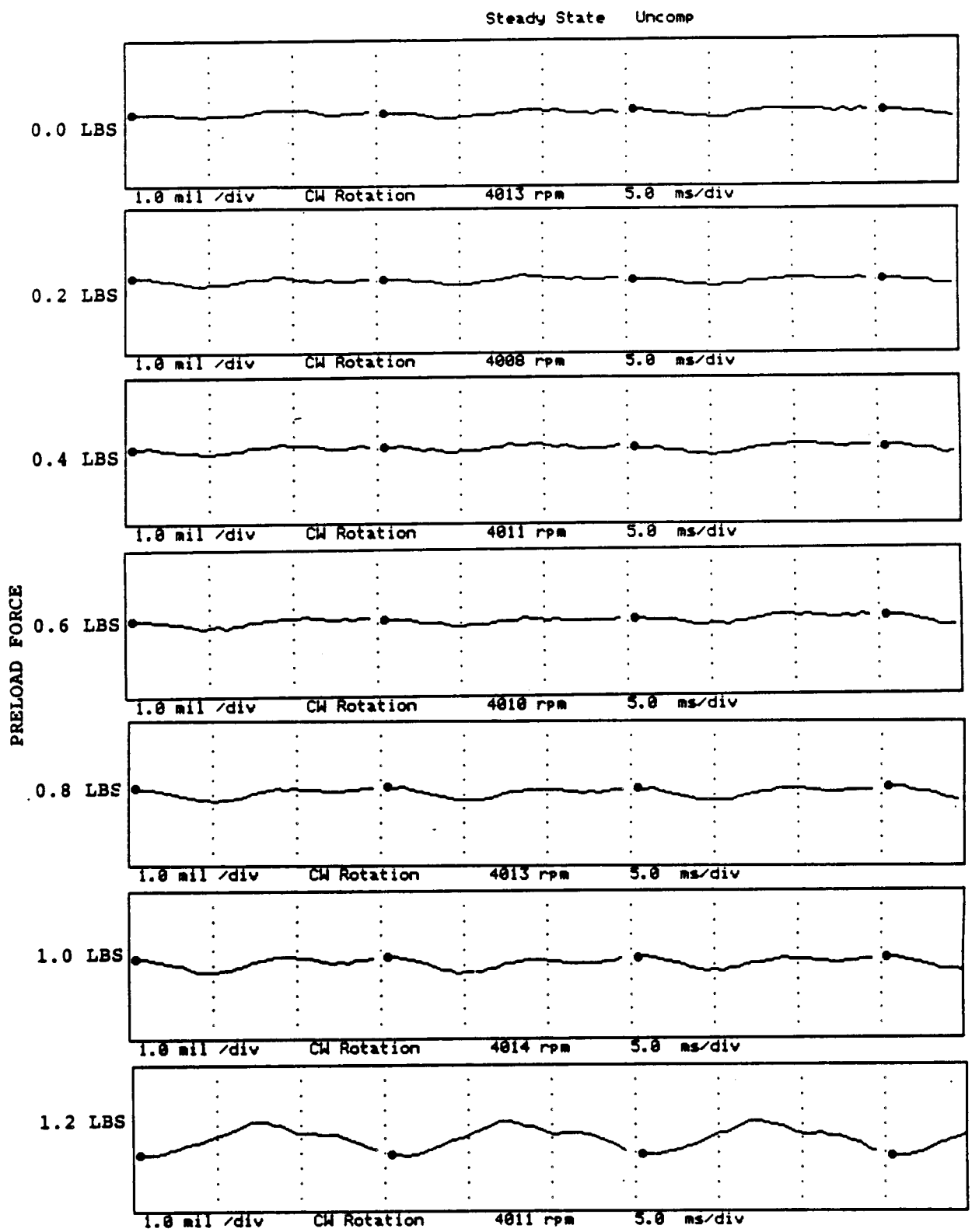

FIGURE 12.299 TIMEBASE FOR VERTICAL PROBE AT LOCATION 4 AT 4000 RPM, 10.0 PSI SEAL OIL PRESSURE, 0.8 IN–GRAM UNBALANCE LOCATED IN THE THIRD PUMP IMPELLER DISK, FOR INCREASING STATIC PRELOADS.

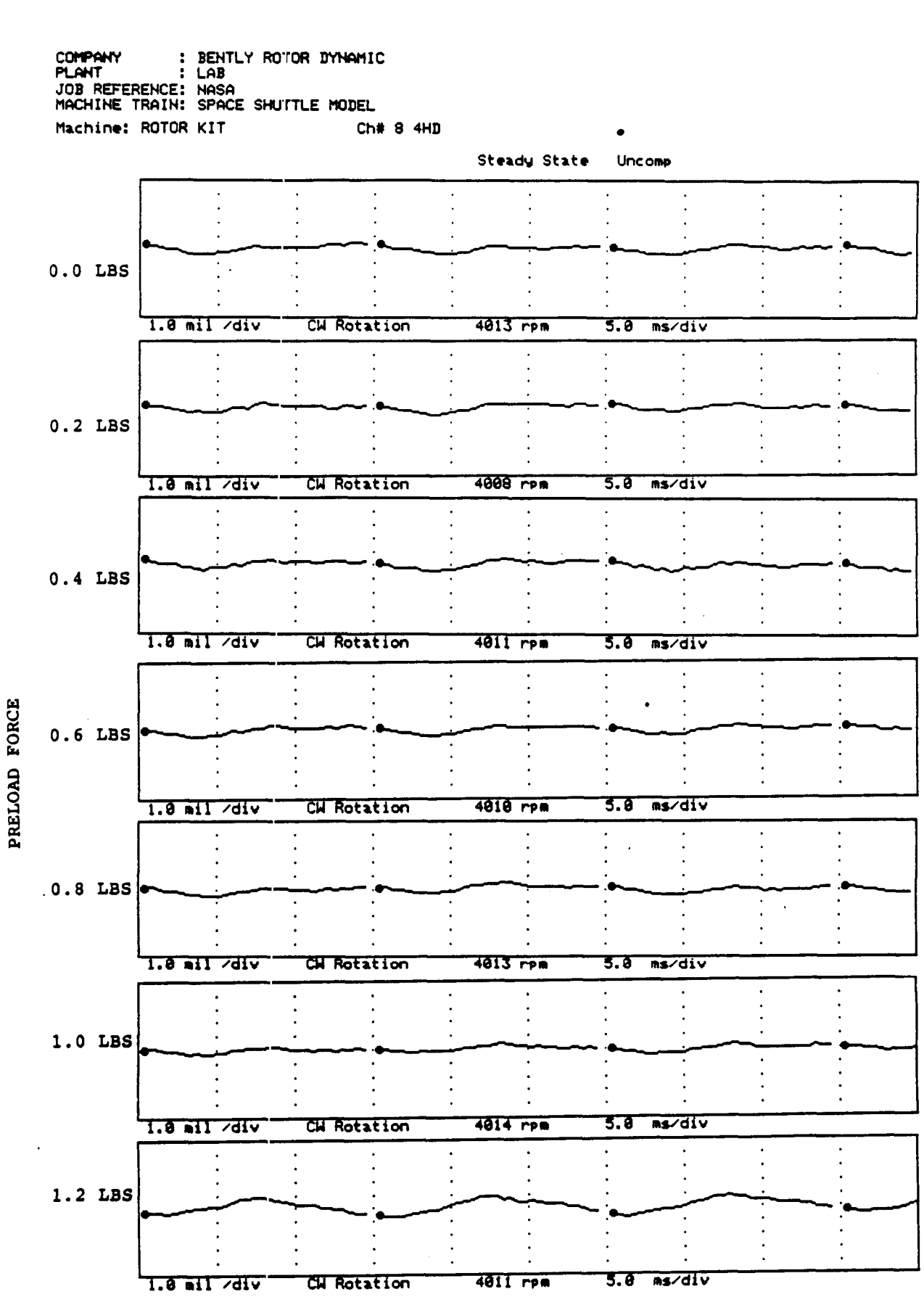

FIGURE 12.300 TIMEBASE FOR HORIZONTAL PROBE AT LOCATION 4 AT 4000 RPM, 10.0 PSI SEAL OIL PRESSURE, 0.8 IN–GRAM UNBALANCE LOCATED IN THE THIRD PUMP IMPELLER DISK, FOR INCREASING STATIC PRELOADS.

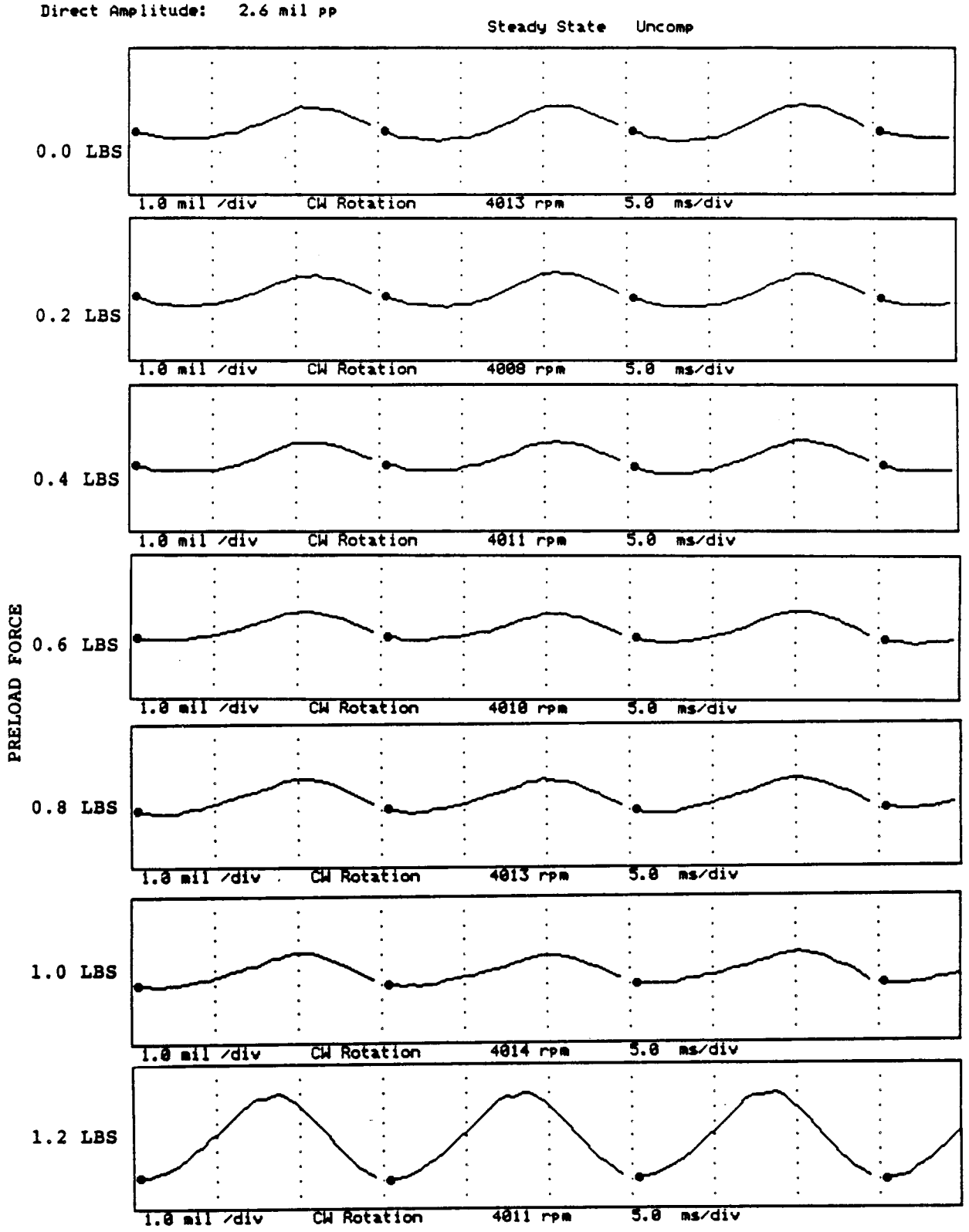

FIGURE 12.301 TIMEBASE FOR VERTICAL PROBE AT LOCATION 5 AT 4000 RPM, 10.0 PSI SEAL OIL PRESSURE, 0.8 IN–GRAM UNBALANCE LOCATED IN THE THIRD PUMP IMPELLER DISK, FOR INCREASING STATIC PRELOADS.

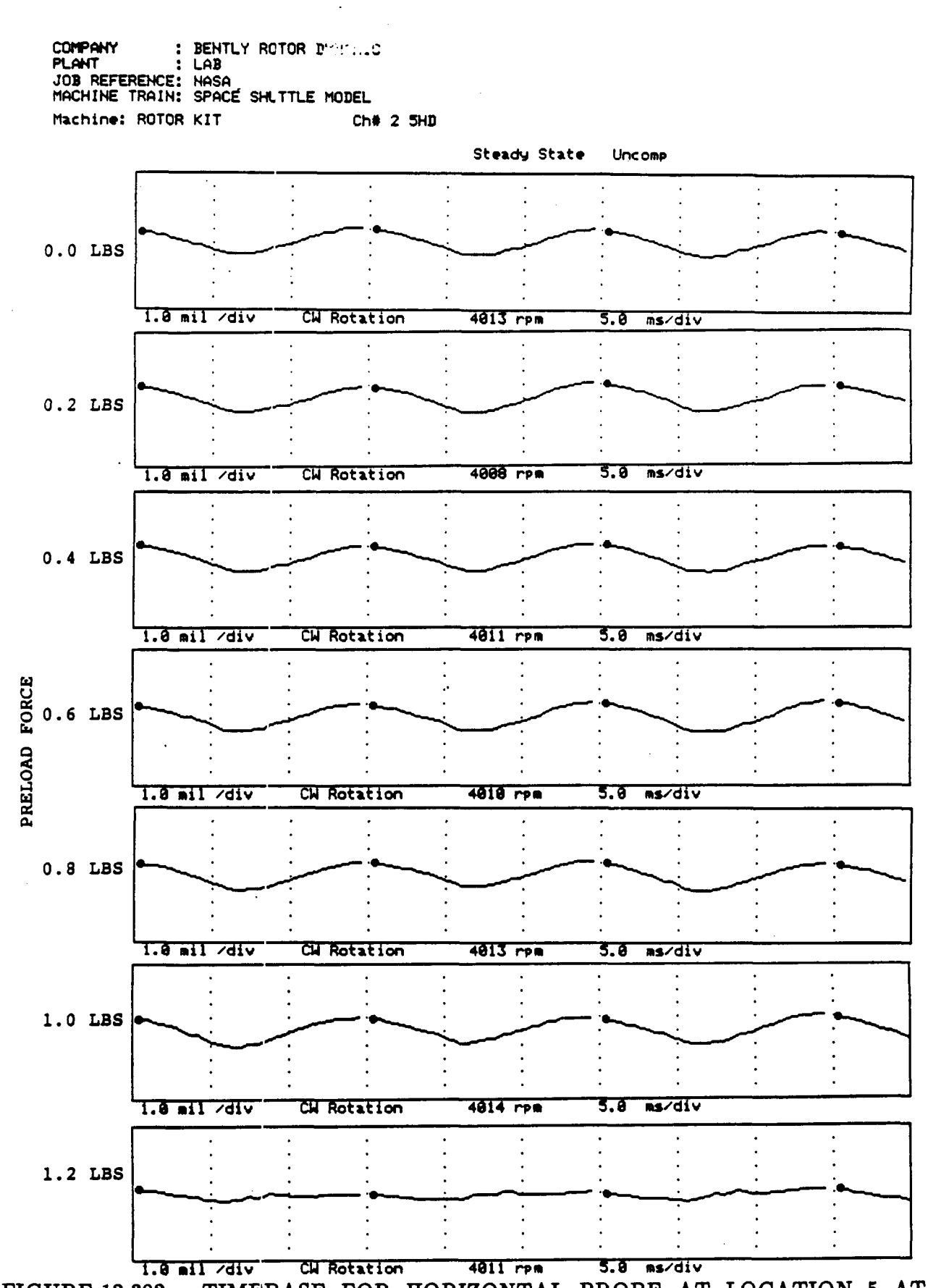

FIGURE 12.302 TIMEBASE FOR HORIZONTAL PROBE AT LOCATION 5 AT 4000 RPM, 10.0 PSI SEAL OIL PRESSURE, 0.8 IN–GRAM UNBALANCE LOCATED IN THE THIRD PUMP IMPELLER DISK, FOR INCREASING STATIC PRELOADS.

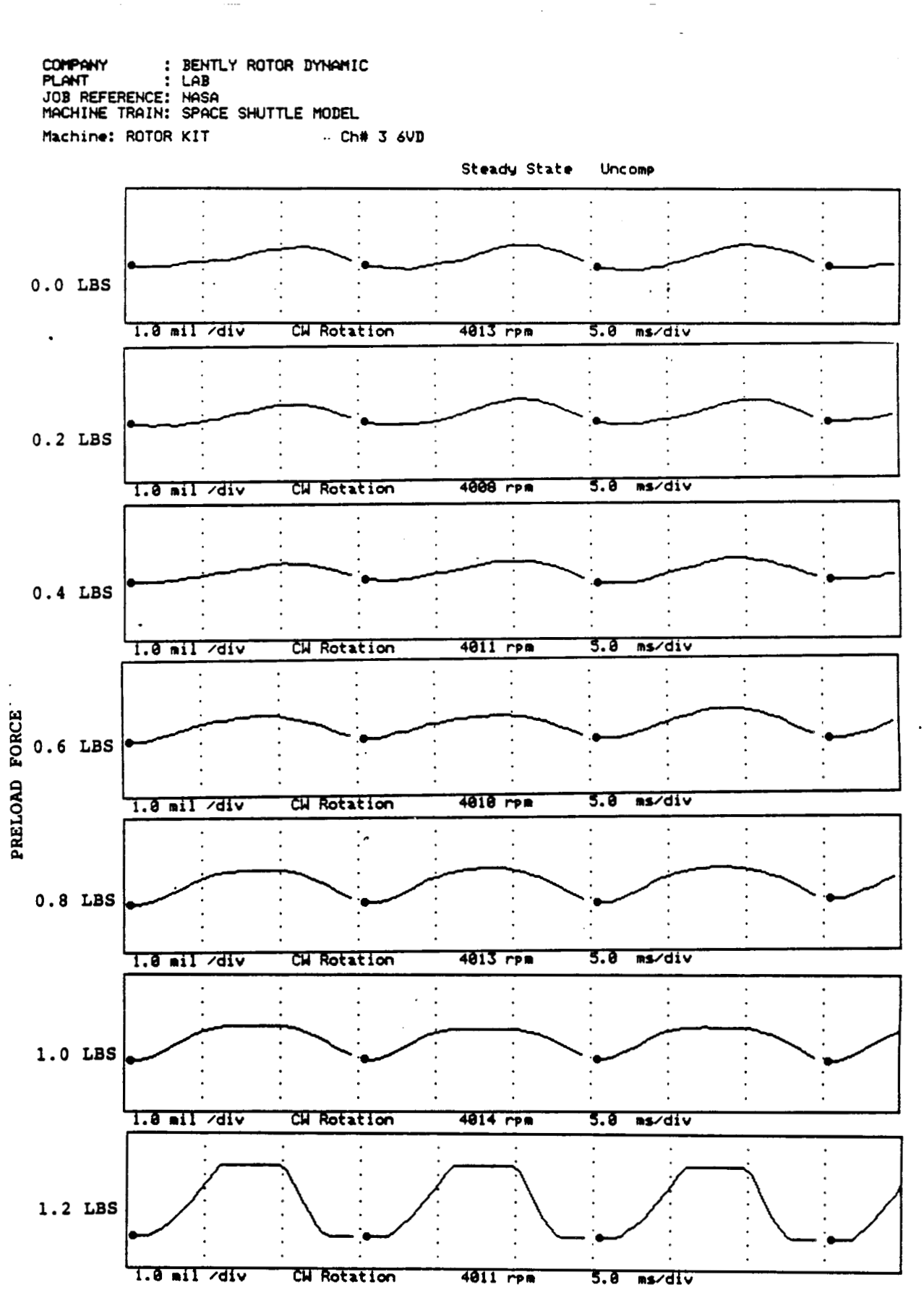

FIGURE 12.303 TIMEBASE FOR VERTICAL PROBE AT LOCATION 6 AT 4000 RPM, 10.0 PSI SEAL OIL PRESSURE, 0.8 IN–GRAM UNBALANCE LOCATED IN THE THIRD PUMP IMPELLER DISK, FOR INCREASING STATIC PRELOADS.

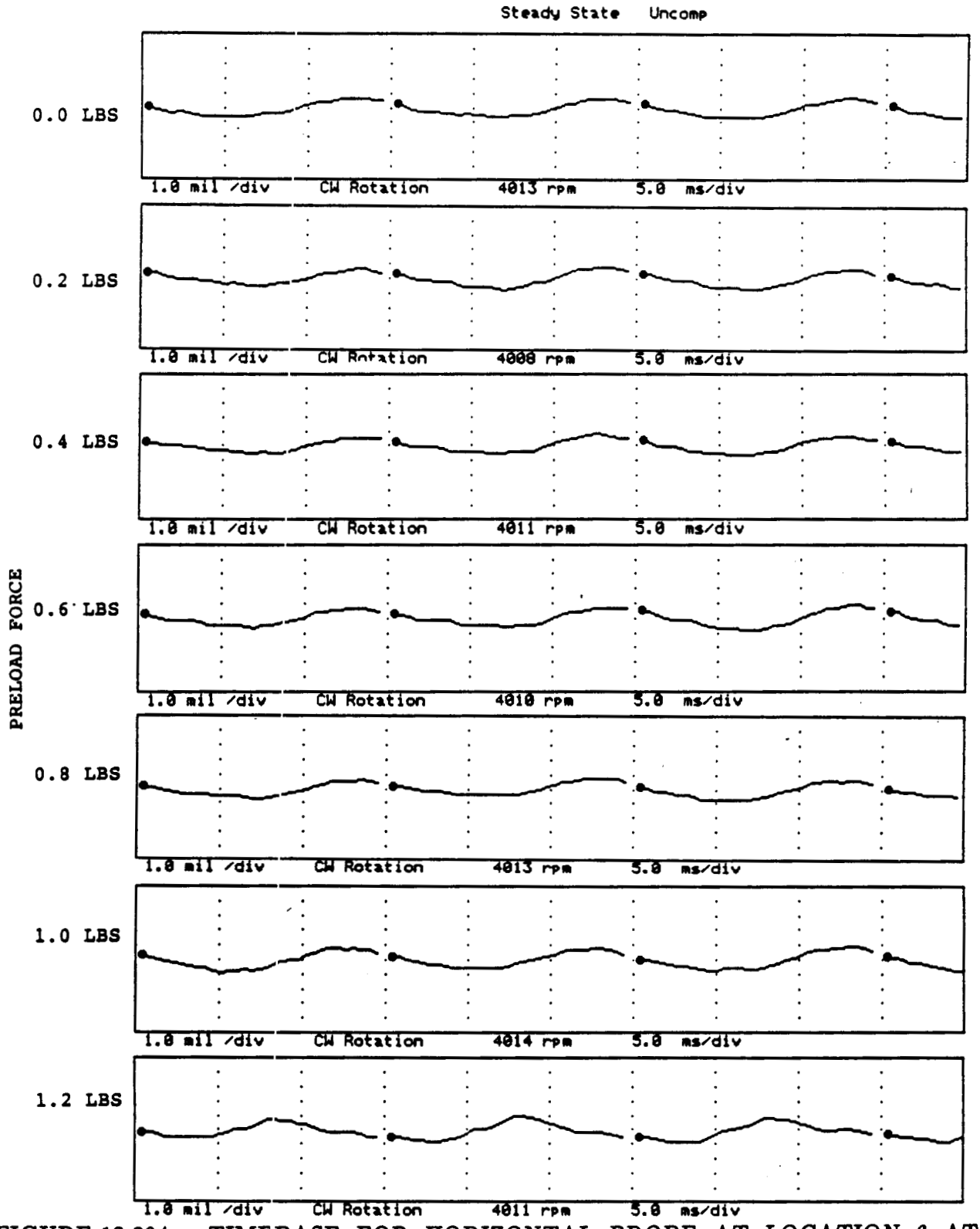

FIGURE 12.304 TIMEBASE FOR HORIZONTAL PROBE AT LOCATION 6 AT 4000 RPM, 10.0 PSI SEAL OIL PRESSURE, 0.8 IN–GRAM UNBALANCE LOCATED IN THE THIRD PUMP IMPELLER DISK, FOR INCREASING STATIC PRELOADS.

NOT AVAILABLE - OIL IN THE CLEARANCE AREA PROHIBITS THE METAL-TO-METAL CONTACT NECESSARY FOR THE CONTACT SENSOR TO OPERATE CORRECTLY.

FIGURE 12.305 TIMEBASE FOR SHAFT TO SEAL 1 CONTACT AT 4000 RPM, 10.0 PSI SEAL OIL PRESSURE, 0.8 IN–GRAM UNBALANCE LOCATED IN THE THIRD PUMP IMPELLER DISK, FOR INCREASING STATIC PRELOADS.

NOT AVAILABLE - OIL IN THE CLEARANCE AREA PROHIBITS THE METAL-TO-METAL CONTACT NECESSARY FOR THE CONTACT SENSOR TO OPERATE CORRECTLY.

FIGURE 12.306 TIMEBASE FOR SHAFT TO SEAL 2 CONTACT AT 4000 RPM, 10.0 PSI SEAL OIL PRESSURE, 0.8 IN–GRAM UNBALANCE LOCATED IN THE THIRD PUMP IMPELLER DISK, FOR INCREASING STATIC PRELOADS.

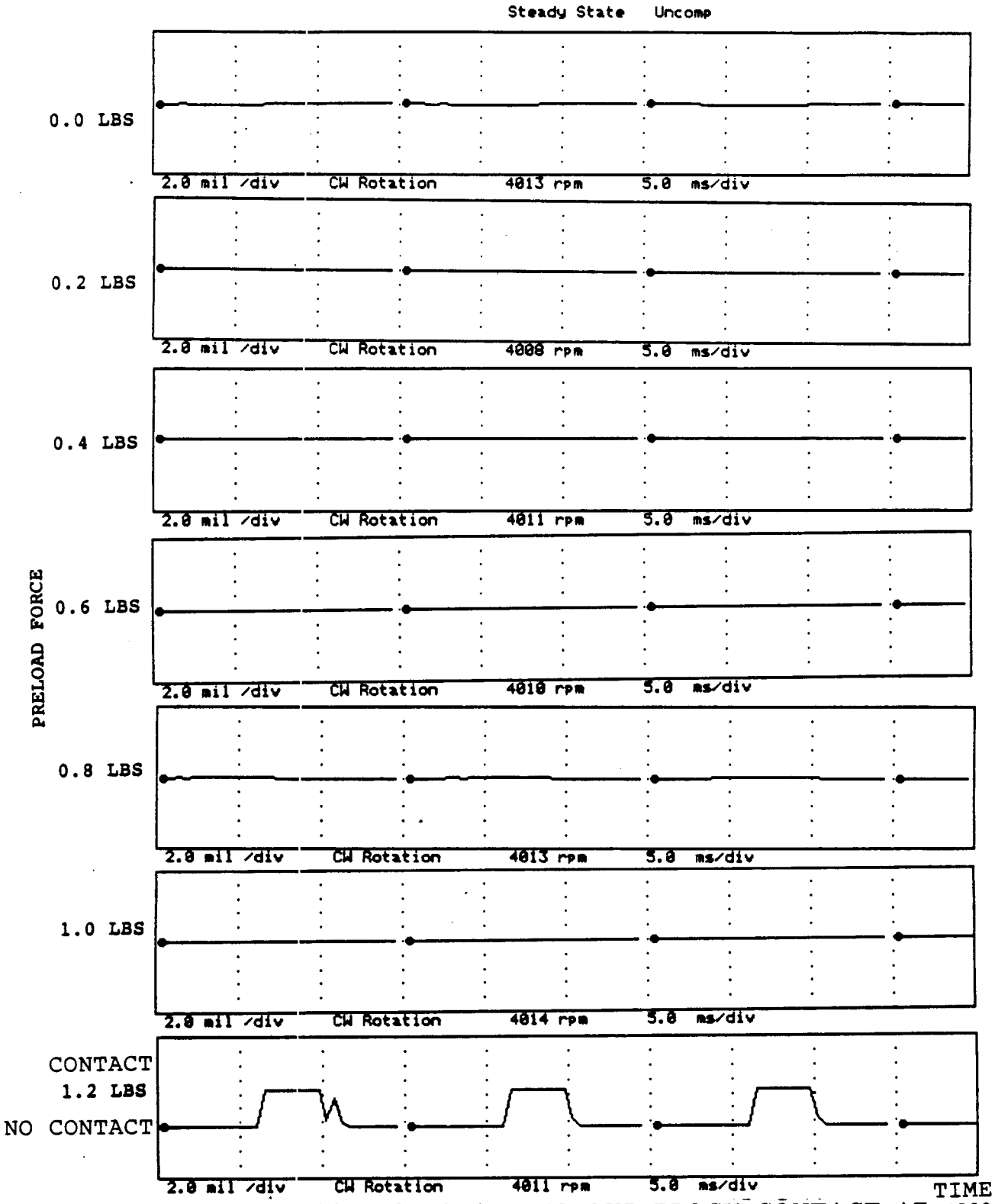

FIGURE 12.307 TIMEBASE FOR SHAFT TO RUB BLOCK CONTACT AT 4000 RPM, 10.0 PSI SEAL OIL PRESSURE, 0.8 IN–GRAM UNBALANCE LOCATED IN THE THIRD PUMP IMPELLER DISK, FOR INCREASING STATIC PRELOADS.

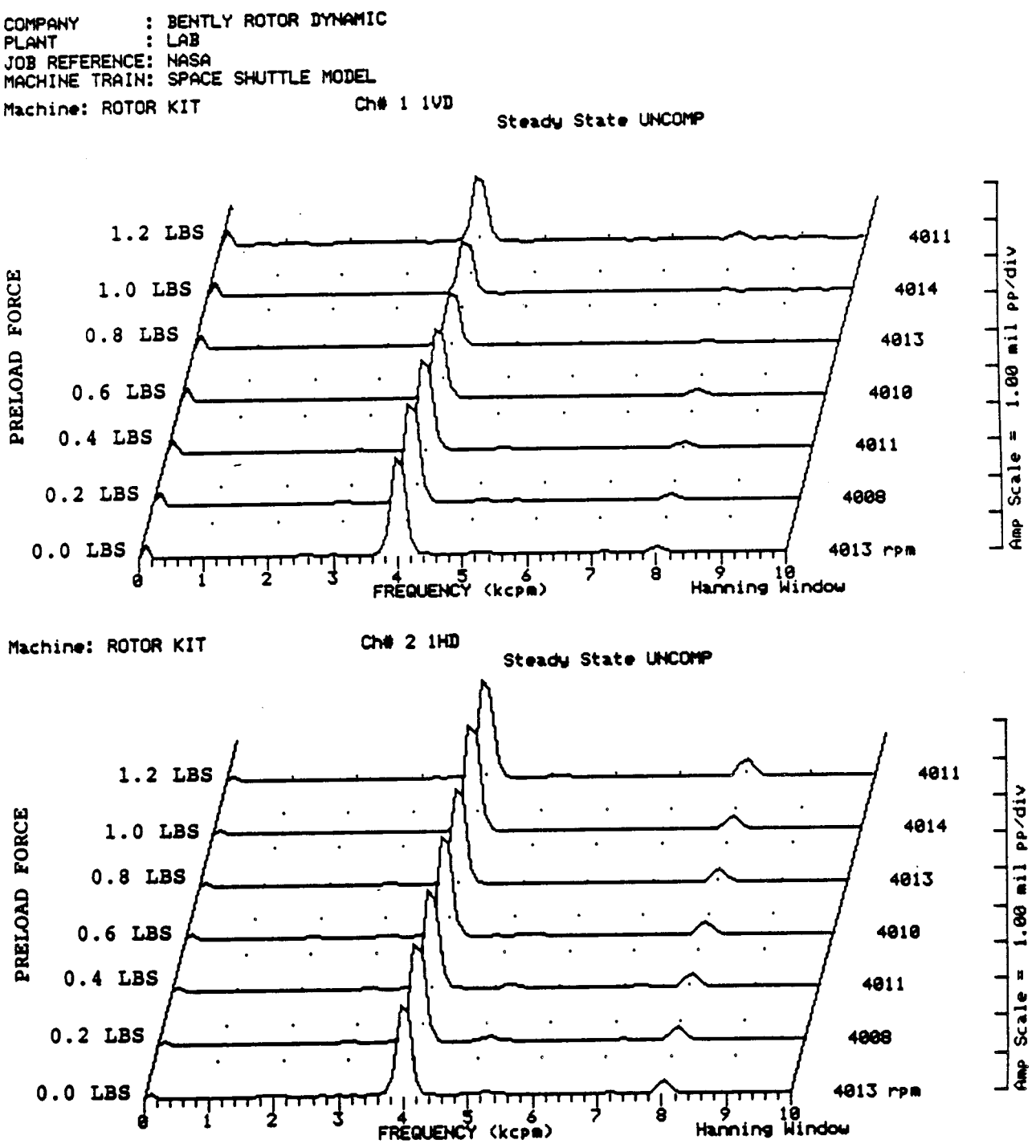

FIGURE 12.308 SPECTRAL CONTENT AT PROBE LOCATION 1 AT 4000 RPM, 10.0 PSI SEAL OIL PRESSURE, 0.8 IN–GRAM UNBALANCE LOCATED IN THE THIRD PUMP IMPELLER DISK, FOR INCREASING STATIC PRELOADS.

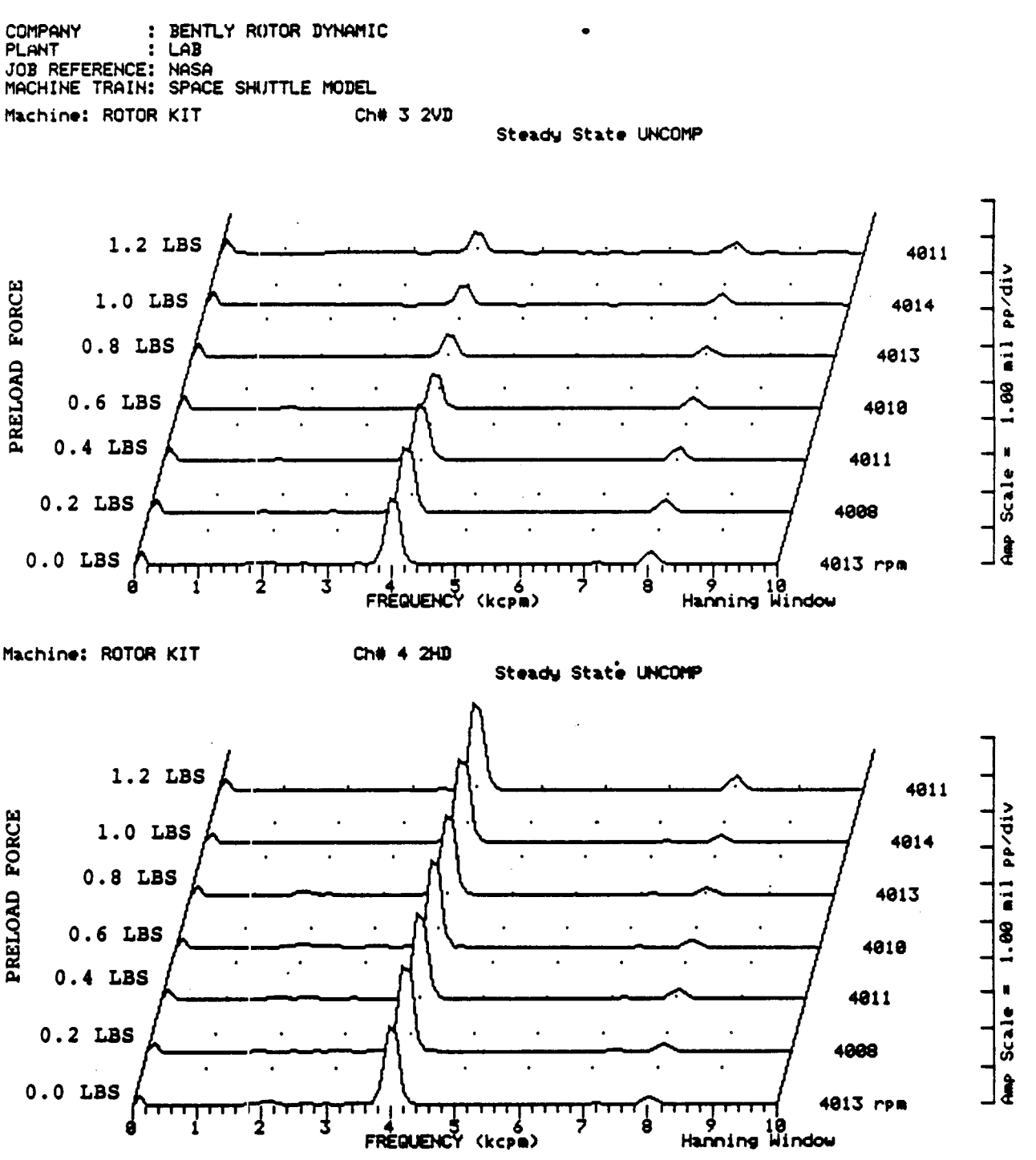

FIGURE 12.309 SPECTRAL CONTENT AT PROBE LOCATION 2 AT 4000 RPM, 10.0 PSI SEAL OIL PRESSURE, 0.8 IN–GRAM UNBALANCE LOCATED IN THE THIRD PUMP IMPELLER DISK, FOR INCREASING STATIC PRELOADS.

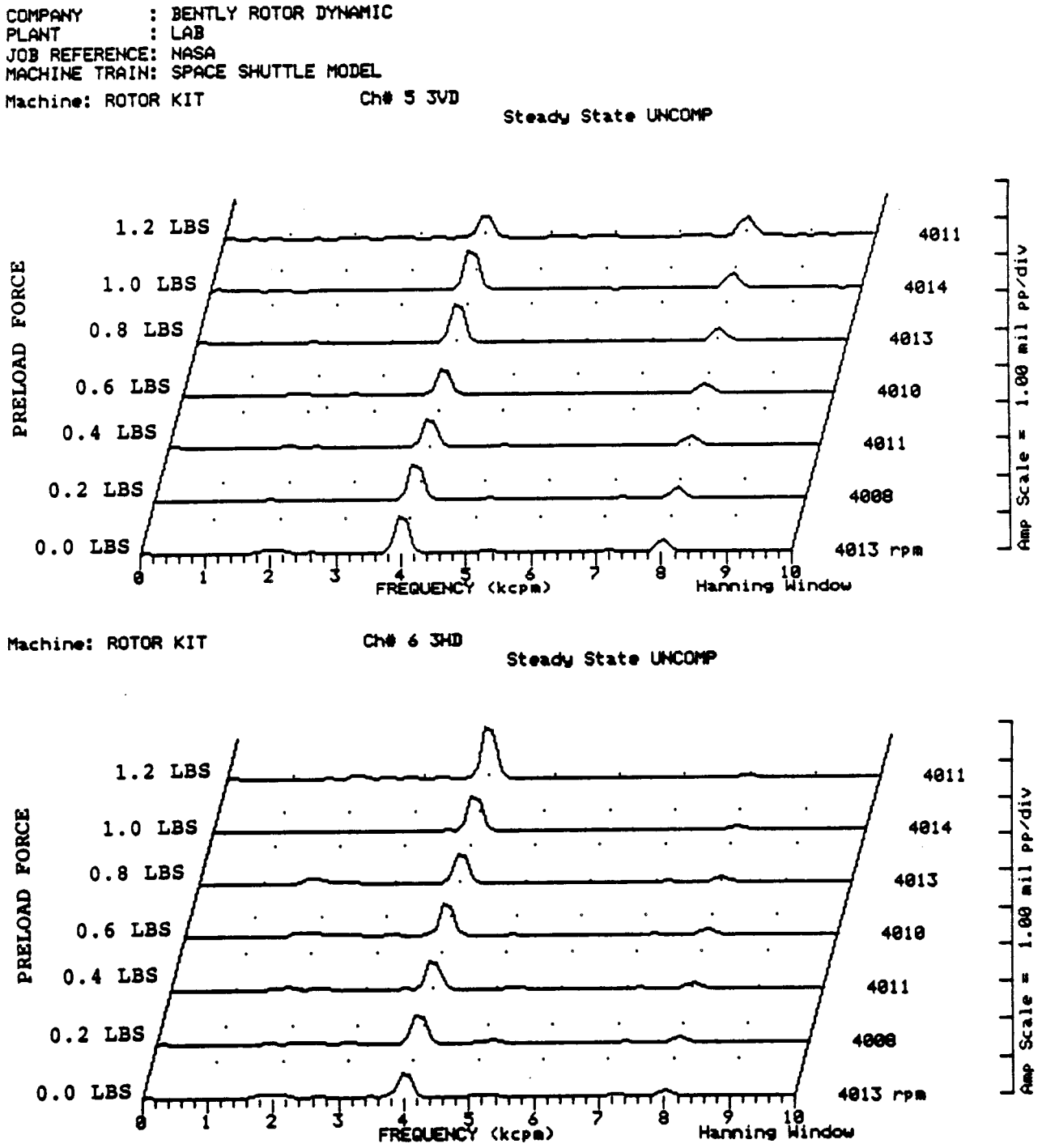

FIGURE 12.310 SPECTRAL CONTENT AT PROBE LOCATION 3 AT 4000 RPM, 10.0 PSI SEAL OIL PRESSURE, 0.8 IN–GRAM UNBALANCE LOCATED IN THE THIRD PUMP IMPELLER DISK, FOR INCREASING STATIC PRELOADS.

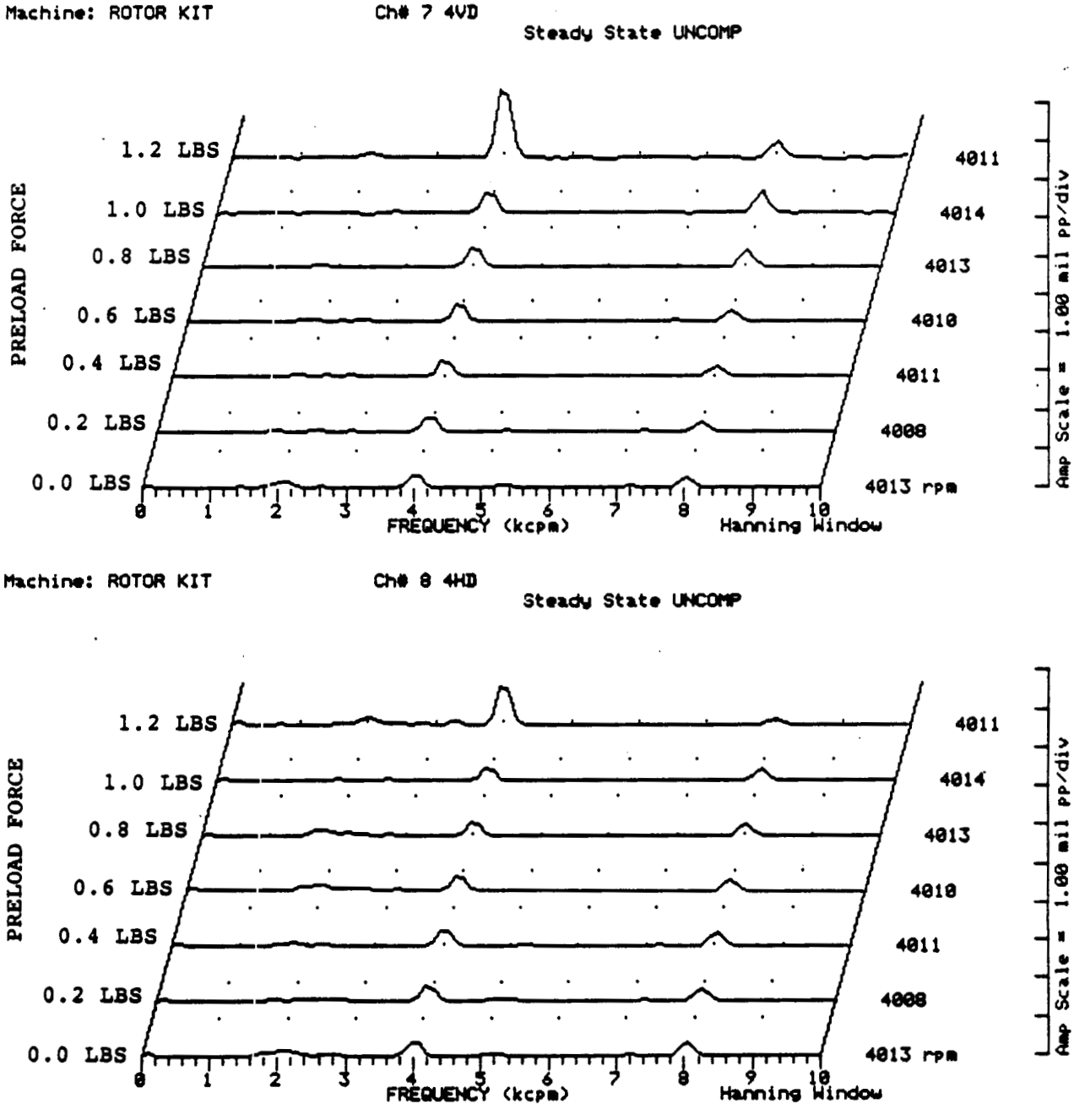

FIGURE 12.311 SPECTRAL CONTENT AT PROBE LOCATION 4 AT 4000 RPM, 10.0 PSI SEAL OIL PRESSURE, 0.8 IN–GRAM UNBALANCE LOCATED IN THE THIRD PUMP IMPELLER DISK, FOR INCREASING STATIC PRELOADS.

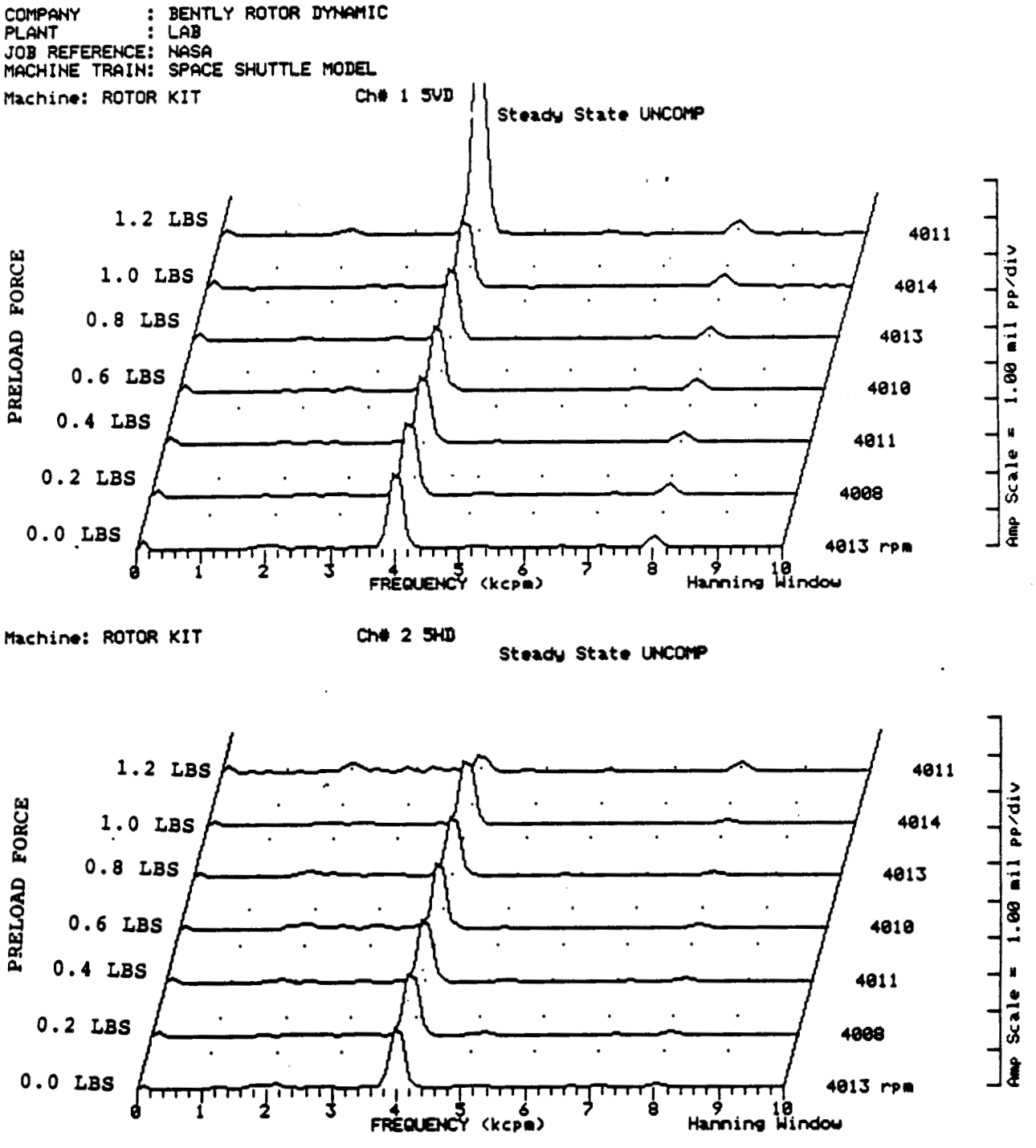

FIGURE 12.312 SPECTRAL CONTENT AT PROBE LOCATION 5 AT 4000 RPM, 10.0 PSI SEAL OIL PRESSURE, 0.8 IN–GRAM UNBALANCE LOCATED IN THE THIRD PUMP IMPELLER DISK, FOR INCREASING STATIC PRELOADS.

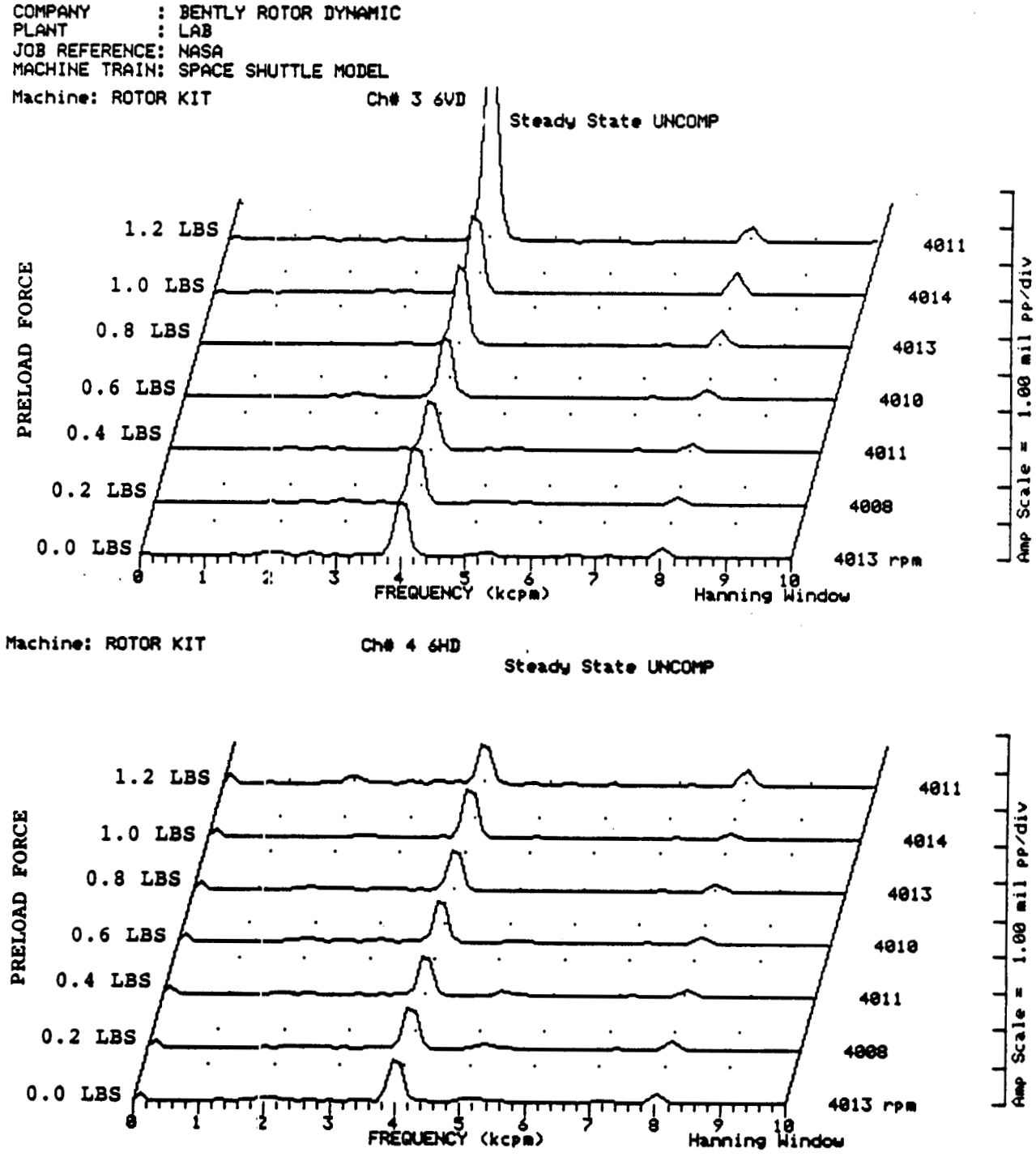

FIGURE 12.313 SPECTRAL CONTENT AT PROBE LOCATION 6 AT 4000 RPM, 10.0 PSI SEAL OIL PRESSURE, 0.8 IN–GRAM UNBALANCE LOCATED IN THE THIRD PUMP IMPELLER DISK, FOR INCREASING STATIC PRELOADS.

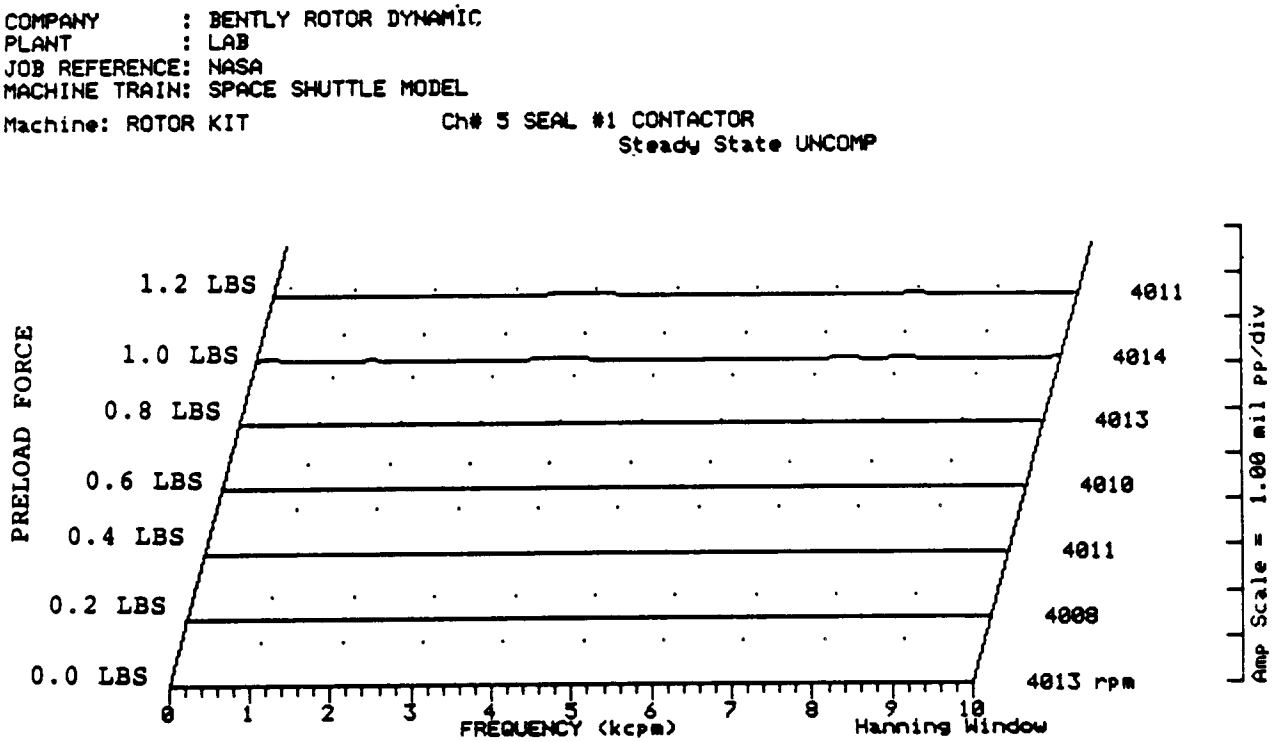

FIGURE 12.314 SPECTRAL CONTENT FOR SHAFT TO SEAL 1 CONTACT AT 4000 RPM, 10.0 PSI SEAL OIL PRESSURE, 0.8 IN–GRAM UNBALANCE LOCATED IN THE THIRD PUMP IMPELLER DISK, FOR INCREASING STATIC PRELOADS.

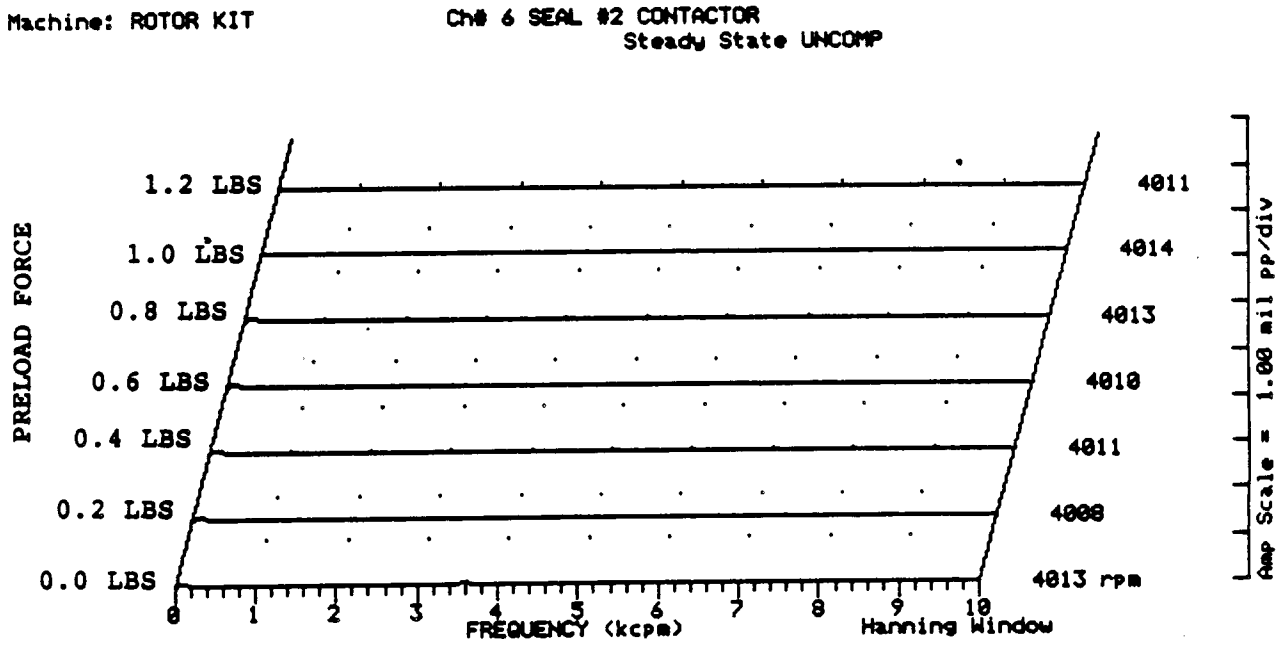

FIGURE 12.315 SPECTRAL CONTENT FOR SHAFT TO SEAL 2 CONTACT AT 4000 RPM, 10.0 PSI SEAL OIL PRESSURE, 0.8 IN–GRAM UNBALANCE LOCATED IN THE THIRD PUMP IMPELLER DISK, FOR INCREASING STATIC PRELOADS.

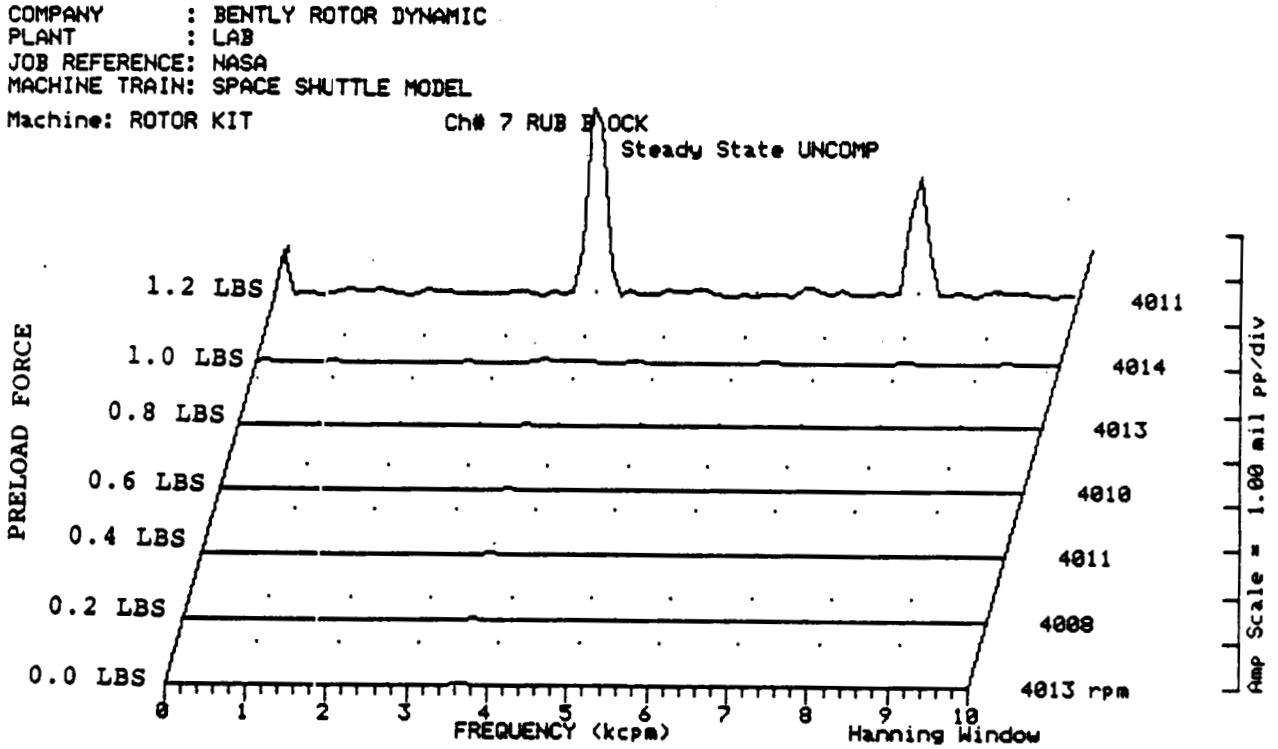

FIGURE 12.316 SPECTRAL CONTENT FOR SHAFT TO RUB BLOCK CONTACT AT 4000 RPM, 10.0 PSI SEAL OIL PRESSURE, 0.8 IN–GRAM UNBALANCE LOCATED IN THE THIRD PUMP IMPELLER DISK, FOR INCREASING STATIC PRELOADS.